FEB - FRESENIUS ENVIRONMENTAL BULLETIN
Founded jointly by F. Korte and F. Coulston
Production by PSP - Vimy Str. 1e, 85354 Freising, Germany in
cooperation with PRT-Parlar Research & Technology
Vimy Str 1e, 85354 Freising
Copyright© by PSP and PRT, Vimy Str. 1e, 85354 Freising, Germany
All rights are reserved, especially the right to translate into foreign language or other processes - or convert to a machine language, especially for data processing equipment - without written permission of the publisher. The rights of reproduction by lecture, radio and television transmission, magnetic sound recording or similar means are also reserved.
Printed in Germany-ISSN 1018-4619

FEB-EDITORIAL BOARD

CHIEF EDITOR:
Prof. Dr. Dr. H. Parlar
Parlar Research & Technology-PRT
Vimy Str.1e
85354 Freising, Germany

MANAGING EDITOR:
Dr. P. Parlar
Parlar Research & Technology
PRT, Vimy Str.1e
85354 Freising, Germany

CO-EDITORS:

Environmental Spectroscopy
Prof. Dr. A. Piccolo
Universita di Napoli "Frederico II"
Dipto. Di Scienze Chemica Agrarie
Via Universita 100, 80055 Portici, Italy

Environmental Biology
Prof. Dr. G. Schuurmann
UFZ-Umweltzentrum
Sektion Chemische Ökotoxikologie
Leipzig-Halle GmbH,
Permoserstr.15, 04318
04318 Leipzig, Germany
Prof. Dr. I. Holoubek
Recetox-Tocoen
Kamenice126/3, 62500 Brno, Czech Republic
Prof. Dr. M. Hakki Alma
Igdir Universitesi
76000, Igdir, Turkey

Environmental Analytical Chemistry
Prof. Dr. M. Bahadir
Lehrstuhl für Ökologische Chemie
und Umweltanalytik
TU Braunschweig
Lehrstuhl für Ökologische Chemie
Hagenring 30, 38106 Braunschweig, Germany
Dr. D. Kotzias
Via Germania29
21027 Barza(Va), Italy

Environmental Management
Dr. K. I. Nikolaou
Env.Protection of Thessaloniki
OMPEPT-54636 Thessaloniki
Greece

Environmental Toxicology
Prof. Dr. H. Greim
Senatkommision – DFG / TUM
85350 Freising, Germany

Environmental Proteomic
Dr. A. Fanous
Halal Control GmbH
Kobaltstr. 2-4
D-65428 Rüsselsheim, Germany

Environmental Education
Prof. Dr. C. Bayat
Esenyurt Üniversitesi
34510 Esenyurt, Istanbul, Turkey

Environmental Medicine
Prof. Dr. I. Tumen
Bartin Üniversitesi
74100, Bartin, Turkey

Advisory Board
K. Bester, K. Fischer, R. Kallenborn
DCG. Muir, R. Niessner,W.Vetter,
A. Reichlmayr-Lais, D. Steinberg,
J. P. Lay, J. Burhenne, L. O. Ruzo

Marketing Manager
Cansu Ekici, B. of B.A.
PRT-Research and Technology
Vimy Str 1e
85354 Freising, Germany
E-Mail: parlar@wzw.tum.de
parlar@prt-parlar.de
Phone: +49/8161887988

Fresenius Environmental Bulletin is abstracted/indexed in:
Biology & Environmental Sciences, BIOSIS, CAB International, Cambridge Scientific abstracts, Chemical Abstracts, Current Awareness, Current Contents/Agriculture, CSA Civil Engineering Abstracts, CSA Mechanical & Transportation Engineering, IBIDS database, Information Ventures, NISC, Research Alert, Science Citation Index (SCI), Scisearch, Selected Water Resources Abstracts

CONTENTS

ORIGINAL PAPERS

SEASONALLY VARIATIONS OF ARSENIC SPECIES IN CHICKEN MEATS CONSUMED BY TURKISH PEOPLE WITH HG-AAS 645
Gokce Kaya, Nagihan M Karaaslan, Mehmet Yaman

BIOREMEDIATION OF Cr(VI)-CONTAMINATED SOIL BY SULFATE-REDUCING BACTERIA (SRB) ENRICHMENT 651
Yuanyuan Han, Chengxu Dong, Yang Cao, Xueping Zhang, Hongwei Ni

CHARACTERIZATION AND COMPARISON OF GROWTH AND TOXICANT PRODUCTION FOR THREE *MICROCYSTIS AERUGINOSA* STRAINS 658
Xiaojian Zhou, Liangyu Tian, Shuyu Liu, Ke Feng, Cuili Jin

SOME HEAVY METALS AND MINERAL NUTRIENTS OF NARROW ENDEMIC *CIRSIUM BYZANTINUM* STEUD., FROM ISTANBUL, TURKEY: PLANT-SOIL INTERACTIONS 668
Ibrahim Ilker Ozyigit, Bulent Eskin, Mehmet Emin Uras, Ugur Sen1, Birsen Eygi Erdogan, Gulbubu Kurmanbekova, Zeki Severoglu, Ibrahim Ertugrul Yalcin

CATIONIC POLYACRYLAMIDE-MODIFIED RIVER SAND FOR EFFICIENT REMOVAL OF *MICROCYSTIS AERUGINOSA* 675
Chenghua Zhong, Yaoyao Huang, Yang Hu, Rui Bai, Ming Yang

PREDICTION OF AFLATOXIN CONTAMINATION ON DRIED FIG (*FICUS CARICA*) SAMPLES BY SPECTRAL IMAGE ANALYSIS IN COMPARISON WITH LABORATORY RESULTS 681
Omer Baris Ozluoymak, Emin Guzel

ULTRASOUND-ASSISTED MODIFICATION OF FLAX WASTES TO REMOVE METHYL VIOLET FROM AQUEOUS SOLUTION 690
Dan Xuanxuan, Li Xiaomin, Lin Jun, Han Ruiming

COMPARING DIFFERENT MOLECULAR SAMPLING METHODS FROM BIRDS VIA MOLECULAR SEXING 703
Ismail Burak Karaceylan, Mehmet Ali Tabur

AN ASSESTMENT OF CARBON DIOXIDE EMISSIONS RELATED TO FUEL CONSUMPTION FOR SUNFLOWER CULTIVATION 710
H Huseyin Ozturk

THE EFFECT OF ACID ON THE SURFACES OF SOME NATURAL STONES FROM TURKEY 720
Halim Cevizci

ALLELOPATHIC EFFECT OF ARTEMISIA VULGARIS ON WINTER WHEAT AND WINTER OILSEED RAPE 727
Ausra Marcinkeviciene, Zita Kriauciuniene, Rimantas Velicka, Robertas Kosteckas, Yoshiharu Fujii

SCREENING FOR HIGH-TEMPERATURE TOLERANT COTTON (*GOSSYPIUM SPP.*) BY USING SOME PHYSIO-MORPHOLOGICAL LEAF TRAITS 733
Remzi Ekinci, Sema Basbag, Emine Karademir, Cetin Karademir

MINERAL CONTENTS AND FATTY ACID COMPOSITIONS OF WILD AND CULTIVATED ROSE HIP (*ROSA CANINA* L.) 744
Suleyman Kizil*, Ozlem Toncer, Tahsin Sogut

PARAMETERS ESTIMATION OF RIVER WATER QUALITY MODEL USING A DIFFERENTIAL EVOLUTION ALGORITHM 749
Hongqin Xue, Xiaodong Liu, Yong Xiong, Li Gu, Ting Yang

INFLUENCE OF IBA TREATMENTS ON ROOT DEVELOPMENT AND MINERAL UPTAKE OF GRAPEVINE CUTTINGS 757
Sezer Sahin, Mustafa Uysal

HEAVY METAL, NITROGEN AND PHOSPHORUS ADSORPTION OF COMPACTED LINER MIXTURES 765
Zeki Gokalp, Ismail Tas, Oguzhan Uzun, Sema Kaplan, Mustafa Basaran

THE PHYSIOLOGY RESPONSE OF BIDENS PILOSA ROOT LEACHATES ON THE *PTERIS MULTIFIDA* GAMETOPHYTE 771
Kai-mei Zhang, Yu Shen, Yan-ming Fang

TEXTILE WASTEWATER TREATMENT USING BIOLOGICAL TRICKLING FILTER WITH NATURAL MEDIA IN COLD WEATHER (CASE STUDY: MOTAHARI TEXTILE FACTORY) 779
Toktam Shahriari, Marjan Shokouhi

LIFE CYCLE ASSESSMENT OF DIRECT AND EXTRUSION SPINNING: A CASE STUDY 787
Sule Altun, Seval Kutlu Akal-Solmaz, Gokhan Ekrem Ustun, Ismail Kagnici

A PRELIMINARY STUDY ON RADIOACTIVITY CONCENTRATIONS AND DOSE ASSESSMENT OF SOME ANTICARCINOGENIC MEDICINAL PLANTS USED IN TURKEY 793
Cumhur Canbazoglu, Suna Ilter, Sultan Sahin-Bal, Sule Karatepe, Mahmut Dogru

PERFORMANCE ASSESSMENT FOR NATURAL WASTEWATER TREATMENT SYSTEMS (CONSTRUCTED WETLAND SYSTEMS) 779
Zeki Gokalp, Mustafa Duygulu

INVESTIGATION OF EPI STRUCTURE IN FRONTAL OF INTAKES ON DIVERSION FLOW IN RIVER BEND WITH CCHE2D MODEL 807
Amir Abbas Kamanbedast, Shatirah Akib, Khodayar Khadem

OXIDATION OF PHENOLIC WASTEWATER WITH KHCO3 ADDITION IN SUPERCRITICAL WATER 815
Fu Yuan, Li Tiejun

MARINE BIOLOGICAL QUALITY ASSESSMENT AND ECOLOGICAL ENVIRONMENT SURVEY IN THE BOHAI BAY, CHINA 820
Wenliang Zhang, Haijiao Liu, Chao Wu, Jun Sun

RECONSTRUCTION OF LOW-FUNCTION FOREST SHIFTS MICROBIAL AND SOIL CARBON POOL 831
Yusong Cao, Huimin Wang, Yi'an Xiao, Cancan Zhao

EFFECT OF ENVIRONMENTAL PARAMETERS ON THE PERSISTENCE OF PROPAMOCARB, FLUOPICOLIDE AND 2,6-DICHLOROBENZAMIDE RESIDUES ON CAULIFLOWER AND SOIL 838
Gourishankar Manikrao, Soudamini Mohapatra, Lekha Siddamallaiah, Radhika Buddidathi, Nagapooja Yogendraiah Matadha

EFFECT OF DIVERSE REGIMES OF IRRIGATION ON METALS ACCUMMULATION IN WHEAT CROP: AN ASSESSESSMENT- DIRE NEED OF THE DAY 846
Kafeel Ahmad, Khalid Nawaz, Zafar Iqbal Khan, Muhammad Nadeem, Kinza Wajid, Asma Ashfaq, Babar Munir, Hafsa Memoona, Madiha Sana, Farzana Shaheen, Robina Kokab, Saif Ur Rehman, Muhammad Fahad Ullah Naunain Mehmood, Hira Muqadas, Zunaira Aslam, Mapara Shezadi, Ijaz Rasool Noorka, Humayun Basir, Hazoor Ahmad Shad, Fauzia Batool, Sana Iqbal, Mudasra Munir, Muhammad Sohail, Muhammad Sher, Saif Ullah, Ilker Ugulu, Yunus Dogan

EFFECTS OF NACL STRESS ON PROLINE METABOLISM, MALONDIALDEHYDE, GLYCINE BETAIN AND CHLOROPHYLL CONTENT IN SUNFLOWER PLANTS 856
Fusun Yurekli

PREPARATION OF IMMOBILIZED PHOTOSYNTHETIC BACTERIA MICROSPHERES AND DEGRADATION OF P-NITROANILINE 863
Zheng Fan, Wei Zheng, Lei Qin, Guo-Liang Zhang

THE FEEDING BEHAVIOUR OF *PLEUROBRACHIA PILEUS* (CTENOPHORA: TENTACULATA) IN THE SOUTHEASTERN BLACK SEA: IN RELATION TO AREA AND SEASON 871
Rahsan Evren Mazlum, Ulgen Aytan, Ertugrul Agirbas

THE PEDOGENIC DEVELOPMENT AND CLASSIFICATION OF SOIL DEVELOPED ON MOUNT HASANDAG'S VOLCANIC MATERIALS IN A SEMI-ARID ENVIRONMENT 880
Hasan Huseyin Ozaytekin, Cihan Uzun, Emel Karaarslan, Mert Dedeoglu

ANALYSIS OF THE WIND POWER TARIFF POLICY IN CHINA: EVOLUTION, PROBLEMS, AND COUNTERMEASURES 898
Shi-Chun Xu, Zheng-Xia He, Chang Gao, Yong-Mei Miao

HYDRAULIC ASSESSMENT OF FLOW IN STEPPED AND LABYRINTH SPILLWAYS TO DETERMINE ENERGY LOSS USING A PHYSICAL MODEL 910
Seyed Ali Banishoaib, Amin Bordbar, Amirabbas Kamanbedast, Alireza Masjedi, Mohammad Heidarnejad

MORPHOLOGICAL AND MOLECULAR CHARACTERIZATION OF AN ENDEMIC AND SIX KNOWN *BILIMNEUS* (HYDRAENIDAE: *LIMNEBIUS*) SPECIES FROM TURKEY 921
Ahmet Kasapoglu, Nesil Ertorun, Mehmet Burcin Mutlu, Erol Atay, Sibel Cilli

IOACCUMULATION OF Al, Cu AND Zn IN COONTAIL (*CERATOPHYLLUM DEMERSUM* L.) AFTER EXPERIMENTAL EXPOSURE TO A METAL COCKTAIL "POLLUTION EVENT" 928
Judith Lize Arnolds, Reinette Georgenie Snyman, James Philander Odendaal

EFFECT OF INFLUENT LOADS ON NITROGEN REMOVAL IN HORIZONTAL SUBSURFACE FLOW CONSTRUCTED WETLANDS WITH *CANNA INDICA* 938
Yan Zhang, Xuelan Liu, Yueming Wang, Peipei Yan, Qingchun Jing, Tianhong Shi, Xuejing Dai

TEMPORAL AND SPATIAL VARIATION OF PHYTOPLANKTON FUNCTIONAL GROUPS AND MAIN DRIVING FACTORS IN THE THREE GORGES RESERVOIR, CHINA 947
Jingya Wang, Shaowen Ye, Zhicong Wang, Jiashou Liu, Tanglin Zhang, Sovan Lek, Zhongjie Li

APPLICATION OF A MULTI-SUBGROUP HYBRID ALGORITHM IN AUTOMATIC PARAMETERIZATION OF A DISTRIBUTED SWAT HYDROLOGICAL MODEL 960
Ye Liu, Li Zhang, Lei Wu, Wen-gang Zhao, Xiao-yi Ma

ASSESSMENT OF SOME QUALITY PARAMETERS OF SPRING WATER IN ERZURUM, TURKEY 971
Banu Tuluk, Figen Orhan

EFFECTS OF SHORT-TERM HIGH-SALT STRESSES ON PHOTOSYNTHETIC CHARACTERISTICS, ACTIVITIES OF PROTECTIVE ENZYME AND COPPER UPTAKE OF ACORUS CALAMUS IN MICROCOSM SUBMERGED WETLANDS 982
Jianqiu Han, Yumei Zhou, Dandan Li, Guangqiang Zhai

THE EFFECT OF DIFFERENT ENVIRONMENTAL CONDITIONS ON YIELD AND OIL RATES OF SAFFLOWER (*CARTHAMUS TINCTORIUS* L.) 989
Ismail Demir, Kamil Kara

EXOGENOUS HYDROGEN PEROXIDE ALLEVIATES COPPER TOXICITY BY STIMULATING ANTIOXIDANT SYSTEM AND INCREASES PHOTOSYNTHESIS EFFICIENCY IN MAIZE SEEDLINGS 996
Rabiye Terzi, Neslihan Saruhan-Guler, Nihan Biskin, Asim Kadioglu

DETERMINATION OF SERA NGAL LEVELS IN PATIENTS WITH LUNG CANCER AND ITS RELATION WITH APOPTOSIS 1006
Bahadır Ozturk, Harun Ciftci, Husamettin Vatansev, Fatma Gul Gun, Guven Sami Sunam, Murat Oncel, Pinar Karabagli

ANTIOXIDANT AND IMMUNOSTIMULANT EFFECTS OF *ORIGANUM MINUTIFLORUM* O. SCHWARZ ET. P.H. DAVIS IN RAINBOW TROUT 1013
Ataman Bilge Sari, Oya Ustuner-Aydal

METHANE OXIDATION BACTERIA COMMUNITY STRUCTURES IN NANLING MOUNTAIN FOREST SOIL OF CHINESE CLIMATIC ECOTONE 1022
Lile Zeng, Huai Chen, NingWu, Zhiying Yan, Linfang Du, Yan Shen, Xu Wang, Jianqing Tian, Yunpeng Luo, Wei Li, Yixin He, Dan Zhu

A NEW WIRELESS BOLUS SENSOR WITH ACTIVE RFID TAG TO MEASURE RUMEN pH 1031
Habib Dogan, Musa Yavuz

APHICIDAL ACTIVITY OF ORANGE OIL TO THE GREEN PEACH APHID *MYZUS PERSICAE* SULZER (HOMOPTERA:APHIDIDAE) 1038
Tawfiq M Al–Antary, Mazen A Ateyyat, Idres H Belghasem, Salaheddin A Alaraj

PORE STRUCTURES CHARACTERISTICS AND POROSITY EVOLUTION OF TIGHT SANDSTONE RESERVOIR: TAKING THE CHANG 6_3 TIGHT SANDSTONES RESERVOIR OF HUAQING AREA IN ORDOS BASIN AS AN INSTANCE 1043
Dengke Liu, Wei Sun, Danchen Li, Jianchao Shi, Dazhong Ren

COMPARATIVE ANALYSIS OF ENERGY USE EFFICIENCY IN FOOD GRAIN PRODUCTION SYSTEMS OF PAKISTAN 1053
Adnan Abbas, Minli Yang, Khurram Yousaf, Khurshied Ahmed Khan, Tahir Iqbal, Shahbaz Gul Hassan

AN EXPERIMENT STUDY OF EFFECTS OF REEZING-THAWING CYCLES ON WATER AND SALT MIGRATION OF SALINE SOIL 1060
Gang Wang, Qing Wang, Xudong Zhang, Wenhua Wang, Chaoyue Li

ANALYSIS OF BACTERIAL COMMUNITY IN SEDIMENT FROM DALIAN MARINE AREA BY PCR-DGGE 1069
Jianfang Yan, Zhiheng Liu, Baixia Zhao, Qiu Liu, Jicheng Yu, Xiaohui Qi, Changjian Liu, Xiang Li

EFFICIENT PROTOCOL FOR MULTIPLE MICRO-SHOOT REGENERATION FROM ENDANGER, ENDEMIC AND ORNAMENTAL PLANT *CENTAUREA FENZLII* REICHARDT. 1076
Nalan Turkoglu, Fethi Ahmet Ozdemir, Nurhan Keskin, Khalid Mahmood Khawar

ENHANCED SIMULTANEOUS SEPARATION OF H_2S AND CO_2 BY AN AMINO ACID SALT-PROMOTED POTASSIUM CARBONATE SOLUTION IN A HOLLOW FIBER MEMBRANE CONTACTOR 1081
Pengrui Jin, Chuan Huang, Yadong Shen, Liao Wang

DIFFERENT EFFECTS OF HEAVY METALS ON PHYSIOLOGICAL AND BIOCHEMICAL PARAMETERS IN WHEAT VARIETIES 1086
Ayse Ak, Ersin Yucel

A RESEARCH ON THE DETERMINATION OF MOLECULAR GENETIC CHARACTERISTICS OF SOME *BEMISIA TABACI* (GENN.) (HEMIPTERA:ALEYRODIDAE) POPULATIONS 1095
Nurdan Topakci, Huseyin Gocmen

HEAVY METAL ACCUMULATION IN THE *MICROTUS GUENTHERI* (DANFORD AND ALSTON, 1880) LIVING NEAR THE MINES AS A BIOMONITOR 1104
Mustafa Yavuz, Ozgur Aktas

ADSORPTION REMOVAL OF METHYLENE BLUE FROM AQUEOUS SOLUTION USING CORNCOB ACTIVATED CARBON: EQUILIBRIUM AND KINETICS STUDIES 1122
Xuefeng Wei, Xiaoyang Wan, Fangzhou Liu, Juan Miao, Shufa Zhu, Qingshan Niu

STATISTICAL EVALUATION OF WATERMELON GENOTYPES EXHIBITING DIFFERENT FEATURES UNDER STRESS CONDITIONS 1131
Muhemet Zeki Karipcin

STUDY ON THE CHARACTERISTICS OF WATER - SOLUBLE ION POLLUTION IN $PM_{2.5}$ IN FULING DISTRICT 1138
Xianghong Wang, Qiong Luo, Lin Qin, Huanbo Wang, Fumo Yang

EFFECT OF HEAT STABILIZED WHEAT GERM ON SOME PROPERTIES OF COOKIES 1145
Hulya Gul, Fatma Hayit, Songul Bicakci, Sultan Acun

STUDY ON COLONIZATION ABILITY IN PLANTS OF ENDOPHYTIC BACILLUS AMYLOLIQUEFACIENS HT-Q6 ISOLATED FROM WALNUT 1152
Mei-qin Wang, Xiao-juan Hao, Yan-ping Yao, Min Xu

COMPARISON OF MAXIMUM RANGE OF POLLUTANTS 1157
Ljiljana Takic, Sonja Ketin, Ranko Marjanovic, Adem Preljevic, Selim Sacirovic

THE EFFECTS OF MANNAN OLIGOSACCHARIDE (MOS) AND VITAMIN B_{12} ADDITIVES ON THE LIVER AND INTESTINE HISTOLOGY OF THE CARP FRY (*CYPRINUS CARPIO* L. 1758) 1164
Mehmet Ates, Hasan Huseyin Atar

INVESTIGATION OF DESMODESMUS ARMATUS FOR LEAD (Pb^{+2}) AND NICKEL (Ni^{+2}) REMOVAL CAPACITY FROM METAL POLLUTED WATER 1169
Cigdem Acar, Ozden Fakıoglu

DETERMINATION OF PHENOLIC COMPOUNDS OF *STACHYS RUPESTRIS* MONTBRET ET AUCHER EX BENTHAM BY LC-MS/MS AND ITS BIOLOGICAL ACTIVITIES 1176
Bulent Ergun, Fatih Goger, Yavuz Bulent Kose, Gokalp Iscan

NUMERICAL COMPARISON OF ANATOMICAL FEATURES IN SOME *ALLIUM* L. 1183
Ali Ozdemir, Canan Ozdemir

THE USE OF ANALYTICAL HIERARCHY METHOD IN FACTORY ESTABLISHMENT PLACEMENT TO PREVENT ENVIRONMENTAL POLLUTION IN FURNITURE INDUSTRY 1191
Yildiz Cabuk

STUDY ON BIODEGRADATION OF CHLORPYRIFOS AND UTILIZATION OF A CHLORPYRIFOS DEGRADING BACTERIUM, *BACILLUS AMYLOLIQUEFACIENS* CZ-5 1196
Jiangwei Zhu, Yan Zhao, Kun Xie, Xiaolou Li, Yi Chen

PRODUCTION OF GHK TRIPEPTIDE EMBEDDED POLY VINYL ALCOHOL-NANOFIBERS 1202
Yasemin Budama Kilinc, Rabia Cakir Koc, Guncem Ozgun Eren, Perihan Kubra Akman, Mustafa Tahsin Yilmaz

THE GENETIC VARIATION OF SEVEN NATURAL CRIMEAN JUNIPER (*JUNIPERUS EXCELSA* BIEB. M.) POPULATIONS AND ITS GROWING ENVIRONMENTAL CONDITIONS IN TURKEY 1210
Cengiz Yucedag, Halil Baris Ozel

SPATIOTEMPORAL CHARACTERISTICS OF HOURLY RAINFALL IN THE UPPER REACHES OF HANJIANG RIVER BASIN 1214
Mingyuan Wang, Weihong Liao, Xiaohui Lei, Yongguang Hu, Tao Qin

EFFECT OF RELATIVE HUMIDITY ON HUMAN INDUCED RESUSPENSION OF PARTICLES 1226
Shuihua Zheng, Lipan Zhao, Weiyuan Du, Yunqing Gu, Jiegang Mou, Jiaxin Tang

DETERMINATION OF MITE SPECIES ON VINEYARDS OF ANKARA – TURKEY 1232
Emre Inak, Sultan Cobanoglu

THE FATTY ACID AND MINERAL COMPOSITIONS OF DIFFERENT CHICKPEA CULTIVARS CULTIVATED 1240
Muharrem Kaya, Asuman Kan, Azime Yilmaz, Ruziye Karaman, Aykut Sener

THE USE OF FURFURAL RESIDUE FOR AQUEOUS-PHASE Cr(VI) REDUCTION 1248
Zhili Wang, Huanzhen Zhang

POST-HARVEST APPLICATION OF SALICYLIC ACID CAN RETAIN THE PHYSICOCHEMICAL ATTRIBUTES OF SWEET ORANGES CV. BLOOD RED 1256
Faheemul Haq, Muhammad Sajid, Amjad Iqbal, Farooq Shah, Ibadullah Jan, Badshah Islam, Zafar Hayat Khan, Mudassar Iqbal, Yousaf Jamal

CHARACTERISTICS OF DEEP SHALE WITH DRILLING FLUID IMMERSION BASED ON RSM 1264
Yuehui Pan, Jingyun Peng

EXPERIMENTAL STUDY ON MECHANICAL PROPERTIES OF HIGH WATER QUICK-SETTING MATERIALS INMARINE ENVIRONMENT 1269
Bingbing Guo,Changwu Liu, Bangwen Lu, Hui Xie, Defeng Liu

STUDY ON DIURNAL VARIATION OF METHANE EMISSION FROM DOMESTIC REFUSE LANDFILL 1282
Wu Xiaoyun, Zheng Youfei, Liu Shengtao, Lin Kesi

NOVEL CVD GROWTH OF LARGE AREA GRAPHENE AND CNTS/GRAPHENE COMPOSITE AT LOW TEMPERATURE AND ITS POTENTIAL APPLICATION 1289
Shu Ye, Won-Chun Oh

© by PSP Volume 27 – No. 2/2018 pages 645-650 Fresenius Environmental Bulletin

SEASONALLY VARIATIONS OF ARSENIC SPECIES IN CHICKEN MEATS CONSUMED BY TURKISH PEOPLE WITH HG-AAS

Gokce Kaya[1,*], Nagihan M Karaaslan[2], Mehmet Yaman[3]

[1]Firat University, Health Sciences Faculty, Department of Nutrition and Dietetic, Elazig, Turkey
[2]Munzur University, Engineering Faculty, Department of Chemical Engineering, Tunceli, Turkey
[3]Firat University, Science Faculty, Department of Chemistry, Elazig, Turkey

ABSTRACT

The aim in this study is speciation and determination of arsenic in chicken meat matrix. For this purpose, chicken meat samples consumed commonly by Turkish people belonging to five different companies in Turkey were obtained from markets once per 15 days during 14 months. The samples were digested in microwave oven by using both nitric and hydrochloric acid. It was found that microwave digestion method can be used successfully in the speciation analysis of arsenic. The determination and speciation of As in solutions were carried out by hydride generation-atomic absorption spectrophotometry (HG-AAS). From the observed results, concentrations of As (V) were ranged between 3.0-14.0 ng g^{-1} (mean 7.3 ng g^{-1}) for breast tissues and 3.0-9.0 ng g^{-1} (mean 5.1 ng g^{-1}) for leg tissues. The concentrations of As (III) in all studied chicken tissues were found lower than the limit of detection (2 ng g^{-1}).

KEYWORDS:
Arsenic speciation, chicken, HG-AAS, meat, microwave digestion.

INTRODUCTION

Heavy metals such as cadmium, lead, arsenic, mercury, and chromium, even in low concentrations in tissues of edible animals, have toxic effects [1]. For example, inorganic arsenic is a human carcinogen even at low-level. Long term exposures to inorganic arsenic have been shown to cause cancers of the lung, bladder, kidney, and skin [2, 3]. Due to these concerns, the USEPA lowered the maximum concentration level (MCL) of drinking water for total arsenic to 10 μgL^{-1} [4]. Further, chronic low-level arsenic exposure has been implicated in adverse health consequences including cardiovascular disease, type2 diabetes, neurocognitive deficits, adverse birth outcomes, and endocrine disruption. Briefly, arsenate (As(V)) and arsenite (As(III)) are believed to be most potent in inducing toxic effects. Basu et al. [3] found angiogenesis associated with vascular disease as well as the growth of new tumors following exposure of human Endothelial cell cultures to 4-hydroxy-3-nitrobenzene arsenic acid (roxarsone) and As(III). Roxarsone was a more potent inducer of angiogenesis than As (III) [3]. As a result; total arsenic content does not give usually enough information if the clinical or environmental importance of this element is to be considered. Therefore, speciation analysis is commonly considered. The distinction between the different species (chemical forms and oxidation states) of this element gives additional information in relation to toxicity and biodistribution. The metabolism of arsenic species in living organisms, including humans, is a complex matter, because the biodistribution of inorganic arsenic species depends on the matrix (e.g. food, water, bewerages) in which they are ingested. It is generally accepted that the toxicity of arsenic is greater for inorganic species (arsenite being more toxic than arsenate) than for organic species (methylated species, arsenobetaine, roxarsone or arsenoribosides) [5].

Roxarsone is an organic arsenical compound containing arsenic. It approved by the U.S. Food and Drug Administration (FDA) in 1944 for use in poultry feed for disease prevention, growth promotion, enhanced feed utilization, and improved meat pigmentation [6].

For several decades, roxarsone (4-hydroxy-3-nitrobenzenearsonicacid) has been approved for use in the feed of broilers (*Gallus gallus domesticus*) and swine (*Susscrofa domesticus*) to control coccidiosis, speed weight gain, and improve meat color [7]. So, the supplies of phenyl arsenic acids (e.g. Nitarsone, Roxarsone) to chicken meat were mentioned to be man-made feed additives. In 2011, the US-FDA released a study that found a higher incidence of carcinogenic inorganic arsenic in livers of roxarsone-treated chickens compared to controls [8]. As of July 2011, the use of roxarsone was banned in the United States because it was discovered that potentially dangerous amounts of As accumulated in meat tissue, particularly in young broilers (up to 0.45 mg As kg^{-1}) [7]. However, roxarsone is still available for use in several other undeveloped countries. In one study, among cooked samples, inorganic arsenic concentrations were higher by greater than a factor of 2 in the

conventional samples (1.8 μg kg^{-1}) than in the antibiotic-free or organic samples, and roxarsone was also detected in 50% of the conventional samples [9].

In speciation studies, the extraction procedure is a crucial step in analytical scheme, because no interconversion of species should occur and quantitative extraction efficiency is necessary. Generally, mild extractants such as water and methanol–water mixtures are used for this purpose. The other used extraction procedures include enzymatic digestion or sonication in an ultrasonic bath [10, 11, 12]. Although sulfuric acid can be employed to break down organoarsenic compounds which are not reduced it is not suggested to study in HG-AAS because hydride is not forming up on reaction with sodium borohydride. For the determination of total arsenic, digestion with nitric acid may be used successfully in many cases. In some studies, nitric acid and hydrogen peroxide digestions have been used successfully to replace the conventional nitric and perchloric acid and sulfuric acid procedures.

In this study, chicken meat samples belonging to 5 different companies in Elazig city-Turkey were obtained from markets once per 15 days during 14 months. The samples were digested in microwave oven by using both nitric and hydrochloric acid. The determination and speciation of As in solutions were carried out by hydride generation-atomic absorption spectrophotometry (HG-AAS).

MATERIALS AND METHODS

Apparatus. The analyses were carried by hydride generation-atomic absorption spectrophotometry (Agilent 240 Duo F-AAS). The operating parameters used in the HG-AAS measurements were chosen as described in the manual handbook. A microwave digestion system (CEM MARSXpress) was used to prepare the samples for the analysis. Doubly distilled water, obtained with a water purification system (Millipore Direct-Q, Millipore Corporation, Bedford, MA, USA) was used for all samples preparations.

Reagents and solutions. Stock standard solutions of arsenic species (1,000 mg L^{-1}, as As) were prepared from arsenic trioxide and arsenic penta oxide in 5 M HCL and distilled water, respectively. HCl, $NaBH_4$, HNO_3, As_2O_3 and As_2O_5 were of analytical-reagent grade (Merck). Standard reference material (NCS ZC73016 chicken-trace elements) was used to check the accuracy. All glass containers were kept clean in order to prevent elemental contamination when they were not in use. Concentrated nitric (65 %, Merck) and hydrochloric (36 %, Merck) acids were used in the digestion procedure. Briefly, unless stated otherwise, all chemicals used throughout the study were of high-purity reagent grade.

Sample collection and preparation. From July 2008 through August 2009, we purchased chicken breasts and legs from markets once per 15 days during 14 months in Elazig, Turkey. The samples belonging to different companies (firms) were cleaned, transported to the laboratory immediately, and stored in a refrigerator prior to analysis. So, approximately, 150 chicken breast and leg samples were analyzed. The samples were digested by using nitric acid to leave total arsenic. The samples were extracted by using hydrochloric acid to leave only arsenic (III) without oxidation to (V)). To determine the best digestion method, the same samples of breast and leg for firm 1 were digested by using both classical wet method and microwave digestion.

In the classical wet method, the samples were treated in 6 M HCl during one night and evaporated in bath water up near to drying, for As(III) extraction. After addition 5 M of HCl to this remaining, the mixture was filtrated and measured. To extract total arsenic from meat sample, concentrated nitric acid was added to the sample and evaporated near to drying. After addition 5 mL of HCl (for HG-AAS determinations), the solution was filtrated, if necessary, and the clear solution measured.

In the microwave digestion, the samples were digested in microwave oven by using both nitric acid (to leave total arsenic) and hydrochloric acid (to extract arsenic (III) without oxidation to (V)). To As(III) determination, 6 M HCl was added to the samples and, the mixtures were irradiated for 30 min as described in manual handbook of microwave oven. After cooling and filtration, if necessary, the solutions were analyzed. To As(V) determination, concentrated nitric acid were added to the samples and digested for 30 min in microwave oven. After evaporating to leave 2-3 mL in water bath, 5 M HCl were added and filtrated. The solid mixture of ascorbic acid and KI (2/1) was added to the obtained clear solution and stirred for 5 min. As a result of this procedure, all of As(V) were reduced to As(III), and probable interference effects from cations such as Ni(II), Cu(II), Fe(III), Cr(III), Mo(II), Bi(III), Se(IV), Se(VI), Sb(III) and Sb(V) were prevented. Then, the determinations were carried out by hydride generation-atomic absorption spectrophotometry (HG-AAS). As(V) concentration was determined from the difference between these results and the results obtained by using 5 M HCl for extraction.

The lowest concentration in the calibration plot for each arsenic species was considered as the limit of quantitation (LOQ). Under the conditions, the limit of quantitation (LOQ) was found to be 0.5 ng mL^{-1} and the limit of detection (LOD) was found to be 0.2 ng mL^{-1}. Blanks were also digested to determine the background contribution of the reagents and treated the same way as the samples.

Related with statistically consideration, One-Way Analyses of Variance (ANOVA) were conducted to test the equality of mean values for each

sample of interest. One of the pairwise comparison tests, Tukey HSD, was carried out to find which of the sample means is different from each other depending on types of meat, firms and collected time. SPSS (version 15) statistical program was used for all statistical computations. Statistical significance was considered when P was equal to=or higher than 0.05.

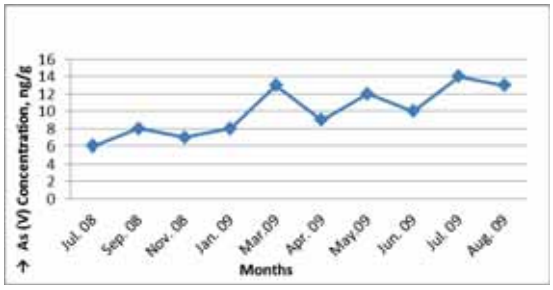

FIGURE 1
Seasonal variations As (V) concentrations of chicken breast tissues from firm 1.

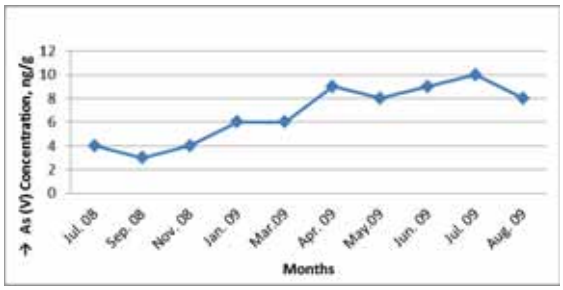

FIGURE 2
Seasonal variations As (V) concentrations of chicken breast tissues from firm 3.

RESULTS AND DISCUSSIONS

Figure 1 indicate that seasonal (July 2008-August 2009) variations As (V) concentrations of chicken breast tissues from firm 1. Figure 2 represent that seasonal (July 2008-August 2009) variations As (V) concentrations of chicken breast tissues from firm 3 and Figure 3 show that seasonal (July 2008-August 2009) variations As (V) concentrations of chicken breast tissues from firm 4. As a result, As (V) concentrations of chicken breast tissues from firm 1, firm 3 and firm 4 higher than firm 2 and 5. We can say that obtained from Figure 1, 2 and 3 indicate specially the concentration values in 2009 year a little higher than in 2008 year concentration values which is As (V) concentrations of chicken breast tissues from all three firms (firm 1, 3 and 4).

Prior to analysis, validation studies were done. Regarding the recovery used for quality control, the arsenic (III) and (V) concentrations were in good agreement, confirming the accuracy of the analytical method applied (Table 1). Moreover, the precision for arsenic (III) and (V) were <15% and <11%, respectively for all analytes. The limit of quantitation (LOQ) is 0.5 ng mL^{-1}. Taking into consideration 1.0 g meat sample and 5 mL of final solution, LOQ for sample was determined to be 2.5 µg kg^{-1}.

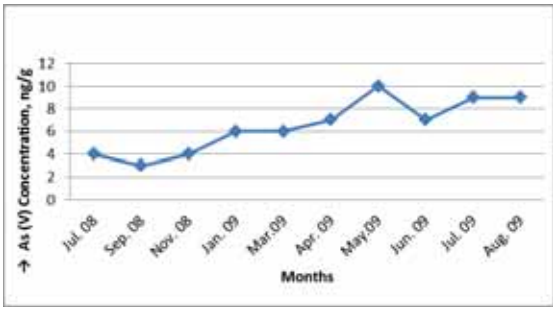

FIGURE 3
Seasonal variations As (V) concentrations of chicken breast tissues from firm 4.

TABLE 1
Comparison of As (V) concentrations (ng g^{-1}) depending on digestion procedures. (The results are mean values ± standard deviation, n=3)

Digestion procedure	As (V) found for firm 1 (May 2009) in breast	As (V) found for firm 1 (May 2009) in legs
Classical	11±1.2	8.4±0.9
MW	12±1.0	9.2±0.9

Comparison of digestion methods. From the Table 1, it was seen that higher concentrations of arsenic in microwave digestion method were found compared to classical method although this difference is slight. So, microwave digestion was preferred for all other samples.

Concentrations of arsenic species in chicken meat. The mean concentrations of arsenic (V) in all studied samples and their standard deviations (SD) are shown in Table 2. The mean concentrations of arsenic (III) in both chicken leg and breast meat samples were found to be below LOQ (2.5 µg kg^{-1}). It was clearly seen that arsenic (V) concentrations in breast samples of Firm 1 are higher than in legs of the same firm ($p<0.05$). Some differences were found in arsenic (V) concentrations among the different firms. Mean Arsenic (V) levels for Firm 1 were significantly higher in both chicken breast and leg samples. Further, the observed As(V) levels in chicken breasts are higher slightly than in the legs for all studied samples. Due to publishing report in recent, the U.S. Food and Drug Administration (FDA) has established tolerance levels for arsenic in by-products of animals treated with veterinary drugs and the permissible level arranged as 0.5 mg kg^{-1} in eggs and uncooked edible tissues of chickens and turkeys [13]. The FDA has not established safety standards for inorganic As in foods, including rice, juice, chicken, or other foods potentially contaminated by arsenic. In 1963, the FDA tolerance for total

TABLE 2
Arsenic concentrations (ng g^{-1}) in chicken meat. (The results are mean values ± standard deviation, n=3)

Collected Time	Species of tissues	As (V)				
		Firm 1	Firm 2	Firm 3	Firm 4	Firm 5
July 08	Breast	6±0.7	4±0.7	4±0.6	4±0.7	4±0.7
September 08		8±0.9	3±0.5	3±0.5	3±0.4	3±0.5
November 08		7±0.8	4±0.6	4±0.7	4±0.5	4±0.6
January 09		8±0.9	6±0.7	6±0.7	6±0.8	6±0.8
March 09		13±1.5	6±.0.8	6±0.8	6±0.7	6±0.7
April 09		9±1.0	7±0.9	9±0.9	7±0.9	8±1.0
May 09		12±1.4	10±1.2	8±1.0	10±1.3	9±1.2
June 09		10±1.1	9±1.0	9±1.1	7±0.8	9±1.1
July 09		14±1.5	8±0.9	10±1.3	9±0.9	10±1.3
August 09		13±1.4	7±0.8	8±1.2	9±1.1	9±1.2
Mean Values		**10.0±2.8**	**6.4±2.3**	**6.7±2.5**	**6.5±2.4**	**6.8±2.5**
July 08	Leg	5±0.6	4±0.7	4±0.7	4±0.7	4±0.6
September 08		5±0.6	4±0.6	4±0.7	4±0.6	4±0.7
November 08		6±0.7	3±0.5	3±0.4	3±0.5	3±0.4
January 09		6±0.5	4±0.7	4±0.6	4±0.7	4±0.6
March 09		5±0.6	3±0.4	3±0.5	3±0.5	3±0.5
April 09		6±0.7	5±.0.5	5±0.7	5±0.7	5±0.7
May 09		7±0.8	6±.0.7	7±0.8	6±0.7	7±0.8
June 09		9±1.1	7±.0.8	6±0.8	4±0.5	6±0.8
July 09		8±0.9	6±.0.6	4±0.5	7±0.9	7±0.9
August 09		8±1.0	5±.0.6	8±1.0	6±0.7	6±0.6
Mean Values		**6.5±1.4**	**4.7±1.3**	**4.8±1.7**	**4.6±1.4**	**4.9±1.5**

arsenic residues in muscle tissues of poultry products of 0.5 mg kg^{-1} was established [14]. In 2011, the FDA Center for Veterinary Medicine (CVM) indicated that the "CVM has determined that a safe level of inorganic arsenic in chicken meat is < 1 μg kg^{-1}", following a roxarsone feeding study [15]. As seen from Table 2, the obtained values in this study are more lover than the permissible levels recommended by FDA-1963. However, these values are higher than the safe level of inorganic arsenic in chicken meat established by FDA-2011 < 1 ng g^{-1}.

Andrade et al. [16] reported that the concentrations of total As element were in ranges of 0.396–12.584 (mean 2.724) mg kg^{-1} for fresh weight (fw) of fish, 0.008–0.783 (mean 0.143) mg kg^{-1} for cereals, nd–0.444 (mean 0.102) mg kg^{-1} for meat and meat by-products taken from south-east Spain using by hydride generation atomic absorption spectrometry [16]. In 2011, Nachman et al. [17] stated that arsenic concentrations in poultry feather meal were found to be between 44 and 4100 μg kg^{-1} [17]. Bordajandi et al. [18] reported that the contents of As were found to be in ranges of ND (not detected)−17.8 ng g^{-1} on fresh weight for chicken. They observed that total mean As level were to be 234 ng g^{-1} on fresh weight canned tuna and were to be 22008 ng g^{-1} on fresh weight tope-sea product taken from different markets across the city of Huelva, located in southwestern Spain and under strong industrial activity [18]. Li et al. [19] reported that the concentrations of As were found to be 303, 289, and 384 ng g^{-1}, in chicken tissue, shrimp and code fish, respectively. They obtained that the concentrations of As in chicken tissue, shrimp and fish were higher three times than carrot (108 ng g^{-1}) and mushroom (107 ng g^{-1}) samples [19]. Julshamn et al. [20] stated that total As concentrations were determined in fish species and prawns from the Barents Sea, Norwegian Sea and North Sea sampled in 1994–2001. In this study, total mean arsenic concentrations were found to be 5.6 mg kg^{-1} for Atlantic cod (*Gadus morhua*), 3.5 (2.1–6.1) mg kg^{-1} for Mackerel (*Scomber scombrus*), 3.6 (2.6–4.5) mg kg^{-1} for Sprat (*Sprattus sprattus*), 1.7 (0.9–2.7) mg kg^{-1} for Horse mackerel (*Trachurus trachurus*), 1.7 (0.8–2.6) mg kg^{-1} for Red fish (*Sebastes marinus*) [20]. Miyashita et al. [21] reported that As (V) and As(III) levels in water and biological samples from the Hayakawa River (Kanagawa, Japan) and high concentrations of total arsenic were obtained to be 2600 μg kg^{-1} in crustacean tissues and were found to be 150–2100 μg kg^{-1} in fish muscle tissues on dry weight [21]. Pizarro et al. [10] reported that total arsenic levels were determined to be 0.182 mg kg^{-1} for rice, 0.168 mg kg^{-1} for chicken, 68.3 mg kg^{-1} for fish [10]. Shah et al. [22] reported that the concentrations of total arsenic in different tissues of broiler chicken were found in the range of 2.19–5.28, 2.15–5.22, 2.97–7.17 and 2.68–6.36 μg g^{-1} for leg, breast, liver and heart tissues, respectively [22]. Sanchez-Rodas et al. [5] conducted that concentrations of total arsenic in chicken tissue were reported to be 270 μg kg^{-1} [5]. Uluozlu et al. [23] determined that arsenic concentrations were found in ranges of 0.06–0.10 μg g^{-1} in chicken samples and chicken products in Turkey [23]. Ysart et al. [24] were reported that mean arsenic levels in UK diet were to be 0.003 mg kg^{-1} for meat products, 4.4 mg kg^{-1} for fish, 0.006 mg kg^{-1} for nuts and 0.004 mg kg^{-1} for poultry samples on fresh weight [24]. In another study, Ghomi [25] reported that As concentrations in common carp muscle was

found to be 0.014 $\mu g g^{-1}$ [25].

CONCLUSIONS

It was found that microwave digestion method can be used successfully in the speciation analysis of arsenic. From the observed results, concentrations of As(V) were ranged between 3.0-14 ng g^{-1} (mean 7.3 ng g^{-1}) for breast tissue and 3.0-9.0 ng g^{-1}(mean 5.1 ng g^{-1}) for leg tissue. On the other hand, concentrations of As(III) in the studied chicken tissues were found to be lower than the limit of detection. The obtained values are higher than the safe level of inorganic arsenic in chicken meat established by FDA-2011 < 1 ng g^{-1}.

ACKNOWLEDGEMENTS

This study was financially supported by The Scientific and Technical Research Council of Turkey (Project number: TUBITAK-106T084).

REFERENCES

[1] Uncumusaoglu, A.A., Sengul, U., Akkan, T. (2016) Environmental contamination of heavy metals in the Yaglidere Stream (Giresun), Southeastern Black Sea. Fresen. Environ. Bull. 25, 5492-5498.

[2] Fisher, D.J., Yonkos, L.T., Staver, K.V. (2015) Environmental concerns of Roxarsone in broiler poultry feed and litter in Maryland, USA. Envir. Sci. Tech. 49, 1999−2012.

[3] Basu, P., Ghosh, R.N., Grove, L.E., Klei, L., Barchowsky, A. (2008) Angiogenic potential of 3-nitro-4-hydroxy benzene arsonic acid (roxarsone). Environ Health Persp. 116, 520−523.

[4] USEPA (2001) National primary drinking water regulations; arsenic and clarifications to compliance and new source contaminants monitoring; final rule. 40 CFR parts 9, 141, and 142,

[5] Sanchez-Rodas, D., Gomez-Ariza, J.L., Oliveira, V. (2006) Development of a rapid extraction procedure for speciation of arsenic in chicken meat. Anal. Bioanal. Chem. 385, 1172-1177.

[6] USFDA (2011) Arsenic: tolerances for residues of new animal drugs in food. 21 CFR 556.60.

[7] Lasky, T., Sun W.Y., Kadry, A., Hoffman, M.K. (2004) Mean total concentration in chicken 1989-2000 and estimated exposures for consumers of chicken. Environ. Health. Persp. 112, 18-21.

[8] Kawalek, J.C, Carson, M., Conklin, S., Lancaster, V., Howard, K., Ward, J., Farrell, D., Myers, M., Swain, H., Jeanettes, P., Frobish, S., Matthews, S. and McDonald, M. (2011) Provide data on various arsenic species present in broilers treated with roxarsone: comparison with untreated birds. Final report on study 275.30.2011; U.S. Food and Drug Administration: Laurel, MD, USA.

[9] Nachman, K.E., Baron, P.A., Raber, G., Francesconi, K.A., Navas-Acien, A., Love, D.C. (2013) Roxarsone, inororganic arsenic, and other arsenic species in chicken: a U.S.-based market basket sample. Environ. Health. Perspect. 121, 818– 824.

[10] Pizarro, I., Gomez, M., Camara, C., Palacios, M.A. (2003) Arsenic speciation in environmental and biological samples extraction and stability studies. Anal. Chim. Acta. 495, 85-98.

[11] Polatajko, A., Szpunar, J. (2004) Speciation of Arsenic in chicken meat by anion-exchange liquid chromatography with inductively coupled plazma-mass spectrometry. J AOAC Int. 87, 233-237.

[12] Al-Aboudi, A.F., Fayyad, M.K., Abu, Zarga, M.H. (2006) Polarographic study of the complexation between the chemical constituents of *Phragmites australis* and heavy metals. Fresen. Environ. Bull. 15, 1271-1275.

[13] Chiou, S., Wen, P., Chen, K.L. (1997) Effects of Roxarsone on performance, toxicity, tissue accumulation and residue of eggs and excreta in laying hens. J Sci. Food. Agr. 74, 229-236.

[14] FDA (Food and Drug Administration) (1963) Food additives resulting from contact with containers or equipment and food additives otherwise affecting food. Fed Reg. 28:10871.

[15] FDA (Food and Drug Administration) (2011b) Final report on study 275.30. Provide data on various Arsenic species present in broilers treated with Roxarsone: comparison with untreated birds.

[16] Andrade, C., Navarro, M., Lopez, H., Lopez, M.C. (2003) Determination of total arsenic levels by hydride generation atomic absorption spectrometry in foods from South-East Spain: Estimation of daily dietary intake. Food Addit Contam. 20, 923-932.

[17] Nachman, K.E., Raber, G., Francesconi, K.A., Navas-Acien, A., Love, D.C. (2012) Arsenic species in poultry feather meal. Sci Total Environ. 417–418, 51– 61.

[18] Bordajandi, L.R., Gomez, G., Abad, E., Rivera, J., Fernandez-Boston, M.D., Blasco J., Gonzalez, M.J. (2004) Survey of persistent organochlorine contaminants (PCBs, PCDD/Fs, and PAHs), heavy metals (Cu, Cd, Zn, Pb, and Hg), and arsenic in food samples from Huelva (Spain): Levels and health implications. J Agr Food Chem. 52, 992-1001.

[19] Li, N., Sun, W.Y., Kadry, A., Hoffman, M.K. (2009) Determination of arsenic in foods by flow injection on-line sorption pre-concentration with hydride generation atomic fluorescence spectrometry. Food Addit Contam. 26, 839–846.
[20] Julshamn, K., Lundebye, A.K., Heggstad, K., Berntssen, M.H.G., Boe, B. (2004) Norwegian monitoring programme on the inorganic and organic contaminants in fish caught in the Barents Sea, Norwegian Sea and North Sea, 1994–2001. Food Addit Contam. 21, 365-376.
[21] Miyashita, S., Shimoya, M., Kamidate, Y., Kuroiwa T., Shikino O., Fujiwara, S., Francesconi, K.A., Kaise, T. (2009) Rapid determination of arsenic species in freshwater organisms from the arsenic-rich Hayakawa River in Japan using HPLC-ICP-MS. Chemosphere. 75, 1065-1073.
[22] Shah, A.Q., Kazi, T.G., Arain, M.B., Jamali, M.K., Afridi, H.I., Jalbani, N., Kandhro, G.A., Baig, J.A., Sarfraz, R.A., Ansari R. (2009) Comparison of electrothermal and hydride generation AAS for the determination of total arsenic in broiler chicken. Food Chem. 113, 1351-1355.
[23] Uluozlu, O.D., Tuzen, M., Mendil, D., Soylak M. (2009) Assessment of trace element contents of chicken products from Turkey. J Hazard. Mater. 163, 982-987.
[24] Ysart G., Miller P., Croasdale, M., Crews, H., Robb, P., Baxter, M., de L'Argy, C. Harrison, N. (2000) 1997 UK Total Diet Study – Dietary exposure to aluminum, arsenic, cadmium, chromium, copper, lead, mercury, nickel, selenium, tin and zinc. Food Addit Contam. 17, 775-786.
[25] Ghomi M.R. (2016) Determination of lead, mercury, arsenic and cadmium level in muscle of common carp (*Cyprinus Carpio*) in Southern Caspian Sea and Gomishan and Anzali Wetlands. Fresen. Environ. Bull. 25, 401-408.

Received: **26.04.2017**
Accepted: **12.10.2017**

CORRESPONDING AUTHOR

Gokce Kaya
Firat University,
Health Sciences Faculty,
Department of Nutrition and Dietetic,
23100, Elazig – Turkey

e-mail: kayag232@hotmail.com

© by PSP Volume 27 – No. 2/2018 pages 651-657 Fresenius Environmental Bulletin

BIOREMEDIATION OF Cr(VI)-CONTAMINATED SOIL BY SULFATE-REDUCING BACTERIA (SRB) ENRICHMENT

Yuanyuan Han[1, 2, 3], Chengxu Dong[2, 3], Yang Cao[2, 3], Xueping Zhang[2, 3], Hongwei Ni[4,*]

[1]Harbin University, Harbin 150086, China
[2]College of Geographical Science, Harbin Normal University, Harbin 150025, China
[3]Key Laboratory of Remote Sensing Monitoring of Geographic Environment, College of Heilongjiang Province, Harbin Normal University, Harbin 150025, China
[4]The Natural Resources and Ecology Institute of Heilongjiang Province Academy, Harbin 150040, China

ABSTRACT

Bioremediation is an environment-friendly and economical technology to remove Cr(VI) from contaminated soils. In this study a set of soil column experiments were designed to determine the bioremediation of Cr(VI)-contaminated soils by sulfate-reducing bacteria enrichments under famine and feast conditions. The dynamics of SRB enrichments in the remediation process both under famine and feast conditions were investigated. The pH value of Cr(VI)-contaminated soils was 8.37, and the total concentrations of Cr(VI) was 437.56 mg/kg. Cr(VI) in contaminated soil were completely removed under both conditions, while a higher removal rate was observed under feast condition. Real-time quantitative PCR revealed that copies of SRB 16S rRNA gene at feast condition were clearly higher than that at famine condition. The results suggest that SRB enrichments are feasible to remediate Cr(VI)-contaminated soil, which provides basis for ongoing refining.

KEYWORDS:
bioremediation, Cr(VI), soil, sulfate-reducing bacteria (SRB)

INTRODUCTION

Discharge of industrial waste and sewage sludge without effective control could induce a large accumulation of heavy metals in soil, resulting in serious public concern and anxiety on food safety [1, 2]. Chromium (Cr), a representative heavy metal, has a wide application in variety of industries, including ore refining, steel and alloys production, metal plating, tannery, pigmentation and other manufactures [3]. Hexavalent chromium (Cr(VI)) and trivalent chromium (Cr(III)) are two of the most stable states of Cr in soil, wherein Cr(VI) displays higher toxicity, carcinogenicity, solubility and mobility [4, 5]. Moreover, Cr(VI) pollution can reduce microbial diversity in soil and alter soil functions, threatening the sustainable development of agriculture [6, 7, 44].

To address these issues, the remediation technologies for Cr(VI)-contaminated soil have been widely studied in recent years. Cr in soil undergoes complex equilibria among the different Cr species and hydrolysis products [8], and thus leads to the Cr speciation in soil with different properties [9]. The complex Cr speciation in soil should have restricted the potential remediation approaches available for Cr (VI)-contaminated soil [10]. Technologies employed to remedy these soils include adsorption [11, 46, 47], electrochemical treatment [12], reduction and precipitation with chemicals [13], and some membrane treatment [45]. However, they are expensive and could also cause the loss of soil fertility [14]. These disadvantages lead to bioremediation, bio-reduction of Cr(VI) to less toxic, less soluble Cr(III), an alternative remediation technology, which is receiving increasing attention due to its environmentally safe and cost-effective properties [15, 16]. Several microorganisms have been tested for Cr(VI) bioremediation, such as *Pseudomonas aeruginosa* A2Chr [17] and *Ochrobactrum anthrophic* [15].

Sulfate-reducing bacteria (SRB), an anaerobic microorganism that typically use sulfate as terminal electron acceptor, are ubiquitous in anoxic habitats [18]. Although named after their ability to use sulfate as a terminal electron acceptor, these organisms can also use many other electron acceptors, for example, Cr(VI) [19, 20, 21] and be beneficial for removing heavy metals from soil. However, most researches on bio-reduction of Cr(VI) were carried out in aqueous solution not in a real contaminated soil [22, 23, 24, 25].

Therefore, in this study we conducted a remediation of Cr(VI)-contaminated soil by SRB enrichments. The contaminated soils were collected at 0-30 cm depth of soil in the vicinity of a mine in southern China. The removal efficiency of Cr(VI) from contaminated soil and remedy conditions were discussed. This work is attempting to provide a promising microbe-mediated approach for Cr(VI)-contaminated soil.

MATERIALS AND METHODS

Soil samples. Samples of soils contaminated by Cr(VI) were collected at 0-30 cm depth of soil in the vicinity of a steel alloy factory in southern China. Soils were air-dried at room temperature, ground and sieved with a 100 mesh size (150 μm) for soil characterization and bioremediation experiment.

Soil characterization. For determining the content of water-soluble Cr(VI), 10 g of soil were suspended into 100 mL of ultrapure water and then shaken at 175 rpm for 2 h. The mixture was filtered and the concentration of Cr(VI) in the filtrate was measured according to Han et al. [26]. The absorbance of the purple complex formed from reacting Cr(VI) with S-diphenylcarbazide (DPC) was measured at $\lambda = 540$ nm by a UV spectrophotometer (Rayleigh Analytical Instrument Corp., China). For determining total contents of Zn, Pb, Mn, Cd, and Cu in soils, 0.5 g soil was digested with an acid mixture (HCl, HNO_3, $HClO_4$, and HF) on the electric heating plate. The concentrations of Zn, Pb, Mn, Cd, and Cu in the digested solution were measured by an inductively coupled plasma-optical emission spectrometer (ICP-OES) (Optima 5300 DV, PerkinElmer Instrument) [14]. For determining As content, 0.5 g soil was digested with HNO_3: HCl (1:3 v/v) in boiling water for 2 h. The concentration of total As in the digested solution was determined with an atomic fluorescence spectrometer (AFS-810, Beijing Titan Instrument). The heavy metal contents of the tested soils were shown in Table 1. Also, Measurements for the concentrations of total organic carbon (TOC) and total nitrogen (TN) were taken by the TOC analyzing instrument (TOC-VCPH, Japan) equipped with platinum catalyst quartz tube. The flow rate of oxygen gas was 130 ml/min and the furnace temperature was 680 °C.

TABLE 1
The heavy metal content of the tested soil

Heavy metals	Concentration (mg/kg)[a]
Cr(VI)	437.56
Zn	622.49
Pb	317.51
Mn	184.09
Cd	93.37
Cu	101.55
As	10.56

[a]Experiments were performed in triplicate and average values were listed herein.

Enrichment and cultivation of sulfate reducing bacteria (SRB). SRB was enriched from wastewater collected from municipal wastewater treatment plant, located at Harbin, China. The composition of the growth medium for enrichment of SRB was prepared as previous described [21]. Briefly, it consisted of 1.2 g/L sodium lactate, 3 g/L sodium citrate, 0.1 g/L yeast extract, 4.5 g/L Na_2SO_4, 0.06 g/L $CaCl_2 \cdot 2H_2O$, 1.0 g/L NH_4Cl, 0.5 g/L KH_2PO_4, 2.0 g/L $MgSO_4 \cdot 7H_2O$, 0.5 g/L $FeSO_4 \cdot 7H_2O$, 0.3 g/L disodium salt and 1 mL of trace element solution. The volume of the medium was made up to 1 L with distilled water and the pH was adjusted to 7.0 ± 0.2. During enrichment, the ratio of COD to sulfate was gradually increased from 1 to 3 over a period of two months. The enriched cultures were used in bioremediation experiments.

Bioremediation experiments. The enriched cultures were grown in sterile Luria Bertani (LB) medium at 30 °C on a rotary shaker (175), harvested after 48 h, washed three times and re-suspended with sterile water to an OD_{600} of 2.0 (bacterial suspension). 200 g of non-sterilized Cr(VI) contaminated soil was placed in soil column (made of plastic) with 5-cm in diameter and 42 cm in height. A plastic mesh (D = 0.2 mm) was placed at the bottom of the column to retain the soil. Then, 200 mL of washing solution circularly washed the contaminated soil at the flow rate of 2.0 mL min^{-1}. The washing solution used in the column contained: SRB enrichment and not-sterile LB liquid medium at the ratio of 1:4 (v/v) (termed as feast condition) (a), SRB enrichment and tap water at the ratio of 1:4 (v/v) (termed as famine condition) (b), and just not-sterile LB liquid medium with the same volume as (a) and (b) (termed as control set) (c). Soil and leachate samples were withdrawn at 24 h intervals within 6 days, the initial soil sample (not washed with washing solution) were named as 0, and the soil samples withdrawn at 1, 2, 3, 4, 5, and 6 day were named as 1, 2, 3, 4, 5, and 6, respectively. The soil samples were air dried before determination of the water-soluble Cr(VI). Leachates were centrifuged at 12000 rpm for 2 min, and the supernatant were used to determine the concentration of Cr(VI).

DNA extraction and Quantitative Polymerase Chain Reaction (qPCR). Total genomic DNA was extracted following the procedures described by Zhou et al. [27]. Crude genomic DNA was purified on an agarose gel and stored at -20 °C until use. To detect the abundance of sulfate-reducing bacteria in the soil during the bioremediation process, the functional gene dissimilatory sulfite reductase (dsrB) was amplified with primer pair DSRp2060F-GC (5' CAACATCGTYCAYACCCA GGG 3') and DSR4R (5' GTGTAGCAGTTACCGCA 3') according to Geets et al. [28]. Conventional PCR with different DNA samples were performed by the ABI Veriti™ Thermal Cycler (Life Tec. Co., USA) and the annealing temperature was 48 °C. The PCR products were checked by 1.0% agarose gel electrophoresis and ethidium bromide staining. The purification of PCR products and the calculation of DNA copy numbers were previously described [29]. The PCR products were serially diluted from 10^7 to 10^1 copies μL^{-1}, which were used as templates DNA to construct standard curves. The threshold cycle (Ct),

i.e. the cycle at which the fluorescence in the sample increases above a pre-defined threshold, was determined. Standard curves were generated by plotting the threshold cycle for each standard, against $\log_{10}$ of the sequence copy number. The qPCR was performed with iCycler iQ real-time PCR detection system (Bio-Rad Laboratories Inc., USA) according to previous study [29]. All tests were performed in triplicate and average results were reported in the tables and figures. More detailed information can be seen in Wang et al. [14].

RESULTS AND DISCUSSION

Soil properties. The pH value of Cr(VI)-contaminated soils was 8.37, and the TOC and TN concentrations were 0.9±0.1 and 0.4±0.05 g kg^{-1}. The total concentrations of Cr(VI) was 437.56 mg kg^{-1}. The soil was also contaminated by Zn, Pb, Mn, Cd, Cu, and As, with the concentrations of 622.49, 317.51, 184.09, 93.37, 101.55 and 10.56 mg kg^{-1}, respectively (Table 1). Cr(VI)-contaminated soil samples tested in the study were collected at 0-30 cm depth of soil in the vicinity of a steel alloy factory, and the surface horizon was subjected from the long-time uncontrolled disposal of chromite ore processing residue. During the conventional chrome ore hydrometallurgy process, soda ash and limestone or dolomite were always supplemented, which generated a large amount of highly toxic chromite ore processing residue of high pH and high concentration of Cr [30]. Chromite ore processing residue typically has an alkaline pH value (>12) and contains high concentrations of total Cr, which may be up to 70000 mg kg^{-1} [31]. The uncontrolled disposal of chromite ore processing residue could lead to the release of the water-soluble, high toxic Cr(VI) and other metals into the soil. The valence state and speciation of Cr(VI) in soil could be influenced by variety of factors, e.g., pH, organic matter in soil, redox potential, and microbial community [8, 32, 33, 34].

Bioremediation experiments. Figure 1 showed the variation of the Cr(VI) concentration in soil and leachate in the bioremediation process. In the bioremediation experiment under feast condition (Figure 1a), Cr(VI) concentration in the soil decreased from 437.56 to 172.84 mg kg^{-1} within the

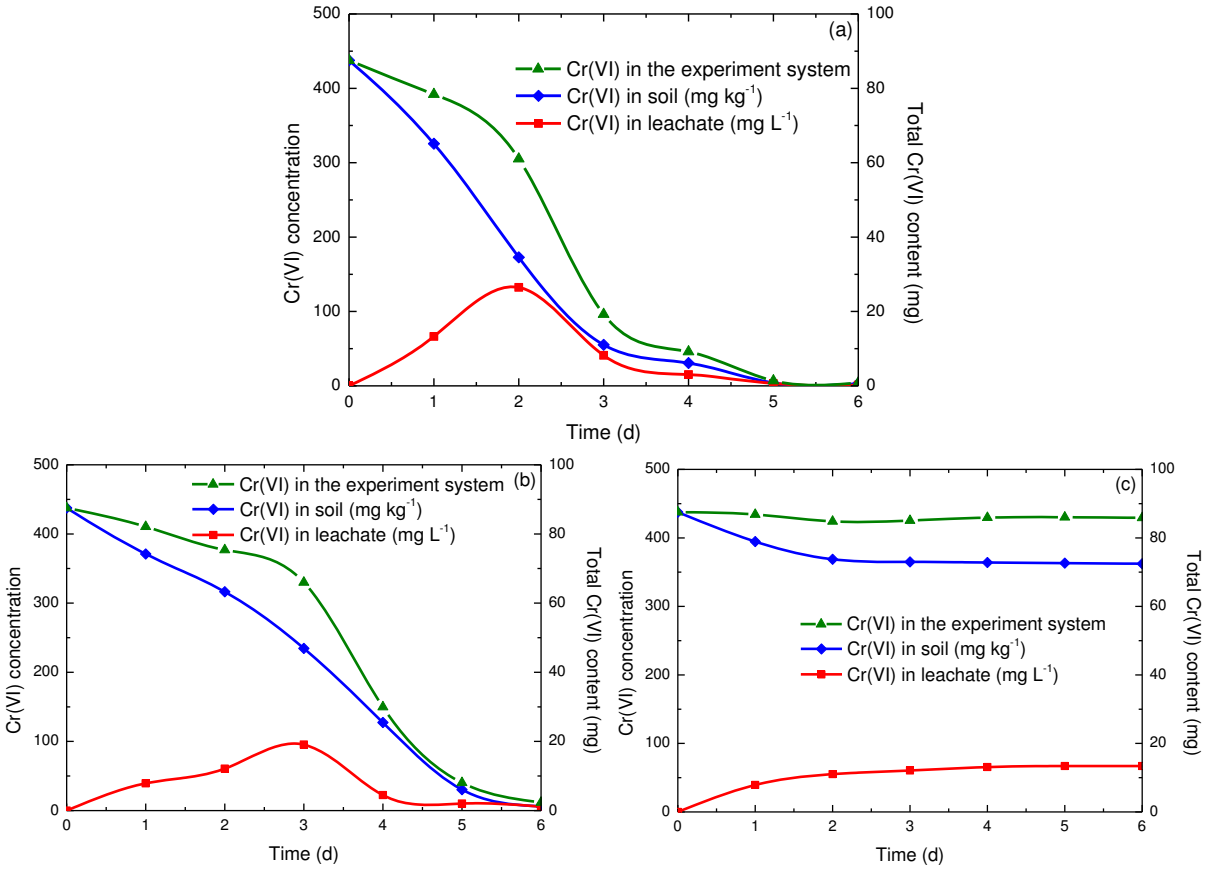

FIGURE 1
Cr(VI) concentration in the bioremediation process, (a) bioremediation experiment under feast condition, (b) bioremediation experiment under famine condition, (c) control experiment

first 2 days, and Cr(VI) in the leachate increased from 0 to 132.36 mg L^{-1}. Thereafter, Cr(VI) concentration in the soil and leachate decreased continuously to the final value of 3.06 mg kg^{-1} and 1.05 mg L^{-1} respectively. Moreover, the total amount of Cr(VI) in the experiment system decreased from 87.51 to 0.82 mg after 6 days remediation.

The variation of Cr(VI) concentration in soil and leachate during the bioremediation experiment under famine condition followed the similar trends to that under feast condition however showed a slow Cr(VI) remediation rate (Figure 1b). Within the first 2 days, only 121.20 mg kg^{-1} of Cr(VI) in the contaminated soil were removed, and Cr(VI) concentration in the leachate peaked 95.47 mg L^{-1} at 3 d. Until the end of the experiment, Cr(VI) concentration in the soil and leachate reached to the final value of 6.13 mg kg^{-1} and 5.75 mg L^{-1} respectively. The total amount of Cr(VI) in the experiment system decreased from 87.51 to 2.38 mg after remediation process. In the control experiment (Figure 1c), Cr(VI) in the soil sample was clearly leached into the leachate within the first 2 day and subsequently Cr(VI) in the soil and leachate maintained stable with the concentration at 362.30 mg kg^{-1} and 67.05 mg L^{-1} respectively. The total amount of Cr(VI) in the control experiment system was slightly decreased from 87.51 to 85.87 mg, which might be related to the organic matter in the LB medium and soil or the indigenous Cr(VI)-reducing bacteria in the soil. The Cr(VI) in the soil was almost completely removed using the SRB enrichments and the removal rate of Cr(VI) in the soil was obviously enhanced under feast condition/with LB medium supplement.

Microbe-mediated remediation approach for Cr(VI)-contaminated soil has been widely studied in recent years [14, 35, 36, 37]. Microorganisms play a key role in the bioremediation process and their activities stronger rely on nutrient/organic matter in the soil. During contaminated soil remediation process, the utilization of inorganic and/or organic supplements is often favored due to their typically unfavorable conditions, e.g., high level of metals, acidic pH, low content in organic matter and nutrients, and poor structure [38]. This especially relevant in mine soils derived from pyritic ores or other metal sulfides, where oxidation or hydrolysis processes may produce a gradual acidification of the medium that increases heavy metal solubility and availability with time [39]. Several cost-effective agroindustrial and farm residues (e.g., animal manures and slurries, urban residues) have been used alone or in combination with liming materials for bioremediation of heavy metal-contaminated soils [40, 41, 42]. These materials may not only modify the solubility and phytotoxicity of heavy metals, but also can provide essential nutrients and organic matter, improving soil microbial activity [38], which would promote the microbe-mediated approach into wide application in heavy metal-contaminated soil remediation.

qPCR analysis. The results of the qPCR were shown in Figure 2. SRB was not detected in the untreated soil sample (0 day), whereas copies of SRB 16S rRNA gene appeared in the treated soils and slowly increased within 5 d (Figure 2).

Moreover, copies of SRB 16S rRNA gene at feast condition was clearly higher than that at famine condition, which was in agreement with a higher Cr(VI) removal rate. However, Cr(VI) both in the soil and leachate were reduced completely within 5 d bioremediation (Fig. 1a). The shift between Cr(VI) reduction and the increase of SRB population might be due to high initial toxicity of Cr(VI) in the initial growth stages of SRB in soil. However, the fast modifications of the complex chemical equilibria of chromium in contaminated soils could also play a role in the chromium speciation during the bio-remediation progress [9]. Relying on the presented results, we concluded that inoculation of SRB capable of reduce Cr(VI) may be an option for the bioremediation of Cr(VI)-contaminated soil, which could replace or complement conventional chemical methods based on the use of Fe-rich compounds [43]. In future more researches are essential to evaluate the potential of SRB for the remediation of other soil types and in relation to their microbial communities.

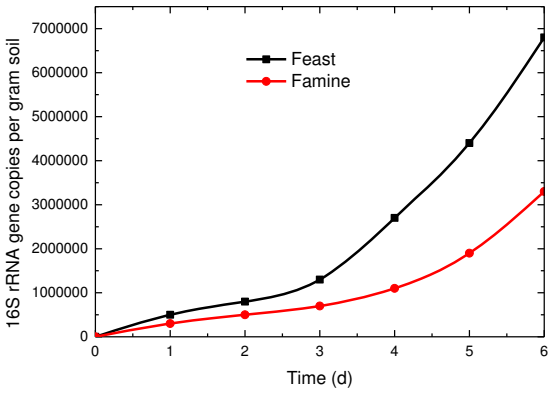

FIGURE 2
Variation of SRB in the bioremediation process

CONCLUSIONS

In this study we successfully utilized SRB enrichments for the bioremediation of Cr(VI)-contaminated soil under both feast and famine conditions. The qPCR analysis revealed that the population of SRB increased quickly after Cr(VI) was completely reduced and copies of SRB 16S rRNA gene at feast condition was clearly higher than that at famine condition, which was in agreement with a higher Cr(VI) removal rate at feast condition. These results demonstrated that SRB has advantages and potential application in bioremediation of Cr(VI)-contaminated soil.

ACKNOWLEDGEMENTS

The authors gratefully acknowledge the financial support provided by National Natural Science Foundation of China (No. 41371072).

REFERENCES

[1] Kumpiene, J., Lagerkvist, A., Maurice, C. (2008) Stabilization of As, Cr, Cu, Pb and Zn in soil using amendments-a review. Waste Manag. 28, 215-225.

[2] Battalia, A., Calace, N., Nardi, E., Petronio, B.M., Pietroletti, M. (2007) Reduction of Pb and Zn bioavailable forms in metal polluted soils due to paper mill sludge addition effects on Pb and Zn transferability to barley. Bioresour. Technol. 98, 2993-2999.

[3] Di, Z.C., Ding, J., Peng, X.J., Li, Y.H., Luan, Z.K., Liang, J. (2006) Chromium adsorption by aligned carbon nanotubes supported ceria nanoparticles. Chemosphere. 62, 861-865.

[4] Gheju, M., Lovi, A. (2006) Kinetics of hexavalent chromium reduction by scrap iron. J. Hazard. Mater. 135, 66-73.

[5] Natale, F.D., Lancia, A., Molino, A., Musmarra, D. (2007) Removal of chromium ions form aqueous solution by adsorption on activated carbon and char. J. Hazard. Mater. 145, 381-390.

[6] D'Ascoli, R., Rao, M.A., Adamo, P., Renella, G., Landi, L., Rutigliano, F.A., Terribile, F., Gianfreda, L. (2006) Impact of river overflowing on trace element contamination of volcanic soils in south Italy: part II, Soil biological and biochemical properties in relation to trace element speciation. Environ. Pollut. 144, 317-326.

[7] Desai, C., Parikh, R., Vaishnav, T., Shouche, Y., Madamear, D. (2009) Tracking the influence of long-term chromium pollution on soil bacterial community structures by comparative analyses of 16S rRNA gene phylotypes. Res. Microbiol. 160, 1-9.

[8] Kotas, J., Stasicka, Z. (2000) Chromium occurrence in the environment and methods of its speciation. Environ. Pollut. 107, 263-283.

[9] Adamo, P., Zampella, M., Gianfreda, L., Renella, G., Rutigliano, F.A., Terribile, F. (2006) Impact of river overflowing on trace element contamination of volcanic soils in south Italy: part I. Trace element speciation in relation to soil properties. Environ. Pollut. 144, 308-316.

[10] James, B.R. (1996) The challenge of remediation chromium-contaminated soil. Environ. Sci. Technol. 30, 248-251.

[11] Baran, A., Bicak, E., Baysal, S.H., Onal, S. (2007) Comparative studies on the adsorption of Cr(VI) ions on to various sorbents. Bioresour. Technol. 98, 661-665.

[12] Lakshmipathiraj, P., Bhaskar Raju, G., Raviatul Basariya, M., Parvathy, S., Prabhakar, S. (2008) Removal of Cr(VI) by electrochemical reduction. Sep. Purif. Technol. 60, 96-102.

[13] Losi, M., Amrhein, C., Frankenberger, W. (1994) Bioremediation of chromate-contaminated groundwater by reduction and precipitation in surface soils. J. Environ. Qual. 23, 1141-1150.

[14] Wang, Y.Y., Ping, B., Yang, Z.H., Chai, L.Y., Liao, Q., Zhang, Z., Li, C. (2015) Bacterial community dynamics during bioremediation of Cr(VI)-contaminated soil. Appl. Soil Ecol. 85, 50-55.

[15] Cheng, Y., Yan, F., Huang, F., Chu, W., Pan, D., Chen, Z., Zheng, J., Yu, M., Lin, Z., Wu, Z. (2010) Bioremediation of Cr(VI) and immobilization as Cr(III) by *Ochrobactrum anthropi*. Environ. Sci. Technol. 44, 6357-6363.

[16] Mistry, K., Desai, C., Lal, S., Patel, K., Patel, B. (2010) Hexavalent chromium reduction by *Staphylococcus* sp. Isolated from Cr(VI) contaminated landfill. J. Biotechnol. Biochem. 6, 117-131.

[17] Ganguli, A., Tripathi, A. (2002) Bioremediation of toxic chromium from electroplating effluent by chromate-reducing *Pseudomonas aeruginosa* A2Chr in two bioreactors. Appl. Microbiol. Biotechnol. 58, 416-420.

[18] Muyzer, G., Stams. A.J.M. (2008) The ecology and biotechnology of sulfate-reducing bacteria. Nat. Rev. Microbial. 6, 441-454.

[19] Lovley, D.R., Phillips, E.J.P. (1994) Reduction of Chromate by *Desulfovibrio vulgaris* and its c3 cytochrome. Appl. Environ. Microbiol. 60, 726-728.

[20] Somasundaram, V., Ligy, P., Bhallamudi, S.M. (2009) Experimental and mathematical modeling studies on Cr(VI) reduction by CRB, SRB and IRB, individually and in combination. J. Hazard. Mater. 172, 606-617.

[21] Somasundaram, V., Ligy, P., Bhallamudi, S.M. (2011) Laboratory scale column studies on transport and biotransformation of Cr(VI) through porous media in presence of CRB, SRB and IRB. Chem. Engineer. J. 171, 572-581.

[22] Fude, L., Harris, B., Urrutia, B.M.M., Beveridge, T.J. (1994) Reduction of Cr(VI) by a consortium of sulfate-reducing bacteria. Appl. Environ. Microbiol. 60, 1525.

[23] Smillie, R.H., Hunter, K., Loutit, M. (1981) Reduction of chromium (VI) by bacterially produced hydrogen sulfide in a marine environment. Water Res. 15, 1351-1354.

[24] Tebo, B.M., Obraztsova, A.Y. (1998) Sulfate-reducing bacterium grows with Cr(VI), U(VI), Mn(IV) and Fe(III) as electron acceptors. FEMS Microbiol. Lett. 162, 193-198.

[25] Smith, W.L., Gadd, G.M. (2000) Reduction and precipitation of chromate by mixed culture sulfate-reducing bacterial biofilms. J. Appl. Microbiol. 88, 983-991.
[26] Han, X., Wong, Y., Wong, M., Tam, N. (2007) Biosorption and bioreduction of Cr(VI) by a microalgae isolate, *Chlorella miniata*. J. Hazard. Mater. 146, 65-72.
[27] Zhou, J., Bruns, M.A., Tiedje, J.M. (1996) DNA recovery from soils of diverse composition. Appl. Environ. Microbiol. 62, 316-322.
[28] Geets, J., Borremans, B., Diels, L., Spingael, D., Vangronsveld, J., Leilie, D.V.D., Vanbroekhoven, K. (2006) DsrB gene-based DGGE for community and diversity surveys of sulfate-reducing bacteria. J. Microbiol. Methods. 66, 194-205.
[29] Zhang, R., Wei, M., Ji, H., Chen, X., Qiu, G., Zhou, H. (2009) Application of real-time PCR to monitor population dynamics of defined mixed cultures of moderate thermophiles involved in bioleaching of chalcopyrite. Appl. Microbiol. Biotechnol. 81, 1161-1168.
[30] Wang, T., He, M., Pan, Q. (2007) A new method for the treatment of chromite ore processing residues. J. Hazard. Mater. 149, 440-444.
[31] Higgins, T.E., Halloran, A.R., Dobbins, M.E., Pittignano, A.J. (1998) In situ reduction of hexavalent chromium in alkaline soils enriched with chromite ore processing residue. J. Air Waste Manage. 48, 1100-1106.
[32] Bartlett, R.J., Kimble, J.M. (1976) Behavior of chromium in soils: II. Hexavalent forms. J. Environ. Qual. 5, 383-386.
[33] Chai, L.Y., Yang, Z.H., Wang, Y.Y., Deng, R., Zhu, W.J., Huang, S.H. (2008) Potential-pH diagram for *Leucobacter* sp. Ch-1-Cr-H2O system. J. Hazard. Mater. 157, 518-524.
[34] He, Z., Gao, F., Sha, T., Hu, Y., He, C. (2009) Isolation and characterization of a Cr(VI)-reduction *Ochrobactrum* sp: strain CSCr-3 from chromium landfill. J. Hazard. Mater. 163, 869-873.
[35] Jeyasingh, J., Philip, L. (2005) Bioremediation of chromium contaminated soil: optimization of operating parameters under laboratory conditions. J. Hazard. Mater. 118, 113-120.
[36] Polti, M.A., Aparicio, J.D., Benimeli, C.S., Amoroso, M.J. (2014) Simultaneous bioremediation of Cr(VI) and lindane in soil by actinobacteria. Int. Biodeterior. Biodegrad. 88, 48-55.
[37] Chai, L.Y., Huang, S.H., Yang, Z.H., Peng, B., Huang, Y., Chen, Y.H. (2009) Hexavalent chromium reduction by *Pannonibacter phragmitetus* BB isolated from soil under chromium-containing slag heap. J. Environ. Sci. Health A. 44, 615-622.
[38] Bernal, M.P., Clemente, R., Walker, D.J. (2007) The role of organic amendments in the bioremediation of heavy metal-polluted soils. In: Gore, R.W. (Ed.) Environmental Research at the Leading Edge. Nova Science Publishers Inc., New York, 1-57.
[39] Navarro, M.C., Perez-Sirvent, C., Martinez-Sanchez, M.J., Vidal, J., Tovar, P.J., Bech, J. (2008) Abandoned mine sites as a source of contamination by heavy metals: a case study in a semi-arid zone. J. Geochem. Explor. 96, 183-193.
[40] Cordova, S., Neaman, A., Gonzalez, I., Ginocchio, R., Fine, P. (2011) The effect of lime and compost amendments on the potential for the revegetation of metal-polluted, acidic soils. Geoderma. 166, 135-144.
[41] Clemente, R., Walker, D.J., Pardo, T., Martinez-Fernandez, D., Bernal, M.P. (2012) The use of a halophytic plant species and organic amendments for the remediation of a trace elements-contaminated soil under semi-arid conditions. J. Hazard. Mater. 223, 63-71.
[42] Pardo, T., Martinez-Fernandez, D., Clemente, R., Walker, D.J., Bernal, M.P. (2014) The use of olive-mill waste compost to promote the plant vegetation cover in a trace element-contaminated soil. Environ. Sci. Pollut. Res. 21, 1029-1038.
[43] Thornton, E.C., Amonette, J.E. (1999) Hydrogen sulfide gas treatment of Cr(VI)-contaminated sediment samples from a plating-waste disposal site-Implications for in-situ remediation. Environ. Sci. Technol. 33, 4096-4101.
[44] Wyszkowski, M., Radziemska, M. (2013) Influence of chromium (III) and (VI) on the concentration of mineral elements in oat (*Avena sativa* L.). Fresen. Environ. Bull. 22, 979-986.
[45] Yari, A.R., Nasseri, S., Mahvi, A.H., Nabizadeh, R., Kalantari, R.R., Yunesian, M. (2013) Application of a forward osmosis membrane in removal of chromium from aqueous solutions. Fresen. Environ. Bull. 22, 2319-2323.
[46] Malkoc, E., Nuhoglu, Y. (2003) The removal of chromium (VI) from synthetic wastewater by *Ulothrix zonata*. Fresen. Environ. Bull. 12, 376-381.
[47] Fronczyk, J., Radziemska, M., Mazur, Z. (2015) Copper removal from contaminated groundwater using natural and engineered limestone sand in permeable reactive barriers. Fresen. Environ. Bull. 24, 228-234.

Received: **28.09.2016**
Accepted: **17.11.2017**

CORRESPONDING AUTHOR

Hongwei Ni
The Natural Resources and Ecology Institute of
Heilongjiang Province Academy,
Harbin 150040 – China

e-mail: hitnhw@163.com

© by PSP Volume 27 – No. 2/2018 pages 658-667 Fresenius Environmental Bulletin

CHARACTERIZATION AND COMPARISON OF GROWTH AND TOXICANT PRODUCTION FOR THREE *MICROCYSTIS AERUGINOSA* STRAINS

Xiaojian Zhou[1,2], Liangyu Tian[1], Shuyu Liu[1], Ke Feng[1], Cuili Jin[1,2,*]

[1]College of Environmental Science and Engineering, Yangzhou University, Yangzhou City, 225127, Jiangsu, China
[2]Marine Science and Technology Institute, Yangzhou University, Yangzhou City, 225127, Jiangsu, China

ABSTRACT

Three strains of *Microcystis aeruginosa* were tested to investigate the differences in their cell growth, contents of chlorophyll-a (Chl-a), phycocyanin (PC), microcystins (MCs), microcystin-LR (MC-LR) and the toxicity produced. The cell density of FACHB-942 increased fastest among three strains. The similar slopes of the linear relationships between cell density and Chl-a content for FACHB-918 and FACHB-905 were approximately 6-fold greater than that of FACHB-942. The slopes of the relationships between the PC content and cell density were lowest and highest for FACHB-942 and FACHB-905, respectively. For the MC-LR and MC contents, FACHB-918 and FACHB-905 had a higher cell quota than FACHB-942 did. However, the total toxicities determined in a bioluminescent bioassay using *Vibrio fischeri* were FACHB-905> FACHB-942> FACHB-918. Strain-specific differences in above characters do exist for these three strains of *M. aeruginosa*. For monitoring and evaluating risks of cyanobacterial blooms, the analyses based on the biomass, pigments, and toxins are not sufficient to accurately describe the actual situations. A bioluminescent bioassay using *V. fischeri* parallel with standard $CuSO_4$ solutions as toxicity markers was proposed to demonstrate the risks and harms.

KEYWORDS:
Microcystis aeruginosa, growth, phycocyanin, microcystin, bioluminescent bioassay

INTRODUCTION

Cyanobacterial blooms have been occurring with increasing frequency and extending geographical distributions, which degrade water quality and pose serious threats to aquatic organisms and human health [1-2]. The genus *Microcystis* is one of the most common bloom formers. The ecology, growth, pigment content, and toxin production were intensively studied for a species of *Microcystis aeruginosa* [3-8].

In many cyanobacterial studies, the monitoring was conducted by cell counts, biomass measurements, phytoplankton pigment extractions, or cyanotoxin analyses [9-10]. These methods are costly and/or time consuming [6]. Chl-a was previously suggested as an indicator representing the biomass. The alert levels of cyanotoxin proposed by European Water Framework Directive and WHO are also derived from Chl-a and cell density [6]. Actually, Chl-a is not a specific cyanobacterial pigment, which makes it poorly informative for evaluating cyanobacterial abundance and cyanotoxin concentrations [11]. Alternatively, phycocyanin (PC), an accessory pigment characteristic of cyanobacteria, was suggested to represent cyanobacterial biomass [6, 11]. MCs are cyclic heptapeptides with more than 100 structural variants and notably hepatotoxic. The methods of HPLC, HPLC-MS, and ELISA were used to analyse MCs [5, 7, 9-10, 12-14]. However, the detected MC concentrations can't represent overall toxicity, due to the potential existence of unknown species-specific and condition-specific toxins [3, 6, 8, 13, 15-16]. Therefore, a simple and convenient method is necessary to quantify the risks of cyanobacterial toxins in addition to biomass monitoring.

In this study, three strains of *M. aeruginosa* frequently used in scientific researches were tested to investigate 1) the cell growth, optical density, the contents of Chl-a, PC, MC, and MC-LR, and total toxicity of each strain of *M. aeruginosa*; 2) existence of significant differences among the different strains; and 3) a bioluminescent bioassay to describe the toxicity in the water caused by cyanobacteria.

MATERIALS AND METHODS

Cyanobacterial cultures. All strains of *Microcystis aeruginosa* were purchased from the Freshwater Algae Culture Collection at the Institute of Hydrobiology, (FACHB-Collection), Chinese Academy of Science, catalogue number WDCM 873 in the World Data Centre for Microorganisms (WDCM). The *M. aeruginosa* strains are catalogue numbers FACHB-905, FACHB-942, and FACHB-

918 in the FACHB-Collection. The strains were maintained for 3 months and then incubated for the experiments in BG-11 medium ($NaNO_3$ 1.5 g L^{-1}, K_2HPO_4 40 mg L^{-1}, $MgSO4 \cdot 7H_2O$ 75 mg L^{-1}, $CaCl_2 \cdot H_2O$ 36 mg L^{-1}, citric acid 6 mg L^{-1}, ammonium ferric citrate 6 mg L^{-1}, EDTA (dinatrium-salt) 1 mg L^{-1}, Na_2CO_3 20 mg L^{-1}, H_3BO_3 2.86 mg L^{-1}, $MnCl_2 \cdot 4H_2O$ 1.81 mg L^{-1}, $ZnSO_4 \cdot 7H_2O$ 0.22 mg L^{-1}, $NaMoO_4 \cdot 5H_2O$ 0.39 mg L^{-1}, $CuSO_4 \cdot 5H_2O$ 80 µg L^{-1}, and $CoCl \cdot 6H_2O$ 40 µg L^{-1}). All of the culture media were sterilised at 121 °C for 20 min. The cultures with at least triplicated samples were incubated at 25 °C with a dark:light ratio = 14 h: 10 h illumination at a light intensity of 25 µmol m^{-2} s^{-1}.

Detection of cell and optical densities. Each culture was inoculated after shaking by sterile pipettor in clean bench. Cell densities in the cultures were detected with a haemocytometer (25×16) under microscopy. Because the initial inoculated cell densities for each culture inevitably varied slightly, the fold changes were calculated by dividing the cell densities at each incubation time by the initial cell density. The growth rate was calculated according to Wu et al. [17]: $\mu = (\ln C_t - \ln C_0)/(T_t - T_0)$. The optical densities of the culture were detected by adding 200 µL of each culture into the wells on transparent 96-well plates, which were read by a 96-well plate reader at 600 nm and shown as OD_{600nm}. For both measurements, at least three samples were independently measured.

Detection of chlorophyll-a (Chl-a) and phycocyanin (PC) contents. The chlorophyll-a (Chl-a) and phycocyanin (PC) contents were extracted and analysed spectrophotometrically as described by Pierangelini et al. [1,15]. Samples were first centrifuged (8000 rpm at 4°C for 10 min). For Chl-a analysis the cells were extracted in the dark with 95% ethanol at 4°C for 48 h, centrifuged for 10 min at 8000 rpm, and the supernatants were collected for measurement of the absorbance at wave lengths of 664 nm and 647 nm. For PC analysis, the cells were mixed with 0.1 M phosphate buffer solution (PBS, pH 7.0), and submitted twice to ultrasonication for 10 min and frozen at -20°C for 12 h; the melted samples were then centrifuged (8000 rpm at 4°C for 10 min) and the supernatants were collected and the absorbance measured at wave lengths of 562, 620 and 652 nm. Quantifications of Chl-a and PC were made according to the equations of Bennett and Bogorad [18] and Jeffrey and Humphrey [19]. For both measurements, at least triplicate samples were independently measured.

Detection of Microcystin-LR (MC-LR) and Microcystins (MCs). Microcystins (MCs) were detected by ELISA as described by the detection kit manufacturer (Beacon Analytical Systems Inc, ME, USA). The MCs in the sample compete with the MC-enzyme conjugate for a limited number of antibody binding sites. The kit does not differentiate between MC-LR (used as kit calibrators) and other MC variants, but detects their presence at various levels. Therefore, the results of the measurement are the total MCs. Each sample was tested at least in triplicate.

The HPLC analyses for MC-LR were carried out as described by Lawton et al. [20] and Ikawa et al. [21]. At least three samples of the algal culture were 0.45 µm filtered and subjected to solid phase extraction (SPE) with a C_{18} column. The column was eluted with methanol containing 0.1% v/v trifluoroacetic acid and the elution was concentrated with a rotary evaporator before being subjected to HPLC analysis using a Hitachi L2000 system. The HPLC system was equipped with a diode array detector (DAD, L-2455, Hitachi, Japan) installed in tandem at the outlet of the column (LaChrom, ODS C_{18}, 5 µm, 4.6 mm × 250 mm, Hitachi, Japan) and mounted with an ODS pre-column. The solvents used were 57% methanol and 43% PBS (0.05 M potassium dihydrogen phosphate adjusted with 20% v/v phosphoric acid to pH 3.0) at a fixed flow rate of 1 ml min^{-1} at 25°C. A 10 µl volume of the sample or the MC-LR standard compound dissolved in methanol was injected into the column using an autosampler (L-2200, Hitachi, Japan). UV absorption was detected at λ = 238 nm.

Analysis for toxicity against the bioluminescence of *Vibrio fischeri.* The 0.45-µm filtered samples run in at least triplicate were subjected to a bioluminescent bioassay using *Vibrio fischeri* as described by Zhou et al. [22]. The freeze-dried *V. fischeri* cells were purchased from Hamamatsu Photon Techniques Inc. (Beijing), catalogue number CS234. The bioluminescent assay was run on white 96-well plates, and the bioluminescence was read by a microplate reader at 490 nm (FLx800, BioTek, USA) at the time the *V. fischeri* cells were exposed to the sample water (T=0) and 15 min afterwards (T=15). To standardize the toxicity quantifications, the toxicities of a wide range of standard $CuSO_4$ solutions were simultaneously measured and a standard curve was established between the inhibition rates against bioluminescence and the $CuSO_4$ concentrations. The toxicities of the samples were converted to $CuSO_4$ concentrations according to the above standard curve. Therefore, the toxicity shown as a concentration of $CuSO_4$ indicates that the toxicity of a sample in terms of inhibitory activity against the bioluminescence of *V. fischeri* was equal to that of the $CuSO_4$ solution at that concentration in the bioassay.

RESULTS

The growth in terms of the OD for the tested *M. aeruginosa* strains were shown in Fig 1. The OD values of three *M. aeruginosa* strains all increased with

increasing incubation time up to 16 days, as shown in Fig 1-A. All growths of the three *M. aeruginosa* strains were in accord with an exponential increase model with R^2>0.92. The difference among the OD values of the three *M. aeruginosa* strains is unclear. The growth in terms of cell density for the tested *M. aeruginosa* strains was shown in Fig 1-B. The cell densities of three *M. aeruginosa* strains also increased with increased incubation time up to 16 days, in accordance with an exponential increase model with R^2>0.95. In contrast to the OD values, the FACHB-942 cell densities increased much more rapidly than those of FACHB-905 and FACHB-918, whose cell densities increased at similar rates.

To eliminate the possible interference by the slight differences in initial cell densities of the three strains tested and to further clarify the growth differences, the cell fold changes were calculated by comparing the cell density at each incubation time with the initial density. The results were shown in Fig 2A. In contrast to those unclear tendencies in the OD values and cell densities, a clear difference among three tested strains was observed. FACHB-942 achieved the highest cell increases, while the FACHB-918 and FACHB-905 cell counts were lower. As shown in Fig 2B, FACHB-942 achieved and maintained the highest growth rate after 4 days' incubation, while FACHB-918 maintained the lowest growth rate throughout the entire incubation period.

The Chl-a and PC contents of the three *M. aeruginosa* strains were also measured. The relationships between the cell density and contents of Chl-a or PC were calculated and shown in Fig 3.

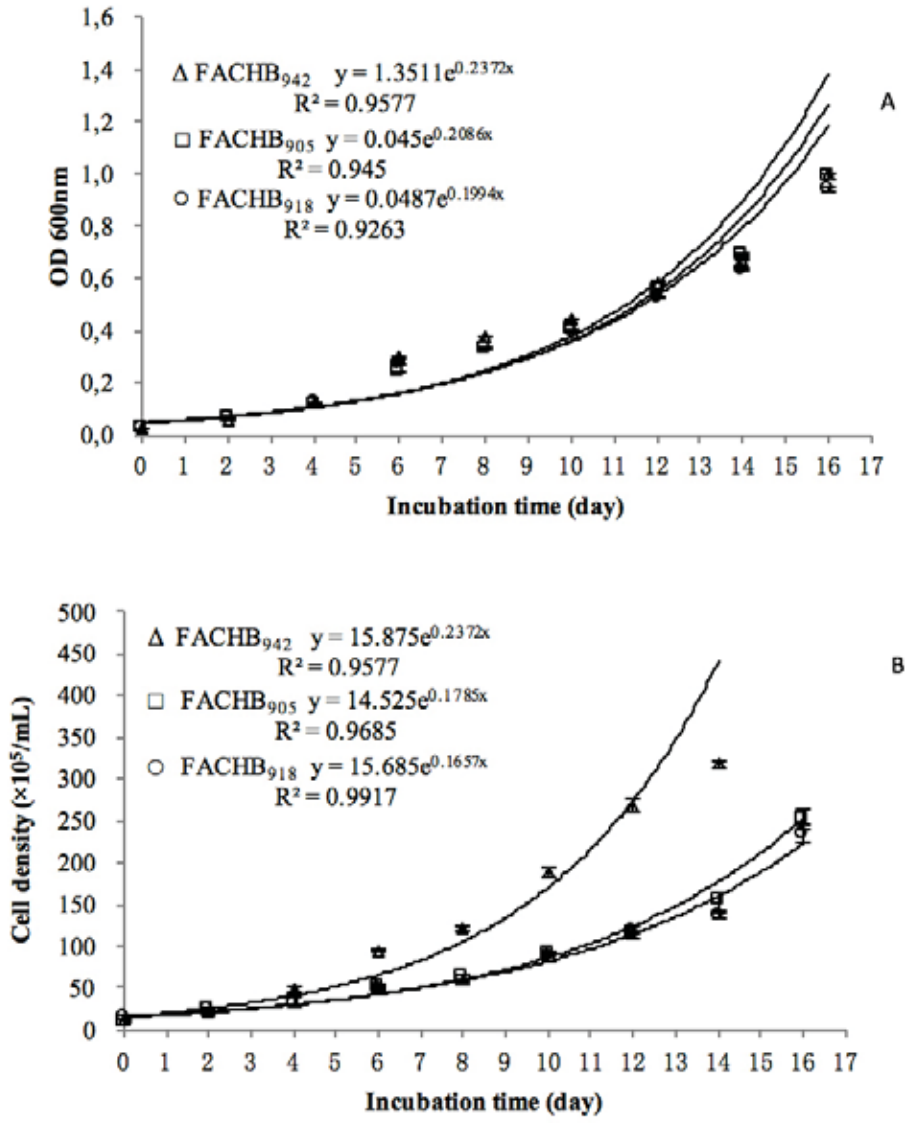

FIGURE 1
Growth in terms of optical densities (A) and cell densities (B) of three tested strains of *Microcystis aeruginosa*.

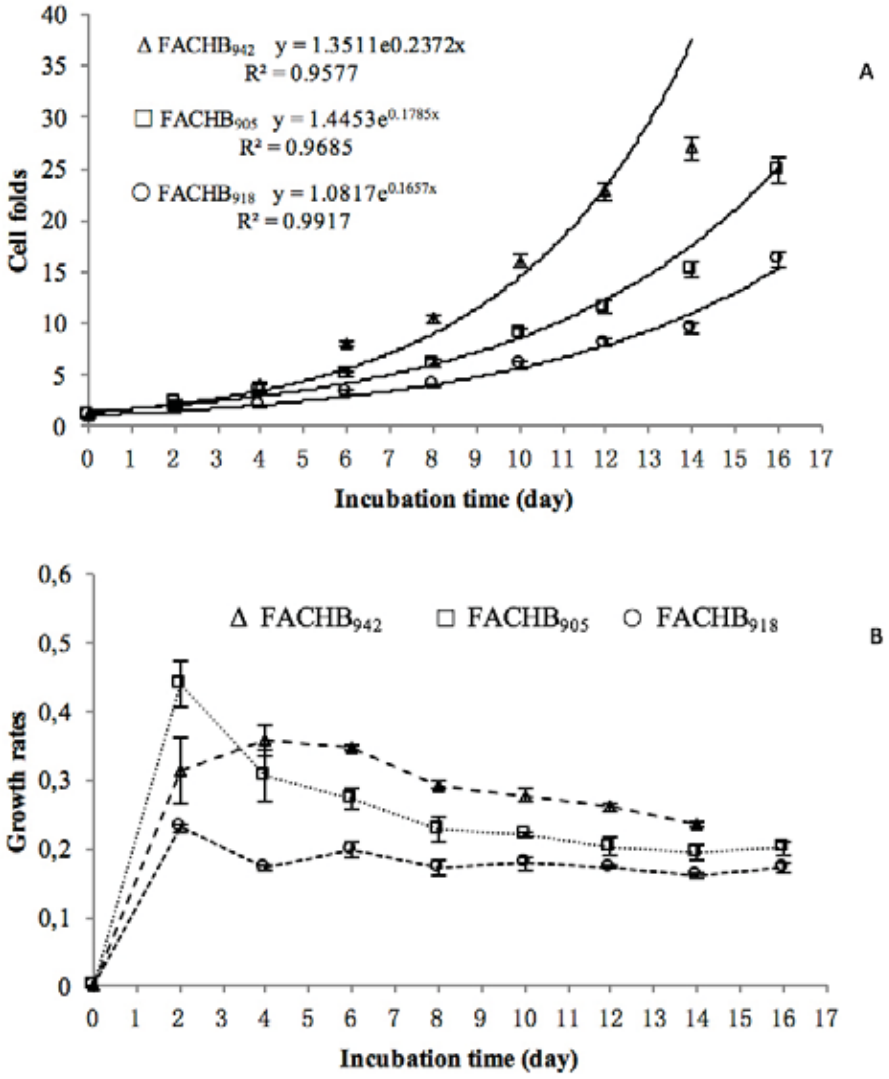

FIGURE 2
Growth in terms of cell fold changes (A) and growth rates (B) of three tested strains of *Microcystis aeruginosa*.

Compared to FACHB-905 and FACHB-918, the Chl-a content of FACHB-942 showed the lowest increase in cell density in accordance with the equation y=1.1903x+12.781 as shown in Fig 3-A. The Chl-a content increase for FACHB-918 and FACHB-905 exhibited a similar pattern, with increasing cell densities following equations y=6.4436x-156.73 and y=6.0927x-120.43, respectively. The PC contents of FACHB-905 increased the fastest, while FACHB-942 increased most slowly with increasing cell density (Fig 3-B). The equations for FACHB-905, FACHB-918, and FACHB-942 were y=0.1508x-2.6736, y=0.0779x-1.2298, and y=0.0408x-0.912, respectively, all with R^2>0.95.

The MC-LR and total MC contents were analysed by HPLC and ELISA. The relationships between the cell density and MC-LR or total MC contents were calculated and shown in Fig 4. FACHB-918 showed the fastest increase in MC-LR content among the three strains, with an equation of y=0.1902x-1.4749 with increasing cell density (Fig 4-A). The FACHB-942 MC-LR content increased most slowly with increasing cell density, resulting in y=0.0263x-1.6789. For the MC content shown in Fig 4-B, FACHB-942 also increased most slowly with increasing cell density, with an equation of y=0.1001x+17.719; FACHB-905 and FACHB-918 behaved similarly, with equations of y=0.6678x-7.3242 and y=0.6103x+6.4153. The lowest R^2 for the equation between total MC content and cell density for three strains was greater than 0.91.

The toxicities of a series $CuSO_4$ solutions with concentrations ranging from 1 to 512 mg L^{-1} were tested by bioluminescent assays using *V. fischeri*,

and the relationship between the toxicities (indicated by the inhibition rates against bioluminescence) and the $CuSO_4$ concentrations was regressed as y= 17.205 ln(x)-1.268 with R^2=0.9674, as shown in Fig 5-A. The culture water of three strains was simultaneously tested by bioluminescent assay and the inhibition rates of the samples were converted to $CuSO_4$ concentrations by the regression equation in Fig 5-A. The relationships between cell density and the total toxicity of the samples were then calculated and were shown in Fig 5-B. The total toxicity of FACHB-905 increased much faster with increasing cell density with a linear equation of y=3.7227x-138.59 (R^2=0.9079) than those of the other two strains. The total toxicity of FACHB-918 remained at a relatively lower level than for the other two strains following a linear equation of y=0.3944x-4.4549 (R^2=0.9739) with increasing cell density. In the case of FACHB-942, the linear equation between the total toxicity and the cell density resulted in a poor correlation, with R^2=0.6998. Meanwhile, the regression equation using the logarithms of the cell densities resulted in a good correlation of y=144.34 ln(x)-518.41, with R^2=0.915.

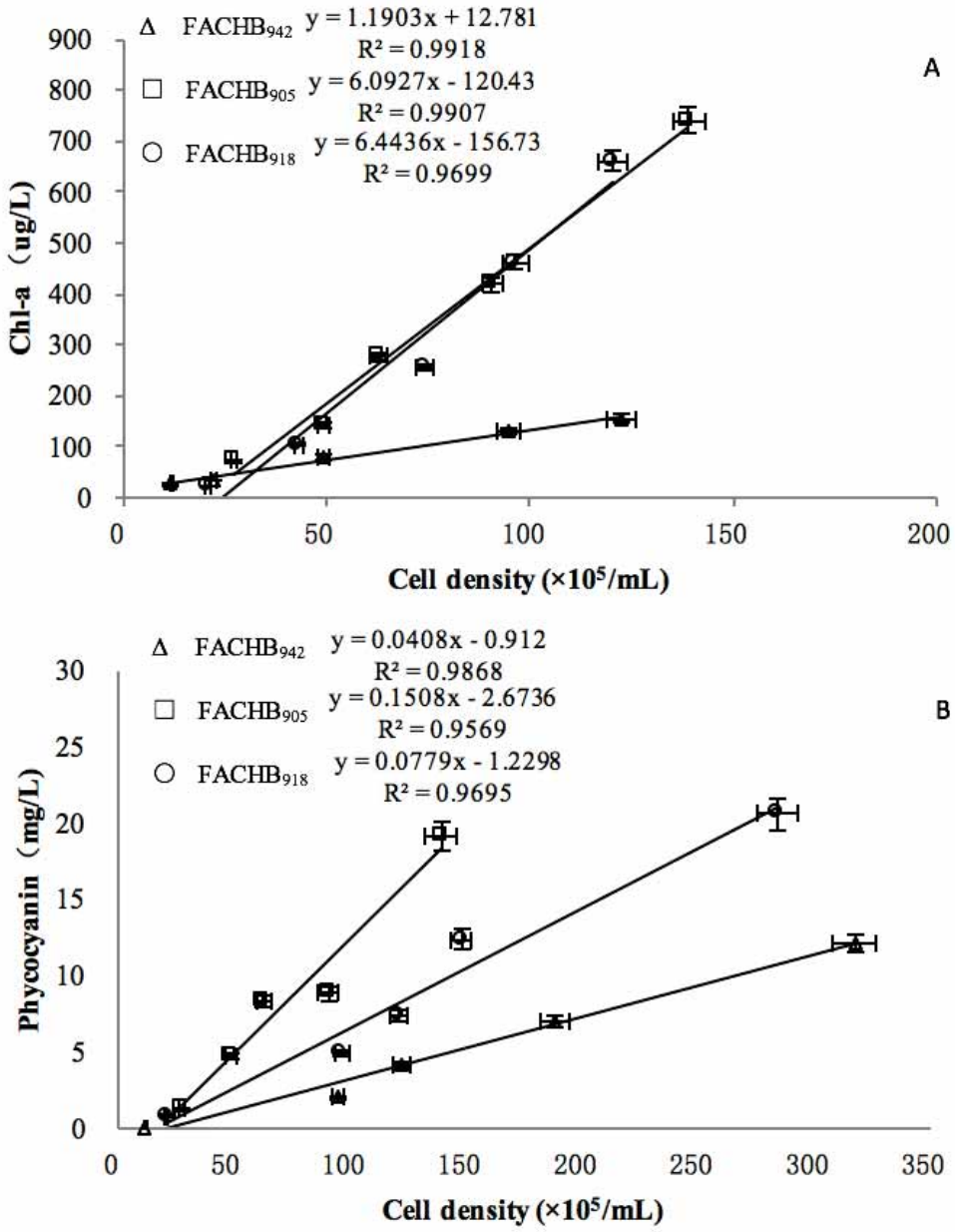

FIGURE 3
Relationships between cell density and the content of chlorophyll-a (A) or phycocyanin (B) for three tested strains of *Microcystis aeruginosa*.

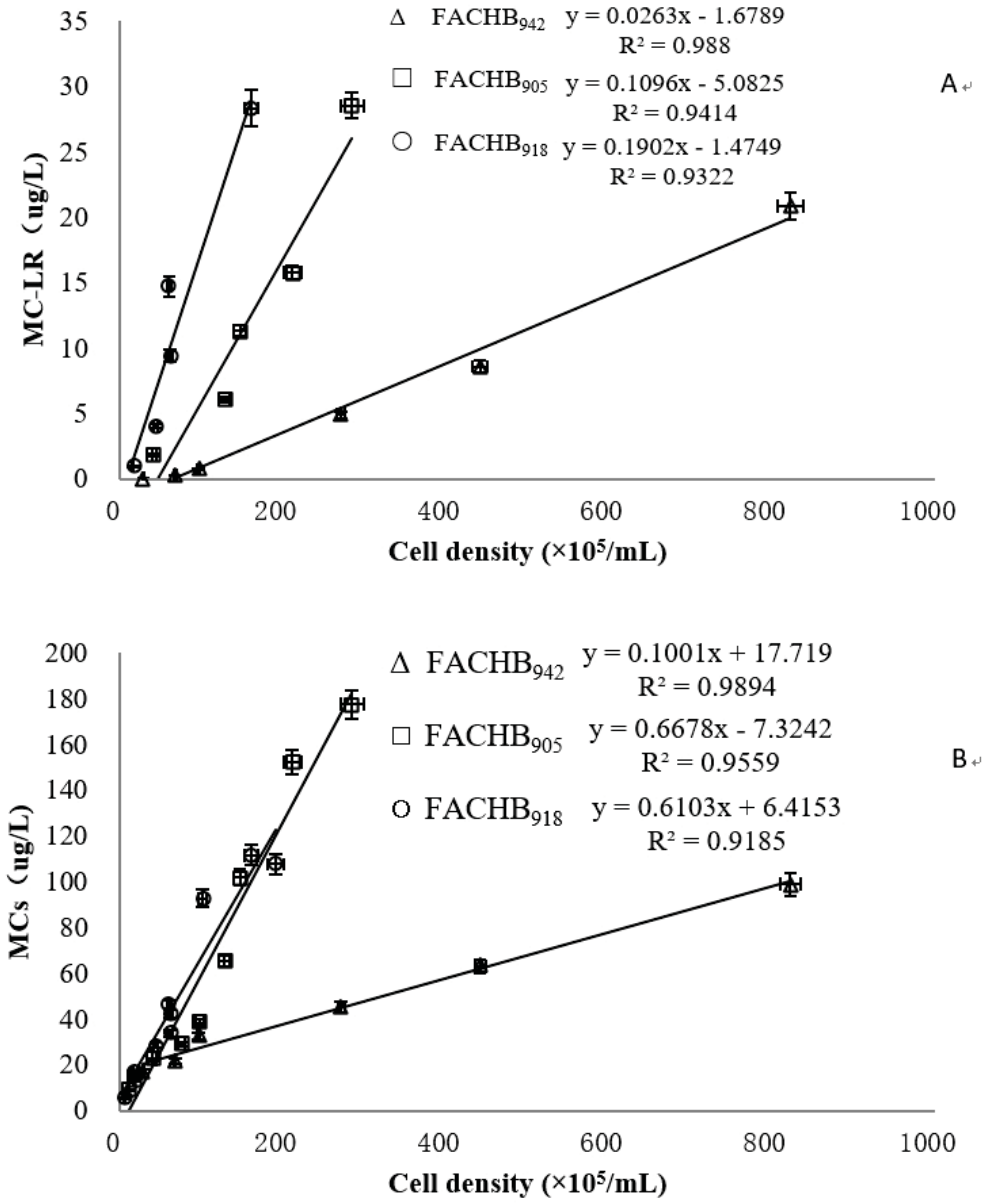

FIGURE 4
Relationship between the cell density and content of MC-LR (A) or MC (B) for three tested strains of *Microcystis aeruginosa*.

DISCUSSION

For the three tested strains, their growth in terms of OD was quite similar (Fig. 1A). But the FACHB-942 strain eventually reached both the highest cell density (Fig. 1B) and the highest cell counts (Fig. 2); FACHB-905 and FACHB-918 achieved similar cell densities (Fig. 1B) over 16 days of incubation, but different cell counts (Fig. 2). Therefore, the three strains of *M. aeruginosa* differed in their cell growth. Cell growth is a fundamental and important feature of microorganisms. Many studies have described the growth of *M. aeruginosa* strains under similar conditions, BG-11 culture medium and approximately 25 °C, but exhibiting various patterns. As reported by Liu et al. [23], the cell density of a strain of *M. aeruginosa* PCC7806 from the Pasteur Culture Collection (Paris France) increased from approximately 4×10^5 cells/mL to a stationary phase of 3.87×10^6 cells/mL after 5-7 days of incubation. Rzymski et al. [24] reported that a *M. aeruginosa* strain, which was isolated from Husinec Reservoir (Czech Republic) and collected in the Culture Collection of the Algal Laboratory, Institute of Botany (Trebon, Czech Republic), grew from 4×10^5 cells/mL to approximately 6.2×10^5 cells/mL after 15 days of incubation. In a study of Ríos et al. [8], two strains of *M. aeruginosa* (PCC7806 and PCC7820,

from Pasteur Culture Collection) exhibited different patterns; one grew constantly from a very low cell density to 60×10^6 cells/mL during 21 days of incubation and the other reached a peak cell density of 40×10^6 cells/mL at day 9 and then decreased to a very low level of 1×10^6 cells/mL. For *M. aeruginosa* grown in BG-11 medium, the reported stationary cell density varied from 6.2×10^5 to 6.0×10^7 cells/mL and the exponential growth periods varied from 5-7 to 20 days [8, 24-26]. In the foregoing studies, slight differences in the incubation temperatures, illumination, medium composition, and dark:light ratios may contribute to the different growth patterns [1, 3, 25]. However, the nature of the differences among the *M. aeruginosa* strains also plays important roles in the various growth patterns [8-9]. In the present study, all culture conditions were exactly the same for all three strains, and the results indicate that strain-specific differences for *M. aeruginosa* do exist in terms of growth pattern for these three strains. Cell numbers or growth rate only would clearly indicate this difference.

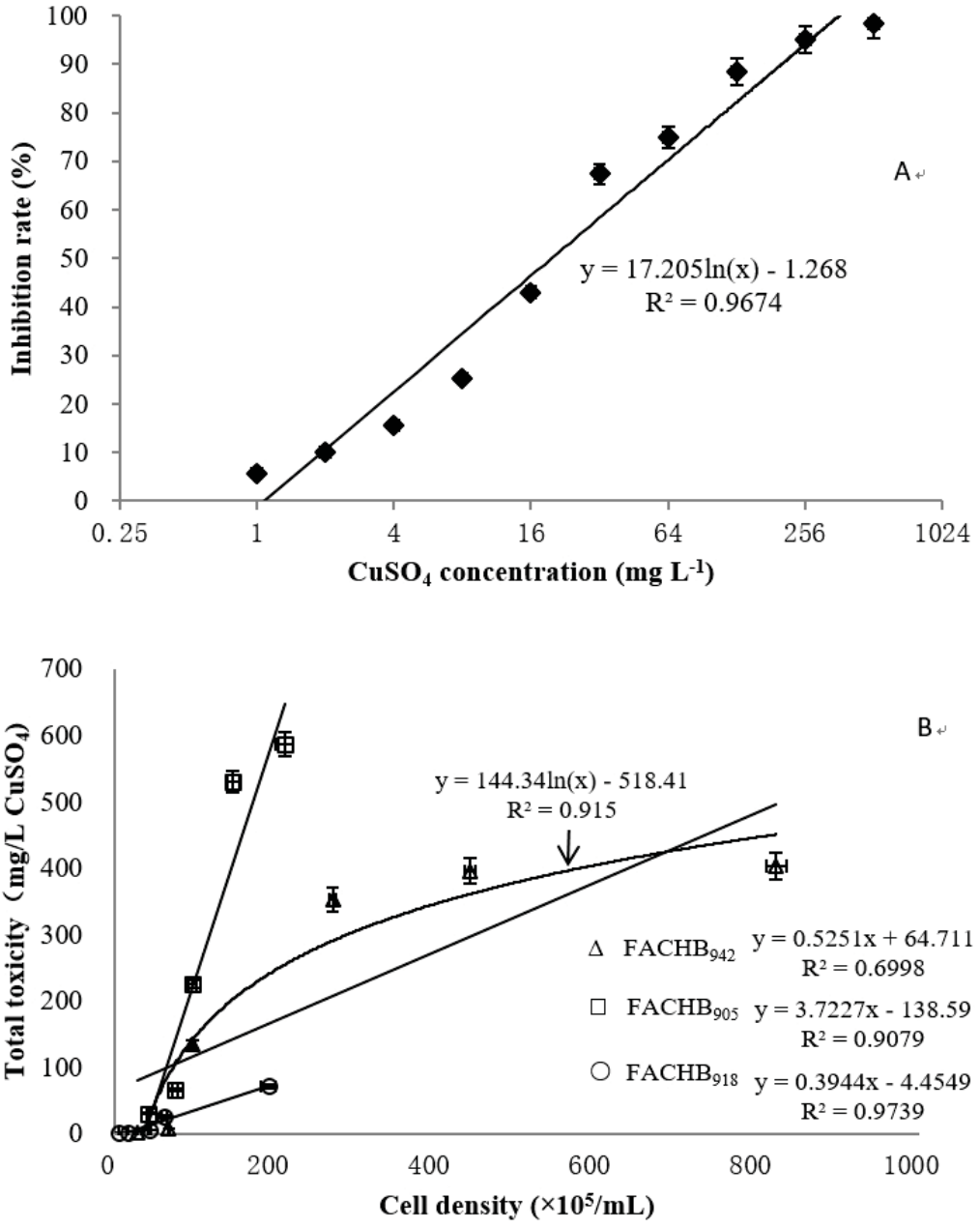

FIGURE 5
Bioluminescent inhibition effect of $CuSO_4$ (A) and the relationship between the cell density and total toxicity of the culture water of three tested *Microcystis aeruginosa* strains (B).

The pigment contents of harmful algae have been used to represent algal biomass and to act as the warning indicators for the toxicity or risk to a water body [6]. It was reported that Chl-a and PC contents of *M. aeruginosa* strain FACHB-911 from FACHB-Collection in Chinese Academy of Science reached 18 μg/L and 1079 μg/L after 12 days of incubation [25]. The Chl-a content of another *M. aeruginosa* strain from the Institute of Hydrobiology of Chinese Academy of Sciences in the study of Li et al. [26] increased from 331 to 523 μg/L after 6 days of incubation. In our study, because three strains showed different cell growth patterns, the comparison of the pigment contents as a function of incubation times could not clarify the difference in the pigment cell quota. Alternatively, pigment contents were used as a function of cell density and increased with increasing cell densities at different rates for each strain. The Chl-a contents of strain FACHB-942 exhibited much lower rates (slopes) than those of FACHB-905 and FACHB-918, indicating that FACHB-942 had the lowest Chl-a cell quota among the three tested three strains. In the case of the PC contents, FACHB-942 also had the lowest cell quota, while FACHB-905 had the higher cell quota than the other two strains. FACHB-942 grew quickly but the low pigment contents might be the main reason for the similar OD value among the three strains. In recent studies, PC was proposed as a predictor for cyanobacterial biomass [6]. Although strong linear relationships were recorded between PC and the cell counts, biovolume or Chl-a for single-species cultures, a significant species-specific variation in the equation of the PC content vs. the cell counts was observed in previous studies, as well as the present study [6]. Therefore, if taking the PC content as the indicator for the risks and harms caused by cyanobacterial blooming, the different cell quotas of the PC content for various species should be taken into account [6].

The risks caused by cyanotoxins are the main reason for the intensive attention given to cyanobacterial blooms. Attempts to chemically measure MCs to evaluate the risks and harms of *Microcystis* spp. blooms have been undertaken for several decades and have identified many cyclic heptapeptides MC variants [5, 12]. Among them, MC-LR is the most studied one and whose concentration in water environments has been of serious concern [13-14, 21, 27]. Our data indicated that three *M. aeruginosa* strains had different cell quotas for MC-LR content, that is, MC-LR was high in FACHB-918 and low in FACHB-942 (Fig. 4A). In contrast to the chemical analysis of MC-LR, ELISA measures all MCs that are able to bind to the designated antibody [8, 10]. In this study, HPLC and ELISA measurements demonstrated that FACHB-942 possessed the lowest MC and MC-LR contents. The MC contents of FACHB-905 and FACHB-918 were similar, indicating that FACHB-905 was rich in MCs other than MC-LR compared to FACHB-918 because FACHB-918 had the highest MC-LR content (Fig. 4B). ELISA detects different MCs in varying degrees, with the most cross-reactive one being MC-LR, which was suggested by the instructional booklet for the Beacon Microcystin Plate Kit. Therefore, the richness of MCs other than MC-LR in FACHB-905 should be higher than the calculation based on the present data. Due to the importance of MCs, recent proposals using mass spectrometry and phosphatase bioassay are directed toward enhancing the accuracy in describing the MC contents [8, 14]. However, del Campo and Ouahid [7] studied the microcystins from three collected strains of *M. aeruginosa,* two from Texas University collection, UTEX-2666 (co-identity with UWOCC-006 and UV-006) and UTEX-2670 (co-identity with UWOCC-MR-A) and one from the Universidad Autónoma de Madrid collection (UAM-1303); they found various microcystin profiles for the tested three strains, and identified several new MCs from algal extracts. Furthermore, Mowe et al. [3] found that certain environmental factors such as temperature changed the microcystin production of *M. aeruginosa* PA20130405MA isolated from Pandan Reservoir of Singapore. Due to new MCs' being continually identified, the production of MCs being affected by environmental factors, and the significant cell quota differences existing among *Microcystis* spp. strains, it is quite challenging to determine comprehensively the risks and harms based on the MCs content [3, 7, 23].

The strain-specific difference was observed among tested three *M. aeruginosa*s strains in the cell growth, optical density, Chl-a content, the PC, MC, and MC-LR contents, and the total toxicity. The significant variations may exist among growth of biomasses, toxin concentrations produced, toxicities brought from different cyanobacteria and even strains belong to *M. aeruginosa* [8, 9-10, 16, 28]. Therefore, the sources and the features of the tested *M. aeruginosa* strains need be distinguished in scientific reports.

A number of researchers went to toxicity evaluation bioassays to find simple and suitable indicators to describe the risks and harms caused by cyanobacterial blooms [5, 29]. Herrera et al. [27] suggested using cladocerans, especially *Daphnia* species, to assess cyanobacterial toxicity. Although cyanobacterial toxicity in different species has been strongly associated with microcystin production and a number of studies have demonstrated the toxic effects of microcystins on these organisms, other compounds can even be more toxic than cyanotoxins [5]. Furthermore, although microcystins are probably toxic to the tested organisms, not every toxic effect can be attributed to them because blooms contain a large number of compounds. It was also suggested that bioactive substances such as lipopolysaccharides (LPS), muegelone and lupenil acetate could be responsible for the high toxicity [27, 29]. These stud-

ies proposed that chemical analyses have some limitations in showing the risks and harms due to *Microcystis* spp. compared with bioassays. We used the bioluminescent bioassay using *V. fischeri* in this study to evaluate the toxicity of cyanobacterial water. FACHB-918 had high contents of MC-LR and MCs in the HPLC and ELISA determinations, but exhibited low toxicity against the bioluminescence of *V. fischeri* compared to the other two strains (Fig. 5B). FACHB-942 had low contents of MC-LR and MCs, but was in the middle in terms of the toxicity cell quota among three strains (Fig. 5B). Our results agreed that some substances other than MCs from the tested strains could be responsible for the high toxicity [27, 29]. *V. fischeri* is a symbiotic bacterium living in the light organs of fish of the family Monocentridae, as well as in the cephalopods *Sepiola* and *Euprymna*, and its bioluminescence intensity is very sensitive to environmental changes and is strictly related to cellular activities [22]. These features ensure that its rapid bioluminescence changes (within 5-15 min) reflect the impact of the surrounding environment and have been widely used for toxicity evaluation [22]. Therefore, the toxicants produced by three tested strains might be quite complicated and should include toxins other than the MCs detected by ELISA [5]. In addition, we suggested a series of standard $CuSO_4$ solutions as both positive controls and as markers of the sample toxicity, which will enhance the standardisation and reproducibility of bioassays. Compared with bioassays using larvae or individual organisms, this bioluminescent bioassay is time and cost effective, easy to perform and standardise, and very sensitive.

CONCLUSIONS

The three tested strains of *M. aeruginosa* cultured in the same experimental conditions exhibited different patterns of growth and toxicant production regardless of the cell density, levels of Chl-a and PC, MC-LR and MCs, or toxicity produced. Among three strains, FACHB-942 showed the fastest cell growth, medium toxicity, and the lowest pigment content and MC production. With a parallel determination of a series of standard $CuSO_4$ solutions as toxicity markers, a bioluminescent bioassay using *Vibrio fischeri* is suggested to indicate the risks and harms of cyanobacterial blooms.

ACKNOWLEDGEMENTS

This study was supported by the National Natural Science Foundation of China (No. 41776156, 41306131, and 41271521), the Key Project of the Chinese Ministry of Education (No. 211065), and the Scientific and Technological Innovation Foundation of Yangzhou University (Environmental Institute 2017-19).

REFERENCES

[1] Pierangelini, M., Stojkovic, S., Orr, P.T. and Beardall, J. (2004) Elevated CO_2 causes changes in the photosynthetic apparatus of a toxic cyanobacterium *Cylindrospermopsis raciborskii*. J Plant Physiol. 171,1091–1098.

[2] Chen, J. and Xie, P. (2008) Accumulation of hepatotoxic microcystins in freshwater mussels, aquatic insect larvae and oligochaetes in a large, shallow eutrophic lake (Lake Chaohu) of subtropical China. Fresen Environ Bull. 17, 849-854.

[3] Mowe, M.A.D., Porojan, C., Abbas, F., Mitrovic, S.M., Lim, R.P., Furey, A. and Yeo, D.C.J. (2015) Rising temperatures may increase growth rates and microcystin production in tropical *Microcystis* species. Harmful Algae. 50, 88–98.

[4] Xing, W., Huang, W. M., Liu, G.H. and Liu, Y. D. (2008) Effects of iron on physiological and biochemical characteristics of *Microcystis wesenbergii* (kom.) Kom. (cyanobacterium). Fresen Environ Bull. 17, 2034-2042.

[5] Smutná, M., Babica, P., Jarque, S., Hilscherová, K., Marsálek, B., Haeba, M. and Bláha, L. (2014) Acute, chronic and reproductive toxicity of complex cyanobacterial blooms in *Daphnia magna* and the role of microcystins. Toxicon. 79, 11-18.

[6] Macário, I.P.E., Castro, B.B., Nunes, M.I.S., Antunes, S.C., Pizarro, C., Coelho, C., Goncalves, F. and de Figueiredo, D.R.A.F. (2015) New insights towards the establishment of phycocyanin concentration thresholds considering species-specific variability of bloom-forming cyanobacteria. Hydrobiologia. 757, 155–165.

[7] del Campo, F.F. and Ouahid, Y. (2010) Identification of microcystins from three collection strains of *Microcystis aeruginosa*. Environ Pollut. 158, 2906-2914.

[8] Ríos, V., Moreno, I., Prieto, A.I., Soria-Díaz, M.E., Frías, J.E. and Cameán, A.M. (2014) Comparison of *Microcystis aeruginosa* (PCC7820 and PCC7806) growth and intracellular microcystins content determined by liquid chromatography–mass spectrometry, enzyme-linked immunosorbent assay anti-Adda and phosphatase bioassay. J Water Health. 12(1), 69-80.

[9] Saker, M.L., Fastner, J., Dittmann, E., Christiansen, G. and Vasconcelos, V.M. (2005) Variation between strains of the cyanobacterium *Microcystis aeruginosa* isolated from a Portuguese river. J Appl Microbiol. 99, 749-757.

[10] Martins, J., Saker, M.L., Moreira, C., Welker, M., Fastner, J. and Vasconcelos, V.M. (2009) Peptide diversity in strains of the cyanobacterium *Microcystis aeruginosa* isolated from Portuguese water supplies. Appl Microbiol Biotechnol. 82, 951-961.

[11] Gregor, J. and Maršálek, B. (2005) A simple in vivo fluorescence method for the selective detection and quantification of freshwater cyanobacteria and eukaryotic algae. Acta Hydroch Hydrob. 33, 142–148.

[12] Mankiewicz-Boczek, J., Izydorczyk, K., Romanowska-Duda, Z., Jurczak, T., Stefaniak, K. and Kokocinski, M. (2006) Detection and monitoring toxigenicity of cyanobacteria by application of molecular methods. Environ Toxicol. 21, 380–387.

[13] Meissner, S., Fastner, J. and Dittmann, E. (2013) Microcystin production revisited: conjugate formation makes a major contribution. Environ Microbiol. 15, 1810–1820.

[14] Foss, A.J. and Aubel, M.T. (2015) Using the MMPB technique to confirm microcystin concentrations in water measured by ELISA and HPLC (UV, MS, MS/MS). Toxicon. 104, 91-101.

[15] Pierangelini, M., Stojkovic, S., Orr, P.T. and Beardall, J. (2004) Photosynthetic characteristics of two *Cylindrospermopsis raciborskii* strains differing in their toxicity. J Phycol. 50, 292–302.

[16] Wilson, A.E., Wilson, W.A. and Hay, M.E. (2006) Intraspecific variation in growth and morphology of the bloom-forming cyanobacterium *Microcystis aeruginosa*. Appl Environ Microbiol. 72, 7386-7389.

[17] Wu, Z., Shi, J. and Li, R. (2009) Comparative studies on photosynthesis and phosphate metabolism of *Cylindrospermopsis raciborskii* with *Microcystis aeruginosa* and *Aphanizomenon flos-aquae*. Harmful Algae. 8, 910–915.

[18] Bennett, A. and Bogorad, L. (1973) Complementary chromatic adaptation in a filamentous blue-green alga. J Cell Biol. 58, 419–435.

[19] Jeffrey, S.W. and Humphrey, G.F. (1975) New spectrophotometric equations for determining chlorophylls a, b, c1 and c2 in higher plants, algae, and natural phytoplankton. Biochem Physiol Pflanz. 167, 191–194.

[20] Lawton, L.A., Edwards, C. and Codd, G.A. (1994) Extraction and High-performance liquid chromatographic method for the determination of microcystins in raw and treat water. Analyst. 119, 1525-1530.

[21] Ikawa, M., Phillips, N., Haney, J.F. and Sasner, J.J. (1999) Interference by plastics additives in HPLC determination of microcystin-LR and -YR. Toxicon. 37, 923-929.

[22] Zhou, X.J., Okamura, H. and Nagata, S. (2006) Applicability of luminescent assay using fresh cells of *Vibrio fischeri* for toxicity. J Health Sci. 52, 811-816.

[23] Liu, Y., Gao, B.Y., Yue, Q.Y., Guan, Y.T., Wang, Y. and Huang, L.H. (2012) Influences of two antibiotic contaminants on the production, release and toxicity of microcystins. Ecotoxicol Environ Safe. 77, 79–87.

[24] Rzymski, P., Poniedzialek, B., Kokociński, M., Jurczak, T., Lipski, D. and Wiktorowicz, K. (2014) Interspecific allelopathy in cyanobacteria: Cylindrospermopsin and *Cylindrospermopsis raciborskii* effect on the growth and metabolism of *Microcystis aeruginosa*. Harmful Algae. 35, 1–8.

[25] Chen, L., Mao, F.J., Kirumba, G.C., Jiang, C., Manefield, M. and He, Y.L. (2015) Changes in metabolites, antioxidant system, and gene expression in *Microcystis aeruginosa* under sodium chloride stress. Ecotox Environ Safe. 122, 126–135.

[26] Li, J., Liu, Y.G., Zhang, P.Y., Zeng, G.M., Cai, X.X., Liu, S.B., Yin, Y.C., Hu, X.J., Hu, X. and Tan, X.F. (2006) Growth inhibition and oxidative damage of *Microcystis aeruginosa* induced by crude extract of *Sagittaria trifolia* tubers. J Environ Sci. 43, 40 – 47.

[27] Herrera, N.A., Echeverri, L.F. and Ferrão-Filho, A.S. (2015) Effects of phytoplankton extracts containing the toxin microcystin-LR on the survival and reproduction of cladocerans. Toxicon. 95, 38-45.

[28] Vezie, C., Rapala, J., Vaitomaa, J., Seitsonen, J. and Sivonen, K. (2002) Effect of nitrogen and phosphorus on growth of toxic and nontoxic *Microcystis* strains and on intracellular Microcystin concentrations. Microb Ecol. 43, 443-454.

[29] Jakobi, C., Rinehart, K.L., Neuber, R., Mez, K. and Weckesser, J. (1996) Cyanopeptolin SS, a disulphated depsipeptide from a water bloom: structural elucidation and biological activities. Phycologia. 35(6), 111-116.

Received: **21.11.2016**
Accepted: **06.11.2017**

CORRESPONDING AUTHOR

Cuili Jin
College of Environmental Science and Engineering, Yangzhou University
196# of Huayang West Street, Hanjiang District, Yangzhou City, Jiangsu Province – China

e-mail: cljin@yzu.edu.cn.

© by PSP Volume 27 – No. 2/2018 pages 668-674 Fresenius Environmental Bulletin

SOME HEAVY METALS AND MINERAL NUTRIENTS OF NARROW ENDEMIC *CIRSIUM BYZANTINUM* STEUD., FROM ISTANBUL, TURKEY: PLANT-SOIL INTERACTIONS

Ibrahim Ilker Ozyigit[1,2,*], Bulent Eskin[3], Mehmet Emin Uras[1], Ugur Sen[1], Birsen Eygi Erdogan[4], Gulbubu Kurmanbekova[2], Zeki Severoglu[1], Ibrahim Ertugrul Yalcin[5]

[1]Marmara University, Faculty of Arts & Science, Biology Department, 34722, Istanbul, Turkey
[2]Kyrgyz-Turkish Manas University, Faculty of Science, Biology Department, 72001, Bishkek, Kyrgyzstan
[3]Aksaray University, Faculty of Economics & Administrative Sciences, Political Science & Public Administration Department, 68100, Aksaray, Turkey
[4]Marmara University, Faculty of Arts & Science, Statistics Department, 34722, Istanbul, Turkey
[5]Bahcesehir University, Faculty of Engineering and Natural Sciences, Molecular Biology and Genetics Department, 34353 Istanbul, Turkey

ABSTRACT

Cirsium species have economic importance because of their botanical and medicinal properties. Thus, this study has aimed to investigate some heavy metal (Fe, Mn and Zn) and mineral nutrient (B, Ca, K, Mg and Na) status of narrow endemic *Cirisum byzantinum*. Plant and soil element concentrations were analyzed by using ICP-OES and the evaluation of plant-soil interactions for heavy metals and mineral nutrients were carried out by statistical methods. The measured element concentrations (in mg/kg) were in ranges of 5.936-19.044 for B, 1862.161-4811.168 for Ca, 12.610-38.474 or Fe, 3421.383-6881.885 for K, 190.984-593.427 for Mg, 3.830-17.301 for Mn, 21.236-62.025 for Na, and 6.183-28.060 for Zn in plant parts. Statistical analysis for element interactions between root/leaf and co-located soil samples revealed that there a was positive correlation between B, Ca, Fe, K, Mg, Mn, Na and Zn found in soil and Na and Zn found in roots, and Fe, Mn and Na found in leaves, respectively. Herein, results of this study could provide preliminary knowledge for future studies to better understand element uptake and heavy metal accumulation status of endemic species. Also, this study could also provide some insights for responsible authorities to develop conservation strategies.

KEYWORDS:
Cirsium, plant-soil interactions, mineral nutrition, autecology, conservation

INTRODUCTION

Cirsium is the largest genus (>250 taxa) in Asteraceae family comprising the annual, biennial and perennial species. Although, mainly populated in mountains of Southern Europe and Caucasia, members of this genus can be seen all around Europe, Asia, Africa and America continents [1-3]. In Turkey, this genus by classified in three main divisions with 78 taxa and 66 species [3].

They are characterized as "Perennial, biennial or rarely annual herbs; plants rarely dioecious; stems spiny-winged or unarmed, branched or not. Leaves spinose at margins, upper surface with or without setae and spinules, entire to pinnatisect. Capitula homogamous, discoid, solitary or crowded. Phyllaries pluriseriate, imbricate, adpressed or ± patent in upper part, with or without a subterminal vitta, sometimes appendaged, usually with a terminal spine, margins entire to spinulose or lacerate. Receptacle long-hairy. Flowers hermaphrodite or rarely unisexual, tubular, usually un-equally 5-fid, white to purple, sometimes yellowish; base of corolla tube slightly widened. Pollen grains globose. Achenes ± oblong, compressed, smooth, glabrous, with ± hemispherical umbo; hilum oval, sub-basal. Pappus pluri-seriate, plumose, connate at base into a ring, deciduous or ± persistent, inner- most hairs longest, often scabrous or thickened at apex; very rarely completely scabrous" [4].

Cirsium members display a wide range of known mating events and are considered as an appropriate model organism for pollination biology [5]. Many *Cirsium* species are also valued for their medicinal importance because of flavonoids, antioxidants and phenolic compounds [6]. In folk medicine, they are also reported to have antidiabetic, antiseptic, diuretic, antihemorrhagic, antihypertensive and antihepatitis activities, and used in treatments of liver and uterine cancers, and leukemia [7-9]. *Cirsium* species are among the best plants for honey production [9]. This genus also includes some invasive species; thereby, comprehensive mechanical, chemical and biological methods have been developed to prevent against their invasive activities [10]. Thus, many species of this genus are under special conservation statues due to their rare distributions and danger of extinction and some members of this genus having invasive nature are also of special concern [5].

TABLE 1
Geographical locations of plant and soil sampling sites

Sampling Site	Location	Altitude (m)	Coordinates
Location 1	Başıbüyük	75	**N** 40° 57′ 11,8″, **E** 29° 8′ 47.8″
Location 2	Roadside, Şile	134	**N** 41° 02′ 02,4″ , **E** 29° 16′ 13.5″
Location 3	Paşaköy Entrance	134	**N** 40° 59′ 07.7″, **E** 29° 19′ 45.0″
Location 4	Paşaköy Wastewater Treatment Facility	137	**N** 40° 59′ 44.9″, **E** 29° 19′ 23.9″
Location 5	Neighborhood Emirli Village	101	**N** 40° 59′ 48.8″, **E** 29° 19′ 06.6″

Most *Cirsium* species have been studied for their ecological, botanical and medicinal properties; however, there is no extensive information about heavy metal uptake and mineral nutrient statuses of this genus. Thus, the aim of this study is to investigate heavy metal and mineral nutrient statuses of this narrow endemic *C. byzantinum* and also is to have information on its plant-soil interactions.

MATERIALS AND METHODS

Botanical Description of Plant Material. *Circium byzantinum* Steud. biennial, about 100-120 cm. Stem stout at base, branched, unwinged, sparsely arachnoid. Median cauline leaves oblong, pinnatisect, lateral lobes bifid, c. 5-8 paired, narrowly triangular to lanceolate, as in *C. ligulare*, lateral and terminal lobes with slender c. 4-7 mm apical spine, spinose-strigose above, with setae 0.6-1.5 mm, otherwise glabrous; sparsely arachnoid below. Lateral branches 2-7, 3-18-capitulate; uppermost leaves 3-7, involucrate, usually longer than involucre, sometimes equalling or shorter than it. Involucres erect, broadly campanulate-obconical to campanulate-obovoid, 15-20 mm. Phyllaries sparsely arachnoid, 6-9-seriate, minutely denticulate at margin (spinules up to 0.2 mm), adpressed in bud, then erecto-patent; median 9-11 mm including 1-1.5x0.20-0.25 mm apical spine without spinules on inner surface; innermost refiexed, gradually narrowed to apical spine. Corollas white, 17-19 mm. Achenes 4.5-5 mm [11].

Pappus 12.5-14 mm. Fl. 7-10. Dry places by roadsides, in fields, dry hills, open places, near sea level.

Type: [Turkey A2(E) Istanbul] circa *Constantinopolim*, Aucher 3392 (G-DC.). Endemic [11].

FIGURE 1
General habitat of *C. byzantinum* plant (A) and branches with flowers (B).

Sample Collection & Analysis. Plant (root, stem, leaf and flower) and soil (~500g from 10cm depth) samples were collected from five different locations in Istanbul/Turkey (Table 1). Plant samples were oven-dried at 80°C for 48h, grounded by micro hammer cutter and fed through a 1.5 mm sieve. Then, 0.3g of plant samples were transferred into Teflon vessels and added of 8ml 65% HNO_3. Soil samples were also oven-dried at 80°C for 24h and fed through a 2 mm sieve. Then, 0.3g of soil samples were transferred into Teflon vessels and added of 5 ml 65% HNO_3, 3 ml 37% HCl and 2ml 48% HF. All samples (plant and soil) were then mineralized in microwave oven (Berghof MWS-2) at 145°C for 5 min, 165°C for 5 min and 175°C for 20 min. Following mineralization and cooling, the samples were filtered using Whattman filters and made up to 50 ml with ultra-pure water and stored in falcon tubes. Multi-element standard solution was prepared from stock solution-1000 ppm (Merck). The concentrations of mineral elements and heavy metals such as boron (B), calcium (Ca), iron (Fe), potassium (K), magnesium (Mg), manganese (Mn), sodium (Na) and zinc (Zn) were measured by using Inductively Coupled Plasma Optical Emission Spectroscopy (ICP-OES; Perkin Elmer Optima 7000 DV).

Statistical Analyses. Multivariate analysis of variance (MANOVA) with Tukey's post-hoc HSD and Pearson correlation were calculated using IBM SPSS Statistics 20 software. The statistical significance was shown as **P<0.01 and *P<0.05 level (2-tailed).

RESULTS AND DISCUSSION

The concentrations of B, Ca, Fe, K, Mg, Mn, Na and Zn were determined by using ICP-OES for understanding of heavy metal accumulation capability and mineral nutrient status of narrow endemic *C. byzantinum*. In plant parts, without standard error consideration, element concentrations (in mg/kg) were 5.936-19.044 for B, 1862.161- 4811.168 for Ca, 12.610-38.474 for Fe, 3421.383-6881.885 for K, 190.984-593.427 for Mg, 3.830-17.301 for Mn, 21.236- 62.025 for Na, and 6.183-28.060 for Zn (Table 2). The average concentration of all elements ranked as flower<stem<leaf<root.

TABLE 2
Heavy metal and mineral element distributions in plant and soil samples.

Cirsium byzantinum		Flower	Leaf	Stem	Root	Soil
B (mg/kg)	**1.Loc**	6.209±0.156^{*ab}	14.524±0.134^{**a}	7.637±0.095^{*ab}	17.681±0.220^{*a}	61.856±0.907^{*b}
	2.Loc	5.981±0.048^{**b}	14.662±0.158^{*a}	8.158±0.080^{*a}	19.044±0.205^{*a}	130.558±3.681^{*a}
	3.Loc	5.936±0.047^{**b}	13.442±0.105^{**b}	5.950±0.057^{**b}	13.658±0.108^{**b}	72.609±2.866^{*b}
	4.Loc	6.503±0.039^{**a}	12.514±0.091^{**b}	6.147±0.071^{*b}	14.032±0.134^{**b}	80.831±1.222^{*b}
	5.Loc	7.127±0.064^{**a}	14.159±0.089^{**a}	6.379±0.073^{*b}	14.052±0.157^{*b}	156.682±5.980^{*a}
Average B		6.351±0.708	13.860±0.115	6.854±0.075	15.693±0.165	100.507±2.931
Ca (mg/kg)	**1.Loc**	2035.736±26.161^{*a}	3200.665±85.611^{*a}	2116.890±28.833^{*a}	4567.892±41.412^{**a}	864.218±2.207^{**b}
	2.Loc	1890.472±15.199^{**b}	3219.086±34.589^{*a}	2218.690±21.666^{**a}	4811.168±51.750^{*a}	934.048±3.325^{**a}
	3.Loc	1889.395±15.047^{**b}	3095.300±24.214^{**b}	1862.161±17.848^{**b}	4041.994±31.832^{**b}	811.769±3.608^{**b}
	4.Loc	2009.195±12.044^{**a}	2874.570±20.799^{**b}	1949.076±22.408^{*b}	4350.039±41.662^{**ab}	834.928±3.542^{**b}
	5.Loc	2316.378±20.710^{**a}	3362.140±21.110^{**a}	2203.049±25.111^{*a}	4560.169±50.869^{*a}	971.930±3.530^{**a}
Average Ca		2028.235±17.832	3150.352±37.264	2069.973±23.173	4466.252±43.505	883.379±3.242
Fe (mg/kg)	**1.Loc**	14.519±0.349^{*b}	32.275±1.061^{*b}	16.259±0.270^{*a}	34.523±0.329^{**a}	1825.700±25.571^{*a}
	2.Loc	16.113±0.130^{**a}	38.009±0.408^{*a}	18.134±0.177^{**a}	37.461±0.403^{*a}	1913.728±24.191^{*a}
	3.Loc	13.767±0.110^{**b}	30.980±0.242^{**b}	12.610±0.121^{*b}	27.370±0.216^{**b}	1730.956±46.654^{*b}
	4.Loc	14.830±0.089^{**b}	28.786±0.208^{*b}	13.912±0.160^{*b}	34.108±0.327^{**a}	1771.874±41.684^{*b}
	5.Loc	17.052±0.152^{**a}	38.474±0.242^{**a}	15.884±0.181^{*ab}	35.394±0.395^{*a}	2035.596±35.583^{*a}
Average Fe		15.256±0.166	33.704±0.432	15.359±8.182	33.771±0.334	1855.570±34.737
K (mg/kg)	**1.Loc**	3672.223±40.318^{*a}	6076.267±38.944^{**a}	3994.433±44.613^{*ab}	6623.114±35.141^{**a}	1245.311±15.585^{*b}
	2.Loc	3422.608±27.517^{**b}	6095.640±65.497^{*a}	4169.967±40.721^{**a}	6881.885±74.023^{*a}	1421.261±23.151^{*a}
	3.Loc	3421.383±27.248^{**b}	5761.344±45.070^{**b}	3488.113±33.432^{**b}	5782.840±45.542^{**b}	1085.570±33.199^{*b}
	4.Loc	3573.108±21.419^{**b}	5322.333±38.509^{**b}	3746.801±43.077^{*b}	6451.708±61.790^{**a}	1159.555±35.734^{*b}
	5.Loc	3677.367±32.879^{**a}	6055.599±38.021^{**a}	4008.102±45.685^{*a}	6708.123±74.829^{*a}	1408.199±20.274^{*a}
Average K		3553.337±29.876	5862.236±45.208	3881.483±41.506	6489.533±58.265	1263.979±25.589
Mg (mg/kg)	**1.Loc**	242.368±11.568^{**a}	499.241±17.753^{*a}	300.927±12.170^{*a}	501.141±11.808^{*a}	5835.326±74.968^{*b}
	2.Loc	266.389±2.142^{**a}	561.459±6.033^{*a}	362.110±3.536^{*a}	593.427±6.383^{*a}	6384.438±80.464^{*a}
	3.Loc	190.984±1.521^{**b}	407.663±3.189^{**b}	227.743±2.183^{**b}	398.949±3.142^{**b}	5805.287±215.544^{*b}
	4.Loc	231.498±1.388^{**ab}	400.026±2.894^{**b}	266.899±3.069^{*b}	471.793±4.519^{**b}	5705.729±53.983^{**b}
	5.Loc	276.628±8.337^{*a}	546.442±3.431^{**a}	338.472±3.858^{*a}	544.688±6.076^{*a}	6655.174±40.243^{*a}
Average Mg		241.573±4.991	483.763±6.660	299.829±4.963	504.153±6.386	6109.591±93.040
Mn (mg/kg)	**1.Loc**	4.453±0.182^{*a}	11.088±0.285^{*b}	5.638±0.260^{*ab}	15.231±0.538^{*b}	148.913±5.666^{*b}
	2.Loc	4.305±0.035^{**a}	14.537±0.156^{*a}	6.365±0.062^{*a}	17.301±0.186^{*a}	181.766±6.877^{*a}
	3.Loc	3.830±0.031^{**b}	10.786±0.084^{**b}	4.359±0.042^{**b}	14.196±0.112^{**b}	117.731±5.970^{*b}
	4.Loc	4.374±0.026^{**a}	10.399±0.075^{**b}	4.990±0.057^{*b}	15.710±0.150^{*b}	124.904±7.623^{*b}
	5.Loc	4.534±0.041^{**a}	13.971±0.088^{**a}	5.932±0.068^{*a}	16.216±0.181^{*a}	206.859±7.780^{*a}
Average Mn		4.298±0.063	12.156±0,138	5.456±0,098	15.730±0.233	156.034±6.783
Na (mg/kg)	**1.Loc**	26.704±1.040^{*b}	42.520±1.392^{*b}	28.447±1.425^{*b}	51.490±1.515^{*ab}	135.744±2.121^{*b}
	2.Loc	29.912±0.240^{**a}	48.464±0.521^{*a}	35.368±0.345^{*a}	62.025±0.667^{*a}	152.598±2.845^{*a}
	3.Loc	21.236±0.169^{**b}	40.865±0.320^{**b}	25.029±0.240^{*b}	44.846±0.353^{**b}	124.204±2.198^{*b}
	4.Loc	23.453±0.141^{**b}	38.196±0.276^{**b}	26.997±0.310^{*b}	49.234±0.472^{**b}	130.449±2.756^{*b}
	5.Loc	32.164±0.288^{**a}	48.058±0.302^{**a}	33.094±0.377^{*a}	59.615±0.665^{*a}	164.981±3.805^{*a}
Average Na		26.693±0,376	43.620±0.562	29.786±0.539	53.441±0.734	141.595±2.745
Zn (mg/kg)	**1.Loc**	8.013±0.382^{*a}	16.022±1.007^{*a}	9.798±0.350^{*b}	21.853±0.845^{*b}	18.679±0.490^{*b}
	2.Loc	8.797±0.071^{**a}	18.764±0.202^{*a}	13.649±0.133^{*a}	28.060±0.302^{*a}	26.456±0.735^{*a}
	3.Loc	6.183±0.049^{**b}	11.496±0.090^{**b}	8.355±0.080^{*b}	16.705±0.132^{**b}	15.506±0.860^{*b}
	4.Loc	7.200±0.043^{**b}	12.338±0.089^{**b}	9.971±0.115^{*b}	19.218±0.184^{*b}	17.263±0.694^{*b}
	5.Loc	8.843±0.079^{**a}	17.775±0.112^{**a}	12.260±0.140^{*a}	26.571±0.296^{*a}	30.525±0.876^{*a}
Average Zn		7.807±0.125	15.278±0.300	10.806±0.164	22.481±0,352	21.685±0.731

The statistical significance was shown as **P<0.01 and *P<0.05 level (2-tailed). Plus-minus sign "±" indicates the standard error.

In relevant studies, acceptable limits/ranges of heavy metals and mineral nutrients in plants have been reported (in mg/kg) as 3.0-100 for B, 2000-30000 Ca, 50-250 for Fe, 1000-50000 for K, 100-1000 for Mg (1500-3500 in field crops), 30-300 for Mn, 100-10000 for Na and 20-150 for Zn [12-17]. Besides, acceptable ranges in soil (in mg/kg) were as 20-200 for B, 50000-150000 for Ca, 5000-50000 for Fe, 12000 for K, 3000-8000 for Mg, 270-525 for Mn, 1000-10000 for Na and 10-300 for Zn [14, 17, 18].

From these elements, Ca involves in modulation of developmental processes and response to various stress factors [19-21]. Herein, in light of relevant literatures, although the concentrations of Ca were found to be within acceptable ranges, their concentrations were slightly lower in the roots (4466.252 mg/kg) and the leaves (3150.352 mg/kg) of the plants. Soil Ca contents of the soils vary depending on soil type, climate and rainfall regimes. For example, Ca contents in sandy soils of rainy regions are very low; in the $CaCO_3$-free soils of rainy and temperate regions, Ca contents are in ranges of 0.7-1.5%; Ca contents in extremely dispersed and fragmented soils of rainy tropical regions are in ranges of 0.1-0.3%; and Ca contents in the calcareous soils vary between 1-25% with their high $CaCO_3$ contents [17]. In this work, soil Ca concentration (883.379 mg/kg) was relatively low. This infers that

plants may reach a metal homeostasis by accumulating sufficient amount of Ca into the various plant organs.

K is another mineral nutrient involving in plant growth and stress tolerance [22,23]. In this study, K level was low but within acceptable limits in all plant organs (3553.337 mg/kg in flower, 5862.236 mg/kg in leaf, 3881.483 mg/kg in stem and 6489.533 mg/kg in root). Also, K content of the soil (1263.979 mg/kg) was found to be relatively low. Like Ca, K can be also speculated to accumulate the sufficient potassium in different plant parts.

Soil salinity is one of the prime stress factors reducing agricultural productivity and low levels of Na concentrations are reported to have beneficial effects in plants [24]. Na was lower than average acceptable limits in all plant organs (26.693 mg/kg in flower, 43.620 mg/kg in leaf, 29.786 mg/kg in stem and 53.441 mg/kg in root). Also, it was lower in soil samples (141.595 mg/kg). This implies that *C. byzantinum* prefers the soils with low Na content.

In plants, B is essential for cell division, maturation and differentiation and its functions are related with growth and development, carbohydrate metabolism and maintenance of cell wall structure [25]. In recent studies, it has been also reported for a possible crosstalk between B and Ca elements [26-27]. In this study, B was within acceptable limits in plant and soil samples (6.351 mg/kg in flower, 13.860 mg/kg in leaf, 6.854 mg/kg in stem and 15.693 mg/kg in root and 100.507 in soil mg/kg).

Fe involves in many biological processes including respiration, photosynthesis, chlorophyll and DNA biosynthesis, hormone production and nitrogen fixation. It also functions as structural component in Fe-sulfur clusters, Fe-binding sites and heme [28-29]. Fe also interferes with ion absorption, Fe-toxicity causes multi-element deficiencies such as Ca, Zn, Mg, K and P [30]. In this work, the levels of Fe in plant and soil samples were quite lower than the acceptable limits such as 15.256 mg/kg in flower, 33.704 mg/kg in leaf, 15.359 mg/kg in stem, 33.771 mg/kg in root, and 1855.570 mg/kg in soil. Low Fe concentrations could be correlated with low soil Fe concentrations. It appears that *C. byzantinum* could be well adapted to its natural habitat in order to produce healthy populations.

Mg is an essential macronutrient for plant growth and reproduction [31]. It serves as a cofactor and/or an allosteric modulator more than 300 enzyme, including ATPases, phosphatases, kinases, carboxylases and RNA polymerases [32-34]. In addition, it weakly adsorbs to soil colloids, especially in acidic soils with low cation exchange capacity; thereby, it is predisposed for leaching [35]. In alkaline soils, the high levels of K, Ca, Na and $MgCO_3$ decrease the availability of Mg for crop species [36-37]. In this study, Mg was within acceptable range in plant parts (241.573 mg/kg in flower, 483.763 mg/kg in leaf, 299.829 mg/kg in stem and 504.153 mg/kg in root) although lower when compared with field crops. Also, it is within the normal limits (6109.591 mg/kg) in soil.

Mn is an essential mineral nutrient for plant growth and development. It involves in photosystem II (PSII) for the catalytic water splitting reaction, participates in lipid, lignin and carbohydrate biosynthesis, and functions as cofactor for various enzymes [38,39]. In this study, Mn in plant and soil samples were found to be lower than the acceptable limits (4.298 mg/kg in flower, 12.156 mg/kg in leaf, 5.456 mg/kg in stem, 15.730 mg/kg in root, and 156.034 mg/kg in soil).

Zn, which is essential for both plant and animals, also a heavy metal with medium toxic effects [40, 41]. It functions as catalytic element for enzymes, including Cu-Zn superoxide dismutase, alkaline phosphatase, carbonic anhydrase and alcohol dehydrogenase. It has also a role in stabilization of many protein motifs such as Zn cluster, Zn finger and RING finger domains [42,43]. In this work, the levels of Zn were found to be lower than the acceptable limits in plant parts (7.807 mg/kg in flower, 15.278 mg/kg in leaf, 10.806 mg/kg in stem and 22.481 mg/kg in root), and its concentration was slightly higher (21.685 mg/kg) than lower acceptable limit in soil samples.

Moreover, correlation coefficients of obtained element concentrations in soil, root and leaf samples were examined for having insights about plant-soil interaction and element accumulation trends. The correlation matrix (Table 3) demonstrated high positive correlations between B, Mg, Mn, Na and Zn in roots and B, Mg, Mn, Na and Zn in leaves (>0.95, >0.74); between Ca, Fe, K, Na and Zn in roots and Mg and Zn in leaves (>0.93, >0.73); between Ca, Mg, Na and Zn in roots and Mn in leaves (>0.93, >0.71); between Mg, Mn and Zn in roots and Na in leaves (>0.93, >0.71); and between Na and Zn in roots and Fe in leaves (>0.85, >0.83). This implies that Na and Zn in roots could positively affect the overall uptake of other elements in leaves. There has also been a positive correlation between the plant roots and leaves for the B, Mg, Mn, Na and Zn.

Correlation matrix (Table 4) also showed high positive correlations between B, Ca, Fe, K, Mg, Mn, Na and Zn in soils and Na and Zn in roots as well as Fe, Mn and Na in leaves (>0.92, >0.70); between K in soils and Ca, Fe, K, Mg and Mn in roots (>0.88, >0.70); between Ca in soils and Ca, Fe, K and Mg in roots (>0.84, >0.72); between Mn, Na and Zn in soils and Mg in roots (>0.78, >0.73); between Ca, Fe, K, Mg, Mn, Na and Zn in soils and Mg in leaves (>0.89, >0.72); and between Ca, Fe, K, Mn, Na and Zn in soils and Zn in leaves (>0.89, >0.72). Findings indicate that B, Ca, Fe, K, Mg, Mn, Na and Zn elements in soil could positively affect concentration of Na and Zn in roots, as well as Fe, Mn and Na concentrations in leaves of *C. byzantinum.*

TABLE 3
Correlation matrix of mineral nutrients and heavy metals between root and leaf samples

Correlation Matrix (R)								
Pearson Correlation	**B Root**	**Ca Root**	**Fe Root**	**K Root**	**Mg Root**	**Mn Root**	**Na Root**	**Zn Root**
B Leaf	.743**	.694**	.463*	.550**	.630**	.461*	.636**	.687**
Ca Leaf	.283	.435*	.319	.416*	.557**	.273	.642**	.661**
Fe Leaf	.380	.692**	.572**	.626**	.762**	.542**	.831**	.847**
K Leaf	.611**	.601**	.378	.479*	.575**	.382	.625**	.670**
Mg Leaf	.609**	.815**	.729**	.774**	.884**	.608**	.893**	.922**
Mn Leaf	.454*	.720**	.646**	.661**	.836**	.749**	.928**	.927**
Na Leaf	.476*	.658**	.556**	.595**	.806**	.714**	.895**	.903**
Zn Leaf	.634**	.824**	.789**	.814**	.931**	.679**	.927**	.948**

** Correlation is significant at level of 0.01 (2-tailed), * Correlation is significant at level of 0.05 (2-tailed).

TABLE 4
Correlation matrix of mineral nutrients and heavy metals between soil and root/leaf samples

Correlation Matrix (R)								
Pearson Correlation	**B Soil**	**Ca Soil**	**Fe Soil**	**K Soil**	**Mg Soil**	**Mn Soil**	**Na Soil**	**Zn Soil**
B Leaf	.350	.597**	.493*	.633**	.524**	.578**	.522**	.503*
B Root	.055	.311	.177	.494*	.166	.275	.224	.220
Ca Leaf	.566**	.677**	.681**	.631**	.673**	.620**	.668**	.609**
Ca Root	.517**	.728**	.626**	.820**	.542**	.657**	.649**	.646**
Fe Leaf	.838**	.906**	.793**	.859**	.843**	.857**	.853**	.876**
Fe Root	.540**	.719**	.609**	.789**	.481*	.632**	.655**	.646**
K Leaf	.406*	.618**	.546**	.619**	.567**	.596**	.550**	.532**
K Root	.540**	.737**	.666**	.809**	.524**	.652**	.674**	.655**
Mg Leaf	.698**	.876**	.756**	.888**	.740**	.813**	.819**	.807**
Mg Root	.697**	.839**	.683**	.884**	.648**	.734**	.777**	.769**
Mn Leaf	.878**	.904**	.722**	.859**	.791**	.826**	.826**	.878**
Mn Root	.634**	.679**	.504*	.704**	.533**	.556**	.627**	.623**
Na Leaf	.787**	.857**	.695**	.805**	.785**	.769**	.811**	.802**
Na Root	.818**	.903**	.742**	.901**	.735**	.794**	.841**	.850**
Zn Leaf	.679**	.855**	.723**	.879**	.691**	.773**	.804**	.779**
Zn Root	.799**	.917**	.741**	.912**	.734**	.821**	.849**	.860**

** Correlation is significant at level of 0.01 (2-tailed), * Correlation is significant at level of 0.05 (2-tailed).

In studies from *C. arvense*, some element concentrations were reported as 21.8 mg/kg for B, 55.4 mg/kg for Fe, 24.0 mg/kg for Mn and 42.9 mg/kg for Zn [44]. These concentrations were higher in herein studied *C. byzantinum* plant. Compared to Muhammad et al. (2013) [45], Ca, Fe, Mn and Na levels in *C. byzantinum* were lower, while K, Mg and Zn were closer than *C. vulgare*. In a different study *C. canum* -grown in serpentine soil- was analyzed for its trace elements, and Ca, Mg, Mn and Zn levels were found higher than *C. byzantinum* [46]. In comparison with our results, higher Fe, Mn and Zn concentrations were found to be in *C. congestum* collected from a mining area [47]. In a similar study, higher Fe, Mn and Zn concentrations were reported in *C. congestum* in comparison with *C. byzantinum* [48].

Findings of this study along with previous reports implicate that narrow endemic *C. byzantinum* represents different accumulation statuses for heavy metals and mineral nutrient elements and prefers different soil properties in comparison with its close relatives (*C. arvense*, *C. congestum*, *C. canum* and *C. vulgare*). Moreover, *C. byzantinum* also differs from other plants for its habitat, element uptake and soil preferences. Therefore, this work will provide future insights for the studies regarding of endemics, narrow endemics and new identified species.

REFERENCES

[1] Kadereit, J.W., Jeffrey, C. (2007) The Families and Genera of Vascular Plants, Vol. 8. Flowering Plants. Eudicots: Asterales. Springer-Verlag, Berlin, 1-635.

[2] Yuksel, E., Kiran, Y., Sahin, A., Yildiz, B., Arabaci, T. (2013) Karyological studies of *Cirsium* sect. *Epitrachys* (Asteraceae) species from Turkey. Turkish Journal of Botany. 37(6), 1085-1092.

[3] Yildiz, B., Arabaci, T., Dirmenci, T., Kostekci, S. (2016) A taxonomic revision of the genus *Cirsium* Mill. sect. *Cirsium* (Asteraceae: Cardueae) in Turkey. Turkish Journal of Botany. 40(5), 514-530.

[4] Davis, P.H., Parris, B.S. (1975a) *Cirsium* Miller. Davis, P.H. (ed.) Flora of Turkey and the East Aegean Islands. 5, 370-411.

[5] Powell, K.I., Krakos, K.N., Knight, T.M. (2011) Comparing the reproductive success and pollination biology of an invasive plant to its rare and common native congeners: a case study in the genus *Cirsium* (Asteraceae). Biological Invasions. 13(4), 905-917.
[6] Ozcan, M., Ayaz, F.A., Ozogul, Y., Glew, R., Ozogul, F. (2016) Fatty acid composition of achenes of *Cirsium* taxa (Asteraceae, Carduoideae) from Turkey. Zeitschrift für Naturforschung C. 71(3-4), 45-54.
[7] Liu, S.J., Luo, X., Li, D.X., Zhang, J., Qiu, D.L., Liu, W., She, L., Yang, Z.R. (2006) Tumor inhibition and improved immunity in mice treated with flavone from *Cirsium japonicum* DC. International Immunopharmacology. 6, 1387-1393.
[8] Yin, J., Heo, S.I., Wang, M.H. (2008) Antioxidant and antidiabetic activities of extracts from *Cirsium japonicum* roots. Nutrition Research and Practice. 2(4), 247-251.
[9] Selvi, S., Sevindik, E., Acar, M. (2013) Polinatörlerin bitkisi *Cirsium* spp., Uludağ Arıcılık Dergisi. 1, 25-27.
[10] Ozcan, M., Hayirlioglu-Ayaz, S., Inceer, H. (2008) Chromosome counts of some *Cirsium* (Asteraceae, Cardueae) taxa from Turkey. Caryologia. 61(4), 375-382.
[11] Davis, P.H., Parris, B.S. (1975b). *Cirsium* Miller. Davis, P.H. (ed.) Flora of Turkey and the East Aegean Islands. 5, 381-382.
[12] Pawlisz, A.V., Kent, R.A., Schneider, U.A., Jefferson, C. (1997) Canadian water quality guidelines for chromium. Environmental Toxicology and Water Quality. 12, 123-183.
[13] Jones, C., Jacobsen, J. (2001) Plant Nutrition and Soil Fertility, Nutrient Management Module No: 2, Montana State University, Extension Service. 4449-2.
[14] Kabata-Pendias, A., Pendias, H. (2001) Trace Elements in Soils and Plants, CRC Press, Boca Raton, USA. 1-432.
[15] Corlett, J.L., Clegg, M.S., Keen, C.L., Grivetti, L.E. (2002) Mineral content of culinary and medicinal plants cultivated by Hmong refugees living in Sacramento, California. International Journal of Food Science and Nutrition. 53, 117-128.
[16] Zayed, A.M., Terry, N. (2003) Chromium in the environment: factors affecting biological remediation. Plant and Soil. 249(1), 139-156.
[17] Kacar, B., Katkat, A.V. (2007). Bitki Besleme. Nobel Publications. 1-379.
[18] Kabata-Pendias, A., Mukherjee, A.B. (2007) Trace Elements from Soil to Human. Springer Science & Business Media. 1-550.
[19] APA Franz, S., Ehlert, B., Liese, A., Kurth, J., Cazalé, A.C., Romeis, T. (2011) Calcium-dependent protein kinase CPK21 functions in abiotic stress response in *Arabidopsis thaliana*. Molecular Plant. 4(1), 83-96.
[20] Short, E.F., North, K.A., Roberts, M.R., Hetherington, A.M., Shirras, A.D., McAinsh, M.R. (2012) A stress-specific calcium signature regulating an ozone-responsive gene expression network in *Arabidopsis*. The Plant Journal. 71(6), 948-961.
[21] Cakmak, I. (2014) Major functions of calcium and magnesium in crop plants. In: 16th World Fertilizer Congress. 16, 30-32.
[22] Ahmad, I., Maathuis, F.J. (2014) Cellular and tissue distribution of potassium: physiological relevance, mechanisms and regulation. Journal of Plant Physiology. 171(9), 708-714.
[23] Zörb, C., Senbayram, M., Peiter, E. (2014) Potassium in agriculture-status and perspectives. Journal of Plant Physiology. 171(9), 656-669.
[24] Flowers, T.J., Colmer, T.D. (2008) Salinity tolerance in halophytes. New Phytologist. 179, 945-963.
[25] Gupta, U.C., Solanki, H.A. (2013) Impact of boron deficiency on plant growth. International Journal of Bioassays. 2(07), 1048-1050.
[26] Koshiba, T., Kobayashi, M., Ishihara, A., Matoh, T. (2010) Boron nutrition of cultured tobacco BY-2 cells. VI. Calcium is involved in early responses to boron deprivation. Plant and Cell Physiology. 51(2), 323-327.
[27] González-Fontes, A., Rexach, J., Quiles-Pando, C., Herrera-Rodríguez, M.B., Camacho Cristóbal, J.J., Navarro-Gochicoa, M.T. (2013) Transcription factors as potential participants in the signal transduction pathway of boron deficiency. Plant Signaling & Behavior. 8(11), e26114.
[28] Kobayashi, T., Nishizawa, N.K. (2012) Iron uptake, translocation, and regulation in higher plants. Annual Review of Plant Biology. 63, 131-152.
[29] Vatansever, R., Filiz, E., Ozyigit, I.I. (2015). Genome-wide analysis of iron-regulated transporter 1 (IRT1) genes in plants. Horticulture, Environment and Biotechnology. 56(4), 516-523.
[30] Quinet, M., Vromman, D., Clippe, A., Bertin, P., Lequeux, H., Dufey, I., Lutts, S., Lefevre, I. (2012) Combined transcriptomic and physiological approaches reveal strong differences between short-and long-term response of rice (*Oryza sativa*) to iron toxicity. Plant, Cell & Environment. 35(10), 1837-1859.
[31] Williams, L., Salt, D.E. (2009) The plant ionome coming into focus. Current Opinion in Plant Biology. 12(3), 247.

[32] Cowan, J.A. (2002) Structural and catalytic chemistry of magnesium dependent enzymes. Biometals. 15, 225-235.
[33] Shaul, O. (2002) Magnesium transport and function in plants: the tip of the iceberg. Biometals. 15, 309-323.
[34] Hawkesford, M., Horst, W., Kichey, T.M.R., Schjørring, J.K., Møller, I.S., White, P. (2012) Functions of macronutrients. In: Marschers, P. (ed.) Marschers's Mineral Nutrition of Higher Plants. Elsevier Science. 135-190.
[35] Grzebisz, W. (2009) Magnesium. In: Handbook of Plant Nutrition. Barker, A.V., Pilbeam, D.J. (Eds.) Boca Raton: CRC Press. 199-260.
[36] Broadley, M.R., White, P.J. (2010) Eats roots and leaves. Can edible horticultural crops address dietary calcium, magnesium and potassium deficiencies? Proceedings of the Nutrition Society. 69(04), 601-612.
[37] Verbruggen, N., Hermans, C. (2013) Physiological and molecular responses to magnesium nutritional imbalance in plants. Plant and Soil. 368(1-2), 87-99.
[38] Law, N., Caudle, M., Pecoraro, V. (1998) Manganese redox enzymes and model systems: properties, structures, and reactivity. Advances in Inorganic Chemistry. 46, 305-440.
[39] Vatansever, R., Filiz, E., Ozyigit, I.I. (2016) *In silico* analysis of Mn transporters (NRAMP1) in various plant species. Molecular Biology Reports. 43(3), 151-163.
[40] Genc, T.O., Yilmaz, F., Inanan, B.E., Yorulmaz, B., Utuk, G. (2015) Application of multi-metal bioaccumulation index and bioavailability of heavy metals in *Unio* sp. (Unionidae) collected from Tersakan River, Muğla, South-West Turkey. Fresen. Environ. Bull. 24, 208-215.
[41] Jusufi, K., Stafilov, T., Vasjari, M., Korca, B., Halili, J., Berisha, A. (2017) Measuring the presence of heavy metals and their bioavailability in potato crops around Kosovo's power plants. Fresen. Environ. Bull. 26, 1682-1686.
[42] Wuana, R.A., Okieimen, F.E. (2011) Heavy metals in contaminated soils: a review of sources, chemistry, risks and best available strategies for remediation. International Scholarly Research Network ISRN Ecology. 1-20.
[43] Vatansever, R., Ozyigit, I.I., Filiz, E. (2016) Comparative and phylogenetic analysis of zinc transporter genes/proteins in plants. Turkish Journal of Biology. 40(3), 600-611.
[44] Győri, Z., Filep, T., Lehoczky, É. (2014) Trace element content of several weed seeds. Carpathian Journal of Earth and Environmental Sciences. 9(2), 251-257.
[45] Muhammad, S., Shah, M.T., Khan, S., Saddique, U., Gul, N., Khan, M.U., Malik, R.N., Farooq M., Naz, A. (2013) Wild plant assessment for heavy metal phytoremediation potential along the mafic and ultramafic terrain in northern Pakistan. BioMed Research International. 1-9.
[46] Salihaj, M., Bani, A., Echevarria, G. (2016) Heavy metals uptake by hyperaccumulating flora in some serpentine soils of Kosovo. Global Nest Journal. 18(1), 214-222.
[47] Cheraghi, M., Lorestani, B., Khorasani, N., Yousefi, N., Karami, M. (2011) Findings on the phytoextraction and phytostabilization of soils contaminated with heavy metals. Biological Trace Element Research. 144(1-3), 1133-1141.
[48] Nouri, J., Lorestani, B., Yousefi, N., Khorasani, N., Hasani, A. H., Seif, F., Cheraghi, M. (2011) Phytoremediation potential of native plants grown in the vicinity of Ahangaran lead-zinc mine (Hamedan, Iran). Environmental Earth Sciences. 62(3), 639-644.

Received: **24.11.2016**
Accepted: **20.11.2017**

CORRESPONDING AUTHOR

Ibrahim Ilker Ozyigit
Marmara University,
Faculty of Arts & Science,
Biology Department,
34722, Istanbul, Turkey

e-mail: ilkozyigit@marmara.edu.tr

© by PSP Volume 27 – No. 2/2018 pages 675-680 Fresenius Environmental Bulletin

CATIONIC POLYACRYLAMIDE-MODIFIED RIVER SAND FOR EFFICIENT REMOVAL OF *MICROCYSTIS AERUGINOSA*

Chenghua Zhong[1,*], Yaoyao Huang[1], Yang Hu[2], Rui Bai[1], Ming Yang[1]

[1]College of Environment and Resources, Chongqing Technology and Business University, Chongqing 400067, China
[2]School of Urban Construction and Environmental Engineering, Chongqing University, Chongqing 400045, China

ABSTRACT

A new method was developed for removal of the algae *Microcystis aeruginosa* using river sand modified with cationic polyacrylamide (CPAM). The effects of CPAM, river sand and *Microcystis aeruginosa* concentrations, pH, and river sand particle size on the removal efficiency of algae were investigated. The highest algae removal efficiency was 99.92% in two hours using 0.5 g L^{-1} of river sand modified with 30 mg L^{-1} CPAM. The pH of the raw algae water affected the percentage of algae removal. Algae removal was efficient in the pH range 7.0–10.0 (>99%). Compared with CPAM alone, the presence of river sand was critical for speeding up the flocculation and sedimentation processes of algal flocs. When the river sand concentration was 0.5 g L^{-1}, the river sand particle size had little effect on the removal efficiency of algae. The algae concentration strongly influenced the flocculation efficiency. An algae concentration of 7.0×10^6 cells mL^{-1} gave the highest removal efficiency of 99.32%. A flocculation mechanism using CPAM-modified river sand was proposed. CPAM as a modifier makes it possible to use river sand for *Microcystis aeruginosa* removal from raw algae water. Economical and environmental concerns are minimized through the use of native sand and biodegradable CPAM.

KEYWORDS:
Cationic polyacrylamide, Modification, River sand, *Microcystis aeruginosa*, Flocculation, Removal efficiency

INTRODUCTION

Owing to the continuous pollution associated with economic and industrial development, the composition of wastewater has become increasingly complex and hence the treatment of sewage has become increasingly difficult. Raw sewage drains into rivers, which increases the nutrient concentration in the water. Accumulation of nutrients in water leads to eutrophication, which brings about algal overgrowth. Algal blooms are mainly caused by the excessive growth of cyanobacteria. The dominant species of algal blooms is the cyanobacteria *Microcystis aeruginosa*. Blooms of *Microcystis aeruginosa* generate unpleasant odors and release toxins into water bodies that are harmful to aquatic life and human health [1, 2]. Therefore, there is an urgent need to find an effective method of algae removal.

Flocculation treatment is a commonly used method to remove algae from water [3–7]. Considerable attention has been focused on the use of clays as a means to remove algal cells from water through flocculation and sedimentation, because the environmental impacts of clay flocculation are generally positive. However, clays are not immediately available at some locations that have algal bloom problems. The cost of transportation may also render this method uneconomical. Clays are exotic materials, so there is also an ecological concern about the negative impacts of using large amounts of clays on aquatic ecosystems. Some studies [8, 9] have shown that the main effect of clay is to accelerate the processes of flocculation and sedimentation of algae flocs, rather than its flocculation ability. Therefore, local river sand has been suggested as a substitute as it has a similar function to clay, but is a native ecological material. As an alternative strategy, the use of local river sand could largely reduce costs and the ecological risks to the aquatic environment. However, the physical characteristics of river sand and clay are quite different, and river sand cannot flocculate to remove algal cells by itself. Hence river sand needs to be modified to enhance its flocculation ability.

Cationic polyacrylamide (CPAM) is an organic polymer with good biocompatibility and biodegradability. It can be dissolved in water, but not in the organic solvents, by the arbitrary proportion. Furthermore, CPAM has the characteristics of a high polymer electrolyte, which can be applied in the treatment of waste water rich in organics with negative charge. CPAM is a linear polymer compound that has many active groups available to form hydrogen bonds by affinity with and adsorption to various substances and hence has adsorption-bridging and adsorption-charge-neutralization abilities in water [10,11]. CPAM has been widely used in sewage treatment, because of its lower cost, lower concentration and better flocculation efficiency [12–15].

Algae secrete acidic polysaccharides, which are formed from the organic colloid layer outside the cell during growth and make the cell surface electronegative [16]. As cationic macromolecules flocculate, cationic polyacrylamide undergoes not only charge neutralization but also adsorption bridging. The effects destabilize algal cells rapidly and form big, thick algae flocs, which dislodges the algae. Therefore, CPAM was chosen as the modifier in this study.

Microcystis aeruginosa, a preponderant algae in algal blooms, was the research object in this study. The effectiveness of flocculation and the removal of *Microcystis aeruginosa* using CPAM-modified river sand in different states were investigated. The CPAM, river sand and algal cell concentrations, pH, and particle size of river sand were studied in detail to optimize the conditions for flocculation and removal efficiency. The proposed mechanism for this approach is (1) adsorption-charge neutralization and adsorption bridging from CPAM to flocculant algal cells followed by (2) acceleration of the settling velocity of algal flocs and reduction of flocs floating to the water surface by the sand. On the basis of these results, an approach for treating raw algae water using CPAM-modified river sand was developed to reduce the extent of algal blooms. The results showed that it is feasible to use modified common river sand to irreversibly remove cyanophyta from natural water bodies.

MATERIALS AND METHODS

Materials. CPAM (molecular weight: 1.2×10^7g mol^{-1}) was obtained from GuangFu Chemical Research Institute Co. (Tianjing, China). River sand was obtained from the Yangtze River in Nan'an District, Chongqing, China. The grinded and sieved sand was washed with 30% H_2O_2 until no gas was emitted and then washed several times with deionized water. The wet sand was put in the oven to dry at 60°C for about 12 h.

Algae species. *Microcystis aeruginosa* was obtained from the Freshwater Algae Culture Collection at the Institute of Hydrobiology in Wuhan, China. It was cultured with BG11 medium at a temperature of (24±2)°C, 4000 lx illumination and a light:dark ratio of 12 h:12 h. The algae were pre-cultured 7 d before the experiment; therefore, all algae in the raw water were in the logarithmic phase.

Modification of river sand. CPAM was dissolved in deionized water to obtain a solution with a concentration of 4 mg mL^{-1} CPAM. River sand was added to the solution and then oscillated on a shaking table for 10 min. It was prepared freshly before each set of experiments.

Flocculation tests. In this study, the number of algal cells was used as an index to investigate the removal of algae in the raw water by flocculation. All flocculation experiments were conducted in 250 mL Erlenmeyer flasks at room temperature. pH was adjusted with HCl (0.1 mol L^{-1}) or NaOH (0.1 mol L^{-1}).

To measure the effect of CPAM dosage, raw algae water (pH 8) was treated with different concentrations of CPAM (without river sand).

To determine the effect of sand dosage, 200 mL of different concentrations of CPAM-modified river sand suspensions (CPAM concentration of 30 mg L^{-1}, pH 8) and a control (river sand concentration 0 mg/L) were pipetted into the raw algae water.

To determine the effect of pH, a series of raw algae water with different pH values was configured and CPAM-modified river sand suspensions (CPAM concentration of 30 mg L^{-1}, river sand concentration of 0.5 g L^{-1}, initial number of algal cells of 1.1×10^7) were added.

To investigate the effect of river sand particle size, different particle sizes of river sand were configured (CPAM concentration of 30 mg L^{-1}, river sand concentration of 0.5 g L^{-1}, pH 8, initial number of algal cells of 9.5×10^7).

To study the effects of different algal concentrations, a series of different concentrations of raw algae water were prepared. Different volumes (20, 60, 100, 140 and 200 mL) of algae fluid were added to conical flasks, BG11 medium was added to make the volume up to 200 mL and CPAM-modified river sand was added (CPAM concentration of 30 mg L^{-1}, river sand concentration of 0.5 g L^{-1}, pH 8, initial number of algal cells of 1.0×10^7 cells mL^{-1}). The algal concentration of each experimental group was 1.0×10^6, 3.0×10^6, 5.0×10^6, 7.0×10^6 and 1.0×10^7.

All mixtures were rapidly for shaken for 30 s and then sedimented for 2 h. Samples were collected at 2 cm below the surface of the tested water sample at 5 min, 1 h and 2 h sedimentation to measure the number of algal cells using an electron microscope (XD30-RFL Inverted fluorescence microscope, China). The tests were conducted three times. The obtained green algae flocs were observed under a microscope.

Analytical methods. The number of algal cells in the supernatant was counted using a blood count plate under a microscope and compared with the initial number of algal cells. The removal efficiency of algae was calculated according to Eq. (1):

$$RE\% = \frac{\text{Initial number of algae cells} - \text{Supernatant number of algae cells}}{\text{Initial number of algaecells}} \times 100\% \quad (1)$$

RESULTS AND DISCUSSION

Effect of CPAM concentration on flocculation efficiency. It is essential to investigate the effect of flocculant concentration on the flocculation effect because different flocculants have different optimal concentrations. As Fig. 1 shows, CPAM concentrations ranging from 10 to 60 mg L^{-1} were used to determine the effect of CPAM concentration on the flocculation efficiency.

Figure 1 indicates that CPAM has a very good flocculation effect. The effect of CPAM concentration on the removal efficiency of algae is shown in Figure 2. Algae removal efficiency increased with increasing CPAM dosage at first and then decreased. The peak efficiency appeared at 30 mg L^{-1}. The removal efficiency gradually increased with sedimentation time, but the removal efficiency showed no significant change after 1 h of settlement. A CPAM dosage of 30 mg L^{-1} resulted in a maximum algae efficiency of 99.81% after 1 h of sedimentation.

(a) (b) (c)

FIGURE 1
Flocculation and sedimentation of algal suspension by CPAM.
(a) Raw algae water. (b) During the flocculation process. (c) After sedimentation.

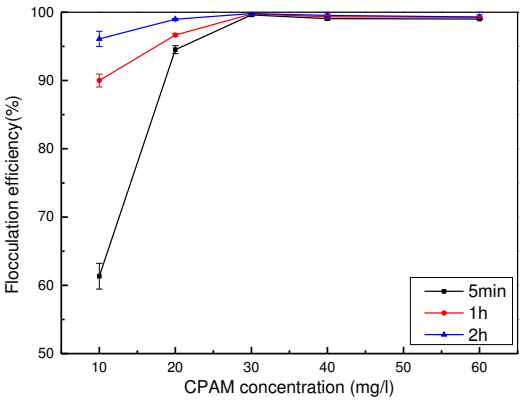

FIGURE 2
Effect of CPAM concentration on the removal efficiency of algae.

The phenomena described above can be explained as follows. CPAM, which is a cationic flocculant, has a high positive charge density. With the addition of CPAM, the negative charge on the algae surface is neutralized. As a result, the algal cells become unstable and flocculate. At low concentrations, CPAM acts as a highly efficient organic flocculant by adsorbing two or more algal cells at the same time and joining them together by bridging. With increasing CPAM concentration, more negative charges are neutralized and the algal cells become more unstable. Therefore, the flocculation becomes more obvious and the distance between algal cells is shortened. As more negatively charged algal cells are neutralized, the electric double layer is compressed, which is more advantageous to the occurrence of bridging [17]. Thus, the optimal removal efficiency is obtained. At extremely high CPAM concentrations, the negatively charged algal cells are absorbed by the excess of CPAM, which is positively charged, resulting in a large number of small and stable flocs that are difficult to precipitate [18,19]. According to the algal removal process, charge neutralization and bridging are the main flocculation mechanisms of CPAM. The optimal concentration of CPAM for the removal of algal is 30 mg L^{-1}.

(a) (b) (c)

FIGURE 3
Influence of river sand on flocculation performance.
(a) Raw algae water. (b) Without river sand. (c) With 0.1 g of river sand added.

Effect of river sand concentration on flocculation efficiency. The effect of river sand concentration on the removal efficiency of algae is shown in Figures 3 and 4, ranging from 0 to 1.0 mg L^{-1}. As can be seen in Figure 3, algae flocs in the group without river sand floated on the water and were dispersed, while algae flocs in the group with river sand were deposited to the bottom in dense flocs. This demonstrates that river sand is able to accelerate the formation and deposition of algae flocs, as well as compact algae flocs and decrease the number of flocs floating on the surface. Figure 4 shows the effect of river sand on the removal efficiency of algae after 1 h and 2 h of sedimentation. In the early stages of the experiment, the algae removal efficiency decreased with increasing river sand dosage (before 1 h of sedimentation). With the extension of precipitation time (after 2 h of sedimentation), the removal efficiency slightly increased. Finally, the removal efficiency remained constant. A concentration 0.5 g L^{-1} of river sand led to the maximum algal removal efficiency of 99.92%. In conclusion, river sand had little effect on the removal rate of algae, but could accelerate the settling velocity of algal flocs and reduce the number of flocs floating on the water surface.

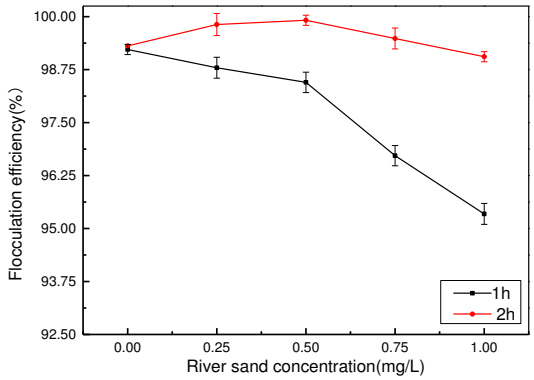

FIGURE 4
Effect of river sand concentration on the removal efficiency of algae.

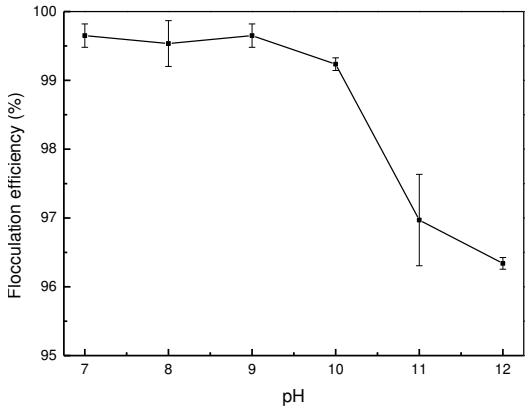

FIGURE 5
Effect of pH value on flocculation efficiency of algae.

Effect of pH value on flocculation efficiency. The surface charge properties of algae can be changed by pH (in the range 7–12); therefore, the pH of algae fluid has a significant effect on the flocculation efficiency of CPAM-modified river sand. As shown in Figure 5, the maximum removal efficiency of algae was 99.65% when the pH value was 7. The removal efficiency decreased slightly above pH 10, but was still at a high level, i.e. 96%. Therefore, CPAM-modified river sand has a wide application scope in terms of pH values.

The flocculation mechanism is essential to the flocculation efficiency [20]. The flocculation performance could be different at different pH values, because pH can change the charge properties of CPAM. When the pH of the algal suspension was between 7 and 10, the algae surface charge was negative charge, so the charges of CPAM and algae were neutralized and colloidal particles were condensed to form adsorption bridges that favored flocculation [21]. At this point, the flocculation mechanism of CPAM may be mainly charge neutralization and adsorption bridging. Under strong alkaline conditions (pH >10), the river sand and algae surface were negatively charged. Flocculation could not neutralize the negative charge [22]. Therefore, the dominant mechanism of CPAM at pH >10 might be bridging, thus, the flocculation efficiency would decrease. Therefore, a pH range of 7–10 is optimal for algae removal.

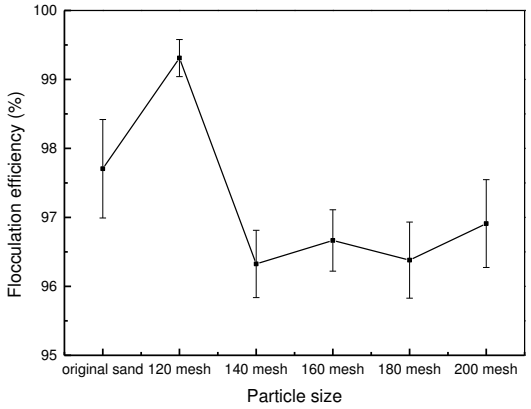

FIGURE 6
Effect of river sand particle size on the removal efficiency of algae.

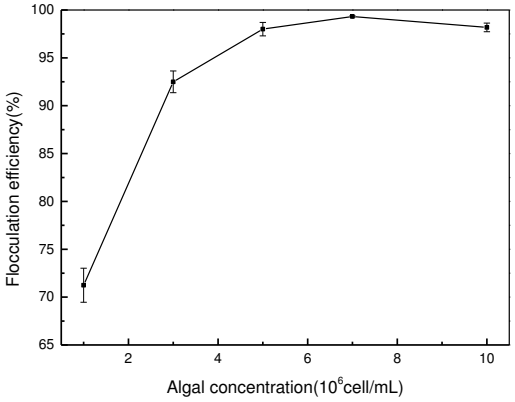

FIGURE 7
Effect of algal concentration on the removal efficiency of algae.

Effect of river sand particle size on flocculation efficiency. The effect of river sand particle size on flocculation is shown in Figure 6. It can be seen that the particle size of river sand had little effect on the flocculation efficiency. The removal efficiency of all sizes reached more than 96%. Influenced by Brownian motion, the smaller particle size of river sand was difficult to settle. Consequently, flocculation efficiency was relatively inferior. Brownian motion of the larger particle size of river sand was faint. Quick subsidence under gravity triggered the good flocculation settling effects. Therefore, the original sand used in the pretreatment was chosen as optimal.

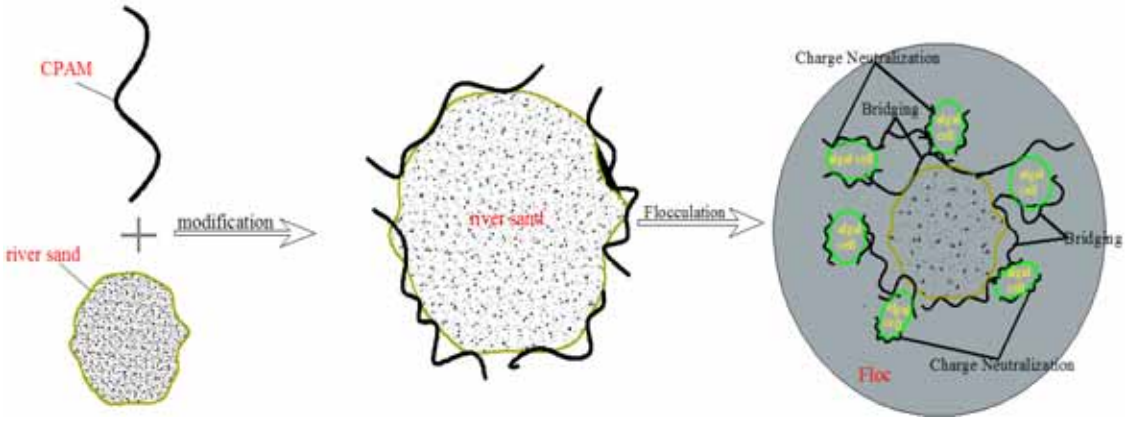

FIGURE 8
Schematic diagram of the proposed CPAM-modified river sand flocculation mechanism.

Effect of algal concentration on flocculation efficiency. Figure 7 shows that the removal efficiency increased quickly with increasing algal concentration and then decreased slightly. An algae concentration of 7.0×10^6 cells mL^{-1} resulted in a maximum algae removal efficiency of 99.32%.

At low algae concentrations, there was an excess of CPAM, according to the CPAM concentration experiment. The flocculation efficiency decreased when CPAM was in excess. With increasing algae concentration, there was less excess CPAM, which contributed to the increase of flocculation efficiency. The CPAM concentration was insufficient at high algae concentrations, which spurred the slight decrease in flocculation efficiency.

Flocculation mechanism of CPAM-modified river sand. According to the experiments, the flocculation efficiency of CPAM-modified river sand is significant. A schematic of the flocculation mechanism of CPAM-modified river sand is presented in Figure 8. After modification with CPAM, the sand surface is covered by CPAM and thus has a positive charge. The negative charge of the algal cell surface is neutralized. When the river sand particles collide with algal cells, it causes the algal cells to become unstable and flocculation. This situation also facilitates bridging between two algal cells or an algal cell and a river sand particle. The collisions of river sand with algal cells are favorable for the formation of algal flocs. Owing to the effect of gravity on sand, the settling velocity of algal flocs is accelerated and the number of flocs floating to the water surface is therefore reduced. In conclusion, this method minimizes potential environmental impacts by using local river sand and a biodegradable polymer, CPAM.

CONCLUSIONS

The use of river sand modified with CPAM achieves high removal efficiency of *Microcystis aeruginosa* cells in a short time. This method minimizes potential environmental impacts by using native ecological materials, such as local river sand, and environmentally friendly materials, such as CPAM. The following conclusions were obtained.

(1) The optimal removal efficiency of algal cells by CPAM-modified river sand is 99.92% with a CPAM concentration of 30 mg L^{-1} and a river sand concentration of 0.5 g L^{-1}. *Microcystis aeruginosa* removal by CPAM-modified river sand results in charge neutralization and adsorption bridging.

(2) The river sand is critical for speeding up sedimentation and reducing the number of flocs floating on the water surface.

(3) The CPAM-modified river sand has a wide application in terms of pH range. The optimal pH range is 7–10. The optimal concentration of algae is 7.0×10^6 cells mL^{-1}.

ACKNOWLEDGEMENTS

This work was supported by the Chongqing Science & Technology Commission Project [grant number cstc2014yykfA20003] and the Innovative Project from Chongqing Technology and Business University [grant number yjscxx2017-066-66].

REFERENCES

[1] Pouria, S., de Andrade, A., Barbosa, J., Cavalcanti, R.L., Barreto, V.T.S., Ward, C.J., Preiser, W., Poon, G.K., Neild, G.H. and Codd, G.A. (1998) Fatal microcystin intoxication in haemodialysis unit in Caruaru, Brazil. Lancet. 352(9121), 21–26.

[2] Wang, J. and Sun, H.-L. (2011) The hazards and treatment of reproductive algae in source water. Southwest Water and Wastewater (China). 32(02), 15–18.

[3] Sample, I. (2000) Clay spray could spell death for algal blooms. New Scientist. 165(2221), 16–16.

[4] Liu, S.-C., Tian, X.-F., Zhao, Y-J., Yi, Z. and Kai, C. (2012) Effect of mixing process on flocculation and removal of algae. China Environmental Science (China). 32(09), 1688-1692.
[5] Lu, G-Y., Song, X-X., Yu, Z.M., Hua, C.X. and Yong, Y.-Q. (2014) Effects of flocculation of *prorocentrum micans* by modified clay on nitrogen and phosphorus. China Environmental Science (China). 34(02), 492-498.
[6] Ahmad, A., Yasin, N., Derek, C. and Lim J. (2011) Optimization of microalgae coagulation process using chitosan. Chemical Engineering Journal. 173, 879-882.
[7] Yang, L., Zhang, G.-K., Tang, D. and Zheng, L. (2015) Removal of *Microcystis aeruginosa* by chitosan-modified red soils. Chinese Journal of Environmental Engineering (China). 09(08), 3745-3750.
[8] Liu, L., Chen, B. and Wang, Z.-h. (2010) Flocculation and removal of algae in algae-bloom water by chitosan-modified clays. Chinese Journal of Environmental Engineering (China). 04(06), 1296-1300.
[9] Pierce, R.-H., Henry, M.-S., Higham, C.-J., Blum, P. and Sengco, M.-R. (2004) Removal of harmful algal cells (Karenia brevis) and toxins from seawater culture by clay flocculation. Harmful Algae. 3(02), 141-148.
[10] Zhang, X.-J., Ji, W., Kang, Z.-J., Sun, D.-Y. and Shan, W. (2008) Characteristics and application of polyacrylamide. Journal of Chemical Industry & Engineering (China). 29(05), 45-49.
[11] Zheng, H., Liao, Y., Zheng, M., Zhu, C. and Ji, F. (2014) Photoinitiated Polymerization of Cationic Acrylamide in Aqueous Solution: Synthesis, Characterization, and Sludge Dewatering Performance. The Scientific World Journal. 11, 465151.
[12] Sun, J., Zhao, X-Z. and Zeng, P. (2013) Adsorption properties of cationic polyacrylamide modified bentonite for indigo blue. Research of Environmental Science (China). 26(09), 1001-1006.
[13] Tang, Z., Chen, J.-T. and Li, Q. (2014) Effect of CPAM Addition on Flocculation and Activity of Anaerobic Sludge. China Biogas (China). 32(05), 3-6.
[14] Mai, Y.-F., Zhu, H., Lin, J.-Y. and Qiu, Z.-H. (2012) Important Technical Progresses of Cationic Polyacrylamide. Polymer Bulletin (China). 08, 105-110.
[15] Guan, Q.-Q., Tang, M., Zheng, H., Teng, H.-K., Tang, X.-M. and Liao, Y. (2016) Investigation of sludge conditioning performance and mechanism by examining the effect of charge density on cationic polyacrylamide microstructure. Desalination & Water Treatment. 57(28), 12988-12997.
[16] Shi, G.-J., Qiao, J.-L., Wang, G.-Q. and Zhang, P. (2009) Research progress on algae removal by flocculants produced from natural materials. Industrial Water & Wastewater. 40(04),1-4.
[17] Chang, Q. (2011) Flocculant and its effectiveness. in: Flocculation of Water Treatment. (The second edition) Chemical Industry Press, Beijing, 113-138.
[18] Zhao, X.-L. and Zhang, Y.-J. (2011) Algae-removing and algicidal efficiencies of polydiallyldimethy lammonium chloride composite coagulants in enhanced coagulation treatment of algae-containing raw water. Chemical Engineering Journal. 173(01), 164-170.
[19] Pan, G., Chen, J. and Anderson, D.-M. (2011) Modified local sands for the mitigation of harmful algal blooms. Harmful Algae. 10(04), 381-387.
[20] Hjorth, M. and Jørgensen, B. (2012) Polymer flocculation mechanism in animal slurry established by charge neutralization. Water Research. 46(04), 1045-1051.
[21] Liu, D., Wang, P., Wei, G., Dong, W. and Hui, F. (2013) Removal of algal blooms from freshwater by the coagulation-magnetic separation method. Environmental Science and Pollution Research. 20(01), 60-65.
[22] Yue, Q.-Y., Gao, B.-Y., Wang, Y., Zhang, H. and Sun, X. (2008) Synthesis of polyamine flocculants and their potential use in treating dye wastewater. Journal of Hazardous Materials. 152(01), 221-227.

Received: **30.11.2016**
Accepted: **27.11.2017**

CORRESPONDING AUTHOR

Chenghua Zhong
College of Environment and Resources,
Chongqing Technology and Business University,
Chongqing 400067 - China

e-mail: zhongchenghua2007@163.com

© by PSP Volume 27 – No. 2/2018 pages 681-689 Fresenius Environmental Bulletin

PREDICTION OF AFLATOXIN CONTAMINATION ON DRIED FIG (*FICUS CARICA*) SAMPLES BY SPECTRAL IMAGE ANALYSIS IN COMPARISON WITH LABORATORY RESULTS

Omer Baris Ozluoymak*, Emin Guzel

Cukurova University, Faculty of Agriculture, Department of Agricultural Machinery and Technology Engineering, Adana, Turkey

ABSTRACT

Aflatoxins are toxic metabolites produced by some fungus (*Aspergillus flavus* and *Aspergillus parasiticus*) that can grow on a wide variety of foodstuffs. The most important factors that play a role in the growth of fungi in foodstuffs and in the formation of aflatoxin are relative to the humidity of the air and the storage temperature. It is also pointed out that aflatoxin, which is passed to humans through food, causes mostly liver cancer, increases the effect of hepatitis (B) and (C) viruses, and breaks the immune system. Traditionally, dried figs have been examined for the evidence of bright greenish-yellow fluorescence (BGYF), which can indicate the possible presence of *Aspergillus flavus*, when illuminated with ultra-violet (UV) light. The BGYF test is typically the first step that leads to a chemical analysis for possible aflatoxin contamination. Naturally, the chemical methods that detect aflatoxins are quite accurate but expensive and destructive. Nowadays, hyperspectral and multispectral imaging are becoming increasingly important for rapid and nondestructive testing for the presence of such contaminants. In this study, a compact machine vision system is being proposed for the detection of aflatoxin contaminated dried figs. An image-processing method is defined for a pixel-based prediction of an aflatoxin contaminated surface area on selected dried figs that is scanned by a Charge Coupled Device (CCD) color camera and under UV lighting in this system. Additionally, naturally contaminated fig test samples are sent to an authorized laboratory in order to determine the amount of aflatoxin B_1 and the total aflatoxins for comparing the actual aflatoxin amounts of dried figs and the pixel values of contaminated samples. The results of this study have shown that there is not a linear correlation between total surface area of aflatoxin contamination on dried figs in pixels and the actual aflatoxin amounts analyzed under laboratory conditions.

KEYWORDS:
Aflatoxin, Digital image processing, Dried fig, UV, Laboratory test results

INTRODUCTION

Aflatoxins are toxic compounds produced by many species of *Aspergillus* molds, especially by *Aspergillus flavus* and *Aspergillus parasiticus*. The term aflatoxin comes from *Aspergillus flavus toxin* [1, 8]. Aflatoxins B_1, B_2, G_1, and G_2 pose a great risk by contaminating a wide range of agricultural products and foodstuffs [8, 17, 21]. These fungi grow whenever the moisture, temperature and relative humidity conditions are favourable for them [13].

Aflatoxin contaminated food and feed grains can potentially cause fatal animal and human diseases. As aflatoxin B_1 has demonstrated carcinogenicity to humans, it has been classified as a class 1 toxin by the International Agency for Research on Cancer (IARC) [2, 3, 8, 13, 14, 17]. Aflatoxin exposure through food in Asia and Africa is linked to liver cancer [23].

Many countries have taken strict regulations and measures to control the level of aflatoxin contamination. The generally accepted level of aflatoxin in food is 20 μg kg^{-1} in Turkey and United States of America. On the other hand, the maximum level of total aflatoxin is determined as 10 μg kg^{-1} and the maximum level of aflatoxin B_1 is determined as 5 μg kg^{-1} in European countries [1, 14, 15].

Aflatoxigenic fungi can grow during the growing, ripening and drying periods on fig fruits, but they thrive especially through the different ripening phases. Toxigenic fungi can be both in the inner cavity and on the surface of the dried figs. Ripening phase of fruits on the tree is the critical period for aflatoxin formation of dried figs [6, 11]. Instantaneous rains, high humidity, and mild temperature may also further the fungal activity. In addition to that, storage is also another phase for mycotoxin production [11].

[1] and [7] stated that although immunological and chemical methods can provide exact quantification of toxins, they require skill and equipment, as well as they are time consuming and expensive.

The development of screening methods for the rapid identification of aflatoxin contaminated crops is very important for the agro-food industry [19]. In recent years, there has been an increase in demand

for specific, accurate, simple, and quick methods for the determination of aflatoxins [21]. [9] stated that fungal growth can cause some chemical changes in forms or colors of nuts and grains. The chemical changes caused by fungal growth in dried figs are similar to those in grains or nuts.

If a food exhibits a BGYF, this indicates that there are aflatoxigenic moulds, and this fluorescence under long-wave ultraviolet (LW-UV) light (365 nm) is probably an indicator for kojic acid, a metabolite of *A. flavus* and *A. parasiticus* or possibly aflatoxin itself [15, 19]. Initially, [20] reported that there is a relationship between BGYF, aflatoxin and *A. flavus* in cottonseed.

For evaluating food and agricultural products, spectral imaging techniques have been developed in recent years [25]. A new image processing based method using a neural network was mentioned for separating aflatoxin contaminated pistachio nuts under the UV light source [18]. [27] controlled the UV absorption with the help of UV photography in which non-aflatoxin-producing molds identified as white colonies, whereas aflatoxin-producing molds were classified as black or gray colonies. Imaging algorithms were developed to identify cashew and pistachio nut samples with fluorescent stains that can be seen with the help of BGYF. Nut samples were classified into two groups as fluorescent stains and non-fluorescent stains according to image analysis results. Non-fluorescent and fluorescent nut samples were analyzed for the contamination of aflatoxin. There was a high correlation between the camera classification and the laboratory analysis results [19]. For the UV-fluorescence imaging application, 365 nm UV band was identified for determination of aflatoxin contamination [26].

This research aimed at determining the correlation between contaminated area predictions through image analysis and laboratory test results for the concentration of the aflatoxin on dried figs.

MATERIALS AND METHODS

Materials. (1) Dried fig samples. Aflatoxin contaminated dried fig samples of the Sarilop cultivar were obtained from a commercial processing facility from the 2014 harvest (İzmir). These contaminated figs had been identified as inappropriate for consuming because bright greenish-yellow fluorescence had been detected when screened under UV light. Thirty individual contaminated figs were randomly selected among a 10 kg sample of dried figs.

(2) Multispectral image acquisition system. An aflatoxin contamination imaging system was designed and built (Figure 1) in a darkened laboratory at the Agricultural Machinery and Technologies Engineering Department of Çukurova University. This contamination does not appear without the UV light source. A small scale imaging system with an empty chamber was used for placing the optical unit. Aflatoxin contaminated dried fig samples were manually placed in this chamber.

The imaging system equipment and performance measures are given in Table 1.

Four 36W UV black-light lamps were used for lightening. An aluminum dome reflector was used to provide the uniform reflectance in the detection area. The background was constructed by using a black rubber material. As a result of the pre-trials, it was found that black color is more effective than other colors when determining aflatoxin contaminated areas with the camera. Fluorescence could be measured perfectly on a black background [22].

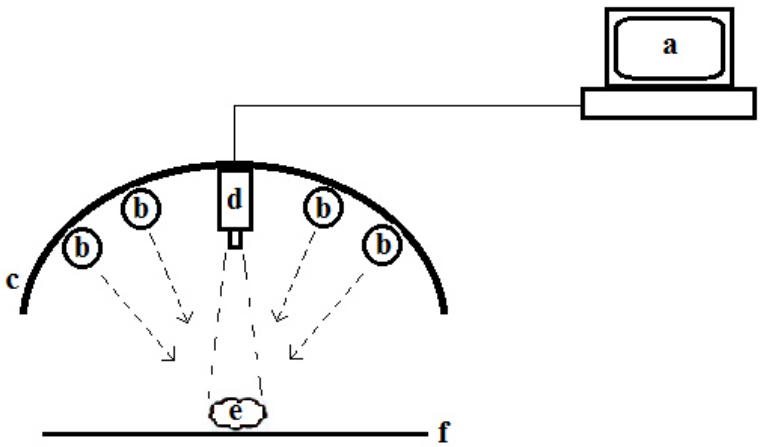

FIGURE 1
Schematic drawing of the imaging system. (a) PC; (b) UV light sources; (c) dome reflector; (d) Firewire (IEEE 1394a) CCD color camera; (e) aflatoxin contaminated dried fig sample; (f) black background

TABLE 1
Equipment and performance measures of the imaging system

Camera	Sensor	Lens for the focal length	Maximum resolution	Working distance	Field of view area	Spatial resolution
AVT Guppy F-033 C Firewire color camera	SONY IT CCD ICX424AL/AQ 1/3" CCD	FUJINON 9 mm	656 (H) x 494 (V) at the full frames	160 mm	91.1 mm x 68.6 mm	7.2 pixels mm^{-1}

TABLE 2
Classification of the prediction values obtained from the imaging system

Class	Ultra-high (UH)	High (H)	Medium (M)	Low (L)
Samples with predicted aflatoxin surface area (pixels)	60000-85000	40000-60000	20000-40000	0-20000

Methods. This study proposes a technique that automatically detects dried figs with aflatoxin contamination. In this method, fluorescence emission spectra of dried figs are reflected under ultraviolet light (365 nm) in a darkened laboratory. Using ultraviolet lights and an imaging system, the system was able to determine the existence of aflatoxin contamination and calculated contaminated surface area on dried figs by using a LabVIEW interface. These same samples were then sent to an accredited independent food control laboratory (TÜRKAK (Turkish Accreditation Agency) Accreditation Number: AB-0328-T) to be analyzed for aflatoxin B_1 and total aflatoxins. The obtained and processed images of contaminated dried figs and analysis test results were compared to each other and according to these results, aflatoxin contamination was also confirmed by the accredited laboratory.

The experimental study was carried out for all aflatoxin contaminated dried figs at the same time. Special gloves were worn to handle contaminated dried figs for protecting from the harmful effects of aflatoxin and UV glasses were worn to avoid the harmful effects of UV lightening. Then, images were acquired by the imaging system described above. Images of contaminated figs were captured from both sides by the camera and analyzed by LabVIEW.

(1) Preparing dried fig samples. Dried figs (*Ficus carica*) were provided from an export company, which is located in İzmir, in 2014. The prediction values of the samples were classified into four classes as shown in Table 2.

To promote the accuracy of training samples, each of the dried fig samples was imaged bilaterally 3 separate times in the experiments. On the imaging system, 30 contaminated dried fig samples were tested. That gave us a total of 180 (= 30 dried figs x 2 sides x 3 iterations) dried fig images to be explored.

The samples were maintained at a refrigerated temperature (4 ºC) and left for 1 hour in the room in order to allow them to reach the room temperature until beginning the image processing analyses.

(2) Fluorescent imaging techniques. Many materials exhibit intrinsic fluorescence which can be triggered by UV or laser radiation. The resulting fluorescence emission has a unique spectral signature for each material [12]. Photoluminescence is divided into two categories: fluorescence and phosphorescence. Short-wavelength light, traditionally in the UV, is required for excitation to activate a luminescence response [24]. Figs are usually affected by AF-producing moulds, which produce kojic acid together with aflatoxin. Kojic acid is a fluorescent compound that exhibits BGYF under the UV light [16].

Using this fluorescence property, the fig samples were monitored under the 365 nm UV lightening. The fluorescence coming from the contaminated dried fig samples was captured and examined with the image processing software. So, aflatoxin contaminated dried figs radiated a longer wavelength by absorbing the incoming light. Aflatoxin contamination was changed from being invisible to visible. Contaminated dried figs radiated BGYF when illuminated with a UV light.

(3) Image processing method. Image thresholding method was utilized in this study. The purpose of the thresholding process is to separate the objects in the image from the image background.

[10] stated that it is possible to evaluate the image in two dominant groups, namely the object pixels and the background pixels. In this case, the easiest way to understand the difference between an object and a background is to compare the pixel values in the image with a selected threshold, *T*, value. Object point is determined if $f(x,y) > T$ for any (x,y)

point in the image; otherwise, this point is determined as background point.

The segmented image, *g(x,y)*, is given in Equation 1.

$$g(x,y) = \begin{cases} 1 & if\ f(x,y) > T \\ 0 & if\ f(x,y) \leq T \end{cases} \quad (1)$$

Where; *g(x,y),* is the processed image; *f(x,y),* is the pixel value of the image and *T,* is the selected threshold value. For color images, threshold values must be specified for red, green and blue color components separately.

The light reflected from the dried fig samples, which absorbed some of the incident light and reflected sufficient light for the camera, was captured by the help of a vision acquisition software integrated with the LabVIEW. Acquired images were analyzed for each contaminated dried fig and they were converted to binary by using thresholding method.

(4) Statistical analysis method. In this study, Spearman's Correlation Coefficient was used to determine the correlation between variables. The result showed that there wasn't a normal distribution and a linear correlation between the variables. Correlation coefficient values take a value between -1 and +1, and the correlations between them become stronger as they get nearer to 1.

(5) Reference test. The dried fruit samples were prepared and assayed by the aforementioned laboratory located in Mersin, Turkey. The aim of this process was to verify the aflatoxin contamination of selected dried figs. Test results of aflatoxin B_1 and total aflatoxins were obtained from this food control laboratory.

RESULTS AND DISCUSSION

Calculation of contaminated areas. Applying image processing method, it was possible to recognize the fluorescent areas on contaminated dried figs. Aflatoxin contamination level is determined according to the number of aflatoxin contaminated particles and the contaminated area which is calculated as pixels. Determination of aflatoxin contaminated surface area by using thresholding method is shown in Figure 2. Otherwise, the sample in the system is determined as uncontaminated.

Determination of efficiency results. After the establishment of the imaging system, its operating efficiency was tested with a sufficient number of recurrences. For this purpose, aflatoxin contaminated areas of figs were grouped in accordance with their areal sizes under the UV light source before capturing images. In this grouping, 4 subgroups were formed between those with extremely small-sized contaminated areas and others with fairly large-sized contaminated areas amongst dried figs with aflatoxin. In this way, determination efficiency of the imaging system was tested according to the size of aflatoxin contaminated surface areas.

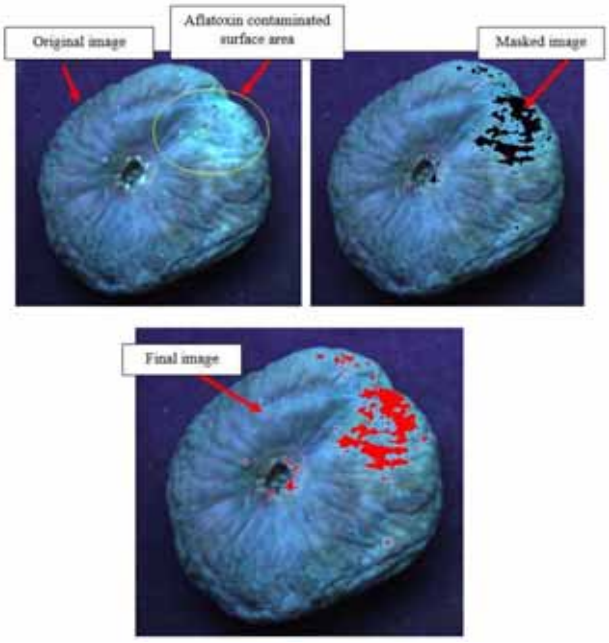

FIGURE 2
Determination of aflatoxin contaminated surface area by using thresholding method

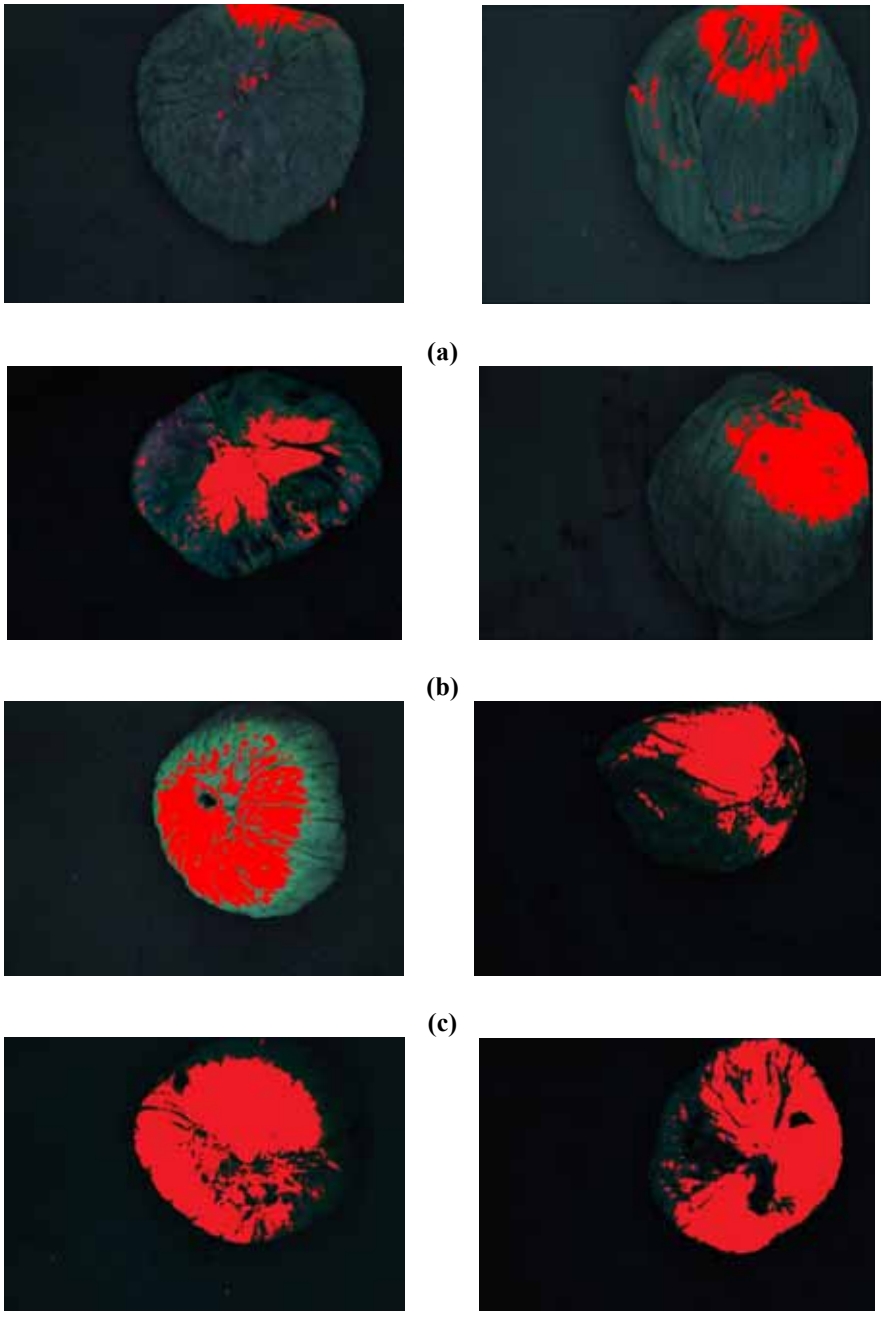

(a)

(b)

(c)

(d)

FIGURE 3
Aflatoxin contaminated dried fig sample classes with applied digital image processing technique: (a) Class L, (b) Class M, (c) Class H and (d) Class UH

Thirty contaminated fig samples were selected from 10 kg sample of aflatoxin contaminated dried figs and they were sent to an authorized food control laboratory to be analyzed for aflatoxin B_1 and total aflatoxins. Image data were captured regarding determination efficiency of the imaging system by investigating the correlation between aflatoxin contamination on dried figs and area information obtained from the image-processing algorithm. As shown in Figure 3, aflatoxin contaminated dried figs are put in order from low to high levels of contamination according to the image processing results.

The graphical representations of correlations are given in Figure 4 and Figure 5, respectively. According to the results, a correlation with the images derived from the contaminated dried figs could be established with aflatoxin amounts per group.

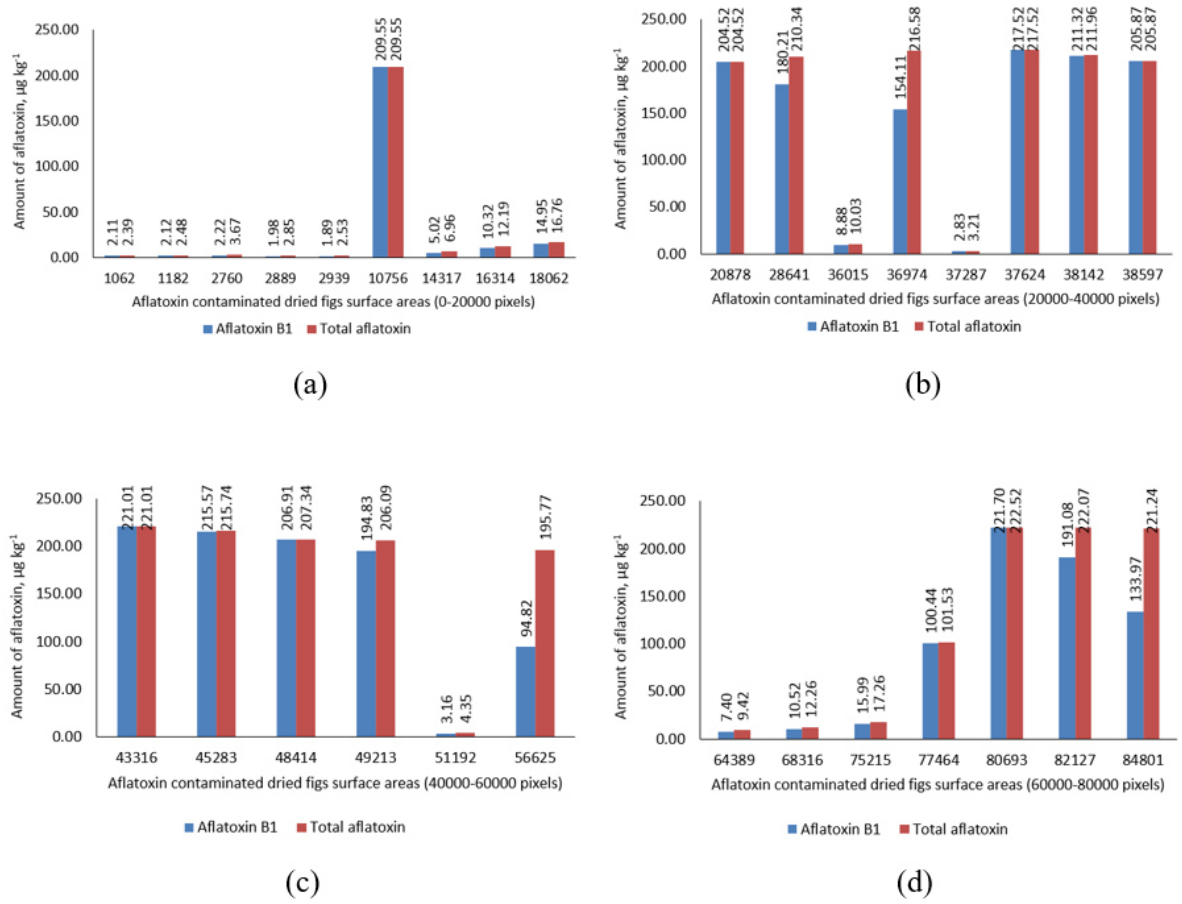

FIGURE 4
Correlation between aflatoxin contaminated dried fig surface areas and Aflatoxin B_1-Total Aflatoxin amounts for per group: (a) Class L, (b) Class M, (c) Class H and (d) Class UH

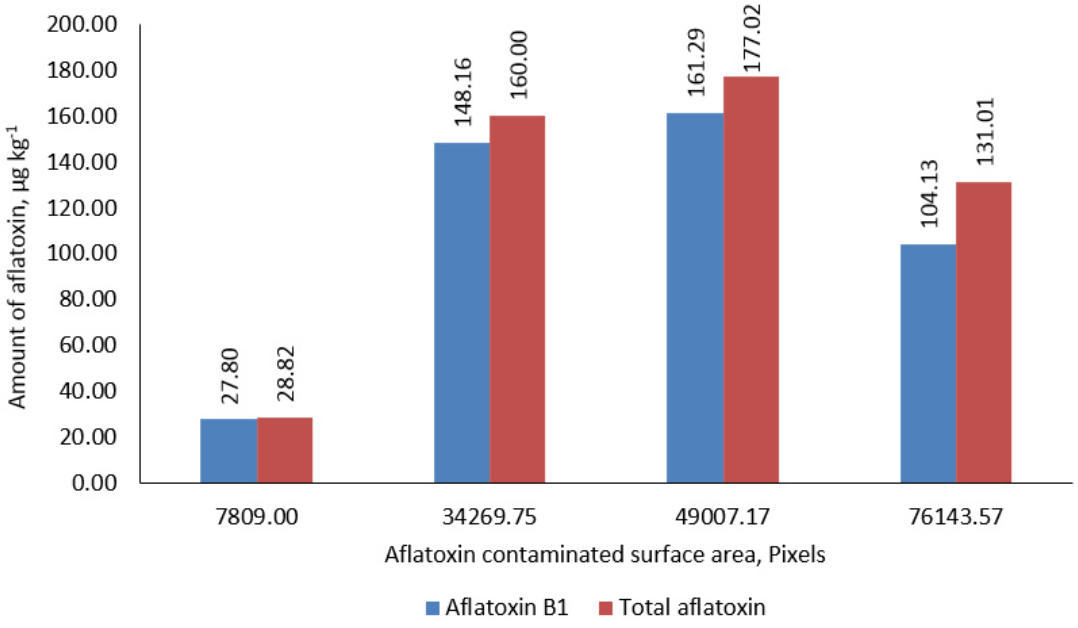

FIGURE 5
Correlation between average aflatoxin contaminated dried fig surface areas and the average aflatoxin amounts

TABLE 3
Tests of normality

	Kolmogorov-Smirnov[a]			Shapiro-Wilk		
	Statistic	df	Significance	Statistic	df	Significance
Pixels	0.088	30	0.200*	0.940	30	0.093
Aflatoxins B_1	0.282	30	0	0.768	30	0
Aflatoxins total	0.292	30	0	0.709	30	0

* This is a lower bound of the true significance.
a Lilliefors Significance Correction

TABLE 4
Spearman's correlation coefficients between aflatoxin B_1, total aflatoxin and pixel data

			Aflatoxins B_1	Aflatoxins total	Pixels
Spearman's rho	Aflatoxins B_1	Correlation Coefficient	1.000		
		Sig. (2-tailed)	.		
		N	30		
	Aflatoxins total	Correlation Coefficient	0.913(**)	1.000	
		Sig. (2-tailed)	0.000	.	
		N	30	30	
	Pixels	Correlation Coefficient	0.460(*)	0.576(**)	1.000
		Sig. (2-tailed)	0.011	0.001	.
		N	30	30	30

** Correlation is significant at the 0.01 level (2-tailed).
* Correlation is significant at the 0.05 level (2-tailed).

Results of statistical analysis. First of all, tests of normality were made for pixel, aflatoxin B_1 and total aflatoxin values. Conformity of data distribution pattern to the normal distribution was tested with Kolmogorov-Smirnov and Shapiro-Wilk tests. The hypotheses related to the data are as follows:

H_0: The data are normally distributed with 95% confidence and H_1: The data are not normally distributed with 95% confidence. The H_0 hypothesis is accepted when the p-value (sig. value) > 0.05 and it is concluded to the result that data has a normal distribution. The H_0 hypothesis is rejected when the p-value (sig. value) < 0.05 and it is concluded to the result that data does not have a normal distribution. Pixel data has a normal distribution, whereas aflatoxin B_1 and total aflatoxin values do not have a normal distribution as shown in Table 3.

As shown in Table 4, there is a strong positive correlation at the level of $r_S = 0.913$ between aflatoxin B_1 data and total aflatoxin data. On the other hand, there is a weak correlation at the level of $r_S = 0.460$ between pixel data and aflatoxin B_1 data, and there is also a weak correlation at the level of $r_S = 0.576$ between pixel data and total aflatoxin data. These correlation results showed that aflatoxin contamination cannot be only on the outer surface of dried fig, but also can be seen inside the fruit.

Aflatoxin contamination may not only occur on the external surface of dried figs, but also inner cavity can be contaminated by fungi. There are many similarities with the literature [5, 4, 9, 11].

CONCLUSIONS

Aflatoxin amount measured from the surfaces of tested dried figs were given as pixels. Then the samples were sent to an accredited laboratory and analyzed for aflatoxin contamination. According to these results, aflatoxin that was detected by imaging system was also confirmed by the accredited laboratory. Although the contaminated surface area data in pixels was explanatory about the aflatoxin amount to some extent, the results showed that there was not a linear correlation between the aflatoxin contaminated areas on dried figs and aflatoxin amounts analyzed under laboratory conditions. We believe that the reason behind this result is the laboratory analysis inspected both the inner cavity and outer skin of the dried fig samples, while this system evaluated only for aflatoxin contaminated area on the fig surface. In other words, aflatoxin could not be identified (unidentifiable) for inner cavity of the dried fig.

According to the results; surface fungus concentration is a deficit indicator for detecting aflatoxin contamination. Although these results are significantly less accurate when compared to chemical analysis, the methodology recommended here provides an easy, rapid and non-destructive operation. For future work, detection performance can be enhanced by using new optical systems, different spectral analysis methods, and other technologies to define internal aflatoxin contamination in dried figs. New prototypes can also be improved by using

novel optical systems in order to be further used under real conditions. As such, a linear correlation can then be reached between aflatoxin contaminated area images (inner and outer) and aflatoxin amounts analyzed under laboratory conditions.

REFERENCES

[1] Ataş, M., Yardimci, Y., Temizel, A. (2012) A New Approach to Aflatoxin Detection in Chili Pepper by Machine Vision. Computers and Electronics in Agriculture. 87, 129-141.

[2] Battilani, P., Leggieri, M.C., Rossi, V., Giorni, P. (2013) Afla-Maize, a Mechanistic Model for Aspergillus Flavus Infection and Aflatoxin B_1 Contamination in Maize. Computers and Electronics in Agriculture. 94, 38-46.

[3] Ceker, S., Agar, G., Alpsoy, L., Nardemir, G., Kizil, H.E. (2013) Protective Role of Essential Oils of *Calamintha Nepeta* L. on Oxidative and Genotoxic Damage Caused by Aflatoxin B_1 in Vitro. Fresen. Environ. Bull. 22, 3265-3270.

[4] Codex Alimentarius Commission (2008) Code of Practice for the Prevention and Reduction of Aflatoxin Contamination in Dried Figs. Doc. Ref. CAC/RCP 65-2008. (Date of access: 03.01.2017)

[5] Doster, M.A., Michailides, T.J. (2007) Fungal Decay of First-Crop and Main-Crop Figs. The American Phytopathological Society. 91(12), 1657-1662.

[6] Embaby, E.M., Hagagg, L.F., Abdel-Galil, M.M. (2012) Decay of Some Fresh and Dry Fruit Quality Contaminated by Some Mold Fungi. Journal of Applied Sciences Research. 8(6), 3083-3091.

[7] Firrao, G., Torelli, E., Gobbi, E., Raranciuc, S., Bianchi, G., Locci, R. (2010) Prediction of Milled Maize Fumonisin Contamination by Multispectral Image Analysis. Journal of Cereal Science. 52, 327-330.

[8] Ghanem, I., Orfi, M., Shamma, M. (2008) Effect of Gamma Radiation on the Inactivation of Aflatoxin B_1 in Food and Feed Crops. Brazilian Journal of Microbiology. 39, 787-791.

[9] Gloria, E.M. (2011) Aflatoxin Contamination Distribution among Grains and Nuts. In: Aflatoxins-Detection, Measurement and Control. Torres-Pacheco, I. (Ed.) InTech.

[10] Gonzalez, R.C., Woods, R.E. (2008) Digital Image Processing (Third Edition). Pearson International Edition, Prentice Hall.

[11] Heperkan, D., Moretti, A., Dikmen, C.D., Logrieco, A.F. (2012) Toxigenic Fungi and Mycotoxin Associated with Figs in the Mediterranean Area. Phytopathologia Mediterranea. 51(1), 119-130.

[12] Hruska, Z., Yao, H., Kincaid, R., Brown, R., Cleveland, T., Bhatnagar, D. (2014) Fluorescence Excitation-Emission Features of Aflatoxin and Related Secondary Metabolites and Their Application for Rapid Detection of Mycotoxins. Food and Bioprocess Technology. 7, 1195-1201.

[13] Iamanaka, B.T., Menezes, H.C., Vicente, E., Leite, R.S.F., Taniwaki, M.H. (2007) Aflatoxigenic Fungi and Aflatoxins Occurrence in Sultanas and Dried Figs Commercialized in Brazil. Food Control. 18, 454-457.

[14] Jin, J., Tang, L., Hruska, Z., Yao, H. (2009) Classification of Toxigenic and Atoxigenic Strains of Aspergillus Flavus with Hyperspectral Imaging. Computers and Electronics in Agriculture. 69, 158-164.

[15] Kalkan, H., Beriat, P., Yardimci, Y., Pearson, T.C. (2011) Detection of Contaminated Hazelnuts and Ground Red Chili Pepper Flakes by Multispectral Imaging. Computers and Electronics in Agriculture. 77, 28-34.

[16] Kalkan, H., Güneş, A., Durmuş, E., Kuşçu, A. (2014) Non-Invasive Detection of Aflatoxin-Contaminated Figs Using Fluorescence and Multispectral Imaging. Food Additives & Contaminants: Part A. 31(8), 1414-1421.

[17] Kamber, U., Gulbaz, G. (2017) The Detoxification Effect of Various Ozone Treatments on Aflatoxin B_1 in Black Pepper (Piper Nigrum L.) and Changes in the Sensory and Microbiological Characteristics of the Black Pepper. Fresen. Environ. Bull. 26, 3314-3324.

[18] Karami, M.A., Mirabolfathy, M. (2006) Neural Network to Separate Aflatoxin Contaminated Pistachio Nuts. Proceedings IVth IS Pistachios and Almonds, Acta Horticulturae. 726, 605-610.

[19] Lunadei, L., Ruiz-Garcia, L., Bodria, L., Guidetti, R. (2013) Image-Based Screening for the Identification of Bright Greenish Yellow Fluorescence on Pistachio Nuts and Cashews. Food Bioprocess Technology. 6, 1261-1268.

[20] Marsh, P.B., Simpson, M.E., Ferretti, R.J., Merola, G.V., Donoso, J., Craig, G.O., Trucksess, M.W., Work, P.S. (1969) Mechanism of Formation of a Fluorescence in Cotton Fiber Associated with Aflatoxin in the Seeds at Harvest. Journal of Agricultural and Food Chemistry. 17, 468-472.

[21] Nilüfer, D., Boyacıoğlu, D. (2002) Comparative Study of Three Different Methods for the Determination of Aflatoxins in Tahini. Journal of Agricultural and Food Chemistry. 50, 3375-3379.

[22] Özlüoymak, Ö.B. (2012) A Research on Separation System Design of Aflatoxin Contaminated Dried Fig. PhD Thesis, Çukurova University, Institute of Natural and Applied Sciences, Department of Agricultural Machinery, Adana, Turkey.

[23] Perz, J.F., Armstrong, G.L., Farrington, L.A., Hutin, Y.J.F., Bell, B.P. (2006) The Contributions of Hepatitis B Virus and Hepatitis C Virus Infections to Cirrhosis and Primary Liver Cancer Worldwide. Journal of Hepatology. 45, 529-538.
[24] Ruiz-Altisent, M., Ruiz-Garcia, L., Moreda, G.P., Lu, R., Hernandez-Sanchez, N., Correa, E.C., Diezma, B., Nicolai, B., Garcia-Ramos, J. (2010) Sensors for Product Characterization and Quality of Specialty Crops-A Review. Computers and Electronics in Agriculture. 74, 176-194.
[25] Qin, J., Burks, T.F., Zhao, X., Niphadkar, N., Ritenour, M.A. (2012) Development of a Two-Band Spectral Imaging System for Real-Time Citrus Canker Detection. Journal of Food Engineering. 108, 87-93.
[26] Steiner, W.E., Rieker, R.H., Battaglia, R. (1988) Aflatoxin Contamination in Dried Figs: Distribution and Association with Fluorescence. Journal of Agricultural and Food Chemistry. 36(1), 88-91.
[27] Yabe, K., Ando, Y., Ito, M., Terakado, N. (1987) Simple Method for Screening Aflatoxin-Producing Molds by UV Photography. Applied and Environmental Microbiology. 53(2), 230-234.

Received: **01.12.2016**
Accepted: **27.11.2017**

CORRESPONDING AUTHOR

Omer Baris Ozluoymak
Çukurova University
Faculty of Agriculture
Department of Agricultural Machinery
and Technology Engineering
01330 Adana – Turkey

e-mail: ozluoymak@cu.edu.tr

© by PSP Volume 25 – No. 4/2016, pages 690-702 Fresenius Environmental Bulletin

ULTRASOUND-ASSISTED MODIFICATION OF FLAX WASTES TO REMOVE METHYL VIOLET FROM AQUEOUS SOLUTION

Dan Xuanxuan, Li Xiaomin*

Key Laboratory at Universities of Education Department of Xinjiang Uygur Autonomous Region, College of Chemical & Environmental Science, Yili Normal University, Xinjiang 835000, China.

ABSTRACT

Preparing an adsorbent to remove methyl violet (MV) from aqueous solution, flax wastes were used as raw material to synthesize new adsorbent via which modified with sodium hydroxide by ultrasound assisted technology. The optimum conditions were studied on the impact of factors such as sodium hydroxide concentration, modified time, modified temperature, modified power, adsorbent dosage, initial dye concentration, adsorption time and temperature. This shown that the adsorption properties of modified flax wastes (MFW) was better than the unmodified flax wastes (FW). The best adsorption capacity and removal rates were 24.80 mg/g and 99.22 %, respectively, which were improved 0.6 mg/g and 2.42%, respectively. Maximum adsorption capacity and removal rate under optimum condition of variables (modified time 60 min and temperature 50 ℃, adsorption time 10 min, adsorbent dosage 0.04 g) by the orthogonal test were 23.83 mg/g and 98.03 %, respectively. Meanwhile, the equilibrium dates were found to fit the Langmuir model better than the Freundlich model (R^2=0.998). Kinetic date reveled that the adsorption process followed the pseudo-second-order equation. The thermodynamic parameters show that the adsorption process belong to spontaneous and endothermic adsorption.

KEYWORDS:
Ultrasound, Methyl violet, Adsorption, Flax wastes, Orthogonal test

INTRODUCTION

Because of the visitations effect in liquid medium that ultrasound could improve a widely variety of chemical and physical processes. Acoustic visitations which caused drastic increasing in the pressure and temperature [1] due to the growth and explosive collapse of microscopic bubbles. The use of ultrasound energy was well documented in many literature in textile coloring, in which it was reported the use of ultrasound could result in increased color yield, lower dyeing temperatures, reduced dyeing time and consumption of dyeing auxiliaries. In the previous studies, researchers have focused their interests on the dyeing of various dyes at different textile substrates with ultrasound, including reactive dyes [2, 3], acid dyes [4], disperse dyes [5], natural dyes [6] and basic dyes [7]. However, the effect of ultrasound on the modifying of flax wastes for removing to MV had not been received attention.

Since a variety of synthetic dyes were used extensively to color their products in the manufacture, large amount of effluents were discharged from the manufactures, which would result in a major environmental pollution problem because many dyes were toxic to some organisms [8]. In up-to-date data, more than 100,000 commercial dyes were known with an annual production of over 7 × 105 tones/ year [9]. The total dye consumption in the textile industry worldwide was more than 10,000 tones/year and approximately 100 tones/year of dyes was discharged into water streams [10].

At present, a number of techniques [11,12] had been employed to remove the dyes from the industrial wastewater, which included coagulation, filtration, ion exchange, biological treatment, advanced oxidation processes, electrolysis, activated sludge, adsorption, and solvent extraction. Among these techniques, adsorption was regarded as a simple, impact and economical method for in the wastewater [9].

Emissions of sewage about 39 billion t/ annual, and which included the 51 % of industrial waste water, and they accounted 35% of industrial waste in dye wastewater [13]. These shown an industrial dye wastewater which was the main sources of wastewater. Due to the poor characteristics of dye wastewater were toxic, high density and color depth, the dye wastewater had been became a major problem for environment treatment.

Adsorption was one of the most effective method of advanced wastewater treatment which industries employed to reduce hazardous inorganic/organic pollutants present in the effluent [14]. Different physical or chemical treatments were applied to the raw biomass adsorbents for improving their adsorption capacity which were also re-

ported by the investigators [15]. Biomass adsorbents received high attention. Many research groups have prepared more efficient and cheaper activate carbon for the removals of organic compounds from the wastewater, such as activate carbon [16], wheat straw [17], pine cones [18], palm kernel [19].

The major component (70%) of flax yarn waste was cellulose, which had been introduced as a basic skeleton of super-absorbent composite in previous studies [20]. So in a continuation of the research in the field of organic – inorganic super-absorbent composite [21], our attention was directed towards providing a novel method for the management of flax yarn waste.

Xinjiang Province was a big country to product the textile flax, and the planting area of the fiber flax had more than 1 × 105 km2. Flax was stripped the surfer and become the best fiber scrap. The millions of tons of annual were used as fuel or livestock with large part, but the utilization was low, which was resulting in a great waste of natural resources were waste, and also were harmful for the environment that risk an increase of security for human [22].

In this work, a good adsorbent was prepared by ultrasonic methods, and then its operating properties such as the concentration of sodium, time, temperature and power were analyzed. The main purpose of this work was to studied the adsorption capacity of the adsorbent from flax wastes. A systematic investigation of the effect of adsorbent dose, initial dye concentration, time and temperature on dye uptake in the single component system was explored in this work. Further, the process variables for dye adsorption by modified flax wastes (MFW) were optimized using the orthogonal test.

MATERIALS AND METHODS

Introduction the dye of MV and experimental materials. MV, used as a cat-ionic dye, was purchased and a pure substance. MV could be used as dyes, acid-base indicator disinfectants, and commonly known as gentian violet or crystal violet which were a series of similar organic compounds. MV was a basic dye which atmosphere mostly were organic bases, and inorganic acids to form salts (chloride). These dyes ionization was the positively charged ions of dye, which may be combined with an acid into a salt.

Main instruments: BAO-150A precision blast oven, SHZ-Ⅲ circulating water pump, FA2104 electronic balance, XYJ-801 electric centrifuge, YB-500A grinder, SHA-A2 multinational thermostatic oscillator, KQ -250DB CNC ultrasonic cleaner, DF-101S-type thermal heating magnetic stirrer, TU-1901 double beam UV/visible spectrophotometer. Major reagents: NaOH, MV, HCl and C_2H_5OH.

Determination of a standard curve for MV. Distilled water as a reference, MV absorbent was measured at 580nm, and evaluated by the standard curve equation:

$$y = 0.0876x + 0.0112 \ ; R^2 = 0.9999 \qquad (1)$$

Where x was the concentration of dye solution, y was the absorbance.

Prepared adsorbent. Flax wastes were picked from agricultural wastes which used 80 mesh during this work. First, flax wastes were repeated washing with distilled water to remove dust. Then the sodium hydroxide solution could be used for modifying flax waste. When the conditions of adsorption were stable (initial MV concentration of 80 mg/l; volume of 25 ml; adsorption dosage of 0.1g; adsorption temperature of 30 ℃; adsorption time of 30 min, adsorption speed of 150 rpm), and the adsorption process of flax wastes with modified by sodium hydroxide solution shown in Table 1. According to the Table 1, we could choose the optimum MFW, and finished the follow-up experiments.

Characterization of adsorbent. In this work, Fourier transform infrared spectroscopy(FTIR)was used to analysis the functional groups. This research were based on the MFW and FW, and after MV adsorption. Fourier transform infrared spectroscopy TU-1901, measured before and after modification and modified flax adsorbed MV infrared spectrum. Scanning electron microscope(SEM) analysis was carried out using a KYKY 2800B scanning electron microscope (China).

TABLE 1
Experimental Design for Batch Modified Study

Set No.	Control parameters	Variable parameters
1	ultrasonic time, 30min; ultrasonic temperature, 25℃; ultrasonic power, 250W	Initial sodium concentration (mol/l): 0.3,0.4,0.5,0.6,0.7,0.8
2	initial sodium concentration, 0.5 mol/l; ultrasonic time, 30min; ultrasonic power, 250W	ultrasonic temperature (℃): 40,50,60,70,80
3	initial sodium concentration, 0.5 mol/l; ultrasonic temperature, 70℃; ultrasonic power, 250W	ultrasonic time(min): 20,30,40,60,70,80,90,120
4	initial sodium concentration, 0.5 mol/l; ultrasonic temperature, 70℃; ultrasonic time, 30min	ultrasonic power(W): 100,125,175,200,225,250

TABLE 2
The design scheme of the Orthogonal test

Variable level	Modified time (min)	Modified temperature (°C)	Adsorption time (min)	Adsorbent dose (g)
	A	B	C	D
1	10	25	40	0.04
2	30	50	60	0.08
3	60	70	100	0.1

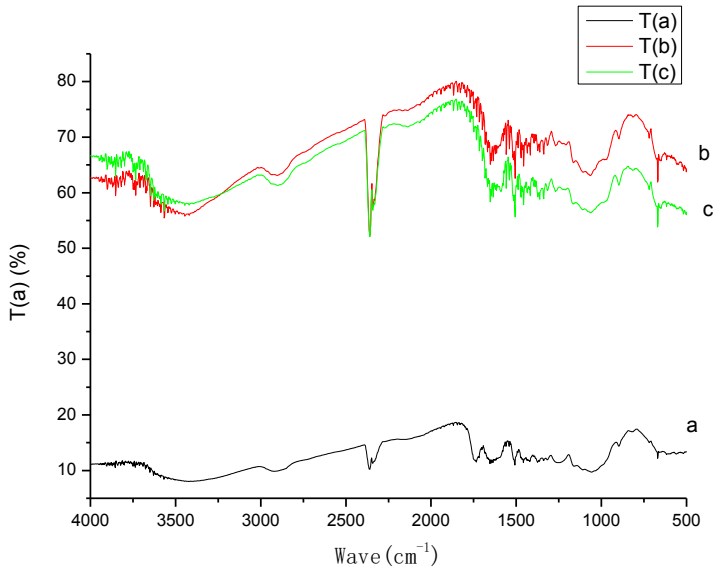

FIGURE 1
FTIR spectra of the unmodified(a)and modified flax(b) and modified flax after(c)dye adsorption

Batch adsorption experiments. Batch adsorption experiments were performed by different dosage (0.02-0.1 g) of MFW in MV solutions of different initial concentrations (40-600 mg/l). The solution were continuously speed (150 rpm) at constant temperature (298-318 K) until equilibrium was reached. At the end of the adsorption process, a certain amount of superannuate to speed 3000 rpm centrifugal 5 min. The concentration of MV in the superannuate was estimated by a UV/visible spectrophotometer at 580 nm, the adsorption capacity (q_e, mg/g) and the removal rate (E, %) of MV adsorbed by MFW from aqueous solution at equilibrium were calculated by the eq. 1. and eq. 1., respectively.

$$q_e = \frac{C_0 - C_e}{W} \times V \quad (2)$$

$$E\% = \frac{C_0 - C_e}{C_0} \times 100\% \quad (3)$$

Where C_0 and C_e were the initial and equilibrium dye concentrations (mg/l), respectively; V was the volume of the solution (L); and W was the adsorbent dosage (g).

Batch desorption experiments. For the desorption study, the MFW was loaded with 80mg/l of dye solution, washed gently with water to remove any unabsorbed dye. The spent adsorbent (0.08 g), suspended in eluting solvents (neutral distilled water, 0.1mol HCl and the perception of 50 C_2H_5OH) was agitated (150 rpm) at 313K for 100min. The concentration was quantified using a UV/ visible spectrophotometer. Desorption efficiency of the adsorbent could be calculated by the eq. 4.

$$D\% = \frac{C_b}{C_a} \times 100\% \quad (4)$$

Where D% was the desorption efficiency; C_a was the concentration of the MV solution (mg/l); C_b was the concentration of departing out the adsorbent for the dye.

Experimental design for orthogonal test. In the single factor experiment, the most significant influence factors for the adsorption of MV solution were selected. The SPAA software were used to design the orthogonal test. Four-factors were applied to evaluate optimum process on three levels and the orthogonal test experimental factors as shown in Table 2.

RESULTS AND DISCUSSION

FTIR spectra analysis of the sorbet. Figure 1 illustrates the FTIR spectra of FW and MFW and after dye adsorption by MFW. The shape of FTIR absorption peak was almost unchanged, but the intensity of an absorption peak changed significant-

ly. A characteristic broad band in the range of 3150-3500cm^{-1} due to hydrogen-bonded –OH stretching was observed for both the FW and MFW. In the range of 1250-1750 cm^{-1}was the vibration peak for - $(CH2)_n$- long chain, and 500-1000cm^{-1} was the stretching vibration peak for -OH and –CHO. Modifying by sodium hydroxide, C-O-C appeared in stretching vibration peak at 843 cm^{-1}. In the range of 2250-2500 cm^{-1} was absorption peak of -CH_2-, and in this section had appeared two peaks, which could due to vibration of the coupling. In the range of 1082.06cm^{-1} was the stretching vibration for unmodified flax. At 2345.51 and 2360.87cm^{-1}, the inner side and the outer surface of vibration peak flex-ion for -CH2-were appeared. Flex-ion characteristic peaks of C-H- and deformation peaks of OH appear in 3425.67cm^{-1}. When the FW were modified by basic, the strength of peak were increased at 1082.06cm^{-1}, 2345.51cm^{-1}, 2930.34cm^{-1} and 2360.87cm^{-1}, which shown that flax modified by sodium hydroxide, the hydrogen bonds in the cellulose, lining and hemicelluloses were breaker, and reduced the crystalline of cellulose and enhanced the intensity of the peak. The MFW adsorbed MV, and the shape of FTIR spectrum peak were almost unchanged and the intensity of the absorption peak had not changed significantly. The different absorption peaks could be seen in some sections. In the range of 3000-3750 cm^{-1} was stretching vibration peak of -OH, but after adsorption MV, the intensity of absorption peak was low, which was due to –OH in MFW and -NH^+ MV solution contact with each, and make the hydrogen bond breaker. In the range of 500-1000cm^{-1} was the stretching vibration peak of -O-H and –CHO. After adsorbing MV, the peak moves to the high frequency region at 915.23 cm^{-1}, which due to the –O-H bonding contact with the MV solution.

SEM analysis of the sorbet. The scanning electron microscope image in Fig,1. A: The stem cuticle of unmodified flax; B: The stem cuticle of flax modified by NaOH; C: The stem cuticle of modified flax after adsorb MV; Bar=10um)

Effect of the modified factors. Effect of initial sodium hydroxide concentration. The Figure 3 could be obtained which was the effect of the different concentration of sodium hydroxide on MFW. It could be found from Figure 3, the adsorption capacity and removal rate increased as the sodium hydroxide concentration rising from 0.3 to 0.5mol. However, when the concentration raised from 0.5 to 0.8 mol/l, the adsorption capacity and removal rate shown reduced. Maximum adsorption capacity and removal rate were at the concentration of 0.5mol/l. This may be due to the fact that the cell walls and nucleus were removed by the solution of sodium hydroxide on the surfer of FW, and thus, the function group of the cellulose, hemicelluloses and lignocelluloses were significantly apparent. With the increasing concentration, the braking on the surfer of FW was more greater. When the MFW contact with the cat-ionic dye of MV, the ion of hydrogen was replaced by the ion of sodium. With the reducing the amount of degradation rate, the adsorption capacity and removal rate were reduced. So the follow-up experiments done to with MFW which were modified by the sodium hydroxide concentration of 0.5 mol / l.

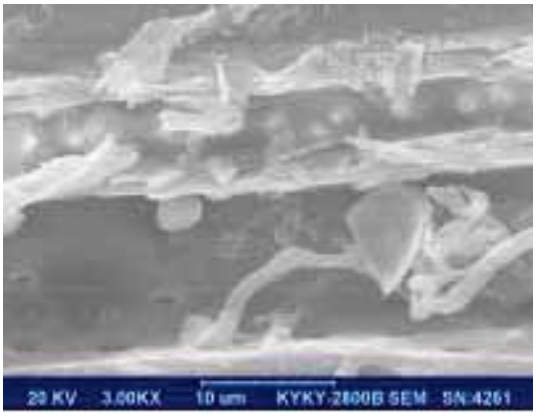

A

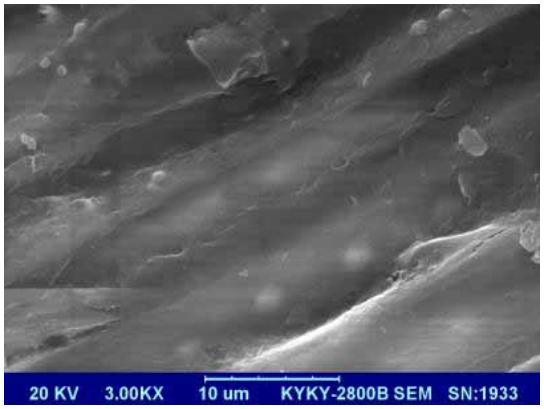

B

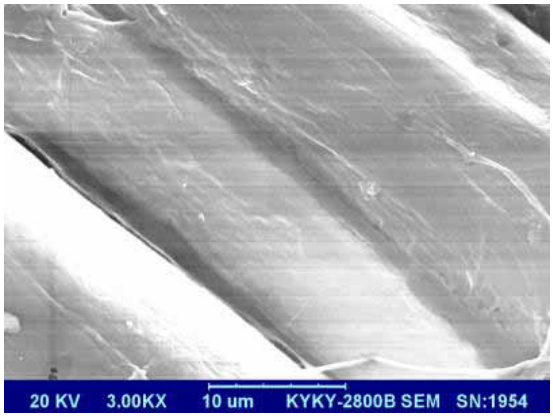

C

FIGURE 2
Hematological changes of flax before and after modified and absorb MV (A: The stem cuticle of unmodified flax; B: The stem cuticle of flax modified by NaOH; C: The stem cuticle of modified flax after adsorb MV; Bar=10um)

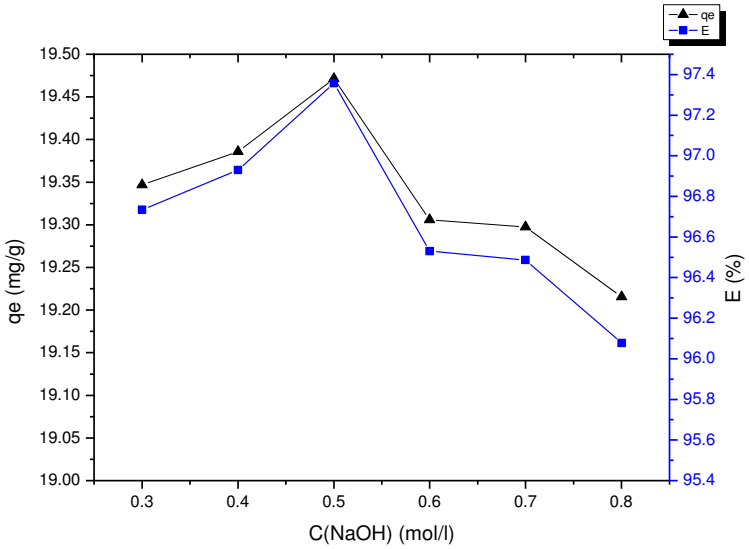

FIGURE 3
The effect of the concentration of sodium hydroxide on MFW

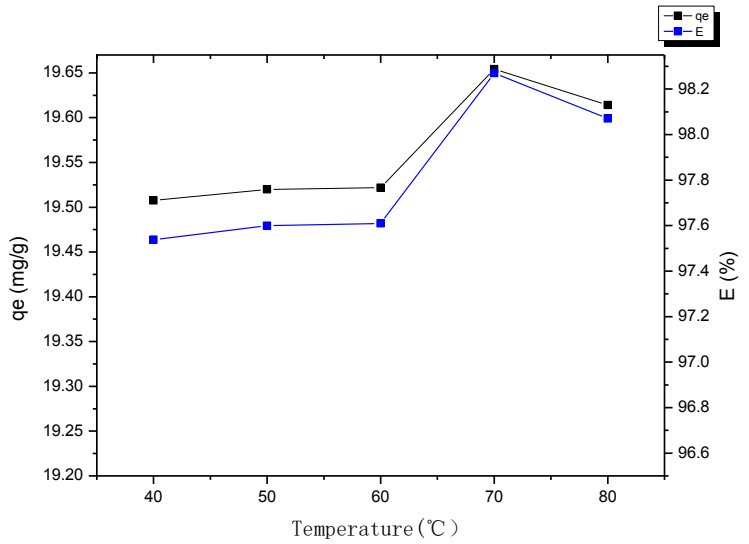

FIGURE 4
The effect of the variable temperature on MFW

Effect of modified temperature. The Figure 4 could be obtained which was the effect of the variable temperature on MFW. It could be seen from Figure 4, with the temperature increasing from 40 ℃ to 60 ℃, the adsorption capacity and removal rate had a little change, but the temperature increasing from 60 ℃ to 70 ℃, the adsorption capacity and removal rate raised quickly. Then with increasing temperature, the adsorption capacity and removal rate were decreased. As the temperature increasing, the pitch of molecular particles in the FW was increased in solution, and the probability of collisions each with every molecules were increased. Under the cavitations of ultrasound, the interaction collision were increased. Thus, some molecule particles with the small competitive were been not sufficiently changed by the solution of sodium hydroxide. Therefore, the adsorption capacity and removal rate were decreased. So the follow-up experiments done to with MFW which were modified under the temperature of 70 ℃.

Effect of modified time. The Figure 5 could be obtained which was the effect of the variable time on MFW. It could be seen from Figure 5, with the time increasing from 20 to 30min, the adsorption capacity and removal rate shown an upward tendency. As the time continues to increasing, the adsorption capacity and removal rate shown a downward tendency. As time increasing, the ultrasonic cavitations were more longer, and the process was handed in much longer time, thus more particles could not be sufficiently modified. Therefore, the adsorption capacity and removal rate were not increased and were instead of downward tendency. So the follow-up experiments were done to with MFW which were modified by the time 30 min.

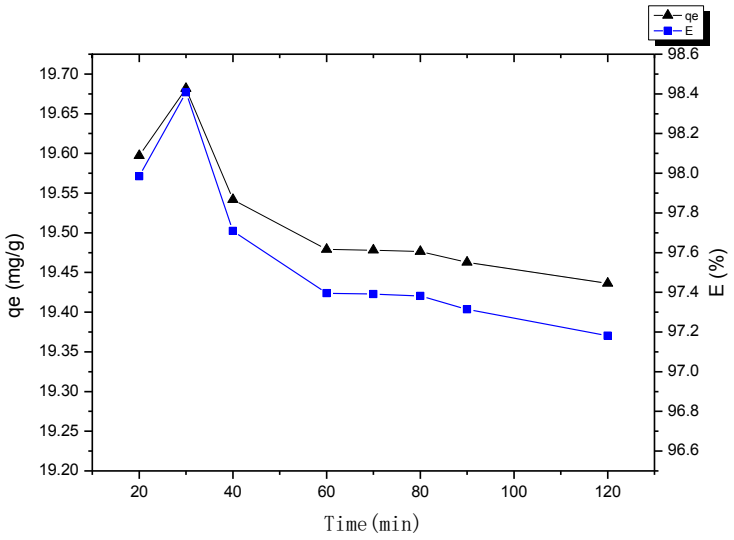

FIGURE 5
The effect of the variable time on MFW

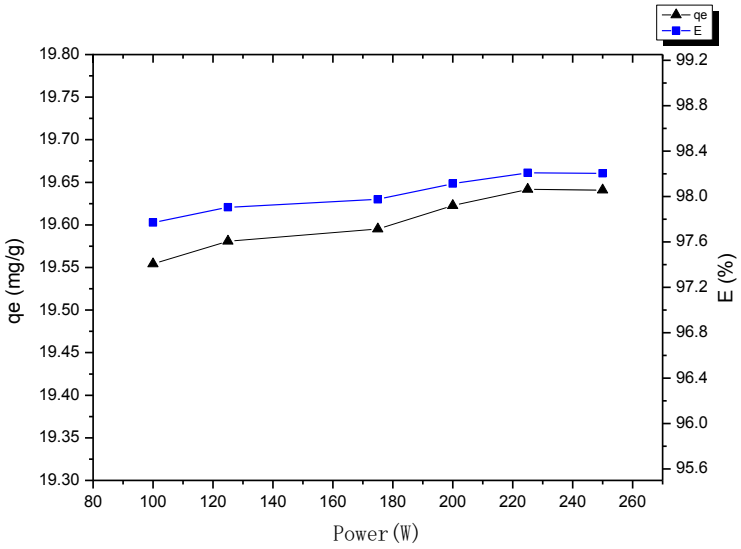

FIGURE 6
The effect of the variable power on MFW

Effect of modified power. The Figure 6 could be obtained which was the effect of the variable time on MFW. It could be seen from Figure 6, with the ultrasonic power increasing, the adsorption capacity and removal rate shown a slow upward tendency, and in the range of 225 W to 250 W, the adsorption reaching equilibrium. With the increasing of ultrasonic power, ultrasonic cavitations increased, thus, the collision in the molecules increased. To be more precise experiment, selecting full-power 250 W.

Effect of the facts of adsorption. Effect of the adsorbent dosage. The Figure 7 of the influence diagram adsorbent dosage on the adsorption of MV by MFW on FW. It could be found from the Figure 7. The adsorbent dosage was increasing, the adsorption capacity was decreased, and the removal rate was raised. The adsorption capacity and removal rate were higher than FW. However, with the adsorbent dosage increasing, MFW and FW had achieved the same effect. The adsorption capacity were increase, as the adsorbent dosage increasing. With increasing the adsorbent dosage, the active sites of dye solution were increase. When the adsorbent dosage increased from 0.02g to 0.08g, the removal rate improved 12.81%. The adsorbent dosage of FW increased from 0.06g to 0.5g, removal rate improved 17.57%. But with increasing adsorbent dosage, the active sites on the surfer of adsorbent were occupied by dye solution and the adsorption reached saturation. This was due to the competitive between the adsorbent and the non-adsorbed of adsorbent. The active sites of adsorbent which could be occupied by dye solution were reduced, and the adsorption capacity were decreased. Selecting the adsorbent dosage 0.08g.

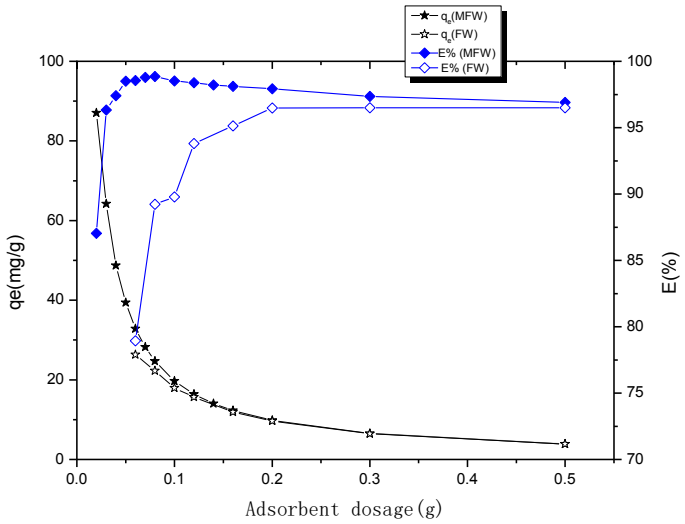

FIGURE 7
Effect of adsorbent dosage on dye adsorption by MFW and FW

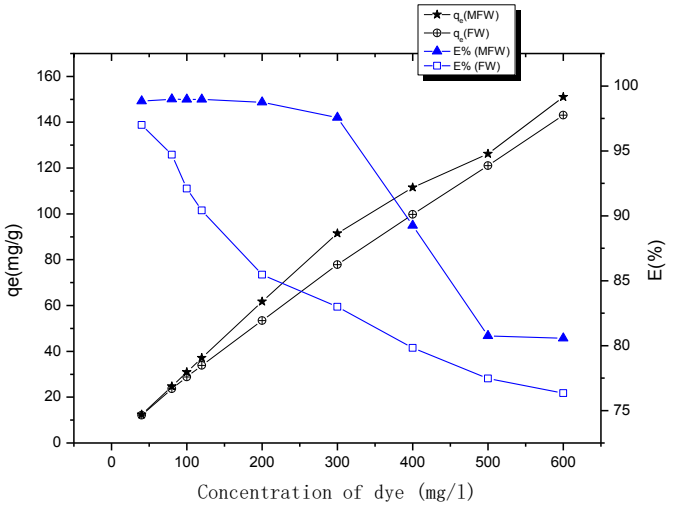

FIGURE 8
Effect of initial dye concentration on dye adsorption by MFW and FW

Effect of initial dye concentration. The Figure 8 of the influence diagram initial dye concentration on the adsorption of MV by MFW on FW. It could be seen from Figure 8, as the concentration of MV dye increasing, the initial removal rate had be in a slow decline, and then the adsorption capacity had an upward tendency. When the concentrations of MV was small, the surfer of adsorbent was not saturated of adsorption conditions, and with the concentration continued increasing, the surface of adsorbent gradually reached saturation which they could no longer adsorbed more dye molecules. When the concentration increased from 50 mg/l to 120 mg/l, the removal rate had declined slowly (14.13%). With the dye concentration increasing, the removal rate decreased significantly (18.23%). Under the experimental conditions in certain circumstances, the removal rate increased, and when the concentration of the dye continued to increase, the removal rate decreased gradually until it reaches adsorption equilibrium. This phenomenon was related with the mass transfer driving force [23]. When the solution of MV concentration increased, and the difference concentration inside and outside of the adsorbent increased which would help to promote the diffusion of the adsorbent from the liquid to the surface and internal on the MFW, thus the removal rate was speeding up. However, the initial concentration was greater than 300 mg/l, the load of the adsorbent gradually increased which replaced the advantages for driving force of adsobate adsorption. Future, with the initial concentration continues to increase, the removal rate had downward tendency. When the initial concentration was much greater, the adsorption capacity was greater on reaching its absorption equilibrium. This was due to the concentration gradient increasing largely, the mass transfer driving force had be more greater, and the amount of MV were adsorbed more greater [24]. Selecting 80 mg/l concentration of MV dye.

TABLE 3
The parameter values of fitting Langmuir and Freundlich isotherm equation

Langmuir wasotherm equation			Freundlich wasotherm equation		
q_m（mg/g）	K_L(l/mg)	R^2	1/n	K_F(l/mg)	R^2
129.199	0.275	0.998	0.383	2321.935	0.812

TABLE 4
Separation factors for adsorption of MV onto MFW

Temp.(K)	Initial concentration(mg/l)								
	40	80	100	120	200	300	400	500	600
298	0.083	0.043	0.035	0.029	0.018	0.012	0.009	0.007	0.006

Adsorption isotherm. The adsorption isotherms, Langmuir and Freundlich were constructed the experimental equilibrium date at initial dye concentration of 40-600 mg/l. In the solid-liquid contact surface, the process of adsorption was usually described by the adsorption isotherm model. From adsorption isotherms were easy to understand the relationship between adsorbent and adsorb systems [24]. Langmuir adsorption isotherm and Freundlich isotherm were the two most commonly adsorption isotherm equation [25].

Langmuir isotherm. The Langmuir adsorption isotherm model assumed that adsorption taken place at specific homogeneous sites within the adsorbent, and it had been used successfully for many adsorption processes of mono-layer adsorption. The Langmuir equation was expressed as follow [26]:

$$\frac{C_e}{q_e} = \frac{1}{K_L q_m} + \frac{C_e}{q_m} \quad (5)$$

where q_m was the maximum mono-layer capacity of adsorbent(mg/g), and K_L was the Langmuir constant that represents the energy of adsorption process(l/mg). q_m and K_L were computed from the slopes and intercepts of the straight line obtained from the plot.

The essential feature of the Langmuir adsorption isotherm could be expressed in terms of a dimensionless constant, separation factor (R_L). The equation defines R_L was as follow [27]:

$$R_L = \frac{1}{1 + K_L C_0} \quad (6)$$

Where R_L values indicate the type of adsorption to be irreversible (R_L=0), favorable (0 < R_L <1), linear (R_L=1) or unfavorable (R_L>1), K_L was the Langmuir constant and C_0 was the initial dye concentration (mg/l).

Freundlich isotherm The Freundlich adsorption isotherm model considers a heterogeneous adsorption surface that had unequal available sites with different energies of adsorption. The Freundlich adsorption isotherm model was as follows [28]:

$$\log q_e = \log K_F + \frac{1}{n} \log C_e \quad (7)$$

where q_e was the amount of MV adsorbed at equilibrium time (mg/g), C_e was the equilibrium concentration of dye in solution (mg/L), K_F was the capacity of the adsorbent and n was the intensity of adsorption constant for Freundlich. The plot of $\log q_e$ versus $\log C_e$ was employed to determine the K_F and n from intercept and slope respectively.

The theoretical monolayer adsorption capacity was calculated to be 129.199mg/g. The Langmuir isotherm equation had a correlation of 0.998 and the Freundlich isotherm equation had a correlation of 0.812(Table 3), so the adsorption process was been fitting very well to Langmuir isotherm equation. Thus the Langmuir isotherm equation could described precisely.

When R_L values were within the range 0 < R_L<1[28], a favorable condition for adsorption was occurred. R_L values obtained for different initial dye concentration were well within the defined range (0.083-0.006) (Table 4). This suggested that the adsorption process was a favorable process under the conditions used for the experiments.

Effect of contact time. The Figure 9 of the influence diagram contact time on the adsorption of MV by MFW and FW. It could be seen from Figure 9, with increasing of adsorption time, the adsorption capacity and removal rate were rising. In the range of 5 to 40 min, the adsorption capacity and removal rate were showed significantly increased. However in 40-200 min interval, the absorption capacity and removal rate had being upward tendency, and in 100-200min interval had reached adsorption equilibrium. As time increasing, monolayer adsorption reached saturation and no more adsorbed dye under certain conditions. Selecting the adsorption time 100min do follow-up experiments.

Adsorption Kinetics. The linearity integral form of the pseudo-first-order model generally expressed as follow [29]:

$$\log(q_e - q_t) = \log q_e - \frac{K_1}{2.303} t \quad (8)$$

where q_t and q_e were the adsorption capacities at time t and at equilibrium, respectively (mg/g), k1 was the rate constant of pseudo-first-order adsorption(min^{-1}) and t was the contact time (min). To plot log (q_e−q_t) versus t gives a linear relationship from which k_1 and predicted q_e could be determined from the slope and intercept of the plot respectively.

The adsorption kinetic may be described by the pseudo-second-order model. The differential equation was generally known and described as follow [30]:

$$\frac{t}{q_t} = \frac{1}{K_2 q_e^2} + \frac{1}{q_e} t \quad (9)$$

Where k^2 was the rate constant of pseudo-second-order adsorption(min−1). The plot of t/qt versus t shows a linear relationship.

The second-order rate constants were used to calculate the initial adsorption rate, given as follow [31]:

$$h = K_2 q_e^2 \quad (10)$$

Values of k^2 and equilibrium adsorption capacity qe were calculated from the intercept and slope of the plot of t/qt versus t according to Eq. (9).

Generally, the value of the linear regression correlation coefficient R^2 given an indication as to which model could be chosen to give the best-fit. In this study, the first-order model had very limited applicability in adsorption kinetics of MV on MFW (q_e=0.393mg/g, R^2=0.820), and that the maximum mono-layer adsorption capacity was 24.783 mg/g and according to the values of the regression correlation coefficient R^2=1 which were well fitting the pseudo-second-order kinetic equation.

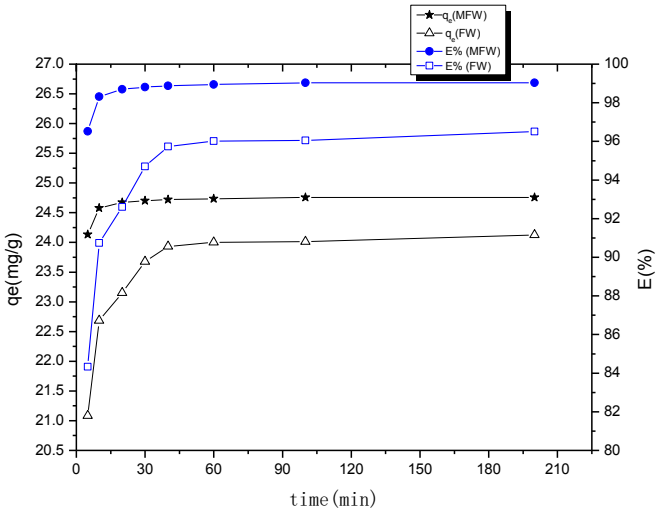

FIGURE 9
Effect of contact time on dye adsorption by MFW and FW

TABLE 5
The kinetic equation parameters

pseudo –first-order model			pseudo –second-order model			
$k_1(min^{-1})$	q_e(mg/g)	R^2	(g/(mg*min)	(mg/(g*min))	q_e(mg/g)	R^2
0.055	0.393	0.820	0.392	240.765	24.783	1

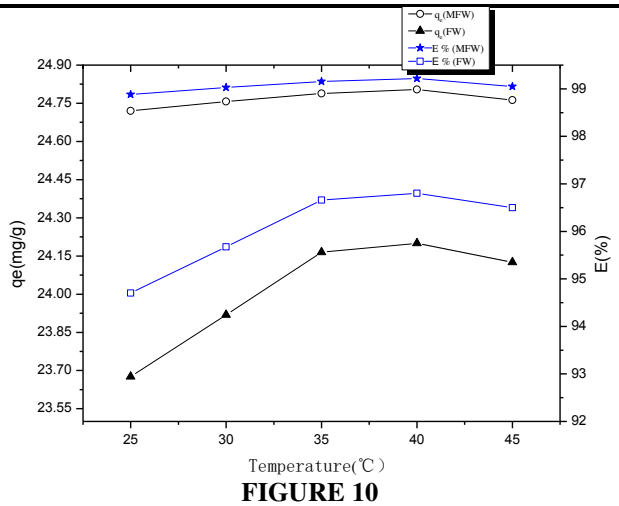

FIGURE 10
Effect of contact temperature on dye adsorption by MFW and FW

Effect of contact temperature. The Figure 10 of the influence diagram contact temperature on the adsorption of MV by MFW and FW. It could be seen from Figure10, as the temperature increasing, the adsorption capacity were relatively flat and the removal rate changed more obviously. When the temperature increasing from 25 ℃ to 35 ℃, the adsorption capacity had been small variation and the removal process increased significantly. As the temperature increasing to 40 ℃, the adsorption capacity and removal rate remained almost stably. In the range of 45-50 ℃, adsorption capacity and removal rate were declining. Selecting 40 ℃ with adsorption conditions.

Thermodynamic calculations. Thermodynamic parameters were calculated from the variation of the equilibrium constant, Kc, was as follow [32]:

$$K_C = \frac{q_e}{C_e} \quad (11)$$

Where Kc (L/g) values were obtained using the method of Khan and Singh (1987) by plotting ln (qe/Ce) versus *q*e and extrapolating to zero *q*e. The intercept of the straight line with the vertical axis gives the values of *K*c.

The Gibbs free energy change（ΔG^0）of the adsorption process was related to Kc as follow [33]:

$$\Delta G^0 = -RT \ln K_C \quad (12)$$

The changes in enthalpy (ΔH^0) and entropy (ΔS^0) for MV adsorption were calculated from the slope and intercept of the plot of lnKc against 1/*T* according to the van't Hoff equation was as follow [33]:

$$\ln K_C = \frac{\Delta S^0}{R} - \frac{\Delta H^0}{RT} \quad (13)$$

Plotting lnKc versus 1/T for adsorbents shows straight lines. From their slope and intercept, ΔH^0 and ΔS^0 were determined.

It could be found that the negative values of ΔG^0 (Table 6) indicate a favorite and spontaneous process [54]. The positive values of ΔH^0 show that MV adsorption was endothermic on both adsorbents. As ΔH^0 values were below 40 kJ/mol, the nature of the adsorption process was physical [44], either caution exchange or hydrogen bonding [34]. The positive value of ΔS^0 indicated an increase in randomness at the solid-solution interface during the adsorption of MV onto MFW.

The Orthogonal experiment. The results and analysis of the orthogonal experiment. According to the orthogonal array of L9(4^3) presented in Table 2, the following experiments were performed (Table 7) and the result of range analysis was shown in Table 8a, 8b.

It could be seen from Table 8a, the influencing order of four factors was D, B, C and A, the adsorbent dosage was became the most significant factor, following the modification temperature, adsorption time and modification time. In the results, we derived the optimum combination of $A_3B_2C_3D_1$, which the combinations were the modification time of 60 min, modification temperature of 50 ℃, adsorption time of 100 min, and adsorbent dosage of 0.04 g. It could be seen from Table 8b, the influencing order was B, C, D and A, the modification temperature was most obvious factors, following by the adsorption time, modification time, and the adsorbent dosage. In the results, we derived the optimal combination of $A_3B_2C_3D_1$, which the combinations were the modification time of 60min, modification temperature of 50 ℃, adsorption time of 100 min, and adsorbent dosage of 0.04 g.

TABLE 6
The parameters for Vant's Hoff equation

Tem. (K)	Kc (l/g)	ΔG^0 (KJ/mol)	ΔH^0(KJ/mol)	ΔS^0(KJ/mol)
298	27.57	-8.217	0.205	35.709
303	31.80	-8.355		
308	36.68	-9.224		
313	39.60	-9.573		

TABLE 7
The design scheme of the orthogonal experiment

set	Modified time	Modified temperature	Contact time	Adsorbent dosage	Adsorption capacity(mg/g)	Removal rate (%)
	A	B	C	D		
1	10	25	40	0.04	48.99	97.98
2	10	50	60	0.0	24.66	98.72
3	10	70	100	0.1	19.69	98.49
4	30	25	60	0.1	19.62	98.12
5	30	50	100	0.04	49.57	99.15
6	30	70	40	0.08	24.55	98.22
7	60	25	100	0.08	24.58	98.35
8	60	50	40	0.1	19.79	98.76
9	60	70	60	0.04	49.38	99.76

TABLE 8a
Analysis of orthogonal experiment for adsorption capacity

	A	B	C	D
K_1[a]	31.116	31.069	31.113	49.318
K_2	31.252	31.342	31.222	24.600
K_3	31.256	31.213	31.289	19.705
R[b]	0.14	0.273	0.176	29.613
Influencing order		D>B>C>A		
Optimal Combination	A_3	B_2	C_3	D_1
		$A_3B_2C_3D_1$		

[a]K_1= (adsorption capacity of single-factor)/4.
[b]R=maxK_1-minK_1.

TABLE 8b
Analysis of orthogonal experiment for removal rate

	A	B	C	D
K_1	98.370	98.154	98.389	98.637
K_2	98.499	98.915	98.506	98.401
K_3	98.696	98.496	98.670	98.527
R	0.197	0.761	0.281	0.236
Influencing order		B>C>D>A		
Optimal Combination	A_3	B_2	C_3	D_1
		$A_3B_2C_3D_1$		

[a]K_1= (removal rate of single-factor)/4.
"[b]R= maxK_1-minK_1.

The verification experiment. Optimum combination of the orthogonal test, its adsorption capacity and removal rate were same with the batch adsorption experiments. The experiment obtained the adsorption capacity of 23.83 mg/g and the removal rate of 98.03 % on MFW, and the adsorption capacity of 19.37 mg/g and the removal rate of 90.21 % on MF, respectively. Optimum combination of conditions for the adsorption capacity and removal rates on MFW were higher than on FW 4.46mg/g, and 7.48%, respectively.

Desorption study. Taking 0.1g MFW were adsorbed the dye of MV which were added 0.1mol / L HCl solution and 50% ethanol each 25mL, and shaking at a temperature of 40 ℃, speed 150rpm and time of 100min. Then the removal rate of MV could be measured were 95.27 % and 88.89%, respectively. It could be found that the absorption effect of 0.1mol / L HCl higher than 50% ethanol solution.

CONCLUSIONS

The results of experimental shown that the FW from agricultural waste could be used as adsorbent for the adsorption of cationic dyes, and also had a good adsorption effect.

(1) The optimum conditions of modified FW were: the concentration of modification reagent of the sodium hydroxide solution of 0.5 mol/l, ultrasonic power of 250 W, modification time of 30 min and modification temperature of 70 ℃.

(2) The optimal modification conditions for MFW which had the better adsorption affections than FW, adsorption capacity and removal rate under optimal adsorption conditions were higher than FW 0.6mg / g and 2.42%, respectively.

(3) This study was found that the model of adsorption isotherm was well fit with the Langmuir isotherm equation and R^2 = 0.998, and the layer of adsorption was the monolayer adsorption; the kinetic equation followed the pseudo-second-order and R^2 = 0.9999, and belong to chemical adsorption; thermodynamic parameter study shows the adsorption was spontaneous endothermic reaction.

(4) The combination of the orthogonal test were modification time of 60min, modification temperature of 50 ℃, adsorption time of 100min, and adsorbent dosage of 0.04g. Under this condition, the adsorption capacity and removal rate compared with FW were increased 4.46mg/g, and7.48%, respectively.

(5) The mechanism of adsorption process by MFW were mainly ion-exchange and hydrogen bonding into the dye.

ACKNOWLEDGEMENTS

This work was supported by the training program of Scientific and Technological talents of Xinjiang Autonomous Region (No: QN2016YX0066).

REFERENCES

[1] Merdan, N., Akalin, M., Kocak, D., Usta, I. (2004) Effects of ultrasonic energy on dyeing of poly amide (microfiber) /Lycia blends. Ultrasonic's Son-Chem. 42, 165–168.

[2] Kan, C.W., Yuen, C.W.M. (2005) Use of ultrasound in textile wet processing. Textile Asia. 36, 47–52.

[3] Ferrero, F., Periolatto, M. (2012) Ultrasound for low temperature dyeing of wool with acid dye. Ultrasonic's Son-Chem. 19, 601–606.

[4] McNeil, S.J., McCall, R.A. (2011) Ultrasound for wool dyeing and finishing. Ultrasonic's Son-Chem. 18, 401–406.

[5] Burkinshaw, S.M., Jeong, D.S. (2012a) The dyeing of poly(lactic acid) fibers with disperse dyes using ultrasound: Part 1 – Initial studies. Dyes and Pigments. 92, 1025–1030.

[6] Ankara, P.S., Shankar, R. (2008) Eco-friendly ultrasonic natural dyeing of cotton fabric with enzyme pretreatments. Desalination. 230, 29–62.

[7] Balci, B. (2016) Basic textile dye adsorption from aqueous solution and synthetic dye bath wastewater by modified bucalyptus barks. Fresen. Environ. Bull. 25, 6124-6131.

[8] Sen, T.K., Afroze, S., Ang, H. (2011) Equilibrium, kinetics and mechanism of removal of methylene blue from aqueous solution by adsorption onto pine cone biomass of Pinusradiata. Water Air Soil Pollution. 218, 499–515.

[9] Yagub, M.T., Sen, T.K., Ang, H. (2012) Equilibrium, kinetics, and thermodynamics of ethylene blue adsorption by pine tree leaves. Water Air Soil Pollution. 223, 5267–5282.

[10] Kant, R. (2012) Adsorption of dye eosin from an aqueous solution on two different samples of activated carbon by static batch method. J. Water Resources Prot. 4, 93–98.

[11] Rehman, M., Kim, T., Han, J. (2012) Adsorption of ethylene blue dye from aqueous solution by sugar extracted spent rice biomass. Carbon Hydrate Poly. 90, 1314–1322

[12] Selvaraj, A., Prabu1, P., Mohan, K., Kumaravel, I., Rajendran, V. (2016) Efficacy of bacterial biopolymeric (EPS) liganded silver mesocage complexes for hexavalent chromium adsorption. Fresen. Environ. Bull. 25, 6030-6037.

[13] Ali, I., Asim, M., Khan, T.A. (2012) Low cost adsorbents for the removal of organic pollutants from wastewater. J. En. Man. 113, 170–83.

[14] Asgher, M., Bhatti, H. (2012) Evaluation of thermodynamics and effect of chemical treatments on adsorption potential of (Citrus) waste biomass for removal of anionic dyes from aqueous solutions. Ecol Eng. 38, 79–85.

[15] Rehman, M., Kim, I., Han, J. (2012) Adsorption of methylene blue dye from aqueous solution by sugar extracted spent rice biomass. Car. Pol. 90, 1314–22.

[16] Giraldo, L., Pirajan, J.C.M., Anal, J. (2014) Adsorption of dye cosine from an aqueous solution on two different samples of activated carbon by static batch method. App. Pyro. 106, 41–47.

[17] Randi, Z., Jinghua, Z, Xiaona, Z., Chanchan, D., Runping, H (2014) Adsorption of Congo red from aqueous solutions using cationic surfactant modified wheat straw in batch mode: Kinetic and equilibrium study. Journal of the Taiwan Institute of Chemical Engineers. 45, 2578–2583.

[18] Nunell, G.V., Fernandez, M.E., Bonelli, P.R., Cukierman, A.L. (2015) Nitrate uptake improvement by modified activated carbons developed from two species of pine cones. Journal of Colloid and Interface Science. 440, 102–108.

[19] Ghaedi, A.M., Vafaei, A. (2016) Principal component analysis-artificial neural network and multiple linear regression for the removal of basic blue dye by alumina nanoparticle loaded on activated carbon prepared from palm kernel. Fresen. Environ. Bull. 25, 6215-6217.

[20] Aloulou, F., Boufi, F., Labidi, J. (2006) Modified cellulose fibers for adsorption of organic compound in aqueous solution. Se. & Pu. Tech. 52, 332–342.

[21] Nogi, M., Yano, H. (2008) Transparent nanacomposites based on cellulose produced by bacteria offer potential innovation in the electronics device industry. Ad. Mate. 20, 1849–1852.

[22] Wu, F., Zhang, Y., Liu, L., Yao, J.M. (2012) Synthesis and characterization of a novel cellulose-g-poly(acrylic acid-co-acrylamide) superabsorbent composite based on flax yarn waste. Car. Po. 87, 2519–2525.

[23] Chunhong, Z., Binh, N., Feng L (2006) Roughing flax waste - pounce Comprehensive Advances in the use. China Re. Com. U. 24, 33-35.

[24] Vamooses, V., Lei, S., Jin, B., Chow, C.W.K., Saint, C. (2009) Adsorption of Congo red by three Australian kaolin. App. Clay Sci. 43, 465-471.

[25] Korkmaz, M., Özmetin, C., Ali Fil, B., Özmetin, E., Yaşar, Y. (2013) Methyl violet dye adsorption onto clinoptilolite (natural zeolite): isotherm and kinetic study. Fresen. Environ. Bull. 22, 1524-1536.

[26] Hu, Z., Chen, H., Ji, F., Yuan, S (2010) Removal of Congo Red from aqueous solution by cattail root. J. Hazard. Mater. 173, 292-303.

[27] Chakra, T.W., Weber, R.K (1974) Pore and solid diffusion model for fixed bed adsorbents. J. Am. Inst. Chem. Eng. 20, 228-232.

[28] Freundlich, H. (1906) Over the adsorption in solution. J. Phys. Chem. 57, 385–470.
[29] Nandi, B., Goswami, A., Purkait, M. (2009) Removal of cationic dyes from aqueous solutions by kaolin: kinetic and equilibrium studies. App. Clay Sci. 42,583–590.
[30] Ho, Y.S., McKay, G. (1999) Pseudo-second order model for sorption processes. Process Bio-Ch. 34, 451–465.
[31] El-Said, I.E., Hide, A.L., Asmara, A.S. (2012) Ciprofloxacin adsorption from aqueous solution onto chemically prepwered carbon from date palm leaflets. J. En. Sci. 24, 1579–1586.
[32] Uslu, H., Inci, I. (2009) Adsorption equilibrium of L-(+)-tartaric acid onto alumina. J. Che. & En. Data. 54, 1997–2001.
[33] Li, Z.H., Hong, H.L., Liao, L.B., Ackley, C.J., Schulz, L.A., MacDonald, R.A (2011) A mechanwastic study of ciprofloxacin removal by kaolin Colloids and Surfaces B: Biointerfaces. 88, 339–344.
[34] Churn, J.M., Wu, C.Y. (2001) Desorption of dye from activated carbon beds: effects of temperature, pH and alcohol. Water Research. 35, 4159–4165.

Received: **08.12.2016**
Accepted: **13.11.2017**

CORRESPONDING AUTHOR

Li Xiaomin
Key Laboratory at Universities of Education
Department of Xinjiang Uygur Autonomous Region, College of Chemical & Environmental Science,
Yili Normal University, Xinjiang 835000 - China

e-mail: lixm228@163.com

© by PSP Volume 27 – No. 2/2018 pages 703-709 Fresenius Environmental Bulletin

COMPARING DIFFERENT MOLECULAR SAMPLING METHODS FROM BIRDS VIA MOLECULAR SEXING

Ismail Burak Karaceylan*, Mehmet Ali Tabur

Suleyman Demirel University, Faculty of Science and Arts, Department of Biology, Isparta, Turkey

ABSTRACT

Molted feathers obtained with noninvasive genetic sampling are valuable tools for genetic analyses on birds. However, the low quality and quantity of DNA obtained from molted feathers poses serious limitations. In this study, we compared the quality (amplification success) of DNA obtained from molted feathers, plucked feathers and blood samples, as well as the feasibility of these methods. Molted feathers of Ruddy Shelduck (*Tadorna ferruginea*) were collected (n=74) around Lake Burdur during 2014-2015. As non-destructive sampling we used feathers plucked (n=12) from chests of domestic chicken (*Gallus gallus*). Blood samples were also taken (n=2) from domestic chickens. Evaluation of DNA was performed by amplification of CHD specific 2550f-2718r markers.

While molted feathers did not yield any DNA, we could successfully amplify all the samples from plucked feathers (♀=10, ♂=2) and blood (♂=2). Blood samples produced stronger bands in gel. In terms of utility and the quality of the obtained DNA we concluded that blood samples yields the best results, followed by plucked feathers and molted feathers.

KEYWORDS:
DNA, NGS, feather, molecular sexing, *Tadorna ferruginea*, Turkey

INTRODUCTION

Turkey forms a very important ecosystem for animals, especially birds, both because it acts as a bridge between Europe and Asia, and because it is situated on a gate to Africa [1]. Furthermore, Turkey is very rich in terms of natural habitats. Therefore its varied geography and climatic conditions provide a suitable habitat for numerous bird species [2].

Birds are the best known major group of organisms, and the conservation status of all bird species have been assessed twice. Even though only a small amount of bird species have gone extinct over the last centuries, the global number of individual birds is reducing significantly faster, which indicates avian populations are declining faster than species extinction rate [3].

An estimated 16 bird species would have gone extinct between 1994 and 2004 were it not for conservation programmes that tackled their threats, reduced rates of population decline and/or increased population sizes. In addition, during this 10-year period, 49 Critically Endangered species (28%) benefited from conservation actions such that they declined less severely (24 species) or improved in status (25 species) [4].

Biodiversity is suffering more than ever due to human impact. Natural habitats of organisms shrink and their populations decline day by day. It is thought that only a few of the extinctions in last centuries were caused by natural processes [5, 6].

Protecting species, communities and ecosystems from excessive extinction is the subject of conservation biology. Aim of this interdisciplinary field is to study and conserve biodiversity [7, 8, 9].

A well accepted objective of conserving nature is conserving biodiversity and this includes genetic diversity [10]. Most important processes at the population level in conserving species' are ultimately genetic and evolutionary as these processes provide the necessary potential to maintain life [5, 8, 10, 11, 12, 13].

Methods like DNA sequencing, MHC, minisatellite, microsatellite, RAPD etc. enables us to identify parents or other relatives, founders of populations, unidentified individuals, population structures, effective population sizes and population specific markers. We can analyze metapopulation structure, hybridization, and delineation of species, subspecies and races, all of which provides important information in setting conservation priorities [14].

With new, improved technologies, DNA polymorphisms became the most popular marker in studying genetic diversity [15]. Any biological material that includes DNA (e.g., blood, tissue samples, plucked hairs, molted feathers, feces, saliva etc.) can be used to measure genetic diversity [12]. This allowed for a method which recently became very popular and called NGS (Non-Invasive Genetic Sampling). This method provides us with DNA samples from hairs, feathers and feces etc. without harming the species. These samples than can be used to identify species that are hard to reach, count them and identify its individuals, identify their sex, feeding

habits, genetic diversity, population structure and reproductive behavior [16].

Most preferred methods of sampling DNA from birds are plucking feathers [17, 18] collecting molted feathers [19, 20, 21] and blood samples [22, 23].

Aim of this study is to compare different genetic sampling methods from birds based on the amplification success of a sex-linked gene CHD. In addition, we discuss the feasibility of the methods in terms of necessary training and suitability to the study that is to be conducted.

MATERIALS AND METHODS

Three different samples that we used in this study are molted feathers collected around Lake Burdur, plucked feathers and blood samples. Molted feathers of ruddy shelduck (*Tadorna ferruginea*) were collected (n=74) along the first 5-15 meters of the lake coast without any intervention to the species. Non-destructive sampling was made with plucking chest feathers (n=12) from chickens (*Gallus gallus*) grown in Suleyman Demirel University Agricultural Research and Application Center and blood samples were collected from chickens that were euthanized as a part of another study. Feathers collected during fieldwork were placed in envelopes without touching the calamus and kept in a dry, cool and dark place until experiments. Blood samples were immediately processed in the laboratory.

DNA extraction was made with Phenol:Chloroform:Isoamyl Alcohol [24] since it is relatively cheaper. However, initial experiments did not yield any DNA from molted feathers. Therefore, experiments were repeated with DNeasy Blood and Tissue Kit (QIAGEN) and it was used for subsequent experiments.

First 1-2 cm of feathers samples belonging to ruddy shelduck and 0.5-1 cm of feather samples of chicken were cut with a sterile lancet and were placed in a container. When observed, blood clot that was identified by Horváth et al. [25] was also added to the container. Different lancets and containers were used for each sample.

For Phenol:Chloroform:Isoamyl Alcohol extraction, lysis buffer was prepared with 500 µL of 1x TNE (H_2O, 50 mM Tris-HCl, 100 mM NaCl, 6.3 mM EDTA), 8% SDS and 10 units of proteinase K. Samples were incubated in the buffer for a week at 37°C and 5 units of proteinase K were added every day [26].

Different versions of this method with using various solution concentrations, adding DTT (dithiothreitol) to the buffer and using different lysis times and temperatures were also tried.

Extraction from blood with DNeasy Blood & Tissue Kit was done using manufacturer's recommended protocol and a user-developed protocol was used for feather samples.

Two methods were used in amplification of DNA extracts. 2550F – 2718R primer pair was used in both methods to amplify CHD gene. In the first method, PCR mix was prepared with 5 µL PCR buffer (10x), 1 µL DNTP (10 mM), 5 µL forward primer (2550F), 5 µL reverse primer (2718R), 5 µL $MgCl_2$ (25 mM), 1 µL template DNA, 0.25 µL *Taq* DNA polymerase (Thermo) and 23.75 µL ddH_2O with a final volume of 50 µL. And the PCR protocol consisted of initial denaturation at 95°C for 1 minute, 30 cycles of denaturation at 95° for 30 seconds, annealing at 60°C for 30 seconds and extension at 72°C for 1 minute, followed by a final extension step at 72° for 5 minutes.

We used Hot Start PCR as the second method. In this method *Taq* DNA polymerase is inactive at lower temperatures thus greatly reducing non-specific amplification. 50 µL of PCR mix was prepared with 4 µL Phire reaction buffer (5x), 1 µL DNTP (10 mM) , 5 µL forward primer (2550F), 5 µL reverse primer (2718R), 1 µL template DNA, 1 µL Phire Hot Start II DNA polymerase (Thermo) and 33 µL ddH_2O. PCR protocol was as follows, initial denaturation at 98°C for 30 seconds, 30 cycles of denaturation at 98°C for 5 seconds, annealing at 58°C for 5 seconds and extension at 72°C for 10 seconds, followed by a final extension step at 72°C for 1 minute.

5 µL of PCR products were mixed with 1 µL loading dye and loaded into 3% agarose gel with GeneRuler 100bp (Thermo) ladder. After electrophoreses, gels were investigated in a UV imager and digital photos were taken.

RESULTS

We could not extract DNA from shed feathers of ruddy shelduck collected around Lake Burdur with neither Phenol:Chloroform:IAA, nor Qiagen DNeasy Blood & Tissue Kit. Even though no bands appeared on the gel after the electrophoresis of genomic DNA, we still tried to amplify the samples, but again couldn't observe any bands.

We successfully extracted DNA from both plucked feathers (♀=10, ♂=2) and blood (♂=2). Blood samples produced stronger bands on the gel suggesting a higher amount of DNA is present as shown in Figures 1 and 2.

Since the bands were very faint after standard PCR application with 2550F/2718R primer we used Hot Start PCR to perform molecular sexing.

Using Hot Start PCR with 2550F/2718R primer sets, we could successfully identify the sexes of the samples shown in Figures 3 and 4.

DNA concentration of blood samples and their pcr products were higher than of plucked feathers as illustrated in Figure 5.

In terms of required laboratory work and quality of the obtained DNA, we think that blood sampling is advantageous over non-destructive sampling that is plucking feathers in this case. Nevertheless, plucked feathers provided enough DNA to be used in molecular studies.

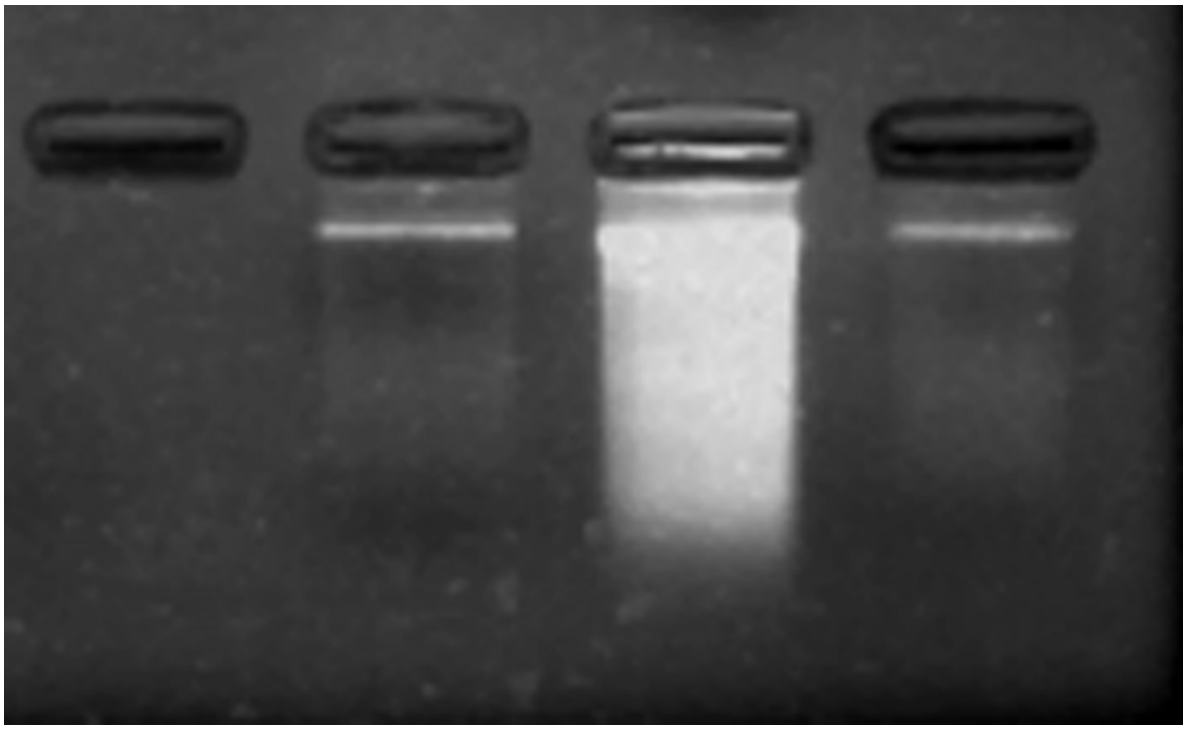

FIGURE 1
Genomic DNA from plucked feathers. First column: negative control.

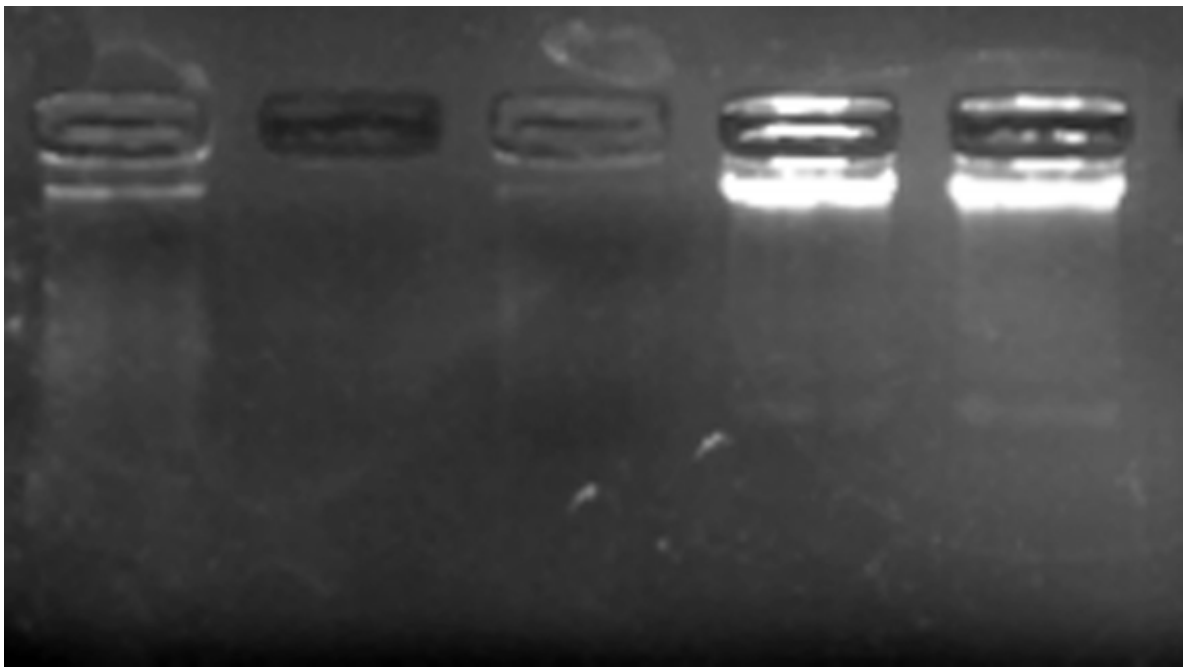

FIGURE 2
Comparing genomic DNA extracted from plucked feathers and blood samples. Last two columns are blood samples

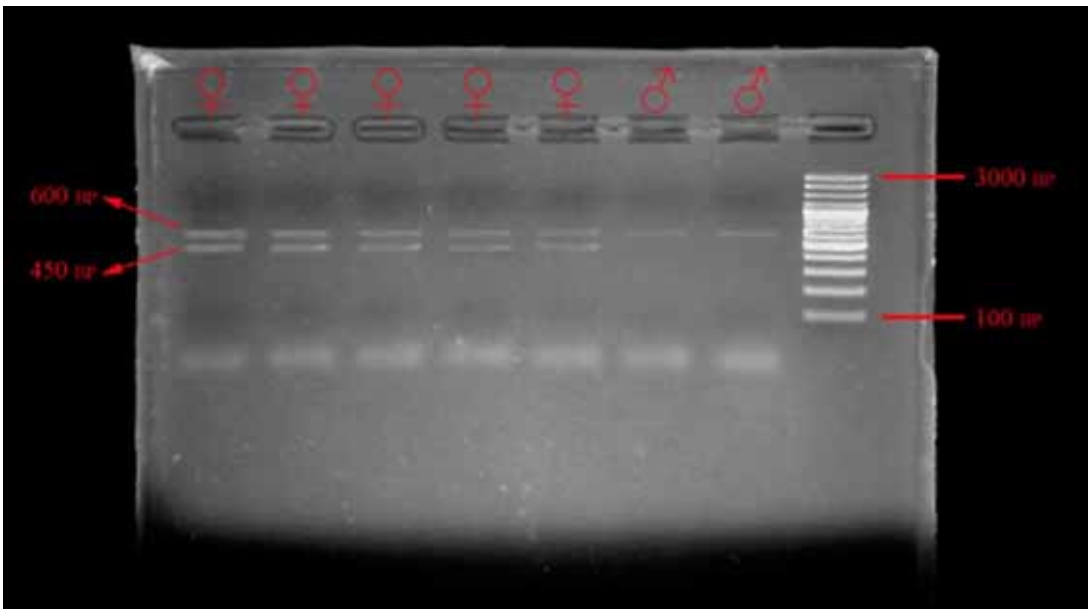

FIGURE 3
Sex identification from plucked feathers and blood. Last two columns are blood samples.

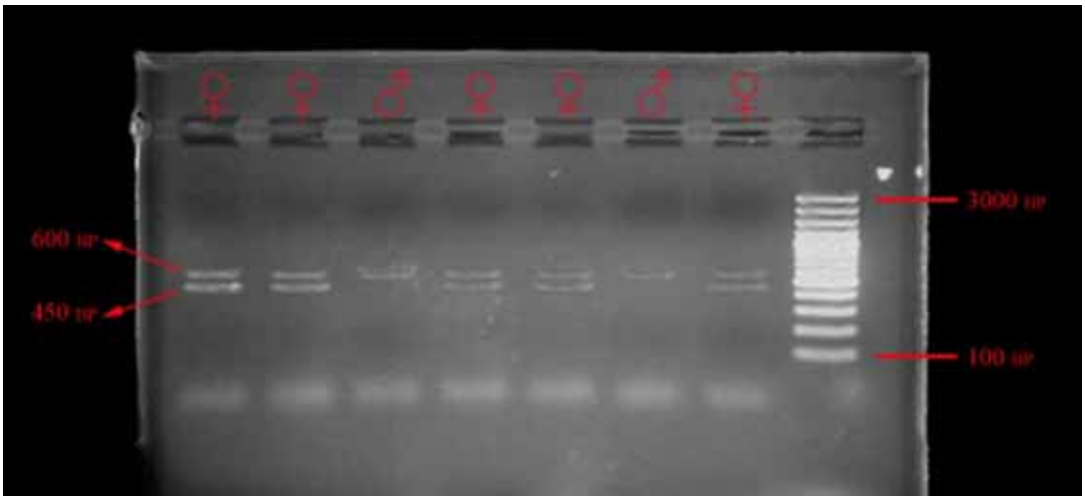

FIGURE 4
Sex identification from plucked feathers and blood.

However, even though it has many advantages, we concluded that non-invasive genetic sampling is not always applicable and also relatively laborious to work with.

DISCUSSION

Because it is possible to collect feathers from large areas and they make it possible to study the species which are hard to study with other methods, non-invasive genetic sampling is an important tool in molecular studies of birds [20, 25]. However, non-invasive genetic sampling has some serious limitations. These are the low quality and the quantity of the obtained DNA. This can lead to getting no PCR product at all or false amplifications [27]. Main cause of this disadvantage is usually environmental conditions. Factors such as sunlight, temperature, humidity and microorganism activity depending on these factors are the main reasons of DNA degradation [28]. Average temperature and sunbathing rate of Burdur city during our field studies (May-November) were 22°C and 9 hours respectively [29]. This suggests that collected feathers were exposed to a lot of sunlight. Since we collected the feathers from the coast very close to the water, highly alkaline and saline characteristic of the lake may have also had negative effects on molted feathers [30]. Environmental conditions around the lake may be the main reason as to why we failed to amplify collected feathers. Presti et al. [31] also failed to obtain PCR products from non-invasively collected feather samples; later

using a different primer set that aims a shorter part of the CHD gene he could successfully identify the sexes of 56% of the samples. Since the introns of the CHD gene are relatively large (450-600 bp) and it's located in nuclear DNA, CHD gene is very sensitive to DNA degradation [25].

Mukesh et al. [32], stated the amount of DNA they could obtain from blood, plucked feathers, and shed feathers as 22:2:1, respectively. In our work, we successfully determined the sexes of individuals using plucked feathers (n=12, ♀=10, ♂=2) and blood samples (n=2, ♂=2), but we failed to amplify any of the molted feathers (n=74). The fact that blood samples produced stronger bands on the gel, suggests that it contains higher amounts of DNA. These findings are in parallel with other studies.

We used gradient PCR to determine the optimum temperatures for 2550F/2718R primer set, however even when the bands were the strongest they were significantly faint. Later on we obtained the brightest bands using Hot Start PCR. This method deactivates the *Taq* polymerase enzyme at lower temperatures to prevent non-specific primer annealing [33]. The reason for the fainter bands we observed using standard PCR protocol might be our working conditions in room temperature.

Molecular methods are used in a lot of different studies like taxonomy, measuring biodiversity, identifying population structure and characteristics, molecular ecology, conservation biology etc. [34]. It is crucial to choose a suitable DNA source while adhering to the aim of the study. This situation is most evident in conservation studies. Causing stress or even damaging the population to obtain DNA material for studying the population genetics of an endangered species is against the very object of the study in the first place. In situations like these, non-invasive sampling should be considered. It is very convenient for the researches to be able to collect genetic material from fieldworks without even needing to observe the species. On the other hand, non-destructive sampling like plucking feathers can provide enough genetic information for molecular studies; therefore they can be used instead of blood sampling. Blood sampling is still the best way to sample DNA from birds in terms of the quality and the quantity of the obtained DNA and it is shown that blood sampling does not affect the mortality of the studied species [35]. However, blood sampling is often more laborious than plucking a few feathers and it is also more stressful to the individuals [36]. Furthermore, when sampling blood, fieldworkers should be trained well. While collecting or plucking feathers, though no prior training is required, fieldworkers should be very careful. Furthermore, laboratory work should also be conducted as sterile and cautious as possible [21]. It is important to conduct a pilot study for non-invasive genetic studies, especially for molted feathers [16, 21, 37].

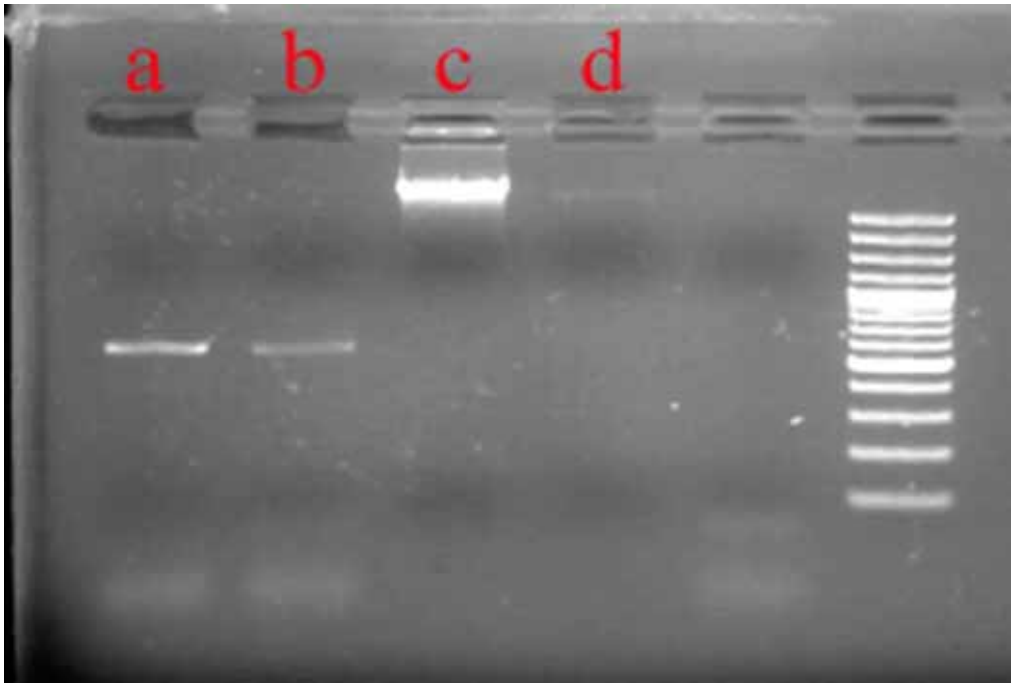

FIGURE 5
Comparing DNA samples obtained from plucked feathers and blood. (a; PCR product of a blood sample (♂), b; PCR product of a plucked feather (♂), c; genomic DNA from a blood sample, d; genomic DNA from a plucked feather.)

Under the light of all these information, molecular sampling method to be chosen depends on the species, environmental conditions, experience of the researchers and ultimately the preference of the researchers. A pilot study can answer all these questions and play a key role in choosing the method. However, it shouldn't be forgotten that despite their disadvantages, non-invasive and non-destructive genetic sampling methods are too valuable to ignore.

ACKNOWLEDGEMENTS

This study was summarized from the results of the masters project numbered 3543-YL1-13. We thank the Scientific Research Project Unit of Süleyman Demirel University (SDÜ-BAP) for their financial support.

REFERENCES

[1] Kiziroğlu, I. (2009) The Pocket Book for Birds of Türkiye. Ankamat Press, Ankara, 534p.
[2] Tabur, M.A. and Ayvaz, Y. (2004) Birds of Lake Beyşehir (Isparta – Konya). Turkish Journal of Zoology. 29, 361-369.
[3] Şekercioğlu, Ç.H., Daily, G.C., Ehrlich, P.R. (2004) Ecosystem consequences of bird declines. Proceedings of the National Academy of Sciences U.S.A. 101, 18042 – 18047.
[4] BirdLife International (2008) Over ten years, action by BirdLife Partners and others prevented the extinction of 16 bird species. http://www.birdlife.org/datazone/sowb/casestudy/268 (Accessed on 17.05.2014).
[5] Frankel, O.H. and Soulé, M.E. (1981) Conservation and Evolution. Cambridge University Press, Cambridge, 366p.
[6] Diamond, J. (1984) Normal extinction of isolated populations. In: Extinctions. Nitecki, M.H. (ed.) 1st ed. University of Chicago Press, Chicago, 191-246.
[7] Soulé, M.E., Wilcox, B.A. (1980) Conservation biology: an evolutionary-ecological perspective. Sinauer Associates, Sunderland, 395p.
[8] Soulé, M.E. (1985) What Is Conservation Biology. Bioscience. 35, 727-734.
[9] Sahney, S. and Benton, M. (2008) Recovery from the most profound mass extinction of all time. Proceedings of The Royal Society B. 275, 759-765.
[10] Spellerberg., I.F. (1996) Themes, terms and concepts. In: Conservation Biology. Spellerberg. I.F. (ed.) 1st ed., Longman, London, 18-35.
[11] Frankham, R. (2003) Genetics and Conservation Biology. Comtes Rendus Biologies. 326, 22-29.
[12] Frankham, R., Ballou, J.D., Briscoe, D.A. (2004) A Primer of Conservation Genetics. Cambridge University Press, Cambridge, 236p.
[13] Frankham, R. (2005) Genetics and extinction. Biological Conservation. 126, 131-140.
[14] Haig, S.M. (1998) Molecular contributions to conservation. Ecology. 79, 413-425.
[15] Somasundaram, S. and Kalaiselvan, M. (2011) Molecular tools for assessing genetic diversity. International Training Course on Mangroves and Biodiversity, Annamalai University, India, 82-91.
[16] Waits, L.P. and Paetkau, D. (2005) Noninvasive genetic sampling tools for wildlife biologists: a review of applications and recommendations for accurate data collection. Journal of Wildlife Management. 69, 1419-1433.
[17] Taberlet, P. and Bouvet, J. (1991) A single plucked feather as a source of DNA for bird genetic studies. Auk. 108, 959-960.
[18] Bello, N., Francino, O., Sánchez, A. (2001) Isolation of genomic DNA from feathers. Journal of Veterinary Diagnostic Investigation. 13, 162-164.
[19] Morin, P.A, Messier, J., Woodruff, D.S. (1994) DNA extraction, amplification, and direct sequencing from hornbill feathers. Journal of The Science Society of Thailand. 20, 31-41.
[20] Hogan, F.E., Cooke, R., Burridge, C.P., Norman, J.A. (2008) Optimizing the use of shed feathers for genetic analysis. Molecular Ecology Resources. 8, 561-567.
[21] Rudnick, J., Katzner, T.E., DeWoody, J.A. (2009) Genetic analyses of noninvasively collected feathers can provide new insights into avian demography and behavior. In: Handbook of Nature Conservation. Aranoff, J.B. (ed.) 1st ed. Nova Science Publishers, New York, 181-197.
[22] Griffiths, R., Double, M.C., Orr, K., Dawson, R.J.G. (1998) A DNA test to sex most birds. Molecular Ecology. 7, 1071-1075.
[23] Irwin, D.E., Bensch, S., Irwin, J.H., Price, T.D. (2005) Speciation by distance in a ring species. Science. 307, 414-416.
[24] Sambrook, J. and Russell, D.W. (2001) Molecular cloning: a laboratory manual. 3rd ed. Cold Spring Harbor Laboratory Press, New York.
[25] Horváth, M.B., Martínez-Cruz, B., Negro, J.J., Kalmár, L., Godoy, J.A. (2005) An overlooked DNA source for non-invasive genetic analysis in birds. Journal of Avian Biology. 36, 84-88.
[26] Isabel Miño, C. and Nassif Del Lama, S. (2009) Molted feathers as a source of DNA for genetic studies in waterbird populations. Waterbirds. 32, 322-329.
[27] Taberlet, P., Waits, L.P., Luikart, G. (1999) Noninvasive genetic sampling: look before you leap. Trends in Ecology and Evolution. 14, 323-327.

[28] Vili, N., Nemesházi, E., Kovács, S., Horváth, M., Kalmár, L., Szabó, K. (2013) Factors affecting DNA quality in feathers used for non-invasive sampling. Journal of Ornithology. 154, 587-595.
[29] MGM (2014) Meteoroloji Genel Müdürlüğü İklim İstatistikleri.
[30] Girgin, S., Kazancı, N., Duegel, M. (2004) On the limnology of deep and saline Lake Burdur in Turkey. Acta Hydrochimica et Hydrobiologica. 32, 189-200.
[31] Presti, F.T., Meyer, J., Antas, P.T., Guedes, N.M., Miyaki, C.Y. (2013) Noninvasive genetic sampling for molecular sexing and microsatellite genotyping of hyacinth macaw (*Anodorhynchus hyacinthinus*). Genetics and Molecular Biology. 36, 129-133.
[32] Mukesh, M.F., Mandhan, R., Sathyakumar, S. (2011) Comparison of different parameters of invasive and noninvasive sampling methods for microsatellite genotyping: A case study from Red Junglefowl and its application for other Galliformes. Journal of Research in Biology. 1, 38-43.
[33] Paul, N., Shum, J., Le, T. (2010) Hot start PCR, RT-PCR Protocols. Methods in Molecular Biology. 630, 301-318.
[34] Haig, S.M., Bronaugh, W.M., Crowhurst, R.S., D'Elia, J., Eagles-Smith, C.A., Epps, C.W., Knaus, B., Miller, M.P., Moses, M.L., Oyler-McCance, S. (2011) Genetic applications in avian conservation. Auk. 128, 205-229.
[35] McDonald, P.G., Griffith, S.C. (2011) To pluck or not to pluck: the hidden ethical and scientific costs of relying on feathers as a primary source of DNA. Journal of Avian Biology. 42, 197-203.
[36] Katzner, T.E., Wheeler, M., Negro, J.J., Kapetanakos, Y., DeWoody, J.A., Horvath, M., Lovette, I. (2012) To pluck or not to pluck: scientific methodologies should be carefully chosen, not "one size fits all". Journal of Avian Biology. 43, 15-17.
[37] Gebhardt, K.J., Waits, L.P. (2008) Cross-species amplification and optimization of microsatellite markers for use in six Neotropical parrots. Molecular Ecology Resources. 8, 835-839.

Received: **11.12.2016**
Accepted: **22.11.2017**

CORRESPONDING AUTHOR

Ismail Burak Karaceylan
Süleyman Demirel University,
Faculty of Science and Arts,
Department of Biology,
Isparta – Turkey

e-mail: burak277@gmail.com

© by PSP Volume 27 – No. 2/2018, pages 710-719 Fresenius Environmental Bulletin

AN ASSESTMENT OF CARBON DIOXIDE EMISSIONS RELATED TO FUEL CONSUMPTION FOR SUNFLOWER CULTIVATION

H Huseyin Ozturk*

Engineering of Agricultural Machinery and Technologies, Faculty of Agriculture, University of Cukurova, 01330 Adana, Turkey

ABSTRACT

The main objective of this study to quantify and evaluate CO_2 emissions related to fuel consumption for the second crop sunflower cultivation in agricultural regions of Turkey. The farms, cultivated sunflower as the second crop, were surveyed in all agricultural regions of Turkey. The total diesel consumption of the tractor and combine harvester was 59.95 L per hectare. The total diesel consumption for seedbed preparation was 29.45 L per hectare. It was found that the total fuel (diesel+lubricant oil), energy consumptions and CO_2 emissions for the second crop sunflower cultivation were 60.62 L/ha, 2249.74 MJ/ha and 166.48 kgCO_2/ha, respectively. The specific values of fuel consumption, seed production, energy consumption related to total fuel and CO_2 emission were to be 32.42 L/t, 30.85 kg/L, 1203.07 MJ/t and 89.03 kgCO_2/t, respectively.

KEYWORDS:
Sunflower cultivation, CO_2 emissions, fuel consumption.

INTRODUCTION

Sunflower is one of the leading oilseed crops cultivated for the production of oil mainly used for human consumption. It has also been considered as an important crop for biodiesel production, particularly in southern European countries [1]. Different studies on the environmental impact of biodiesel produced from sunflower were published. The effective savings of CO_2 emissions of first generation biofuels are limited by the high energy input required for crop cultivation and biomass conversion to fuel [2]. De Marco et al., [3] performed an environmental analysis of biodiesel production on pilot scale from sunflower oil. The higher emissions of biodiesel production are due to the high "land consumption" for the agricultural phase, to the carbon dioxide emissions from diesel engines, which burn the fuels in the agricultural phase. Kallivroussis et al., [1] aimed to study the energy input and output per hectare for the production of sunflower and to evaluate the crop as a source of biodiesel in Greece. The total fuel and fuel energy consumed were calculated to be 64 kg and 3558 MJ per hectare.

In Turkey, sunflower was cultivated in total of 685 317.4 hectares area in Turkey. The total production was 1 680 700 tons in 2015 [4]. Production values of sunflower cultivation for oil production in dry and irrigated conditions are given in Table 1. Sunflower as the second crop was cultivated in 961 ha area in 2015.

Sunflower cultivation in Turkey heavily depends on fossil fuels which in turn lead to many environmental problems. The approximately 35% of the total agricultural production inputs are mechanization inputs. The 20% of total mechanization inputs belongs to purchase of agricultural tools/machines and 15% of these inputs are related to fuel consumptions of tools/machines. First of all the selection of agricultural tools/machines have appropriate capability and capacity is very important for mechanization planning. Another factor in this regard is the tractor selection according to farm size. These two factors are the most important criteria for fuel consumption accounts for about half of the total operating costs of agricultural machinery. Selecting the proper tractor for agricultural farms is important, the selection of appropriate tools/machines for the tractors is also important. The highest priority processing steps are tillage and sowing stages to increase crop yield and to reduce the negative impacts on the environment. Fuel and time consumptions are too high in these process steps. About 70% and 50% of the total fuel and time consumptions takes place in these processes in dry and irrigated agriculture, respectively. In addition, about 30% and 25% of the total production costs relate to tillage and sowing operations in irrigated agriculture in dry and irrigated agriculture, respectively. Tillage and sowing stages are operation steps that lead to environmental pollution.

The biggest problem in use of tractor completed its economic life is fuel costs. According to field works, old tractors causes more fuel consumption by 30% compared to new one. When using a tractor has completed its useful life, about 700 liters more fuel are consumed in a year. Therefore, 1816 kg more CO_2 emissions are released. In addition, toxic emissions such as 80 kgNOx/year, 56

kgCO/year and 82 kgHC/year are released. In case of renewal of farm tractors who have completed their economic life, exhaust and noise emissions are reduced [5].

Comprehensive studies have been performed by several authors regarding to assessment of the environmental impacts and CO_2 emissions for different processes and industries in different countries of all over the world [6–31]. Regarding environmental sustainability, in recent years it has become of major interest to evaluate cropping systems in terms of energy consumption. The reduction of energy consumption in agriculture became particularly relevant partly because fossil energy is a limited resource to be conserved for future generations [32] and it contributes to greenhouse gas emissions in the atmosphere [33].

Fossil energy used and CO_2 emissions released in cultivation of any crop could be used as one of the relevant factors to indicate the crop long-term sustainability. The energy input and output of three energy crops (rapeseed, soybean and sunflower) in low input system (LIS) and high input system (HIS) in Europe has been reviewed by Venturi and Venturi [34]. They determined that energy inputs related to fuel consumption for rapeseed, soybean and sunflower were to be 5-19 GJ/ha, 10-16.1 GJ/ha and 9-19 GJ/ha in LIS and HIS, respectively. Sheikh Davoodi and Houshyar [35] evaluated energy consumption of canola and sunflower production. Energy inputs related to diesel consumption per hectare for different practices of canola and sunflower cultivation were determined as follows: seed bed preparation 2739.81 MJ and 3122.71 MJ, sowing 2283.92 MJ and 1973.43 MJ, fertilizer application and spraying 361.39 MJ and 248.16 MJ and harvesting 818.86 MJ and 1050.15 MJ, respectively. Cavalaris et al., [36] compared conservation tillage with conventional to investigate the potential for energy reduction. Tillage energy was estimated by field measurements of the consumed power for sunflower cultivation. Fuel consumptions were measured to be 49.21 L/ha, 7.16 L/ha and 8.77 ML/ha for mouldboard plough, disc harrow and field cultivator, respectively.

Rodrigues et al [37] developed a model and various scenarios were considered in order to assess the impacts on the crops' energy balance of (1) full and deficit irrigation, (2) climatic demand scenarios, and (3) upgrading irrigation systems performance. Iriarte et al. [38] used Life Cycle Assessment (LCA) to compare environmental impacts and energy and water demand of rapeseed (*Brassica napus* L.) and sunflower (*Helianthus annuus* L.) in Chile. The results indicate that, compared to sunflower, rapeseed production has a better environmental performance in 9 out of the 11 impact categories evaluated, and lower water consumption. The energy demand of rapeseed is 4.9 GJ/t seed, 30% less than that of sunflower.[2] greenhouse gas emissions and energy balance of sunflower biodiesel. Nassoa et al., [39], compared the energy use of a 12-year rainfed cropping system, located in Tuscany, Italy. The system is cultivated under two different management intensities: a conventional system (CS) and a low input system (LIS) for a six-year crop rotation that included sugar beet, durum wheat, sorghum, sunflower and durum wheat. The direct energy input was 7.6 GJ/ha and 5.3 GJ/ha for CS and LIS, respectively. While the direct energy input for soil tillage was 4.5 GJ/ha for CS, it was 3.2 GJ/ha for LIS.

The main objective of this study to quantify and evaluate CO_2 emissions related to fuel consumption for the second crop sunflower cultivation in agricultural regions of Turkey. The farms, cultivated sunflower as the second crop, were surveyed in all agricultural regions of Turkey in 2015. Taking actual farm size as the variable, the total 332 farms was randomly selected by using stratified random sampling. The data were obtained related to energy inputs used for different field operations and yield. The energy related to fuel and lubricant oil consumed by agricultural tractor used with agricultural implements/machinery during cultivating operations was evaluated as a direct energy input. The CO_2 emissions associated with direct fuel and lubricant oil consumptions are estimated according to the Intergovernmental Panel on Climate Change (IPCC) approach. The specific values for fuel consumption, seed production, energy consumption and CO_2 emission were defined to analyze the relationship between fuel consumption and CO_2 emission for the second crop sunflower production.

TABLE 1
Production values of sunflower cultivation for oil production in Turkey [4]

First crop				*Second crop*			
Dry		Irrigated		Dry		Irrigated	
Area (ha)	Production (ton)	Area (ha)	Production (ton)	Area (ha)	Production (ton)	Area (ha)	Production (ton)
420 390.6	958 000	137 835.9	514 320	961	1 520	9 713.8	26 160

MATERIALS AND METHODS

In this study, the farms, cultivated sunflower as the second crop, were surveyed in all agricultural regions of Turkey. The data were obtained related to energy inputs used for different field operations and yield. The sample size has been calculated following equation. The permissible error was defined to be 5 % for 95 % reliability [40].

$$n = \left(\sum N_h S_h\right)^2 / \left(N^2 D^2 + \sum N^h S_h^2\right) \quad (1)$$

where; n is the required sample size, N is the number of holdings in target population, N_h is the number of population in h the stratified, S_h is the variance of h the stratified, and D is the precision where (x-X).

Cultivation practices for sunflower production. Cultural practices applied in the conventional system for the second crop sunflower are given in Table 2. Sunflower cultivation analyzed in this study corresponds to representative practices in Turkey. Sunflower is normally grown in crop rotation and under intensive farming. Two power categories of tractors have been used in field operations. Tractor has two wheels drive and 55 kW power has been used for the light tasks such as secondary tillage, sowing, spraying and fertilizing applications. On the other hand, tractor has four wheels drive and 75 kW power has been used for the heavier tasks such as tillage with a plough.

TABLE 2
Cultivation practices and mechanization implements for sunflower production

Cultivation practices	Implements
Tillage at a depth of 26-30 cm	Plough, 3 furrows of 35 cm width
Fertilizing, 25-30 kgP_2O_5/ha	Centrifugal fertilizing machine, 2 discs
Tillage at a depth of 3-4 cm	Disc harrow, 20 discs, 3 m width
Sowing at 4-5 cm depth, 10 kg/ha	Pneumatic sowing machine, four rows
Hoeing for weed control	Hoeing machine, five rows
Fertilizing, 70-80 kgN/ha	Hoeing machine with fertilizing, five rows
Herbicide application	Sprayer, 10-14 m width, 800-1000 L capacity
Harvesting	Combine harvester

Determination of fuel energy inputs. The energy related to fuel and lubricant oil consumed by agricultural tractor used with agricultural implements/machinery during cultivating operations was evaluated as a direct energy input. In this sense, the calculation methods for the direct energy inputs per hectare are given.

Diesel energy input. The fuel energy inputs per hectare related to diesel fuel consumed by agricultural tractor and combine harvester have been calculated as follows:

$$E_{FC} = M_f \times LHV_f \quad (2)$$

where;
E_{FC}=the fuel energy input per hectare (MJ/ha),
M_f=diesel fuel consumed by tractor or combine harvester (L/ha) and
LHV_f=the lower heating value of diesel fuel (MJ/L).

The lower heating values depending on fuel types were taken from IPCC, 1996, Volume 2, Section 1 [41]. The lower heating values used in calculations for the diesel fuel and lubricant oil are given in Table 3.

TABLE 3
Emission factors and heating values for diesel fuel and lubricant [41]

Fuel type	Lower heating value (GJ/L)	Emission factors (kg CO_2/GJ)
Diesel	0.0371	74.01
Lubricants	0.0382	73.28

Lubricant oil energy input. The direct energy inputs related to lubricant oil consumptions were determined taking into account hourly lubricant oil consumption values of agricultural tractor used for cultivation operations and combine harvester used for harvesting operations in the second crop sunflower production. Therefore, the total energy input related to lubricant oil consumption per unit production area (ha) was determined as follows:

$$E_{TLC} = E_{LC,T} + E_{LC,C} \quad (3)$$

where;
E_{TLC}=the total lubricant oil energy input (MJ/ha),
$E_{LC,T}$= energy input for lubricant oil consumed by agricultural tractor (MJ/ha) and
$E_{LC,C}$= energy input for lubricant oil consumed by combine harvester (MJ/ha).

The energy inputs related to lubricant oil consumed by agricultural tractor and combine harvester were estimated multiplying the oil consumption with the lower heating value of the lubricant oil.

$$E_{LC} = M_l \times LHV_l \quad (4)$$

where;
E_{LC}=the lubricant oil energy input (MJ/ha),
M_l=the lubricant oil consumed by tractor or combine harvester (L/h) and
LHV_l=the lower heating value of oil (MJ/L).

The hourly lubricant oil consumption of agricultural tractors, depending on the maximum power take off (PTO) for the tractor, has been calculated as follows [42]:

$$M_{l,T} = 0.00059 \times PTO_{\max} + 0.02169 \quad (5)$$

where;

$M_{l,T}$=the lubricant oil consumed by tractor (L/h) and PTO_{max}=the max. power take off for tractor (kW).

The maximum PTO for tractor used in cultivation operations was estimated based on the nominal power of tractor (NP) [42].

$$PTO_{\max} = 0.88 \times NP \quad (6)$$

where; *NP* is the power of tractor (kW).

The hourly lubricant oil consumption of combine harvester, depending on the engine power, has been calculated as follows [42]:

$$M_{l,C} = 0.004 \times P_e \quad (7)$$

where;

$M_{l,C}$=the lubricant oil consumed by combine harvester per hour (L/h) and

P_e=engine power of combine harvester (kW).

Calculation methodology used for CO_2 emissions. The CO_2 default emission factors depending on fuel type based on lower heating values are from IPCC, 1996, Volume 2, Section 1 [41] (Table 3). The methods for calculating CO_2 emissions recommended by the *GHG Protocol - Mobile Guide (03/21/05) v1.3 (Calculating CO2 Emissions from Mobile Sources Guidance to calculation worksheets)* were used in this study. The following equations the suggested approach to calculating CO_2 emissions based on fuel use.

CO_2 emissions = Fuel used x Heating value x Emission factor
Diesel-based CO_2 emissions = Diesel used x Heating value x Emission factor
Diesel-based CO_2 emissions = L/ha x 0.0371 GJ/L x 74.01 kgCO_2/GJ (8)
Diesel-based CO_2 emissions = kgCO_2/ha
Lubricant oil-based CO_2 emissions = Oil used x Heating value x Emission factor
Lubricant oil-based CO_2 emissions = L/ha x 0.0382 GJ/L x 73.28 kgCO_2/GJ (9)
Lubricant oil-based CO_2 emissions = kgCO_2/ha

The specific fuel consumption. The specific fuel consumption (S_{FC}) and specific seed production (S_{SP}) were defined to analyze the relationship between fuel consumption and sunflower production. The value of the specific fuel consumption (S_{FC}) indicates the amount of fuel consumed (L) to produce the unit quantity (t) of seed product.

$$S_{FC} = FC / GY \quad (10)$$

where S_{FC} is the specific fuel consumption (L/t), *FC* is fuel consumption (L/ha) and *GY* is seed yield (ton/ha).

The specific seed production. The specific seed production (S_{SP}) is the ratio of fuel consumption to corn yield and indicates fuel consumption (L) per kg of sunflower seed.

$$S_{SP} = SP / FC \quad (11)$$

where S_{SP} is the specific seed production (kg/L), *SP* is seed production per hectares (kg/ha) and *FC* is fuel consumption per hectares (L/ha).

The specific energy consumption. The specific energy consumption (S_{EC}) is the ratio of energy consumption to seed yield and indicates energy consumption (GJ) per ton of sunflower seed.

$$S_{EC} = EC / FC \quad (12)$$

where S_{SP} is the specific energy consumption (GJ/t), *EC* is energy consumption per hectares (GJ/ha) and FC is *GY* is seed yield (ton/ha).

The specific carbon dioxide emission. The specific carbon dioxide emission (S_{CO2}) was defined to analyze the relationship between CO_2 emissions and corn production. The S_{CO2} is the ratio of total CO_2 emissions to corn grain yield and indicates CO_2 emissions (kgCO_2) per ton of sunflower seed.

$$S_{CO2} = CO_2 / GY \quad (13)$$

where S_{CO2} is the specific carbon dioxide emission (kgCO_2/ton), CO_2 is carbon dioxide emissions (kgCO_2/ha) and *GY* is seed yield (ton/ha).

RESULTS AND DISCUSSION

Diesel fuel consumption and CO_2 emissions for sunflower cultivation. The change of diesel fuel consumptions, CO_2 emissions and related energy consumptions for sunflower cultivation is given in Fig. 1 and Fig. 2, respectively. The diesel and related energy consumptions with the agricultural implements and machines for sunflower cultivation are given in Table 4. The total diesel consumption of the tractor with the implements/machines and combine harvester was 59.95 L per hectare. Considering diesel consumption with the implements and machines for the second crop sunflower cultivation, the following results can be drawn:

- The total diesel consumption for seedbed preparation was 29.45 L per hectare. This value corresponds to 49.12% of the total fuel consumption for sunflower cultivation.
- The 61.62% of the total fuel for seedbed preparation was consumed during tillage with plough. The fuel consumption with plough was 18 L per hectare. Since the plough was pulled at the greatest depth, it was the most fuel consuming implement.
- The chisel had lower energy demand than the other tillage implements. The fuel consumption with disk harrow and chisel were 8.2 L/ha and 3.25 L/ha, respectively.
- Fuel consumption with combine harvester was 17 L per hectare during harvesting. This consumption corresponds to 28.36% of the total fuel consumption for sunflower cultivation.
- The 77.48% of the total fuel (46.45 L/ha) was consumed for seedbed preparation with tillage implements and harvesting with combine harvester.

The total CO_2 emissions for sunflower cultivation were calculated as 164.61 $kgCO_2$ per hectare (Fig.1). As it might be expected, CO_2 emissions increased linearly as the amount of fuel consumption increased. The highest CO_2 emission released during tillage operations followed by harvesting with the combine harvester. The total 80.86 $kgCO_2$ per hectare was released during the tillage operations.

In response to amounts of diesel fuel used for per unit area (59.95 L/ha), the totally 2224.15 MJ fuel energy was consumed per unit area (ha) (Fig. 2). This result lower than that of [1]. They found that the total fuel and fuel energy consumed were calculated to be 64 kg and 3558 MJ per hectare. However, [43] the fuel energy consumption in sunflower production processes is realized depending on the amount of diesel fuel consumed in these production processes. The maximum fuel energy consumption was realized during tillage with plough (667.8 MJ/ha). The tillage operation with plough are followed by harvesting with combine harvester (630.7 MJ/ha) disc harrow application (304.22 MJ/ha) and hoeing and fertilizing application (222.6 MJ/ha), respectively. On the other hand, Sheikh Davoodi and Houshyar [35] evaluated energy inputs related to diesel consumption per hectare for different practices of sunflower cultivation. They determined as follows: seed bed preparation 3122.71 MJ, sowing 1973.43 MJ, fertilizer application and spraying 248.16 MJ and harvesting 1050.15 MJ, respectively.

Lubricant oil consumption and CO_2 emissions for sunflower cultivation. The change of the lubricant oil consumptions and related CO_2 emissions for sunflower cultivation is given in Fig. 3 and Table 5. The total lubricant oil consumption of the tractor with the implements/machines and combine harvester was 0.67 L per hectare. [43] In response to these amounts of lubricant oil used for per unit area (ha), the totally 25.59 MJ oil energy was consumed per unit area (ha) (Table 5). The total CO_2 emissions related to lubricant oil consumptions were found to be 1.88 $kgCO_2$ per hectare (Fig.3).

TABLE 4
Diesel consumptions and CO_2 emissions for implements and machines

Tools and machines	Diesel Consumption		Fuel energy (MJ/ha)	CO_2 emission ($kgCO_2$/ha)
	L/ha	%		
Plough	18.00	30.03	667.8	49.42
Chisel	3.25	5.42	120.575	8.92
Disk harrow	8.20	13.68	304.22	22.52
Sowing machine	5.05	8.42	187.355	13.87
Hoeing+fertilizing	6.00	10.01	222.6	16.47
Sprayer	2.45	4.09	90.895	6.73
Combine harvester	17.00	28.36	630.7	46.68
Total	***59.95***	***100***	***2224.15***	***164.61***

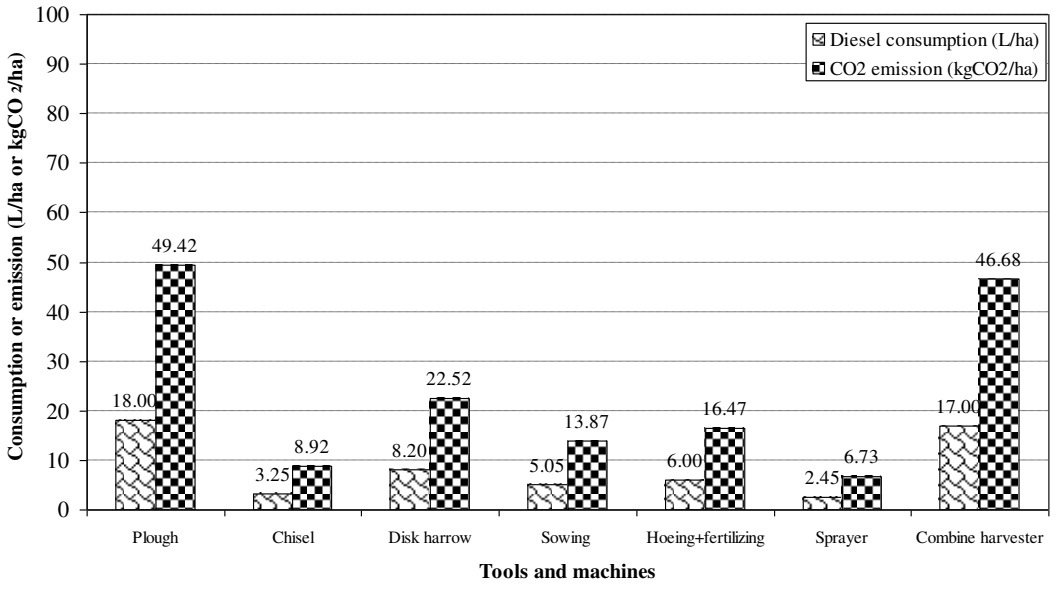

FIGURE 1
The change of diesel consumptions and CO_2 emissions for tools and machines

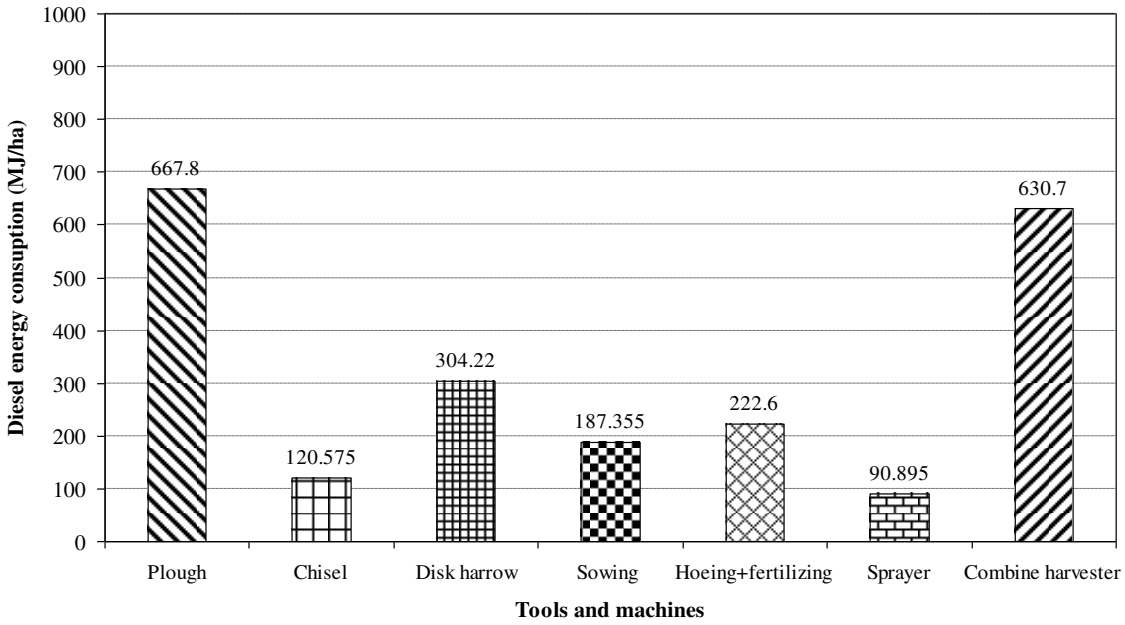

FIGURE 2
The change of diesel energy consumptions for tools and machines

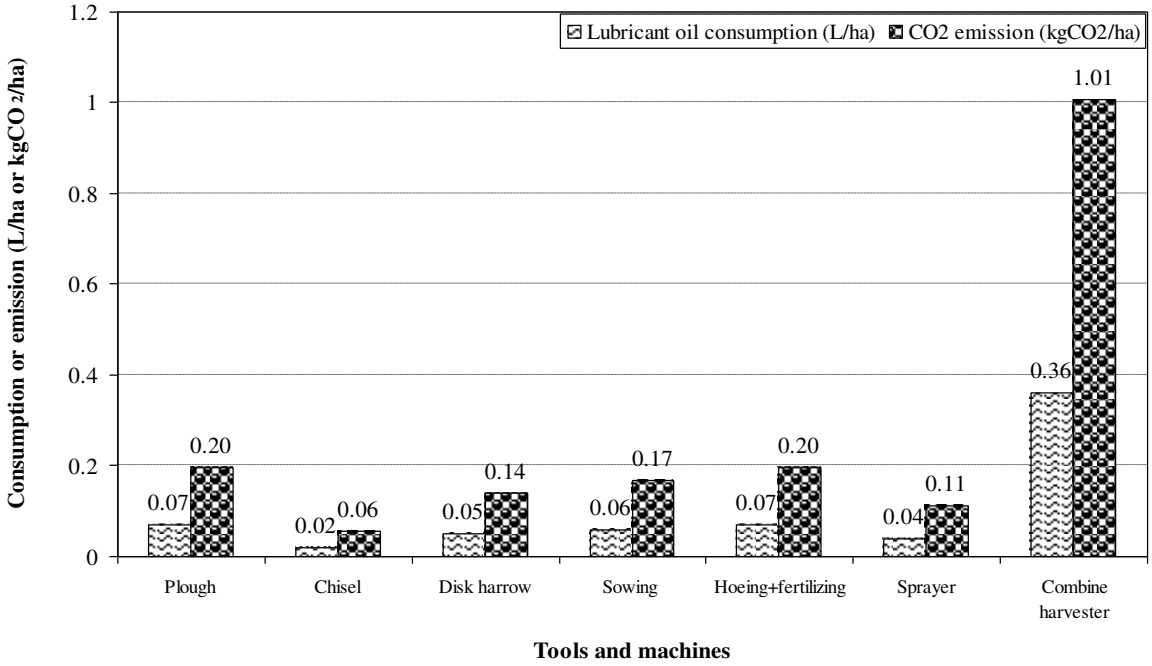

FIGURE 3
The change of oil consumptions and CO_2 emissions for tools and machines

TABLE 5
The lubricant oil consumptions and CO_2 emissions for implements and machines

Tools and machines	Lubricant oil consumption		Fuel energy (MJ/ha)	CO_2 emission ($kgCO_2$/ha)
	L/ha	%		
Plough	0.07	10.45	2.67	0.20
Chisel	0.02	2.99	0.76	0.06
Disk harrow	0.05	7.46	1.91	0.14
Sowing machine	0.06	8.96	2.29	0.17
Hoeing+fertilizing	0.07	10.45	2.67	0.20
Sprayer	0.04	5.97	1.53	0.11
Combine harvester	0.36	53.73	13.75	1.01
Total	***0.67***	***100***	***25.59***	***1.88***

The 0.36 kg lubricant oil was consumed for harvesting operation with combine harvester. Thus, the highest CO_2 (1.01 kg per hectare) released for this operation due to highest oil consumption.

Specific parameters for sunflower cultivation. It was found that the total fuel (diesel+lubricant oil), energy consumptions and CO_2 emissions for the second crop sunflower cultivation were 60.62 L/ha, 2249.74 MJ/ha and 166.48 kgCO_2/ha, respectively. The specific parameters for the second crop sunflower cultivation are given in Table 6.

The specific fuel consumption. The specific values of fuel consumption, seed production and CO_2 emissions were calculated for sunflower cultivation and given in Fig. 4. The specific fuel consumption (L/t) defined as the ratio of the total amount fuel (L) consumed in the production process to the total amount of harvested product (t). The specific fuel consumption can be calculated based on dividing fuel consumption (L) by seed yield (tone=1000 kg). The value of the specific fuel consumption indicates the amount of fuel consumed (L) to produce the unit quantity (t) of seed product. The specific value of fuel consumption was 32.42 L per ton sunflower seed. The lower value of the specific fuel consumption means the energy efficiency of production is higher. Taking into account the values of specific fuel consumption, 32.42 L fuel (diesel+lubricant oil) was consumed to produce 1 tone sunflower seed.

The specific seed production. The average seed yield was found to be 1870 kg per hectare for the second crop sunflower cultivation. Some research results in Turkey indicated that the average seed yield can be in the range of 1500–1600 kg/ha, 2250–2500 kg/ha, 2750–3000 kg/ha and 3500–4000 kg/da for dry conditions, one time irrigated, two times irrigated and three times irrigated, respectively. Kallivroussis et al., [1] determined that seed yield 1800 kg per hectare for normally fertilized conditions in Greece. The average seed yield in Europe and Italy was to be 1500 kg and 1800–2000 kg per hectare.

The specific seed production (kg/L), as the inverse of the specific fuel consumption value, was defined as the ratio of the total amount of harvested seed product (kg) to the total amount of fuel (L) used in the cultivation process. The specific value of the seed production indicates the total amount of harvested product (kg) from the unit production area (ha) corresponds to the unit amount of fuel (L) consumed for the unit production area (ha). The specific seed production was 30.85 kg/L for the second crop sunflower cultivation (Fig. 4). The higher value of the specific seed production means the energy efficiency of production is higher. Considering the specific value of seed production, 1 L fuel (diesel+lubricant oil) was consumed to produce 30.85 kg sunflower seed.

TABLE 6
The specific parameters for sunflower cultivation

Yield (kg/ha)	Diesel + oil consumption (L/ha)	Energy (Diesel+oil) consumption (MJ/ha)	CO_2 emissions (kgCO_2/ha)	S_{FC} (L/t)	S_{SP} (kg/L)	S_{EC} (MJ/t)	S_{CO2} (kgCO_2/t)
1870	60.62	2249.74	166.48	32.41711	30.8479	1203.069	89.02914

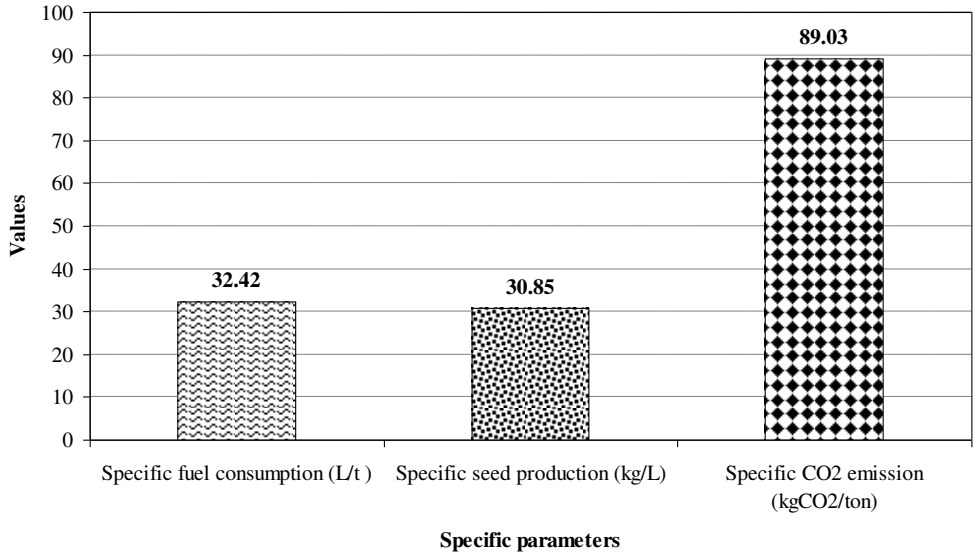

FIGURE 4
The specific parameters for sunflower cultivation

The specific energy consumption. The specific energy consumption (S_{EC}) defined as the ratio of energy consumption (GJ/ha) to the total amount of obtained seed per hectares (t/ha). The specific value of the energy consumption indicates the amount of energy consumed (L) to produce the unit quantity (t) of seed product. It was found that the specific value of energy consumption related to total fuel (diesel+lubricant oil) was to be 1203.07 MJ per ton seed (Fig. 4). The lower value of the specific fuel consumption means the energy efficiency of production is higher. Taking into account the specific value of energy consumption, 1203.07 MJ fuel energy (diesel+lubricant oil) was consumed to produce 1 tone sunflower seed.

The specific carbon dioxide emission. The specific carbon dioxide emission (S_{CO2}) was defined to analyze the relationship between CO_2 emissions and seed yield. The S_{CO2} is the ratio of total CO_2 emissions to sunflower seed yield and indicates CO_2 emissions ($kgCO_2$) per ton of sunflower seed. The specific value of CO_2 emission was calculated as 89.03 $kgCO_2$/t (Fig. 4). The lower value of the specific CO_2 emissions means cultivation system in terms of CO_2 emissions is efficient. Taking into account the specific value of CO_2 emission, 89.03 kg CO_2 was released to produce 1 tone sunflower seed.

CONCLUSIONS

The diesel and lubrication oil consuptions for CO_2 emissions were two of the most significant determinants of the total energy input for sunflower cultivation. Especially field operations consuming more fuel should be applied based on scientific data to reduce fuel consumption. To reduce fuel consumption in soil tillage practices, unnecessary operations should be avoided in tillage. Consideration should be given to conservative and reduced tillage practices. The land size, production patterns and soil structure should be considered in the selection of agricultural mechanization tools. Agricultural machinery and equipments are required to be renewed at the end of a given study periods. Use of tractors completed economic life cause a lot of environmental pollution as well as economic losses. The precision farming techniques can be used utilized in all stages of plant production until tillage to harvest. For this purpose, decision support system is required. However, sensing, monitoring, control and data transfer systems are necessary for precision farming operations.

Agricultural policies should emphasize development of new technologies and alternative energy resources aiming efficient use of energy. In addition to these, the results imply that Turkish field crop production might be considered as sensitive to changes in prices and availability of fossil fuels due to mainly its significant share in total consumed energy in field crop production. The results of this study can be used by policy makers and other relevant agencies for recommendations to farmers in order to use energy more efficiently.

REFERENCES

[1] Kallivroussis, L., Natsis A. and Papadakis, G. (2002) The energy balance of sunflower production for biodiesel in Greece. Biosystems Engineering. 81(3), 347–354.

[2] Iriarte, A. and Villalobos, P. (2013) Greenhouse gas emissions and energy balance of sunflower biodiesel: Identification of its key factors in the supply chain. Resources, Conservation and Recycling. 73, 46–52.

[3] De Marco, I., Miranda, S., Riemma, S. and Iannone, R. (2016) Biodiesel production from sunflower: an environmental study. Chemical Engineering Transactions. 49, 331–336.

[4] TURKSTAT (2016) Turkish Statistic Foundation. Ankara, Turkey.

[5] Evcim, H.U., Ulusoy, E., Gülsoylu, E. and Tekin, B. (2007) Agricultural mechanization in Turkey: Problems and solutions. Technical Congress of Agricultural Engineering, 1–20, Ankara, Turkey.

[6] Bacenetti, J. and Fiala, M. (2015) Carbon footprint of electricity from anaerobic digestion plants in Italy. Environmental Engineering and Management Journal. 14(7), 1495–1502.

[7] Farcas, V., Ilies, N. and Cot, R. (2013) CO_2 and energy footprint of different retaining walls solutions. Environmental Engineering and Management Journal. 14(6), 1323–1326.

[8] Popiţa, G.E., Frunzeti, N., Ionescu, A., Lazăr, AL., Baciu, C., Popovici, A., Pop, C., Faur, VC. and Proorocu, M. (2013) Evaluation of carbon dioxide and methane emission from Cluj-Napoca municipal landfill, Romania. Environmental Engineering and Management Journal. 14(6), 1389–1398.

[9] Robu, B., Zaharia, C. and Macoveanu, M. (2005) Environmental impact assessment for steel processing. Environmental Engineering and Management Journal. 4(1), 51–66.

[10] Mitran, G. and Ilie, S. (2014) Method for inventorying CO emissions from road traffic in urban areas through transport modeling. Environmental Engineering and Management Journal. 13(8), 1945–1956.

[11] Szabo, G., Fazekas, I., Szabo, S., Szabo, G., Buday, T., Paladi, M., Kisari, K. and Kerenyi A. (2014) The carbon footprint of a biogas power plant. Environmental Engineering and Management Journal. 13(11), 2867–2874.

[12] Yang, L., Wang, J.M. and Pan, H. (2014) Relationship between energy consumption, economic development and carbon emissions in China. Environmental Engineering and Management Journal. 13(5), 1173–1180.
[13] Tang, Z., Shang, J. and Shi, C. (2013) Estimation of carbon dioxide emissions and spatial variation from tourism accommodation in China. Environmental Engineering and Management Journal 12(10), 1921–1926.
[14] Soceanu, A., Dobrinas, S., Stanciu, G., Coatu, V. and Epure, D.T. (2009) Residues of polycyclic aromatic hydrocarbons in different stages of Capsicum annuum (pepper) and Solanum lycopersicum (tomato) growing. Environmental Engineering and Management Journal. 8(1), 49–54.
[15] Liu, M., Li, W., Cheng, Q., He, Y. and Cao, X. (2011) Life cycle assessment for carbon emission of plate glass industry. Environmental Engineering and Management Journal. 10(6), 739–744.
[16] Chiriac, R. and Descombes, G. (2010) Fuel consumption and pollutant emissions reduction for diesel engines by recovery of wasted energy. Environmental Engineering and Management Journal. 9(10), 1335–1340.
[17] Dumitrascu, G. and Horbaniuc, B. (2010) Solar-assisted Joule-Brayton engines used to reduce carbon dioxide emissions. Environmental Engineering and Management Journal. 9(10), 1431–1436.
[18] Iosip, A., Hortal, M., Dobón, A. and Bobu E. (2010) Comparative environmental impact assessment of corrugated board production. Environmental Engineering and Management Journal. 9(9), 1281–1288.
[19] Quesada, J.M., Villar, E., Madrid-Salvador, M. and Molina, V. (2010) The gap between CO_2 emissions and allocation rights in the Spanish industry. Environmental Engineering and Management Journal. 9(9), 1161–1164.
[20] Zaharia, M., Robu, T. and Irimia, N. (2010) Ecological agriculture: Dynamics of the biological activities in soils cultivated with maize under the influence of organic fertilization. Environmental Engineering and Management Journal. 9(10), 1437–1442.
[21] Dinca, C., Badea, A.A., Apostol, T. and Lazaroiu, *G.* (2009) GHG emissions evaluation from fossil fuel with CCS. Environmental Engineering and Management Journal. 8(1), 81–89.
[22] Grec, A., Dumescu, F. and Maior, C. (2009) Assessment of the environmental impacts generated by rubber processing activity. Environmental Engineering and Management Journal. 8(6), 1533–1540.
[23] Gaba, A., Iordache, S., Vladescu, M., Ungureanu, D. and Vizureanu, P. (2009) Reducing of pollutants emissions and heavy liquid fuels consumption in boilers by using of additives. Environmental Engineering and Management Journal. 8(5), 1241–1246.
[24] Meghea, I., Mihai, M., Lacatusu, I. and Apostol, T. (2009) Environmental monitoring of CO emissions: statistical character of acquired data. Environmental Engineering and Management Journal. 8(3), 575–582.
[25] Mihailescu, N., Daescu, V., Holban, E., Badea, M.N. and Paceagiu, J. (2009) Energy conservation and CO_2 emissions reduction for clinker portland cement manufacturing process. Environmental Engineering and Management Journal. 8(4), 947–952.
[26] Rem, P.C., Olsen, S., Welink, J.H. and Fraunholcz, N. (2009) Carbon dioxide emission associated with the production of plastics –a comparison of production from crude oil and recycling for the Dutch case. Environmental Engineering and Management Journal. 8(4), 973–980.
[27] Soceanu, A.D., Dobrinas, S., Popescu, V., Stanciu, G. and Epure, D.T. (2012) OCPs and PAHs distribution in different stages of tomato growing. Environmental Engineering and Management Journal. 11(2), 457–462.
[28] Ţenu, I., Jităreanu, G., Muraru-Ionel, G., Cojocariu, P. and Muraru, V.G. (2009) The impact of mechanization technologies on soil. Environmental Engineering and Management Journal. 8(5), 1263–1268.
[29] Gavrilescu, D. (2008) Carbon dioxide generation - implications for Romanian pulp and paper industry. Environmental Engineering and Management Journal. 7(2), 111–117.
[30] Robu, B., Jitar, O., Teodosiu, C., Strungaru, S.A., Nicoara, M. and Plavan, G. (2015) Environmental impact and risk assessment of the main pollution sources from the Romanian Black Sea coast. Environmental Engineering and Management Journal. 14(2), 331–340.
[31] Zaharia, C. and Surpateanu, M. (2002) The impact of energy production on environment in Romania. Environmental Engineering and Management Journal. 1(3), 313–324.
[32] WCED. (1987) World Commission on Environment and Development. Our common future (The Brundtland Report). Oxford University Press, Oxford.
[33] Seguin, B., Arrouays, D., Balesdent, J., Soussana, J.F., Bondeau, A. and Smith, P. (2007) Moderating the impact of agriculture on climate. Agr. Forest. Meteorol. 142(4), 278–287.
[34] Venturi, P. and Venturi, G. (2003) Analysis of energy comparison for crops in European agricultural systems. Biomass and Bioenergy. 25, 235–255.

[35] Davoodi, M.J.S. and Houshyar, E. (2009) Energy consumption of canola and sunflower production in Iran. American-Eurasian J. Agric. & Environ. Sci. 6(4), 381–384.
[36] Cavalaris, C., Karamoutis C., Fountas, S. and Gemtos, TA. (2008) Sunflower oil energy budget for in-farm oil production under four tillage systems. Eurageng 2008 World Congress. Crete.
[37] Rodrigues, G.C., Carvalho, S., Paredes, P., Silva, F.G. and Pereira, L.S. (2010) Relating energy performance and water productivity of sprinkler irrigated maize, wheat and sunflower under limited water availability. Biosystems Engineering. 106(2), 195–204.
[38] Iriarte, A., Rieradevall, J. and Gabarrell, X. (2010) Life cycle assessment of sunflower and rapeseed as energy crops under Chilean conditions. Journal of Cleaner Production. 18(4), 336–345.
[39] Nasso, N.N., Bosco, S., Di Bene, C., Coli, A., Mazzoncini, M. and Bonari, E. (2011) Energy efficiency in long-term Mediterranean cropping systems with different management intensities. Energy. 36(4), 1924–1930.
[40] Yamane, T. (1967) Elementary Sampling Theory. N.J., USA. Prentice Hall Englewood Cliffs.
[41] IPCC. (1996) The Intergovernmental Panel on Climate Change. Volume 2, Section 1.
[42] [Ozturk, H.H. (2010) Energy Management in Plant Production. Hasad Publication. Istanbul, Turkey.
[43] Spinelli, D., Jez, S., Pogni, R. and Basosi, R. (2013) Environmental and life cycle analysis of a biodiesel production line from sunflower in the province of Siena (Italy). Energy Policy. 59, 492–506.

Received: **01.12.2017**
Accepted: **22.11.2017**

CORRESPONDING AUTHOR

H. Huseyin Ozturk
Engineering of Agricultural Machinery and Technologies, Faculty of Agriculture,
University of Cukurova,
01330 Adana – Turkey

e-mail: hhozturk@cu.edu.tr

© by PSP Volume 27 – No. 2/2018 pages 720-726 Fresenius Environmental Bulletin

THE EFFECT OF ACID ON THE SURFACES OF SOME NATURAL STONES FROM TURKEY

Halim Cevizci*

Suleyman Demirel University, Mining Engineering Department, Isparta, Turkey

ABSTRACT

In this study, the effect of HCl acid solution on some carbonate stones from Turkey is investigated. It is known that stone plates used for outdoor and indoor covering applications can be been exposed to acid effects. For example, some chemical cleaning substances or drinks that contain acid can come in contacted with stone surfaces inside a building or acid rains outside can alter surface characteristics of stone plates. The calcite within the marble or limestone reacts with acid and is dissolved. In this way, it can be seen significant changes in the surface quality of stones. The surfaces of stone material losses its glossiness and its beauty.

Nineteen kinds of Turkish natural stone were used for this study. Specimens were immersed in a solution which contains 1% diluted HCl acid. Process continued for twenty days. Weight, glossiness and roughness changes were recorded. Also, chemical and thin section analyses, point load index tests, seismic velocity measurements and Shore hardness tests were carried out. From this study, it was found that acidic substances changes surface characteristics of carbonate stones significantly. Detailed results and discussion on HCl acid effects on stones are presented in the paper.

KEYWORDS:
Acid effect, carbonate stones, roughness, glossiness, stone decay

INTRODUCTION

The Surface quality of marbles is important, especially to for use in floors or natural facing stone in the building sector. In addition, the quality of surface features is an important point in terms of increasing export sales. Natural stone usage is increasing day to day as cladding the outside walls and the floors of buildings. Marble usage is increasing day to day. So, knowing the acid effect on marbles is very important for determining the place of use. Surface quality, in other words surface roughness and gloss quality, is very important for usage of marble or other natural face stones.

When a natural stone is used outside, acid effect is possible on natural stone with rain or like similar ways. In addition to this, at in a kitchen or where like that area, some chemical cleaning substances or drinks that contain acid can be contacted oncome in contact with the stone surfaces. Experiments were carried out to investigate the acid effect according to a Turkish Standard [1].

Viles et al. [2], Camuffo [3], Caneva et al. [4], O'Brien et al. [5], Okuda et al. [6], Sikiotis and Kirkitsos [7], Wilkins et al. [8], Winkler [9], Thomson and White [10], Winkler [11], Thornbush and Viles [12], Marinoni et al. [13], Thomas et al. [14] investigated the effects of acid on stone surface detorioration, strength and like other parameters.

In this study, the change of surface quality with acid contact was measured mainly in terms of surface roughness and surface glossiness. Shore hardness values were measured for a tile and their average of them calculated. Point load index [15], bulk density and p-wave velocity were measured too. In addition to this, chemical analyses were carried out and thin sections of the stones were prepared and examined on under microscope.

Experiments for HCl acid effects on stones were carried out on the nineteen different Turkish natural stones. An acid solution which contains 1% diluted HCl was prepared. Firstly, original weights, gloss and roughness values, Shore hardness, bulk density and p-wave velocity values were recorded. Specimens were immersed in acid solution. The process continued for twenty days. Then weights, gloss, roughness, point load index, bulk density and p-wave velocity were measured again. Since changes in point load index, bulk density, Shore hardness and p-wave velocity values after acid application are not significant. So, they are not shown in this paper.

At immersing HCl acid solution, the main chemical reactions are as follows:

$CaCO_3(s) + 2\ HCl(aq) \rightarrow CaCl_2(aq) + CO_2(g) + H_2O(l)$

$CaMg(CO_3)_2(s) + 4\ HCl(aq) \rightarrow CaCl_2(aq) + MgCl_2(aq) + 2CO_2(g) + 2\ H_2O(l)$

MATERIALS AND METHODS

Thin sections of the nineteen stones were prepared and shown in Fig. 1. Besides, chemical analyses of the stones were carried out. A summary of evaluations of the thin sections is as follows:

FIGURE 1
Thin sections of the stones

a- Mugla Green	**b- Elazig Cherry**	**c- Beige I**	**d- Emprador Light**
e- Burdur Beige	**f-Lilac**	**g- Onix**	**h- Marmara dolomite**
i- Blue Grey	**j- Red Limestone**	**k- Breccia Lim.**	**l- Silver**
m- Mugla White	**n- Beige II**	**o- Antrasite**	**p- Sedef**
r- Toros Black	**s- Dolomitical Marble**	**t-Mooncream**	

- Mugla Green: It is a marble. It is made up of calcite (as abundant), dolomite, muscovite and chlorite. Mugla Green has lepido-granoblastic texture.
- Elazig Cherry: It is altered serpentinite with calcite wein. Boulder-sized serpentinites clast are cemented by calcite. Calcite levels are white-coloured and have sparcalcite sized-crystals. Surprisingly, serpentinite levels are red coloured because the iron included by serpentinite altered hematite.
- Beige I: It is a limestone. It is composed of micritic and sparitic-sized calcites.
- Emperador Light: It is a dolostone and consists of dolomite mineral. The rock was fractured due to deformation but fractions of it reunited due to recrystallization. Textural feature of it likes a view of spider web. Rare iron causes yellow-brown colour.
- Burdur Beige: It is a limestone. The limestone consists of sparitic and micritic-sized calcite and contains small sized pellet.
- Lilac: It is a marble. The marble has granoblastic texture. Calcite minerals are approximately circular in form. Sizes of particles are up to 1 mm.
- Onyx: The stone consists of aragonites. It has big sized prismatic crystals.
- Marmara Dolomite: It is a marble. It is composed of medium sized dolomite crystals.
- Blue Grey: It is a fossiliferous limestone. Fossil fragments (bioclasts) are abundant and a part of them is nummulite fossil. Blue Grey contains 1-3% quartz fragments.
- Red Limestone: It is limestone. It forms from micritic-sized calcite. There is also oxidized iron (by volume1-3%). So, red colour is caused by oxidized iron.
- Breccia Limestone: It is limestone. The limestone consists of fragments of limestone (breccias) and calcite cement. Calcite cement has sparitic-sized crystals. Breccias have micritic-sized calcite.
- Silver: It is a marble. It consists of mainly calcite and rarely graphite. It has granoblastic texture. Particle sizes are heterogeneous.
- Mugla White: It is a marble. It forms from calcite and has granoblastic texture. The size of the calcite minerals are 1 - 2 mm.
- Beige II: It is a limestone. The limestone consists of sparitic and micritic-sized calcite. Size of crystals is heterogeneous.
- Antrasite: It is a fossiliferous limestone. Bioclasts which forms micritic-sized calcite are cemented micritic-sized calcite.
- Sedef: It is a marble and likes Lilac sample. The rock includes pure calcite.
- Toros Black: It is a limestone and contains micritic-sized calcite. Bituminous contents are abundant and there are ferrous minerals, which cause its dark colour.
- Dolomitic marble: It is a marble and composed of same-medium sized dolomite minerals.
- Mooncream: It is dolomitic limestone. The stone is made up of firstly micritic calcite and secondly sparitic-sized dolomite.

The nineteen different types of stones were studied and shown in Table 1. Diluted acid solution that contains % 1 HCl was used for the tests. Marble tiles that are 150 mm x 150 mm in width and 20 mm in thickness were used. Thirty grids were drawn on surfaces of tiles for measuring place.

Effect of acid solution was assessed by measuring weights, roughness and glossiness of samples before and after acid treatment. Values of glossiness and roughness were measured in thirty grids for each natural stone. The arithmetic mean of the values is was calculated. In this paper, the rough-

TABLE 1
Some physical and mechanical properties of the stones

Stone name (Code)	Stone type	Bulk density (kg/m^3)	Effective porosity (%)	Point load index (MPa)	Seismic velocity (m/s)	Schmidt hardness value
Mugla Green	Marble	2746	0.258	3.921	4907	43
Elazig Cherry	Altered serpentinite calcite	2687	0.890	5.266	7518	52
Beige I	Limestone	2685	0.309	4.276	5835	53
Emprador Light	Dolomite	2720	3.149	7.773	6104	43
Burdur Beige	Limestone	2680	0.423	5.831	6698	54
Lilac	Marble	2717	0.181	3.849	5108	38
Onyx	Onyx	2699	0.219	4.947	6494	50
Marmara Dolomite	Dolomite	2815	0.526	4.506	3787	29
Blue Grey	Fossiliferous Limestone	2665	1.221	6.289	5049	48
Red Limestone	Limestone	2698	0.470	5.033	3268	51
Breccia Limestone	Limestone	2634	1.630	4.394	5873	50
Silver	Marble	2722	0.395	3.966	5165	43
Mugla White	Marble	2715	0.229	2.897	5474	40
Beige II	Limestone	2672	0.131	6.006	5721	58
Antrasite	Limestone	2704	0.117	5.914	7146	56
Sedef	Marble	2820	0.564	2.628	5785	35
Toros Black	Limestone	2683	0.605	5.443	5748	57
Dolomitic Marble	Limestone	2694	0.291	4.452	5584	54
Mooncream	Limestone	2711	0.256	6.566	4118	37

ness of the samples was measured with a Mitutoya surftest SJ-201 P portable surface roughness tester. Roughness such as Ra, Rz and Rq values were measured in terms of surface roughness. Ra described as the arithmetic mean of the absolute departures of the roughness profile from the mean line was used in this study, since this value is a universally accepted surface roughness value and the best choice for evaluating the effect of factors on the surface quality [16].

Glossiness is the ratio of the density of the incoming light to the density of the reflected light. Roughness and irregularities inhibit the proper reflection of the light and decrease the brightness. According to the material properties, it is also possible that light can be partially refracted through the stone, thus causing loss of reflection capacity [17]. In this study, Tasco model digital gloss meter, which has a measurement range of 0-100 gloss units with a resolution of 1 gloss unit, was used for gloss measurements. Gloss meter measures light reflected from a surface illuminated and measured at equal but opposite angles. An increase in surface roughness generally results in reduced gloss.

Tasco model digital gloss meter enables measurement with 60◦ for standard measurement or 20◦ angles for measuring high-gloss levels. The measuring area at 60◦ and at 20◦ is 6mm×3mm and 4mm×3mm, respectively. A 60° angle of incidence was chosen in this study.

Dry weights (W_{d1} and W_{d2}) of samples for both before and after acid process were determined by leaving them in 105 ^{o}C oven during 24 hours (Table 2). In addition, all of nineteen stones chemical analyses were done.

Firstly, values of bulk densities, effective porosities were determined for all kinds of stones (Table 1). The surface roughness and the surface gloss were measured in 30 grid points on the surfaces of tiles. Mean values were calculated and given in Tables 3 and 4, respectively.

TABLE 2
Weight changes with HCl acid treatment

Stone name (Code)	Original Dry Weight(W_{d1})(g)	Dry Weight after acid treatment(W_{d2}) (g)	Change in weight (%)
Mugla Green	1185.98	1184.64	0.113
Elazig Cherry	1195.52	1195.30	0.018
Beige I	1175.03	1155.83	1.634
Emprador Light	1173.47	1166.39	0.603
Burdur Beige	1200.08	1183.74	1.362
Lilac	1172.45	1100.28	6.155
Onyx	1252.02	1234.95	1.363
Marmara Dolomite	1311.95	1303.68	0.630
Blue Grey	1198.61	1174.25	2.032
Red Limestone	1009.8	990.28	1.933
Breccia Limestone	1181.82	1151.2	2.591
Silver	1268.05	1242.66	2.002
Mugla White	1130.96	1052.12	6.971
Beige II	1184.28	1170.83	1.136
Antrasite	1206.91	1205.99	0.076
Sedef	1278.5	1249.7	2.253
Toros Black	1139.76	1139.30	0.040
Dolomitic Marble	1235.78	1235.06	0.058
Mooncream	1167.54	1166.61	0.080

TABLE 3
Roughness (Ra) changes of tiles before and after acid treatment

Sample	Original roughness (Ra) values of samples (μm)	Roughness (Ra) values of samples after acid treatment (μm)	Change in roughness (%)
Mugla Green	1.534	2.627	71
Elazig Cherry	0.214	2.332	990
Beige I	0.177	1.958	1006
Emprador Light	0.593	8.559	1343
Burdur Beige	0.411	1.350	228
Lilac	0.410	1.247	204
Onyx	0.141	1.347	855
Marmara Dolomite	0.502	14.985	2885
Blue Grey	0.309	5.262	1603
Red Limestone	1.248	1.626	30
Breccia Limestone	0.207	2.882	1292
Silver	0.218	4.465	1948
Mugla White	0.066	1.132	1615
Beige II	0.136	2.502	1740
Antrasite	0.231	0.672	191
Sedef	0.436	0.962	121
Toros Black	0.090	1.173	1203
Dolomitic Marble	0.942	1.884	100
Mooncream	0.401	1.144	185

RESULTS

Weight changes. The weights of all stone samples decreased after acid treatment as shown in Table 2. But the degree of weight loss is different for each stone type. Maximum weight loss was measured for Mugla White and Lilac as 6.155 % and 6.971%, respectively. Whereas, minimum weight loss was occurred for Elazig Cherry as 0.018 %. The average weight loss for the samples of nineteen stone types is about 1.2 %. In addition to this, increase in SiO_2 content causes decrease in weight loss due to resistance of silicates to acid erosion effect.

Roughness changes. All of measured roughness values increased significantly with acid treatment (Table 3). Changes in roughness values mean that acid contact is very important for stones due to decrease in quality of the surface. The effect of acid treatment on each stone was different levels. Maximum change in roughness was measured for Marmara Dolomite as 2885 %. Average change of roughness for all stones was 388 %. Fig. 2 shows that the surface roughness profile of the red limestone tile for in the original state and after acid treatment.

Gloss changes. Glossiness of all types of stones decreased significantly after immersing in the acid solution as shown in Table 4. Decrease in gloss values means that acid contact alters surface quality and appearance of the stone tiles. Gloss changes of stone tile surfaces after acid treatment is at varying levels depending on types and mineralogy of the stone. Maximum decrease in glossiness measured for Onyx was 98.74%. Average value of gloss change was 94.53 % for all stone types.

Chemical analyses. Major oxide examination was carried out (Table 5).

TABLE 4
Glossiness changes of tiles before and after acid treatment

Sample	Original glossiness values of samples	Glossiness values of samples after acid treatment	Change in glossiness (%)
Mugla Green	11.00	4.10	-63
Elazig Cherry	72.23	14.47	-80
Beige I	56.80	2.03	-96
Emprador Light	36.80	1.90	-95
Burdur Beige	7.60	2.13	-72
Lilac	11.13	3.03	-73
Onyx	81.77	1.03	-99
Marmara Dolomite	39.70	1.00	-97
Blue Grey	59.20	1.73	-97
Red Limestone	2.40	1.73	-28
Breccia Limestone	66.33	2.03	-97
Silver	21.63	1.23	-94
Mugla White	102.67	2.53	-98
Beige II	78.43	2.00	-97
Antrasite	76.10	1.13	-99
Sedef	39.23	6.00	-85
Toros Black	85.93	1.17	-99
Dolomitic Marble	7.33	5.97	-19
Mooncream	15.90	2.03	-87

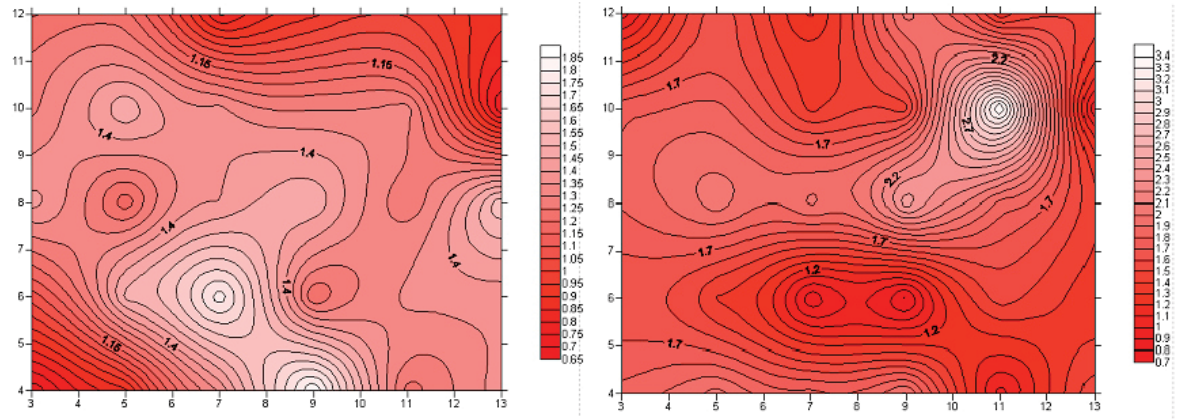

a) Original b) After acid treatment

FIGURE 2
Roughness contours for the red limestone tile surface

TABLE 5
Chemical analyses of the natural stones

Sample	SiO_2 (%)	Al_2O_3 (%)	Fe_2O_3 (%)	MgO (%)	CaO (%)	Na_2O (%)	K_2O (%)	TiO_2 (%)	P_2O_5 (%)	MnO (%)	LOI (%)	Total (%)
Mugla Green	<0,01	0,09	0,14	5,88	49,73	0,03	0,03	<0,01	0,03	<0,01	43,77	99,72
Elazig Cherry	15,08	0,28	5,49	15,43	33,07	0,10	0,08	<0,01	0,03	0,07	29,70	99,33
Beige I	<0,01	0,04	0,05	0,35	55,61	0,08	0,05	<0,01	0,04	<0,01	43,21	99,43
Emprador Light	<0,01	0,03	0,03	17,31	35,69	0,09	0,03	<0,01	0,03	<0,01	46,11	99,32
Burdur Beige	<0,01	0,03	0,03	0,19	56,00	0,04	0,02	<0,01	0,04	<0,01	42,67	99,03
Lilac	<0,01	0,06	0,03	0,33	55,26	0,02	0,02	<0,01	0,06	<0,01	43,29	99,07
Onyx	<0,01	0,10	1,02	0,15	53,54	0,03	0,02	<0,01	0,04	0,13	43,88	98,90
Marmara Dolomite	<0,01	0,07	0,03	17,57	36,58	0,03	0,02	<0,01	0,04	<0,01	45,23	99,57
Blue Grey	0,18	0,40	0,22	0,88	55,37	0,02	0,03	<0,01	0,04	<0,01	42,74	99,89
Red Limestone	0,10	0,23	0,27	0,51	55,40	0,03	0,01	<0,01	0,03	<0,01	43,25	99,84
Breccia Limestone	0,02	0,12	0,05	0,16	55,15	0,03	0,02	<0,01	0,04	<0,01	43,46	99,04
Silver	<0,01	0,04	0,06	0,83	55,44	0,08	0,02	<0,01	0,03	<0,01	42,70	99,19
Mugla White	<0,01	0,03	0,04	0,23	55,96	0,05	0,02	<0,01	0,03	<0,01	42,69	99,06
Beige II	<0,01	0,03	0,02	0,11	56,07	0,05	0,01	<0,01	0,03	<0,01	43,04	99,36
Antrasite	<0,01	0,05	0,05	0,33	55,89	0,04	0,01	<0,01	0,04	<0,01	42,70	99,10
Sedef	<0,01	0,04	0,03	0,07	55,54	0,07	0,02	<0,01	<0,01	<0,01	43,24	99,00
Toros Black	0,03	0,12	0,12	1,67	54,98	0,01	0,01	<0,01	<0,01	<0,01	42,60	99,54
Dolomitic marble	<0,01	0,02	0,02	17,22	36,96	0,02	0,01	<0,01	<0,01	<0,01	45,54	99,79
Mooncream	<0,01	0,03	0,02	0,94	55,71	0,02	0,02	<0,01	<0,01	<0,01	42,68	99,41

CONCLUSIONS

The weights of all stone samples decreased after acid treatment. But the degree of weight loss is different for each stone type. We can say that acidic material has an important erosion effect in erosion on stone material. A maximum weight loss was occurred for with Mugla White. Because the CaO rate is high in Mugla White and the calcite crystals are the biggest sized. Minimum weight loss was occurred in Elazig Cherry. Because, it has highest level of SiO_2 content (silicates prevent stone erosion due to the acid effect), weight loss is minimum. In spite of the high level CaO rate, the weight loss rate is low at Antrasite. Because it has both bioclast and cement forming micritic-sized calcite.

Also, the weight loss rate was low in Toros Black with acid treatment in spite of the high level CaO rate. It contains micritic-sized calcite. Bituminous (carbon) contents are abundant and there are ferrous minerals. It is possible that graphite prevents the acid effect. One of the low level weight losses is occurred at in Mugla Green. Because, it is made up of calcite (as abundant), dolomite, muscovite and chlorite. Mugla Green has lepidogranoblastic texture. Among the all dolomitic stones having the same content of MgO, which are Emparador Light, Marmara Dolomite and Dolomitic marble, the weight loss level of weight loss for Dolomitic marble is lesser than the others. Because, Dolomitic marble has small sized particles and interlock of it is well.

However, according to mineralogical and petrographic properties, chemical content and crystal size, rates of weight loss are different. Two similar stones which like each other can have different weight loss because of particle sizes.

All of the measured roughness values increased significantly with acid treatment. Changes in roughness values mean that acid contact is very important for stones due to decrease in quality of the surface. The effect of the acid treatment on each stone was had a different level.

Glossiness of all types of stones decreased significantly after immersing in the acid solution. Decrease in gloss values means that acid contact alters surface quality and appearance of the stone tiles. Gloss changes of stone tile surfaces after acid treatment is at varying levels depending on types and mineralogy of the stone. Between variables of CaO rate, MgO rate, ignition loss rate and weight loss, roughness, glossiness there are positive and negative correlations. However, it is not significant in statistically ($p<0.05$).

ACKNOWLEDGEMENTS

Author thanks to Alaaddin Sakçali for his encouragement and help.

REFERENCES

[1] TS 699 (2009) Natural building stones- methods of inspection and laboratory testing, Turkish Standard Institute, Ankara 88p (In Turkish).

[2] Viles, H.A. (2002) Implications of future climate change for stone deterioration. In Natural Stone, Weathering Phenomena, Conservation Strategies and Case Studies, Siegesmund, S., Vollbrecht, A., Weiss, T. (eds.), Special Publication 205, Geological Society, London, 407–418.

[3] Camuffo, D. (1992) Acid rain and deterioration of monuments: how old is the phenomenon? Atmospheric Environment. 26B, 241–247.
[4] Caneva, G., Gori, E.T. (1995) Montefinale, Biodeterioration of monuments in relation to climatic changes in Rome between 19–20th centuries, Science of the Total Environment. 167, 205–214.
[5] O'Brien, P.F., Bell, E., Orr, T.L.L., Cooper, T.P. (1995) Stone loss rates at sites around Europe, Science of the Total Environment. 167, 111–121.
[6] Okuda, T., Iwase, T., Ueda, H., Suda, H., Tanaka, S., Dokiya, Y., Fushimi, Hosoe, K.M. (2005) Long-term trend of chemical constituents in precipitation in Tokyo metropolitan area, Japan, from 1990–2002, Science of the Total Environment 339, 127–141.
[7] Sikiotis, D, Kirkitsos, P (1995) The adverse effects of nitrates on stone monuments, Science of the Total Environment. 171, 173–182.
[8] Wilkins, S.J., Compton, R.G., Viles, H.A., Taylor, M.P. (2002) A new technique to evaluate and quantify modified solution kinetics of calcareous materials after sulphuric acid pretreatment and urban exposure, Studies in Conservation. 47, 88–94.
[9] Winkler, E.M. (1970) The importance of air pollution in the corrosion of stone and metals, Engineering Geology. 4, 327–334.
[10] Thomson, G., White, R. (1974) The pH of rain and the destruction of alkaline stone, Studies in Conservation. 19, 190–191.
[11] Winkler, E.M. (1977) Stone Decay in Urban Atmospheres, Geological Society of America, Engineering Geology Case Histories Number 11, 53–58.
[12] Thornbush, M.J., Viles, H.A. (2007) Simulation of the dissolution of weathered versus unweathered limestone in carbonic acid solutions of varying strength, Earth Surface Processes and Landforms, School of Geography, University of Oxford. 32, 841–852.
[13] Marinonia, N., Pavesea, A., Rivac, A., Cellad, F., Cerullid, T. (2007) Chromatic weathering of black limestone quarried in Varenna (Lake Como, Italy), Building and Environment. 42, 68–77.
[14] Thomas, C., Lombillo, I., Setien, J., Polanco, J.A., Villegas, L. (2013) Characterization of Materials with Repellents and Consolidants from a Historic Building, Journal of Materials In Civil Engineering. 25, 1742-1751.
[15] ISRM. (1985) Suggested Method for determining point load strength, Int. J. Rock Mech.Min.Sci. Geomech. Abstr. 22, 51-60.
[16] Yavuz, H., Ozkahraman, H.T, Demirdag, S. (2011) Polishing experiments on surface quality of building stone tiles, Construction and Building Materials. 25, 1707-1711.
[17] Erdogan, M. (2000) Measurement of polished rock surface brightness by image analysis method. Eng. Geol. 57, 65-72.

Received: **14.12.2016**
Accepted: **22.11.2017**

CORRESPONDING AUTHOR

Halim Cevizci
Suleyman Demirel University,
Mining Engineering Department,
Isparta – Turkey

e-mail: halimcevizci@sdu.edu.tr

© by PSP Volume 27 – No. 2/2018 pages 727-732 Fresenius Environmental Bulletin

ALLELOPATHIC EFFECT OF *ARTEMISIA VULGARIS* ON WINTER WHEAT AND WINTER OILSEED RAPE

Ausra Marcinkeviciene[1,2], Zita Kriauciuniene[1,*], Rimantas Velicka[1,2], Robertas Kosteckas[1], Yoshiharu Fujii[3]

[1]Experimental Station, Aleksandras Stulginskis University, Rapsu str. 7, LT-53363 Noreikiskes, Kaunas distr., Lithuania
[2]Institute of Agroecosystems and Soil Science, Faculty of Agronomy, Aleksandras Stulginskis University, Studentu str. 11, LT-53361, Akademija, Kaunas dist., Lithuania
[3]International Agro-biological Resources, Faculty of Agriculture, Tokyo University of Agriculture and Technology, 4-8-5, Saiwai-cho, Fuchu, Tokyo, Japan

ABSTRACT

In recent years spread of common mugwort (*Artemisia vulgaris* L.) among agricultural crops has increased significantly. The object of this research was to determine the allelopathic effect of the mugwort on winter wheat and winter oilseed rape germination and early growth. For the experiments aqueous extracts of aboveground part and the root biomass of mugwort at different concentrations were used. It was found that the highest total amount of phenolic compounds was in the mugwort leaves. Investigations showed that aqueous extracts of mugwort had no significant ($P \geq 0.05$) influence on winter wheat seed germination while winter oilseed rape germination was significantly ($P \leq 0.05$) inhibited by aqueous extract of mugwort roots at the 1:10 concentration. Winter wheat shoot and root growth was inhibited by all concentrations of aqueous extracts of the mugwort roots compared with the control. Winter oilseed rape shoot growth was significantly ($P \leq 0.05$) stimulated, but the root growth significantly ($P \leq 0.05$) inhibited by the highest concentration (1:10) of mugwort aboveground parts aqueous extracts.

KEYWORDS:
allelopathy, common mugwort, phenolic compounds, germination, early growth

INTRODUCTION

Common mugwort (*Artemisia vulgaris* L.) is a perennial herbaceous plant of the Asteraceae family. It adapts to a wide range of climatic conditions: it can be found in high mountain regions and warm climates. Its population can be found in soils with a range of granulometric composition (sand, loam, and clay) and different pH. *A. vulgaris* is frequently found along waterway, railroad, and road rights-of-way [1]. The perennial species *A. vulgaris* became more common in agricultural crops (cereals, grain legumes, root crops, vegetables and ornamentals, etc.) in Europe and is difficult to control it [2, 3].

Weeds can often interfere with germination and growth of crops, because of their physiologically active exudates [4-7]. Allelopathy includes both interactions among plants, stimulating, as well as inhibitory, because of the release of biologically active compounds called allelochemicals [8, 9]. Allelochemicals can be immediately effective after being released but can also persist in soils, resulting in a legacy effect [10]. *A. vulgaris* has allelopathic impacts on other plant growth and development [11-13]. It was determined by Barney et al. [14] that mugwort biomass toxicity depends on interacting phytotoxic terpenes. He identified the composition of terpenes, constituting essential oils: the monoterpenes: α-pinene, β-pinene, limonene, eucalyptol (1.8-cineole), camphor, β-myrcene, santolina triene, and camphene. Zhigzhitzhapova et al. [15] investigated the volatile organic compounds (VOCs) composition in *A. vulgaris*. Monoterpenes (80.33%) were the main components of VOCs. The major components of essential oil were monoterpenes (44.49%) and sesquiterpenes (29.98%). An experiment by Li et al. [16] of the allelopathic influence of mugwort aqueous extracts showed strong inhibition on *Triticum aestivum*, *Brassica campestris* and *Raphanus sativus* seed germination energy and seedling growth. *B. campestris* and *R. sativus* were more sensitive to the mugwort allelopathic effect than *T. aestivum*. The germination of *B. campestris*, *R. sativus*, and *T. aestivum* decreased by 100.0, 87.3 and 61.1 % respectively at 0.0125 g/mL concentration of mugwort aqueous extract. Research on the allelopathic influence of mugwort aqueous extracts from the biomass (leaves, stems, and buds) on seed germination and growth of *T. aestivum*, *Lolium multiflorum*, and *Sinapis alba* showed that the mugwort biomass aqueous extracts had no effects on the germination and growth of *T. aestivum*, but inhibited *L. multiflorum* seed germination and growth. Mugwort root and stem aqueous extracts had lower inhibitory effects on *S. alba* seed germination, seedling height, and root length than the leaf extract [12].

Other researchers identified allelopathic influ-

ence of various weeds on cultivated crops as well [7]. It is shown, that germination of *Hordeum vulgare* may be inhibited by number of weeds: *Plantago major*, *Convolvulus arvencis, Equisetum arvense*, *Cirsium arvense* [17], *Rumex crispus* [18]. Aqueous extracts of *C. arvense* have an inhibitory allelopathic effect on *T. aestivum* germination. *Rumex crispus* inhibits germination of *Zea mays*, *Helianthus annuus* and *T. aestivum* [19].

More detailed studies of the allelopathic properties of mugwort should be carried out, as this weed has started to spread in agricultural crops. The objective of this research was to determine the allelopathic influence of mugwort aboveground parts and root biomass on winter wheat and winter oilseed rape germination and early growth.

MATERIALS AND METHODS

The allelopathic effect of the aboveground parts (leaves, stems, and inflorescences) and root biomass of the common mugwort (*Artemisia vulgaris* L.), at various aqueous extract concentrations, on the germination and early growth of the winter form of common wheat (*Triticum aestivum* L.) cv. 'Ada', and the winter form of oilseed rape (*Brassica napus* L. spp. *oleifera biennis* Metzg.) cv. 'Sunday', was studied at the Experimental Station of Aleksandras Stulginskis University. Experiment treatments were: 1) distilled water (control); 2) 1:6,250 (mugwort biomass and distilled water ratio); 3) 1:1,250; 4) 1:250; 5) 1:50; 6) 1:10. These concentrations were chosen according to the methodology used by Grodzinski [4].

Mugwort samples (aboveground parts and roots) were taken from a certified organic farm at the flowering stage and were chopped into 3 mm chaffs. The biomass was kept for 24 hours in distilled water (biomass and water ratio 1:10) at 18°C. Other concentrations of the prepared aqueous extract were obtained by dilution: 1:6,250, 1:1,250, 1:250 and 1:50. Winter wheat and winter oilseed rape seeds (30 units) were germinated for four days on filter paper in Petri dishes moistened with aqueous extracts at different concentrations in a RUMED 1301 climatic chamber (Rubarth Apparate GmbH, Germany) at 25°C and 65% humidity. Germinated wheat and oilseed rape percentages were estimated, and shoot height and root lengths measured. Experiments were carried out in four replications.

The total amounts of phenolic compounds in the different morphological parts of the mugwort (inflorescences, leaves, stems, and roots) were determined in the flowering stage using the Folinic spectrophotometric method [20]. The total amounts of phenolic compounds were expressed in gallic acid equivalents, mg g^{-1}.

Research data were statistically evaluated using the t-test and the Fisher criterion. Significant differences were established by calculating the least significant difference $LSD_{0.05}$ with a probability level of ($P \leq 0.05$) [21].

RESULTS AND DISCUSSION

The total amount of phenolic compounds in different morphological parts of the mugwort. The maximum amount of phenolic compounds was determined in mugwort leaves (1.93 mg g^{-1}) (Fig. 1). The mugwort inflorescences, stems, and roots, accumulated significantly ($P \leq 0.05$) less (from 19.7% to 54.4%) phenolic compounds compared with the leaves. Phenolic compounds accumulated by 59.1% more in mugwort roots than in stems, but significantly ($P \leq 0.05$) by 9.7% less in inflorescences.

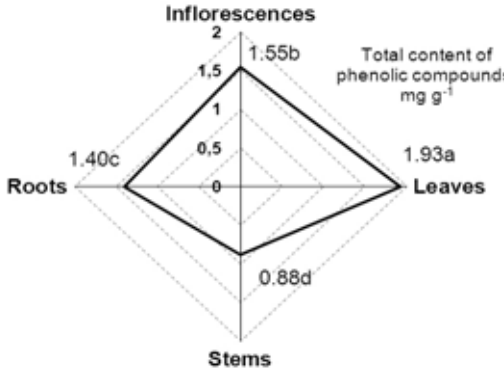

FIGURE 1
The total amounts of phenolic compounds in different morphological parts of the mugwort Note. Between the value means, those marked with different letters (a, b, c, d), were significantly different ($P \leq 0.05$)

Phenolic compounds, as secondary plant metabolites, are important in plant allelopathic activity [22,7]. Mugwort contains biologically active compounds such as sterols, terpenes, flavonoids, saponins, and tannins [14,15]. It has been shown that allelochemicals accumulate most in plant leaves, compared with the other morphological parts [23].

Mugwort allelopathic effect on winter wheat. Aqueous extracts of the aboveground morphological parts and roots of mugwort, at each concentration, compared with the control, had no significant effect on winter wheat germination (Fig. 2). Other authors have stated that the mugwort leaves and roots inhibit the germination of wheat [16,24]. These differences may occur due to variations in VOC composition in mugwort which depends on its growing conditions as it was explained by principal component analysis based on the types of components of essential oils of *A. vulgaris* collected from different countries [15].

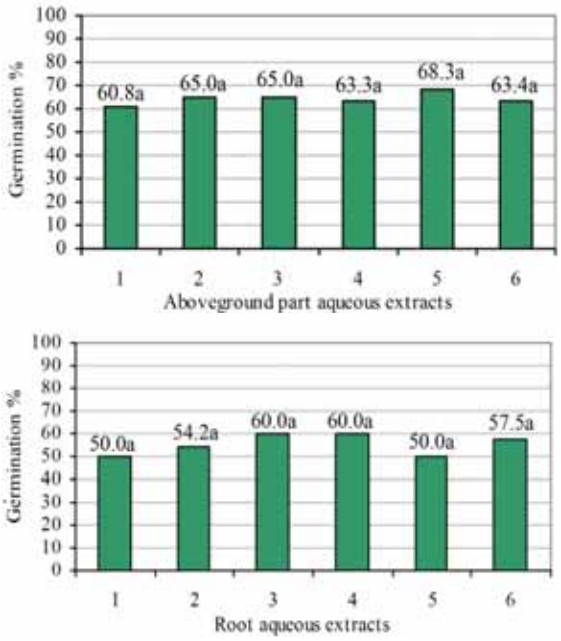

FIGURE 2
Allelopathic effects of aqueous extracts of mugwort aboveground parts and root on winter wheat germination
Note. Aqueous extracts: 1) distilled water, 2) 1: 6,250 (mugwort and distilled water ratio); 3) 1:1,250, 4) 1:250, 5) 1:50 and 6) 1:10; there were no significant differences ($P > 0.05$)

Mugwort aqueous extracts, at different concentrations, had a greater allelopathic impact on wheat shoot and root growth than grain germination (Figs 2 and 3). Wheat shoot growth, compared with distilled water, was significantly ($P \leq 0.05$) inhibited (13.6%) by the highest concentration (1:10) of mugwort root aqueous extract. With the other aqueous extracts of different concentrations wheat shoots' growth did not differ significantly ($P \geq 0.05$) from the shoots of wheat grown in distilled water. Aqueous extracts of mugwort aboveground parts, at 1:1,250, 1:250 and 1:50 concentrations increased wheat root length significantly ($P \leq 0.05$) from 13.9% to 24.3% compared to the controls. The lowest (1:6,250) and the highest (1:10) concentrations of aboveground part mugwort aqueous extracts did not affect root length significantly ($P \geq 0.05$) compared to controls.

A stronger inhibitory impact on the wheat shoot height and root length was found when using mugwort root aqueous extracts. Compared to controls, wheat shoot height significantly decreased ($P \leq 0.05$) from 15.5% to 21.9%, and the root length from 33.4% to 47.8% in all the concentrations of aqueous root extracts. According to Abdel-Fattah et al. [25] stronger mugwort concentrations of aqueous extracts inhibited not only winter wheat germination, but also their shoot and root growth.

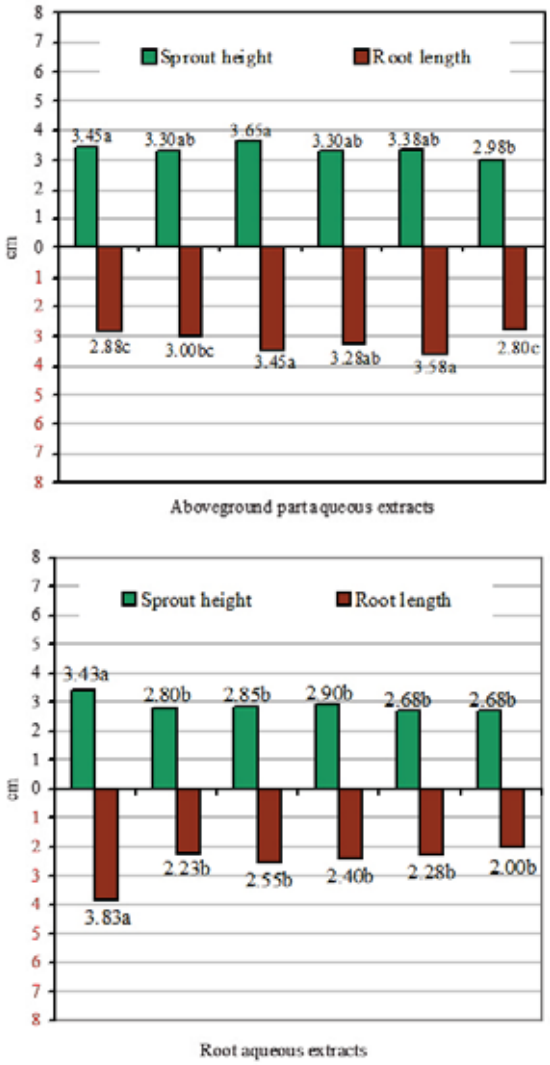

FIGURE 3
Mugwort aboveground parts and root aqueous extracts' allelopathic effects on initial winter wheat growth
Note. Concentrations of mugwort aboveground parts and root aqueous extracts: 1) distilled water, 2) 1:6,250, 3) 1:1,250, 4) 1:250, 5) 1:50 and 6) 1:10; the value means marked with different letters (a, b, c) were significantly different ($P \leq 0.05$)

Mugwort allelopathic effects on winter oilseed rape. Lower concentrations of aqueous extracts from the aboveground parts of mugwort had a tendency to stimulate winter oilseed rape germination, compared to controls, but effect was not significant (Fig. 4). Winter oilseed rape germination was inhibited with increasing mugwort root aqueous extracts concentration, but a significant ($P \leq 0.05$) inhibition (32.1%) compared to distilled water, was found only at the highest concentration (1:10) of the aqueous extract.

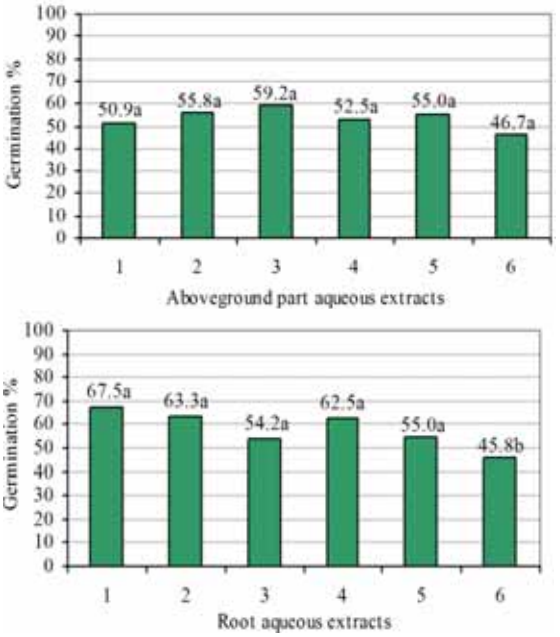

FIGURE 4
Mugwort aboveground parts and root aqueous extracts' allelopathic effects on winter oilseed rape germination
Note. Concentrations of aqueous extracts: 1) distilled water, 2) 1:6,250 (mugwort and distilled water ratio), 3) 1:1,250, 4) 1:250, 5) 1:50 and 6) 1:10; the value ($P \leq 0.05$) means marked with different letters (a, b) were significantly different ($P \leq 0.05$)

Mugwort aboveground parts' aqueous extracts at 1:50 and 1:10 concentrations, compared with controls, stimulated winter oilseed rape shoot growth significantly ($P \leq 0.05$): the shoot heights increased from 28.4% to 43.9%; while the 1:1,250 aqueous extracts inhibited the growth significantly ($P \leq 0.05$); the shoot heights decreased by 15.5% (Fig. 5). Winter oilseed rape root growth, compared to controls, was significantly ($P \leq 0.05$) inhibited (by 28.8%) only at the highest concentration (1:10) of the mugwort aboveground parts' aqueous extract.

Mugwort root extract concentrations affected winter oilseed rape shoot development differently: the 1:250 and 1:50 concentrations of aqueous extracts inhibited growth significantly ($P \leq 0.05$), by 13.7% to 16.3%, respectively, while the 1:10 concentration aqueous extract stimulated it significantly ($P \leq 0.05$), by 24.2%, compared to controls. Concentrations of aqueous extracts of mugwort root at 1:6,250 and 1:1,250 significantly increased ($P \leq 0.05$) winter oilseed rape root length from 32.3% to 34.8%, compared with controls, while at higher concentrations of aqueous extracts the differences were not significant ($P > 0.05$). Winter oilseed rape, compared to winter wheat, was less susceptible to the allelopathic effects of mugwort. Many authors have stated that oilseed rape itself has allelopathic properties, as a result of the presence of various alleloche-mical compounds [26-29].

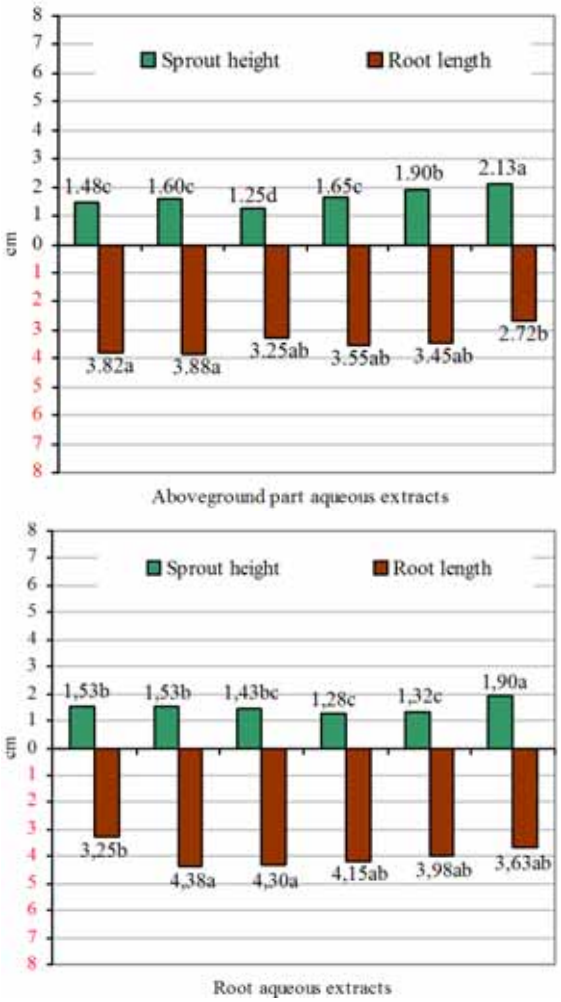

FIGURE 5
Mugwort aboveground parts and root aqueous extracts' allelopathic effects on initial winter oilseed rape growth
Note. Mugwort aboveground parts and root aqueous extracts: 1) distilled water, 2) 1:6,250, 3) 1:1,250, 4) 1:250, 5) 1:50 and 6) 1:10; the value means marked with different letters (a, b, c) were significantly different ($P \leq 0.05$)

CONCLUSIONS

1. The maximum amount of phenolic compounds was in the mugwort leaves. Phenolic compounds in the mugwort inflorescences, stems, and roots, compared with leaves, accumulated significantly ($P \leq 0.05$) from 19.7% to 54.4% less.
2. Winter wheat seed germination in the mugwort aboveground parts and root aqueous extracts were not significantly ($P \geq 0.05$) different. Winter oilseed rape germination was significantly ($P \leq 0.05$) inhibited (by 32.1%) by the aqueous extract of mugwort roots at the 1:10 concentration.
3. Winter wheat shoot growth, compared with controls, was inhibited (from 13.6% to 21.9%) by all concentrations of aqueous extracts of the mugwort root, and also by the highest concentration

of the aqueous extract of the aboveground part. Root growth of winter wheat was reduced (from 33.4% to 47.8%) by all the concentrations of the mugwort root aqueous extracts.

4. Winter oilseed rape shoot growth was inhibited (from 13.7% to 16.3%) by the mugwort aboveground parts at 1:1,250 concentration, and by the roots – at 1:250 and 1:50 concentrations of aqueous extracts, compared with controls. Winter oilseed rape root growth was inhibited (28.8%) by the mugwort aboveground parts' aqueous extract at the highest concentration. Winter oilseed rape shoots growth was significantly ($P \leq 0.05$) stimulated by the highest concentrations of mugwort aboveground parts and root aqueous extracts, and root growth by the lower concentrations of the aqueous extracts.

ACKNOWLEDGEMENTS

Research was funded by a grant (No. SIT-8/2015) from the Research Council of Lithuania. The authors want to express their appreciation to Aleksandras Stulginskis University. Authors are deeply grateful to Prof. Dr. David Richard Arney for revising the English language of the manuscript.

REFERENCES

[1] Barney, J.N. (2006) North American history of two invasive plant species: phytogeographic distribution, dispersal vectors, and multiple introductions. Biological Invasions. 8(4), 703–717.

[2] Weber, E., Gut, D. (2005) A survey of weeds that are increasingly spreading in Europe. Agronomy for Sustainable Development, Springer Verlag/EDP Sciences/INRA. 25(1), 109–121.

[3] Andreasen, C., Stryhn, H. (2008) Increasing weed flora in Danish arable fields and its importance for biodiversity. Weed Research. 48(1), 1–9.

[4] Grodzinski, A.M. (1965) Allelopathy in life of plants and their communities. Kiev, Ukraine. (In Russian).

[5] Colquhoun, J.B. (2006) Allelopathy in weeds and crops: myths and facts. Wisconsin Fertilizer, Aglime and Pest Management Conference. 45, 318–320.

[6] Delabays, N., Slacanin, I., Bohren, D. (2008) Herbicidal potential of artemisinin and allelopathic properties *Artemisia annua* L.: from the laboratory to the field. Journal of Plant Diseases and Protection. XXI (special iss.), 317–322.

[7] Zohaib, A., Abbas, T., Tabassum, T. (2016) Weeds cause losses in field crops through allelopathy. Notulae Scientia Biologicae. 8(1), 47–56.

[8] Inderjit, Duke, S.O. (2003) Ecophysiological aspects of allelopathy. Planta. 217, 529–539.

[9] Rice, E.L. (2013) Allelopathy. Academic Press, New York.

[10] Del Fabbro, C., Prati, D. (2015) The relative importance of immediate allelopathy and allelopathic legacy in invasive plant species. Basic and Applied Ecology. 16(1), 28–35.

[11] Inderjit, Foy Ch.L. (1999) Nature of the interference mechanism of mugwort (*Artemisia vulgaris*). Weed Technology. 13(1), 176–182.

[12] Pannacci, E., Pettorossi, D., Regni, L., Tei, F. (2011) Allelopathic effects of *Artemisia vulgaris* L. (mugwort) on seed germination and growth of *Sinapis alba* L., *Triticum aestivum* L. and *Lolium multiflorum* Lam. 1 p. [accessed 18. 11.2015]

[13] Pannacci, E., Pettorossi, D., Regni, L., Tei, F. (2015) Allelopathic potential of mugwort (*Artemisia vulgaris* L.) to control the Italian ryegrass (*Lolium multiflorum* Lam.) in winter wheat. Allelopathy Journal. 36(2), 257–272.

[14] Barney, J.N., Hay, A.G. Weston, L.A. (2005) Isolation and characterization of allelopathic volatiles from mugwort (*Artemisia vulgaris* L.). Journal of Chemical Ecology. 31(2), 247–263.

[15] Zhigzhitzhapova, S.V., Radnaeva, L.D., Gao, Q., Chen, S., Zhang, F. (2016) Chemical composition of volatile organic compounds of *Artemisia vulgaris* L.(Asteraceae) from the Qinghai–Tibet Plateau. Industrial Crops and Products. 83, 462–469.

[16] Li, M., Gao, X., Gao, Z., Wang, Q. (2010) Primary study on allelopathy of *Artemisia vulgaris*. Acta Prataculturae Sinica. 19(6), 114–119.

[17] Lazauskas, P. (1990) Agrotechnology against weeds. Vilnius, Lithuania. (In Lithuanian).

[18] Pilipavičius, V., Romaneckas, K., Šarauskis, E., Vaiciukevičius, E., Kerpauskas, P. (2011) Phytotoxicity effects of *Rumex crispus* L. grounded biomass on spring barley grain germination, African Journal of Agricultural Research. 7(12), 1819–1826.

[19] Khan, R., Khan, M.A., Waqas, M., Haroon, M., Hussain, Z., Khan, N., Bashir, S. (2012) Bioherbicidal activity of some winter weeds against some crops. Pakistan Journal of Weed Science Research. 18(4), 561–569.

[20] Ragaee, S., El-Sayed, M.A.A., Noaman, M. (2006) Antioxidant activity and nutrient composition of selected cereals for food use. Food Chemistry. 98, 32–38.

[21] Quinn, G.P., Keough, M.J. (2006) Experimental design and data analysis for biologists. Cambridge, UK.

[22] Rodzynkiewicz, E.S., Dabkowska, T., Stoklosa, A., Hura, T., Dubert, F., Lepiarczyk, A. (2006) The effect of selected phenolic compounds on the initial growth of four weed species. Journal of Plant Diseases and Protection. 20, 479–486.
[23] Gill, L.S., Anoliefo, G.O., Iduoze, U.V. (2009) Allelopathic effects of aqueous extract from Siam weed on the growth of cowpea. University of Benin, Nigeria.
[24] Sharangi, A.B. (2011) In search of allelopathy from common alliaceae crops for managing weeds in coriander: An overview. International Journal of Agricultural Research. 6(3), 209–217.
[25] Abdel-Fattah, I.R., Abou-Zeid, A.M., Altalhi, A.D. (2011) Allelopathic effects of *Artemisia princeps* and *Launae sonchoids* on rhizospheric fungi and wheat growth. African Journal of Microbiology Research. 5(4), 419–424.
[26] Jafariehyazdi, E., Javidfar, F. (2011) Comparison of allelopathic effects of some *Brassica* species in two growth stages on germination and growth of sunflower. Plant Soil and Environment. 57(2), 52–56.
[27] Velička, R., Marcinkevičienė, A., Pupalienė, R., Čepulienė, R., Kriaučiūnienė, Z. (2012) Allelopathic effects of aqueous extracts of rape residues on winter wheat seed germination and early growth. Journal of Food, Agriculture & Environment. 10(3-4), 1053–1057.
[28] Ibrahim, R.A., Abustueit, E.O., Shaban, S.A. (2014) Allelopathic activity and chemical composition of rapeseed extracts on Jungle rice. International Journal of Advanced Research. 2(10), 150–154.
[29] Aliki, H.M., Reade, J.P., Back, M.A. (2014) Effects of concentrations of *Brassica napus* (L.) water extracts on the germination and growth of weed species. Allelopathy Journal. 34(2), 287–298.

Received: **15.12.2016**
Accepted: **03.12.2017**

CORRESPONDING AUTHOR

Zita Kriauciuniene
Experimental Station,
Aleksandras Stulginskis University,
Rapsu str. 7, LT-53363 Noreikiskes,
Kaunas distr. – Lithuania

e-mail: zita.kriauciuniene@asu.lt

© by PSP Volume 27 – No. 2/2018 pages 733-743 Fresenius Environmental Bulletin

SCREENING FOR HIGH-TEMPERATURE TOLERANT COTTON (*GOSSYPIUM SPP.*) BY USING SOME PHYSIO-MORPHOLOGICAL LEAF TRAITS

Remzi Ekinci[1], Sema Basbag[1,*], Emine Karademir[2], Cetin Karademir[2]

[1]Department of Field Crops, Faculty of Agriculture, University of Dicle, Diyarbakir, Turkey.
[2]Department of Field Crops, Faculty of Agriculture, University of Siirt, Siirt, Turkey.

ABSTRACT

One hundred sixty cotton genotypes obtained from genetic stocks were evaluated for high temperature tolerance based on some physio-morphological leaf traits under field conditions and controlled condition. Genotypes showed differences for all investigated traits. In the study, stomal density ranged from 83.49-128.35 stomata. $(mm^2)^{-1}$, stomatal conductance ranged from 140.77-394.90 $mmol.m^{-2}.s^{-1}$, stomal width ranged from 92.39-154.01 μm, stomatal rate of width/length ranged from 0.42-0.58, canopy temperature ranged from 20.24-52.00 ^oC, leaf area ranged from 67.50-173.05 cm^2, leaf SPAD value ranged from 31.80-63.73, and leaf photosynthesis yield ranged from 12.72-33.05 $\mu mol.m^{-2}s^{-1}$. The results showed that high temperature stress did not influence stoma numbers, whereas it decreased stomatal conductance, stomatal width, stomatal width/length, leaf area, leaf SPAD and leaf photosynthesis yield; and that it increased canopy temperature values. The Fantom was determined to be tolerant with respect to stomatal conductance trait and the Tropikal-225 genotype with respect to stoma width and width/length traits.

KEYWORDS:
Cotton, stress, high temperature tolerance, physio-morphological traits

INTRODUCTION

Crops face many stress factors during their lifetimes. Stress factors that may rarely effect on crops by themselves usually have simultaneous impacts. Abiotic stresses such as high temperature, drought, salinity and chemical toxicity threaten the crop growth and thus the world agricultural production. According to numerous climate models, it is estimated that the increase in CO_2 and other greenhouse gases would increase the air temperature and that this increase would be on average 1.4–5.8 ˚C in 2050; and a great number of climate models estimate that the mean temperature rise would be 3.5 – 5.9 ˚C [1]. It is an inevitable macro result that probable climate changes impact the crop structure in the region. This situation will cause reductions in 25% of the production of crop species/varieties [2]. However, it was noted in many researches that improvements to be introduced thanks to breeding of new heat-tolerant varieties and particularly agronomic practices would be able to reduce the risks caused by climate change in short term [3].

Adaptation capabilities of crops are closely related to transpiration and photosynthesis taking place in leaves. The number of stomata in unit leaf area has an effect on gas interchange [4]. Genotypes and ecological factors have also influence over the stoma size and density of crops [5, 6, 7, 8, 9].

The primary environmental factor affecting the germination, growth, development and fruit maturation of the cotton plant is heat [10, 11]. The optimum development temperature for cotton varies according to species and variety. Temperature requirements for cotton vary according to phenological stages, occurrence time of temperature, physio-morphological and genetic traits of the crop [12, 13]. Photosynthesis and respiration continuing throughout the development of the cotton plant are related and linked in many aspects. In the cotton plant, the temperatures of 22 – 40 ˚C, through temperature increase, reduce the respiration and photosynthesis by 15 – 50% [14]. Determination of high-temperature tolerances of cotton varieties will be useful for both present and future climates [15]. In high temperature conditions, variations occur in many physio-morphological traits of cotton leaf such as stoma conductivity, photosynthesis, leaf size, leaf chlorophyll content and leaf temperature. By variations in these traits, sensitivity and tolerance levels of the genotype against high temperature conditions can be determined.

This study was conducted in order to determine how and at what level physio-morphological traits of the leaves of cotton plant are affected by the abiotic stresses caused by the heat that has risen due to global climate change and is foreseen to rise further in the future and the resistance/tolerance levels of cotton genotypes against heat stress; and contribute to that genetically resistant cotton genotypes could

be used in breeding programs to be carried out in the future.

MATERIALS AND METHODS

Materials of this study were composed of 160 cotton genotypes obtained from genetic stocks. The study was conducted separately in controlled and field conditions under normal temperature (N) and high temperature stress (S) conditions. The field condition (FC) study was carried out in the trial fields of the Southeastern Anatolian Project International Agricultural Research and Training Center, whereas controlled condition (CC) studies under greenhouse conditions in which temperature and moisture could be controlled in 2010 and 2011.

Trials were laid out in augmented design with 7 replications, 6 standard genotypes (Stoneville-474, Stoneville-468, Teks, Fantom, DP-90, Fibermax-832) in the lengths of 12 m. (field) and 2 m. (controlled), in plots consisting of 2 rows each (70 cm interrow spacing; 20 cm intrarow spacing). FC trial sowings were conducted on April 9 and June 14; and controlled condition trials on April 9. CC trials were carried out for normal temperature (N) trial in 2010 (long term averages of hourly temperatures are parallel) and for high temperature stress (S) trial in 2011 (+5 °C higher than the long term average of the highest hourly temperature). To ensure CC, the greenhouse to be used was transformed into closed system temperature and moisture controlled one after air conditioning and automation works. Infrared technology was used for heating system; ventilation fans for air ventilation system; moist panels for cooling and moisturizing; curtain system for shading; and drip irrigation system for irrigation. In the established system, moisture and temperature value changes in hourly periods between 00:00–24:00 were achieved by entering weekly automation.

Daily high temperature variation graphs of the FC and CC trials during cotton growing season of 2010-2011 are shown in Fig.1.

Before the soil tillage prior to sowing, 7 kg.da^{-1} N and 7 kg.da^{-1} P (in complex 20-20-0 form) were applied; and the remaining portion of 7 kg.da^{-1} N in the form of 33% Ammonium Nitrate with the first irrigation water as top dressing. Irrigation was applied 10 times in total using the drip irrigation system. In both years, hand hoe for weed control and soil aerating was applied 3 times a year to let the cotton plant to develop.

Measurement of Physiological Traits. Within the scope of the study, the following traits were studied: stomatal conductance (mol.m^2.s^{-1}), number of stoma quantity.(mm^2)$^{-1}$, width of stoma, width.length-1 of stoma, leaf photosynthesis yield, single leaf area (cm^2), leaf SPAD value, canopy temperature (°C). All physio-morphological traits were metered day after planting 90. Measurements were obtained during mid-day on the fifth fully expanded leaf below with three reading per leaf of the plant [16]. Photosynthetic yield (µmol.CO_2.m^{-2}s^{-1}) was measured by the EARS-PPM Plant Photosynthesis System. Stomatal conductance (mol.m^{-2}s^{-1}) and leaf temperature were measured by a leaf porometer (Model SC-1), canopy temperature was measured by an infrared thermometer (DT-8811H) and leaf chlorophyll contents were obtained by a Minolta SPAD-502 chlorophyll meter [17]. Number of stoma and width of stoma and length of stoma (for stoma rate of Width.Length^{-1}) were obtained using the Nikon-S5 microscope. Single leaf area was calculated by NetCAD 5.0 software.

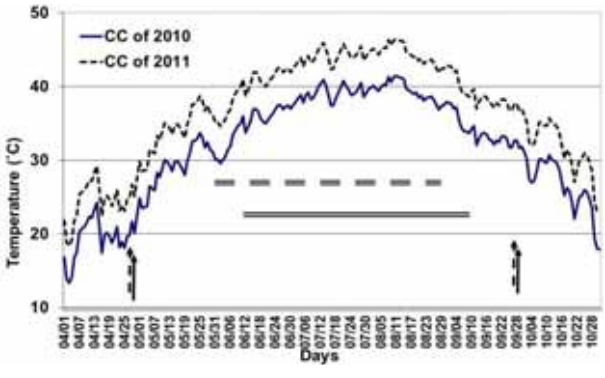

FIGURE 1a
High temperature variation graphs of the CC trials during cotton growing season of 2010 and 2011.

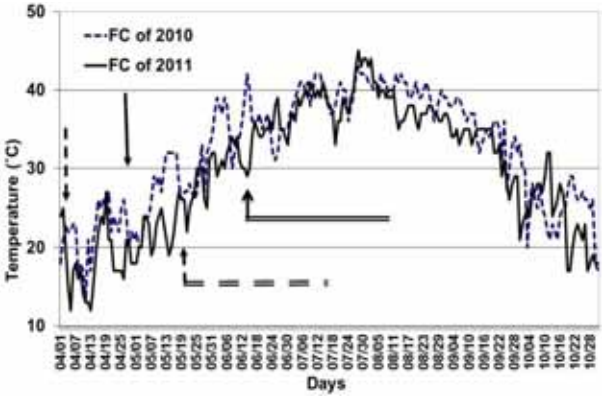

FIGURE 1b
High temperature variation graphs of the FC trials during cotton growing season of 2010 and 2011.

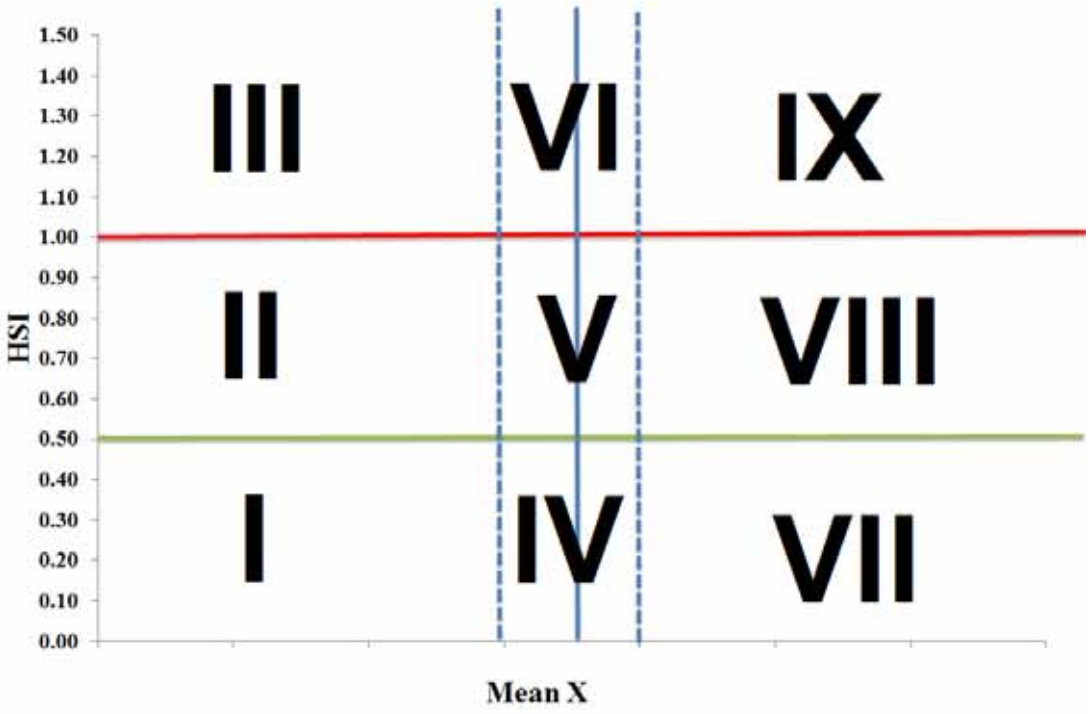

FIGURE 2
Distribution graph based on the Normal Conditions Mean Value and HSI Value of the genotypes as material
I Region: X<Mean and HSI≤0.05; II Region: X<Mean and 0.05<HSI≤1.00;
III Region: X<Mean and HSI>1.00; IV Region: X=Mean and HSI≤0.05;
V Region: X=Mean and 0.05<HSI≤1.00; VI Region: X=Mean and HSI>1.00 ;
VII Region: X>Mean and HSI≤0.05; II Region: X>Mean and 0.05<HSI≤1.00;
III Region: X>Mean and HSI>1.00

Heat Stress Index (HSI) for all the traits studied was calculated using the following equation.

$$HSI = \frac{\frac{G_N - G_S}{G_N}}{\frac{M_N - M_S}{M_N}}$$

(HSI: Heat Stress Index; G: Genotype; M: Mean; N: Normal Condition; S: Stress Condition) [18].

Genotypes were rated as follows; HSI≤0.50 high tolerant, HSI 0.5-1.0 middle tolerant; HSI>1.0 sensitive [19].

It was constructed with respect to the Normal Conditions Mean Value and HSI Value of the trait being studied of the genotypes as material in Fig.2. Statistical analyses were performed using JMP 7.0.1 statistical software.

RESULTS

The graph on the stoma density for genotypes is given in Figure 3; the one on leaf stomatal conductance in Figure 4; the one on stoma width in Figure 5; the one on stoma length/width ratio in Figure 6; the one on canopy temperature value in Figure 7; the one on single leaf area in Figure 8; the one on leaf SPAD value in Figure 9 and the one on leaf photosynthesis yield in Figure 10.

Stomatal Density (stomata.mm^{-2}): Whereas the values for the stomatal density vary in the range of 83.49-128.35 stomata.(mm^2)$^{-1}$ under CC_N and in the range of 81.73-126.59 stomata.(mm^2)$^{-1}$ under CC_S, 83.71-128.08 stomata.(mm^2)$^{-1}$ under FC_N and 83.71-128.08 stomata.(mm^2)$^{-1}$ under FC_S. Mean stomata numbers were determined to be 105.04±11.64 stomata.(mm^2)$^{-1}$,103.43±11.62 stomata.(mm^2)$^{-1}$, 106.13±12.24 stomata.(mm^2)$^{-1}$, 105.25±12.05 stomata.(mm^2)$^{-1}$ under CC_N, CC_S, FC_N, FC_S, respectively of the genotypes, 70 were determined as sensitive (3 in region III, 32 in region VI, 35 in region IX); 90 as middle tolerant (28 in region II, 60 in region V, 2 in region VIII) (Fig.3). Our findings support those reported by Kliewer et al., (1985) [5], Rana and Chadha (1990) [6], Şahin and Soylu (1991) [7], Çağlar and Tekin (1999) [8] that stomata number in unit leaf area (stomata density) had varied with respect to plant species and varieties.

TABLE 1
Analysis of Variance for investigated traits in Field Condition (FC) and Controlled Condition (CC) 2010-2011

Traits		Years		Source of Variation				
				Std. Genotypes	Blok	Error	Total	CV (%)
			DF	5	6	30	41	
Stomatal Conductance	FC	2010	S	1741.85	123.15	2335.33	4200.32	**19.57**
			N	1630.16	321.33	2012.13	3963.62	**16.20**
		2011	S	1640.55	91.58	2226.22	3958.35	**18.60**
			N	1699.06	220.96	2194.25	4114.27	**16.67**
	CC	2010	S	1303.49	707.75	3095.25	5106.49	**24.18**
		2011	N	1297.38	1108.97	876.07	3282.41	**10.21**
Single Leaf Area	FC	2010	S	127.29	7.56	172.19	307.05	**12.45**
			N	229.85	72.77	261.48	564.10	**12.38**
		2011	S	175.11	7.94	238.69	421.74	**13.35**
			N	258.26	106.86	264.87	629.99	**12.04**
	CC	2010	S	213.14	167.84	469.78	850.76	**19.43**
		2011	N	337.92	348.96	175.03	861.92	**10.29**
Leaf SPAD Value	FC	2010	S	16.68	0.78	22.72	40.18	**9.94**
			N	19.21	0.18	26.92	46.31	**10.02**
		2011	S	17.34	0.75	23.67	41.77	**10.03**
			N	19.55	3.85	23.74	47.13	**9.36**
	CC	2010	S	9.17	13.46	14.42	37.06	**9.85**
		2011	N	9.87	10.66	4.13	24.66	**3.76**
Canopy Temperature	FC	2010	S	4.85	1.83	5.55	12.23	**7.87**
			N	5.51	1.07	6.98	13.56	**7.89**
		2011	S	4.95	1.27	6.46	12.68	**8.93**
			N	6.29	1.59	7.78	15.66	**8.65**
	CC	2010	S	12.20	2.40	33.68	48.28	**16.73**
		2011	N	17.35	0.68	24.44	42.46	**10.47**
Leaf Photosynthesis Yield	FC	2010	S	2.80	0.40	3.56	6.76	**11.91**
			N	7.25	0.23	9.99	17.47	**16.09**
		2011	S	2.73	0.49	3.39	6.61	**11.55**
			N	7.27	0.40	9.85	17.53	**15.77**
	CC	2010	S	0.40	0.21	0.99	1.59	**6.56**
		2011	N	7.71	2.12	8.88	18.71	**10.47**
Stomatal Density	FC	2010	S	136.03	285.42	67.66	489.11	**7.37**
			N	150.61	315.83	75.09	541.53	**7.56**
		2011	S	135.62	286.30	65.89	487.81	**7.27**
			N	149.82	354.93	34.20	538.94	**5.10**
	CC	2010	S	139.64	23.46	312.89	475.99	**16.35**
		2011	N	140.03	23.80	313.53	477.36	**16.12**
Stomatal Width	FC	2010	S	79.71	63.78	52.25	195.74	**6.04**
			N	104.19	98.86	54.29	257.34	**5.67**
		2011	S	88.63	53.59	74.63	216.85	**7.27**
			N	118.01	96.49	75.85	290.35	**6.75**
	CC	2010	S	71.61	45.21	164.87	281.68	**10.89**
		2011	N	103.98	77.53	75.71	257.21	**6.63**
Stomatal Rate of Width/Length	FC	2010	S	0.00012	0.00070	0.00007	0.00089	**1.72**
			N	0.00009	0.00086	0.00007	0.00101	**1.59**
		2011	S	0.00038	0.00069	0.00143	0.00251	**7.91**
			N	0.00046	0.00078	0.00180	0.00304	**8.17**
	CC	2010	S	0.00009	0.00011	0.00042	0.00061	**4.19**
		2011	N	0.00002	0.00001	0.00012	0.00016	**2.04**

S: Stress, N: Normal; FC: Field Condition; CC: Controlled Condition

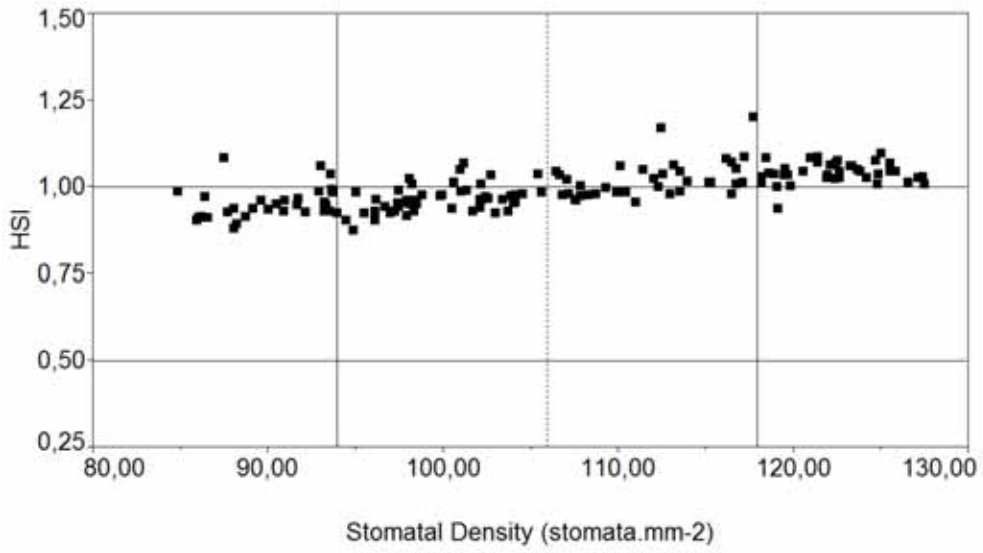

FIGURE 3
The graph on the stoma density for genotypes

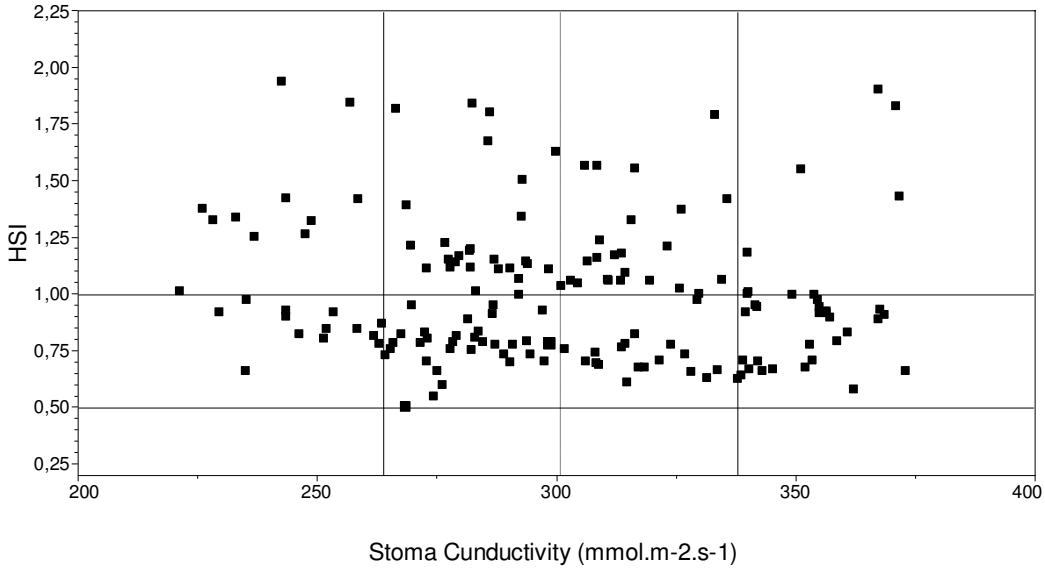

FIGURE 4
The graph on the stoma conductance for genotypes

Stomatal Conductance (mmol.m^{-2}.s^{-1}). However leaf stomatal conductance values varied in the range of 240.92-394.90 mmol.m^{-2}.s^{-1} under CC_N and 140.77-310.56 mmol.m^{-2}.s^{-1} under CC_S, they varied in the range of 154.16-383.46 mmol.m^{-2}.s^{-1} under FC_N and 154.16-378.44 mmol.m^{-2}.s^{-1} under FC_S. The mean leaf stomatal conductance values were determined to be 317.54±36.12 mmol.m^{-2}.s^{-1}, 228.76±35.62 mmol.m^{-2}.s^{-1}, 277.12±45.70 mmol.m^{-2}.s^{-1}, 259.84±46.17 mmol.m^{-2}.s^{-1} under CC_N, CC_S, FC_N, FC_S, respectively. Of the genotypes, 68 were determined to be sensitive (11 in region III, 50 in region VI, 7 in region IX); 91 medium tolerant (13 in region II, 51 in region V, 27 in region VIII); and 1 tolerant (1 in region IV) (Fantom) (Fig.4).

Stomatal Width (μm): While stomatal width values varied in the range of 103.20-154.01 μm under CC_N and 92.39-136.52 μm under CC_S; 94.35-155.08 μm under FC_N conditions and 92.54-152.59 μm under FC_S. The mean stomatal width values were determined to be 134.33±10.11 μm; 119.45±8.36 μm; 128.88±11.49 μm; 124.97±10.96 μm under CC_N, CC_S, FC_N, FC_S, respectively. Of the genotypes, 80 were determined to be sensitive (14 in region III, 50 in region VI, 16 in region IX); 79 medium tolerant (12 in region II, 56 in region V, 11 in region VIII); and 1 tolerant (Tropikal 225 in region IV) (Fig.5).

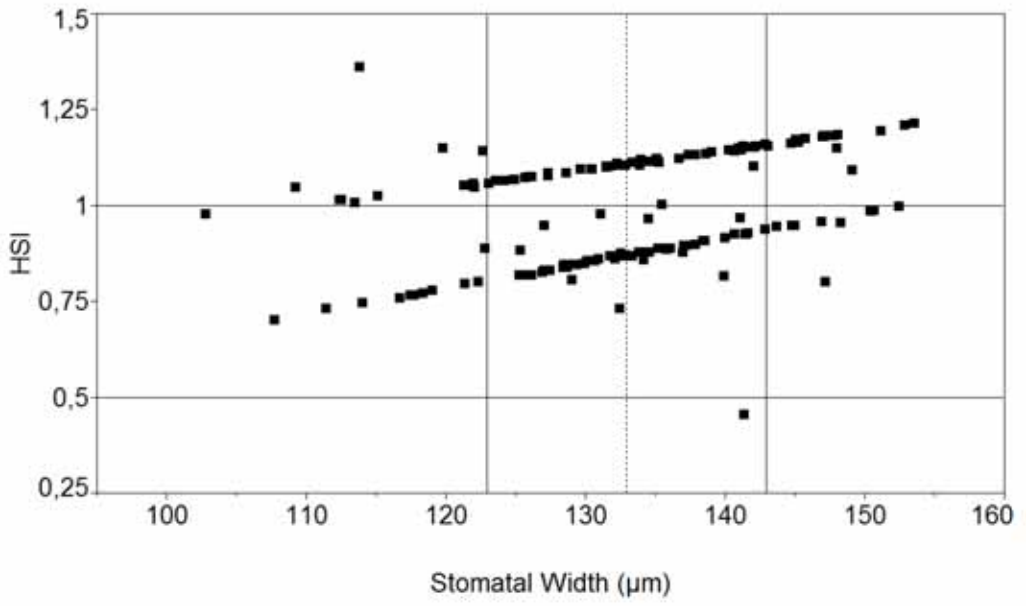

FIGURE 5
The graph on the stoma width for genotypes

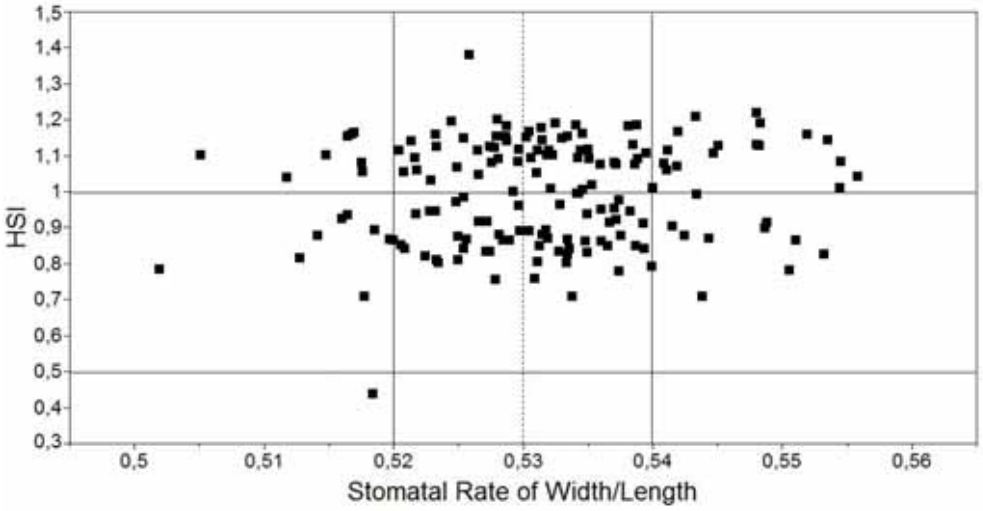

FIGURE 6
The graph on the stomal rate of width/length for genotypes

Stomatal Rate of Width/Length. Whereas stomatal rate of width/length values varied in the range of 0.42-0.55 under CC_N and 0.45-0.50 under CC_S, 0.52-0.58 under FC_N and 0.42-0.55 under FC_S. The mean stomatal rate of width/length values were determined to be 0.53±0.004; 0.47±0.009; 0.51±0.028; 0.49±0.027 under CC_N, CC_S, FC_N, FC_S, respectively. Of the genotypes, 83 were determined to be sensitive (13 in region III, 56 in region VI, 14 in region IX); 76 medium tolerant (12 in region II, 55 in region V, 9 in region VIII); and 1 tolerant (Tropikal 225 in region I) (Fig.6).

Canopy Temperature (°C). However canopy temperature values varied in the range of 23.1-38.84 °C under CC_N and 33.7-52.00 °C under CC_S, 20.24-36.01 °C under FC_N and 20.24-38.00 °C under FC_S. The mean canopy temperature values were determined to be 26.74±4.10 °C; 30.79±3.46 °C; 28.50±3.40 °C; 29.28±3.48 °C under CC_N, CC_S, FC_N, FC_S, respectively of the genotypes, 82 were determined to be sensitive (11 in region III, 57 in region VI, 14 in region IX); 78 medium tolerant (12 in region II, 53 in region V, 13 in region VIII) (Fig.7). Our findings agree with those of Brown (2008) [20], Brown and Zeiher (1998) [21], and Zeiher et al. [22,

23] who pointed out that the canopy temperature were lower compared to air temperature.

Single Leaf Area (cm^2): Whereas single leaf area values varied in the range of 83.87-170.00 cm^2 under CC_N and 67.50-146.52 cm^2 under CC_S, 83.20-173.05 cm^2 under FC_N and 81.40-169.60 cm^2 under FC_S. The mean single leaf area values were determined to be 81.39±18.51 cm^2; 103.55±14.54 cm^2; 131.9±18.45 cm^2; 120.77±18.67 cm^2 under CC_N, CC_S, FC_N, FC_S, respectively. Of the genotypes, 82 were determined to be sensitive (15 in region III, 57 in region VI, 10 in region IX); 78 medium tolerant (7 in region II, 58 in region V, 13 in region VIII) (Fig.8). Our findings support the findings of Khan et al. (2008) [24], Gerik et al., (1996) [25] and Pettigrew, (2004) [26] who reported that leaf areas had decreased under stress conditions.

Leaf SPAD Value (SPAD Value): Whereas leaf SPAD values varied in the range of 45.93-63.73 under CC_N and 31.8-45.8 under CC_S, 32.34-63.22 under FC_N and 31.85-62.60 under FC_S. The mean leaf SPAD values were determined to be 55.00±3.13; 39.16±3.03; 51.45±4.69; 49.81±4.62 under CC_N, CC_S, FC_N, FC_S, respectively. Of the genotypes, 82 were determined to be sensitive (16 in region III, 52 in region VI, 14 in region IX); 78 medium tolerant (6 in region II, 55 in region V, 17 in region VIII) (Fig.9). Our findings support the findings of Burke and Mahony (2001) [27] who stated that high temperature had decreased the leaf chlorophyll amount.

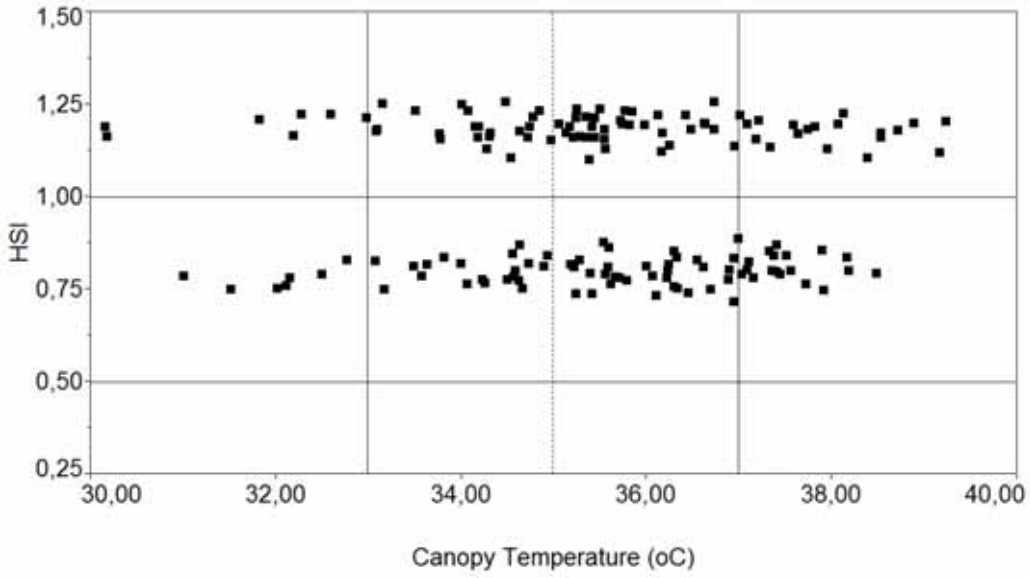

FIGURE 7
The graph on the canopy temperature for genotypes

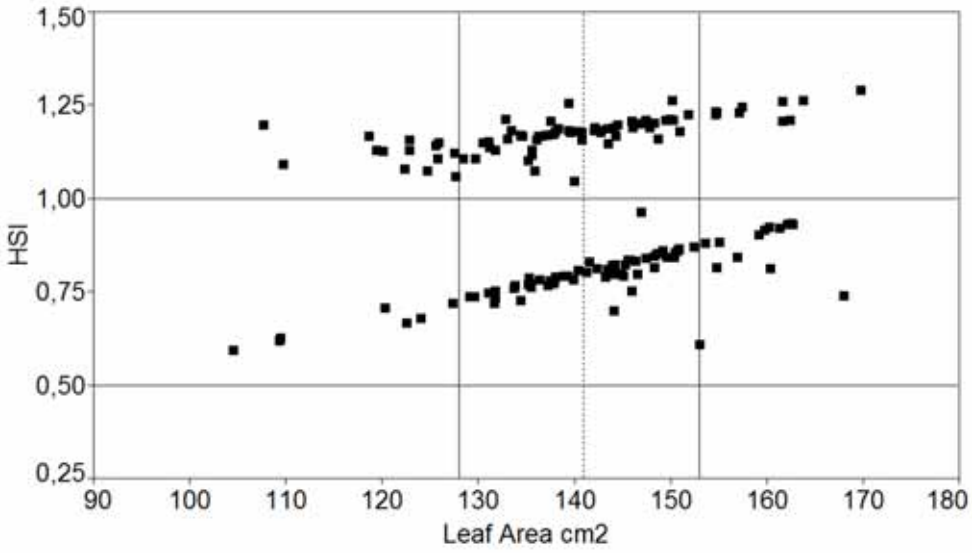

FIGURE 8
The graph on the leaf area for genotypes

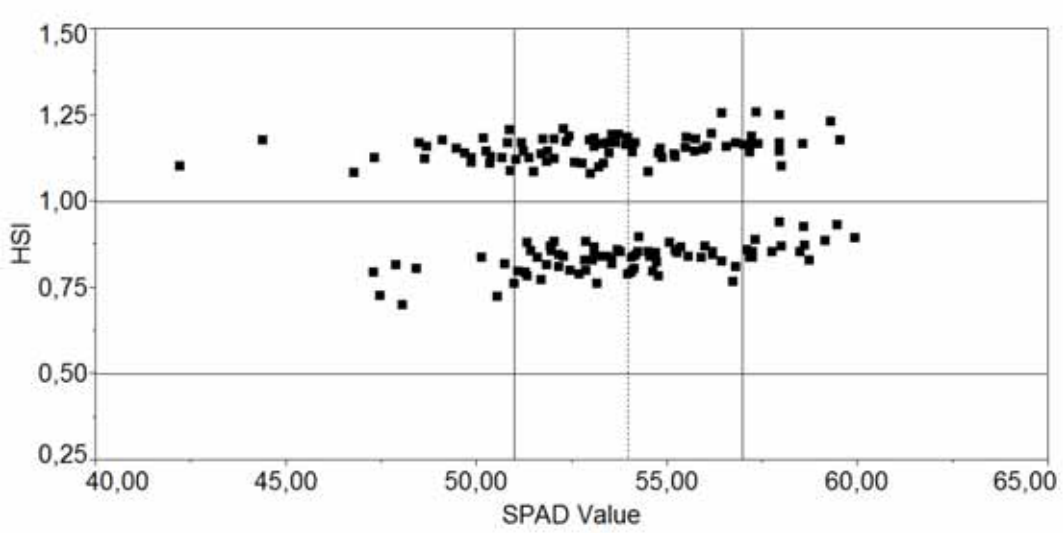

FIGURE 9
The graph on the leaf SPAD value for genotypes

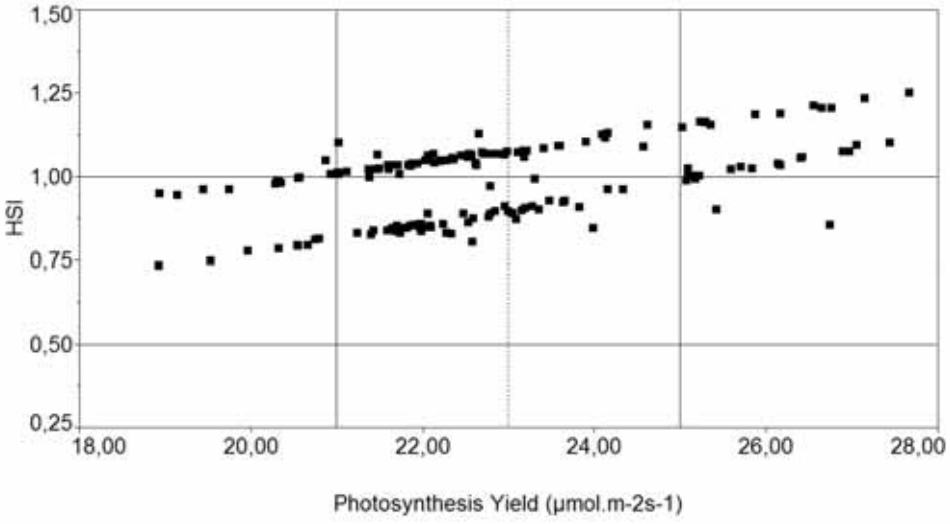

FIGURE 10
The graph on the leaf photosynthesis yield for genotypes

Leaf Photosynthesis Yield (µmol.m^{-2}s^{-1}): Whereas leaf photosynthesis yield values varied in the range of 20.42-33.05 µmol.m^{-2}s^{-1} under CC_N and 12.72-15.47 µmol.m^{-2}s^{-1} under CC_S, 13.16-27.08 µmol.m^{-2}s^{-1} under FC_N and 13.12-26.97 µmol.m^{-2}s^{-1} under FC_S. The mean leaf photosynthesis yield values were determined to be 28.38±2.72 µmol.m^{-2}s^{-1}; 14.68±0.63 µmol.m^{-2}s^{-1}; 18.59±3.14 µmol.m^{-2}s^{-1}; 17.09±2.88 µmol.m^{-2}s^{-1} under CC_N, CC_S, FC_N, FC_S, respectively. Of the genotypes, 86 were determined to be sensitive (2 in region III, 57 in region VI, 27 in region IX); 74 medium tolerant (19 in region II, 51 in region V, 4 in region VIII) (Fig.10).

DISCUSSION

It is seen that high temperature stress did not influence stoma numbers, whereas it decreased stomatal conductance, stomatal width, stomatal width/length, leaf area, leaf SPAD and leaf photosynthesis yield; and that it increased canopy temperature values.

As a result of the analysis conducted, among the genotypes constituting the material, whereas tolerant genotypes were not determined with respect to stoma number, it is seen that 90 medium tolerant genotypes were identified.

Stomatal conductance, stomatal width, stomatal width/length and plant canopy temperature are

the traits relevant to the opening conditions of stomata. Cotton plant can apply different attitudes/mechanisms towards reducing the effect of high temperature occurring. It aims at having the canopy temperature reach the optimal values so as to mitigate the damage caused by the high temperature occurred. This condition is closely related with the magnitudes of stress, soil moisture conditions and the air circulation factors in the canopy. In insufficient soil moisture conditions, cotton plant shows a tendency to close its stomata in order to reduce the water losses under the stress conditions caused by high temperature. In the study, decreasing values of stomatal conductance, width and width/length indicates the insufficient soil moisture level. However, it has to be considered that the mean canopy temperature under controlled conditions increased only 4.04 ^{o}C due to the effect of the stress. In the cotton plant, enabling this mechanism to deliver the desired benefit is largely associated with the soil moisture. The sufficiency level of the moisture content in the soil may affect the stoma opening of the plant and the escape mechanism of the cotton plant. In this condition, provided that other parameters are high, the genotypes with high stomatal conductance, width and width/length values under stress conditions are considered to be studied. Our findings support the findings of Hall (1992) [28] who reported that heat tolerance was achieved by selection of plants with more stomatal conductance; and those of Cornish et al. (1991) [29], Hutmacher and Krieg (1983) [30], Radin et al. (1987) [31]; Lu et al. (1994) [32], Nijs et al (1997) [33], Rahman (2004) [34] who noted that stomatal conductance and opening were highly related with the soil moisture.

As a result of the analysis done, the Fantom variety being an early genotype with respect to stomatal conductance trait and the Tropikal-225 genotype with respect to stoma width and width/length traits were determined to be tolerant; 91 varieties with respect to stomatal conductance trait, 79 varieties with respect to stoma width, and 76 with respect to width/length trait were determined to be medium tolerant.

Leaf area, leaf SPAD value and leaf photosynthesis yield are the traits relevant to the physiological development of the cotton plant. As a result of decreases in leaf area, leaf chlorophyll level and photosynthesis yield due to high temperature stress, decreases occur in the formation of photosynthesis products. In this condition, provided that other parameters are high, the genotypes with high leaf area, SPAD value and photosynthesis yield values under stress conditions are considered to be studied. Our findings support the findings of Reddy et al., (1991) [35] and Cottee et al., (2007) [36] who reported that photosynthesis yield dropped under high temperature stress conditions; those of Reddy et al., (2000) [37] who stated that the genotypes showing fast growing and photosynthesis at high temperature values had to be studied; and those of Cornish et al., (1991) [29] who noted that photosynthesis capacity is important for high yield. As a result of the analysis done, among the genotypes forming the material, whereas no tolerant genotype was determined with respect to leaf area, leaf SPAD value and photosynthesis yield traits, 78 genotypes were determined to be medium tolerant with respect to leaf area and leaf SPAD traits, and 74 genotypes were determined to be medium tolerant with respect to leaf photosynthesis yield trait.

It is thought that considering also the genotypes placed in the medium tolerant group in region VIII with respect to the traits studied (excluding canopy temperature), those in region II with respect to canopy temperature trait would be beneficial.

CONCLUSION

It was determined that high temperature stress did not affect the stoma numbers, whereas it decreased stomatal conductance, stomatal width, stomatal width/length, leaf area, leaf SPAD and leaf photosynthesis yield; and that it increased canopy temperature values. Cotton plant can apply different attitudes/mechanisms towards reducing the effect of high temperature occurring. Achieving the desired benefit by this mechanism in the cotton plant is largely related with the moisture content in the soil. As a result of decreases in leaf area, leaf chlorophyll level and photosynthesis yield due to high temperature stress, decreases occur in the formation of photosynthesis products. The Fantom was determined to be tolerant with respect to stomatal conductance trait and the Tropikal-225 genotype with respect to stoma width and width/length traits.

It is considered that it would be beneficial to pay attention to the following genotypes as medium tolerant genotypes: Nektarsız and STG-14 with respect to **stoma number trait**; 2421-A, Acala Prema, Bahar-82, Barut-2005, DKG-658, DPL-419, DPL-493, DPL-529, DPL-5409, Gossypolsüz Nazilli, GSN-12, HGPIG14QH-1-94, HT-1, LGQWILBCGS-1-95, Mc Nair-235, Nazilli-143, Nazilli-954, Nieves, PI-528420, Siokra-133, SPNXHQBPIS-1-94, STG-14, Stoneville-132, Şahin-2000, Tamcot-SP37-H, Taşkent-6, Zeta-2 with respect to **stomatal conductance trait**; 152-F, Çoşkun-1, DPL-419, Ekşi-911, Garant, Kurak-2, Nazilli-84, Paymaster-330, Stoneville-KC-311, Şahin-2000 and Tamcot-SP37-H with respect to **stomatal width trait**; 93-FF-01, Aleppo-1, DPL-419, Kurak-1, Lachata, Nazilli-87, PD-0648, Tamcot Sphinx and Stoneville-468 with respect to **stomatal width/length trait**; 2421-A, Acala 1517-99, Aleppo-40, BA-525, DKG-658, DPL-396, DPL-5111, DPL-5409, Nazilli-84, Siokra-133, STN-8A, Şahin-2000, Zeta-2 with respect to **leaf area trait**;

152-F, 93-FF-01, BA-525, Blightmaster, DPL-5111, DPL-529, GSN-22, Lachata, Özbek-142, NAPA-122, Paymaster-2379 (RR), Paymaster-330, R-5, SİVON, Sphinx V, STN-8A, Zeta-2 with respect to **leaf SPAD value trait**; NAPA-122, Nazilli M-342, PD-0648 and Şahin-2000 with respect to **photosynthesis yield trait**; 152-F, 2421 A, Acala 3080, Aleppo 40, Blightmaster, DPL 529, Kurak-1, Paymaster 330, Sphinx V, STN-8A, Stoneville 132 and Vulcano with respect to **canopy temperature trait**.

ACKNOWLEDGEMENTS

This work was supported by the Scientific and Technical Research Council of Turkey (TUBITAK) under Grant No. TOVAG-109O339.

REFERENCES

[1] Reddy, K.R., Hodges, H.F. and. Mc Kinion, J.M. (1997) Crop modeling and applications: a cotton example. Advance in Agronomy. 59, 225-290.
[2] Lawlor, D.W. (1997) Response of crops for environmental change conditions: Consequences for World food production. J. Agric. Meterol. 52(5), 769-778.
[3] Downing, T.E., Ringius, L., Hulme, M. and Waughray, D. (1997) Adapting to climate change in Africa. Mitigation and Adaptation Strategies for Global Change. 2, 19–44.
[4] Brownlee, C. (2001) The Long and Short of Stomatal Density Signals. Trends in Plant Sci. 6, 441-442.
[5] Kliewer, W.M., Kobriger, J.M., Lira, R.H., Lagier, S.T., Collalto, G. (1985) Performance of Grapevines Under Wind and Water Stress Conditions. Proc. of the International Symposium on Cool Climate Viticulture and Enology. 198-216.
[6] Rana, H.S. and Chadha, T.R. (1990) Relationship Between Stomatal Density and Vigor in Clones of Some Prunus Species. XXIII. International Hort. Cong. Firenze (Italy) Abst. of Contributed Papers. No.1232.
[7] Şahin, T. and Soylu, A. (1991) A research on the leaf morphology and stomata frequency of some important selected chestnut cultivars. Uludağ University Graduate School of Natural Sciences, Scientific Report Series: 10.
[8] Çağlar, S. and Tekin, H. (1999) The stomata density of Pistachio cultivars on different Pistacia rootstocks. Tr. J. Agric. Forest. 23, 1029-1032 (Turkish).
[9] Pekşen, E., Pekşen, A., Artık, C. (2006) Comparison of Leaf and Stomatal Characteristics in Faba Bean (Vicia faba L.). Journal of Biological Sciences. 6(2), 360-364, 2006.
[10] Baker D.N. (1965) The effects of certain environmental factors on net assimilation in cotton. Crop. Sci. 5, 53-56
[11] Surendra B., Oğuz, M.C., Özcan, S.F., Anayol, E., Ahmed, H.A., Khawar, K.M. and Özcan, S. (2016) Effect of Temperature Germination, Seed Vigor Index and Seedling Growth Of Five Turkish Cotton (Gossypium hirsutum L.) Cultivars. Fresen. Environ. Bull. 24(8a), 2561-2566.
[12] Barutcular, C., Yildirim, M., Koc, M., Dizlek, H., Akinci, C., El Sabagh, A., Saneoka, H., Ueda, A., Islam, M.S., Toptas, I., Albayrak, O., Tanrikulu, A. (2016) Quality Traits Performance of Bread Wheat Genotypes Under Drought and Heat Stress Conditions. Fresen. Environ. Bull. 25(12a), 6159-6165.
[13] Oosterhuis, D.M. (2002) Day or night high temperatures: A major cause of yield variability. Cotton Grower. 46, 8–9.
[14] Perry, S.W., Krieg, D.A. and Hutmacher, R.B. (1983) Photosynthetic rate control in cotton. Plant Physiol. 73, 662–665.
[15] Kakani, V.G., Reddy, K.R., Koti, S., Wallace, T.P., Prasad, P.V.V., Reddy, V.R., Zhao, D. (2005) Differences in in vitro Pollen Germination and Pollen Tube Growth of Cotton Cultivars in Response to High Temperature. Ann. Bot. 96:59-67.
[16] Johnson, J.R. and Saunders, J.R. (2003) Evaluation of Chlorophyll Meter for Nitrogen Management in Cotton. http://msucares.com/nmrec/reports/2002/
[17] Anonymous (2015) http://www.plantstress.com/methods/index.asp
[18] Fischer, R.A. and Maurer, R. (1978) Drought resistance in spring wheat cultivars. I. Grain yield response. Aust. J. Agric. Res. 29, 897-907.
[19] Khanna-Chopra, R. and Viswanathan, C. (1999) Evaluation of heat stress tolerance in irrigated environment of *T. aestivum* and related species. I. Stability in yield and yield components. Euphytica. 106, 169-180.
[20] Brown, P.W. (2008) Cotton Heat Stress. AZ1448, 02/08, This information has been reviewed by university faculty. cals.arizona.edu/pubs/crops/az1448.pdf, The University of Arizona College of Agriculture and Life Sciences Tucson, Arizona, 85721.
[21] Brown, P.W. and Zeiher, C.A. (1998) A model to estimate canopy temperature in the desert southwest. In: Proceedings of 1998 Beltwide Cotton Conferences, 5-9 Jan. 1998. San Diego, CA. Natl. Cotton Council. Memphis, TN. Vol. 2, 1734.
[22] Zeiher, C.A., Brown, P.W., Silvertooth, J.C., Matumba, N. and Mitton, N. (1994) The effect of night temperature on cotton reproductive development. In: Cotton: A College of Agriculture Report. Series P-96. University of Arizona, Tucson, AZ. 26-32.

[23] Zeiher, C.A., Matumba, N., Brown, P. and Silvertooth, J. (1995) Response of Upland cotton to elevated night temperature II. In: Proceedings of 1995 Beltwide Cotton Conferences, 4-7 Jan. 1995, San Antonio, TX. National Cotton Council, Memphis, TN. Vol. 2: 1129.
[24] Khan, A.I., Khan, I.A., Sadaqat, H.A. (2008) Heat tolerance is varıable in cotton (*Gossypium hirsutum* L.) and can be exploited for breedıng of better yielding cultivars under high temperature regimes. Pak. J. Bot., 40(5), 2053-2058.
[25] Gerik T.J., Faver, K.L., Thaxton, P.M. and Elzik, K.M. (1996) Late season water stress in cotton Plant growth, water use, and yield. Crop Sci. 36, 914-921.
[26] Pettigrew W.T. (2004) Physiological consequences of moisture deficit stress in cotton. Crop Sci. 44, 1265-1272.
[27] Burke, J.J. and Mahony, J.O. (2001) Protective role in acquired thermotolerance of developmentally regulated heat shock proteins in cotton seeds. The Journal of Cotton Sci. 5, 174-183.
[28] Hall, A.E. (1992) Breeding for heat tolerance. Plant Breeding Reviews. 10, 129168.
[29] Cornish, K., Radin, J.W., Turcotte, E.L., Lu, Z., Zeiger, E. (1991) Enhanced Photosynthesis and Stomatal Conductance of Pima Cotton (*Gossypium barbadense* L.) Bred for Increased Yield. Plant Physiol. (1991)97, 484-489.
[30] Hutmacher, R.B., Krieg, D.R. (1983) Photosynthetic rate control in cotton. Stomatal and nonstomatal factors. Plant Physiol. 73, 658-661.
[31] Radin, J.W., Kimball, B.A., Hendrix, D.L., Mauney, J.R. (1987) Photosynthesis of cotton plants exposed to elevated levels of carbon dioxide. Photosyn Res. 12, 191-203.
[32] Lu, Z.M., Radin, J.W., Turcotte, E.L., Percy, R.G. and Zeiger, E. (1994) High yields in advanced lines of pima cotton are associated with higher stomatal conductance, reduced leaf area and lower leaf temperature. Physiol. Plant. 92, 266-272.
[33] Nijs, I., Ferris, R., Blum, H., Hendrey, G., Tmpens, I. (1997) Stomatal regulation in a changing climate - a field study using free air temperature increase (FATI) and free air CO2 enrichment (FACE). Plant, Cell & Environ. 20, 1041-1050.
[34] Rahman, H. (2004) Genetic Basis of Heat Resistance in Upland Cotton Gossypium hirsutum L. (PhD. Thesis), Institute of Pure & Applied Biology, Bahauddin Zakariya University. Multan, Pakistan.
[35] Reddy, V.R., Baker, D.N. and Hodges, H.F. (1991) Temperature effects on cotton canopy growth, photosynthesis and respiration. Agronomy Journal. 83, 699-704.
[36] Cottee, N.S., Tan, D.K.Y., Cothren, T., Bange, M.P., Campbell, L.C. (2007) Screening Cotton Cultivars for Thermotolerance under Field Conditions. https://www.icac.org/wcrc/Paper2234.pdf.
[37] Reddy, K.R., Hodges, H.F. Kimball, B.A. (2000) Crop Ecosystem Responses to Climatic Change: Cotton. In: Reddy, K.R. and Hodges, H.F. (eds.) Climate Change and Global Crop Productivity. CAB International. 161-187.

Received: **07.07.2017**
Accepted: **03.12.2017**

CORRESPONDING AUTHOR

Sema Basbag
Department of Field Crops,
Faculty of Agriculture,
University of Dicle,
Diyarbakır – Turkey

e-mail: sbasbag@dicle.edu.tr

© by PSP Volume 27 – No. 2/2018 pages 744-748 Fresenius Environmental Bulletin

MINERAL CONTENTS AND FATTY ACID COMPOSITIONS OF WILD AND CULTIVATED ROSE HIP (*ROSA CANINA* L.)

Suleyman Kizil*, Ozlem Toncer, Tahsin Sogut

Department of Field Crops, Faculty of Agriculture, Dicle University, 21280 Diyarbakir, Turkey

ABSTRACT

Wild Rose hip (*Rosa canina* L.) clone samples were collected from Dicle, district of Diyarbakir, and conserved by planting since 2002 in the Department of Field Crops, Agriculture Faculty, Dicle University, Diyarbakir, Turkey. Morphological characteristics of fruits together with mineral contents, oil yield, protein contents, ash and fatty acid contents of wild and cultivated forms of the plant were determined. Thousand seed weight were determined as 27.5 g for wild and 22.5 g for cultured rose hips. Ca concentrations were found higher in fruits compared to seeds both in wild and cultivated forms. Whereas, Fe was lower in seeds than fruits. Zn and Na concentrations were 26.7 mg kg^{-1} and 129.1 mg kg^{-1} in wild seeds and 39.4 mg kg^{-1} and 129.4 mg kg^{-1} in cultivated seeds. The fruits had Zn, Na concentrations as 16.5 mg kg^{-1} and 140.9 mg kg^{-1} for wild and 33.8 mg kg^{-1} and 148.7 mg kg^{-1} for cultivated forms, respectively. Major fatty acids of rose hip fruit and seed oil of wild and cultivated forms were oleic, linoleic, palmitic, stearic and linolenic, respectively. The fruits had main fatty acid component as linoleic acid, while in the seeds it was determined as oleic acid.

KEYWORDS:
Rose hip, fruit characteristics, fatty acid composition, mineral content, oleic and linoleic acids

INTRODUCTION

The genus *Rosa* contains approximately 100 species that are widely distributed in Europe, Asia, the Middle East, and North America [1]. Matured and dried fruits of *Rosa canina* L. (Rosaceae) are consumed as herbal tea and used for making jam in the South east Anatolia Region, Turkey.

Plant height of this species ranged between 1.5 to 3 m and the plant is shown as a sub shrub plant. Flowers of plant are white and pink colour, and plant is widespread on borders of roads and gardens. Fruits of plant are plucked during autumn. Fruits consist sugar, organic acids, tannin and vitamin (A, B, C), especially vitamin C with range of 500 to 1700 mg/100 g [2] and 0.24 to 1.25% depending on sources [3]. Rose hip fruits are used throughout the world. Rose hip species are mainly used as a source of natural vitamin C and used as an herb tea ingredient.

It is reported that the major fatty acids of rose hip seed oils growing wild were palmitic (between 1.71% and 3.17%), stearic (1.69% and 2.47%), oleic (14.71% and 18.42%), linoleic (48,64% and 54.41%), linolenic (16.42%, and 18.41%), and arachidic (1.87%, and 2.61%). Moreover, it is reported that the seeds were rich in oil and minerals [4]. Fatty acids extracted from peel and seeds also show significant antibacterial [5], antioxidant, anti-inflammatory and anti-cyanobacterial activity [6].

Due to high vitamin C content, plant is well known for efficacy in human body defence against infections, particularly the common cold. Whole fruits or rose hip powders are boiled in water and used as diuretics and therapy against common cold remedies. The recommended daily intake for vitamin C is 90 mg for male adults and 75 mg for female adults [7].

The main objective of this study was to compare and determine some morphological characteristics, nutritional content and fatty acid compositions of the rose hip under wild and cultivated conditions.

MATERIALS AND METHODS

This study was carried out at the Department of Field Crops, Faculty of Agriculture, Dicle University, Diyarbakir, Turkey.

Plant Materials. Cuttings of rose hip plant for cultivation were collected from the district of Dicle, Diyarbakir province. Care was taken to collect plant material far from industrial activities, human waste accumulations, road traffic and chemicals used in agriculture (fertilizers and pesticides). Initially, the cuttings were rooted in sandy media (October 2002) for rooting, which were transplanted to the Medicinal and Aromatic Plants Collection Garden of Department of Field Crops, to grow until they showed well developed leaves over the cuttings (April 2003). The plants were watered when planted followed by watering during summer as and when required. No fertilizers were applied and required

care was made when needed. When the plants flowered in the field, they were identified in the taxonomy section of the Department of Biology, Dicle University, Diyarbakir, Turkey.

Rose hip fruits were harvested manually from *Rosa canina* shrubs cultivated during November 2008. The fruits in wild (district of Dicle, Diyarbakir) were also picked up at the same time for proper comparison with cultivated plants at ripe stage. The seeds were obtained from both types of fruits.

Oil Extraction. Ground samples were extracted in a Soxhlet extraction apparatus with petroleum ether (Merck) as solvent. Then the solvent was removed completely by rotary evaporation.

Protein Content. Protein contents of the samples were determined with LECO FP-528 (Leco Instruments, St Joseph, MI, USA) protein analyser.

Mineral Content. Mineral content of the plants were determined by Perkin Elmer Optima 2100 DV ICP OEMS.

Ash Content. Ash contents of the samples were determined at 600°C for 6 hour.

Lipid Extraction. Three gram seeds were used for each analysis. The samples were homogenised in chloroform-methanol (2:1, v/v) [8]. Autoxidation of unsaturated components was minimized by adding 50 µl of 2% butylated hydroxytoluene in chloroform. The total lipid extracts were dried under a stream of N_2 and measured gravimetrically. For subsequent analyses, the dry extracts were scraped into reaction vials, and the associated fatty acids were trans-methylated by refluxing the fractions in acidified methanol for 90 min at 85 °C. The fatty acid methyl esters (FAMEs) were extracted from the reaction vials three times with hexane [9]. Each sample was analysed in three replications.

Gas Chromatography/Mass Spectrometry (GC/MS) Analysis. Fatty acids of rose hip fruit and seed were analysed using a Finnigan–Trace GC-MS equipped with an auto sampler. One micro litre of the sample volume was injected using the split method with a 50 split ratio. Chromatographic separations were accomplished with a Thermo TR-MS 5 capillary column (5% phenyl–95% dimethylpolysiloxane, 0.25 mm i.d. × 60 m, film thickness 0.25 mm). Analysis was carried out using helium as the carrier gas with flow rate of 1.0 mL/min. The column temperature was programmed from 1 min in 50 ºC to 50 ºC to 300 ºC at 3 ºC/min for 5min. The injection port temperature was 250 ºC. The ionisation voltage applied was 70 eV with mass range m/z of 41–400 amu. The separated components were identified tentatively by matching with the GC-MS results of the National Institute of Standards and Technology (NIST 05) and Wiley 7 mass spectral library data. The quantitative determination was carried out based on peak area integration.

RESULTS AND DISCUSSION

The results of morphological characteristics, mineral and fatty acid contents of wild and cultivated rose hip are given in Table 1, 2, 3 and 4.

Thousand seed weight of wild and cultivated plants was recorded as 27.5 g and 22.5 g, hundred fruit weight as 123.5 g and 105.8 g, fruit length 22.1 mm and 21.5 mm, fruit width as 10.9 mm and 11.4 mm and moisture content as 14 and 12%, respectively. Wild plants had higher thousand seed weight, a hundred fruit weight, fruit length & width and moisture content compared to cultivated plants (Table 1). Fruit sizes of the present study are in accordance with Rosu et al. [10] who reported different populations of *Rosa canina* fruit length ranging 16.8 and 24 mm, and fruit width of 11.4 and 14.8 mm.

Mineral contents and chemical values of the rose hip fruits are given in Table 2 and 3. Quantitative results indicated important differences between mineral contents of wild and cultivated fruits of rose hip. Protein, oil contents, Al, Fe, K, Mg and Ni content of wild plants were higher compared to the cultivated plants. Contrarily, ash and Na content of wild plant were lower compared to the cultivated plants. Crude protein and oil contents of the seeds were considerably lower than those of fruits (Table 2 and 3). The protein content results of both fruits and the seeds are higher compared to Rosu et al. [10] who reported protein content of ten different Rosa species between 0.25% and 0.47%. Ash content was also found more than that reported by Leahu et al. [11] as 2.14 100 g^{-1}.

Ca, K and Mg content of seeds were also lower compared to their ratio in fruits. Ca (3704.3 mg kg^{-1}) Na (148.7 mg kg^{-1}) and Zn (33.8 mg kg^{-1}) of fruit concentration under cultivated conditions were higher compared to their concentration in the wild population. The mineral contents (K, Mg, and Na) of the wild and cultivated fruits contained higher concentrations compared to their concentrations in the seeds. Rose hip contained the optimum minerals in the fruits, and it is apparent that these are good sources of minerals both under wild and cultivated conditions.

The plant materials used in this study was collected very carefully to avoid pollution lead problems, the analytical studies carried out did not show any polluted chemical due to industrial, agricultural and other human anthropological activities that was reflected in the analysed samples that were far below the limits as described in legislation on Turkish and European food standards [7, 12].

TABLE 1
Some morphological characteristics of wild and cultivating forms of rose hip.

Characteristics	Wild	Culture
1000 seed weight (g)	27.5	22.5
100 fruit weight (g)	123.5	105.8
Fruit length (mm)	22.1	21.5
Fruit width (mm)	10.9	11.4
Moisture content (%)	14.0	12.0
Dry matter (%)	84.0	84.0

TABLE 2
Nutrition contents of wild and cultivated forms of rose hip.

Constituents	Wild		Culture	
	Fruit (mg kg^{-1})	Seed (mg kg^{-1})	Fruit (mg kg^{-1})	Seed (mg kg^{-1})
Al	101.4	66.6	70.3	55.2
Ca	3351.0	2141.0	3704.3	2430.3
Cd	-0.6	-0.6	-0.6	-0.5
Cr	-0.9	-1.0	-0.7	-0.9
Cu	2.8	4.0	5.4	4.2
Fe	117.5	83.1	89.7	87.2
K	6258.3	2906.3	4673.7	2455.0
Mg	1435.0	781.4	1301.5	877.7
Na	140.9	129.1	148.7	129.4
Ni	0.91	1.2	0.4	0.8
Pb	0.81	0.5	0.3	0.6
Zn	16.5	26.7	33.8	39.4

TABLE 3
Ash, protein, oil and essential oil contents of wild and cultivated forms of rose hip.

	Wild		Culture	
	Fruit	Seed	Fruit	Seed
Ash content (%)	4.0	2.5	7.5	2.5
Protein content (%)	3.4	4.3	2.2	4.4
Oil content (%)	5.4	7.4	4.8	10.4
Essential oil content (%)	0.05	0.05	0.05	0.05

Ercisli et al. [1] determined that the oil yield of seed was between 4.79% (*Rosa villosa*), 5.37% (*Rosa canina*), 5.13% (*R. pulverulanta*), 4.84% (*R. dumalis boissieri*), 4.60% (*R. pisiformis*), 5.22% (*R. dumalis*), and 5.01% (*R. dumalis antalyensis*). Seed oil content of present study ranged 7.4 and 10.4% that was higher compared to the results of above mentioned studies, and was in agreement with the results of Yunusova et al. [13]; who determined it as 7.2%. In contrast, oil yield reported in this study was higher compared to the Fan et al. [7] who reported rose hip oil yield of 1.74%.

Ozcan et al. [14] reported that rose hip contains Al (13.7 mg kg^{-1}), Ca (3479.3 mg kg^{-1}), Cd (0.000 mg kg^{-1}), Cr (1.33 mg kg^{-1}), Cu (0.71 mg kg^{-1}), Fe (8.85 mg kg^{-1}), K (5316.8 mg kg^{-1}), Mg (1018.2 mg kg^{-1}), Na (280.1 mg kg^{-1}), Ni (0.67 mg kg^{-1}), Pb (0.17 mg kg^{-1}) and Zn (3.96 mg kg^{-1}). Al, Cu and Fe contents of wild plants were clearly higher, and Cr and Pb content also were considerably lower compared to the findings of Ozcan et al. [14]. Ca, Cd and Mg contents of these researchers are in agreement with results of this study. Moreover, Demir and Ozcan [15] reported that *R. canina* contents Na in range of 3.97 to 4.67 mg kg^{-1}, K 890.5 to 1023.9 mg kg^{-1}, P 1850 to 2200 mg kg^{-1}, Fe 59.4 to 72.9 mg kg^{-1}, Zn 3.69 to 4.51 mg kg^{-1}, Mn 22.4 to 44.8 mg kg^{-1}, Mg 162.7 to 183.9 mg kg^{-1} and Ca 133.3 to 146.7 mg kg^{-1}. The seeds and fruits of wild and cultivated rose hip are rich in microelements, when compared to the previous studies [4, 7, 10]. These differences could be attributed to variations in environmental, growth conditions, time of harvesting and storage conditions.

TABLE 4
Fatty acid compositions (%) of wild and cultivated forms of rose hip.

Fatty acids	RT	Wild		Culture	
		Fruit	Seed	Fruit	Seed
Suberic acid	39.51	–	–	–	0.16
Citric acid	40.29	–	–	–	1.31
Lauric acid	42.54	0.12	0.16	0.20	0.1
Azelaic acid	43.66	–	0.50	–	1.19
Tetradecanoic acid	50.27	0.25	0.23	0.11	0.25
7-Hexadecenoic acid	56.62	–	–	–	0.19
Palmitic acid	57.32	7.21	–	7.44	24.79
Hexadecanoic acid ethyl ester	59.42	0.13			0.31
14-Methyl-hexadecanoic acid	60.51	–	0.14	–	0.17
Linoleic acid	62.75	37.07	34.43	23.09	17.07
Oleic acid	62.95	17.58	40.66	10.49	38.83
Linolenic acid	63.07	9.78	–	10.98	–
Stearic acid	63.62	2.66	6.03	2.93	7.05
Linolelaidic acid	65.58	0.11	0.41	0.24	–
Acetic acid. octadecyl ester	66.00	–	1.27	–	–
11.13-Eicosadienoic acid	68.66	–	1.20	–	0.45
11-Eicosenoic acid	68.78	0.25	0.48	–	0.46
Cis-9.10-epoxystearic acid	69.00	–	–	–	0.27
Arachidic acid	69.43	0.60	0.39	0.69	0.57
Erucic acid	74.23	–	–	–	–
Behenic acid	74.78	0.15	–	0.32	0.18
Dotriacontane	76.36	0.18	0.76	1.10	–
Tetracosanoic acid	79.78	0.10	–	0.48	0.31
Total		**76.19**	**86.66**	**58.07**	**93.66**

RT: retention time

Wild and cultivated rose hip fruit oil possess major fatty acids like oleic, linoleic, palmitic, stearic and linolenic acid contents of 74.60% and 54.93%, respectively (Table 4). In previous study, it is reported that rose hip fatty acid components represent 99.93% (*Rosa canina*) of total oil [1]. The fatty acid of wild and cultivated rose hip fruit oil has palmitic, linoleic, oleic, linolenic and stearic acid as major components. The highest fatty acid in fruit, linoleic acid, was noted as 37.07% from wild samples, while it was recorded as 23.09% from cultivated samples.

Similarly, oleic, palmitic, linoleic, linolenic and stearic acids were found as major oil components in rose hip seed. The highest oil component was found to be oleic acid in wild (40.66%) and cultivated plant seeds (38.83%). Conversely, Yunusova et al. [13] and Ercisli et al. [1] reported that linoleic acid was the main fatty acid component of *R. canina*.

CONCLUSION

The present study emphasise that the native rose hip species of South East Anatolia is extremely rich in fatty acids (linoleic and oleic acid) and some essential minerals both under wild and cultivated conditions. This suggests that these fruits have large potential for their effective use in the food industry.

REFERENCES

[1] Ercisli, S., Orhan, E., Esitken, A. (2007) Fatty acid composition of *Rosa* species seeds in Turkey. Chem. Nat. Compd. 43(5), 605-606.

[2] Baytop, T. (1984) Therapy with Medicinal Plants in Turkey (past and present) (1st ed.). Istanbul, Turkey: Publications of the Istanbul University, No. 3255 (In Turkish).

[3] Leung, A.Y., Foster, S. (2003) Encyclopaedia of Common Natural Ingredients Used in Food, Drugs and Cosmetics. John Wiley & Sons, USA, 649p.

[4] Ozcan, M. (2002) Nutrient composition of rose (*Rosa canina* L.) seed and oils. Journal of Medicinal Food. 5(3), 137-140.

[5] McGaw, L.J., Jager, A.K., Van Staden, J. (2002) Mini review: Antibacterial effects of fatty acids and related compounds from plants. S. Afr. J. Bot. 68, 417-423.

[6] Wang, H., Xi, B., Cheng, S., Wang, Y., Zhang, L. (2015) Phenolic and fatty acids from pomegranate peel and seeds: Extraction, identification and determination of their anti-algal activity. Fresen. Environ. Bull. 24, 3921-3915.

[7] Fan, C., Pacier, C., Martirosyan, D.M. (2014) Rose hip (*Rosa canina* L): A functional food perspective. Functional Foods in Health and Disease. 4(11), 493-509.

[8] Bligh, E.G., Dyer, W.J. (1959) A rapid method of total lipid extraction and purification. Canadian Journal of Biochemistry and Physiology. 37(8), 911–917.
[9] Stanley-Samuelson, D.W., Dadd, R.H. (1983) Long-chain polyunsaturated fatty acids: Patterns of occurrence in insects. Insect Biochemistry. 13(5), 549-558.
[10] Rosu, C.M., Manzu, C., Olteanu, S., Oprica, L., Oprea, A., Ciornea, E., Zamfirache, M.M., (2011) Several fruit characteristics of *Rosa* sp. genotypes from the Northeastern Region of Romania. Not. Bot. Horti Agrobo. 39(2), 203-208.
[11] Leahu, A., Damian, C., Oroian, M., Ropciuc, S., Rotaru, R. (2014) Influence of processing on vitamin C content of Rosehip fruits. Scientific Papers: Animal Science and Biotechnologies. 47(1), 116-120.
[12] Tuna, B., Gecgel, U. (2011) Determination of heavy metals and micronutrients in olives grown under different conditions. Fresen. Environ. Bull. 20, 2883-2889.
[13] Yunusova, S.G., Sitnikova, F.Kh., Karimova, A.R., Yunusov, M.S. (1998) Determination of fatty acid compositions by the direct transesterification of seed lipids. Chem. Nat. Com. 34(2), 137-140.
[14] Ozcan, M.M., Unver, A., Ucar, T., Arslan, D. (2008) Mineral content of some herbs and herbal teas by infusion and decoction. Food Chem. 106(3), 1120-1127.
[15] Demir, F., Ozcan, M. (2001) Chemical and technological properties of rose (*Rosa canina* L.) fruits grown wild in Turkey. J. Food Eng. 47(4), 333-336.

Received: **20.12.2016**
Accepted: **01.11.2017**

CORRESPONDING AUTHOR

Suleyman Kizil
Department of Field Crops,
Faculty of Agriculture,
Dicle University,
21280 Diyarbakır – Turkey

e-mail: suleymankizil@gmail.com

© by PSP Volume 27 – No. 2/2018 pages 749-756 Fresenius Environmental Bulletin

PARAMETERS ESTIMATION OF RIVER WATER QUALITY MODEL USING A DIFFERENTIAL EVOLUTION ALGORITHM

Hongqin Xue[1], Xiaodong Liu[2,*], Yong Xiong[2], Li Gu[2], Ting Yang[2]

[1]School of Civil Engineering, Nanjing Forestry University, Nanjing 210037, P.R. China
[2]Key Laboratory of Integrated Regulation and Resource Development on Shallow Lake of Ministry of Education, College of Environment, Hohai University, Nanjing 210098, P.R. China

ABSTRACT

To avoid the shortcomings of traditional optimization algorithms, a new multi-parameters estimation model based on Differential Evolution(DE) algorithm coupled with water quality model was proposed in this paper. The computational results of three numerical cases indicate the proposed parameter estimation model has high accuracy and good anti-noise properties. It can give precise results under both steady flow and unsteady flow. It can be used to identify parameters for both 1D and 2D water quality model, including analytical solution model and numerical model. Comparison results show that the method based on DE has roughly same accuracy as that on GA, but has higher convergence speed and better anti-noise property. This work contributes to the parameter estimation for river systems.

KEYWORDS:
Differential evolution (DE), Parameter estimation, River, Water quality model

INTRODUCTION

River system sustains a complex interaction and exchange of mass and energy within its biotic and abiotic components. It offers resilience to change and also recovers itself from the minor changes imposed on it from the polluting surroundings. Growing population, urbanization and industrialization have magnified the amount of total wastewater generated which threatens the health of river ecosystems when discharged into it. Rivers are increasingly getting polluted due to large scale withdrawal of fresh water and increased discharge of wastewater. Many nations have already initiated resource intensive river quality restoration projects [1]. Knowledge of dispersion of pollutants in streams is necessary for the determination of both the acceptable limits of effluent input and the concentration along the river course in these projects. Planning of these projects requires application of river water quality models. For many decades, river water quality models have been developed worldwide.

When the pollutant enters streams intentionally or unintentionally, it disperses in every direction due to diffusion and spatial velocity distribution. First the pollutant mixes completely in the vertical direction and then in the transverse direction. Most rivers have a high width/depth ratio and pollutants become mixed vertically within a short distance from the source. Vertical mixing is only important in the so-called near field and is often neglected when considering subsequent transverse and longitudinal mixing. When dealing with the practical engineering problems, it is not computationally efficient to use three-dimensional (3D) models. Instead, researchers applied two-dimensional (2D) water quality models to simulate the transverse mixing in channels. After the transverse mixing has taken place, the primary variation of concentration is in one direction; dispersion from that section onwards is referred to as longitudinal dispersion and is independent of the geometrical configuration and type of source. In natural channels, 1D mathematical models are commonly adopted to model the longitudinal dispersion process. Whichever model is chosen, the selection of proper parameters is the most important and also the most difficult task. The dispersion coefficient represents the rate of pollution and it is the most desired parameter in any water pollution modeling study. In many practical and natural situations, one or two dimensional dispersion coefficients are often required for modeling. Besides dispersion coefficients, some other parameters, i.e. degradation coefficient, also must be obtained. It is a relatively simple task to use a measured dispersion coefficient, if it is known. However, for streams where mixing and dispersion characteristics are unknown, the water quality coefficients can only be estimated using theoretical equations, empirical equations or inversion method.

A theoretical method to predict the longitudinal dispersion coefficient was first proposed by Taylor [2] and expanded by Elder [3], who derived an equation to compute the longitudinal coefficient for a uniform flow in an infinitely wide open channel, assuming a logarithmic velocity profile. Fischer et al. [4] found that the transverse profile of the longitudinal

velocity is 100 or more times as important in producing longitudinal dispersion as the vertical profile in the natural streams. Fischer [5] and Fischer et al. [4] gave the following quantitative estimate of longitudinal dispersion coefficient in a real stream by neglecting the vertical velocity profile entirely and applying Taylor's analysis to the transverse velocity profile.

$$E_x = -\frac{1}{A}\int_0^W U'h(y)\int_0^y \frac{1}{\varepsilon_t h(y)}\int_0^y U'h(y)dydydy \quad (1)$$

where A is flow area; y is distance in transverse direction; W is width of channel; U' is deviation of local depth-averaged velocity from the cross-sectional averaged velocity U; and ε_t is local transverse mixing coefficient. Equation (1) is rather difficult to use because detailed transverse profiles of both velocity and cross-sectional geometry are required. Some researchers developed different equations using different velocity profiles for the Equation (1) [6-10]. Thus, the theoretical method is not encouraging in terms of data requirement. A number of investigators have developed empirical equations for predicting the dispersion coefficient based on experimental and field data [11-14]. The longitudinal dispersion coefficient can be estimated by using flow and channel parameters. But since most studies have been conducted based on specific assumptions and channel conditions, the behavior of existing equations varies widely even for the same flow conditions and streams. Comparatively, the parameter inversion method, which is based on concentration profile, is thought to be more accurate and reliable. The method would be called tracer test method if the concentration data is obtained by using tracer test. Many tracer test methods have been published. For example, the longitudinal dispersion coefficient can be obtained by using curves of the temporal variation of concentration (C–t curves) at two or more stations downstream of the tracer injection point. The moment method [4, 15], routing procedure [5], fitting method [16], and the optimization method [17] are available for the determination of longitudinal dispersion coefficient using C–t curves and other properties of the stream. Besides tracer test method, sometimes, the concentration data is from field water quality measurement without expensive tracer test. For example, trial-and-error is the most common method used in parameters identification. With this approach, an initial group of estimated values for the parameters is assumed and inserted into the numerical model, and then the simulated results are compared with field data. If the deviation is significant, the parameters are repeatedly adjusted until the deviation is acceptable. It is not feasible if the studied river has a complicated topography. To address this, researchers have proposed a number of auto-calibration models [18] by using optimization method. Its optimizing process largely avoids the calculation errors caused by field measurements. Traditional optimization algorithms sometimes cannot get satisfactory coefficients with observation data with noise for their limitations, such as high demand for objective function, local convergence, and the convergence speed decreasing by geometric progression with the increase of the number of parameters. This limits their application in multi-parameter identification for complicated models. To address this, artificial intelligence techniques, such as artificial neural network (ANN), adaptive neuro-fuzzy inference system, genetic algorithm (GA) and Bayesian networks(BA) have shown promising performance in predicting longitudinal dispersion [19-22].

Recently, as another evolutionary technique, differential evolution (DE), has been proposed for unconstrained continuous optimization problems in 1995 [23]. Although the original objective in the development of DE was for solving the Chebychev polynomial problem, it has been found to be an efficient and effective solution technique for complex functional optimization problems [24]. In 1996, DE algorithm has been proved to be the optimization algorithm with the highest convergence speed during the First International Contest on Evolutionary Computation. Due to its simple concept, easy implementation and quick convergence, the algorithm has attracted much attention and wide applications [25]. However, until now, there have been few published work on DE for parameters estimation of water quality models.

In this present study, a DE approach is applied to estimate the parameters of river water quality models. Numerical cases and comparisons demonstrate the effectiveness and robustness of DE.

MATERIALS AND METHODS

Parameter Estimation Method Based on DE. The problem of parameter estimation could be converted to an extremum problem by defining a object function J. The agreement between the measured results and simulated values is one of the most important indicators as to how well a model is calibrated [26]. The object function J, which is Expressed with the norm, is defined as follows:

$$J(C,X) = \int_0^T \frac{1}{2}\left\|C - C^*\right\|^2 dt \quad (2)$$

where C is calculated value vector, C^* is observed value vector, X is unknown parameter vector. In parameter identification, model parameters are adjusted to achieve minimize J for all variables simultaneously. The extremum problem can be described mathematically as follows:

$$\text{Minimize } J = f(X) = f(x_1, x_2, ..., x_n) \quad (3)$$

$$\text{Subject to } x_{ilow} \le x_i \le x_{iup} \quad i = 1, 2, ..., n \quad (4)$$

where, $X = (x_1, x_2, ..., x_n)$ is the parameter vector, *n* is the number of parameters to be identified, x_{ilow} and x_{iup} represent the lower bound and upper bound of the parameter x_i. The *J* is a non-linear function, and its minimization problem can be solved by multidimensional non-linear optimization methods. DE algorithm coupled with water quality model was used here for its high efficiency and robustness.

DE is a population-based evolutionary computation technique, which uses simple differential operator to create new candidate solutions and one-to-one competition scheme to greedily select new candidate. The general steps of the estimation method are as follows:

(1) Parameters set for the DE: the parameters include the number of parameters (n), population size (NP), scaling factor (F), the probability of crossover operator (*CR*), the maximal number of generations (T_m). NP is at least 4 so that the mutation can be applied.

(2) Initialization: the initial population is generated from specified ranges of parameters by random methods, which is usually preferred to keep a suitable balanced distribution in the initial population. $x_i^0 = x_{ilow} + rand \times (x_{iup} - x_{ilow})$, where *rand* is a random number between 0 and 1.

(3) Selection of water quality model: According to the river flow condition and pollutant emission mode, suited water quality model is necessary to be established correctly.

(4) Calculation of fitness: since the DE can only make the individual evolution in the direction where the fitness increases, so the fitness function can be designed as follows:

$$Fit(X) = 1/(J(X)) = (\int_0^T \frac{1}{2} \left\| C - C^* \right\|^2 dt)^{-1} \quad (5)$$

Where, *C* is calculated by using water quality model, C^* is obtained by measurement. Calculate the fitness of the current *X*. Check $T > T_m$, where *T* is the number of generation. If so, output the current value of *X* as the final parameter estimation results. Otherwise continue.

(5) Mutation. The purpose of mutation is to broaden the search scope. After a current individual X_j was selected, the new individual Y_j is generated as follows.

$$Y_j = X_{r1}(t) + F(X_{r2}(t) - X_{r3}(t)) \qquad j = 1, 2, ..., NP \quad (6)$$

Where $r1, r2, r3$ are randomly chosen and $r1 \neq r2 \neq r3 \neq i$. $F \in [0, 2]$ is a constant called scaling factor which controls amplification of the differential variation $X_{r2}(t) - X_{r3}(t)$.

(6) Crossover. The crossover operator is applied to increase the diversity of the population. Thus, for each target individual $X_j(t) = (x_{j1}, x_{j2}, ..., x_{jn})$, a crossover vector $Z_j = (z_{j1}, z_{j2}, ..., z_{jn})$ is generated by the following equation:

$$z_{ji} = \begin{cases} y_{ji}, & \text{if } (rand_i \leq CR \vee j = k(i)) \\ x_{ji}, & else \end{cases} \quad (7)$$

Where $rand_i$ is the *i*th independent random number uniformly distributed in the range of [0,1]. $k(j)$ is a randomly chosen index from the set $\{1, 2, ..., n\}$. $CR \in [0,1]$ is a constant called probability of crossover operator that controls the diversity of the population.

(7) Selection. An individual of the given population is selected according to its fitness to form the next generation by selection operator. After the crossover operation, the member of the population of the next generation is generated by the following one-to-one based greedy selection criterion:

$$X_j(t+1) = \begin{cases} Z_j, & \text{if } (Fit(Z_j) \geq Fit(X_j(t)) \\ X_j(t), & otherwise \end{cases} \quad (8)$$

where $X_j(t+1)$ is the individual of the new population. After this go back to step 4.

The flow chart of the parameter identification model can be seen in Fig.1.

RESULT AND DISSCUSION

Case 1. Test data are taken from the literature [20, 27]. The case was a numerical test not an actual test. The river cross-section area *A* was 20 m^2, and the average velocity *u* was 0.5 $m \cdot s^{-1}$. The tracer (10 kg) was released in the upper reaches of the river. Assuming that the longitudinal dispersion coefficient E_x was 50 $m^2 \cdot s^{-1}$ and degradation coefficient *K* was 0.3 d^{-1} in the case Tracer concentration (to three decimal places) at different times in the downstream 500 m was calculated by 1D water quality model, and are shown in Table 1. Treating the data in Table 1 as observational data and *A*, *u*, E_x and *K* as unknown parameters to be identified, this case can be used to verify the reliability of parameter estimation method.

Observation Data with Noise. No matter how high accuracy measuring instruments are used, observation noise can not be avoided in measurement. Since the noise is usually random, some random noise was added to the values in Table 1. The observational data with noise can be expressed as: $C_j^\delta = C_j^*(1 + \beta * \delta)$. Where C_j^* is true concentration, β is random number between -1 and 1, δ is noise (disturbance) level.

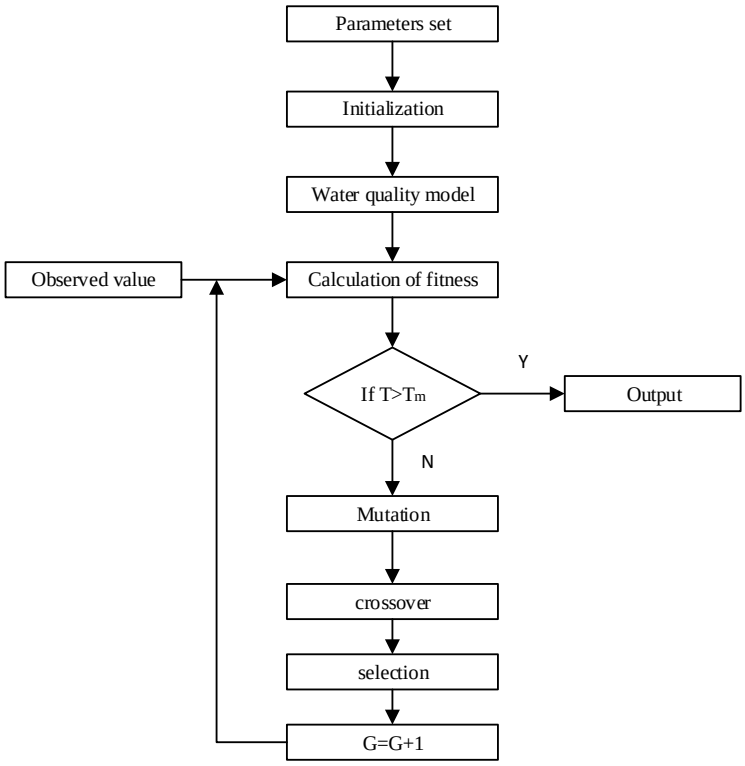

FIGURE 1
Flow chart diagram for the parameter estimation model

TABLE 1
Tracer test data in instantaneous source

t_i/min	2	6	10	12	14
c_i/(mg·L^{-1})	0.001	0.254	0.583	0.649	0.663
t_i/min	16	20	24	36	40
c_i/(mg·L^{-1})	0.642	0.552	0.444	0.197	0.147

TABLE 2
Results under different noise level

Parameter	*method*	*GA*			*DE*		
	noise level	*mean value*	*standard deviation*	*relative standard deviation*	*mean value*	*standard deviation*	*relative standard deviation*
A	$\delta=1\%$	19.9282	0.0699	0.35%	19.9533	0.0728	0.36%
	$\delta=5\%$	19.9299	0.1708	0.85%	19.9808	0.2114	1.06%
	$\delta=10\%$	19.8866	0.3818	1.91%	19.9750	0.4431	2.22%
	$\delta=30\%$	20.0991	1.3008	6.50%	20.0672	1.2877	6.44%
u	$\delta=1\%$	0.4993	0.0012	0.24%	0.4995	0.0011	0.22%
	$\delta=5\%$	0.4997	0.0049	0.98%	0.4997	0.0046	0.92%
	$\delta=10\%$	0.4992	0.0092	1.84%	0.4984	0.0094	1.88%
	$\delta=30\%$	0.4983	0.0284	5.68%	0.5021	0.0282	5.64%
E_x	$\delta=1\%$	50.0087	0.2519	0.50%	49.9913	0.2573	0.51%
	$\delta=5\%$	50.0905	1.2288	2.46%	49.9721	1.2468	2.49%
	$\delta=10\%$	50.1091	2.4866	4.97%	50.0237	2.3365	4.67%
	$\delta=30\%$	49.6296	8.0001	16.00%	49.6516	7.7054	15.41%
K_1	$\delta=1\%$	0.6167	0.3056	101.87%	0.5184	0.2394	79.80%
	$\delta=5\%$	0.5860	0.3869	128.97%	0.4838	0.2346	78.20%
	$\delta=10\%$	0.5791	0.4196	139.87%	0.5013	0.2318	77.27%
	$\delta=30\%$	0.5691	0.4323	144.10%	0.5067	0.2377	79.23%

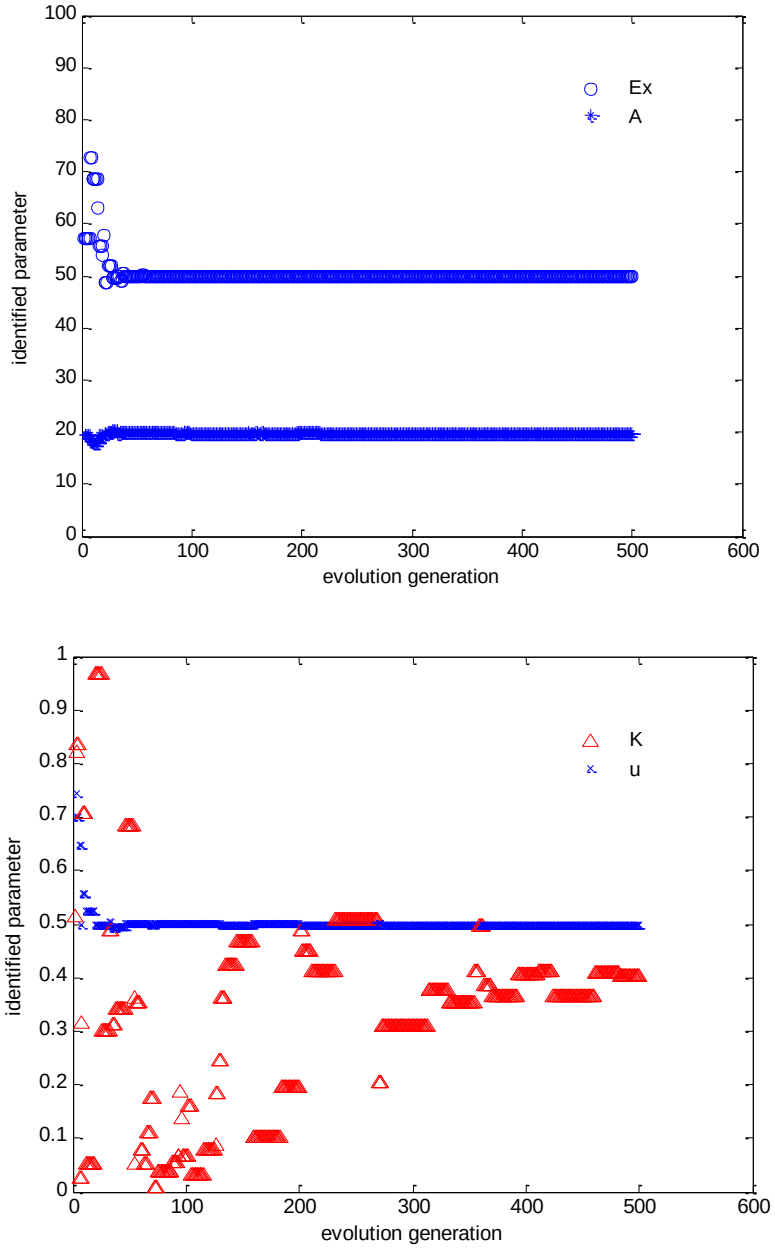

FIGURE 2
Parameters evolution process by DA

Parameter Estimation. Under the condition of instantaneous source and steady flow, analytic solutions of 1D water quality model are used here. Using the parameter estimation method on DE, the result compared with the results on GA [20] can be obtained in Table 2, where F is0.8, CR is 0.8, T_m is 500. The result shows that both methods have high accuracy and good anti-noise property at a similar level. The parameters evolution process can be shown in Fig 2. From Fig 2, it can be concluded that DA has better convergence speed than GA.

Case 2. The numerical test is given to test the parameter identification approach when the flow is unsteady [20]. The length of studied river is 3 km. The variations of the stream discharge with time can be expressed as $Q(t)=10+0.001*t$ $m^3 \cdot s^{-1}$. The river can be separated into six stream sections. Upstream concentration C_0=1.0 $mg \cdot L^{-1}$, and the initial concentration in the studied river is assumed to be 0 $mg \cdot L^{-1}$. Denoting the longitudinal dispersion coefficients of each section as 50 $m^2 \cdot s^{-1}$, 70 $m^2 \cdot s^{-1}$, 90 $m^2 \cdot s^{-1}$, 110 $m^2 \cdot s^{-1}$, 130 $m^2 \cdot s^{-1}$ and 140 $m^2 \cdot s^{-1}$ respectively, the concentrations of the final section of six segments (to three decimal places) can be obtained by a FDM water quality model, shown in Table 3. The longitudinal dispersion coefficients of the six sections are supposed to be unknown parameters, which should be

identified by parameter identification model if the proposed model is correct. The test has been used to verify the method based on GA by Liu et al. [20], so Comparison results between GA and DE for parameter estimation are discussed here.

Parameters Identification on Observation Data without Noise. The data in Table 3 are calculated concentrations without noise added. The parameter estimation results by parameter identification model on DE and GA are shown in Table 4. The values by using the two methods are very close to the denoting values, and the errors are 0.01%~0.97% and 0.03%~1.38% respectively. There are no significant different precision between the two methods.

Parameter Identification on $\delta = 10\%$ Observation Data with Noise. Some random noise is added in Table 3, where the data are assumed to be measured concentrations with noise. Using the Matlab program for 500 iterations, the statistical results by DE and GA are shown in Table 5. From Table 5 it can be concluded that satisfactory results can be obtained by DE or GA when $\delta \le 10\%$, which indicate that both of them have good global convergence and robustness. However, the relative standard deviation of the parameters by DE are less than those by GA, which indicate that DE has better anti-noise abilities for parameter estimation.

TABLE 3
Concentration values used in parameter identification (mg·L^{-1})

t/min	The number of stream section					
	1	2	3	4	5	6
5	0	0	0	0	0	0
10	0.213	0.028	0.003	0	0	
15	0.399	0.100	0.020	0.003	0	
20	0.555	0.203	0.058	0.014	0.003	0.001
25	0.684	0.323	0.121	0.039	0.011	0.005
30	0.787	0.448	0.205	0.081	0.028	0.014
35	0.867	0.570	0.306	0.142	0.059	0.035
40	0.925	0.681	0.417	0.222	0.105	0.070
45	0.965	0.777	0.530	0.317	0.168	0.126
50	0.991	0.856	0.638	0.422	0.245	0.204
55	1.000	0.917	0.737	0.530	0.334	0.305

TABLE 4
Inversion result of parameters by DE and GA under no noise

The number of stream segment		1	2	3	4	5	6
true value		50	70	90	110	130	140
GA	Identified value	50.0042	70.0193	89.9807	109.8955	130.4208	141.3565
	relative deviation	0.01%	0.03%	0.02%	0.10%	0.32%	0.97%
DE	Identified value	50.0163	70.0350	90.0162	109.9824	130.5442	141.9283
	relative deviation	0.03%	0.05%	0.02%	0.02%	0.42%	1.38%

TABLE 5
Inversion result of parameters by genetic algorithm under 10% noise level

Stream segment		1	2	3	4	5	6
true value		50	70	90	110	130	140
GA	mean value	48.7907	69.4851	97.8049	111.9494	125.2322	110.2591
	standard deviation	3.7558	9.2667	20.9430	26.1876	25.4049	53.3514
	relative standard deviation	7.51%	13.24%	23.27%	23.81%	19.54%	38.11%
DE	mean value	50.2546	64.5020	84.6603	117.8943	127.2391	131.7230
	standard deviation	3.7156	5.4940	11.6601	23.4915	18.4143	29.4398
	relative standard deviation	7.43%	7.85%	12.96%	21.36%	14.16%	21.03%

TABLE 6
Result of parameters under different sampling time scale

Iteration steps	E_x ($m^2 \cdot s^{-1}$)		E_y ($m^2 \cdot s^{-1}$)		K_1 (d^{-1})	
	Value	Relative deviation	Value	Relative deviation	Value	Relative deviation
47	0.995745	0.43%	0.100104	0.10%	0.295544	1.49%
100	1.000115	0.01%	0.099997	0.00%	0.300266	0.09%

Case 3. This numerical test [26] is given to test the parameter identification approach for 2D water quality model. The length of the studied river was 2 km. The river width B was 100 m. The upstream discharge was 60 $m^3 \cdot s^{-1}$. The variations of downstream water level with time can be expressed as follows:

$$z = z_0 + A \cdot \sin\left(\frac{2 \cdot \pi t}{T}\right) \tag{9}$$

where wave amplitude A is 0.1, z_0 is 1.0 m, cycle T is 12 h. A point source released pollutants continuously with the speed of 15 $g \cdot s^{-1}$. Upstream concentration and the initial concentration in the studied river is assumed to be 0 $mg \cdot L^{-1}$. 200 meshes were distributed in the studied area which can be seen in the literature [26]. Denoting E_x as 1.0 $m^2 \cdot s^{-1}$, E_y as 0.1 $m^2 \cdot s^{-1}$, and K as 0.3 d^{-1}, the pollutant concentration of five points (to three decimal places) every 1 hour in the downstream 1000 m can be calculated by water quality ADI model [26]. Treating the data as observational data and u, E_x, E_y and K as unknown parameters to be identified, this case can be used to verify the reliability of parameter estimation method.

Parameters Estimation for 2D Water Quality Model. Using target function $J \le 0.000001$ as termination condition, the parameter estimation results by parameter identification model are shown in Table 6（T=47）. Using maximum iteration step is 100 as termination condition, the parameter estimation results are shown in Table 6. The calculated values are very close to the denoting values. By this method, successful calculation of parameters of 2D water quality model can be achieved.

CONCLUSIONS

To avoid the shortcomings of traditional optimization algorithms, a new multi-parameters estimation model based on DE algorithm coupled with water quality model was proposed in this paper. The computational results of three numerical cases indicate the proposed parameter estimation model has high accuracy and good anti-noise properties. It can give precise results under both steady flow and unsteady flow. It can be used to identify parameters for both 1D and 2D water quality model, including simple analytical solution model and complicated numerical model. Comparison results show that the method based on DE has roughly same accuracy as that on GA, but has higher convergence speed and better anti-noise property.

ACKNOWLEDGEMENTS

This research was supported by the National Nature Science Foundation of China (Grant No. 51479064, 51379058, 51379060), a Project Funded by the Priority Academic Program Development of Jiangsu Higher Education Institutions（PAPD） and Qing Lan Project.

REFERENCES

[1] Sharma, D. and Kansal, A. (2013) Assessment of river quality models: a review. Rev Environ Sci Biotechnol. 12, 285–311.
[2] Taylor, G.I. (1954) The dispersion of matter in turbulent flow through a pipe. Proceedings of Royal Society of London. 223A, 446–468.
[3] Elder, J.W. (1959) The dispersion of marked fluid in turbulent shear flow. Journal of Fluid Mechanics. 5(4), 544–560.
[4] Fischer, H.B., List, E.J., Koh, R.C.Y., Imberger, J. and Brooks, N.H. (1979) Mixing in Inland and Coastal Waters. Academic Press, New York.
[5] Fischer, H.B. (1967) The mechanics of dispersion in natural streams. Journal of Hydraulic Division. 93(6), 187–216.
[6] Deng, Z.Q., Singh, V.P. and Bengtsson, L. (2001) Longitudinal Dispersion Coefficient in Straight Rivers. Journal of Hydraulic Engineering. 127(11), 919–927.
[7] Ahmad, Z. (2003) Estimation of longitudinal dispersion coefficients. Journal of Hydraulic Engineering. 9(1), 14–28.
[8] Seo, I.W., Gadalrab, M.S. (1999) Estimation of Dispersion Coefficient Using Different Forms of Lateral Velocity Distribution. Proc. WEESHE-99 Conf.217–226.
[9] Seo, I.W., Baek, K.O. (2004) Estimation of the Longitudinal Dispersion Coefficient Using the Velocity Profile in Natural Streams. Journal of Hydraulic Engineering. 130(3), 227-236.
[10] Wang, Y.F., Huai, W.X. (2016) Estimating the longitudinal dispersion coefficient in straight natural rivers. Journal of Hydraulic Engineering. 142(11), 04016048.

[11] Tayfur, G., Singh, V.P. (2005) Predicting longitudinal dispersion coefficient in natural streams by artificial neural network. Journal of Hydraulic Engineering. 131(11), 991–1000.
[12] Sahay, R.R., Dutta, S. (2009) Prediction of longitudinal dispersion coefficients in natural rivers using genetic algorithm. Hydrology Research. 40(6), 544–552.
[13] Zeng, Y., Huai, W.X. (2014) Estimation of longitudinal dispersion coefficient in rivers. Journal of Hydro-environmental Research. 8(1), 2–8.
[14] Disley, T., Gharabaghi, B., Mahboubi, A. and McBean, E. (2015) Predictive equation for longitudinal dispersion coefficient. Hydrological Processes. 29(2), 161–172.
[15] Naidoo, N., Kumarasamy, M. (2016) Sensitivity Analysis of Model Parameters for Water Quality Simulation. Polish Journal of Environmental Studies. 25(4), 1655-1660.
[16] Wen, J., Guo, J.Q., Zai, S.M. and Wang, H.S. (2008) Linear analytic method for determining water quality parameters of river according to the observation data obtained from two sections. Journal of Hydraulic Engineering. 39(10), 618-622.
[17] Ho, D.T., Schlosser, P. and Caplow, T. (2002) Determination of longitudinal dispersion coefficient and net advection in the tidal Hudson River with a large-scale, high resolution SF6 tracer release experiment. Environmental Science & Technology. 36(15), 3234-3241.
[18] Liu, X.D., Hua, Z.L., Xue, H.Q., Gu, L. and Xie, Z.F. (2011) Inverse optimization method to determine longitudinal dispersion coefficient and selection of sampling time in tracer test. Fresen. Environ. Bull. 20, 1149-1154.
[19] Toprak, Z.F., Cigizoglu, H.K. (2008) Predicting longitudinal dispersion coefficient in natural streams by artificial intelligence methods. Hydrological Processes. 22, 4106–4129.
[20] Liu, X.D., Zhou, Y.Y., Hua, Z.L., Chu, K.J., Wang, P., Gu, L. and Chen, L.Q. (2014) Parameter identification of river water quality models using a genetic algorithm. Water Science & Technology. 69(4), 687-693.
[21] Ahmad, Z. (2013) Prediction of longitudinal dispersion coefficient using laboratory and field data: relationship comparisons. Hydrology Research. 44(2), 362–376.
[22] Mohamad, J.A., Hosein, S., Mohammad, R.K., Hamid, S. and Reza, B. (2017) Prediction of longitudinal dispersion coefficient in natural rivers using a cluster-based Bayesian network. Environmental Earth Science. 76, 86.
[23] Storn, R., Price, K. (1995) DE- A simple and efficient adaptive scheme for global optimization over continue space. Technical Report TR-95-012, ICSI.
[24] Khazraee, S.M., Jahanmiri, A.H. and Ghorayshi, S.A. (2010) Model reduction and optimization of reactive batch distillation based on the adaptive neuro-fuzzy inference system and differential evolution. Neural Comput Applic. 20(2), 239–248.
[25] Peng, B., Liu, B., Zhang, F.Y. and Wang, L. (2009) Differential evolution algorithm-based parameter estimation for chaotic systems. Chaos, Solitons and Fractals. 39, 2110–2118.
[26] Liu, X.D., Tu, Q.L., Hua, Z.L., Huang, W.R., Xing, L.H. and Zhou, Y.Y. (2015) Multi-parameter identification of a two-dimensional water-quality model based on the Nelder–Mead Simplex algorithm. Hydrology Research. 46(5), 711-720.
[27] Guo, J.Q., Wen, J. (1990) The liner graphic method for determining longitudinal dispersive coefficient of the streams by tracer test. Environmental Science. 11(2), 24-27.

Received: **21.12.2016**
Accepted: **27.12.2017**

CORRESPONDING AUTHOR

Xiaodong Liu
College of Environment Hohai University (HHU)
Xikang Road 1
Nanjing 210098 – P.R. China

e-mail: xdliu@hhu.edu.cn

© by PSP Volume 27 – No. 2/2018 pages 757-764 Fresenius Environmental Bulletin

INFLUENCE OF IBA TREATMENTS ON ROOT DEVELOPMENT AND MINERAL UPTAKE OF GRAPEVINE CUTTINGS

Sezer Sahin[1,*], Mustafa Uysal[2]

[1]Gaziosmanpasa University, Faculty of Agriculture, Department of Soil Science and Plant Nutrition, Tasliciftlik Campus, 60200, Tokat, Turkey
[2]Alasehir Commodity Exchange Soil Laboratory, Manisa, Turkey

ABSTRACT

The present study was conducted to determine the effects of different indole butyric acid concentrations (IBA, 0, 1000 and 2000 ppm) on root development and mineral uptake of cuttings of three different grapevine cultivars (Redglobe, Sultani and Superyol) and 41-b rootstock over soils with three different pH levels (5, 7 and 8). A pot experiment was conducted in a completely randomized block design with 3 replications. Cuttings were planted in pots and 150 mg kg^{-1} N, 50 mg kg^{-1} P and 100 mg kg^{-1} K were supplied to each pot to support the growth of saplings. Fresh and dry root and leaf weights were measured and leaf nitrogen, phosphorus and potassium contents were analyzed. Compared to control (0 ppm IBA) treatment, significant increases were observed in root and leaf weights with increasing IBA concentrations. Increased N, P and K uptakes were also observed at 1000 and 2000 ppm IBA treatments. The results clearly demonstrated that IBA treatments improved biomass and mineral uptake of grapevine cuttings.

KEYWORDS:
Grapevine, indole-3-butyric acid, root development, mineral uptake

INTRODUCTION

Grapevine (*Vitis vinifera L.*) is one of the most important edible and beverage fruits cultivated worldwide. Vineyard sites are ever increasing in the world and old vineyards are re-planted with the new ones. In renewals, either the rootstocks or cultivars resistant especially against to phyloxera disease should be planted or a well root development should be provided proper plant nutrition and other cultural practices. Auxin treatments, especially IAA, NAA and IBA, are applied commonly to improve rooting and root quality of saplings and scions. Auxin is one the most important hormones used on stem cuttings for accelerating the formation of adventitious roots [1]. Primary task of auxin is to initiate root formation. Plants are able produce auxins in their roots and young leaves but scions should be treated with auxins to prevent deaths [2]. Auxins, particularly indole-3-butyric acid (IBA), are one of the most common and effective means to enhance rooting of cultures [3].

IBA is a plant growth regulator used to promote and accelerate root formation of plant clippings and to reduce transplant shock of non-food ornamental nursery stock [4]. Various researchers reported positive impacts of IBA on root development and rooting of various plants [5-6, 7, 8, 9, 10, 11, 12].

Positive impacts of IBA treatments on root development and rooting also increase plant nutrient uptake from the soil. Nitrogen exists in structure of IAA (indole-3-acetic acid) through existence in structure of tryptophan amino acid forming indole-3-acetic acid [13]. IAA synthesis is retarded under nitrogen deficient conditions. With the existence of potassium in the ambient, increases are observed in indole acidic acid, cytokine and gibberellic acid activities [14]. Some growth hormone (IAA, GA_3, ABA and Cytokine) treatments decreased P concentration in tomato plant tissues [15]. Such increase or decreases in mineral uptakes result in variations in vegetative developments of the plants. In grapevines, high rooting rates and well-growth in the initial year will positively affect the later growth and development of the plants.

While IBA treatments had positive impacts on root development of sage scions, they decreased N, P, K and Mn concentrations and increased Ca, Mg, Fe and Zn concentrations during root formation [16]. Different IBA doses and putrescine treatments increased N, P and K concentrations of chickpea [17]. There is a need to investigate the effects of plant growth regulators on nutrient uptake from the soil through. Therefore in the present study, minerals uptake of plants and responses of grapevine rootstocks to different IBA concentrations in three different soils were investigated.

MATERIALS AND METHODS

This study was carried out in Manisa-Alaşehir in the year 2013. The physical and chemical characteristics of experimental soils are provided in Table 1. Grapevine cultivars of R. Globe, Sultani, Superyol and 41-b rootstock were used as the plant material of the experiments. Grapevine cuttings were planted into pots on 15th of April. Leaf samples were taken and experiments were terminated on 15th of September. The experiments were carried out in 108 pots with 3 different soils (pH 5.04, 7.07 and 8.07), 4 different grape cultivars and rootstock, 3 different IBA concentrations (0, 1000 and 2000 ppm) in net greenhouse and according to a completely randomized block design with 3 replications. Cuttings were dipped in IBA solution on 15 seconds. A cutting was planted in each pot and 150 mg kg^{-1} N, 50 mg kg^{-1} P and 100 mg kg^{-1} K were supplied to each pot. Ammonium nitrate, monoammonium phosphate and potassium nitrate fertilizers were applied as basal fertilizers.

TABLE 1
Physical and chemical characteristics of experimental soils

Characteristics	pH 8.07	pH 5.04	pH 7.07
Total N	0.04	0.15	0.11
Available K_2O (kg da^{-1}) [25]	24.98	18.02	21.08
Mg (mg kg^{-1})	189.3	81.6	182.9
Available P_2O_5 (kg da^{-1}) [26]	5.19	8.94	5.84
Zn (mg kg^{-1}) [27]	0.11	0.28	0.25
Fe (mg kg^{-1}) [27]	2.7	3.22	3.48
Mn (mg kg^{-1}) [27]	1.36	1.51	0.61
Cu (mg kg^{-1}) [27]	0.34	017	0.34
Lime (%)	18.7	2.3	5.7
Total salt	0.03	0.02	0.11
Organic matter (%) [28]	1.45	1.89	1.55
Texture	Loam	Sandy-loam	Loam

TABLE 2
Effects of IBA treatments on root and leaf weights in soil 1 (pH 8.07)

Characteristics	Grapevine Cultivar	IBA treatments, ppm			Average
		0	1000	2000	
Root fresh weight (gr)	**R. Globe**	11.96	13.76	16.50	**14.07 cd**
	41 b	12.80	14.56	19.10	**15.48 ab**
	Sultani	12.20	15.45	16.75	**14.80 c**
	Superyol	12.13	16.13	25.43	**17.90 a**
	Average	**12.27 c**	**14.99 b**	**19.43 a**	
Root dry weight (gr)	**R. Globe**	3.33	3.53	3.76	**3.54 ab**
	41 b	3.06	3.16	3.90	**3.37 ab**
	Sultani	3.13	3.63	3.50	**3.42 b**
	Superyol	2.80	3.53	5.43	**3.92 a**
	Average	**3.08 c**	**3.46 b**	**4.15 a**	
Leaf fresh weight (gr)	**R. Globe**	13.10	13.73	15.56	**14.13 b**
	41 b	11.90	13.66	15.93	**13.83 c**
	Sultani	11.73	15.06	17.36	**14.72 b**
	Superyol	13.73	18.40	21.96	**18.03 a**
	Average	**12.61 c**	**15.21 b**	**17.70 a**	
Leaf dry weight (gr)	**R. Globe**	4.26	3.70	4.63	**4.20 b**
	41 b	2.63	2.46	4.13	**3.07 c**
	Sultani	2.46	3.10	5.13	**3.56 bc**
	Superyol	3.16	4.80	5.76	**4.57 a**
	Average	**3.13 c**	**3.51 b**	**4.91 a**	
Total Dry Biomas (gr)	**R. Globe**	7.59	7.23	8.39	**7.73 b**
	41 b	5.69	5.62	8.03	**6.44 c**
	Sultani	5.59	6.73	8.63	**6.98 c**
	Superyol	5.96	8.33	11.19	**8.49 a**
	Average	**6.20 c**	**6.97 b**	**9.06 a**	

Root fresh weight; Cultivars*, IBA treatments**, Ç x IBA*; Root dry weight; Cultivars*, IBA treatments**, C x IBA*; Leaf fresh weight; Cultivars**, IBA treatments**, C x IBA**; Leaf dry weight; Cultivars**, IBA treatments**, C x IBA**; NS: Non-Significant; * P<0.05 and **P<0.01. Possibility is significant. Total Dry Biomas; Cultivars**, IBA treatments**, Ç x IBA*, Total Dry Biomas: Root dry weigth + leaf dry weight (gr)

Grapevine cuttings planted in April 15 to pots and cutting harvested in 15 September 2013. Root and leaf weights of grapevine saplings were measured. Leaf samples were then washed with distilled water and dried at 65 °C and grinded. Nitrogen analysis was carried out in accordance with Kjeldahl distillation method [18]. Grinded samples were dry-ashed [19], P and K contents were measured by using an ICP-OES (Perkin-Elmer) device. Data were statistically analyzed by using MSTAT-C software.

RESULTS

Effects of IBA treatments on root and leaf weights. IBA treatments significantly increased root fresh weights, root dry weights, leaf fresh weights and leaf dry weights of grapevine saplings ($p < 0.01$) (Tables 2, 3 and 4). Cultivars exhibited significantly different performances from each other ($p < 0.01$, $p < 0.05$) (Tables 2, 3 and 4).

In soil 1, the cultivar Superyol yielded the highest values of all parameters. While root fresh weight of Superyol was 12.13 g in control treatment, the value increased to 25.43 g with 2000 ppm IBA treatment. In soil 2, the cultivar Superyol also had the highest values of entire parameters except for leaf fresh weight. Increasing IBA treatments increased average root fresh weights of soil 2 from 12.42 to 18.93 g. In soil 3, effects of treatments on investigated parameters were found to be significant at different significance levels (Table 4). In general, results revealed increasing parameter values with increasing IBA doses in 3 different soils. It was observed that cultivars exhibited significantly different performances under IBA treatments in different soils.

Effects of IBA treatments on leaf N, P and K content. Significant variations were observed in N, P and K contents of different grapevine cultivars with 0, 1000 and 2000 ppm IBA treatments (Tables 5, 6 and 7). With regard to measured values, effects of treatments were significantly different in different soils. Such a case was mainly because of soil characteristics. Nutrient contents of plants were determined in a dry matter-base and therefore the dry matter contents and plant nutrient uptakes were different in each soil. Nitrogen content in soil 1 varied between 1.78-2.25%. With regard to average values, nitrogen content was 1.82% in control treatment, 1.75% in 1000 ppm IBA treatment and 2.04% in 2000 ppm IBA treatment. In soil 2, cultivars exhibited significantly different N contents. On the other hand, N contents of cultivars were not significantly different from each other in soil 3 and increasing N contents were observed with increasing IBA treatments ($p < 0.01$).

TABLE 3
Effects of IBA treatments on root and leaf weights in soil 2 (pH 5.04)

Characteristics	Grapevine Cultivar	IBA treatments, ppm			Average
		0	1000	2000	
Root fresh weight (gr)	**R. Globe**	12.34	14.46	16.58	**14.46 c**
	41 b	12.86	15.56	19.26	**15.89 b**
	Sultani	12.28	15.64	16.89	**14.93 c**
	Superyol	12.21	16.35	23.01	**17.19 a**
	Average	**12.42 c**	**15.50 b**	**18.93 a**	
Root dry weight (gr)	**R. Globe**	2.73	3.80	4.96	**3.83 cd**
	41 b	3.60	4.13	5.23	**4.32 c**
	Sultani	3.70	5.43	6.36	**5.16 ab**
	Superyol	5.40	5.83	6.46	**5.90 a**
	Average	**3.85 c**	**4.80 b**	**5.75 a**	
Leaf fresh weight (gr)	**R. Globe**	15.76	16.73	21.36	**17.95 d**
	41 b	18.56	25.60	22.60	**22.25 b**
	Sultani	19.43	20.13	22.66	**20.74 c**
	Superyol	19.43	24.56	26.96	**23.65 a**
	Average	**18.30 c**	**21.75 b**	**23.40 a**	
Leaf dry weight (gr)	**R. Globe**	4.46	3.53	4.73	**4.24 b**
	41 b	3.96	6.20	5.20	**5.12 a**
	Sultani	3.53	3.50	4.80	**3.94 c**
	Superyol	3.73	4.33	5.06	**4.37 b**
	Average	**3.92 a**	**4.39 b**	**4.95 a**	
Total Dry Biomas (gr)	**R. Globe**	7.19	7.33	9.69	**8.07**
	41 b	7.56	10.33	10.43	**9.44**
	Sultani	7.23	9.33	11.16	**9.24**
	Superyol	9.13	10.16	11.52	**10.27**
	Average	**7.77**	**9.28**	**10.70**	

Root fresh weight; Cultivars*, IBA treatments**, C x IBA*; Root dry weight; Cultivars*, IBA treatments**, C x IBA**; Leaf fresh weight; Cultivars**, IBA treatments**, C x IBA**; Leaf dry weight; Cultivars**, IBA treatments**, C x IBA**; NS: Non-Significant; * P<0.05 and **P<0.01. Possibility is significant. Total Dry Biomas; Cultivars**, IBA treatments**, Ç x IBA**. Total Dry Biomas: Root dry weigth + leaf dry weight (gr)

TABLE 4
EFFECTS of IBA treatments on root and leaf weights in soil 3 (pH 7.07)

Characteristics	Grapevine Cultivar	IBA treatments, ppm			Average
		0	1000	2000	
Root fresh weight (gr)	**R. Globe**	11.48	14.76	15.01	**13.75 c**
	41 b	12.45	15.03	15.67	**14.38 b**
	Sultani	12.67	14.78	15.03	**14.16 b**
	Superyol	13.14	16.66	16.34	**15.38 a**
	Average	**12.43 b**	**15.30 a**	**15.51 a**	
Root dry weight (gr)	**R. Globe**	2.70	5.76	6.83	**5.10 b**
	41 b	3.76	5.40	5.73	**4.96 c**
	Sultani	4.26	5.20	5.50	**4.98 c**
	Superyol	5.63	6.56	5.56	**5.92 a**
	Average	**4.09b**	**5.73 a**	**5.90 a**	
Leaf fresh weight (gr)	**R. Globe**	16.43	20.10	24.20	**20.24 c**
	41 b	25.53	23.83	26.36	**25.24 b**
	Sultani	27.03	26.76	29.70	**27.83 a**
	Superyol	20.86	31.43	25.96	**26.08 b**
	Average	**22.46 c**	**25.53 b**	**26.55 a**	
Leaf dry weight (gr)	**R. Globe**	3.40	4.43	4.73	**4.18 c**
	41 b	4.50	5.13	5.10	**4.91 a**
	Sultani	5.03	4.83	4.93	**4.93 a**
	Superyol	4.53	5.06	5.10	**4.90 a**
	Average	**4.36 c**	**4.86 a**	**4.96 a**	
Total Dry Biomas (gr)	**R. Globe**	6.1	10.19	11.56	**9.28**
	41 b	8.26	10.53	10.83	**9.87**
	Sultani	9.29	10.03	10.43	**9.91**
	Superyol	10.16	12.16	10.66	**10.99**
	Average	**8.45 b**	**10.72 a**	**10.87 a**	

Root fresh weight; Cultivars, NS; IBA treatments*, C x IBA: NS; Root dry weight; Cultivars: NS, IBA treatments*, C x IBA: NS; Leaf fresh weight; Cultivars*, IBA treatments**, C x IBA: NS; Leaf dry weight; Cultivars*, IBA treatments*, C x IBA*; NS: Non-Significant; * P<0.05 and **P<0.01. Possibility is significant.
Total Dry Biomas; Cultivars: NS, IBA treatments*, Ç x IBA:*
Total Dry Biomas: Root dry weigth + leaf dry weight (gr)

TABLE 5
Effects of IBA treatments on leaf N, P and K concentrations and total content in soil 1 (pH 8.07)

Characteristics	Grapevine Cultivar	IBA treatments, ppm						M.C.	T.C.
		Mineral Concentration (%)			Total Content (mg pot^{-1})			Av.	Av.
		0 ppm	1000 ppm	2000 ppm	0 ppm	1000 ppm	2000 ppm		
Leaf N con. (%)	R. Globe	1.78	2.02	2.25	135.1	146.5	188.7	2.02	157
	41 b	1.94	1.88	1.97	110.3	105.6	158.1	1.96	125
	Sultani	2.10	1.98	1.82	117.3	133.2	157.0	1.97	136
	Superyol	1.45	1.92	2.12	86.4	159.9	237.2	1.83	161
	Average	1.82 b	1.75 b	2.04 a	112 c	136 b	185 a		
Leaf P con. (%)	R. Globe	0.17	0.19	0.23	12.9	15.9	18.4	0.19	15.7
	41 b	0.22	0.22	0.23	10.8	12.9	13.6	0.22	12.4
	Sultani	0.16	0.22	0.22	12.8	10.7	17.2	0.20	13.6
	Superyol	0.17	0.20	0.19	13.1	18.3	21.2	0.19	17.5
	Average	0.18 b	0.21 a	0.22 a	12.4c	14.5b	17.6a		
Leaf K con. (%)	R. Globe	1.50	1.43	1.45	113.9	103.4	121.7	1.46c	113
	41 b	2.02	1.64	1.67	114.9	92.2	134.1	1.77a	113
	Sultani	1.50	1.73	1.66	83.9	116.4	143.3	1.6a	114
	Superyol	1.43	1.44	1.70	85.2	120.0	190.2	1.52c	132
	Average	1.61	1.56	1.62	99c	108b	147a		

Leaf N content; Cultivars: NS; IBA treatments**, C x IBA*; Leaf P content; Cultivars: NS; IBA treatments**, C x IBA: NS; Leaf K content; Cultivars**, IBA treatments: NS; C x IBA*; Total N content; Cultivars: NS; IBA treatments**, C x IBA*; Total P content; Cultivars: NS; IBA treatments**, C x IBA: NS; Total K content; Cultivars: NS, IBA treatments: *; C x IBA: NS. NS: Non- Significant; * P<0.05 and **P<0.01. Possibility is significant. Total Content: total dry matter x mineral concentration/100:mg pot^{-1}

TABLE 6
Effects of IBA treatments on leaf N, P and K concentrations and total content in soil 2 (pH 5.04)

Characteristics	Grapevine Cultivar	IBA treatments, ppm						M.C.	T.C.
		Mineral Concentration (%)			Total Content (mg pot^{-1})			Av.	Av.
		0 ppm	1000 ppm	2000 ppm	0 ppm	1000 ppm	2000 ppm		
Leaf N con. (%)	R. Globe	2.07	2.35	1.91	148.8	172.3	185.1	2.11a	168.7
	41 b	2.12	1.98	1.79	160.3	204.5	186.7	1.96 b	183.8
	Sultani	1.96	1.84	1.88	141.7	171.7	209.8	1.89 bc	174.4
	Superyol	1.63	1.81	1.99	148.8	183.9	229.2	1.81 c	187.3
	Average	1.94 a	1.99 a	1.89 b	149.9c	183.1b	202.7a		
Leaf P con. (%)	R. Globe	0.16	0.21	0.19	11.5	15.4	18.4	0.19 b	15.1c
	41 b	0.20	0.16	0.19	15.1	16.5	19.8	0.18 b	17.1c
	Sultani	0.22	0.25	0.23	15.9	23.3	25.7	0.23 a	21.6b
	Superyol	0.24	0.23	0.23	21.9	23.4	26.5	0.23 a	23.9a
	Average	0.20	0.21	0.21	16.1c	19.65b	22.6a		
Leaf K con. (%)	R. Globe	1.41	1.55	1.67	101.4	113.6	161.8	1.54 c	125.6
	41 b	1.57	1.70	1.82	118.7	175.6	189.8	1.69 b	161.4
	Sultani	1.40	1.66	1.66	101.2	154.9	185.3	1.57 c	147.1
	Superyol	1.71	1.84	1.78	156.1	186.9	205.1	1.77 a	182.7
	Average	1.52 c	1.69 b	1.73 a	119.3c	157.7b	185.5a		

Leaf N content; Cultivars*; IBA treatments**, C x IBA*; Leaf P content; Cultivars**; IBA treatments: NS; C x IBA: NS; Leaf K content; Cultivars**, IBA treatments**; C x IBA**; NS: Non- Significant; * P<0.05 and **P<0.01. Possibility is significant. Total N content; Cultivars: NS; IBA treatments**, C x IBA*; Total P content; Cultivars: * IBA treatments*, C x IBA: NS; Total K content; Cultivars: NS, IBA treatments: *; C x IBA: NS.
NS: Non- Significant; * P<0.05 and **P<0.01. Possibility is significant.
Total Content: total dry matter x mineral concentration/100:mg pot^{-1}

TABLE 7
Effects of IBA treatments on leaf N, P and K concentrations and total content in soil 3 (pH 7.07)

Characteristics	Grapevine Cultivar	IBA treatments, ppm						M.C.	T.C.
		Mineral Concentration (%)			Total Content (mg pot^{-1})			Av.	Av.
		0 ppm	1000 ppm	2000 ppm	0 ppm	1000 ppm	2000 ppm		
Leaf N con. (%)	R. Globe	1.70	1.93	1.92	103.7	196.7	222.0	1.85	174.1
	41 b	1.59	1.89	1.93	131.3	199.0	209.0	1.80	179.8
	Sultani	1.60	1.79	1.63	148.6	179.5	170.0	1.67	166.0
	Superyol	1.59	1.86	1.90	161.5	226.2	202.5	1.78	196.7
	Average	1.62 b	1.87 a	1.84 a	136.3c	200.4a	200.9a		
Leaf P con. (%)	R. Globe	0.22	0.23	0.22	13.4	23.4	25.4	0.23	20.7
	41 b	0.23	0.23	0.22	19.0	24.2	23.8	0.22	22.3
	Sultani	0.19	0.23	0.22	17.7	23.1	22.9	0.21	21.2
	Superyol	0.20	0.23	0.22	20.3	28.0	23.5	0.22	23.9
	Average	0.21	0.23	0.22	17.6	24.7	23.9		
Leaf K con. (%)	R. Globe	1.68	1.66	1.79	102,5	169,2	206,9	1.71	159,5
	41 b	1.62	1.74	1.79	133,8	183,2	193,9	1.71	170,3
	Sultani	1.63	1.67	1.81	151,4	167,5	188,8	1.70	169,2
	Superyol	1.38	1.63	1.77	140,2	198,2	188,7	1.59	175,7
	Average	1.58 c	1.67 b	1.79 a	132,0c	179,5b	194,6a		

Leaf N content; Cultivars: NS; IBA treatments**, C x IBA: NS; Leaf P content; Cultivars: NS; IBA treatments: NS; C x IBA: NS; Leaf K content; Cultivars: NS; IBA treatments**: C x IBA: NS; NS: Non- Significant; * P<0.05 and **P<0.01. Possibility is significant. Total N content; Cultivars: NS; IBA treatments**, C x IBA*; Total P content; Cultivars: NS; IBA treatments: NS, C x IBA: NS; Total K content; Cultivars: NS, IBA treatments: *; C x IBA: NS.
NS: Non- Significant; * P<0.05 and **P<0.01. Possibility is significant.
Total Content: total dry matter x mineral concentration/100:mg pot^{-1}

With regard to P contents of plant leaves, significant increases were observed in soil 1 with IBA treatments. In soil 2, effects of cultivars on phosphorus contents were significant. On the other hand in soil 3, effects of treatments on phosphorus contents were not found to be significant. Except for soil 1, IBA treatments yielded significant increases in plant K contents in the other soils. Leaf K contents varied between 1.43-2.02% in soil 1, between 1.40 - 1.84% in soil 2 and between 1.38-1.82% in soil 3. It was thought that general variations in soil physical and chemical characteristics might affect the K contents of plants.

Effects of IBA treatments on total N, P and K content of plant biomass. Significant variations were observed in total N, P and K contents of plant biomass of different grapevine cultivars with 0, 1000 and 2000 ppm IBA treatments (Tables 5, 6 and 7). Plant's total N content is correlated with created total dry matter and results are parallel with plant's N concentrations in three soil (Table 5, 6 and 7). The total phosphorus and potassium contents of the plant show parallel results as in nitrogen. The N, P and K content removed by the plant from the soil has shown an increase with IBA treatments (Table 5, 6 and 7). Superyol vine varieties have lifted more nutrient elements applied to the soil when compared to other root stocks in all three soil. The rootstock lifting more nutrient elements from the soil in the first year is an important parameter for its development in subsequent years.

DISCUSSION

There are several factors affecting the plant growth and development. The basic soil nutrients (N, P, and K) should be available at sufficient levels especially during the initial root development periods. In case of limiting impacts of soil characteristics, cultural measurements should be taken to inhibit such limiting impacts and to provide a well plant development. Livestock manure, various soil regulators, humic substances and especially root-developing hormones may provide positive outcomes. For instance, auxin treatments may improve rooting of various plants [20]. Among the auxins, IBA is the most commonly used one [21]. he present study revealed that IBA treatments had significant impacts on rooting and total biomass (root + leaf) of different grapevine cultivars and increased the measured values. Compared to control treatment, the increase in total biomass with 2000 ppm IBA treatments was 51.2% in soil 1, 56% in soil 2 and 34% in soil 3. The main reason for such increase was stimulation of meristematic cells of root region and augmentation of adventive root development by IBA. Results of the previous researches on this issue also support the findings of the present study [6-8, 9, 10, 11].

Compared to control treatment, 1000 ppm and 2000 ppm IBA-treated grapevine saplings had higher N, P and K uptake rates from the soil. Similar effects of IBA treatments were also observed in previous studies investigating the relationships between IBA treatments and nutrients [16, 17]. Cultivars of the present study had varying performances with regard to investigated parameters in different soils. The reason to select the soils with different pH levels was to see the impacts of IBA treatments on plant development when pH was a limiting factor. Plants usually have different responses against different pH levels [22] and such responses indicate the genetic diversity among the plants. Total biomass of Superyol cultivar was higher than the other cultivars. Nutrient uptakes of cultivars were also different from each other.

Total biomass values observed in soil 1 with higher pH and lime levels were significantly lower than that of the other soils. In alkaline soils with higher pH levels, availability of P, Fe, B, Zn and Mn like elements decreases and deficiency is observed in those elements [23]. Lime (CaCO3) increases soil pH level and the basic reason of week growth and development of *L. angustzfolius* and *L. pilosus* in alkaline soils was increasing pH levels rather than high Ca levels and ionic strength [24].

The present study revealed improved root development and nutrient uptake from the soils with IBA treatments. Performance of the cultivars with regard to investigated characteristics was different from each other and varying values were observed in different soils. Superyol grapevine cultivars attained higher root and leaf weights in three soils (pH .07, 5.04, 7.07), in comparison to other varieties. This results from the difference of biochemical characteristics of the variety. Differences are mainly observed in the plant's capacity for using nutritional elements and generating biomass, even among the genotypes of the varieties. In our study, it is seen in plant leaf results that the plants to which 2000 ppm IBA treatment is applied has uptake more N. Soil characteristics should also be taken into consideration and limiting factors should be eliminated for desired success in rooting. High amount of lime, a characteristic of soil, decreases plants' taking advantage of phosphorus. In our study, the lime content in soil is 18% and pH 8.07 value. The root improvement through IBA treatment in that soil caused the plant to grow more P from the soil. It was concluded here in that IBA treatments should be carried out and plant nutrients should be supplied during the initial rooting of grapevine cultivars.

REFERENCES

[1] Hartmann, H.T., Kester, D.E., Davies, F.T. and Geneve, R.L. (1997) Plant Propagation: Principles and Practices. Prentice-Hall, Inc., Englewood Cliffs, New Jersey. Sixth edition.

[2] Stefanic, M., Stamper, F., Veberic, R. and Osterc, G. (2006) The level of IAA, IAAsp and some phenolics in cherry rootstock 'Gisela 5', leafy cutting pretreated with IAA and IBA. Sci Hort. 112, 399-405.

[3] Leaky, R.R.B. (2004) Physiology of vegetative reproduction. In: Burley, J., Evans, J., Youngquist, J.A. (eds.) Encyclopaedia of Forest Sciences. Academic Press, London. 1655–1668.

[4] Anonymous (1992) Indole-3-butyric acid. United States Environmental Protection Agency, Office of Prevention, Pesticides and Toxic Substances (H-7508W), EPA-738-F-92-001, August 1992.

[5] Al-Sagri, F. and Alderson, P.G. (1996) Effect of IBA, cutting type and rooting media on rooting of *Rosa centifolia*. Journal Hort. Sci. 71, 729-737.

[6] Chhun, T., Takcta, S., Tsurumi, S. and Masahiko, I. (2004) Different behavior of indole-3-acetic acid and indole-3-butyric acid in stimulating lateral root development in rice (*Oryza sativa* L.). Plant Gro. Reg. 43, 135-143.

[7] Kaya, Ş.S., Büyükkartal, H.N., Algan, G. and Ercoşkun, T. (2005) Farklı oksinlerin turp (*Raphanus sativus* L.) yumrusunun anatomik yapısı ve gelişimi üzerine etkileri. Tarım Bilimleri Dergisi. 11(2), 165-172 (in Turkish).

[8] Gomez, F. and Canhoto, J.M. (2009) Micropropagation of strawberry tree (*Arbutus unedo* L.) from adult plants. In Vitro Cellular and Dev Biology-Plant. 45, 72–82.

[9] Şeker, M., Akçal, A., Sakaldaş, M. and Güngoğdu, M.A. (2010) Farklı çelik alma dönemleri ile oksin dozlarının Kocayemişin (*Arbutus unedo* L.) köklenme oranı üzerine etkilerinin belirlenmesi. U. Ü. Ziraat Fakültesi Dergisi, 24(1), 99-108 (in Turkish).

[10] Rahbin, A., Aboutalebi, A. and Hasanzadeh, H. (2012) Study on the effect of cutting location on shoot and IBA on rooting of 'Night Jessamine' (*Cestrum nocturnum*) stem cuttings. Int Res J of App and Basic Sci. 3(11), 2345-2348.

[11] Bidarigh, S. and Azarpour, E. (2013) Study effect of IBA hormone levels on rooting in micro cuttings of tea (*Camellia sinensis* L.). ARPN Journal of Agri and Bio Sci. 8(1), 1-5.

[12] Galavi, M., Karimian, M.A. and Mousavi, S.R. (2013) Effects of different auxin (IBA) concentrations and planting-beds on rooting Grape cuttings (*Vitis vinifera*). Ann Review & Research in Bio. 3(4), 517-523.

[13] Ünsal, P.N. (1993) Bitki Büyüme Maddeleri. İstanbul Teknik Üniversitesi. Üni. Yayın No: 3677, Enst. Yay. No: 4, ISBN 975-404-254-3 (in Turkish).

[14] Marschner, H. (1986) Mineral nutrition of higher plants. Institute of Plant Nutrition University of Hohenheim Federal Republic of Germany. Academic Press. 850 p.

[15] Gemici, M., Güven, A., Yürekli, K.A. and Katmer, P. (2000) Effect of some growth regulators and commercial preparations on the chlorophyll content and mineral nutrition of *Lycopersicum esculentum Mill*. Turk J. Bot. 24, 215-219.

[16] Ayanoğlu, F. and Özkan, C.F. (2000) Tıbbi adaçayı (*Salvia officinalis L.*) çeliklerinde kök oluşumu ve gelişimi esnasında mineral element konsantrasyonunda meydana gelen değişikler ve IBA etkisi. Turk J Agric For. 24, 677-682 (in Turkish). Record Number 20003032675.

[17] Amin, A.A., Gharib, F.A., Abouziena, H.F. and Dawood, M.G. (2013) Role of indole-3-butyric acid or/and putrescine in improving productivity of chickpea (*Cicer arientinum* L.) plants. Pakistan J of Bio Sci. 16, 1894-1903.

[18] Bremner, J.M. (1965) Methods of soil analysis. Part II. Chemical and microbiological properties. Ed. A.C.A. Black. Amer. Soc. of Agron. Inc. Pub. Agron. Series No:9 Madison USA.

[19] Kacar, B. and. Inal, A. (2008) Plant Analysis. Nobel Publications. No: 1241.

[20] Marks, T.R. and Simpson, S.E. (2000). Interaction of explant type and indole-3-butyric acid during rooting *in vitro* in a range of difficult and easy-to-root woody plants. Plant Cell, Tissue and Organ Cul. 62, 65-74.

[21] Kotis, M., Yupsanis, T.A., Syros, T.D. and Economou, A.S. (2009) Peroxidase, acid phosphatase, RNase and DNase activity and isoform patterns during *in vitro* rooting of *Petunia×hybrida* microshoots. Biologia Plantarum. 53, 530-538.

[22] Fageria, N.K. and Baligar, V.C. (1999) Growth and nutrient concentrations of common bean, lowland rice, corn, soybean and wheat at different soil ph on an inceptisol. Journal of Plant Nut. 22(9), 1495-1507.

[23] Alam, S.M., Naqvi, S.S.M. and Ansari, R. (1999) Impact of soil pH on nutrient uptake by crop plants. In: Pessarakli, M. (Ed.) Handbook of Plant and Crop Stress. 2. Edition. Marcel Dekker Pub. New York, USA, 51-60.

[24] Tang, C., Robson, A.D. and Adams, H. (1995) High Ca is not the primary factor in poor growth of *Lupinus angustifolius* L. in high pH soil. Aust J of Agri Res. 46, 1051–1062.

[25] Richards, L.A. (1954) Diagnosis and improvement of saline and alkaline soils. U.S.D.A. Handbook. No: 60.

[26] Olsen, S.R., Cole, V., Watanabe, F.S. and Dean, L.A. (1954) Estimation of available phosphorus in soils by extraction with sodium bicarbonate. Agricultural Handbook, US, Soil Department 939, Washington, D.C.
[27] Lindsay, W.L., Norvell, W.A. (1978) Development of a DTPA soil test for zinc, iron, manganese and copper. Soil Sci Amer J. 42, 421-428.
[28] Nelson, D.W. and Sommers, L.E. (1982) Methods of soil analysis, Part 2. Chemical and microbiological properties. Page, A.L., Miller, R.H. Keeney, D.R. (eds.) 2nd edition. S.S.S. of America Inc. Publisher, Madison, Wisconsin.

Received: **30.12.2016**
Accepted: **17.11.2017**

CORRESPONDING AUTHOR

Sezer Sahin
Gaziosmanpasa University,
Faculty of Agriculture,
Department of Soil Science and Plant Nutrition,
Taşlıçiftlik Campus,
60200, Tokat – Turkey

e-mail: sezer.sahin@gop.edu.tr

© by PSP Volume 27 – No. 2/2018 pages 765-770 Fresenius Environmental Bulletin

HEAVY METAL, NITROGEN AND PHOSPHORUS ADSORPTION OF COMPACTED LINER MIXTURES

Zeki Gokalp[1,*], Ismail Tas[2], Oguzhan Uzun[1], Sema Kaplan[1], Mustafa Basaran[1]

[1]Erciyes University Agricultural Faculty, Melikgazi, 38038 Kayseri, Turkey
[2]Canakkale Onsekiz Mart University Agricultural Faculty, 17018, Canakkale, Turkey

ABSTRACT

Nitrate, phosphorus and heavy metals are among the most common pollutants and create potential dangers for groundwater contamination. In this research, a liner design was proposed for waste repository sites, constructed wetland basins and manure management lagoons to prevent groundwater contamination by seepages from the bottom of these facilities. For this purpose, sand-bentonite and pumice-bentonite mixtures with pre-defined grain size range (1.00-0.50 mm) and bentonite content (30%) was used. The mixtures were compacted at optimum moisture content and maximum dry weight and then permeability tests were carried out over compacted mixtures. Various concentrations of nitrate, phosphorus (25, 50, 100, 150 and 200 ppm) and heavy metal (Cd, Ni, Pb, Cr and Cu) solutions (10, 20, 30, 40 and 50 ppm) were used to saturate the permeability test samples. Extracts of permeability tests were used to investigate the adsorption characteristics of proposed mixtures for liner design. With regard to heavy metal adsorption, bentonite had the best performance because it is a clay mineral. Sand and pumice exhibited similar performances in lead and cadmium adsorption, but pumice had much better performance than sand in chrome, copper and nickel adsorption. Although sand-bentonite and pumice-bentonite mixtures exhibited similar performance in nitrate adsorption, again pumice-bentonite mixtures had much better performance than sand-bentonite mixtures in phosphorus adsorption. Current results revealed that pumice with macro-micro pore structure and resultant adsorptive surface characteristics could be used as an alternative of sand in liner design.

KEYWORDS:
Adsorption, Bentonite, Compacted liner, Heavy metal, Pumice, Phosphorus.

INTRODUCTION

Soil and water resources are greatly influenced and polluted by seepage from the bottoms or through the liners of waste repositories. Therefore, increasing awareness on preservation of surface and groundwater supplies brought about a need for the design of well-isolated contaminant structures [1]. The liners placed beneath these structures should be so designed that they should provide sufficient impermeability and should meet the national or international standards set for liners of such structures. Besides synthetic liners, various materials were studied with respect to their mineral composition and physical properties for buffers, backfills [2], with respect to their swelling characteristics [3] and with respect to geotechnical characteristics to be used in earth-fill dams [4].

Compacted sand-bentonite mixtures are commonly used to create an impervious layer or barrier for waste repositories [5], constructed wetland basins and livestock waste storage lagoons [6]. The compacted bentonite-sand mixture is generally used as a buffer material for their quite low permeability, self-sealing characteristics due to its swelling capacity and adsorption of various heavy metals [7]. Several other types of cement based materials are also used in engineered barrier systems to prevent seepage and resultant pollutions.

Bentonite is a type of clay with quite high cation exchange capacity, swelling potential and considerably low hydraulic conductivity. Compacted bentonite–sand, bentonite–crushed rock or bentonite–ballast mixtures possess higher structural integrity, thermal conductivity and stiffness and such mixtures are usually more economic than pure bentonite. When combined in proper proportions, those mixtures can form an excellent barrier or liner that is dimensionally stable and has a low hydraulic conductivity [8].

Akgun [9] carried out a study to investigate the geotechnical characteristics (compaction, hydraulic conductivity, swelling and strength parameters) and performance of sand-bentonite mixtures to be used in sealing of underground waste repository and recommended 30% bentonite mixture with the lowest hydraulic conductivity. Al-Rawas et al. [10] investigated potential use of sand-attapulgite clay mixtures as a landfill liner and also recommended 30% clay mixture to satisfy the requirements for landfill liners. Mollamahmutoglu and Yılmaz [11] investigated potential use of fly ash and bentonite mixtures as liner or cover at waste disposal areas and recommended 20% bentonite-fly ash mixtures as a suitable liner or

cover material at waste disposal sites. Several other researchers assessed the geotechnical characteristics of sand-bentonite mixtures for various purposes [12, 13, 14].

Beside waste repositories, sand-bentonite mixtures are also used as a liner for constructed wetland basins and livestock waste storage lagoons. Natural wastewater treatment systems, also called as constructed wetlands, have been used as an alternative low-cost method for controlling water pollution from various sources. They often require a liner of low permeability beneath the wetland basin to prevent the contamination of groundwater or to prevent groundwater intrusion into the wetland [15]. Commonly synthetic materials such as polyvinylchloride (PVC) and high-density polyethylene and in some cases clay-bentonite mixtures are used in liner design for these structures. Synthetic liners are potentially expensive and are prone to damages, so clay or sand-bentonite liners are preferred [16].

TABLE 1
Physical and chemical properties of bentonite and pumice

Bentonite Property	Value	Pumice Property	Value
SiO_2	62.1%	SiO_2 (%)	53.50%
Al_2O_3	15.21%	Al_2O_3 (%)	10.75%
Fe_2O_3	6.58%	CaO (%)	3.78%
MgO	2.28%	Fe_2O_3 (%)	3.22%
Na_2O	1.59%	K_2O (%)	3.15%
CaO	1.19%	MgO (%)	1.95%
K_2O	1.1%	Na_2O (%)	1.60%
pH	9.5	pH	6.5
Moisture content	9.50%	Moisture Content (%)	10.9%
Density	0.9 g/cm^3	Lime (%)	6.6%
Liquid Limit (%)	630%	Water Hold. Cap.	90.2
Compressibility (%)	40%	Total N	0.028 ppm
Fresh Strength	24.5 (N/cm^2)	Soluble P	0.004 ppm
Dry Strength	42 (N/cm^2)	Soluble K	4.79 ppm
Shear Strength	6.25 (N/cm^2)	Soluble Ca	14.019 ppm
CEC	80-90 (meq/100g)	Soluble Mg	1.077 ppm

Pumice is a porous, spongy and glassy material formed by volcanic processes and resistant to physical and chemical impacts. It includes several macro and micro-scale pores formed by sudden release of gases inside it during the formation process. Since the pores are discontinuous, it has relatively low permeability and high heat and noise insulation capacity. Turkey has enormous pumice reserves especially around the extinguished volcanoes. Pumice sources around the extinguished volcanic mountain Erciyes in Kayseri, Turkey are commercially utilized by local enterprises. Pumice in the region is widely used to make lightweight concrete or insulated low-density breeze blocks [7]. The present research was conducted primarily to investigate adsorption characteristics of pumice-bentonite mixtures and compare them with sand-bentonite mixtures to assess potential use of pumice in mixtures for liners.

MATERIALS AND METHODS

Bentonite used in this study was supplied from a commercial bentonite facility located in Cankiri Province of Turkey. It is powdered Na-bentonite with at least 78% montmorillonite. Some physical and chemical properties of powdered bentonite are provided in Table 1. Sand for experiments was supplied from construction department of Erciyes University. It was washed and pre-sieved river sand used for construction. Since it was washed through and sieved, there was not any soil particles left among sand grains. Pumice was supplied from material storages of a commercial pumice manufacture and trade company in Develi, Kayseri. Some physical and chemical properties of pumice are provided in Table 1.

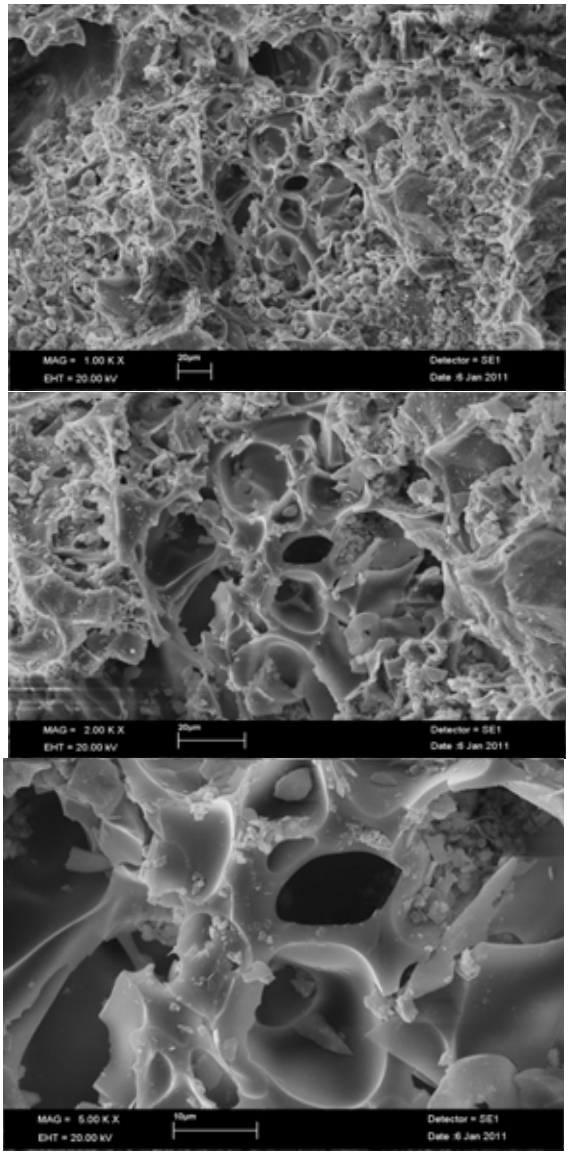

FIGURE 1
SEM images for pumice samples

TABLE 2
Heavy metal concentrations of permeability leachates (ppm)

Heavy Metal	Cd		Cr		Cu		Pb		Ni	
Influent (ppm)	Sand	Pumice	Sand	Pumice	Sand	Pumice	Sand	Pumice	Sand	Pumice
	0.311	0.214	0.048	0.011	0.032	0.065	0.117	0.031	0.289	0.324
10	0.425	0.198	0.081	0.018	0.052	0.049	0.165	0.041	0.345	0.280
	0.337	0.178	0.065	0.008	0.048	0.083	0.181	0.030	0.303	0.179
	0.337	0.199	0.090	0.032	0.092	0.100	0.321	0.120	0.421	1.925
20	0.318	0.214	0.102	0.050	0.121	0.146	0.200	0.075	0.405	2.376
	0.349	0.186	0.098	0.045	0.103	0.128	0.275	0.097	0.352	2.599
	1.021	0.557	0.174	0.041	0.194	0.389	0.621	0.164	0.612	3.841
30	0.830	0.621	0.149	0.067	0.255	0.507	0.702	0.213	0.507	4.328
	0.821	0.650	0.156	0.052	0.228	0.492	0.667	0.251	0.537	4.110
	0.792	0.865	0.245	0.069	0.197	0.384	0.915	0.450	0.718	4.925
40	1.012	0.912	0.207	0.110	0.222	0.632	0.701	0.637	0.699	5.314
	0.915	0.826	0.211	0.089	0.258	0.512	0.718	0.436	0.679	4.712
	1.952	2.185	0.387	0.117	0.291	0.764	1.489	1.032	1.962	9.004
50	1.795	2.257	0.321	0.148	0.319	0.912	1.821	0.841	2.194	7.248
	1.945	2.252	0.333	0.123	0.325	0.687	1.717	0.994	2.201	8.225

Scanning electron microscopy images of pumice samples were taken to present porous nature of the pumice used in experiments (Figure 1). The inter-particular and inner-particular pores, continuous or discontinuous, improved the specific surface and then the adsorption capacity of the material.

Since the materials are to be used in impervious liner design, sand and pumice samples were mixed with bentonite at certain mixture ratio. The bentonite ratio was selected as 30% just based on previous researches [7, 9]. Mixtures were compacted in standard proctor molds in accordance with ASTM D698 [17] as to have maximum dry unit weight with optimum moisture content. Optimum moisture content was obtained as 13.80% for sand-bentonite mixtures and 19.00% for pumice-bentonite mixtures. Maximum dry unit weight was identified as 1.770 t/m^3 for sand-bentonite and 1.491 t/m^3 for pumice-bentonite mixtures.

Compacted samples were subjected to permeability tests in accordance with ASTM D5084 [18]. Permeability tests were carried out to get leachate from compacted specimens. Test specimens were saturated with different heavy metal (Cd, Ni, Pb, Cr, Cu), phosphorus and nitrate solutions at different concentrations as to represent the pollutants. Test concentrations for heavy metals were selected as 0, 10, 20, 30, 40 and 50 ppm and test concentrations for phosphorus and nitrate were selected as 0, 25, 50 100, 150 and 200 ppm. Pollutant solutions leached through permeability columns and resultant leachates were subjected to heavy metal, phosphorus and nitrogen analyses to determine the adsorption capacities of sand-bentonite and pumice-bentonite mixtures.

The material size (0.50 – 1.00 mm for sand and pumice), bentonite mixture ratio, compaction parameters (maximum dry unit weight and optimum moisture content) and permeability coefficient (3.21×10^{-8} cm/s for sand-bentonite and 1.88×10^{-8} cm/s for pumice-bentonite mixtures) were all selected based on a previous research [6].

RESULTS AND DISCUSSION

Sand-bentonite and pumice-bentonite mixtures were compacted at optimum moisture content and maximum dry unit weight and samples were saturated with 10, 20, 30, 40 and 50 ppm Cd, Cr, Cu, Pb and Ni solutions and permeability leachates were obtained through the samples. Heavy metal concentrations were measured from these leachates (Table 2). Leachate cadmium (Cd) concentrations of sand-bentonite mixtures varied between 0.311 – 1.952 ppm and cadmium concentrations of pumice-bentonite mixtures varied between 0.178 – 2.257 ppm. Although Cd adsorption capacity of mixtures was quite close to each other, pumice-bentonite mixtures slightly had higher adsorption capacity (Figure 2a).

Leachate chrome (Cr) concentrations of sand-bentonite mixtures varied between 0.048 – 0.387 ppm and concentrations of pumice-bentonite mixtures varied between 0.008 – 0.148 ppm. Increasing leachate concentrations were observed with increasing influent concentrations. Pumice-bentonite mixtures had almost three times higher Cr adsorption than sand-bentonite mixtures (Figure 2b). With regard to copper (Cu), leachate concentrations of sand-bentonite mixtures varied between 0.032 – 0.325 ppm and concentrations of pumice-bentonite mixtures varied between 0.049 – 0.917 ppm. Contrary to Cd and Cr, sand-bentonite mixtures exhibited better performance in adsorption of Cu (Figure 2c).

While the leachate nickel (Ni) concentrations of sand-bentonite mixtures varied between 0.289 – 2.201 ppm, Ni concentrations of pumice-bentonite mixtures varied between 0.179 – 9.004 ppm. Nickel concentrations of pumice-bentonite mixtures were

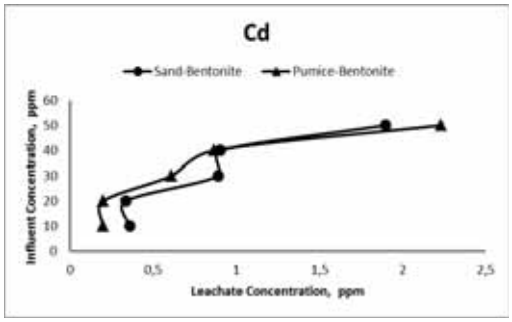

(a)

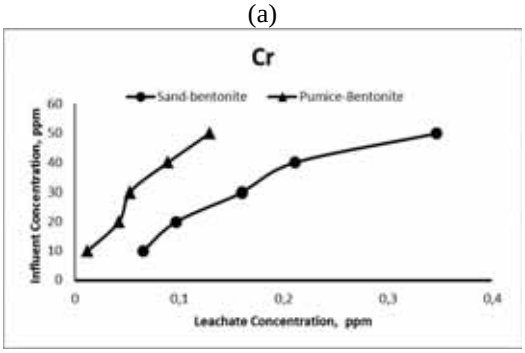

(b)

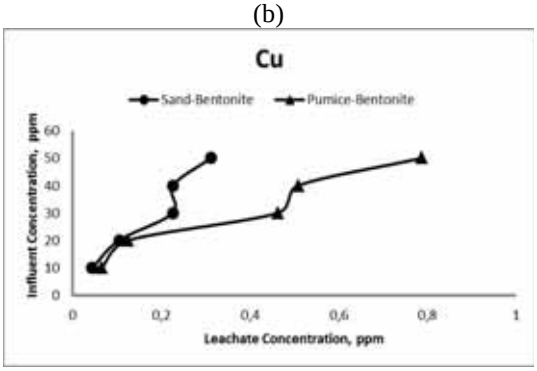

(c)

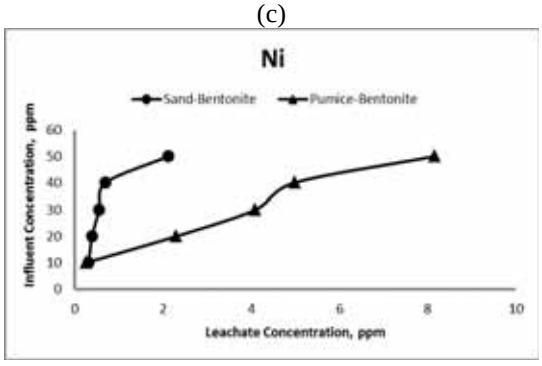

(d)

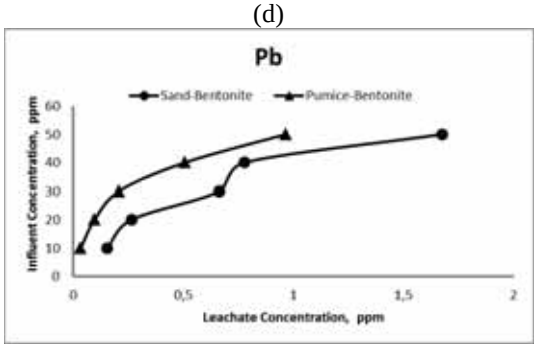

(e)

FIGURE 2
Variation in heavy metal adsorption of proposed mixtures

almost three times higher than the Ni concentrations of sand-bentonite mixtures (Figure 2d). This means that sand-bentonite mixtures exhibited quite better performance than pumice-bentonite mixtures in Ni adsorption (Figure 2d). The leachate lead (Pb) concentrations were between 0.117 – 1.821 ppm in sand-bentonite mixtures and between 0.030 – 1.032 ppm in pumice-bentonite mixtures. Pumice-bentonite mixtures had better Pb adsorption than sand-bentonite mixtures (Figure 2e).

Compacted sand-bentonite and pumice-bentonite mixtures were saturated with 25, 50, 100, 150 and 200 ppm phosphorus (P) and nitrate (NO_3) solutions to test P and N adsorption capacities of the mixtures (Table 3). While leachate P concentrations of sand-bentonite mixtures varied between 3.102 – 11.719 ppm, P concentrations of pumice-bentonite mixtures varied between 0.761 – 4.772 ppm. Pumice-bentonite mixtures exhibited quite better performance than sand-bentonite mixtures in P adsorption (Figure 3a). NO_3 concentrations of pumice-bentonite mixtures varied between 4.973 – 18.629 ppm and the concentrations of san-bentonite mixtures varied between 4.758 – 16.281 ppm. Both mixture types exhibited quite similar performance in NO_3 adsorption with slightly better performance of pumice-bentonite mixtures (Figure 3b).

TABLE 3
Phosphorus and nitrogen concentrations of permeability leachates (ppm)

Concentration	P		NO_3	
	Sand	Pumice	Sand	Pumice
25	3.102	0.761	4.973	4.758
	4.287	0.907	6.007	5.147
	3.485	0.937	6.637	5.921
50	4.990	1.046	8.715	6.492
	5.018	1.452	10.384	5.925
	5.621	1.328	9.448	6.352
100	7.772	1.837	12.754	10.762
	8.007	2.079	11.937	11.146
	8.391	1.973	13.548	11.895
150	9.126	3.021	16.348	13.782
	10.114	2.492	15.027	14.892
	9.627	2.470	15.957	14.559
200	10.927	3.880	17.485	14.941
	11.719	4.455	18.117	16.281
	11.382	4.772	18.629	15.367

McBride [19] indicated that soil Cd, Cu, Ni and Zn adsorptions varied from soil to soil and greatly influenced by soil pH, organic matter content, cation exchange capacity and especially type of clay mineral. In present research, bentonite played the dominant role in heavy metal adsorption. Scheidegger et al. [20] in a study investigating the effects of phrohyllite, kaolinite, gypsum and montmorillonite on Ni adsorption indicated the significance of heavy metal adsorption of soil minerals for the environment and reported faster Ni adsorption for montmorillonite. Bentonite is adsorbent aluminum phyllosilicate clay consisting mostly of montmorillonite, thus played also a significant role in Ni adsorption in present study. Therefore, current findings comply with those earlier ones. Adriano [21] carried out a study about

heavy metal adsorption of different soil minerals and indicated that heavy metal adsorption of soils mostly related to their clay, organic matter, Fe and Mn oxide contents, Pb and Cr were mostly adsorbed by organic matter and Cu and Cd were mainly adsorbed by clay minerals (especially by calcite-dolomite). Morera et al. [22] investigated heavy metal (Cd, Cu, Ni, Pb and Zn) mobility in soils and indicated that Pb and Cu were more related to soil surface activities than Cd, Ni and Zn. Vega et al. [23] carried out a study to investigate the metal ion abruption behaviors of soil and soil components (clay minerals, metal hydroxides and soil organic matter) and indicated that carbonate contents played a dominant role in Pb adsorption. Present findings comply with the findings of [24, 25, 26] about treatment performance of different materials.

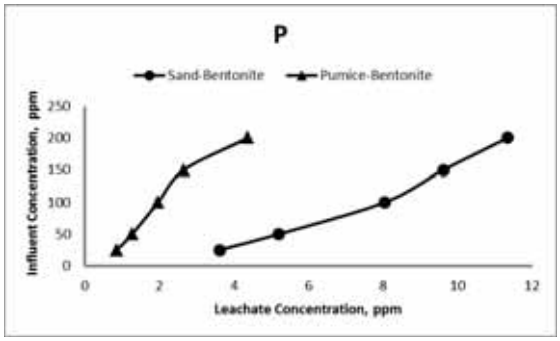

(a)

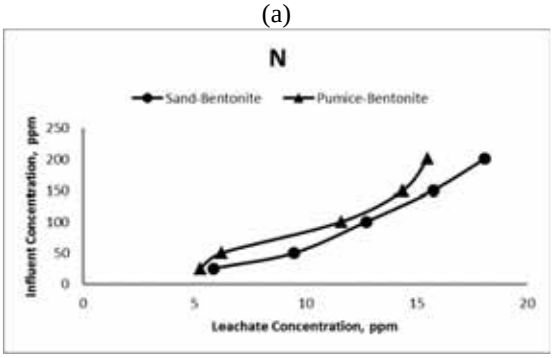

(b)

FIGURE 3
Variation in phosphorus and nitrogen adsorption of proposed mixtures

CONCLUSION

The primary objective of the present study was to elucidate adsorption behaviors of pumice-bentonite mixtures through comparisons with sand-bentonite mixtures and to present a potential use of naturally abundant pumice material. The following conclusions can be drawn from the present study carried out with sand and pumice samples with certain size range and mixed with bentonite clay at certain ratio to be used in liner design for waste repositories, constructed wetland wastewater treatment basins and waste storage lagoons of livestock facilities to prevent possible leakage and resultant groundwater pollution:

1. Bentonite played a dominant role in heavy metal adsorption since it is a clay mineral. Sand and pumice exhibited similar performance for Pb and Cd, but pumice had quite better performance in adsorption of Cr, Cu and Ni.
2. While sand-bentonite and pumice-bentonite mixtures had similar performance in nitrate adsorption, pumice-bentonite mixtures had again quite better performance in phosphorus adsorption. Higher surface area of pumice grains yielded quite higher phosphorus adsorption than sand grains.
3. Pumice with several macro-micro pores and much higher surface area can be used as an alternative to sand in mixtures to be used in liner design.

The single size range (0.50-1.00) and a single bentonite mixture ratio (30%) were used in current mixtures based on findings of a previous study. In further studies, different material sizes, different bentonite mixture ratios, greater heavy metal, nitrate and phosphorus doses and other clay minerals can be used for better presentation of adsorption characteristics of those materials.

ACKNOWLEDGEMENTS

This work was supported by TUBITAK (The Scientific and Technological Research Council of Turkey) with a project number of TOVAG – 111O713.

REFERENCES

[1] Sallfors, G. and Oberg-Hogsta, A.L. (2002) Determination of hydraulic conductivity of sand bentonite mixtures for engineering purposes. Geotechnical and Geological Engineering. 20, 65-80.
[2] Pusch, R. (2001) The buffer and backfill handbook. Part 2: Materials and Techniques. Geodevelopment AB, Technical Report. TR-02-12.
[3] Agus, S.S. and Schanz, T. (2005) Effects of shrinking and swelling on microstructures and fabric of compacted bentonite-sand mixture. In: Proceedings of International Conference on Problematic Soils. Cyprus, 2, Pp. 543550.
[4] Gokalp, Z. (2009) Engineering characteristics of sand-clay mixtures used for clay cores of earthfill dams. Clay Minerals. 44, 319-326.
[5] Akgun, H., Kockar, M.K., Akturk, O. (2006) Evaluation of compacted bentonite/sand seal for underground waste repository isolation. Environmental Geology. 50, 331-337.

[6] Gokalp, Z., Basaran, M., Uzun, O. (2012) Permeability characteristics of pumice-bentonite mixtures in comparison with sand-bentonite mixtures. Scientific Research and Essays. 7 (31), 2816-2826.
[7] Gokalp, Z., Basaran, M., Uzun, O. (2011) Compaction and swelling characteristics of sand bentonite and pumice-bentonite mixtures. Clay Minerals. 46(3), 449-459.
[8] Chapius, R.P. (1990) Sand-bentonite liners: Predicting permeability from laboratory tests. Canadian Geotechnical Journal. 27, 47-57.
[9] Akgun, H. (2009) Geotechnical characterization and performance assessment of bentonite/sand mixtures for underground waste repository sealing. Applied Clay Science. 49, 394-399.
[10] Al-Rawas, A.A., Mohamedzein, Y.E., Al-Shabibi, A.S., Al-Katheiri, S. (2006) Sand attapulgite clay mixtures as a landfill liner. Geotechnical and Geological Engineering. 24, 1365-1383.
[11] Mollamahmutoglu, M. and Yılmaz, Y. (2001) Potential use of fly ash and bentonite mixtures as liner or cover at waste disposal areas. Environmental Geology. 40, 1316-1324.
[12] Villar, M.V. (2006) Infiltration tests on a granite/bentonite mixture: Influence of water salinity. Applied Clay Science. 31, 96-109.
[13] Mishra, A.K., Dhawan, S., Rao, S.M. (2008) Analysis of swelling and shrinkage behavior of compacted clays. Geotechnical and Geological Engineering. 26, 289-298.
[14] Sun, D.A., Cui, H., Sun, W. (2009) Swelling of compacted sand-bentonite mixtures. Applied Clay Science. 43, 485-492.
[15] Kadlec, H.R. and Knight, R.L. (1996) Treatment Wetlands. Lewis Publisher, Florida, USA.
[16] Kadlec, R.H., Knight, R.L., Vymazal, J., Brix, H., Cooper, P., Haberl, R. (2000) Constructed wetlands for pollution control; processes, performances, design and operation. Scientific and Technical Report No. 8, IWA Publishing. London, England.
[17] Anonymous (2000a) ASTM D698 Standard Test Method for Laboratory Compaction Characteristics of Soil using Standard Effort. American Society for Testing and Materials. Section 4, 04.08(1), 78-85.
[18] Anonymous (2000b) ASTM D5084 Standard Test Method for Measurement of Hydraulic Conductivity of Saturated Porous Materials using a Flexible Wall Permeameter. American Society for Testing and Materials. Section 4, 04.08(1), 125-132.
[19] McBride, M.B. (1989) Reactions controlling heavy metal solubility in soils. Advances in Soil Science. 10, 1-56.
[20] Scheidegger, A.M., Lamble, G.M., Sparks, D.L. (1996) Spectroscopic evidence for the formation of mixed-cation hydroxide phases upon metal sorption on clays and aluminum oxides. Journal of Colloid and Interface Science. 186, 118–128.
[21] Adriano, D.C. (1986) Heavy metals in the terrestrial environment. Springer-Verlag, New York.
[22] Morera, M.T., Echecerria J.C., Mazkiaran, C., Garrido J.J. (2001) Isotherms and sequential extraction procedures for evaluating sorption and distribution of heavy metal in soils. Environmental Pollution. 113, 135-144.
[23] Vega, F.A., Covelo, E.F., Andrade, M.L., Marcet, P. (2004) Relationship between heavy metals content and soil properties in mine soils. Analytic Chemistry Acta. 524, 141-150.
[24] Kavak, D. (2017) Adsorption of Cr(III) from aqueous medium by hazelnut shell and batch design. Fresen. Environ. Bull. 26, 1784-1790.
[25] Yuhui, L., Fei, L., Diyi, X., Xiujie, Z., Pengfei, Z., Xin, W., Lichao, Z., Changyu, S. (2017) Thermodynamic test on antimony adsorption performance of modified activated carbon. Fresen. Environ. Bull. 26, 2271-2276.
[26] Wu, F., Wang, Y., Xia, C., Hau, J., Wei, B. (2016) Sorption of ammonia nitrogen on suspended sediments in Lanzhou section of the yellow river China. Fresen. Environ. Bull. 25, 4-13.

Received: **10.01.2017**
Accepted: **08.09.2017**

CORRESPONDING AUTHOR

Zeki Gokalp
Erciyes University,
Agricultural Faculty Biosystems
Engineering Department
Melikgazi 38038 Kayseri – Turkey

e-mail: zekigokalp@yahoo.com

© by PSP Volume 27 – No. 2/2018 pages 771-778 Fresenius Environmental Bulletin

THE PHYSIOLOGY RESPONSE OF *BIDENS PILOSA* ROOT LEACHATES ON THE *PTERIS MULTIFIDA* GAMETOPHYTE

Kai-mei Zhang[1,2,3], Yu Shen[4], Yan-ming Fang[1,2,*]

[1]Co-Innovation Center for Sustainable Forestry in Southern China, Nanjing Forestry University, Nanjing, Jiangsu, 210037, China
[2]College of Biology and the Environment, Nanjing Forestry University, Nanjing, Jiangsu, 210037, China
[3]Department of Botany, Smithsonian Institution, Washington, DC, 20013, USA
[4]College of Resources and Environmental Sciences, Nanjing Agricultural University, Nanjing, Jiangsu, 210095, China

ABSTRACT

Bidens pilosa, a common invasive species, has allelopathic effects on the local vegetation growth in China. In this study, we examine the allelopathy of *B. pilosa* to the fern's (*Pteris multifida*) gametophyte, and explain its phytotoxicity mechanisms caused by invasive plants. This report has investigated effects on the roots leachates of invasive *B. pilosa* on photosynthesis and the cell membrane in *P. multifida* gametophytes. Compared to the control, fluorescence parameters are reduced by gametophytes exposed to root leachates of *B. pilosa*, except non-photochemical quenching. There are increasing inhibitory effects on these parameters when leachate concentrations of *B. pilosa* increased, showing that the greatest inhibition is taken place at day 10. *B. pilosa* leachates take negative dose-dependent (that is, exposure-dependent) effects on Chlorophyll *a*, Chlorophyll *b*, carotenoid and total chlorophyll in the gametophytes. The damage is increased by gametophytes exposed to *B. pilosa* to cell membranes as expressed in aspects of electrolyte leakage (membrane permeability) and certain degree of damage to the cell membrane. The damage is caused due to the stress from root leachates to two chief mechanisms of photosynthesis, which reduces carriers of light and electron transmit in Photosystem I and the production of photochemical quantum output in Photosystem II. The gametophyte's osmotic potential is also destroyed by the chemicals from the root leachates. With treatment concentration increasing, electrolyte leakage and the degree of injury present a trend to become worsen, which suggests that the cell structure suffered from a negative effect by the allelopathy effects of *B. pilosa* root leachates. Conclusion is drawn that the chief allelopathic of *B. pilosa* might influence the *P. multifida* gametophyte in terms of durable and irreversible inhibition.

KEYWORDS:
Pteris multifida, gametophyte, *Bidens pilosa*, chlorophyll fluorescence, electrolyte leakage.

INTRODUCTION

In view of the investigation of the plants responses to environmental stress and the uncovering of associated mechanisms for these responses, the gametophyte has more particular benefits than the sporophyte and other higher plants. Farrant and Moore has studied the desiccation tolerance of the fern gametophyte [1]. Recently, there were few studies about the allelopathy effects which native fern species could bring by exotic invasive plants, as well as the gametophyte. It is released that the allelopathic effects can adversely affect the surrounding vegetation [2, 3]. For instance, *Eupatorium adenophorum* can have inhibitory impacts on the fern gametophytes of *Pteris finotii, Macrothelypteris torresiana*, and *Cibotium barometz* consisting of inhibition of spore germination, development, and rhizoid growth [4, 5, 6]. To date, the effects of invasive plants on ferns have received less attention compared to the attention paid to their effects on other types of vegetation, such as mangrove forests [7, 8] and crops [9, 10]. As the growth and development of fern gametophytes could be affected by the invasion species in the environment, it is critical to decide the allelopathic impacts of invasive plants on fern gametophytes. Thus this study can be helpful for researchers to know the fern gametophytes respond to the environment and to exotic species of invasive vegetarian, which will offer a potential guidepost to guard Chinese rare fern resources, and focus on allelopathy study to decide the impacts on other harmful invasive vegetarians.

B. pilosa is one of the main invasive plant species found in China and is part of the plant family that includes *E. adenophorum.* It can reduce agricultural production and alter plant community structures [11]. Most studies of *B. pilosa* have focused on its deleterious effects on spermatophytes. It excretes allelochemicals and delivers them into the rhizosphere through root exudates and leaching from the leaves and other aerial plant parts via different pathways that includes volatile emissions, root exudation, and leaf litter. These allelochemicals hinder the germination and seedling growth of potential competitors [12].

Allelopathic activity is more readily observed when vegetarian grew in the sensitive period. Zhang et al. suggests that it is easy for ferns to detect the activity in the period of spore germination and gametophyte growth [13]. However, there are no studies concerning to the potential allelopathic effects of *B. pilosa* on ferns. Based on our field observations, it is shown that some ferns cannot succeed in setting up pure patches of *B. pilosa*. The distribution of *Pteris multifida* overlaps with that of *B. pilosa* in China. This study aims to evaluate the potential allelopathic impacts of *B. pilosa* on the gametophytes of *P. multifida*.

Weir et al. suggest that physiological and biochemical results are helpful to show the mechanisms of phytotoxicity caused by allelochemicals in recipient/susceptible vegetarians [14]. In allelopathy study, phytotoxic activity was evaluated through the secondary physiological procedures like germination, seedling growth, and/or biomass of test species for most bioassays [15, 16, 17]. Bigot et al. thinks that people hardly understand the response of the physiological and primary processes (like photosynthesis and osmotic potential) in native species impacted by invasive species [18]. For the procedures are the first time that it is necessary to have the adverse allelopathic impacts of invasive vegetarians, investigation to respond to these impacts.

In this study the release of photosynthesis and cell membranes in the *P. multifida* gametophyte would be necessary to decide the potential involvement of allelopathic mechanisms caused by *B. pilosa* root leachates.

MATERIALS AND METHODS

Root leachates. *B. pilosa* were cultured and collected from Nanjing Forestry University, the seeds of *B. pilosa* were gathered in Xishuangbanna, Yunnan, China. Root leachates were prepared by every 1 g gently washed fresh samples loading into 10 mL distilled water, and then soaked for 72 h at 130 rpm. Then the leachates were filtered through filter paper pulp under vacuum conditions and stored at –20 °C. The leachates were sterilized by Durapore® PVDF membrane (0.45 μm, Carrigtwohill, Co. Cork. Ireland).

Gametophyte culture. Spores of *P. multifida* were collected on September 2014 from 15-20 fertile mature fronds at Nanjing Forestry University. Spores were collected and screened using a 0.088-mm diameter mesh (Zhejiang Shangyu Yarn and Sieve Factory, Shangyu, China). Then the spores were spread evenly in plastic trays (size 25 cm × 20 cm × 5 cm) with a sieved mixture of dark soil and sand with an average density of 100-150 spores per cm^2 [19]. The trays were covered with transparent plastic film to avoid contamination and desiccation, with fluorescent light (photon flux density 1000 μ mol $m^{-2}\cdot s^{-1}$) at 25°C with a 12 h light photoperiod. Twenty days after the spores were sowed, healthy and uniform gametophytes (10 × 5 mm) were selected and rinsed carefully and thoroughly with distilled water.

Treatment applications. Root leachates of *B. pilosa* were diluted with distilled water to create five different concentrations (0, 12.5, 25, 50, and 100%); distilled water was used as the control. Afterwards, all gametophytes were treated with 5 mL of leachates in a Petri dish (60-mm diameter). One hundred gametophytes were grown in each Petri dish with fluorescent light (37.5 μ mol $m^{-2}\cdot s^{-1}$) at 25°C with a 12-h light photoperiod.

Fluorescence and pigment measurements. The fluorescence and pigments of the fern gametophytes were analyzed every two days when the experiment starts. The gametophytes were collected immediately before the fluorescence measurement. Samples were dark-adapted for 2 min. Junior PAM (Heinz Walz GmbH, D91090, Effeltrich, Germany) was applied to perform fluorescence measurements. The fluorometer was connected to a PAM Data Acquisition System PDA 100 (Walz) controlled by the software WINCONTROL v3 (Heinz Walz GmbH). Actinic light intensity (PAR) was 66 μ mol $m^{-2}\cdot s^{-1}$. Data were recorded and calculated for quantum yield of photosystem II (Φ_{PSII}), lower quantum efficiency of open PSII reaction centers (*Fv*/*Fm*), photochemical fluorescence quenching (*qP*), electron transport rate (ETR) and non-photochemical quenching (NPQ) by following the formulas of Hoegh-Guldberg et al. [20]. The efficiency of dark-adapted PSII was calculated by $Fv/Fm = (Fm - F_0)/Fm$, where Fm and F0 are the maximum and the minimum fluorescence of dark-adapted samples, respectively.

Plant samples (0.025 g of fresh weight) from each plant species were used for the pigment measurements. Chlorophyll was extracted in darkness with a 5-mL mixture of ethanol and acetone (1:1, v/v). This colorimetric procedure was performed until the samples were visibly colorless. The optical densities of the extracts were determined at 470, 647, and 663 nm with a SP-2100P spectrophotometer (Spectroscopic Instruments Inc., Shanghai, China). Subsequently, the optical densities were converted to Chlorophyll *a* (Chl *a*), Chlorophyll *b* (Chl *b*), carotenoid (Car), and total chlorophyll, following the formulas of Moran (1982). Five fluorescence indexes were recorded of photosystem II (PS II) and the chlorophyll pigments (Chl *a*, Chl *b* and Car) of gametophytes with exposure of the plant samples to *B. pilosa* root leachates.

Electrolyte leakage. Electrolyte leakage (membrane permeability) was estimated as described by Sánchez-Viveros et al. with modifications

[21]. The initial electrical conductivity (*C*1) of the medium with *P. multifida* was measured at time zero, with variable electrical conductivities (*C*n) determined at 12, 24 and 36 h, respectively. Finally, the samples were autoclaved at 100°C for 20 min to release all electrolytes; the final electrical conductivity (*C*F) was measured after cooling of the samples to 25°C. The degree of electrical leakage (ET) was calculated from the following equation: ET = (*C*n − *C*1)/*C*F × 100. The degree of injury was estimated by the following equation: degree of injury = (L_t − L_{CK})/(1 − L_{CK}) × 100; where L_t and L_{CK} are the values of (*C*n − *C*1) in the treatments and the control, respectively. All data were measured for electrolyte leakage in gametophytes during treatment with leachates and collected every other day (days 2, 4, 6, 8 and 10).

Statistical analysis. The effects of root leachates of *B. pilosa* on photosynthesis and cell membranes in *P. multifida* gametophytes were analyzed by one-way analysis of variance (ANOVA). All statistical analyses were carried out with SPSS v.20.0 for Windows; graphical work was performed using Origin 8.0 (Origin Lab, USA). All results are expressed as means with corresponding standard deviations.

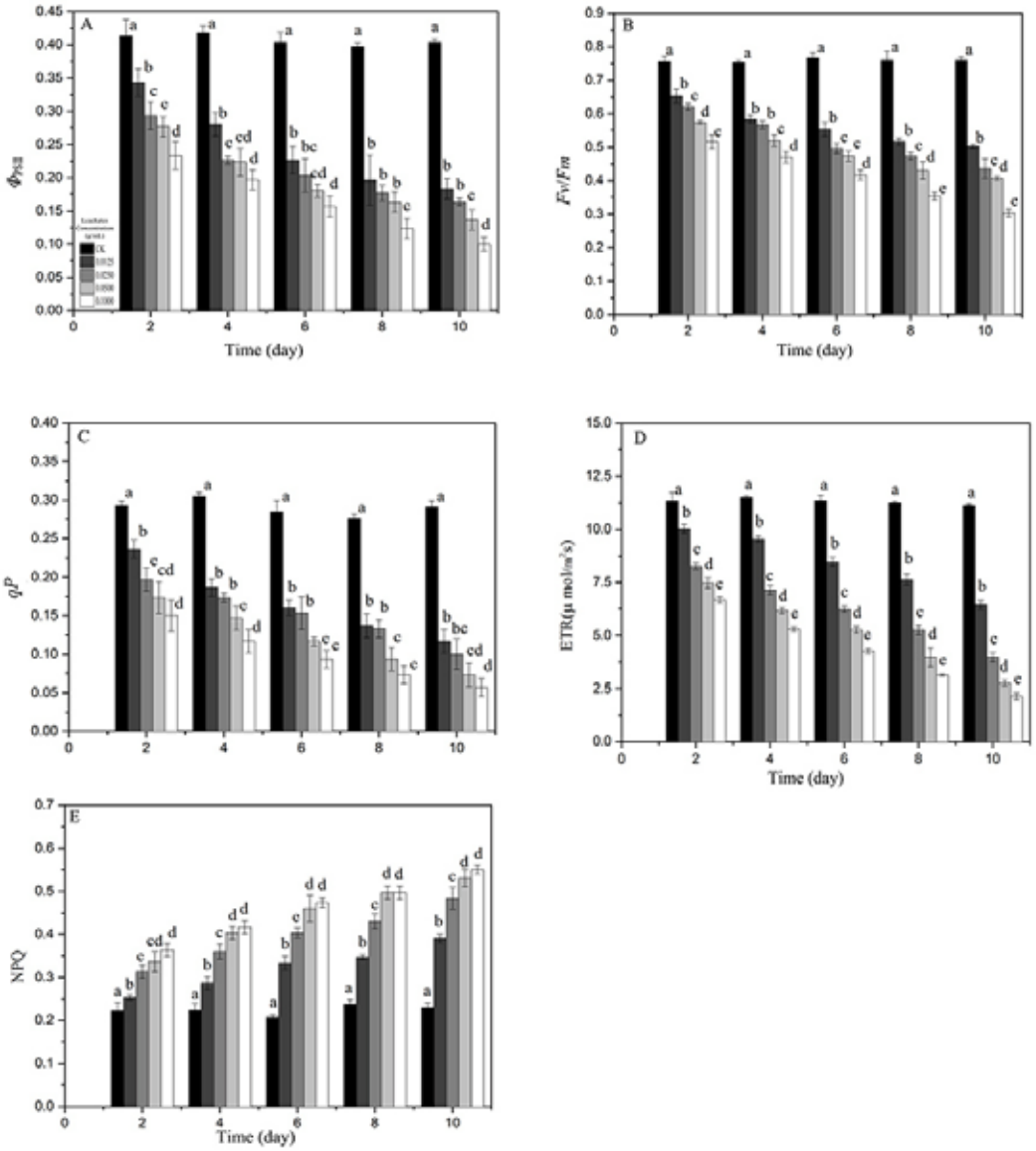

FIGURE 1
A, B, C, D, E
Impact of time and root leachates of *Bidens pilosa* on Φ_{PSII}, *Fv*/*Fm*, *qP*, ETR and NPQ of *Pteris multifida* gametophytes. Statistically significant differences among treatments are indicated by letters above or below lines. Two similar letters indicate no significant difference between treatments, and dissimilar letters indicate a significant difference between treatments ($P < 0.05$).

RESULTS AND DISCUSSION

Fluorescence of gametophytes. Φ_{PSII} of *P. multifida* reduced with root leachate concentrations of *B. pilosa* and treated time increasing (Fig. 1A). Compared to the control, after *B. pilosa* was applied, a big difference in the Φ_{PSII} of *P. multifida* was recorded at day 2 at the 0.0125 g/mL concentration. Under the exposure of 0.1000 g/mL *B. pilosa* root leachates at day 10, the Φ_{PSII} of the gametophyte got the minimum at 0.10 (Fig. 1A). *Fv/Fm* in *P. multifida* gametophyte was inhibited under *B. pilosa* root leachates and presented a similar trend with Φ_{PSII} (Fig. 1B). When the root leachate concentrations increasing, *Fv/Fm* decreased gradually, the inhibitory impacts of *B. pilosa* leachates, and the value got the bottom at day 10. While, the similar effects happened on the *qP* in the gametophyte, when the treatments concentrations increasing, the negative dose-dependent impacts were applied on the decrease of *qP* (Fig. 1C). The variation in ETR had similarities to that for *qP*, which reduced when root leachate concentrations of *B. pilosa* increased (Fig. 1D). *P. multifida* showed its lowest ETR level (2.13 μ mol·m^{-2}·s^{-1}) with treatment with 0.1000 g/mL of the *B. pilosa* root leachate at day 10. NPQ of *P. multifida* was promoted with root leachate of *B. pilosa* increasing (Fig. 1E). Under the 0.1000 g/mL *B. pilosa* leachate treatment, NPQ values took a 0.64-fold reduction at day 2 and a 1.39-fold increase at day 10 than that of the control. Particularly, NPQ was significant influenced by root leachates of *P. multifida* increasing at day 10.

Pigment content. Chl *a*, Chl *b*, Car, and total chlorophyll contents reduced when root leachates concentrations got increasing (Fig. 2 A-D). This change was also reflected by the change in color of the gametophyte. Car content showed the lower level than that of the control under 0.1000 g/mL root leachates treatment in experiment time. At day 2, the total chlorophyll reduced by 22.33% and 30.98% when the root exudate concentration increased from 0.0250 g/mL to 0.0500 g/mL (Fig. 2D). At days 2 and 10, 36.10% and 48.76% decrease in the total chlorophyll than that of the control were recorded when the 0.100 g/mL root exudate was added.

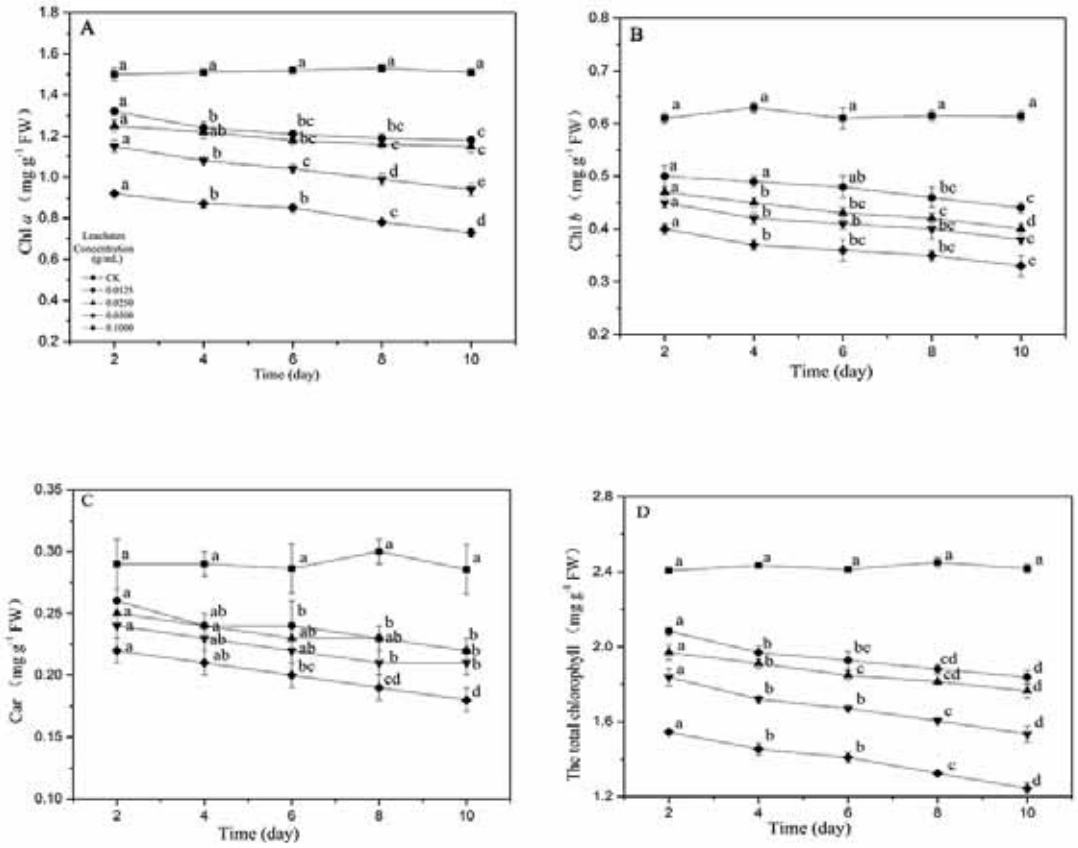

FIGURE 2
The values of A) Chlorophyll *a*, B) Chlorophyll *b*, C) carotenoid and D) the total chlorophyll in the control and treated with *B. pilosa* root leachates. Statistically significant differences among treatments are indicated by different letters ($P < 0.05$).

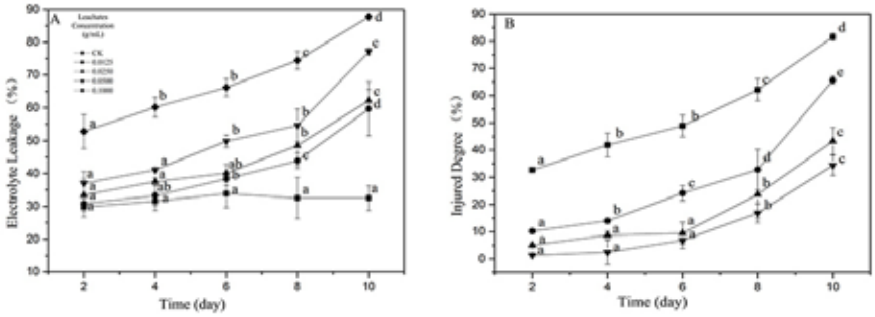

FIGURE 3
The strength(%) of A) electrolyte leakage and B) injured degree in the control and treated with *B. pilosa* root leachates. Statistically significant differences among treatments are indicated by different letters ($P < 0.05$).

Electrolyte leakage. Figure 3A shows the impact of root leachate on electrolyte leakage of *P. multifida*. Electrolyte leakage raised obviously up when various root leachate treating from day 8 to day 10 than that of the control group ($P < 0.05$). It was found that the electrolyte leakage got the peak at 87.73% when root leachate treat got the 0.1000 g/mL than that of the control group at day 10. The change of degree of injury followed a similar pattern as that for electrolyte leakage in Fig. 3B, as the trend presented a correlation with root leachate concentrations. At day 2, 1.36% degree of damage to the control was tested under root leachates treatments. The gametophyte seemed to suffer the highest degree of damage with treatment getting 0.1000 g/mL root leachate at day 10. The degree of damage increased by 137.10% with the 0.1000 g/mL root leachate treatment when compared to the 0.0125 g/mL root leachate treatment.

Fv/*Fm*, Φ_{PSII}, *qP* and ETR took negative trends when *B. pilosa* root leachates increasing. Φ_{PSII} and *Fv*/*Fm* were regarded as the indexes to indicate photochemical quantum output and relative outcome in PS II reaction centers. According to the results above, the chemicals of root leachates suppressed the gametophyte PS II center gaining and storing photochemical quanta, as the quantum output caused the decrease of photosynthesis efficiency. This tendency of the index endured, for the values of Φ_{PSII} and *Fv*/*Fm* became both lower under root leachates treatments. At the same time, the weakened electron transport could lead one to infer that the process of conversion from light to electrons was blocked due to the root leachates being absorbed into the gametophyte. And the reduced photochemical quantum production and yield might be one reason for it. The final NPQ amount is more heavily influenced by the non-photochemical quenching that reflects heat dissipation of excitation energy in the antenna system. Furthermore, the results of NPQ reflect the fact that the remainder of the energy in PS II may be converted into heat and finally dissipate into the system. The results of the photo-protection index, *qP*, also descend with increasing root leachate concentration, signifying that the negative effects caused by the chemicals is irreversible. In addition, chlorophyll pigments (Chl *a*, Chl *b*, and Car) also decrease with increase in root exudate concentrations; this is particularly true for Chl *a* and Chl *b*, which are important parts in photosystem I (PS I). This implies that the components of the root exudates have the function of hindering the synthesis of chlorophyll.

Meanwhile, the study reveals that the electron transport from PS II to PS I is interrupted and the effective quantum yields in PS II reaction centers are also limited, resulting in the disruption of photosynthesis. The chlorophyll fluorescence of *P. multifida* was adversely affected by *B. pilosa* leachates, similar to the description of the chlorophyll fluorescence analysis of photosynthetic efficiency, quantum yield, and photon energy dissipation in PS II antennae of *Lactuca sativa* leaves exposed to cinnamic acid in Hussain and Reigosa [22]. And Zhang et al. also has described the photosystem would be destroyed by the root exudates [23].

Chlorophyll plays an important role in the absorption, transfer and transformation of light energy. Car is the indispensable component of chromoprotein in photosynthesis, which is important for the protection of photosynthesis from injury of singlet oxygen. Our results showed that chlorophyll and Car decreased upon exposure of *P. multifida* to *B. pilosa* root leachates. The reduced sensitivity of *Fv*/*Fm* to *B. pilosa* leachates was due to the conserved F_0 in relation to lower chlorophyll content, indicating a low-level functioning of PS II with a low absorption rate of light in the gametophytes. The results for the chlorophyll contents align with those from preliminary studies on *Chlorella vulgaris* by Qian et al. [24] and *Microcystis aeruginosa* NIES-843 (Cyanobacteria) by Shao et al. [25].

The extent of membrane damage, also of interest in this study, could be assessed indirectly by conductometric measurements of solute leakage from cells. In this study, the electrolyte leakage and the

degree of injury increase significantly with increasing root leachate concentrations, implying that the chemicals damage the membrane and the osmotic potential of the cell, especially the balance of the cellular ions. The significant increase in cellular injury demonstrates that the root leachates have enduring negative effects on the cell membrane; the structure of the cell would be destroyed by these effects over time and with the increase of the concentration of the chemicals [26, 27, 28]. This mechanism would cause broader destructive effects, as the condition of the soil (with its varying pH ranges and nutrient content) would be permanently changed by the invasive plants [29]. The fading of native species caused by these chemicals would be the outcome of the allelopathy in the soil.

Our experiments show that cell membranes are the component severely affected by the root leachates of *B. pilosa* in *P. multifida* gametophytes. Membrane permeability alteration mediates an increase in electrolyte leakage. This result is in line with a previous report, which revealed that this allelopathic effect can lead to increased cell membrane permeability, leakage of cellular contents, increased lipid peroxidation, and ultimately slow growth or death of plant tissue [30]. Comparisons can be drawn with the damage caused by heavy metals, for which the response is faster and repair is difficult in terms of removal from the cells [31], while the stress caused by chemicals seems more durable, and the damage is also harmful in plant cells.

The donor invasive plant species can have fatal, weak or non-allelopathic effects on several target species that belong to different taxonomic families. As a result, small but important differences associated with the allelochemical mode of action are expected in their physiology [32]. The observed loss of fern species in *B. pilosa* patches in the field, together with the findings in our laboratory tests, imply that the effects of *B. pilosa* on native species are deleterious and allelopathy may be partly responsible for the adverse effects. According to the Novel Weapons Hypothesis, which attempts to explain the remarkable success of many exotic invasive species, invasive plant species may possess novel chemicals that are more phytotoxic to plants in the invaded range than to adapted species in the invader's native range [33]. With regard to *B. pilosa*, many secondary metabolites (phenolics, polyacetylenes, and triterpens) involved in allelopathic action were found. Of these, phenylheptatriyne (PHT) and its derivatives were highest in concentration in *B. pilosa* oil [12]. A total of 23 phenolic compounds (including salicylic acid, vanillin, *p*-hydroxybenzoic acid, *p*-coumaric acid, and ferulic acid) were identified and isolated in *B. pilosa* shoots and roots. Contents of caffeic acid were highest (117.4, 298.7, and 350.3 μg g^{-1} in leaves, stems and roots), followed by pyrocatechin [12]. The organics from *B. pilosa* could also result in damage to non-adapted plants, such as *P. multifida* in this study. Furthermore, the effects of the stem, leaf and flower of *B. pilosa* on the *P. multifida* gametophyte should be addressed due to the possible variety and concentrations of allelochemicals in different plant parts. Although we are still in the early stages of comprehending the gametophyte responses of *P. multifida* to *B. pilosa*, this study opens the door to understanding of the physiological response of the fern to invasive plant species.

CONCLUSION

In conclude, *B. pilosa* root leachates enduringly and irreversibly affect the photosynthesis of *P. multifida* via allelopathic interference and damage the cell membrane. The decrease of the carriers of light and electron transport in PS I and of the production of photochemical quantum yield in PS II are the main mechanisms through which *B. pilosa* leachates damage the photosynthetic process in *P. multifida*. The changed osmotic potential of the cells in *P. multifida* indicates that the root leachates negatively affect plant growth, mainly through the cell structure. In a word, the main allelochemicals in the root leachates of *B. pilosa* could have negative effects on the growth of the *P. multifida* gametophyte.

ACKNOWLEDGEMENTS

This work was supported by the National Natural Science Foundation of China (31200233), the Priority Academic Program Development of Jiangsu Higher Education Institutions (PAPD), Collaborative Innovation Plan of Jiangsu Higher Education, the Jiangsu Government Scholarship for Overseas Studies and the Laboratories of Analytical Biology of the National Museum of Natural History, the Smithsonian Institution.

REFERENCES

[1] Farrant, J.M. and Moore, J.P. (2011) Programming desiccation-tolerance: from plants to seeds to resurrection plants. Current Opinion in Plant Biology. 14, 340-345.

[2] Bais, H.P., Vepachedu, R., Gilroy, S., Callaway, R.M. and Vivanco, J.M. (2003) Allelopathy and exotic plant invasion: from molecules and genes to species interactions. Science. 301, 1377-1380.

[3] Yang, R., Zhou, G., Zan, S., Guo, F., Su, N. and Li, J. (2011) Arbuscular mycorrhizal fungi facilitate the invasion of *Solidago canadensis* L. in southeastern China. Acta Oecologica. 61, 71-77.

[4] Zhang, K., Shi, L., Jiang, C. and Li, Z. (2007) Influence of root, stem and leaf leachates of *Ageratina adenophora* weed on the gametophyte development of *Pteris finotii*. Allelopathy Journal. 20, 203-212.
[5] Zhang, K., Shi, L., Jiang, C. and Li, Z. (2008a) Inhibition of *Ageratina adenophora* on spore germination and gametophyte development of *Macrothelypteris torresiana*. Journal of Integrative Plant Biology. 50, 559-564.
[6] Zhang, K., Shi, L., Jiang, C. and Li, Z. (2008b) Allelopathic effects of *Eupatorium adenophorum* on spore germination and gametophyte development in *Cibotium barometz*. Acta Pratacult Urae Sinica. 17, 19-25.
[7] Biswas, S.R., Choudhury, J.K., Nishat, A. and Rahman, M.M. (2007) Do invasive plants threaten the Sundarbans mangrove forest of Bangladesh? Forest Ecology and Management. 245, 1-9.
[8] Hai, R., Guo, Q., Liu, H., Zhang, Q., Xu, F. and Xu, H. (2014) Patterns of Alien Plant Invasion across Coastal Bay Areas in Southern China. Journal of Coastal Research. 295, 448-455.
[9] Naylor, R. (1996) Invasions in Agriculture: Assessing the Cost of the Golden Apple Snail in Asia. AMBIO. 25, 443-448,
[10] Kankanala, P., Czymmek, K. and Valent, B. (2007) Roles for rice membrane dynamics and plasmodesmata during biotrophic invasion by the blast fungus. Plant Cell. 19, 706-724.
[11] Hao, J., Liu, Q. and Qiang, S. (2009) Reproductive traits associated with invasiveness in *Bidens pilosa*. Chinese Bulletin of Botany. 44, 656-665.
[12] Khanh, T.D., Cong, L.C., Xuan, T., Uezato, Y., Deba, F., Toyama, T. and Tawata, S. (2009) Allelopathic plants: 20. hairy beggarticks (*Bidens pilosa* L.). Allelopathy Journal. 24, 243-253.
[13] Zhang, K., Liu, J., Cheng, X., Zhang, G., Fang Y. and Zhang, H. (2012) Effects of *Ageratina adenophora* on spore germination and gametophyte development of *Neocheiropteris palmatopedata*. American Fern Journal. 102, 208-215.
[14] Weir, T.L., Park, S.W. and Vivanco, J.M. (2004) Biochemical and physiological mechanisms mediated by allelochemicals. Current Opinion in Plant Biology. 7, 472-479.
[15] Li, H., Qiang, S. and Qian, Y. (2008) Physiological response of different croftonweed (Eupatorium adenophorum) populations to low temperature. Weed Science. 56, 196-202.
[16] Ruan, X., Li, Z., Wang, Q., Pan, C., Jiang, D. and Wang, G. (2011) Autotoxicity And Allelopathy of 3, 4-Dihydroxyacetophenone isolated from Picea schrenkiana needles. Molecules. 16, 8874-8893.
[17] Iqbal, A. and Fry, S.C. (2012) Potent endogenous allelopathic compounds in *Lepidium sativum* seed exudate: effects on epidermal cell growth in *Amaranthus caudatus* seedlings. Journal of Experimental Botany. 63, 2595–2604.
[18] Bigot, A., Fontaine, F., Clement, C. and Vaillant-Gaveau, N. (2007) Effect of the herbicide flumioxazin on photosynthetic performance of grapevine (*Vitis vinifera* L.). Chemosphere. 6, 1243-1251.
[19] Zhang, K., Liu, B., Fang, Y., Shi, L. and Tang, S. (2011) Studies on the gametophytes of eight Chinese species of *Dryopteris* (Dryopteridaceae). American Fern Journal. 101, 12-24.
[20] Hoegh-Guldberg, O. and Jones, R. (1997) Photoinhibition and photoprotection in symbiotic dinoflagellates from reef-building corals. Marine Ecology Progress Series. 183, 73-86.
[21] Sánchez-Viveros, G., González-Mendoza, D., Alarcón, A. and Ferrera-Cerrato, R. (2010) Copper effects on photosynthetic activity and membrane leakage of *Azolla filiculoides* and *A. caroliniana*. Journal of Integrative Plant Biology. 12, 365-368.
[22] Hussain, M.I. and Reigosa, M.J. (2011) A chlorophyll fluorescence analysis of photosynthetic efficiency, quantum yield and photon energy dissipation in PSII antennae of *Lactuca sativa* L. leaves exposed to cinnamic acid. Plant Physiology and Biochemistry. 49, 1290-1298.
[23] Zhang, K., Shen, Y., Zhou, X., Ma, L. and Fang, Y. (2016a) Photosynthetic electron-transfer reactions in the gametophyte of Pteris multifida reveal the presence of allelopathic interference from the invasive plant species Bidens pilosa. Journal of Photochemistry and Photobiology, B. 158, 81-88.
[24] Qian, H., Li, J., Sun, L., Chen, W., Sheng, D., Liu, W. and Fu, Z. (2009) Combined Effect of Copper and Cadmium On *Chlorella vulgaris* growth and photosynthesis-related gene transcription. Aquatic Toxicology. 94, 56-61.
[25] Shao, J., Wu, Z., Yu, G., Peng, X. and Li, R. (2009) Allelopathic mechanism of pyrogallol to *Microcystis aeruginosa* PCC7806 (Cyanobacteria): from views of gene expression and antioxidant system. Chemosphere. 75, 924-928.
[26] Hare, P.D. and Cress, W.A. (1997) Metabolic implications of stress-induced proline accumulation in plants. Plant Growth and Regulation. 2, 79-102.
[27] Malíková, L., Mudrák, O. and Klimešová, J. (2012) Adventitious sprouting enables the invasive annual herb *Euphorbia geniculata* to regenerate after severe injury. Ecology Research. 27, 841-847.

[28] Zhang, K., Shen, Y., Fang, Y. and Liu, Y. (2016b) Changes in gametophyte physiology of *Pteris multifida* induced by the leaf leachate treatment of the invasive *Bidens pilosa*. Environment Science and Pollution Research. 23(4), 3578-3585.
[29] Sołtysiak, J. and Brej, T. (2014) Invasion of Fallopia Genus Plants in Urban Environment. Polish Journal of Environmental Studies. 23, 449-458.
[30] Campos, P.S., Quartin, V.N., Ramalho, J.C. and Nunes, M.A. (2003) Electrolyte leakage and lipid degradation account for cold sensitivity in leaves of Coffea sp. plants. Journal of Plant Physiology. 3, 283-292.
[31] Eleftheriou, E.P., Adamakis, I.D.S., Panteris, E. and Fatsiou, M. (2015) Chromium-Induced Ultrastructural Changes and Oxidative Stress in Roots of Arabidopsis thaliana. International Journal of Molecular Sciences. 16, 15852-15871.
[32] Lorenzo, P., Palomera-Pérez, A., Reigosa, M.J. and González, L. (2011) Allelopathic interference of invasive *Acacia dealbata* Link on the physiological parameters of native understory species. Plant Ecology. 212, 403-412.
[33] Zhu, X., Zhang, J. and Ma, K. (2011) Soil biota reduce allelopathic effects of the invasive *Eupatorium adenophorum*. Plos One. 6, e25393.

Received: **12.01.2017**
Accepted: **08.09.2017**

CORRESPONDING AUTHOR

Yan-ming Fang
Co-Innovation Center for Sustainable Forestry in Southern China,
Nanjing Forestry University,
Nanjing, Jiangsu, 210037 – China

e-mail: jwu4@njfu.edu.cn

© by PSP Volume 27 – No. 2/2018 pages 779-786 Fresenius Environmental Bulletin

TEXTILE WASTEWATER TREATMENT USING BIOLOGICAL TRICKLING FILTER WITH NATURAL MEDIA IN COLD WEATHER (CASE STUDY: MOTAHARI TEXTILE FACTORY)

Toktam Shahriari*, Marjan Shokouhi

Faculty of Environment, University of Tehran, Tehran, Iran

ABSTRACT

Start-up of a biological trickling filter used with natural rock media and suitable hydraulic retention time (HRT) for the treatment of the wastewater from Motahhari textile factory was investigated. The pilot trickling filter column was filled with lava rocks with average diameter of 5 cm and porosity of 65%. For start-up operation, the textile wastewater and the activated sludge from treatment facilities of the textile factory were used for 25 days to reach a steady state. The textile wastewater, with average chemical oxygen demand (COD) of 2850 mg/L, was then pumped into the column. HRTs of the trickling filter were 5, 4, 3, 2 and 1 day, which were then reduced to 12, 8, 6, and 4 h. The influent and effluent wastewater parameters were measured at ambient temperatures of 5-10 °C. Reducing HRT from 5 days to a few hours led to the COD elimination with average efficiency of 90%. At HRT=6h, COD of the treated wastewater reached 85 mg/L.

KEYWORDS:
Biodegradation, biological treatment, COD, lava rock, textile wastewater, trickling filter

INTRODUCTION

High costs of industrial wastewater treatment, especially textile wastewater treatment, have directed many concerns towards finding the new and less costly methods for wastewater treatment [1-10]. Biological processes allow for reducing the high COD in industrial wastewater because of the suitable growth of microorganisms on lava rock [11,12]. High COD, temperature and pH of the influent wastewater; accurate system start-up; type of media and its specific surface area; and suitable growth of microorganisms are among the factors which influence the wastewater treatment by biological trickling filters [13]. These filters usually include organic media, microorganisms, and nutrients that can decompose water pollutants [14,15]. Moreover, non-submerged biological trickling filters with fixed media are used to induce biofilm growth for removing organic matter or nitrification of domestic or industrial wastewater [16, 17]. Wastewater passing through a media filled with porous material, forms biofilm on the media surface through biological degradation of pollutants in the wastewater. Pollutants are transferred from wastewater to biofilm where continuous biological degradation takes place [15, 18, 19, 20]. Biological trickling filter systems are simple reactors filled with solid materials, such as wood chips, lava rock, plastic, manure and compost, on which the biofilms with suitable microbial populations are formed [16, 21, 22, 23, 24, 25, 26]. In a biological tricking filter, the media filling the filter provides a buffer environment and a background (or a field) for the satisfactory growth of microorganisms [27]. The main pollutants in textile wastewater include high levels of total suspended solid, COD, BOD_5, dyes, alkalinity, and other dissolved substances [28, 29]. If the untreated textile wastewater is added to the surface water, the following will occur:

- Dissolved oxygen in water will rapidly decline.
- Sludge will be formed on riverbeds.
- Fungal growth in wastewater will substantially increase.
- Water pH will gradually decrease.

Since biodegradation of organic matter in wastewater requires oxygen, it increases the sludge mass and causes hydraulic flow problems in various parts of the region [30]. The production process in textile factories involves four stages of spinning, weaving, dyeing and finalizing the cloth. Bleaching, dyeing, printing and finalizing the cloth are the most important water-consuming processes in a textile factory. The wastewater produced in these sections contains high levels of COD, BOD_5 and dyes along with the daily manufactured products.

Since the time of microbial stabilization in biological trickling filter is high especially in cold seasons, it has not received much attention in most of the studies. Therefore, this study attempted to investigate the performance of biological trickling filter with lava rocks substrate in reducing the parameters that influence wastewater in cold weather

(5-10 °C). The suitable and optimal start-up and HRT for the filter to reduce COD and suspended solids are also investigated.

MATERIALS AND METHODS

The used pilot biological trickling filter was an unpainted steel column with a height of 2.1 m and average diameter of 21 cm (the diameter at the top and bottom was 32 cm). 160 cm of the height of the column was filled with lava rocks (with diameters of 3-7 cm, porosity of 65%, and specific surface area of 75 m^3/m^2). Two liquid sampling valves were installed at the column heights of 60 and 110 cm from the bottom (Fig. 1). The liquid distributor was a perforated metallic plate for pouring the wastewater uniformly and slowly onto the lava rocks media.

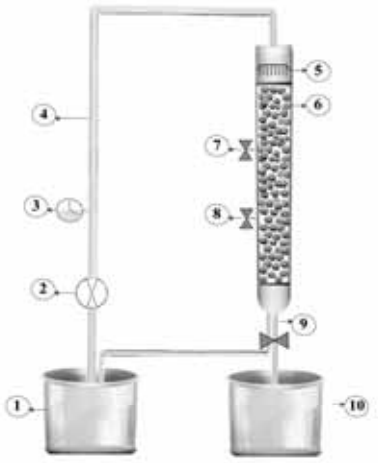

FIGURE 1
Schematic diagram of the biological trickling filter with lava rocks media
(1) Liquid storage tank, (2) Liquid pump, (3) Liquid flow meter (L/min), (4) Return of the liquid, (5) Liquid distributor, (6) Lava rocks media, (7) Sampling valve at the height of 60 cm, (8) Sampling valve at the height of 110 cm, (9) Sampling valve at the end of the column and, (10) Sedimentation tank

The total volume of the column (including rock substrate) was 55 L and that of the tank for returning liquid was 52 L. 10-20% of the volume of the tank for returning liquid was filled with activated sludge during the start-up process. The pilot was launched in a cold weather and stabilized at the temperature range of 5 to10 °C. The influent wastewater flow to the treatment facilities at Motahari textile factory is 400 m^3/day. The wastewater produced in the factory contains BOD_5 of 1400-1500 mg/L, and COD of 2800-3000 mg/L. The produced wastewater also contains fats, total suspended solids and dyes, which vary depending on the processes used in the factory.

Lava rocks, which can be obtained easily and at low cost, were collected from the mountains around Tehran and used to prepare a suitable media for the growth of biofilm. Activated sludge from the aeration tank and effluent wastewater from the wastewater treatment facilities of Motahari textile factory, located on the Buin Zahra road to Ghazvin, were used for start-up of the pilot biological trickling filter. Finally, it was observed that microorganisms could grow and adapt themselves to the pilot more quickly.

Samples were taken from sampling valves of the influent and effluent flows at the heights of 60 and 110 cm from the substrate to measure the parameters such as chemical oxygen demand (COD), dissolved oxygen (DO), total suspended solid (TSS) and pH. To measure COD, a Hack DT-500 spectrophotometer, capable of measuring high, average, and low ranges, was used at the wavelength of 420 nm. The TSS values of the samples were measured based on the standard methods and using filter paper at oven temperature of 105 °C. DO and pH were determined by a DO meter and a Metrohm 691 pH meter, respectively. All the tests were conducted based on the standard methods developed in 2005 [30].

RESULTS AND DISCUSSION

Sludge from the wastewater treatment facilities of Motahari textile factory, where the activated sludge method is employed, was used to start-up the pilot biological trickling filter. 20-30% of the 52 L feeding tank (up to15 L) was filled with the sludge with an MLSS of 6150 mg/L. The activated sludge from the treatment facilities was used for the formation of biological mass on the media made up of lava rocks. It should be noted that formation of biological mass on the bed reduced the pollutants in wastewater through microorganisms feeding. The biological growth on the media was started with the continuous flow of the activated sludge pumped from the tank to the top of pilot column. To examine the formation of biological mass, at first, three samples were taken from the lowermost sampling valve daily. The values of COD, TSS, pH and temperature were measured in each daily sample. Values of COD and TSS samples exhibited a descending trend on consecutive days. The reactor start-up was conducted under continuous operation using a returning liquid flow at the loading rate of 1.494 kg/m^3/day COD. The COD concentration in the activated sludge of Motahari textile factory is averagely 14920 mg/L. Table 1 shows COD reduction in the activated sludge in the first stage of system start-up. This stage lasted for 10 days during which COD elimination with the efficiency of 85% was achieved.

TABLE 1
COD elimination on the lava rocks media in the first stage of system start-up

Hydraulic Retention time (days)	Influent COD (mg/L)	Effluent COD (mg/L)	COD elimination efficiency (%)
1	14920	11250	25
2	14930	8690	42
3	14925	4790	68
4	14922	3820	74
5	14915	3000	80
6	14925	2755	81.5
7	14930	2555	83
8	14930	2375	84
9	14920	2160	85.5
10	14920	2000	87

TABLE 2
COD elimination on the lava rocks media in the second stage of system start-up

Hydraulic Retention time (days)	Influent COD (mg/L)	Effluent COD (mg/L)	COD elimination efficiency (%)
1	4550	1790	61
2	4575	1410	69
3	4650	1230	73
4	4670	1190	74
5	4480	1150	74
6	4500	1030	77
7	4750	930	80
8	4700	875	81

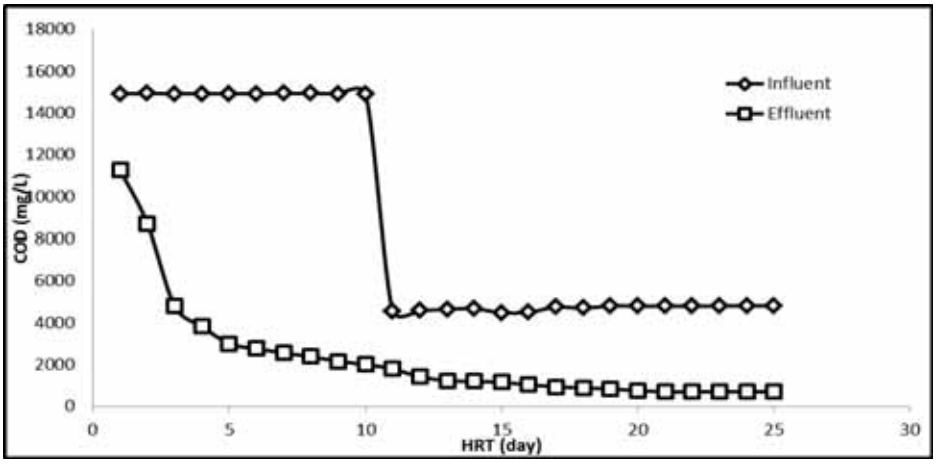

FIGURE 2
COD changes in the textile wastewater during the pilot start-up period

Since the stable conditions for the system start-up were not established, the second stage continued until the 18th day and textile wastewater was added to the low amount of sludge with the COD of 2000 mg/L which was left in the tank for returning liquid. The organic load during this period was 0.559-0.592 kg/m^3/day COD. In this stage, by adding the textile wastewater produced during the manufacture of colored products at the textile factory, a descending trend in COD was observed from the first day. The results of the experiments are presented in Table 2.

The final stage started with the organic load of 0.957 kg/m^3/day COD. In this stage, with HRT of 7 days, stabilization trend of COD values occurred immediately. COD value of the liquid returning to the tank was equal to 695 mg/L and the COD elimination percentage remained constant at 85.5%. Therefore, the process of biofilm growth on the porous lava rocks followed a constant trend and a biofilm with suitable thickness and sufficient number of microorganisms required for treatment was formed. At this time, the wastewater from the textile factory was added to the liquid tank to fill it, and the HRT and the capacity of the system for the treatment of the textile wastewater were studied.

As shown in Fig. 2, the best time duration, in terms of day and hour, for wastewater treatment at the textile factory was determined and the obtained results were compared with each other. First, HRT of 5-day was selected to be tested, and next, HRTs of 4-, 3-, 2-, and 1-day were tested. Since the pilot biological trickling filter had passed a 25-day start-up period for microorganisms to start their growth and the pilot had become stable, feeding carbon and nitrogen sources in the wastewater was started with the growth of microorganisms, which reduced COD and suspended solids in the wastewater.

TABLE 3
Characteristics of wastewater at different HRTs

Hydraulic Retention time (days)	Influent COD (mg/L)	Effluent COD (mg/L)	COD elimination efficiency (%)
5	2950	142	95
4	2965	110	96
3	2940	102	97
2	2945	98	97
1	2950	95	97

TABLE 4
Wastewater characteristics at different HRTs

Hydraulic Retention time (hours)	Influent COD (mg/L)	Effluent COD (mg/L)	COD elimination efficiency (%)
12	2960	95	97
8	2970	95	97
7	2975	96	97
6	2690	96	97
4	2955	120	96
2	2960	119	96

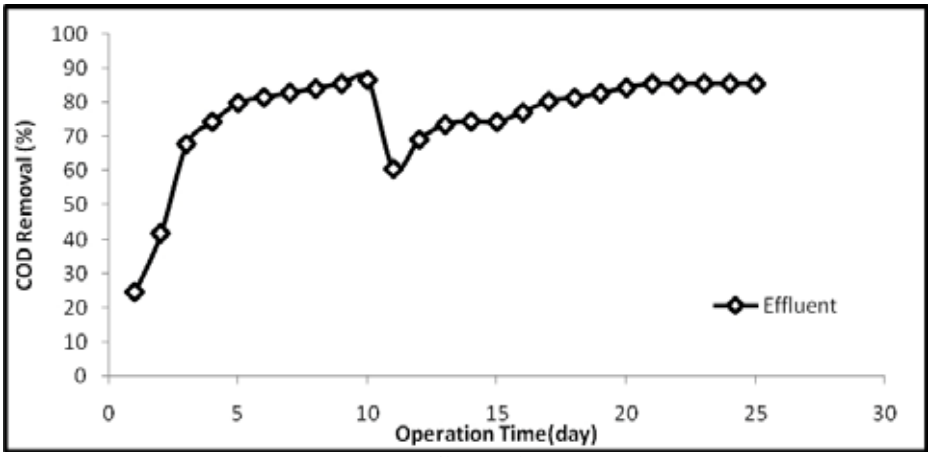

FIGURE 3
Changes in COD elimination efficiency during the start-up period

At HRT of 5-day, COD of textile wastewater declined from 2950 to 95 mg/L, which meant COD elimination of 97% from the textile wastewater. At this HRT, TSS of the wastewater decreased from 355 to 20 mg/L. When HRT reduced, the COD elimination percentage remained at 96% and it continued until HRT was lowered to 6 h. Table 3 shows the characteristics of the influent and effluent wastewater at various retention times. As can be seen, the efficiency of COD elimination remained over 96% even at retention time of 1 day. The temperatures and pH values at these retention times were 5 to 10 °C and 7 to 7.5, respectively. Changes of pH values in wastewater should always be studied to be able to take the necessary measures when dissolved oxygen deficiency and acidic wastewater are observed. In this study, pH value was kept within the neutral range and the DO under aerobic conditions was measured without using air pumps.

Considering the high efficiency of COD elimination at the given hydraulic retention times, it was decided to further reduce the HRT and study the obtained results. First, by lowering HRT to 12 h, COD elimination efficiency remained over 96% and continued to be at this level even when hydraulic retention time was decreased to 6 h. Next, HRT of 4-hour was tried, at which the efficiencies severely declined and the COD and total suspended solids in the effluent wastewater increased. Therefore, HRT of 4-hour (or shorter HRTs) was concluded to be economically undesirable for COD elimination. Table 4 shows a summary of wastewater characteristics at different HRTs.

Table 4 indicates that HRTs can be used for designing the biological trickling filters with natural stone media in order to achieve the best elimination parameters for the wastewater from Motahari textile factory. In this way, the economic costs which affect the selection of process types at wastewater treatment facilities can be lowered.

Since stabilization of parameters in the liquid leaving the column occurred during 5 days, the total period for the column start-up and reaching the stable conditions in the biological tricking filter was 25 days, and COD of the effluent liquid in the last day was 695 mg/L. Therefore, elimination efficiency of 85.5% and effluent liquid COD concentration of 695 mg/L indicated that the reactor is working well and it is ready for the treatment of dairy wastewater. Figure 3 shows the changes in COD elimination efficiency during the start-up period.

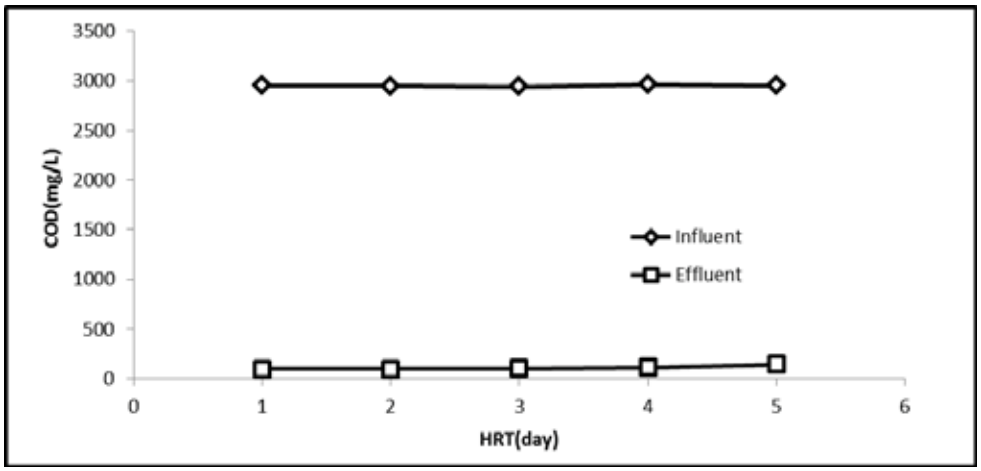

FIGURE 4
Effects of HRT reduction on wastewater COD

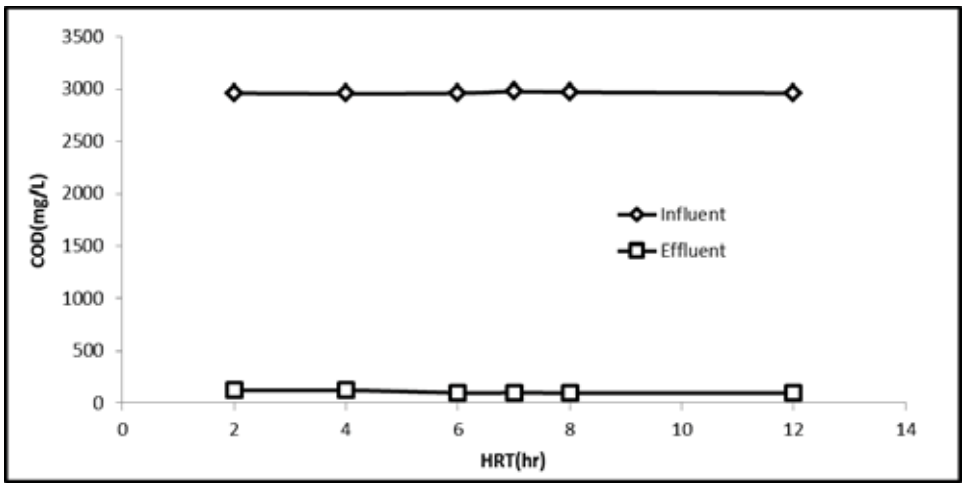

FIGURE 5
COD changes with reduction of HRT in hours

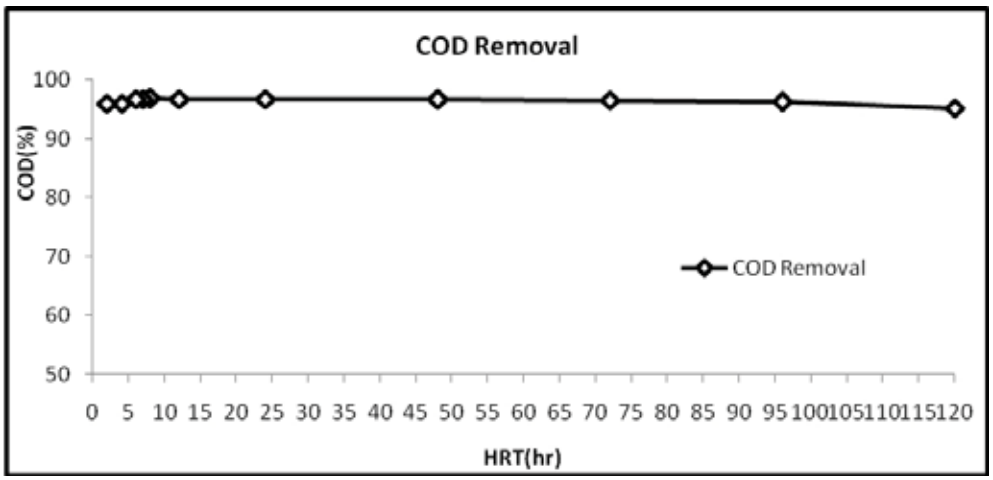

FIGURE 6
Changes in COD elimination efficiency at various HRTs

Figure 4 shows the effects of HRT changes on the influent and effluent COD concentrations. By maintaining the COD almost constant, the effluent COD increases slightly. As shown in Fig. 4, reduction of efficiency was negligible, and COD elimination remained over 96%. Therefore, it was possible to reduce HRT, because reduction of the retention time and increase of the wastewater flow rate entering the pilot column decreased the contact area between the liquid and the microorganisms formed on media, with the reduction of COD elimination percentage being negligible.

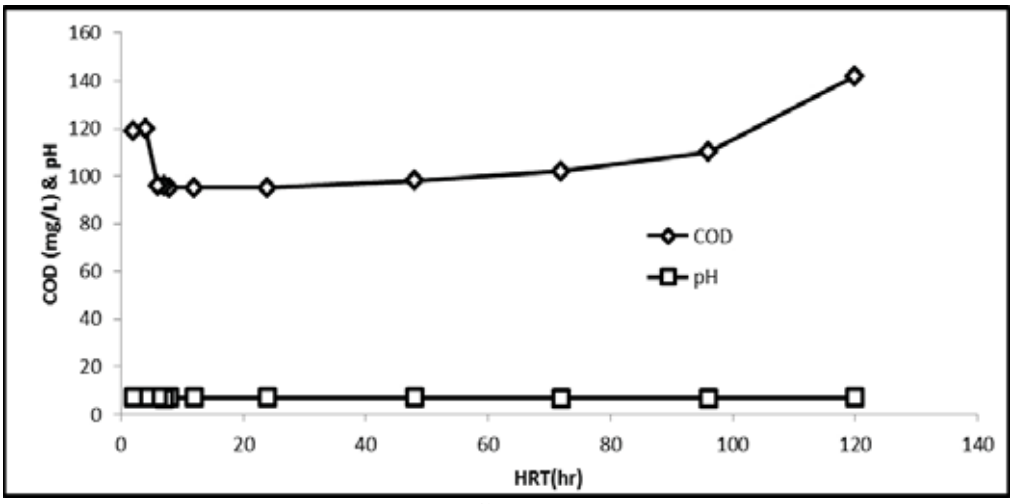

FIGURE 7
Changes in COD and pH values at various HRTs

Figure 5 shows the output COD changes with respect to HRT in hours. COD of the effluent wastewater slightly increased with the reduction of HRT. This increase was negligible because the efficiency of COD elimination remained over 96% at HRT of 6 h (Fig. 5). COD elimination of 96% at HRT of 6 h was considered suitable for designing the biological trickling filters because COD elimination efficiency would dramatically decrease at HRTs of less than 6 h.

In Fig. 6, COD values are plotted versus all of the studied HRTs. As shown in Fig. 6, COD elimination starts at HRT of 5 days and ends at HRT of 4 h. Even at HRT of 6 h, COD elimination efficiency remains over 96%. However, at HRT of less than 6 h, COD elimination efficiency in the wastewater from the textile factory declines considerably. Therefore, the optimal hydraulic retention time for eliminating COD from the textile wastewater is considered to be 6 h.

The tests were conducted at 5-10 °C, and the ambient cold weather was controlled to ensure that the biological trickling filter can reach a desirable efficiency in treating the textile wastewater at the given temperatures. It was therefore concluded that the obtained results could be applied in the cold regions of the country on actual scales.

The major problem associated with textile wastewater treatment is alkalinity or acidity of the wastewater, which, to some extent, disrupt the biological treatment system. Because of acidity or alkalinity of textile wastewater, a neutral pH must be achieved to create suitable conditions for biological growth on the media [14]. In the presented pilot, the type of media itself adjusted the pH, and pH-reducing effects of the products were neutralized accordingly. The pH changes were minor and did not adversely affect the wastewater treatment. According to Fig. 7, the pH always remained within the neutral range and this prevented the growth of harmful microorganisms such as Sphaerotilus [31]. Therefore, in the biological trickling filters particularly used for the treatment of industrial wastewater, maintaining the pH within the neutral range is important to achieve a suitable system performance [31]. In the tests conducted in this study, the effluent wastewater had a lower turbidity than the influent wastewater due to the decrease of suspended solids in the output wastewater. This led to the production of less sludge in the sedimentation pool after wastewater exit from the trickling filter. Because of the column height, the porosity of the media and the suitable growth of the microorganisms, a considerable reduction was observed in the amount of suspended particles, and the output liquid leaving the bottom of the pilot column was a wastewater with a very low turbidity. The remaining turbidity could be reduced further at the next stage in the sedimentation phase. In the common systems used for the treatment of textile wastewater, long aeration periods are required, but in this method, there was no need for sludge return (required in the active sludge method) because the media was fixed and the microorganisms could grow on it. Considering the results obtained in this study, the wastewater containing higher levels of organic matter was treated in a much shorter time. This can be very useful because of reducing electricity consumption and lowering the economic costs.

CONCLUSION

A pilot biological trickling filter was launched in three stages and reached a stable condition in 25 days. This study was conducted on a natural substrate consisting of volcanic rocks with an average diameter of 5 cm, porosity of 65% and specific surface area of 75 m^3/m^2. The pilot was used for the treatment of the textile wastewater from Motahhari textile factory in a cold weather (5-10 °C). Active

sludge and textile wastewater from the wastewater facilities of the textile factory were used for start-up of the column and treatment of the textile wastewater after taking three samples. In this study, the suitable HRT and pH were 6 h and 7 to 7.5, respectively. COD elimination efficiency of over 96% was achieved at HRT of 6 h. The sludge produced at the end of the wastewater treatment process and the volume of liquid entered the sedimentation pool declined considerably due to the reduction of suspended solids. The results showed that the wastewater containing high levels of organic matter could be treated in a short time in cold weather.

ACKNOWLEDGEMENTS

The authors wish to thank the authorities of Motahhari textile factory, Ghazvin, Iran, for their support during this study.

REFERENCES

[1] Mobarak-Qamsari, E., Kasra-Kermanshahi, R., Nosrati, M. and Amani, T. (2012) Enzymatic prehydrolysis of high fat content dairy wastewater as a pretreatment for anaerobic digestion. Int. J. Environ. Res. 6(2), 475-480.

[2] Nikolaeva, S., Sanchez, E. and Borja, R. (2013) Dairy wastewater treatment by anaerobic fixed bed reactors from laboratory to pilot scale plant: A case study in Costa Rica Operating at ambient temperature. Int. J. Environ. Res. 7(3), 759-766.

[3] Onodera, T., Sase, S., Choeisai, P., Yoochatchaval, W., Sumino, H., Yamaguchi, T., Ebie, Y., Xu, K., Tomioka, N., Mizuochi, M. and Syutsubo, K. (2012) Evaluation of process performance and sludge properties of an up flow staged sludge blanket (USSB) reactor for treatment of molasses wastewater. Int. J. Environ. Res. 6(4), 1015-1024.

[4] Pattananuwat, N., Aoki, M., Hatamoto, M., Nakamura, A., Yamazaki, S., Syutsubo, K., Araki, N., Takahashi, M., Harada, H. and Yamaguchi, T. (2013) Performance and microbial community analysis of a full scale hybrid anaerobic–aerobic membrane system for treating molasses based bioethanol wastewater. Int. J. Environ. Res. 7(4), 979-988.

[5] Senturk, E., Ynce, M. and Onkal Engin, G. (2013) Assesment of kinetic parameters for thermophilic anaerobic contact reactor treating food processing wastewater. Int. J. Environ. Res. 7(2), 293-302.

[6] Vazquez-Palma, D.E., Netzahuatl-Munoz, A.R., Pineda-Camacho, G. and Cristiani-Urbina, E. (2017) Biosorptive removal of nickel(II) ions from aqueous solutions by Hass Avocado (*Persea Americana* Mill. Var. Hass) shell as an effective and low-cost biosorbent. Fresen. Environ. Bull. 26, 3501-3513.

[7] Huang, C.F., Huang, A.C., Pai, T.Y., Ni, R.X., Chu, F.J., Wan, T.J. and Shi, D.H. (2017) Prediction and diagnosis of extraordinary situatiovs for wastewater treatment systems using neural network approach. Fresen. Environ. Bull. 26, 3293-3299.

[8] Chen, Y.H., Wang, Y.T., Dai, J.L. and Wang, R.Q. (2017) Prokaryotic community structure and composition in a full-scale wastewater treatment system for the high-efficiency biodegradation of polyvinyl alcohol. Fresen. Environ. Bull. 26, 1847-1857.

[9] Gholami-Borujeni, F., Mahvi, A.H. and Nejatzadeh-Barandoozi, F. (2013) Removal of heavy metal ions from aqueous solution by application of low cost materials. Fresen. Environ. Bull. 22, 655-658.

[10] Ozer, A., Turabik, M. and Akkaya, G. (2009) Biosorption of acid dyes by brown alga *Dictyota dichotoma*: equilibrium, kinetic and thermodynamic studies. Fresen. Environ. Bull. 18, 1798-1808.

[11] Akadar, A.B., Bourioug, M., Mohamed, N., Alaoui-Sosse, B. and Cavalli, E. (2014) Evaluation of effectiveness of domestic wastewater treatment by infiltration through sand and pozzolana in PVC columns. Int. J. Environ. Res. 8(3), 515-522.

[12] Akker, B.V., Holmes, M., Pearce, P., Cromar, N.J. and Fallowfield, H.J. (2011) Structure of nitrifying biofilms in a high-rate trickling filter designed for potable water pre-treatment. Water Res. 45(11), 3489-3498.

[13] Liu, C., Liu, J., Li, J., He, H., Peng, S., Li, C. and Chen, Y. (2013) Removal of H2S by co-immobilized bacteria and fungi biocatalysts in a biotrickling filter. Process Saf. Environ. Prot. 91(1–2), 145-152.

[14] Fortin, N.Y. and Deshusses, M.A. (1999) Treatment of methyl tert-butyl ether vapors in biotrickling filters. 1. Reactor startup, steady-state performance, and culture characteristics. Environ. Sci. Technol. 33(17), 2980-2986.

[15] Ottengraf, S.P. and Van Den Oever, A.H. (1983) Kinetics of organic compound removal from waste gases with a biological filter. Biotechnol. Bioeng. 25(12), 3089-3102.

[16] Chou, M.S. and Huang, Y.S. (1999) Treatment of ethylether in air stream by biotrickling filter packed with slags. J. Air Waste Manage. Assoc. ASCE. 49(5), 533- 543.

[17] Mehrdadi, N., Keshavarzi Shirazi, H., Azimi, A.A. and Mirmohammadi, M. (2010) Removal of Triethylamine vapor from waste gases by biotrickling filter. Iranian J. Environ. Health Sci. Eng. 7(4), 337-344.
[18] Almstrand, R., Lydmark, P., Sorensson, F. and Hermansson, M. (2011) Nitrification potential and population dynamics of nitrifying bacterial biofilms in response to controlled shifts of ammonium concentrations in wastewater trickling filters. Bioresour. Technol. 102(17), 7685-7691.
[19] Novotny, C., Svobodova, K., Benada, O., Kofronova, O., Heissenberger, A. and Fuchs, W. (2011) Potential of combined fungal and bacterial treatment for color removal in textile wastewater. Bioresour. Technol. 102(2), 879-888.
[20] Puhulwella, R.G., Beckers, L., Delvigne, F., Grigorescu, A., Thonart, P. and Hiligsmann, S. (2014) Mesophilic biohydrogen production by Clostridium butyricum CWBI1009 in trickling biofilter reactor. Int. J. Hydrogen Energy. 39(30), 16902-16913.
[21] Chen, R., Liao, Q., Tian, X., Wang, Y.Z., Zhu, X. and Miao, J.H. (2012) Characterization of the start-up behavior and steady-state performance of biotrickling filter removing low concentration toluene waste gas. Sci. China Technol. Sci. 55(6), 1701–1710.
[22] Dorado, A.D., Rodriguez, G., Ribera, G., Bonsfills, A., Gabriel, D., Lafuente, J. and Gamisans, X. (2009) Evaluation of mass transfer coefficients in biotrickling filters: experimental determination and comparison to correlations. Chem. Eng. Technol. 32(12), 1941-1950.
[23] Estrada, J.M., Lebrero, R., Quijano, G., Perez, R., Figueroa-Gonzalez, I.A., Garcia-Encina, P. and Munoz, R. (2014) Methane abatement in a gas-recycling biotrickling filter: Evaluating innovative operational strategies to overcome mass transfer limitations. Chem. Eng. J., 253, 385–393.
[24] Niu, H., Leung, D.Y.C., Wong, C., Zhang, T., Chan, M. and Leung, F.C.C. (2014) Nitric oxide removal by wastewater bacteria in a biotrickling filter. J. Environ. Sci. 26(3), 555–565.
[25] Philip, L. and A. Deshusses, M. (2008) The control of mercury vapor using biotrickling filters. Chemosphere. 70(3), 411–417.
[26] Zapotocky, L. and Svab, M. (2012) Removal of ammonia emissions from waste air in a biotrickling filter: pilot-scale demonstration in real conditions. Central Eur. J. Chem. 10(4), 1049-1058.
[27] Zhao, Q., Zhong, H., Wang, K., Wei, L., Liu, J. and Liu, Y. (2013) Removal and transformation of organic matters in domestic wastewater during lab-scale chemically enhanced primary treatment and a trickling filter treatment. J. Environ. Sci. 25(1), 59-68.
[28] Sarkar, B., Chakrabarti, P.P., Vijaykumar, A. and Kale, V. (2006) Wastewater treatment in dairy industries possibility of reuse. Desalination. 195(1–3), 141–152.
[29] Mirmohammadi, M., Bayat, R., Keshavarzi Shirazi, H. and Sotoudeheian, S. (2014) Effect of empty bed residence time on biotrickling filter performance: case study-triethylamine. Int. J. Environ. Sci. Technol. 11(1), 183–190.
[30] Eaton, A.D. and Franson, M.A.H. (2005) Standard Methods for the examination of water and wastewater. Prepared and published jointly by American public health association. American water works association. Water environment federation, 21st Ed, 1200pp.
[31] Kornaros, M. and Lyberatos, G. (2006) Biological treatment of wastewaters from a dye manufacturing company using a trickling filter. J. Hazard. Mater. 136(1), 95-102.

Received: **28.01.2017**
Accepted: **18.11.2017**

CORRESPONDING AUTHOR

Toktam Shahriari
Faculty of Environment,
University of Tehran,
Tehran – Iran

e-mail: Tshshahriari@ut.ac.ir

© by PSP Volume 27 – No. 2/2018 pages 787-792 Fresenius Environmental Bulletin

LIFE CYCLE ASSESSMENT OF DIRECT AND EXTRUSION SPINNING: A CASE STUDY

Sule Altun[1], Seval Kutlu Akal-Solmaz[2], Gokhan Ekrem Ustun[2,*], Ismail Kagnici[3]

[1]Bursa Technical University, Department of Fiber and Polymer Engineering, Osmangazi, Bursa, Turkey
[2]Uludag University, Department of Environmental Engineering, Faculty of Engineering, Gorukle, Bursa, Turkey
[3]Korteks Textile Industry and Trade Inc., Organized Industrial District Yellow St. No:3, 16159 Bursa, Turkey

ABSTRACT

This study assessed the status of direct and extrusion spinning in Bursa, Turkey. Sensitivity analysis of Life Cycle Assessment (LCA) methods and dominant processes were conducted to validate the results. The results of this study increase the life cycle inventory database for Poly(ethylene terephthalate) (PET) fibre production, provide basic and necessary information for evaluating environmental impacts of international chemical products, and facilitate the decision making of policymakers regarding the establishment, reconstruction, expansion, or technological transformation of industries. However, the combined assessment of economic, social and management factors warrants further research to provide a more systematic and sustainable assessment.

KEYWORDS:
Environmental impact, Life cycle assessment, PET fibre production, Spinning

INTRODUCTION

Humans have long been concerned with the environmental issues. Although there are some tangible signs of these efforts like eco-labels and eco-standards, climate change is still a big challenge for manufacturers, users and state economies. Thus, more strategic and systematic approaches must be developed and/or implemented to address this acute problem more effectively. LCA is one of the available techniques which can be used to contribute the solution of this issue.

LCA is a methodology to assess environmental impacts of products, services and works through their life cycle from extraction and production of raw materials, production, distribution, use (including reuse and maintenance) to recycling and final disposal [1-5]. LCA addresses to the direct and potential environmental impacts such as climate change, stratospheric ozone depletion, tropospheric ozone (smog) creation, eutrophication, acidification, toxicological stress on human health and ecosystems, resource depletion, water use, land use and the others, throughout a product's life cycle [6, 7]. All activities, or processes, in a product's life result in environmental impacts due to consumption of resources, emissions of substances into the natural environment, and other environmental exchanges [6]. In textiles, the production and use phases also have some environmental effects. High pesticide and water usage in cotton cultivation, high energy consumption in spinning, weaving, knitting and dyeing processes, high chemical content of textile wastewaters are well known problems. LCA has been implemented to textile processes and products for a long time [8-10] for various reasons; among others, to find "hot spots" [11] to compare products or processes, [9, 12, 13] to develop new products, [14] establishing eco-label criteria.

Poly(ethylene terephthalate) (PET) is a condensation polymer. In the polymerization stage, the pure reactants, terapthalic acid (TPA) and ethylene glycol (EG) are fed to form a paste. PET is used for different applications in the forms of films and fibers [15, 16]. When the polymer reaches the target intrinsic viscosity, the molten polymer may be pumped directly to a spinning unit to obtain drawn polyester yarns (continuous process) or to the spinnerets to have belts (discontinuous process). Then the belts are cooled, cut and dried. The obtained chips are conveyed to the extruders, and then the melted material is pumped to the spinning unit. The continuous process is more economic since drying/melting of granulates and mechanical complexity of process are eliminated. However, in terms of taking variations in demand, process flexibility and storage holding into account, discontinuous process is preferable [17].

Environmental impacts of textile fibers, including PET, were dealt with in some studies; recycled and original fibers, organic and conventional fibers were compared using LCA [18, 21]. However, studies investigating two main polyester fiber processes are yet to be carried out.

World fiber consumption reached 95.6 million tons in 2015, 55% of which were polyester fibres [22, 23]. Huge production volume of PET materials, non-renewability of them, high energy consumption used in manufacturing processes cause significant

contribution to the carbon footprint of textile industry.

In this study continuous and discontinuous PET fibre processes were analyzed using LCA method to disclose their environmental impacts.

MATERIALS AND METHODS

The present study was conducted according to ISO 14044 standard [7] which specifies requirements and provides guidelines for LCA. There are four phases in an LCA study:

a) The goal and scope definition phase,
b) The inventory analysis phase,
c) The impact assessment phase, and
d) The interpretation phase (ISO 14044 [7]).

The Goal and scope definition phase. The main goal of this study was to analyze the environmental profiles of the continuous and discontinuous PET fibre production processes.

Functional unit. According to ISO 14044, [24] functional unit is defined as quantified performance of a product system for use as a reference unit. The functional unit of this LCA was 1 ton partially oriented yarn (POY). One ton POY was produced both in discontinuous and continuous processes.

System boundary. The environmental impacts were assessed according to "gate-to-gate" model, including only the impacts resulting from the production of processes and not the use or disposal of the product. The simplified process flow diagrams are given in Figure 1. The excess ethylene glycol (EG) recycled and then reused in the polymerization stage. It was assumed that, EG was added only the beginning of the production process. EG recycling process was also included in the study.

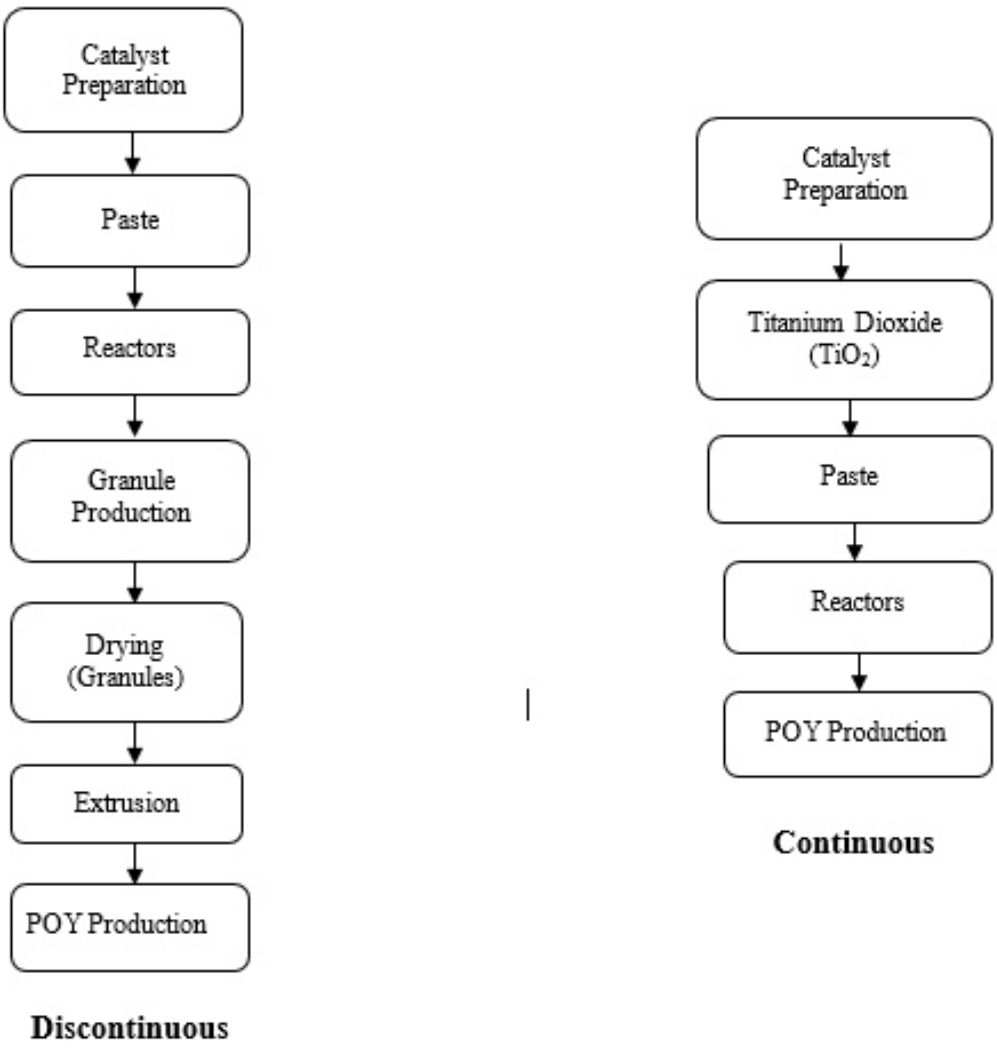

FIGURE 1
Discontinuous and continuous process flow diagrams

TABLE 1
Inputs and outputs of the systems

INPUT				
Catalyst Preparation	**Titanium Dioxide Suspension**	**Paste Preparation**	**Reactors**	**Granules**
Electricity	Electricity	Electricity	Paste	Demineralized water
Monoethylene glycol (MEG)	TiO_2	PTA	TiO_2 suspension	Electricity
Antimony (III) acetate	MEG	DEG	Electricity	Natural Gas
		Recycled (waste) MEG	Natural gas	Polymer
		Catalyst	Demineralized water	
			Recycled EG	
OUTPUT				
Filter	Waste Titan Out of Filter	Emissions	MEG	Polymer
Contaminated package (PP)	Big Bag (PP)	Big Bag (PP)	Wastewater	Wastewater
		Container(PE)	Steam	
			Oligomer	
			Polymer (waste)	
			Packaging wastes (PE, PP, cardboard, wood)	
			Recycled EG	

TABLE 2
Environmental profiles of discontinuous and continuous processes

Impact categories	Units	Discontinuous	Continuous
Acidification (A)	kg SO_2 eq	10.2	9.7
Eutrophication (E)	kg PO_4 eq	38	37
Global warming (GWP)	kg CO_2 eq	3018	2334
Human toxicity (HT)	kg 1.4-DB eq	3579	3507
Fresh water aquatic ecotox. (FE)	kg 1.4-DB eq	89	85
Marine aquatic ecotoxicity (ME)	kg 1.4-DB eq	280101	248726
Terrestrial ecotoxicity (TE)	kg 1.4-DB eq	6.6	6.5
Photochemical oxidation (POF)	kg C_2H_4 eq	0.48	0.43

The inventory analysis phase. All data were collected through active surveillance within the business processes. The company got all of its electricity from a natural gas power plant. The analysis involves catalyst preparation, TiO_2 preparation, paste, polymerization, granules production, drying (granules), extrusion and POY production steps for discontinues and continuous processes. Inputs and outputs of the systems are summarized in Table 1.

Impact assessment phase. Only the classification and characterization stages amongst the steps defined by the impact assessment phase in the LCA method were considered [24]. A retrospective LCA for PET yarn production was carried out according to the CML 2 baseline 2000 V2.05 method. This method results in the definition of an environmental profile for the assessed product/process/service by quantifying the environmental impact on different categories. The impact categories analyzed in this study are: abiotic resources depletion (AD), global warming (GW), ozone layer depletion (OLD), photochemical oxidants formation (POF), acidification (A) and eutrophication (E). In addition, toxicological impact categories (human toxicity (HT), fresh water aquatic ecotoxicity (FE), marine aquatic ecotoxicity (ME) and terrestrial ecotoxicity (TE)) were also analyzed. The LCA software SimaPro 7.3.3 was used to perform the impact assessment stage.

RESULTS AND DISCUSSION

The result of the comparison of discontinuous and continuous processes is given in Table 2.

Relative contributions for per subsystem to each impact category in discontinuous and continuous processes are shown respectively in Figures 2 and 3.

AD is one of the impact categories in LCA which is advised to be taken into account [25] as it considers the depletion of natural resources (including energy resources) such as minerals or fossil fuels, among others. According to the results, which are shown in Table 1, drying of granules, extrusion and reactors have a contribution over 75 %. In discontinuous process the drying stage and in continuous process the polymerization stages have the significant contributions (Figures 2 and 3).

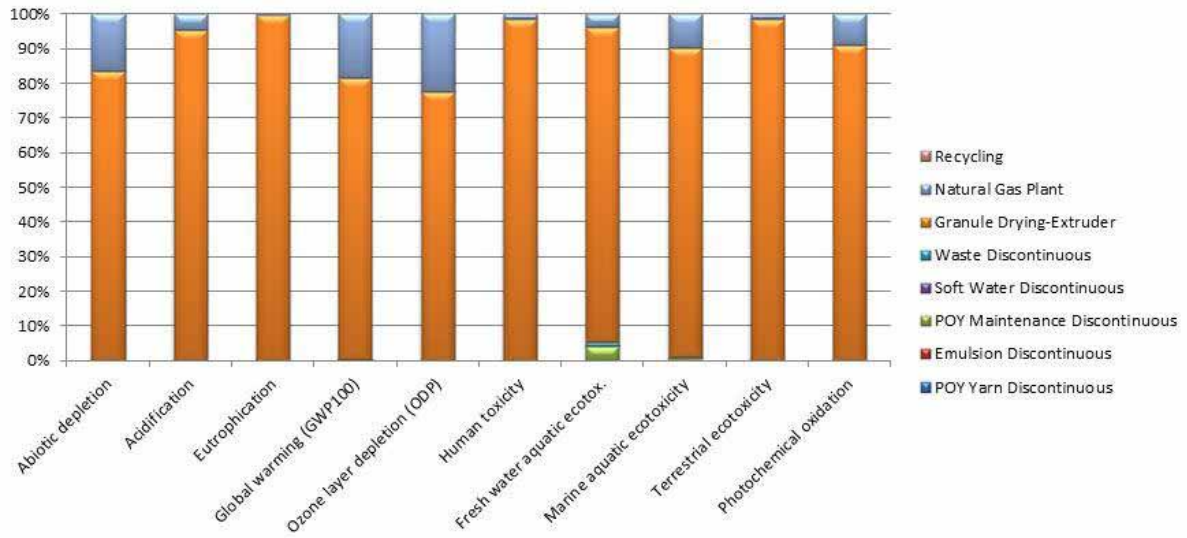

FIGURE 2
Relative contributions per subsystems (in %) to each impact category (Discontinuous)

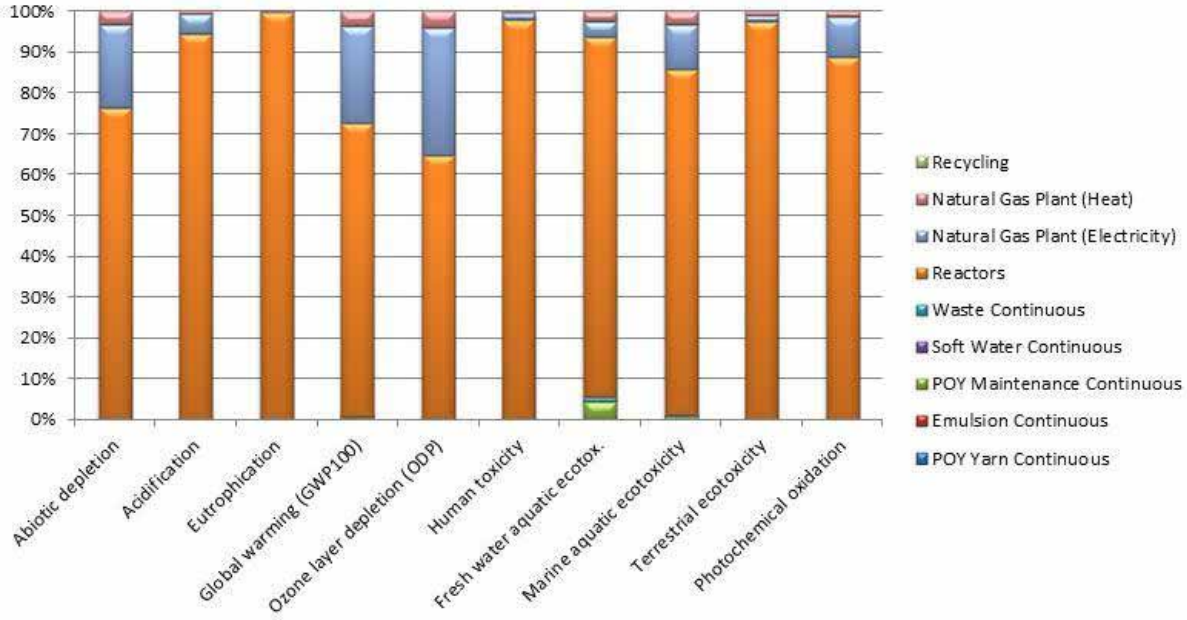

FIGURE 3
Relative contributions per subsystems (in %) to each impact category (Continuous)

In the context of GWP, is important to note that only the CO_2 originated during non-renewable fuel combustion was considered because the CO_2 released from renewable sources is assumed to be balanced with CO_2 absorption in the photosynthesis stage [2]. The results indicated a release of 3 and 2.3 tons of equivalent CO_2 per ton of discontinuous and continuous PET polymer production respectively. It is clear that chips drying and extrusion stages are the major contributors of CO_2 emissions because of high natural gas based energy consumption. In the continuous process, the main CO_2 emission comes from polymerization stage (75 %) because of huge energy consumption.

Eutrophication (E) is generally associated with the environmental impacts of excessively high levels of nutrients that lead to shifts in species composition and increased biological productivity, for example for algal blooms [26]. Actual eutrophication varies greatly geographically, but to simplify the model the geographical variation has been disregarded which means the potential reflect maximum eutrophying effect of a substance, simulating that all airborne nutrients end up in aquatic systems. In the present study, the eutrophication potential of two processes is almost equal. The process is differentiated after the polymerization process; same chemicals are used in the processes and the wastewaters contain almost same chemicals.

Fresh water aquatic ecotoxicity, marine aquatic ecotoxicity and terrestrial ecotoxicity are all expressed in kg 1.4-DB eq, marine aquatic ecotoxicity in discontinuous process is higher than the continuous process. Electricity production was the main contributor to the marine aquatic ecotoxicity. Production of one kg POY in discontinuous process consumed 2.8 kwh electricity, whereas, production of 1 kg POY in continuous process consumed only1.28 kwh of electricity.

In this study cumulative energy demand (CED) of polymer production was 47.9 MJ. CED reduced, for both process, almost 49% because of EG recycling.

CONCLUSIONS

This LCA study was carried out compare the most significant environmental impacts of the continuous and discontinues PET fibre production processes. It was proved here that consumption of enormous electrical energy and chemical substances during polymerization and melting stages of PET fibre production were the main reasons of significant environmental impacts. The potential environmental impacts of continuous process were lower than that of discontinuous process especially in AD, GWP and ME categories. The high electricity consumption of discontinuous process was the main source of potential for environmental impacts. This subsystem is an important contributor of air emissions as well as fossil fuels consumption.

ACKNOWLEDGEMENTS

This study was supported by the Korteks Textile Industry and Trade Inc.

REFERENCES

[1] Madival, S., Auras, R., Singh, S.P. and Narayan, R. (2009) Assessment of the environmental profile of PLA, PET and PS clamshell containers using LCA methodology. J. Cleaner Prod. 17, 1183-1194.

[2] Garcia, S.G., Moreira, M.T., Artal, G., Maldonado, L. and Feijoo, G. (2010) Environmental impact assessment of non-wood based pulp production by soda- anthraquinone pulping process. J. Cleaner Prod. 18, 137-145.

[3] Gironi, D. and Piemonte, V. (2011) Life cycle assessment of polylactic acid and polyethylene terephthalate bottles for drinking water. Environ Prog. and Sustain. Energy. 30(3), 459-468.

[4] Hong, J., Chen, W., Wang, Y., Changqing, X., Xu, X. (2014) Life cycle assessment of caustic soda production: a case study in China. J. Cleaner Prod. 66, 113-120.

[5] Saer, A., Lansing, S., Davitt, N.H. and Graves, R.E. (2013) Life cycle assessment of a food waste composting system: environmental impact hotspots. J. Cleaner Prod. 52, 234-244.

[6] Rebitzer, G., Ekvall, T. and Frischknechtc, R. (2004) Life cycle assessment Part 1: Framework, goal and scope definition, inventory analysis, and applications. Environ Int. 30, 701-720.

[7] ISO 14044 (2006) International Organization for Standardization, Environmental Management, Life cycle Assessment-Requirements and Guidelines, first ed. On line at: http://www.iso.org/iso/home.htm. ISO 14044.

[8] Dahllöf, L. (2003) Life Cycle Assessment (LCA) applied in the textile sector: the usefulness, limitations and methodological problems-a literature review. ESA-Report 2003:9, ISSN: 1404-8167, Revised Nov. 10th 2004.

[9] Laursen, S.E., Hansen, J., Knudsen, H.H., Wenzel, H., Larsen, H.F. and Kristensen, F.M. (2007) EDIPTEX-Environmental assessment of textiles. Working Report No. 24. The Danish Environmental Protection Agency.

[10] Nieminen, E., Linke, M., Tobler, M. and Beke, B.V. (2007) EU COST Action 628: Life cycle assessment (LCA) of textile products, eco-efficiency and definition of best available technology (BAT) of textile processing. J. Cleaner Prod. 15, 1259-1270.

[11] Barber, A. and Pellow, G. (2006) Life cycle assessment New Zealand Merino Industry Merino wool total energy use and carbondioxide emissions. The AgriBusiness Group, Pukekohe, Auckland.

[12] Kalliala, E.M. and Nousiainen, P. (1999) Life cycle assessment envıronmental profile of cotton and polyester-cotton fabrics. AUTEX Res J. 1(1), 8-20.

[13] Woolridge, A.C., Ward, G.D., Phillips, P.S., Collins, M. and Gandy, S. (2006) Life cycle assessment for reuse/recycling of donated waste textiles compared to use of virgin material: an UK energy saving perspective. Resour Conserv Recy. 46, 94-103.

[14] Intini, F. and Kühtz, S. (2011) Recycling in buildings: an LCA case study of a thermal insulation panel made of polyester fiber, recycled from post-consumer PET bottles. Int. J. Life. Cycle. Ass. 16(4), 306-315.

[15] Ward, I.M. and Hadley, D.W. (1995) An introduction to the mechanical properties of solid polymers. Chichester, England: John Wiley and Sons.

[16] Rudolf, A., Gersak, J. and Smole, M.S. (2011) The effect of heat treatment conditions using the drawing process on the properties of PET filament sewing thread. Textile Res J. 82(2), 161-171.
[17] Bauer, K.H. (1993) Manufacturing Yarn and Fibre. In: Brunnschweiler, D., Hearle, J. (eds.) Polyester 50 Years of Achievement. Textile Institute, Manchester, UK. ISBN:978-1870812498, 64.
[18] Cherrett, N., Barrett, J., Clemett, A., Chadwick, M. and Chadwick, M.J. (2005) Ecological Footprint and Water Analysis of Cotton, Hemp and Polyester, Bio Regional Development Group and WWF Cymru, SEI.
[19] Shen, L., Worrell, E., Patel, M.K. (2010) Open-loop recycling: A LCA case study of PET bottle-to-fibre recycling. Conserv Recy. 55(1), 34-52.
[20] Tabone, M.O., Cregg, J.J. and Beckman, E.J. (2010) Sustainability metrics: life cycle assessment and Green design in polymers. Environ Sci Technol. 44, 8264-8269.
[21] Muthu, S.S., Li, Y., Hu, J.Y. and Ze, L. (2012) Carbon footprint reduction in the textile process chain: Recycling of textile materials. Fibers and Polymers. 13(8), 1065-1070.
[22] http://www.lenzing.com/en/investors/equity-story/global-fiber-market.html, access date 21.11.2016
[23] http://textileexchange.org/wp-content/uploads/2016/07/2016-TE-Preferred-Fiber-and-Materials-Market-Report.pdf, access date 21.11.2016
[24] ISO 14040 (1997) International Organization for Standardization, Environmental Management, Life cycle Assessment- Principles and Framework, Geneva, Switzerland.
[25] Guinée, J.B., Gorrée, M., Heijungs, R., Huppes, G., Kleijn, R., Koning, A., Oers, L. Van, L., Wegener Sleeswijk, A., Suh, S., Udo de Haes, H.A., Bruijn, H., Duin, R. and Huijbregts, M.A.J. (2002) Handbook on life cycle assessment: operational guide to the ISO standards. Kluwer Academic Publisher, Dordrecht.
[26] Baumann, H. and Tillman, A.M. (2004) The hitch hikers guide to LCA - An orientation in life cycle assessment methodology and application. Student literature. ISBN 91-44-02364-2, Lund, Sweden.

Received: **06.02.2017**
Accepted: **17.11.2017**

CORRESPONDING AUTHOR

Gokhan Ekrem Ustun
Uludag University,
Department of Environmental Engineering,
Faculty of Engineering,
Gorukle, Bursa – Turkey

e-mail: gokhaneu@uludag.edu.tr

© by PSP Volume 27 – No. 2/2018 pages 793-798 Fresenius Environmental Bulletin

A PRELIMINARY STUDY ON RADIOACTIVITY CONCENTRATIONS AND DOSE ASSESSMENT OF SOME ANTICARCINOGENIC MEDICINAL PLANTS USED IN TURKEY

Cumhur Canbazoglu[1,*], Suna Ilter[1], Sultan Sahin-Bal[2], Sule Karatepe[2], Mahmut Dogru[2]

[1]Department of Physics, Faculty of Arts and Sciences, Kilis 7 Aralik University, 79000 Kilis, Turkey
[2]Department of Physics, Faculty of Arts and Sciences, Bitlis Eren University, Bitlis, Turkey

ABSTRACT

The medicinal plants have been traditionally used to treat illnesses for many years all over the world. Determining radioactivity levels in the medicinal plants is of great importance for the protection of human health. However, there are limited number of research related to radioactivity levels of medicinal plants in Turkey. The aim of this study is to determine the radioactivity levels in some anticarcinogenic medicinal plants that are often used to treat illnesses in Turkey. The analysis of ^{226}Ra, ^{232}Th, ^{40}K and ^{137}Cs activity concentration of medicinal plants was performed using a high resolution gamma-ray spectrometer with HpGe detector. The average activity concentrations for the medicinal plants were calculated as 10.87 ± 1.61, 18.02 ± 2.06, 1025.75 ± 15.53 and 1.14 ± 0.36 Bq kg^{-1} for ^{226}Ra, ^{232}Th, ^{40}K and ^{137}Cs, respectively. Total committed effective dose value due to ingestion was determined as 55.04 µSv y^{-1} for these medicinal plants and has no risk to public health.

KEYWORDS:
Medicinal plants, Gamma spectrometry, Radiation dose, Natural and Artificial Radioactivity

INTRODUCTION

Human beings are continuously exposed to ionizing radiation arising from terrestrial radionuclides (^{238}U series, ^{232}Th series and ^{40}K) and cosmic rays. The radiation dose taken both internally and externally from these natural radiation sources is approximately 2.4 mSv. Internal exposure due to ingestion and inhalation arise from terrestrial radionuclides in the environment. These radionuclides are accumulated in various organs in time and create a dose effect. Besides, fission products spread to the environment due to nuclear activities also create a dose effect on people. The most important fission product is ^{137}Cs because it is rapidly transferred to the foodstuffs and has long term effects [1]. Ingestion exposure occurs when radionuclides in the environment enter food chains. The primary recipients of radioactive contamination to the food chain are plants. The plants might be subjected to direct and indirect contamination. Direct contamination is deposition of the radionuclide in the atmosphere on above-ground part of the plants. Indirect contamination is sorption of radionuclides from the soil by the root system of plants, as well. Consequently, the radionuclides accumulated in the plants transfer to human through the food chain. Hence, the radiation dose due to the ingestion depends on consumption amount and radionuclide concentration of the foodstuffs [1].

The medicinal plants have been used for treatment of diseases all over the world for centuries. They are widely used in the kitchens for adding taste to the meals, as well. The medicinal plants naturally grow in the nature and a great majority of them are not cultivated. Some medicinal plants that have anticarcinogenic activity heal diseases without toxic effect. Along with that, anticarcinogenic medicinal plants have also immunomodulatory effects. Therefore, anticarcinogenic medicinal plants are consumed by taking these effects into consideration [2, 3]. In addition, there are limited number of studies in the literature considering determination of the natural and artificial radionuclides in medicinal plants. Beside that, the advantage of medicinal plants for the treatment of various illnesses contributes to the importance of such studies [4-10].

In this study, we report the determination of ^{226}Ra, ^{232}Th, ^{40}K and ^{137}Cs radionuclide concentrations in some medicinal plants for the treatment of various illnesses in Turkey. The radiation dose exposed through ingestion was calculated. The significance of the study is that it is the first study related to determine the radioactivity levels in some anticarcinogenic medicinal plants in Turkey and will provide data for future studies. Also the data obtained from this study may make contribution to determination of contamination level in case of any nuclear accident or nuclear fallout like Chernobyl.

TABLE 1
Scientific name of selected medicinal plants and their common use in treatment of illnesses.

Medicinal plant	Scientific name	Supplied From	Common use	Part used
Sage	*Salvia officinalis*	Hatay*	N, Res, D	Leaves, flowers
Anise	*Pimpinella anisum*	Denizli*	D, Res	Fruits
Rosemary	*Rosmarinus officinalis*	Mersin*, Gaziantep*	D, U	Leaves, flowers
Yarrow	*Achillea millefolium*	Malatya*, Hatay*, Mersin*	D, U	Leaves, flowers
Black seed	*Nigella sativa*	Syria, India	D, U	Seeds
Laurel leaf	*Laurus nobilis*	Hatay*	D, Res	Leaves, Fruits
Echinacea	*Echinacea species*	Mersin*	Res, U	Flowers
Black pepper	*Piper nigrum*	Vietnam	D	Fruits
Cumin	*Cuminum cyminum*	Konya*	D, U, Res	Fruits
Coriander	*Coriandrum sativum*	Denizli*, Syria	D, U, N	Fruits
Licorice root	*Glycyrrhiza glabra*	Syria, Hatay*, Harran*, Maraş*, Adıyaman*	Res, U	Roots
Mint	*Mentha spicata*	Nizip*	N, D	Leaves
Chili pepper	*Capsicum species*	Maraş*, Islahiye*	D, U	Fruits
Basil	*Ocimum basilicum*	Elbistan*, Siirt*	N, U, D	Leaves
Fennel	*Foeniculum vulgare*	Denizli*	D	Fruits
Garlic	*Allium sativa*	Germany, Holland, Maraş*	U, D	Corm
Sumac	*Rhus coriaria*	Kilis*, Mardin*, Midyat*, Nizip*	D	Fruits
Sesame	*Sesamum indicum*	Throughout Turkey, India	D	Seeds
Ginger	*Zingiber officinale*	Brazil, India	N, D	Roots

*: supplied from Turkey
D digestive system, *Res* respiratory system, *U* urinary system, *N* nervous system

MATERIALS AND METHODS

Sample selection and preparation. Selected anticarcinogenic medicinal plants are used as traditional medicine in the Anatolian culture. Details of medicinal plants and common use in the treatment of digestive, respiratory, urinary and nervous system illnesses are given in Table 1. Nineteen medicinal plant samples were purchased from herbalist markets in Kilis (Turkey) province as ready to be consumed and their scientific names were identified. Activity measurements of medicinal plant samples were carried out in Bitlis Eren University Nuclear Physics Research Laboratory. The samples were dried at 80 ^{0}C in oven for dehumidification. Then they were put into 1 liter marinelli beakers and then weighed. Prepared samples were hermetically sealed to prevent escape of the radon gas. The sealed samples were stored for 1 month to attain radioactive equilibrium between ^{226}Ra and its short-lived decay products before radioactivity measurement procedure.

Gamma Spectrometric Measurements. The radiation levels of the medicinal plant samples were analyzed by a high resolution gamma-ray spectrometer at nuclear physics laboratory in Bitlis Eren University. The gamma spectrometry system consisted of a coaxial p-type HPGe detector (ORTEC GMX50P4-83-A) having 51% relative efficiency and a multi-channel analyzer. The HPGe detector's energy resolution is 2.1 keV at 1332 keV. To reduce environmental gamma background radiation, the detector was shielded by a cylindrical lead shield. Efficiency calibration of the system was made by using RGU-1, RGTh-1 and RGK-1 reference materials. The gamma ray spectrum was analyzed by using ORTEC MAESTRO 32 software program. The medicinal plant samples were placed on top of the detector and counted for 86000 s. Background measurements were taken under the same conditions. The radionuclide activities of each sample were determined using the total net counts under the corresponding peaks in the energy spectrum. The gamma ray energies of the 609.3 keV from ^{214}Bi were used to determine the activity of ^{226}Ra. The gamma ray energies of the 911.2 keV from ^{228}Ac were used to determine the activity of ^{232}Th. ^{40}K and ^{137}Cs activity concentrations were measured directly from the 1460.8 keV and 661.7 keV photopeak energies, respectively.

Radioactivity and Dose Calculations. The activity concentration in medicinal plant samples was calculated using Eq. (1)

$$A\ (Bq\ kg^{-1}) = \frac{C}{M_s \varepsilon P_\gamma} \quad (1)$$

where A is the mean activity concentration of radionuclide, C is the net count rate of radionuclide (counts s^{-1}), M_s is the mass of the sample (kg), ε is the efficiency of the detector at the energy of the measured gamma-ray and P_γ is the absolute transition probability of gamma decay [6, 11-13].

The internal dose due to ingestion is calculated with the following equation (Equation 2) and depends on radionuclide concentration in the foodstuffs and consumption rate [1, 14, 15].

$$H_{T,r} = \sum(U^i\ C_r^i\ )\ g_{T,r} \quad (2)$$

where i symbolizes foodstuff group, U^i and C_r^i are annual consumption rate (kg) and activity concentration of radionuclide (Bq kg^{-1}), respectively, and $g_{T,r}$ is dose conversion coefficient for r radionuclide (Sv Bq^{-1}). For adult members of the community, dose conversion coefficients for ^{226}Ra, ^{232}Th, ^{40}K and

^{137}Cs radionuclide are 4.5 x 10^{-8}, 2.3 x 10^{-7}, 6.2 x 10^{-9} and 1.3 x 10^{-8} Sv Bq^{-1}, respectively [14, 16, 17].

RESULTS AND DISCUSSION

In this study, natural (^{226}Ra, ^{232}Th and ^{40}K) and artificial (^{137}Cs) radionuclide concentrations of some anticarcinogenic medicinal plants were determined. The internal radiation dose occurring through consumption of these plants was calculated. The radioactivity concentrations of nineteen medicinal plant samples were measured using high resolution gamma spectrometer with HpGe detector.

^{226}Ra, ^{232}Th, ^{40}K and ^{137}Cs activity concentrations of nineteen medicinal plant samples purchased from herbalist markets in Kilis province are given in Table 2. ^{226}Ra activity concentrations ranged from 1.78 ± 0.29 to 33.46 ± 5.2 Bq kg^{-1} and average activity value was 10.87 ± 1.61 Bq kg^{-1}. The highest activity concentration of ^{226}Ra was measured for *Sage* whilst *Nigella sativa* medicinal plant had the lowest activity concentration. ^{232}Th concentrations of medicinal plants varied from 1.46 ± 0.34 to 65.25 ± 5.2 Bq kg^{-1} with an average value of 18.02 ± 2.06 Bq kg^{-1}. The lowest and highest activity concentration for ^{232}Th were measured in *Chili pepper* and *Sage* medicinal plants, respectively. The activity concentrations for ^{40}K ranged from 312.55 ± 4.38 to 2211.80 ± 28.50 Bq kg^{-1} with an average value of 1025.75 ± 15.53 Bq kg^{-1}. The highest and lowest activity of ^{40}K were found in *Basil* and *Sesame*, respectively. ^{137}Cs activity of medicinal plant samples varied from 0.27 ± 0.15 to 6.30 ± 0.74 Bq kg^{-1} and average value was 1.14 ± 0.36 Bq kg^{-1}. The highest activity for ^{137}Cs was measured in *Basil* while the lowest activity was measured in *Anise*. ^{137}Cs activity concentrations of ten medicinal plant samples were below detection limit. The mean value of minimum detectable activity (MDA) calculated for ^{137}Cs was estimated to be 0.05 Bq.

TABLE 2
^{226}Ra, ^{232}Th, ^{40}K and ^{137}Cs activity concentrations of medicinal plant samples.

Medicinal plant	Scientific name	Activity concentrations of medicinal plants (Bq kg^{-1})			
		^{226}Ra	^{232}Th	^{40}K	^{137}Cs
Sage	*Salvia officinalis*	33.46 ± 5.2	65.25 ± 5.2	1300.95 ± 41.01	0.8731 ± 0.5
Anise	*Pimpinella anisum*	2.49 ± 0.43	6.53 ± 0.58	1035.07 ± 6.68	0.27 ± 0.15
Rosemary	*Rosmarinus officinalis*	11.67 ± 1.53	29.31 ± 2.57	941.49 ± 13.02	0.63 ± 0.27
Yarrow	*Achillea millefolium*	8.32 ± 1.26	27.51 ± 3.13	1049.31 ± 21.73	BDL
Black seed	*Nigella sativa*	1.78 ± 0.29	5.13 ± 0.43	456.10 ± 4.33	BDL
Laurel leaf	*Laurus nobilis*	30.53 ± 3.60	60.28 ± 4.22	669.31 ± 31.05	BDL
Echinacea	*Echinacea species*	9.82 ± 1.49	10.77 ± 1.21	1218.69 ± 16.90	0.99 ± 0.60
Black pepper	*Piper nigrum*	10.42 ± 0.62	7.56 ± 0.53	846.80 ± 6.36	0.27 ± 0.21
Cumin	*Nigella sativa um cyminum*	2.83 ± 0.62	4.17 ± 0.51	1072.24 ± 7.08	BDL
Coriander	*Coriandrum sativum*	5.22 ± 0.98	13.68 ± 1.34	1078.03 ± 10.17	BDL
Licorice root	*Glycyrrhiza glabra*	20.28 ± 2.30	25.69 ± 2.26	470.01 ± 17.64	BDL
Mint	*Mentha spicata*	12.86 ± 1.49	8.68 ± 0.97	1227.56 ± 14.39	BDL
Chili pepper	*Capsicum species*	3.42 ± 0.45	1.46 ± 0.34	2042.78 ± 9.90	0.33 ± 0.27
Basil	*Ocimum basilicum*	18.24 ± 3.06	36.38 ± 3.39	2211.80 ± 28.50	6.30 ± 0.74
Fennel	*Foeniculum vulgare*	4.32 ± 0.77	7.49 ± 0.65	1231.01 ± 8.82	0.33 ± 0.26
Garlic	*Allium sativa*	13.99 ± 4.53	15.76 ± 9.95	1002.53 ± 39.80	BDL
Sumac	*Rhus coriaria*	7.16 ± 0.82	9.18 ± 0.95	465.16 ± 6.73	0.27±0.25
Sesame	*Sesamum indicum*	4.99 ± 0.53	4.29 ± 0.48	312.55 ± 4.38	BDL
Ginger	*Zingiber officinale*	4.65 ± 0.59	3.29 ± 0.40	857.81 ± 6.60	BDL
Average		10.87 ± 1.61	18.02 ± 2.06	1025.75 ± 15.53	1.14 ± 0.36

BDL below detection limit

TABLE 3
Dose coefficients and calculated effective dose values for ^{226}Ra, ^{232}Th, ^{40}K and ^{137}Cs.

Radioisotopes	Activity intake (Bq)	Effective dose coefficient (μSv Bq^{-1})	Committed effective dose (μSv y^{-1})	
			Range	Average
^{226}Ra	54.35	0.045	0.40 ± 0.07 – 7.53 ± 1.17	2.45 ± 0.36
^{232}Th	90.1	0.23	1.68 ± 0.39 – 75.04 ± 5.98	20.72 ± 2.37
^{40}K	5128.75	6.2 x 10^{-3}	9.69 ± 0.14 – 68.57 ± 0.88	31.80 ± 0.48
^{137}Cs	5.7	1.3 x 10^{-2}	0.02 ± 0.01 – 0.41 ± 0.05	0.07 ± 0.02

TABLE 4
Comparison of ^{226}Ra, ^{232}Th, ^{40}K and ^{137}Cs activity concentrations in the medicinal plants and committed effective dose values with the values reported for some countries.

Country	Activity Concentration (Bq kg^{-1})							Committed Effective Dose (μSv y^{-1})		Ref.
	^{226}Ra		^{232}Th		^{40}K		^{137}Cs			
	Range	Mean	Range	Mean	Range	Mean	Range	Range	Mean	
Italy[a]	<0.3-16.6	---	---	---	66-3582	---	<0.3-10.7	---	---	[4]
Nigeria[a]	10.8-42.5	25	27.8-41	35.1	75-324	172	---	4.3-6.9	5.4	[18]
Ghana[a]	20.4-46.9	31.8	42-70.6	56.2	566-1093	840	---	26-42	35	[19]
Serbia[a]	0.6-8.2	---	1.7-15.1	---	126-1244	---	0.3-8.8	1-10.6	---	[20]
Turkey[a]	BDL-15.1	5.9	1.6-3.5	2.8	50-1312	500	<BDL	0.3-9	4.5	[21]
Turkey[b]	1.8-33.5	10.9	1.5-65.3	18	313-2212	1026	BDL-6.3	11.8-151.6	55	This work

a: medicinal plants, b: anticarcinogenic medicinal plants

Effective dose values due to ingestion of ^{226}Ra, ^{232}Th, ^{40}K and ^{137}Cs through the medicinal plants were estimated. Committed effective dose values were obtained by multiplying consumption rate, effective dose coefficient and average activity concentration for each radionuclide. Annual foodstuff consumption (dairy products, meat products, cereal products, vegetables, fruit and fish products) has been accepted as 500 kg worldwide by UNSCEAR [1]. We have not found any significant data in the literature concerning the consumption amounts of medicinal plants in Turkey. Therefore consumption amount of medicinal plants in Turkey was taken as 1% of the world average and dose estimations were calculated regarding this consideration. Calculated dose estimations for the medicinal plants are presented in Table 3. The average committed effective dose values were calculated as 2.45 ± 0.36, 20.72 ± 2.37, 31.80 ± 0.48 and 0.07 ± 0.02 μSv y^{-1} for ^{226}Ra, ^{232}Th, ^{40}K and ^{137}Cs, respectively. Two main contributions to effective dose values were originated from ^{40}K and ^{232}Th radioisotopes, respectively. Effective dose values for ^{226}Ra, ^{232}Th, ^{40}K and ^{137}Cs in the medicinal plants varied from 0.40 ± 0.07 to 7.53 ± 1.17, 1.68 ± 0.39 to 75.04 ± 5.98, 9.69 ± 0.14 to 68.57 ± 0.88 and 0.02 ± 0.01 to 0.41 ± 0.05 μSv y^{-1}, respectively. Total committed effective dose was calculated as 55.04 μSv in a year. This value is lower than 300 μSv that is accepted as world average of annually committed effective dose value in the UNSCEAR report and has no risk to public health [1].

Radioactivity concentrations and committed effective dose values of the medicinal plants reported for some countries are shown in Table 4 [4, 18-21]. It can be seen in Table 4 that our results are in accordance with other reported values. However, total committed effective dose values reported for anticarcinogenic medicinal plants are relatively higher than reported values for Turkey and other countries.

CONCLUSION

In this study, ^{226}Ra, ^{232}Th, ^{40}K and ^{137}Cs activity concentrations of some anticarcinogenic medicinal plants were determined with gamma spectrometric method. The activity measurements were carried out using gamma spectrometry system with a HpGe detector. Average activity concentrations of medicinal plants were calculated as 10.87 ± 1.61 Bq kg^{-1} for ^{226}Ra, 18.02 ± 2.06 Bq kg^{-1} for ^{232}Th, 1025.75 ± 15.53 Bq kg^{-1} for ^{40}K, and 1.14 ± 0.36 Bq kg^{-1} for ^{137}Cs. The highest ^{226}Ra and ^{232}Th activity were measured in the *Sage* medicinal plant sample (33.46 ± 5.2 Bq kg^{-1} for ^{226}Ra and 65.25 ± 5.2 Bq kg^{-1} for ^{232}Th). The lowest ^{226}Ra and ^{232}Th activity were measured in the *Nigella sativa* (1.78 ± 0.29 Bq kg^{-1}) and *Chili pepper* (1.46 ± 0.34 Bq kg^{-1}), respectively. The highest and lowest activity for ^{40}K were measured in *Basil* (2211.80 ± 28.50 Bq kg^{-1}) and *Sesame* (312.55 ± 4.38 Bq kg^{-1}), respectively. The highest ^{137}Cs activity was determined in *Basil* (6.30 ± 0.74 Bq kg^{-1}) and the lowest activity was determined in *Anise* (0.27 ± 0.15 Bq kg^{-1}). ^{137}Cs activity concentrations of ten medicinal plant samples were below detection limit.

The average effective dose values that people are exposed through consumption of medicinal plant samples were calculated as 2.45 ± 0.36 μSv y^{-1} for ^{226}Ra, 20.72 ± 2.37 μSv y^{-1} for ^{232}Th, 31.80 ± 0.48 μSv y^{-1} for ^{40}K, and 0.07 ± 0.02 μSv y^{-1} for ^{137}Cs. Total committed effective dose due to the ingestion was determined as 55.04 μSv in a year. This value is lower than 300 μSv that is accepted as world average of annually committed effective dose value stated in UNSCEAR 2000 report and has no risk to public health.

ACKNOWLEDGEMENTS

This study was supported by the Scientific Research Projects Department (Project no: 2012/1/LTP/04) at Kilis 7 Aralik University. We would like to express our thanks to Muhittin Kulak

for his contributions in identification of the medicinal plants.

REFERENCES

[1] UNSCEAR (2000) Sources and effects of ionizing radiation. Report of the United Nations Scientific Committee on the Effects of Atomic Radiation to the General Assembly, with scientific annexes, United Nations, New York.

[2] Kaur, R., Singh, J., Singh, G. and Kaur, H. (2011) Anticancer Plants: A Review. J Nat Prod Plant Resour. 1, 131-136.

[3] Madhuri, S. and Pandey, G. (2009) Some anticancer medicinal plants of foreign origin. Curr Sci. 96, 779-783.

[4] Desideri, D., Meli, M.A. and Roselli, C. (2010) Natural and artificial radioactivity determination of some medicinal plants. J Environ Radioact. 101, 751-756.

[5] Sussa, F.V., Damatto, S.R., Alencar, M.M., Mazzilli, B.P. and Silva, P.S.C. (2013) Natural radioactivity determination in samples of Peperomia pellucida commonly used as a medicinal herb. J Environ Radioact. 116, 148-151.

[6] Espinosa, G., Golzarri, J.I. and Navarrete, J.M. (2016) Determination of the natural and artificial radioactivity of a selection of traditional Mexican medicinal herbs by gamma spectrometry. J Radioanal Nucl Chem. 307, 1717-1721.

[7] Chandrashekara, K. and Somashekarappa, H.M. (2016) Estimation of radionuclides concentration and average annual committed effective dose due to ingestion for some selected medicinal plants of South India. J Radiat Res Appl Sci. 9, 68-77.

[8] Desideri, D., Meli, M.A., Roselli, C., Forini, N., Rongoni, A. and Feduzi, L. (2014) Natural radionuclides in Italian diet and their annual intake. J Radioanal Nucl Chem. 299, 1461-1467.

[9] Bakım, M. and Görgün, A.U. (2015) Radioactivity in soils and some terrestrial foodstuffs from organic and conventional farming areas in Izmir, Turkey. J Radioanal Nucl Chem. 306, 237-242.

[10] Priharti, W., Samat, S.B., Yasir, M.S. and Garba, N.N. (2016) Assessment of radiation hazard indices arising from natural radionuclides content of powdered milk in Malaysia. J Radioanal Nucl Chem. 307, 297-303.

[11] Canbazoglu, C. and Dogru, M. (2013) A preliminary study on ^{226}Ra, ^{232}Th, ^{40}K and ^{137}Cs activity concentrations in vegetables and fruits frequently consumed by inhabitants of Elazıg Region, Turkey. J Radioanal Nucl Chem. 295, 1245-1249.

[12] Al-Absi, E., Manasrah, R., Wahsha, M. and Al-Makahleh, M. (2016) Radionuclides levels in marine sediment and seagrass in the northern Gulf of Aqaba, Red Sea. Fresen. Environ. Bull. 25, 3461-3474.

[13] Canbazoglu, C. and Dogru, M. (2013) A Preliminary study on determination of radiological parameters of soil samples collected from central Elazıg, Turkey. Fresen. Environ. Bull. 22, 3377-3382.

[14] ICRP (1996) Age-dependent doses to members of the public from intake of radionuclides: part 5. Compilation of ingestion and inhalation dose coefficients. Annals of the ICRP 26(1). ICRP Publication 72. Pergamon Press, Oxford.

[15] Till, J.E. and Moore, R.E. (1998) A pathway analysis approach for determining acceptable level of contamination of radionuclides in soil. Health Phys. 55, 541-548.

[16] ICRP (1994) Age-dependent doses to members of the public from intake of radionuclides: part 2. Ingestion dose coefficients. Annals of the ICRP 23(3/4). ICRP Publication 67. Pergamon Press, Oxford.

[17] IAEA (2005) Derivation of activity concentration values for exclusion, exemption and clearance. In: Safety reports series. IAEA Publication, Vienna.

[18] Njinga, R.L., Jonah, S.A. and Gomina, M. (2015) Preliminary investigation of naturally occurring radionuclides in some traditional medicinal plants used in Nigeria. J Radiat Res Appl Sci. 8, 208-215.

[19] Tettey-Larbi, L., Darko, E.O., Schandorf, C., Appiah, A.A. (2013) Natural radioactivity levels of some medicinal plants commonly used in Ghana. SpringerPlus. 2, 157.

[20] Jevremovic, M., Lazarevic, N., Pavlovic, S. and Orlic, M. (2011) Radionuclide concentrations in samples of medicinal herbs and effective dose from ingestion of ^{137}Cs and natural radionuclides in herbal tea products from Serbian market. Isot Environ Health Stud. 47, 87-92.

[21] Parmaksız, A. and Agus, Y. (2014) Activity concentrations of ^{226}Ra, ^{232}Th, ^{40}K and ^{137}Cs radionuclides in Turkish medicinal herbs, their ingestion doses and cancer risks. Radiat Eff Defects S. 169, 980-988.

Received: **22.02.2017**
Accepted: **23.08.2017**

CORRESPONDING AUTHOR

Cumhur Canbazoglu
Department of Physics,
Faculty of Arts and Sciences,
Kilis 7 Aralik University,
79000 Kilis – Turkey

e-mail: canbazoglu@kilis.edu.tr

© by PSP Volume 27 – No. 2/2018 pages 799-806 Fresenius Environmental Bulletin

PERFORMANCE ASSESSMENT FOR NATURAL WASTEWATER TREATMENT SYSTEMS (CONSTRUCTED WETLAND SYSTEMS)

Zeki Gokalp[1,*], Mustafa Duygulu[2]

[1]Erciyes University Agricultural Faculty Biosystems Engineering Department, 38038, Kayseri, Turkey
[2]Kayseri Sugar Company, 38036, Kayseri, Turkey

ABSTRACT

The present research was conducted to assess the treatment performance of two natural treatment systems constructed in Kayseri province of Turkey. Influent and effluent wastewater samples were subjected to biological oxygen demand (BOD), chemical oxygen demand (COD), total suspended solids (TSS), pH, electrical conductivity (EC), total kjeldahl nitrogen (TKN) and total phosphorus (TP) analyses. Effluent BOD_5 concentrations varied between 40-110 mg/L, COD concentrations varied between 287-402 mg/L, pH values between 7.18-8.04, EC values between 1571-2870 µS/cm. The pH values of all samples met the discharge criteria specified in water pollution control regulations. COD and pH values exhibited an irregular trend with the months. Influent TSS values varied between 75-99 mg/L and effluent TSS values varied between 64-84 mg/L and effluent TSS concentrations were meeting the discharge criteria. Effluent COD concentrations of one of the systems were also meeting the discharge criteria. Effluent total phosphorus values were above the discharge limits. Considering the parameters not able to meet the discharge criteria, it was concluded that these systems should either be repaired or rehabilitated to eliminate the deficiencies experienced in practice.

KEYWORDS:
Water treatment, domestic wastewater, constructed wetlands, effluent, BOD_5, pollution.

INTRODUCTION

World population is continuously increasing and reached to almost 7.5 billion. Parallel to rapid increase in world population and food demands of this increasing population, water demands are also rapidly increasing to produce food to feed this huge population. Despite increasing demands, fresh water resources are continuously depleting worldwide. Basic water-user sectors (agricultural, domestic and industrial) are in ever-aggravating competition for limited water resources. Continuously polluted waters, decreasing fresh water resources because of climate change and resultant global warming, increasing labor and energy costs all brought the water and treatment technologies into the first place in the agendas of the world countries. To solve water-related problems, initially water losses in agricultural, domestic and industrial uses should be prevented, efficient water use should be provided in agricultural practices and possible use of wastewater and treated water should be investigated.

Untreated wastewaters are usually discharged into seas, rivers and other receiving water bodies because of high treatment costs in Turkey. According to the results of Municipal Wastewater Statistics Survey, which was applied to all municipalities, 1 309 out of 1 396 municipalities were served by sewage systems in 2014 in Turkey. Out of 4.3 billion m^3 of wastewater discharged via sewage system, 3.5 billion m^3 was treated in wastewater treatment plants. The rate of advanced treatment was 41.6%, while the rate of biological treatment was 33.2%, the rate of physical treatment was 25.0% and the rate of natural treatment was 0.2% [1].

Natural treatment systems, also called as constructed wetlands or treatment wetlands, are quite cheaper and easy-to-construct systems with low energy and labor costs, easy operation, maintenance and monitoring [2]. These natural systems were also specified as the primary issue in rural development strategy document of State Planning Organization of Turkey [3]. Today, constructed wetlands are widely used to treat domestic wastewaters [4], agricultural wastewaters [5], industrial wastewater and runoff waters [6]. Constructed wetland technology is relatively new in Turkey and the first one was constructed in the year 2004 in a village of Ankara [7]. These natural treatment systems are mostly used for sewage treatment of villages in Turkey. Influent and effluent rates, water quality criteria, hydraulic water level and biological conditions should continuously be monitored and assessed. In Turkey, almost none of them are monitored and none of them have an operation, maintenance, monitoring and assessment programs. Therefore, majority of them either not operating or operating with quite low performance outcomes. The present study was conducted to assess

the performance of two natural treatment systems constructed in Kayseri province of Turkey.

MATERIALS AND METHODS

Natural treatment systems constructed in Kayseri province of Turkey between the years 2006-2015 were visited onsite (51 of them were visited) and two of them were selected for performance assessment. Most of them were either not operating or already out of order. Therefore, only two of them were able to be selected since they were already operating and available for water sampling from influent and effluent discharge sections. Location of the selected systems (Seyhsaban and Subasi villages) is presented in Figure 1, the constructed images of them are presented in Figure 2 and design projects are presented in Figure 3. Influent and effluent water samples were taken at the beginning of each month for 5 months (April, May, June, July and August) in accordance with Water Pollution Control Guidelines issued by Ministry of Environment of Turkey [8]. Then, water samples were subjected to pH, electrical conductivity (EC), biological oxygen demand (BOD_5), chemical oxygen demand (COD), total suspended solids (TSS), total kjeldahl nitrogen (TKN) and total phosphorus (TP) analyses. Water samples were transported to laboratory immediately and subjected to pH and EC analyses with a pH (Hanna Instruments, pH 211 model) and EC (Hanna 98107 model) meter. BOD analyses were performed with BOD measurement apparatus (WTW- Oxitop). COD analyses were performed with a COD measurement set (WTW CR2200 model thermo reactor). TSS suspended solids were determined with a vacuumed filtration apparatus. Kjeldahl method was used to determine total kjeldahl nitrogen content of water samples. ICP-MS device (model 7700 Agilent Inc., Tokyo, Japan) was used to determine total phosphorus content of water samples.

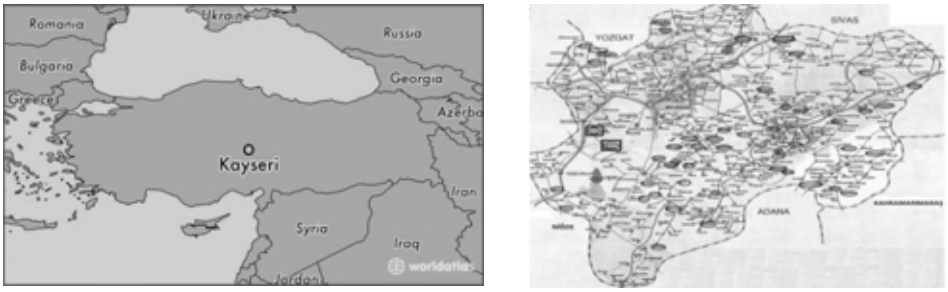

FIGURE 1
Location of natural treatment systems

FIGURE 2
Natural treatment systems

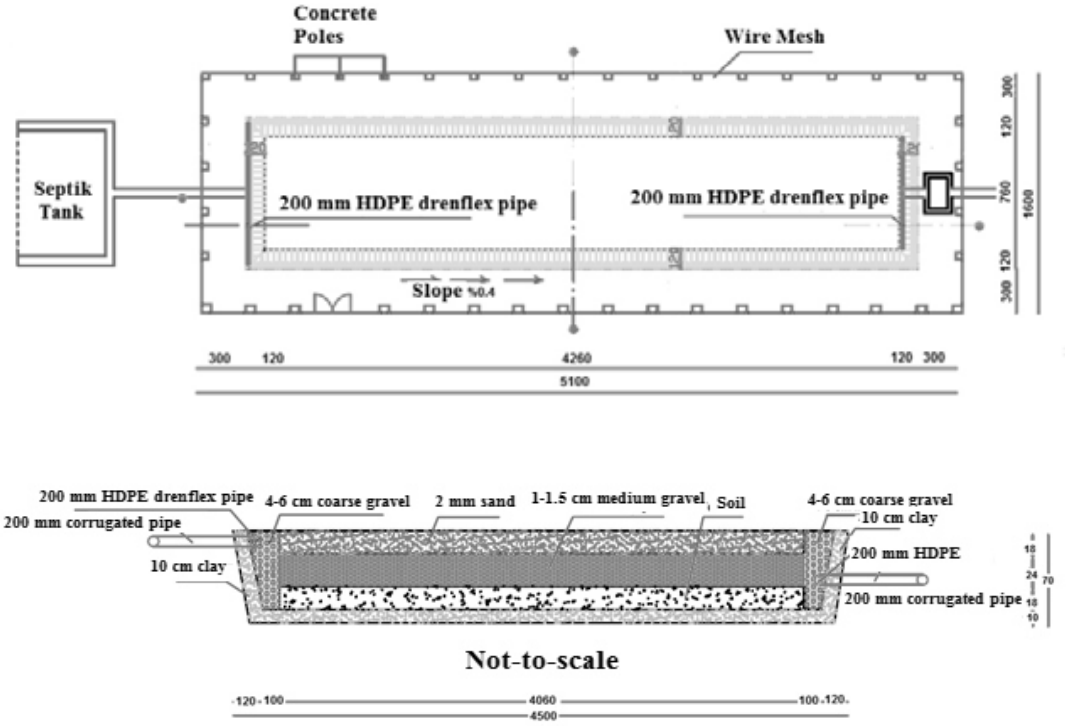

FIGURE 3
Design project of natural treatment systems

RESULTS AND DISCUSSION

Biological oxygen demand (BOD_5), chemical oxygen demand (COD), pH, electrical conductivity (EC), total suspended solids (TSS), total kjeldahl nitrogen (TKN) and total phosphorus content of influent and effluent water samples are provided in Table 1. Influent BOD values varied between 118-190 mg/L and effluent BOD values varied between 40-110 mg/L. The monthly variations in BOD values are presented in Figure 4a. Both influent and effluent BOD values increased with increasing temperatures. According to effluent discharge standards set by the Ministry of Environment [8], effluent BOD value should be maximum 50 mg/L. The natural treatment systems considered in this study were quite far from meeting the effluent discharge standards.

Biological oxygen demand is an indicator of how fast the microorganisms in water consume oxygen in water and it is a common parameter used in design of wastewater treatment systems. Higher values indicate higher pollution levels [9]. Demirors [10] assessed the performance of a natural treatment system in Cukurova region of Turkey and reported the average effluent BOD value as 13 mg/L with about 91% BOD removal efficiency. Since the system investigated in that study was totally designed for BOD removal, the system was able to meet the discharge criteria. Natural treatment systems are commonly designed based on the population to be served. Usually 5 m^2 basin area is recommended per capita, but this value is most of the time applied as 3-5 m^2 [11, 12]. The treatment systems investigated in present study were designed with 0.9 m^2 basin area per capita. Therefore, there was an excessive BOD loading rate and the system was not able to meet the discharge criteria set for wastewater effluents. The BOD removal efficiency of the current treatment systems was calculated as about 49%. Akratos & Tsihrintzis [13] investigated BOD removal efficiency of natural treatment systems under different temperature, plantation and hydraulic retention conditions and reported the average value as 89%.

Influent chemical oxygen demand (COD) values varied between 351-460 mg/L and effluent COD values varied between 266-402 mg/L (Table 1). The monthly variations in COD values are presented in Figure 4b. Both influent and effluent COD values exhibited irregular changes with months. The effluent discharge criterion is set as 100 mg/L in relevant standards [8]. Thus, both systems were not able to meet the discharge criteria. COD is not a design parameter, but a pollution parameter. Contrary to BOD values, COD may include some substances not biologically degraded, therefore, COD values of wastewaters usually higher than BOD values of the same samples [14]. The primary reason for failure in COD removal performance was again improper design of the systems since the natural treatment systems of the present study were design without taking

wastewater influent characteristics into consideration and only the previously prepared pilot projects were used. Demirors [10] in a study carried out with natural treatment systems, reported quite low effluent COD values (24 mg/L) and high COD removal efficiencies (71%). Since the natural treatment systems of that study were designed especially for BOD removal, researchers were able to achieve high removal efficiencies for COD. The average COD removal efficiency of the present study was calculated as around 20%. However, Kotti *et al*. [15] carried out a study with different basin geometries, temperatures and hydraulic retention times (6, 8, 14 and 20 days) and reported an average COD removal efficiency of 67.9%.

Influent pH values varied between 7.12-7.99 and effluent pH values varied between 7.18-8.04 (Table 1). Monthly variations in influent and effluent pH values are presented in Figure 4c. As it was in COD values, pH values also exhibited irregular variations in months. The discharge standard was set as to be between 6-9 for domestic wastewater effluents from natural treatment systems [8]. So, the effluent pH values of both treatment systems were meeting the discharge criteria. While influent EC values varied between 1587-2403 µS/cm, effluent EC values varied between 1571-2870 µS/cm. The monthly variations in EC values of the natural treatment systems are presented in Figure 4d. Again the trend was irregular in EC values. The discharge criteria were set as to be between 750-2000 µS/cm in relevant standards [8]. Considering this standard value, it was observed that one of the systems (Subası) was meeting the discharge criteria, whereas the other (Seyhsaban) was not. In similar previous studies, effluent pH values were reported as between 6.5-7.9 [10] and 6.5-8.5 [16]. Current effluent pH values well comply with these earlier findings. Especially the EC values of Subası natural treatment system (1571-1911 µS/cm) were quite similar with the values reported by [17].

TABLE 1
Physico-chemical wastewater characteristics

	Months				
	April	May	June	July	August
	BOD (mg/L)				
Subası Influent	170	160	140	169	175
Subası Effluent	110	105	76	71	110
Seyhsaban Influent	130	120	190	126	118
Seyhsaban Effluent	40	50	67	63	68
	COD (mg/L)				
Subası Influent	363	351	360	460	390
Subası Effluent	318	318	304	402	310
Seyhsaban Influent	398	378	409	450	450
Seyhsaban Effluent	287	266	327	320	345
	pH				
Subası Influent	7.12	7.18	7.21	7.25	7.82
Subası Effluent	7.71	7.86	7.89	7.82	7.31
Seyhsaban Influent	7.51	7.99	7.60	7.18	7.43
Seyhsaban Effluent	7.95	7.61	8.04	7.47	7.18
	EC (mmhos/cm)				
Subası Influent	1829	1752	1597	1587	1652
Subası Effluent	1826	1732	1594	1571	1911
Seyhsaban Influent	2403	2340	2380	2393	2303
Seyhsaban Effluent	2470	2387	2330	2870	2353
	TSS (mg/L)				
Subası Influent	83	82	79	77	75
Subası Effluent	73	71	67	65	64
Seyhsaban Influent	99	94	91	89	89
Seyhsaban Effluent	84	83	77	77	75
	TKN (mg/L)				
Subası Influent	28	29	27	25	26
Subası Effluent	14	14	16	15	17
Seyhsaban Influent	26	23	24	20	25
Seyhsaban Effluent	11	13	14	12	15
	TP (mg/L)				
Subası Influent	9	8	8	7	6
Subası Effluent	7	4	6	6	5
Seyhsaban Influent	11	9	9	8	7
Seyhsaban Effluent	8	8	7	6	6

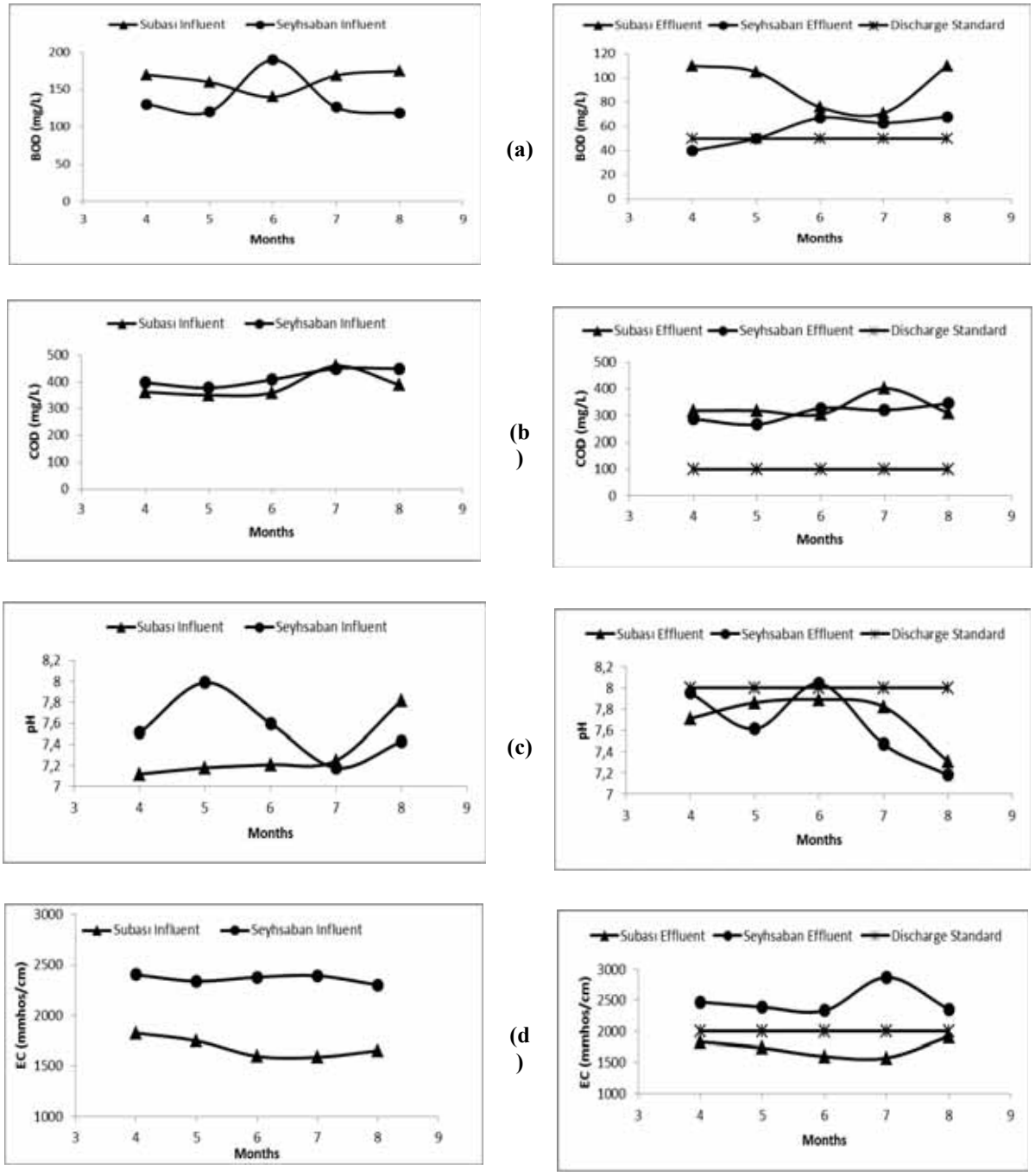

FIGURE 4
Monthly variations in (a) BOD, (b) COD (c) pH and (d) EC values of influent and effluent wastewater samples

Influent total suspended solid (TSS) values varied between 75-99 mg/L and effluent TSS values varied between 64-84 mg/L. The variations in TSS values with months are presented in Figure 5a. The discharge limit value was set as 150 mg/L, so both systems were meeting the discharge criteria. Since septic tanks were used in front of the inlet sections, TSS values were quite lower than expectations. Septic tanks provided a pre-settlement for suspended solids before they get into to treatment system as influent. Demirors [10] in a study carried out in Cukurova region of Turkey, indicated that the system under consideration was not able to meet TSS removal standards. The average TSS removal performance of the present systems was calculated as 14% and both systems were well meeting the discharge standards set for effluent TSS values of natural treatment systems. Since there was a four-cell concrete septic

tanks in front of the inlet section of the natural treatment systems of the present study, majority of suspended solids settled down in septic cells and thus quite low TSS values were observed. Therefore, low TSS values were an expected case in these systems with pre-treatment septic tanks [7].

Influent total kjeldahl nitrogen (TKN) values varied between 20-29 mg/L and effluent TKN values varied between 11-17mg/L. Monthly variations in TKN values are presented in Figure 5b. The discharge criteria set for effluent TKN is 15 mg/L [8]. Except for couple months of Subası treatment system, effluent waters were meeting the discharge criteria. Organic nitrogen is used in photosynthesis process of the plants [17]. Nitrogen removal performance of natural treatments systems are greatly influenced by hydraulic loading rates and hydraulic retention times, so each system may have different removal performances [18]. The average nitrogen removal performance of the present systems was calculated as about 44%. Influent nitrogen concentrations were quite high in this study because wastewaters of livestock facilities are also entered into the treatment systems. While influent total phosphorus (TP) values varied between 6-11 mg/L, effluent TP values varied between 4-8 mg/L (Table 1). The variations in TP values with months are presented in Figure 5c. Both systems were not able to meet the discharge criteria set for total phosphorus concentration of domestic wastewater effluents (2 mg/L). Detergents in domestic wastewaters may increase influent phosphorus concentrations. The phosphorus removal performance of the present systems was calculated as 22.8%. Since phosphorus removal usually occurred through absorption and plant use, it is quite usual to have low phosphorus removal performance for natural treatment systems [19].

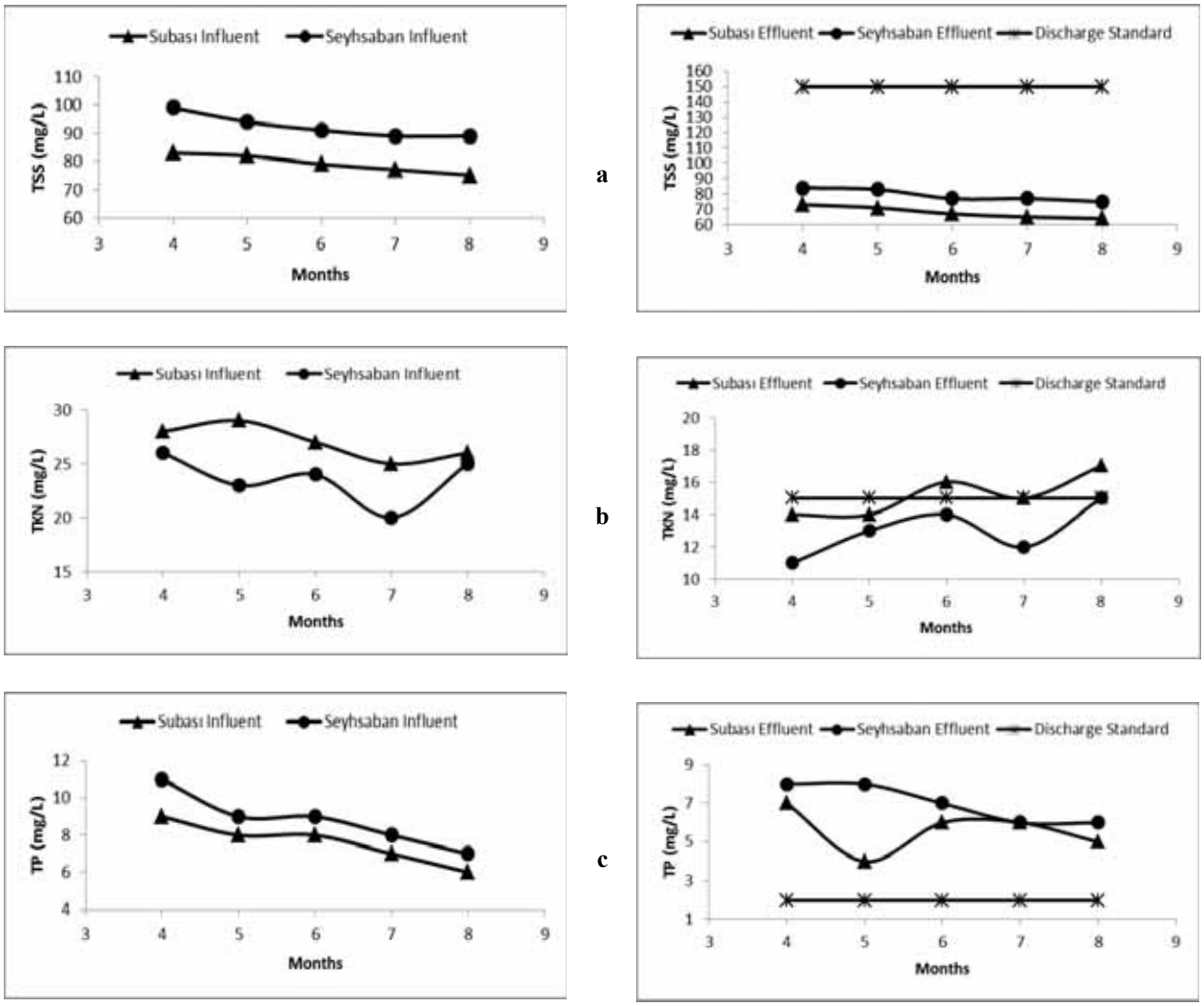

FIGURE 5
Monthly variations in (a) TSS, (b) TKN and (c) TP values of influent and effluent wastewater samples

CONCLUSIONS

Considering the current impacts of climate change and resultant global warming of fresh water resources, re-use of treated wastewaters play a significant role in sustainable and efficient use of water resources. As it was in all developing countries, agriculture is the greatest water-user sector in Turkey. Therefore, measures like water sawing and wastewater re-use should be initiated in agriculture. Discharge of untreated wastewaters creates significant threats on both environment and human health. Wastewaters should be treated before to discharge them into receiving bodies or before to re-use them. Natural treatment systems are preferred for domestic wastewater treatment especially in rural sections, in villages of Turkey. These systems were also indicated as the primary issue in Rural Development Strategy Document of State Planning Organization of Turkey. Usually pilot projects are used in construction of natural treatment systems. Influent wastewater characteristics, local climate conditions and relevant discharge standards have not been taken into consideration. Therefore, majority of already constructed ones either not operating or are not able meet effluent discharge criteria. Current performance assessments also revealed that the natural treatment systems of the present study were also far away from meeting the effluent discharge criteria specified in relevant standards. The natural treatment systems should be rehabilitated urgently to get the desired performance outcomes from them. The new ones to be constructed should be designed by taking specific design criteria and local conditions into consideration.

ACKNOWLEDGEMENTS

The present study was supported by Scientific Research Department of Erciyes University (with a project number of FBA-12-3859).

REFERENCES

[1] Anonymous (2014) Municipality Wastewater Statistics. Turkish Institute of Statistics Bulletin. 74 (in Turkish).

[2] EPA (1993) Constructed wetlands for waste water treatment and wild life habitat: 17 Case Studies. EPA 832-R-93-005 8.

[3] Anonymous (2006) National Development Strategy, State Planning Organization.

[4] Cooper, P., Smith, M. and Maynard, H. (1997) The design and performance of a nitrifying vertical-flow reed bed treatment system. Water Science and Technology. 35, 215–221.

[5] Rivera, R., Warren, A., Curds, C.R., Robles, E., AGutierrez, A., Gallegos, E. and Caldeffin, A. (1997) The application of the root zone method for the treatment and reuse of high strength abattoir waste in Mexico. Water Science and Technology. 35(1997) 271–278.

[6] Trautmann, N.M., Martin, Jr. H., Porter, K.S. (1989) Use of artificial wetlands for treatment of municipal solid waste land fillleachate. In: Hammer, D.A. (Ed.) Constructed Wetlands for Wastewater Treatment. Lewis, Chelsea. 245–251.

[7] Gokalp, Z., Uzun, O. and Çalış, Y. (2014) Common failures of the natural treatment systems (Constructed Wetlands) of Kayseri, Turkey. Ekoloji. 23(92), 38-44.

[8] Anonymous (2004) Official Gazette Date: 31.12.2004 Issue: 25687 Water Pollution Control Regulations (in Turkish).

[9] Anonymous, (2015a) Biochemical oxygen demand https://tr.wikipedia.org (in Turkish).

[10] Demirors, B. (2006) Possible use of constructed wetland technology in rural sections of Cukurova Region. Institute of Natural and Applied Sciences. Cukurova University (in Turkish).

[11] EPA (2000) Guiding Principles for Constructed Wetland Treatment. United States Environmental Protection Agency, Office of Wetlands, Oceans and Watersheds, EPA 843-B-00-003.

[12] Knight, R.L., McKim, T.W. and Kohl, H.R. (1987) Performance of natural wetland treatment system for wastewater management. Journal of Water Pollution Control. 59, 746-754.

[13] Akratos, C.S. and Tsihrintzis, V.A. (2007) Effect of temperature, HRT, vegetation and porous media on removal efficiency of pilot-scale horizontal subsurface flow constructed wetlands. Ecological Engineering. 29(2), 173-191.

[14] Anonymous (2015b) Chemical oxygen demand, https://tr.wikipedia.org (in Turkish).

[15] Kotti, I.P., Gikas, G.D. and Tsihrintzis, V.A. (2010) Effect of operational and design parameters on removal efficiency of pilot-scale FWS constructed wetlands and comparison with HSF systems. Ecological Engineering,

[16] Koottatep, T., Polprasert, C., Koanh, N.T., Heinss, U., Montangero, A. and Strauss, M. (2001) Septage Dewatering in Vertical–Flow Constructed Wetlands Located in the Tropics. Water Science and Technology. 44(2–3), 181–185.

[17] Anonymous, (2015c) Biochemical oxygen demand https://tr.wikipedia.org (in Turkish).

[18] Kadlec, H.R., Knight, R.L. (1996) Treatment Wetlands. Lewis, Boca Raton, New York, London, Tokyo, p. 893.

[19] EPA (1999) Manual, Constructed Wetlands Treatment of Municipal Wastewaters, EPA/625/R-99/010, U.S. Environmental Protection Agency, Cincinnati, Ohio, USA.

Received: **23.02.2017**
Accepted: **06.09.2017**

CORRESPONDING AUTHOR

Zeki Gokalp
Erciyes University
Agricultural Faculty
Biosystems Engineering Department,
38038, Kayseri – Turkey

e-mail: zekigokalp@yahoo.com

© by PSP Volume 27 – No. 2/2018 pages 807-814 Fresenius Environmental Bulletin

INVESTIGATION OF EPI STRUCTURE IN FRONTAL OF INTAKES ON DIVERSION FLOW IN RIVER BEND WITH CCHE2D MODEL

Amir Abbas Kamanbedast[1,*], Shatirah Akib[2], Khodayar Khadem[1]

[1]Department of Water Science and Engineering, Ahvaz Branch, Islamic Azad University, Ahvaz, Iran*
[2]School of Energy, Geoscience, Infrastructure and Society (EGIS), Heriot-Watt University Malaysia, Putrajaya 62200, Malaysia

ABSTRACT

Rivers have long been regarded as one of the most important water supplies to human beings, since the major civilizations of human beings were formed near rivers to take advantage of the water's blessings. Along with the water, rivers carry sediment, which is created by erosion of the riverbed and erosion caused by rainfall or surface runoff flowing over the catchment area. Groins are simple hydraulic components that are used for organizing bends in rivers or directing them in some other way and to control erosion and protect the shoreline. In this project, CCHE2D software was used to prepare a numerical model of flow patterns around an Epi in a setting with one simple groin related to the flow direction of frontal intake in a 90-degree bend. Such a bend causes vortex flow around the groin to add to the entry of the water intake, which would make new challenges. In this study, simulation of the discharge and groin structure input into these intakes was investigated to analyze and evaluate the hydraulic conditions of flow in an intake with different locations of 45, 60, 75 degree of bend and that has a sinusoidal-like turn. In addition, the variation of various parameters, such as velocity, Froude number, shear stress, river bed elevation, and total discharge of the river were calculated and discussed. The impact of these different locations on hydraulic flow was studied. The results of these tests indicated that an intake with Epi can improve the flow patterns at the inlet.

KEYWORDS:
Location of Intake, River Bend, Epi(groin), CCHE2D

INTRODUCTION

River is a dynamic process and its behavioral pattern is changing all the time. These changes greatly affect the river morphology and the hydraulic condition of the river flow. Understanding of river characteristics has many applications in planning, designing and constructing hydraulic structures in the river. Unlike many countries, Iran has very limited water resources and therefore right and planned utilization of the rivers is very crucial. Different kinds of studies have been done on Iranian rivers, such as water resources management, flood control and sediment balance. The hydrodynamic simulation of the unsteady flow pattern in a river is studied in [2, 3]. The place of a lateral intake in the extrados (outer curve of an arc) of the river is identified using the CCHE2D model in [7]. Also, [8] uses the same model to simulate the flow and sediment pattern in rivers with the assumption that the flow is unsteady. In [6, 18], the numerical simulation of flow in an arch with a 90 degree angle is conducted using the CCHE2D model. The simulation of flow and sedimentation patterns around the river cutwater in an arch with a 180 degree angle is done in [1, 5]. Kamanbedast et al. [4,10] investigate the river Karkheh on flood discharge by the CCHE2D model.

In an unsteady flow, time parameters also interfere the changes in the flow toward the time are contradicted to zero. In unsteady flows within waterways, at least one value of two main parameters (i.e. depth and flow discharge) change together with the time. This change could happen because of natural events, planned factors or incidents and these events consist of frequent waves, tidal flows and flood as a result of dam breakage. Every unsteady flow is a wave that is changed according to the situation like depth, discharge or both of them. These two factors change from place to place and time to time. Unsteady flows fall into two categories: gradual variable and rapidly variable. Examples of gradual variables are flood waves, tidal waves and waves that are made by slow operations of the flow control structures. Rapidly variable flows can be made by sudden opening and closing of flow control structures.

In river morphology, rivers are three types according to their figures: straight, meander and braided. This classification was made by Leopold and Lemon in 1957 as is shown in Table 1. They used two factors: winding factor and the scale factor between width and depth of the flow to create these categories. When the winding factor is higher than 1.4 or 1.5, the river is swirly (winding) and the lower factors indicate the straightness of the river.

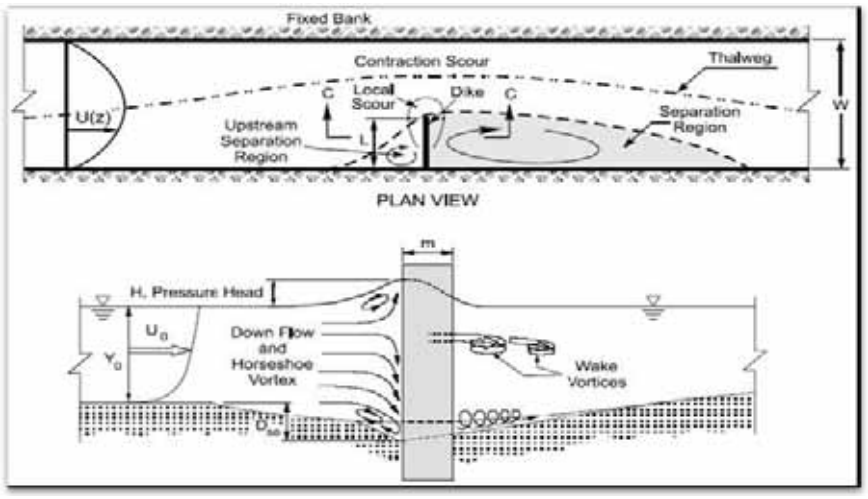

FIGURE 1
Flow around Epi, vortex flow pattern and secondary flow

TABLE 1
Turning factor for different types of river meanders

Turning factor	1-1.05	1.06-1.25	1.25-2	Higher than 2
River figure				
River type	Straight	Sinus-oidal	Meander	Extreme Meander

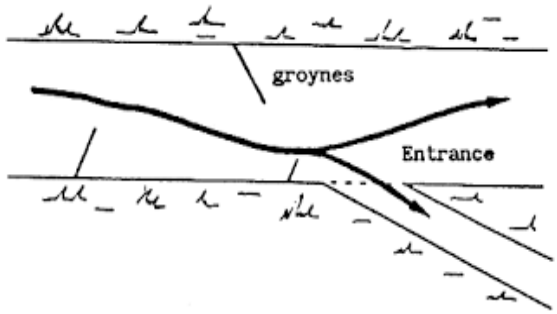

FIGURE 2
Flow around groins frontal intake

In general, it is assumed that the forces governing the flow in a bend are centrifugal forces. In rivers, the velocity of flow in upper areas near the free surface is high, and this leads to non-uniform velocity profile in vertical direction. Due to the centrifugal force and interaction with lateral pressure gradients caused by side slope of water surface, a flow is formed known as the secondary flow. In such a flow, the water in upper part is expelled to the outside and in lower part moves toward the inner bend. Due to the interaction between the secondary flows and non-uniform velocity profile in depth, a flow pattern is formed called the spiral flow. This flow pattern causes serious disturbance in the flow and has a great effect on the river bend morphology. So that high velocity of flow in the outer bend will result in erosion of the river bed and outer bank and consequently its destruction. The river width is not constant at the bends, but is gradually reduced and the bend has a convergent Shape. Investigating the features and flow behavior and related component is one of the complex phenomena that make using of software inevitable. Groin is simple hydraulic component that used for organizing the rivers in bend or direct way and erosion control and protecting of shores. Figure 1. Also flow around groins frontal intake shows in fig 2.

In this paper numerical study of position effect and adding groins and their influence flow regime of location of 90° degree bend. Studied scientifically to achieve this purpose, 2 different discharges are modeled too. Numerical models (CCHE2D) are work at actual size condition and for determination velocity of turbulent flow and bed scouring here been utilize. In the paper CCHE2Dsoftware which is my complete and suitable for complicated flows here my stable applied. Ghodsian, M. [9] studied Experimental study on scour and flow field in a scour hole around a T-shape spur dike in a 90° bend. Kamanbedast, A. [11] investigated the Scour around Bridge Pile in Flood with Hec-Ras Software. Masjedi et al [15] studied effect of, nose shape effect of: T-shape-spur dike on: Scouring depth of 180° bend with tree: spur dike shape %. (Such as: straight, semi-cylinder and: triangular) with experimental tests. Masjedi, et al [16] studied investigation on the time development of local scour at a spur dike is presented. Spur dikes have been used extensively for erosion control in the outer bank of river bends. Experimental investigation on scouring and determination of depth of scouring are among the most important issues in spur dike designation. The overall objective of the research is to study the temporal development of the scour for a spur dike. The study was conducted using a 180° laboratory flume bend with a relative radius of R/B = 4.67 operated under clear-water

conditions. The median size and geometric standard deviation of bed material were equal to d50= 2 mm and σg = 1.7, respectively. Tests were conducted using one spur dike with 110 mm length in position of 60° under four flow conditions. In this study, the time development of the local scour around the spur dike plates was studied. The effects of various flow intensities (u*/u*c) on the temporal development of scour depth at the spur dike were also studied. The time development of the scour hole around the model spur dike installed was compared with similar studies on spur dikes. The results of the model study indicated that the maximum depth of scour is highly dependent on the experimental duration. It was observed that as flow intensities (u*/u*c) increases, the scour increases. Measuring time and depth of scouring based on experimental observation, an empirical relation was developed with a high regression coefficient of 97. Matinfard, A. [13] shows Effect of Changes in the Hydraulic Conditions on the Velocity Distribution around L-Shaped Spur Dike at the River Bend Using Flow-3D model. Saki, A. et al [18] tried to instigate and designed rectangular weir for flow regulation at river fork through a physical model (case studies of Karkheh), and numerical way through clear water condition. As a result, in normal mode without any weirs installed, however, there will be associated with the flow controlled by the weir.

MATERIALS AND METHODS

CCHE2D Model –The model strictly enforces the mass conservation within the computational domain through the user of control volume approach. This property is of fundamental importance in achieving reliable and accurate results. Wetting and drying of the domain as the nodes are submerged under high flows and exposed during low flows. This feature is particularly important during unsteady flows. The wet and dry nodes are distinguished based on the critical depth specified by the user. During the simulation process any node having flow depth less than the critical depth is considered dry. The turbulent eddy viscosity is approximated using three different approaches. The first one is based on the depth average parabolic eddy viscosity model; the second approach employs depth-averaged mixing length model; and the last approach is based on depth-averaged scheme. The last two approaches are particularly suitable for recirculation flows and flow around hydraulic structures. The user has the option to simulate a given case with any of the above turbulent closure scheme.

The user can provide no-slip, total-slip, partial-slip, or log-law boundary condition at the no-flow boundaries. The log-law approach results in an accurate prediction of shear stresses near the hydraulic structures that are important for computing flow and sediment transport in the vicinity of hydraulic structure. The model supports both steady and unsteady boundary conditions for flow with multiple inlets and outlets. At any inlet the user can specify specific discharge, total discharge, or discharge hydrograph boundary condition. At an outlet the model accepts open boundary, water surface level, stage-discharge relationship, or stage hydrograph as a boundary condition. In case of open boundary the model uses kinematic wave approximation to assess the water surface level at the outlet. This condition should be applied judiciously and is useful in cases when water surface level at the outlet is not available. The model is capable of handling supercritical flow. In addition, mixed flow regime (combination of subcritical and supercritical flow) in a channel reach can be simulated using the CCHE2D model.

CCHE2D is an aggregated software package created in 2005 by Wang, Jia and San in the National Centre of Calculation and Hydraulic Engineering (NCCHE) under the supervision of University of Mississippi, USA. This model is a two dimensional hydraulic model that is created for analyzing and simulation of flow hydraulic, sediment transport and morphology processes in open flows. The model uses average equations of Reynolds for solving flow area in depth. Two zero models of parabolic distributed equations and the prantels mix length model and also the model of two equations k-ε are used for modeling of distributed flow. The network used in this model is curved and not orthogonal. This model is applicable for both steady and unsteady flow. Based on [23], we used effective Element method (a kind of limited Element), the control volume for solving the equations and dry surfaces method for simulation of unsteady flows and border motions. The CCHE2D has two important categories: CCHE2D Mesh generator and CCHE2D GUI (Graphical User Interface). The Mesh generator allows the user to introduce the geometric condition and structures of environment to the model and then proceeds to create the structure's network. Then, using the GUI model, user can observe hydraulic parameters of flow, sediment, boundary condition, parameters needed for simulation and also the output results [23].

Equations for Modeling. Equations which are used in CCHE2D software are the equations for flow and sediment in open channels and rivers as the followings. Equations for wave dynamic model in an open channel are Saint-Venant equations. Equation 1 is the Continuity equation and Equation 2 is the Momentum equation.

$$\frac{\partial A}{\partial t} + \frac{\partial Q}{\partial x} = q \quad (1)$$

$$\frac{\partial}{\partial t}\left(\frac{Q}{A}\right) + \frac{\partial}{\partial x}\left(\frac{\beta Q^2}{2A^2}\right) + g\frac{\partial h}{\partial x} + g(S_f - S_0) = 0 \quad (2)$$

In these equations, x and t represents time and place axles. A is flow space, Q is flow discharge, h is flow depth, S_0 is steep of the river bed, b is correction factor of momentum factor, g is gravity speed, q is discharge to width unit and S_f represents frictional steep. In the dynamic wave method, we use the complete momentum equation. Complete momentum equation together with the continuity equation can be only solved by numeric methods. The momentum equation for wave spreading model is Equation 3. The equation for non uniform sediment transport is Equation 4.

$$\frac{\partial h}{\partial x} + S_f - S_0 = 0 \quad (3)$$

$$\frac{\partial (AC_{tk})}{\partial t} + \frac{\partial Q_{tk}}{\partial x} + \frac{1}{L_s}(Q_{tk} - Q_{t*k}) = q_{lk} \quad (4)$$

Where C_{tk} is the mean (average) of sediment density for the size of k units, Q_{tk} is the rate of actual carried alluvia for the size of k units, Q_{t*k} is the capacity for carrying sediments, L_s the length of the distance that sediment is carried inconstantly and q_{lk} the side discharge or output sediments in width unit. This research is made base on the physical model. Fig2. By this software, five stages should be followed: mesh making, flow ridge condition adjustment, flow initial adjustment and/or sediment adjustment, model execution and illustrating of the program execution results.

Calibration. Table 2 shows the parameter of physical modeling. Sketch of physical model is shown in fig 3. Different discharges, geometric and hydraulic specifications were entered to software. Initial conditions and boundary conditions were determined for the software. Particle percentage of suspended sediment, bed sediment, suspended sediment discharge and bed load discharge were entered to software. Initial conditions and sediment boundary conditions were determined for the software and the sediment load was analyzed. Depth of Discharge rate for the 25 and 42 liters per second respectively 11 and 18 cm. Also Calibration test in software model is shown in tab 3, fig4.

TABLE 2
Characteristic of river bend (physical model)

Q(M3/s)	Angle (degree)	High of canal (m)	Wide (m)	Radial of canal (m)	Length of outlet (m)	Length of inlet (m)
different	90	0.4	0.5	2	0.5	3

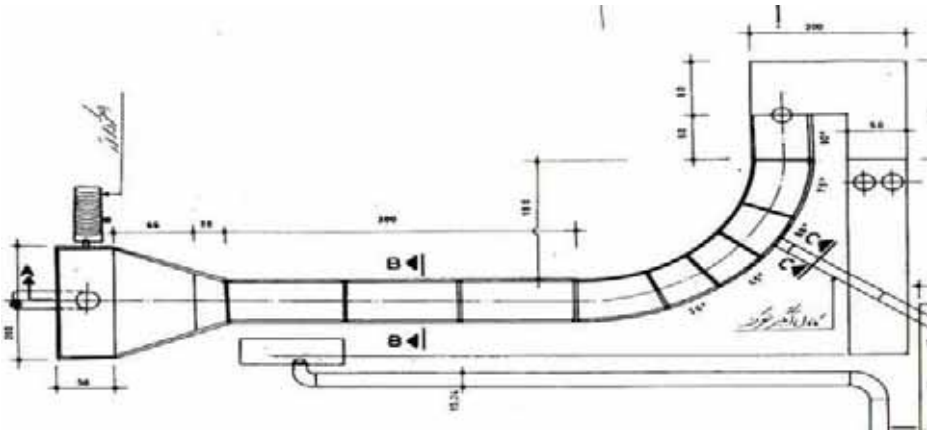

FIGURE 3
Sketch of physical model

TABLE 3
Calibration test result

test	Turbulence model	(n) Manning's coefficient
1	Parabolic Eddy Viscosity Model	0.02
2	Mixing Length Model	0.02
3	K-Epsilon Model	0.02
4	Parabolic Eddy Viscosity Model	0.025
5	Mixing Length Model	0.025
6	K-Epsilon Model	0.025
7	Parabolic Eddy Viscosity Model	0.03
8	Mixing Length Model	0.03
9	K-Epsilon Model	0.03
10	Parabolic Eddy Viscosity Model	0.035
11	Mixing Length Model	0.035
12	K-Epsilon Model	0.035
13	Parabolic Eddy Viscosity Model	0.04
14	Mixing Length Model	0.04
15	K-Epsilon Model	0.04

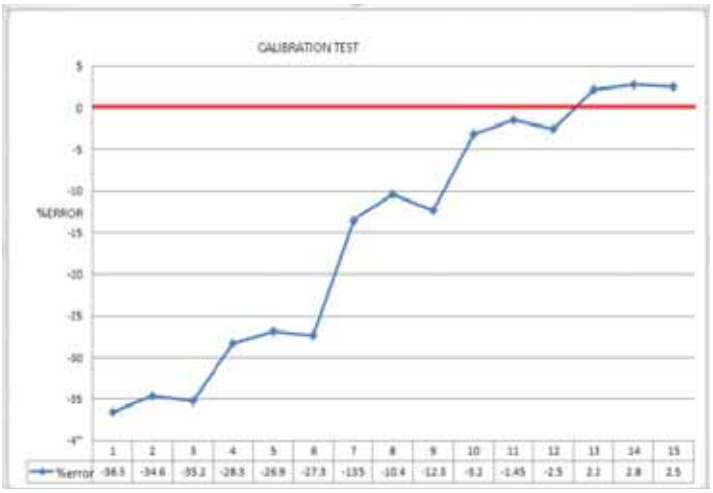

FIGURE 4
Calibration test in software model

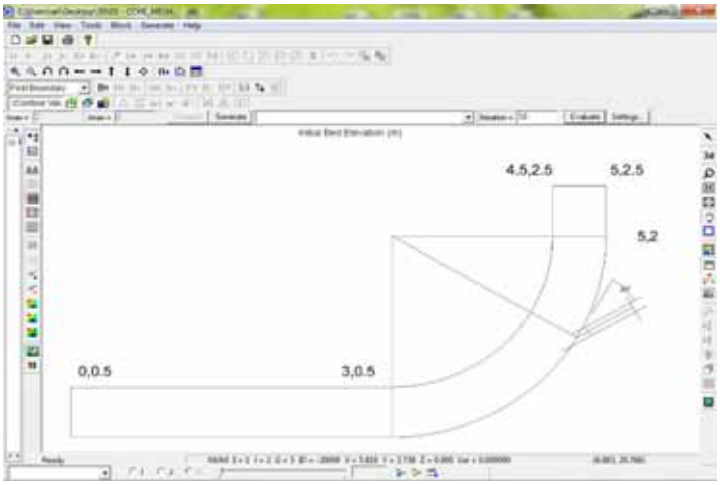

FIGURE 5
Simulation of canal, bend and intake in CCHE2D model

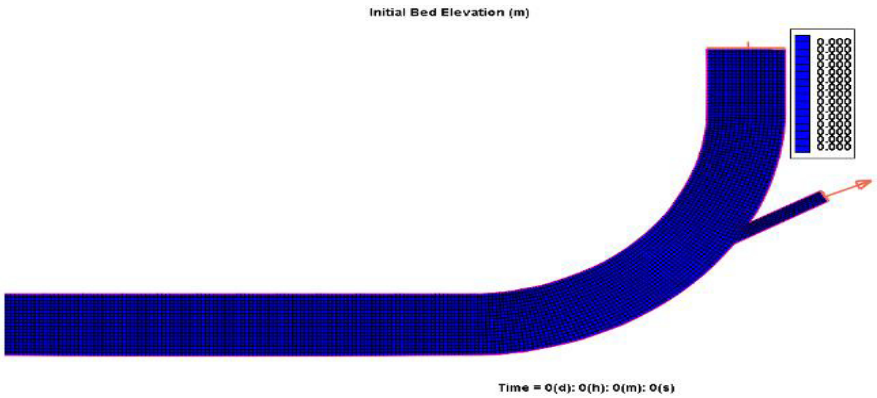

FIGURE 6
Sample of initial data and intake's mesh lines

Geometry and Networking. This stage is the first step in flow simulation and it is important because creating an appropriate network increases the accuracy of final results. In desirable mesh making, the areas locations are specified thoroughly in networks and the relation between them will be preserved. Created cells are almost uniform with equal aggregation. Input and output ridges of flow must be far enough from the center spots so that the flow becomes normal (balanced). Mesh lines must be as flat as possible and must not be vertical towards each other. The mesh lines should also go the same as the flow direction as illustrated. Figure5.

TABLE 4
Result of cche2D model for diversion of water intake (Qd)

Angle	location	Total discharge Q0(L/S)	diversion discharge $Q_{d\ (L/S)}$	rate of Q%	diversion discharge Q_d with adding $groin_{(L/S)}$	rate of Q%
45	45	25	3.3	13.2	3.45	13.8
	60		3.5	14	3.9	15.6
	75		3.35	13.4	3.5	14
	45	42	5.2	12.4	6	14.2
	60		5.8	13.8	6.6	15.7
	75		5.4	12.8	6.5	15.4

Assigning Initial Flow Parameters and Boundary Conditions. To assign initial parameters we set constant value for the input and output value in the related windows. After model calibration the manning coefficient is set to 0.035. Fig6.

In order to invest the effect of adding epi structure, first Simulation time and calculated time scale is specified from currants number is set. After completing other adjustments and inserting necessary information, the software starts getting many runs for different discharges. . Sample of intakes streamlines and influences of epi is shown in Figure 7 to 9.

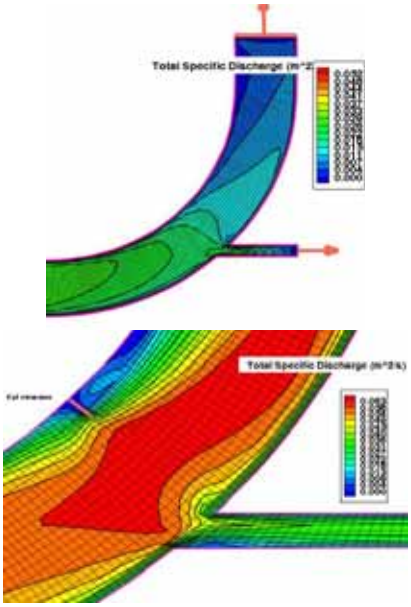

FIGURE 7
Sample of intakes streamlines (left: without structures, right: with Epi (45º location))

RESULTS AND DISCUSSION

After introducing geometric and hydraulic specifications of flow to the model and running the model, one can observe the modeling results in different forms. In this research, the effects of parameters like velocity, shear tension, water surface profile on the location of intake and river bend also the effect of adding a structures (epi) in front of intake will be studied. The results of velocity distribution and their values for different locations and discharges before the epi and after epi structure is show in table4. Table 4 shows the results for 2 discharges and 3 locations (45, 60, 75 degree). It is seen that diversion discharges (Q_d).

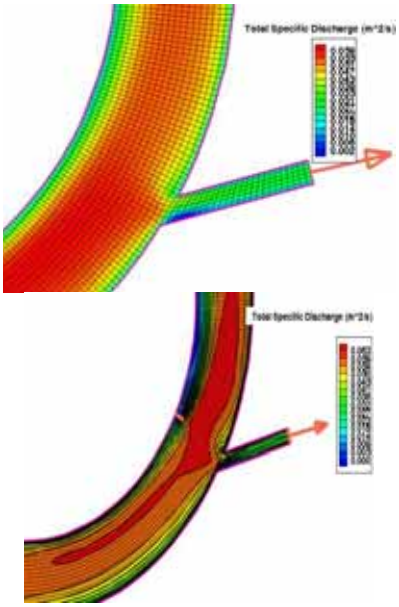

FIGURE 8
Sample of intakes streamlines (left: without structures, right: with Epi (60º location))

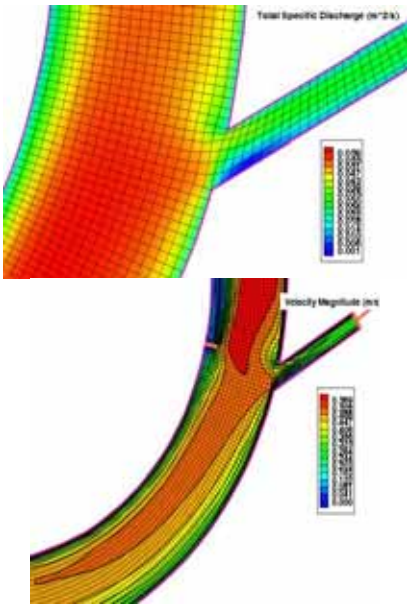

FIGURE 9
Sample of intakes streamlines (left: without structures, right: with Epi (75º location))

The percentage of diversion discharges rate (Q_d) without groin and after adding groin structures (Epi) in simulation modeling are shown in Figure 10 and 11, respectively.

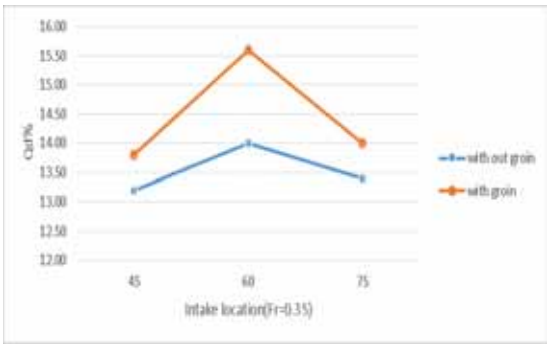

FIGURE 10
Results intake discharge rate with the Froude number=0.35

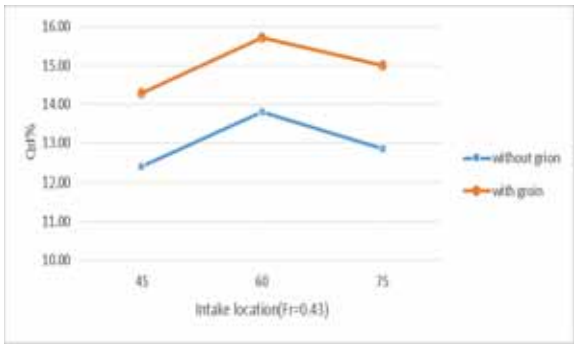

FIGURE 11
Results intake discharge rate with the Froude number=0.43

According to the diagram the simulation results can be well seen in the intake with location of 60° can have the highest rate of intake. This is because the separation of flow was minimized in simulation, so the stream lines were easier to entrance intake. Comparing the simulation results by physical model can be found, the simulations have been performed with high accuracy. To compare the simulation results with respect to the physical model, we find that the simulation is performed with high accuracy and intake with 60 degree location is the highest diversion rate. Also in both of figures the effect of adding groin structures is completely clear, in other words adding epi structure causes to move streamlines to intake, so the rate of diversion discharge is increased. Figure 10, 11.

CONCLUSION

This paper investigates the steady pattern of bend River flow as well as variations of location of intakes and adding epi in front of intakes in bend of rivers due to two discharges events and 3 locations of intakes using CCHE2D. It was found that velocity, Froude number and shear stress for 2 discharges. It was also found that diversion rate for 2 discharges and 3 location before adding epi and after it. The dominant phenomenon in 60 degree causes to conveyance water to intake entrance. Conclusions which can be drawn from this research through investigating and analyzing the above tables and figures are as follows: In this research, after identification of significant and effective parameters affecting discharge rate of intakes with different location using CCHE2D methods and finally performing about 24 tests on intakes with range of discharges, it reached the following results, Results of this research are summarized as follows:

1. Diversion rate: intakes with location of 60 degree have the highest rate of diversion rate.
2. Effect of Epi : also intakes with groin (Epi) has more percentage of diversion rate intakes than toward without it.
3. The intakes, with a location 60 degrees with approximate high diversion rate of least percent of energy loss best designed and implemented. In general, it can be observed that increase or decrease angle than 60° causes to separate of flow.

ACKNOWLEDGEMENTS

This paper is taken from sabbatical project conducting by Amir Abbas Kamanbedast. The authors wish to thank the Ahvaz Branch, Islamic Azad University (IAU) for the financial support. The authors would like to thank all the editors, reviewer, and University of Malaya for their comment in the development and improvement of this paper.

REFERENCES

[1] Abbasi, S., Kamanbedast, A.A. and Ahadian, J. (2011) Numerical Investigation of Angle and Geometric of L-Shape Groin on the Flow and Erosion Regime at River Bends. World Applied Sciences Journal. 15 (2), 279-284.
[2] Abdoshah Nejhad, A. (2010) Determination of flood plain in river with CCHE2D model. Master Thesis, Islamic Azad University, Ahvaz branch, Iran.
[3] Aziaian, A., Gholizadeh, M. Amiri Tokaladany, E. (2010) Simulation of meandering rivers migration processes using CCHE2D. In the proceedings of the 8th International River Engineering Conference, Iran.
[4] Elyasi, M. and Kamanbedast A.A. (2014) The Effect of Angle of Intakes on Diversion sediments in River Bend with CCHE2D Model. Advance in environmental biology. AENSI Journal. 8(22), 180-186.

[5] Faghiholislam Jahromi, A. and Mosavi Jahromi, S.H. (2010) Simulation of flow and sedimentation patterns in 180o River bends using CCHE2D. In the proceedings of the 8th International River Engineering Conference, Iran.
[6] Fazli, M. and Ghodsian, M. and Neyshabouri, S.A.A. (2008) Scour and flow field around a spur dike in a 90° bend. International Journal of Sediment Research. 23(1), 56-68.
[7] Forozam, F. and Karimy Pasha, M.H. (2010) Hydrodynamic Simulation of unsteady flow in rivers using CCHE2D. In the proceedings of the 2nd National Conference on Water, Iran.
[8] Geravandi, E., Kamanbedast, A.A., Masjedi, A., Heidarnejad, M., Bordbar, A. (2018) Laboratory investigation of the impact of armor dike simple and L-shape in upstream and downstream intake of the hydraulic flow of the Kheirabad River to help physical model. Fresen. Environ. Bull. 27, 263-276.
[9] Ghodsian, M. and Vaghefi, M. (2009) Experimental study on scour and flow field in a scour hole around a T-shape spur dike in a 90° bend. International Journal of Sediment Research. 24(2), 145–158.
[10] Kamanbedast, A.A., Nasrollahpour, R. and Mashal, M. (2013) Estimation of Sediment Transport in Rivers Using CCHE2D Model (Case Study: Karkheh River). Indian Journal of Science and Technology. 6(2), 4112-4115.
[11] Kamanbedast, A.A., Ghahremani, A. (2014) Evaluation of Scour Around Bridge Pile in Flood with Hec-Ras Software. Journal of River Engineering, 2.
[12] Kamanbedast, A. (2012) The Investigation of Discharge Coefficient for the Morning Glory Spillway Using Artificial Neural Network. World Applied Sciences Journal. 17(7), 913-918.
[13] Matinfard, A., Heidarnejad, M., Ahadian, J. (2013) Effect of Changes in the Hydraulic Conditions on the Velocity Distribution around a L-Shaped Spur Dike at the River Bend Using Flow-3D model. Tech J Engin &App Sci., 13(6), 1862-1868.
[14] Marelius, F., Sinha, S.K. (1998) Experimental Investigation of Flow Past Submerged Vanes. Journal of Hydraulic Engineering, ASCE. 124(5), 542-545
[15] Masjedi, A., Shafai.M. and Rahnavard, P. (2010) Reduction of Local at Single T- Shape Spour Dike Whit Wing Shape in a 180 Degree Flume Bend. World Applied sciences Journal. 8(9), 1122-1128. Issn 1818- 4952.
[16] Masjedi, A., Shafai Bejestan, M. and Moradi, A. (2010) Experimental study on the time development of local scour at a spur dike in a 180° flume bend. Journal of Food, Agriculture & Environment. 8(2), 904-907.
[17] Rouzegar, J., Kamanbedast, A.A., Masjedi, A., Heidarnejad, M., Bordbar, A. (2017). The Experimental Investigation of Flow Hydraulics In Zigzag Morning Glory Spillways. Fresen. Environ. Bull. 26, 2389-2396.
[18] Saki, A., Kamanbedast, A.A., Masjedi, A., Heidarnejad, M., Bordbar, A. (2017) A newly designed rectangular weir for flow regulation at river fork through a physical model (case studies of karkheh/hufel/nissan streams). Fresen. Environ. Bull. 26, 7400-7410.
[19] Shahidan, N. F., Hasan, Z. A., Abdullah, M. Z., & Ghani, A. A. (2012). Mathematical Modelling of Flow and Sediment Pattern at Ijok Intake, Ijok River, Perak, Malaysia. International Journal of Modelling and Simulation, 32(3), 165-170.
[20] Shirali, M., Kamanbedast, A.A., Masjedi, A., Bordbar, A., Heidarnejad, M. (2017) An experimental investigation on the effects of the shape of the cross section in morning glory spillways. Fresen. Environ. Bull. 26, 6532-6542.
[21] Taebi, H., Shafai Bajestan, M. and Kaheh, M. (2010) Simulation of flow in 90o bends using CCHE2D software. In the proceedings of the 8th International River Engineering Conference, Iran.
[22] Zeraat, B., Heidarnejad, M., Masjedi, A., Kamanbedast, A., Hasoonizadeh, H. (2017) Hydraulics of Arch Plan Labyrinth Weirs with Two Different Cycles. Fresen. Environ. Bull. 26, 2862-2867.
[23] Zhang, Y. (2005) CCHE2D-GUI-graphical user interface for the CCHE2D model. Technical Report No. NCCHE-TR-2005-03, University of Mississippi.

Received: **09.03.2017**
Accepted: **14.08.2017**

CORRESPONDING AUTHOR

Amir Abbas Kamanbedast
Department of Water Science and Engineering, Ahvaz Branch,
Islamic Azad University,
Ahvaz, Iran

e-mail: ka57_amir@yahoo.com

© by PSP Volume 27 – No. 2/2018 pages 815-819 Fresenius Environmental Bulletin

OXIDATION OF PHENOLIC WASTEWATER WITH $KHCO_3$ ADDITION IN SUPERCRITICAL WATER

Fu Yuan[1,*], Li Tiejun[2]

[1] Department of Chemical Engineering. Inner Mongolia Chemical Engineering Professional College, Huhhot 010070, China
[2]Marine Fisheries Research Institute of Zhejiang Province, Scientific Observing and Experimental Station of Fishery Resources for Key Fishery Grounds, Ministry of Agriculture, Zhejiang Province Key Laboratory for Technology Research on Sustainable Utilization of Marine Fishery Resources, Zhoushan 316021, China

ABSTRACT

Phenolic wastewater is a typical kind of industrial effluents with high toxicity and poor biodegradability. Huge quantities of phenol-polluted waters are formed from many chemical operations including coking, coal gasification, oil refineries, plastics, pesticides, steel and phenolic resin production. This paper deals with treating high phenol-concentrated wastewater by supercritical water oxidation (SCWO) method. The effects of H_2O_2 dosage, reaction time, temperature, and concentration of $KHCO_3$ on removal efficiency of phenol were studied with laboratory bench-scale experiments. The results indicated that the removal process was more effective under the experimental conditions. The best removal efficiency of phenol reached 99.8%. This investigation will provide fundamental method for developing a pretreatment method of industrial phenolic wastewater with flexibility, simplicity and high activity.

KEYWORDS:
Supercritical water oxidation, Phenolic wastewater, $KHCO_3$, Removal

INTRODUCTION

Phenolic wastewater is a typical kind of industrial effluents with high toxicity and poor biodegradability. Huge quantities of phenol-polluted waters are formed from many chemical operations including coking, coal gasification, oil refineries, plastics, pesticides, steel and phenolic resin production [1, 2]. Phenolic compounds and their derivatives are considered preferred controlled pollutants in water since they can pose a severe health hazard as mutagens and carcinogens and cause serious damage to aquatic animals and microorganisms even at low concentrations [3–6]. Various species of phenolic pollutants at high concentrations from hundreds to thousands mg/L are identified in the industrial wastewaters especially from heavy chemical or petrochemical industries. Once released into the environment, they may have adverse effects on ecological health and represent a serious environmental problem [7]. Therefore, removal of phenolic compounds from wastewater becomes urgent in the field of practical industrial wastewater treatment.

Traditionally, efficient treatment of phenolic wastewater can be conducted by either conventional physical-chemical [8, 9] or biological techniques [10]. However, these treatments are very complex and expensive. This situation is triggering the development of new treatment technologies for phenolic wastewater, especially technologies claiming a small production of additional waste sludge [11].

Supercritical water oxidation (SCWO) shows a substantial promise for clean and efficient decontamination of many aqueous organic wastes [12–15]. SCWO can rapidly and efficiently destroy organic substances into H_2O and CO_2 in significantly short residence times.

The ability of an oxygenate additive to enhance the oxidation rate of a targeted organic compound an mixtures is well known in combustion [16], but only recently have several studies showed similar effects in SCWO reactions [17-19]. In SCWO, the oxidation mechanism is assumed to be similar with that involved in combustion and the former process can take advantage of the vast scientific database of the latter.

In this work, the treatment of the phenolic wastewater is performed using hydrogen peroxide as an oxidant in a flow reactor at sub- and supercritical conditions of water. We report experimental oxidation results of the phenolic wastewater via SCWO, and to examine the feasibility of the technology as a pre-treatment for biological remediation to reduce toxic organic compounds. The effects of H_2O_2 dosage, reaction time, temperature, and concentration of $KHCO_3$ on removal efficiency of phenol were studied.

MATERIALS AND METHODS

Characteristics of phenolic wastewater. The phenolic wastewater sample is taken from a gasification plant, China. The main characteristics are intensive violet-dark brown color, strong specific offensive smell, a large number of bubbles and high degree of organic pollution. Some relevant indices of

water quality are shown in Table 1.

Experimental Procedure. The general set up of the system including the SCWO reactor is shown in Fig.1.

SCWO experiments were performed in a continuous-flow reactor system. The oxidant feed stream was prepared by dissolving hydrogen peroxide with deionized water in a feed tank. Another feed tank was loaded with the phenolic wastewater. The two feed streams were pressurized in two different lines using two high-pressure pumps and then they were separately pre-heated, until the reactor temperature had reached the desired value (±0.1 ◦C). After pre-heating, two lines were mixed at the reactor inlet using a mixing tee. Upon exiting the reactor, the effluent was cooled rapidly by passing through a heat exchanger. Afterwards the particles, which would be formed presumably, were filtered out by a 0.5 min line filter, before the effluent was depressurized by a back-pressure regulator. The flow rates of the oxidant and wastewater were ranged from 1 to 7 mL/min at pump conditions. The system pressure was maintained at desired pressures (±0.1MPa) by the back-pressure regulator. The product stream was then separated into liquid and vapor phases. The liquid products were collected in a graduated cylinder.

TABLE 1
Some water quality indices of phenolic wastewater from coal gasification

Water quality index	Original wastewater
Total phenols (mg/L)	1000
Chemical oxygen demand (COD, mg/L)	6000
Biochemical oxygen demand (BOD, mg/L)	120
BOD/COD	0.02
pH	7.45

RESULTS AND DISCUSSION

Effect of temperature and reaction time on phenol removal. The results are presented in Fig. 2. As it is expected, rising temperature increased the phenol removal. Phenol removal reached about 82 and 93% after 1 and 9 min at 445°C, respectively. Therefore, temperature had a significant impact on the oxidation of phenolic wastewater.

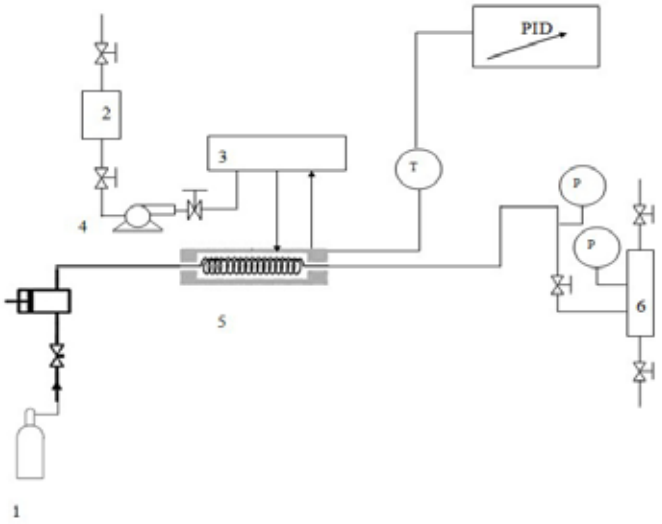

FIGURE 1
Schematic diagram of the experimental setup
1. Nitrogen tank 2. Oxidant tank 3. Heater 4. High pressure pump 5 Reactor. 6 Gas-liquid separator; PID: Proportional Integral Derivative

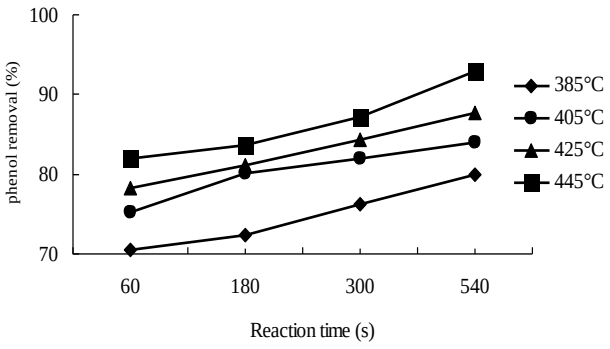

FIGURE 2
Effect of temperature and reaction time on phenol removal

That is because when the temperature increased, the reaction rate accelerated. Eventually, it led to increasing oxidation rates of organic matter degradation of phenolic wastewater. Therefore, it is shown that phenol removal increases when temperature increases.

Fig. 2 showed phenol removal for SCWO of phenolic wastewater at different temperatures. The results appeared that reaction time had a significant effect on phenol removal of phenol wastewater. Within each set of isothermal experiments, the phenol removal increased rapidly during the first 1 min of reaction and slowed down afterwards.

Effect of H_2O_2 dosage on phenol removal. Fig. 3 shows that phenol removal is affected by H_2O_2 dosage. The phenol removal increased with increasing H_2O_2 dosage from Fig. 3, the COD removal increasing trend is gentle when H_2O_2 dosage is over 5000mg/L, so the appreciate H_2O_2 dosage is 5000mg/L.

Effect of $KHCO_3$ on phenol removal. Table 2 shows the phenol removal of phenolic wastewater in supercritical water oxidation in relation to the effect of temperature from 385°C to 445°C without $KHCO_3$, or with $KHCO_3$. Experimental results show that the phenol removal increased with the increasing reaction temperature.

Experimental results show that the supercritical water oxidation of phenolic wastewater system by adding a small amount of $KHCO_3$ can raise the phenol removal. The high concentration of phenol causes an increase in the phenol removal when temperature is 445°C, reaction time is 540 s, and H_2O_2 dosage is 5000 mg/L from 90.8% without $KHCO_3$ present to 99.8% with 50 mg/L of $KHCO_3$, the phenol removal increases 9%.

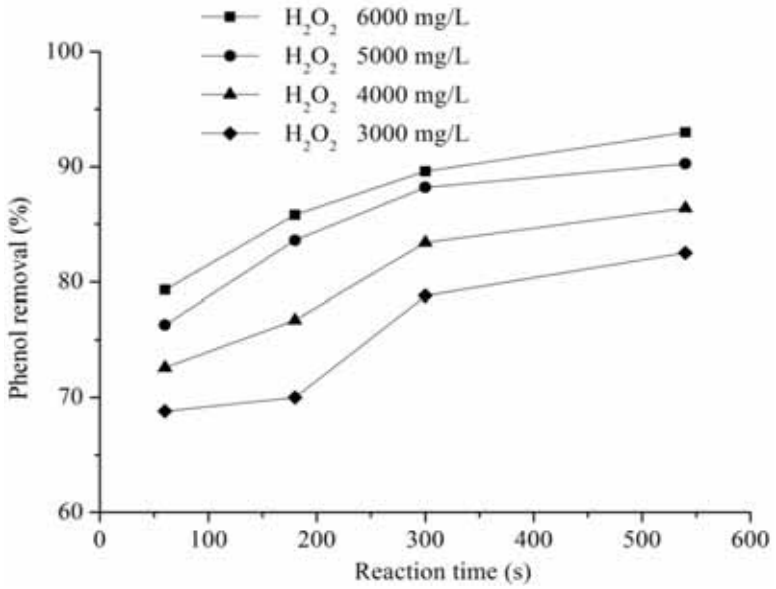

FIGURE 3
Effect of H_2O_2 dosage on phenol removal

TABLE 2
Effect of glycol on phenol removal

Temperature (°C)	H_2O_2 dosage (mg/L)	Reaction time (s)	Phenol removal without $KHCO_3$ (%)	Phenol removal with 50 mg/L of $KHCO_3$ (%)
385	5000	60	70.66	70.97
		180	71.43	73.54
		300	75.23	79.55
		540	78.89	81.63
405	5000	60	75.24	76.41
		180	80.16	84.65
		300	82.56	85.96
		540	82.89	86.52
425	5000	60	80.57	83.88
		180	81.35	88.66
		300	84.64	91.63
		540	89.63	96.64
445	5000	60	81.77	88.65
		180	83.78	90.97
		300	87.46	93.97
		540	90.8	99.8

CONCLUSIONS

This paper deals with treating high phenol-concentrated wastewater by supercritical water oxidation (SCWO) method. The effects of H_2O_2 dosage, reaction time, temperature, and concentration of $KHCO_3$ on removal efficiency of phenol were studied with laboratory bench-scale experiments. Experimental results indicated that in the SCWO process, 90.8% phenol removal was obtained after 540s at temperature of 445°C, H_2O_2 dosage of 5000 mg/L. Adding the $KHCO_3$ accelerates the destruction of phenolic wastewater. The best removal efficiency of phenol reached 99.8%.

ACKNOWLEDGEMENTS

This work was supported by the Science and technology project of Zhejiang Province (Grant No. 2014F30024).

REFERENCES

[1] Fajardo, A.S., Rodrigues, R.F., Martins, R.C., Castro, L.M. and Quinta-Ferreira, R.M. (2015) Phenolic wastewaters treatment by electrocoagulation process using Zn anode. Chem Eng. J 275, 331-341.

[2] Shokri, A., Mahanpoor, K. and Soodbar, D. (2016) Degradation of 2-nitrophenol from petrochemical wastewater by UV/$NiFe_2O_4$/ Clinoptilolite process. Fresen. Environ. Bull. 25, 500-508.

[3] Peng, R.C., Yu, P. and Luo, Y.B. (2016) A comparative study of Fenton and electro-Fenton treatment for COD removal from coking industry wastewater. Fresen. Environ. Bull. 25, 3987-3992.

[4] Bazrafshan, E., Biglari, H. and Mahvi, A.H. (2012) Phenol removal by electrocoagulation process from aqueous solutions. Fresen. Environ. Bull. 21, 364-371.

[5] Cavalieri, E., Li, K., Balu, N., Saeed, M., Devanesan, P., Higginbotham, S., Zhao, J., Gross, M. and Rogan, E. (2002) Catechol ortho-quinones: the electrophilic compounds that form depurinating DNA adducts and could initiate cancer and other diseases. Carcinogenesis. 23, 1071-1077.

[6] Bukowska, B., Michalowicz, J., Krokosz, A. and Sicinaska, P. (2007) Comparison of the effect of phenol and its derivatives on protein and free radical formation in human erythrocytes (in vitro). Blood Cell Mol Dis. 39, 238-244.

[7] Szabó, E., Zügner, G.L., Farkas, M., Szilágyi, I. and Dóbé, S. (2012) Direct Kinetic Study of the OH-radical Initiated Oxidation of Pivalaldehyde, $(CH_3)_3CC(O)H$, in the Gas Phase. Oxid Commun. 35, 538-544.

[8] Orak, H.H., Karamac, M. and Amarowicz, R. (2015) Antioxidant Activity of Phenolic Compounds of Red Bean (Phaseolus vulgaris L.). Oxid Commun. 38, 67-76.

[9] Zilli, M., Converti, A., Lodi, A., del Borghi, M. and Ferraiolo, G. (1993) Phenol removal from waste gases with a biological filter by Pseudomonas putida. Biotechnol Bioeng. 41, 693-699.

[10] Moussavi, G., Mahmoudi, M. and Barikbin, B. (2009) Biological removal of phenol from strong wastewaters using a novel MSBR. Water Res. 43, 1295-1302.

[11] González, G., Herrera, M.G., García, M.T. and Peña, M.M. (2001) Biodegradation of phenol in a continuous process: comparative study of stirred tank and fluidized-bed bioreactors. Bioresour Technol. 76, 245-251.

[12] Zhao, X.J., Wu, X.M. and Zhang, W.X. (2015) Gasification of Petrochemical Sludge in Supercritical Water for Hydrogen Production. Oxid Commun. 38, 175-182.

[13] Zhang, Y.R., Zhang, L.J. and Zhao, T.T. (2015) Supercritical Water Gasification of Oily Wastewater. Oxid Commun. 38(2), 803-807.

[14] Yan, Z.Y. and Tan, X.Y. (2015) Hydrogen generation from oily wastewater via supercritical water gasification (SCWG). Journal of Industrial and Engineering Chemistry. 23, 44-49.

[15] Lv, W.Y. and Shuang, H.Q. (2015) Oxidation of Phenolic Wastewater with Glycol in Supercritical Water. Oxid Commun. 38, 796-802.

[16] Yakaboylu, O., Harinck, J., Smit, K.G. and de Jong, W. (2015) Testing the constrained equilibrium method for the modeling of supercritical water gasification of biomass. Fuel Processing Technology. 138, 74-85.

[17] Civan, F., Özaltun, D.H., Kıpçak, E. and Akgün, M. (2015) The treatment of landfill leachate over Ni/Al_2O_3 by supercritical water oxidation. The Journal of Supercritical Fluids. 100, 7-14.

[18] Dong, X.Q., Gan, Z.D., Lu, X.L., Jin, W.Z., Yu, Y.Z. and Zhang, M.H. (2015) Study on catalytic and non-catalytic supercritical water oxidation of p-nitrophenol wastewater. Chem Eng J. 277, 30-39.

[19] Lu, Y.D. and Savage, P.E. (2015) Supercritical water gasification of lipid-extracted hydrochar to recover energy and nutrients. Journal of Supercritical Fluids. 99, 88-94.

Received: **28.03.2017**
Accepted: **21.06.2017**

CORRESPONDING AUTHOR

Fu Yuan
Department of Chemical Engineering.
Inner Mongolia Chemical Engineering
Professional College,
Huhhot 010070 – China

e-mail: liyanxia12009@163.com

© by PSP Volume 27 – No. 2/2018 pages 820-830 Fresenius Environmental Bulletin

MARINE BIOLOGICAL QUALITY ASSESSMENT AND ECOLOGICAL ENVIRONMENT SURVEY IN THE BOHAI BAY, CHINA

Wenliang Zhang[1,2], Haijiao Liu[3],Chao Wu[3], Jun Sun[4, 5,*]

[1]School of Environmental Science and Engineering, Tianjin University, 300072 Tianjin, China
[2]Tianjin Bohai Marine Monitoring and Surveillance Management Center, 300480 Tianjin, China
[3]Institute of Marine Science and Technology, Shandong University, 27 Shanda Nan Road, Jinan 250110, China
[4]Tianjin Key Laboratory of Marine Resources and Chemistry, Tianjin University of Science and Technology, Tianjin 300457, China
[5]College of Marine and Environmental Sciences, Tianjin University of Science and Technology, Tianjin 300457, China

ABSTRACT

This study discussed and assessed the 12 biological quality elements (heavy metals and persistent organic pollutants, POPs) in marine commercial organism residues and its adjacent area of ecological environment in the Bohai Bay (BB) undertaken in 2007 and 2009 spring and autumn. Benthos was prominently dominated by the mollusc, and followed by crustacean, polychaetes, and echinoderm. Dominant phytoplankton was *Skeletonema*, *Ditylum brightwelli*, *Nitzschia longissima*, *Thalassiosira excentrica*, *Thalassiosira rotula*, etc. The abundant chain-formed *Skeletonema* is typically considered as a biological indicator of water quality, particularly, in relation to coastal environmental pollutions. 5 and 12 commercial species were detected in 2007 spring and autumn survey respectively and assessed by single factor pollution index method. The investigation of pollutant residual levels within these commercial organisms in BB indicated that heavy metals such as Cd, Cu, Zn, Pb, and Cr were extremely over-standard (type I standard). This investigation and assessment have vital importance for recognizing marine environment status and commercial organism health in the coastal region.

KEYWORDS:
Heavy metal, commercial organism, biological quality, pollutant, assessment, Bohai Bay.

INTRODUCTION

Semi-enclosed systems are invariably suffered multiple stressors with increasing urbanization and industrialization [1]. Coastal zones connecting terrene and sea have experienced serious pollution discharged by the river into the sea since last ten years [2, 3]. They act as filters holding diverse elements and compound, afterwards, threaten the indigenous biocenose and water health [4]. As the only semi-enclosed system in China, the Bohai Bay is situated in a multi-river environment, especially influenced by the Haihe River and the Yongding River [5-7]. The eutrophication of Bohai Bay is accelerated in decade years, which is closely related to the human activities and global climate change [8-9]. As one of a staple industrial base of China, Tianjin has been built into the national 11th five-year program, with all this going on, the environmental problem comes along [10].

Many trace metals act as a micronutrient for marine organisms, but toxic and harmful to their metabolic growth under excessive quantities [11]. Ag (silver), Cd (cadmium), Cr (chromium), Cu (copper), Hg (mercury), Pb (plumbum), Ni (nickel) and Zn (zinc) are classified as heavy metals. Heavy metals in coastal ecosystems can be accumulated from sediments, subsequently accumulated (biological magnification) and converted by marine organisms [12, 13]. Besides heavy metals, DDT (2,2-bis-(chlorophenyl)-1,1,1-trichloroethane), persistent organic pollutants (POPs), e.g., PAHs (polycyclic aromatic hydrocarbon) and PCBs (Polychlorinated Biphenyl), can also be bioaccumulated through marine organisms at the different trophic level and pose a great risk to aquatic ecosystem [14-17]. All the pollutants act as indicators for evaluating environment status and guiding of restoration engineering [18]. There are several studies reporting the pollutants in surface sediments, yet relatively few concerning those matters in the water body in the Bohai Bay [14, 19, 20].

As one of the most contaminated coastal city in China, Tianjin captures more and more interests and attentions. The comprehensive survey and assessment on the Bohai Bay is a critical component for marine coastal comprehensive studies of China, aimed at supplying authentic and reliable marine environment and resource information, specifically, has profound realistic and historical significances on accelerating marine ecological development.

Knowledge of the status of marine resources, water quality, can shed light on the management of the coastal ecological environment and sustainable development of Tianjin marine economy. The present work helps us better understand the environmental status of marine resources in the Bohai Bay

[21]. By investigating of the chemical status of Tianjin marine environment factors, especially the status of marine pollution, provide basic data and foundation for marine economic development, the use of sea areas, marine policies and regulations as well as the development of marine environmental protection, sustainable use of marine resources and marine macro-managements.

MATERIALS AND METHODS

Survey area. Regional setting was performed in the Bohai Bay. Specific survey area lied in the Bohai Bay inshore shallower than 10 m isobath, a total of 45 sites during 4 cruises were investigated for marine biological quality and ecological environment, as illustrated in Figure 1.

Survey parameters. Commercial marine organisms and their pollutant residuals were collected in 2007 spring and autumn in BB, meanwhile, their adjacent area of ecological environment was also investigated in 2009 spring and autumn, including heavy metal in water, chlorophyll *a*, plankton abundance and biomass and primary productivity; survey analysis has two parts, field investigation and laboratory analysis. Pollutant residuals include: petroleum, heavy metals (mercury, cadmium, lead, zinc, arsenic, copper, chromium), BHC (666, benzene hexachloride), DDT (dichlorodiphenyltrichloroethane), PCBs, PAHs.

Sampling method and preservation. All organisms sampled were washed by field seawater and enclosed by polyethylene plastic, marked, and kept refrigerated, till back to the laboratory, body length and shell length were measured by vernier caliper and weighed by electronic scales. Then, soft tissues and body fluids were taken after processing dissection, and put into polyethylene plastic, marked, and kept refrigerated. During the sampling, any operation resulting in contamination should be avoided as much as possible.

Prior to analysis, frozen organism samples thawed at room temperature, and was minced homogenates by high-speed tissue masher, each 500 g was put into 500 ml wild-mouth bottle till to be analyzed. Pollutants residue analysis was in accordance with the 'technical protocols' (GB17378.6) monitoring standards, biometric analysis method, as shown in Table 1.

Quality control. Quality management agencies were established to be responsible for the overall quality management and system formulation, quality supervision, inspection procedures, and system implementation.

Personnel and equipment must meet the following requirements: examination certificate. ① All analysts must pass the examination qualified, and possess a national grade examination certificate. ② Analytical instruments and equipment should be approved by the relevant measure departments and used within test period. ③ Laboratories which undertake sample analysis, possess Grade A quality certification certificate.

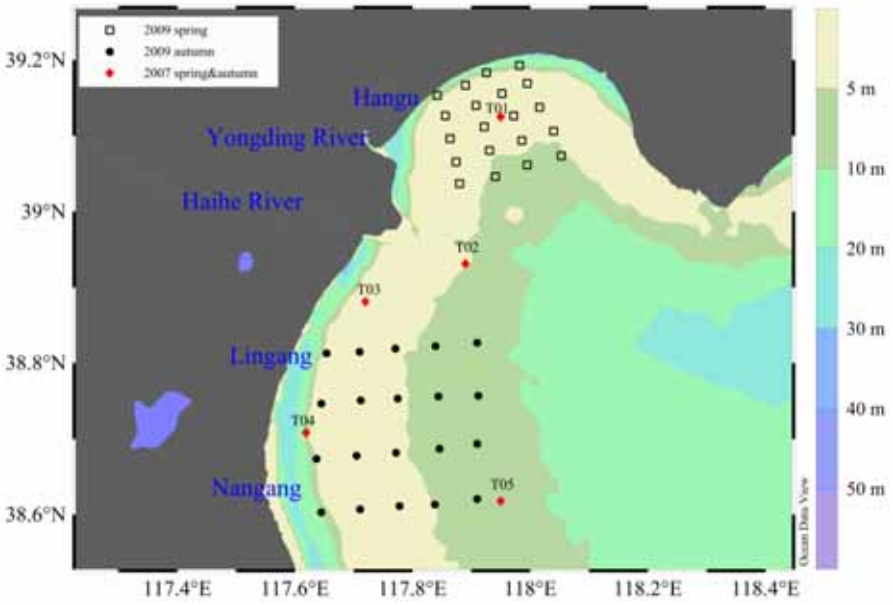

FIGURE 1
Location of sampling sites in the Bohai Bay during 4 cruises. Note: marine biological quality analysis was conducted in 2007 spring and autumn shown as those five red diamond; black square and dots represented various background parameters of the local ecological environment.

TABLE 1
Sample measurements of the marine biological quality

No.	Factors	Method	Detection limit	Reference
1	Petroleum	UV spectrophotometer	3 μg/g	GB17378.5
2	As	Atomic fluorescence Spectrometer	0.06 μg/g	GB12763
3	Hg	Atomic fluorescence spectrometer	--	GB12763
4	Cu	Flameless atomic absorption spectrophotometry	0.5 μg/g	GB17378.5
5	Pb	Flameless atomic absorption spectrophotometry	1.0 μg/g	GB17378.5
6	Cd	Flameless atomic absorption spectrophotometry	0.04 μg/g	GB17378.5
7	Zn	Flameless atomic absorption spectrophotometry	6.0 μg/g	GB17378.5
8	Cr	Flameless atomic absorption spectrophotometry	2.0 μg/g	GB17378.5
9	BHC	Gas chromatography	23.8～52.1 pg/g	GB17378.5
10	PCBs	Capillary column gas chromatography	29.2～67.5 pg/g	GB17378.5
11	PAHs	Capillary column gas chromatography	0.51～7.06 ng/g	GB17378.5

TABLE 2
Sampling record of marine biological quality.

Site	Species	Date	Weight (G)	Shell high (MM)	Body length (MM)	Total catch (Kg)
T01	*Oratosquilla oratoria*	9th May	30.5	-	113.5	6.15
T01	*Saccostrea cucullata*	9th May	45.6	25	-	15
T01	*Rapana venosa*	9th May	5.0-57.8	18-45	-	5
T02	*Octopus variabilis*	29th May	11.0-16.0	30-35	-	3.6
T05	*Scomberomorus niphonius*	23rd May	667	-	350	16
T03	*Mactra quadrangularis*	30th May	9.03	1.93	-	2
T04	*Bullacta exarata*	30th May	9.4-11.8	18-20	-	1.5
T04	*Mactra quadrangularis*	5th Nov	9.3	2.81	-	-
T04	*Neverita didyma*	5th Nov	4.5	2.27	-	-
T03	*Synechogobius hasta*	5th Nov	156	-	32	3
T02	*Rapana venosa*	5th Nov	76.8	68.10	-	4
T02	*Charybdis japonica*	5th Nov	123.1	59.5	-	4
T02	*Synechogobius hasta*	5th Nov	153.8		31.7	3
T01	*Scapharca subcrenata*	6th Nov	22.5	34.6		5
T01	*Odontamblyopus rubicundus*	6th Nov	44	-	30.8	1.5
T01	*Saccostrea cucullata*	6th Nov	48	27	-	15
T01	*Octopus variabilis*	6th Nov	144.4	-	-	3
T05	*Lateolabrax japonicus*	5th Nov	361.9	-	299.2	2
T05	*Oratosquilla oratoria*	5th Nov	34.5	-	143.5	13

Note: shellfish and crab were measured as weight and shell height; fish and shrimp were measured as weight and body length; *Octopus variabilis* was measured as weight and ketone body lengths.

Sample determination according to the following provisions: ① Instructions of "the Specification for Marine Monitoring (GB 17378.6) were regarded as standard methods. ② Prescribed format should be followed for a data record and measurement results calculation when sample determined. ③ 10% samples were selected randomly for two-sample measurements, with assurance to meet the requirements; ④ Adding 10% biological standard materials into the batch samples for contrast analysis, guarantee the accuracy of sample analysis.

RESULTS AND DISCUSSIONS

Ecological effects of the marine biological quality analysis. Biological residues are not only related to pollutant level, pollutant property, environmental factors such as temperature and salinity, etc., but also organism species, life stage and trophic level. Generally, bivalves body pollutant concentrations were positively correlated with ambient concentrations, while fish and crustaceans have an active enzyme system for xenobiotics degradation, some organic pollutants, such as PCBs with low concentration. Pollutants stability in organism body was expressed as half-life period, longer half-life period

made organic matter more difficult in the environment, they also retained in organism body for a very long time.

Marine animals can absorb pollutants directly from seawater, and also ingest contaminated food, suspended particles and deposited silt. It can be grouped into the following characteristics: ① smaller animals (or larvae) or lower trophic level organisms, direct pollutants absorption from the water is a major way; and larger animals or higher trophic level organisms always feed on pollutants; ② the same kind animal, has different ways to absorb varied pollutants; ③ under acute pollution, animals mainly absorb from the water; reversely, chronic pollution is more important for feeding ways; ④ when food is plentiful, absorption occurred in feeding way, reversely, them absorb pollutants from deposition.

Species composition of marine biological quality survey. Table 2 showed the commercial species composition identified in 2007. In 2007 spring, 7 species of commercial organisms were collected, they were *Mactra veneriformis*, *Bullacta exarata*, *Octopus variabilis*, *Rapana venosa*, *Saccostrea cucullata*, *Oratosquilla oratoria*, and *Scomberomorus niphonius*; the same year in autumn, 11 species were collected, namely *M. veneriformis*, *Scapharca subcrenata*, *Neverita didyma*, *O. variabilis*, *R. venosa*, *S. cucullata*, *O. oratoria*, *Charybdis japonica*, *Synechogobius hasta*, *Lateolabrax japonicus*, and *Odontamblyopus rubicundus*, specifically, *S. hasta* was found at station T03 and T02.

Residual levels in marine organisms. Pb, Cd, Hg, As, Cu, Zn, Cr, petroleum, BHC, DDT, PCBs, and PAHs, were detected in all organisms sampled at five sites of 2007 spring and autumn (Table 3-4). And their residual levels dependent on their different behaviours and ambient water quality.

TABLE 3
Marine organism residual levels in spring (fresh weight)

Station	Species	Petroleum (10^{-6})	Hg (10^{-6})	Cu (10^{-6})	Pb (10^{-6})	Zn (10^{-6})	Cd (10^{-6})
T04	*Bullacta exarata*	1.010	0.0013	22.97	0.0359	3.242	0.1153
T03	*Mactra quadrangularis*	4.720	-	8.040	0.5764	2.291	0.2908
T02	*Octopus variabilis*	3.419	0.0040	46.70	0.3018	22.73	1.623
T01	*Rapana venosa*	4.298	0.0102	36.91	0.0491	74.00	3.289
T01	*Saccostrea cucullata*	3.881	0.0017	89.05	0.0498	71.38	1.470
T01	*Oratosquilla oratoria*	2.040	0.0057	48.36	0.1214	7.283	2.815
T05	*Scomberomorus niphonius*	0.9997	0.0117	11.77	0.3705	-	0.2311
Maximum		4.720	0.0117	89.05	0.5764	73.95	3.289
Minimum		0.9997	0.0000	8.040	0.0359	0.0000	0.1153
Mean		2.910	0.0049	37.69	0.2150	25.84	1.404

Station	Species	Cr (10^{-6})	As (10^{-6})	666 (10^{-9})	DDT (10^{-9})	$\sum PCBs$ (10^{-9})	$\sum PAHs$ (10^{-9})
T04	*Bullacta exarata*	0.8754	0.0775	7.562	5.400	0.1789	135.3
T03	*Mactra quadrangularis*	1.6540	0.1403	3.196	-	5.936	62.76
T02	*Octopus variabilis*	0.6799	0.0108	12.73	-	-	45.29
T01	*Rapana venosa*	0.5614	0.0944	4.570	11.17	0.5914	71.28
T01	*Saccostrea cucullata*	0.6453	0.0503	1.683	4.583	0.0130	21.54
T01	*Oratosquilla oratoria*	0.5443	0.0299	1.748	3.699	-	93.57
T05	*Scomberomorus niphonius*	1.797	-	4.242	-	0.0920	90.79
Maximum		1.797	0.1403	12.73	11.17	5.936	135.3
Minimum		0.5443	0.0000	1.683	0.0000	0.0000	21.54
Mean		9.654	0.0576	5.105	3.550	0.9730	74.36

Note：“-” means undetectable

TABLE 4
Marine organism residual levels in autumn (fresh weight)

Station	Species	Petroleum (10^{-6})	Hg (10^{-6})	Cu (10^{-6})	Pb (10^{-6})	Zn (10^{-6})	Cd (10^{-6})
T04	*Mactra quadrangularis*	5.341	0.0028	3.320	0.2361	7.776	0.4340
T04	*Neverita didyma*	4.390	0.0038	37.26	0.3073	19.53	1.157
T03	*Synechogobius hasta*	2.081	0.0033	1.883	0.0222	4.756	0.0311
T02	*Rapana venosa*	4.210	0.0017	162.4	0.1431	155.1	11.92
T02	*Synechogobius hasta*	2.060	0.0404	1.402	0.0132	1.956	0.0264
T02	*Charybdis japonica*	2.480	0.0037	41.28	0.2379	41.28	2.577
T01	*Odontamblyopus rubicundus*	1.979	0.0098	2.032	0.0964	2.971	0.0257
T01	*Scapharca subcrenata*	5.460	0.0002	2.960	0.1196	8.729	2.502
T01	*Saccostrea cucullata*	6.969	0.0014	64.06	0.1113	95.81	2.299
T01	*Octopus variabilis*	4.670	0.0039	22.26	0.0599	22.36	0.8977
T05	*Lateolabrax japonicus*	1.969	0.0316	2.961	0.0706	4.944	0.0236
T05	*Oratosquilla oratoria*	3.880	0.0179	25.92	0.0871	25.11	4.006
Maximum		6.969	0.0404	162.4	0.3073	155.1	11.92
Minimum		1.969	0.0002	1.883	0.0132	1.956	0.0236
Mean		3.791	0.0100	30.65	0.1254	32.53	2.158

Station	Species	Cr (10^{-6})	As (10^{-6})	666 (10^{-9})	DDT (10^{-9})	$\sum$PCBs (10^{-9})	$\sum$PAHs (10^{-9})
T04	*Mactra quadrangularis*	0.7744	0.0436	5.795	1.292	5.899	173.9
T04	*Neverita didyma*	0.3537	0.0388	1.5430	2.095	2.183	69.90
T03	*Synechogobius hasta*	0.1736	-	-	1.447	1.995	196.0
T02	*Rapanavenosa*	0.2028	0.0954	0.2459	15.19	3.656	193.7
T02	*Synechogobius hasta*	0.1620	0.0003	0.0000	1.863	1.326	176.7
T02	*Charybdis japonica*	0.2946	0.0431	1.148	6.193	2.377	89.62
T01	*Odontamblyopus rubicundus*	0.0117	0.0010	0.0000	0.7530	0.9090	145.3
T01	*Scapharca subcrenata*	0.4092	0.0308	3.838	4.014	3.564	81.03
T01	*Saccostrea cucullata*	0.3638	0.0494	4.950	9.304	0.0000	390.1
T01	*Octopus variabilis*	0.1821	0.0099	3.477	18.70	3.682	98.00
T05	*Lateolabrax japonicus*	0.3625	0.0061	2.487	17.56	6.097	109.2
T05	*Oratosquilla oratoria*	0.1748	0.0367	0.7270	2.206	1.791	80.28
Maximum		0.7744	0.0954	5.795	18.70	6.097	390.1
Minimum		0.0117	0.0000	0.0000	0.7530	0.0000	69.90
Mean		0.2888	0.0296	2.018	6.718	2.790	150.3

Marine biological quality survey results and analysis in spring. Different heavy metals and POPs contents in 7 marine species were analyzed (data not shown). Cu and Zn levels showed different trends with the other heavy metals. And *R. venosa and O. oratoria* could accumulate higher Cd level. Overall, *B. exarata* has relatively lower accumulating ability to heavy metals, but the higher accumulating ability to PAHs related to their different ingestive behavior. This toxic organic compound is also popular in airborne particles and has an adverse effect on human health [22]. PCBs was relatively lower in organism body.

Marine biological quality survey results and analysis in autumn. Different heavy metals contents in 12 marine species were displayed in Figures 2-4. The first 8 species have higher heavy metal concentrations. PAHs still remains highest among POPs.

Ecological environment conditions in the ambient area of 2009 spring and autumn. In 2009 spring, benthos and plankton were surveyed in Hangu area. Their surface distributions were displayed in Figures 5-6. It can be seen that benthos richness matched well with its *H'* index value, and having lowest richness in inshore area. Figure 7 showed the distribution of benthos, phytoplankton and zooplankton in 2009 autumn. It turned out that Lingang area showed more abundant benthos and plankton that that of Nangang area. It revealed that large water discharge represented a major pollutant source. As a whole, benthos was prominently dominated the by mollusc and followed by crustacean, polychaetes, and echinoderm (data not shown).

Many observations on phytoplankton were accumulated in the Bohai Sea [23-25]. Dominant phytoplankton was *Skeletonema*, *Ditylum brightwelli*, *Nitzschia longissima*, *Thalassiosira excentrica*, *Thalassiosira rotula*, etc. The abundant chain-formed *Skeletonema* is typically considered as a biological indicator of water quality, particularly, in relation to coastal environmental pollutions. Actually, plankton examination has been an effective candidate for determining the water quality since the chemical method has various limits [26]. Besides, different heavy metals were detected as shown in Figures 8-9. The ambient heavy metal level had a direct effect on body residuals in the marine commercial organism. Most of them showed increasing concentration from offshore to the inshore area. Lingang and Nangang area were greatly influenced by Haihe River.

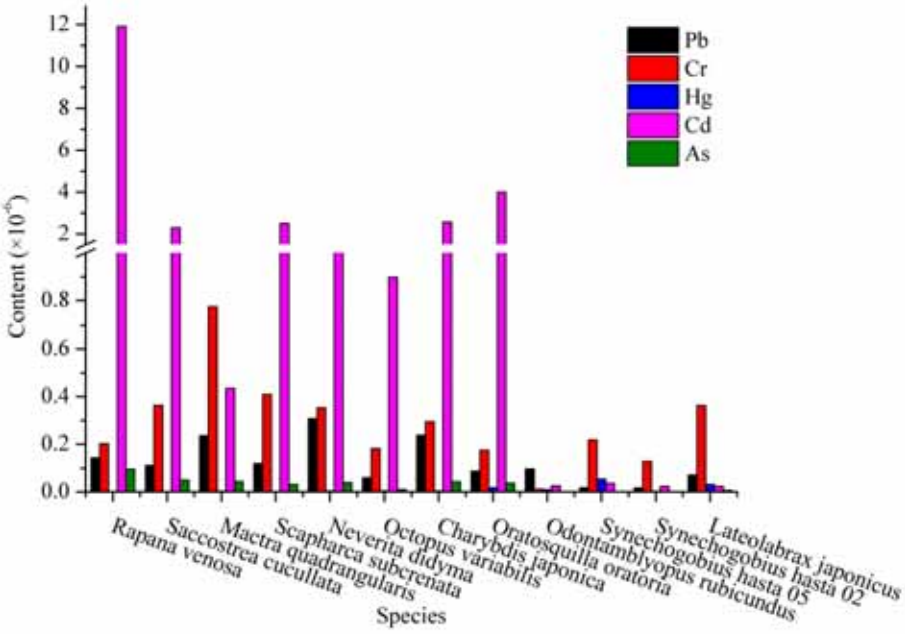

FIGURE 2
Pb, Cr, Hg, Cd, As residue levels and differences of 12 marine species in 2007 autumn

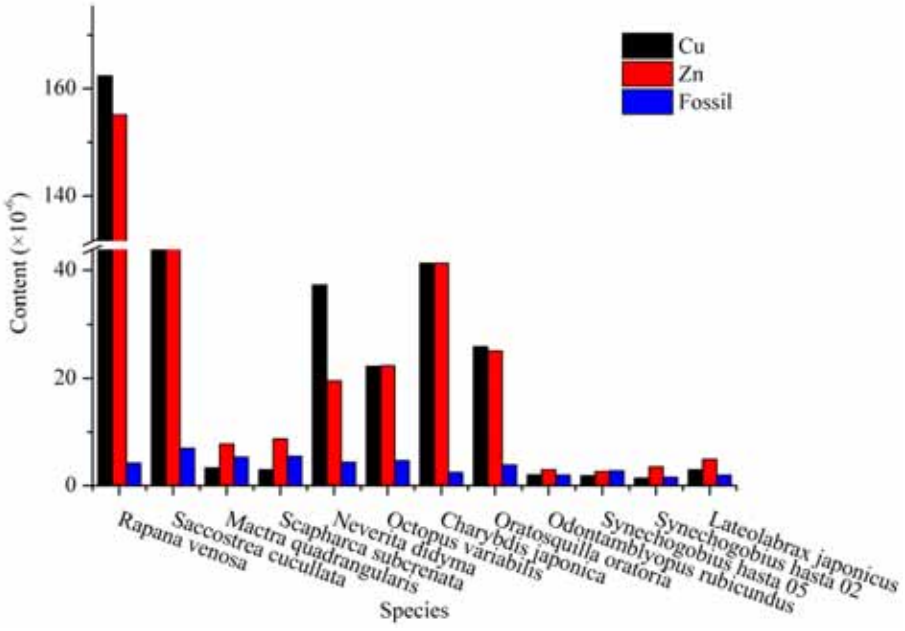

FIGURE 3
Cu, Zn and petroleum residue levels and differences of 12 marine species in 2007 autumn

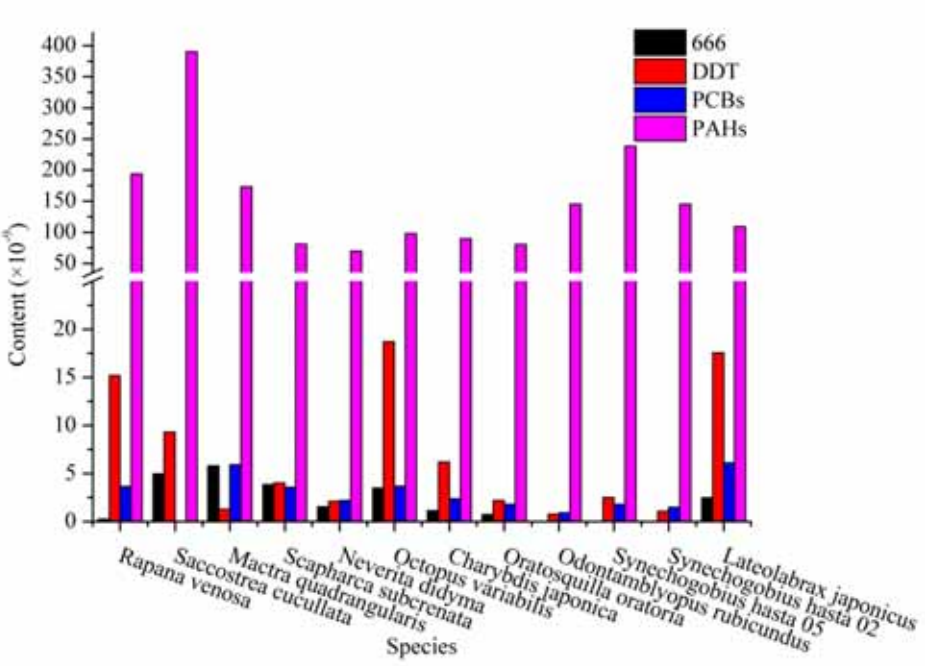

FIGURE 4
666, DDT, PCBs and PAHs residue levels and differences of 12 marine species in 2007 autumn

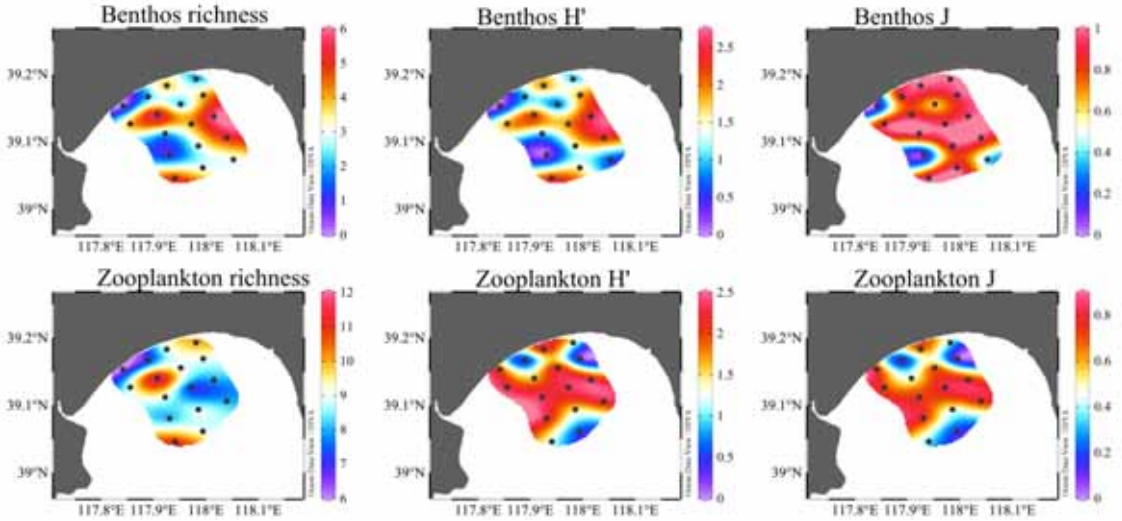

FIGURE 5
Benthos, zooplankton and their biodiversity indices distributions in 2009 spring cruise

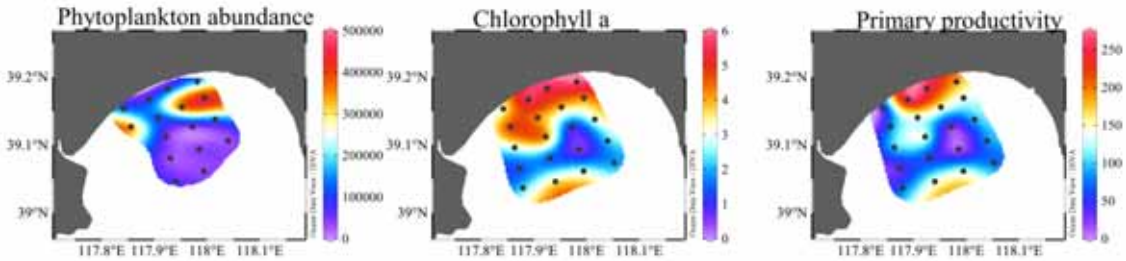

FIGURE 6
The distribution of phytoplankton abundance, chlorophyll *a* and primary productivity (PP) in 2009 spring cruise

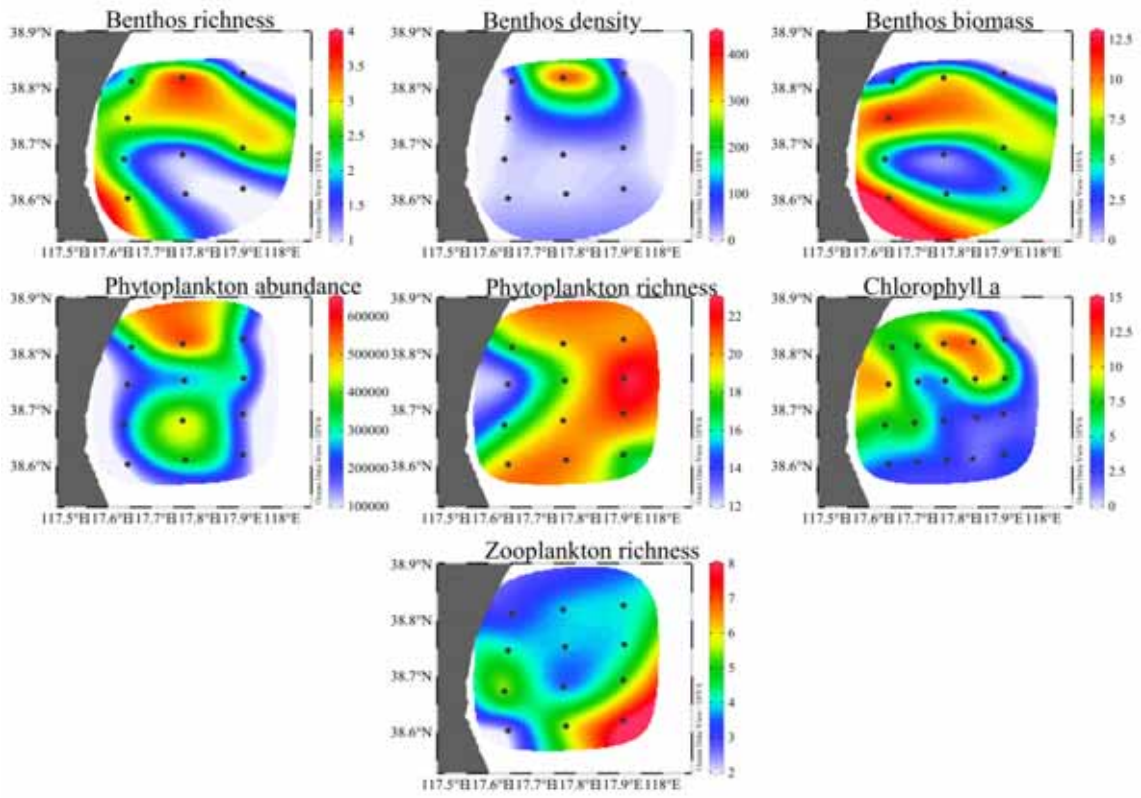

FIGURE 7
The distribution of benthos, phytoplankton, Chla and zooplankton in 2009 autumn cruise

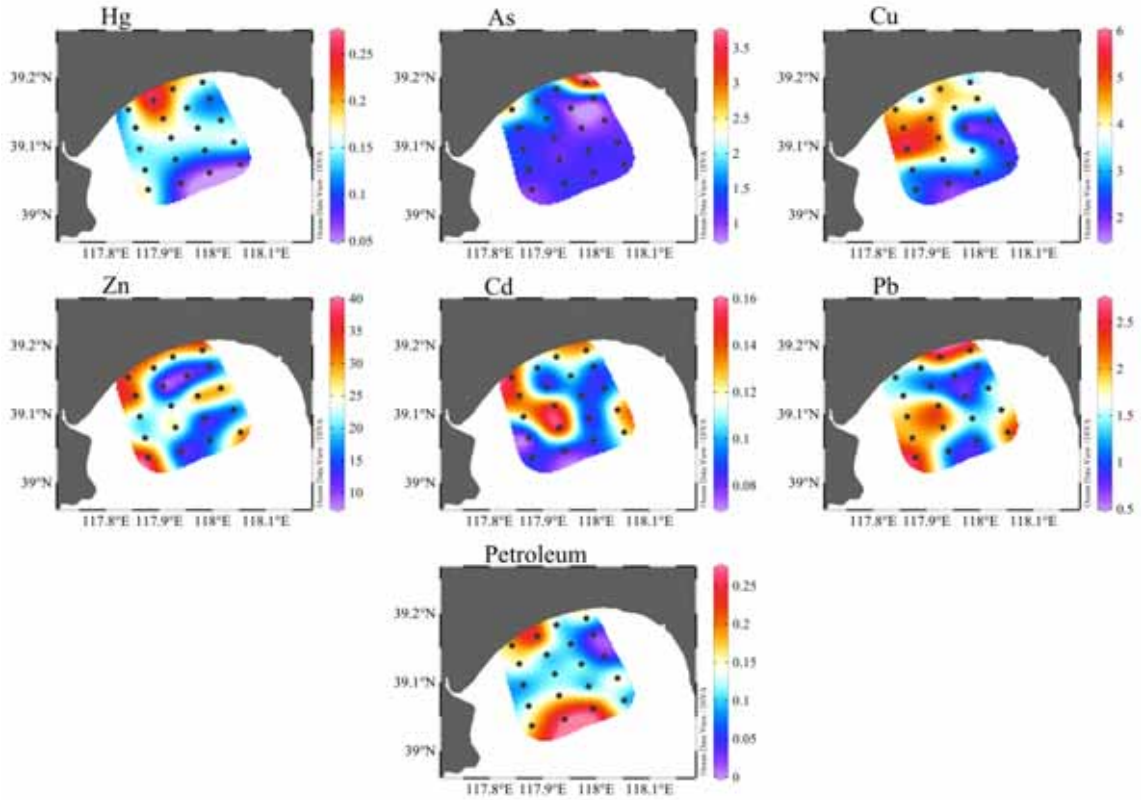

FIGURE 8
The horizontal distribution of heavy metal pollutants and petroleum in 2009 spring

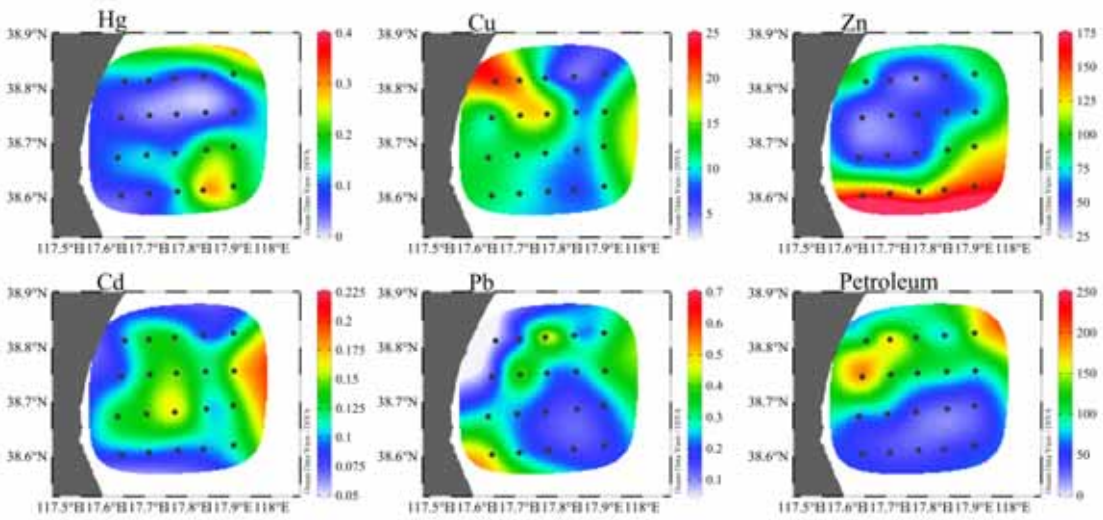

FIGURE 9
The horizontal distribution of heavy metal pollutants and petroleum in 2009 autumn cruise

Assessment standard and methods. Take the GB18421 'Marine biological quality' as the quality evaluation criteria of marine organisms.

Single factor pollution index method was used for assessing marine biological quality, calculated as follows:

$P_i=C_i/S_i$……(1)

P_i——pollutant index of pollutant i;

C_i——measured value of pollutant I;

S_i——standard value of pollutant i.

Marine biological quality was determined by pollution index value. When P_i> 1 biological quality exceeds the standard; when Pi <1 biological quality meets the standard.

Horizontal distributions and assessment results of marine biological quality. Contaminant residues of marine organisms were comparatively analyzed in two surveys. Figures 2-9 showed the value variations at different stations and the comparisons with one to three standard value (no domestic uniform criteria for PAHs). Petroleum, Hg, As, 666, and PCBs at 5 sites were all under Ⅰ standard value. The other heavy metals largely exceeded the criteria and ordered by Cd, Cu, Pb, Cr and Zn. The over-standard rates of these five heavy metals were compared to confirm pollution level in BB. Pollution level of spring cruise was ordered as T02 > T03 = T05 > T01 > T04. Pollution level of autumn cruise was ordered as T02 = T04 > T01 > T05 > T03, T03 meet the standard value.

To sum up, site T02 was mostly over-standard. This is due to its location within the downstream of Haihe River, while, site T01 located in Hangu shallow molluscs resource recovery within the proliferative zone, which lied in the southern margin of special marine protection area, such as Cd, Cu and Zn were heavily over-standard. It is speculated that large variations between site T04 and T03 of two seasons may be related to biological species.

According to GB18421 "Marine biological quality" standard, commercial biological quality in the Bohai Bay was assessed.

Comparison of marine biological quality with historical data. Comparing the present survey results and findings of Hebei Province in 2004 and the Second National Marine Pollution Baseline Survey findings Tianjin Sea in 1997, petroleum, Hg, Cd and as residues in the organism, body shared a decreasing trend, while, Pb, DDT and PCBs displayed a slightly increasing trend [27].

Marine biological quality of health safety assessment. Using the state health standards was referred to assess marine biological test in spring and autumn, Cd was over-standard at all five stations in spring, Cu and Zn were slightly over-standard at site T01, Cd only meets the standard at site T03, Cu and Zn were over-standard at site T02.

The investigation of pollutant residual levels within several commercial organisms in BB indicated that heavy metals such as Cd, Cu, Zn, Pb, and Cr were extremely over-standard (type standard). Compared to the result of Second National Marine Pollution Baseline Survey, Cd showed a decreased trend, however, it was still higher than the standard of food health requirement, Pb, DDT and PCBs showed an increasing tendency.

According to Tianjin marine function zoning, site T01 located in oil-gas region and Hangu shallow molluscs resource recovery, Cd, Cu and Zn residues were over-standard, that were not suitable for marine fisheries, aquaculture, marine conservation, and marine function zoning to industrial water related to

human consumption; site T04 and T03 were relatively lower in residue level.

CONCLUSIONS

The marine biological quality survey is in full accordance with the 'Marine Survey and Assessment Project' and its relevant provisions on the coastal waters survey, with strict implementation of quality control procedures to ensure the quality of survey data.

The survey results showed that heavy metals such as Cd, Cu, Zn, Pb, and Cr extremely exceeds the type I standard value, shared similar result with the survey of Hebei province in 2004, and Pb detection within *M. quadrangularis* of Tianjin marine environmental quality report in September 2006; compared with the second National marine pollution baseline survey in 1997, petroleum, Hg, Cd, and As residues reduced, Pb, DDT and PCBs were slightly increased. Survey results showed that Cd at most stations, Cu and Zn at minority stations were over the food health standard. Benthos was prominently dominated by the mollusc, and followed by crustacean, polychaetes, and echinoderm. Dominant phytoplankton were *Skeletonema*, *Ditylum brightwelli*, *Nitzschia longissima*, *Thalassiosira excentrica*, *Thalassiosira rotula*, etc.

The present study investigated the marine biological quality and ecological environment in the Bohai Bay furnishing valuable data for assessing Tianjin marine pollution biological residues and for monitoring marine environment. This has vital importance for recognizing marine environment status and assessing pollution spatial-temporal variations.

ACKNOWLEDGEMENTS

This work was supported by the Natural Science Foundation of China (41676112), the Key Project of Natural Science Foundation for Tianjin (17JCZDJC40000), the strengthening the ocean by science and technology for Tianjin (KJXH2013-22), the University Innovation Team Training Program for Tianjin (TD12-5003), and the Program for Changjiang Scholars to Jun Sun. Special thanks to Dr. Satheeswaran Thangaraj for his language improvement.

REFERENCES

[1] Li, Y., Zhao, Y., Peng, S., Zhou, Q. and Ma, L.Q. (2010) Temporal and spatial trends of total petroleum hydrocarbons in the seawater of Bohai Bay, China from 1996 to 2005. Marine Pollution Bulletin. 60(2), 238-243.

[2] Shao, C., Guan, Y., Chu, C., Shi, R., Ju, M. and Shi, J. (2014) Trends analysis of ecological environment security based on DPSIR model in the coastal zone: a survey study in Tianjin, China. International Journal of Environmental Research. 8(3), 765-778.

[3] Tian, X., Ju, M., Shao, C. and Fang, Z. (2011) Developing a new grey dynamic modeling system for evaluation of biology and pollution indicators of the marine environment in coastal areas. Ocean & coastal management. 54(10), 750-759.

[4] Gao, X., Zhou, F. and Chen, C.T.A. (2014) Pollution status of the Bohai Sea: An overview of the environmental quality assessment related trace metals. Environment International. 62, 12-30.

[5] Sun, J., Liu, D.Y., Zhang, C. and Zhong, H. (2003) The preliminary study on size - fractionated biomass of phytoplankton in the central Bohai Sea, the Bohai Straits and its adjacent area. Acta Oceanologica Sinica. 25(5), 103-112. [in Chinese].

[6] Zou, S., Xu, W., Zhang, R., Tang, L., Chen, Y. and Zhang, G. (2011) Occurrence and distribution of antibiotics in coastal water of the Bohai Bay, China: impacts of river discharge and aquaculture activities. Environment Pollution. 159(10), 2913-2920.

[7] Liu, C., Wang, Z.Y., and He, Y. (2003) Water pollution in the river mouths around Bohai Bay. International Journal of Sediment Research. 18(4), 326-332.

[8] Sun, J, Liu, D.Y., Chai, X.Y., and Qian, S.B. (2002) The distribution of phytoplankton biomass and primary productivity in the Laizhou Bay and estuary of the Weihe River in summer. Acta Oceanologica Sinica. 24(5), 81-90. [in Chinese].

[9] Sun, J. and Liu, D.Y. (2005) Net - phytoplankton community of the Bohai Sea in the autumn of 2000. Acta Oceanologica Sinica. 27(3), 124-132. [in Chinese].

[10] Shi, J.B., Liang, L.N., Jiang, J.B. and Jin, X.L. (2005) The speciation and bioavailability of mercury in sediments of Haihe River, China. Environment International. 31(3), 357-65.

[11] Santomauro, G., Sun, W.L., Brümmer, F. and Bill, J. (2016) Incorporation of zinc into the coccoliths of the microalga *Emiliania huxleyi*. BioMetals. 29(2), 225-234.

[12] Bastami, K.D., Bagheri, H., Kheirabadi, V., Zaferani, G.G., Teymori, M.B., Hamzehpoor, A., Soltani, F., Haghparast, S., Harami, S.R.M. and Ghorghani, N.F. (2014) Distribution and ecological risk assessment of heavy metals in surface sediments along southeast coast of the Caspian Sea. Marine Pollution Bulletin. 81(1), 262-267.

[13] Xu, R., Yang, Y. and Li, Z. (2007) Diffusion of heavy metals from marine environment to shellfish. Marine Science Bulletin-Tianjin-Chinese Edition-. 26(5), 117-120. [in Chinese].
[14] Lu, X., Chen, C., Zhang, S., Hou, Z. and Yang, J. (2013) Concentration levels and ecological risks of persistent organic pollutants in the surface sediments of Tianjin coastal area, China. The Scientific World Journal. 2013, 1-8.
[15] Mirsadeghi, S.A., Zakaria, M.P., Yap, C.K. and Shahbazi, A. (2011) Risk assessment for the daily intake of polycyclic aromatic hydrocarbons from the ingestion of cockle (*Anadara granosa*) and exposure to contaminated water and sediments along the west coast of Peninsular Malaysia. Journal of Environmental Sciences. 23(2), 336-345.
[16] Liu, W., Chen, J., Lin, X., Fan, Y. and Tao, S. (2007) Residual concentrations of micropollutants in benthic mussels in the coastal areas of Bohai Sea, North China. Environmental Pollution. 146(2), 470-477.
[17] Wan, Y., Hu, J.Y., Liu, J.L., An, W., Tao, S. and Jia, Z.B. (2005) Fate of DDT-related compounds in Bohai Bay and its adjacent Haihe Basin, North China. Marine Pollution Bulletin. 50(4), 439-45.
[18] Ma, C., Zhang, G.Y., Zhang, X.C. and Li, Y.J. (2012) Application of multiple indicators in environment evaluation of coastal restoration engineering: a case study in Bohai Bay in China. Applied Mechanics & Materials. 170-173, 2228-2232.
[19] Gao, X. and Chen, C.T. (2012) Heavy metal pollution status in surface sediments of the coastal Bohai Bay. Water Research. 46(6), 1901-1911.
[20] Wang, H.Z., He, M.C., Lin, C.Y., Quan, X.C., Guo, W. and Yang, Z.F. (2007) Monitoring and assessment of persistent organochlorine residues in sediments from the Daliaohe River Watershed, Northeast of China. Environmental Monitoring and Assessment. 133(1-3), 231-242.
[21] Giordano, M. (2003) An Anaplerotic Role for Mitochondrial Carbonic Anhydrase in Chlamydomonas reinhardtii. Plant Physiology. 132(4), 2126-2134.
[22] Wu, S.P., Tao, S., Zhang, Z.H., Lan, T. and Zuo, Q. (2005) Distribution of particle-phase hydrocarbons, PAHs and OCPs in Tianjin, China. Atmospheric Environment. 39(38), 7420-7432.
[23] Jin, H., Feng, Y., Li, X., Zhai, W. and Sun, J. (2015) Spring and autumn living coccolithophores in the Bohai Sea and Yellow Sea, China. Acta Oceanologica Sinica. 34(10), 132-46.
[24] Sun, J., Liu, D. and Qian, S.B. (2000) Estimating biomass of phytoplankton in the Jiaozhou Bay I. Phytoplankton biomass estimated from cell volume and plasma volume. Acta Oceanologica Sinica. 19(2), 97-110.
[25] Sun, J., Liu, D.Y., and Qian, S.B. (2001) Preliminary study on the seasonal succession and development pathway of phytoplankton community in the Bohai Sea. Acta Oceanologica Sinica. 20(2), 251-60.
[26] Bianchi, F., Acri, F., Aubry, F.B., Berton, A., Boldrin, A., Camatti, E., Cassin, D. and Comaschi, A. (2003) Can plankton communities be considered as bio-indicators of water quality in the Lagoon of Venice? Marine Pollution Bulletin. 46(8), 964-971.
[27] Fink, C., Baumann, K.H., Groeneveld, J. and Steinke, S. (2010) Strontium/Calcium ratio, carbon and oxygen stable isotopes in coccolith carbonate from different grain-size fractions in South Atlantic surface sediments. Geobios. 43(1), 151-164.

Received: **01.04.2017**
Accepted: **05.12.2017**

CORRESPONDENCE AUTHOR

Jun Sun
Tianjin Key Laboratory of Marine Resources and Chemistry,
Tianjin University of Science and Technology,
Tianjin 300457 – P.R. China

e-mail: phytoplankton@163.com

© by PSP Volume 27 – No. 2/2018 pages 831-837 Fresenius Environmental Bulletin

RECONSTRUCTION OF LOW-FUNCTION FOREST SHIFTS MICROBIAL AND SOIL CARBON POOL

Yusong Cao[1], Huimin Wang[2], Yi'an Xiao[1], Cancan Zhao[3,*]

[1]School of Life sciences, Jinggangshan University, Ji'an, Jiangxi, China
[2]Institute of Geographic Sciences and Natural Resources Research, Chinese Academy of Sciences, Beijing, China
[3]International Joint Research Laboratory for Global Change Ecology, College of Life Sciences, Henan University, Kaifeng, Henan, China

ABSTRACT

Soil microbial biomass regulates plant litter decomposition and provides a sensitive measure of change in organic matter status. Reconstruction of low-function forest by inter-planting broadleaved trees change the composition of plant community, but how this change would affect microbial biomass and soil carbon and nitrogen pools are unclear. We reconstructed low-function forests by inter-planting broadleaved trees under *Pinus massoniana* which is the typical coniferous and low-function forest in China. The treatments included *P. massoniana* pure forest (*PM*), *P. massoniana* inter-planted with *Schima superba* (*PMSS*) and *Liquidambar formosana* (*PMLF*), respectively. The results showed that soil microbial biomass carbon and organic matter in *PMSS* were significantly lower than that in *PM*. However, soil soluble carbon contents in *PMSS* was higher than that in *PM.* These results indicate that the reconstruction mode of *PMSS* accelerate decomposition of soil organic matter. There was no obvious change of soil microbial biomass between *PMLF* and *PM*. Both soil organic matter and soluble carbon in *PMLF* were higher than that in *PM*, suggesting that the reconstruction mode of *PMLF* facilitate soil organic carbon accumulation as carbon sink.

KEYWORDS:
low-function plantation, microbial biomass carbon, soil organic matter, carbon source/sink

INTRODUCTION

Forest ecosystems cover more than 4.1×10^9 hectares, and globally store 1146 Pg of carbon (C) [1]. It is predicted that the existing forest biomass C storage in China would increase from 5.86 Pg C in 1999-2003 to 10.23 Pg C in 2050, resulting in a increase of 4.37 Pg C. Newly planted forests by reforestation and afforestation would have the sequestration potential of 2.86 Pg C in biomass [2]. However, the large area low-function forests restricted sustainable development of forestry and greatly reduced the carbon sequestration function and ecological benefits [3]. There are several forest management modes of reconstruction of low efficiency forest, including forest tending, intermittent cutting of forest thinning, and close-to-nature forest management, etc. [4-6]. Many studies focus on the effects of different forest management approaches on natural regeneration, species diversity, and soil physical and chemical properties [7-8]. However, little attention has been paid to the effect of reconstruction of low efficiency forests on soil biota.

Soil microorganisms play a major roles in litter decomposition and nutrients transformation process [9]. Microbial biomass serve as a source or a sink of available plant nutrients and regulate plant litter decomposition in soil [10]. In addition, microbial biomass provides a more sensitive measurement of changes in organic matter status [11]. Microbial biomass and community composition are commonly regulated by plant diversity directly and indirectly. Moreover, microbial biomass and community composition can be even affected by different cultivars of the same species in agricultural systems in both temperate and tropic regions [12-14]. A better understanding of the effects of reconstruction of low-function forest, i.e., changing forest species composition, on soil microbial biomass and regulatory organic matter is critical for dynamically predicting soil carbon and nitrogen pools and ecological services [15-16].

The southern forest region is one of the most important four major forest regions in China, in which *Pinus massoniana* is the typical coniferous tree species. The area of *P. massoniana* in China is up to 1.13×10^7 ha, accounting for 20% of the total afforested area in China [17-18]. However, due to long-term pure forest operation, *P. massoniana* plantation ecosystems have become fragile and vulnerable to pine moth, and led to decreasing of productivity and ecosystem stability, and increasing of forest fires risk [19-21]. In order to improve *P. massoniana* pure forest service function, we inter-planted *Schima superba* and *Liquidambar formosana* under *P. massoniana*. The specific objectives of this study were to examine effects of reconstruction of low-function forest on microbial biomass and other soil carbon and nitrogen pools, and subsequently to estimate the ecological service functions of low-benefit forest reconstruction.

MATERIALS AND METHODS

Study Site. The study was conducted at the Qianyanzhou Experimental Station, Chinese Academy of Sciences, Jiangxi, China (115°04′13″E, 26°44′48″N, 20-50 m a.s.l.). The climate is typical subtropical monsoon climate. The average annual temperature and precipitation are 17.9 °C and 1489 mm, respectively. The main soil type of the region is red soil. The representative vegetation is central subtropical evergreen broad-leaved forest. However, native vegetation has been completely destroyed, and now dominated by artificial forest, developed from grassland slopes as a result of restoration of degraded ecosystem. The main vegetation types are *Pinus massoniana, Cunninghamia Lanceolata*, *Schima superba,* and *Liquidambar formosana* plantation.

Experimental Design. The experiment used a randomized block design with 3 replications of *P. massoniana* pure forests. We set up 3 treatments, including *P. massoniana* pure forest (*PM*), *P. massoniana* inter-planted with *S. superba* (*PMSS*), and *P. massoniana* inter-planted with *L. formosana* (*PMLF*). Nine plots of 30 × 30 m^2 were established. All of the broad-leaved tree species were planted in 2009 and are 6 years-old when we sampled soil.

Sampling and Analysis. Soil samples were collected from all plots on August of 2015. In each plot, 5 cores of soil were randomly taken using an auger boring with a diameter of 10 cm. Soil of 0-20 cm depth were collected and divided into 2 layers of 0-10 cm and 10-20 cm. Five same layer of soil were mixed to obtain a composite sample per plot. After visible roots and stones removed, samples were transported to the laboratory and subsequently stored at 4 °C until analysis.

A 30 g field moist soil subsample was adjusted to 50% of maximum water holding capacity and analyzed for microbial biomass carbon (MBC) and nitrogen (MBN) using the chloroform fumigation incubation method [22]. Soil organic matter (SOM) was determined using the potassium dichromate oxidation method. We determined NH_4^+-N by the potassium chloride leaching - indophenol blue colorimetric method, and NO_3^--N by the copperized cadmium reduction - diazotization coupling colorimetric method. Available phosphorus (P) was determined using the hydrochloric acid - ammonium fluoride leaching - molybdenum antimony colorimetric method. Cation exchange capacity (CEC) was determined using the ammonium acetate exchange method. Soil moisture was measured by the oven-drying method. Soil pH was determined in a soil water mixture of 1:2.5 ratio with a pH meter [23].

Statistical Analysis. The effects of reconstruction mode and soil depth on microbial and soil properties were analyzed using two-way ANOVAs. One-way ANOVAs were used to examine the effects of reconstruction mode on microbial and soil properties in each soil layer. Simple linear regressions were performed to assess the relationships of microbial biomass and organic matter with soil physicochemical properties. These analyses were conducted using SPSS 17.0 (SPSS Inc., Chicago, USA) with an alpha of 0.05. Assumptions of normality of residuals were met for all analyses.

Relationships of carbon pools with soil properties. Across all the plots, MBC (r = 0.486; P = 0.041) and SOM (r = 0.614; P = 0.007) linearly increased with TSN (Fig. 5). SOM showed a positive correlation with CEC (r = 0.710; P = 0.001), but a negative correlation with soil pH (r = -0.720; P = 0.001; Fig. 5).

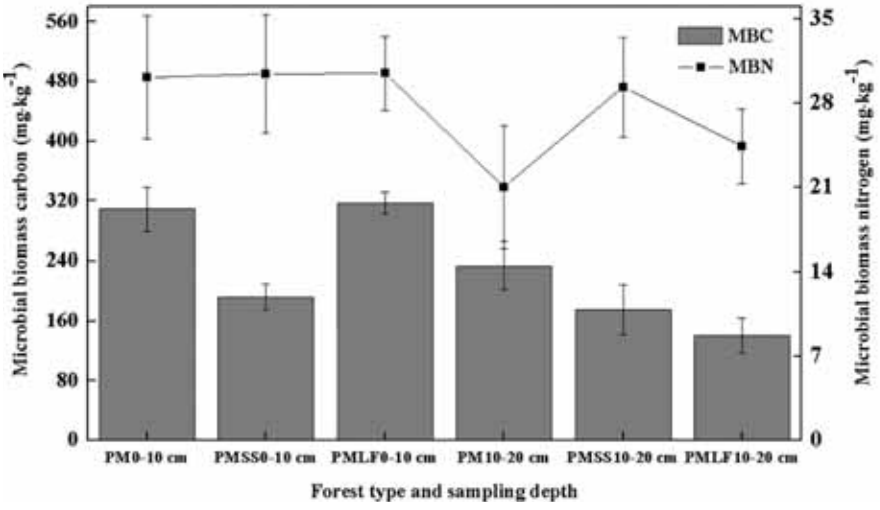

FIGURE 1

Soil microbial biomass carbon and nitrogen contents in *PM*, *PMSS*, and *PMLF*. *PM*, *PMSS*, and *PMLF* represent *P. massoniana* pure forest, *P. massoniana* inter-planting with *S. superba* and *P. massoniana* inter-planting with *L. formosana* mixed forest, respectively.

RESULTS

Soil Microbial Carbon and Nitrogen. Both mean MBC and MBN in 0-10 cm soil layer were higher than that in 10-20 cm soil layer (Fig. 1). In 0-10 cm layer, MBC in *PMSS* (192.57 mg kg^{-1}) was significantly lower than that in *PM* (308.81mg kg^{-1}). However, MBC in *PMLF* did not show any differences with *PM* (Fig. 1). In 10-20 cm layer, MBC in *PMSS* (175.36 mg kg^{-1}) and *PMLF* (141.11 mg kg^{-1}) was markedly lower than that in *PM* (233.83 mg kg^{-1}; Fig. 1). Reconstruction mode had no impacts on MBN in 0-10 cm layer. MBN in *PMSS* was significantly higher than that in *PM* (Fig. 1).

Soil Characteristics. SOM in 0-10 cm soil layer was much higher than that in 10-20 cm layer. SOM in *PMSS* was lower than that in *PM*, however, SOM in *PMLF* were markedly higher than that in *PM* in the both two soil layers (Fig. 2). Both available K and CEC showed similar patterns with SOM (Fig. 2). Available P in both *PMSS* and *PMLF* were higher than that in *PM* in 10-20 cm layer (Fig. 2). Soluble carbon content in 0-10 cm soil layer was much higher than that in 10-20 cm layer. Soluble carbon content in both *PMSS* and *PMLF* were higher than that in *PM* in the both two soil layers (Fig. 3). Soil moisture content had similar patterns with soluble carbon except without differences of soil layers (Fig. 3). Soil pH in *PMSS* was higher than that in *PM* in the both two soil layers (Fig. 3). Ammonium N, nitrate N, and total soluble N (TSN) in 0-10 cm soil layer were all higher than that in 10-20 cm soil layer (Fig. 4). Ammonium N in *PMLF* was lower than in *PM* in 0-10 cm layer. Nitrate N in *PMLF* was much higher than in *PM* in the both two soil layers (Fig. 4).

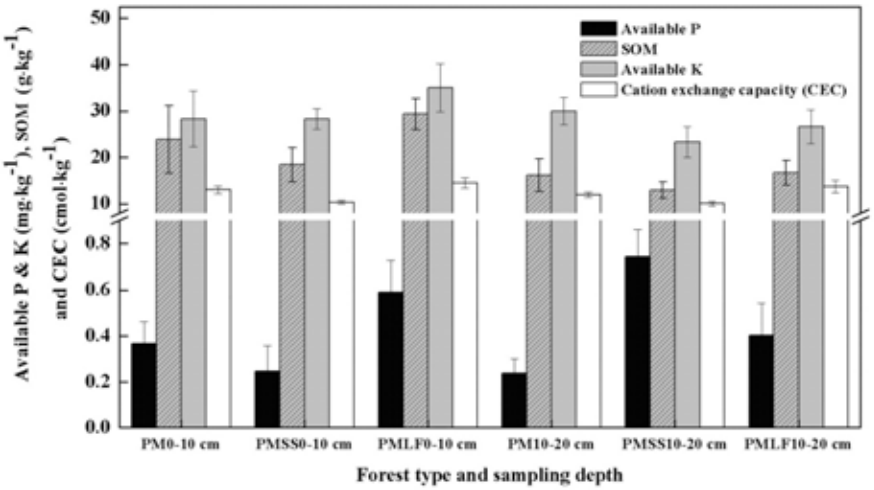

FIGURE 2

Soil available P, K contents, soil organic matter, and cation exchange capacity in *PM*, *PMSS*, and *PMLF*. *PM*, *PMSS*, and *PMLF* represent *P. massoniana* pure forest, *P. massoniana* inter-planting with *S. superba* and *P. massoniana* inter-planting with *L. formosana* mixed forest, respectively.

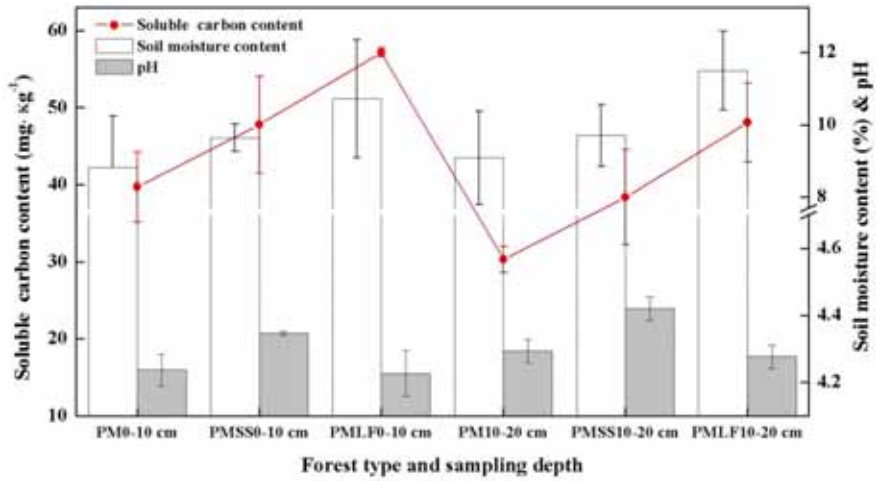

FIGURE 3

Soluble carbon, soil moisture content, and pH value in *PM*, *PMSS*, and *PMLF*. *PM*, *PMSS*, and *PMLF* represent *P. massoniana* pure forest, *P. massoniana* inter-planting with *S. superba* and *P. massoniana* inter-planting with *L. formosana* mixed forest, respectively.

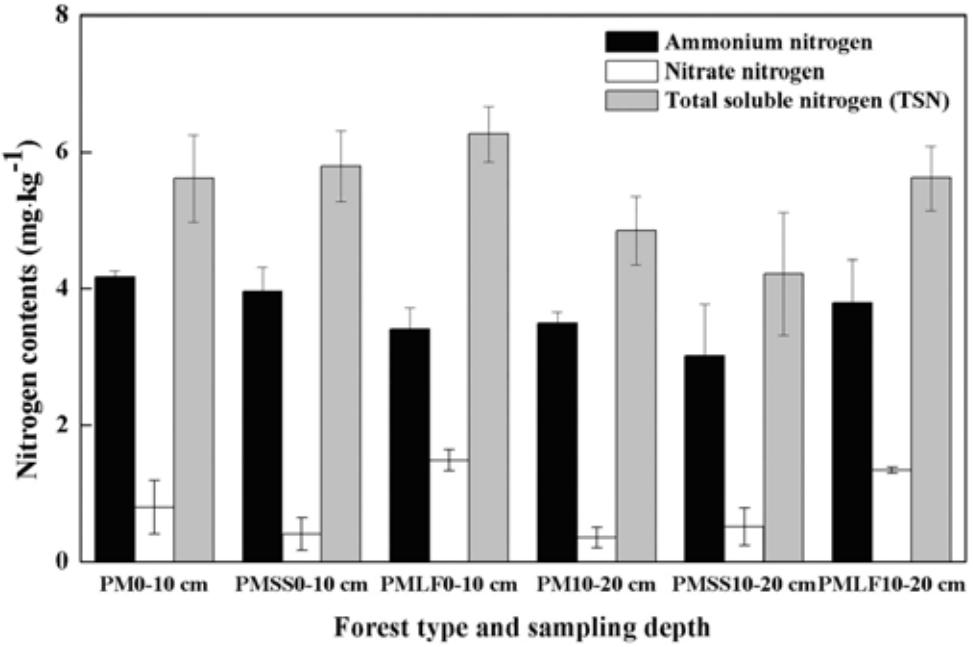

FIGURE 4

Soil total soluble nitrogen and inorganic nitrogen contents in *PM*, *PMSS*, and *PMLF*. *PM*, *PMSS*, and *PMLF* represent *P. massoniana* pure forest, *P. massoniana* inter-planting with *S. superba* and *P. massoniana* inter-planting with *L. formosana* mixed forest, respectively.

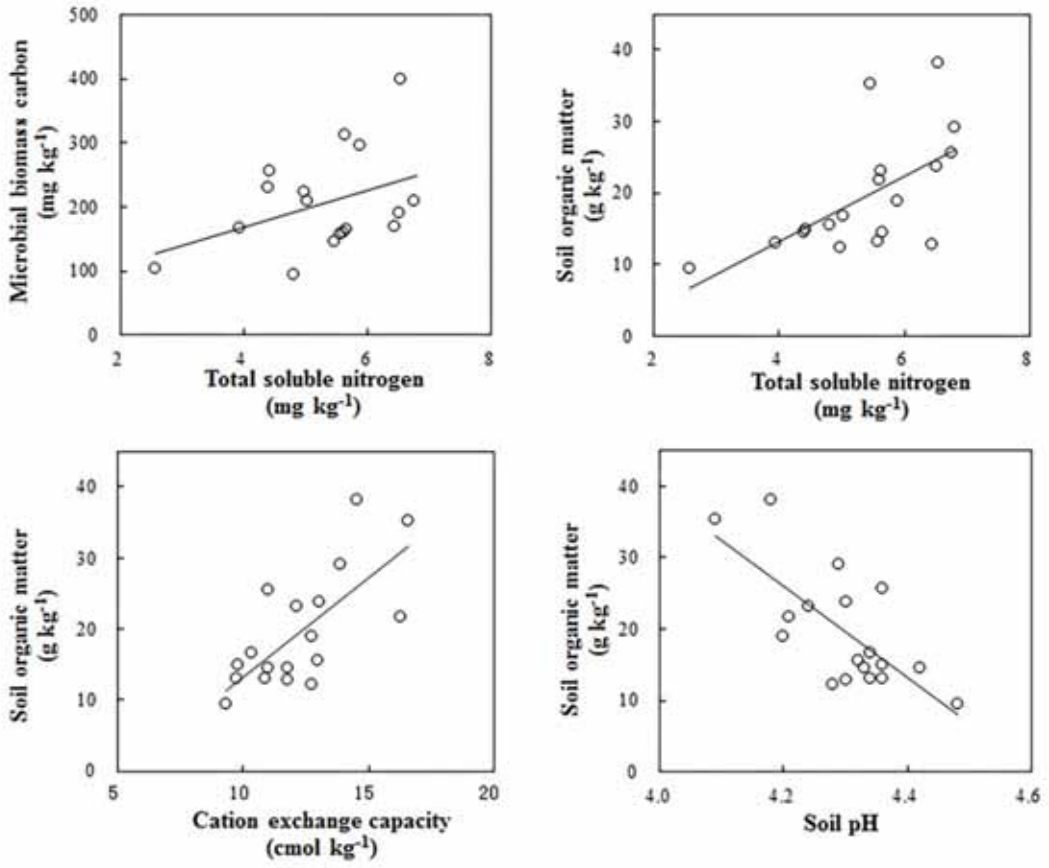

FIGURE 5

Dependence of microbial biomass carbon and soil organic matter on total soluble nitrogen, cation exchange capacity, and soil pH across all the plots.

DISCUSSION

In the present study, soil organic matter, microbial biomass, and soil soluble carbon and nitrogen contents of 0-10 cm layer were all higher than 10-20 cm layer (Fig. 1-4), suggesting that topsoil support more roots biomass, soil animals and microorganisms, and consequent organic carbon and microbial activity than subsoil.

Reconstruction of low-function forest by interplanting with broad-leaved tree species can increase species diversity, root biomass production and change litter resource heterogeneity, sequentially change microbial biomass and organic carbon storage [24]. Most previous studies suggest that plant diversity facilitate accumulation of microbial biomass carbon and new carbon pool in soil [25-28]. Lower organic carbon of *PMSS* soil and higher organic carbon of *PMLF* soil in our study suggest that the effects of elevating species diversity through interplanting with different broad-leaved tree species on soil carbon pools are inconsistent (Fig. 2). The accumulation of organic carbon in *PMLF* soil is consistent with findings of most studies. On one hand, *PMLF* treatment facilitate a greater amount and more diverse organic resources input via litter and root exudates [29-31]. On the other hand, diverse organic resources from higher plant diversity might provide various substrates (Fig. 3,5) to increase microbial respiration [32], accelerate decomposition of existing soil carbon (positive priming effect), and reduce carbon storage [33]. A denser vegetation in highly diverse plant communities can reduce soil erosion and evaporation and enhance moisture (Fig. 3) of the topsoil, which in turn promotes higher soil microbial activity and growth [34]. Increasing diversity of soil microbial communities in rhizosphere could also increase microbial respiration [35]. As a result, the storage of organic carbon in *PMLF* treatment is caused by the larger formation of new soil organic carbon that exceed the continued decomposition of inherited soil organic carbon [36-37]. The amount of soil microbial biomass plays a major role in driving the balance between the release of soil carbon and its sequestration in soil organic matter in terrestrial ecosystems [27, 38].

The uncommon patterns that soil organic matter and microbial biomass carbon in *PMSS* were lower than that in *PM* in our study could be interpreted in two ways. First, nitrogen is a fundamental nutrient for plant growth and metabolism but limited in most terrestrial ecosystems, causing strong competition for available N between roots and soil microorganisms [39-40]. Some previous studies have showed that rhizosphere microorganisms are stronger competitors for available nitrogen than plant roots in the rhizosphere in the short-term time [41-42]. However, there are also a few studies have suggest that some plant species are better able to acquire organic or inorganic nitrogen in the face of microbial competition [43-44]. *S. superba* is a pioneer tree species of degraded ecosystems in the subtropical region by virtue of its preferable adaptation. *S. superba* which have developed root systems, can acquire more nitrogen (Fig. 4,5) for their productivity purpose and reduce soil nutrients sequestration. Second, both *P. massoniana* and *L. formosana* excrete organic acids, resulting in relatively higher soil pH in *PMSS* treatment (Fig. 3). Increasing soil pH could create better environmental conditions for the development of acid-intolerant microorganisms, resulting in higher microbial growth, respiration and extracellular enzyme activities [45-46]. More carbon are released into the atmosphere through microbial decomposition.

Forest soil store the vast majority of terrestrial carbon, and increased soil carbon storage may counteract the increase in atmospheric carbon dioxide [47]. Reconstructed low-function *P. massoniana* forests by inter-planting *L. formosana* is an effective way of increasing biodiversity, forestry production, and organic carbon sequestration.

ACKNOWLEDGEMENTS

We thank Shenglei Fu and Yanqiu Liu for sharing their experimental fields and guiding this project. We also thank Qingkang Li for experiment design, Peide Zhang and Zhenquan Wang for assistance in field investigation. We thank Haihong Zong, Lixia Zhou, and Xiaoli Wang for help laboratory analyses. This work was supported by the National Natural Science Foundation of China (31640011, 31360138), International (regional) cooperation and exchange program (31210103920), and Natural Science Foundation of Jiangxi Province (20142BAB204-005).

REFERENCES

[1] Dixon, R.K., Brown, S., Houghton, R.A., Solomon, A.M., Trexler, M.C. and Wisniewski, J. (1994) Carbon pools and flux of global forest ecosystems. Science. 263, 185-190.

[2] Xu, B., Guo, Z.D., Piao, S.L. and Fang, J.Y. (2010) Biomass carbon stocks in China's forests between 2000 and 2050: A prediction based on forest biomass-age relationships. Sci. China Life Sci. 53, 776-783.

[3] Guner, S.T. and Comez, A. (2017) Biomass equations and changes in carbon stock in afforested black pine (*Pinus nigra* Arnold. subsp. *pallasiana* (Lamb.) Holmboe) stands in Turkey. Fresen. Environ. Bull. 26, 2368-2379.

[4] Cojzer, M., Diaci, J. and Brus, R. (2014) Tending of young forests in secondary succession on abandoned agricultural lands: An experimental study. Forests. 5, 2658-2678.

[5] Lundqvist, L., Chrimes, D., Elfving, B., Mörling, T. and Valinger, E. (2007) Stand development after different thinnings in two uneven-aged *Picea abies* forests in Sweden. Forest Ecol. Manag. 238, 141-146.
[6] Van Gossum, P., Luyssaert, S., Serbruyns, I. and Mortier, F. (2005) Forest groups as support to private forest owners in developing close-to-nature management. Forest Policy Econ. 7, 589-601.
[7] Sutinen, R., Närhi, P., Herva, H., Piekkari, M. and Sutinen, M.L. (2010) Impact of intensive forest management on soil quality and natural regeneration of Norway spruce. Plant Soil. 336, 421-431.
[8] Schulze, E.D., Aas, G., Grimm, G.W., Gossner, M.M., Walentowski, H., Ammer, C., Kühn, I., Bouriaud, O. and Von Gadow, K. (2016) A review on plant diversity and forest management of European beech forests. Eur. J. Forest Res. 135, 51-67.
[9] Zhao, C., Miao, Y., Yu, C., Zhu, L., Wang, F., Jiang, L., Hui, D. and Wan, S. (2016) Soil microbial community composition and respiration along an experimental precipitation gradient in a semiarid steppe. Sci. Rep. 6, 24317.
[10] Friedel, J.K., Gabel, D. and Stahr, K. (2001) Nitrogen pools and turnover in arable soils under different durations of organic farming: II: Source-and-sink function of the soil microbial biomass or competition with growing plants? J. Plant Nutr. Soil Sc. 164, 421-429.
[11] Anderson, T.H. and Domsch, K.H. (1989) Ratios of microbial biomass carbon to total organic carbon in arable soils. Soil Biol. Biochem. 21, 471-479.
[12] Aneja, M.K., Sharma, S., Fleischmann, F., Stich, S., Heller, W., Bahnweg, G., Munch, J.C. and Schloter, M. (2006) Microbial colonization of beech and spruce litter - influence of decomposition site and plant litter species on the diversity of microbial community. Microb. Ecol. 52, 127-135.
[13] Gessner, M.O., Swan, C.M., Dang, C.K., Mckie, B.G., Bardgett, R.D., Wall, D.H. and Hättenschwiler, S. (2010) Diversity meets decomposition. Trends Ecol. Evol. 25, 372-380.
[14] Carney, K.M. and Matson, P.A. (2006) The influence of tropical plant diversity and composition on soil microbial communities. Microb. Ecol. 52, 226-238.
[15] Durkaya, A., Durkaya, B., Makineci, E., Orhan, I. (2015) Aboveground biomass and carbon storage relationship of Turkish pines. Fresen. Environ. Bull. 24, 3573-3583.
[16] Cevik, I. and Sagliker, H.A. (2017) Soil carbon mineralization in *Arbutus andrachne* and *Cupressus sempervirens* growing on the different elevations. Fresen. Environ. Bull. 26, 6078-6084.
[17] Yang, H., Wang, S., Zhang, J., Fan, B. and Zhang, W. (2011) Biomass and nutrients of *Pinus massoniana* plantations in southern China: Simulations for different managing practices. J. Food Agric. Environ. 9, 689-693.
[18] [Chen, L.C., Liang, M.J. and Wang, S.L. (2016) Carbon stock density in planted versus natural *Pinus massoniana* forests in sub-tropical China. Ann. Forest Sci. 73, 461-472.
[19] Xu, X.N. and Hirata, E. (2002) Forest floor mass and litterfall in *Pinus luchuensis* plantations with and without broad-leaved trees. Forest Ecol. Manag. 157, 165-173.
[20] Xiang, W., Fan, G., Lei, P., Zeng, Y., Tong, J., Fang, X., Deng, X. and Peng, C. (2015) Fine root interactions in subtropical mixed forests in China depend on tree species composition. Plant Soil. 395, 335-349.
[21] Garcia-Gonzalo, J., Zubizarreta-Gerendiain, A., Ricardo, A., Marques, S., Botequim, B., Borges, J.G., Oliveira, M.M., Tomé, M. and Pereira, J.M.C. (2012) Modelling wildfire risk in pure and mixed forest stands in Portugal. Allg. Forst. Jagdztg. 183, 238-248.
[22] Voroney, R.P. and Paul, E.A. (1984) Determination of k_C and k_N *in situ* for calibration of the chloroform fumigation-incubation method. Soil Biol. Biochem. 16, 9-14.
[23] Zhao, J., Wang, F., Li, J., Zou, B., Wang, X., Li, Z. and Fu, S. (2014) Effects of experimental nitrogen and/or phosphorus additions on soil nematode communities in a secondary tropical forest. Soil Biol. Biochem. 75, 1-10.
[24] Steinbeiss, S., Beβler, H., Engels, C., Temperton, V.M., Buchmann, N., Roscher, C., Kreutziger, Y., Baade, J., Habekost, M. and Gleixner, G. (2008) Plant diversity positively affects short-term soil carbon storage in experimental grasslands. Global Change Biol. 14, 2937-2949.
[25] Wen, L., Lei, P., Xiang, W., Yan, W. and Liu, S. (2014) Soil microbial biomass carbon and nitrogen in pure and mixed stands of *Pinus massoniana* and *Cinnamomum camphora* differing in stand age. Forest Ecol. Manag. 328, 150-158.
[26] Thakur, M.P., Milcu, A., Manning, P., Niklaus, P.A., Roscher, C., Power, S., Reich, P.B., Scheu, S., Tilman, D. and Ai, F.X. (2015) Plant diversity drives soil microbial biomass carbon in grasslands irrespective of global environmental change factors. Global Change Biol. 21, 4076-4085.
[27] Lange, M., Eisenhauer, N., Sierra, C.A., Bessler, H., Engels, C., Griffiths, R.I., Mellado-Vázquez, P.G., Malik, A.A., Roy, J., Scheu, S., Steinbeiss, S., Thomson, B.C., Trumbore, S.E. and Gleixner, G. (2015) Plant diversity increases soil microbial activity and soil carbon storage. Nat. Commun. 6, 6707.

[28] Mellado-Vázquez, P.G., Lange, M., Bachmann, D., Gockele, A., Karlowsky, S., Milcu, A., Piel, C., Roscher, C., Roy, J. and Gleixner, G. (2016) Plant diversity generates enhanced soil microbial access to recently photosynthesized carbon in the rhizosphere. Soil Biol. Biochem. 94, 122-132.
[29] Knops, J.M.U., Bradley, K.L. and Wedin, D.A. (2002) Mechanisms of plant species impacts on ecosystem nitrogen cycling. Ecol. Lett. 5, 454-466.
[30] Liang, C., Cheng, G., Wixon, D.L. and Balser, T.C. (2011) An absorbing Markov chain approach to understanding the microbial role in soil carbon stabilization. Biogeochemistry. 106, 303-309.
[31] Fornara, D.A. and Tilman, D. (2008) Plant functional composition influences rates of soil carbon and nitrogen accumulation. J. Ecol. 96, 314-322.
[32] Manzoni, S., Taylor, P., Richter, A., Porporato, A. and Ågren, G. (2012) Environmental and stoichiometric controls on microbial carbon-use efficiency in soils. New Phytol. 196, 79-91.
[33] Fontaine, S., Barot, S., Barré, P., Bdioui, N., Mary, B. and Rumpel, C. (2007) Stability of organic carbon in deep soil layers controlled by fresh carbon supply. Nature. 450, 277-280.
[34] Lange, M., Habekost, M., Eisenhauer, N., Roscher, C., Bessler, H., Engels, C., Oelmann, Y., Scheu, S., Wilcke, W., Schulze, E. and Gleixner, G. (2014) Biotic and abiotic properties mediating plant diversity effects on soil microbial communities in an experimental grassland. PLoS One. 9, e96182.
[35] Bell, T., Newman, J.A., Silverman, B.W., Turner, S.L. and Lilley, A.K. (2005) The contribution of species richness and composition to bacterial services. Nature. 436, 1157-1160.
[36] Soussana, J.F., Loiseau, P., Vuichard, N., Ceschia, E., Balesdent, J., Chevallier, T. and Arrouays, D. (2004) Carbon cycling and sequestration opportunities in temperate grasslands. Soil Use Manage. 20, 219-230.
[37] Sun, O.J., Campbell, J., Law, B.E. and Wolf, V. (2004) Dynamics of carbon stocks in soils and detritus across chronosequences of different forest types in the Pacific Northwest, USA. Global Change Biol. 10, 1470-1481.
[38] Miltner, A., Bombach, P., Schmidt-Brücken, B. and Kästner, M. (2012) SOM genesis: microbial biomass as a significant source. Biogeochemistry. 111, 41-55.
[39] Hodge, A., Stewart, J., Robinson, D., Griffiths, B.S. and Fitter, A.H. (2000) Competition between roots and soil micro-organisms for nutrients from nitrogen-rich patches of varying complexity. J. Ecol. 88, 150-164.
[40] Liu, Q., Qiao, N., Xu, X., Xin, X., Han, J.Y., Tian, Y., Ouyang, H. and Kuzyakov, Y. (2016) Nitrogen acquisition by plants and microorganisms in a temperate grassland. Sci. Rep. 6, 22642.
[41] Bardgett, R.D., Steeter, T.C. and Bol, R. (2003) Soil microbes compete effectively with plants for organic-nitrogen inputs to temperate grasslands. Ecology. 84, 1277-1287.
[42] Cheng, X. and Bledsoe, C.D. (2004) Competition for inorganic and organic N by blue oak (*Quercus douglasii*) seedlings, an annual grass, and soil microorganisms in a pot study. Soil Biol. Biochem. 36, 135-144.
[43] Jaeger, C.H. III, Monson, R.K., Fisk, M.C. and Schmidt, S.K. (1999) Seasonal partitioning of nitrogen by plants and soil microorganisms in an alpine ecosystem. Ecology. 80, 1883-1891.
[44] Xu, X., Stange, C.F., Richter, A., Wanek, W. and Kuzyakov, Y. (2008) Light affects competition for inorganic and organic nitrogen between maize and rhizosphere microorganisms. Plant Soil. 304, 59-72.
[45] Chen, D., Li, J., Lan, Z., Hu, S. and Bai, Y. (2016) Soil acidification exerts a greater control on soil respiration than soil nitrogen availability in grasslands subjected to long-term nitrogen enrichment. Funct. Ecol. 30, 658-669.
[46] Zhao, C., Fu, S., Mathew, R.P., Lawrence, K.S. and Feng, Y. (2015) Soil microbial community structure and activity in a 100-year-old fertilization and crop rotation experiment. J. Plant Ecol. 8, 623-632.
[47] Chen, D., Zhang, C., Wu, J., Zhou, L., Lin, Y. and Fu, S. (2011) Subtropical plantations are larger carbon sinks: Evidence from two monoculture plantations in South China. Agr. Forest Meteorol. 151, 1214-1225.

Received: **10.04.2017**
Accepted: **05.12.2017**

CORRESPONDING AUTHOR

Cancan Zhao
International Joint Research Laboratory for Global Change Ecology,
College of Life Sciences,
Henan University,
Kaifeng, Henan 475004 – China

e-mail: cczhao2008@163.com

© by PSP Volume 27 – No. 2/2018 pages 838-845 Fresenius Environmental Bulletin

EFFECT OF ENVIRONMENTAL PARAMETERS ON THE PERSISTENCE OF PROPAMOCARB, FLUOPICOLIDE AND 2,6-DICHLOROBENZAMIDE RESIDUES ON CAULIFLOWER AND SOIL

Gourishankar Manikrao[1,2], Soudamini Mohapatra[1,*], Lekha Siddamallaiah[1], Radhika Buddidathi[1], Nagapooja Yogendraiah Matadha[1]

[1]Pesticide Residue Laboratory, ICAR- Indian Institute of Horticultural Research, Hessaraghatta Lake P.O., Bangalore, 560089, India
[2]Center for Nano and Material Sciences, Jain University, Jakkasandra, Kanakpura, Bangalore, 562112, India

ABSTRACT

Effect of environmental parameters on the residue persistence of fluopicolide, its metabolite, 2,6-dichlorobenzamide and propamocarb was evaluated on cauliflower and soil over two years (2013 and 2014). Initial residues of fluopicolide on cauliflower (1.495 and 1.275 mg/kg) at the standard dose of 100 g a.i./ha were less than the EU MRL (2 mg/kg). Propamocarb initial residue at the standard dose (1000 g a.i./ha) reached below EU MRL (10 mg/kg) within 1 day in the first study and in the second study it was less than the MRL. The residue dissipation followed first order rate kinetics and the half-life (DT_{50}) of fluopicolide was 4.5-6.2 days and that of propamocarb, 4.4-6.2 days. Spray drift caused by wind speed could be the reason for difference in the residue deposits in the two studies. The dissipation pattern of propamocarb and fluopicolide remained the same in spite of high rainfall during the second study.

KEYWORDS:
2,6-Dichlorobenzamide, Fluopicolide, Half-life, Propamocarb, Risk assessment

INTRODUCTION

Fluopicolide (2,6-dichloro-*N*-[3-chloro-5-(trifluoromethyl)-2-pyridylmethyl] benzamide) belongs to the new chemical class of acylpicolide fungicides which effectively controls a large number of oomycete diseases [1]. The acute toxicity of fluopicolide is low with the oral LD_{50} being > 5000 mg/kg bw (body weight) in rats [2]. Fluopicolide translocated to stems and leaves when applied to the soil for control against *Phytophthora capsici* of tomato [3]. The metabolite 2,6-dichlorobenzamide was more toxic than fluopicolide in a single dose and a long-term study [4]. For risk assessment purpose fluopicolide and 2,6-dichlorobenzamide are considered separately [5]. The metabolite is a common groundwater contaminant and persistent in topsoil and subsurface deposits [6].

Propamocarb (propyl 3-(dimethylamino) propylcarbamate), is a carbamate fungicide active against Oomycete species that causes seedling, root, and stem rots and foliar diseases in a number of edible crops [7]. Propamocarb is effective against *Phytophthora infestans* as an individual compound and in combination with other fungicides [8]. Propamocarb exhibits low acute toxicity and the oral LD_{50} is >2000 mg/kg bw in the rat [9]. The combination product of fluopicolide with propamocarb hydrochloride was used effectively to control diseases of vegetable crops [10]. This combination product also gives good control of cauliflower downy mildew.

Cauliflower crop suffers from higher rates of pest infestation compared to other crops and requires frequent pesticide application [11]. Downy mildew is a serious disease of cauliflower which can reduce the yield drastically [12]. When market samples of vegetables were monitored, the pesticide residues were above MRL in cauliflower [13]. Multiple pesticide residues were detected in *Brassica* vegetables [14]. Cauliflower crop is highly sensitive to weather conditions and fluctuations in the temperature leads to variations in the net curd weight. Crops grown during high temperature periods result in maximum curd diameter, whereas, the crops planted under lower temperature regimes give significantly lower curd diameter [15]. Pesticide dissipation on crops is likely to be affected by temperature, humidity, light intensity and rainfall [16]. As growth dilution effect is a major factor for pesticide residue dissipation from crops; variations in the curd diameter and curd weight will have an impact on pesticide dissipation rates [17, 18]. Pesticide dissipation may vary under different environmental conditions in different locations and in successive years in one location. The present study was conducted to evaluate the residue persistence of fluopicolide and propamocarb on cauliflower and their risk assessment under semi arid climatic conditions of India over a period of two years.

TABLE 1
Environmental parameters recorded during the study period

Year	Period	Average maximum temperature (°C)	Average minimum temperature (°C)	Average maximum relative humidity (%)	Average minimum relative humidity (%)	Total cumulative rainfall (mm)	Average maximum wind speed (km/hr)
2013	July	28.0	18.3	78.6	46.4	51.0	6.0
	August	28.3	18.0	82.8	51.8	55.5	4.2
	September	30.1	18.8	83.7	50.4	290.5	4.5
2014	July	28.8	19.4	70.3	43.4	166.8	9.0
	August	30.6	20.6	73.2	53.5	149.0	7.0
	September	29.7	20.8	70.2	45.4	185.5	5.4

MATERIALS AND METHODS

Certified reference materials of 2,6-dichlorobenzamide (purity 99.9%), fluopicolide (purity 99.9%) and propamocarb (purity 96.8%) were procured from Sigma Aldrich Chemicals Pvt. Ltd, India. The commercial formulation, fluopicolide 6.25% + propamocarb hydrochloride 62.5% (Infinito 68.75% SC) was obtained from Bayer Crop Science Ltd, Mumbai, India. Primary secondary amine (PSA), particle size 40 µm, was procured from Agilent Technologies (Bangalore, India). Acetonitrile (HPLC grade), anhydrous sodium sulphate, magnesium sulphate, sodium acetate, analytical grade hexane and analytical grade acetone were procured from Ranbaxy Fine Chemicals, Bangalore, India.

Field study of fluopicolide and propamocarb on cauliflower was carried out as per good agricultural practices (GAP) at the experimental field of ICAR-IIHR (Indian Institute of Horticultural Research, latitude, $13^0 7^1$ N; Longitude, 77^0 29^1E), Bangalore, India. The study was undertaken on cauliflower variety, Titris, during July-September, 2013 using randomised block design of 5M×5M plots with three replications each. The environmental parameters such as temperature, humidity, rainfall and wind speed were recorded (Table 1). Fluopicolide 6.25% + propamocarb hydrochloride 62.5% -Infinito 68.75% SC application was given at the standard and double doses of 100+1000 and 200+2000 g a.i./ha at the curd initiation stage twice at 10-day intervals. Fluopicolide, propamocarb and 2,6-dichlorobenzamide residue analysis in cauliflower curd was carried out after 0 (1h), 1, 3, 5, 7, 10, 15, 20, 25 and 30 day (harvest) of treatment. The experimental field soil was analyzed at harvest. The study was repeated at the same location in a similar manner during July-September, 2014.

Cauliflower curd samples (4-5) were collected at random from each treatment and pooled to form a sample size of approximately 5 kg. Each cauliflower curd was cut into 4 pieces. A quarter of each cauliflower curd cut into small pieces was mixed to form a sub-sample of approximately 1 kg. The samples were homogenized in a Waring blender and the representative samples of 15 g in 3 replicates were taken for analysis of propamocarb and fluopicolide along with its metabolite 2,6-dichlorobenzamide. Soil samples were collected at 0-15 cm depth at harvest. The soil samples from all the treated plots were mixed to form a sample size of approximately 5 kg. The soil samples were air dried in the laboratory at room temperature (25 ± 2^0C), powdered and passed through 2 mm sieve. A represantative 20 g sample in triplicate was taken for analysis. Cauliflower grown without pesticide application was used for spiking.

Cauliflower sample extraction and purification was carried out as per methodology described by Manikrao et al. (2015) [19]. The samples (15 g) were placed in 50mL polypropylene centrifuge tubes and treated with 15 mL HPLC grade acetonitrile. Anhydrous magnesium sulphate (6 g) and anhydrous sodium acetate (1.5 g) were added to the tubes and mixed for 2 min. The contents of the tube were centrifuged in a Restek centrifuge (Q-Sep 3000, Bellefonte, PA 16823, USA) at 4100 rpm for 10 min. Three mL of acetonitrile extract was transferred to centrifuge tubes (15mL) and subjected to solid phase extraction clean-up. To the extracts, 150 mg primary secondary amine (PSA) sorbent and 450 mg anhydrous magnesium sulphate was added and mixed for 2 min, centrifuged. Two mL extract was concentrated to dryness, and re-dissolved in 2 mL of hexane: acetone (9:1, v/v). Extraction of the soil samples (20 g) was carried out with 30 mL acetonitrile: water (2:1, v/v) as described above. The upper solvent layer was transferred to a 50-mL measuring cylinder with stopper and mixed with 10 mL saturated sodium chloride solution. Four mL of the acetonitrile extract was subjected to solid phase extraction clean-up as described above. Two mL of acetonitrile extract was concentrated and re-dissolved in hexane: acetone (9:1, v/v) for analysis by GC and GC-MS.

Fluopicolide and 2,6-dichlorobenzamide analysis was carried out in a Bruker gas chromatograph, GC-450 (Model 1177 S/SL), equipped with Ni^{63} electron capture detector (ECD) and auto-sampler. DB-5MS (30m × 0.25 mm i.d. × 0.25µm; stationary

phase, 5% phenyl 95% methyl polysiloxane) capillary column was used for separation of the analytes. Ultra high pure nitrogen, (99.999% purity) at 1 mL/min was used as the carrier gas. The column temperature program started at 80ºC (with hold time of 5 min) and ramped up at 15ºC/ min to 150ºC (hold time 5 min), 4ºC/min to 250ºC and 10ºC/min to 280ºC with hold time of 17 min. Injector and detector temperatures were 280ºC and 300ºC, respectively. The sample injection volume was 1 µL and split ratio was 20. Propamocarb analysis was carried out in Agilent GC, Model 7890B, equipped with nitrogen phosphorous detector (NPD) with a DB-5 capillary column (30m × 0.25mm, 0.25µm film thickness; stationary phase, 5% phenyl / 95% dimethyl polysiloxane) column. The carrier gas (ultra high pure nitrogen) flow rate was 1 mL/min; hydrogen and air, 3 and 60 mL/min, respectively. Confirmatory studies were carried out by analyzing cauliflower samples in a Shimadzu gas chromatograph mass spectrometry (GC-MS with a QP2010 Plus detector). The GC-MS was operated in full scan mode (40-450 m/z) at the ionization energy of 70 eV. The gas chromatograph was operated in split less mode with injector temperature of 250^0C and ion source temperature of 200^0C. The capillary column, Restek RXI-5ms (30m × 0.25 mm i.d. × 0.25 µm; stationary phase**,** 5% diphenyl/ 95% dimethyl polysiloxane) was used for separation of the analytes and the oven temperature program similar to GC analysis. Ultra high pure helium (99.999%) was used as the carrier gas with a flow rate of 1 mL/min.

Before analysis of the field samples, a recovery study was carried out by spiking fluopicolide, propamocarb and 2,6-dichlorobenzamide in cauliflower and soil at different levels. The spiking levels for fluopicolide and 2,6-dichlorobenzamide were 0.01, 0.05, 0.1 and 0.5 mg/kg and propamocarb, 0.1, 0.5 and 1.0 mg/kg. The lowest concentration of the analyte in the sample that gave satisfactory recovery at the signal: noise ratio of 10:1 was considered the LOQ. The lowest concentration at which the analytes that could be detected corresponding to a signal: noise ratio of 3:1 was considered the LOD.

RESULTS AND DISCUSSION

The LOD obtained for fluopicolide and 2,6-dichlorobenzamide using GC-ECD was 0.003 µg/mL, while the LOQ was 0.01mg/kg. The LOD obtained for propamocarb using GC-NPD was 0.03µg/mL, while the LOQ was 0.1mg/kg. The average recoveries of fluopicolide from cauliflower and soil were between 78.04-97.80% and 2,6-dichlorobenzamide between 80.20-92.72% (Table 2). The average recoveries of propamocarb from cauliflower and soil were between 87.62-99.84% (Table 2). The recoveries obtained for all compounds were within the satisfactory range of 70.0-120.0% [20].

Fluopicolide residue level on cauliflower was 1.495 mg/kg from treatment at the standard dose of 100 g a.i./ha and 2.654 mg/kg from treatment at the double dose of 200 g a.i./ha in the first study (2013) (Table 3). Faster dissipation of fluopicolide in the initial stages and slow dissipation in the later stages was observed for both treatments. Within the first 5 days, 45-50% fluopicolide residues had dissipated from cauliflower and after 10 days the residue dissipation was 74.2 and 70.1%. Further, the residue dissipation of fluopicolide was a slow process. After 25 days the residue levels were 0.025 and 0.147 mg/kg from treatments at the standard and double doses, and after 30 days it was <LOQ and 0.071 mg/kg, respectively. Residues of the major metabolite, 2,6-dichlorobenzamide was <LOQ in all samples. In the field soil (analyzed on the 30^{th} day) residues of fluopicolide and 2,6-dichlorobenzamide were <LOQ. Residues of fluopicolide in the second study (2014) were 1.275 and 2.1 mg/kg from treatments at the standard and double doses of 100 and 200 g a.i./ha, respectively (Table 3). Fluopicolide residues were detected on cauliflower for 25-30 days and the residue dissipation was similar to the first study. Residues of 2,6-dichlorobenzamide was always <LOQ. The initial residues at standard dose treatment were always less than the MRL of 2 mg/kg notified by European Union [21]. The field soil was free from residues of fluopicolide and 2,6-dichlorobenzamide residues after 30 days. Dissipation of fluopicolide from cauliflower over time is presented in Fig. 1.

TABLE 2
Recovery and measurement of uncertainty of fluopicolide, 2,6-dichlorobenzamide and propamocarb from cauliflower and soil

Spiked level (mg/kg)	Average recovery (%) ± SD*					
	Fluopicolide		2,6-dichlorobenzamide		Propamocarb	
	Cauliflower	Soil	Cauliflower	Soil	Cauliflower	Soil
0.01	78.04 ± 9.6	86.60 ± 8.8	80.20 ± 7.2	80.55 ±10.6	-	-
0.05	81.82 ± 7.8	88.70 ± 7.0	81.58 ± 6.8	82.78 ± 5.1	-	-
0.10	89.53 ± 7.0	91.70 ± 6.2	88.73 ± 6.2	86.38 ± 4.7	87.62 ± 8.2	90.53 ± 10.0
0.50	95.90 ± 5.7	97.80 ± 5.5	90.55 ± 4.5	92.72 ± 4.5	91.44 ± 6.5	95.68 ± 7.9
1.00	-	-	-	-	94.70 ± 4.0	99.84 ± 7.2

*Average of 6 replicate analyses ± SD

TABLE 3
Residues of fluopicolide and propamocarb on cauliflower and soil

Days after Treatment	Untreated control	Residues± SD (mg/kg) * 1st year			
		Fluopicolide		Propamocarb	
		Application at 100 g a.i./ha	Application at 200 g a.i./ha	Application at 1000 g a.i./ha	Application at 2000 g a.i./ha
0	ND	1.495 ±0.045	2.654 ±0.232	11.556±0.954	20.600±2.026
1	ND	1.325 ±0.035 (11.7)	2.411 ±0.072 (9.15)	9.634±0.844 (16.6)	18.327±1.452 (11.0)
3	ND	1.054 ±0.060 (29.5)	1.949 ±0.034 (26.9)	7.226±0.605 (37.5)	15.163±0.753 (26.4)
5	ND	0.817 ±0.030 (45.3)	1.329 ±0.040 (50.3)	5.163±0.301 (55.3)	10.242±0.853 (50.3)
7	ND	0.581 ±0.025 (61.1)	0.982 ±0.077 (63.0)	3.425±0.424 (70.4)	7.748±0.876 (62.4)
10	ND	0.385 ±0.025 (74.2)	0.793 ±0.061 (70.1)	2.104±0.155 (81.8)	5.860±0.687 (71.5)
15	ND	0.203 ±0.013 (86.4)	0.526 ±0.067 (80.2)	1.412±0.132 (87.8)	3.884±0.294 (81.1)
20	ND	0.105±0.011 (93.0)	0.316±0.017 (88.1)	0.578±0.072 (95.0)	2.026±0.163 (90.1)
25	ND	0.025±0.004 (98.1)	0.147±0.010 (93.9)	0.185±0.014 (98.4)	1.200±0.095 (94.2)
30	ND	<LOQ	0.071±0.011 (96.3)	<LOQ	0.436±0.052 (97.9)
Soil (30-d)	ND	<LOQ	<LOQ	<LOQ	<LOQ
Days after Treatment	Untreated control	Residues± SD (mg/kg) * 2nd year			
		Fluopicolide		Propamocarb	
		Application at 100 g a.i./ha	Application at 200 g a.i./ha	Application at 1000 g a.i./ha	Application at 2000 g a.i./ha
0	ND	1.275±0.049	2.100±0.116	9.846±1.023	17.788±1.560
1	ND	1.155±0.048 (9.41)	1.875±0.063 (10.7)	8.853± 0.612 (10.1)	16.082±1.628 (9.6)
3	ND	0.853±0.018 (33.0)	1.430±0.055 (31.9)	6.572± 0.726 (33.3)	13.550±0.833 (23.8)
5	ND	0.665±0.082 (44.8)	1.150±0.153 (45.2)	4.842± 0.387 (50.8)	11.474±0.972 (35.5)
7	ND	0.425±0.024 (66.6)	0.893±0.039 (57.5)	3.047± 0.186 (69.1)	9.337±0.626 (51.9)
10	ND	0.285±0.050 (77.6)	0.667±0.063 (68.2)	1.875± 0.096 (80.9)	7.753±0.533 (73.3)
15	ND	0.136±0.005 (89.3)	0.382±0.060 (81.8)	0.961± 0.073 (90.2)	3.147±0.175 (82.3)
20	ND	0.093±0.012 (92.7)	0.235±0.007 (88.8)	0.743± 0.076 (92.5)	2.182±0.082 (87.7)
25	ND	0.056±0.007 (95.1)	0.118±0.006 (93.7)	0.324±0.025 (96.7)	1.226±0.160 (95.1)
30	ND	<LOQ	0.072±0.010 (95.0)	<LOQ	0.622±0.074 (97.1)
Soil (30-d)	ND	<LOQ	<LOQ	<LOQ	<LOQ

*Average of 3 replicate analyses ± SD
Values in the parenthesis are the percent dissipation of residues

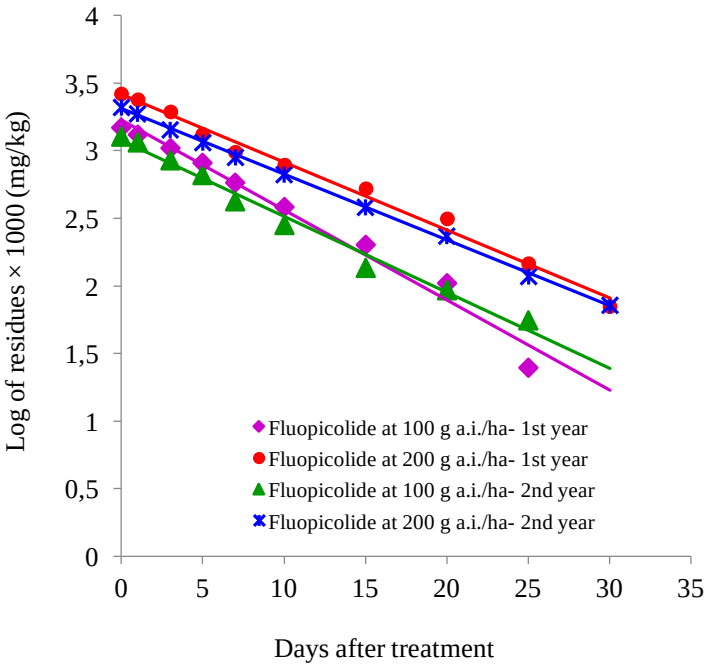

FIGURE 1
Residue dissipation of fluopicolide on cauliflower over 2 years

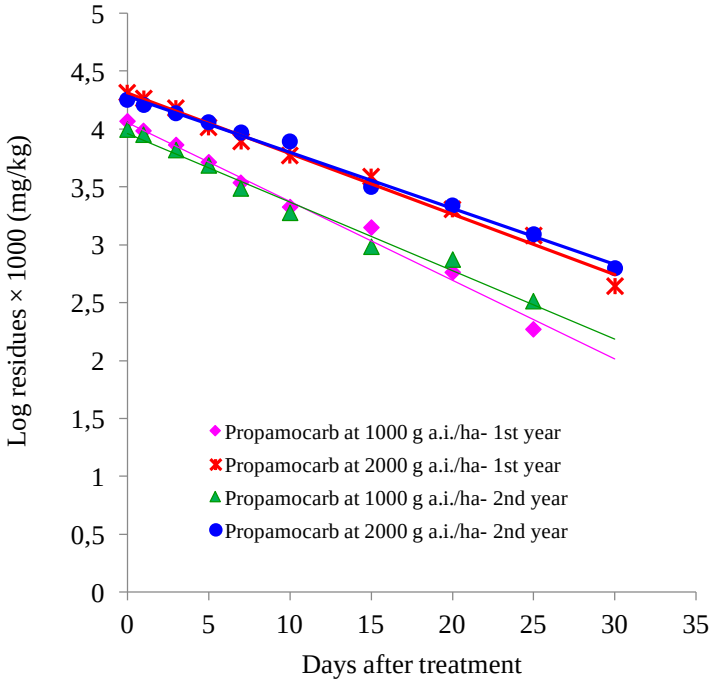

FIGURE 2
Residue dissipation of propamocarb on cauliflower over 2 years

Propamocarb residue levels on cauliflower were much higher than that of fluopicolide. In the first study (2013) the residue was 11.556 mg/kg from treatment at the standard dose of 1000 g a.i./ha and 20.6 mg/kg from treatment at the double dose of 2000 g a.i./ha (Table 3). Residue dissipation was faster initially where more than 50% residues degraded within 5 days. After 10 days, 81.8 and 71.5% propamocarb residues had dissipated from standard and double dose treatments. The residue levels reached <LOQ at the standard dose treatment after 30 days, whereas at the double dose the residues were 0.436 mg/kg on the 30th day. Though the initial

residue levels of propamocarb were much higher than that of fluopicolide both compounds remained on cauliflower for 25 and 30 days at the standard and double dose treatments. In the second study (2014), initial residue deposit of propamocarb at the standard dose was 9.846 mg/kg, which was less than the MRL value. At the double dose treatment, propamocarb residue was 17.788 mg/kg. As in case of fluopicolide, the initial residue levels of propamocarb in the second study was less than that of the first study. There was no significant difference in the dissipation pattern of propamocarb in the two studies. At the double dose treatment propamocarb residue was 0.622 mg/kg which was less than the MRL value. The field soil analyzed after 30 days was free from propamocarb residues in the two studies. Dissipation of propamocarb from cauliflower over time is presented in Fig. 2.

As both studies were carried out in a similar manner the difference in the initial residue deposits could be due to the spray drift. One of the most decisive factors influencing the total spray drift was the wind speed [22, 23]. The spray drift is affected by adjuvant, wind direction, wind speed, air stability, relative humidity, temperature, etc. [24]. The adjuvant used was same in both studies and the relative humidity and temperature was about the same during the study period in 2013 and 2014 (Table 1). Therefore spray drift affected by higher wind speed during 2014 could be the possible reason for lower initial residue deposits.

Fluopicolide and propamocarb dissipation pattern remained similar irrespective of the initial residue deposits in the two studies. This could be due to the similarity in the environmental parameters (relative humidity and temperature) in the two studies (Table 1). The higher rainfall (501.3 mm) during the study period in 2014 did not facilitate faster dissipation of the fungicides. In both studies the residues remained on cauliflower for 25 and 30 days from treatments at 100+1000 and 200+2000 g a.i./ha. Though residues of fluopicolide persisted on cauliflower up to 25 days, the initial residue deposits at the standard dose were below the tolerance limit (MRL). Propamocarb initial residue deposit in the first study was slightly above MRL and in the second study it was less than the MRL. In both studies the metabolite 2,6-dichlorobenzamide was not detected. Fluopicolide was not metabolised to any great extent in plant and the parent compound was the major component of the radioactive residues [2]. Fluopicolide and propamocarb are systemic fungicides and likely to get absorbed by the cauliflower tissues. The surface pesticide residues may degrade faster and the amount adsorbed by the plant may degrade slowly [25].

Residues of fluopicolide, propamocarb or 2,6-dichlorobenzamide were not detected in the soil after 30 days of foliar application to cauliflower plants. Pesticide degradation in soil is influenced by pesticide characteristics, organic matter content of soil, soil pH and soil microbial community [26]. Photodegradation of pesticide may occur in soil [27]. Fluopicolide is steadily degraded in soil by a combination of chemical and microbial transformation processes [28]. Propamocarb degradation was enhanced in the presence of *B. amyloliquefaciens* IN937a and *B. pumilus* SE34 [29]. In the current study the fungicides were applied to cauliflower plants and the thick foliage of the cauliflower plant could have reduced spillage of pesticide solution on soil during spray. The residues in the soil could have dissipated due to various environmental factors including rainfall and are unlikely to remain after 30 days.

The half-life (DT_{50}) for fluopicolide was 4.5 days from treatment at 100 g a.i./ha and 6 days from treatment at 200 g a.i./ha in the first study. In the second study the half-lives were 5.4 days and 6.2 days. Propamocarb residues degraded at the half-life of 4.4 and 5.1 days from treatments at 1000 and 2000 g a.i./ha, respectively in the first study (2013). In the second study (2014) the half-lives were 5.7 and 6.2 days. The half-life of the two compounds in the two studies did not vary much and it was in the range of 4.4-6.2 days. The reported half-lives of fluopicolide on tomato were 2.3-2.5 days and that of propamocarb, 1.4-2.0 days [30]. The half-life of fluopicolide on grapes was 10.2-12.3 days [31]. The floral structure of cauliflower may retain pesticides longer and increase their persistence. The difference in the half-lives in the current study and that reported for grapes could be the dilution effect resulting from crop growth. Dilution due to growth (decrease in the residues) was reported to be the major reason for reduction of pesticides on various crops [32, 33].

The PHI is defined as the interval between the last application of a pesticide to a crop and harvesting of that crop. PHI of fluopicolide and propamocarb was calculated from the residue data and MRL as per statistical analysis by Hoskins [34]. This interval is allowed for degradation of pesticide residues in the harvested crop to an acceptable level, which is defined as the MRL or legal limits. The residue levels of fluopicolide in the two studies were below its MRL at the recommended dose (100 g a.i. ha^{-1}). Therefore, a PHI of 1 day was required for this treatment. By doubling the treatment dosage (200 g a.i. ha^{-1}) the required PHIs for fluopicolide were 2.3 days and 1 day, respectively (first and second study). The required PHI for propamocarb treatment at the standard dose of 1000 g a.i./ha was 1 day for both studies. For double dose treatment the required PHI was 6 days. For treatment of the combination formulation, fluopicolide 6.25% + propamocarb hydrochloride 62.5% (Infinito 68.75% SC), at 100+1000 g a.i./ha the PHI was 1 day to reduce the risk to human health. When treatment was doubled the PHI re-

quired was 6 days. Except wind speed other environmental parameters were about the same in the two studies, so was the dissipation pattern. It indicates that fluopicolide and propamocarb dissipation is likely to be influenced by different environmental conditions, but under similar environmental conditions its behaviour may remain the same.

CONCLUSIONS

Validation of the analytical method for analysis of fluopicolide, propamocarb and 2,6-dichlorobenzamide in cauliflower and soil gave satisfactory results for all parameters studied. The initial residue deposits of fluopicolide and propamocarb on cauliflower varied to some extent in the two studies. The initial residue levels of fluopicolide at the standard dose treatment remained below its MRL. Propamocarb initial residues were slightly above MRL in the first study and below MRL in the second study. Dissipation pattern of the two compounds was about the same in the two studies. The wind speed during the study period seemed to affect the initial residue deposits of the two compounds on cauliflower. Higher rainfall did not accelerate degradation of fluopicolide or propamocarb. The half-life of degradation of both compounds was within 4.4-6.2 days. For treatment of fluopicolide + propamocarb at the standard dose 100+1000 g a.i./ ha 1 day PHI was required for the residues to reduce below their respective MRLs. When the treatment was doubled the required

ACKNOWLEDGEMENTS

The authors thank Director, ICAR-Indian Institute of Horticultural Research, Bangalore, India and Indian Council of Agricultural Research, New Delhi, for providing the facilities to carry out this study.

REFERENCES

[1] Stepanovic, M., Rekanovic, E., Todorovic, B., Potocnik, I., Milijasevic-Marcic, S. (2011) Field evaluation of new fungicide mixture against Phytophthora infestans (Mont.) de Bary on tomato. Acta Horticulturae. 914, 377-379.

[2] Anonymous (2009) Joint meeting on pesticide residues: fluopicolide, pesticide residues in food. FAO plant production Protection paper. 235, 350-406.

[3] Jiang, L.L., Wang, H.Y., Xu, H., Qiao, K., Xia, X.M., Wang, K.Y. (2015) Transportation behaviour of fluopicolide and its control effect against *Phytophthora capsici* in greenhouse tomatoes after soil application. Pest Management Science. 71, 1008-1014.

[4] Douglas, B.M., Roland, S. (2009) Fluopicolide. The Joint FAO/WHO Meeting on Pesticide Residues (JMPR). 269-356.

[5] EFSA (2010) Conclusion on the peer review of the pesticide risk assessment of the active substance dichlobenil. European Food Safety Authority. EFSA J. 8, 1705.

[6] Leake, C., Mackenzie, E., Kley, C. (2006) Mobility assessment of fluopicolide and its metabolites. Pflanzenschutz-Nachrichten-Bayer. 59, 225-242.

[7] Caldas, E.D. (1984) Propamocarb (148), first draft prepared by Eloisa Dutra Caldas, University of Brasilia, Brasilia, Brazil, 719.

[8] Reiter, B., Wenz, M., Buschhau, H., Buchenauer, H. (1995) Effect of propamocarb hydrochloride on *Phytophthora infestans in vitro* and in potato and tomato.Gesunde Pflanzen. 47, 43-50.

[9] Wolterink, G., Tasheva, M. (2005) Propamocarb. Joint FAO/WHO Meeting on Pesticide Residues (JMPR), 417.

[10] Cooke, L.R., Little, G. (2006) Evaluation of fluopicolide containing formulation for the control of potato late blight in Northern Ireland. Pflanzenschutz-Nachrichten Bayer. 59, 303-316.

[11] Weinberger, K., Ramasamy, S. (2009) Farmers' management of cabbage and cauliflower pests in India and their approaches to crop protection. Journal of Asia-Pacific Entomology. 12, 253-259.

[12] Ziadi, S., Barbedette, S., Godard, J.F., Monot, C., Corre, D.L., Silue, D. (2008) Production of pathogenesis-related proteins in the cauliflower (*Brassica oleracea* var. *botrytis*)–downy mildew (*Peronospora parasitica*) pathosystem treated with acibenzolar-S-methyl. Journal of Plant Pathology. 50, 579-586.

[13] Srivastava, A.K., Trivedi, P., Srivastava, M.K., Lohani, M., Srivastava, L.P. (2011) Monitoring of pesticide residues in market basket samples of vegetable from Lucknow city, India: QuEChERS method. Environmental Monitoring and Assessment. 176, 465-472.

[14] Lozowicka, B., Jankowska, M., Kaczynski, P. (2012) Pesticide residues in *Brassica* vegetables and exposure assessment of consumers. Food Control. 25, 561-575.

[15] Thakur, B.S. (2014) Studies on effect of temperature on curd yield under year round production system of cauliflower (*Brassica oleracea Var. botrytis* L.) under mid hills of Himachal Pradesh. Asian Journal of Horticulture. 9, 319-323.

[16] Bloomfield, J.P., Williams, R.J., Gooddy, D.C., Cape, J.N., Guha, P. (2006) Impacts of climate change on the fate and behaviour of pesticides in surface and groundwater- a UK perspective. Science of the Total Environment. 369, 163–177.

[17] Cabras, P., Angioni, A., Garau, V.L., Melis, M., Pirisi, F.M., Cabitza, F., Cubeddu, M., Minelli, E. (1996) Pesticide residues in artichokes: effect of different head shape. Journal of Environmental Science and Health Part B. 31, 1189-1199.
[18] Zongmao, C., Haibin, W. (1988) Factors affecting residues of pesticides in tea. Journal of Pesticide Science. 23, 109-118.
[19] Manikrao, G., Mohapatra, S., Lekha, S., Radhika, B. (2015) Validation of GC and GC-MS methodologies for analysis of fluopicolide and 2,6-dichlorobenzamide in vegetables and soil. Fresen. Environ. Bull. 24, 2985-2994.
[20] SANCO (2013) Guidance document on analytical quality control and validation procedures for pesticide residues analysis in food and feed. Document SANCO/12571/201. 3, 1-46.
[21] EU pesticide database. Available at http://ec.europa.eu/food/plant/pesticides/eu-pesticides-database/public/?event=pesticide.residue.CurrentMRL&language=EN.
[22] Hewitt, A.J., Johnson, D.R., Fish, J.D., Hermansky, C.G., Valcore, D.L. (2002) Development of the spray drift task force database for aerial applications. Environmental Toxicology and Chemistry, 21, 648-658.
[23] Arvidsson, T., Bergstrom, L., Kreuger, J. (2011) Spray drift as influenced by meteorological and technical factors. Pest Management Science. 67, 586-598.
[24] Felsot, A.S., Unsworth, J.B., Linders, J.B., Roberts, G., Rautman, D., Harris, C., Carazo, E. (2011) Agrochemical spray drift; assessment and mitigation-a review. Journal of Environmental Science and Health Part B. 46, 1-23.
[25] Holland, J., Sinclair, P. (2004) Environmental fate of pesticides and the consequences for residues in food and drinking water. In: Hamilton, D. (ed.) Pesticide Residues in food and drinking water human exposure and risks. Crossley, S., John Wiley & Sons Ltd, England. 27-62.
[26] Gavrilescu, M. (2005) Fate of pesticides in the environment and its bioremediation. Engineering in Life Sciences. 5, 497-526.
[27] Katagi, T. (2004) Photodegradation of pesticides on plant and soil surfaces. Reviews of Environmental Contamination and Toxicology. 182, 1-189.
[28] Mackenzie, E., Leake, C., Kley, C. (2006) Metabolism of fluopicolide in soil and water. Pflanzenschutz-Nachrichten Bayer. 59, 209-224.
[29] Myresiotis, C.K., Vryzas, Z., Papadopoulou-Mourkidou, E. (2012) Biodegradation of soil-applied pesticides by selected strains of plant growth-promoting rhizobacteria (PGPR) and their effects on bacterial growth. Biodegradation. 23, 297-310.
[30] Sahoo, S.K., Mandal, K., Kumar, R., Singh, B. (2014) Analysis of fluopicolide and propamocarb residues on tomato and soil using QuEChERS sample preparation method in combination with GLC and GCMS. Food Analytical Methods. 7, 1032-1042.
[31] Mohapatra, S., Ahuja, A.K., Deepa, M., Jagdish, G.K., Rashmi, N., Kumar, S., Prakash, G.S. (2011) Persistence and dissipation of fluopicolide in/on grape berries and soil under semi arid tropical climatic conditions of India. Bulletin of Environmental Contamination and Toxicology. 86, 238-241.
[32] Hill, B.D., Charnetski, W.A., Schaalje, G.B., Schaber, B.D. (1982) Persistence of fenvalerate in alfalfa: effect of growth dilution and heat units on residue half-life. Journal of Agricultural and Food Chemistry. 30, 653-657.
[33] Xia, H.L., Wang, Y.G., Wan, H.B., Ma, H.Q., Chen, Z.M. (1992) Growth dilution by tea plants during the degradation of pesticides in tea plants. Journal of Tea Science.12, 1-6.
[34] Hoskins, W.M. (1961) Mathematical treatment of loss of pesticide residues. Plant Protection Bulletin. 9, 163-168.

Received: **21.04.2017**
Accepted: **20.11.2017**

CORRESPONDING AUTHOR

Soudamini Mohapatra
Pesticide Residue Laboratory,
ICAR-Indian Institute of Horticultural Research,
Hessaraghatta Lake P.O.,
Bangalore 560089 – India

e-mail: soudamini_mohapatra@rediffmail.com

© by PSP Volume 27 – No. 2/2018 pages 846-855 Fresenius Environmental Bulletin

EFFECT OF DIVERSE REGIMES OF IRRIGATION ON METALS ACCUMMULATION IN WHEAT CROP: AN ASSESSESSMENT- DIRE NEED OF THE DAY

Kafeel Ahmad[1], Khalid Nawaz[3], Zafar Iqbal Khan[1,*], Muhammad Nadeem[4], Kinza Wajid[1], Asma Ashfaq[1], Babar Munir[1], Hafsa Memoona[6], Madiha Sana[6], Farzana Shaheen[1], Robina Kokab[1], Saif Ur Rehman[5], Muhammad Fahad Ullah[5], Naunain Mehmood[2], Hira Muqadas[2], Zunaira Aslam[1], Mapara Shezadi[7], Ijaz Rasool Noorka[10], Humayun Basir[1], Hazoor Ahmad Shad[8], Fauzia Batool[1], Sana Iqbal[1], Mudasra Munir[1], Muhammad Sohail[1], Muhammad Sher[9], Saif Ullah[11], Ilker Ugulu[12], Yunus Dogan[12]

[1]Department of Botany, University of Sargodha, Sargodha, Pakistan
[2]Department of Zoology, University of Sargodha, Pakistan
[3]Department of Botany, University of Gujrat, Gujrat, Pakistan
[4]Institute of Food Science and Nutrition, University of Sargodha, Pakistan
[5]Department of Earth Sciences, University of Sargodha, Sargodha, Pakistan
[6]Department of Zoology, Lahore College for Women University, Lahore, Pakistan
[7]Department of Plant breeding and Genetics, Ghazi University, Dera Ghazi Khan, Pakistan
[8]Department of Chemistry, Government Post Graduate College, Jhang, Pakistan
[9]Department of Chemistry, University of Sargodha, Pakistan
[10]Plant Breeding and Genetics, Agriculture College, University of Sargodha, Pakistan
[11]Department of Economics, University of Sargodha, Pakistan
[12]Buca Faculty of Education, Dokuz Eylul University, Izmir, 35150, Turkey

ABSTRACT

Wastewater irrigation causes possible contamination of soil and crops and is responsible for health hazards to consumers. Current research was undertaken to observe the extent of contamination in wheat irrigated with wastewater and its possible consequences on humans. A pot experiment was performed in this regard to assess the concentration of metals in soil, water and grain samples. The level of heavy metals (mg kg^{-1}) in wheat grains ranged from 1.18 to 1.64 for Cd, 0.07 to 0.20 for Pb, 0.74 to 1.28 for Cu, 0.44 to 0.60 for Cr, and 0.02 to 0.22 for Co. The values of all heavy metals were within the permissible limit of 0.3 mg kg^{-1} for Pb, 73.3 mg kg^{-1} for Cu, 2.3 mg kg^{-1} for Cr, and 50 mg $kg^{-1}$for Co, while the Cd content in wheat surpassed the tolerable limit of 0.2 mg kg^{-1} indicating its mobility. A significant and positive correlation was obtained for Cd, Pb Cu, and Co (0.90, 0.85, 0.79, 0.89; $p<0.01$) while Cr showed non-significant correlation (0.52; $p>0.05$) between soil and wheat grains. The values of health risk index for all heavy metals were below 1 except for Cd. Regular monitoring of wheat crop is suggested in light of these findings to minimize the health risks in humans.

KEYWORDS:
Triticum aestivum L., Wastewater, Contaminated soil, Physicochemical parameters, Health risk index

INTRODUCTION

Since the period of industrial revolution, safety of food has become one of the imminent challenges throughout the globe. In developing countries, increasing demand of food has pressurized farmers to use inexpensive methods which help in increasing crop yield. Among such methods, wastewater irrigation is gaining much more importance all over the world. Approximately, 10% population of world relies on wastewater irrigated crops [1].

Wastewater contains large amount of significant plant nutrients but it may also contain large amount of contaminants such as synthetic chemicals, pathogens and heavy metals e.g., lead, chromium, cadmium, and nickel etc. which pollute environment and cause various health hazards to human [2].

Soil is an important reservoir for heavy metals and these heavy metals accumulate in eatable parts of plants. Food chain contamination is one of the considerable pathways by which human bodies get exposed to toxic heavy metals [3]. However, some plants develop various adaptations to control the absorption of metals at the boundary of soil and root. Selection of limited metal absorbing varieties of cereal crops may help in safer production of crops on wastewater contaminated soils [4].

Wheat (*Triticum aestivum* L.), belongs to family Poaceae, is an essential crop throughout the globe. Wheat is a staple food and vital component of human diet. It plays significant role in growth of humans by providing inorganic micronutrients, proteins and carbohydrates. Wheat is an indispensable

part of diet of more than 35% of the total population of the world so there is a constant need to get the higher yield of wheat to meet the demand of people [5].

Heavy metal accumulation in different plant parts increases after wastewater irrigation. So the consumption of contaminated wheat crop may cause serious health hazards to humans. Consumption of contamination-free food crop is the vital feature of food quality [3].

Therefore, current study focused on the impact of wastewater irrigation on heavy metal buildup in soil and wheat and its impact on wheat growth as well as human health. Bio-concentration factor (BCF), pollution load index (PLI), correlation, daily intake of metal (DIM) and health risk index (HRI) due to metals via consumption of *Triticum aestivum* were also calculated.

MATERIALS AND METHODS

Plant cultivation. Current research work was carried out at Botanical Garden, University of Sargodha, Sargodha, during the year 2015-2016. Seeds of wheat variety (Faisalabad-2008) were sown in November, 2015 in plastic pots (10 cm in height and 25 cm in diameter) and harvested at the start of April, 2016. About 5 kg of soil was added in each pot. Contaminated soil was collected from wastewater irrigated area. Different contaminated soil amendments used for pot experiment were: 100% pure soil; 50% contaminated soil and 50% pure soil; 75% contaminated soil and 25% pure soil; 100% contaminated soil. Four pots with three replications of each treatment were labeled. Each pot was sown with eight seeds. Wastewater irrigation with different combinations was used. The wastewater was taken from a sewage pond in Sargodha, along with ground water with different concentrations: T1: Irrigated with 100% ground water, T2: Irrigated with 50% wastewater and 50% ground water, T3: Irrigated with 75% wastewater and 25% ground water, T4: irrigated with 100% wastewater. Experimental design used for this study was randomized block design (RBD). Wastewater and ground water were analyzed for multiple physico-chemical parameters such as pH, electrical conductivity (EC), Magnesium (Mg^{+2}), calcium (Ca^{+2}) and heavy metals: chromium (Cr), lead (Pb), cadmium (Cd), copper (Cu) and cobalt (Co).

Sample collection and preparation. After threshing, seeds were powdered ground. Soil was taken from top 5 cm for sampling. Oven dried soil samples were eventually analyzed for various physico-chemical parameters. Digestion of soil, water and grain samples was done through "wet digestion method" [6].

Analysis of some physico-chemical parameters of water and soil samples. Soil and water characteristics such as electrical conductivity (EC), pH, calcium, magnesium, and organic matter were determined. pH and EC were determined by pH meter and EC meter [7]. Titration method was used for calculation of Ca^{+2} and Mg^{+2} content. Soil OM was determined by Walkley and Black acid digestion method [8].

Statistical analysis. Analysis of variance was performed for treatments in support of water, soil and wheat grains with the help of software package SPSS.16. Correlation between soil and wheat grains for each heavy metal was calculated.

Bio-concentration factor (BCF) was calculated following [9]. Pollution load index (PLI) was calculated by following [10]. Daily intake of metal (DIM) was calculated by following formula [11] to assess metal intake by considering daily consumption of wheat as 0.242 kg $person^{-1}$ [12] and average body weight of 55.9 kg [13]. Health risk index (HRI) values depend on daily intake of metals and oral reference dose (R_fD). HRI was determined by using equation described by [9].

RESULTS

ANOVA exhibited significant effect ($p<0.05$) of water treatments on heavy metal levels such as Cd, Co, Pb and Cu while non-significant effect ($p>0.05$) on Cr. Significant effect ($p<0.05$) of treatments was noticed on heavy metals (Cu, Pb, Cr, Cd, Co) in soil used to grow wheat. Significant effect ($p<0.05$) of treatments on levels of Cd, Pb, Cu, and Co was observed in wheat grains while non-significant effect ($p>0.05$) in grains of wheat was obtained for Cr (Table 1).

Physico-chemical parameters of water. Mean values of EC (dSm^{-1}) among four treatments ranged from 1.48 to 7.15. The values of Ca^{+2} and Mg^{+2} (meq L^{-1}) in four treatments were 5.43-24.76. The values of Na^{+} ranged from 9.96 to 49 meq L^{-1}. The value of Na^{+} was lowest in treatment-I while highest in treatment-IV. Concentration of Cl^{-} (meq L^{-1}) in all treatments ranged from 4.8 to 44.5. The values of SAR among four treatments were 1.8, 4.76, 10.3 and 13.86 respectively (Table 2).

Mean concentrations (mg L^{-1}) of heavy metals in water. In water samples, mean levels of heavy metals (mgL^{-1}) ranged from 0.018 to 0.074 for Pb, 1.69 to 1.88 for Cd, 0.53 to 0.74 for Cu, 0.54 to 0.65 for Cr, and 0.31 to 0.46 for Co respectively. The order of concentration of heavy metals at treatment-I was: Cd>Cr>Cu>Co>Pb; while at treatment-II, III and IV it was in following sequence:

Cd>Cu>Cr>Co>Pb (Table 3, Figure 1). The concentration of Cd was highest while Pb was lowest in all treatments.

Physico-chemical parameters of soil. Loamy texture of soil was noticed in all treatments. Mean values of soil pH was 8.1, 7.8, 7.8, and 7.7 in four treatments. E.C. of soil was in the range of 6.65 dSm^{-1} to 13.27 dSm^{-1}. The range (%) of OM in four treatments was 0.96-1.11. The mean values of available P (mg kg^{-1}) among four treatments were 6.66, 14.36, 18.33 and 25.4 respectively. The values of available K (mg kg^{-1}) among four treatments were 331, 356.33, 368.33 and 277.3 respectively (Table 4).

Mean concentrations (mg kg^{-1}) of heavy metals in soil. In soil samples, concentrations (mg kg^{-1}) of heavy metals varied from 0.14 to 0.35 for Pb, 1.85 to 1.98 for Cd, 1.25 to 2.04 for Cu, 1.01 to 1.2 for Cr, and 0.63 to 0.76 for Co respectively. The trend of heavy metals among four treatments was: Cd>Cu>Cr>Co>Pb (Table 5, Figure 2). Mean concentrations of Cd and Cu were found to higher while Pb was lowest among four treatments.

Mean concentrations (mg kg^{-1}) of heavy metals in wheat grains. In wheat grains, concentrations of heavy metals (mg kg^{-1}) ranged from 0.07 to 0.2 for Pb, 1.18 1.64 for Cd, 0.44 to 0.6 for Cr, and 0.02 to 0.22 for Co respectively. At treatment-I, II and III the sequence of heavy metal concentration was: Cd>Cu>Cr>Pb>Co; while at treatment-IV it was found in following order: Cd>Cu>Cr>Co>Pb (Table 6, Figure 3). Concentration of Cd was found to be highest while Co and Pb were low in all treatments.

TABLE 1
Analysis of variance of heavy metals in water, soil, and wheat grains

	Mean Square				
Heavy metals	**Pb**	**Cd**	**Cu**	**Cr**	**Co**
Water	0.002***	0.021***	0.025***	0.005^{ns}	0.014***
Soil	0.009***	0.166***	0.331***	0.020***	0.029***
Wheat grains	0.009***	0.166***	0.185^{ns}	0.017^{ns}	0.023***

*, **, *** = Significant at 0.05, 0.01, 0.001 level, **ns** = non-significant

TABLE 2
Physico-chemical parameters of water

Treatments	**Physico-chemical parameters**				
	EC (dSm^{-1})	**Calcium, Magnesium (Ca^{+2}, Mg^{+2}) ($meqL^{-1}$)**	**Sodium (Na^{+}) ($meqL^{-1}$)**	**Chloride (Cl^{-}) ($meqL^{-1}$)**	**Sodium Adsorption Ratio (SAR)**
I	1.48±1.4	5.43± 1.2	9.96±1.2	4.80±1.3	1.8±0.9
II	3.47±1.7	10.33±1.2	29.43±1.5	19.2±1.4	4.76±1.2
III	5.87±1.6	17.3±1.3	39.23±1.7	30.3±1.2	10.3±1.2
IV	7.15±2.7	24.76±1.4	49±1.6	44.5±1.4	13.86±1.3
Standard limits	5.1[a]	200[a], 150[a]	900[b]	-	15[b]

Source [a]MWE [44]; Source [b]FAO (46), T-I = Treatment-I, T-II = Treatment-II; T-III = Treatment-III, T-IV, Treatment-IV, EC= Electrical conductivity

TABLE 3
Mean concentrations (mg L^{-1}) of heavy metals (Mean ± SE) in water

Heavy metals	**T-I**	**T-II**	**T-III**	**T-IV**	**PML (mg L^{-1})[a]**
Pb	0.130±0.08	0.271±0.12	0.355±0.11	0.503±0.13	5.00
Cd	1.693±0.1	1.790±0.12	1.840±0.14	1.886±0.18	0.01
Cu	0.530±0.07	0.596±0.09	0.660±0.1	0.743±0.12	0.20
Cr	0.549±0.08	0.580±0.09	0.594±0.13	0.650±0.15	0.10
Co	0.318±0.06	0.373±0.08	0.441±0.1	0.467±0.13	0.05

Source [a] FAO/WHO [17], T-I = Treatment-I, T-II = Treatment-II; T-III = Treatment-III, T-IV, Treatment-IV, SE = Standard Error, PML = Permissible Limit

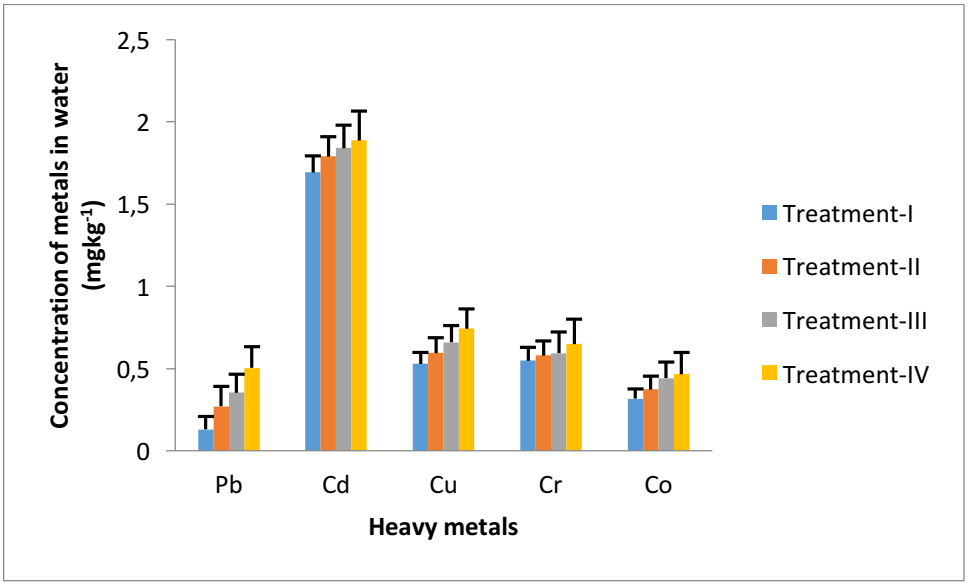

FIGURE 1
The fluctuation of heavy metals in water of four treatments

TABLE 4
Physico-chemical parameters of soil

Treatments	Physico-chemical parameters					
	pH	EC (dSm^{-1})	Organic matter (%)	Available Phosphorus (mg kg^{-1})	Available Potassium (mg kg^{-1})	Texture
I	8.1±0.05	6.65±0.02	0.96±0.01	6.66±0.08	331±0.57	Loam
II	7.8±0.03	11.6±10.01	1.06±0.01	14.36±0.14	356.3±1.2	Loam
III	7.8±0.03	13.04±0.01	1.07±0.02	18.33±0.14	368.3±0.88	Loam
IV	7.7±0.06	13.27±0.28	1.11±0.08	25.4±0.11	377.3±0.66	Loam

TABLE 5
Mean concentrations (mg kg^{-1}) of heavy metals (Mean± SE) in soil

Metals	T-I	T-II	T-III	T-IV	PML (mg kg^{-1})[a]
Pb	0.146±0.06	0.240±0.11	0.298±0.12	0.356±0.15	100
Cd	1.855±0.08	1.916±0.09	1.938±0.14	1.983±0.16	3
Cu	1.251±0.09	1.531±0.12	1.698±0.2	2.046±0.17	100
Cr	1.011±0.08	1.060±0.12	1.120±0.13	1.201±0.16	50
Co	0.631±0.08	0.678±0.09	0.706±0.12	0.761±0.15	100

Source [a] FAO/WHO [17], T-I = Treatment-I, T-II = Treatment-II; T-III = Treatment-III, T-IV, Treatment-IV, SE = Standard Error, PML = Permissible Limit

TABLE 6
Mean concentrations (mg kg^{-1}) of heavy metals (Mean ± SE) in grains of *Triticum aestivum*

Metals	T-I	T-II	T-III	T-IV	PML (mg kg^{-1})[a]
Pb	0.076±0.03	0.121±0.05	0.155±0.06	0.206±0.06	0.3
Cd	1.181±0.05	1.385±0.08	1.501±0.06	1.646±0.08	0.2
Cu	0.745±0.06	0.791±0.08	1.025±0.07	1.286±0.06	73.3
Cr	0.441±0.05	0.490±0.06	0.573±0.06	0.603±0.08	2.3
Co	0.026±0.03	0.07±0.04	0.115±0.06	0.228±0.04	50

Source [a] FAO/WHO [17], T-I = Treatment-I, T-II = Treatment-II; T-III = Treatment-III, T-IV, Treatment-IV, SE = Standard Error, PML = Permissible Limit

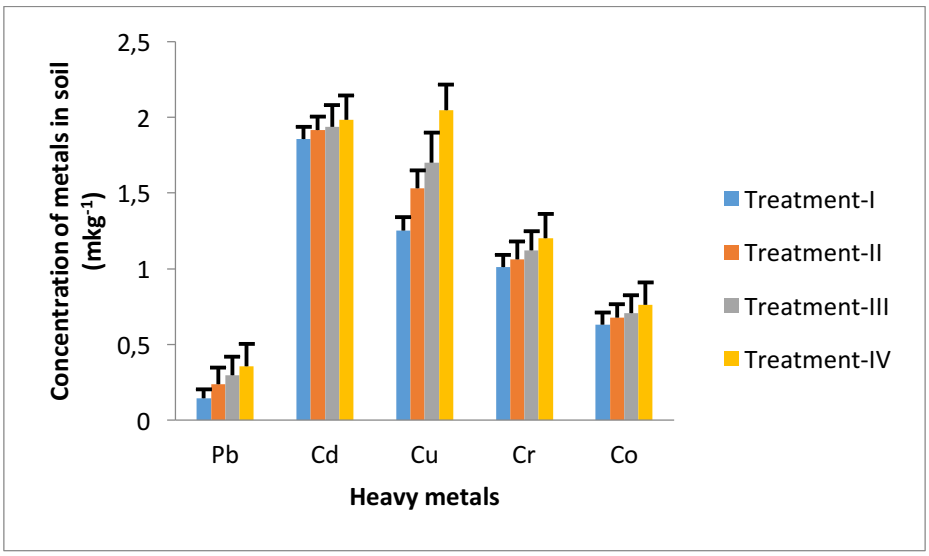

FIGURE 2
The fluctuation of heavy metals in soil of four treatments

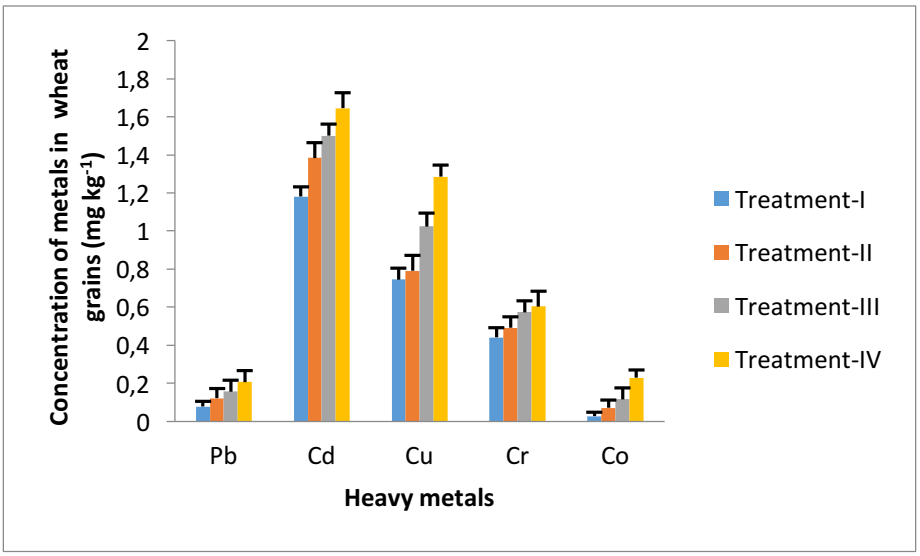

FIGURE 3
The fluctuation of heavy metals in grains of four treatments

TABLE 7
Bio-concentration factor for wheat grain/soil

Treatments	Heavy metals				
	Pb	Cd	Cu	Cr	Co
I	0.5205	0.6366	0.5955	0.4362	0.0412
II	0.5041	0.7228	0.5166	0.4622	0.1032
III	0.5201	0.7733	0.6036	0.5116	0.1628
IV	0.5786	0.8300	0.6285	0.5020	0.2996

TABLE 8
Correlation between soil and grain metal concentrations

	Correlation				
Heavy metals	Pb	Cd	Cu	Cr	Co
Soil-Grains	0.902**	0.856**	0.799**	0.526^{ns}	0.898**

*, **= Correlation is significant at 0.05 and 0.01 level, **ns** = Correlation is non-significant

TABLE 9
Pollution load index for heavy metals in soil

Treatments	Heavy metals				
	Pb	Cd	Cu	Cr	Co
I	0.0179	1.2449	0.1491	0.1114	0.0693
II	0.0294	1.2859	0.1824	0.1168	0.0745
III	0.0365	1.3026	0.2023	0.1234	0.0775
IV	0.0436	1.3308	0.2438	0.1324	0.0836

TABLE 10
Daily intake of metals

Treatments	Heavy metals				
	Pb	Cd	Cu	Cr	Co
I	0.0003	0.0051	0.0032	0.0019	0.0001
II	0.0005	0.0059	0.0034	0.0021	0.0003
III	0.0006	0.0064	0.0044	0.0024	0.0004
IV	0.0008	0.0071	0.0055	0.0026	0.0009

TABLE 11
Health risk index of metal contents via intake of *Triticum aestivum*

Treatments	Heavy metals				
	Pb	Cd	Cu	Cr	Co
I	0.094	5.113	0.0806	0.0012	0.0026
II	0.1497	5.996	0.0856	0.0014	0.0070
III	0.1917	6.498	0.1109	0.0016	0.0115
IV	0.2548	7.126	0.1391	0.0017	0.0229

Bio-concentration factor (BCF). BCF was used to determine the transfer of metals from soil to edible parts of plants. The decreasing order of BCF among four treatments was: Cd>Cu>Pb>Cr>Co. The values of BCF for Cd were highest while Co showed lowest values of BCF (Table 7).

Correlation Correlation between soil and wheat grain for each metal such as Pb, Cd, Ni, Fe, Mn, Cu, Zn, and Co was positive and significant while that for Cr was positive and non-significant between soil and wheat grains (Table 8).

Pollution load index (PLI) Pollution severity was determined by PLI. The PLI at treatment-I, II, III and IV was found in following sequence: Cd>Cu>Cr>Co>Pb. The values of PLI for Cd were highest while Pb had lowest value in all treatments (Table 9).

Daily intake of metals (DIM). The value of DIM for Cd was highest while Pb and Co showed low DIM values. At treatment-I, II, and III the values of DIM were in following sequence: Cd>Cu>Cr>Pb>Co; while at treatment-IV it was found in decreasing order of: Cd>Cu>Cr>Co>Pb (Table 10).

Health risk index (HRI). The values of HRI for Cd was greater than 1, while that of Pb, Co, Cu, and Cr were less than 1. The values of HRI among all treatments was found in decreasing order of: Cd>Pb> Cu>Co>Cr (Table 11).

DISCUSSION

Water salinity can be well indicated by electrical conductivity. Wastewater contains high salt content. Current results were in agreement to the findings of Singh et al. [14]. SAR is more consistent index, which is the affinity of irrigation water to form exchangeable sodium in soil [46]. Balkhair and Ashraf [15] reported higher values of Ca^{+2} and Na^{+} while lower values of EC and SAR as compared to current investigation. EC in current investigation was greater than the findings of Alghobar et al. [16].

The mean values of heavy metals such as Pb, Cu, Co, Cr and Cd in water samples were above the permissible level recommended by FAO/WHO [17]. Mojiri and Aziz [18] suggested lower level of Cd in wastewater as compared to present investigation. The values of Pb, Cd, Cr, and Cu in current investigation were above the values of Singh et al. [19]. Sherif et al. [20] reported lower values of Co, Cu, Cd, Cr and Pb as compared to the present values.

Soil texture has significant effect on physico-chemical properties of soil. Wastewater irrigation considerably increased the soil OM, EC, available P, and available K and decreased the soil pH. Organic matter breaks down and generates organic acids in soil and affects its properties [21]. The values of OM and pH in present investigation were above the values reported by Naz et al. [22]. Soil OM content is an important indicator of soil fertility [23]. EC of soil increased after wastewater irrigation. Current data were similar to the results of Khai et al. [24] for soil properties. In present investigation the value of OM was lower while phosphorus and potassium were higher in contrast to study of Yang et al. [25].

The mean level of all heavy metals found in soil was within the PML suggested by Balkhair and Ashraf [15]. This might be due to the high values of soil pH. In soil, distribution of heavy metals is affected by various properties of soil for example pH, EC and OM content [26]. Yu et al. [27] suggested higher values of Cr Cu, Pb and lower level of Cd in contrast to the present findings. The soil Cd contents were above while Cr Cu, and Pb were below the obtained data of Wang et al. [28]. The exchangeable capacity of Cd is higher as compared to other metals so that's why it easily becomes available and accumulates in edible parts of plants [29]. The soil Cd concentration was above as reported by Ashfaq et al. [30] and lower as suggested by Liu et al. [31]. Bio-availability of heavy metals in wastewater irrigated soil was higher as compared to ground water irrigated soil [32].

The mean values of all heavy metals found in wheat grains were within the PML except for Cd as recommended by FAO/WHO [17]. The level of Cd and Cu was above while the concentration of Zn was below in present study in wheat grains while Pb and Cr level was similar to that analyzed by Yu et al. [27].

Cadmium concentration in grains was above the PML of 0.2 $mgkg^{-1}$suggested by Balkhair and Ashraf [15], meaning that wheat had been polluted by cadmium. Cadmium poisoning in man can cause bone disorder, lung cancer and anemia [12].

In humans, BCF is the basic component to determine the level of exposure through food chain. Amongst various metals in wheat grains Cd exhibited highest BCF values while Co showed lowest BCF values. High value of BCF depicted a high movement of this metal toward plant and vice versa. Balkhair and Ashraf [15] reported that Cd is more mobile as compared to other heavy metals hence it binds weakly to soil. The differences in BCF may be due to the binding of heavy metals to plant roots, interaction between physico-chemical parameters, available metals in soil, and type of plant species [7]. BCF values for Cu, Zn, Ni and Cr in present investigation was above as than the findings of Verma et al. [34].

A strong positive correlation for Pb, Cd, Cu, and Co showed that these metals could be coming from same wastewater source. In present investigation, a positive and non-significant correlation for Cr was due to the feeble association between wheat grains and soil. Ekmekyapar et al. [35] also demonstrated a non-significant correlation between concentrations of heavy metals in soil and wheat grains.

To estimate the contamination status and inconsistency in soil, PLI was determined. The values of PLI (>1) indicate that soil is contaminated; values lower than 1 were considered as uncontaminated [36]. The PLI for Cd was greater than 1 among all treatments. The values of PLI greater than 1 indicated that this metal can potentially cause ecological hazard. High PLI values could be due to different factors such as agricultural runoff, human activities and industrial activities [37].

The DIM for Pb, Cd, Cu, Co, and Cr were below the tolerable daily intake limit [38, 39, 40, 41, 42]. In present investigation the values of DIM by consumption of wheat grains were found less than 1. Jaishree and Khan [43] reported higher values of DIM for Pb, Cu, Cd, and Cr as compared to present investigation.

HRI is an important parameter for estimating the risks related with consumption of metal contaminated food crop [1]. Value >1 suggested serious health risks to public [43] which in present study was obtained for Cd. In present study, HRI values for Cr and Pb were lower while those of Cd were higher as reported by Ministry of water and electricity, Saudi Arabia [44]. Health hazard due to Cd in present investigation was above as contrast to the findings of Singh et al. [45].

CONCLUSION

Wastewater irrigation causes buildup heavy metals in soil, crop and contaminates food chain. The values of heavy metals in wheat grains were within the acceptable limits except for Cd. The greater level of cadmium in wheat grains indicated stronger transfer capability of Cd from soil to edible part of plants. The discrepancy in level of heavy metals in wheat grains reflected the differences in accumulating capability of heavy metals by wheat plant. So it is concluded that quality of wastewater irrigated wheat was poor and cannot be considered safe for human health because of high concentration of Cd. Therefore, steps should be taken for efficient treatment of wastewater to reduce health risks in human.

REFERENCES

[1] Corcoran, E. (2010) Sick water: The central role of wastewater management in sustainable development: A rapid response assessment. UNEP/Earth print.

[2] Shahid, M., Dumat, C., Pourrut, B., Abbas, G., Shahid, N. and Pinelli, E. (2015) Role of metal speciation in lead-induced oxidative stress to *Viciafaba* roots. Russian Journal of Plant Physiology. 62(4), 448-454.

[3] Khan, S., Cao, Q., Zheng, Y.M., Huang, Y.Z. and Zhu, Y.G. (2008) Health risks of heavy metals in contaminated soils and food crops irrigated with wastewater in Beijing, China. Environmental Pollution. 152(3), 686-692

[4] Chamon, A.S., Gerzabek, M.H., Mondol, M.N., Ullah, S.M., Rahman, M. and Blum, W.E.H. (2005) Influence of cereal varieties and site conditions on heavy metal accumulations in cereal crops on polluted soils of Bangladesh. Communication Soil Sciences and Plant Analysis. 36, 889-906.

[5] Khakwani, A.A., Dennett, M.D., Munir, M. and Abid, M. (2012) Growth and yield response of wheat varieties to water stress at booting and anthesis stages of development. Pakistan Journal of Botany. 44, 879-886.

[6] Allen, S., Grimshaw, H. and Rowland, A. (1986) Chemical analysis, Moore P.D., Chapman, S.B. Methods in Plant Ecology, Blackwell Scientific Publications, Oxford. 285-344.

[7] Jackson, M.L. (1973) Soil Chemical Analysis. Jackson Prentice Hall of India, New Delhi, India.

[8] ASA. (1982) Methods of Soil Analysis. Part 2. Chemical and Microbiological Properties, 2nd edition, Page, A.L. (Ed.) Agronomy Society of America.

[9] Cui, Y.J., Zhu, Y.G., Zhai, R.H., Chen, D.Y., Huang, Y.Z., Qui, Y. and Liang, J.Z. (2004) Transfer of metals from near a smelter in Nanning, China. Environment International. 30, 785-791.

[10] Liu, W.H., Zhao, J.Z., Ouyang, Z.Y, Soderlund, L. and Liu, G.H. (2005) Impacts of sewage irrigation on heavy metals distribution and contamination in Beijing, China. Environment International. 31, 805-812.

[11] Sajjad, K., Farooq, R., Shahbaz, S., Khan, M.A. and Sadique, M. (2009) Health risk assessment of heavy metals for population via consumption of vegetables. World Applied Science Journal. 6, 1602-1606.

[12] Wang, X., Huan, G.W., Tian, H.G., Dong, S.R., Yin, H.G. and Cao X.H. (2007) Investigation on dietary of urban residents in Tianjin from 2000-2004, China. Journal of Public Health. 23, 1245.

[13] Wang, X., Sato, T., Xing, B. and Tao, S. 2005. Health risks of heavy metals to the general public in Tianjin, China via consumption of vegetables and fish. Science of the Total Environment. 350, 28.

[14] Singh, S.N., Srivastav, G. and Bhatt, A. (2012) Physico-chemical determination of pollutants in wastewater in Dheradun. Current World Environment.7, 133-138.

[15] Balkhair, K.S. and Ashraf, M.A. (2016) Field accumulation risks of heavy metals in soil and vegetable crop irrigated with sewage water in western region of Saudi Arabia. Saudi Journal of Biological Sciences. 23, 32-44.

[16] Alghobar, M.A. and Suresha, S. (2015) Evaluation of nutrients and trace metals and their enrichment factors in soil and sugarcane crop irrigated with wastewater. Journal of Geoscience and Environment Protection. 3, 46-56.

[17] FAO/WHO. (2001) Codex Alimentarius Commission. Food additive and contaminants. Joint FAO/ WHO Food Standards Programme, ALINORM 01/ 12A. 1-289.

[18] Mojiri, A. and Aziz, H.A. (2011) Effects of municipal wastewater on accumulation of heavy metals in soil and wheat (*Triticum aestivum* L.) with two irrigation methods. Romanian Agricultural Research. 28, 217-222.

[19] Singh, K.P., Mohon, D., Sinha, S. and Dalwani, R. (2004) Impact assessment of treated/untreated wastewater toxicants discharge by sewage treatment plants on health, agricultural, and environmental quality in wastewater disposal area. Chemosphere. 55, 227-255.

[20] Sherif, A.E.A., El-Kholy, M.M. and Salem, T.M. (2015) Risk assessment of trace elements toxicity through edible plants from irrigation canal at Giza Governorate, Egypt. Iranica Journal of Energy & Environment. 6(1), 47-55.

[21] Mojiri, A. and Jalalian, A. (2011) Relationship between growth of *Nitrariaschoberi* and some soil properties. Journal of Animal and Plant Sciences. 21(2), 246-250.

[22] Naz, H., Naz, A. and Ashraf, S. (2015) Impact of heavy metal toxicity to plant growth and nodulation in chickpea grown under heavy metal stress. International Journal for Research in Emerging, Science and Technology. 2(5), 248-260.

[23] Song, C.Y., Zhang, X.Y., Liu, X.B. and Gao, C.S. (2008) Effect of soil organic matter on soil fertility and crop productivity. Syst Sci Comp Stud Agric. 24, 357-362.

[24] Khai, N.M., Tuan, P.T., Vinh, C.N. and Oborn, T. (2008) Effects of using wastewater as nutrient sources on soil chemical properties in peri-urban agricultural systems. VNU Journal of Science, Earth Sciences. 24, 87-95.

[25] Yang, B., Kong, X., Cui, B., Jin, D., Deng, Y., Zhuang, X., Zhuang, G. and Bai, Z. (2015) Impact of rural domestic wastewater irrigation on the physicochemical and microbiological properties of pakchoi and soil. Water. 7, 1825-1839.

[26] Zhou, L., Yang, B., Xue, N., Li, F., Seip, H.M., Cong, X., Yan, Y., Liu, B., Han, B. and Li, H. (2014) Ecological risks and potential sources of heavy metals in agricultural soils from Huanghuai Plain, China. Environmental Science and Pollution Research. 21, 1360-1369.

[27] Yu, X., Wang, Z., Lynn. A., Cai, J., Huangfu, Y., Geng, Y., Tang.J. and Zeng, X. (2016) Heavy metals in wheat grown in sewage irrigation: A distribution and prediction model. Polish Journal of Environmental Study. 25(1), 413-418.

[28] Wang, Z., Zeng, X., Geng, M., Chen, C., Cai, J., Yu, X., Hou, Y. and Zhang, H. (2015) Health risks of heavy metals uptake by crops grown in a sewage irrigation area in China. Polish Journal of Environmental Study. 24(3), 1379-1386.

[29] Luo, C., Liu, C., Wang, Y., Liu, X., Li, F., Zhang, G. and Li, X. (2011) Heavy metal contamination in soils and vegetables near an e-waste processing site, south China. Journal of Hazardous Materials. 186(1), 481-490.

[30] Ashfaq, A., Khan, Z.I., Bibi, Z., Ahmad, K., Ashraf, M., Mustafa, I., Akram, N.A., Perveen, R. and Yasmeen, S. (2015) Heavy metals uptake by *Cucurbita maxima* grown in soil contaminated with sewage water and its human health implications in peri-urban areas of Sargodha city. Pakistan Journal of Zoology. 47(4), 1051-1058.

[31] Liu, Z., Zhang, Q., Han, T., Ding, Y., Sun, J., Wang, F. and Zhu, C. (2016) Heavy metal pollution in a soil-rice system in the Yangtze River region of China. International Journal of Environmental Research and Public Health.13(63), 1-16.

[32] Mahmood, A. and Malik, R.N. (2014) Human health risk assessment of heavy metals via consumption of contaminated vegetables collected from different irrigation sources in Lahore, Pakistan. Arabian Journal of Chemistry. 7(1), 91-99.

[33] Bose, S. and Bhattacharyya, A.K. (2008) Heavy metal accumulation in wheat plant grown in soil amended with industrial sludge. Chemosphere. 70, 1264-1272.

[34] Verma, S., Yadav, S., Yadav, S.K., Kadyan, P.S., Singh, I. and Singh, D. (2015) Heavy metals in wheat grains of Haryana (India) and their health implications. Journal of Chemical and Pharmaceutical Research. 7(10), 342-351.

[35] Ekmekyapar, F., Sabudak, T. and Seren, G. (2012) Assessment of heavy metal contamination in soil and wheat (*Triticum aestivum L.*) plant around the Corlu-Cerkezkoy highway in Thrace region. Global NEST Journal. 14(4), 496-504.

[36] Harikumar, P.S., Nasir, U.P., Mujeebu, M.P. and Rahma. (2009) Distribution of heavy metals in the core sediments of a tropical wetland system. International Journal of Environment Science and Technology. 6(2), 225-232.

[37] Uwah, E.I., Ndahi, N.P. and Ogugbuaja, V.O. (2009) Study of the levels of some agricultural pollutants in soils, and water leaf (*Talinum triangulare*) obtained in Maiduguri, Nigeria. Journal of Applied Sciences and Environmental Sanitation. 4(2), 71-78.

[38] Food and Nutritional Board. (2004) Recommended Intake for Individuals, Dietary Reference Intakes [DRIs]. National Academy of Sciences, Washington, DC: USA.

[39] USEPA (United State Environmental Protection Agency). (2002) Region 9, Preliminary Remediation Goals.

[40] USEPA (United State Environmental Protection Agency). (2010) Integrated Risk Information System.

[41] WHO (World Health Organization). (1994) Quality Directive of Potable Water, Geneva, second ed. p. 197.

[42] WHO/FAO. (2007) Joint WHO/FAO Food Standards Program Code Alimentarius Commission 13th Session," Report of the Thirty Eight Session of the Codex Committee on Food Hygiene, Houston, Texas, USA, ALINORM 07/30/13.

[43] Jaishree, and Khan T.I. (2015) Assessment of heavy metals risk on human health via dietary intake of cereals and vegetables from effluent irrigated land Jaipur district, Rajasthan. International Journal of Innovative Research in Science, Engineering and Technology. 4(7), 5142-5148.

[44] MWE. (2005) MWE (Ministry of water and Electricity) National wastewater Regulations, Section III – 2.2 and 3.2.3 Riyadh, Saudi Arabia.

[45] Singh, A., Sharma, R.K. and Agarwal, M. (2010) Risk assessment of heavy metal toxicity through contaminated vegetables from wastewater irrigated area of Varanasi. Tropical Ecology. 51, 375-87.

[46] FAO. (1985) Water quality for agriculture, FAO irrigation and drainage paper No. 29, Rome, FAO, Rome.

Received: **25.04.2017**
Accepted: **28.09.2017**

CORRESPONDING AUTHOR

Zafar Iqbal Khan
Department of Botany
University of Sargodha
Sargodha –Pakistan

e-mail: zikhan11@gmail.com

© by PSP Volume 27 – No. 2/2018 pages 856-862 Fresenius Environmental Bulletin

EFFECTS OF NaCl STRESS ON PROLINE METABOLISM, MALONDIALDEHYDE, GLYCINE BETAIN AND CHLOROPHYLL CONTENT IN SUNFLOWER PLANTS

Fusun Yurekli*

Inonu University, Arts and Science Faculty, Department of Biology, 44280 Malatya, Turkey

ABSTRACT

The effects of NaCl changes in the free proline, pyrroline-5-carboxylate reductase (P-5-CR), proline oxidase (PO) and proline dehydrogenase (PDH) enzyme activities, glycine betaine and chlorophyll contents in salt tolerant and sensitive cultivars of sunflower. Significant proline accumulation was observed in both cultivars but it was more in salt tolerant sunflower plants under salt stress. PO, P-5-CR and PDH activities increased in tolerant cultivar and inhibited under salt stress in sensitive cultivar. The study indicated that while more glycine betaine, malondialdehyde accumulation was much less in tolerant cultivar. The levels of pigments, were similar amounts in both cultivars under salt stress. With these results, we can say that enhancing enzyme activities and proline levels during salt stress contributes significantly to the survival of plants. The salt tolerance of A-6535 is more pronounced in salt stress than in A-2517 when glycine betain (GB) is accumulated at high levels. In addition, the salt tolerance of A-6535 was shown in lower amounts of chlorophyll degredation. The physiological significance of these alterations can be assessed together with the functions of these enzymes in plant metabolism under salt stress.

KEYWORDS:
Glycine-betaine, NaCl stress, proline, sun flower

INTRODUCTION

Salinity is an ecological and abiotic stress factor of considerable importance, influencing the agriculture of culture plants. Cultivated areas are affected by salt stress and salinity increases progresively. According to their evolutionary adaptation, plants generally divide into two major groups, halophytes and glycophytes. Most of the important agricultural species are in the second group and salinity is considered as an important environmental stress factor in this group of plants [1-5]. Proline and glycine-betaine osmolytes accumulation is occuring, due to decrasing water potentials. Plants can prevent the destructive effect of water shortages by taking water from the environment by osmoregulation mechanism. A high level of proline maintains the plant survive at low water potentials. It has been reported that proline serves as a source of energy that regulates redox potential, as a hydroxy radical scavenger, as a substance that protects macro molecules against denaturation, as a means to reduce acidity in the cell, and as a storage compound and nitrogen source for post-stress rapid growth [6]. Proline has accumulated in response to stress such as salinity and freezing but at the same time it has been found to be in small quantities in response to heavy metal toxicity [7, 8], plant pathogenic interactions [9] and other abiotic and biotic stimuli. There are significant correlations between high proline level and stress factor are symptomatic of injury, which is a consequence of extreme growth and reduced metabolism rahter than an adaptive response to proline [10]. Indeed, the production of carbohydrates in restricted quantities by photosynthesis limits growth and reproductive performance, while plants accumulate large quantities of proline in the drought period [11]. Proline metabolism is actively regulated by stress stimuli, using reverse genetics (such as p5cs1 mutants; [12] makes it possible to test how much proline is needed to cope with stress. Such literature data show widely that proline metabolism is regulated by abiotic stress and it is a definite proof that the accumulation of stress-induced proline is an adaptive response. It is difficult to answer how the proline contributes to the stress tolerance of the plant, the metabolic regulation that causes proline accumulation in high amounts, and whether it is beneficial for the biotechnological improvement of plants.

The proline is synthesized in two ways, the glutatamate and the ornithine pathway in plants. During osmotic stress a high amount of proline accumulation occurs with the glutamate pathway. Δ'-pyrroline-5-carboxylate synthetase (P5CS) and Δ'-pyrroline-5-carboxylate reductase (P5CR) enzymes synthesize proline from glutamic acid [13, 14, 15]. Prolin degradation occurs in mitochondria with proline dehydrogenase or proline oxidase enzyme (PDH or POX) [16-19]. PDH transcription is activated by rehydration and proline, it is suppressed by dehydration, thereby inhibiting proline degradation during

abiotic stress [20, 21, 22]. It has been suggested that the accumulation of the prolin contributes to stress tolerance in many ways. The proline acts as a protective molecule that increases the activity of different enzymes and protects protein integrity [23].

Glycine betaine and proline are important organic molecules that accumulate in various plant species under abiotic stress conditions such as salinity, drought, high temperature, heavy metal. It is known that the accumulation of organic molecules, such as glycine betaine, in cells, protects organisms through osmoregulation against the abiotic stress. The tolerant and sensitive species exhibit different tolerance levels according to the accumulation levels of these compounds during abiotic stress. It has been reported that plants naturally accumulate glycine betaine in arid and saline environments [24-27]. In the present study, we have investigated the effects of salt stress on the activity of P5CR, PDH and PO enzymes; malondialdehyde, prolin and total cholorophyll content in salt tolerant and sensitive sunflower cultivars, in order to better understand their differences on salt stress tolerance.

MATERIALS AND METHODS

Plant materials and salinity treatments. In this study, the 2517-A ve 6535-A (*Helianthus annuus* L.) seeds are used as experimental material, was obtained from Trakya Agricultural Research institute. These varieties were developed and registered by the Trakya Agricultural Research institute. A-6535 and A-2517 varieties were selected as tolerant and sensitive varieties respectively. Sterilization of seeds in 0.5 % sodium hypochlorite solution for 5 minutes was performed and then washed 4-5 times with sterile dH_2O. After the seeds are sterilized and stored in distilled water overnight. One night in distilled water held sunflower seeds, 10 pieces were planted in plastic pots containing perlite. Seeds were germinated in perlite, 12 hr dark / 12 hr light, 25 ° C temperature, with 60% humidity and grown for 25 days watered with Hoagland's solution. Growth of 25 days; pots of both sunflower varieties were exposed to 100 mM NaCl, 200 mM NaCl, 400 mM NaCl in prepared in Hoagland solution. After application, samples from leaf tissue 2 times at 2 day intervals for each concentrations. Immediately before the applications (day 0) and applications made after 2 and 4 days at the end of the mature leaves for use in analyzing samples taken in liquid nitrogen frozen and stored in a freezer at -40 ° C.

Proline Assay. Sunflower leaves (0.5 gr) exracted in 3% (w/v) sulphosalicylic and free proline content measured using ninhydryn reagent. The mixture is heated in a water bath at 100 ° C for 1 hour after addition of ninhydrin and glacial acetic acid. Then the reaction was stopped by using an ice bath. To this mixture 3 mL of toluene was added and toluene fraction was aspirated from the liquid phase then absorbance was read at 520 nm in a spectrophotometer. Proline concentration is figured out using a calibration curve and displayed as nmol/g fresh weight [28].

Pyrroline-5-carboxylate Reductase (P-5-C R) Activity Assay. Pyrroline-5-carboxylate reductase was extracted and measured in leaf tissues [29]. Briefly, the enzyme was extracted in a reaction mixture containing 100 mmol/L PBS (pH 7.4), 1.0 ml 128 mmol/l l-pyrroline-5-carboxylate and enzyme activity was evaluated the decrease in absorbance at 340nm.

Proline Oxidase Activity Assay. In the measurement of proline oxidase enzyme activity dichlorophenolindophenol (DCPIP) reduction was monitored in mitochondrial preparation containing 50 mM Tris–HCl (pH 8.5), 5.0 mM MgCl2, 0.5 mM FAD, 1.0 mM phenazine methosulphate, 0.06 mM DCPIP and 100 mM proline in a total volume of 1 mL reaction mixture [30].

Proline Dehydrogenase Activity Assay. Proline dehydrogenase was extracted containing 100 mM phosphate buffer (pH 8.0) 1.0 mM cystine and 0.1 mM EDTA and activity assayed by following NAD reduction in 1.0 mL of reaction medium containing 100mM Na_2CO_3–$NaHCO_3$ buffer (pH 10.3), 20 mM l-proline and 10 mM NAD+ [29].

Glycine betaine. Glycine betaine extraction was performed from 0.20 g of dry plant material in 10 mL of distilled water under stirring for 24 h. Extract was filtered and added 2 mL of 2 N H_2SO_4, the solution was incubated 16 h at 4 ◦C. Then solution was centrifuged at 9200 × g 15 min at 0 ^oC. The pellet was resuspended in 1,2 dichloroethane. The level of glycine betaine was calculated after 2 h and absorbance vaules obtained at 365 nm against a standard curve of glycine betaine. The amount of glycine betaine was displayed as $\mu g\ g^{-1}DW$ [31].

Total Chlorophyll content. The chlorophyll amounts of the leaves were measured. The pigments were extracted from 0.1 g fresh leaves by using 80% acetone [32].

Malondialdehyde content. Lipid peroxidation level was assayed in leaf samples as the malondialdehyde (MDA) content. The MDA content, was determined by using the thiobarbituric acid reaction and concentration was calculated from the absorbance at 532 nm. In determination of the MDA concentration an extinction coefficient of 155 mM^{-1} cm^{-1} was used [33].

Statistical analysis. The data obtained from the studies were calculated according to the significance of the two-way ANOVA p <0.05 (5%) in the SPSS 15 package program. The results were compared using the Tukey's test. All experiments were done in triplicate.

RESULTS

Amounts of free proline in the leaves of the two varieties exposed to NaCl salt stress were measured in control plants and on days 2 and 4. Results are shown in Table 1. The amount of free proline was significantly increased on days 2 and 4 compared to the control plant due to application of NaCl salt stress in both cultivated plants. There was an obvious increase in the amount of free proline, increased salt concentration and time.

However, there was a difference in the amount of free proline between the two varieties. It was observed that there was more proline increase in the A-6535 variety than in the A-2517 variety. More increased proline content was observed at 400 mM NaCl in the A-6535 and A-2517 varieties and proline increased about 4-6 times on the 4th day respectively.

Pyrroline-5-carboxylate reductase activity was determined in the leaves of control and NaCl stressed in both cultivars and the results are presented in Table 2. P-5-C reductase activity was increased significantly during all NaCl consantrations and on 2and 4 days. Obviously elevation in enzyme activity was increased as the concentration of NaCl and duration of stress increased. Nevertheless, higher P-5-C reductase activity was observed in the leaves of A-6535 than in A-2517.

A decrease in proline oxidase activity was observed in both cultivars types in stress conditions (Table 3). In all stress applications, the enzyme activity was significantly reduced. The rate of decline depended on the severity and duration of the stress. Relatively, a greater inhibition of enzyme activity was observed in the A-6535 variety. The enzyme activity was inhibited at 92% of the control in the A-6335 variety and the control was reduced to 62% at the A-2517 on day 4 of the NaCl (400 mM) stress conditions.

TABLE 1
Free proline amount (nmol gFW^{-1}) in the leaves of control and NaCl stressed cultivars. Results are means from three replications. Statistically differences (P≤0.05) are presented by different letters.

	Cultivar A-6535		Cultivar A-2517	
	48h	96 h	48 h	96 h
Control	12,65±0,65[a]	15,86±0,74[a]	13,94±0,55[a]	16,89±1,54[a]
100 mM NaCl	17,29±0,98[a]	37,91±1,78[c]	13,61±0,78[a]	28,47±1,54[b]
200 mM NaCl	25,51±1,02[b]	62,92±2,02[d]	22,51±0,92[b]	43,04±1,74[e]
400 mM NaCl	33,98±1,23[c]	119,35±3,45[f]	26,79±1,55[b]	65,16±1,86[d]

TABLE 2
Activity of pyrroline-5-carboxylate reductase activity (nmol min^{-1}) in leaves of control and NaCl stressed sunflower cultivars. Results are means from three replications. Statistically differences (P≤0.05) are presented by different letters.

	Cultivar A-6535		Cultivar A-2517	
	48h	96 h	48 h	96 h
Control	37,21±3,55[a]	45,61±3,08[a]	34,51±2,87[a]	57,76±4,59[b]
100 mM NaCl	85,51±5,41[c]	113,24±7,25[d]	72,52±5,02[c]	93,33±6,74[c]
200 mM NaCl	86,05±6,25[c]	144,06±6,18[d]	73,58±6,35[c]	108,72±8,05[e]
400 mM NaCl	106,56±7,36[d]	195,75±7,38[f]	91,82±7,34[c]	134,12±8,65[d]

TABLE 3
Proline oxidase activity (nmol min^{-1}) in leaves of control and NaCl stressed sunflower plants. Results are means from three replications. Statistically differences (P≤0.05) are presented by different letters.

	Cultivar A-6535		Cultivar A-2517	
	48h	96 h	48 h	96 h
Control	588,57±17,25[a]	628,48±12,18[b]	570,28±15,32[a]	588,25±22,47[a]
100 mM NaCl	474,28±15,37[c]	280,52±16,35[d]	525,71±14,45[a]	351,42±15,81[e]
200 mM NaCl	388,45±13,42[e]	160,54±18,52[f]	451,42±16,28[c]	302,85±12,24[e]
400 mM NaCl	331,42±16,68[e]	108,26±17,21[g]	354,28±11,35[e]	225,71±14,02[d]

TABLE 4
Proline dehydrogenase activity (nmol min-1) in leaves of control and NaCl stressed sunflower plants. Results are means from three replications. Statistically differences (P≤0.05) are presented by different letters.

	Cultivar A-6535		Cultivar A-2517	
	48h	96 h	48 h	96 h
Control	39,25±2,35[a]	40,12±3,02[a]	37,03±2,89[a]	38,51±4,67[a]
100 mM NaCl	23,71±1,56[b]	18,51±2,74[b]	31,11±3,17[a]	20,74±2,88[b]
200 mM NaCl	17,03±2,27[b]	8,14±1,62[c]	23,71±2,47[b]	15,55±2,12[b]
400 mM NaCl	10,37±1,38[c]	5,92±0,95[d]	16,29±1,45[b]	10,37±1,35[c]

TABLE 5
Glycine betaine levels (μg g^{-1}DW) in leaves of control and NaCl stressed sunflower plants. Results are means from three replications. Statistically differences (P≤0.05) are presented by different letters.

	Cultivar A-6535		Cultivar A-2517	
	48h	96 h	48 h	96 h
Control	2,65±065[a]	5,86±0,74[b]	3,94±0,55[a]	6,89±0,65[b]
100 mM NaCl	7,29±1,98[b]	17,91±2,78[c]	3,61±0,18[a]	8,47±0,52[b]
200 mM NaCl	15.51±1,02[c]	42,14±3,27[d]	7,51±1,52[b]	3,02±0,47[a]
400 mM NaCl	23,98±2,23[e]	79,35±5,18[f]	7,79±0,85[b]	46,02±4,32[d]

TABLE 6
The effect of increasing NaCl concentration on the chlorophyll a and b (mg g-1 FW) content of sunflower plants. Results are means from three replications. Statistically differences (P≤0.05) are presented by different letters.

	Cultivar A-6535		Cultivar A-2517	
	48h	96 h	48 h	96 h
Control	2,1±0,20[a]	0,32±0,03[b]	2,12±0,20[a]	0,35±0,03[b]
100 mM NaCl	1,8±0,18[a]	0,27±0,02[b]	1,73±0,17[a]	0,22±0,02[c]
200 mM NaCl	1,6±0,16[a]	0,21±0,02[b]	1,27±0,12[d]	0,18±0,02[c]
400 mM NaCl	1,2±0,12[d]	0,18±0,01[c]	0,74±0,07[e]	0,11±0,01[f]

TABLE 7
The effect of increasing NaCl concentration on the MDA (μM mg-1 FW) content of sunflower plants. Results are means from three replications. Statistically differences (P≤0.05) are presented by different letters.

	Cultivar A-6535		Cultivar A-2517	
	48h	96 h	48 h	96 h
Control	6,1±0,98[a]	6,4±0,87[a]	6,2±0,55[a]	9,5±0,48[b]
100 mM NaCl	6,7±1,11[a]	8,1±1,10[c]	8,3±0,75[c]	12,3±1,14[d]
200 mM NaCl	6,9±0,78[a]	8,5±0,92[c]	9,2±0,78[b]	14,6±1,07[d]
400 mM NaCl	7,2±0,85[a]	9,1±0,78[b]	10,4±0,68[b]	17,2±1,62[d]

Proline dehydrogenase activity was significantly inhibited in stressed plants (Table 4). The decrease in enzyme activity was proportional to the severity of stress and the continuity of stress. Also, the decrease in A-6535 was higher when compared to A-2517. Proline dehydrogenase activity decreased to 86% under 400 mM NaCl stress on day 4 in day A-6535 leaves, while the decrease in enzyme activity in A-2517 was 74% at the same NaCl stress level.

Glycine betain levels were estimated on days 2 and 4 of the leaves of both sunflower species under control and salt stress conditions and the results are shown in Table 5. Glycine betaine content increased markedly in the salty stressed leaves of both varieties. Glycine betaine accumulation increased with stress intensity and the duration of NaCl application. However, the growth rate of A-6535 varieties was higher than that of A2517 varieties. The amount of glycine betaine in the stressed leaves of the A-6535

strain was increased 6-fold in the A-2517 range when compared to the corresponding controls during the 4 day's 400 mM NaCl stress conditions. These results show that the levels of glycine betaine were higher in the A-6535 cultivar than in the A-2517 at each stage of salt stress.

In this study, it was found that the application of NaCl reduced the content of chlla and chlb in both types. The contents of chla and chLb in A-6335 were reduced by 43% and 44% and in A-2517 decreased 66% and 69% compared to the control groups, respectively, within 4 days in salt stressed treatment (Table 6).

The MDA content of the two sunflower varieties was different (Table 7). The amount of MDA increases to A-6335 with the increase in the concentration of A-2517 NaCl (Figure 7). The difference between control and 400 mM NaCl was not significant in A-6335. In A-2517, lipid peroxidation significantly increased when salt stress reached 400 mM NaCl on day 4. However, A-6335 had the same amount of MDA at all salt stress levels (Figure 7). The content of MDA in A-2517 increased by 85% on day 4 and 400 mM NaCl treatment.

DISCUSSION

Plants respond to a variety of physiological and developmental changes to various water stresses such as drought, high salinity and low temperature. During stress water can cause changes in plant cells, concentrations of solutes in cell volume and cell membranes, gradient-dependent disruption of water potential, loss of turgor, impairment of membrane integrity, and denaturation of proteins. It has been shown that high proline accumulation negatively affects plant growth in stress-free plants and at the same time causes cell death [34,35]. However, when these plants are exposed to stress, toxicity due to proline accumulation is reduced. Prolin itself is known to reduce cell death at low concentrations, but P5C metabolism triggers cell death [36,37]. The content of proline has increased in roots and foliage with increasing water stress intensity. The proline has increased steadily in both root and foliage with mild stress. The proline accumulation in response to the stress is more than the leaves in the roots.

Soluble proline is likely to be considered as an osmoprotector associated with osmotic regulation and membrane stability under stress [38]. Although its role under salt stress is not well known, there are many reports such as supporting a function for proline in osmotic regulation of salt stress in rice and wheat [39, 40]. On the other hand, proline accumulation is accompanied by salinity-dependent destruction of the rice plant [41]. Prolin accumulation is seen as a sign of salinity damage, not as an indicator of stress tolerance. Pyrroline-5-carboxylate (P5C) reductase (P5CR) catalyzes the last step of proline synthesis in plants. In fact, high salt concentrations inhibit proline dehydrogenase (PRODH) activity. In response to other conditions, proline storage is produced by reduced pyrroline-5-carboxylate dehydrogenase (P5CDH) activity [42, 43].

Glycine betaine and proline, are commonly osmolyte accumulated in plants under stress. Proline accumulation and correlation of stress tolerance has been reported in several studies. During salt stress in plants proline serves as an osmotic regulator of gene expression [44]. Proline accumulation is known to have an important role in stress tolerance [16]. Proline accumulation is known to be one of the key parametric indicators of stress conditions in plants an increase in the accumulation of proline in our study it was found that both cultivars occur [16, 41].

Photosynthesis and transpiration are common salt stress symptoms. The amount of chlorophyll decreased in salt sensitive plants such as tomatoes, potatoes and peas, but the amount of salt-resistant mustard and chlorophyll in wheat increased [45]. In our study, it can be concluded that as salinity level increased, chlorophyll a, b contents linearly decreased in both cultivars. Results based on increasing NaCl concentration, showed that among the two sunflower varieties, A-6535 could be ranked as a salt tolerant and A-2517 as a salt sensitive.

It also showed a general increase with the increase in the severity of NaCl stress with respect to their respective controls. Lipid peroxidation in the cell membranes is mentioned to be one of the most coping with NaCl stress in the membranes of all the cells exposed to varied degree of stress as reported other researchers [46, 47].

According to the results of our study, the effects of salt stress caused various levels of antioxidative enzyme activities, salt stress induction of oxidative stress and hence increase in MDA content (lipid peroxidation), degradation of chlorophyll molecule in both varieties. 6535-A varietycould be evaulated, one of the two types of study, showed much more pronounced antioxidant mechanisms after salt stress induction and thus protected from harmful effects or damage caused by stress.

ACKNOWLEDGEMENTS

Our study was supported by a grant (Project No: BAPB 2013/211) from The Scientific Research Project Units of Inonu University.

REFERENCES

[1] FAO, High Level Expert Forum-How to Feed the World in 2050. (2009) Economic and Social Development, Food and Agricultural Organization of the United Nations, Rome, Italy.

[2] Flowers, T.J. (2004) Improving crop salt tolerance. Journal of Experimental Botany. 55 (396), 307-319.
[3] Munns, R., Tester, M. (2008) Mechanisms of salinity tolerance. Annual Review of Plant Biology. 59, 651–681.
[4] Ediga, A.S., Hemalatha, S., Meriga, B. (2013) Effect of salinity stress on antioxidant defense system of two finger millet cultivars (Eleusine coracana (L.) Gaertn) differing in their sensitivity. Advances in Biological Research. 7(5), 180-187.
[5] Siddiqui, Z.S., Shahid, H., Cho, J.I., Park, S,H., Ryu, T.H., Park, S.C. (2016) Physiological responses of two halophytic grass species under drought stress environment. Acta Botanica Croatica. 75(1), 31–38.
[6] Kumar, G., Reddy., S.G., Sudhakara, A.M. (2003) NaCl effects on proline metabolism in two high yielding genotypes of mulberry (Morus alba L.) with contrasting salt tolerance. Plant Science. 165, 1245–1251.
[7] Verslues, P.E., Agarwal, M., Katiyar-Agarwal, S., Zhu, J., Zhu, J.K. (2006) Methods and concepts in quantifying resistance to drought, salt and freezing, abiotic stresses that affect plant water status. The Plant Jornal. 45(4), 523-39.
[8] Sharma, S.S., Dietz, K.J. (2009) Review The relationship between metal toxicity and cellular redox imbalance. Trends in Plant Science. 14(1), 43-50.
[9] Fabro, G., Kovacs, I., Pavet, V., Szabados, L., Alvarez, M.E. (2004) Proline accumulation and AtP5CS2 gene activation are induced by plant-pathogen incompatible interactions in Arabidopsis. Molecular Plant-Microbe Interaction. 17, 343–350.
[10] Stewart, C.R., Hanson, A.D. (1980) Proline accumulation as a metabolic response to water stress. In: Turner, N.C., Kramer, P.J. (ed.) Adaptation of Plants to Water and High Temperature Stress. John Wiley and Sons, New York, 173–189.
[11] Boyer, J.S. (2010) Drought decision-making. Journal of Experimental Botany. 61, 3493–3497.
[12] Szekely, G., Abraham, E., Csepio, A., Rigo, G., Zsigmond, L., Csiszar, J., Ayaydin, F., Strzhov, N., Jasik, J., Schmelzer, E., Koncz, C., Szabados, L. (2008) Duplicated P5CS genes of Arabidopsis play distinct roles in stress regulation and developmental control of proline biosynthesis. The Plant Journal. 53, 11-28.
[13] Carter, C., Shafir, S., Yehonatan, L., Palmer, R.G. (2006) Thornburg R. A novel role for proline in plant floral nectars. Naturwissenschaften. 93, 72–79.
[14] Vendruscolo, E.C.G., Schuster, I., Pileggi, M., Scapim, C.A., Correa Molinari, H.B., Marur, C.J., Esteves Vieira, L.G.(2007) Stress-induced synthesis of proline confers tolerance to water deficit in transgenic wheat. Journal of Plant Physiology. 64, 1367–1376.
[15] Chiang, H.H., Dandekar, A.M. (1995) Regulation of proline accumulation in Arabidopsis thaliana (L) Heynh during development and in response to desiccation. Plant Cell and Environment. 18, 1280–1290.
[16] Delauney, A.J., Verma, D.P.S. (1993) Proline biosynthesis and osmoregulation in plants. The Plant Journal. 4, 215–223.
[17] Kishor, P.B.K., Hong, Z., Miao, G.H., Hu, C.A.A., Verma, D.P.S. (1995) Overexpression of pyrroline-5-carboxylate synthetase increase proline production and confers osmotolerance in transgenic plants. Plant Physiol. 108, 1387–1394.
[18] Tarczynski, M.C., Jensen, R.G., Bohnert, H.J. (1993) Stress protection of transgenic tobacco by production of the osmolyte mannitol. Science. 259, 508–510.
[19] Madan, S., Nainawate, H.S., Jain, R.K., Chowdhury, J.B. (1995) Proline and proline metabolising enzymes in in vitro selected NaCl-tolerant Brassica juncea L. under salt stress. Annals of Botany. 76, 51–55.
[20] Grieve, C.M., Grattan, S.R. (1983) Rapid assay for determination of water soluble quaternary ammonium compounds. Plant Soil. 70, 303–307.
[21] Sudhakar, C., Reddy, P.S., Veeranjaneyulu, K. (1993) Effect of salt stress on the enzymes of proline synthesis and oxidation in green gram (Phaseolus aureus Roxb.) seedlings. Journal of Plant Physiology. 141, 621–623.
[22] Ashraf, M. (1994) Breeding for salinity tolerance in plants. Critical Reviews in Plant Science. 13, 17-42.
[23] Mattioni, C., Lacerenza, N.G., Troccoli, A., De Leonardis, M., Di Fonzo, N. (1997) Water and salt stress-induced alterations in proline metabolism of Triticum durum seedlings. Physiologia Plantarum. 101, 787-792.
[24] Cha-Um, S., Kirdmanee, C. (2010) Effect of glycinebetaine on proline, water use, and photosynthetic efficiencies, and growth of rice seedlings under salt stress. Turkish Journal of Agriculture and Forestry. 34, 517-527.
[25] Yurekli, F. (2014) The Effect of salinity and glycine-betaine application on some plant hormones production by different rice varieties. International Journal of Agriculture and Forestry. 4(2), 67-72.
[26] Sakamoto, A., Murata, N. (2002) The role of glycine betaine in the protection of plants from stress: clues from transgenic plants. Plant, Cell and Environment. 25, 163-171.

[27] Giri, J. (2011) Glycinebetaine and abiotic stress tolerance in plants. Plant Signaling & Behavior 6(11), 1746-1751.
[28] Bates, L.S., Waldren, R.P., Teare, I.D. (1973) Rapid determination of free proline for water-stress studies. Plant and Soil. 39(1), 205-207.
[29] Rena, A.B., Splittstoesser, W.E. (1975) Proline dehydrogenase and pyrroline5-carboxylate reductase from pumpkin cotyledons. Phytochemistry. 14, 657-661.
[30] Huang, A.H.C., Cavalieri, A.J. (1979) Proline oxidase and water stress induced proline accumulation in spinach leaves. Plant Physiol. 63, 531-535.
[31] Lichtenthaler, H.K., Wellburn, A.R. (1983) Determinations of total carotenoids and chlorophylls a and b of leaf extracts in different solvents. Biochemical Society Transactions. 11(5), 591-592.
[32] Madhava, R.K.V, Sresty, T.V.S. (2000) Antioxidative parameters in the seedlings of pigeon pea (Cajanus Cajan L. Millspaugh) in response to Zn and Ni stresses. Plant Science. 157, 113-28.
[33] Hellmann, H., Funck, D., Rentsch, D., Frommer, W.B. (2000) Hypersensitivity of an Arabidopsis sugar signaling mutant toward exogenous proline application. Plant Physiology. 122(2), 779-789.
[34] Verbruggen, N., Hermans, C. (2008) Proline accumulation in plants: a review. Amino Acids. 35(4), 753-759.
[35] Deuschle, K., Funck, D., Forlani, G., Stransky, H., Biehl, A., Leister, D., van der Graaff, E., Kunze, R., Frommer, W.B. (2004) The role of Δ1-pyrroline-5-carboxylate dehydrogenase in proline degradation. Plant Cell. 16, 3413-3425.
[36] Bhusan, D., Das, D.K., Hossain, M., Murata, Y., Hoque, Md.A. (2016) Improvement of salt tolerance in rice (Oryza sativa L.) by increasing antioxidant defense systems using exogenous application of proline. Australian Journal of Crop Science. 10(1), 50-56.
[37] Maggio, A., Raimondi, G., Martino, A., De Pascale, S. (2007) Salt stress response in tomato beyond the salinity tolerance threshold. Environmental and Experimental Botany. 59(3), 276–282.
[38] Lutts, S., Kinet, J.M., Bouharmont, J. (1996) Effects of various salts and of mannitol on ion and proline accumulation in relation to osmotic adjustment in rice (Oryza Sativa L.) callus cultures. Journal of Plant Physiology. 149(1–2), 186-195.
[39] Poustini, K., Siosemardeh, A., M. Ranjbar, M. (2007) Proline accumulation as a response to salt stress in 30 wheat (Triticum aestivum L.) cultivars differing in salt tolerance. Genetic Resources and Crop Evolution. 54(5), 925-934.
[40] Garcia, A.B., Engler, A. J., Iyer, S., Gerats, T., Van Montagu, M., Caplan, A.B. (1997) Effects of osmoprotectant upon NaCl stress in rice. Plant Physiology. 115(1), 159-169.
[41] Yoshiba, Y., Kiyosue, T., Nakashima, K., Yamaguchi-Shinozaki, K., Kazuo Shinozakj, K. (1997) Regulation of levels of proline as an osmolyte in plants under water stres. Plant Cell Physiology. 38(10), 1095-1102.
[42] Stein, H., Honig, A., Miller, G., Erster, O., Eilenberg, H., Csonka, L.N., Szabados, L., Koncz, C., Zilberstein, A. (2011) Elevation of free proline and proline-rich protein levels by simultaneous manipulations of proline biosynthesis and degradation in plants. Plant Science. 181(2), 140-50.
[43] Koskeroglu, S., Tuna, A.L. (2010) The investigation on accumulation levels of proline and stress parameters of the maize (Zea mays L.) plants under salt and water stress. Acta Physiologiae Plantarum. 32, 541-549.
[44] Sudhir, P., Murthy, S.D.S. (2004) Effects of salt stress on basic processes of photosynthesis. Photosynthetica. 42(4), 481-486.
[45] Thankamani, C.K., Chempakam, B., Ashokan, P.K. (2003) Water stress induced changes in enzymatic activities and lipid peroxidation in black pepper (Piper nigrum). Journal of Medicinal and Aromatic Plant Sciences. 25, 646-650.
[46] Turkan, I., Bor, M., Ozdemir, F., Koca, H. (2005) Differential response of lipid peroxidation and antioxidants in the leaves of drought-tolerant P. Acutifolius Gray anddrought-sensitive P. vulgaris L. subjected to polyethylene glycol mediated water stress. Plant Science. 168, 223-231.

Received: **05.05.2017**
Accepted: **07.12.2017**

CORRESPONDING AUTHOR

Fusun Yurekli
Inonu University,
44280 Malatya – Turkey

e-mail: fusun.yurekli@inonu.edu.tr

© by PSP Volume 27 – No. 2/2018 pages 863-870 Fresenius Environmental Bulletin

PREPARATION OF IMMOBILIZED PHOTOSYNTHETIC BACTERIA MICROSPHERES AND DEGRADATION OF P-NITROANILINE

Zheng Fan[1], Wei Zheng[2], Lei Qin[1], Guo-Liang Zhang[1,*]

[1]Institute of Oceanic and Environmental Chemical Engineering, Ocean College, Zhejiang University of Technology, 18, Chaowang Road, Hangzhou, 310014, P.R. China
[2]College of Chemical Engineering, Zhejiang University of Technology, 18, Chaowang Road, Hangzhou, 310014, P.R. China

ABSTRACT

Immobilized photosynthetic bacteria (PSB) for degrading p-nitroaniline wastewater were prepared with different embedding materials. By comparing several kinds of immobilization process, optimal embedding materials containing diatomite, sodium alginate, polyethylene glycol (PEG), and PVA were obtained. The influence of various operating conditions on the biodegradation of p-nitroaniline was systematically analyzed. Optimization of parameters revealed that the optimal operating conditions of immobilized PSB for degradation of p-nitroaniline wastewater are as follows: light, aerobic, particle size 3–4 mm, embedding ratio 14%, and microsphere dosing quantity 150 g L^{-1}. The degradation rate of immobilized cells was higher than that of free cells. When the concentration of p-nitroaniline is 100 mg L^{-1}, the removal rate was 99.2% by the immobilized cells biodegradation after 3 days. Furthermore, the immobilized bacteria maintained a high degradation rate following storage for 35 days and eight repetitions of the degradation experiment, which shows that immobilized microspheres can be widely used in p-nitroaniline degradation applications.

KEYWORDS:
photosynthetic bacteria, immobilized, biodegradation, p-nitroaniline

INTRODUCTION

P-nitroaniline is an important raw material used in azo dyes, corrosion inhibitors, pesticides, antioxidants, antiseptic agents, and in other industries [1]. It is highly toxic, can be readily absorbed through the skin, causes long-term damage to the environment, and is potentially fatal to aquatic organisms. Its threshold limit value (TLV) is 0.001 kg m^{-3}, which is even more toxic than aniline (TLV of 0.002 kg m^{-3}) [2]. There are multiple methods of dealing with toxic and harmful chemicals [3, 4, 5, 6]. At present, the general treatment methods of p-nitroaniline wastewater are chemical oxidation [7], electrochemistry [8], photo-catalysis [9], adsorption [10, 11], biological [12], microorganism biological [13, 14] and so on. The biochemistry method is receiving increased attention because of its advantages over physical and chemical methods; it is low cost, requires less investment, and has high efficiency and no secondary pollution. Studies show that photosynthetic bacteria (PSB) are commonly used microorganisms due to their distinctive ability to use a variety of organic compounds as carbon sources [15, 16]. Free PSB is susceptible to be washed away when in flowing water, and can be out-competed by other bacteria. Therefore, combining and immobilizing PSB with a carrier and ensuring that the embedded bacteria predominates over other species is very important.

This immobilized cell system can improve settling properties, poison resistance and tolerance, and can easily realize solid-liquid separation. In the early 1960s, immobilized cell technology received increasing interest as a new biological engineering technology because of its advantages, such as high processing efficiency [17], smaller floor space requirements, and lower sludge production during wastewater treatment. However, light diffusion and difficulty in diffusion and mass transfer over the substrate and product are challenging. Currently, cell immobilization occurs through use of a polymer to form a gel, with the microbial agent fixed within it. The choice of suitable embedding media and conditions are crucial for the success of the immobilization technology. The embedding agent should satisfy the following demands: lower microbial activity loss and good stability when immobilized, high mechanical strength, and good mass transfer performance. Sodium alginate is widely considered to be a suitable embedding medium. Polyethylene glycol (PEG) and PVA are usually used as additives to improve immobilized cell performance [18, 19].

Immobilized PSB are widely used in hydrogen production [20, 21], however, using PSB to degrade toxic substances is more challenging. Recent research on embedding conditions is not sufficiently detailed. In this study, gels of varying compositions containing diatomite, sodium alginate, PEG, and

PVA were used as fixed material. Several factors were studied, including changes in the tiny holes inside immobilized microspheres, different particle dosing quantities, and different embedding ratios of immobilized materials and PSB, which would all impact degradation. The impact of the adsorption film phenomenon on microchannels and of some operating parameters, such as light intensity, pH, and substrate concentration on the degradation characteristics of a microchannel reactor were studied based on the growth and mass transfer characteristics of microorganisms immobilized in embedded tiny holes. Immobilized PSB were used to degrade p-nitroaniline wastewater, laying a foundation for the screening of effective microbial agents to treat p-nitroaniline wastewater and the improvement of research into immobilization technology.

MATERIALS AND METHODS

Microorganisms and cultivation. The PSB used for degrading p-nitroaniline were isolated from Zhejiang Dinglong, China [22]. The bacteria were grown and enriched in a synthetic medium, the contents of which are listed in Table 1. The incubators were stirred at 150 rpm at 30 °C. The cells were cultivated at an illumination intensity of approximately 3000 lux.

TABLE 1
Growth media for photosynthetic bacteria cultivation and for batch experiments

Component	Concentration (mg L^{-1})
p-nitroaniline	50
$K_2HPO_4•3H_2O$	500
NaH_2PO_4	400
NH_4Cl	550
$MgSO_4•7H_2O$	200
$CaCl_2$	50
$Fe_2SO_4•7H_2O$	200
Nicotinic acid	0.002
Pantothenic acid	0.002
Riboflavin	0.002
Biotin	0.002
Sucrose	6000

Immobilization of bacteria microspheres. After cultivation, PSB were collected by centrifugation (5000 rpm, 15 min) and then washed twice with sterile phosphate buffer solution. Dead PSB were obtained by autoclaving centrifuged bacteria at 121 °C for 20 min [23]. Three different microspheres were prepared as carriers for the immobilized bacterial cells (A, B, C; Table 2). Firstly, the immobilization solution was prepared by adding the mixture of carriers to distilled water according to a given proportion. This was slowly heated to 80 °C in a thermostatic bath until dissolved, and the mixed slurry was cooled to 25–30 °C. Subsequently, the centrifuged PSB cells were mixed into the prepared solutions using a magnetic stirrer. Finally, the dissolved slurry was extruded from a sterile syringe and dropped into the crosslinked solution to form single microspheres with 3–4 mm diameter, and crosslinked in the refrigerator for 24 h. The microspheres were then washed thoroughly with physiological brine under sterile conditions for 15 minutes.

Experimental methods. In order to choose an optimum additive from activated carbon, diatomaceous earth, and polyamide, the degradation rate of p-nitroaniline by gel granules was demonstrated. Three immobilized microspheres (A, B, and C) are briefly described in Table 2. The medium used for batch experiments is shown in Table 1. All batch experiments were carried out at 30 °C, 3000 lux, and 150 rpm in triplicate. The initial concentration of p-nitroaniline was 50.0 mg L^{-1}. The optimum additive was used in subsequent experiments.

TABLE 2
Three immobilized microspheres with different additives

	Microsphere A	Microsphere B	Microsphere C
Activated carbon (%)	1	0	0
Diatomaceous earth (%)	0	1	0
Polyamide (%)	0	0	1
Sodium alginate (%)	2	2	2
PVA (%)	2	2	2
Polyethylene glycol (%)	0.5	0.5	0.5

The effects of sodium alginate, PVA, and PEG on biodegrading p-nitroaniline were examined by orthogonal test L9 (3, 3), as was the influence of crosslinking conditions, including concentrations, temperature, and time. In the two experiments, biomass content was 10%, the immobilized microspheres were at a concentration of 100 g L^{-1}, and reaction conditions were maintained at 30 °C, 3000 lux, and 150 rpm. Biomass content is an important factor, so under the optimum conditions we examined the influence of varying biomass content.

Different initial concentrations of p-nitroaniline were subjected to immobilized PSB microspheres and studied under optimum conditions. To validate the superiority and adsorption of immobilized PSB, 200 mL fresh bacteria microspheres, dead bacteria microspheres, and free bacteria was added to each of the 250 mL flasks.

Degradation conditions such as dissolved oxygen (DO), light intensity, and the initial concentration of p-nitroaniline may affect the activity of PSB. Thus, these three conditions are discussed in this study. Experiments were carried out in 1000 mL wastewater, to which was added 100 g immobilized PSB microspheres. The aeration, light intensity and initial concentration conditions in the reactor were controlled. After 72 h of reaction, we analyzed p-nitroaniline removal rate.

Under optimum immobilization and degradation conditions, we examined reusability using batch experiments. The storage stability of the immobilized bacteria was studied after storage of the mixture for 0, 7, 14, 21, 28, and 35 d. Microspheres were stored at 4 °C in distilled water.

Analytical methods. Samples collected from reactors were centrifuged at 10 000 rpm for 15 min. Supernatant was used to test p-nitroaniline concentration, which was analyzed by HPLC (Jasco LC2000) using an ODS-C18 reversed phase chromatographic column (250mm × 4.6 mm, 5 μm). The HPLC was run with mobile phase methanol/water (55:45, v/v), flow rate 0.8 mL min^{-1}, injection volume 20 ml, and monitoring absorption wavelength 254 nm. All experiments were performed in triplicate. The degradation rate of p-nitroaniline was calculated using Eq. (1):

$$\text{Degradation rate} = \frac{C_1 - C_2}{C_1} \times 100\% \quad (1)$$

where C_1 is the initial concentration of p-nitroaniline and C_2 is the concentration of p-nitroaniline in the supernatant.

Illumination intensity was measured with a digital lux meter (AS831). The structure of the immobilized bacteria microspheres was analyzed by a scanning electron microscope (SEM; TM-1000, Hitachi, Japan). The microspheres were washed twice with deionized water, then fixed with 2.5% calcium chloride and left for 1 h at 4 °C. They were then dehydrated by successive passages through 50%, 70%, 80%, 90%, and 100% ethanol. Each dehydrating step took 10 min. The dried samples were photographed by SEM.

RESULTS AND DISCUSSION

Influence of microsphere additives. Figure1-A shows that microspheres embedded with activated carbon, sodium alginate, PVA, and PEG are not closely packed, and transmission of light for the microspheres is bad. The binding force between activated carbon and sodium alginate is weak, which can cause the spheres to damage easily. Even though activated carbon has a certain adsorption effect, experimental results show that it is not suitable for embedding packing. As shown in Figure 1-B, the surface of microsphere B immobilized with diatomite, sodium alginate, PVA, and PEG is uneven. Diatomite is embedded on the particle surface and internally. Diatomite has empty skeleton structures, thus creating many cavity channels where PSB can easily grow. Moreover, p-nitroaniline can also adsorb to the diatomite cavities, increasing the transfer between PSB and p-nitroaniline wastewater, thus enhancing the efficiency of PSB to degrade p-nitroaniline. Figure 1-C shows that the surface of microsphere particle C is relatively smooth. Although sodium alginate and polyamide have good compatibility, the particle lacks pores, making microbe reproduction difficult and causing poor particle mass transfer performance i.e., low p-nitroaniline degradation rate.

Diatomite microspheres improve embedding and adsorption, resulting in the removal rate of p-nitroaniline by microsphere B being higher than that of other embedding carriers. This kind of structure is advantageous for internal bacterial growth. PVA-immobilized microspheres have good mass transfer performance, which improves p-nitroaniline contact with bacteria.

Figure 2 shows that p-nitroaniline degradation rates by the three immobilized microspheres varies. The highest degradation rate for immobilized activated carbon microspheres (A; 42.6%) was obtained after 72 h, but the resulting microspheres lacked strength; they were easy to dissolve and break up. The microspheres showed some swelling after 3 d, and had partially decomposed after 6 d. Performance of the polyamide microsphere (C) is relatively similar, but the degradation efficiency is low, thus C is not appropriate for the embedding of PSB for p-nitroaniline degradation. The diatomite microspheres (B) show good integrity and the degradation rate reached 59.1% after 72 h. Fig. 1-B shows good crosslinking and the presence of many internal pores. Distribution of bacteria in internal pores is suitable for microorganism activity, thus enhancing degradation efficiency. Therefore, diatomite microspheres were used for the following experiments.

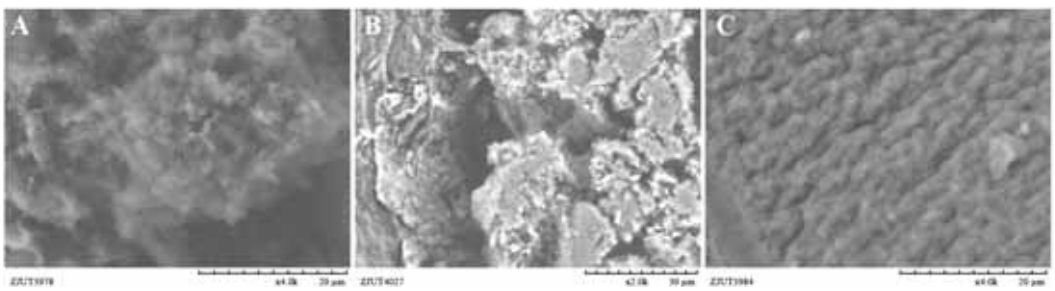

FIGURE 1
SEM of three different microspheres

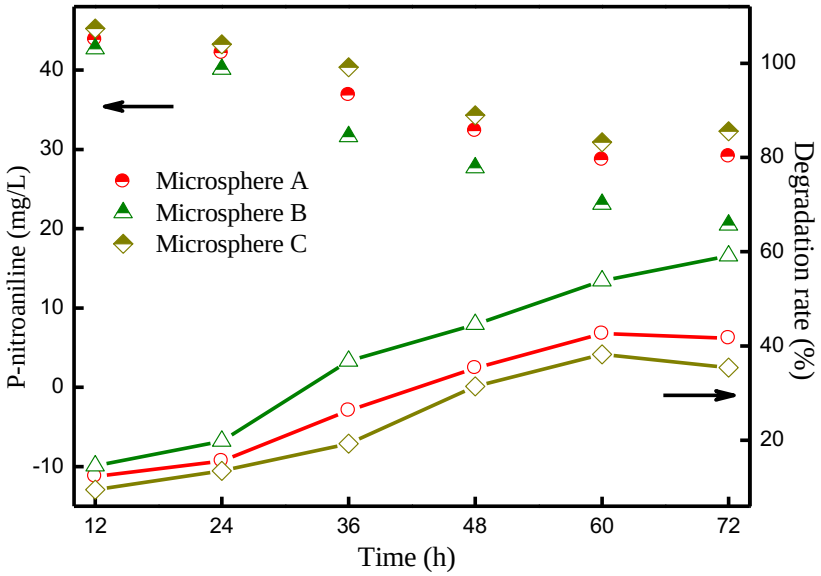

FIGURE 2
Biodegradation of p-nitroaniline with three microspheres

TABLE 3
Factors and levels of orthogonal test for embedding agent

Level	Factor (%)		
	A: Sodium alginate	B: PVA	C: Polyethylene glycol
1	1.5	3.0	0.3
2	2.0	4.0	0.5
3	2.5	5.0	0.7

TABLE 4
Results of orthogonal experiments for embedding agent

Serial number	A: Sodium alginate (%)	B: PVA (%)	C: Polyethylene glycol (%)	Removal rate of p-nitroaniline (%)
1	1.5	3.0	0.3	53.5
2	1.5	4.0	0.5	62.4
3	1.5	5.0	0.7	41.6
4	2.0	3.0	0.5	53.1
5	2.0	4.0	0.7	49.1
6	2.0	5.0	0.3	54.3
7	2.5	3.0	0.7	48.0
8	2.5	4.0	0.3	44.7
9	2.5	5.0	0.5	58.9
K1	157.5	154.6	147.3	
K2	156.5	156.2	174.4	
K3	151.6	154.8	138.7	
R	5.9	1.6	35.7	

Effect of immobilized carriers on degradation of p-nitroaniline wastewater. Immobilized carrier composition and concentration are critical factors affecting degradation of p-nitroaniline. The carriers used were sodium alginate, PVA, and PEG. To obtain the optimal composition, different proportions of the three carriers were analyzed by orthogonal test L9 (3, 3). The levels of the factors and the degradation rate of p-nitroaniline are shown in Table 3, the results of orthogonal experiments is shown in Table 4. The higher the R value obtained, the greater the effect. The effect order is C > A > B, showing that PEG content is the most important factor. Furthermore, the optimal conditions for p-nitroaniline degradation are A1, B2, C2, or sodium alginate 1.5%, PVA 4.0%, and PEG 0.5%. Increased sodium alginate and PEG increases liquid viscosity, thus making the microspheres denser. This affects the mass transfer of substrates and products, reducing the activity of PSB, and thereby reducing the rate of degradation. On the other hand, the lower the sodium alginate and PEG content, the looser the microspheres, which means that they can break down more easily.

Effect of crosslinking conditions on degradation of p-nitroaniline wastewater. Crosslinking is a key parameter affecting microsphere degradation rate of p-nitroaniline. Crosslinking concentrations, temperature, and time greatly influence p-nitroaniline degradation rate. In order to find the optimal crosslinking conditions, different conditions were analyzed by orthogonal test L9 (3, 3). Factor levels and p-nitroaniline degradation rate are shown in Table 5, the results of orthogonal experiments is shown in Table 6. Illumination intensity was set to 3000 lux, and temperature to 30 °C. As shown in Table 4, the effect order is B > A > C; crosslinking temperature is the most important factor. The optimal conditions for degrading p-nitroaniline are A1, B1, and C2.

TABLE 5
Factors and levels of orthogonal test for crosslinking conditions

Level	Factor		
	A: CaCl2 (%, w/w)	B: Temperature (°C)	C: Time (h)
1	2	4	0.5
2	3	18	4
3	4	30	12

TABLE 6
Results of orthogonal experiments for crosslinking conditions

Serial number	CaCl 2 (%, w/w)	T (°C)	Time (h)	Removal rate of p-nitroaniline (%)
1	2	4	0.5	70.2
2	2	18	4	67.8
3	2	30	12	59.3
4	3	4	4	67.9
5	3	18	12	58.5
6	3	30	0.5	63.8
7	4	4	12	60.7
8	4	18	0.5	57.6
9	4	30	4	54.5
K1	195.3	198.8	178.5	
K2	190.2	183.9	190.2	
K3	172.8	175.6	176.5	
R	22.5	23.2	13.7	

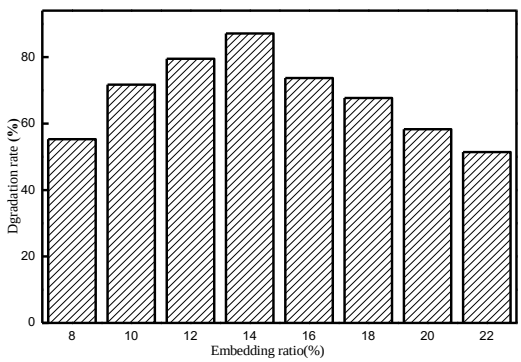

FIGURE 3
Effect of embedding ratio of photosynthetic bacteria in microspheres on the degradation rate of p-nitroaniline

Effect of embedding ratios on degradation rate of p-nitroaniline. The degradation rate of the granules depends on the amount of PSB. Experimental results under illumination intensity of 3000 lux, temperature 30 °C, and 150 rpm are shown in Fig. 3. The degradation rate achieved by the microspheres is sensitive to the embedding ratio. Degradation rate initially increases with increasing embedding ratio, but after reaching a certain threshold the degradation rate decreases with increasing embedding ratio. This may be because excessive bacteria would inhibit PSB metabolism, thereby affecting degradation rate. Embedding large amounts of bacteria may cause the microspheres to break down more easily. The highest removal rate was obtained at an embedding ratio of 14%. After 72 h, the degradation rate reached 87.1%.

Figure 4 shows the integrity of the PSB microspheres after 72 h of p-nitroaniline degradation, when the degradation rate reached 87.1%. The surface crosslinking of the diatomite embedding medium is good and there are still many pores present inside the microspheres. Therefore, diatomite microspheres were used for the following experiments.

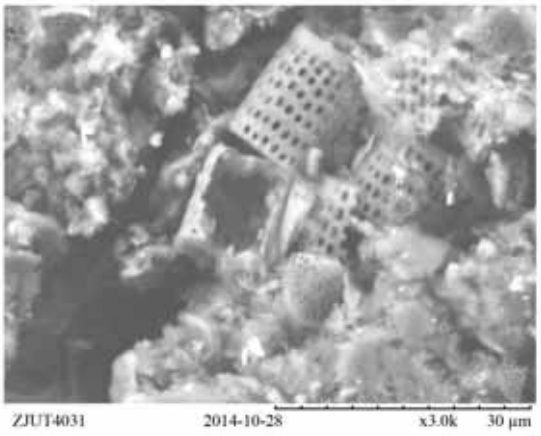

FIGURE 4
Photosynthetic bacteria microspheres after 72 h degradation experiment

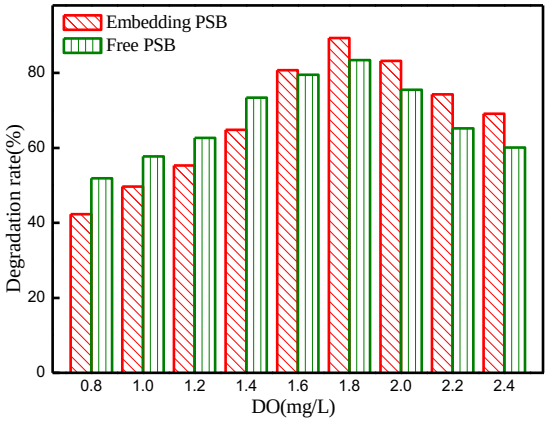

FIGURE 5
Effect of different dissolved oxygen (DO) concentrations on degradation rate of p-nitroaniline

Effect of degradation conditions on degradation rate. Effect of dissolved oxygen. DO in the bioreactor was controlled by regulating the volume of aeration. Figure 5 shows that the removal rate of p-nitroaniline gradually rises with increasing DO. This is because PSB need sufficient oxygen to metabolize p-nitroaniline into small molecule. Increasing DO results in a high p-nitroaniline removal rate. I think the reason is that there are many holes and immobilized channel, as shown in figure 4. The degradation rate of the microspheres reached a maximum value of 89.3% for a DO value of 1.8 mg·L^{-1}. Increasing micro bubbles can increase gas-liquid contact areas, prompting p-nitroaniline to be evenly suspended in wastewater. This is conducive to the absorption of nutrients and dispersion of metabolites. On the other hand, if DO exceeds a threshold, the degradation rate is reduced. This may be because oxygen inhibition occurs. As a consequence, DO concentration should be controlled at around 1.8 mg L^{-1}.

Effect of illumination intensity. Figure 6 suggests that the degradation rate is sensitive to illumination intensity. Increasing illumination intensity promotes degradation of bacteria up to a certain value, after which the degradation rate decreases. The optimum illumination intensity is 5000 lux; photo-inhibition of the degradation reaction will occur at intensities higher than this threshold.

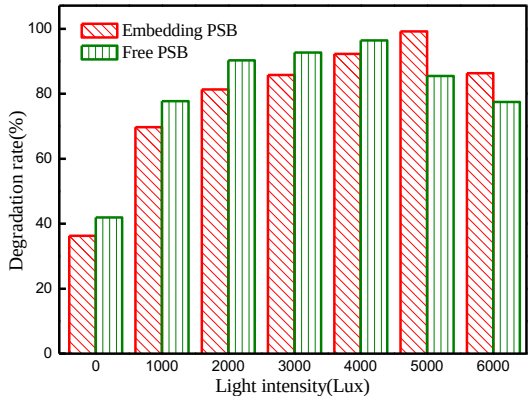

FIGURE 6
Effect of different light intensities on degradation rate of p-nitroaniline

Effect of p-nitroaniline initial concentration. The p-nitroaniline initial concentrations investigated were 10.0, 20.0, 40.0, 60.0, 80.0, and 100.0 mg L^{-1}. As shown in Fig. 7, as the concentration of p-nitroaniline increases, degradation by PSB takes longer. When the p-nitroaniline concentration is 10.0 or 20.0 mg L^{-1}, immobilized PSB can fully biodegrade p-nitroaniline in 48 hours. When the concentration of p-nitroaniline is 40.0 or 60.0 mg L^{-1}, immobilized PSB biodegrade p-nitroaniline within 56 or 64 hours, respectively. when the concentration of p-nitroaniline is 100 mg L^{-1}, the removal rate was 99.2% after 3 days, show that immobilized PSB need 72 hours to almost completely biodegrade p-nitroaniline. This shows that p-nitroaniline has strong toxicity; at high concentrations in aqueous solution it has an inhibitory effect on PSB and the degradation ability of PSB is reduced.

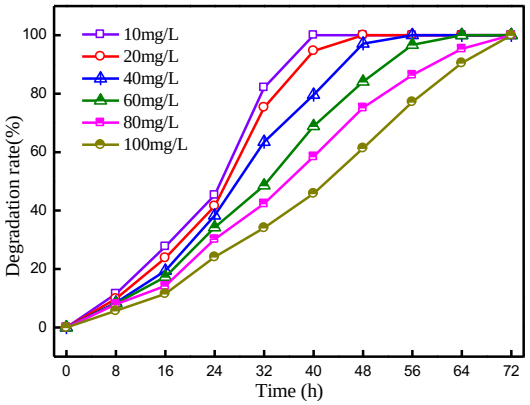

FIGURE 7
Effect of different initial concentrations of p-nitroaniline on p-nitroaniline degradation

Reusability and storage stability of immobilized PSB microspheres. We repeated tests to ascertain the recovery and recycling of immobilized bacteria for degrading p-nitroaniline. The PSB microspheres tested were composed of the following components: diatomite 2%, sodium alginate 1.5%, PVA 4.0%, and PEG 0.5%. The PSB embedding ratio was 14% (M/M). The experiment was performed at an illumination intensity 5000 lux, temperature 30 °C and 150 rpm with 72 h degradation time. As shown in Fig. 8, immobilized PSB microspheres were used in eight consecutive experiments. The last experiment shows a p-nitroaniline degradation rate of 88.7%. In each batch test the initial p-nitroaniline concentration was 50.0 mg L^{-1}.

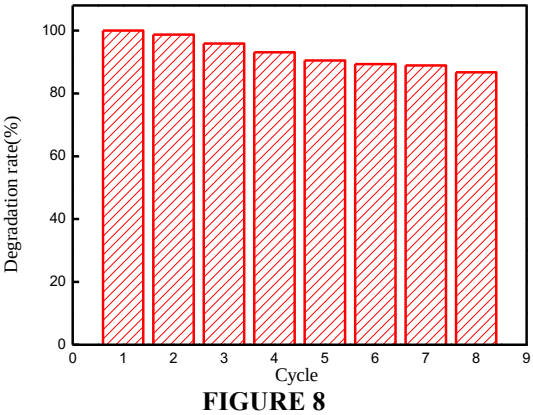

FIGURE 8
Repeated p-nitroaniline degradation by reusing immobilized microspheres

The experiments show that immobilized PSB microspheres can be reused without reducing their ability to degrade p-nitroaniline. High mechanical strength and operating stability can allow the immobilized microspheres to be widely used in industry.

Stability is an important factor for practical application of immobilized bacteria systems during long-term storage. As shown in Fig. 9, the stability of beads remained high following storage for 35 days at 4 °C. Degradation rates of p-nitroaniline by immobilized bacteria reached 90.3% during the 35th day. Immobilization does not affect bacterial activity; observed activity loss is small. Immobilized bacteria in storage can be reactivated [23]. In conclusion, the excellent degradation rate obtained from the immobilized bacteria microsphere indicates good prospects for application of immobilized PSB systems more widely.

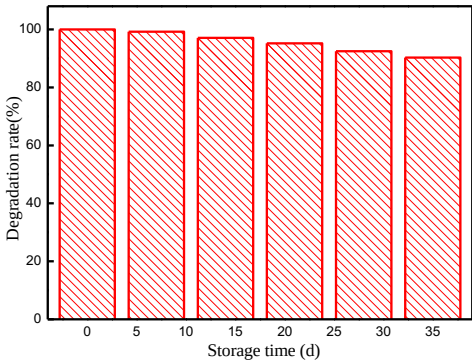

FIGURE 9
Storage stability and activity of photosynthetic bacteria (PSB) microspheres in p-nitroaniline degradation

CONCLUSIONS

This study clearly demonstrates that immobilized PSB is effective in enhancing the degradation rate of p-nitroaniline. PSB grows in the diatomite gaps on microspheres and p-nitroaniline adsorbs on the surface of the diatomite from the surface to the interior. This promotes biodegradation of p-nitroaniline. Furthermore, mechanical stability and rich porous microspheres can effectively increase contact between oxygen and bacteria [24,25], forming an aerobic environment, thus maintaining the vitality of the bacteria, and allowing PSB to dominate. This also increases degradation of p-nitroaniline [26]. The main conclusions are:

(1) Optimum conditions for preparing immobilized microspheres are 1.0% diatomite, 1.5% sodium alginate, 4.0% PVA, 0.5 % PEG, with 2% calcium chloride as the crosslinking agent, fixed at 4 °C for 4 hours.

(2) Optimum conditions for treatment of p-nitroaniline wastewater are 5000 lux illumination, 1.8 mg L^{-1} dissolved oxygen, 3–4mm particle size, and an embedding ratio of 14%. Furthermore, when the concentration of p-nitroaniline is 100 mg L^{-1}, the removal rate was 99.2% after 3 days. The degradation rate of immobilized PSB is better than that of free PSB.

ACKNOWLEDGEMENTS

This work was financially supported by the the National Natural Science Foundation of China (No. 21736009, 21506193, 21476206 and 21236008), Zhejiang Provincial Natural Science Foundation of China (Grant No. LY18B060010), Zhejiang Provincial Bureau of Science and Technology (Grant No. 2016C33007), China Postdoctoral Science Foundation (Grant No. 2015M581958) and Zhejiang Provincial Postdoctoral Science Foundation.

REFERENCES

[1] Sun, J.H., Sun, S.P., Fan, M.H., Guo, H.Q., Qiao, L.P. and Sun, R.X. (2007) A kinetic study on the degradation of p-nitroaniline by Fenton oxidation process. J Hazard Mater. 148, 172-177.

[2] Ma, H.J., Wang, M., Pu, C.Y., Zhang, J., Zhao, S.F., Yao, S. and Xiong, J. (2009) Transient and steady-state photolysis of p-nitroaniline in aqueous solution. J Hazard Mater. 165, 867-873.

[3] Masomboon, N., Lu, M.C. and Ratanatamskul, C. (2008) Effect of hydrogen peroxide on the degradation of 2,6-dimethylaniline by Fenton processes. Fresen. Environ. Bull. 17, 1073-1081.

[4] Ekici, P., Leupold, G. and Parlar, H. (2001) Degradability of selected azo dye metabolites in activated sludge systems. Chemosphere. 44, 721-728.

[5] Sogut, O.O. and Akgun, M. (2008) Degradation of aqueous Disperse Orange 25 by supercritical water oxidation. Fresen. Environ. Bull. 17, 864-871.

[6] Vlyssides, A.G., Loukakis, H.N. and Karlis, P.K. (2004) Olive mill wastewater detoxification by applying pH related Fenton oxidation process. Fresen. Environ. Bull. 13, 501-504.

[7] Zhao, Y.S., Sun, C., Sun, J.Q. and Zhou, R. (2015) Kinetic modeling and efficiency of sulfate radical-based oxidation to remove p-nitroaniline from wastewater by persulfate/ Fe_3O_4 nanoparticles process. Sep Purif Technol. 142, 182–188.

[8] Wang, Y.B., Zhang, Y.N., Zhao, G.H., Wu, M.F., Li, M.F., Li, D.M., Zhang, Y.G. and Zhang, Y.L. (2013) Zhang, Electrosorptive photocatalytic degradation of highly concentrated p-nitroaniline with TiO_2 nanorod-clusters/carbon aerogel electrode under visible light. Sep Purif Technol. 104, 229–237.

[9] Wu, W.M., Liang, S.J., Chen, Y., Shen, L.J., Zheng, H.R. and Wu, L. (2012) High efficient photocatalytic reduction of 4-nitroaniline to p-phenylenediamine over microcrystalline $SrBi_2Nb_2O_9$. Catal Commun. 17, 39–42.

[10] Li, K.Q., Zheng, Z., Feng, J.W., Zhang, J.B., Luo, X.Z., Zhao, G.H. and Huang, X.F. (2009) Adsorption of p-nitroaniline from aqueous solutions onto activated carbon fiber prepared from cotton stalk. J Hazard Mater. 166, 1180–1185.
[11] Xiao, G.Q., Wen, R.M., Wei, D.M. and Wu, D. (2014) Effects of the steric hindrance of micropores in the hyper-cross-linked polymeric adsorbent on the adsorption of p-nitroaniline in aqueous solution. J Hazard Mater. 280, 97–103.
[12] Khalid, A., Arshad, M. and Crowley, D.E. (2009) Biodegradation potential of pure and mixed bacterial cultures for removal of 4-nitroaniline from textile dye wastewater. Water Res. 43, 1110–1116.
[13] Qureshi, A., Verma, V., Kapley, A. and Purohit H.J. (2007) Degradation of 4-nitroaniline by Stenotrophomonas strain HPC 135. International Biodeterioration & Biodegradation. 60, 215–218.
[14] Silambarasan, S. and Vangnai, A.S. (2016) Biodegradation of 4-nitroaniline by plant-growth promoting *Acinetobacter* sp. AVLB2 and toxicological analysis of its biodegradation metabolites. J Hazard Mater. 302, 426–436.
[15] Mekjinda, N. and Ritchie, R.J. (2015) Breakdown of food waste by anaerobic fermentation and non-oxygen producing photosynthesis using a photosynthetic bacterium. Waste Manage. 35, 199–206.
[16] Suzuki, H., Shimada, Y., Kobayashi, M., Kudo, M., Nozawa, T. and Wang, Z.Y. (2005) Isotopic labeling of proteins by utilizing photosynthetic bacteria. Anal Biochem. 347, 324–326.
[17] Li, J., Dang, Z., Guo, C., Lu, G. and Lu, J. (2012) Removal of pyrene using immobilized microorganism. Environ Chem. 31, 1036–1042.
[18] Mao, Y.H. and Wang, J.L. (2013) Immobilization of activated sludge in PVA matrix using innovative methods. Acta Scientiae Circumstantiae. 33, 370–376.
[19] Wang, X., Xu, L., Gao, J. and Liu, G. (2014) Study on preparation and properties of PVA immobilized microorganism hydrogel beads. China Plast Ind. 42, 89–92.
[20] Zhang, C., Zhang, H., Zhang, Z.P., Jiao, Y.Z. and Zhang, Q.G. (2014) Effects of mass transfer and light intensity on substrate biological degradation by immobilized photosynthetic bacteria within an annular fiber-illuminating biofilm reactor. J Photochem Photobiol B. 131, 113–119.
[21] Zhang, C.A., Zhu, X., Liao, Q.A., Wang, Y.Z., Li, J., Ding, Y.D. and Wang, H. (2010) Performance of a groove-type photobioreactor for hydrogen production by immobilized photosynthetic bacteria. Int J Hydrogen Energ. 35, 5284–5292.
[22] Qin, L., Liu, Q.H., Meng, Q., Fan, Z., Liu, T. Shen, C. and Zhang, G. (2017) Anoxic oscillating MBR for photosynthetic bacteria harvesting and high salinity wastewater treatment. Bioresour Technol. 224, 69–77.
[23] Lin, C., Gan, L., Chen, Z., Megharaj, M. and Naidu, R. (2014) Biodegradation of naphthalene using a functional biomaterial based on immobilized Bacillus fusiformis (BFN). Biochem Eng J. 90, 1–7.
[24] Ha, J., Engler, C.R. and Wild, J.R. (2009) Biodegradation of coumaphos, chlorferon, and diethylthiophosphate using bacteria immobilized in Ca-alginate gel beads. Bioresour Technol. 100, 1138–1142.
[25] Manohar, S., Kim, C.K. and Karegoudar, T.B. (2001) Enhanced degradation of naphthalene by immobilization of Pseudomonas sp. strain NGK1 in polyurethane foam. Appl Microbiol Biotechnol. 55, 311 – 316.
[26] Tao, X.Q., Lu, G.N., Liu, J.P., Li, T. and Yang, L.N. (2009) Rapid degradation of phenanthrene by using Sphingomonas sp. GY2B immobilized in calcium alginate gel beads. Int J Environ Res Public Health. 6, 2470 – 2480.

Received: **12.05.2017**
Accepted: **21.11.2017**

CORRESPONDING AUTHOR

Guo-Liang Zhang
Institute of Oceanic and Environmental Chemical Engineering,
Ocean College,
Zhejiang University of Technology,
18, Chaowang Road,
Hangzhou, 310014 – P.R. China

e-mail: guoliangz@zjut.edu.cn

© by PSP Volume 27 – No. 2/2018 pages 871-879 c Fresenius Environmental Bulletin

THE FEEDING BEHAVIOUR OF *PLEUROBRACHIA PILEUS* (CTENOPHORA: TENTACULATA) IN THE SOUTHEASTERN BLACK SEA: IN RELATION TO AREA AND SEASON

Rahsan Evren Mazlum*, Ulgen Aytan, Ertugrul Agirbas

Faculty of Fisheries, Recep Tayyip Erdoğan University, TR-53100, Rize, Turkey

ABSTRACT

The diet composition of *Pleurobrachia pileus* (Müller, 1776) was studied in five stations (İyidere, Rize, Çayeli, Pazar and Fındıklı) located along the Southeastern Black Sea coast of Turkey. The diet of *P. pileus* was also investigated in relation to seasonal variations. Overall, the diet of *P. pileus* was dominated by prey groups from phytoplankton followed by zooplankton. Also, seasonal diet of *P. pileus* is exclusively dominated by phytoplankton only during autumn and winter periods. Dendrogram, multidimensional scaling plots, ANOSIM and SIMPER analysis indicated an extremely identical diet of *P. pileus* between spring and summer. Autumn and winter have distinct prey assemblages and revealed low diet similarities with the two other seasons. Such trend was not found between different regions indicating a similar diet. The study suggested that *P. pileus* is miscellaneous feeder and its diet composition may evince the availability of different prey groups in the ambient environment. The results obtained from this study would assess not only to describe the diversity of prey species to a certain extent but may also determine interspecific competition for food in the Southeastern Black Sea.

KEYWORDS:
Black Sea, ctenophores, *Pleurobrachia pileus*, predation

INTRODUCTION

Three gelatinous species of the phylum Ctenophora are common in the Black Sea: *Mnemiopsis leidyi*, *Beroe ovata* and *Pleurobrachia pileus* [1, 2, 3, 4]. The *M. leidyi* was invaded to the Black Sea during the early 1980s via ballast water of ships from the north-western Atlantic coastal region which has dramatically affected the population of zooplankton resulting into an abrupt decline in the icthyo- and mesozooplankton abundance of the Black Sea [5, 6]. The swarms/population of *M. leidyi* was controlled once a voracious predator *B. ovata* was introduced in the region [7].

P. pileus has been described as a cosmopolitan species occurring in marine waters of the North-West Atlantic [8, 9], the North-East Atlantic [1, 10, 11] and the Black Sea [2]. Similar to *M. leidyi*, *P. pileus* also fed primarily on copepods (zooplankton) and is considered as a key species of the German Bight ecosystem to control the populations of copepod during maximum abundance regarded as a second trophic control system [12]. However, the presence of *P. pileus* in high densities result in the reduction of zooplankton and after the reduction of zooplankton they may start to consume eggs and larvae of fishes [1, 13, 14] becoming a major competitor with pelagic and larvae fish for zooplankton [15].

Since the diet composition of *P. pileus* mostly depend on the structure of different prey availability and the abundance of the *P. pileus* themselves [16], therefore, their diet composition reflects the ambient food environment [1]. Though it is obvious that *P. pileus* generally fed on copepods however the information on its diet composition in the Black Sea is limited.

In this paper, the diet composition of *P. pileus* was investigated during spring, summer, autumn and winter from five stations along the Southeastern Black Sea. The results of this study will provide a baseline data for future work to assess the proper management of aquatic resources and to estimate the tropic levels in the Black Sea ecosystem.

MATERIALS AND METHODS

Study area. The sampling sites include five offshore stations located two miles from shore. All sampling sites are located in the Southeastern Black Sea (Figure 1). The established five stations for *P. pileus* sampling during spring (May 2014), summer (July 2014), autumn (November 2014) and winter (February 2015) were İyidere (41° 02' 38" N- 40° 21' 46" E), Rize (41° 03' 25" N- 40° 31' 15" E), Çayeli (41° 07' 12" N- 40° 43' 29" E), Pazar (41° 12' 38" N- 40° 53' 07" E) and Fındıklı (41° 18' 21" N- 41° 08' 49" E). Each time the *P. pileus* was sampled from stations. Recep Tayyip Erdoğan University, Faculty of Fisheries research vessel 'R/V RIZESUAR' with an overall length of 12 m (140 HP) was used during *P. pileus* sampling. The vertical temperature of seawater (*in-situ*) was obtained by using SBE 19 CTD probe.

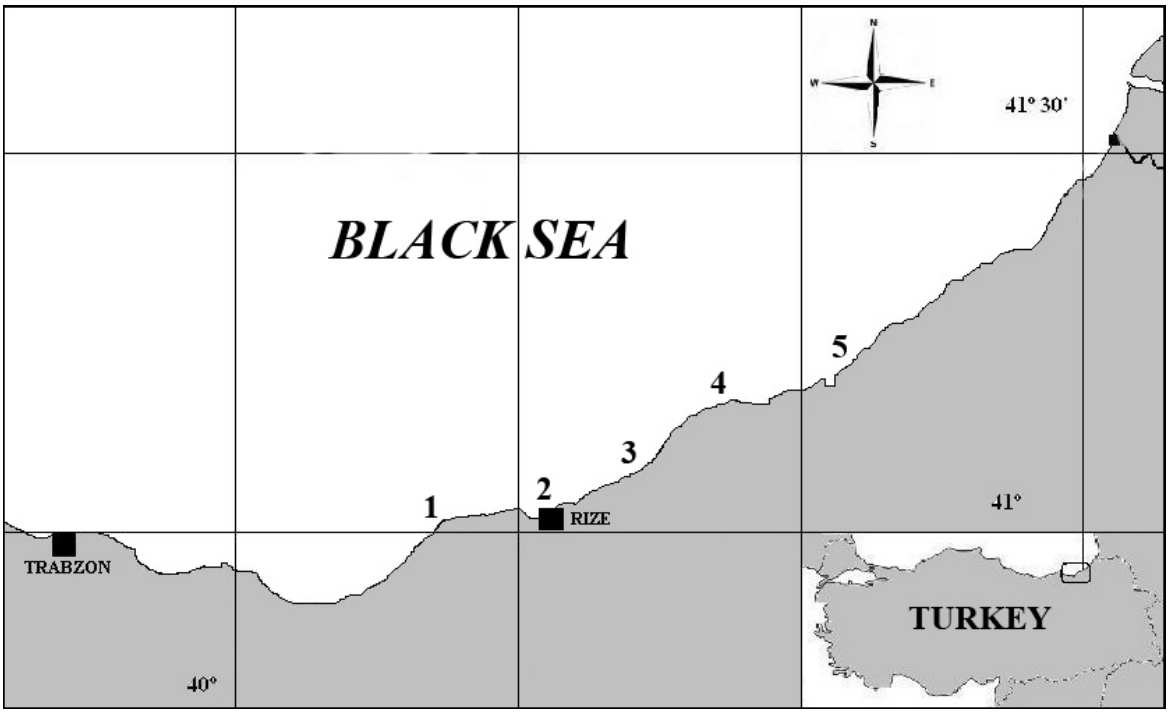

FIGURE 1

Map of the study area showing the five established stations for the collection of *Pleurobrachia pileus*. 1(İyidere) : 41° 02' 38" N- 40° 21' 46" E, 2 (Rize) : 41° 03' 25" N- 40° 31' 15" E, 3 (Çayeli) : 41° 07' 12" N- 40° 43' 29" E, 4 (Pazar) : 41° 12' 38" N- 40° 53' 07" E, 5 (Fındıklı) : 41° 18' 21" N- 41° 08' 49" E.

Sampling and laboratory investigation. *P. pileus* specimens were collected using a plankton net (Hydrobios, 200µm mesh size; vertically between surface and 100 m). They were immediately preserved in 4% formaldehyde [13, 17]. During laboratory investigation, *P. pileus* samples were weighted to the nearest 0.001 g using digital balance and measured to 1.0 mm using electronic digital calliper. The gut contents were then studied under Nikon SMZ1000 stereomicroscope, identified to the lowest possible taxonomic level (mostly genus) and, were counted.

Qualitative dietary analysis. Food composition was expressed as the percentage of prey groups occurrence frequency (*F%*) and percentage of prey groups numerical frequency (*N%*) methods [18, 19]. The *N%* and *F%* were calculated as:

$$F\% = \frac{n}{N_s} \times 100 \quad (1)$$

where, *n* is number of fish with particular food type, N_s is a total number of fish containing food in their stomach

$$N\% = \frac{n'}{N_p} \times 100 \quad (2)$$

where n' is the total number of a food group, N_p is the total number of all prey groups.

Statistical analysis. Dendrogram and multidimensional scaling plots (MDS) analysis based on *F%* and *N%* values were used to determine the percentage similarities or dissimilarities among seasons and stations. The logarithmic transformed data were used in MDS. One-way analysis of similarity (ANOSIM) was used to test the null hypothesis of no difference in the diet composition of *P. pileus* among stations and seasons [20]. The typifying prey and discriminating prey for each study area and season were determined using the SIMPER. The SIMPER also determines the average contribution of each prey to the dissimilarity between different study area and seasons. The multivariate function of the PRIMER 6.0 software package and PAST (version 2.14) were used to carry out the statistical tests.

TABLE 1
The mean length (± standard error) minimum and maximum length of *Pleurobrachia pileus* specimen collected from different season

Season	Body length (cm)			
	Mean ± SE	Min.	Max.	Observations (n)
Spring	0.59 ± 0.03	0.2	1.1	70
Summer	0.41 ± 0.02	0.1	0.7	37
Autumn	0.80 ± 0.05	0.4	1.2	25
Winter	0.95 ± 0.03	0.5	1.5	61

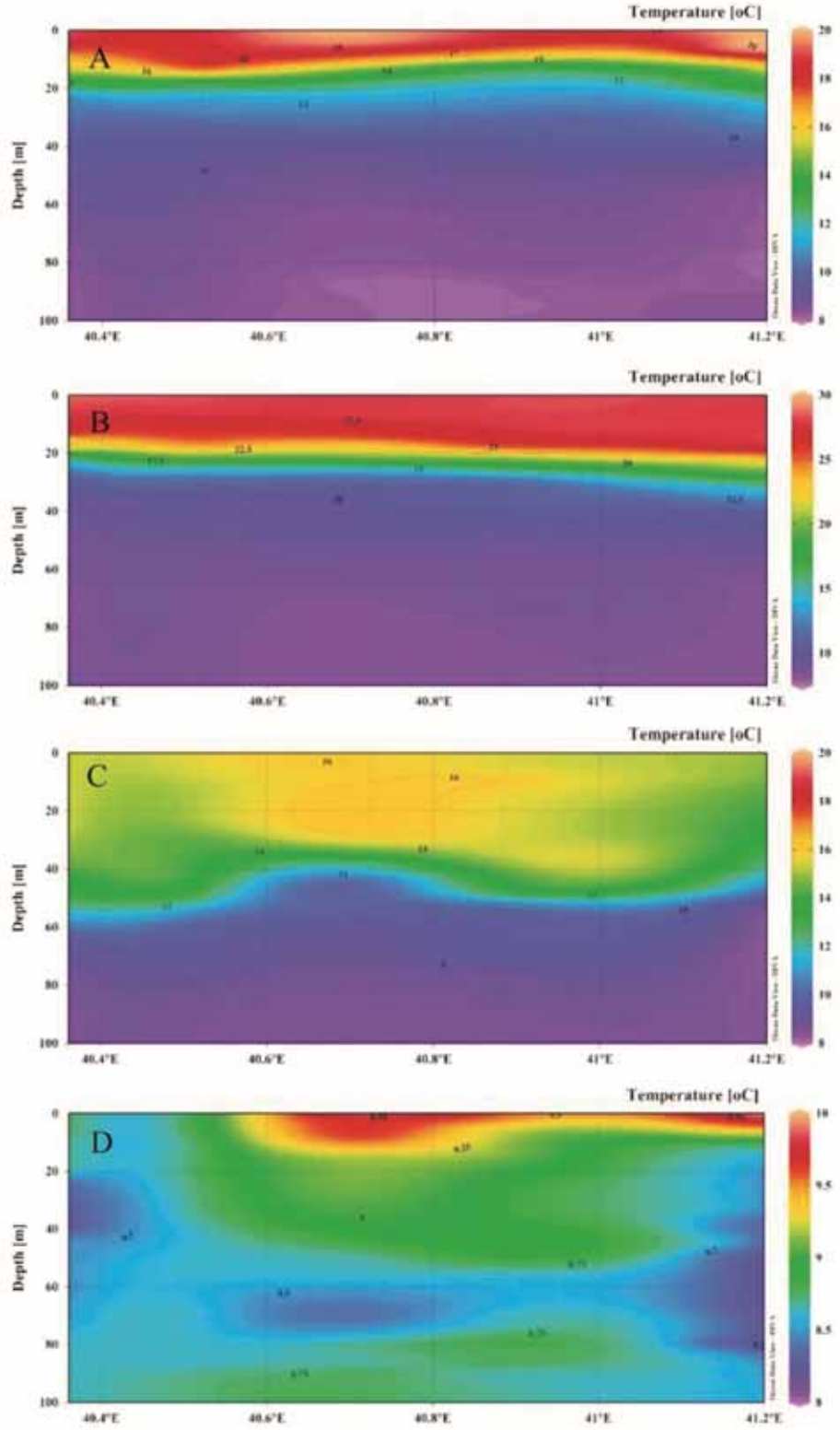

FIGURE 2
The seawater temperature in relation to water depth (A: Spring, B: Summer, C: Autumn, D: Winter)

RESULTS

Figure 2 shows the vertical temperature of seawater in relation to water depth during different seasons. The temperature is mostly constant during winter.

A total of 193 specimens of *P. pileus* were examined during the study (Table 1). Above 80% of *P. pileus* specimens had food in their gut collected from five established stations during different seasons [Figure 3(A) and 3(B)].

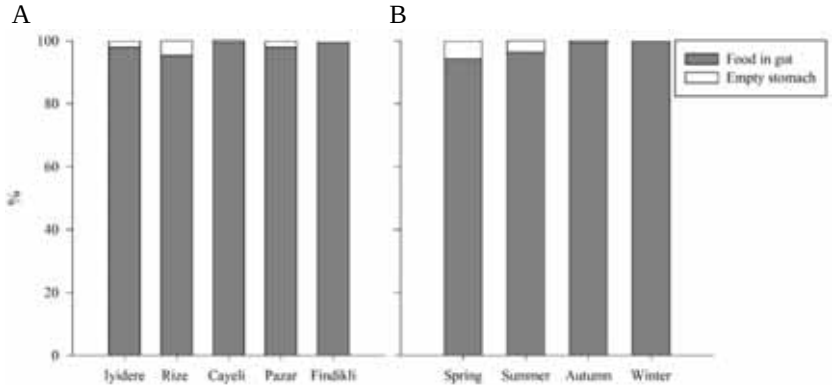

FIGURE 3
The percentage of *Pleurobrachia pileus* specimens with food in gut collected from different study areas (A) and during different season (B).

TABLE 2
The diet composition of *Pleurobrachia pileus* in the Southeastern Black Sea region of Turkey. The contribution of each prey item is given as percentage of prey group numerical frequency (*N %*) and percentage of prey group occurrence frequency (*F%*).

Prey groups	Overall		Spring		Summer		Autumn		Winter	
	%N	*%F*	*%N*	*%F*	*%N*	*%F*	*%N*	*%F*	*%N*	*%F*
PHYTOPLANKTON										
Dinophyceae										
Ceratium fusus	6.60	10.46	0.42	0.53	—	—	61.69	27.16	5.24	13.90
Ceratium furca	1.21	4.04	—	—	—	—	5.19	12.35	1.29	5.08
Ceratium tripos	2.84	7.11	—	—	—	—	2.60	8.64	3.52	11.76
Noctiluca scintilans	0.45	2.51	3.22	7.37	0.45	2.78	—	—	0.03	0.53
Protoperidinum sp.	0.75	2.93	—	—	—	—	3.90	7.41	0.77	4.01
Alexandrium sp.	0.05	0.42	—	—	—	—	0.65	2.47	0.03	0.27
Dinophysis sp.	0.03	0.28	—	—	—	—	0.65	2.47	—	—
Prorocentrum sp.	0.03	0.28	—	—	—	—	—	—	0.03	0.53
Bacillariophyceae										
Chaetoceros sp.	0.04	0.14	0.31	0.53	—	—	—	—	—	—
Navicula sp.	0.04	0.28	0.31	1.05	—	—	—	—	—	—
Proboscia sp.	5.66	0.14	—	—	—	—	—	—	7.28	0.27
Pseudanitzchia delicatisima	55.91	6.83	—	—	—	—	—	—	71.90	13.10
Rhizosolenia sp.	0.93	3.49	—	—	—	—	—	—	1.20	6.68
Thallassionema nitzschi-oides	0.05	0.42	—	—	—	—	—	—	0.07	0.80
PROTOZOA										
Stenosemella nivalis	0.01	0.14	—	—	—	—	—	—	0.02	0.27
ZOOPLANKTON										
Isopoda										
Isopot larvae	0.05	0.56	0.42	2.11	—	—	—	—	—	—
Copepoda										
Acartia sp.	0.22	1.95	—	—	—	—	1.95	6.17	0.18	2.41
Acartia sp. naupli	0.06	0.70	—	—	—	—	—	—	0.08	1.34
Calanus sp.	2.74	5.16	12.98	10.53	14.93	16.67	6.17	4.94	0.02	0.27
Calanus sp. copopodit	0.35	2.51	—	—	—	—	0.97	2.47	0.40	4.28
Oithona sp.	0.08	0.42	—	—	1.13	2.78	0.32	1.23		
Chaetognatha										
Sagitta setosa	0.27	1.39	1.66	3.68	1.13	4.17	—	—	—	—
Appendicularian										
Oikopleura sp.	0.65	2.37	4.05	5.26	1.13	2.78	—	—	0.10	1.34
Nemertea										
Nemertea sp.	0.09	0.70	—	—	—	—	—	—	0.12	1.34
Bivalvia										
Mytilus sp. veliger	0.90	5.72	4.26	13.16	4.98	15.28	—	—	0.10	1.34
Micrometazoan egg-larvae			—	—	—	—	—	—		
Jellyfish egg	0.62	1.95	—	—	—	—	—	—	0.80	3.74
Jellyfish planula	1.47	3.35	10.18	10.00	2.49	5.56	—	—	0.07	0.27
Polychaete larvae	0.26	1.67	1.66	4.74	0.23	1.39	—	—	0.05	0.53
Shrimp larvae	0.01	0.14	0.10	0.52	—	—	—	—		
Fish egg	4.76	6.97	24.92	14.21	21.04	16.67	0.32	1.23	0.55	2.67
Microplastic							—	—		
Particle plastic	10.91	17.85	35.51	26.32	52.49	31.94	15.58	23.45	3.64	9.63
Fiber	0.30	1.95	—	—	—	—	—	—	0.38	3.74
Other										
Fecal pellet	1.65	5.16	—	—	—	—	—	—	2.13	9.89

Overall diet composition. The overall contribution of each prey item to the total bulk of the diet of *P. pileus* is summarized in Table 2. The diet of *P. pileus* is mainly composed of phytoplankton and zooplankton. On the basis of *N%* and *F%* the most predominate prey group was phytoplankton that constituted to the maximum portion of diet followed by zooplankton. Moreover, microplastic was also found in the gut of *P. pileus*.

Food items in relation to season and area. ***Phytoplankton.*** The winter season encompasses a wide variety of phytoplankton that contributed to the total diet bulk of *P. pileus* (11 prey items) whereas only a single phytoplankton species was observed in the gut content of *P. pileus* during summer (Table 2).

On the basis of stations, the numbers of different phytoplankton species were 8-12 and maximum variety was found in the gut content of *P. pileus* collected from Rize (Table 3).

Zooplankton. Similar to phytoplankton, a wide variety of zooplankton was found during winter (11 prey items) whereas during autumn only 5 prey items belonging to zooplankton was observed in the gut of *P. pileus* (Table 2).

The gut content of *P. pileus* collected from Rize had a wide variety of zooplankton with 13 different prey items (Table 3). The variety of different zooplankton decreased in the study areas of Pazar and Fındıklı (10 prey items).

TABLE 3
The diet composition of *Pleurobrachia pileus* in relation to different study areas.

	Study area									
	İyidere		Rize		Çayeli		Pazar		Fındıklı	
Prey groups	***N%***	***F%***	***N%***	***F%***	***N%***	***F%***	***N%***	***F%***	***N%***	***F%***
PHYTOPLANKTON										
Dinophyceae										
Ceratium fusus	12.92	10	5.64	10.96	13.16	12.27	2.08	10.09	2.78	7.98
Ceratium furca	0.32	2.94	2.00	2.05	8.08	7.36	0.27	4.59	0.23	2.45
Ceratium tripos	4.56	7.65	2.11	6.16	6.02	6.75	0.91	7.34	1.45	6.13
Noctiluca scintilans	0.13	1.18	0.07	1.37	0.19	1.23	0.64	6.42	0.98	3.07
Protoperidinum sp.	0.51	2.94	0.64	3.42	0.66	1.23	0.05	0.92	1.39	4.91
Alexandrium sp.			0.14	2.05						
Dinophysis sp.	0.06	0.59			0.09	0.61				
Prorocentrum sp.			0.04	0.68			0.05	0.92		
Bacillariophyceae										
Chaetoceros sp.									0.17	0.61
Navicula sp.			0.04	0.68					0.12	0.61
Proboscia sp.			15.57	0.68						
Pseudanitzchia delicatisima	47.18	8.24	53.73	6.16	46.15	5.52	79.93	9.17	62.34	4.91
Rhizosolenia sp.	1.33	3.53	0.82	4.11	0.66	1.84	0.59	3.67	0.58	3.68
Thallassionema nitzschioides	0.06	0.59	0.11	1.37						
PROTOZOA										
Stenosemella nivalis			0.04	0.68						
ZOOPLANKTON										
Isopoda										
Isopot larvae	0.06	0.59			0.09	0.61	0.11	1.83		
Copepoda										
Acartia sp.	0.63	4.12	0.18	3.42	0.19	1.23				
Acartia sp. naupli	0.13	1.18	0.04	0.68	0	0	0.05	0.92	0.05	
Calanus sp.	2.28	3.53	0.93	4.11	1.60	2.45	2.40	6.42	0.37	
Calanus sp. copopodit	0.25	1.76	0.21	2.74	1.32	5.52	0.16	1.83	0.11	
Oithona sp.			0.04	0.68						
Chaetognatha										
Sagitta setosa			0.07	0.68	0.47	1.23	0.32	2.75	0.46	2.45
Appendicularian										
Oikopleura sp.	0.82	4.12	0.04	0.68	0.47	1.84	1.66	5.50		
Nemertea										
Nemertea sp.	0.38	2.35	0.04	0.68						
Bivalvia										
Mytilus sp. veliger	1.27	5.88	0.25	2.05	0.56	2.45	0.43	6.42	1.62	10.43
Micrometazoan egg-larvae										
Jellyfish egg	0.44	1.76	1.04	2.74	0.66	2.45			0.29	1.84
Jellyfish planula	0.44	1.18	0.14	0.68	2.16	21.47	0.16	0.92	5.45	9.82
Polychaete larvae	0.44	2.35	0.11	1.37	0.19	0.61	0.32	2.75	0.12	1.23
Shrimp larvae									0.06	0.61
Fish egg	3.10	4.71	6.39	10.27	2.44	4.29	3.15	7.34	5.21	7.36
OTHER										
Particle plastic	19.63	19.41	8.78	22.60	8.27	7.98	5.82	13.76	10.78	20.86
Fiber	0.44	2.35	0.29	2.74	0.38	1.84	0.16	1.83	0.06	0.61
Fecal pellet	2.60	7.06	0.54	3.42	6.20	9.20	0.75	4.59		

N %, percentage of prey group numerical frequency; *F%*, percentage of prey group occurrence frequency

TABLE 4

One-way ANOSIM results of the gut content for *Pleurobrachia pileus* in relaiton to different season periods (*R* values and significance level *p*). SIMPER results showed that the average dissimilarities (%) and the four species contributing most to the dissimilarity and their contribution ratios to the average dissimilarities between seasons.

Season	One-way ANOSIM		SIMPER						
	R value	*p* value	Average Dissimilarity %	Discriminating species 1	Contr. (%)	Discriminating species 2	Contr. (%)	Discriminating species 3	Contr. (%)
Spring-Autumn	0.2459	0.0002	81.95	*Ceratium fusus*	50.32	Particle plastic	31.63		
Spring-Winter	0.4609	0.0001	94.04	*P. delicatisima*	61.05	Particle plastic	18.18	*Ceratium fusus*	13.27
Summer-Autumn	0.3545	0.0001	85.9	*Ceratium fusus*	48.08	Particle plastic	37.82		
Summer-Winter	0.5303	0.0001	93.65	*P. delicatisima*	60.04	Particle plastic	19.21	*Ceratium fusus*	12.86
Autumn-Winter	0.3471	0.0001	85.29	*P. delicatisima*	56.92	*Ceratium fusus*	18.35	Particle plastic	8.50

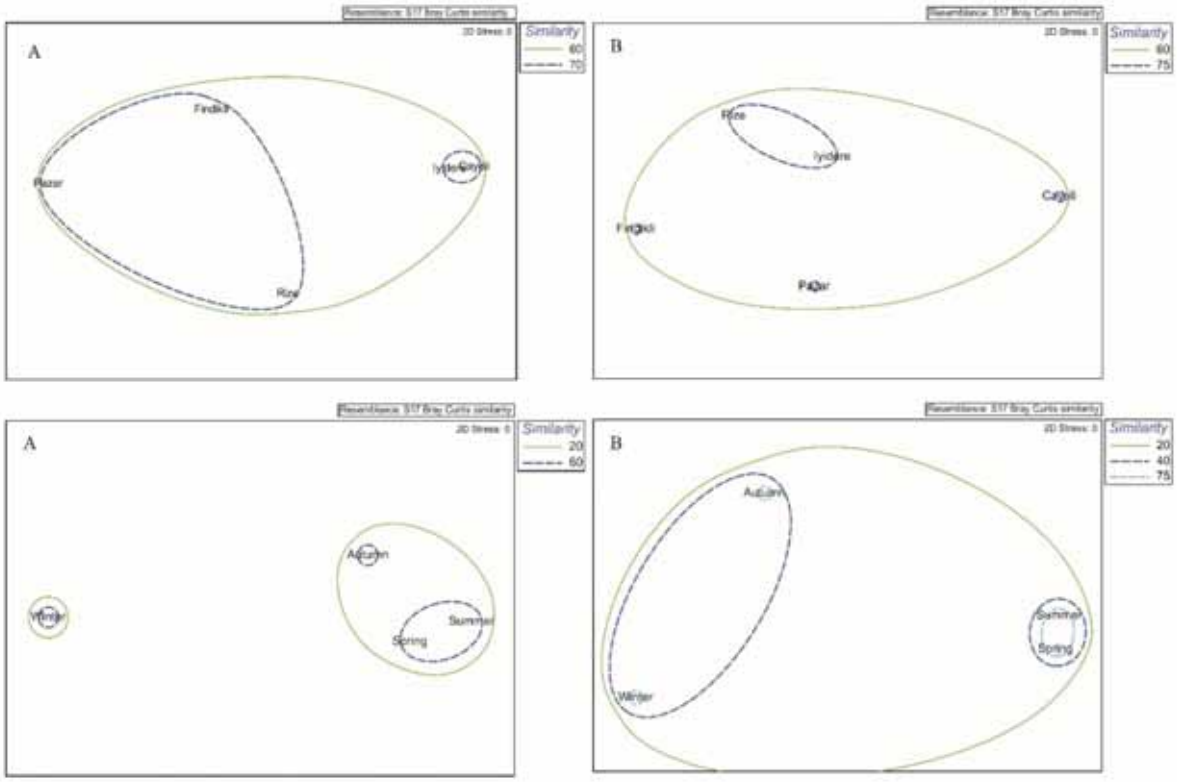

FIGURE 4

Multi-dimensional scaling (MDS) plot of similarity for the diet of *Pleurobrachia pileus* among different study areas and seasons based on: (A) percentage of prey groups numerical frequency *N%* and (B) percentage of prey groups occurrence frequency *F%*. The logarithmic transformed data of *N%* and *F%* were used in MDS.

Dendrogram, MDS, ANOSIM and SIMPER analysis. Diet variation due to seasons. Dendrogram and MDS based on either *N%* or *F%* values showed that spring and summer group together with high similarities (>80%) indicating extremely similar diet (Figure 4 and 5 for season). While the autumn and winter grouped separately from the spring and summer with low similarities indicating differences between the diets at these two periods. Based on *N%*, the diet composition of *P. pileus* in winter showed extremely different diet; shared only 8.0% similarity with spring, summer and autumn. The result of SIMPER analysis indicated that the dissimilarity among different seasons were primarily due to *Pseudonitzschia delicatissima, Ceratium fusus* and particle plastic (Table 4).

Diet variation due to study area. The dendrogram and MDS based on *N%* values showed high percentage of similarity among all study areas indicating a similar diet (Figure 4A and 5A for areas). This was confirmed by ANOSIM, that show low R

values (0.12 – 0.18) showing low differentiation between different study areas (Table 5). However dendrogram based on *F%* values revealed that four different stations (İyidere, Rize, Pazar and Fındıklı) showed high percentage of similarity indicating a similar diet, while the Çayeli station showed lower percentage of similarity with the other stations indicating a different diet (Figure 5B). The MDS based on *F%* showed high percentage of similarity between Rize and İyidere (see Figure 4B for different area). The SIMPER analysis indicated that the dissimilarity between different study areas was primarily due to *P. delicatisima*, plastic particle, *C. fusus* and fish egg (Table 5).

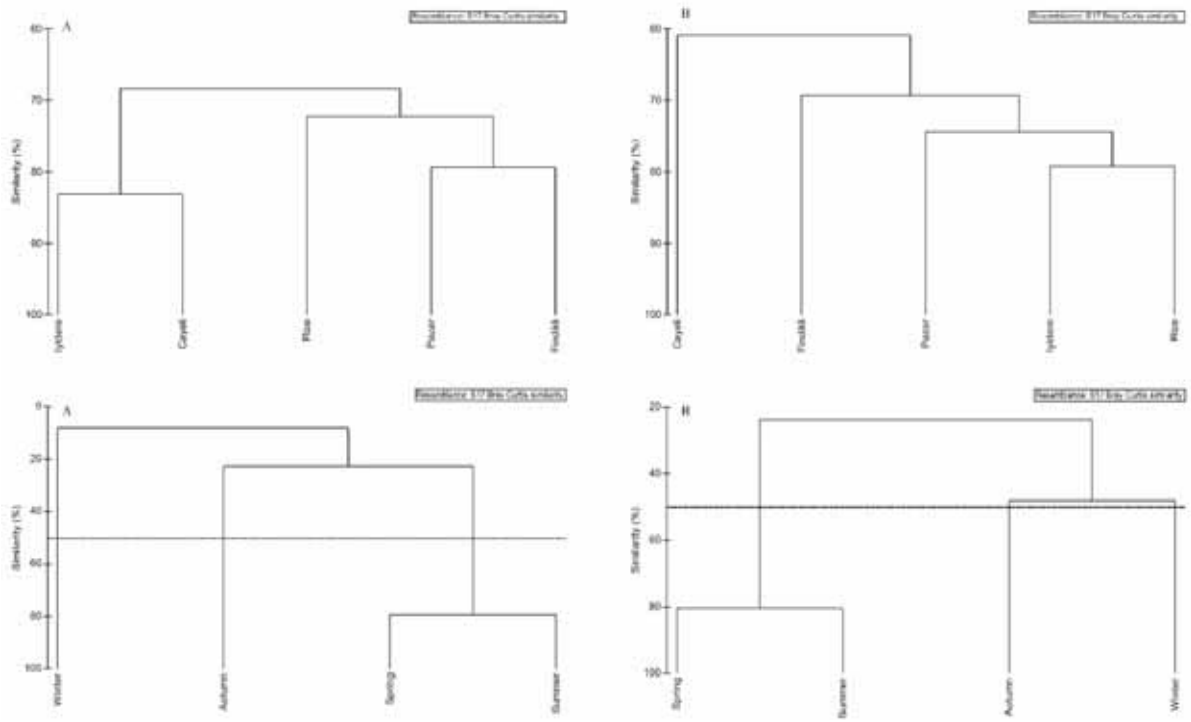

FIGURE 5
Dendrogram of diet similarities of *Pleurobrachia pileus* among different study areas and seasons based on: (A) percentage of prey groups numerical frequency *N%* and (B) percentage of prey groups occurrence frequency *F%*.

TABLE 5
One-way ANOSIM results of the gut content for *Pleurobrachia pileus* in relation to different study areas. SIMPER results showed the average dissimilarities (%) and the contribution of different food items to the dissimilarities.

Stations/ Location	One-way ANOSIM		SIMPER									
	R value	*p* value	Average Dissimilarity %	Discriminating species 1	(%)	Discriminating species 2	(%)	Discriminating species 3	(%)	Discriminating species 4	(%)
İyidere - Rize	0.1602	0.0001	86.23	*P. delicatisima*	36.12	Particle plastic	33.95	*Ceratium fusus*	21,3	Fish egg	7.44
İyidere - Pazar	0.1602	0.0001	84.53	*P. delicatisima*	45.52	Particle plastic	31.45	Fish egg	9,77	*Ceratium fusus*	9.69
İyidere - Fındıklı	0.0308	0.0466	78.63	*P. delicatisima*	38.32	Particle plastic	33.01	*Ceratium fusus*	15,34	Fish egg	13.33
Rize – Çayeli	0.1481	0.0001	88.25	*P. delicatisima*	32.80	Particle plastic	31.24	*Ceratium fusus*	21,22	Fish egg	14.74
Rize – Pazar	0.1265	0.0005	85.11	*P. delicatisima*	41.15	Particle plastic	30	Fish egg	17,47	*Ceratium fusus*	11.39
Çayeli - Fındıklı	0.1829	0.0001	87.55	*P. delicatisima*	34.06	Particle plastic	28.92	*Ceratium fusus*	19,95	Fish egg	17.08
Pazar - Fındıklı	0.1500	0.0002	84.43	*P. delicatisima*	42.71	Particle plastic	29.25	Fish egg	19,57	*Ceratium fusus*	8.46

DISCUSSION

The overall diet of *P. pileus* was dominated by phytoplankton. In relation to different seasons, the diet of *P. pileus* during autumn and winter was mainly dominated by phytoplankton followed by zooplankton, however the diet of *P. pileus* during spring and summer periods were mainly composed of zooplankton. Thus the results reaffirmed the opportunistic feeding habits of *P. pileus* and no prey type preferences suggest that *P. pileus* is miscellaneous feeder eat anything encountered that falls within the parameters of prey. This result is concur with a number of similar investigations [1, 13, 21, 22, 23, 24]

The contribution of fish eggs was found to be high during spring and summer periods whereas its contribution to the total diet bulk of *P. pileus* decreased abruptly and showed comparatively little importance during autumn and winter periods. The *Pleurobrachia* collected from Scottish sea during 1967 has also reported fish eggs only in spring period [1].

Differences between the food items taken by *P. pileus* at five different stations do not differ greatly from each other. The dominate food items of *P. pileus* was found to be phytoplankton in all five study areas.

Up to 20% of *P. pileus* sampled during spring and summer periods had empty guts that gradually decreased till autumn (only 4% empty gut) and winter (no empty gut). Yip [13] also reported a similar gradually decreased in the percentage of empty gut from May to November.

Both overall diet composition and the diet of *P. pileus* in relation to stations showed that the phytoplankton was the dominate prey group in the diet of *P. pileus* in the Southeastern Black Sea. According to earlier studies, different prey group was found to be the dominate prey group in the diet of *P. pileus* at different places. For example, the research work published during 1948, 1962, 1970 and 1971 showed that the dominate prey group in the total diet bulk of *P. pileus* in the Black Sea included fish larvae, *Sagitta* spp., copepods and larvae of benthic organisms while the dominate prey group in the diet of *P. pileus* collected from Hawaiian waters, northern North Sea and Galway Bay was salp, *Oikopleura longicauda* and barnacle nauplii (for Hawaiian waters), Crustaceans, especially copepods and the cladoceran *Evadne* sp. (for northern North Sea and Galway Bay) [cited in 13].

CONCLUSIONS

In conclusion, most of the studies have reported that zooplankton as the main prey items in the diet of *P. pileus*, however, in the Southeastern Black Sea the dominant prey groups in the diet of *P. pileus* is phytoplankton (overall diet). As the diet of *P. pileus* actually shows the availability of different prey groups in the ambient environment and thus the zooplankton fauna of the Black Sea seems to be limited that could possibly cause the collapse of whole ecosystem in near future just similar to the 1980s era during which the icthyo- and mesozooplankton abundance/production of the Black Sea was badly affected due to the shortage of zooplankton. The Black Sea contributes to a larger portion of the total Turkish fisheries yield and according to a recent report published by the Turkish Statistical Institute (TÜİK) the production of fishing industry of Turkey has been gradually shrinking since 2011 with a decrease of around 21.5% with respect to the previous year [25]. The results reported from Mazlum et al. [4] and present study showed that the population of zooplankton in the Southeastern Black Sea is limited compare to other regions and the inadequate of zooplankton especially copepods might be the possible reason in the recent reduction of Turkey fisheries production.

The Southeastern Black sea is reported as one of the hotspot of microplastic pollution [26]. In this study, the presence of microplastics in the diet of *P. pileus* shows bioavailability of these particles for marine biota.

It is believed that the results of this study will provide a baseline data for future work to understand the tropic levels that will assess the proper management of aquatic resources in the Black Sea.

ACKNOWLEDGEMENTS

This study was founded by Recep Tayyip Erdogan University Scientific Research Projects Unit (Project Number: 2013.103.03.2).

REFERENCES

[1] Fraser, J. (1970) The ecology of the ctenophore *Pleurobrachia pileus* in Scottish waters. Journal du Conseil. 33(2),149-168.

[2] Mutlu, E., Bingel, F., Gücü, A., Melnikov, V., Niermann, U., Ostr, N., Zaika, V.E. (1994) Distribution of the new invader Mnemiopsis sp. and the resident *Aurelia aurita* and *Pleurobrachia pileus* populations in the Black Sea in the years 1991–1993. ICES Journal of Marine Science: Journal du Conseil. 51, 407-421.

[3] Anninsky, B., Finenko, G., Datsyk, N. and Ignatyev S. (2013) Gelatinous macroplankton in the Black Sea in the autumn of 2010. Oceanology. 53, 676-685.

[4] Mazlum, R.E., Solak, E. and Bilgin S. (2017) Diet composition of European anchovy (*Engraulis encrasicolus* L., 1758) in Eastern Black Sea region of Turkey: diet variation by season and body size. Cahiers de Biologie Marine. (In press).
[5] Shiganova, T. (1998) Invasion of the Black Sea by the ctenophore *Mnemiopsis leidyi* and recent changes in pelagic community structure. Fisheries Oceanography. 7(3-4), 305-310.
[6] Siapatis, A., Giannoulaki, M., Valavanis, V.D., Palialexis, A., Schismenou, E., Machias, A. and Somarakis S. (2008) Modelling potential habitat of the invasive ctenophore *Mnemiopsis leidyi* in Aegean Sea. Hydrobiologia. 612(1), 281-295.
[7] Rapoza, R., Novak, D. and Costello, J. (2005) Life-stage dependent, in situ dietary patterns of the lobate ctenophore *Mnemiopsis leidyi* Agassiz 1865. Journal of Plankton Research. 27, 951-956.
[8] Frank, K.T. (1986) Ecological significance of the ctenophore *Pleurobrachia pileus* off southwestern Nova Scotia. Canadian Journal of Fisheries and Aquatic Sciences. 43, 211-222.
[9] Suthers, I.M., Frank, K.T. (1990) Zooplankton biomass gradient off south-western Nova Scotia: nearshore ctenophore predation or hydrographic separation? Journal of Plankton Research. 12(4), 831-850.
[10] Fransz, H. and Gieskes, W. (1984) The unbalance of phytoplankton and copepods in the North Sea. ICES Journal of Marine Science / J. Cons. int. Explor. Mer. 183, 218-225.
[11] Williams, R. and Collins, N. (1985) Chaetognaths and ctenophores in the holoplankton of the Bristol Channel. Marine Biology. 85(1), 97-107.
[12] Greve, W. and Reiners, F. (1988) Plankton time—space dynamics in German Bight—a systems approach. Oecologia. 77, 487-496.
[13] Yip, S.Y. (1984) The feeding of *Pleurobrachia pileus* Mueller (Ctenophora) from Galway Bay. Paper presented at the Proceedings of the Royal Irish Academy. Section B: Biological, Geological, and Chemical Science.
[14] Attrill, M.J. (1998) A rehabilitated estuarine ecosystem: The environment and ecology of the Thames estuary: Springer Science & Business Media, 124p.
[15] Fish, J.D. and Fish S. (2011) A student's guide to the seashore: Cambridge University Press, 123p.
[16] Møller, L.F., Canon, J.M. and Tiselius, P. (2010) Bioenergetics and growth in the ctenophore *Pleurobrachia pileus*. Hydrobiologia. 645(1), 167-178.
[17] Båmstedt, U. (1998) Trophodynamics of *Pleurobrachia pileus* (Ctenophora, Cydippida) and ctenophore summer occurrence off the Norwegian north-west coast. Sarsia. 83, 169-181.
[18] Hyslop, E. (1980) Stomach contents analysis—a review of methods and their application. Journal of Fish Biology. 17, 411-429.
[19] Cortés E. (1997) A critical review of methods of studying fish feeding based on analysis of stomach contents: application to elasmobranch fishes. Canadian Journal of Fisheries and Aquatic Sciences. 54, 726-738.
[20] Clark, K.R. and Warwick, R.M. (1994) Changes in marine communities: an approach to statistical analysis and interpretation. Natural Environment Research Council. UK, 144p.
[21] Mayor, A.G. (1912) Ctenophores of the Atlantic coast of North America: Carnegie institution of Washington.
[22] Ralph, P.M. and Kaberry, C. (1950) New Zealand Coelenterates Ctenophores from Cook Strait: Victoria University College, Department of Zoology.
[23] Lazareva, L. (1962) On the feeding of the Black Sea ctenophore *Pleurobrachia pileus* Müller. Trudy Karadags1 ka Biol. St. 18, 71-84.
[24] Martinez, J. (2009) Feeding and growth in the ctenophore *Pleurobrachia pileus*. Master Thesis. Department of Marine Ecology University of Gothenburg.
[25] TÜİK (Turkish Statistical Institute). (2015) Fishing in our seas is decreasing [Press news]. Retrieved from http://tuik.gov.tr/basinOdasi/haberler/2015_42_20150707.pdf [Turkish version].
[26] Aytan, U., Valente, A., Senturk, Y., Usta, R. and Esensoy, Sahin F.B., Mazlum, R.E., Agirbas, E. (2016) First Evaluation of Neustonic microplastics in Black Sea Waters. Marine Environmental Research. 119: 22-30.

Received: **24.05.2017**
Accepted: **02.12.2017**

CORRESPONDING AUTHOR

Rahsan Evren Mazlum
Faculty of Fisheries,
Recep Tayyip Erdoğan University,
TR-53100, Rize – Turkey

e-mail: evren.mazlum@erdogan.edu.tr

© by PSP Volume 27 – No. 2/2018 pages 880-897 Fresenius Environmental Bulletin

THE PEDOGENIC DEVELOPMENT AND CLASSIFICATION OF SOIL DEVELOPED ON MOUNT HASANDAG'S VOLCANIC MATERIALS IN A SEMI-ARID ENVIRONMENT

Hasan Huseyin Ozaytekin[1,*], Cihan Uzun[2], Emel Karaarslan[1], Mert Dedeoglu[1]

[1]Selcuk University, Agriculture Faculty, Department of Soil Science and Plant Nutrition, 42079 Konya, Turkey
[2]Directorate of Provincial Food Agriculture and Livestock Konya Turkey

ABSTRACT

In comparison with Andisols from humid regions, very little information is available regarding the volcanic soils of semi-arid climates. The objectives of this research were to discuss the extent to which these soils meet the requirements of real Andisols, as defined by Soil Taxonomy and to investigate the physical and chemical properties, as well as to define the weathering processes and pedogenic products, of the soils formed over the volcanic materials of Mt. Hasandag in a semi-arid environment.

For this purpose, 4 representative soil profiles were evaluated; after morphological identifications were completed, the soil samples were collected from the horizons to investigate the physical, chemical, geochemical and mineralogical properties to analyze the soil formation over time in a semiarid region. The soils also underwent FT-IR and Scanning Electron Microscope (SEM) analysis in the range of 4000 to 400 cm^{-1} with pellets and at magnifications ranging from 250 to 20.000 X.

The results indicated that the content of the sand and coarse silt fractions were higher than 30% in all soils. Phosphate retention is generally low, and it is lower than 85% in all profiles. The pH values in NaF are lower than 9.5, in general. The bulk density is higher than 0.90 $gr.cm^{-3}$ in all profiles. The Al + ½ Fe percentages (by ammonium oxalate) are lower than 2% in all profiles. Selective extraction in all of the horizons in profile 5 exhibited the following relationships: $Fe_o > Fe_d > Fe_p$ and in other profiles, and in most horizons, $Al_p > Al_d > Al_o$. Selective extraction indicated that in contrast to the soils usually forming on volcanic material worldwide, these soils lack noncrystalline minerals, such as allophone, imogolite and iron humus complexes. The only noncrystalline minerals that are present in great quantities are Al-humus complexes and Ferrihydrite. The crystallized Fe minerals were higher than the other Fe minerals. Feldspar (anorthite and albite), amphibole (diopside, Actinolite, tremolite, hornblende) apatite, hematite, olivine and biotite were more common primer minerals. X-ray diffraction indicates smectite, kaolinite and illite were dominant minerals in the clay fraction. Furthermore, a considerable quantity of chlorite-smectite interstrafied was identified in the clay fraction. The results indicated that the dominant soil-forming processes include the following: 1. desilication and the loss of base cations and Al from the solum; and 2. transformation of iron and aluminum from the sand and silt-size fractions into secondary clay and crystalline Fe minerals. The climate, topography and the nature of the parent materials affected by the leaching regime and weathering rates were identified as the major factors determining soil genesis on Mt. Hasandag. The studied soils were not classified as Andisol because of their lack of andic properties.

KEYWORDS:
Andisols, Soil weathering, Soil Formation, Soil Classification, Hasandag

INTRODUCTION

Volcanic soils were not recognized among international soil scientists until the middle of the 20th century. Volcanic ash soils were identified for the first time in an international system of soil classification by Soil Survey Staff [1]. The FAO Andosol major soil group is even younger [2]. This group was created in 1974 during preparation of the FAO/UNESCO Soil Map of the World. The definition of this group was originally drawn from the Andept suborder in Soil Taxonomy [3], but has subsequently undergone substantial development. Although Andisols account for less than 1% of the soils in the world, they are very productive [4] [5] [2].

Andisols are soils derived from volcanic materials and have a number of unique features that differentiate them from other soils [6] [4]. In general, volcanic soils are dominated by the presence of allophane-imogolite, ferrihydrite, volcanic glasses and Al-(Fe)-humus complexes [7] [8] [2]. More specifically, among the features that make Andisols unique are high phosphate retention, variable charge, high water retention, low bulk density, high friability and highly-stable soil aggregates [9] [10] [2]. In appropriate environmental conditions, the "andosolization" [11] processes usually result in the formation and accumulation in the finer soil fraction of non-

crystalline constituents, such as allophane, imogolite, ferrihydrite, together with organic matter and Al-, Fe-humus complexes [12] [2] [13] as weathering proceeds and soil develops, there is a progressive enrichment of the reactive colloidal components [14].

In addition to the common characteristics that differentiate them from other orders [15] or soil reference groups [16], there are also notable differences among Andisols, which can be attributed to their genesis and management [4] [2]. From a climatic viewpoint, the most common conditions for Andisols formation are a humid environment, with a relatively young, weatherable parent material, under forest vegetation. However, Andisols can occur in a variety of soil temperature regimes – including thermic and hyper thermic – provided that soil moisture regimes are adequately wet enough to allow sufficient weathering and to produce the characteristic key taxonomic requirements [17]. In Mediterranean environments, such as Turkey, the climate may appear to be too hot and too dry for andosolization [18] despite the widespread occurrence of both passive and active volcanic areas.

Previous studies clearly indicate that in addition to parent material, climatic conditions are an important factor in weathering because climate determines the weathering product of volcanic materials and, therefore, the type of noncrystalline minerals that will be formed [19] [20]. The fact that noncrystalline mineral formation is the result of oversaturation of the soil solution with Si, Al, and Fe, which control the soil solution concentration, makes the influence of climate on volcanic soil characteristics easily understood.

In particular, the lengthy hot, dry season, which typically lasts 3 to 4 months, may hamper the conservation of primary glasses, the genesis of allophane [8] [21], the formation of Al-Fe-organomineral complexes, and the subsequent development of andic properties [22]. Conversely, the genesis of well-organized clays is favored [18]. On this basis, research has begun that aims to elucidate the factors and processes discriminating andosolization and the mineralogy of soils developed on volcanic materials under a xeric Mediterranean climate. Previous investigations [23] have shown a wide pedovariability of soils developed on a same parent material, suggesting that environmental factors prevail over the nature of parent materials in addressing pedogenesis.

There are many volcanic areas found in Turkey; a considerable area of central Anatolia is covered by volcanic rocks that are notably andesitic in character. In the semiarid region of central Anatolia, the weathering products from the volcanic materials are quite different from those in humid climates, and soil formation is not yet clearly understood in this environment. Quaternary and Tertiary eruptions have created a belt of volcanic rocks extending west to east through the center of Anatolia. Nevertheless, the question of whether Andisols occur in Turkey remains open. Up until now, very few soil studies have been carried out on the occurrence and properties of soils developed on volcanic material in Turkey. More information is needed about the soils derived from the volcanic parent material in Turkey because only a few studies have been conducted on this subject [24] [25] [26] [27].

This study has been conducted with the aim of defining the role of climate and Al-Fe- compounds in the differing expressions of the andic properties and allophane content in the soils coexisting in a semi-arid area on the same andesitic parent material, under homogeneous xeric, mesic conditions. The aims of this study were to (i) investigate the pedogenetic development of the soils in a semi-arid environment and (ii) show whether soils developed in the Hasandag volcanic parent materials are Andisols

MATERIALS AND METHODS

Site Description. Hasandag, situated 155 km southeast of Konya, is a volcanic mountain in central Anatolia. It forms part of the Cenozoic central Anatolia volcanism. The area investigated lies between 38°01'N and 38°11'N and 34°02'E and 34°17'E in the central portion of Anatolia. Mount Hasan is a double-peaked stratovolcano, located in Central Anatolia, Turkey. The magmas erupted from this multicaldera complex range from basalt to rhyolite, but are dominated by andesite and dacite. Two terminal cones, Big Mt. Hasan and Small Mt. Hasan, culminate at 3253 m and 3069 m, respectively. In the past 13 Ma, a number of different volcanoes have been built in the Mt. Hasan complex. However, the main volcanic activity occurred during the Quaternary period. There are four evolutionary stages in the history of the volcanic complex: stage 1, Kecikalesi volcano, 13 Ma; stage 2, Palaeovolcano, 7 Ma; stage 3, Mesovolcano and stage 4, Neovolcano. The eruptive products consist of lava flows, lava domes, and pyroclastic rocks. The latter include ignimbrites, phreatomagmatic intrusive breccias and pyroclastic flow, sometimes reworked as lahars. The total volume is estimated to be 354 km^3 and the area extent is estimated to be 760 km^2. The textural and mineralogical data suggest that both magma mixing and fractional crystallization were involved in the generation of the andesites and dacites. The magmas that erupted from the central volcanoes show a transition with time from tholeite to calc-alkaline. Three generations of basaltic strombolian cones and lava flows were emplaced contemporaneously with the central volcanoes. The corresponding lavas are alkaline with a sodic tendency [28]. The annual rainfall is 321.30 millimeters, and the annual evaporation rate is 1317.90 millimeters. The mean annual temperature is 9.68 ºC, and the mean soil temperature at a depth

of 50 cm is 13.59 ºC [29]. According to the climate data, the soil moisture and temperature regimes are xeric and mesic [30].

Sampling and analysis. For this study, 4 soil profiles were sampled from four andesitic lava flows or domes. From 2 to 3 kg of soil was collected per soil horizon. The soil samples were air-dried at 20°C for one week, stones were crushed using a wooden pestle and mortar and the fine fraction (< 2 mm) was separated from the gravel (>2 mm) with sieving; additionally, the plant debris, and pebbles were removed and stored in plastic bags for future use.

To characterize the soil profiles, a variety of the physical, chemical and mineralogical properties were determined. The soil pH was measured with a combined electrode in a soil-water (w/v) suspension and 0.01 N KCl with a soil/ solution ratio of 1:2.5. Measurements were taken of (NaF) pH 1 M (1:50) after 2 min of equilibration, as prescribed by the USDA [31]. Measurements were taken of (NaF) pH 1 M (1:50) after 2 min of equilibration, as described by Fieldes and Perrott [32]. The electrical conductivity (EC) was potentiometrically determined in a 1:2.5 soil-water suspension [31]. The bulk density (BD) was determined by weighing soil cores [33]. The water retention at - 33 and – 1500KPa was measured in the disturbed soil samples using a pressure plate extractor [34]. The soil texture was determined using a hydrometer method [35], after the removal of organic matter using H_2O_2 and after the soil was stirred into a sodium hexametaphosphate solution. The P retention was determined in an acidic potassium dihydrogen phosphate solution (1 mg P ml^{-1}) at a pH of 4.6, buffered by sodium acetate with the method described in the Soil Survey Laboratory Methods Manual [31]. The samples were shaken for 16 h, centrifuged and filtered. The P concentration in the supernatant was measured photometrically. The total soil organic carbon (C_{org}) was determined using the Walkley-Black wet digestion method [36]. The exchangeable bases were extracted with a neutral 1 M NH4-acetate, and the bases were determined using atomic absorption spectroscopy [37] [38]. The cation exchange capacity (CEC) was determined using ammonium acetate (1 N, at pH 7), and the quantity was determined using a flame photometer [39]. The amount of carbonate in the soil was measured with a Scheibler calcimeter [31]. The percent base saturation was determined by dividing the sum of the K, Mg, Ca, and Na in mEq 100 g^{-1} soil by the CEC. The short-range order constituents were characterized by selective chemical dissolution. For this purpose, dark ammonium oxalate, dithionite-citrate bicarbonate (DCB), and sodium pyrophosphate-extractable Si, Al, and Fe were determined according to the [31] and using an AAS for quantification. The cations were designated by the subscripts o, d and p for the respective methods. The total elemental analysis of the soil and rock samples was conducted through fusion with lithium metaborate (LiBO2) and dilution in a HNO_3-HF solution according to the procedure outlined by Chao and Sanzolone [40] samples were taken into solution by alkaline fusion using a mixture of 0.25 g soil or sediment powder and 0.75 g flux (lithium tetra and metaborate), with 0.2 N HNO3 solutions diluted to 1:1000. An aliquot of the sample solution was analyzed for the trace elements and REE, on a combination simultaneous/sequential (ICP-MS). The detection limits were 0.002 to 0.01 ppm for all major elements and 0.1 to 1 ppm for all trace elements. The instrument was calibrated using certified standard reference materials (OREAS24P and G1) and then the contents were measured by inductively-coupled argon plasma (ICP).

The bulk and clay mineralogy assessments were conducted using X-ray diffraction (XRD) on powdered samples as randomly-oriented powder mounts with a Shimadzu XRD-6000 with a Cu anticathode and K filter (40 kV, 35 mA). The bulk samples were powdered to 40 μm using a sintered Al oxides mortar grinder. An aliquot was separated and mounted as unoriented powder using the back-side method [41]. The powder was submitted to XRD between 2° and 40° 2θ, and the data were analyzed in a semi-quantitative manner following [42]. The clay fraction (<2 μm) was obtained from the soil after the destruction of organic matter with dilution and Na-acetate-buffered H_2O_2 (pH 5), followed by dispersion with Calgon and sedimentation in water. The oriented specimens of the clay-size fraction were realized using a glass-slide method and were analyzed using X-ray diffraction with Cu Kα radiation from 2° to 15° 2θ, with steps of 0.02° 2θ at 2 s $step^{-1}$. The following treatments were performed: Mg saturation, ethylene glycol solvation (EG), and K saturation, followed by heating for 2 h at 550 °C. The minerals and relative abundance were identified by their diagnostic XRD spacing and were evaluated by their XRD relative peak intensities in the XRD diagram.

Fourier transform infrared analysis (FTIR) was only performed on the <2 μ fractions with pellets made from a 1 mg sample of each sample and 250 mg of KBr. The infrared spectra were recorded with a spectrometer (Perkin Elmer universal ATR probe) in the 4000 to 400 cm^{-1} wavelength range with 1 cm^{-1} resolution [43]. The morphological features of the allophane were observed by scanning electron microscopy (SEM) after the samples were mounted onto aluminum stubs after being coated with carbon and then gold. This double coating was superior to a coating of carbon or gold alone. Each specimen was studied at magnifications ranging from 250 to 20,000. The volcanic glass contents from the coarse silt plus sand fraction (0.02-2.00 mm) were also observed using a glass slide with a polarizing microscope [44] [45].

RESULTS

A description of the study sites and the 4 respective representative soil profiles are summarized in Table 1 and table 2. Profiles 2, 3 and 4 are situated on steep slopes, while profile 1 is situated on a piedmont in a xeric moisture and mesic temperature regime. Horizon differentiation was poor. The solum depth ranged from 55 to 189 cm. In profiles 2, 3 and 4, there are no diagnostic horizons other than an A horizon, whereas a cambic B horizon, in addition to an A horizon, was identified in profile 1. A continuous R was present below the C-horizon in profile 3, and a continuous C layer lay was identified under the A or B horizon in other profiles. Of the profiles, Profile 1 and Profile 2 were medium textured, and Profile 3 and Profile 4 were coarse textured. The structural development was poor or no development was present in all of the analyzed profiles, except in the surface horizons. All profiles had from slightly to moderately developed granular A horizons. Profile 1 had a moderately to highly-developed angular blocky structure in the B horizons. The soil structure was massive in the C layers in all profiles. The colors in the profiles in the Hasandag range from 2.5 Y to 10 YR and generally have high values when it is dry and were characterized by higher values in the deeper layers.

The rate of organic matter accumulation on the surface was higher than in the lower layers, and significant differences were observed between the surface horizons and sub-surface horizons. These differences resulted from differences in the organic matter, roots and the levels of biological activity. No reaction with HCl was observed in the horizons in any of the profiles. The fact that the horizon differences are not high and that the parent material exhibits low-weathering rates indicates that soil evolution is in the preliminary stages.

TABLE 1
Selected site characteristics of the studied profiles.

Pedon	Coordinates		Parent material	Elevation (m)	Phyzyography	Slope (%)	Land use
	Latitude	Longitude					
I	37° 51’35’’	33° 51’47’’	Andesite-basalt	1539	Piedmont	2	Forest
II	37° 51’35’’	33° 51’47’’	Andesite-basalt	1894	steep slopes	30	Grasland
III	37° 51’35’’	33° 51’47’’	Andesite-basalt	1537	steep slopes	15	Forest
IV	37° 51’35’’	33° 51’47’’	Andesite-basalt	1563	steep slopes	20	Forest

TABLE 2
Selected morphological characteristics of profiles.

Profile	Horizon	Depth (cm)	Color (dry)	Color (moist)	Structure[a]	Field texture[b]	Roots[c]	Boundary	Biological activity[d]
I	A1	0-28	10YR4/4	10YR4/3	gr	SC	3-k	gradual, smooth	h
	A2	28-76	10YR4/3	10YR2/3	gr	SC	2-o	gradual, smooth	h
	Bw1	76-164	10YR4/3	10YR2/3	ab	C	2-i	gradual, smooth	m
	Bw2	164-189	10YR4/3	10YR2/3	ab	C	1	gradual, smooth	w
	BC	189-209	10YR5/4	10YR3/4	ab	C	1	clear, wavy	w
	C	+209	10YR5/4	10YR4/4	mas	C	1	...	n
II	A1	0-34	10YR5/3	10YR4/4	gr	SiL	3-k	clear - smooth	m
	A2	34-55	10YR5/3	7.5YR4/3	gr	SiL	3-o	abrubt- smooth	m
	R	+55	-	-	-	-	1	gradual - smooth	n
III	A1	0-27	10YR6/2	7.5YR3/3	gr	CSL	3-k	gradual - smooth	h
	A2	27-61	10YR5/4	10YR4/4	gr	CSL	2-o	clear - smooth	h
	A3	61-101	2.5Y7/2	10YR4/3	gr	SL	2-i	gradual -irregular	m
	C1	101-149	2.5Y7/2	10YR5/1	mas	SL	1	-	w
	C2r	149-174	2.5Y7/1	10YR4/2	mas	SL	1		w
	R	+174	-	-	-	-	1		n
IV	A1	0-11	10YR6/4	10YR4/3	gr	CSL	3-o	clear - smooth	h
	A2	11-65	10YR7/3	10YR4/3	gr	SiL	2-o	abrubt - smooth	h
	A3	65-101	10YR7/3	10YR4/4	gr	S	1	abrubt - smooth	w
	C1	101-144	10YR7/2	10YR4/3	ma	SA	1	abrubt -irregular	w
	C2r	+144	10YR7/1	10YR5/1	ma	SA	1	...	w

a Structure: mas, massive; gr, granular; ab, angular blocky; p, prismatic **b** Field texture: SC: sandy clay, C: clay.; SL: sandy loam; CSL: clayey sandy loam, SA: Sandy weathering material S: Sand, SiL: Silty loam **c** Roots: 1, none; 2, few; 3, moderate; 4, common; i, fine (<2 mm); o, medium (2-5 mm); k, coarse (>5 mm). **d** Biological activity: n, none; w, weak; m, moderate; h, high.

TABLE 3
Some chemical properties of studied profiles.

Profile	Horizon	Depth (cm)	pH (H2O) (1:2.5)	$pH_{(KCL)}$ (1/2.5)	ΔpH KCl-H_2O	$pH_{(NaF)}$ (1/50)	EC (µS/cm)	Organic matter (%)	$CaCO_3$ (%)
I	A1	0-28	6.56	7.13	-0.58	9.66	166	2.99	1.0
	A2	28-76	6.79	6.59	-0.21	9.57	60	1.41	1.1
	Bw1	76-164	6.94	6.51	-0.43	9.68	59	2.04	0.8
	Bw2	164-189	7.01	6.45	-0.57	9.49	39	1.08	0.8
	BC	189-209	7.06	6.47	-0.58	9.56	72	0.70	0.8
	C	+209	7.43	6.48	-0.95	9.62	91	0.60	0.3
II	A1	0-34	7.22	6.26	-0.96	9.29	69	3.23	0.7
	A2	34-55	7.02	6.31	-0.71	9.57	58	1.69	1.1
	R	+55	-	-	-	-	-	-	-
III	A1	0-27	6.61	6.09	-0.52	9.58	72	4.11	0.5
	A2	27-61	6.60	5.95	-0.65	9.59	50	1.30	0.5
	A3	61-101	6.93	6.03	-0.90	9.64	39	0.29	1.4
	C1	101-149	6.67	6.35	-0.33	9.37	51	0.07	0.9
	C2r	149-174	6.92	6.41	-0.51	9.44	55	0.10	0.8
	R	+174	-	-	-	-	-	-	-
IV	A1	0-11	6.78	6.19	-0.59	9.38	69	1.57	0.7
	A2	11-65	6.43	5.84	-0.60	9.54	56	0.60	0.8
	A3	65-101	6.67	5.71	-0.97	9.05	29	0.17	1.8
	C1	101-144	6.55	6.14	-0.41	8.96	24	0.04	1.1
	C2r	+144	6.56	6.29	-0.27	8.97	34	0.01	1.1

TABLE 4
Some chemical and physical properties of studied profiles.

Profile	Horizon	Depth (cm)	Particle size distribution (%)			K.D.K. ($me.100gr^{-1}$)	Base saturation	Exchangeable cations (cmol.kg-1)			
			Sand	Clay	Silt			Ca	Mg	Na	K
I	A1	0-28	41.9	26.1	32.0	15.80	100	11.60	5.14	0.29	1.12
	A2	28-76	38.9	34.1	27.0	18.79	100	11.91	6.13	0.16	1.32
	Bw1	76-164	39.9	35.1	25.0	25.20	100	15.31	10.96	0.34	0.70
	Bw2	164-189	46.9	29.1	24.0	21.92	100	12.83	9.26	0.35	0.67
	BC	189-209	49.9	25.1	25.0	22.27	100	12.55	11.55	0.39	0.69
	C	+209	51.9	21.6	26.5	21.61	74	13.92	0.91	0.51	0.64
II	A1	0-34	53.9	20.1	26.0	11.17	78	7.49	0.34	0.17	0.68
	A2	34-55	54.9	19.1	26.0	9.13	82	6.22	0.35	0.19	0.73
	R	+55	-		-	-	-	-	-		-
III	A1	0-27	61.9	16.1	22.0	10.21	80	7.20	0.29	0.10	0.62
	A2	27-61	71.9	12.1	16.0	5.73	85	4.12	0.16	0.13	0.45
	A3	61-101	82.9	8.1	9.0	2.95	81	1.79	0.08	0.21	0.31
	C1	101-149	89.9	5.1	5.0	0.49	100	0.25	0.01	0.12	0.23
	C2r	149-174	88.9	5.1	6.0	0.94	95	0.54	0.07	0.08	0.20
	R	+174	-		-	-	-	-	-		-
IV	A1	0-11	58.9	17.1	24.0	7.54	80	5.16	0.24	0.13	0.52
	A2	11-65	66.9	17.1	16.0	5.40	78	3.39	0.26	0.16	0.43
	A3	65-101	76.9	7.6	15.5	3.47	69	1.70	0.21	0.15	0.35
	C1	101-144	82.9	5.1	12.0	0.93	88	0.48	0.07	0.09	0.18
	C2r	+144	83.9	1.1	15.0	0.71	100	0.49	0.06	0.08	0.18

Some chemical and physical properties of studied profiles are described in Table 3 and Table 4. The profiles evaluated showed similar textural classes (loam or sand), although their sand, silt and clay contents were different. The textures of the soils are loamy in profiles 1 and 2, and sandy in profiles 3 and 4. The clay content of the soils ranged from 1.1% to 35.1%, the sand content ranged between 38.9% and 89.9%, and the silt content ranged between 5.0% and 32.0%. The relatively high clay content of profiles 1 and 2 emerged as a result of the alteration of the primary minerals into clay minerals. Profiles 3 and 4 had high sand content, and their clay contents generally decreased with depth. The pH (H_2O) was alkaline in the subsurface horizons and the C layer of profile 1 and profile 2, whereas it was acidic in the surface horizons of profile 1 and all horizons of profiles 3 and 4. The soil pH (H_2O) values ranged from 6.43 to 7.43 with no regular distribution, whereas the pH in KCl ranged from 5.71to 7.13 and was consistently less than pH (H_2O). The ΔpH (pH_{KCl} - pH_{H2O}) was negative in all of the horizons. This signals the presence of a net negative charge in all of the horizons, pH in NaF values ranged from 8.96 to 9.68, with values <9.5 in some soils, indicating the absence of Al activity. However, in some horizons the pH values in NaF were over 9.5. Anions such as florid and phosphate undergo specific anion adsorption in allophone and imogolite, and they emit high amounts of OH^- to the environment when these minerals react with NaF. However, the test is only applicable to soils without free carbonates. Free carbonates in the profile cause NaF pH values to measure high; therefore, the test involved is not used to determine the mineralogy class in which the free carbonates are present. The presence of a net negative load in the soils in the area of the study and the resulting pH_{NaF} > 9.5 due to the small amount of carbonates in the surface horizons indicate that there is

no allophone or imogolite in the studied soils. The electrical conductivity of the soils ranged from 24 µS cm^{-1} to 166 µS cm^{-1}. All of the profiles were salt-free. All the soils followed the general trend of having the highest organic matter content on the surface. The organic matter content declined rapidly with depth in all of the profiles, and it increased to proportionally high values, particularly in the surface horizon of profiles 1, 2 and 3. The organic matter content was low in the other horizons. The organic matter content in the profiles ranged from 0.01% to 4.11%. The lowest values were observed in the Cr horizons.

The $CaCO_3$ content was close to the detection limit in the profiles and ranged from 0.3% to 1.8%. No trend was observed with depth. The CEC values ranged from 0.49 to 25.20 $cmol_c$ kg^{-1}. The CEC value varied with the amount of clay and organic matter in the horizons and decreased with depth, whereas an increase was observed in the cambic horizons in profile 1. The exchangeable cations in the soils were identified to be Ca>Mg>K>Na. The exchangeable Ca varied between 0.48 and 15.31 me 100 g^{-1}, the Mg ranged between 0.01 and 11.55 me 100 $g^{-1,}$ the Na ranged between 0.08 and 0.51 me 100 g^{-1} and the K ranged between 0.18 and 1.32 me 100 g^{-1}. The amount of exchangeable cations generally decreased with the soil depth. The base saturation values ranged between 69% and 100% with high values. This indicated that the active forms of Al and Fe do not accumulate in the soil. The andic properties of the studied soils are described in Table 5. All profiles showed a bulk density of >0.9 g cm^{-3} in the studied soils. The bulk density (BD) values of the soils ranged from 1.07 to 1.82 g·cm^{-3}, with surface soils generally having lower BD values than subsurface soils. The BD values were generally high because of the high sand content of the soils in profiles 3 and 4. Phosphate retention ranged from 0.32% to 30.93% and was below 85% in all horizons. It was higher than 25% only in the deeper horizons of profile 1. Phosphate retention was not within the range of Andisols in any of the profiles. The amount of water retention at -1500 kPa was comparatively low and ranged between 0.8% and 15.4%. This value was lower than the expected value when compared with Andisols worldwide. Similarly, low rates of water retention were also observed at -33 kPa. The water retention at this pressure was between 3.6 and 23.7. The first requirement formulated in WRB [46] for andic properties is an Al+½ Fe content (by ammonium oxalate) in the fine earth (0–2 mm) fraction equal to 2.0% or more on an oven-dried (105 °C) basis [47], indicating the presence of amorphous or short-range-order (SRO) materials, such as allophane, imogolite, and ferrihydrite. The Al+½Fe content of the studied soils ranged from 0.23 to 0.64% and did not meet the requirements of Andisols in any of the profiles. The distributions of volcanic glass in the horizons, which have been obtained with the study, were conducted using a polarized microscope technique. The volcanic glass content values ranged from 2% to 13 % in the profiles studied. The highest value was observed in profile 1.

The results of the selective dissolution analysis are given in Table 6. The Si_o content was smaller than 0.2% in all horizons and ranged from 0.029% to 1.210%. The Si_o values did not show a regular trend with depth. The Al_o and Fe_o values ranged from 0.0014% to 0.048% and from 0.318% to 1.321%, respectively. The Al_o and Fe_o did not exhibit an obvious trend in the profile distributions or in the surface and sub-surface horizons. The Fe_p and Al_p values were notably low in the studied profiles and ranged from 0.0013 to 0.0430% and from 0.004 to 0.254%, respectively.

TABLE 5
Index values of the andic properties of studied soils

Profile	Horizon	Phosphorous Retention (%)	Volcanic glass (%)	Al_o+1/2Fe_o (%)	Water retention (% w/w)		Bulk density (g cm–3)	2-0.02 mm Fraksiyon (%)
					-33 kPa	-1500 kPa		
I	A1	22.71	13	0.47	14.5	10.1	1.55	54.8
	A2	27.65	11	0.31	14.7	12.4	1.52	57.5
	Bw1	30.55	6	0.36	19.2	15.4	1.73	54.5
	Bw2	26.13	3	0.23	17.5	15.1	1.61	56.9
	BC	29.16	4	0.20	19.2	13.2	1.63	62.4
	C	30.93	5	0.24	23.7	13.3	1.62	62.5
II	A1	15.75	8	0.56	16.9	5.9	1.07	70.2
	A2	19.04	3	0.64	16.1	5.6	1.34	70.1
	R	-		-	-		-	-
III	A1	11.20	4	0.53	15.1	5.1	1.38	75.9
	A2	11.58	9	0.52	10.4	5.0	1.45	84.7
	A3	8.17	3	0.42	6.5	3.5	1.72	89.5
	C1	0.45	2	0.42	3.6	1.4	1.82	94.2
	C2r	0.32	4	0.37	4.4	1.7	1.72	93.1
	R	-		-	-		-	-
IV	A1	12.34	2	0.71	8.4	5.7	1.56	76.8
	A2	14.11	3	0.57	8.6	4.9	1.65	80.1
	A3	4.88	5	0.31	4.6	3.7	1.66	89.0
	C1	1.33	2	0.24	5.4	1.0	1.78	92.7
	C2r	0.83	3	0.26	6.4	0.8	1.76	93.2

TABLE 6
Selective dissolution analyses of <2 mm of soils of studied soils (%).

Profile	Horizon	Fe_d	Fe_o	Fe_p	Al_d	Al_o	Al_p	Si_o
I	A1	0.925	0.866	0.0428	0.057	0.036	0.254	0.925
	A2	1.148	0.553	0.0111	0.059	0.036	0.229	1.172
	Bw1	1.105	0.634	0.0218	0.062	0.047	0.239	1.210
	Bw2	0.982	0.380	0.0038	0.054	0.037	0.248	0.929
	BC	0.754	0.318	0.0032	0.052	0.040	0.058	0.814
	C	0.982	0.387	0.0028	0.068	0.048	0.047	1.136
II	A1	0.628	1.023	0.0430	0.051	0.048	0.020	0.492
	A2	0.765	1.189	0.0426	0.049	0.044	0.038	0.505
	R	-	-		-		-	-
III	A1	0.486	0.983	0.0405	0.042	0.038	0.037	0.236
	A2	0.318	0.971	0.0354	0.035	0.031	0.024	0.173
	A3	0.267	0.760	0.0041	0.033	0.035	0.065	0.59
	C1	0.123	0.783	0.0026	0.035	0.028	0.004	0.035
	C2r	0.153	0.690	0.0013	0.030	0.027	0.021	0.037
	R	-	-		-		-	-
IV	A1	0.509	1.321	0.0299	0.040	0.045	0.028	0.385
	A2	0.506	1.069	0.0271	0.042	0.033	0.053	0.257
	A3	0.278	0.568	0.0179	0.039	0.024	0.038	0.044
	C1	0.102	0.441	0.0028	0.022	0.014	0.004	0.029
	C2r	0.091	0.471	0.0046	0.022	0.023	0.020	0.035

TABLE 7
The results of total element analysis of studied profiles (%).

Pedon	Horizon	SiO_2	Al_2O_3	Fe_2O_3	MgO	CaO	Na_2O	K_2O	TiO_2	P_2O_5	MnO	LOI	Total
I	A1	57.35	17.21	5.85	2.09	4.24	2.62	1.66	0.87	0.13	0.14	7.6	99.80
	A2	56.76	18.15	6.44	2.19	3.88	2.38	1.71	0.91	0.14	0.14	7.1	99.81
	Bw1	56.37	17.93	6.41	2.26	3.83	2.16	1.55	0.87	0.14	0.14	8.1	99.79
	Bw2	56.71	18.26	6.42	2.42	3.93	2.40	1.70	0.85	0.12	0.12	6.8	99.81
	BC	56.41	18.31	6.57	2.56	3.90	2.32	1.71	0.84	0.14	0.12	6.9	99.81
	C	55.98	18.50	6.66	2.64	4.10	2.37	1.63	0.85	0.15	0.11	6.8	99.80
II	A1	57.88	17.63	5.09	2.20	4.62	3.11	1.64	0.69	0.14	0.10	6.7	99.82
	A2	57.88	18.16	5.47	2.37	4.66	3.14	1.54	0.74	0.11	0.10	5.6	99.83
	R	63.53	16.29	4.27	2.33	5.20	3.59	2.08	0.56	0.16	0.08	1.7	99.84
III	A1	58.33	16.77	5.02	2.33	4.65	3.24	1.77	0.68	0.15	0.10	6.8	99.82
	A2	60.24	17.24	5.13	2.41	4.72	3.47	1.79	0.67	0.12	0.09	3.9	99.83
	A3	61.68	16.90	5.09	2.57	4.85	3.57	1.89	0.65	0.13	0.09	2.4	99.83
	C1	62.73	16.50	5.01	2.61	5.11	3.69	2.06	0.68	0.16	0.09	1.2	99.83
	C2r	63.37	16.18	4.65	2.49	4.95	3.57	2.00	0.61	0.14	0.08	1.8	99.84
	R	63.42	16.23	4.05	2.18	5.08	3.78	2.19	0.54	0.16	0.07	2.1	99.85
IV	A1	58.18	17.90	5.67	2.40	4.96	3.29	1.54	0.79	0.10	0.10	4.9	99.82
	A2	59.59	18.08	5.42	2.27	4.95	3.44	1.58	0.74	0.08	0.09	3.6	99.84
	A3	63.23	16.39	4.34	2.05	4.70	3.40	1.94	0.56	0.11	0.07	3.0	99.85
	C1	63.53	16.39	4.29	2.31	5.05	3.73	2.09	0.57	0.14	0.08	1.7	99.84
	C2r	62.81	16.44	4.61	2.42	5.07	3.72	2.11	0.60	0.15	0.08	1.8	99.83

Such low values were a result of the low organic matter content, in contrast to the values found in volcanic areas in wet regions of the world. Dithionite-citrate-bicarbonate, unlike other solutions, has a stronger effect on compounds that are in crystalline form. In the studied profiles, Fe_d ranged from 0.091% to 1.148%, and Al_d ranged from 0.022% to 0.068%. In general, both Fe_d and Al_d decreased with depth.

The distributions of the measured elemental oxides (total element analysis) are given in Table 7. The Si and Al values differed in the profiles, depending on the sand and clay content of the profiles. The SiO_2 content ranged from 55.98% to 63.53%. The amount of Al in the soil is directly related to the distribution of clay, and the amount of Al_2O_3 increases in mature soils. The Al_2O_3 content varied between 16.18% and 18.50% and tended to decrease with depth in profiles 3 and 4. Due to the low rate of weathering, the amount of Al_2O_3 in the studied soils was close to that of the parent material in solution. The amount of Fe_2O_3 ranged from 4.05% to 6.66%. The highest value of Fe_2O_3 was observed on the surface horizons, except in profile 1. The percentage of CaO exhibited higher levels in the parent material compared with the upper horizons. The CaO values were higher in the C layers than in the other horizons. The percentage of CaO exhibited a distribution between 3.83 and 5.20, whereas the MgO values ranged from 2.05 to 2.64%. The MgO values showed no clear trend in terms of the distribution with depth. The generally high values of MgO resulted from the presence of substantial amounts of minerals with ferro magnesium. High amphibole and biotite peaks were also observed in the primary mineral analyses.

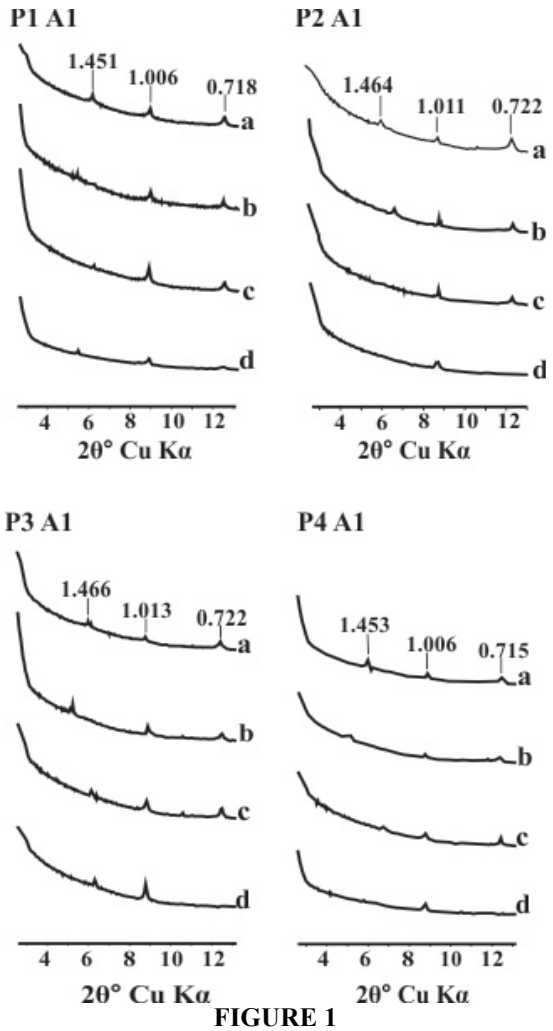

FIGURE 1
X-ray diffractograms of clay factions of selected samples *d*-values in nm.
a: Mg^{+2} saurated ; b: Mg^{+2} + Gliserol saurated; c: K^{+1} saurated; d: K+550 ^{o}C heated

The percentages of K_2O and Na_2O were between 1.54% and 2.11 % and 2.16 % and 3.73 %, respectively. This is closely related to the distribution of the feldspars that are present in andesite and basalt. Titanium is a mineral resistant to, and used for identification of, chemical change. The TiO_2 content in the soils ranged between 0.54 and 0.91 %, the MnO_2 content ranged between 0.07 % and 0.14 %, and the P_2O_5 content ranged between 0.08 % and 0.16 %. A regular trend was not observed between the horizons in the distribution of other major elements generally.

X-ray diffraction of the whole soil body and the clay fraction to determine the mineralogical properties of the profiles was undertaken in the study area and the results are shown in figures 1 and 2. Infrared spectroscopy graphs are shown in Figure 3, and SEM images are shown in Figure 4. Very clean and distinct peaks could not be obtained in the profiles. As seen from the figures, diverse fillo silicates formed in diverse levels of crystallization and in differing amounts in the profiles. In the samples saturated with Mg in the profiles, the peaks, which are seen in the form of a plateau and are poorly crystallized at 1.45 nm, expanded to 1.7 nm in a Mg+Gl (glycerol) application. This indicated that these peaks belong to smectite. The peaks that were observed between 0.710 and 0.720 nm in the samples saturated with Mg, Mg+Gl and K disappeared when heated at 550℃. These peaks belonged to kaolinite. The peaks that were observed at 1.0 nm in all applications belonged to illite. No distinct differences in the clay mineral distribution with depth were observed, and pedons from all geomorphic surfaces had similar mineral components.

Thus, the weak peaks stemmed from too low an amount of clay content of the profiles, especially in the C horizons. The X-ray diffraction (XRD) patterns of powdered samples used to identify primary minerals indicated the presence of feldspar (anorthite and albite), amphibole and pyroxene (diopside, actinolite, tremolite, and hornblende) apatite, hematite, olivine and biotite. The IR spectrums were taken from the horizons to detect the presence of amorphous structures, such as allophone, and they are presented in Figure 4. As seen from these spectrums, peaks were identified in the mono, dimer and triple

bond areas. The IR spectra of the soil showed 5 principal peaks: 712-798, 910-1027, 1409-1449, 1631-1643, 3355-3621 cm^{-1} of the profile. In the IR spectra with a large band structurally, OH peaks of H were observed at 3355-3621 cm^{-1}. The bent vibration peaks belonging to H were found at 1631-1643 cm^{-1}, and a Si-C single vibration band was present at 712-798 cm^{-1}.

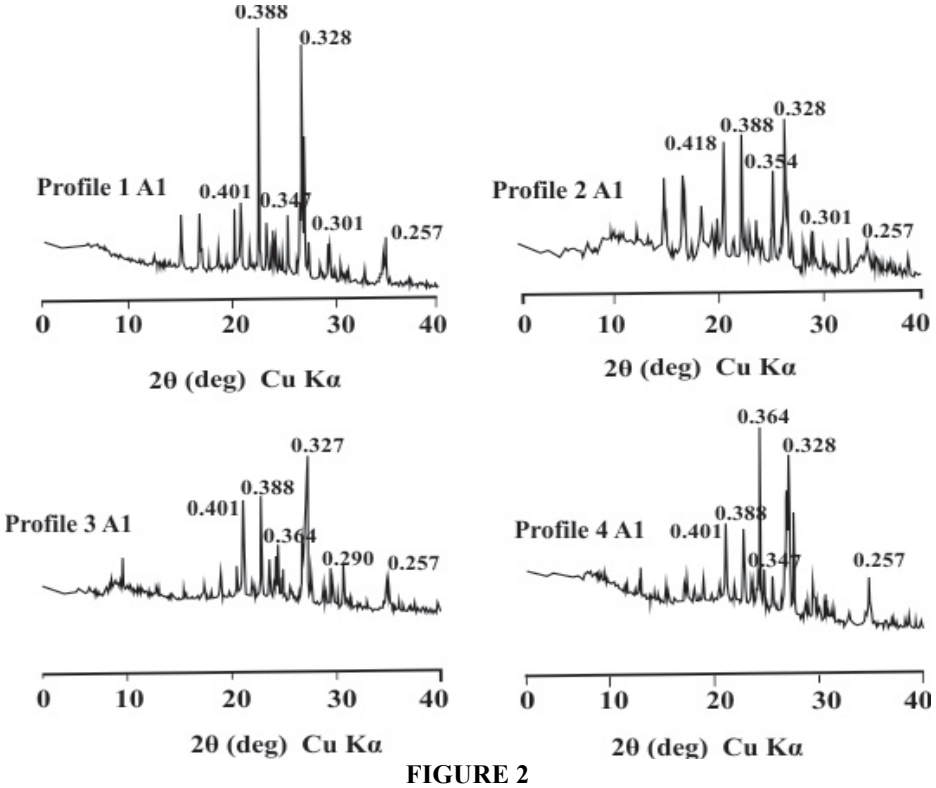

FIGURE 2
X-ray diffractograms of whole soils of representative horizons, *d*-values in nm.

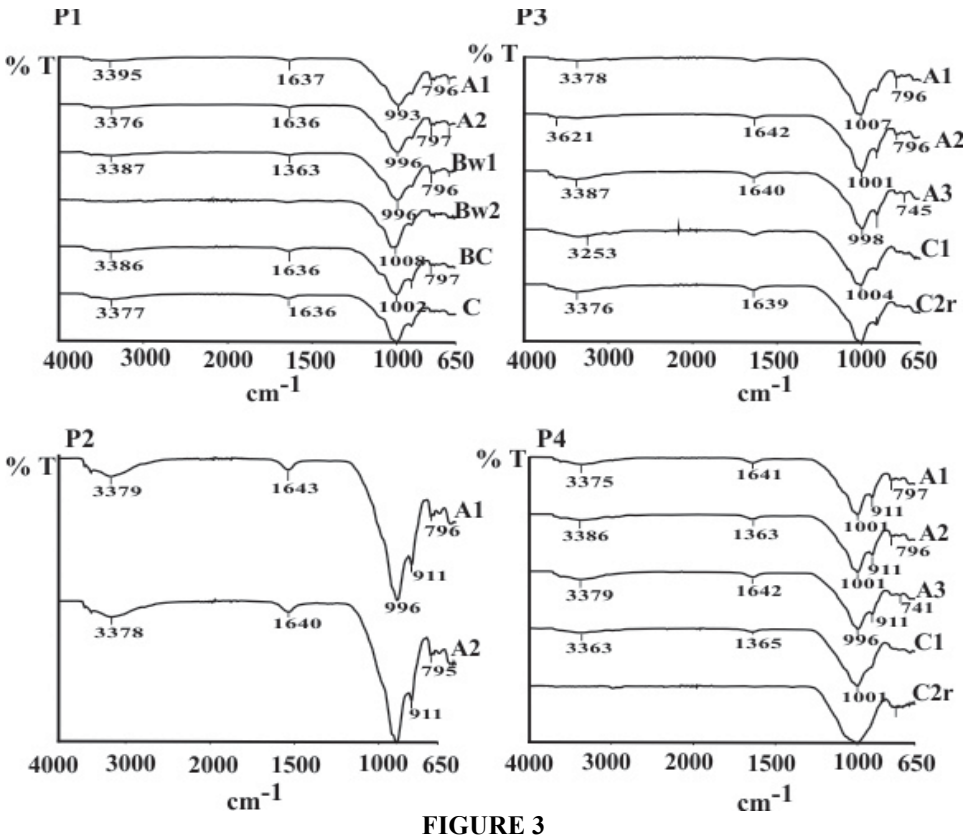

FIGURE 3
Infrared spectra of clay samples.

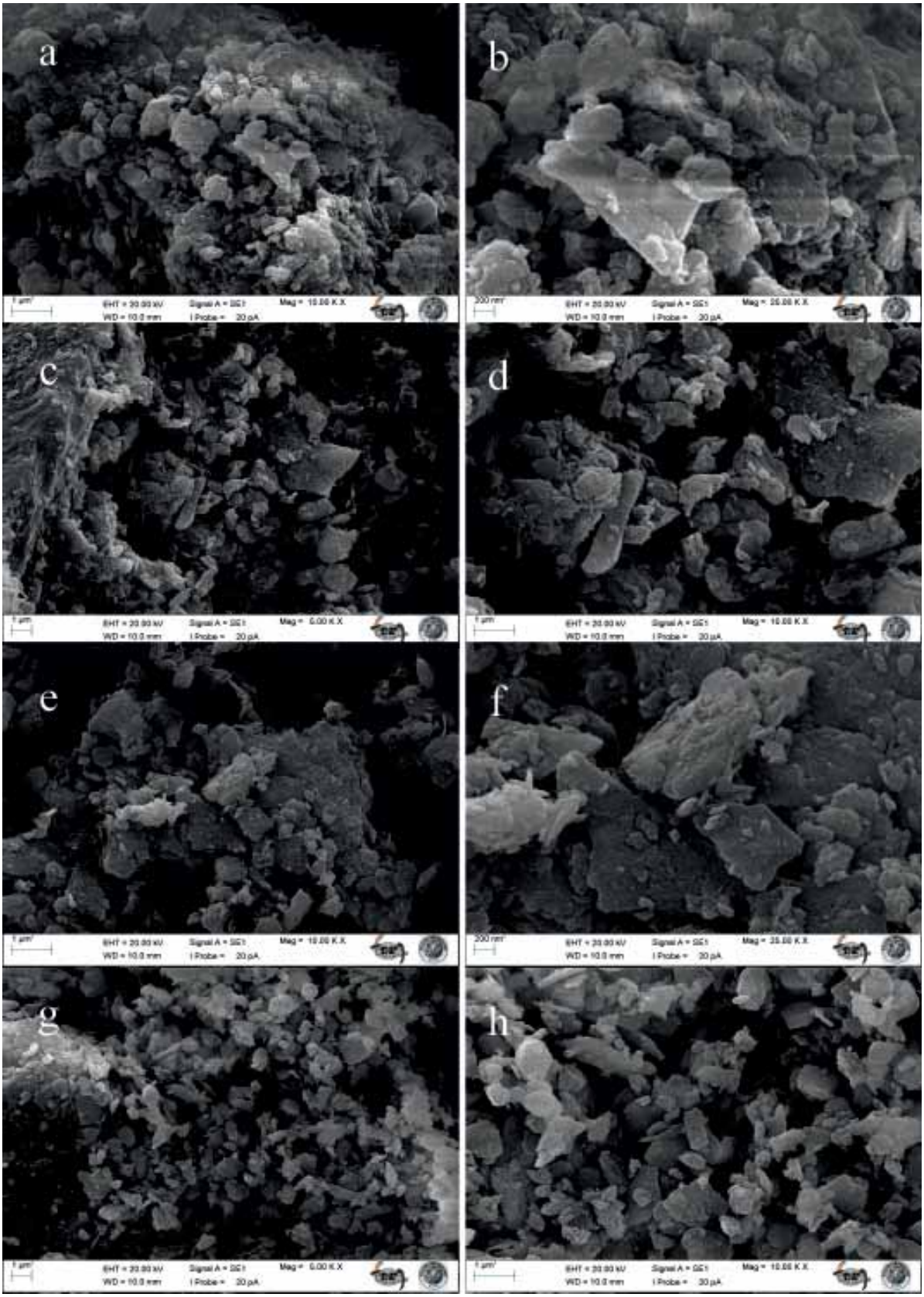

FIGURE 4

SEM photograph of selected samples. Porous, weathered volcanic glass vesicular encased with silt and clay particles or ferrihydrite and vesicular of volcanic glass, and Fe-oxide (hematite) and, ferrihydrite coating, Clay coating on sand grains. a) Image from profile 1-A1. b) Area from (a) enlarged. c) Image from profile 2-A1 d) Area from (c) enlarged. e) Image from profile 3-A1, f) Area from (e) enlarged. g) Image from profile 4-A1 h) Area from (g) enlarged.

DISCUSSION

Morphological, Physical and Chemical Properties. The profile descriptions indicated that there are no diagnostic horizons in profiles 2, 3 and 4, except in the A horizon. The generally high content of sand in the soil, the loamy or sandy-loamy texture in the profiles and the high sand content seen in the textured profiles indicated a low weathering rate, in the soils. The lack of a significant differentiation indicates that the parent material disintegrated slowly; this finding, in turn, suggests that soil formation in the region is in its initial stage. The reason that disintegration was so low is because of climatic factors; low precipitation, high evaporation, and a long dry season limited the weathering process.

All of the horizons of the studied profiles showed a bulk density > 0.9 $g \cdot cm^{-3}$, which is characteristic of Andisols. The bulk density of the soil is lower on the surface and increases in the subsurface horizons. These results from the presence of organic matter on the surface and the lack of smaller particle densities such as allophane and imogolite, factors considered responsible for the lower bulk density [48]. Furthermore, the fact that the C horizons are in the form of weathered or softened main rocks has had an effect on the bulk density values. For this reason, the bulk density values have increased with depth.

When the amount of water retention at -1500 kPa and at -33 kPa in the study area soils is compared with other Andisols in the world; the values are lower than expected. Andisols have the capacity to retain large quantities of water as a result of meso and micro pores that have the ability to retain water at high suction [2], this water-retention capacity is because of the typical spherical and hollow structure of the allophane and allophane-like minerals. However, in the studied soils, water retention at - 1500 and - 33 kPa is very low compared with that expected for Andisols worldwide. The water retention was lower than 20% for all profiles.

In the soils in the study field, the content of organic material especially on the surface horizons reached 4.11%, which can be regarded as high for a dry region in Turkey. The organic carbon concentrations decreased with depth in all the profiles. The organic matter was limited because of the low rate of clay content in most horizons and the scarcity of humus-metal complexes, which can be understood from the Al_p and Fe_p values because the humus-metal complexes and fine fractions protect the organic matter from microbial decomposition and therefore improve its stability. While the organic matter content is relatively high in the surface horizons compared with the arid regions of Turkey, compared with other Andisols in the world, the organic matter content is very low. Low precipitation and a long dry season limited the level of organic matter. High organic matter content caused an anti-allophonic effect to be limited because it hinders the bonding of Al and Fe by organic matter in the Andisols. However, despite low organic matter content, there is no allophone formation in these soils.

When the soil reaction in the soil profiles was examined, it was observed that most soils were weakly acidic but some were weakly alkaline (profile 1 and 2). The higher $pH_{(H2O)}$ values might be related to lower Al activity and lower organic matter content. The pH values (in most cases between 6.5 and 7.0) were relatively high considering the nature of the parent material and the absence of carbonates. Whereas the pH in KCl in all of the horizons was lower than that of pure water. The ΔpH (pH_{KCl}- pH_{H2O}) was negative (-) in all horizons, which indicated a negative charge in all horizons. Determining (NaF) pH is based on the release of OH^- ions into the soil solution by the exchange of OH^- for F^-, which increases the pH and forms fluoaluminate. This exchange occurs mainly in the presence of non-crystalline clays, which is high when these colloids dominate the clay fraction, thus determining the amount of OH−released [32] [49]. The amount of OH^- ions released is related to how much active Al is present [50]. In soils with allophane, fluorides release hydroxyl ions continuously in amounts much larger than in other clays [51]. (NaF) pH ≥ 9.4 is a strong indicator that short-range ordered materials dominate the exchange complex [31]. (NaF) pH is used to differentiate between soils with crystalline and short-range ordered mineralogy, although few studies have evaluated whether this test can assess the spatial variability of volcanic soils with different characteristics. Nevertheless, (NaF) pH has shown significant correlations with various clay minerals (kaolinite, gibbsite, hematite, goethite, allophane, Fe_o and Al_o) in different soil types [52] [53] [54]. In this study, (1 M NaF) pH and the other concentrations that were evaluated were able to differentiate among the four soils; however, Honorato and Pinochet [55] affirmed that when soils are close to the threshold value to be considered as an Andisol (NaF pH ≥ 9.4), this chemical parameter is not useful to adequately discriminate among the soils. Additionally, the test is only applicable to soils without free carbonates. In this study, the pH values in NaF are notably close to the threshold value or below 9.5. Additionally, this value turned out to be over 9.5, especially in the surface horizons where the free carbonate contents were higher than those in the subsurface layers. For this reason, free carbonates in the profile cause NaF pH values to measure high; therefore, the test involved is not used to determine the mineralogy class in which the free carbonates are present. The presence of a net negative load in the soils in the area of the study and the resulting pH_{NaF} > 9.5 due to carbonates indicate that there is no allophone or imogolite in the studied soils. Furthermore, another reason that the NaF test is not always valid

is that Al is attached to the organic matter. These findings are in agreement with the very low amounts of oxalate-extractable Si (Si_o) in the soils, further confirming their nonallophanic nature.

Among the profiles investigated, all profiles contain a small amount of lime. The profiles contain a relatively high amount of calcium carbonate, especially in the upper horizons. A low $CaCO_3$ content was detected in the profiles because the soils in the study area have a volcanic origin.

Phosphate retention (P retention) is also used as a classification criterion in Andisols because of their short-range ordered material [2] [56]. Allophane and imogolite are considered to be the main minerals associated with P retention [57]. Thus, there are several significant relationships between P retention and short-range ordered materials in Andisols [58] [54]. P retention shows a high variability in Andisols, depending on the quantity and type of P forms (organic or inorganic) and the Al and Fe content [59] [60]. In this study, all samples showed very low P retention that remained below the required limits for Andisols, confirming that these soils are not dominated by allophane [61]. Nevertheless, relatively high P retention in some horizons of profile 1 was attributed to the presence of Fe oxides [62].

The CECs of these soils ranged from 0.49 to 25.20 me.100 g^{-1}, and in certain areas (in profile 1), high values were obtained despite the low organic matter content. The CEC increased with the depth in profile 1, which was related to the clay content. The highest CEC value was found in the cambic B horizons of profile 1 due to the high clay content among the horizons. The increase in the CEC to these high values indicated the presence of alumina silicates (smectite) with layers of high charge density. In the XRD's of the clay fractions of the samples, 1.45 nm reflections in the Mg-saturated samples were expanded towards 1.70 nm in glycerol applications. This result explains the high CEC values in profile 1. In other profiles, very low CEC values were observed because of the very low clay content of the horizons, and CEC decreased with the depth related to the clay content. The base saturation values were higher than 50%, in all profiles. The high base saturation indicates that precipitation is inadequate for the leaching of bases. A high exchangeable Ca and Mg content was detected in the profiles of the study area. Several minerals with Ca and Mg, such as diopside, augite and plagioclase are present in the soils, which was evident from the primary mineral analysis of the soils in the study area.

In all four profiles, the clay contents are low and the texture classes are loam or sand, indicating a low rate of weathering. Under climatic conditions of low precipitation and long dry seasons, the weathering process is not easily facilitated. The elevated concentrations of clay, especially in the B horizons of profile 1, are the result of the transformation of primary minerals to clay minerals [63]. The flat topography observed in profile 1 has encouraged the clay formation.

An important criterion used to determine andic properties in the World Reference Base is Al+½Fe content (by ammonium oxalate) equal to 2% or more. Very low Al+½Fe values were observed in the studied soils. Considering the values of volcanic glass, Al+½ Fe values were below the threshold value for Andisols.

TABLE 8
Index values of selective dissolution analysis of the studied soils

Pedon	Horizon	$(Fe_d - Fe_o)^* 100/Fe_d$	Fe_o/Fe_d	Fe_d/Fe_t	Fe_p/Fe_o	Fe_p/Fe_d	$(Al_o - Al_p)/Si_o$	Al_p/Al_d	Al_o/Al_d	Al_p/Al_o
I	A1	6.38	0.94	0.16	0.05	0.046	-0.24	4.46	0.63	7.06
	A2	51.83	0.48	0.18	0.02	0.010	-0.16	3.88	0.61	6.36
	Bw1	42.62	0.57	0.17	0.03	0.020	-0.16	3.85	0.76	5.09
	Bw2	61.30	0.39	0.15	0.01	0.004	-0.23	4.59	0.69	6.70
	BC	57.82	0.42	0.11	0.01	0.004	-0.02	1.12	0.77	1.45
	C	60.59	0.39	0.15	0.01	0.003	0.00	0.69	0.71	0.98
II	A1	-62.90	1.63	0.12	0.04	0.068	0.06	0.39	0.94	0.42
	A2	-55.42	1.55	0.14	0.04	0.056	0.01	0.78	0.90	0.86
	R	-	-	-	-	-	-	-	-	-
III	A1	-102.26	2.02	0.10	0.04	0.083	0.00	0.88	0.90	0.97
	A2	-205.35	3.05	0.06	0.04	0.111	0.04	0.69	0.89	0.77
	A3	-184.64	2.85	0.05	0.01	0.015	-0.05	1.97	1.06	1.86
	C1	-536.59	6.37	0.02	0.00	0.021	0.69	0.11	0.80	0.14
	C2r	-350.98	4.51	0.03	0.00	0.008	0.16	0.70	0.90	0.78
	R	-	-	-	-	-	-	-	-	-
IV	A1	-159.53	2.60	0.09	0.02	0.059	0.04	0.70	1.13	0.62
	A2	-111.26	2.11	0.09	0.03	0.054	-0.08	1.26	0.79	1.61
	A3	-104.32	2.04	0.06	0.03	0.064	-0.32	0.97	0.62	1.58
	C1	-332.35	4.32	0.02	0.01	0.027	0.34	0.18	0.64	0.29
	C2r	-417.58	5.18	0.02	0.01	0.051	0.09	0.91	1.05	0.87

Selective Dissolution Analysis. Different extractable forms of Al, Fe and Si have been used to characterize different types of soils and have, therefore, also been used to characterize Andisols [54] [64]. Index values derived from the selective dissolution analyses results were given in Table 8. These values obtained with the help of these data helped to elucidate whether amorphous materials, such as allophone, imogolite and ferrihydrite were available.

The acid–ammonium oxalate-extractable Fe (Fe_o) is supposed to be a reliable estimator of ferrihydrite, and the Fe substituting Al in allophane and not to extract other Fe oxides, such as goethite and hematite, to any significant extent [65] [66]. The Al_o and Si_o values determined in the acid oxalate in the study area were below those seen in Andisols that are rich in allophone. Therefore, these low values indicated a low level, or total absence, of amorphous compounds, such as allophone and imogolite. The low amount of Fe_o in comparison with Fe_d is an indicator of the thermodynamic conversion of metastable ferrihydrite into stable Fe-oxides, such as gotite and hematite [67]. In general, Fe_o was also low compared with Fe_d in the studied profiles. The very small amount of Fe_o also indicates that Fe oxides are mainly crystallized. Furthermore, the presence of hematite in certain profiles across all soil mineralogy confirms the presence of Fe oxides. Low pH (NaF) values are in agreement with very low amounts of oxalate-extractable Si (Si_o). The pyrophosphate-extractable Al (Al_p) and Fe (Fe_d) provided significant information about the organometallic complex forms of Fe and Al. Al_p and Fe_p are very high in Andisols; however, in the studied soils, these values were very low compared with those of other Andisols because of the very low organic matter content of the studied soils; the low precipitation and long and dry summer season in the study area prevent the organic matter from reaching high levels. The Fe_p, and Al_p values were also observed to be low. However, the Al_p values in the study area, especially in the surface horizons, were observed to be higher than those of Al_o and Al_d. This indicates that the Al-complexes were found in the profiles at a higher rate than the allophone or crystallized Al compounds or reached substantial amounts, whereas the Fe humus complexes were identified far less than the other Fe fractions. The Fe_d rates in the studied profiles appeared to be generally higher than in the other extracts. The extremely small amounts of Al_o and Si_o compared with Fe_d suggest that crystalline aluminosilicates with high charge density could be occurring through neoformation, consuming both the Al and Fe released from the weathered parent material. The Al_d values were higher than the general Al_o. This indicated that Al was identified more often in crystallized compounds than in allophone. High Fe_d values indicate that Fe is found in the form of crystallized compounds. As mentioned above the index values provide very important information about the status of amorphous materials in the soils. The high Fe_o/Fe_d rates observed in the profiles support this finding. The Fe_p/Fe_d values in the soils were also fairly low. Such low values are additional evidence of the presence of crystallized Fe compounds. The ratio of Al_p/Al_o yields information about the relative composition of the colloidal fraction, with a ratio of < 0.5 separating the Al - humus complexes from the allophanic materials. The rate of Al_p/Al_o was used to measure a characteristic of Andisols whereby an Al_p-to-Al_o ratio lower than 0.1 confirms the absolute presence of allophane. The Al_p/Al_o value was found to be very high in the studied soils. The fact that these values were > 0.5 in all profiles suggests that much of the extractable Al was present in Al - humus complexes rather than in allophane. Fe_p/Fe_d values were quite small, as were Fe_o/Fe_d values, probably because crystalline Fe - oxides were more abundant than ferrihydrite. The concentrations of Fe_o were consistently higher than the concentrations of Fe_p. A low Fe_p-to-Fe_o ratio (<0.9 in all horizons) indicates that Fe-humus complexes are limited. Consequently, all selective dissolution analysis results and the index values of selective dissolution analysis indicate that noncrystalline minerals, such as allophane and imogolite, have not formed in these soils. Many researchers who found similar results reported that allophones are rarely found in soils under ustic, xeric, or aridic moisture regimes due to the restricted leaching of silica [68] [26].

Mineralogical Properties. Because most of the differences among Andisols are primarily determined by their clay fraction, it would be useful to know in detail the type and amount of clay in these soils. There are several chemical tests associated with the minerals of the clay fraction in volcanic soils, including the reactivity of sodium fluoride (NaF), phosphate retention and the content of Al, Fe and Si extracted with ammonium oxalate (Al_o, Fe_o and Si_o) [15] [52] [53] [54] [68] [69] [70] In this study, X-ray diffractograms, infrared spectroscopy and SEM images were used to characterize and confirm the mineralogical properties of the soils. The results of the X-ray analysis are shown in Figures 1 and 2. The X-ray diffractograms showed only weak and often not very clear signals in the region of 2-15 °2θ. There is no significant difference in the amount of minerals that exist deep in the profile. The similarity of the minerals to one another in the solum, and the lack of significant differentiation in their amounts, indicated that these soils are young; however, the prevalence of the clay minerals with an intermediate layer in the solum demonstrated that the profile has a more developed composition than that of a primary stage profile. As illustrated in Figure 1, the presence of kaolinite and illite in the profile indicates that the feldspars turned directly into kaolinite and illite, most likely due to mineral weathering. Illite, which was encountered in all profile horizons,

probably formed through the conversion of minerals that contain K in an environment where chemical reactions occur. The fact that the illite was almost uniform in the profile supports the view that it was formed from feldspars that are commonly found in basalts and andesites. Additionally, 2.1 type clay minerals were found in the study area. This finding is noted because the basic cations, which emerged from the weathering of pyroxene and amphiboles, raised the pH and because the Si and Ca could not be sufficiently leached, which encouraged smectite formation accompanied by a high Si/Al ratio and Ca. The presence of such minerals as augite and diopside, which are among the primary minerals, reinforces this theory. In light of all of these data, the clay minerals in the studied soils likely formed as the products of conversion and weathering of the minerals, feldspars, pyroxene and amphibole, which are heavily detected in the basalt and andesitic materials derived from the parent material. Hematite was found in small amounts of sesquioxide in all profiles. Hematite is a common minor constituent of volcanic ash, especially from volcanoes that are very hot when erupting, leading to the oxidation of iron compounds at high temperatures to produce hematite. The presence of crystalline Fe oxides is in agreement with the low Fe_o-to-Fe_d ratios, indicating that a considerable amount of Fe is released from the weathering of Fe-bearing minerals and transformed to crystalline Fe oxides. Wada [71], and Bingham et al. [72] reported that hematite is related to magnetite and maghemite, that magnetite can easily formed from maghemite under forest vegetation and in the presence of organic matter and that gibbsite is available in the well-disintegrated volcanic ash soil in Hawaii.

The infrared spectroscopy charts (Figure 3) and SEM images (Figure 4) have been taken to confirm the existence of amorphous materials, but neither allophane nor imogolite were found in the IR spectra and SEM. Allophones have 4 major IR absorption regions. The first region is at 3475 to 3500 cm^{-1} due to the OH stretching vibrations of the Al-OH octahedral and SiOH tetrahedral groups and/or adsorbed water called the functional group region. The second region, appearing at 1400 to 1440 cm^{-1} is due to the HOH deformation vibration of adsorbed water. The third region (800 to 1400 cm^{-1}), called the fingerprint, is attributed to Al-OH and/or Si-O linkages [48] [70] [73]. Allophane shows a single absorption band, while imogolite shows two absorption maxima at approximately 940 to 1000 cm^{-1} [48]. Such vibrations could not be obtained in the soil samples from the study area. The samples from Mt. Hasandag did not show any absorption in regions 1, 2 and 3. The maxima in the 1630 to 1650 and 600 to 800 cm^{-1} region are typical of metal-organo complexes and fillo silicates, respectively. The results of the infrared spectra of the clay samples of the studied soils do not show the usual features for allophane and imogolite in the spectrum, thereby indicating an absence of allophane and imogolite. The data were consistent with SEM images taken to confirm the presence of allophones and imogolite in the samples. In the SEM images, the images observed were not in the shape of rings belonging to allophones and imogolite or belonging to the morphology of spherical and tubular shapes in varying sizes. Consequently, the relatively lower degree of leaching in this semiarid climate with alternating dry and wet seasons is believed to cause higher Si contents in the soil solution and to limit allophane and imogolite formation. The small differences in the clay mineral type and amount, the similar content of primary minerals, the high sand content in the profiles, and the existence of an A-C, A-R or A-Bw-C horizon arrangement indicate small pedogenetic differences.

Classification. The requirements for a soil to be classified as an Andisol are described in Soil Survey Staff [15]. The index values belonging to the andic properties for the studied soils can be seen in table 5. The Al_o+1/2 Fe_o values in all of the profiles are rather low and below 0.64 % in all of the horizons. The phosphorus fixation capacity in the soils is lower than 85 %, and shows that active Al and Fe complexes do not accumulate in the soil. The bulk density is higher than 0.9 gr/cm^{-1} in all of the horizons. For all soils, it can be observed that the studied soils do not meet all the requirements for andic properties [15]. As a result, the soils developed at Mt. Hasandag cannot be classified as Andisols. According to Soil Taxonomy, profiles 2, 3 and 4 are classified as Entisols because they have no diagnostic surface or subsoil horizons, except for ochric epipedon; therefore, they are classified as Orthent because they have no other suborder properties of Entisols. According to the polarizing microscope study using glass slides, soils contain volcanic glass and this value satisfies the requirements of vitric or andic subgroups. Because they are in a xeric moisture regime and meet the necessary requirements for the vitrandic subgroup, they are classified as Vitrandic Xerorthent. Conversely, in profile 1, in addition to the surface mollic epipedon, the soil is classified in the Inceptisol order because of the absence of a cambic horizon in the profile. Because it does not contain plagen and antropic epipedon, it is classified in the subgroup Xerept. Finally, because the soil does not involve a duripan, calcic or petrocalcic horizon and fragipan, and has a base saturation of over 60 %, it is classified in the Haploxerept great group. This profile is classified as Vitrandic Haploxerept at the sub-group level.

CONCLUSIONS

In this study, we evaluated soil formation by analyzing 4 profiles developed on volcanic materials in the semi-arid climatic conditions in Central Anatolia. The physical, chemical and mineralogical properties of the profiles were identified, and it was determined whether the soils formed in the study area could be classified as Andisols. The low precipitation rates, the long and dry summer, low rate of weathering, and the inadequate Si leaching in the study area restricted noncrystalline minerals, such as allophane and imogolite, in these soils. The local climate has a dry season, and the very small amount of precipitation negatively affected soil moisture. None of the studied profiles achieved the requirements for Andisols in Soil Taxonomy [15] and no andic properties were identified in the profiles. The soils of Mount Hasandag did not show andic properties and were not classified as Andisol, but rather as Vitrandic Xerorthent or Vitrandic Haploxerept. From the obtained data, we established that the climate determines the concentration of such cations as Al, Si, and Fe in the soil solutions by affecting both the accumulation of organic matter and the amount of weathering products from volcanic materials in the formation of andic properties, as described in Soil Taxonomy. The semi-arid climate and the long and dry summer season of the volcanic areas, a low rate of weathering, inadequate Si leaching as a result of low precipitation and the small amount volcanic glass content of the parent materials of the soil studied prevented andic soil properties. Consequently, in the studied environment, it was found that the climate (precipitation) and the volcanic glass content of the parent materials are more influential in Andisols formation than the parent material.

ACKNOWLEDGEMENTS

This study is a part of a Ph.D. Thesis produced by Cihan Uzun and was supported by TUBITAK (Scientific and Technological Research Council of Turkey, Project No: TOVAG 110O301) and the Selcuk University BAP Office (Coordinating Office of Scientific Research Projects, Project No: 10201007).

REFERENCES

[1] Soil Survey Staff (1960) A Comphensive System 7th Approximation. Soil Conservation Service USDA Washington D.C.

[2] Shoji, S., Dahlgren, R. and Nanzyo, M. (1993) Genesis of Volcanic Ash Soils. In: Soils Shoji, S., Nonzyo, M., Dahlgren, R. (eds.) Volcanic Ash Genesis, Properties and Utilization Elsevier, Amsterdam, 37-71.

[3] Soil Survey Staff (1975) Soil Taxonomy: A Basic System of Soil Classification for Making and Interpreting Soil Surveys. U.S. Dept. of Agric. Handb. 436. U.S. Govt. Print. Off. Washington, DC. 754p.

[4] Dahlgren, R.A., Saigusa, M. and Ugolini, F.C. (2004) The nature, properties and management of volcanic soils. Adv. Agron. 82, 113–182.

[5] Leamy, M.L., Smith, G.D., Clomet-Daage, F. and Otowa, M. (1980) Themorphological characteristics of Andisols. In: Tan, K.H. (Ed.) Andosols. Van Nostrand Reinhold Company. 34-51.

[6] Besoain, E. (1985) Mineralogía de los suelos volcánicos del centro sur de Chile. In: Tosso, J. (ed.) Suelos Volcánicos de Chile Instituto de Investigaciones Agropecuarias, Chile (INIA). 109–151.

[7] Malucelli, F., Terribile, F. and Colombo, C. (1999) Mineralogy, micromorphology and chemical analysis of andosols of the Island of Sao Miguel (Azores). Geoderma. 88, 73–98.

[8] Mizota, C. and Van Reeuwijk, L.P. (1989) Clay Mineralogy and Chemistry of Soils Formed in Volcanic Material in Diverse Climatic Regions. International Soil Refence and Information Centre Soil Monograph, Vol. 2, ISRIC, Wageningen, the Netherlands.

[9] Armas-Espinel, S., Hernández-Moreno, J., Muñoz-Carpena, R. and Regalado, C. (2003) Physical properties of “sorriba”- cultivated volcanic soils from Tenerife in relation to andic diagnostic parameters. Geoderma. 117, 297–311.

[10] Dorner, J., Dec, D., Peng, X. and Horn, R. (2010) Effect of land use change on the dynamic behavior of structural properties of an Andisol in southern Chile under saturated and unsaturated hydraulic conditions. Geoderma. 159, 189–197.

[11] Duchaufour, P. (1977) Pedolgy. Masson, Paris.

[12] Shoji, S. and Ono, T. (1978) Physical and chemical properties and clay mineralogy of Andosols from Kitakami, Japan. Soil Science. 126, 297–312.

[13] Monteiro, F., Kleber, M., Fonseca, M., Madeira, M. and Jahn, R. (2007) Crystalline clay constituents of soils from European volcanic systems. In: Arnalds, Ó., Bartoli, F., Buurman, P., Óskarsson, H., Stoops, G., García-Rodeja, E. (Eds.) Soils of Volcanic Regions in Europe. Springer, Berlin. 181–195.

[14] Taboada, T., García, C., Martínez-Cortizas, A., Nóvoa, J.C., Pontevedra, X. and García-Rodeja, E. (2007) Chemical weathering of Reference European volcanic soils. In: Arnalds, Ó., Bartoli, F., Buurman, P., Óskarsson, H., Stoops, G., García-Rodeja, E. (Eds.) Soils of Volcanic Regions in Europe. Springer, Berlin, 307–323.

[15] Soil Survey Staff, (2010) Keys to Soil Taxonomy, 11th ed. USDA-Natural Resources Conservation Service, Washington, DC, USA.
[16] FAO/IUSS/ISRIC (2006) World Reference Base (WRB) for Soil Resources. A framework for international classification and communication. World Soil Resources Report 103. FAO, Rome.
[17] Kimble, J.M., Ping, C.L., Sumner, M.E. and Wilding, L.P. (2000) Andisols. In: Sumner, M.E. (Ed.) Handbook of Soil Science. CRC Press, Boca Raton, FL. pp. 209–224.
[18] Lulli, L. (2007) Italian volcanic soils. In: Arnalds, Ó., Bartoli, F., Buurman, P., Óskarsson, H., Stoops, G., García-Rodeja, E. (Eds.) Soils of Volcanic Regions in Europe. Springer, Berlin. 51–67.
[19] Egli, M., Mirabella, A., Nater, M., Alioth, L. and Raimondi, S. (2008) Clay minerals, oxyhydroxide formation, element leaching and humus development in volcanic soils. Geoderma. 143, 101-114.
[20] Özaytekin, H.H. and Özcan, S. (2012) Mass Balance of Soil Evolution on Mt. Erenler Volcanic Materials In Central Anatolia - A Case Study. Carpathian Journal of Earth Science. 8(1), 5-18.
[21] Singer, A., Zarei, M., Lange, F.M. and Stahr, K. (2004) Halloysite characteristics and formation in the northern Golan Heights. Geoderma. 123, 279–295.
[22] Southard, S.B. and Southard, R.J., (1989) Mineralogy and classification of Andic soils in northeastern California. Soil Sci am. 53, 1784-1791.
[23] Vacca, S., Buondonno, A., Capra, G.F., Coppola, E., Rubino, M., Odierna, P., Madrau, S., Colella, A. and Langella, A. (2008) Pedovariability and expression of andic soil properties on the basalts of macomer (Sardinia): influence of vegetal cover. In Soils Changing in a Changing World. Advances in GeoEcolgy. (Eds. Dazzi, C., Costantini, E. The Soils of Tomorrow: vol. 39. Catena Verlag, Reiskirchen. 81–99.
[24] Kapur, S. (1980) Pedogenesis and Classification of Soils Developed on Basalt Rock around the Mt. Karacadağ. Assoc. Professorship Thesis. Çukurova University, Adana, Turkey, 115p. (in Turkish with English abstract).
[25] Özaytekin, H.H., (2002) Physical, Chemical, Mineralogical Properties and Classifıcation Of The Soils Developed On The Karadağ (Karaman) Volcanics. Ph. D. Thesis, Selçuk Univ. Agricultural Faculty Konya Turkey, 134p.
[26] Alp, S. and Ozaytekin, H.H. (2011) Soil Formation overlying Volcanic Materials at Mt. Erenler, Konya, Turkey. Turkish Journal of Agriculture and Forestry . 35(5), 545-562.
[27] Dingil, M. (2003) Soil properties and genesis on probable Andisols in Turkey. Ph. D. Thesis, Çukurova Univ. Adana Turkey.
[28] Aydar, E. and Gourgaud, A. (1998) The geology of Mount Hasan stratovolcano, central Anatolia, Turkey. Journal of Volcanology and Geothermal Research. 85, 129–152.
[29] DMI (1994) Meteorology Bulletin. Prime Ministry Printing Establishment, Ankara.
[30] Soil Survey Staff (1999) Soil Taxonomy. A Basic System of Soil Classification for Making and Interpreting Soil Survey. USDA Agriculture Handbook No. 436, Washington DC, USA.
[31] USDA (2004) Soil Survey Laboratory Methods Manual. United States Department of Agriculture-Natural Resources Conservation Service, Soil Survey Investigations Report No. 42, Washington DC, USA.
[32] Fieldes, M. and Perrott, K.W. (1966) The nature of allophane in soils. Part 3. Rapid field and laboratory test for allophane. N. Z. J. Sci. 9, 623–629.
[33] Blake, G.R. and Hartge, K.H. (1986) Bulk Density. In: Klute, A. (ed.) Methods of soil analysis, part 1. Physical and mineralogical methods. Agronomy Monograph No: 9. SSSA, Madison, WI, S: 393, 363-375.
[34] Peters, D.B. (1965) Water availability. In: Black, C.A. (ed.) Methods of Soil Analysis, Part I American Society of Agronomy, Madison, WI, USA, 279-285.
[35] Bouyoucos, G.J. (1951) A recalibration of the hydrometer method for making mechanical analysis of soils. Agron J. 43, 434-438.
[36] Van Lagen, B. (1993) Manual for Chemical Soil Analyses. Department of Soil Science and Geology, Wageningen University, Netherlands. volcanic soils. Adv. Agron. 82, 113–182.
[37] Sumner, M.E. and Miller, W.P. (1996) Cation exchange capacity and exchange coefficients. In: Sparks D.L. (ed.) Methods of Soil Analysis. Part 3. Chemical Analysis. Soil Sci. Soc. Am. Book.
[38] Tan, K.H. (1996) Soil Sampling Preparation and Analysis. Marcel Dekker, New York. 408 p.
[39] Schollenberger, C.J. and Simon, R.H. (1954) Determination of exchange capacity and exchangeable bases in soil-ammonium acetate method. Soil Science. 59, 13-24.
[40] Chao, T.T. and Sanzolone, R.F. (1992) Decomposition techniques. Journal of Geochemical Exploration. 44, 65-106.
[41] Brindley, G.W. and Brown, G. (1980) Crystal Structures of Clay Minerals and Their X-ray Identification. Mineralogical Society, London. 495p.

[42] Cook, H.E., Johnson, P.D., Matti, J.C. and Zemmels, I. (1975) Methods of sample preparation and x-ray diffraction data analysis, x-ray mineralogy laboratory. In: Kaneps, A.G. (ed.) Initial reports of the DSDP. Washington DC, 997-1007.
[43] White, J.L. and Roth, C.B. (1986) Infrared spectroscopy. In: Klute, A. (ed.) Methods of Soil Analysis, Part 1: Physical and Mineralogical Methods, 2nd ed. Soil Science Society of America, Madison, WI, USA, 291-330.
[44] Erkan, Y. (1994) Investigation of important Rock-forming minerals on Microscope (in Turkish).
[45] Tinsley, J. (1970) A Manuel of experiments for student of soil science. Department of Soil Science University of Aberdeen, 128p.
[46] FAO/IUSS/ISRIC (2014) World Reference Base (WRB) for Soil Resources. International soil classification system for naming soils and creating legends for soil maps World Soil Resources Report 106. FAO, Rome.
[47] Blakemore, L.C., Searle, P.L. and Daly, B.K. (1987) Methods for Chemical Analysis of Soils. N.Z. Soil Bureau Scientific Report. Vol: 80. N.Z. Soil Bureau, Lower Hutt, New Zeland, 1390p.
[48] Wada, K. (1989) Allophane and imogolite. In: Dixon, B., Weed, S.B. (eds.) Minerals in Soil Environment J. Soil Sci. Soc. of America, Madison, WI, USA, 1051-1087.
[49] Perrot, K.W., Smith, F.L. and Inkson, R.H.E. (1976) The reaction of fluoride with soils and soil minerals. J. Soil Sci. 27, 58–67.
[50] Parfitt, R.L. and Henmi, T. (1982) Comparison of an Oxalate – Extraction Method and a infrared Spectroscopic Method for Determining Allophane in Soil Clays. Soil Sci. Plant Nutr. 28(2), 183-190.
[51] Egawa, T., Sato, A. and Nishimura, T. (1960) Release of OH ions from clay minerals treated with various anions with special reference to the structure and chemistry of allophane. adv. Clay Sci. 2, 252–262.
[52] Alves, M.E. and Lavorenti, A. (2004) Remaining phosphorus and sodium fluoride pH in soils with different clay contents and mineralogies. Pesq. Agropec. Bras. Brasilia. 39(3), 241–246.
[53] Campos, A., Oleschko, K., Cruz, L., Etchevers, J. and Hidalgo, C. (2000) Estimación de alofano ysu relación con otros parámetros químicos en Andisoles de montaña del Volcán Cofre de Perote. Terra. 19, 105–116.
[54] Garcia–Rodeja, E., Novoa, J.C., Pontevedra, X., Martinez-Cortizas, A. and Burman, P. (2004) Aluminium fractionation of European volcanic soils by selective dissolution techniques. Catena. 56, 155-183.
[55] Honorato, R. and Pinochet, D. (1986) Classification of Chilean soils originated from volcanic materials using andic tests proposed by ICOMAND. Cienc. Investig. Agraria. 13(2), 121–133.
[56] Parfitt, R.L. and Kimble, J.M. (1989) Conditions for formation of allophane in soils. Soc. am. J. 53, 971 - 977.
[57] Wada K. (1985) The distinctive properties of Andosol. In: Stewart, B.A. (ed.) Advances in Soil Science. Vol. 2. Springer, New York, 173-229.
[58] Alcalá de Jesús, M., Hidalgo, C. and Gutiérrez, M. (2009) Mineralogía y retención de fosfatos en Andisoles. Terra Latinoamericana. 27, 275–286.
[59] De Browere, K., Thijs, A., Hens, M. and Merckx, R. (2003) Forms and availability of soil phosphorus in temperate forests in southern Chile and Flanders. Gayana Bot. 60(1), 17–23.
[60] Wada, K. (1980) Soils with variable charge. In: Theng B.K.G. (ed.) New Zealand Society of Soil Science. Lower Hutt. 87-107.
[61] Honorato, R., Galindo, G. and Pinochet, D. (1984) Application of some tests of Andic properties to Chilean soils derived from volcanic materials. Cienc. Investig. Agraria. 11(3), 179–190.
[62] Gunjigake, N. and Wada, K. (1981) Effects of phosphorus concentration and pH on phosphate retention by active aluminium and iron of Ando soils. Soil Science. 132, 347–352.
[63] Beckmann, G.G., Thompson, C.H. and Hubble, G.D. (1974) Genesis of red and black soils on basalt on the Darling Downs, Queensland, Australia. Journal of Soil Science. 25(3), 265-281.
[64] Matus, F., Garrido, E., Sepulveda, N., Carcamo, I., Panichini, M. Hubble. Zagal, E. (2008) Relationship Between Extractable Al and Organic C in Volcanic Soils of Chile. Geoderma. 148, 180-188.
[65] Schwertmann, U. (1964) Differenzierung der Eisenoxide des Bodens durch Extraktion mit Ammoniumoxalat Loesung.Z. Pflanzenernaehrung Duengung Bodenk. 105, 194–202.
[66] Schwertmann, U. (1973) Use of oxalate for Fe extraction from soils. Canadian Journal of Soil Science. 53(2), 244–246.
[67] Dahlgren, R., Shoji, S. Hubble. Nanzyo, M. (1993) Mineralogical Characteristic of Volcanic Ash Soils. In: Shoji, S., Nanzyo, M., Dahlgren, R. (eds.) Volcanic Ash Soils. Developments in Soil Science. Elsvier, Amsterdam. 101-143.
[68] Moustakas, N.K. Hubble. Georgoulias, F. (2005) Soils developed on volcanic materials in the Island of Thera, Greece. Geoderma. 129, 125-138.

[69] Algoe, C., Stoops, G., Vandenberghe, R.E., Van Ranst, E. (2012) Selective dissolution of Fe–Ti oxides—extractable iron as a criterion for andic properties revisited. Catena. 92, 49–54.
[70] Fieldes, M. and Claridge, G.G.C. (1975) Allophane. In soil components. Vol.2 Inorganic components. Berlin: Springer –Verlag, 351-393.
[71] Wada, K. (1987) Minerals Formed and Mineral Formation from Volcanic Ash by Weathering. Chemical Geology. 60, 17-28.
[72] Bigham, J.M., Fitzpatrick, R.W. and Schulze, D.G. (2002) Iron Oxides. In: Dixon, J.B., Schulze, D.G. (eds.) Soil Mineralogy with Environmental Applications. SSSA Book Ser. No. vol. 7. Soil Sci. Soc. Am., Madison, WI, 323-366.
[73] Tan, K.H. (1993) Principles of soil chemistry. New York and Basel: Marcel Dekker Inc.

Received: **09.05.2017**
Accepted: **18.11.2017**

CORRESPONDING AUTHOR

Hasan Huseyin Ozaytekin
Selcuk University,
Agriculture Faculty,
Department of Soil Science and Plant Nutrition, 42079 Konya – Turkey

e-mail: hhuseyin@selcuk.edu.tr

© by PSP Volume 27 – No. 2/2018 pages 898-909 Fresenius Environmental Bulletin

ANALYSIS OF THE WIND POWER TARIFF POLICY IN CHINA: EVOLUTION, PROBLEMS, AND COUNTERMEASURES

Shi-Chun Xu[1], Zheng-Xia He[2,*], Chang Gao[1], Yong-Mei Miao[1]

[1]Management School, China University of Mining and Technology, Xuzhou 221116, China
[2]College of Economics and Management, Nanjing Forestry University, Nanjing 210037, China

ABSTRACT

China is now at the forefront of the development of wind power throughout the world. By the end of 2016, the cumulative installed capacity and newly installed capacity for wind power in China accounted for 34.7 % and 42.7 % of the global total. However, by 2015, wind curtailment intensified with an average rate of 15 %, where the gap in funding for renewable energy subsidies hit a new record high at a total of about 30 billion RMB yuan, which is still increasing compared with previous years. Thus, the Chinese government has proposed to strengthen overall planning by actively promoting a series of market-oriented reforms and innovation of institutions and policy to solve the wind power consumption problem and subsidies gap problem. In particular, the wind power tariff policy reform is one of the most effective methods. This study focuses on the evolution, implementation status and problems of the wind power tariff policy in China. A series of countermeasures and recommendations are proposed, which will be important for achieving the wind power development target during the 13th five-year plan period.

KEYWORDS:
Wind power, Tariff policy, Evolution, Problems, Countermeasures

INTRODUCTION

In recent years, due to the impact of oil prices and global climate change, the development and utilization of renewable energy have attracted the attention of nternational community. Thus, many countries have proposed clear development goals, as well as formulating regulations and policies to support the development of renewable energy. The Chinese government has realized that the exploitation and utilization of renewable energy is an important way of solving the problems of environmental pollution and energy shortages [1, 2]. During the 11th five-year plan (FYP) period (2006–2010), China's wind power industry experienced a rapid growth period in scale and manufacturing ability, while during the 12th FYP period (2011–2015), China's wind power industry increased in quality and a competitive industrial system was established. However, the 13th FYP period (2016–2020) will be the most important period for the wind power industry system and tariff reform because various contradictions affect the development of the wind power industry and tariffs. The objective of this study is to review the evolution of China's wind power tariff policy, to analyze the existing problems, and propose suitable countermeasures.

EVOLUTION OF THE WIND POWER TARIFF POLICY

The main issue that will affect the development of wind power is the formulation of wind power tariffs. This section reviews the evolution of the feed-in tariff policy, the tariff surcharge subsidy policy, and the grid connection expenses policy.

Feed-in tariff policy for wind power. (1) The first stage was the cost pricing stage (1990–1998). During this stage, the profit margins were not considered when determining wind power tariffs and only the maintenance cost of wind farms was considered. For example, the tariff for the Dabancheng wind farm, which was built in the early 1990s, was less than 0.3 CNY/KWh. In the initial stage of exploration, China's wind power tariff policy was mainly based on cost accounting, whereas specific reference standards were not defined for the cost, loan interest, profit rate, etc. In addition, there was no consideration of regional resources and economic differences, so it was difficult to achieve a fair and reasonable wind power tariff policy. The cost pricing policy did not fundamentally remove the obstacles that hinder the development of renewable energy. These deficiencies led to a failure to implement China's wind power strategic planning during this period and ultimately the cost pricing policy was phased out [3].

(2) The second stage was the regional approved stage (1998–2003). From 1998 to 2003, the

tariffs for wind power were no longer determined by the central government, but instead they were set by the local price authorities and reported to the central government for recording, so this stage was called the regional approved stage. Based on cost pricing, the regional approved tariffs considered the regional differences in wind resources and economic conditions.

(3) The third stage was the coexistence of bidding and approved stage (2003–2006). The change to this stage from the previous stage was marked by the introduction of first concession bidding in 2003. In this stage, two types of pricing methods emerged for wind power. The tariffs for large-scale wind power projects organized by central government were determined by public bidding, whereas the tariffs for wind power projects within the scope of provincial and regional approval were still determined by local government.

(4) The fourth stage was the bidding plus approved stage (2006–2009). In this stage, the tariffs for renewable energy comprised government pricing or the government guidance price. The point that marked the change to this stage from the previous stage was the issuance of "Interim Measures on Renewable Energy Electricity Prices and Cost Sharing Management" that was released by the National Development and Reform Commission (NDRC) in 2006 [4].

(5) The fifth stage is the fixed benchmark stage (from 2009 to the present). The 7th Document issued in 2006 established pricing and cost sharing mechanisms for renewable energy power generation in China, and it vigorously promoted the development of the renewable energy power generation industry. However, the policy has been unable to meet actual needs during the rapid development of China's wind power industry. The fixed benchmark tariff policy is conducive to changing the current non-unified situation of the wind power pricing mechanism. Due to improvements in wind power technology and cost reductions, the NDRC has reduced the fixed feed-in tariff twice.

Tariff surcharge subsidies. The evolution of renewable energy tariff surcharge policy is as follows: in January 2006, the 7th Document made provisions: renewable energy tariff surcharge is approved by the price authorities of the State Council, and levied according to the actual quantity of electricity used by electricity users, and the whole country will carry out the uniform standards; the tariff subsidies actually paid by the provincial power grid companies, the grid connection expenses of renewable energy power generation projects together with the difference of renewable energy tariff surcharge shared among various provincial power grid enterprises should be in unified deployment throughout the country [4]. In January 2007, "the Interim Measures for Revenue Allocation of Renewable Energy Tariff Surcharge" clearly defined the quota trading mode: the provincial power grid enterprises include the levied renewable energy tariff surcharge revenue in the income of the enterprise, and the revenue should be firstly used for paying renewable energy tariff subsidy for their respective province (autonomous regions and municipalities directly under the central authority), the difference of which will be balanced across the country by quota trading [5]. "The Interim Measures on Collection and Utilization Management for Renewable Energy Development Funds" implemented in January 2012 included the renewable energy tariff surcharge revenue in renewable energy development fund management. The renewable energy tariff surcharge should be levied by the Ministry of Finance on a monthly basis to power grid enterprises, the full amount of which should be turned over to the central treasury [6]. In March 2012, "The Interim Measures for Renewable Energy Tariff Surcharge Subsidies Funds Management" clearly determined: the projects which apply for renewable energy tariff surcharge subsidies must be confirmed by the NEA for approval; the subsidized funds should be allocated in advance quarterly, and liquidated at the end of the year in principle [7].

TABLE 1
The adjustment of levying standard of renewable energy tariff surcharge from 2006 to 2016

The Time of Issuance	Policy document	Levying standard (CNY / KWh)	The Time of Implementation
June 28th, 2006	NDRC Price [2006] 1228 [28], NDRC Price [2006] 1229 [29]	0.001	June 30th, 2006
June 29th, 2008	NDRC Price [2008] 1677[30], NDRC Price [2008]1678[31], NDRC Price [2008]1682 [32]	0.002 **(the levying standard of electricity used by residents and fertilizer production remains unchanged)**	July 1st, 2008
November 18th, 2009	NDRC Price [2009]2919 [33], NDRC Price [2009]2920 [34]	0.004	November 20th, 2009
November 29th, 2011	NDRC Price [2011]2619[35], NDRC Price [2011]2620[36]	0.008	December 1st, 2011
August 27th, 2013	NDRC Price [2013]1651 [24]	0.015	September 25th, 2013
January 5th, 2016	Finance and Tax [2016]4 [25]	0.019	January 1st, 2016

In general, as shown in Table.1, the levying standard of renewable energy tariff surcharge subsidies start from 0.001 CNY / KWh in 2006. With the rapid development of renewable energy, the renewable energy tariff surcharge funds were unable to make ends meet, the gap of which continues to increase, up to present (from January 1st, 2016), the levying standard of renewable energy tariff surcharge has risen to 0.019 CNY / KWh.

Grid connection expenses. According to the 7th Document and "the Interim Measures for Revenue Allocation of Renewable Energy Tariff Surcharge" released by the NDRC in 2006 and 2007 respectively, the grid connection expenses of renewable energy refers to transmission investment and operation and maintenance costs for renewable energy power generation projects to be connected to the power grid, which will be shared through levying tariff surcharge on electricity users and in nationwide unified deployment [8]. Depends on transmission distances and the subsidies for grid connection expenses will be collected at 0.01RMB/kWh for within 50km, 0.02RMB/kWh for 50–100km, and 0.03RMB/ kWh for 100 km or longer distances [5]. "The Interim Measures on Collection and Utilization Management for Renewable Energy Development Funds" implemented in January, 2012 included renewable energy tariff surcharge in renewable energy development funds management and stipulated that the part of reasonable grid connection expenses and other reasonable relevant expenses paid by power grid companies can be funded through renewable energy tariff surcharge revenue if they cannot been recovered from the sales price of the electricity [9]. In March, 2012, the Ministry of Finance, the NDRC, and the NEA jointly issued "the Interim Measures for Renewable Energy Tariff Surcharge Subsidies Funds Management", which stipulated: the engineering investment and operation and maintenance costs for renewable energy power generation projects to be connected to the power grid can be compensated from renewable energy development fund according to the on-grid electricity, and the subsidy standard is as follows: 0.01RMB/kWh for within 50km, 0.02RMB/kWh for 50–100km, and 0.03RMB/ kWh for 100 km or longer distances [7].

PROBLEMS WITH THE WIND POWER TARIFF POLICY

Frequent reductions to the feed-in tariff weakened the investment incentives for wind power producers. As the most important policy for supporting the wind power industry, the continuity and stability of the tariff policy is related directly to the investment decisions made by enterprises, so the most difficult situation faced by investors is a lack of expectations and frequent changes in the tariff policy [8]. According to the China Wind Energy Association, the reduction in the feed-in tariff might make wind power investment unprofitable in some zones, while some zones such as Shanxi and Anhui may progress to a new wind power development scenario. The reduction in the feed-in tariff will inevitably have negative effects on the internal rate of return (IRR) and net rate of return (NRR) for the main wind power generating groups. According to annual report data provided by these groups, the average annual operating time for wind power in China is 1903 hours, the average tariff is 0.568 CNY/kWh including tax, and the average life cycle of onshore wind farms is 20 years, so the following estimates can be made for a scenario where capital accounts for 20 %, bank loans account for 80 %, the loan period is 15 years, and the loan interest rate is 7.2 %. Prior to the tariff adjustment, the IRR for wind power investment by each power group was 10.77 % and the NRR was 7.43 %, which are slightly higher than the interest rates on bank loans [10]. On December 22, 2015, the NDRC issued "The Notice on Improving the Benchmark Feed-in Tariff Policy of Onshore Wind Power and Solar Photovoltaic Power" and they decided to implement a tariff policy where the benchmark feed-in tariff for onshore wind power decreases gradually with the scale of development. Thus, in 2016, the tariff for the first three resource zone categories was reduced by 0.02 CNY/KWh. In 2018, the tariff for the first three resource zone categories will be reduced by 0.03 CNY/KWh compared with 2016, and the tariff for category IV will be reduced by 0.02 CNY/KWh relative to 2016, as shown in Table 2. And shown in Fig.1, from 2009 to 2018, the feed-in tariff for the category I zone will be reduced from 0.51 CNY/KWh in 2009 to 0.44 CNY/KWh in 2018, the feed-in tariff for the category II zone will be reduced from 0.54 CNY/KWh in 2009 to 0.47 CNY/KWh in 2018, the feed-in tariff for the category III zone will be reduced from 0.58 CNY/KWh in 2009 to 0.51 CNY/KWh in 2018, and the feed-in tariff for the category IV zone will be reduced from 0.61 CNY/KWh in 2009 to 0.58 CNY/KWh in 2018.

According to the "Statistical Evaluation Report of Chinese Wind Power Construction in 2014" released by the NEA, the national average construction cost per KW of wind farms in 2014 was 8618.87 CNY, and the average construction costs per KW for wind farms from Category I–IV zones were 8100 CNY, 8300 CNY, 8600 CNY, and 9200 CNY respectively. Without considering the cost reduction due to technological progress and other factors, and under the given conditions, for a wind farm with an installed capacity of 50 MW, loan period of 15 years, and long-term interest rate of 4.9 %, the financial IRR and capital IRR for wind farms belonging to the four zone categories under

different feed-in tariff scenario were calculated, which is shown in Table.3. Table.3 indicates that the financial IRR and capital IRR for wind farms in the first three zone categories decrease significantly after the reduction of feed-in tariffs, where the capital IRR for the category II and category III zones even become negative under the tariff in 2018. By contrast, due to the smaller decline in the tariff, the negative effects on the financial IRR and capital IRR are lower for wind farms in category IV zone.

TABLE 2
The benchmark feed-in tariff for onshore wind power in 2016 and in 2018

Resource Zone	Benchmark feed-in tariff (CNY/KWh) 2016	2018	Administrative areas included
Category I	0.47	0.44	**Inner mongolia autonomous region except:** Chifeng, Tongliao, Xing'anmeng, Hulunbeier; **xinjiang uygur autonomous region:** Urumqi, Yili, Changji, Karamay, Shihezi
Category II	0.50	0.47	**Hebei province:** Zhangjiakou, Chengde; **Inner Mongolia Autonomous Region:** Chifeng, Tongliao, Xing'anmeng, Hulunbeier; **Gansu province:** Zhangye, Jiayuguan, Jiuquan
Category III	0.54	0.51	**Jilin province:** Baicheng, Songyuan; **Heilongjiang province:** Jixi, Shuangyashan, Qitaihe, Suihua, Yichun, Daxinganling region, **Gansu province except:** Zhangye, Jiayuguan, Jiuquan, **Xinjiang autonomous region except:** Urumqi, Yili, Changji, Karamay, Shihezi, **Ningxia Hui autonomous region**
Category IV	0.60	0.58	Other parts of China not mentioned above

Source: Notice on Improving the Benchmark Feed-in Tariff Policy of Onshore Wind Power and Solar Photovoltaic Power" (NDRC Price [2015]3044). http://www.sdpc.gov.cn/gzdt/201512/t20151224_768582.html

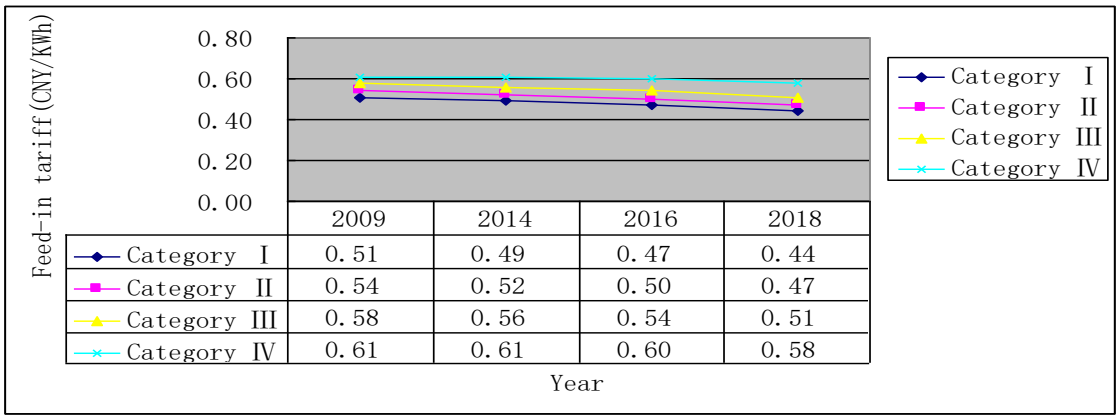

FIGURE 1
Adjusted feed-in tariffs for Chinese onshore wind power from 2009 to 2018

TABLE 3
Financial IRR and capital IRR of the wind farm of 50 MW under different feed-in tariffs

Resource Zone	Current Tariff (CNY /KWh)	Financial IRR	Capital IRR	Tariff in 2016 (CNY /KWh)	Financial IRR	Capital IRR	Tariff in 2018 (CNY /KWh)	Financial IRR	Capital IRR
Category I	**0.49**	5.32%	6.74%	**0.47**	4.59%	4.74%	**0.44**	3.41%	1.78%
Category II	**0.52**	3.89%	2.95%	**0.50**	3.29%	1.47%	**0.47**	2.26%	-0.89%
Category III	**0.56**	4.09%	3.47%	**0.54**	3.45%	1.87%	**0.51**	2.60%	-0.11%
Category IV	**0.61**	6.07%	8.92%	**0.60**	5.79%	8.08%	**0.58**	5.27%	6.59%

Source: What is the impact of the decrease in feed-in tariff of wind power and solar photovoltaic? http://www.nandudu.com/article/17718[11]

The fixed feed-in tariff mechanism causes various problems and risks related to wind power grid connection. (1) Lack of a risk sharing mechanism. On December 29, 2015, the "Management Measures for Full Protection of Acquisition of Renewable Energy Power Generation (Draft for Comments)" issued by the NEA identified that the grid enterprises should sign contracts for priority power generation with enterprises that have completed renewable energy on-grid power generation projects by the end of the previous year. Power grid enterprises should give priority to the implementation of the renewable energy power generation plan and electricity trading contracts to secure wind energy, solar energy, biomass energy, and other renewable energy sources as the highest priority for power generation, but they are not allowed to obtain the priority rights for power generation by making payments to power generation projects with the lower priority. However, the full protection of acquisition did not formulate detailed measures to compensate for the risk and additional costs borne by the grid companies when solving various technical problems related to the operational control of power grids caused by wind power grid connections, such as peak regulation, frequency modulation, and voltage regulation. Under the current benchmark fixed feed-in tariff policy and the management measures implemented to provide full protection to the acquisition of wind power, the risks caused by fluctuations in wind power were borne completely by the grid companies. Thus, due to the lack of an effective risk sharing mechanism, the enthusiasm of power grid enterprises cannot be fundamentally mobilized.

(2) Lack of policy incentives for providing supplementary services. Under the current benchmark fixed feed-in tariff policy, the risks and costs of providing peak load regulation services borne by the conventional hydropower and thermal power units cannot receive compensation. Due to the intermittency, randomness, and volatility of wind power, it is necessary for other hydropower, thermal power, and conventional energy sources with considerable scale to participate in peak load regulation for the power system to secure its safe and stable operation. Therefore, connecting wind power to the grid will inevitably increase the burden in terms of providing supplementary services such as peak load regulation via other conventional energy units as well as increasing energy consumption and the cost of power generation. However, there has been no appraisal or economic compensation policies for all of the supplementary services provided by hydropower and thermal power units, which is unfair and it could decrease the enthusiasm of conventional energy units to participate in peak load regulation with wind power grid connections [12].

It is difficult to reflect the environmental value of renewable energy. Fixed pricing methods based on cost mark-up are currently applied to fix the price of renewable energy power generation. These methods aim to maintain a reasonable rate of return on investment for the renewable energy development projects, thereby reducing the risk of investment and stimulating the scale of investment. This has the advantage that the price level is only related to the level of technology, the scale of the application, and the expected profit margin from renewable energy, which can be estimated easily. However, at the same time, it also has many disadvantages, where most importantly, the electricity price for renewable energy has no direct contacts with price changes and the environmental costs of traditional fossil energy under this method, so it is difficult to reflect the total value of reduced greenhouse gas emissions, environmental value, and social preferences due to renewable energy power generation. Therefore, this pricing method cannot accurately and completely solve the problem of negative externalities caused by fossil energy consumption [13]. In addition, the current renewable energy tariff policy in China mainly employs a fixed pricing method, which has certain advantages in terms of convenience for tariff management and the stability of investment returns, but this type of pricing method does not consider the market price and it may have negative effects on the development of renewable energy.

The imperfect tariff transmission mechanism and the deep-seated contradictions of the power market mechanism are the root causes of wind power curtailment problems. Since 2010, China has surpassed the USA for six consecutive years and become the world's largest wind power market. The installed wind power capacity in China is ranked first in the world, but the generating capacity share of wind power among the national power generating structure is still relatively low. The wind power generating capacity in China increased by 16.6 % in 2015, but it only accounts for 3.3 % of the national generating capacity, whereas over the same period, the thermal power generating capacity still accounted for 74.94 % of the national generating capacity, thereby demonstrating that China lags far behind European countries in terms of wind power consumption. Due to the advance of the 13th FYP of China, the target for wind power development is expected to be raised further. However, the "abandonment of wind power" has become the main bottleneck that hinders the healthy development of China's wind power industry.

The large-scale abandonment of wind power began to appear frequently in the northeast and northwest regions of China, where the abandoned wind power in Gansu, Inner Mongolia, Jilin, and Heilongjiang reached 5.304 TWh, thereby account-

ing for 50 % of the total nationwide. The issue became most serious in 2012, when the abandoned wind power reached 20.8 TWh and the curtailment rate reached 17.12 %, as the peak calendar year. In addition, the issue became even more serious in the "Three Norths" Region of China, which has rich wind resources, where the issue was most prominent in the east of Inner Mongolia and Jilin because the wind power utilization hours comprised less than 1500 hours and the curtailment rate was more than 50 % in the winter. The wind power curtailment situations are shown in Fig.2.

The issue of "abandonment of wind power" indicates that the current electric power development and operation model in China cannot adapt to the development of wind power, as well as reflecting the deep-seated contradictions of the power operation mechanism and market mechanism in China, which are affected by the following two main issues. First, the market mechanism for renewable energy power consumption has not yet been fully implemented. The developmental scale of hydropower, wind power, and solar energy power will continue to grow in the southwest and the "Three Norths" regions of China in the future, but the market space for consumption has gradually become the biggest bottleneck that hinders renewable energy consumption. Thus, the current electric power operation system characterized by "power generation planning" and a "fixed price" cannot adapt to the development of renewable energy. In addition, the current electric power operation in China is managed by the provinces as entities, but cross-provincial and regional power transmission was not included in the long-term regional power transmission plan developed in the national energy strategy, which indicates that there is a lack of enthusiasm for the consumption of renewable energy in the regions of China [14]. Second, the marketization of the power market is low and the system for regulation and legal construction is weak. Electric power system reform has not yet been completed in China, so a large number of power plants do not assume responsibility for power peak regulation, thereby leading to an imperfect mechanism for Electric Peak shaving and other auxiliary services. Although the "Renewable Energy Law" stipulates that priority should be given to the scheduling and full acquisition of renewable energy power generation, the energy-saving generation dispatch of renewable energy is still restricted by the original power operation mechanism and rigid pricing mechanism, which makes it difficult to fully implement administrative regulations such as renewable energy priority scheduling [15].

Lack of sufficient support for technical progress. The wind power industry in China has just started and it lacks core technology, where R & D is far behind that in other advanced countries and the industrial chain is yet to be cultivated. In the field of whole machine equipment for wind power production with high technology contents, Chinese enterprises basically lack their own core technology and their wind power equipment is mainly derived from assembled production. The core components for wind power equipment such as spindle bearings and electrical control systems are still in their initial stages. By contrast, the installed wind power capacity in China has been growing very rapidly in recent years although the core technology is very weak [16].

The most important reasons why the Chinese wind power industry has failed to grasp core technology are as follows. First, the R & D inputs into wind power industry have been insufficient for a long time, where wind power technology is considered an emerging high-technology field with high risks and wind power companies have not become the main centers for technology R & D due to the relatively low enthusiasm for investment. Second, compared with developed countries in Europe and the USA, there has been very limited support from the Chinese government for wind power technology R & D. In order to support key R & D in technology for wind power equipment and to accelerate the development of the industry, China's Ministry of Finance has implemented "Substitute Subsidies with Rewards" to support the industrialization of wind power equipment. In 2008, the Ministry of Finance promulgated the "Interim Measures for the Administration of Special Funds for the Industrialization of Wind Power Equipment" and this is the first time that the Chinese government has provided cash subsidies to wind turbine manufacturers. It is stipulated that the first 50 sets of MW class wind turbine units with a unit capacity more than 1.5 MW will be granted subsidies according to the standard of 600 CNY/KW, where whole machine manufacturing enterprises and key component manufacturing enterprises account for 50 % respectively. This subsidy policy has played a significant role in guiding and encouraging the localization of wind power equipment technology, but only a small number of enterprises meet the criteria for this award and the application restrictions are demanding, so the support for technological progress in wind power industry is still low [17].

From the perspective of the wind power tariff policy, the current tariff subsidies policy is aimed at providing wind power manufacturing enterprises with some investment support, where the aim is to financially support increased mass production, but there is obviously insufficient support for technological improvement. The purpose of financial support is to promote the overall effectiveness of wind power consumption, but the high volume of subsidies has only helped China to increase mass production, with little technological improvement.

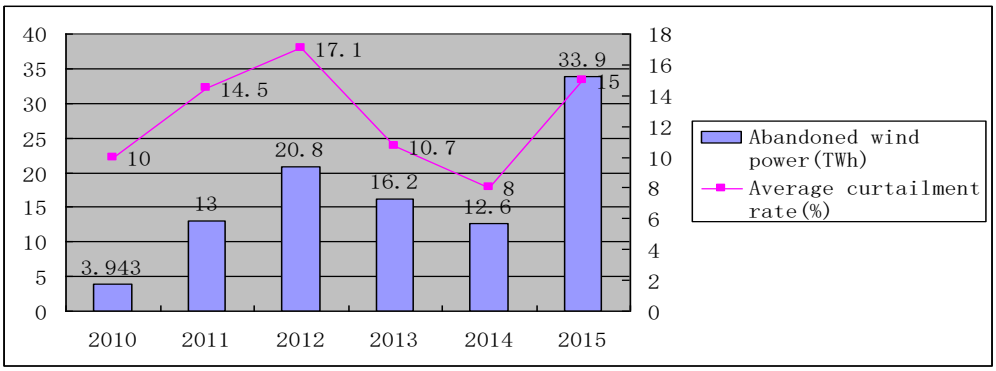

FIGURE 2
Wind power curtailment situation in China from 2010 to 2015

Without policy incentives, little investment is flowing into technological innovations [18].

The tariff subsidy policy for grid connection projects is not reasonable. First, the subsidy standard for wind power grid connection project is rather low. According to "The Interim Measures for Renewable Energy Tariff Surcharge Subsidies Funds Management" released in March 2012, the project investment, operation, and maintenance costs incurred by grid connection for renewable energy power generation projects can receive compensation from the renewable energy development fund according to on-grid electricity, where the detailed subsidy standards are as follows: 0.01 CNY/kWh for within 50 km, 0.02 CNY/kWh for 50–100 km, and 0.03CNY/ kWh for 100 km or longer distances. Overall, the current subsidy standard of 0.01–0.03 CNY/kWh for the grid connection of renewable energy power generation projects is low, which makes it difficult to meet the debt service needs of grid connection projects and this will have negative effects on the enthusiasm for investment among power grid enterprises.

Second, the tariff subsidy policy for grid connection projects is not reasonable. The current policy only considers the construction and operation costs for grid connection projects related to the local consumption of the renewable energy generating capacity, whereas it fails to address the long-distance transmission of electric energy, grid expansion at the sending and receiving ends, and other factors involved with a large-scale renewable energy power generation base. The large scale renewable energy power generation base is distributed mainly in the "Three Norths" regions as well as other remote and underdeveloped regions, where compensation is received by increasing the local sales price of electricity if the construction and operation costs of grid supporting projects exceed that of grid connection projects for conventional energy sources. However, this method significantly increases the burden on local users and restricts the development of the local economy. Furthermore, if the compensation is provided by increasing renewable energy electricity prices, this would greatly reduce the competitiveness of renewable energy consumption. Both of these methods will affect the enthusiasm for renewable energy development and consumption, which is not conducive to the healthy and rapid development of renewable energy sources [19].

The tariff surcharge subsidy of renewable energy cannot be fully in place in time with the gap growing constantly. First, the tariff surcharge involves many departments, and the application and circulation processes are time-consuming. The Ministry of Finance, NDRC, and NEA are currently the co-heads for the application and approval of subsidy projects and subsidy funds for renewable energy tariff surcharges, but the focus of approval differs for each department according to their particular perspectives, which make the process time-consuming.

Second, the allocation of funds is not performed in a timely manner and there is a heavy financial burden on power generation enterprises. The application for the approval of subsidy funds involves a number of departments and the renewable energy tariff surcharge collected nationwide each year does not completely match with the funds needed by the subsidy projects, so the allocation of subsidy funds has lagged behind since 2012. Before receiving their financial allocation, the power grid enterprises cannot advance the huge subsidies funds and transferred them to renewable energy power generation enterprises on a quarterly basis, which restricts their cash flow and they constantly need to raise funds through bank loans as well as other ways to maintain their normal operation.

Third, the current collection standard for the renewable energy tariff surcharge is rather low, which will make it difficult to meet the needs of renewable energy development in the future. Thus, China has already met the installed capacity target proposed in the 12th FYP for Wind Power. However, the "13th Five-Year Development Plan of Renewable Energy (Drafts for Comments)" issued by

the NEA, proposed that the proportion of non-fossil energy among the total energy consumption should reach 15 % by 2020 and 20 % by 2030, and that new investment during the 13th FYP period should reach about 2.3 trillion yuan. In particular, by the end of 2020, the development and utilization goals are 380 GW for hydropower, 160 GW for solar power (solar photovoltaic accounts for 150 GW), and 250 GW for wind power [20]. The growth rate of renewable energy will be far greater than that of electricity, which forms the basis for collecting the tariff surcharge, so the subsidies gap becomes increasingly obvious.

COUNTERMEASURES TO TACKLE THE WIND POWER TARIFF POLICY

Establishing a flexible adjustment mechanism for the feed-in tariff for renewable energy to support the stable expectations of investors. Frequent changes or the lack of stable expectations regarding the renewable energy feed-in tariff will weaken the incentives for wind power investors. However, due to changes in the electric power market and technological innovation, it will be necessary to revise and adjust the fixed feed-in tariff policy in China in order to pass on the benefits of technological innovation to consumers, achieve grid connections for renewable energy at parity price, and ultimately realize market-oriented tariff reform. Thus, considering the incentive factors for investors, much attention should be paid to the establishment of a flexible adjustment mechanism for the feed-in tariff policy when adjusting the fixed feed-in tariff, thereby supporting the stable expectations of investors.

The establishment of a declining price mechanism for the fixed feed-in tariff with stable expectations can encourage technical progress and falling costs for renewable energy power projects, as well as preventing enterprises with cost advantages from gaining long-term windfall profits, thereby ultimately improving the dynamic efficiency of the feed-in tariff mechanism in an effective manner. In particular, the establishment of a flexible adjustment mechanism should clearly adjust the tariff regularly based on time or the generating capacity, or make corresponding adjustments to the tariff with technological progress. Some EU countries have established a periodic evaluation and reduction mechanism for the feed-in tariff. Therefore, based on the experiences of Germany and other European countries, China can establish a declining price mechanism for the fixed feed-in tariff on a time-dependent basis, i.e., by linking with the newly or cumulative installed capacity, the price decline rate can be adjusted according to the actual situation for renewable energy development either quarterly or yearly, thereby supporting the stable expectations of investors and minimizing the negative impact of a fixed feed-in tariff reduction on renewable energy investment.

Countermeasures for tackling the issue of wind power grid connection caused by a fixed feed-in tariff. (1) Establishing a reasonable risk sharing mechanism. Given the specific situation in China, the following measures may be implemented. First, the dispatch department should deal with the power fluctuation components that are outside the specified range (e.g., 25 %). Second, the wind farm should balance the power fluctuation components. Third, assuming a hybrid energy storage system mechanism for stabilizing the output power fluctuations of wind farms and their effects on the feed-in tariff, China should also consider the introduction of a regulatory method for the wind power feed-in tariff based on a revised benchmark tariff and a power fluctuation coefficient. The implementation of this feed-in tariff mechanism based on a power fluctuation coefficient could drive wind farms to improve the stability of their output power using energy storage technology, thereby obtaining a higher power fluctuation coefficient and more tariff subsidies.

(2) Establishing an auxiliary service compensation mechanism to promote the development of renewable energy. In order to ensure the smooth acquisition of renewable energy, an auxiliary service compensation mechanism that promotes renewable energy development must be established to make the relevant bodies provide compensation for auxiliary services. The solutions can be divided into two steps as follows. In the short term, according to other conventional energy practices, an auxiliary service compensation mechanism must be set up to provide hydropower and thermal power units that participate in peak shaving with appropriate compensation. In the long term, the auxiliary service market should be established gradually by combining it with the construction and development of the electric power market to motivate the power plants to regulate their ability to actively participate in the system balance, thereby increasing the enthusiasm of power plants, as well as promoting the formation of an auxiliary service market with good liquidity, reducing costs for providing peak load regulation services, and ensuring the maximization of social benefits.

A comprehensive pricing mechanism should be established to reflect the costs, market supply and demand, environmental value, as well as government tax incentives and subsidies. From the perspective of power generation, the cost-oriented pricing method can be applied to wind power, i.e., the feed-in tariff = power generation cost + tax + after tax profits. Obviously, the produc-

tion costs of wind power enterprises can be compensated for by using this method, but there is a lack of incentive and restraint mechanisms to promote enterprises to reduce costs. A competition-oriented pricing method can also be applied to wind power. Bidding pricing will help reduce the cost and tariff for wind power, but it may lead to excessive competition, which is not conducive to the sustainable development of the wind power industry. From the perspective of the demand side, a demand-oriented pricing method can be adopted, i.e., the wind power tariff can be formulated according to the electricity users' demand and affordability [21]. Given the regional nature of wind power production, the indirectness of wind power consumption, and the environmental benefits of wind power, it is recommended that a comprehensive pricing mechanism should be established for wind power based on an overall consideration of various factors, such as the power generation side, demand side, power grid, government, cost of wind power, market supply and demand, the interests of the power grid, and the tax incentives and subsidies provided by the government [22].

Market-oriented reform of the wind power tariff policy is required. The experiences of other countries in the advanced development of wind power demonstrate that market-oriented institutional reform is an inevitable requirement, and the core of the reform is to establish an open, competitive, and orderly modern power market system. Therefore, the vigorous development of wind power in China should adhere to market-oriented electricity reform; in particular, measures should be taken to ensure that the market plays a decisive role in the allocation of resources through the wind power tariff policy reform. Based on the experiences of Spain, Germany, and Denmark, China should reform the renewable energy feed-in tariff mechanism in a timely manner, as well as promoting renewable energy sources to participate in on-grid bidding similar to other conventional energy sources, thereby transforming the pure governmental pricing mode (i.e., the fixed feed-in tariff mechanism) into a "Double Track System" where the fixed feed-in tariff mechanism can coexist with a premium feed-in tariff mechanism to combine government support policies with a market competition mechanism. Based on the cost of the project plus a certain rate of return, the government mandates power grid enterprises to acquire the renewable energy generating capacity within the power grid coverage according to a certain tariff level during a specific period of time, which should be implemented within 15 to 20 years. This tariff level does not change with price fluctuations on the power market. Based on the experiences of Germany and other EU countries, China has currently developed and implemented a fixed feed-in tariff mechanism for renewable energy power generation such as wind power and solar photovoltaic power. The transition from the fixed feed-in tariff mechanism to the "Double Track System" and the eventual move toward full marketization of renewable energy electricity prices should be a trend during the development of China's renewable energy tariff reform [23]. In particular, China's electric power market mechanism, especially reform of the tariff formation mechanism, should combine with China's power dispatch reform to obtain a pricing mechanism that is determined by the market supply and demand as well as marginal costs, which would allow the generation of all types of units via competition, and cancelling the planned management system for the generating capacity. The fixed benchmark tariff and the plan for the generating capacity should be replaced by the market price and energy-saving dispatch [23]. There should be strict controls on the approval and construction of wind power projects in regions with severe wind power curtailment issues, as well as adjusting the wind power tariff policy, slowing down the speed of wind power development, and setting aside the consumption capacity for stock projects. It is necessary to reduce the feed-in tariff for incremental projects in regions with severe wind power curtailment issues and to control the scale of the installed capacity. We recommend giving full play to the price adjustment mechanism, reducing the feed-in tariff for newly developed wind power projects in regions with a severe curtailment issue, weakening the profitability of these projects, slowing down the impetus for wind power development enterprises to continue to seize wind resources and expand the installed capacity, as well as slowing down the speed of wind power development in these regions.

Support new technological applications. In order to improve the overall manufacture of wind power technology, China can extract funds from the renewable energy tariff surcharge and special national finance funds to set up specific funds for wind power equipment industrialization, thereby providing subsidies to wind turbine units >2 MW to promote the improvement and localization of wind power technology. Based on the experiences of the fixed feed-in tariff mechanism for renewable energy in EU countries, China can provide additional tariff incentives to power generation projects that first apply new technology. Tariff policy support should be given to wind farms that apply grid-friendly technology and other new types of technology to encourage R&D and the application of innovative wind power technology. It is recommended that the specific rules for the full implementation of subsidies related to energy storage technology and offshore wind power technology R&D, as well as other applications based on renewable energy development funds should be released,

which would improve the effect on promoting technological innovation by levying the renewable energy tariff surcharge.

Increasing the expenses standards for renewable energy power generation grid connection and improving the pricing methods. Different policies can be adopted to recover the investment and operation expenses to support grid engineering projects in the wind power bases. Thus, for relatively small scale wind power bases, the benchmark methods can be adopted and the expenses can be recovered according to the on-grid electricity of wind power. For relatively large scale wind power bases, the long-distance transmission of electricity, grid expansion at the sending and receiving ends, and other factors involved with renewable energy power generation bases should be considered. The tariff subsidy standards for grid supporting projects in the large scale renewable energy power generation bases should be approved separately. It is necessary to clarify that compensation for the difference in the construction and operation expenses for supporting grid projects in renewable energy power generation bases compared with those for conventional energy power generation bases should be shared among the national power grids by levying the renewable energy tariff surcharge [24].

Simplifying the application process, exploring a multiple cost sharing mechanism, and establishing an exit mechanism for the dynamic adjustment of subsidies. To address the problem of the growing renewable energy subsidies gap, the following measures can be implemented. First, simplifying the application process and shortening the funds allocation cycle is necessary. We propose that the application process for subsidized projects and subsidy funds should be further simplified by increasing the announcement frequency, shortening the allocation cycle for subsidized funds, and ensuring that renewable energy tariff surcharge policies actually become an effective method for promoting the development of renewable energy power generation [25]. Second, it is important to explore a diversified cost sharing mechanism to broaden the sources available for renewable energy subsidies. In terms of new energy subsidies, there are three main sources: financial funds, carbon taxes, and tariff surcharges; but at present, the new energy tariff subsidies funds in European countries and the USA come mainly from tariff surcharges paid by electricity consumers. In China, due to the rapid development of the renewable energy industry, there will be great pressure on the original tariff surcharge funds, and a growing "subsidies deficit" may even appear. At present, China has not levied carbon taxes, so there are only two ways to ease the pressure on subsidies funds: increasing the tariff surcharge, and extracting a certain amount of funds from the financial income. From a practical perspective, these two methods are both feasible. Considering the welfare effects and social justice issues related to different sources of funds, formulating a reasonable standard for the tariff surcharge by extracting a certain amount of funds from individual tax sources to support the development of renewable energy industry, such as enterprise income tax and environmental tax, could also be a policy alternative. Third, a dynamic adjustment mechanism for subsidies should be established according to renewable energy development goals determined by the national energy development strategy and the tariff subsidy standards, which must be adjusted according to the speed required for achieving renewable energy development goals. According to price decline stages, renewable energy development should be supported by the tariff subsidies policy during the price decline and price protection stages, and when the accumulated renewable energy technology allows the shift from quantity to quality, tariff subsidies should be abolished and renewable energy will finally enter a phase of free competition with other energy sources.

CONCLUSIONS

In terms of renewable energy development, it is clear that tariff reform and the electric power market-oriented reform of renewable energy will become the focus during the 13th FYP period, where wind power generation is one of the most mature technologies with the largest scale and it is suitable for commercialization. The focus of the 13th FYP is no longer targeting installed capacity and grid connection. Instead, it is concerned with policy adjustment, i.e., policy stability and solving the problem of "abandoned wind power and electricity rationing." Financial support will be provided by exploring a diversified cost sharing mechanism for funding renewable energy subsidies. Abandoned wind power and electricity rationing are the main factors that restrict the development of wind power in China. The market-oriented reform in electric power market, especially ensuring the decisive role of the market in the allocation of resources via the market-oriented reform of wind power tariff policies, the reform of electric power dispatching model, and implementing full protection for the acquisition system for renewable energy power generation will alleviate the problems related to "abandoned wind power" and remove the constraints on wind power development to a great extent.

In this study, we outlined and analyzed the status of China's wind power tariff policies, including the evolution of policy, problems, and countermeasures, which will be of great importance for the

development of wind power. The wind power tariff policy is only one effective measure for ensuring the sustainable and rapid development of wind power, and it will be necessary to consider other supporting policies and reform measures in order to successfully achieve the target of the 13th FYP in terms of wind power in China. Therefore, studies of policy choices that might promote wind power development can be conducted in the following areas in the future. (1) Planning connections between wind power and other conventional power sources, between wind power and power grids, coordinating development planning and tariff subsidies funds, and coordinating the sustained large-scale development and utilization of wind power and the construction of supporting infrastructure. It is necessary to study the scientific planning of the overall layout of energy and electric power in China to ensure the effective implementation and full protection of the acquisition system for renewable energy. (2) Creating an "Energy Internet" to improve efficiency and reduce costs. As technology matures and the capacity for technological improvement becomes limited, the use of Internet-based technology will be important for achieving cost reductions for wind power in the future. In addition, studies should determine how to adopt emerging technologies and tools to improve the reliability and utilization of wind turbines. (3) Development of distributed wind power. Future research should focus on supporting policies for distributed wind power in China, particularly the design of a tariff policy for distributed wind power. It is necessary to consider the consumption capacity of distribution networks, as well as the development and coordination of a reasonable overall development target and the acquisition system for distributed wind power.

In the future, there is vast capacity for developing wind power to meet reduction targets for greenhouse gas emissions and energy transformation. As technology improves and supporting policies are implemented, wind power will enter a stage of sustainable, rapid, and healthy development during the 13th FYP period. Therefore, given the establishment of a clean, low-carbon, safe, and efficient modern energy system, as proposed in the 13th FYP Outline, related power system innovation and market-oriented reform, including the reform of the wind power tariff mechanism, should be actively promoted to generate a favorable policy environment to facilitate the large-scale development and utilization of wind energy, as well as industrial development, which will help China to meet its emissions reduction commitments, together with optimizing and upgrading the energy structure.

ACKNOWLEDGEMENTS

This study was financially supported by the Fundamental Research Funds for the Central Universities (grant No. 2017XKQY100).

REFERENCES

[1] He, J.K., Yu, Z.W. and Zhang, D. (2012) China's strategy for energy development and climate change mitigation. Energy Policy. 51, 7–13.

[2] Huang, C., Su, J., Zha, X.Y. Sui, J., Ru, P., Zhang, H.W. and Wang, X. (2012) Government funded renewable energy innovation in China. Energy Policy. 51, 121–127.

[3] Xu, S.C., Zhang, W.W., Gao, C., Long, R.Y. and Chen H. (2017) Impacts of carbon tariffs on China's economic structure and carbon intensity: Simulation analysis using a dynamic CGE model. Fresen. Environ. Bull. 26, 4742-4756.

[4] gov. cn. Interim Measures on Renewable Energy Electricity Prices and Cost Sharing Management (NDRC Price[2006]7). http://www.gov.cn/ztzl/2006-01/20/content_165910.htm

[5] Newenergy.in-en.com. Interim Measures on Revenue Allocation from Renewable Surcharges"(NDRCprice[2007]44) http:// newenergy.in-en.com/html/newenergy-939715.shtml

[6] Zeng, M., Liu, X.M., Li, N. and Xue, S. (2013) Overall review of renewable energy tariff policy in China: Evolution, implementation, problems and countermeasures. Renewable and Sustainable Energy Reviews. 25, 260-271.

[7] jjs.mof.gov.cn. Notice on issuing interim measures on the management of renewable energy tariff surcharge subsidies. http://jjs.mof.gov.cn/zhengwuxinxi/zhengcefagui/201203/t20120329_638930.html

[8] Liu, M. and Wu, F.L. (2009) Wind power investment decision-making strategy based on real options theory. Automation of Electric Power Systems. 33(21), 19-23. (in Chinese)

[9] zhs.mof.gov.cn. Notice on issuing interim measures on the collection and use of renewable energy development fund. http://zhs.mof.gov.cn/zhengwuxinxi/zhengcefabu/201112/t20111212_614767.html

[10] 21st Century Business Herald. NDRC lowered the feed-in tariffs of wind power and the execution periods remained largely unknown. http://money.163.com/15/0112/04/AFO01C7M00253B0H.html.

[11] www.nandudu.com What is the impact of the decrease in feed-in tariff of wind power and solar photovoltaic? http://www.nandudu.com/article/17718

[12] Zhao, S.S., Zhang, D.X., Yin, Y.H. and Shen, H. (2011) Pricing policy and risk management strategy for wind power considering wind integration. Power System Technology. 35(5), 142-145. (in Chinese)
[13] Cory, K., Couture, T. and Kreycik, C. (2009) Feed-in Tariff Policy: Design, Implementation, and RPS Policy Interactions. Office of Scientific and Technical Information Technical Reports.
[14] Shi, D., and Yang, S. (2015) Research on perfecting renewable energy tariff policy: Review based on tariff subsidy policy and policy implementation effect. Price, Theory and Practice. 6, 24-28. (in Chinese).
[15] Zhao, Y.Q. and Wang, H.F. (2015) The analysis and countermeasures of renewable energy curtailment in China. Energy of China. 37(12), 15-20. (in Chinese).
[16] Bai, X.J. and Li, Y. (2012) The development of Chinese strategies emerging industries and avoiding the low-end locking: Taking wind power equipment manufacturing industry as an example. Forum on Science and Technology in China. 3, 50-55 (in Chinese).
[17] Hu, Z., Wang, J.H., Byrne, J. and Kurdgelashvili, L. (2013) Review of wind power tariff policies in China. Energy Policy. 53, 41-50.
[18] He, J., Zhao, X. and Yang, S. (2011) China's off-shore wind power development and policy recommendations. Yangtze River. 42(1), 1–6 (in Chinese).
[19] Liu, Y.Q. (2015) Analysis of China's renewable energy tariff surcharge policy. Journal of Shanxi Institute of Economic Management. 23(1), 65-68. (in Chinese).
[20] BJX NEWS CENTER. Renewable energy planning in the 13th Five -Year Plan: New investments of 2.3 trillion yuan, and wind power with newly installed capacity of 250 GW. http://news.bjx.com.cn/html/20160129/705742.shtml
[21] Cullen, J.A. (2013) Measuring the environmental benefits of wind-generated electricity. American Economic Journal Economic Policy. 5, 107-133.
[22] Huang, H. (2011) Research on the ways of optimizing the price formation mechanism of wind power in China. Price, Theory and Practice. 3, 25-26 (in Chinese).
[23] Wang, Q.K., Jiang, L.P. and Li, Q.H. (2012) Analysis on feed-in tariff mechanism for generations from renewables in EU and its implications for China. Renewable Energy Resources. 30, 109-113 (in Chinese).
[24] Rowlands, I.H. (2005) Envisaging feed-in tariffs for solar photovoltaic electricity: European lessons for Canada. Renewable and Sustainable Energy Reviews. 9, 51-68.
[25] Bürer, M.J. and Wüstenhagen, R. (2009) Which renewable energy policy is a venture capitalist's best friend? empirical evidence from a survey of international cleantech investors. Energy Policy. 37(12), 4997-5006.

Received: **09.06.2017**
Accepted: **14.12.2017**

CORRESPONDING AUTHOR

Zheng-Xia He
College of Economics and Management
Nanjing Forestry University,
Nanjing 210037 – China

e-mail: hezhengxia79@163.com

© by PSP Volume 27 – No. 2/2018 pages 910-920 Fresenius Environmental Bulletin

HYDRAULIC ASSESSMENT OF FLOW IN STEPPED AND LABYRINTH SPILLWAYS TO DETERMINE ENERGY LOSS USING A PHYSICAL MODEL

Seyed Ali Banishoaib[1,2], Amin Bordbar[2,*], Amirabbas Kamanbedast[2], Alireza Masjedi[2], Mohammad Heidarnejad[2]

[1]Department of Water Science and Engineering, Khuzestan Science and Research Branch, Islamic Azad University, Ahvaz, Iran.
[2]Department of Water Sciences and Engineering, Ahvaz Branch, Islamic Azad University, Ahvaz, Iran.

ABSTRACT

A 'spillway' is a structure used to provide controlled release of flood water from upstream into downstream area of a dam. As an important component of every dam, a spillway should be constructed strongly, reliably, and efficiently to be used at any moment. Labyrinth and stepped spillways are presented as appropriate modifications to those spillways hardly capable of managing maximum potential discharge. Owing to their nonlinear crests for a given width, labyrinth and stepped spillways have a larger discharge rate than linear-crest spillways at an identical height. Compared to other energy dissipaters, the combination of stepped and labyrinth spillways is known as a very strong energy dissipater. In the following part, the combination of these two structures and their dimensional change for increasing water-energy dissipation are addressed. To conduct this laboratory study, an experimental flume with a 90-degree bend in the Islamic Azad University of Ahwaz was used. In total, 90 experiments were conducted on three different labyrinth-shape stepped spillway models with two different lengths, three different widths, and five different discharges. Analysis of results showed a greater energy loss reduction in triangular than rectangular than trapezoidal labyrinth-shape stepped spillways. In addition, energy loss is greater in labyrinth spillways with two cycles than with one cycle. Energy loss increases by increasing the Froude number from 0.05 to 0.1; whereas energy loss decreases with increasing the Froude number from 0.1 to 1.0, which is due to the submergence of steps, a decrease in roughness of steps, and an increase in the intensity of aeration.

KEYWORDS:
Labyrinth Spillway, Stepped Spillway, Energy Dissipation, Physical Model

INTRODUCTION

Each dam is composed of several substructures, including spillways as one of the most important ones. Spillways in large dams are often used for flood discharge. Typically, they should be able to drain the maximum discharge from the dam during the probable maximum flood in a short length of time. Accordingly, it can be said that the hydraulic design of spillways is very important. Spillways and rapids are among important hydraulic structures with a major role in maintaining the stability of dams. Labyrinth spillways are important hydraulic structures for handling water level and flow rate in channels, rivers, and dam reservoirs, and also for flow aeration in main sewer networks (Figure 1). The main assumption for the development of labyrinth spillways has been to increase their discharge capacity by increasing the crest length for a given width.

FIGURE 1
Labyrinth spillway

Labyrinth spillways are characterized by a crest with nonlinear axis in plan. Labyrinth spillways are a combination of walls constructed with triangular, trapezoidal, rectangular, or U-shape geometries in plan-view. These geometric shapes may be repeated alternatively across the flow width with a labyrinth cycle. The upstream of labyrinth spillways has a subcritical flow. Due to the presence of a contraction section in the channel, flow constriction occurs and water surface level drops. On the other hand, water surface level elevates across the upstream channel because of the continuous discharge from side walls of the spillway. Combination of these two hydraulic conditions gradually increases water surface level in the upstream channel almost up to the water surface

level before flowing into upstream channel of the spillway. Spillway body is typically considered in form of a vertical wall. The spillway crest may have sharp-edged, flat, semicircular, or quadrant shape.

Stepped spillways are composed of several steps, which start from around the spillway crest and continue to the downstream heel. Such spillways have been receiving increasing attention due to the significant effect of steps on energy loss. Energy loss in the stepped spillways occurs by water flow striking the steps. Therefore, less energy loss is needed at the end of the spillway and thus a smaller energy dissipater is needed. Larger kinetic energy in downstream should be handled proportionally by constructing larger stilling basin or by using further energy dissipation systems, which subsequently increases the costs associated with the implementation and maintenance, and affects the stability of dams. Given the amount of skin friction, velocity will be lower than above number. Ultimately, the ratio of actual velocity to maximum velocity of the flow depends on the type of flow channel. This velocity reduction partially results in energy dissipation. Therefore, the need for such energy dissipating structures as stilling basins at the downstream toe is eliminated or their size can be decreased by dissipating the overflow energy uniformly and continuously through increasing roughness. One way to increase roughness is to construct stepped spillway, which is a spillway with steps on its chute (Figure 2). Such spillways have been receiving increasing attention due to their significant effect on energy loss by causing greater energy dissipation as compared to broad-crested (flat) spillways. Steps increase roughness and subsequently are effective in increasing energy dissipation. They also eliminate the need for energy dissipaters at the downstream or significantly reduce their dimensional requirements.

FIGURE 2
Stepped spillway

Previous studies on hydraulic models of stepped spillways showed that energy loss increases up to 84% at their toes. Moreover, energy loss in such spillways is approximately by 75% greater than in non-ogee stepped spillways. Horner [25] was the first one who scientifically studied stepped spillway. The most significant studies on such spillways were conducted by Chanson [17], who introduced an equation to determine energy loss in stepped spillways with horizontal steps in a nappe flow regime. Chamani and Rajaratnam [16, 15] investigated nappe flow and developed an equation to estimate energy loss on horizontal steps based on the number of steps. Chinnarasri and Wongwises [22] developed an equation to determine energy loss in stepped spillways with reverse inclined steps and/or end sill. The important problem in this regard is increasing the effect of steps on energy dissipation.

Combination of Stepped Spillways with Other Types of Spillways. The labyrinth spillways and piano key weirs can be combined with step spillways at the same time. This combination allows for relatively higher amount of discharge through spillways with narrow width and shallow depth, as compared to conventional spillways. In addition, they can be simply installed on the crest of gravity dams. Stepped spillways are typically used in roller-compacted concrete (RCC) gravity dams. Among the most important advantages of this combination are (i) good compatibility of spillway structure with RCC dam construction method, (ii) reduction of water energy on steps, and (iii) reduction of construction costs and still basin dimensions at the downstream. Results show the effectiveness of laboratory study into combination of these two types of spillways, indicating that this combination can be used as a new model to determine optimal hydraulic dimensions in a large scale. Specific geometric characteristics of labyrinth spillways produce different jets and flows at the downstream, and subsequently affect energy loss and aeration. According to hydraulic and hydrodynamic principles and results from previous studies on stepped spillways, the use of a labyrinth or a piano key plan for handling upstream flow can improve energy loss in the downstream channel equipped with a stepped spillway. Cassidy [14] was among the leading researchers who used Laplace's equation and its solution through finite difference method to analyze ogee spillway overflow. He used potential flow theory to analyze free water surface and pressure of the crest. His findings are in good consistency with laboratory results. Sorensen and Chanson [21, 55] conducted several laboratory experiments on flow patterns and energy dissipation in stepped spillways and developed a number of equations to determine the flow type and the amount of energy loss on them. Olsen and Kjellesvig [46] modeled and solved flows over ogee spillways in 3D and 2D spaces using numerical methods and obtained the coefficient of discharge for ogee spillways. Chen et al. [36] employed Navier-Stokes equations with K-epsilon turbulence model. Tabara et al. [56] used finite volume method to analyze stepped spillway overflow and employed K-epsilon turbulence model to determine the turbulence of the flow. Chen et al. [36] modelled and analysed stepped spillways using the finite element method. Afshoon et al. [3]illustrate

after analysing the results in step spillways, it was found that in the stepped spillway combined with respectively a triangular, rectangular, and trapezoidal barrier, a decrease in dissipation and energy loss is observed. An increase in the length and width of the barriers results in an increase in dissipation and energy loss. Abbasi S., and Kamanbedast, A.A.[1], investigated the effect of changes in dimension and the hydraulics of stepped spillways for maximization of energy dissipation. They were among the first researchers to use flow3D to obtain a solution based on the method for the flow analysis of stepped spillways. The velocity and height of downstream flow were obtained using numerical methods, and then energy dissipation along K-epsilon turbulence of the spillway was computed. Results from numerical analysis were compared to laboratory results from the stepped spillway model, and the efficiency of the numerical model was discussed. Rostami, H. et al. [50] investigate labyrinth spillways and showed that increasing the weir hydraulic head ratio (H_d/P) would decrease the discharge coefficient (C_d). Rouzegar, J. et al. [51] find out that the increase in length of spillway and number of zigzag will increase the flow rate.

Governing Flow Equations. Flow Regimes. The majority of researchers have mentioned two different flow regimes for energy dissipation, namely nappe and skimming flow regimes. The first type occurs for small discharges and large step heights. The second type occurs for large discharges and small step heights (Osri and Horner, [25] Rajatnam, Chanson, Chamani and Rajaratnam,) [15, 16] these regimes are presented in Figure 3. In this figure, horizontal length and vertical height of each step are presented with l and h, respectively.

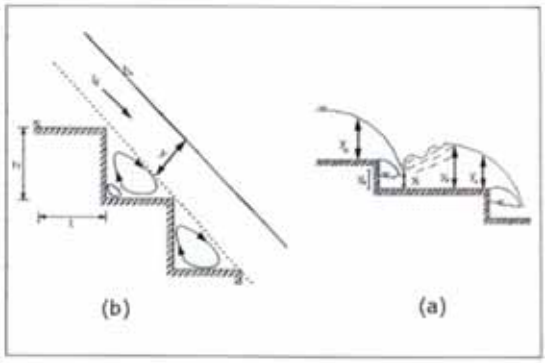

FIGURE 3
Flow regimes over stepped spillways: a) nappe regime, b) skimming regime (Chanson, 1994)

According to the experiments on stepped spillways with broad slope change, conversion of nappe regime to skimming regime occurs approximately at $y_c/h =$ 0.8 (Rajaratnam, 1990). [15]

Considerations concerning nappe and skimming regimes. In nappe flow regime, the total drop heights of the stepped spillway can be divided into a number of vertical drops. Therefore, depending on the horizontal length of the step, flow may have complete or incomplete hydraulic jumps when striking consecutive steps.

In general, the continuity and momentum equations in isochoric flow are expressed as follows:

$$\frac{\partial p}{\partial t}+\frac{\partial p u_i}{\partial x_i}=0 \tag{1}$$

$$\frac{\partial \rho u_i}{\partial x_i}+\frac{\partial}{\partial x_j}(\rho u_i u_j)=-\frac{\partial p'}{\partial x_i}+\frac{\partial}{\partial x_j}\left[(\mu+\mu_t)\left\langle\frac{\partial u_i}{\partial x_j}+\frac{\partial u_j}{\partial x_i}\right\rangle\right] \tag{2}$$

Where, t is time, u_i is velocity, x_i is coordinate, ρ is density, μ is dynamic viscosity, and μ_t is turbulence viscosity.

Energy dissipation in spillways and vertical drops. Energy dissipation means the difference between upstream energy of spillway with vertical drop and downstream (toe) on the depth before hydraulic jump (initial depth):

$$\Delta H = H_t - H_1 = (1.5 y_c + H_{dam}) - \left(y_t - \frac{V_1^2}{2g}\right) \tag{3}$$

In addition, relative energy dissipation $\left(\frac{\Delta H}{H_t}\right)$ is defined as follows:

$$\frac{\Delta H}{H_t}=\frac{H_t-H_1}{H_t}=1-\frac{H_1}{H_t}=1-\frac{\left(y_t-\frac{V_1^2}{2g}\right)}{1.5y_c+H_{dam}} \tag{4}$$

In above equations, H_t is overall upstream energy, H_1 is energy in toe before hydraulic jump, H_{dam} is overall spillway height, h is step height, y_c is critical depth, y_1 is depth before hydraulic jump, and V_1 is mean velocity before hydraulic jump. Figure 4 shows the cross-section of the vertical drop and stepped spillway, as well as different hydraulic parameters on them.

Dimensional analysis to determine energy loss. To this end, the parameters affecting energy dissipation should be determined. According to previous studies, energy dissipation in stepped spillways ΔH depends on the following factors (Chanson, 1994) [18, 19, and 20]:

H_0: Overall upstream energy; q: discharge per unit width; h: step height; l: step length; ρ_w: specific fluid density; σ: fluid surface tension; f_e: roughness coefficient of the bed; N: number of steps; μ: fluid dynamic viscosity; g: acceleration of gravity.

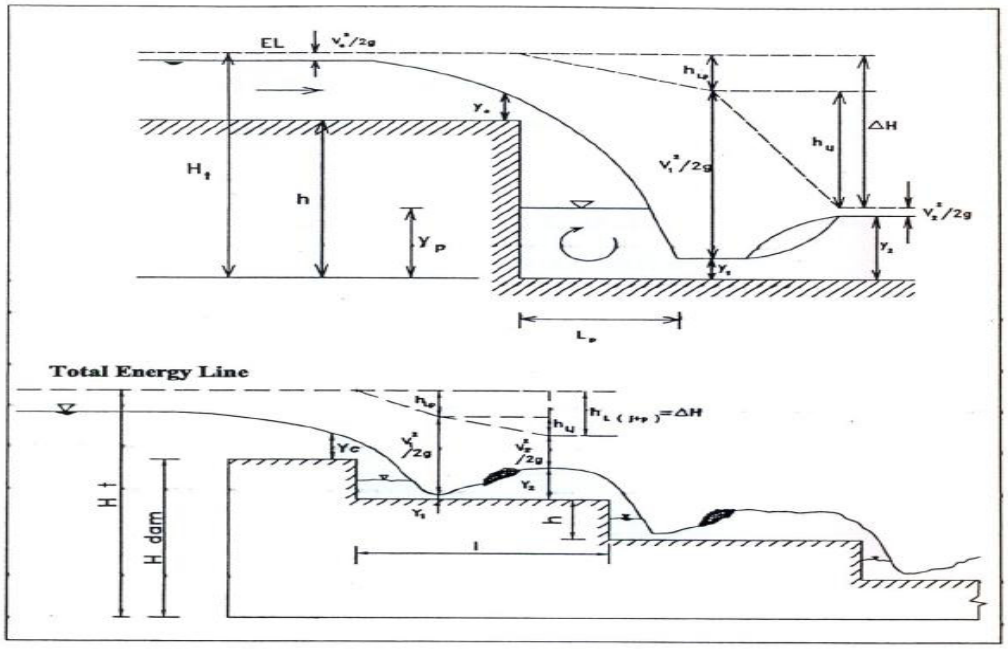

FIGURE 4
Cross-section of vertical drop and stepped spillway

Therefore, the following relationship exists between these parameters:

$$F\left(\Delta H, H_0, q, h, l, \rho_w, \sigma, f_e, N, \mu, g\right)=0 \quad (5)$$

$$f\left(\frac{\Delta H}{h}, \frac{H_0}{h}, \frac{y_c}{h}, \frac{h}{l}, \frac{\sigma}{\rho_w g h^2}, f_e, \frac{\mu}{\rho_w \sqrt{g h^3}}, N\right)=0 \quad (6)$$

Dimensionless parameters affecting energy loss in stepped spillway can be rewritten as follows by ignoring the effect of fluid viscosity μ and surface tension σ, undergoing slight manipulation of aforementioned parameters:

$$\frac{\Delta H}{H_0}=f\left(\frac{y_c}{h}, \frac{h}{l}, N, f_e\right) \quad (7)$$

To test the combination of stepped and labyrinth spillways, combinable and replaceable Plexiglass models were made. In this way, totally 90 experiments were conducted with 18 stepped labyrinth spillways with three steps and five different discharges.

$$\frac{\Delta H}{H_0}=\left(\frac{y_c}{H}, \frac{W}{B}, \frac{L}{W'}, \frac{L'}{W'}\right) \quad (8)$$

In this study, Froude number, change in labyrinth crest length, change in width of labyrinth cycles, and even change in labyrinth configuration and its effect on energy loss were evaluated. Variables included:

1. Five different discharges (five variables)
2. Spillway length change (two variables)
3. Step width change (three changes)
4. Configuration of labyrinth weir steps (three variables).

In total 90 physical model were studied.

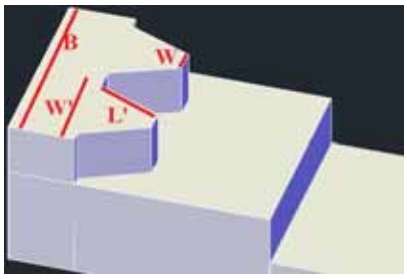

FIGURE 5
Schematic of stepped-labyrinth spillway combination

TABLE 1
Experimental variables

Step shape	L'/W	W/B	y_c/H
3	3	2	5 discharge

Experiments were conducted with 18 stepped-labyrinth spillway with three steps and five different discharges (90 experiments in total). Experimental results are discussed below. Specifications of labyrinth spillways are presented in Table 2.

MATERIALS AND METHODS

To perform this study in a laboratory setting, an experimental flume with the following characteristics was used in Islamic Azad University of Ahwaz. The experimental flume has open rectangular inlet and outlet channels with side walls made of Plexiglass. The length of inlet channel at the inlet section of the flume and that of outlet channel at the outlet

section of the flume are 4.5m and 2.5m long, respectively. The width and height of the flume are 0.5m and 0.6m, respectively. The flume is located 0.7m above the floor. The bed and side walls of the straight inlet channel are made of metal sheets (3mm in thickness) and Plexiglass (10mm in thickness and 4.5m in length), respectively. This way, the effect of the side wall roughness has decreased and hydraulic phenomena can be observed. The bed and side walls of the straight outlet channel are made of metal sheets (3mm in thickness) and Plexiglass (10mm in thickness and 2.5m in length), respectively. The flume has a fixed bed with no slope (Figure 6).

TABLE 2
Specification and dimensions of labyrinth spillways

L′/ W	L′/ W′	W	L′	W′	Type of labyrinth spillway	Schematic of labyrinth spillway	Number of labyrinth spillway
-	0.55	-	25.5	46			1
-	0.71	-	32.5	46	A		2
-	0.77	-	35.5	46			3
-	0.7	-	16	23			4
-	0.89	-	20.5	23	B		5
-	1.1	-	25.5	23			6
-	0.35	10	16	46			7
-	0.53	10	24.5	46	C		8
-	0.65	10	30	46			9
-	0.52	5	12	23			10
-	0.7	5	16	23	D		11
-	0.91	5	21	23			12
0.52	-	23	12	-			13
1	-	23	23	-	E		14
1.24	-	23	28.5	-			15
1	-	11.5	11.5	-			16
1.48	-	11.5	17	-	F		17
1.74	-	11.5	20	-			18

FIGURE 6
View of the flume

FIGURE 7
90-degree triangular notch spillways at the inlet and outlet of flume

FIGURE 8
Centrifugal pump

FIGURE 9
Labyrinth and stepped spillway models

There is a slide valve right after the flume tank to adjust discharge at inlet, a 90-degree triangular spillway to measure inlet discharge, a slide valve at the inlet of lateral basin to control the inflow, and a 90-degree triangular spillway to measure discharge at outlet. The valves are made of metal sheets. A mesh was used after the initial spillway to prevent the wave entry into the channel (Figure 7).

A centrifugal pump (power: 11KW, diameter of suction and delivery pipe: 6 inches) was used to circulate water in the experimental flume. The suction and delivery heights of the pump were approximately 2m and 6m, respectively; in addition, the maximum discharge of the pump was 60L/s (Figure 8).

Figure 9 presents fabricated labyrinth and stepped spillway models.

RESULTS

Results from evaluation of Froude number, change in labyrinth crest length, change in the width of labyrinth cycles, and even change in labyrinth shape and its effect on energy loss are presented in three classes:

1. Effects of change in the length and width of labyrinth cycles on energy dissipation and loss
2. Effects of change in the shape and number of labyrinth cycles on energy dissipation and loss
3. Effect of Froude number on energy dissipation and loss

Effects of change in the length and width of labyrinth cycles on energy dissipation and loss. The data required for analysis of results were obtained from the experiments and presented in the following diagrams. In the following section, results from relative energy loss for different Froude number and L'/W' ratios in combination of stepped spillway with different types of labyrinth spillways were addressed.

According to the diagrams (Diagram 1 and 2), relative energy loss increases by increasing L'/W' ratio from 0.55 to 0.77 in combination of stepped spillway with type A of labyrinth spillway. In addition, relative energy loss increases by increasing L'/W' ratio from 0.7 to 1.1 in combination of stepped spillway with type B of labyrinth spillway. It is also obvious that relative energy loss increases by increasing the Froude number to 0.1; whereas, relative energy loss decreased with further increase in Froude number, which can be attributed to the submergence of steps, reduced roughness of steps, and increased air entrainment. The comparison between type A of labyrinth spillway and type B of labyrinth spillway shows an increase in energy loss, which can be attributed to the presence of two cycles in the triangular section.

According to Diagram 3 and 4, relative energy loss increases by increasing L'/W' ratio from 0.35 to 0.65 in combination of stepped spillway with type C of labyrinth spillway. In addition, relative energy loss increases by increasing L'/W' ratio from 0.52 to 0.91 in combination of stepped spillway with type D of labyrinth spillway. It is also obvious that the relative energy loss increases by increasing the Froude number to 0.1; whereas, the relative energy loss decreased with further increase in Froude number, which can be attributed to the submergence of steps, reduced roughness of steps, and increased air entrainment. The comparison between type C of labyrinth spillway and type D of labyrinth spillway shows an increase in energy loss, which can be attributed to the presence of two cycles in trapezoidal section.

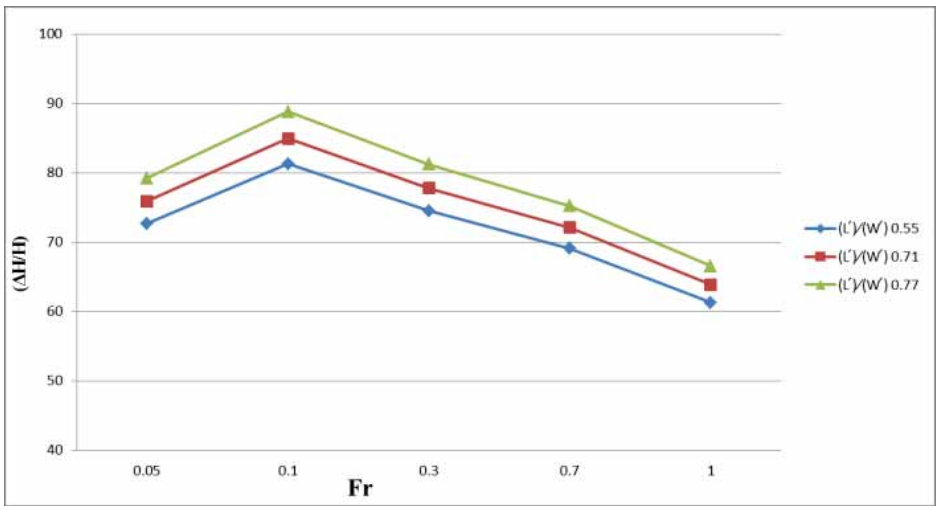

DIAGRAM 1
Comparative diagram of relative energy loss in combination of stepped spillway with type A of labyrinth spillway

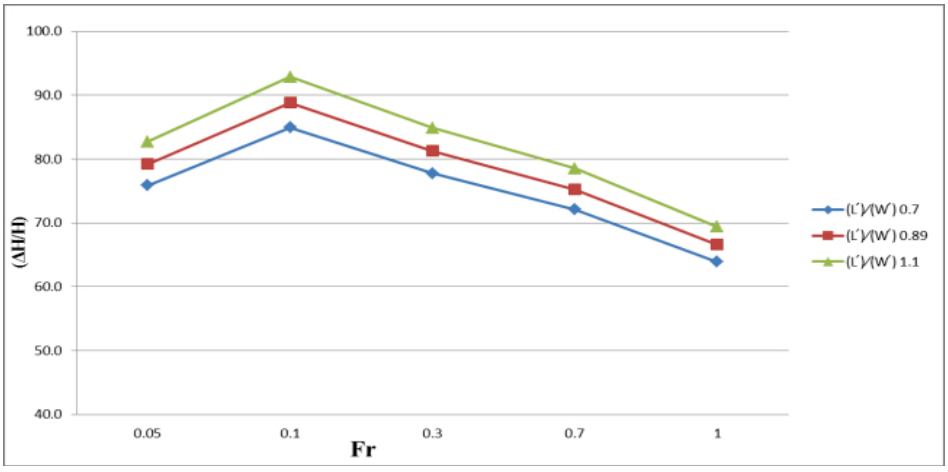

DIAGRAM 2
Comparative diagram of relative energy loss in combination of stepped spillway with type B of labyrinth spillway

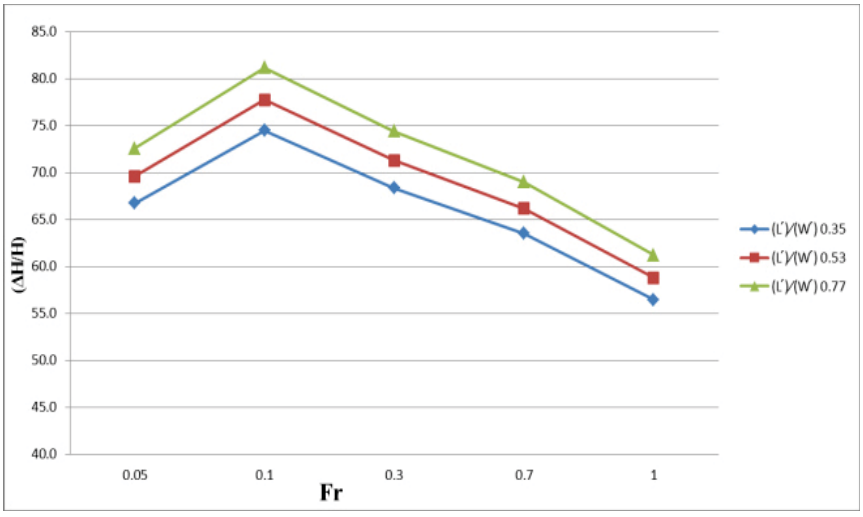

DIAGRAM 3
Comparative diagram of relative energy loss in combination of stepped spillway with type C of labyrinth spillway

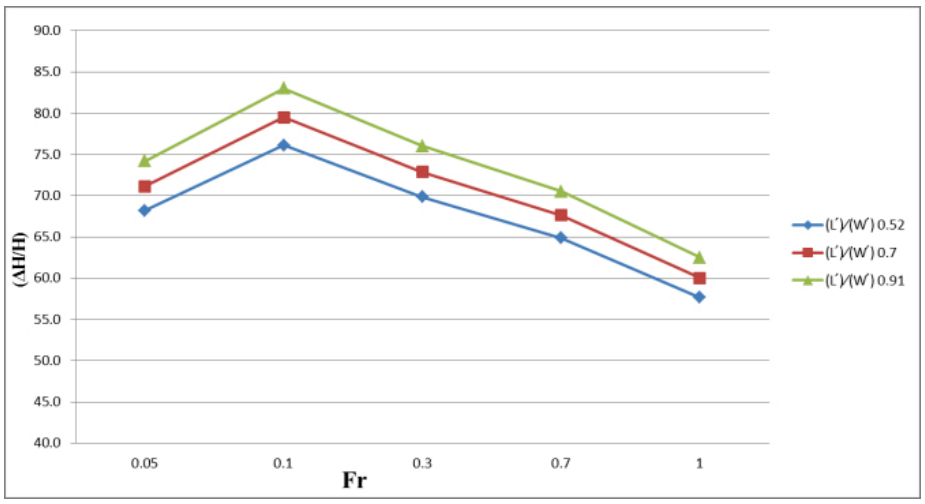

DIAGRAM 4
Comparative diagram of relative energy loss in combination of stepped spillway with type D of labyrinth spillway

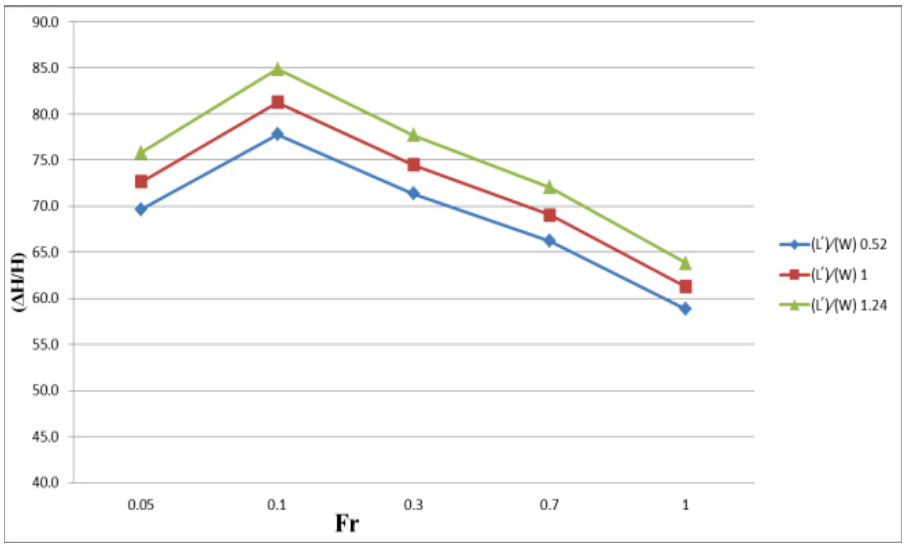

DIAGRAM 5
Comparative diagram of relative energy loss in combination of stepped spillway with type E of labyrinth spillway

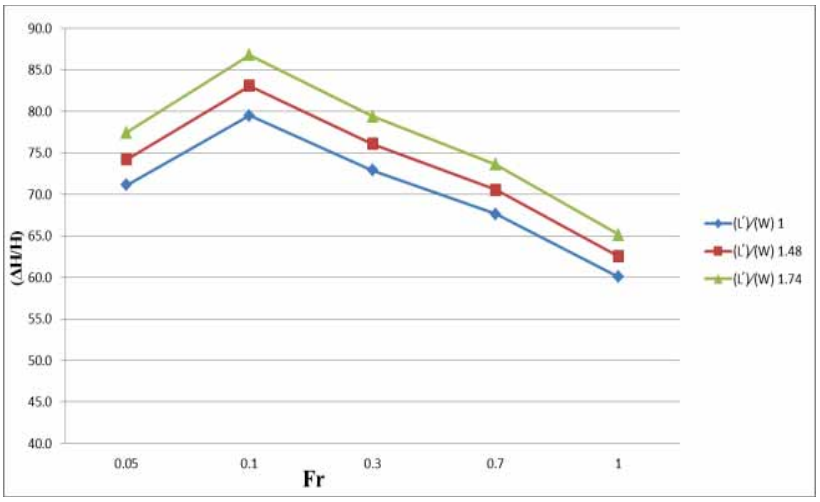

DIAGRAM 6
Comparative diagram of relative energy loss in combination of stepped spillway with type F of labyrinth spillway

According to the diagrams (Diagram 5 And 6), relative energy loss increases by increasing L′/W′ ratio from 0.52 to 1.24 in combination of stepped spillway with type E of labyrinth spillway. In addition, relative energy loss increases by increasing L′/W′ ratio from 1 to 1.74 in combination of stepped spillway with type F of labyrinth spillway. It is also obvious that relative energy loss increases by increasing the Froude number to 0.1; whereas, relative energy loss decreased with further increase in the Froude number, which can be attributed to the submergence of steps, reduced roughness of steps, and increased air entrainment. The comparison between type E of labyrinth spillway and type F of labyrinth spillway shows an increase in energy loss, which can be attributed to the presence of two cycles in rectangular section.

CONCLUSIONS

The combination of stepped spillway with labyrinth spillway can increase energy dissipation. Therefore, this study addressed the combination of stepped spillway with one- and two-cycle triangular, trapezoidal, and rectangular labyrinth.

1. Energy dissipation and loss reduction are greater in triangular than rectangular than trapezoidal labyrinth-shape stepped spillways.
2. Energy dissipation and loss are greater in labyrinth spillways with two cycles than with one cycle.
3. Energy loss and dissipation increase by increasing the Froude number from 0.05 to 0.1.

ACKNOWLEDGEMENTS

The present paper is based on PhD dissertation of Seyed Ali Banishoaib, PhD student of aqueous structures of Science and Research Branch of Islamic Azad University of Khuzestan and Ahvaz branch. In addition, the contributions of this university is warmly appreciated.

REFERENCES

[1] Abbasi, S., Kamanbedast, A.A. (2012) Investigation of effect of changes in dimension and hydraulic of stepped spillways for maximization energy dissipation. World Applied Sciences Journal. 18(2), 261-267.

[2] Aletaha, A., Rajae, T., Hassanzadeh Y. (2007) Hydraulic efficiency of stepped spillways in terms of dimensions and optimal number of steps. The 7th International Conference in Civil Engineering.

[3] Afshoon, H., R., Kamanbedast, A.A., Masjedi, A., Heidarnejad, M., Bordbar, A. (2018).Evaluation of the effect of the geometry of the barriers on stairs on energy loss in step spillways using physical model, Fresen. Environ. Bull. 27, 346-356.

[4] Azhdarymoghaddam, M. (1997) The hydraulics of ogee-stepped spillway profile, PhD Thesis, Ottawa, Canada.

[5] Barani, Gh. E., Sadra, A. (2003a) Energy dissipation in inclined stepped spillways. The 6th International Conference in Civil Engineering, Isfahan University of Technology, Iran.

[6] Barani, Gh. E., Sadra, A. (2003b) Energy dissipation in edged stepped spillways. The 6th International Conference in Civil Engineering, Isfahan University of Technology, Iran.

[7] Betts, P.L. (1979) A variation principle in terms of stream function for free surface flows and its application to finite element method. Computers and fluids. 7(2), 145-153.

[8] Beyrami, M.K. (2010) Water transmission structures. Isfahan University of Technology, Iran. Isfahan: Isfahan University of Technology Publisher.

[9] Bina, M., Moradisabzkohi, A., Kashefipoor, S.M. (2006) Laboratory study into the amount of energy dissipation in stepped drops. The 7th International Seminar on River Engineering, Shahid Chamran University of Ahwaz, Iran.

[10] Bina, M., Mousavijahromi, H., Salmasi, F. (2002) Laboratory study into energy loss over stepped spillways. The 6th International Conference on Civil Engineering, Isfahan University of Technology.

[11] Bina, M., Mousavijahromi, H., Salmasi, F. (2004) Effect of geometry of stepped spillway in energy dissipation. The 5th Conference in Hydraulics, Shahid Bahonar University of Kerman, Iran.

[12] Boes, R.M., Hager, W.H. (2003a) Hydraulic design of stepped spillways. Journal of hydraulic engineering, ASCE. 129(9).

[13] Boes, R.M., Hager, W.H. (2003b) Tow-phase flow characteristics of stepped spillways. Journal of hydraulic engineering, ASCE. 129(9), 661-670.

[14] Cassidy, J.J. (1965) Irrational flow over spillways of finite height. J. mecheng div. 91(6), 155-173.

[15] Chamani, M-R., Rajaratnam, N. (1999) Characteristics of skimming flow over stepped spillway. Journal of Hydraulic Eng. 125(4), 361-367.

[16] Chamani, M.R., Rajaratnam, N. (1994) Jet flow on stepped spillway. Journal of hydraulic engineering, ASCE. 12(5), 441-448.

[17] Chanson, H. (1994b) Comparison of Energy dissipation between nappe and skimming flow Regimes on stepped chutes. Journal of Hydraulic Research. 32(2), 213-218.
[18] Chanson, H. (1995) Hydraulic Design of stepped Cascades, Channels, Weirs and Spillway. Pergamon, Oxford, UK.
[19] Chanson, H. (1994a) Hydraulics of skimming flows over stepped channels and spillways. Journal of hydraulics Research. 32(3), 445-460.
[20] Chanson, H. (1994c) Jet flow on stepped spillways, Discussion. Journal of hydraulic engineering. 120(2), 443-444.
[21] Chanson, H. (2001) The hydraulic of stepped chutes and spillway. TC. 555, C.4623.
[22] Chinnarasi, C., Wongwisess, S. (2006) Flow patterns and energy dissipation over various stepped chutes. Journal of irrigation and drainage engineering, ASCE. 132(1).
[23] Christodoulou, G.C. (1999) Design of stepped spillway for optimal energy dissipation. Hydropower and dam. 5, 90-93.
[24] Erfanian Azmodeh, M.H., Kamanbedast, A.A. (2013) Determine the Appropriate Location of Aerator System on Gotvandoliadam's Spillway Using Flow 3D. JAES, 13(3), 378-383.
[25] Essery, I.T.S., Horner, M.W. (1971) The hydraulic design of stepped spillway, Report 33, Constr. Industry Res. And Information Assoc., London, England.
[26] Gharibvand, R., Heidarnejad, M., Kashkouli, H., Hasoonizadeh, H., Kamanbedast, A.A. (2016) An experimental study into hydraulic coefficient in trapezoidal labyrinth weir and piano key weir. Fresen. Environ. Bull. 25, 5590-5598.
[27] Geravandi, E., Kamanbedast, A.A., Masjedi, A., Heidarnejad, M., Bordbar, A. (2018) Laboratory investigation of the impact of armor dike simple and L-shape in upstream and downstream intake of the hydraulic flow of the Kheirabad River to help physical model. Fresen. Environ. Bull.,27, 263-276.
[28] Guo Y, Wen X, Wu C, Fang D. (1998) Numerical modeling of spillway flow with drop and initially unknown discharge. Journal of hydraulic engineering. 36(5), 785-801.
[29] Hoseinisohi, S.M. (2005) Hydraulic simulation of flow in stilling basin with Flow3D (thesis). Library of Shahid Modarres University.
[30] Ikegawa, M., Washizu, K. (1973) Finite element method applied to analysis of flow over a spillway crest. Journal of hydraulic engineering. 6, 179-189.
[31] Johnson, M., Savage, B. (2006) Physical and numerical comparison of flow over ogee spillway in the presence. Journal of hydraulic engineering. 132(2),1353-1357.
[32] Kamanbedast, A.A. Gholizade, B. (2012) The study of siphon spillway Hydraulic by Modeling (physical and software). Journal of Applied sciences Research, 8(5), 2548-2553.
[33] Kamanbedast, A.A. (2012) The Investigation of Discharge Coefficient for the Morning Glory Spillway Using Artificial Neural Network. World Applied Sciences Journal. 17(7), 913-918.
[34] Kamanbedast, A.A. (2014) Handbook of hydraulic structures engineering. Published in Islamic Azad University, Ahvaz, Iran.
[35] Kavianpoor, M.R., Hoseini, M., Roshan, R. (2009) Characteristics of two-phase flows on stepped spillways. The 8th International Conference on Civil Engineering, Shiraz University.
[36] Li, W., Xie, Q. and Chen, C.J. (1989) Finite analytic solution of flow over spillways. Journal of hydraulic engineering, ASCE. 115(12), 2635-2648.
[37] Majdzadehtabatabae, M.R., Shorabi, H. (2001) Designing stepped spillways: a suitable energy dissipater. The 3rd Conference on Hydraulic, Engineering Faculty of Tehran University, Iran.
[38] Mansoori, A., Pedram, A.H. (2009) Energy dissipation on edged stepped spillway. The 7th Conference on Hydraulics, Power and Water University of Technology (Shahid Abbaspoor).
[39] Matos, J., Quintela, A. (1995) Flow resistance and energy dissipation in skimming flow over stepped spillways. Conference on water resources engineering, ASCE. Texas, USA. 2, 1121-1126.
[40] Matos, J., Quintela, A. (1994) Jet flow on stepped spillways, Discussion. Journal of hydraulic engineering. 120(2), 443-444.
[41] Maynord, S.T. (1985) General spillway investigation, Technical Report, HL-85-1, United States Army Corps of Engineers, Waterways Experimental Station, Vicksburg, MS.
[42] Mousavi-Jahroumi, H., Karimi, M. (2009) Modeling skimming flow on stepped spillway with ANSYS. The 1st National Engineering and Management Conference, Engineering Campus of Tehran University
[43] Mousavi-Jahromi, S.H., Heidariarjlo, S., Farazmand, S. (2009) Effect of slope on energy loss in stepped spillways using physical models. The 8th International Conference on Civil Engineering, Shiraz University, Iran
[44] Mousavi -ahromi, S.H., Heidariarjlo, S., Farazmand, S. (2009) Investigation into initiation of skimming flow in stepped spillways using physical models. The 8th International Conference on Civil Engineering, Shiraz University, Iran.
[45] Dezfoli, M.H.N., Kamanbedast, A.A., Masjedi, A., Heidarnejad, M., Purmohammadi, M.H. (2017) Comparing Methods of Estimating Hydraulic Jumps Stilling Basins' divergent Parameters. Fresen. Environ. Bull. 26, 2231-2236.

[46] Olsen, N.R., Kjellesving, H.M. (1998) Three-dimensional numerical flow modeling for estimation of spillway, capacity. Journal of hydraulic engineering, the Netherland. 36(5), 775-784.
[47] Rajaratnam, N. (1990) Skimming flow in stepped spillway. Journal of hydraulic engineering, ASCE. 116(4).
[48] Rice, C.E., Kadavy, K.C. (1996) Model study of a roller compacted concrete stepped spillway. Journal of hydraulic engineering, ASCE. 122(6).
[49] Rodi, W. (1980) Turbulence models and their application in hydraulics, monograf. International Association for Hydraulic Research. Delft, The Netherlands, 27-30.
[50] Rostami, H., Heidarnejad, M., Purmohammadi, M. H., Kamanbedast, A., Bordbr, A. (2016) An Experimental Study into Discharge Coefficient of Labyrinth Weirs with Rectangular-Shaped Plans. Fresen. Environ. Bull. 25, 5138-5144.
[51] Rouzegar, J., Kamanbedast, A. A., Masjedi, A., Heidarnejad, M., Bordbar, A. (2017) The Experimental Investigation of Flow Hydraulics in Zigzag Morning Glory Spillways. Fresen. Environ. Bull. 26, 2389-2396.
[52] Savege, B.M., Johnson, C.M. (2001) Flow over ogee spillway physical and numerical model case study. Journal of hydraulic engineering, ASCE. 127(8), 640-649.
[53] Shamsae, A. (2004) Design and construction of storage dams. Tehran: Iran University of Science and Technology Publisher.
[54] Silva-Araya, W.F., Chaudhry, M.H. (1997) Computation or energy dissipation in transient flow. Journal of hydraulic engineering, ASCE. 123(2)
[55] Sorensen, R.M. (1985) Stepped spillway hydraulic model investigation. Journal of hydraulic Engineering. 111(12), 1461-1472,
[56] Tabbara, M., Chatila, J., Awwad, R. (2005) Computational simulation of flow over stepped spillways, Department of civil engineering, Lebanese American University, Lebanon.
[57] Tozzi, M.J. (1994) Residual energy in stepped spillways. Int. Water power and dam Construction. 46(5), 32-34.
[58] Yasuda, Y., Ohutso, L. (1998) Flow resistance of skimming flow stepped channels, Dept. of civil Eng. Nihon Uni. 6.
[59] Zeraat, B., Heidarnejad, M., Masjedi, A., Kamanbedast, A., Hasoonizadeh, H. (2017) Hydraulics of Arch Plan Labyrinth Weirs with Two Different Cycles. Fresen. Environ. Bull. 26, 2862-2867.

Received: **11.06.2017**
Accepted: **25.11.2017**

CORRESPONDING AUTHOR

Amin Bordbar
Department of Water Science and Engineering,
Ahvaz Branch,
Islamic Azad University,
Ahvaz – Iran

e-mail: Asefmn@yahoo.com

© by PSP Volume 27 – No. 2/2018 pages 921-927 Fresenius Environmental Bulletin

MORPHOLOGICAL AND MOLECULAR CHARACTERIZATION OF AN ENDEMIC AND SIX KNOWN *BILIMNEUS* (HYDRAENIDAE: *LIMNEBIUS*) SPECIES FROM TURKEY

Ahmet Kasapoglu[1,*], Nesil Ertorun[2], Mehmet Burcin Mutlu[2], Erol Atay[1], Sibel Cilli[1]

[1]Mustafa Kemal University, Science and Art Faculty, Department of Biology, 31060, Hatay, Turkey
[2]Anadolu University, Faculty of Science, Department of Biology, 26470, Eskisehir, Turkey

ABSTRACT

Limnebius has a worldwide distribution with more than 150 described species and 21 of them from Turkey, four of them are endemic for the Turkish fauna. Limnebius species are small water beetles which their morphologies are very uniform with oval and drop-like body shape. For this reason, taxonomists use male sex organs called aedeagi for classical taxonomical identification of Limnebius species. Molecular techniques have been widely applied in many disciplines of biological sciences including insect identification. These techniques improved over traditional morphological identification and allowed timely and unambiguous identification of insects. The enzyme cytochrome c oxidase is a large transmembrane protein complex found in mitochondrion of eukaryotes and bacteria, and cytochrome c oxidase I is the main subunit of the cytochrome c oxidase complex (COX 1).

The aim of this study is to determine the evolutionary relationships of some *Limnebius (Bilimneus)* species (Coleoptera: Hydraenidae: *Limnebius*) (*Limnebius atomus, Limnebius corfidius, Limnebius corybus, Limnebius myrmidon, Limnebius paranuristanus, Limnebius* subunit 1 (COX 1) nucleotide sequences.

Here, we present the first study on some *Limnebius (Bilimneus)* species from Turkey (1 of them is an endemic species) and their taxonomic identification was performed based on both classical morphological identification and DNA barcoding by using a near-complete DNA sequences of COX1 gene.

KEYWORDS:
Hydraenidae, *Limnebius*, *Bilimneus*, Cytochrome C Oxidase, Turkey

INTRODUCTION

Insects in the animal kingdom have a wide variety. Diagnosis of species in this rich variety can be quite difficult in some groups. For this reason, many taxonomic analyzes of insect groups usually use sex organs, especially male sex organs. The genital organs play a key role in species identification, except some special situation such as for neutral geographic variations or local adaptations [1].

The genus Limnebius forms a well-defined, distinctive group of small water beetles with a rather similar external morphology. Limnebius adults have uniform morphology with oval and drop-like body shape [2]. Most of the Limnebius species can only be reliably distiguished based on aedeagi [3]. Except Antarctica and South America, the genus has a worldwide distribution with more than 150 described species [1].

Turkey *Limnebius* fauna is represented by 21 species and *L. ferroi* is an endemic species for the Turkish fauna [4]. Body length is 1.15 - 1.4 mm long and shape is parallel-sided.

Limnebius ferroi is very closely related to *L. paranuristanus* and there are no significant distinguishing characters between *L. paranuristanus* and *L. ferroi.* Shagrination and punctation on head and pronotum usually more distinctly pronounced in *L. paranuristanus.* Aedeagus of *L. ferroi* is very similar to *L. paranuristanus* but less sinuous on lateral aspect than in *L. paranuristanus*. Body length is 1.2 - 1.5 mm long in *L. paranuristanus* [2].

Male ventrite VII of *L. corfidius* as in *L. corybus*. *L. atomus* is very similar to *L. perparvulus*. *L. myrmidon* is very similar to *L. perparvulus* with which it generally it agrees body form and size [2]. Aedeagus of *L. perparvulus* is very similar to *L. atomus*.

DNA barcoding is the use of a short-standardized DNA sequence (a 658 bp fragment of the mitochondrial cytochrome c oxidase (COX I) gene in insects) for identification and assign a taxonomic position of unknown specimens. This is also useful for facilitating the discovery of new species.

Recent molecular analysis related with insect species have been done by using several marker gene such as the rDNA internally transcribed spacer region 2 (ITS-2), cytochrome c oxidase subunit 1 (COX 1), NADH dehydrogenase subunit 1 (nadH1) and cytochrome b (sitB) markers. These studies were quite helpful for understanding the phylogenetic relationships between insect species [5]. However, the cytochrome c oxidase subunit 1 (COX 1) has been extensively used by molecular biologists around the world to identify insect species [6]. COX 1 is a well-conserved gene that is present in all mitochondrial genomes encoding the largest subunit of cytochrome c oxidase, an element of complex IV in the respiratory chain [7].

The aim of this study is to determine the evolutionary relationships of some *Limnebius (Bilimneus)* species (Coleoptera: Hydraenidae: *Limnebius*) of living in Turkey using cytochrome c oxidase subunit 1 (COX 1) nucleotide sequences.

MATERIALS AND METHODS

Collection and Identification. Materials of this study were collected using sieves from various ecosystems across Turkey. At each site, the specimens were transferred to collection tubes containing 96 % alcohol.

Specimens were examined with the following microscopes: Wild M5A stereoscopic microscope with direct lighting and Wild M 10 stereoscopic microscope with diffuse lighting. In addition to these stereoscopic microscopes, aedeagi were also examined with an Olympus BH-2 transmitted light microscope. Male genitalia were placed in concentrated lactic acid in a cavity slide for at least several hours before they were examined. Beside identification made in Naturhistorisches Museum (Wien/Austria) by first author by compared with museum materials. The specimens were identified to species level and distributed into their respective families to obtain a clear phylogenetic signal immediately upon their collection. The specimens, thus collected and morphologically identified, were used for COX 1 barcoding.

FIGURE 1
Distribution maps for the chosen *Limnebius (Bilimneus)* species that was used in this study, (a) Map of Turkish provinces, (b) Reported by different studies of used *Bilimneus* species (Shaded areas are the provinces of collected and used specimens for COX 1 in this study).

TABLE 1
Collected and used specimens for COX 1 and their representative symbols on the map.

Species name	Sampling Locality	Symbols on the Map
Limnebius (Bilimneus) atomus	Bursa-Karacabey	♦
Limnebius (Bilimneus) corfidius	Balıkesir-Kepsut	⊗
Limnebius (Bilimneus) corybus	Erzurum-Çat	∇
Limnebius (Bilimneus) ferroi	Hatay-İskenderun	∗
Limnebius (Bilimneus) myrmidon	Erzurum-Çat	+
Limnebius (Bilimneus) paranuristanus	Erzurum-Tortum	θ
Limnebius (Bilimneus) perparvulus	Erzurum-Tortum	X

TABLE 2
COX 1 gene sequences used for the primer design

Limnebius	
Organism	**Accession No**
Limnebius zaerensis	EU365868.1
Limnebius truncatellus	HQ165290.1
Limnebius nitidus	HE610238.1
Limnebius montanus	HE610237.1
Limnebius ordunyai	HE610239.1
Limnebius monfortei	HE610236.1
Limnebius millani	HE610235.1
Limnebius maurus	HE610234.1
Limnebius irmelae	HE610233.1
Limnebius hilaris	HE610232.1

Figure 1 shows the distribution of Bilimneus species in Turkey. *Limnebius atomus*: were reported from Bursa, Kırklareli and Samsun in Turkey [4]. The sequence analysis has been performed by the sample which was collected from Bursa.

Limnebius corfidius has been reported from Balıkesir, Bursa, Çanakkale, Istanbul and Muğla from Turkey [4]. The sequence analysis has been performed by the sample which was collected from Balıkesir.

Limnebius corybus has been reported from Aydın, Balıkesir, Bursa, Bitlis, Çanakkale, Denizli, Erzurum, Gümüşhane, İzmir, Muğla and Ordu in Turkey [4]. The sequence analysis has been performed by the sample which was collected from Erzurum.

Limnebius ferroi is an endemic species for Turkey and has been reported from Antalya, Hatay and Mersin [4]. The sequence analysis sample was collected from Hatay.

Limnebius myrmidon has been reported from Artvin, Balıkesir, Bursa, Bitlis, Çanakkale, Erzurum, Istanbul, Muğla, Muş and Ordu [4]. The sequence analysis sample was collected from Erzurum.

Limnebius paranuristanus has been reported from Bitlis, Erzincan, Erzurum, Gaziantep and Kilis [4]. The sequence analysis sample was collected from Erzurum.

Limnebius perparvulus has been reported from Ankara, Antalya, Balıkesir, Çanakkale, Diyarbakır, Erzincan, Erzurum, Hatay, İzmir, Kocaeli, Mardin, Mersin, Muğla and Tekirdağ [4]. The sequence analysis has been performed by the sample which was collected from Erzurum.

All the sequence analysis samples were shown on Table 1.

Examined material. DNA extraction. Biospeedy™ DNA-Tricky Purification Kit (Bioeksen Ltd. Co., Turkey) was used for the DNA extraction. Briefly, the samples were homogenized at 6000 rpm for 2 minutes in a buffer (2% CTAB -hexadecyltrimethylammonium bromide-, 100 mM Tris-HCl pH 8, 20 mM EDTA, 1.4 M NaCl) containing 0.1 mm diameter glass beads. The samples were then incubated at 98°C for 10 minutes. The samples were centrifuged and the supernatant was combined with a binding buffer (final concentration of 3.4 M Guanidinium thiocyanate, 8 mM Tris-HCl pH 8.0, 25% isopropanol). The extracted DNA was captured using silica columns and then washed twice with a buffer containing 20 mM NaCl, 2 mM Tris-HCl, pH 7.5; 80% v/v Ethanol. The DNA was eluted in 100 mM Tris-HCl pH 8.0 and stored at -20°C.

Primer design. PCR primers were designed based on comparison of the available *Limnebius* Cytochrome c oxidase subunit I (COX 1) sequences retrieved from Genbank. CO1 gene sequences used for the primer design were given in Table 2. The sequences were aligned using Clustal Omega

(www.ebi.ac.uk) and the degenerate primers were designed manually. The specifity of the designed primers were tested using Primer-Blast (www.ncbi.nlm.nih.gov). The CO1 targeted primer set was forward 5'-CATATTATYAGMCAA-GAAAG-3' and reverse 5'-AAATCTTTCTCAAATRATDAAWA-3' sequences.

Real time PCR (Q-PCR). Biospeedy™ EvaGreen Master Mix (Bioeksen Ltd. Co., Turkey) and Roche Light Cycler Nano (Roche Diagnostics GmbH, Germany) were utilized for all reactions. Reaction mixes contained 25 ng template DNA, 6mg/ml BSA, 5 mg/ml PEG 400, 0.25% Tween 20, 20 mM Tris-HCl pH 8.4, 50 mM KCl, 1.5 mM $MgCl_2$, 0.2 mM dNTP mix, 0.1U Proof Reading Hot-Start DNA Polymerase and 200 nM of each primer. The following thermo cycling program was applied: 98°C, 3 min; 35 cycles of 10 s at 95°C, 5 s at 52 °C and 20 s at 72°C. A melt curve analysis was performed from 65°C to 95°C to determine if only one amplified product was generated during Q-PCR. Q-PCR runs were analyzed using Roche Light Cycler Nano Software.

DNA sequencing and phylogenetic analysis. The Q-PCR products larger than 100 bp were purified using Biospeedy™ PCR Product Purification Kit (Bioeksen Ltd. Co., Turkey). The purified DNAs were sequenced using the ABI prism Big Dye Terminator Cycle Sequencing Ready Reaction Kit on an ABI Prism 377 DNA sequencer (Applied Biosystems, USA). The sequences were analyzed in Chromas (www.technelysium.com) and manually checked for reading errors. Homology searches of the sequences in DNA databases were performed with BLAST (www.ncbi.nlm.nih.gov). The COX1 sequences and their closest matches in GenBank were aligned using Clustal Omega (www.ebi.ac.uk) followed by manual adjustments. Only unambiguously aligned base positions were used in the analysis. Maximum-likelihood method was performed with the MEGA software (www.megasoftware.net) to construct an unrooted phylogenetic tree.

RESULTS

The performance of COX 1 as a molecular marker to appreciate the identification of endemic Limnebius species was tested in this study. Two primers were designed according to 10 COX 1 gene sequences from NCBI, to specifically amplify these taxa.

As can be seen in Figure 2, especially the species *Limnebius ferroi* has a lot of mismatches against to other species such as the nucleotide position 96 to 102, 132 to 141, and 373 to 381. These positions could be used as a signature sequence for identification of this endemic species.

When we look at the morphology of aedagus, it is seen that *L. corybus* and *L. corfidius* are similar to each other. However, COX 1 gene dendogram (Fig. 3) of these species showed the opposite of what morphological taxonomy told us.

DISCUSSION AND CONCLUSION

Biogeographical studies focused on different organisms were reported recently from different parts of Turkey [8-9]. In our study examined materials were collected from different parts of Turkey such as Bursa, Balıkesir, Erzurum and Hatay.

Limnebius species are morphologically very similar to each other. This is why the detailed patterns of aedeagi are used in the diagnosis of the species. In order to understand the evolutionary relations of an insect group that shows so much similarity, molecular analysis needs to be done. This work is planned for this purpose. After the molecular analyzes of all the species sequences have been uploaded to the NCBI data bank, we believe that evolutionary interrelationships between species can be evaluated more healthily.

Sequences from organelle genomes have been adopted as bar codes for species identification. Plants have different plastid encoding genes (CBOL Plant Working Group, 2009, http://www.barcoding.si.edu/plant_working_group.html) and a 648 bp region of mitochondrial cytochrome c oxidase 1 (COX1 or CO1) [10-11].

Currently, identification of insects by using morphological characteristics is time consuming and requires expert knowledge. The identification of adult specimens is usually possible for relatively inclusive taxonomic stages such as family or order, and the identification of immature or larval specimens is even more challenging. As a result, publicly owned databases (GenBank and BOLD) are filled with poorly defined DNA barcode sequences [12]. For this reason, the use of such sequences in gene banks may lead to erroneous interpretations.

COX1 has increasing attention as a sequence for species identification in the insect groups [13-14]. However, it was reported that one of the major obstacles facing the use of COX1 for barcoding living organisms (in the case of Fungi) is the frequent occurrence of either group I or II introns in mitochondrial genes [15]. Therefore, these introns, whose positions in mitochondrial genes are not conserved, vary in size from 100 bp to 4.3 kb [16], thus making amplification of coding sequences difficult in many cases.

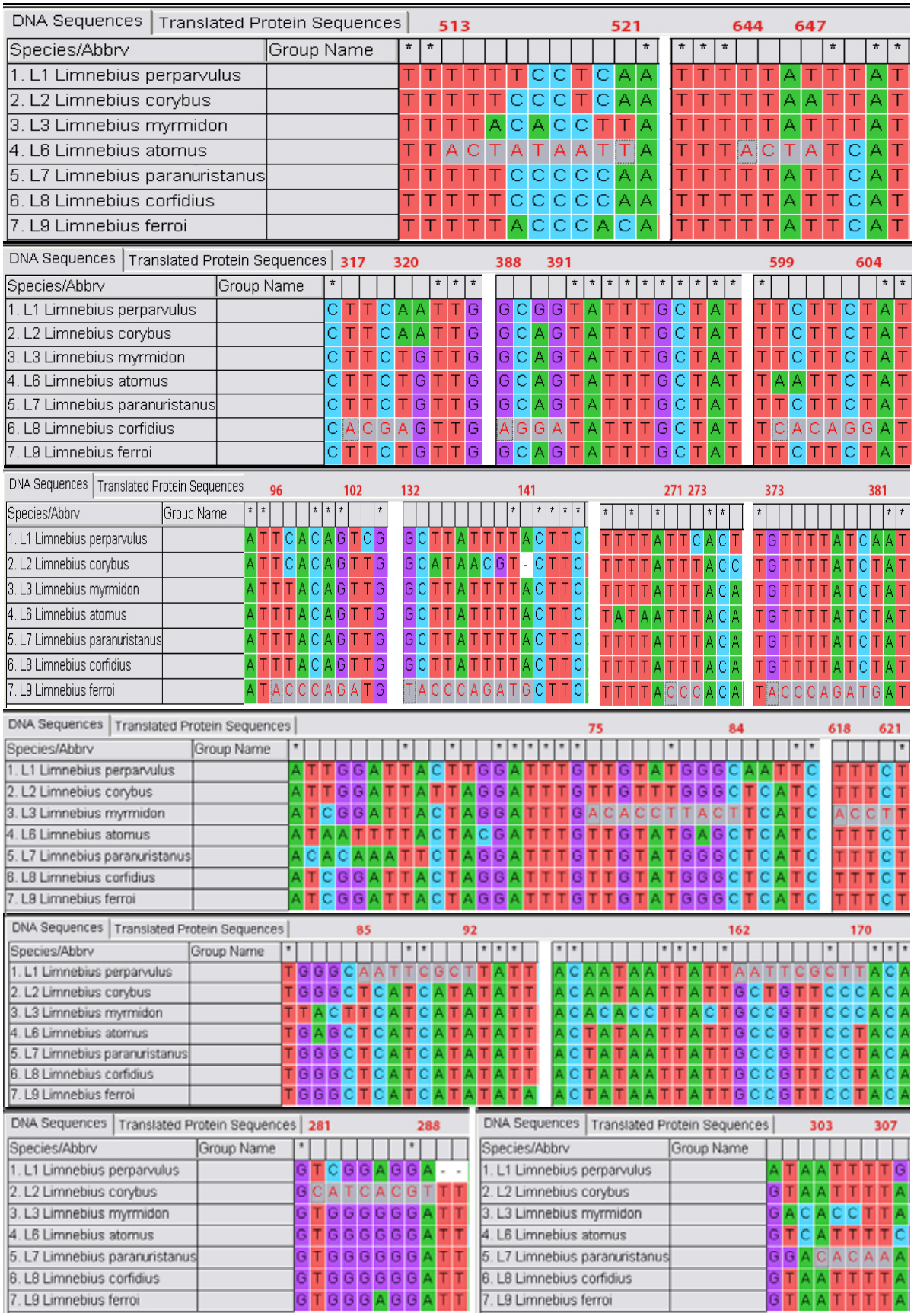

FIGURE 2
Alignment of sequences of COX 1 gene and some of the mismatches between these sequences in different nucleotide positions

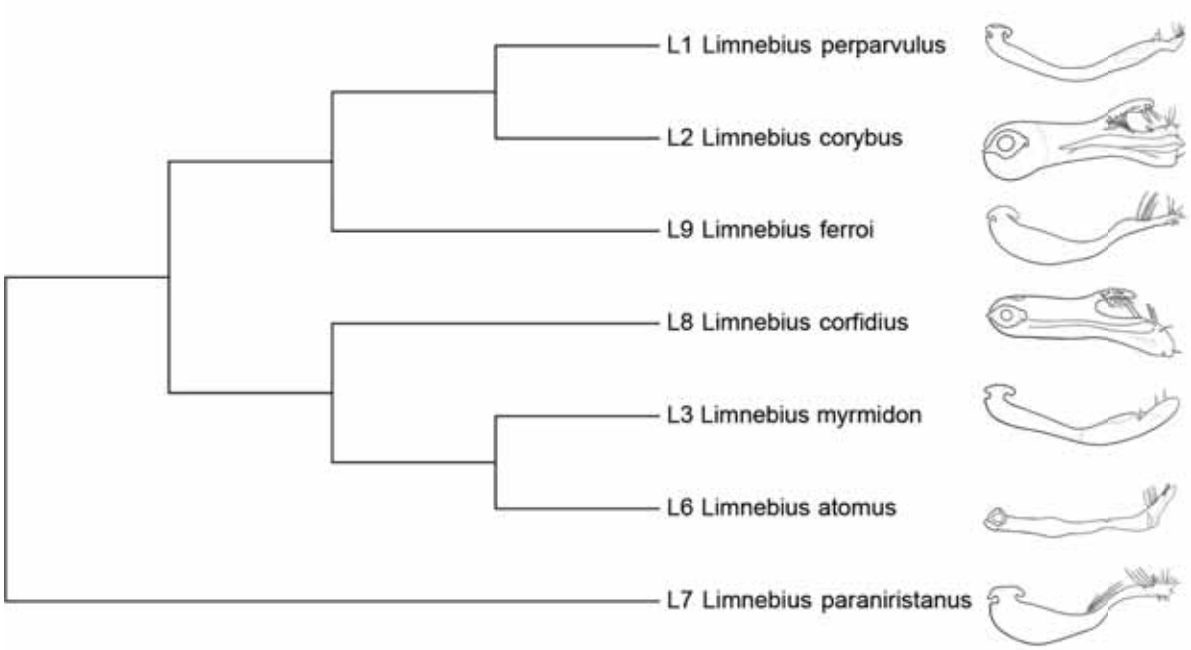

FIGURE 3
UPGMA dendrogram based on COX1 sequences (500 bp) of examined *Limnebius* samples and their aedeagi structures (Aedeagi figures from [2]).

As with the ITS sequence [17], in which intraspecific and intraspecific variant levels are reported, these inconsistencies are either due to sequence-specific sequence evolution rates or to recent or ancient speciation events.

COX1 is a powerful tool for predicting large-scale species richness in sequence data, ecology and b-diversity research and has great potential for determining conservation priorities. However, Hendrich et al. [18] reported that individual error rates could be high.

Similar to these studies, assigning taxonomic position to our samples by using results coming from morphological differences of their aedeagi structures and the results coming from COX 1 sequence of the examined species is not overlapping in our study.

The quality of the taxonomic identification of samples ultimately determines the usefulness of DNA barcode sequences in the reference databases. This motivated us to carefully inspect all the specimens in the dataset again for possible taxonomic misidentifications. Our dataset included seven (one of them endemic species for Turkey) species discovered through an iterative process of morphospecies sorting. Molecular approach has shown that some of the nucleotide positions in the COX 1 gene of the *L. ferroi* could be used as a signature sites to identify this endemic species of Turkey.

In recent years, molecular taxonomy as well as classical taxonomy has been utilized to a great extent. Molecular taxonomy data is recorded in the NCBI data bank and offers benefits such as accuracy testing in a sense for classical taxonomy. The species belonging to the *Bilimneus* genus used in this study have previously been used in a faunistic study in Turkey [4]. It is aimed to reveal the molecular differences of these species morphologically separated from each other very difficult.

Here, we present the first study on some *Limnebius (Bilimneus)* species from Turkey (1 of them is an endemic species) and their taxonomic identification. Our study was performed based on both classical morphological identification and DNA barcoding by using a near-complete DNA sequences of COX1 gene.

ACKNOWLEDGEMENTS

This study was financially supported by the Scientific Research Projects of Mustafa Kemal University (Project number: BAP-331). The authors sincerely thank to Dr. Manfred Jäch (NHM Wien) for his invaluable efforts for identification of the specimens.

REFERENCES

[1] Rudoy, A. and Ribera, I. (2017) Evolution of sexual dimorphism and Rensch's rule in the beetle genus Limnebius (Hydraenidae): is sexual selection opportunistic? Peer J. 5, e3060.

[2] Jäch, M.A. (1993) Taxonomic revision of the Palearctic species of the genus Limnebius Leach, 1815 (Coleoptera: Hydraenidae). Koleopterologische Rundschau. 63, 99–187.
[3] Hernando, C., Aguilera, P. and Ribera, I. (2008) *Limnebius zaerensis*, a new species from Pays Zaer-Zaiane, central Morocco (Coleoptera: Hydraenidae). Koleopterologische Rundschau. 78, 195-198.
[4] Ertorun, N., Jäch, M.A., Kasapoğlu, A. and Darılmaz, M.C. (2011) Checklist of the Hydraenidae (Coleoptera) of Turkey, with notes on distribution. Zootaxa. 3055, 22–42.
[5] Ashok, K.A., Reddy, V.S., Ramaiah, B., Sanjana, Reddy, P., Sahrawat, K.L. and Upadhyaya, H.D. (2009) Genetic variability and plant character association of grain Fe and Zn in selected core collections of sorghum germplasm and breeding lines. Journal of SAT Agricultural Research (ejournal.icrisat.org). 7, 1–4.
[6] Jalali, S.K., Ojha, R. and Venkatesan, T. (2015) DNA Barcoding for identification of agriculturally important insects. In: Chakravarthy, A.K. (ed.) New Horizons in Insect Science: Towards Sustainable Pest Management, Springer, India.
[7] Capaldi, R.A., Malatesta, F. and Darley-Usmar, V.M. (1983) Structure of cytochrome c oxidase. Biochim. Biophys. Acta. 726(2), 135-48.
[8] Osma, E., Ozyigit, I.I., Demir, G. and Yaşar, U. (2014) Assesment of some heavy metals in wild type and cultivated purslane (*Portulaca oleracea* L.) and soils in Istanbul, Turkey. Fresen. Environ. Bull. 23, 2181-2189.
[9] Baba, H., Zumre, M. and Ozyigit, I.I. (2016) A comperative biogeographical study of myxomycetes in four different habitats of Eastern Mediterranean part of Turkey. Fresen. Environ. Bull. 25, 1449-1460.
[10] Hebert, P.D.N., Penton, E.H., Burns, J.M., Janzen, D.H. and Hallwachs, W. (2004) Ten species in one: DNA barcoding reveals cryptic species in the neotropical skipper butterfly *Astraptes fulgerator*. Proc. Natl. Acad. Sci. USA. 101, 14812–14817.
[11] Hajibabaei, M., Janzen, D.H., Burns, J.M., Hallwachs, W. and Hebert, P.D.N. (2006) DNA barcodes distinguish species of tropical Lepidoptera. Proc. Natl. Acad. Sci. USA. 103, 968–971.
[12] Porter, T.M., Gibson, J.F., Shokralla, S., Baird, D.J., Golding, G.B. and Hajibabaei, M. (2014) Rapid and accurate taxonomic classification of insect (class Insecta) cytochrome coxidase subunit 1 (COI) DNA barcode sequences using a naïve Bayesian classifier. Molecular Ecology Resources. 14(5), 929-942.
[13] Rudoy, A. and Ribera, I. (2016) The macroevolution of size and complexity in insect male genitalia. Peer J. 4, e1882
[14] Rudoy, A., Beutel, R. and Ribera, I. (2016) Evolution of the male genitalia in the genus *Limnebius* Leach, 1815 (Coleoptera, Hydraenidae). Zoological Journal of the Linnean Society. 178(1), 97-127.
[15] Vialle, A., Feau, N., Allaire, M., Didukh, M., Martin, F., Moncalvo, J.M. and Hamelin, R.C. (2009) Evaluation of mitochondrial genes as DNA barcode for Basidiomycota. Mol. Ecol. Resour. 9(s1), 99-113.
[16] Damon, C., Barroso, G., Férandon, C., Ranger, J., Fraissinet-Tachet, L. and Marmeisse, R. (2010) Performance of the *COX1* gene as a marker for the study of metabolically active Pezizomycotina and *Agaricomycetes* fungal communities from the analysis of soil RNA. FEMS Microbiology Ecology. 74, 693–705.
[17] Nilsson, R.H., Ryberg, M., Abarenkov, K., Sjokvist, E. and Kristiansson, E. (2008) The ITS region as a target for characterization of fungal communities using emerging sequencing technologies. FEMS Microbiol. Lett. 296, 97–101
[18] Hendrich, L., Pons, J., Ribera, I. and Balke, M. (2010) Mitochondrial cox1 sequence data finds patterns of insect dendritic reliably uncover patterns of insect diversity but suffer from high lineage-idiosyncratic error rates. PLos ONE. 5(12), e14448.

Received: **13.06.2017**
Accepted: **02.12.2017**

CORRESPONDING AUTHOR

Ahmet Kasapoglu
Mustafa Kemal University,
Science and Art Faculty,
Department of Biology,
TR-31060, Hatay – Turkey

e-mail: aksp25@yahoo.com

© by PSP Volume 27 – No. 2/2018 pages 928-937 Fresenius Environmental Bulletin

BIOACCUMULATION OF Al, Cu AND Zn IN COONTAIL (*CERATOPHYLLUM DEMERSUM* L.) AFTER EXPERIMENTAL EXPOSURE TO A METAL COCKTAIL "POLLUTION EVENT"

Judith Lize Arnolds[1,3,*], Reinette Georgenie Snyman[2], James Philander Odendaal[1]

[1]Department of Environmental and Occupational Studies, Faculty of Applied Sciences, Cape Peninsula University of Technology, PO Box 652, Cape Town, 8000, South Africa
[2]Department of Conservation and Marine Sciences, Faculty of Applied Sciences, Cape Peninsula University of Technology, PO Box 652, Cape Town, 8000, South Africa
[3]South African National Biodiversity Institute, Private Bag X7, Claremont, 7735, Cape Town, South Africa

ABSTRACT

Metal pollution is of major concern because metals can be bioaccumulated in aquatic organisms and have high toxicity. Metal concentrations can be increased along the food chain and could potentially threaten environmental and human health. As the coontail (*Ceratophyllum demersum* L.) is rootless, it is advantageous for use in laboratory bioassays as this would eliminate the complication of soil-root-continuum and shoot-root metal partitioning. It thus has the potential to be a suitable model for investigating metal stress in plants. The research objective was to determine the degree of Al, Cu and Zn bioaccumulation in *C. demersum* L. after exposure to a metal cocktail in a simulated "pollution event" under laboratory conditions over a five week exposure period. Plants were divided into four experimental treatment groups, each with different exposure concentrations of Al ($AlSO_4$), Cu ($CuSO_4$) and Zn ($ZnSO_4$) in mixture. A fifth uncontaminated group of plants served as the control. Aluminium, Cu and Zn concentrations were determined in water and plant samples by means of nitric acid digestion and ICP-MS analysis. This macrophyte proved highly effective in the accumulation of these metals at all four exposure concentrations. The results showed that concentrations of the metals in the water varied in all treatments over time with no specific patterns emerging amongst the treatment groups. The metal bioaccumulation in *C. demersum* was also variable between consecutive weeks per treatment and between consecutive treatments per week. This may be due to *C. demersum* being able to regulate Al, Cu, and Zn throughout the exposure period. The plant accumulated metals in the order: Zn>Al>Cu.

KEYWORDS:
Aquatic, exposure concentrations, metal bioaccumulation, plants, pollution event

INTRODUCTION

Metal pollution in aquatic ecosystems and aquatic plants. Metal pollution is of major concern because metals can be bioaccumulated in aquatic organisms and have high toxicity. Metal concentrations can be increased along the food chain and could potentially threaten environmental and human health [1, 2, 3]. Metals from geological origin can naturally enter the river system by weathering or erosion [4] or be produced by the slow leaching from soil/rock water at low concentrations with no serious toxic effects on human health [5]. They can also be produced through anthropogenic activities due to industrial processing, mining, agricultural, urban activities and sewage disposal. Metals have proven to be very damaging to aquatic habitats and species [6]. Small concentrations of trace metals are utilized by living organisms to stabilize protein structures, facilitate electron transfer reactions and catalyze enzymatic reactions, amongst other functions [7, 8]. Copper, Zn and Fe are essential constituents of catalytic sites for several enzymes, while other metals such as Pb, Hg and Cd may displace or substitute for essential trace metals and interfere with correct functioning of enzymes and associated cofactors [7].

Macrophytes can cover large areas and are the dominant primary producers in aquatic environments. Submerged macrophytes growing in polluted water bodies can absorb the toxic substances that enter the food chain and can pose a serious threat to environmental and human health [9]. *Ceratophyllum demersum* L. (family Ceratophyllaceae), a coontail, is a submerged, free floating rootless macrophyte. It is a perennial plant of cosmopolitan distribution and grows rapidly in shallow, muddy, quiescent water bodies with low light intensities. As *C. demersum* L. is rootless, it is advantageous for use in laboratory bioassays as this would eliminate the complication of soil-root-continuum and shoot-root metal partitioning. It thus has the potential to be a suitable

model for investigating metal stress in plants [10].

Aluminium is released to the environment mainly by natural processes such as erosion of rock and via various industrial processing that utilise Al. Aluminium is a potentially toxic metal and is probably not an important nutrient in organisms [11, 12]. It is well known for its toxic effect on plant growth and metabolism but their toxicity thresholds are highly variable [13].

Copper is associated with mines, industry, landfills and waste disposal. Most water soluble Cu is due to agricultural runoff, as Cu is an important ingredient of many fungicides [14]. Copper is found in surface water, groundwater, seawater and drinking water but it is primarily present in complexes or as particulate matter [15]. It is an essential trace element and is needed by plants as a micronutrient [16]. It is a constituent of hormones, vitamins, enzymes and nucleoprotein complexes. Copper is regulated by living organisms but excessive concentrations in organisms due to Cu pollution in the environment can potentially cause toxic effects [17].

Zinc is released into the environment in considerable amounts by both natural processes and anthropogenic activities [18,19]. Zinc is an essential element for plant metabolism although high levels of Zn inhibit many plant metabolic functions. This can result in limited growth and cause senescence [20]. Zinc pollution in freshwater bodies has been previously reported by various studies to exceed the environmental limit by up to 100 times [19, 21, 22].

It is unknown as to how quickly metals are bioaccumulated in this species, and to what degree, as well as whether there is a pattern of metal exchange between plant and water over time. The time factor is a particularly poignant question, when considering a "pollution event" in a river. Previous laboratory studies with aquatic plants have mostly been conducted over short exposure periods (e.g. 15 days) [23] or 7 days [24] but in the present study the exposure period is 5 weeks, and the water is only contaminated once, so as to simulate a "pollution event" and to study the metal exchange between the plants and the medium, a time period after the "event". This has not been attempted in a laboratory study before to the authors' knowledge.

The research objective was therefore to determine the degree of Al, Cu and Zn bioaccumulation in *C. demersum* L. after exposure to a metal cocktail in a simulated "pollution event" under laboratory conditions over a five week exposure period.

MATERIALS AND METHODS

Experimental design and growing conditions. For this greenhouse study *C. demersum* L. plants were collected from a reasonably clean and unpolluted fishpond at the greenhouse nursery, situated on the Cape Town campus of the Cape Peninsula University of Technology (CPUT), Cape Town, where it flourishes in a pond community with other macrophytes and fish. These plants occupy most of the available pond space and appear to be healthy. 150 plants were carefully removed from the pond and washed in deionized water to remove any debris that could be attached to the plants. Excess water was shaken off and each plant was weighed on a two decimal place Mettler balance (PC2200). Plants (± 8.5g each) were placed in 68L hydroponic containers (a total of 5 containers with thirty plants per container). Before metal exposure, plants were acclimatized for one week under laboratory conditions. The metals used (Al, Cu and Zn) were selected for this study as they are some of the most abundant metals previously measured in Western Cape river systems [25, 26, 27, 28, 29]. Plants were exposed to different exposure concentrations of Al ($AlSO_4$), Cu ($CuSO_4$) and Zn ($ZnSO_4$) in mixture (Table 1). These preparations were added to 10% Hoagland solution [30] in hydroponic containers. The plants were exposed for a period of 5 weeks. A fifth uncontaminated group of plants served as the control. Plants were kept in the same 10% Hoagland solution for the entire experimental period to simulate a single pollution event. Aeration in containers was achieved by using small pumps. There was no overcrowding of plants in the containers and the initial water volume was 68L. Additional stress factors were kept at a minimum.

Sampling procedures and metal analysis. Pre-exposure and during exposure electrical conductivity, pH, salinity and temperature of the water in each container were measured with a handheld multi-parameter instrument (Eutech PCSTEST35-01X441506 / Oakton 35425-10). Samples were collected every week from week 0 to week 5 from the containers in the greenhouse. During each sampling occasion, water samples were taken from each treatment group and the control, for metal analysis. Water samples were digested with 65% nitric acid using the method described by [31].

Five plants per treatment group and 5 plants from the control group were randomly harvested for metal analysis each week. The plants were individually washed in deionised water and blotted with paper. The plant samples were dried in an oven at 60°C for 48h. The dried plants were then weighed to obtain the dry weight. These samples were digested with 65% nitric acid using the method set out by [31].

Aluminium, Cu and Zn concentrations were determined using the ICP-MS (Inductively Coupled Plasma-Mass Spectrophotometer). The plant metal concentrations were expressed as mg/kg and the water metal concentrations as mg/L.

Statistical analysis. MediCalc Version 15.2.2 was used for all statistical analysis. ANOVA on Ranks was used to test for significant differences between metal concentrations. Post hoc analyses were done using the Student-Newman-Keuls (SNK) Test to determine statistical differences between treatment groups and between weeks ($P<0.05$).

RESULTS AND DISCUSSION

Physico-chemical parameters of the water. Electrical conductivity, pH, salinity and temperature of the water were measured in each treatment group during each sampling occasion. The electrical conductivity ranged from 0 to 535.41 mS/cm, the pH ranged from 6.33 to 8.45, the salinity ranged from 150.26 to 201.22 ppm and the temperature ranged from 20.82 to 29.06 °C.

Metals in water and plant samples. Aluminium. Comparisons of the mean Al concentrations in water and plant samples between weeks per treatment and between treatments per week are shown in Tables 2 and 3.

Aluminium concentrations varied in all the treatments in the water over all five weeks of exposure. However, no significant differences in Al concentrations were found between the start and the end of the experimental period in the different treatments. Only in the control, a significant decrease was found between the start and the end of the experiment. Significant increases in Al concentrations were detected in treatments T2 and T4 and a significant decrease in Al concentrations was detected in treatment T1 during week 1 (Table 2). After week 1 the Al concentrations decreased and increased on a weekly basis in the different treatments and the control. The Al concentrations in terms of the pooled data differed in the different treatment groups. The highest Al concentrations were found in the highest dosage treatment (T4) and the lowest Al concentrations were found in treatment T2 in terms of the pooled data (Table 2).

TABLE 1
Exposure concentrations (mg/l) of metals provided to the different experimental treatment groups

Treatments (T)	T1	T2	T3	T4
AlSO4	25.5	51.0	102.0	204.0
CuSO4	0.85	1.7	3.4	6.8
ZnSO4	8.5	17.0	34.0	68.0

TABLE 2
Mean (±SD) Al concentrations (mg/L) measured in the water from the experimental treatments, per week. n=5

	Treatments				
Weeks	**Control**	**T1**	**T2**	**T3**	**T4**
0 (baseline)	$^{a}1.54^{a}$ ±0.22	$^{a}1.11^{b}$ ±0.48	$^{a}0.00^{c}$ ±0.00	$^{a}0.00^{c}$ ±0.00	$^{a}0.77^{d}$ ±0.10
1	$^{*b}0.00^{a}$ ±0.00	$^{*b}0.01^{b}$ ±0.01	$^{*b}2.06^{c}$ ±0.23	$^{a}0.76^{d}$ ±0.27	$^{*b}2.02^{e}$ ±0.28
2	$^{*c}0.03^{a}$ ±0.04	$^{*b}0.10^{a}$ ±0.04	$^{c}0.00^{a}$ ±0.00	$^{*b}0.90^{b}$ ±0.09	$^{*c}0.17^{b}$ ±0.05
3	$^{c}2.07^{a}$ ±0.40	$^{*b}0.01^{b}$ ±0.01	$^{c}0.01^{b}$ ±0.03	$^{*c}1.84^{c}$ ±0.19	$^{*d}0.22^{d}$ ±0.03
4	$^{*d}0.00^{a}$ ±0.00	$^{b}0.04^{a}$ ±0.08	$^{c}0.00^{a}$ ±0.00	$^{d}0.00^{a}$ ±0.00	$^{*d}0.00^{a}$ ±0.00
5	$^{*c}0.02^{a}$ ±0.05	$^{c}2.62^{b}$ ±0.46	$^{c}0.00^{c}$ ±0.00	$^{d}0.40^{d}$ ±0.12	$^{e}1.37^{e}$ ±0.19
Pooled data for entire experimental period	**0.61^{a} ±0.11**	**0.66^{a} ±0.18**	**$^{b}0.35^{b\#}$ ±0.04**	**0.65^{c} ±0.11**	**0.76^{d} ±0.11**

Different letters on the left side of mean values indicate statistical significant differences between consecutive weeks per treatment and significant differences between week 0 and other weeks are indicated by *. Different letters on the right side of mean values indicate statistical significant differences between consecutive treatments per week and significant statistical differences between the control and consecutive treatments are indicated by # (Student-Newman-Keuls (SNK) post hoc test ($p<0.05$)). 0 = week 0 (start of experiment/baseline); 1 = week 1 of exposure; 2 = week 2 of exposure; 3 = week 3 of exposure; 4 = week 4 of exposure; 5 = week 5 of exposure.

TABLE 3
Mean (±SD) Al concentrations (mg/kg) measured in *Ceratophyllum demersum* L. from the experimental treatments, per week. n=5

	Treatments				
Weeks	**Control**	**T1**	**T2**	**T3**	**T4**
0 (baseline)	$^{a}3054.50^{a}$ ±1336.74	$^{a}3983.20^{a}$ ±812.47	$^{a}2511.75^{a}$ ±678.35	$^{a}2764.82^{a}$ ±703.12	$^{a}2462.83^{a}$ ±359.19
1	$^{a}2820.05^{a}$ ±536.75	$^{a}4155.08^{b}$ ±939.55	$^{*b}5311.53^{b}$ ±1345.83	$^{*b}4048.75^{b}$ ±2036.90	$^{*b}4457.82^{b}$ ±1982.52
2	$^{a}2145.77^{a}$ ±334.35	$^{*b}2506.37^{a}$ ±613.09	$^{c}2536.65^{a}$ ±376.74	$^{*b}4826.92^{b}$ ±1170.06	$^{*b}4476.17^{b}$ ±721.55
3	$^{b}3056.20^{a}$ ±1521.92	$^{*c}6026.11^{b}$ ±1807.53	$^{*d}4279.51^{b}$ ±743.88	$^{b}3580.79^{b}$ ±1924.17	$^{*c}9245.92^{c}$ ±2175.70
4	$^{*b}5067.31^{a}$ ±1021.68	$^{*d}2291.91^{b}$ ±589.05	$^{e}2189.13^{b}$ ±218.60	$^{b}5677.85^{c}$ ±1386.06	$^{*d}2376.46^{d}$ ±659.99
5	$^{*c}1348.85^{a}$ ±261.65	$^{e}3903.26^{b}$ ±1065.56	$^{*f}4434.84^{b}$ ±854.32	$^{*b}4722.93^{b}$ ±1381.44	$^{*e}7153.18^{c}$ ±1005.67
Pooled data entire experimental period	**2915.45^{a} ±1130.10**	**$3810.99^{b\#}$ ±971.21**	**3543.90^{b} ±702.95**	**$4270.34^{c\#}$ ±1433.63**	**$5028.73^{c\#}$ ±1150.67**

Different letters on the left side of mean values indicate statistical significant differences between consecutive weeks per treatment and significant differences between week 0 and other weeks are indicated by *. Different letters on the right side of mean values indicate statistical significant differences between consecutive treatments per week and significant statistical differences between the control and consecutive treatments are indicated by # (Student-Newman-Keuls (SNK) post hoc test ($p<0.05$)). 0 = week 0 (start of experiment/baseline); 1 = week 1 of exposure; 2 = week 2 of exposure; 3 = week 3 of exposure; 4 = week 4 of exposure; 5 = week 5 of exposure.

The Al concentrations increased in all the treatments and decreased in the control in week 1 in the plants and generally fluctuated thereafter from week to week during the experimental period. This fluctuating trend corresponds with that of the water concentrations (Table 2). The Al concentrations in the plants declined after week 1 and increased significantly at week 3 in the control. The Al concentrations in all the other treatments varied between the weeks. The highest accumulation occurred during week 3 in treatment T4 (9245.92 ± 2175.70 mg/kg). Significant increases in Al concentrations were found between the start and the end of the experiment in treatments T2, T3 and T4. A significant decrease in Al concentrations was found between week 0 and week 5 in the control. The fluctuating Al concentrations in the water and plant samples are indicative of a regulation system where Al bioaccumulates in the plants up to a point and where excess Al is released into the water from the plants [32]. After reaching a certain threshold concentration in the plant, the Al is eliminated by physiological mechanisms [33].

The pooled data revealed that Al accumulation in plants increased with higher Al exposure. After five weeks of exposure to Al the plants in three of the treatments (T2, T3 and T4) showed significantly higher Al concentrations compared to the control plants. There is thus a positive relationship between Al exposure concentration and Al bioaccumulation in *C. demersum* L. The results of this study are similar to the results found in common buckwheat (*Fagopyrum esculentum*) [34] and also in both tartary buckwheat (*Fagopyrum tataricum Gaertn cv. Rotundatum*) and wild buckwheat (*Fagopyrum homotropicum Ohnishi cv. Mianshawan*) [35]. The present study has found high Al accumulation that could possibly be attributed to the uptake and xylem loading of aluminium [35]. [36] reported a 25 to 43-fold increase in uptake of Al following exposure to Al in duckweed (*Lemna minor* L.). Many variables influence the uptake and storage of metals within plants, especially that of the bioavailability of metals. The other metals in the water could have influenced the bioaccumulation of Al in the plants [37].

Copper. Comparisons of the mean Cu concentrations in water and plants between weeks per treatment and between treatments per week are shown in Tables 4 and 5.

The Cu concentrations varied in all the treatments in the water over all five weeks of exposure. However, no significant differences in Cu concentrations were found between the start and the end of the experimental period in the different treatments, except for the control where a significant increase in Cu concentrations was found. A significant increase in Cu concentrations in the control and significant decreases in Cu concentrations in treatments T1 and T4 were found during week 1. After week 1 the Cu concentrations decreased and increased from week to week in the different treatments and the control. The pooled data also revealed differences in Cu concentrations in the water for some of the treatments compared to the control (Table 4).

TABLE 4
Mean (±SD) Cu concentrations (mg/L) measured in the water from the experimental treatments, per week. n=5

	Treatments				
Weeks	**Control**	**T1**	**T2**	**T3**	**T4**
0 (baseline)	$^{a}0.00^{a}$ ±0.00	$^{a}1.79^{b}$ ±0.26	$^{a}0.55^{c}$ ±0.04	$^{a}1.95^{d}$ ±0.04	$^{a}0.05^{e}$ ±0.03
1	$^{*b}1.59^{a}$ ±0.05	$^{*b}0.07^{b}$ ±0.08	$^{a}0.49^{c}$ ±0.06	$^{*b}0.37^{d}$ ±0.07	$^{a}0.05^{e}$ ±0.04
2	$^{*c}0.36^{a}$ ±0.42	$^{*b}0.00^{a}$ ±0.00	$^{*b}0.28^{a}$ ±0.09	$^{*c}0.00^{a}$ ±0.00	$^{*b}0.42^{a}$ ±0.07
3	$^{*d}1.38^{a}$ ±0.67	$^{*c}0.49^{b}$ ±0.00	$^{*c}0.01^{c}$ ±0.03	$^{*d}0.92^{d}$ ±0.08	$^{*b}0.67^{e}$ ±0.12
4	$^{*d}0.90^{a}$ ±0.71	$^{*d}0.00^{b}$ ±0.00	$^{*d}0.31^{c}$ ±0.08	$^{*e}0.46^{d}$ ±0.16	$^{*b}0.71^{e}$ ±0.10
5	$^{*e}0.37^{a}$ ±0.08	$^{d}0.00^{b}$ ±0.00	$^{e}0.01^{b}$ ±0.01	$^{f}0.99^{c}$ ±0.11	$^{b}0.79^{d}$ ±0.07
Pooled data for entire experimental period	**0.77^{a} ±0.45**	**$0.39^{b\#}$ ±0.06**	**$0.27^{c\#}$ ±0.05**	**0.78^{d} ±0.08**	**0.45^{d} ±0.07**

Different letters on the left side of mean values indicate statistical significant differences between consecutive weeks per treatment and significant differences between week 0 and other weeks are indicated by *. Different letters on the right side of mean values indicate statistical significant differences between treatments per week and significant statistical differences between the control and treatments are indicated by # (Student-Newman-Keuls (SNK) post hoc test ($p<0.05$)). 0 = week 0 (start of experiment/baseline); 1 = week 1 of exposure; 2 = week 2 of exposure; 3 = week 3 of exposure; 4 = week 4 of exposure; 5 = week 5 of exposure.

TABLE 5
Mean (±SD) Cu concentrations (mg/kg) measured in *Ceratophyllum demersum* L. from the experimental treatments, per week. n=5

	Treatments				
Weeks	**Control**	**T1**	**T2**	**T3**	**T4**
0 (baseline)	$^{a}1237.74^{a}$ ±261.59	$^{a}607.66^{b}$ ±170.34	$^{a}315.78^{c}$ ±82.74	$^{a}333.65^{c}$ ±85.49	$^{a}204.72^{d}$ ±32.35
1	$^{*b}291.29^{a}$ ±49.32	$^{a}487.44^{b}$ ±112.831	$^{*b}1485.83^{c}$ ±262.23	$^{*b}694.91^{d}$ ±68.91	$^{*b}1258.83^{e}$ ±45.86
2	$^{*c}539.62^{a}$ ±84.42	$^{a}481.79^{a}$ ±116.41	$^{*c}845.33^{b}$ ±72.53	$^{*c}2729.60^{c}$ ±750.56	$^{*c}3190.04^{c}$ ±540.19
3	$^{*d}305.48^{a}$ ±28.37	$^{b}672.92^{b}$ ±115.84	$^{*d}1158.31^{c}$ ±216.625	$^{*d}749.70^{d}$ ±100.41	$^{*d}1170.39^{e}$ ±272.40
4	$^{e}755.82^{a}$ ±55.82	$^{*c}310.52^{b}$ ±79.50	$^{*e}479.59^{c}$ ±120.04	$^{*e}1594.33^{d}$ ±426.87	$^{*e}2564.83^{e}$ ±351.23
5	$^{*f}222.52^{a}$ ±39.55	$^{*d}2259.71^{b}$ ±345.91	$^{*f}644.34^{c}$ ±120.86	$^{*e}2001.79^{d}$ ±539.20	$^{*e}2083.86^{d}$ ±293.01
Pooled data for entire experimental period	**558.75^{a} ±86.51**	**803.34^{a} ±156.81**	**$821.53^{a\#}$ ±145.84**	**$1350.66^{a\#}$ ±270.09**	**$1745.44^{a\#}$ ±255.84**

Different letters on the left side of mean values indicate statistical significant differences between consecutive weeks per treatment and significant differences between week 0 and other weeks are indicated by *. Different letters on the right side of mean values indicate statistical significant differences between consecutive treatments per week and significant statistical differences between the control and consecutive treatments are indicated by # (Student-Newman-Keuls (SNK) post hoc test ($p<0.05$)). 0 = week 0 (start of experiment/baseline); 1 = week 1 of exposure; 2 = week 2 of exposure; 3 = week 3 of exposure; 4 = week 4 of exposure; 5 = week 5 of exposure.

According to [38] Cu is more soluble in acidic waters at pH values below 6.5. A possible explanation for the variation in the results of the present study could be that the pH of the water in the control and different treatments changed from slightly acidic during week 0 to slightly alkaline during week 3 and to more neutral during week 5. This variation of pH from one week to another may affect the bioavailability of metals. The uptake of metals by plants is dependent on the bioavailability of metals in water

[39]. The Cu concentrations in the plants varied between weeks in all the treatments and the control. This may be due to the varying pH values of the water, resulting in varying bioavailability of Cu. The lowest pH in this study (6.33) and the highest Cu concentrations were found during week 2 in treatment T4 (3190.04 ± 540.19 mg/kg). This is evidence of the effect of lower pH values on the bioaccumulation of Cu. Accumulation of metals in various parts of higher plants is often accompanied by an induction of a variety of cellular changes, some of which directly add to metal tolerance capacity of plants [40]. Copper appears to be relatively mobile in plants [41]. The varying Cu concentrations between the weeks per treatment and between treatments per week in *C. demersum* L. in the present study could be indicative of bioaccumulation and the plants releasing Cu into the water through the leaves over time or when decaying started [32]. However, in general, significant increases in Cu concentrations in plants were found between the start and the end of the experiment in all the treatments, while Cu concentrations in plants significantly decreased between week 0 and week 5 in the control (Table 5). The pooled data also revealed an increase in Cu concentrations in the plants with higher Cu dosage, compared to the control. Therefore, Cu bioaccumulated, overall in Cu-exposed *C. demersum* over the experimental period. Significant accumulation of Cu has also been observed in other macrophytes, such as *Lemna trisulca* [42], *Vallisneria spiralis* [43], *Potamogeton pectinatus* and *Potamogeten malaianus* [44].

A possible reason for the rapid uptake (see week 1 concentrations in Table 5) of Cu in treatments T2, T3 and T2 was that the plants were not physiologically adapted to the polluted environment and was more vulnerable to taking up Cu during the first week of exposure. After week 1 the plants might have adapted physiologically to the environment and could regulate the uptake and accumulation of Cu in the plants, resulting in fluctuations in Cu concentrations in plants over the rest of the exposure period. A possible reason for this fluctuation could be that a down regulation mechanism for Cu uptake might exist. Another reason for the fluctuations of the Cu concentrations between weeks in the different treatments might be due to the plant attempting to internally regulate concentrations of the metal over time to reduce the toxicity. Some metals such as Cu negatively affect cell membrane integrity causing an increase in electrical conductivity of water [17,45], as observed in this study. The toxicity of Cu in combination with other metals in water can also cause oxidative stress over time, resulting in lipid peroxidation and ion leakage [17].

Zinc. Comparisons of the mean Zn concentrations in water and plant samples between weeks per treatment and between treatments per week are shown in Tables 6 and 7.

TABLE 6
Mean (±SD) Zn concentrations (mg/L) measured in the water from the experimental treatments, per week. n=5

	Treatments				
Weeks	**Control**	**T1**	**T2**	**T3**	**T4**
0 (baseline)	$^{a}0.29^{a}$ ±0.06	$^{a}0.38^{a}$ ±0.14	$^{a}0.03^{b}$ ±0.02	$^{a}0.11^{c}$ ±0.02	$^{a}0.61^{d}$ ±0.13
1	$^{*b}0.15^{a}$ ±0.04	$^{*b}3.58^{a}$ ±0.73	$^{*b}0.88^{b}$ ±0.06	$^{a}0.18^{c}$ ±0.09	$^{a}0.71^{d}$ ±0.07
2	$^{*c}0.56^{a}$ ±0.12	$^{c}0.33^{a}$ ±0.03	$^{*c}0.13^{b}$ ±0.05	$^{*b}1.27^{c}$ ±0.08	$^{*b}0.21^{d}$ ±0.12
3	$^{c}0.29^{a}$ ±0.01	$^{c}0.54^{a}$ ±0.06	$^{*d}2.09^{a}$ ±0.15	$^{*c}0.39^{a}$ ±0.06	$^{c}0.58^{a}$ ±0.35
4	$^{c}0.32^{a}$ ±0.07	$^{*c}1.00^{a}$ ±0.52	$^{*c}0.60^{b}$ ±0.17	$^{*d}0.22^{c}$ ±0.08	$^{*d}0.00^{d}$ ±0.00
5	$^{*d}0.31^{a}$ ±0.23	$^{d}0.05^{a}$ ±0.00	$^{*c}0.66^{a}$ ±0.17	$^{*c}0.81^{a}$ ±0.18	$^{c}0.33^{a}$ ±0.10
Pooled data for entire experimental period	**0.32^{a} ±0.09**	**0.98^{a} ±0.25**	**0.48^{a} ±0.29**	**0.50^{a} ±0.09**	**0.41^{a} ±0.13**

Different letters on the left side of mean values indicate statistical significant differences between consecutive weeks per treatment and significant differences between week 0 and other weeks are indicated by *. Different letters on the right side of mean values indicate statistical significant differences between treatments per week and significant statistical differences between the control and treatments are indicated by # (Student-Newman-Keuls (SNK) post hoc test ($p<0.05$)). 0 = week 0 (start of experiment/baseline); 1 = week 1 of exposure; 2 = week 2 of exposure; 3 = week 3 of exposure; 4 = week 4 of exposure; 5 = week 5 of exposure.

TABLE 7
Mean (±SD) Zn concentrations (mg/kg) measured in *Ceratophyllum demersum* L. from the experimental treatments, per week. n=5

	Treatments				
Weeks	**Control**	**T1**	**T2**	**T3**	**T4**
0 (baseline)	$^{a}23761.87^{a}$ ±4682.74	$^{a}4682.74^{b}$ ±1562.26	$^{a}4002.61^{c}$ ±1079.67	$^{a}6577.51^{d}$ ±513.38	$^{a}4549.14^{e}$ ±435.56
1	$^{*b}4778.22^{a}$ ±840.04	$^{a}7170.24^{b}$ ±958.83	$^{*b}12825.28^{c}$ ±1984.40	$^{*b}10776.28^{c}$ ±1183.40	$^{*a}7887.63^{d}$ ±609.60
2	$^{c}13789.37^{a}$ ±1469.12	$^{*b}2833.40^{b}$ ±509.10	$^{*c}5618.93^{c}$ ±826.41	$^{*c}20943.08^{d}$ ±5677.53	$^{*b}11548.90^{e}$ ±1501.15
3	$^{*c}9770.83^{a}$ ±3122.60	$^{*c}8404.34^{a}$ ±1435.38	$^{*d}10586.33^{a}$ ±1806.18	$^{d}5897.71^{a}$ ±2754.29	$^{*c}9136.63^{a}$ ±200.74
4	$^{*d}4447.00^{a}$ ±539.48	$^{*d}3037.53^{a}$ ±871.17	$^{*c}6480.33^{b}$ ±1574.26	$^{*e}8319.49^{c}$ ±165.59	$^{*d}8274.97^{c}$ ±937.16
5	$^{*d}5064.29^{a}$ ±920.22	$^{*e}16279.74^{b}$ ±2315.86	$^{f}4331.57^{c}$ ±1019.55	$^{*e}12847.43^{d}$ ±1619.00	$^{*e}16518.26^{d}$ ±2344.67
Pooled data for entire experimental period	^{a}**10268.60** ±1929.03	^{a}**5227.45** ±1275.43	^{a}**7307.51** ±1381.74	^{b}**10893.58** ±1985.53	^{b}**9652.60** ±1004.81

Different letters on the left side of mean values indicate statistical significant differences between consecutive weeks per treatment and significant differences between week 0 and other weeks are indicated by *. Different letters on the right side of mean values indicate statistical significant differences between consecutive treatments per week and significant statistical differences between the control and consecutive treatments are indicated by # (Student-Newman-Keuls (SNK) post hoc test ($p<0.05$)). 0= week 0 (start of experiment/baseline); 1 = week 1 of exposure; 2 = week 2 of exposure; 3 = week 3 of exposure; 4 = week 4 of exposure; 5 = week 5 of exposure.

The Zn concentrations in water samples decreased significantly in the control and increased significantly in the lower exposure treatment groups during week 1, relative to week 0 (Table 6). No significant differences in Zn concentrations were found in the higher exposure treatment groups during week 1, relative to week 0. Significant differences were found between the start and the end of the experiment after the five week exposure period for some of the treatments (Table 6).

Zinc concentrations differed in all the treatments between weeks. The lowest mean Zn concentration was found in week 2 (2833 ± 509.10 mg/kg) in treatment T1 and the highest mean concentration among the experimental treatment groups was measured in week 2 (20943 ± 5677.53 mg/kg) in treatment T3 in the plants (Table 7). Such high concentrations of Zn may affect physiological processes in the plants [46]. Growth inhibition and chlorosis may be possible consequences of Zn toxicity [20]. The Zn concentrations in all the treatments except for the control increased after week 1 of exposure, although not all increases were statistically significant, and then fluctuated in all the other weeks compared to week 0. Zn concentrations varied per week in the different treatments compared to the control. Significant increases between the start and the end of the experiment were found in treatments T1, T3 and T4. A significant decrease between the start and the end of the experiment was found in the control. The pooled data revealed that higher Zn exposure concentrations lead to greater bioaccumulation. Greater accumulation of Zn than Al in *Lemna minor* was found in a study by [36]. The results of this study are similar to the results found by [36]. In studies by [48] and [49] significant Zn accumulation in *Hydrilla verticillata* plants were also found. The mixture of metals in the water and their interactions may have played a role in the bioavailability of Zn and its bioaccumulation in *C. demersum*. Interactions between a combination of metals in solution are often complex and are dependent on the metal concentration and pH of the growth medium [46].

CONCLUSION

Ceratophyllum demersum was tested for the bioaccumulation of metals (Al, Cu, Zn) over a 5 week period under laboratory conditions. Contrary to how many other experimental exposure studies on aquatic plants were done, as seen in the literature, the water was contaminated once off in the beginning of the experiments to simulate a "pollution event". The 5 week exposure period was also longer than in most other studies in order to investigate variability over time. This macrophyte proved highly effective in the accumulation of these metals at all four exposure concentrations. The results showed that concentrations of the metals in the water varied in all treatments over time with no specific patterns emerging

amongst the treatment groups. The metal concentrations in the plants were much higher compared to the metal concentrations in the water. The metal bioaccumulation in *C. demersum* was also variable between consecutive weeks per treatment and between consecutive treatments per week over a five week exposure period. This may be due to *C. demersum* being able to regulate Al, Cu, and Zn throughout the exposure period. The plant accumulated metals in the order: Zn>Al>Cu. The results show that metals are bioaccumulated quickly by *C. demersum* after the water is contaminated with metals, i.e. after the "pollution event". However, over time, metals are continuously exchanged between the plants and the water, accounting for the fluctuations in metal concentrations observed over time. Therefore, the authors are of the opinion that should this species be used as a phytoremediator, the plants need to be removed from the contaminated water a week or two after the pollution event. It may be necessary to replace remediator plants until the metal levels are reduced to acceptable concentrations in the contaminated water. Further research is required on the use of *C. demersum* as a phytoremediator.

ACKNOWLEDGEMENTS

The authors wish to thank the Cape Peninsula University of Technology for financial support.

REFERENCES

[1] Jin, L. (1992) Environment. Bionomy (1st Ed.) High Education Press, Beijing.

[2] Zhou, Q., Zhang, J., Fu, J., Shi, J., Jiang, G. (2008) Review: Biomonitoring: an appealing tool for assessment of metal pollution in the aquatic ecosystem. Analytica Chimica Acta. 606, 135-150.

[3] Kaushik, A., Kansal, A., Meena, S., Kumari, S., Kaushik, C.P. (2009) Heavy metal contamination of river Yamuna, Haryana, India. Assessment by metal enrichment factor of the sediments. Journal of Hazardous Materials. 164(1), 265-270.

[4] Zhang, J., Huang, W.W. (1993) Dissolved trace metals in the Huanghe: the most turbid large river in the World. Water Research. 27(1), 1-8.

[5] Abbasi, S.A., Abbasi, N., Soni, R. (1998) Heavy metals in the environment. Metal publications. New Delhi, India.

[6] Ash, C., Stone, R. (2003) A question of dose. Science. 300, 925.

[7] Torres, M.A., Barros, M.P., Campos, S.C.G., Pinto, E., Rajamani, S., Sayre, R.T., Colepicolo, P. (2008) Biochemical biomarkers in algae and marine pollution: A review. Ecotoxicology and Environmental Safety. 71, 1-15.

[8] Gupta, M., Chandra, P. (1998) Bioaccumulation and toxicity of mercury in rooted-submerged macrophyte Vallisneria spiralis. Environmental Pollution. 103, 327-332.

[9] Aravind, P., Prasad, M.N.V., Malec, P., Waloszek, A., Strzałka, K. (2009) Zinc protects Ceratophyllum demersum L. (free-floating hydrophyte) against reactive oxygen species induced by cadmium. Journal of Trace Elements in Medicine and Biology. 23, 50-60.

[10] Department of Water Affairs and Forestry (DWAF) (1996) South African Water Quality Guidelines. Volume 7: Aquatic Ecosystems. Department of Water Affairs and Forestry.

[11] Fodor, F. (2002) Physiological responses of vascular plants to heavy metals. In: Prasad, M.N.V., Strzatka, K. (Eds.) Physiology and Biochemistry of metal Toxicity and Tolerance in Plants. Kluwer Academic Publisher, Netherlands, 149-177.

[12] Umebese, C.E., Motajo, A.J. (2008) Accumulation, tolerance and impact of aluminium, copper and zinc on growth and nitrate reductase activity of *Ceratophyllum demersum* (Hornwort). Journal of Environmental Biology. 29(2), 197-200.

[13] Walker, C.H., Hopkin, S.P., Sibly, R.M., Peakall, D.B. (2006) Principles of Ecotoxicology. 3rd Edition. Taylor and Francis. London.

[14] Agency for Toxic Substances and Disease Registry (ATSDR). (2008) Toxicological profile for aluminium. Atlanta, GA, US Department of Health and Human Services, Public Health Service (TP-91/01).

[15] Brown, B.T., Rattigan, B.M. (1979) Toxicity of soluble copper and other metal ions to *Elodea canadensis*. Environmental Pollution. 20, 303–314.

[16] Devi, S.R., Prasad, M.N.V. (1998) Copper toxicity in *Ceratophyllum demersum* L. (Coontail), a free floating macrophyte: response of antioxidant enzymes and antioxidants. Plant Science. 138, 157-165.

[17] Gensemer, R.W., Playle, R.C. (1999) The bioavailability and toxicity of aluminium in aquatic environments. Critical Reviews in Environmental Science and Technology. 29, 315–450.

[18] Shikazono, N., Zakir, H.M., Sudo, Y. (2008) Zinc contamination in river water and sediments at Taisyu Zn-Pb mine area, Tsushima Island Japan. Journal of Geochemical Exploration. 98, 80-88.

[19] Rout, G.R., Das, P. (2003) Effect of metal toxicity on plant growth and metabolism: I. Zinc. Agronomie. 23, 3-11.

[20] Srikanth, R., Madhumohan Rao, A., Shravan Kumar, C.H., Khanum, A. (1993) Lead, cadmium, nickel and zin contamination of groundwater around Hussain Sagar Lake, Hyderabad, India. Bulletin of Environmental Contamination and Toxicology. 50, 138–143.

[21] Pistelok, F., Galas, W. (1999) Zinc pollution of the Przemsza River and its tributaries. Polish Journal of Environmental Studies. 8, 47–53.
[22] Rai, U.N., Sinha, S., Tripathi, R.D., Chandra, T.P. (1995) Wastewater treatability potential of some aquatic macrophytes: removal of heavy metals. Ecological Engineering. 5, 5-12.
[23] Malar, S., Vikram, S.S., Favas, P.J.C., Perumal, V. (2014) Lead heavy metal toxicity induced changes on growth and antioxidative enzymes level in water hyacinths (*Eichhornia crassipes* (Mart.)). Botanical Studies. 55, 54.
[24] Jackson, V.A., Paulse, A.N., Van Stormbroek, T., Odendaal, J.P., Khan, W. (2007) Investigation into the predominant metals contaminating the Berg River, Western Cape, South Africa. Water SA. 33(2), 175-182.
[25] Shuping L.S. (2008) Biomonitoring of metal contamination in the lower Diep River, Milnerton, Western Cape. M. Tech. thesis. Cape Peninsula University of Technology, South Africa.
[26] Ayeni, O.O., Ndakidemi, P.A., Snyman, R.G. and Odendaal, J.P. (2010) Metal contamination of soils collected from four different sites along the lower Diep River, Cape Town, South Africa. International Journal of the Physical Sciences. 5(13), 2045 – 2051.
[27] Erasmus, D.V. (2012) Metal Bioaccumulation, Membrane Integrity and Chlorophyll Content in the Aquatic Macrophyte Ceratophyllum Demersum from the Diep River, Western Cape. Thesis (M.Tech. (Horticulture))-Cape Peninsula University of Technology.
[28] Jackson, V.A., Paulse, A.N., Odendaal, J.P. and Khan, W. (2013) Identification of point sources of metal pollution in the Berg River, Western Cape, South Africa. Water, Air and Soil Pollution. 224, 1477.
[29] Hoagland, D.R., Arnon, D.I. (1950) The water-culture method for growing plants without soil. California Agricultural Experiment Station. 347(2), 32.
[30] Shuping, L.S., Snyman, R.G., Odendaal, J.P., Ndakidemi, P.A. (2011) Accumulation and distribution of metals in *Bolboschoenus maritimus* (Cyperaceae), from a South African River. Water, Air and Soil Pollution. (216), 319-328.
[31] Kähkönen, M.A., Manninen, P.K.G. (1998) The uptake of nickel and chromium from water by *Elodea canadensis* at different nickel and chromium exposure levels. 36, 1381–1390.
[32] Wright, D.A., Welbourn, P. (2002) Environmental toxicology. Cambridge Environmental Chemistry Series 11. Cambridge University Press. Cambridge.
[33] Ma, J.F., Zheng, S.J., Matsumoto, H. (1997) Specific secretion of citric acid induced by Al stress in *Cassia tora* L. Plant and Cell Physiology. 38(9), 1019-1025.
[34] Wang, H., Chen, R.F., Iwashita, T., Shen, R.F., Ma, J.F. (2015) Physiological characterization of aluminium tolerance and accumulation in tartary and wild buckwheat. New Phytologist. 205, 273–279.
[35] Radić, S., Babić, M., Škobić, D., Roje, V., Branka, P-K. (2010) Ecotoxicological effects of aluminium and zinc on growth and antioxidants in *Lemna minor* L. Ecotoxicology and Environmental Safety. 73, 336-342.
[36] Robinson, B.H., Lombi, E., Zhao, F.J., McGrath, P. (2003) Uptake and distribution of nickel and other metals in the hyperaccumulator *Berkheya coddii*. New Phytologist. 158(2), 279-285.
[37] Jones, G.B., Belling, G.B. (1967) The movement of copper, molybdenum and selenium in soils as indicated by radioactive isotopes. Australian Journal of Agricultural Research. 18, 733-740.
[38] Tangahu, B.V., Abdullah, S.R.S., Basri, H., Idris, M., Anuar, N., Mukhlisin, M. (2011) A review of heavy metals (As, Pb and Hg) uptake by plants through phytoremediation. International Journal of Chemical Engineering. 2011, Article ID 939161.
[39] Phillips, D.J.H. (1977) The use of biological indicator organisms to monitor trace metal pollution in marine and estuarine environments – a review. Environmental Pollution. 13, 281- 317.
[40] Mal, T., Andorran, P., Corbett, A. (2002) Effect of copper on growth of an aquatic macrophyte *Elodea canadensis*. Environmental Pollution. 120, 307-311.
[41] Prasad, M.N.V., Malec, P., Waloszek, A., Bojko, M., Strzalka, K. (2001) Physiological responses of *Lemna trisulca* L. (duckweed) to cadmium and copper bioaccumulation. Plant Science. 161, 881–889.
[42] Vajpayee, P., Rai, U.N., Ali, M.B., Tripathi, R.D., Kumar, A., Singh, S.N. (2005) Possible involvement of oxidative stress in copper-induced inhibition of nitrate reductase activity in *Vallisneria spiralis* L. Bulletin of Environmental Contamination and Toxicology. 74, 745-754.
[43] Peng, K., Luo, C., Lou, L., Li, X., Shen, Z. (2008) Bioaccumulation of heavy metals by the aquatic plants *Potamogeton pectinatus* L. and *Potamogeton malaianus* Miq. and their potential use for contamination indicators and in wastewater treatment. Science of the Total Environment. 392(11), 22-29.
[44] Kumar, G.P., Prasad, M.N.V. (2004) Cadmium Toxicity to *Ceratophyllum demersum* L.: Morphological symptoms, membrane damage, and ion leakage. Bulletin of Environmental Contamination and Toxicology. 72, 1038-1045.

[45] Balsberg-Påhlsson, A.-M. (1989) Mineral nutrients, carbohydrates and phenolic compounds in leaves of beech (*Fugus sylvatica* L.) in southern Sweden as related to environmental factors. Tree Physiology. 5, 485-495.
[46] Radić, S., Babić, M., Škobić, D., Roje, V., Branka, P-K. (2010) Ecotoxicological effects of aluminium and zinc on growth and antioxidants in *Lemna minor* L. Ecotoxicology and Environmental Safety. 73, 336-342.
[47] Srivastava, S., Mishra, S., Tripathi, R.D., Dwivedi, S., Trivedi, P.K., Tandon, P.K. (2007) Phytochelatins and antioxidant systems respond differentially during arsenite and arsenate stress in *Hydrilla verticillata* (L.f.) Royle. Environmental Science and Technology. 41(8), 2930–2936.
[48] Bakar, A.F.A., Yusoff, I., Fatt, N.T., Othman, F., Ashraf, M.A. (2013) Arsenic, zinc, and aluminium removal from gold mine wastewater effluents and accumulation by submerged aquatic plants (*Cabomba piauhyensis*, *Egeria densa*, and *Hydrilla verticillata*). BioMed Research International. Hindawi Publishing Corporation.

Received: **23.06.2017**
Accepted: **29.09.2017**

CORRESPONDING AUTHOR

Judith L Arnolds
South African National Biodiversity Institute,
Private Bag X7, Claremont, 7735,
Cape Town – South Africa

e-mail: j.arnolds@sanbi.org.za

© by PSP Volume 27 – No. 2/2018 pages 938-946 Fresenius Environmental Bulletin

EFFECT OF INFLUENT LOADS ON NITROGEN REMOVAL IN HORIZONTAL SUBSURFACE FLOW CONSTRUCTED WETLANDS WITH *CANNA INDICA*

Yan Zhang[1,*], Xuelan Liu[1], Yueming Wang[1], Peipei Yan[1], Qingchun Jing[1], Tianhong Shi[1], Xuejing Dai[2]

[1]Poultry Institute, Shandong Academy of Agricultural Science, Jinan 250023, P.R. China
[2]Jinan Environmental Monitoring Center, Jinan 250014, P.R. China

ABSTRACT

The discharge of livestock and poultry breeding wastewaters (LPWs) with high pollution load, particularly wastewater from broiler houses, has increased. This study performed simulation experiments on horizontal subsurface constructed wetlands (HF-CWs) with *Canna indica* to examine the effect of influent loads on the efficiency of nitrogen removal from wastewater from broiler houses. The results indicated that the removal of different forms of nitrogen was influenced by microorganisms, plants, influent loads and retention time. Plants and retention time accelerated the removal rate of nitrogen; however, high influent loads decelerated the nitrogen removal rate, particularly for ammonium nitrogen (NH_4^+-N). Moreover, organic matter in water promoted total nitrogen (TN) removal and, in particular, nitrate nitrogen (NO_3^--N) removal, by enhancing the activity of denitrifying bacteria. This enhanced removal might explain the low NO_3^--N concentrations observed in wastewaters from livestock and poultry breeding. Furthermore, our results indicate that HF-CWs with *Canna indica* may be suitable for treating wastewater from livestock and poultry breeding that meet the "Discharge Standard of Pollutants for Livestock and Poultry Breeding" (GB18596-2001). However, HF-CWs with *Canna indica* should not be used to treat wastewaters from livestock and poultry breeding directly; certain improvements are still needed for their application.

KEYWORDS:
Livestock and poultry breeding wastewaters, Constructed wetlands, Nitrogen removal, Organic matter, Retention time

INTRODUCTION

Currently, livestock and poultry breeding wastewaters (LPWs), in addition to industrial wastewater and domestic sewage, have been a considerable source of pollution. The pollution loads of LPWs exceed the accumulated pollution loads of industrial wastewater and domestic sewage in China [1]. The chemical oxygen demand (COD) and total nitrogen (TN) discharge volumes from livestock and poultry breeding in China are approximately 1.3×107 and 1.0×106 t/year, respectively, accounting for approximately 95.8% and 37.9%, respectively, of the total discharge volume of pollutants from agriculture and 41.9% and 21.7%, respectively, of the total discharge volume of pollutants in China; however, over 90% of pollutants from livestock and poultry breeding are untreated [2]. Untreated livestock and poultry breeding wastewaters (ULPWs) typically exhibit high concentrations of organic matter, ammonium nitrogen (NH_4^+-N), TN, phosphate, and suspended solids, acting as the key pollution sources of surface water bodies in China [3]. However, the NO_3^--N concentrations in ULPWs are relatively low. According to the "Discharge Standard of Pollutants for Livestock and Poultry Breeding" (GB18596-2001), organic matter and NH_4^+-N are still present at high concentrations (400 and 80 mg/L, respectively) in treated wastewater from wastewater treatment projects. The effluent water may influence the quality of surface and ground water if discharged directly into surface waters or if used to irrigate farmland. Thus, effective approaches for the advanced treatment of LPWs are urgently needed.

The pollution loads of livestock wastewater are markedly higher than those of poultry wastewater due to the high discharge from each head of livestock and the total amount of livestock in China. Furthermore, an increasing number of researchers have focused on livestock wastewater treatment; however, few studies have focused on poultry wastewater treatment, particularly the wastewater from high-intensity chicken farms [4,5]. The economic benefits of high-intensity chicken farms are smaller than those of livestock farms; as a result, most high-intensity chicken farms in China lack efficient wastewater treatment and integrated utilization facilities [6]. In addition, although some high-intensity chicken farms have wastewater treatment and integrated utilization facilities, there are typically high operation and maintenance costs and energy requirements for

these wastewater treatment systems. As a result, the wastewater is not treated as thoroughly in the high-intensity chicken farms with integrated utilization facilities, resulting in the direct discharge of wastewater from chicken farms into adjacent receiving waters and farmland, which may, in turn, affect the quality of adjacent surface waters [7, 8]. Hence, constructed wetlands for poultry wastewater treatment should be proposed due to their moderate capital cost and low operating costs.

Horizontal subsurface constructed wetlands (HF-CWs), which are often recognized as a sustainable wastewater treatment system with relatively low energy consumption and operation and maintenance costs, could potentially play multi-functional roles in water treatment, landscapes, biodiversity, recreation and education and are also an appropriate eco-system to remove pollutants, such as NH_4^+-N, from wastewaters [9-11]. In recent years, many studies have been focused on the water treatment function of HF-CWs [12-14], primarily for the treatment of municipal, domestic, agricultural, and industrial wastewater, as well as landfill leachate [15]. However, the application of HF-CWs in treating LPWs, particularly poultry wastewater, is increasing slowly due to the high concentration of pollutants and lack of dissolved oxygen (DO) in filtration beds [11]. Various internal and external factors, such as the hydraulic retention time, hydraulic and nutrient mass loading rates, substrates, plants, microbial communities, inflow ways, climate, pH, and dissolved oxygen, can affect the efficiency of nitrogen removal in HF-CWs [16-18]. Microbial activities are typically regarded as one of the dominant influential factors [19-21]. Plant species can also be a significant influencing factor. *Canna indica* was found to be a suitable plant species option in HF-CWs where nitrogen mainly occurs as NH_4^+-N [22, 23]. The concentrations of NH_4^+-N and organic matter were still rather high in the treated LPWs; however, few studies have reported on LPWs treated in HF-CWs with *Canna indica* because of the lack of investigation regarding different influent nitrogen concentrations. The forms of nitrogen (TN, NH_4^+-N, NO_3^--N), oxidation-reduction potential (ORP) and pH in wastewater with high pollutant concentrations remain unknown.

This study aimed to determine the effect of influent C/N ratios due to influent loads and plants on nitrogen removal in HF-CWs under experimental conditions, to discuss the reasons for low nitrate nitrogen (NO_3^--N) concentrations, to analyze the pH and ORP variations, and to assess whether HF-CWs are suitable for treating livestock and poultry breeding wastewater. This study will provide a reasonable reference for increasing the rate of nitrogen removal in constructed wetlands (CWs) and improving the management of livestock and poultry breeding wastewater.

MATERIALS AND METHODS

Experimental design. Three outdoor HF-CWs (W1, W2 and W3) were operated using the intermittent method. Each treatment was performed in triplicate. The wetland beds were made of PVC cuboids that were 10 mm thick, 1.3 m long, 0.5 m wide and 0.8 m high. These wetland beds were filled with a 0.55-m layer of large slag (5-30 mm in diameter) at the bottom and a 0.1 m layer of small slag (<5 mm in diameter) on top. The wetland beds were approximately 0.15 m long in the inlet sections, 1.0 m long in the work sections, and 0.15 m long in the outlet sections. The inlet and outlet sections were filled with gravel (20-30 mm). *Canna indica* was planted in the wetlands at a density of 40 cuttings per m^2. Experiments were performed from June to September 2015 to track plant growth and bacteria communities accommodating the wetland environment. The formal experiment started after three months. Influent water was first prepared in three feed tanks (per approximately 2 m^3) by dissolving ammonium nitrate, sodium hydrogen phosphate and glucose in each wetland. The influent water was introduced into the three wetlands at the same time. Low load, middle load and high load were immitted into W1, W2 and W3 during the formal experiment (Table 1), respectively. The residence time of the influent water in the wetlands was 9 d.

Water samples were collected from each wetland using perforated tubes (20 mm in diameter) and combined using the inverted siphon method. Three perforated tubes used to collect water samples were embedded into the substrate to a depth of 0.3 m, and their range of perforated parts was 0.15 m to 0.20 m apart from the subsurface of the wetland substrate to collect water samples from the top layer. Three additional tubes were driven into the substrate to a depth of 0.45 m, and the range of perforated parts was 0.30 m to 0.35 cm apart from the subsurface of the wetland substrate to collect water samples from the middle layer. Other perforated tubes supplied to gather water samples from the bottom layer were driven into the substrate to a depth of 0.60 m, and the ranges of the perforated parts were 0.15 m to 0.20 m apart from the bottom of the wetland.

Water sample collection and analyses. Water samples were collected daily from the perforated tubes using the inverted siphon method. Collected water samples were immediately stored in an ice chest and transported to the laboratory. Portions of the water samples were filtered through 0.45-μm Whatman filters, and the remaining samples were filtered into separate polyvinyl vials. All water samples were completely analyzed within 2 days. Water samples were analyzed for TN, total phosphorus (TP), NH_4^+-N, NO_3^--N, chemical oxygen demand (COD_{Cr}), pH and ORP. TN was analyzed by the test-in-tube alkaline persulfate digestion method. The

persulfate digestion method was used for TP, Nessler's reagent colorimetric method was used for NH_4^+-N, the cadmium reduction method was used for NO_3^--N, and the potassium dichromate method was used for COD_{Cr}. Water sample analyses were performed using a UV–Vis spectrophotometer (UV-8000S, METASH, China). A Sension ORP electrode and Piccolo pH meter were used to measure the ORP and pH of the water samples, respectively. The characteristics of real wastewater samples (washing water) from the septic tank of high-intensity chicken farms were as follows: NH_4^+-N, 302.9-458.1 mg/L; NO_3^--N, 67.5-132.4 mg/L; TN, 416.1-663.2 mg/L; COD_{Cr}, 314.5-530.6 mg/L; TP, 43.5-73.0 mg/L; orthophosphate phosphorus (PO_4^{3-}-P), 40.5-70.4 mg/L; and pH range, 7.31-8.46. However, the characteristics were variational with retention time in the septic tank. And the real wastewater has much changing factors. Hence, Synthetic wastewater was used for the sake of revealing the effect of influent C/N ratios due to influent loads and plants on nitrogen removal. Synthetic wastewater was prepared based on the real poultry wastewater composition to accurately observe the performance of HF-CWs.

Statistical analysis. Origin 7.5 software and the SPSS 16.0 statistical package were used for drawing and for the statistical analysis of the data, respectively. Analysis of variance (ANOVA) was performed to test the differences in TN, NH_4^+-N and NO_3^--N among different wetlands and different substrate layers.

TABLE 1
Mean concentrations (±SD) of the main parameters of influent water (mg/L, excluding pH and C/N) and plant biomass at the end of the experiment (kg/m^2).

Parameter	W1	W2	W3
TN	58.25±3.06	124.36±4.83	253.15±6.71
TP	18.31±1.02	19.40±0.45	20.16±1.38
NH_4^+-N	27.86±1.31	57.06±3.04	119.61±6.02
NO_3^--N	26.81±1.27	61.48±3.15	122.33±3.94
COD_{Cr}	647±5.38	650±8.72	659±7.75
pH	7.45	7.54	8.19
C/N	11.1	5.2	2.6
biomass	8.27	10.87	4.04

RESULTS

TN removal under different influent loads. As shown in Table 1, the COD_{Cr} and TP concentrations were similar in the influent water of different treatments. The TN concentrations were different in W1, W2 and W3, with mainly NH_4^+-N and NO_3^--N and a small fraction of nitrite or organic nitrogen present, which led to different C/N ratios in the influent water of the three wetlands. Consequently, the plant biomasses were also different at the end of the experiment. As shown in Figure 1, the TN removal efficiencies all increased with retention time in W1, W2 and W3 during the 9 d. The TN removal efficiencies were 6.0-20.8% and 14.7-30.2% greater in W1 than in W2 and W3, respectively, at the same retention time, and they were 8.6-12.5% greater in W2 than in W3. The highest removal efficiency was 94.48% in W1, 88.4% in W2 and 79.8% in W3. However, a significant difference in TN removal efficiency was only observed between W1 and W3 ($p<0.05$). Hence, the influent TN concentrations clearly affected the TN removal efficiencies.

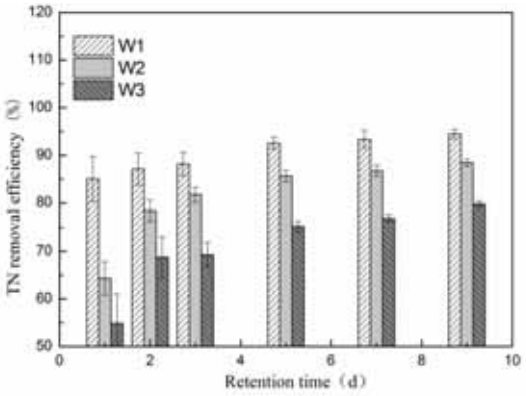

FIGURE 1
Change in TN removal efficiency of the three wetlands with retention time.

NH_4^+-N and NO_3^--N removal. The NH_4^+-N removal efficiency generally increased with retention time in the three wetland systems. The NH_4^+-N removal efficiency was significantly higher in W1 than in W2 ($p<0.05$) and W3 ($p<0.001$), and it was significantly higher in W2 than in W3 ($p<0.05$) (Fig. 2). In W1 and W2, the NH_4^+-N removal efficiency in the middle layers was higher than in both the top and bottom layers, and the top and bottom layers had similar removal efficiencies. In W3, the NH_4^+-N removal efficiency in the middle layer was slightly lower than in the top and bottom layers from day 2 onward. However, there were no significant differences in NH_4^+-N among the top, middle and bottom layers in the three CWs. Thus, in the current study, increasing the retention time could clearly enhance the NH_4^+-N removal efficiency, and the influent NH_4^+-N concentrations clearly affected the NH_4^+-N removal efficiencies. However, layer effects for the NH_4^+-N removal efficiencies were not observed in the HF-CWs with *Canna indica.*

No significant difference in NO_3^--N removal efficiency was observed between W1 and W2 ($p>0.05$) (Fig. 3). However, a significant difference existed between the NO_3^--N removal efficiencies of W1 and W3 ($p<0.001$) and of W2 and W3 ($p<0.001$). In W1, the NO_3^--N removal efficiencies among the three layers were nonsignificant ($p>0.05$), and the efficiencies were all close to 100 percent during the retention period. In W2, the NO_3^--N removal efficiency in the middle layers were higher than those in

the top and bottom layers on day 1. The NO_3^--N removal efficiencies were not significantly different among the three layers with increasing retention time ($p>0.05$); the efficiencies exceeded 98.5 percent and leveled off. In W3, variations in the NO_3^--N removal efficiencies could be clearly observed with increasing retention time. The NO_3^--N removal efficiencies initially increased, then decreased, increased again, and then leveled off with increasing retention time. However, no differences in the efficiencies were observed among the three layers, and the average efficiency was 91.0 percent on day 9. Therefore, retention time exerted a limited influence on the NO_3^--N removal efficiencies under lower influent NO_3^--N concentrations; however, higher influent NO_3^--N concentrations significantly affected the NO_3^--N removal efficiencies. The three experiment wetland systems with *Canna indica* did not display layer effects for the NO_3^--N removal efficiency.

pH and ORP variation in the different substrate layers of wetlands. Figure 4 shows the variations in the pH values of the different layers of the three wetlands with retention time. The pH values were significantly lower in W1 than in W2 ($p<0.001$) and W3 ($p<0.001$), and the pH values were lower in W2 than in W3 ($p<0.05$). At the same retention time, the pH value ranking of the three wetlands was observed to be W3>W2>W1. Nevertheless, the pH values among the three layers in each wetland system were not significantly different at the same retention time (all $p>0.05$). All wetland systems exhibited an increasing trend in pH values with increasing retention time. However, the pH range was from 7.1 to 8.0, 7.3 to 8.6 and 8.1 to 8.8 in W1, W2 and W3, respectively.

The ORP ranking of the three wetlands was W1>W2>W3 at a given retention time (Fig. 5; all $p<0.001$). The ORPs of the three wetlands were different, with decreasing trends for W1 and W2 and a flat trend for W3. In W2, the ORP was reduced because DO was consumed on day 1. Thereafter, the ORP initially increased with increasing DO and then gradually decreased. The highest ORP values were 499.50, 460.15, and 400.70 mV in W1, W2 and W3, respectively. In addition, no significant differences for ORP among the three layers in each wetland were observed with increasing retention time ($p>0.05$).

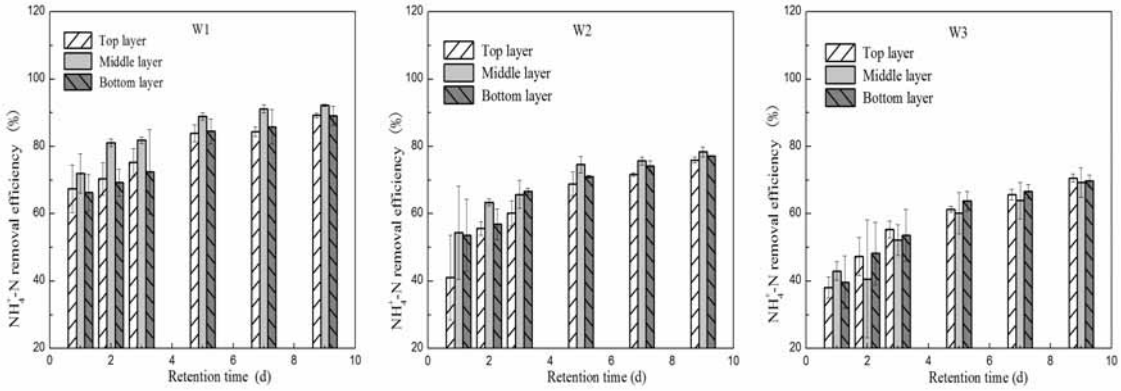

FIGURE 2
Changes in NH_4^+-N removal efficiency in the different layers of the three wetlands with retention time.

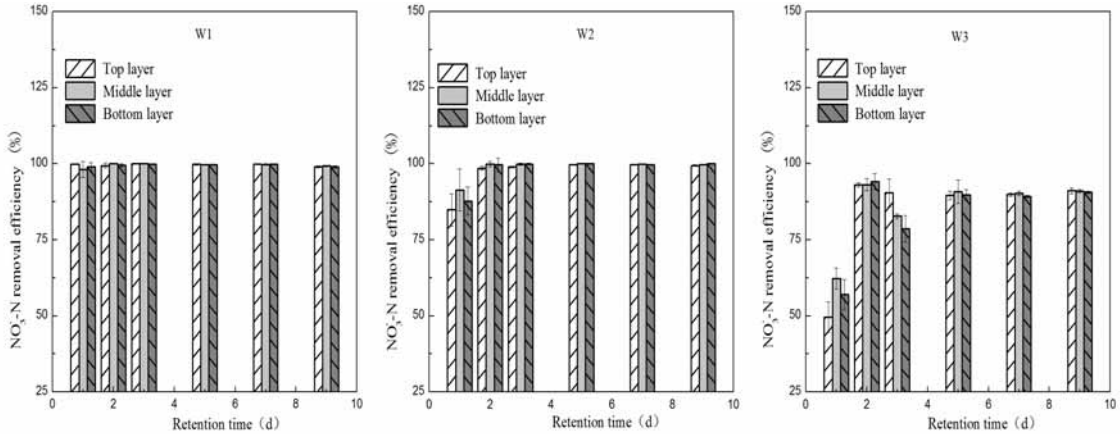

FIGURE 3
Changes in NO_3^--N removal efficiency in the different layers of the three wetlands with retention time.

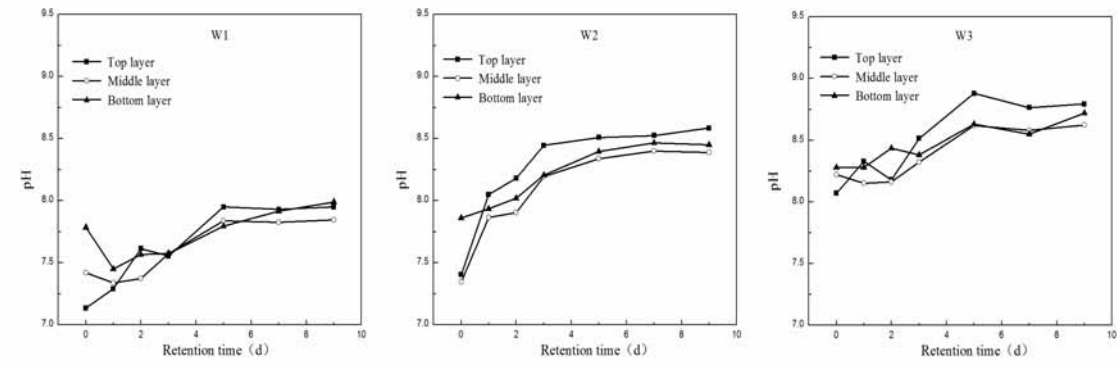

FIGURE 4
Changes in the pH in the three layers of the three wetlands with retention time.

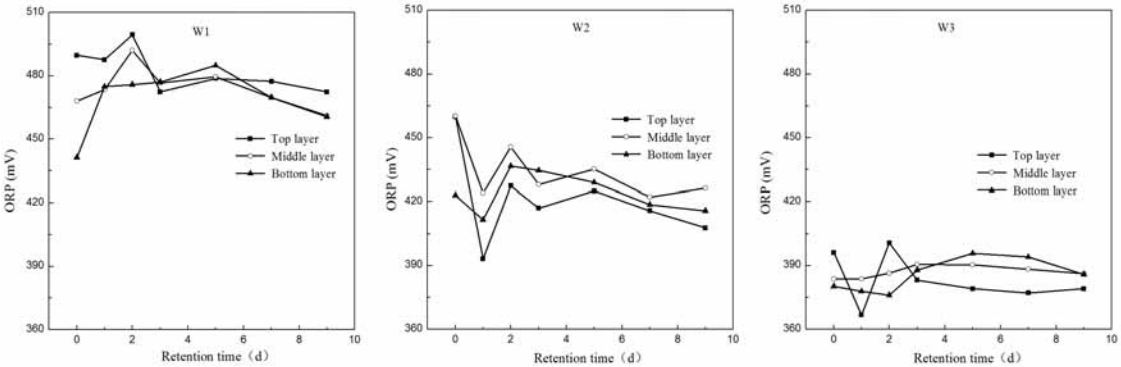

FIGURE 5
Change in the ORP in the different layers of the three wetlands with retention time.

DISCUSSION

NH_4^+-N and NO_3^--N removal in wetland systems. NH_4^+-N removal is affected by substrate adsorption, plant and microbial uptake, ammonia volatilization, microbiological nitrification, and NO_3^--N reduction to NH_4^+-N, among other factors [24, 25]. Slag substrate with a large bonding surface area for microbes has a cation exchange capacity and can provide sites for adsorption, which is favorable for the adsorption of ammonium ions (NH_4^+) [26]. However, the NH_4^+ adsorption of slag was generally low and only temporary, and the adsorbed NH_4^+ was utilized in other ways. Kronzucker et al. [27] noted that NH_4^+ was the predominating form of available inorganic nitrogen for plant uptake at low pH or in reduced oxygen conditions. Nevertheless, the amount of NH_4^+-N uptake by plants and microbes was limited during the 9 days of this study. The amount of ammonia volatilization in the wetland systems was low because surface water and algal activity were lacking, which would increase the pH of the water, and was negligible in HF-CWs under pH 7.0-9.0 [15]. The pH values were optimal for the growth of nitrifying bacteria and nitrite bacteria based on the efficiency of the nitrification process [28,29]. Some researchers have indicated that NH_4^+-N removal depends mainly on nitrification activated by nitrifying bacteria [30,31]. There were many aerobic zones in the wetland systems due to the influent water carrying DO, atmosphere reaeration and the oxygen released from the plant rhizosphere [32]. In the aerobic zones, NH_4^+ was first oxidized into nitrite (NO_2^-) and then further transformed into nitrate (NO_3^-) [33,34], which led to reduced NH_4^+-N concentrations and enhanced NH_4^+-N removal efficiencies. Moreover, the concentrations differed between aerobic zones and the other zones, which accelerated the diffusion of NH_4^+ to aerobic zones and subsequently increased NH_4^+-N removal, particularly in the middle layers of W1 and W2. In addition, prolonging the retention time of water in wetland systems promoted all the above processes, which increased NH_4^+-N removal.

The NO_3^--N removal in wetland systems was mainly caused by nitrification-denitrification processes and plant uptake [35]. In nitrification processes, NH_4^+-N is ultimately transformed into NO_3^--N in aerobic zones, after which denitrifying bacteria convert NO_3^--N into NO_2 or N_2. Hence, nitrification only converts nitrogen forms and does not reduce the nitrogen content in wetland systems; denitrification is considered the dominant nitrogen removal mechanisms in CWs [15,21,36]. In this study, the fluctuation of NO_3^--N removal efficiencies before three days in W3 was the accumulation of NO_3^--N by nitrification processes, in which plentiful NH_4^+-N was translated into NO_3^--N. In W1 and W2, NO_3^--N did not accumulate because of the relative deficiency in

NH_4^+-N. Meanwhile, prolonging the retention time was also optimal for NO_3^--N removal in CWs. Prolonging the retention time can provide time for nitrification-denitrification processes, plant uptake and increased chemical residence time in wetlands. A pH of 7.0-9.0 was favorable for nitrification-denitrification occurring in CWs [37,38]. In addition, the experiment was performed in summer and early autumn, and the weather was rather warm in Jinan, China, which may have accelerated bacterial activity and benefitted the nitrification-denitrification processes. Although the amount of NO_3^--N uptake by plants was limited, plant uptake was also useful for NO_3^--N removal.

Effect of the influent load on nitrogen removal. The COD_{Cr} concentrations were similar in the influent water of the three wetlands, and the TN concentrations were different, resulting in different C/N ratios with the order of W1>W2>W3. The C/N ratios represent the relative amounts of carbon and nitrogen sources in wetland systems. C/N ratios can affect microorganisms' nitrification and denitrification functions, the microbiological degradation of organic matter, and microbial communities in wetland systems [39, 40]. The NH_4^+-N removal efficiencies in the three wetlands increased with increasing C/N ratios. This observation disagreed with the results obtained by Zhu et al. [21], in which the COD_{Cr} concentrations were adjusted and the TN concentrations were uniform in influent water. In contrast, the TN concentrations in influent water were adjusted and the COD_{Cr} concentrations were invariant in this study. However, the degradation of organic matter demanded more oxygen in the CWs, leading to the DO in water to decrease rapidly, the ORP in water to decrease, the transformation of NH_4^+-N to be inhibited, and the occurrence anoxic and anaerobic environments, which favored NO_3^--N removal. As a result, TN removal was enhanced.

Denitrification processes are considered the dominant mechanisms of nitrogen removal in CWs. Glucose as a carbon source is the major electron donor for denitrification, consumes hydrogen ions (H^+) and is converted into carbonate (CO_3^{2-}) in denitrification processes, which subsequently lead to an increase in the pH of the CWs. A sufficient carbon source increases the denitrification process, whereas the lack of a carbon source inhibits the denitrification process [41,42]. In this study, the high C/N ratios in W1 and W2 indicated sufficient carbon sources and accelerated the denitrification in CWs, resulting in higher TN removal efficiencies. In W3, the low C/N ratio restrained the denitrification process due to the lack of a carbon source; consequently, the TN removal efficiencies were lower due to insufficient electron donors for denitrification by microorganisms. Hence, the TN and NO_3^--N removal efficiencies increased with increases in the C/N ratio, which was in agreement with the results reported by Ding et al. and Zhu et al. [12, 21]. The results further revealed the reason behind the low NO_3^--N contents in untreated wastewater from livestock and poultry breeding.

Effect of plants on nitrogen removal. Plants are important to nitrogen removal in wetland systems. The plants in wetland systems, such as *Canna indica*, can not only remove nitrogen via direct uptake for plant growth but also transport oxygen through their leaves and stems and into rhizomes, which leads to the appearance of aerobic, anoxic, and anaerobic zones, in that order, around the plant roots [43]. In aerobic zones, the activity of nitrifying bacteria is promoted in the rhizosphere [44]; the activity of denitrifying bacteria is accelerated in anaerobic zones. Moreover, the roots of *Canna indica* can also act as rough and adherent media for microbes and released organic matter, which enhances denitrification [45, 46]. In this study, the biomass of *Canna indica* in W3 was 43.7% and 39.3% lower than that in W1 and W2 (Table 1), respectively, leading to a decrease in nitrogen removal efficiency. The higher influent ammonium concentrations in W3 suppressed plant growth; induced symptoms of NH_4^+ toxicity, including leaf chlorosis and a reduction in root to shoot ratios [47]; and reduced the biomass of *Canna indica*, ultimately affecting nitrogen removal. However, surplus NO_3^--N is not harmful for plant growth [22, 48]. In addition, the root systems of *Canna indica* were confined in an approximately 0.35-m-deep substrate layer, which led to increased NH_4^+-N removal in the middle layer of W1 and W2 because of the aerobic zones. The roots of *Canna indica* were damaged because of high influent ammonium concentrations, which limited NH_4^+-N removal in the middle layer of W3. However, a significant layer effect in NH_4^+-N and NO_3^--N removal was not observed in this study.

Nitrogen for plant uptake mainly depends on the availability of different inorganic nitrogen forms in the environment. Growing plants predominantly absorb the NH_4^+-N form in wetlands. Konnerup and Brix [26] found that *Canna indica* not only took up NH_4^+-N at faster rates than NO_3^--N but also had higher contents of nitrogen in the tissues and higher photosynthetic rates when supplied with NH_4^+-N. However, excess NH_4^+-N inhibited plant growth. Hence, the results further indicate that HF-CWs with *Canna indica* were unfit for directly treating wastewater from livestock and poultry breeding. Nevertheless, according to the "Discharge Standard of Pollutants for Livestock and Poultry Breeding" (GB18596-2001), NH_4^+-N was still higher (80 mg/L) in the treated wastewater from livestock and poultry breeding. Hence, HF-CWs with *Canna indica* are suitable for treating the treated wastewater from livestock and poultry breeding.

In the HF-CWs, TN, and NH_4^+-N removal efficiencies decreased with decreasing C/N ratios due to

the different influent TN concentrations. Organic matter enhanced NO_3^--N removal due to the intense activities of denitrifying bacteria and, to a certain extent, reduced dissolved oxygen content in wastewaters, which may have caused the low NO_3^--N concentrations in LPWs. Carbon and nitrogen sources significantly increased the pH and decreased the ORP in CWs. Furthermore, the presence of *Canna indica* and a prolonged retention time also promoted nitrogen removal in the CWs. Hence, HF-CWs are suitable for the downstream treatment of the treated wastewater from livestock and poultry breeding with higher organic matter and NH_4^+-N, which is advantageous for protecting regional water resources. Additionally, the experimental results did not support a layer effect of nitrogen removal in HF-CWs with *Canna indica*.

ACKNOWLEDGEMENTS

The authors gratefully acknowledge funding from the National Natural Science Foundation of China (No. 41501520), the Youth Science Foundation of Shandong Academy of Agriculture Sciences (No. 2014QNM44), the Agriculture Important Application Technology Innovation Program of Shandong Province in 2014, and the Agricultural Science and Technology Innovation Foundation of Shandong Academy of Agriculture Sciences (No. CXGC2016A08). The authors also thank Jiaoyue Wang at the Institute of Applied Ecology, Chinese Academy of Sciences, for constructive suggestions and language editing of the manuscript.

The authors have declared no conflicts of interest.

REFERENCES

[1] Wang, F.H., Ma, W.Q., Dou, Z.X., Ma, L., Liu, X.L., Xu, J.X. and Zhang, F.S. (2006) The estimation of the production amount of animal manure and its environmental effect in China. China Environmental Science. 26(5), 614-617 (in Chinese).

[2] Zhang, T., Bu, M.D. and Geng, W. (2012) Pollution status and biogas-producing potential of livestock and poultry excrements in China. Chinese Journal of Ecology. 31(5), 1241-1249 (in Chinese).

[3] Xiao, H., Yang, P., Peng, H., Zhang, Y.Z., Deng, S.H. and Zhang, X.H. (2010) Nitrogen removal from livestock and poultry breeding wastewaters using a novel sequencing batch biofilm reactor. Water Science and Technology. 62(11), 2599-2606.

[4] Wei, X.M., Lin, C., Duan, N., Peng, Y.X. and Ye, Z.Y. (2010) Application of aerobic biological filter for treating swine farms wastewater. Procedia Environmental Sciences. 2, 1569-1584.

[5] Othman, I., Anuar, A.N., Ujang, Z. and Rosman, N.H. (2013) Livestock wastewater treatment using aerobic granular sludge. Bioresource Technology. 133, 630-634.

[6] Song, W., Zang, H.L., Zhang, F., Liu, C.Q. and Bi, X.J. (2013) Study on feasibility of emission reaching standared for treatment of washing wastewater of large-scale chicken farms by three-stage process. Ecological Engineering. 31(S), 307-309, 328 (in Chinese).

[7] Hao, Q.B. (2014) Harms and treatment measures of wastewater from poultry farms. Poultry Science 6, 46-49 (in Chinese).

[8] Zhu, D.L., Sun, C., Zhang, H.H., Wu, Z.L., Jia, B. and Zhang, Y. (2012) Roles of vegetation, flow type and filled depth on livestock wastewater treatment. Ecological Engineering. 39, 7-15.

[9] Becerra-Jurado, G., Harrington, R. and Kelly-Quinn, M. (2012) A review of the potential of surface flow constructed wetlands to enhance macroinvertebrate diversity in agricultural landscapes with particular reference to Integrated Constructed Wetlands (ICWs). Hydrobiologia. 692(1), 121-130.

[10] Wu, S., Kuschk, P., Brix, H., Vymazal, J. and Dong, R. (2014) Development of constructed wetlands in performance intensifications for wastewater treatment: a nitrogen and organic matter targeted review. Water Research. 57, 40-55.

[11] Wu, S.B., Lei, M., Lu, Q.M., Guo, L.C. and Dong, R.J. (2016) Treatment of pig manure liquid digestate in horizontal flow constructed wetlands: Effect of aeration. Engineering in Life Sciences. 16(3), 263-271.

[12] Ding, Y., Song, X.S., Wang, Y.H. and Yan, D.H. (2012) Effects of dissolved oxygen and influent COD/N ratios on nitrogen removal in horizontal subsurface flow constructed wetland. Ecological Engineering. 46, 107-111

[13] Ávila, C., Reyes, C., Bayona, J.M. and García, J. (2013) Emerging organic contaminant removal depending on primary treatment and operational strategy in horizontal subsurface flow constructed wetlands: Influence of redox. Water Research. 47(1), 315-325

[14] Wu, S.B., Kuschk, P., Brix, H., Vymazal, J. and Dong, R.J. (2014) Development of constructed wetlands in performance intensifications for wastewater treatment: A nitrogen and organic matter targeted review. Water Research. 57, 40-55.

[15] Vymazal, J. and Kröpfelová, L. (2009) Removal of nitrogen in constructed wetlands with horizontal sub-sureface flow: a review. Wetlands. 29(4), 1114-1124.
[16] García, J., Chiva, J., Aguirre, P., Álvarez, E., Sierra, J.P. and Mujeriego, R. (2004) Hydraulic behaviour of horizontal subsurface flow constructed wetlands with different aspect ratio and granular medium size. Ecological Engineering. 23(3), 177-187.
[17] Akratos, C.S. and Tsihrintzis, V.A. (2007) Effect of temperature, HRT, vegetation and porous media on removal efficiency of pilot-scale horizontal subsurface flow constructed wetlands. Ecological Engineering. 29(2), 173-191.
[18] Tunçsiper, B. (2009) Nitrogen removal in a combined vertical and horizontal subsurface-flow constructed wetland system. Desalination. 247(1-3), 466-475.
[19] Khangembam, C.D. (2016) Effect of temperature on nitrifying microbes, emphasizing on ammonia oxidizing archaea and bacteria. Journal of Biological Sciences and Medicine. 2(2), 7-14
[20] Wang, R., Baldy, V., Périssol, C. and Korboulewsky, N. (2012) Influence of plants on microbial activity in a vertical-down flow wetland system treating waste activated sludge with high organic matter concentrations. Journal of Environmental Management. 95, 158-164.
[21] Zhu, H., Yan, B.X., Xu, Y.Y., Guan, J.N. and Liu, S.Y. (2014) Removal of nitrogen and COD in horizontal subsurface flow constructed wetlands under different influent C/N ratios. Ecological Engineering. 63, 58-63.
[22] Konnerup, D. and Brix, H. (2010) Nitrogen nutrition of *Canna indica*: Effects of ammonium versus nitrate on growth, biomass allocation, photosynthesis, nitrate reductase activity and N uptake rates. Aquatic Botany. 92(2), 142-148.
[23] Chen, B.Q., Liu, D., Han, W.J., Fan, X., Cao, H.Q., Jiang, Q.S., Liu, Y., Chang, J. and Ge, Y. (2014) Nitrogen-removal ability and niche of *Coix lacryma-jobi* and *Reineckia carnea* in response of NO_3^-/NH_4^+ ratio. Aquatic Botany. 120, 193-200.
[24] Zhang, Y., Zhu, H., Yan, B.X., Ou, Y. and Li, X.H. (2013) Nutrient removal in different overlying water layers and their variation in pore water of drainage ditches in Sanjiang Plain, Northeast China. Desalination and Water Treatment. 51(28-30), 5599-5607.
[25] Wu, H.M., Zhang, J., Ngo, H.H., Guo, W.S., Hu, Z., Liang, S., Fan, J.L. and Liu, H. (2015) A review on the sustainability of constructed wetlands for wastewater treatment: Design and operation. Bioresource Technology. 175, 594-601.
[26] Saeed, T. and Sun, G. (2012) A review on nitrogen and organics removal mechanisms in subsurface flow constructed wetlands: dependency on environmental parameters, operating conditions and supporting media. Journal of Environmental Management. 112, 429-448.
[27] Kronzucker, H.J., Siddiqi, M.Y. and Glass, A.D.M. (1997) Conifer root discrimination against soil nitrate and the ecology of forest succession. Nature. 385, 59-61.
[28] Villaverde, S., García-Encina, P.A. and Fdz-Polanco, F. (1997) Influence of pH over nitrifying biofilm activity in submerged biofilters. Water Research. 31(5), 1180-1186.
[29] Jampeetong, A., Konnerup, D., Piwpuan, N. and Brix, H. (2013) Interactive effects of nitrogen form and pH on growth, morphology, N uptake and mineral contents of *Coix lacryma-jobi* L. Aquatic Botany. 111, 144-149.
[30] Mayo, A.W. and Mutamba, J. (2004) Effect of HRT on nitrogen removal in a coupled HRP and unplanted subsurface flow gravel bed constructed wetland. Physics and Chemistry of the Earth, Parts A/B/C. 29(15-18), 1253-1257.
[31] Ruiz-Rueda, O., Hallin, S. and Bañeras, L. (2008) Structure and function of denitrifying and nitrifying bacterial communities in relation to the plant species in a constructed wetland. FEMS Microbiology Ecology. 67, 308-319.
[32] Winter, P., Pearce, P. and Colquhoun, K. (2012) Contribution of nitrous oxide emissions from wastewater treatment to carbon accounting. Journal of Water and Climate Change. 3(2), 95-109.
[33] Metcalf and Eddy, revised by Tchobanoglous, G., Burton, F.L., Stensel, H.D. (2003) Wastewater Engineering: Treatment and Reuse. 4th ed. McGraw-Hill, Boston, USA, 611-616.
[34] Gray, N.F. (2004) Biology of Wastewater Treatment. 2nd ed. Imperial College Press, London, UK, 282-290.
[35] Zhang, Y., Zhu, H., Yan, B.X., Li, X.H. and Ou, Y. (2014) Effects of Plant and Water Level on Nitrogen Variation in Overlying and Pore Water of Agricultural Drainage Ditches in Sanjiang Plain, Northeast China. Clean – Soil Air Water. 42(4), 386-392.
[36] Ayaz, S.C., Aktas, Ö, Findik, N., Akca, L. and Kinaci, C. (2012) Effect of recirculation on nitrogen removal in a hybrid constructed wetland system. Ecological Engineering. 40, 1-5.
[37] Vymazal, J., Brix, H., Cooper, P.F., Haberl, R., Perfler, R. and Laber, J. (1998) Removal mechanisms and types of constructed wetlands in Europe. Leiden: Backhuys Publishers, 17-66.
[38] Jayaweera, G.R. and Mikkelsen, D.S. (1991) Assessment of ammonia volatilization from flooded soil systems. Advances in Agronomy. 45, 303-365.

[39] Deng, H.H., Ge, L.Y., Xu, T., Zhang, M.H., Wang, X.D., Zhang, Y.L. and Peng, H. (2011) Analysis of the metabolic utilization of carbon sources and potential functional diversity of the bacterial community in lab-scale horizontal subsurface-flow constructed wetlands. Journal of Environmental Quality. 40(6), 1730-1736.
[40] Wang, W., Ding, Y., Ullman, J.L., Ambrose, R. F., Wang, Y.H., Song, X.S. and Zhao, Z.M. (2016) Nitrogen removal performance in planted and unplanted horizontal subsurface flow constructed wetlands treating different influent COD/N ratios. Environmental Science and Pollution Research. 23(9), 9012-9018.
[41] Meng, P., Pei, H., Hu, W., Shao, Y. and Li, Z. (2014) How to increase microbial degradation in constructed wetlands: influencing factors and improvement measures. Bioresource technology. 157, 316-326.
[42] Gajewska, M., Jóźwiakowski, K., Ghrabi, A. and Masi, F. (2015) Impact of influent wastewater quality on nitrogen removal rates in multistage treatment wetlands. Environmental Science and Pollution Research. 22(17), 12840-12848.
[43] Liu, S.Y., Yan, B.X. and Wang, L.X. (2011) The layer effect in nutrient removal by two indigenous plant species in horizontal flow constructed wetlands. Ecological Engineering. 37, 2101-2104.
[44] Vymazal, J. (2011) Plants used in constructed wetlands with horizontal subsurface flow: a review. Hydrobiologia. 674, 133-156.
[45] Picek, T., Cizkova, H. and Dusek, J. (2007) Greenhouse gas emissions from a constructed wetland-plants as important sources of carbon. Ecological Engineering. 31, 98-106.
[46] Hu, L.M., Hu, W.P., Deng, J.C., Li, Q.Q., Gao, F., Zhu, J.G. and Han, T. (2010) Nutrient removal in wetlands with different macrophyte structures in eastern Lake Taihu, China. Ecological Engineering. 36, 1725-1732.
[47] Equiza, M.A. and Zwiazek, J.J. (2014) Nitrogen form affects physiological responses and root expansigenous honeycomb aerenchyma in the emergent macrophyte Acorus americanus. Botany. 92(8), 541-550.
[48] Britto, D.T. and Kronzucker, H.J. (2013) Ecological significance and complexity of N-source preference in plants. Annals of Botany. 112(6), 957-963.

Received: **23.06.2017**
Accepted: **09.12.2017**

CORRESPONDING AUTHOR

Yan Zhang
Poultry Institute,
Shandong Academy of Agricultural Science,
Jinan 250023 – P.R. China

e-mail: swallow928@126.com

© by PSP Volume 27 – No. 2/2018 pages 947-959 Fresenius Environmental Bulletin

TEMPORAL AND SPATIAL VARIATION OF PHYTOPLANKTON FUNCTIONAL GROUPS AND MAIN DRIVING FACTORS IN THE THREE GORGES RESERVOIR, CHINA

Jingya Wang[1, 2], Shaowen Ye[1], Zhicong Wang[1], Jiashou Liu[1], Tanglin Zhang[1], Sovan Lek[3], Zhongjie Li[1,*]

[1]State Key Laboratory of Freshwater Ecology and Biotechnology, Institute of Hydrobiology, Chinese Academy of Sciences, Wuhan 430072, China
[2]University of Chinese Academy of Sciences, Beijing 100049, China
[3]Universite´ de Toulouse, UPS, UMR5174 EDB, 31062 Toulouse, France

ABSTRACT

The Three Gorges Reservoir (TGR) is a deep, canyon-reservoir created in consequence of the Changjiang (Yangtze) River's impoundment by the Three Gorges Dam in southwest China. To study the spatio-temporal dynamics of phytoplankton functional groups and the main driving factors in this large subtropical reservoir, field samplings were conducted in five sections along the longitudinal axis of the TGR in summer (August 2012), autumn (December 2012), winter (January2013), and spring (April 2013), respectively. Twenty-nine phytoplankton functional groups were identified among 246 phytoplankton species. There were obvious seasonal and spatial differences in both the biomass and composition of the phytoplankton functional groups. The algal biomass in the mainstream was at low level during the study period and the dominant functional groups included groups B, D, P, and MP, which adapted to mixed and turbid water condition. In comparison with the mainstream, the algal biomass in the tributaries was higher in during the flood seasons (spring and summer) and the dominant groups switched to X2, L_O, and P, which prefer meso-eutrophic environments and standing water. In the dry seasons (autumn and winter), the dominant groups in the tributaries were B, D, P, L_O, and Y. Group L_O and Y can swim to optimal light and nutrients layers with the help of flagella. The study suggests that hydrological regimes such as mixing, water flow, water temperature, and thermal structure played an important role in determining the biomass and community structure of phytoplankton, and shows the value of phytoplankton functional groups in studying algal spatio-temporal dynamics in the TGR.

KEYWORDS:
Phytoplankton, Functional group, Community structure, Three Gorges Reservoir

INTRODUCTION

In aquatic ecosystem, hydrodynamics takes an important part in the water quality formation, and biological productivity by affecting the movement of suspended substance and dissolved matter, heat; the intensity of internal circulation of the aquatic ecosystem, the speed of pollution processes, and self-purification capacity [1]. Hence, hydrologic regimes may influence the community structure and biomass of phytoplankton directly (e.g. water column stability and water retention time) [2, 3, 4] and indirectly (e.g. light and nutrient availability) [5, 6].

The concept of "functional groups" was put forward by Grime [7] and introduced into aquatic ecosystems by Reynolds [8]. Following Grime's [7] seminal work on the classification of terrestrial vegetation, several phytoplankton functional groups were defined by Reynolds that may potentially be dominant or co-dominant species in a certain habitat by using the morphological, physiological, and ecological traits of the phytoplankton species [8, 9]. To date, 40 phytoplankton functional groups have been identified [8, 10, 11]. Phytoplankton functional groups are useful in aquatic environment research by their preference, tolerance, and dislike to the habitat [12]. So that, in recent years, there has been a growing interest in phytoplankton functional groups versus species [13, 14]. The functional group approach has been applied worldwide in many different lakes and reservoirs [8, 11].

The Three Gorges Reservoir (TGR) is a deep, subtropical canyon-reservoir, created in consequence of the Changjiang (Yangtze) River's impoundment by the Three Gorges Dam in southwest China. It has a 30 m fluctuation in the water level and the capacity of the TGR in checking working condition is 45 billion cubic meters. It plays an important role in flood control, power generation, navigation, and water diversion. The impoundment changed stretches of inflow tributaries into reservoir-bays in downstream of the TGR, and algal blooms often occur in these bays, especially during warm springs

[15, 16]. Because of the importance of the TGR project, there has been a great deal of research on seasonal phytoplankton community variation [17], algal blooms, eutrophication [15], and the main factors affecting algae growth in it, especially in the important tributaries and bays, such as the Daning River [18, 19], Xiangxi Bay [16, 20, 21, 22] and Xiaojiang River [23]. However, the approach about phytoplankton functional groups in the whole reservoir, giant as TGR with dramatic water level fluctuations and complex water regimes, are still lacking.

In the present study, we applied the concept of phytoplankton functional groups to study phytoplankton community composition, structure, and its temporal and spatial variation in the mainstream and important tributaries in five sections along the longitudinal axis of the TGR. We assumed that the hydrological regime would be the main factor influencing the changes in biomass and composition of phytoplankton in the TGR. The intention of our study is to contribute useful information for improving aquatic environment and reservoir regulation in the TGR and other similar reservoir systems.

MATERIALS AND METHODS

Study area. The TGR is located in southwest China, and stretches from Sandouping of Hubei, to Jiangjin district of Chongqing Municipality (29°16′–31°25′ N, 106°–110°50′ E) (Fig. 1) [18, 24]. It is canyon-shaped, 663 km long and very deep (the maximum depth is about 160m). This region of China has a humid subtropical climate, with hot rainy summers and warm winters, early springs and cold autumns. The mean annual temperature was 18.4 °C and the mean annual precipitation was about 1050mm [24, 25].

In the present study, we chose five sections from downstream to upstream of the TGR: Zigui (ZG), Wushan (WS), Yunyang (YY), Zhongxian (ZX) and Mudong (MD). There were 10 sampling sites distributing in three different habitats, i.e. mainstream (M), main tributaries (T) and confluences (C) in each section (Fig. 1).

Sampling and processing. Sampling was carried out seasonally, in August, December 2012 and January, April 2013 respectively. One-liter samples were collected at a depth of 0.5m beneath the water surface, preserved with 1% neutral Lugol's solution and settled in a cylindrical bottle for more than 48 hours. We siphoned the supernatant off with a 2mm diameter hose, and collected the residue (50 mL) for counting algae.

Conductivity (Cond), pH, dissolved oxygen (DO, %), water temperature (Temp, °C) and turbidity (Turb, NTU) at each sampling site were measured with an YSI 6600 V2 multi-parametric sonde. Water transparency was measured with a Secchi disk. The data of total nitrate (TN), total phosphorus (TP), nitrate (NO- 3-N), soluble reactive phosphorus (SRP) and chlorophyll-a (Chl-a) were cited from Wang et al. [26] who took water samples at each samples sections simultaneously with us.

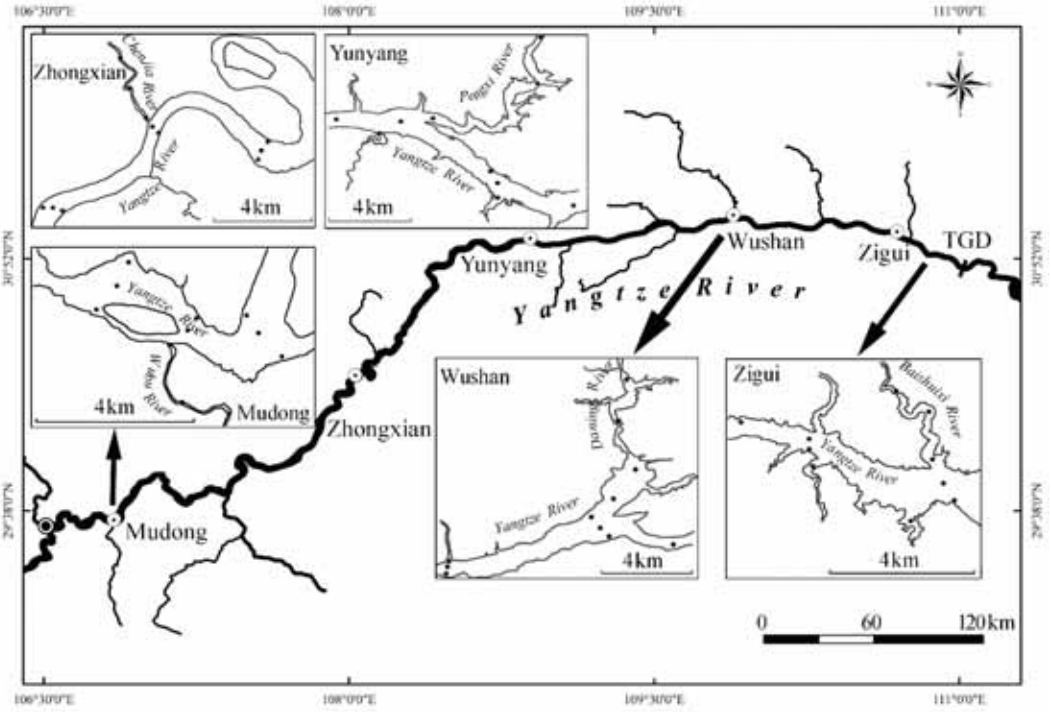

FIGURE 1
Distribution of sampling sites in the TGR

Sample analysis. We counted the phytoplankton with a light microscope (Leica DM 1000) at 400× magnification. Taxonomic identification of phytoplankton species was done according to Hu and Wei [27]. Phytoplankton functional groups were identified according to the criteria of Reynolds et al. [8] and Padisák et al. [11]. We calculated the phytoplankton bio-volume by the geometric shapes formulae [28]. Algae biomass was expressed in fresh weight, and 1 mm^3 L^{-1}= 1 mg L^{-1} was assumed [29, 30].

Calculations. Secchi depth (SD) was multiplied by 2.7 to provide an estimate of euphotic zone depth (Zeu) [31]. Depth of the mixing zone (Zmix) was equivalent to the depth of epilimnetic zone when water body was stratified. In the case of the absence of stratification, Zmix was equal to the actual depth at the sampling site [32]. The ratio of Zeu to Zmix was used as an index of light availability in the mixing zone [33]. Real-time water level data were obtained from the website of the China Three Gorges Corporation (http://www.ctgpc.com /sxjt/sqqk/index.html).

Relative water column stability (RWCS) was computed by using the following formula: RWCS= $(D_h-D_s)/ (D_4-D_5)$, where D_h is the bottom water density, D_s is the surface water density, D_4 and D_5 are the density of pure water at 4 °C and 5 °C, respectively [34]. In the present study, the depth of 0.5 m was considered as the "surface". The actual depth was considered as the "bottom" when it was less than 50 m, otherwise, while the depth of 50 m was considered as the "bottom" for depths of 50 m or more, because data from deeper strata were not measured.

The values of M, T, and C in each section were the average of the sampling sites data in the corresponding habitats.

Data analysis. Principal component analysis (PCA) was used to determine which physicochemical variables contributed to the temporal and spatial variation of phytoplankton. The PCA analysis was performed using the software CANOCO version 4.5 on the variables including Temp, Cond, DO (%), Turb, pH, Zeu, Zmix, Zeu/Zmix, RWCS, TP, TN, N/P, $NO^{3-}N$, and SRP. All variables were all transformed by log (x + 1).

Statistical analysis was carried out using the SPSS 18.0 package. Variance analysis (ANOVA) was employed for comparing means. In order to determine whether unimodal or linear ordination methods should be used we performed a detrended correspondence analysis (DCA) of the phytoplankton species and main environmental variables. Canonical correspondence analysis (CCA) was utilized to ordinate phytoplankton functional groups data with environmental variables, and this was tested using Monte Carlo simulation. DCA and CCA were run using the software CANOCO 4.5 [35] with the environmental and phytoplankton variables which were transformed to log (x + 1).

RESULTS

Hydrodynamics. Water level fluctuation and water flow variation of the TGR during the study period are shown in Fig. 2. As a consequence of hydraulic operations, the water level varied between 145.9 m and 172.5 m, with a range of 26.6 m. In the flood season (from June to September), water level of the TGR was maintained the lowest at 145 m by hydrologic regulation to achieve a capacity of flood storage of 22.15 billion m^3. At the end of the flood season (from August to September), the water level rose to 175 m rapidly, and was kept until the end of the dry season (February). The water level dropped to 145 m slowly during the transition period (March to May) before the next flood season. Water flow was higher in the flood season than in the dry season.

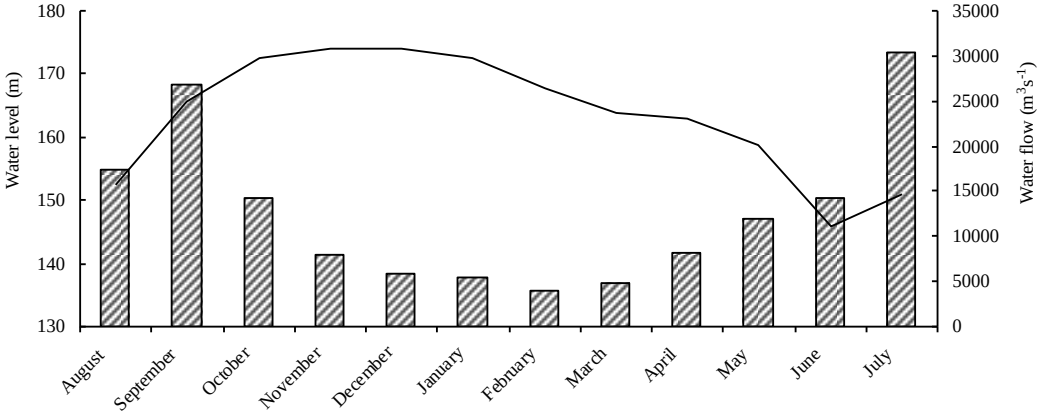

FIGURE 2
Water level fluctuations (solid line) and water flow variation (gray bars) of the Three Gorges Reservoir in the monitoring period (data from http://www.ctgpc.com/sxjt/sqqk/index.html)

The relative water column stability (RWCS) was higher in the tributaries during summer and was lower during autumn and winter (p<0.05), and intermediate in spring. The RWCS maintained a lower level during the sampling period in Zigui (ZG) and the mainstream of Wushan (WS), Yunyang (YY), Zhongxian (ZX) and Mudong (MD). It was relatively high in the confluences of WS and YY, and comparatively low at the confluences of ZG, ZX, and WS. (Fig. 3)

From the variation in RWCS, the mixing regime could be identified: the water column was stratified during summer in the tributaries and confluences, and was mixed in the autumn and winter. Spring was a transition period with the water column condition was transformed from mixing to stratification. The water column was mixed well in the mainstream during the whole year in the five sections.

Physical and chemical scenarios. Water temperature, euphotic zone, light availability, and turbidity showed significant spatial and temporal differences in the TGR (Figs. 4–7). Water temperature was higher in the upstream than in the downstream in spring (p<0.05), while in autumn and winter the reverse conditions prevailed (p<0.05), and in summer there was no significant spatial differences (p>0.05) (Fig. 4). The euphotic zone (Zeu) (Fig. 5) and light availability (Zeu/Zmix) (Fig. 6) of the water column were higher in tributaries than in the confluences and mainstream, and higher in the flood season than in the dry season. In addition, these values were higher in midstream (from Yunyang to Zhongxian) than in upstream (Mudong) and downstream (Zigui), while Turb values presented an opposite result (p<0.05) (Fig. 7).

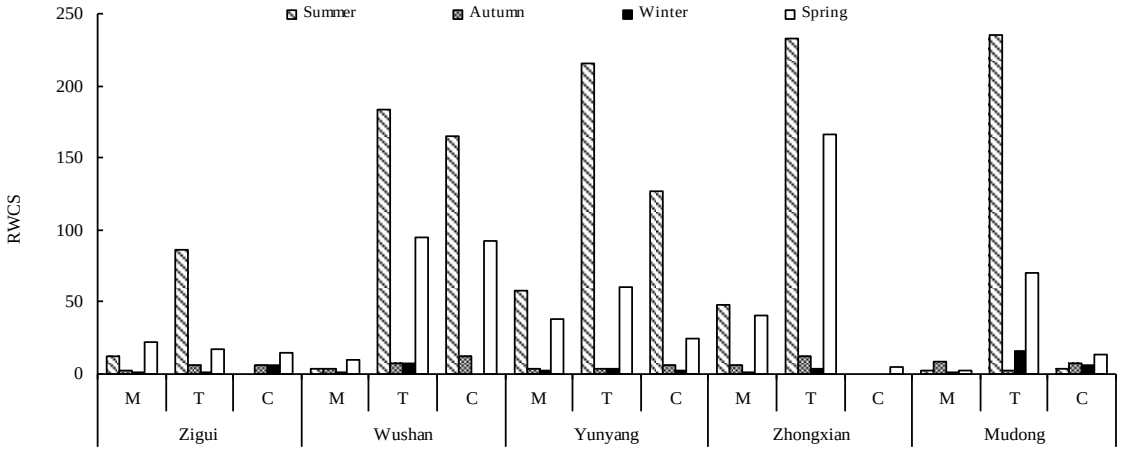

FIGURE 3
Seasonal and spatial variation of relative water column stability (RWCS) in the TGR (M-mainstream, T-tributary, C-confluence)

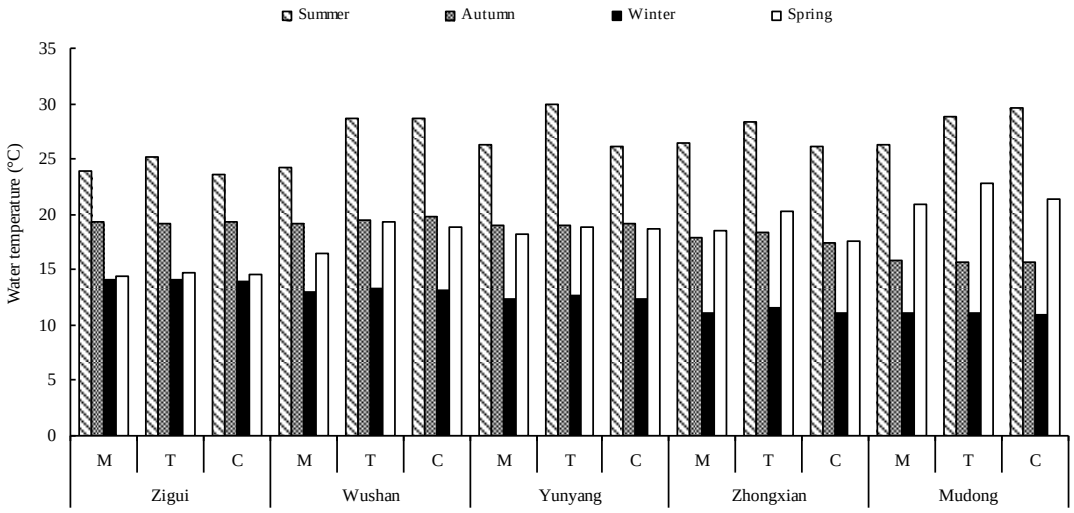

FIGURE 4
Seasonal and spatial variation of water tempreature in the TGR

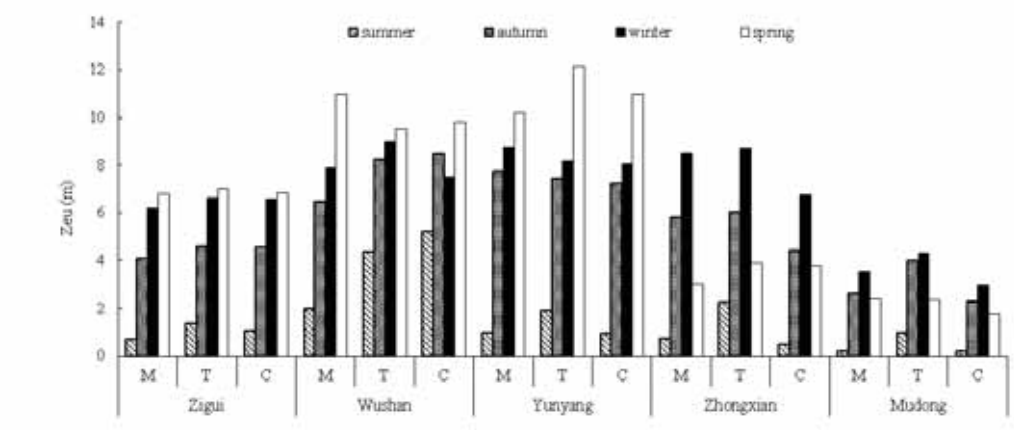

FIGURE 5
Seasonal and spatial variation of euphotic zone (Zeu) in the TGR

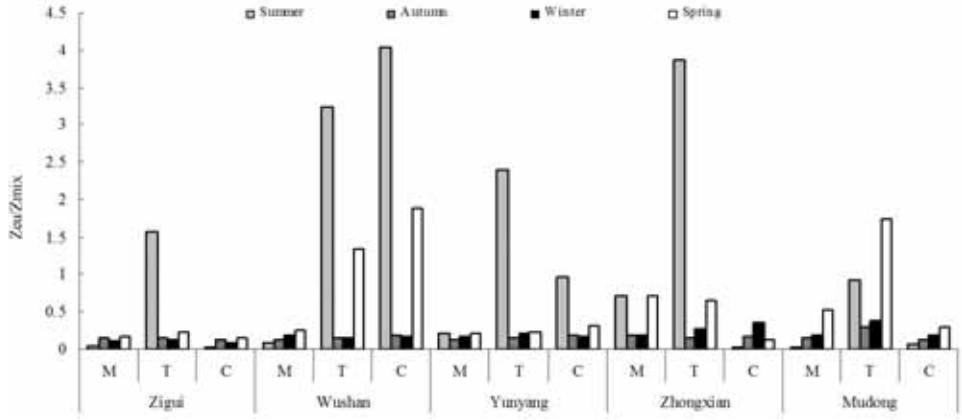

FIGURE 6
Seasonal and spatial variation of light availability (Zeu/Zmix) in the TGR

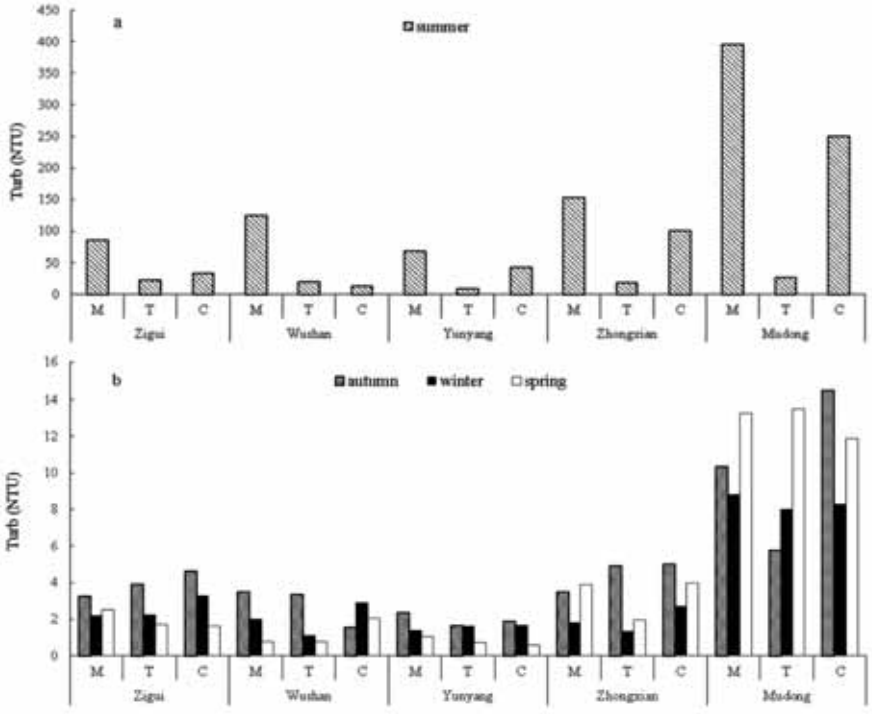

FIGURE 7
Seasonal and spatial variation of turbidity in the TGR, (a) summer; (b) autumn, winter, spring

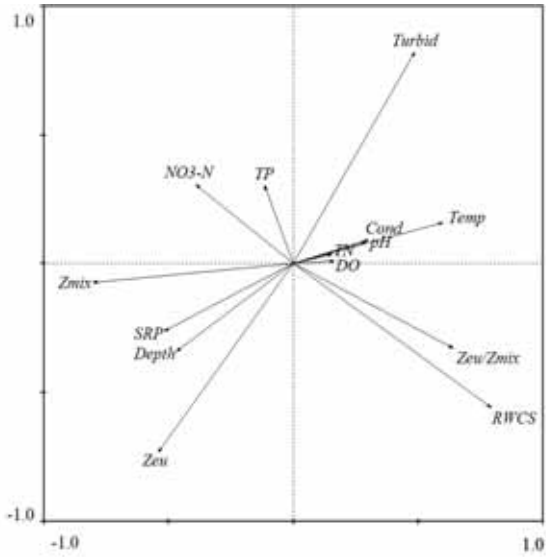

FIGURE 8
Principal components analysis of environmental variables in the TGR

PCA using fourteen abiotic variables explained 68.9% of the data variations in the first two axes (axis 1 = 39.9%, axis2 = 29%). The first principal component reflected the seasonal gradient and the mixing regime. The most important variables for axis 1 ordination were Zmix (−0.76), RWCS (0.87), Zeu/Zmix (0.67), and Temp (0.60). The second axis showed the gradient of the transparency of the water column; with the most important variables for its ordination were euphotic zone depth (Zeu) (−0.79) and Turb (0.90) (Fig. 8).

Phytoplankton dynamics. The average phytoplankton biomass in summer and spring was 8.36 mg L^{-1} and 6.29 mg L^{-1}, respectively, which was higher than that in autumn (0.49 mg L^{-1}) and winter (3.03 mg L^{-1}) (p<0.05). Furthermore, the phytoplankton biomass in the tributaries was higher than in the mainstream and confluences during the four seasons (p<0.05) (Fig. 9).

A total of 246 taxa of phytoplankton species were identified in the TGR, belonging to eight major taxonomic categories: Chlorophyta (122), Cyanophyta (31), Bacillariophyta (67), Cryptophyta (5), Pyrrrophyta (4), Euglenophyta (5), Chrysophyta (5), and Xanthophyta (1). The 246 phytoplankton taxa identified were members of 29 functional groups (Table 1). We considered functional groups which account for not less than 5% of total biomass at least one time during the sampling period as main groups. Twenty one main groups were recognized in our study(namely group B, C, D, E, F, G, H1, J, L_O, M, MP, N, P, S1, S_N, T_B, T_D, W1, X1, X2, and Y); collectively contributed more than 90% of total phytoplankton biomass in each sample. Most of the groups appeared in all the four seasons. The composition of the phytoplankton community and the process of succession were analyzed using these 21 prevailing functional groups. The typical traits of these main functional groups are shown in Table 2.

TABLE 1
Phytoplankton functional groups in the TGR

Group code	Genus included in the group	Group code	Genus included in the group
A	Rhizosolenia	M	Microcystis
B	Cyclotella, Coscinodiscus	P	Closterium, Closteriopsis, Melosira, Fragilaria
C	Melosira, Asterionella	T	Planctonema
Y	Cryptomonas	T_B	Melosira, Pinnularia
E	Dinobryon, Mallomonas	T_D	Oedocladium
G	Eudorina, Pandorina	W1	Gonium, Euglena, Phacus
H1	Aphanizomenon, Anabeana	W2	Trachelomonas
K	Aphanothece, Aphanocapsa	X1	Chlorella, Ankistrodesmus, Monoraphidium
D	Stephanodiscus, Nitzschia, Synedra, Cymatopleura	X2	Chroomonas, Chlamydomonas, Pteromonas, Dysmorphococcus, Ochromonas, Chromulina, Kephyrion
S1	Phormidium, Lyngbya	X3	Sphaerellopsis, Schroederia
S2	Spirulina	X_{PH}	Phacotus
S_N	Raphidiopsis, Cylindrospermopsis, Dactylococcopsis, Anabeana	N	Desmid, Spondylosium, Staurastrum, Gonatozygon, Tabellaria
L_O	Synechocystis, Chroococcus, Merismopedia, Ceratium, Peridinium, Peridinium, Gymnodinium	MP	Oscillatoria, Pseudanabaenaceae, Chlorococcum, Ulothrix, Melosira, Anomoeneis, Rhopalodia, Amphora, Epithemia, Navicula, Stauroneis, Cocconeis, Diatoma, Achnanthes, Cymbella, Diploneis, Surirella, Neidium, Gomphonema, Eunotia, Gyrosigma, Hantzschia, Caloneis, Amphiprora
J	Scenedesmus, Sorastrum, Actinastrum, Coronastrum, Pediastrum, Tetraedron, Crucigenia, Coelastrum, Chodatella, Franceia, Tetrastrum, Acanthosphaera, Golenkinia, Westellopsis, Tetradesmus	F	Sphaerocystis, Kirchneriella, Dictyosphaeria, Selenastrum, Palmella, Coccomyxa, Planktosphaeria, Treubaria, Botryococcus, Quadrigula, Elakatothrix, Westella, Oocystis, Nephrocytium, Micratinium, Gloeocystis, Asterococcus, Schizochlamys, Echinosphaerilla
T_C	Gloeocapsa		

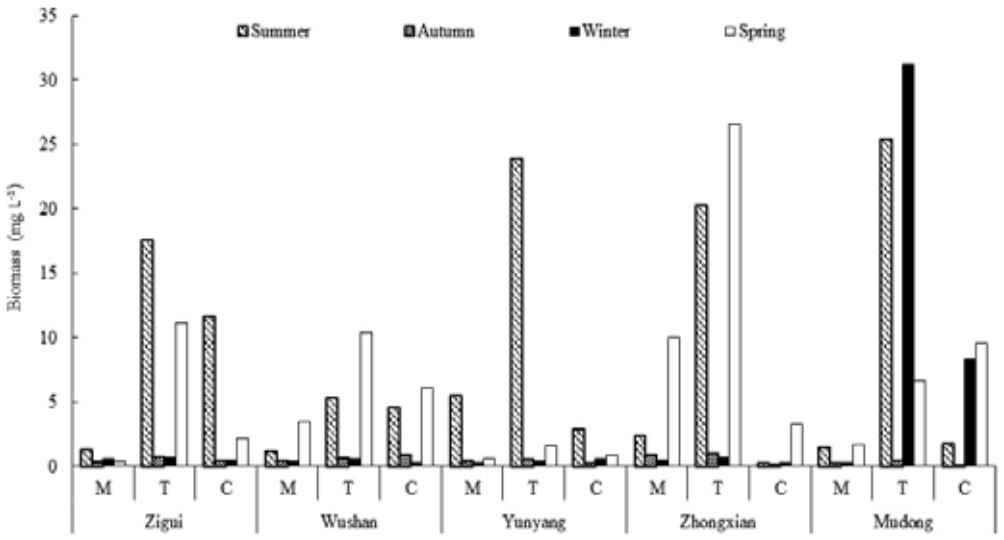

FIGURE 9
Seasonal and spatial variation of phytoplankton biomass (mg L^{-1}) in the TGR .

TABLE 2
Trait (quoted from Reyonlds et al. [8] and Padisák et al. [11]) of main phytoplankton functional groups (≥5% to the total biomass) detected in the TGR

Codon	Habitat template	Tolerances	Sensitivities
B	Mesotrophic small-medium-sized lakes	Light deficiency	pH rise, Si depletion, stratification
C	Eutrophic small- and medium-sized lakes	Light, C deficiencies	Si exhaustion, stratification
D	Shallow turbid waters including rivers	Flushing	Nutrient depletion
E	Eutrophic to hypertrophic, small- to medium-sized water bodies	Low nutrients (resort to mixotrophy)	CO_2 deficiency
F	Clear, deeply mixed and meso-eutrophic lakes	Low nutrients, high turbidity	CO_2 deficiency
G	Stagnating water columns with nutrient-rich conditions; small eutrophic lakes, and stable stages in larger reservoirs and river-fed basins	High light	Nutrient deficiency
H1	Eutrophic, both stratified and shallow lakes with low nitrogen content	Low nitrogen, low carbon	Mixing, poor light, low phosphorus
J	Shallow, mixed, highly enriched systems (including many low-gradient rivers)		Setting into low light
L_O	Deep and shallow, oligo to eutrophic, medium to large lakes	Segregated nutrients	Prolonged or deep mixing
M	Eutrophic to hypertrophic, small- to medium-sized water bodies	High insolation	Flushing, low total light
MP	Frequently stirred up, inorganically turbid shallow lakes		
N	Continuous or semi-continuous mixed layer of two to three meters in thickness. This group can live in shallow lakes which the mean depth is within this regulation or greater, and also in the mixing phases in stratified lakes epilimnia	Nutrient deficiency	Stratification, pH rise
P	Similar to that of codon N but at higher trophic states	Mild light and C deficiency	Stratification, Si depletion
S1	Turbid mixed environments. This codon includes only shade-adapted cyanoprokaryotes	High light Deficient conditions	flushing
S_N	Warm mixed environments	Light-nitrogen-deficient condition	flushing
T_D	Mesotrophic standing waters or slow-flowing rivers with emergent macrophytes		
T_B	Highly lotic environments (streams and rivulets)		
W1	Ponds, even temporary, rich in organic matter from husbandry or sewages	High BOD	grazing
Y	Including large cryptomonads and small dinoflagellates, can live in wide range of habitats, and its representative species could exist in almost all lentic habitats with low grazing pressure	Low light	Phagotrophs
X1	Shallow, eu-hypertrophic environments	stratification	Nutrient deficiency, filter feeding
X2	Shallow, meso-eutrophic environments	stratification	Mixing, filter feeding

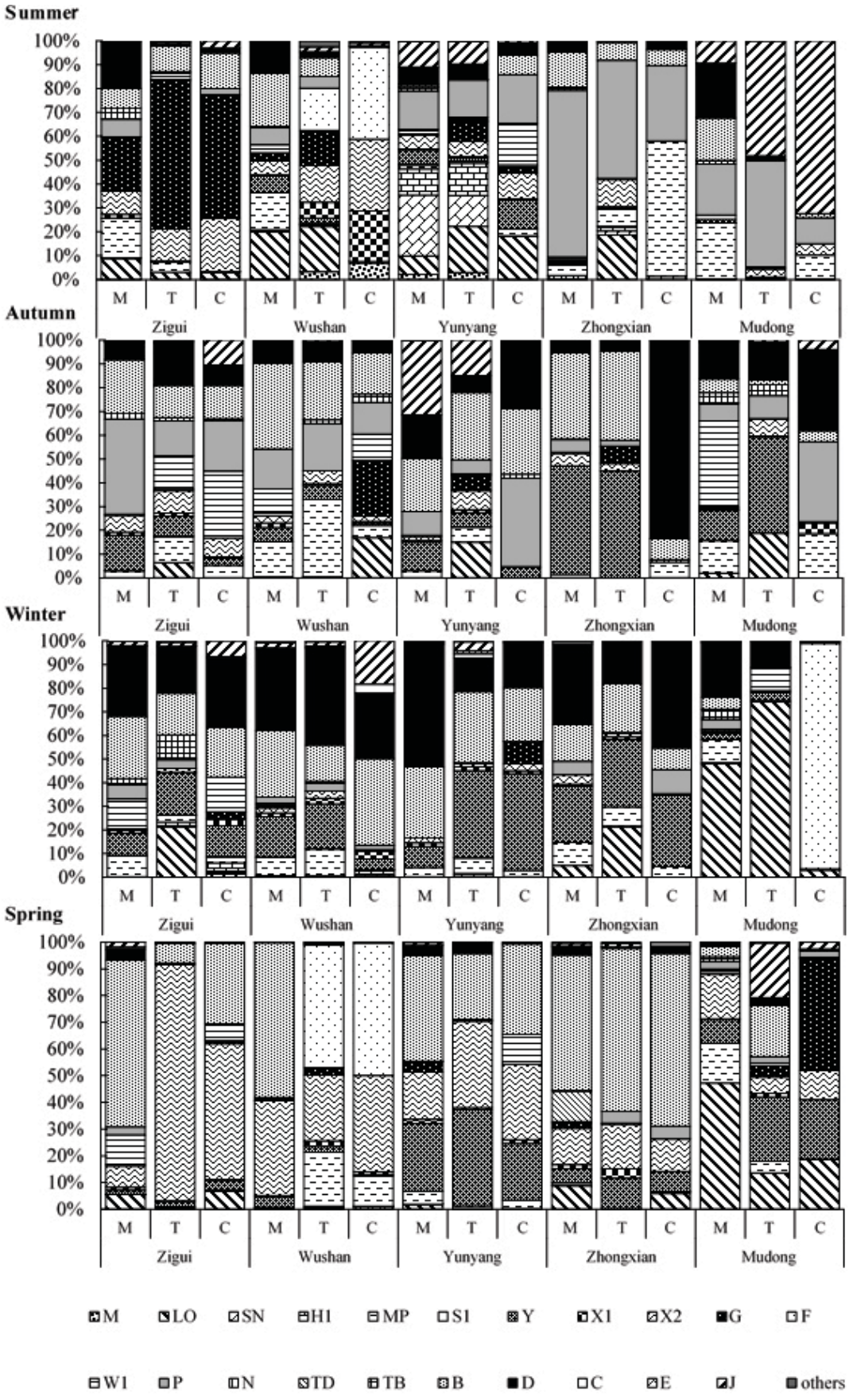

FIGURE 10
Spatial variation in relative biomass (%) of the 21 major phytoplankton functional groups in the four seasons of the TGR

There were marked seasonal variations in the representation of each of the 21 main phytoplankton functional groups (Fig. 10). During summer, groups S_N, P, B, and D dominated in the mainstream (58% of total biomass), L_O, G, and J dominated in the tributaries (54%) and X2, G, B, J dominated in the confluences (69%). In autumn, the mainstream was dominated by groups Y, P, and B (66%), the tributary was dominated by Y, B, D (57%) and the confluence was dominated by Y, P, B and D (68%). In winter groups Y, B, and D dominated in the mainstream (70%), groups L_O and D dominated in the tributaries (82%) and L_O, F, D dominated in the confluences (81%). In spring groups L_O, X2, B dominated in the mainstream (77%), Y, X2, B dominated in the tributaries (75%) and X2, F, B dominated in the confluences.

Canonical correspondence analysis. A DCA of the prevailing phytoplankton functional groups revealed that the gradient length of the first axis was 3.6, and therefore CCA was performed to reveal the relationships between environmental variables and phytoplankton functional groups. The CCA ordination results on axes 1 and 2 are showed in Figs. 11a and b. Automatic forward selection was used for the six main environmental variables. The Monte Carlo permutation test (499 random permutations) revealed that the first axis and all axes were significant (F = 17.14, P = 0.002; F = 7.84, P = 0.002).

The CCA ordination for phytoplankton functional groups and environmental variables on all canonical axes cumulatively accounted for 94.2% of the variance in phytoplankton-environment relationships, 41.6% and 30.4% of the variance were explained by the first two CCA axes. The relative eigenvalues of axis 1, 2, 3, and 4 were 0.238, 0.174, 0.074, and 0.053, respectively. All the six environmental variables were selected as significant variables (Temp p = 0.002, F = 16.40; Zeu/Zmix p = 0.006, F = 12.82; Turbid p = 0.006, F = 4.94; RWCS p = 0.002, F= 4.19; Zeu p = 0.01, F = 3.47, Zmix p = 0.034, F =2.29).

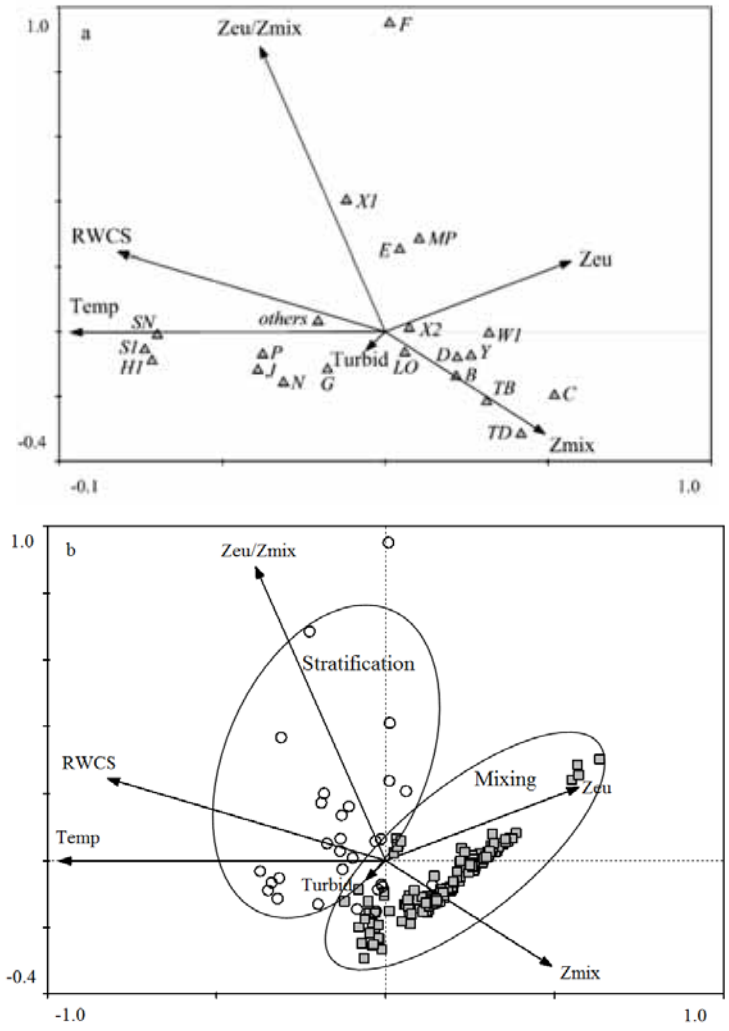

FIGURE 11

CCA Biplot of the relationship between 6 environmental variables (black lines) and (a) phytoplankton functional groups, and (b) sampling time. In (a) the functional groups are shown by gray triangles. In (b) the sample times are: white circle, stratification period; gray square, mixing period.

DISCUSSION

The growth of phytoplankton is usually limited by the combined net effects of nutrient availability, major ions, pH, light availability, water temperature, and other physicochemical factors, especially nutrient and light availability [36, 37, 38, 39]. All the above factors may be strongly related to the water flowing, morphology and hydrology of the water body [32]. In reservoirs, the hydraulic regime generally affects the structure and abundance of the phytoplankton community by influencing the availability of nutrient and light [32, 40, 41, 42].

After the impoundment of the TGR, the water level and water depth increased, and temperature stratification in tributaries during the wet season occurred. Water flow velocity was reduced and the water environment of the reservoir area has changed from a typical river water to a kind of water body like lake. During our study, the water regime of the TGR showed obvious spatial and seasonal heterogeneity. In the mainstream, water flow velocity was relatively high, and large amounts of sediment were transported from the bare shoreline by surface runoff and river flow [43]. This caused high turbidity, low Zeu, and low RWCS during the study period, especially in summer. The concentration of TP and TN in the mainstream was not lower than in the tributaries [26], but the biomass of phytoplankton maintained low level in the mainstream in our study. Therefore, we speculate that light availability may be the most important limiting factor in the growth of phytoplankton in the TGR's mainstream. This may explain why phytoplankton biomass was low in the mainstream during the whole sampling period.

In the tributaries and confluences, sediment sunk to the bottom because of the low flow velocity, creating conditions where turbidity was lower and Zeu was higher than in the mainstream. There was a period of stratification in the tributaries during the wet season, which could inhibit the internal circulation of nutrients. In turn, nutrient availability would decrease as surface water temperature and water column stability increase, and limit the growth of phytoplankton in the euphotic zone [44, 45]. However, the frequent precipitation in summer and spring brings external nutrients from the terrestrial ecosystem into the reservoir and increases nutrient availability in the surface water. The biomass of phytoplankton was high in such a condition, and there was a higher frequency of algal blooms in tributaries and reservoir-bays [15].

Phytoplankton functional groups under stratification condition and mixing condition were separated in the result of CCA (Fig. 11b). Stratification condition was characterized by a high value of light availability, water column stability and water temperature and low turbidity, while mixing condition was on the contrary.

There are riverine, transitional, and lacustrine, three major zones in typical reservoirs [46]. And this theory is applied to conditions in the mainstream of the TGR. The Zigui section, in the head region of the TGR, very close to the Three Gorges Dam, may be the region most affected by reservoir impounding and water level fluctuations, in summer and spring of the TGR, although the inflows were relatively higher than in autumn and winter, the velocity was still low [19]. When the water level was stable, the relative stability of the water column increased, and thermal stratification developed in the tributaries. In the tributary of the Zigui section, the phytoplankton functional groups G and X2 were dominant in summer and spring, respectively. The two groups consisting of Chlorophyta (*Eudorina elegans*, *Pandorina morum* and etc.) and Cryptophyta (*Chroomonas*) which are well adapted to live in nutrient–rich conditions in standing water [11]. The competitiveness of the two groups is enhanced by the possession of flagella, which may significantly decrease its sinking rate and allow vertical migration between water layers with optimal light conditions and nutrient concentrations [47, 48].

Spring was the beginning of the wet season, and thermal stratification developed as the water warmed up. However, this was a transition period and stratification in the tributaries was not stable. Group B and X2, which are well adapted to low light availability conditions, showed high relative biomass in this low Zeu/Zmix. Group B included larger centric diatoms (GALD>10 μm), and their shape makes contribution to the high surface/volume for light harvesting efficiently. Furthermore, their dependence on turbulence for suspension makes them sensitive to mixing depth and the seasonal water column stratification [8], which may explain the relatively low biomass of group B observed in summer.

In autumn, the water level rose rapidly and the backwater from the Changjiang River disrupted the thermal stratification and caused rapid water body mixing in the tributaries. Moreover, there was no significant spatial heterogeneity in the hydrological regimen between the mainstream and tributaries (p>0.05). Low Zeu/Zm values recorded in autumn and winter indicate that light was an important limiting factor for phytoplankton growth. A community consisting of diatoms (groups B, D, and P) and Cryptophyta (group Y) dominated in autumn. The CCA biplot diagram (Fig. 11a) showed that these groups were well adapted to mixing and low light availability conditions. The shape of the diatoms in groups B, D and P contributes to the maintenance of high surface/volume and efficient light harvesting. Group Y could live in a wide range of habitats. However, phytoplankton in this group are vulnerable to the feeding activities of lots kinds of crustacean zooplankton, a few rotifers, and protistans [8]. However, the grazing pressure in the TGR during the dry season was relatively low [49, 50, 51].

In winter, the dominant groups in the TGR were the same as in autumn, except for the Mudong section. The biomass of phytoplankton was relatively high in the Mudong tributary and reached 0.8 mg L^{-1}, group L_O (*Peridiniopsis* sp.) had absolute predominance (74%). *Peridiniopsis* sp. is a kind of eurythermic alga that can multiply rapidly in a wide range of water temperature (10–28 °C) [52]. The mild temperature (about 10 °C), calm water column, and domestic sewage rich in organic nutrients discharged by Mudong Town provided a good growing condition for the mass propagation of *Peridiniopsis* sp. [53, 54].

CONCLUSION

In the TGR, temperature, water-level fluctuation and water flow have a major effect on the structure and abundance of phytoplankton functional groups because of their influence on the stability and turbidity of the water body. The functional groups approach provides a practical way of describing the seasonal variations in phytoplankton in the large and deep subtropical reservoir.

Data Availability Statement. The data that support the findings of this study are available from the corresponding author upon reasonable request.

ACKNOWLEDGEMENTS

This study was financially supported by the Special Scientific Research Fund of Agriculture Public Welfare Profession of China (No. 201303056), the State Key Laboratory of Freshwater Ecology and Biotechnology (Grant No. 2011FBZ28), and the Science and Technology Research Project of China Three Gorges Corporation (CT-12-08-01). And we thank all colleagues and Mr. CHEN at the fisheries ecology lab for their assistance in the field.

REFERENCES

[1] Dubnyak, S. and Timchenko, V. (2000) Ecological role of hydrodynamic processes in the Dnieper reservoirs. Ecological Engineering. 16, 181–188.

[2] Naselli-Flores, L. and Barone, R. (1997) Importance of water level fluctuation on population dynamics of cladocerans in a hypertrophic reservoir (Lake Arancio, south-west Sicily, Italy). Hydrobiologia. 360, 223–232.

[3] Huszar, V., Kruk, C. and Caraco, N. (2003) Steady-state assemblages of phytoplankton in four temperate lakes (NEUSA). Hydrobiologia. 502, 97–109.

[4] Borges, P.A.F., Train, S. and Rodrigues, L.C. (2008) Spatial and temporal variation of phytoplankton in two subtropical Brazilian reservoirs. Hydrobiologia. 607, 63–74.

[5] Naselli-Flores, L. and Barone, R. (2000) Phytoplankton dynamics and structure: a comparative analysis in natural and manmade water bodies of different trophic state. Hydrobiologia. 438, 65–74.

[6] Costa, L.S., Huszar, V.L.M. and Ovalle, A.R. (2009) Phytoplankton functional groups in a tropical estuary: hydrological control and nutrient limitation. Estuaries & Coasts. 32, 508–521.

[7] Grime, J.P. (1977) Evidence for the existence of three primary strategies in plants and its relevance to ecological and evolutionary theory. American Naturalist. 111, 1169–1194.

[8] Reynolds, C.S, Huszar, V., Kruk, C., Naselli-Flores, L. and Melo, S. (2002) Towards a functional classification of the freshwater phytoplankton. Journal of Plankton Research. 24, 417–428.

[9] Kruk, C., Mazzeo, N., Lacerot, G. and Reynolds, C.S. (2002) Classification schemes for phytoplankton: a local validation of a functional approach to the analysis of species temporal replacement. Journal of Plankton Research. 24, 901–912.

[10] Borics, G., Várbíró, G., Grigorszky, I., Krasznai, E., Szabó, S. and Kiss, K.T. (2007) A new evaluation technique of potamo-plankton for the assessment of the ecological status of rivers. Large Rivers. 161, 465–486.

[11] Padisák, J., Crossetti, L.O. and Naselli-Flores, L. (2009) Use and misuse in the application of the phytoplankton functional classification: a critical review with updates. Hydrobiologia. 621, 1–19.

[12] Xiao, L.J., Wang, T., Hu, R., Han, B.P., Wang, S., Qian, X. and Padisák, J. (2011) Succession of phytoplankton functional groups regulated by monsoonal hydrology in a large canyon-shaped reservoir. Water Research. 45, 5099–5109.

[13] Cadotte, M.W., Carscadden, K. and, Mirotchnick, N. (2011) Beyond species: functional diversity and the maintenance of ecological processes and services. Journal of Applied Ecology. 48(5), 1079–1087.

[14] O'Gormann, E.J., Yaersley, J.M., Crowe, T.P., Emmerson, M.C., Jacob, U. and Petchey, O.L. (2011) Loss of functionally unique species may gradually undermine ecosystems. Proceedings Biological Sciences. 278, 1886–1893.

[15] Cai, Q.H. and Hu, Z.Y. (2006) Studies on eutrophication problem and control strategy in the Three Gorges Reservoir. Acta Hydrobiologica Sinica. 30, 7–11. (in Chinese with English abstract).

[16] Xu, Y.Y., Cai, Q.H., Ye, L., Zhou, S.C. and Han, X.Q. (2009) Spring diatom blooming phases in a representative eutrophic Bay of the Three-Gorges Reservoir, China. Journal of Freshwater Ecology. 24, 191–198.
[17] Wang, J.Y., Wang, Z.C., Li, C., Ye, S.W., Lian, Y.X., Liu, J.S., Zhang, T.L. and Li, Z.J. (2015) The spatio-temporal dynamic of phytoplankton community structure in the head region of the Three Gorges Reservoir. Acta Hydrobiologica Sinica. 39(5), 877–884. (in Chinese with English abstract).
[18] Huang, C., Zhong, C.H., Deng, C.G., Xing, Z.G., Li, Y.J., Wang, D.R. and Meng, W.L. (2006) Preliminary study on correlation between flow velocity and algae along Daning River's backwater region at sluice initial stages in the Three Gorges Reservoir. Journal of Agro-Environment Science. 25(2), 453–457. (in Chinese with English abstract).
[19] Zhu, K.X., Bi, Y.H. and Hu, Z.Y. (2013) Responses of phytoplankton functional groups to the hydrologic regime in the Daning River, a tributary of Three Gorges Reservoir, China. Science of the Total Environment. 450–451, 169–177.
[20] Li, F.Q., Ye, L., Liu, R.Q., Cao, M. and Cai, Q.H. (2008) Dynamics of main nutrient input to Xiangxi Bay of the Three-Gorges Reservoir. Acta Ecologica Sinica. 28(5), 2073–2097.
[21] Wang, L., Cai, Q.H., Tan, L. and Kong, L.H. (2011) Longitudinal differences of phytoplankton community during a period of small water level fluctuations in a subtropical reservoir bay (Xiangxi Bay, Three Gorges Reservoir, China). International Review Hydrobiology. 96, 381–396.
[22] Yang, M., Bi, Y.H., Hu, J.L., Zhu, G.X. and Hu, Z.Y. (2011) Seasonal variation in functional phytoplankton groups in Xiangxi Bay, Three Gorges Reservoir. Chinese Journal of Oceanology and Limnology. 29(5), 1057–1064.
[23] Guo, J.S., Chen, J., Li, Z., Fang, F., Zhang, C. and Tian, G. (2008) Investigation of phytoplankton and assessment of algal diversity on backwater area of Xiaojiang River in Three Gorges Reservoir after its initiate impounding to the water level of 156 m in spring. Environmental Science. 29(10), 2710–2715. (in Chinese with English abstract)
[24] Chinese Research Academy of Environmental Sciences (C.R.A.E.S). (2004) Studies report on the assessment standards and methods for trophic status in the Three Gorges Reservoir. (in Chinese).
[25] Deng, C.G. (2007) Studies on Entrophication in the Three Gorges Reservoir. Environmental Science Press, Beijing, China. 197p. (in Chinese).
[26] Wang, S.Y., Zhou, Z.J., Wang, Z.C., Li, H., Chao, X.Y., Song, C.L. and Zhou, Y.Y. (2015) The distribution of nutrients in the Three Gorges Reservoir and the effects on the growth of algae. Acta Hydrobiologica Sinica. 39(5), 910–919. (in Chinese with English abstract)
[27] Hu, H.J. and Wei, Y.X. (2006) The Freshwater Algae of China–Systematics, Taxonomy and Ecology. Science Press, Beijing, China. P. 1–1023. (in Chinese)
[28] Hillebrand, H., Dürselen, C.D., Kirschtel, D., Pollingher, U. and Zohayr, T. (1999) Biovolume calculation for pelagic and benthic microalgae. Journal of Phycology. 35, 403–424.
[29] Zhang, Z.S. and Huang, X.F. (1991). The Research Methods for Freshwater Plankton. Science Press, Beijing, China. 414p. (in Chinese).
[30] Wetzel, R.G. and Likens, G.E. (2000) Limnological Analyses. 3rd edn. Springer, New York, America. 147–174.
[31] Cole, G.A. (1994) Textbook of Limnology. Waveland Press Inc., Illinois, America. 1–412.
[32] Naselli-Flores, L. (2000) Phytoplankton assemblages in twenty-one Sicilian reservoirs: relationships between species composition and environmental factors. Hydrobiologia. 424, 1–11.
[33] Jensen, J.P., Jeppensen, E., Olrik, K. and Kristensen, P. (1994) Impact of nutrients and physical factors on the shift from cyanobacterial to chlorophyte dominance in Danish lakes. Canadian Journal of Fisheries & Aquatic Sciences. 51, 1692–1699.
[34] Padisák, J., Barbosa, F., Koschel, R. and Krienitz, L. (2003) Deep layer cyanoprokaryota maxima in temperate and tropical lakes. Advances in Limnology. 58, 175–199.
[35] Lepš, J. and Šmilauer, P. (2003) Multivariate Analysis of Ecological Data Using CANOCO. Cambridge University Press, New York, America. 269p.
[36] Tilman, D., Kilham, S.S. and Kilham, P. (1982) Phytoplankton community ecology: the role of limiting nutrients. Annual Review of Ecology & Systematics. 13, 349–372.
[37] Reynolds, C.S. (1998) What factors influence the species composition of phytoplankton in lakes of different trophic status? Hydrobiologia. 369(370), 11–26.
[38] Reynolds, C.S. (1999) Phytoplankton Assemblages in Reservoirs. In: Tundisi, J.G., Straskraba, M. (eds.) Theoretical Reservoir Ecology and Its Applications. Backhuys, Leiden, Netherlands. 439–56.
[39] Xing, W., Huang, W.M., Liu, G.H., and Liu, Y.D. (2008) Effect of iron on physiological and biochemical characteristics of *Microcystis wesenbergii* (Kom.) Kom. (Cyanobacterium). Fresen. Environ. Bull. 17, 2034–2042.

[40] Reynolds, C.S. (2006) The Ecology of Phytoplankton. Cambridge Univ. Press, Cambridge, UK. 550p.
[41] Wilk-Wożniak, E. and Pociecha, A. (2007) Dynamics of chosen species of phyto- and zooplankton in a deep submontane dam reservoir in light of differing life strategies. Oceanological and Hydrobiological Studies. 36, 35–48.
[42] Sönmez, F., Kutlu, B., Sesli, A. (2017) Spatial and temporal distribution of phytoplankton in Karkamis Dam Lake (Sanliurfa/ Turkey). Fresen. Environ. Bull. 26, 6234–6245.
[43] Shi, D.M., Yang, Y.S., Lv, X.X. and Liang, Y. (1991) An analysis of soil erosion rules and sediment producing sources in the region of Three-Gorge of the Yangtze River. Journal of Soil & Water Conservation. 5(3), 9–21. (in Chinese with English abstract).
[44] Arfi, R. (2005) Seasonal ecological changes and water level variations in the Sélingué Reservoir (Mali, West Africa). Physics and Chemistry of the Earth. 30, 432–441.
[45] Becker, V., Caputo, L., Ordóñez, J., Marcé, R., Armengol, J., Crossetti, L.O. and Huszar, V.L.M. (2010) Driving factors of the phytoplankton functional groups in a deep Mediterranean reservoir. Water Research. 44, 3345–3354.
[46] Kimmel, B.L. and Groeger, A.W. (1984) Factors controlling primary production in lakes and reservoirs: a perspective. Lakes Lake & Reservoir Management. 1, 277–81.
[47] Klaveness, D. (1988) Ecoloy of Cryptomonadida: A First Review. In: Sandgren, C.D. (ed.) Growth and Reproductive Strategies of Freshwater Phytoplankton. Cambridge University Press, Cambridge, UK. 105–133.
[48] Bovo-Scomparin, V.M. and Train, S. (2008) Long-term variability of the phytoplankton community in an isolated floodplain lake of the Ivinhema River State Park, Brazil. Hydrobiologia. 610, 331–344.
[49] Yao, J.L., Xue, J.Z., Wang, D.Y., Cai, Q.H., Huang, X.F. and Liu, J.K. (2007) Seasonal variation and longitudinal distribution of copepods in the main river area of the Three Gorges Reservoir. Biodiversity Science. 15(3), 300–305. (in Chinese with English abstract).
[50] Wu, H.X., Yao, J.L., Xue, J.Z., Cai, Q.H. and Liu, J.K. (2009) Seasonal variation and longitudinal distribution characters of cladocerans in the Three Gorges Reservoir. Biodiversity Science. 17(5), 512–517. (in Chinese with English abstract).
[51] Chen, Y. (2009) Studies on Structure of Phytoplankton and Rotifer Community in the Three Gorges Reservoir. Chongqing: Southwest University. 39–52 (in Chinese with English abstract).
[52] Tang, H.B., Hu, S., Hu, Z.Y., Kuang, Q.J. and Liu, G.X. (2007) Relationship between *Peridiniopsis* sp. And environmental factor in Lake Donghu, Wuhan. Journal of Lake Sciences. 19(6), 632–636. (in Chinese with English abstract).
[53] Pollingher, U. and Zemel, E. (1981) In situ and experimental evidence of the influence of turbulence on cell division processes of Peridinium cinctum forma westii (Lemm.) Lefèvre. British Phycological Journal. 16, 281–287.
[54] Sun, J. and Guo, S.J. (2011) Dinoflagellate heterotrophy. Acta Ecologica Sinica. 31(20), 6270–6286. (in Chinese with English abstract).

Received: **25.06.2017**
Accepted: **22.10.2017**

CORRESPONDING AUTHOR

Zhongjie Li
State Key Laboratory of Freshwater Ecology and Biotechnology,
Institute of Hydrobiology,
Chinese Academy of Sciences,
No. 7, Donghu South Road, Wuchang District,
Wuhan, 430072 – China

e-mail: zhongjie@ihb.ac.cn

© by PSP Volume 27 – No. 2/2018 pages 960-970 Fresenius Environmental Bulletin

APPLICATION OF A MULTI-SUBGROUP HYBRID ALGORITHM IN AUTOMATIC PARAMETERIZATION OF A DISTRIBUTED SWAT HYDROLOGICAL MODEL

Ye Liu[1,2], Li Zhang[1,2], Lei Wu[1,2], Wen-gang Zhao[1,2], Xiao-yi Ma[1,2,*]

[1]College of Water Resources and Architectural Engineering, Northwest A&F University, Yangling, Shaanxi 712100, P.R. China
[2]Key Laboratory of Agricultural Soil and Water Engineering in Arid and Semiarid Areas of Ministry of Education, Northwest A&F University, Yangling, Shaanxi 712100, P.R. China

ABSTRACT

The complexity of parameters in a physically based distributed hydrological system increases the difficulty of model calibration and validation. The accuracy of SWAT hydrological parameters calibration is crucial for effectively simulating water, sediments and nutrients. Genetic algorithms (GAs) have a broad global-searching ability, and particle swarm optimization (PSO) has an accurate local-searching ability, so we developed a multi-subgroup GA-PSO hybrid algorithm that combined the characteristics of good generalization and fast convergence. We then comparatively evaluated GA-PSO with GA, PSO and SUFI-2 in a SWAT-CUP model for the Daxi River watershed. Calibration was good for PSO and SUFI-2, but the precision of validation was slightly deficient. The performance of GA was stable in the two periods, but was poor for the evaluation indices and peak flows. The hybrid GA-PSO algorithm, however, obtained the best streamflow line and precise peak flow, with Nash-Sutcliffe coefficients of 0.91 and 0.92 and coefficients of determination of 0.91 and 0.93 during the calibration and validation periods, respectively. This algorithm provides an important theoretical and practical reference for the popularization and application of the automatic calibration of hydrological models.

KEYWORDS:
Genetic algorithms, particle swarm optimization, multi-subgroup, parameter calibration, SWAT model

INTRODUCTION

The Soil and Water Assessment Tool (SWAT) [1] is a distributed hydrological model with strong hydrological physical mechanisms. Accurate calibration of SWAT hydrological parameters is crucial for applying the model to effectively simulate water, sand, and nutrients [2-4]. Manual calibration and computerized automatic optimization have recently been introduced to guide the parameterization of hydrological models [5, 6]. Automatic parameterization can greatly increase the speed of parameter optimization, and the objectivity and reliability of simulations due to the subjectivity and slowness of manual parameterization [7, 8].

Some studies have applied parallel or hybrid algorithms for global optimization to calibrate hydrological parameter [9-11] in order to reduce the time required and improve premature convergence. Wang [12] first applied a GA for calibrating the parameters of a hydrological model, and GAs have since become an active global-searching tool with highly parallel, random and adaptive optimization capabilities [13, 14]. And the later PSO algorithm, with simpler structures, has the advantages of fast evolutionary search efficiency by accurate local-searching abilities, which GAs lack [15-17].

Combined the advantages of the strong global-searching ability (GAs) and the fast convergence (PSO), this paper introduced a multi-subgroup hybrid GA-PSO algorithm to automatically calibrate the parameters of a distributed SWAT hydrological model. This algorithm economizes the calibration time and overcomes the shortages of the lower efficiency of late evolution and premature convergence, which improves the efficiency and stability of hydrological parameterization. The objectives of this study were therefore to: 1) propose a multi-subgroup hybrid algorithm combining a GA and PSO for the automatic parameter calibration of SWAT models; 2) compare simulations using the hybrid algorithm with those by SWAT-CUP, GA, and PSO; 3) assess the applicability of the proposed hybrid algorithm in the Daxi River basin.

MATERIALS

Study area. The Daxi River (107°00'-107°57'E, 34°54'-35°14'N) is a secondary tributary of the Jinghe River. The basin originates in Baoji in Shaanxi Province, runs through Lingtai in Gansu Province, and finally merges with the Heihe River in Shaanxi Province. The catchment area of the basin is 2537 km^2, the river is 127 km long, the mean annual precipitation in the basin is 555.9 mm, and the aver-

age runoff is 1.6×10^8 m^3. The basin has a warm temperate semi-arid continental monsoon climate. The average annual temperature is 8.6°C, the mean annual frost-free period is 159 days, the mean annual hours of sunshine is 2452, and the sunshine percentage is 53%.

Data sources. A digital elevation model, land-use types, and soil types for the Daxi River basin, pretreated by ArcGIS, are shown in Fig. 1-3 respectively. The attribute data, mainly meteorological information, included daily rainfall at three national meteorological stations and daily meteorological data measured by 10 stations with rain gauges. The environmental database in this study depicts in Table 1, and the soil types and land use types with each area statistics show in Table 2 and 3.

In this application process, the Daxi River basin was divided into 33 sub-basins (Fig. 4) using a SWAT model. The average monthly streamflow, for the first sub-basins from the Zhang Jiagou hydrological station, were divided into three stages: a buffer period in 1980, a calibration period from 1981 to 1985 and a verification period from 1986 to 1988.

METHODS

SUFI-2. SWAT-CUP, a SWAT calibration and uncertainty program developed by the Swiss Federal Institute of Water Science and Technology, is a public computer program for analyses of parameter sensitivity and uncertainty, parameter calibration and validation. The SUFI-2 (Sequential Uncertainty Fitting, ver.2) algorithm is a kind of comprehensive optimization and gradient search method developed by Abbaspour et al [18], which is one of the most widely used approaches for hydrological model uncertainty analysis.

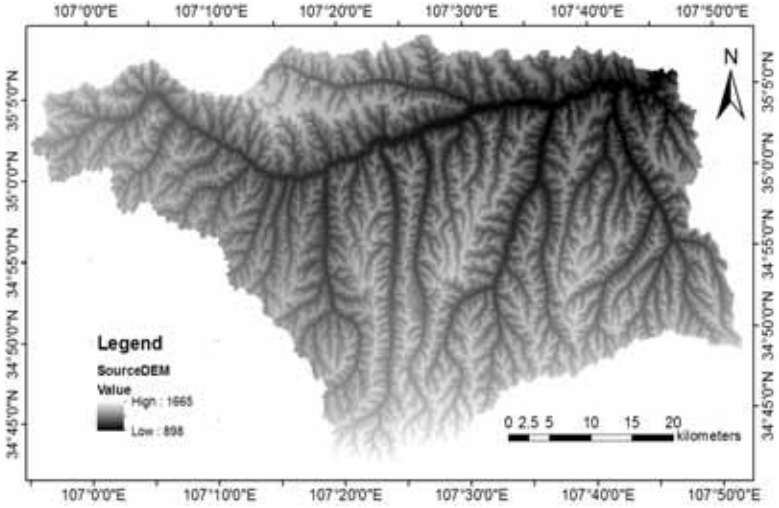

FIGURE 1
Digital Elevation Model (DEM) of the Daxi River basin.

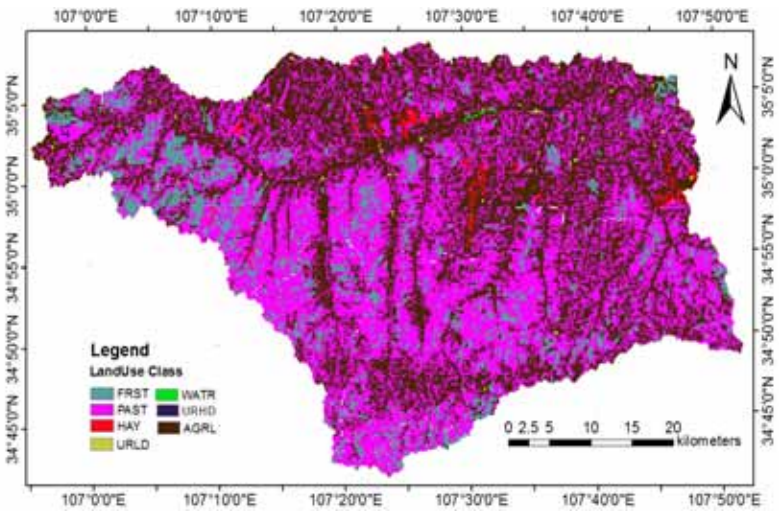

FIGURE 2
Land use types of the Daxi River basin.

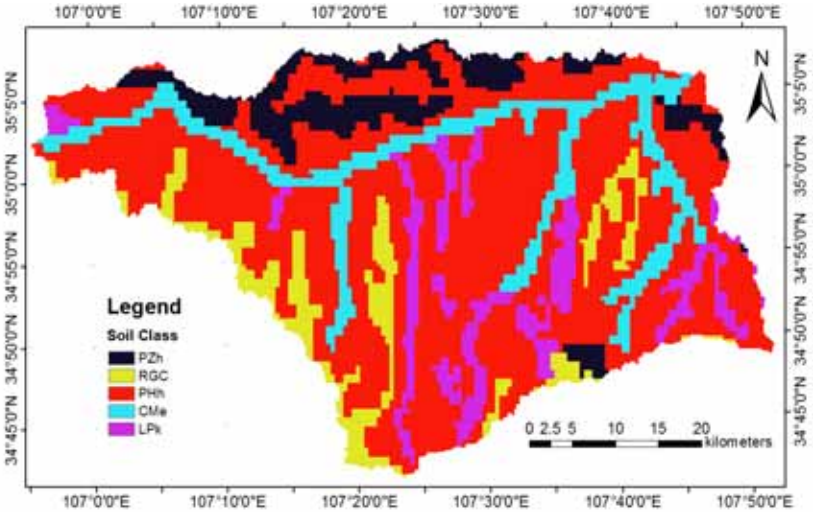

FIGURE 3
Soil types of the Daxi River basin.

TABLE 1
Descriptions and sources of the environmental database for the Daxi River basin.

Data type	Data Accuracy	Format	Website Sources
Digital Elevation Model (DEM)	30 meters	ESRI GRID	http://www.gscloud.cn
Land use map	1:105	ESRI GRID	http://westdc.westgis.ac.cn
Soil type map	1:106	ESRI GRID	http://westdc.westgis.ac.cn
Climate data	0.1 °C	txt	http://data.cma.cn/site/index.html
Precipitation data	0.1 mm	xls	http://loess.data.ac.cn/index.html
Digital River map	30 meters	Shape	DEM extraction based on ArcGIS

TABLE 2
Soil types and area statistics in the Daxi River basin.

Coding	soil types	SWAT Code	Area /km^2	Area Percentage /%
1	Eutric Cambisols	CMe	273.60	11.12
2	Rendzic Leptosols	LPk	232.56	9.45
3	Haplic Phaeozems	PHh	1512.35	61.46
4	Haplic Podzols	PZh	234.73	9.54
5	Calcaric Regosols	RGc	207.57	8.44

TABLE 3
Land use types and area statistics in the Daxi River basin.

Coding	land use types	SWAT Code	Area /km2	Area Percentage /%
1	Forest-Mixed	FRST	245.44	9.97
2	Pasture	PAST	1197.23	48.65
3	Hay	HAY	21.73	0.88
4	Water	WATR	1.17	0.05
5	Residential-High Density	URHD	1.59	0.06
6	Residential-Low Density	URLD	6.40	0.26
7	Agricultural Land-Generic	AGRL	987.26	40.12

In this method, parameter sensitivities were calculated by multiple regression model, which regresses the Latin hypercube [19] generated parameters against the objective function values, utilizing T-test to identify the relative significance of each parameter. To compare the search performance of each algorithm, the initial ranges of calibration parameters should be settled at the maximum scope, using the default parameter changing identifiers in order to avoid manual calibration and save required time.

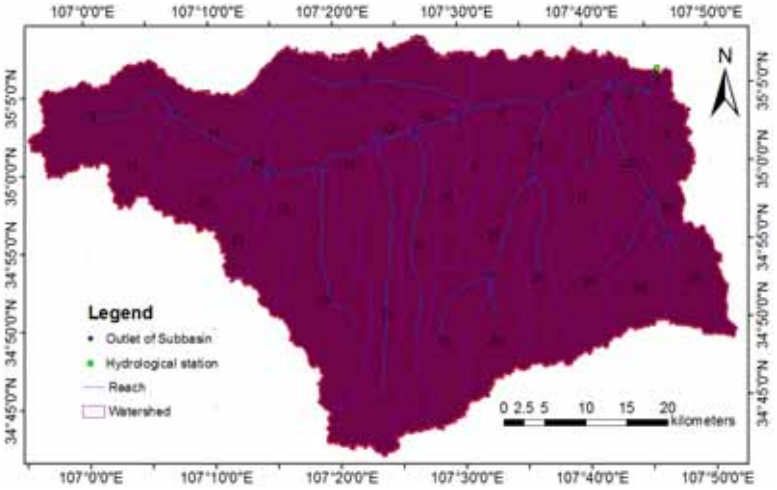

FIGURE 4
Divisions of sub-basins in the Daxi River basin.

Genetic Algorithm. A GA is a global stochastic search technique inspired by natural selection and genetics of evolutionary biology [20, 21]. GAs use Darwin's principle of 'survival of the fittest' for obtaining optimal solutions by the iterative use of genetic manipulation for possible solutions for a continuously evolving population by selection, crossover and mutation. GAs are global and robust and have been successfully applied to many fields [22, 23], such as hydrological parameter calibration, optimized design, neural-network training, pattern recognition and time-series prediction.

The implementation of a GA begins with initializing a population of candidate solutions (called chromosomes) randomly sampled from a feasible parameter space. Each chromosome is evaluated in each generation by a fitness function. The fittest chromosomes, which repeatedly use crossover and mutation, are preferentially selected to reproduce new promising offspring during population iteration. The crossover operator choses parental solutions and exchanges important building blocks between two parental chromosomes to generate new offspring solutions, which are randomly mutated with a low probability to ensure the diversity of the new population. This iterative evolution of the parameter solutions ends only when an optimal goal of model evaluations is reached.

Particle Swarm Optimization. PSO is an evolutionary optimization algorithm derived from the study of bird foraging behavior [24]. The PSO algorithm finds potential solutions by using each particle to adjust its position based on its own flying experience and the flying experiences of all companions. PSO searches for the best solution for each individual and the global populations during each iteration, so that each particle can update its information by its own previous best position and the best neighborhood or global position. PSO has been widely used in many fields, including engineering optimization and image processing, due to its advantages of a simple structure and fast convergence compared to GA.

Each particle, P_i, in the original PSO algorithm represents a candidate solution of a multi-dimensional search space, which has two features: position X_i and velocity V_i. Each particle updates itself during the iteration by tracking two extremes: the current optimal position found by the particle (P_{best}), and the current best position found by the global population (G_{best}). The criterion for terminating the iterations is determined when the maximum generation or a designated fitness is reached. The PSO can be updated by:

$$V_i^{new} = wV_i^{old} + c_1 r_1 \left(P_{best} - X_i^{old}\right) + c_2 r_2 \left(G_{best} - X_i^{old}\right) \quad (1)$$

$$X_i^{new} = X_i^{old} + V_i^{new} \quad (2)$$

where w<1 is the inertial weight, c_1 and c_2 are learning factors, r_1 and r_2 are the random numbers between 0 and 1 of uniform distribution.

Coupling of the multi-subgroup hybrid GA-PSO algorithm and a SWAT model. This multi-subgroup hybrid GA-PSO algorithm changes the organization structure of individuals to isolate the global and partial searches towards the GA and PSO, respectively. The structure of the multi-subgroup separates the entire population, which can guarantee the independent of each population, ensuring the diversity of individuals, and is convenient for the allocation of parallel computing. Specifically, the entire populations are divided into some independent subgroups, using GA respectively to evolve in a comprehensive search to ensure the robustness of optimal populations. The best individuals simulated from all subgroups were collected together into the claimed 'elite group', using PSO alone for a precise search to obtain more optimal solutions, then updating the individuals and improving the convergence

in each subgroup. This method can speed up the convergence under the premise of population diversity and hence overcome the contradiction between global-search ability and convergence efficiency.

Fig. 5 illustrates parameter calibration by coupling the multi-subgroup hybrid GA-PSO algorithm with a SWAT model. The specific steps are:

Step 1: Generate enough initial parameter individuals and copy all files that SWAT needs in each parallel process for preparation.

Step 2: Introduce each individual as a parameter into the SWAT model and simulate the data results, using the defined fitness function to evaluate the quality. Note that this step would be executed when the particle is updated.

Step 3: Rank the fitness evolution of each individual in each subgroup and use GA to evolve in several generations; then collect the best individuals to form the elite group and use PSO to update in a limited iteration. This entire evolution process is defined as a coupling cycle.

Step 4: If the calibration criterion is not satisfied and the maximum number of coupling cycles is not reached, some of the worse individuals in each subgroup will be replaced by the best individual particle obtained from step 3, thus start the next coupling cycles.

Parameter settings of intelligent algorithms. With the hardware support of a 28-core server, the population size (*Popsize*) should be <28 to ensure the reasonable allocation of the CPU and RAM. *Popsize* was finally determined as *25*, which could be easily parallelized to save time and improve the efficiency. The conception of sub-group in the hybrid GA-PSO algorithm increases the diversity of species but multiply increases the time required, so the number of *Generations* in GA and *Iterations* in PSO should decrease as *Popsize* increases.

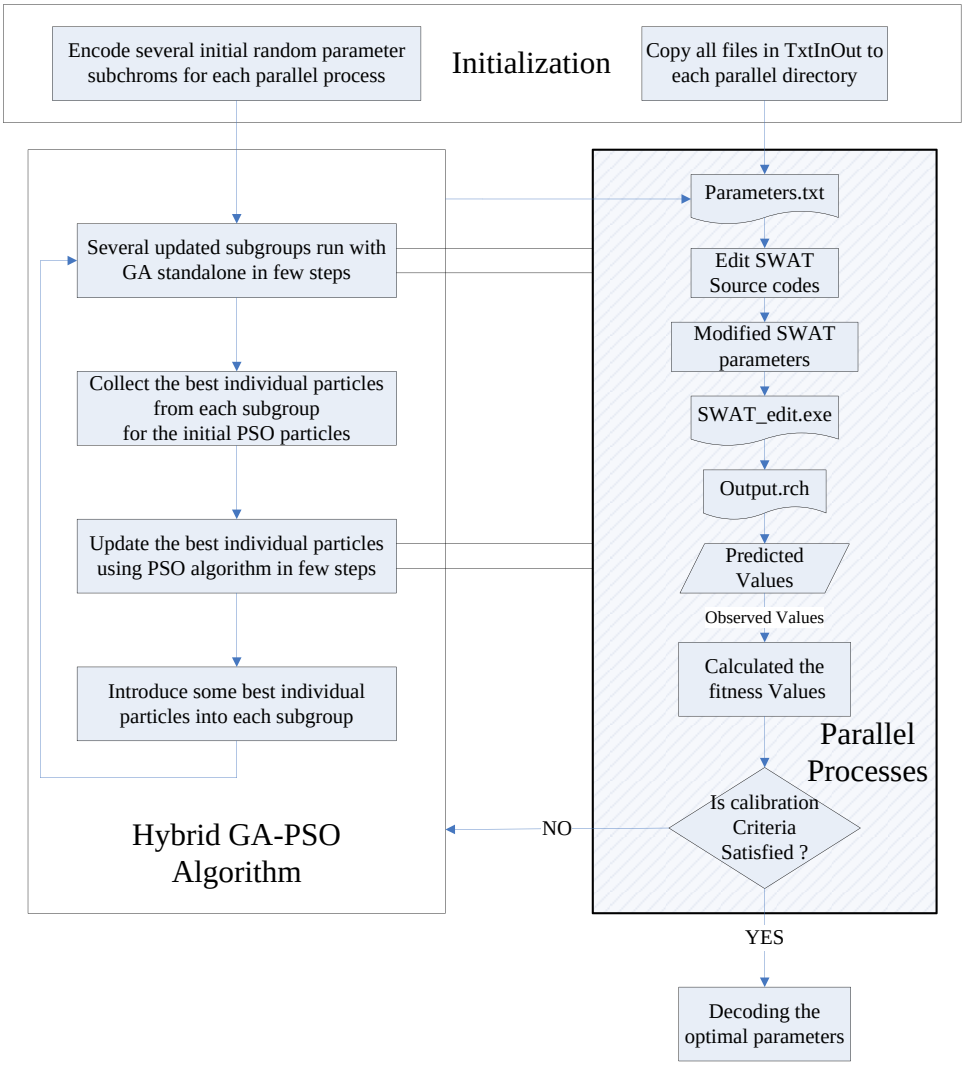

FIGURE 5
Schematic of the hybrid GA-PSO algorithm for parameter calibration in SWAT model.

TABLE 4
Parameter settings in different algorithms.

Algorithm	P_s	P_c	P_m	w	c_1	c_2	*PopSize*	*Generations*	*Iterations*	Total
GA	80%	0.80	0.07	-	-	-	25	1500	-	37500
PSO	-	-	-	0.729	2.0	2.0	25	-	1500	37500
GA-PSO	80%	0.80	0.07	0.729	2.0	2.0	25×10	20×6	5×6	37500

TABLE 5
The 12 selected calibration parameters by sensitivity analysis.

Parameter	Type	Briefly description	t-stat	p-value
SOL_K*	.sol	Soil conductivity (mm/h)	-6.3280	0.0000
HRU_SLP*	.hru	Average slope steepness (m/m)	-5.2279	0.0000
SOL_Z*	.sol	Soil depth	3.8951	0.0001
SLSUBBSN*	.hru	Average slope length (m)	3.6706	0.0003
CANMX	.hru	Maximum canopy index	2.8243	0.0048
GW_DELAY	.gw	Groundwater delay (days)	1.5699	0.1167
SOL_AWC*	.sol	Available soil water capacity	-1.4798	0.1392
SFTMP	.bsn	Snow melt base temperature (°C)	-1.3360	0.1819
ESCO	.hru	Soil evaporation compensation factor	0.7209	0.4712
CH_N2	.rte	Manning coefficient for channel	-0.6162	0.5379
CN2*	.mgt	Curve number	-0.5035	0.6147
CH_K2	.rte	Effective hydraulic conductivity (mm/hr)	0.4016	0.6881

Note: *The every distributed parameter varies with other parameters, which maintains the spatial relationship.

The number of subgroups in this hybrid algorithm was defined as *10*, and each subgroup had the same *Popsize* of *25*. For each individual, we set *20* as the *Generations* number and *5* as the *Iterations* number for once coupling cycle, and the total number of coupling cycles was set as *6*. The total number of calculation iterations by the entire population should therefore be 25 × 10 × (20+5) × 6 = 25 × 1500 = 37 500. The total calculation and algorithm complexities must be set at the same level to ensure consistency and the comparability of the calibration results calculated by each intelligent algorithm. The total number of iterations should thus be set as *1500* in the simple GA and PSO algorithms and SUFI-2, and *Popsize* was set as *25*. The detailed parameter settings in the different algorithms are shown in Table 4. Notice that P_s, P_c and P_m represent the probability of selection, crossover and mutation respectively; and w, c_1 and c_2 are the constant coefficients in Eq.1.

Evaluation index of optimization parameters. In SWAT-CUP calibration, Nash-Sutcliffe efficiency coefficient (E_{ns}) [25] was generally chose as the objective function. To limit the non-uniqueness of parameter calibration, the objective function should include more indices. Mean absolute error (*MAE*) and average relative error (*ARE*) are the most representative statistical indices in data processing, so the fitness function F was defined as the quotient in Eq.3, which is *ARE* multiplied by *MAE*. We used the Nash-Sutcliffe efficiency coefficient (E_{ns}) and the coefficient of determination (R^2) [26] as statistical indices to evaluate the simulations of the SWAT hydrological model after parameter optimization for comparing the accuracy of the optimized parameters by the arithmetic means and medians. The formulas for the above indices were:

$$F = \frac{1}{N}\sum\left|\frac{Q_{obs,i}-Q_{sim,i}}{Q_{sim,i}}\right| \times \frac{1}{N}\sum\left|Q_{obs,i}-Q_{sim,i}\right| \quad (3)$$

$$E_{ns} = 1 - \frac{\sum\left(Q_{obs,i}-Q_{sim,i}\right)^2}{\sum\left(Q_{obs,i}-\bar{Q}_{obs}\right)^2} \quad (4)$$

$$R^2 = \frac{\left[\sum\left(Q_{obs,\mathrm{i}}-\bar{Q}_{obs}\right)\left(Q_{sim,\mathrm{i}}-\bar{Q}_{sim}\right)\right]^2}{\sum\left(Q_{obs,i}-\bar{Q}_{obs}\right)^2\sum\left(Q_{sim,i}-\bar{Q}_{sim}\right)^2} \quad (5)$$

where $Q_{obs,i}$ is the measured value for the i-th rainfall, $Q_{sim,i}$ is the simulated value for the i-th rainfall, $\bar{Q}_{obs}$ is the average of all measured values, and $\bar{Q}_{sim}$ is the average of all simulated values.

APPLICATION RESULTS

Analysis of parameter sensitivity by SWAT-CUP. Distributed parameters in SWAT models generally have different values in each hydrologic research unit, depending on the spatial heterogeneity of the underlying surface. Increasing the number of parameters thus greatly increases the difficulty of calibration. The total number of parameters for streamflow in this SWAT model was as high as 26, so calibrating all these parameters was time-consuming and reduced the efficiency of calibration. Almost halved parameters did not have a large impact on the

simulations via T-test, so the 12 representative parameters for calibration selected using the sensitivity analysis are listed in Table 5.

Results of parameter calibration. The simulated parameter values after calibration, including their ranges of each model, are listed in Table 6. The parameter values diverged strongly amongst the three intelligent algorithms (PSO, GA and GA-PSO). For example, SOL_K*, obtained by the relative method (r__), ranged from -45.1% to +47.5%; and GW_DELAY, calculated by the replace method (v__), ranged between 67.30 and 497.9. Each algorithm thus effectively used its inherent characteristics for the complicated SWAT parameter calibrations. The parameters calibrated by SUFI-2 were more similar to the results obtained by PSO, implying that fast convergence might be the more important feature in SWAT-CUP, similar to the PSO algorithm.

Streamflow calibration and validation. Fig. 6 displays the observed runoff process line and precipitation bar for the study area. The normal flow was 10-20 m^3/s around September in the flooding season almost every year in this watershed. The attractive oversized peak flows, however, were >30 m^3/s three times, in 1981 and 1983 during the calibration period and in 1988 during the validation period. Maximum streamflow in particular was as high as 54.8 m^3/s in October 1981. Streamflow during the calibration period (1981-1985) was simulated well, with normal flooding seasons and two completely different peak flows. One of the peak flows in 1981 was due mostly to the high precipitation >8.0 mm/day in the previous month, similar to the peak flow in 1988. Another peak flow in 1983 was partly attributed to the continuous six-month precipitation near 4.0 mm/day.

TABLE 6
Parameter values for the calibration models.

Parameters	Ranges		Calibration results			
	Min	Max	SUFI-2	PSO	GA	GA-PSO
r__SOL_K*	-50%	+50%	+47.5%	+39.9%	+2.2%	-45.1%
r__HRU_SLP*	-50%	+50%	+27.3%	+14.2%	+50.0%	-44.0%
r__SOL_Z*	-50%	+50%	+44.1%	+47.2%	-45.4%	+0.6%
r__SLSUBBSN*	-50%	+50%	-23.4%	-13.6%	+28.3%	+47.6%
v__CANMX	0	100	27.51	14.16	6.256	11.19
v__GW_DELAY	0	500	67.30	156.0	342.2	497.9
r__SOL_AWC*	-50%	+50%	+27.2%	+38.9%	-1.0%	-7.7%
v__SFTMP	-5	5	-1.628	-1.416	2.424	1.560
v__ESCO	0	1	0.490	0.406	0.624	0.202
v__CH_N2	-0.01	0.3	0.215	0.175	-0.004	0.021
r__CN2*	-50%	+50%	-30.1%	-11.1%	+7.8%	+10.4%
v__CH_K2	-0.01	500	394.2	455.8	62.74	206.1

Note: In SWAT-CUP calibration, v__ means the existing parameter value is to be replaced by the given value; r__ means the existing parameter value is multiplied by 1+ a given value.

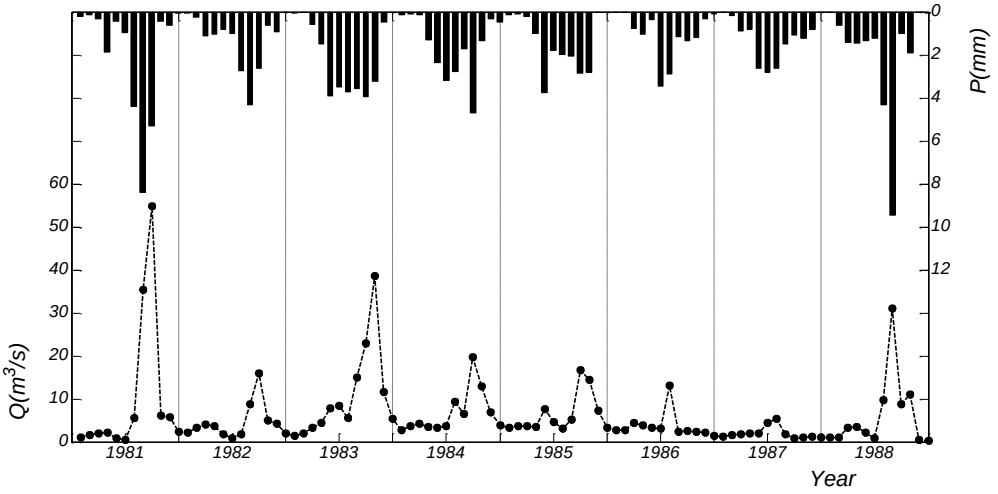

FIGURE 6
Observed monthly values of runoff and precipitation.

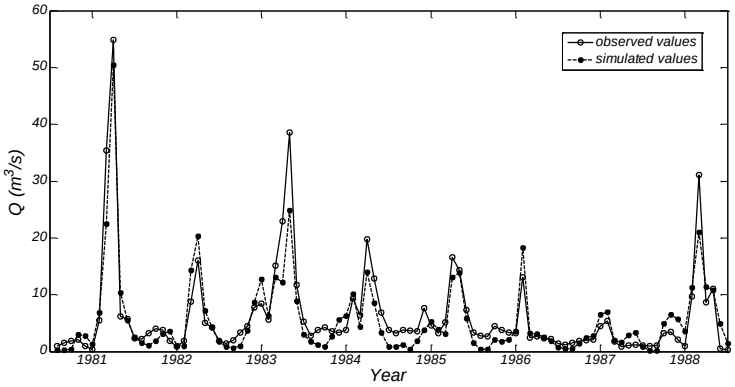

a. SWAT-CUP

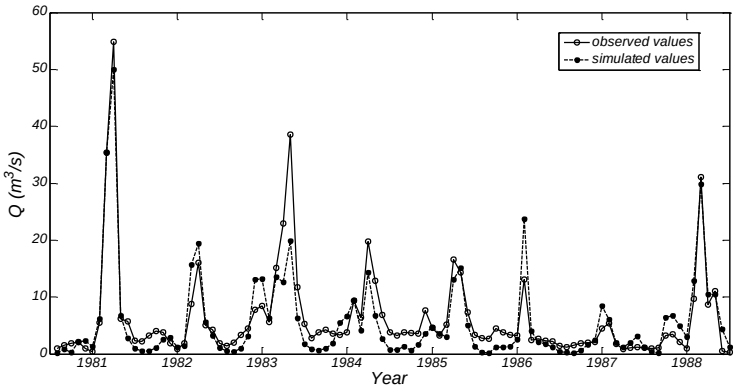

b. PSO

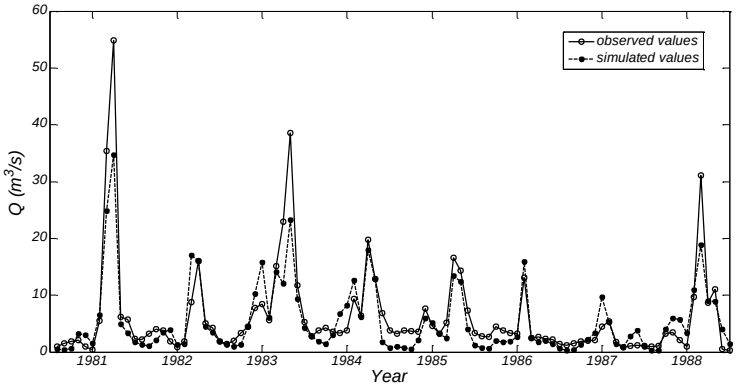

c. GA

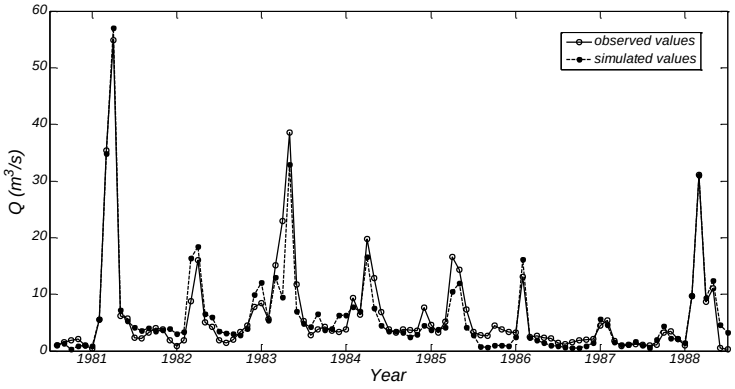

d. GA-PSO

FIGURE 7

(a, b, c, d) Simulated monthly streamflow values by different methods.

TABLE 7
The simulated monthly flood data via each method.

Time (Year. Month)	Observed streamflow (m^3/s)	Simulated streamflow (m^3/s)			
		SUFI-2	PSO	GA	GA-PSO
1981. 7	**35.429**	**22.470**	**35.380**	**24.860**	**34.800**
1981. 8	**54.830**	**50.440**	**49.960**	**34.670**	**57.000**
1982. 9	16.034	20.320	19.440	16.040	18.400
1983. 8	15.076	13.100	13.560	14.070	13.000
1983. 9	22.868	12.180	12.570	12.060	9.420
1983. 10	**38.526**	**24.810**	**19.860**	**23.320**	**32.900**
1983. 11	11.668	8.851	6.323	9.300	6.920
1984. 9	19.780	14.010	14.320	17.960	16.600
1984. 10	12.844	8.562	6.681	12.850	7.490
1985. 9	16.611	13.030	13.130	13.450	10.500
1985. 10	14.347	13.820	15.060	12.410	12.000
1986. 7	13.093	18.270	23.670	15.880	20.100
1988. 8	**31.055**	**21.050**	**29.840**	**18.860**	**31.000**
1988. 10	11.046	10.820	10.420	8.860	12.400
ARE in normal flood (%)		24.005	31.010	**15.713**	30.472
ARE in peak flow (%)		28.100	15.345	36.334	**5.128**

TABLE 8
Evaluation coefficients for each algorithm.

Methods	Calibration		Validation	
	E_{ns}	R^2	E_{ns}	R^2
SUFI-2	0.85	0.88	0.78	0.79
PSO	0.84	0.86	0.77	0.84
GA	0.78	0.84	0.75	0.76
GA-PSO	**0.91**	**0.91**	**0.92**	**0.93**

Monthly streamflow was calibrated and validated by different methods for depicting the details of runoff simulation (Fig. 7). The flood data exceeding 10 m^3/s are presented in Table 7. The SWAT-CUP model using SUFI-2 algorithm simulated acceptable process lines and normal flood values and predicted the maximum peak flow in August 1981 well but could not obtain enough peak flow >30 m^3/s. The simulated process line for the PSO algorithm was similar to that for SUFI-2, and the simulated normal flood data were slightly worse than the outcomes of SUFI-2. The peak flows in 1981 and 1988, which were caused by heavy but brief rains, were accurately forecasted. The PSO method produced the worst values, and the peak flow in October 1983 was underestimated by nearly half, during the continuous flooding from prolonged precipitation in 1983. The simulated process line obtained by GA was the ideal streamflow trend, but without the exceptional values in the peak-flow season. GA was stable and produced better results for normal floods, which had the lowest *ARE* (15.7%). All simulated peak flows >30 m^3/s, however, were badly underestimated, with the highest *ARE* (36.3%), and thus could easily be mistaken as normal floods.

Finally, the runoff process line simulated by the hybrid GA-PSO algorithm coincided mostly with the observed streamflow line. All four peak flow values could be exactly predicted, with the lowest *ARE* (5.1%), although normal floods were not simulated as well as by SUFI-2 and GA. The prolonged continuous precipitation produced the most underestimated values for normal floods, especially in 1983, but accurate predictions of the times and values of peak flows were more important for forecasting floods.

The evaluation coefficients for the monthly streamflows simulated with different methods for the Daxi River basin are presented in Table 8. E_{ns} and R^2 calculated by GA for the calibration period were obviously lower than those calculated by the other methods, perhaps due to premature convergence during calibration. The evaluation index calculated by GA were much more similar between the calibration and validation periods, implying that GA was stable and generalized well for promoting the application of runoff simulation. E_{ns} and R^2 calculated by the SUFI-2 and PSO methods were acceptable near 0.85 during the calibration period but were significantly lower during the validation period. These methods had good convergence but were likely to tend to-

wards the local optimal solution, so could not precisely and reliably validate and popularize this streamflow process. More importantly, the GA-PSO algorithm reliably simulated the process during both the calibration and validation periods, and then produced results with the highest E_{ns} and R^2 >0.90. In additions, this hybrid GA-PSO algorithm could get the highest evaluation indices via the different fitness function, indicating this method could be more effective than the SWAT-CUP method to alleviate the non-uniqueness problem. Overall, this hybrid algorithm combined the generalization ability of GA, the convergence performance of PSO, and the diversity that the multi-subgroups provided, thus providing a new technique for parameter calibration in SWAT simulations.

DISCUSSION AND CONCLUSIONS

We proposed a multi-subgroup hybrid algorithm combining GA and PSO to calibrate the parameters with a SWAT model applied to the Daxi River watershed. The results were compared to those from the SWAT-CUP auto-calibration module, the GA and PSO algorithm. The new hybrid algorithm calibrated the parameters faster in parallel, accurately and stably predicted the streamflows. The main conclusions are:

1) The number of calibration parameters were reduced to 12 before calibration by a sensitivity analysis using SWAT-CUP, and parallel calculations were introduced to save time and increase effectiveness. Four methods, SUFI-2, GA, PSO and a multi-subgroup hybrid GA-PSO algorithm, were used to calibrate the parameters and optimize the streamflow in hydrological processes. The different models produced different parameter values, indicating different characteristics of calibration.

2) GA well simulated normal floods and overall streamflow trends, and the evaluation index was strongly consistent between the calibration and validation periods, highlighting its stable global-searching ability and reliable generalization. GA was unable to accurately predict the peak flows, E_{ns} and R^2 were lower than with the other methods, indicating that this algorithm could not easily or quickly converge into the global extreme point, thus affecting the efficiency or accuracy of the calibration.

3) The results simulated by the SUFI-2 algorithm in SWAT-CUP were largely similar to the results simulated by PSO. The streamflow process line simulated by PSO during the calibration period was ideal, except for the peak flow in 1983, and E_{ns} and R^2 were near 0.85, indicating that the PSO algorithm had the advantage of fast and precise convergence, which GA lacks. The evaluation index during the validation period, however, decreased, and the simulated values for floods in 1986 were overestimated with an observed bias. The results implied that PSO might quickly tend towards the local extreme point and would be unable to escape for determining global optimal resolutions. Without the ability of global searching, only fast but premature convergence cannot ensure the accuracy and reliability of the validation.

4) The runoff line simulated by the multi-subgroup GA-PSO algorithm was closest to the observed line, and E_{ns} and R^2 were >0.90. This algorithm best simulated streamflow and had the highest calibration accuracy. All its advantages, including the global-searching ability and reliable generalization provided by GA and the local-searching efficiency and fast convergence provided by PSO, were combined successfully in this hybrid algorithm when applied to this SWAT model. The diversity of individuals due to the multi-subgroups ensured the stability of parameter calibration. The proposed hybrid algorithm provides a new method for general-purpose automatic parameter optimization and may be generalized to other complex hydrological models, such as for nutrient transport and the non-point source pollution.

ACKNOWLEDGEMENTS

This study was supported by the National Science & Technology Pillar Program during the 12th Five-year Plan Period [2012BAD08B01], Non-profit Industry Financial Program of Ministry of Water Resources [201301016], the National Natural Science Foundation of China [51279167], and the National Natural Science Foundation of China [51309194].

REFERENCES

[1] Arnold, J.G., Srinivasan, R., Muttiah, R.S., Williams, J.R. (1998) Large area hydrologic modeling and assessment part 1: model development. Journal of the American Water Resources Association. 34(1), 73-89.

[2] Rahman, M.M., Thompson, J.R., Flower, R.J. (2016) An enhanced SWAT wetland module to quantify hydraulic interactions between riparian depressional wetlands, rivers and aquifers. Environmental Modelling & Software. 84, 263-289.

[3] Tomy, T., Sumam, K.S. (2016) Determining the Adequacy of CFSR Data for Rainfall-Runoff Modeling Using SWAT. Procedia Technology. 24, 309-316.

[4] Golmohammadi, G., Rudra, R., Dickinson, T., Goel, P., Veliz, M. (2017) Predicting the Temporal Variation of Flow Contributing Areas using SWAT. Journal of Hydrology. 547, 375-386.

[5] Francés, F., Vélez, J.I., Vélez, J.J. (2007) Split-parameter structure for the automatic calibration of distributed hydrological models. Journal of Hydrology. 332(1), 226-240.
[6] Jiang, Y., Li, X., Huang, C. (2013) Automatic calibration a hydrological model using a master-slave swarms shuffling evolution algorithm based on self-adaptive particle swarm optimization. Expert Systems with Applications. 40(2), 752-757.
[7] Eckhardt, K., Arnold, J.G. (2001) Automatic calibration of distributed catchment model. Journal of Hydrology. 251(1-2), 103-109.
[8] Wu, K., Johnston, C.A. (2007) Hydrologic response to climatic variability in a Great Lakes Watershed: A case study with the SWAT model. Journal of Hydrology. 337(1-2), 187-199.
[9] Cheng, C.T., Ou, C.P., Chau, K.W. (2002) Combining a fuzzy optimal model with a genetic algorithm to solve multi-objective rainfall-runoff model calibration. Journal of Hydrology. 268(1), 72-86.
[10] Wang, H., Fu, X.D., Wang, G.Q., Li, T.J., Gao, J. (2011) A common parallel computing framework for modeling hydrological processes of river basins. Parallel Computing. 37(6-7), 302-315.
[11] Wu, Y.P., Li, T.J., Sun, L.Q., Chen, J. (2013) Parallelization of a hydrological model using the message passing interface. Environmental Modelling & Software. 43(3), 124-132.
[12] Wang, Q.J. (1991) The genetic algorithm and its application to calibrating conceptual rainfall-runoff models. Water Resources Research. 27(9), 2467-2471.
[13] Ho, T., Fieser, M., Danheiser, R., Roush, W., Fieser, L. (1996) Use of genetic algorithm combined with a local search method for the automatic calibration of conceptual rainfall–runoff models. Hydrological Sciences Journal. 41(1), 21-39.
[14] Franchini, M., Galeati, G. (1997) Comparing several genetic algorithm schemes for the calibration of conceptual rainfall-runoff models. Hydrological Sciences Journal. 42(3), 357-379.
[15] Kao, Y.T., Zahara, E. (2008) A hybrid genetic algorithm and particle swarm optimization for multimodal functions. Applied Soft Computing. 8(2), 849-857.
[16] Kuo, R.J., Han, Y.S. (2011) A hybrid of genetic algorithm and particle swarm optimization for solving bi-level linear programming problem - A case study on supply chain model. Applied Mathematical Modelling. 35, 3905-3917.
[17] Soleimani, H., Kannan, G. (2015) A hybrid particle swarm optimization and genetic algorithm for closed-loop supply chain network design in large-scale networks. Applied Mathematical Modelling. 39(14), 3990-4012.
[18] Abbaspour, K.C., Yang, J., Maximov, I., Siber, R., Bogner, K., Mieleitner, J., Zobrist, J., Srinivasan, R. (2007) Modelling hydrology and water quality in the pre-alpine/alpine Thur watershed using SWAT. Journal of Hydrology. 333(2), 413-430.
[19] McKay, M.D., Beckman, R.J., Conover, W.J. (2000) A comparison of three methods for selecting values of input variables in the analysis of output from a computer code. Technometrics 42(1), 55-61.
[20] Holland, J.H. (1975) Adaptation in Natural and Artificial Systems, University of Michigan Press, Michigan, US.
[21] Goldberg, D.E. (1989) Genetic Algorithms in search optimization & machine learning. Addison-Wesley, Reading, MA.
[22] Reca, J., Martínez, J. (2006) Genetic algorithms for the design of looped irrigation water distribution networks. Water Resources Research. 42(5), 110-119.
[23] Zhang, X., Srinivasan, R., Bosch, D. (2009) Calibration and uncertainty analysis of the SWAT model using Genetic Algorithms and Bayesian Model Averaging. Journal of Hydrology. 374(3-4), 307-317.
[24] Kennedy, J., Eberhart, R.C. (1995) Particle swarm optimization. In: 1995 IEEE International Conference on Neural Networks, Proceedings. 4, 1942–1948.
[25] Nash, J.E., Sutcliffe, J.V. (1970) River flow forecasting through conceptual models, part I: A discussion of principles. Journal of Hydrology. 10(3), 282-290.
[26] Nearing, M.A., Liu, B.Y., Risse, L.M., Zhang, X. (1996) Curve numbers and Green-Ampt effective hydraulic conductivities. Water Resources Bulletin. 32, 125-136.

Received: **28.06.2017**
Accepted: **05.12.2017**

CORRESPONDING AUTHOR

Xiao-yi Ma
College of Water Resources and
Architectural Engineering,
Northwest A&F University,
No. 23 Weihui Road, Yangling District,
Shaanxi, 712100 – P.R. China

e-mail: xma@nwsuaf.edu.cn

© by PSP Volume 27 – No. 2/2018 pages 971-981 Fresenius Environmental Bulletin

ASSESSMENT OF SOME QUALITY PARAMETERS OF SPRING WATER IN ERZURUM, TURKEY

Banu Tuluk[1,*], Figen Orhan[2]

[1]Ataturk Univesity, Faculty of Engineering, Department of Environmental Engineering, Erzurum, Turkey
[2]Ataturk University, Health Services Vocational Training School Erzurum, Turkey

ABSTRACT

Although spring waters occur naturally underground their quality can be controlled by combined interactive natural and anthropogenic factors. This factors may cause pollution of existing water resources. Drinking water is also mostly supplied from the spring water fountains in Erzurum(Turkey). Snow water and rainwater can interfere with water resources and they may cause pollution and illnesses. This study was carried out to determine qualities of the most used spring waters in Erzurum, to monitor the changes in water quality and to determine the effects of possible sources of pollution. Water samples taken from ten different public fountains have a clean appearance, normal odor, color, and taste. pH and electrical conductivity (EC) are 7,14-8,25 and 96-662 µs/cm respectively. Fluoride (F), chloride (Cl), nitrite (NO_2), nitrate (NO_3), sulphate (SO_4) and ammonia (NH_4) values are 0,16-0,40; 0,84-52,62; <0.05; 1,03-82,79; 3,02-83,85 and 0,05-0,19 mg/L respectively. Some fountains are not suitable for human consumption in terms of nitrate contents and microbiologically.

KEYWORDS:
Spring water, physical, chemical, microbiological, water quality, Turkey, Erzurum

INTRODUCTION

Spring waters occur naturally underground and they are transferred to surface spontaneously or technical methods. They have natural protection against pollution by the covering layers [1]. Temperature, flow, and characteristics vary slightly from season to season. They are not significantly affected by precipitation surface water and groundwater. Spring, well, gallery etc. are defined as underground spring waters [2]. Underground waters are important resources, unlike surface waters, they are usually less polluted or even unpolluted [3].

Groundwater constitutes 97% of global freshwater [4]. Natural springs are significant sources of water for people around the world [5]. They are major sources of drinking water in rural as well as urban areas, particularly in the developing countries and they are the major sources of water for domestic, agricultural and industrial purposes in many countries [4, 6]. Treatment, including disinfection, is often not required [4]. Springs are easily accessible at the surface [5]. They are inexpensive to protect and they do not require a pump to bring the water to the surface [7]. Their quality depends on a number of factors such as geology, the degree of chemical weathering of the various rock types, quality of recharge water, and water-rock interaction [6]. They vary from place to place [8]. Chemical characteristics of groundwater play an important role in assessing and classifying the quality of water [6].

Although ground waters have a natural protection against pollution, their quality can be controlled by combined interactive natural (including lithologic, tectonic, topographic, climatic, edaphic) and anthropogenic factors [9]. They may have some acceptability problems based on concentration level of certain chemical parameters [8].

Population growth, rapid urbanization, mixing of domestic-industrial and agricultural wastes into waters without treatment, pesticides used in agriculture, biological cycle, natural transport cause pollution of existing water resources [10,11]. They might contain undesired substances that are deleterious to human health when they polluted [12].

Once the groundwater is contaminated, its quality cannot be restored by stopping the pollutants from the sources. Drinking water should not contain toxic substances, biological organisms and an excessive amount of minerals in terms of human health [12, 13]. Therefore it becomes imperative to regularly monitor the quality of groundwater and develop devices to protect it [13].

According to the World Health Organization (WHO), 80% of all illnesses in developing countries are caused by drinking water [11]. Exposure to physical, chemical and biological pollution of drinking water significantly affects the quality of water and public health [10]. Non-hygienic waters may cause many illnesses and they may cause major health problems [11]. Therefore drinking water has to comply with certain physical, chemical and microbiological standards, which is designed to ensure that the water is palatable and safe for drinking [8]. Standards set by international organizations

such as the WHO, Environmental Protection Agency (EPA) and the European Union (EU) on drinking water have been adopted by many countries. Drinking water standards in Turkey are compatible with these standards.

Groundwater resources are limited. For this reason, it is inevitable to use surface waters today [14].

The drinking water requirement in Erzurum province was supplied from 61 water wells until 2008. After the Palandöken Dam activated, the drinking water requirement was supplied from the surface waters [15]. The people of Erzurum have not fully accepted the water obtained from the dam as drinking water. For this reason, drinking water is mostly supplied from the spring water fountains. They are cold and thought to be clean. Their taste is liked. However, at the beginning of the summer months, snow water and rainwater can interfere with water resources and cause pollution. There was no study on the evaluation of spring waters covering June, July, and August in Erzurum. Especially in these months complaints of diarrhea are increasing. This situation required the examination of spring water in terms of drinking water standards in summer. Our studies differ from the previous studies done by other researchers.

This study was carried out to determine the physical, chemical and microbiological qualities of the most used spring waters in the province of Erzurum and to monitor the changes in water quality, to determine the effects of possible sources of pollution.

MATERIALS AND METHODS

Description of The Study Area. The province of Erzurum is located in the east of Turkey, in Asia. The city lies between the latitude of 39,9 N and longitude of 41,27 E and covers an area of 25.066 km². The altitude is 1859 meters above sea level. It is one of the highest and coldest cities in Turkey and has a continental climate. The temperature is highest in summer (+35ºC) and lowest in winter (-30ºC). The region receives an average rainfall is 460 mm/m² on every year [16]. While the least rainfall is seen in the winter season, the most rainfall is seen in spring and summer seasons [15]. The rivers in the region are strengthening with snowwater [16].

Sampling, Sample Preparation, and Analysis. Water samples were collected from 10 spring fountains of Erzurum in the summer months(June–July–August) of 2015 (once a month/on the 15th day of each month). Spring fountains were numbered. A total of 30 water samples were collected from 10 different water sources. The location of the spring fountains are marked on the aerial photograph of Erzurum in Figure 1.

Coordinates and altitudes of the spring fountains are shown in Table 1.

FIGURE 1
Locations of the spring fountains in Erzurum

TABLE 1
Spring fountain names, number coordinates, and altitudes

Fountain name	Number	Co-ordinates		Altitude
		East	North	
Cennet F.	1	41°16′ 21.37″E	39°54′ 29.28″K	1905 m
Yazıcı F.	2	41°16′ 08.88″E	39°54′ 12.85″K	1913 m
Dabakhane F.	3	41°16′ 44.38″E	39°54′ 26.74″K	1911 m
Şabakhane F.	4	41°16′ 44.38″E	39°54′ 26.74″K	1911 m
Paşapınarı1F.	5	41°20′ 46.09″E	39°55′ 08.69″K	1998 m
Paşapınarı2 F.	6	41°20′ 36.23″E	39°55′ 01.36″K	1992 m
Palandöken F.	7	41°17′ 19.02″E	39°50′ 52.32″K	2506 m
Solakzade F.	8	41°15′ 58.69″E	39°53′ 27.72″K	1961 m
Yıldızkent F.	9	41°14′ 35.16″E	39°52′ 47.65″K	1954 m
Dadaşkent F.	10	41°11′ 18.24″E	39°55′ 03.36″K	1789 m

For chemical analysis, samples were taken directly into polypropylene bottles (250 ml) from flowing water and transferred to the laboratory in ice and analyzed within 4 h after collection.

For microbiological analysis, samples were taken directly into sterile bottles from flowing water and transferred to the laboratory in ice. The time between sampling and microbiological analysis did not exceed 2 hours.

The collected water samples were analyzed for their physical, chemical and microbiological constituents.

The physical and chemical analyses were carried out at the Department of Environmental Engineering and Medical Microbiology Department laboratories in Atatürk University in Erzurum.

The analyzed parameters were turbidity, odor, color, taste, pH, electrical conductivity (EC), fluoride (F), chloride (Cl), nitrite (NO_2), nitrate (NO_3), sulfate (SO_4), ammonia (NH_4), total coliform and *E.coli.*

All chemicals obtained from commercial

sources were of super pure grade unless otherwise stated. All aqueous solutions were prepared using double distilled water. [17].

The organoleptic analyses were carried out by a sensory method based on human perception of water quality.

pH and electrical conductivity (EC) were measured using portable WTW MultiLine P4 conductivity meters according to TS EN ISO 10523 and SM 2510B at the sampling points [18, 19]. These parameters are closely related to the environment of water that they are likely to be altered by sampling and storage, and a meaningful value can be obtained only at the sampling point.

Fluoride (F), chloride (Cl), nitrite (NO_2), nitrate (NO_3), sulfate (SO_4) analyses were analyzed using Dionex-ICS 3000 Ion chromatography device according to EPA 300.1 after samples filtered through 0.45 µM membrane filters [20].

Ammonia (NH_4) parameters were analyzed by specific kits using Merck- PHARO 300 spectrophotometer [21].

Total coliform, *E.coli* analyses were analyzed according to TS EN ISO 9308-1 standard [22]. For this purpose, 100 ml of water sample was filtered through 0.45 µm pore size a membrane filter (Sartorius) and settled on a chromogenic CCA agar (Hyper Aqua). 36 ± 2 °C for 21±3h incubation. Also, *E.coli* strain ATCC 25922 was used as a quality control strain.

Statistical Analyses. The data of our study collected for 3 months. Shapiro Wilk test is used to analyze the normal distribution in the samples. To compare the variables which are more than two group; If it is normal distribution; t-test is used if it is not; Friedman test is used. Statistical significance is p 0,05.

RESULTS AND DISCUSSION

The parameters that analyzed and the limit values specified in Turkısh Standard, Directıve Of European Communities (EC), United States Environmental Protection Agency (EPA), World Health Organization (WHO) are shown in Table 2.

Samples taken from all spring waters have clean appearance, normal odour, colour and taste. pH and electrical conductivity (EC) values are 7,14-8,25 and 96-662 µS/cm respectively. Fluoride (F), chloride (Cl), nitrite (NO_2), nitrate (NO_3), sulfate (SO_4) and ammonia (NH_4) values are 0,16-0,40; 0,84-52,62; <0.05; 1,03-82,79; 3,02-83,85 and 0,05-0,19 mg/L respectively.

The physical- chemical-microbiological and statistical analyses of data for samples are presented in Figures 2, 3, 4, 5, 6, 7, 8, Table 3 and Table 4.

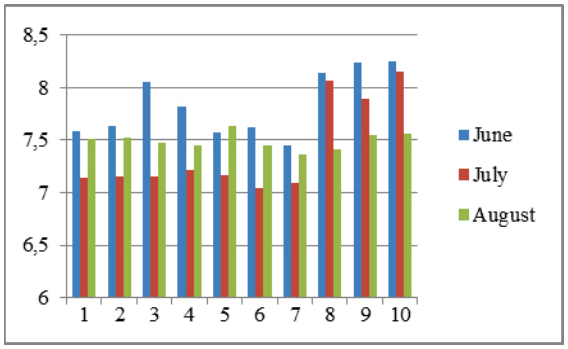

FIGURE 2
pH value of spring fountains

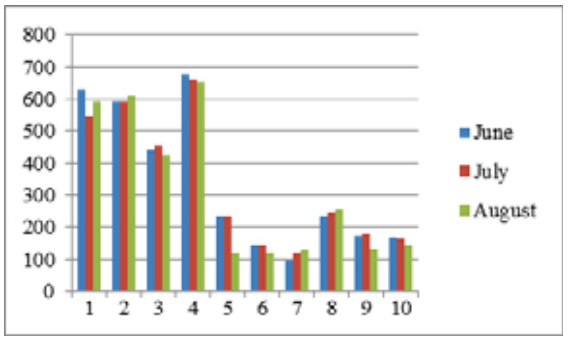

FIGURE 3
EC value of spring fountains(µS/cm)

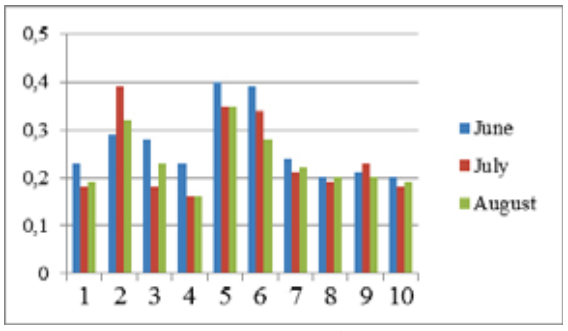

FIGURE 4
F value of spring fountains(mg/L)

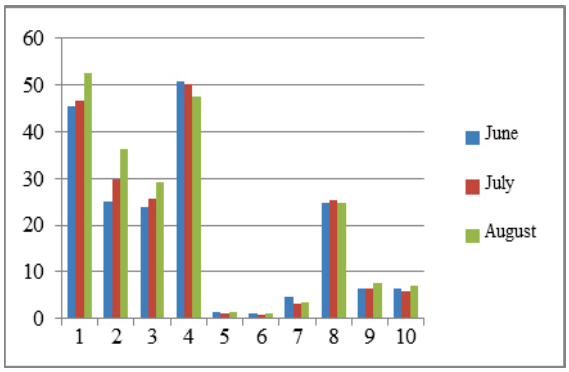

FIGURE 5
Cl value of spring fountains(mg/L)

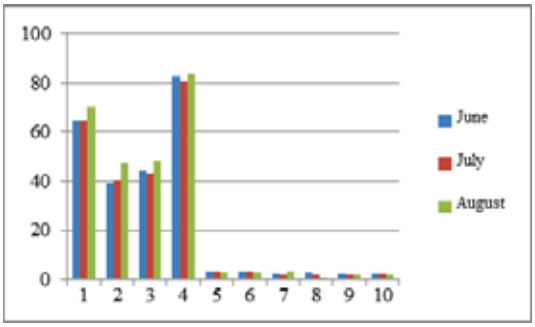

FIGURE 6
NO_3 value of spring fountains(mg/L)

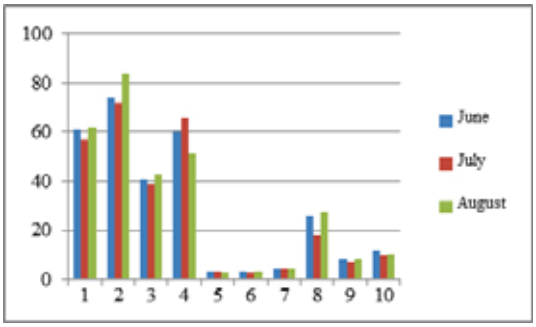

FIGURE 7
SO_4 value of spring fountains(mg/L)

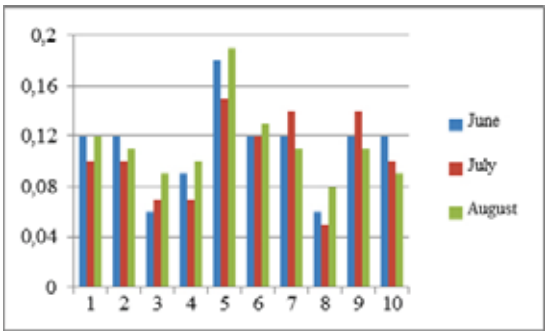

FIGURE 8
NH_4 value of spring fountains(mg/L)

TABLE 2
Standards and limit values

	Regulation Concerning Water Intended for Human Consumption, 2005 [23]	EC, 1998 [24]	EPA, 2009 [25]	WHO, 2011 [26]
Turbidity	Acceptable to consumers and no abnormal change	Acceptable to consumers and no abnormal change	1	
Odor	Acceptable to consumers and no abnormal change	Acceptable to consumers and no abnormal change	3 TON (threshold odor number)	should be acceptable to the consumer
Color	Acceptable to consumers and no abnormal change	Acceptable to consumers and no abnormal change	15 color units	
Taste	Acceptable to consumers and no abnormal change	Acceptable to consumers and no abnormal change		should be acceptable to the consumer
pH	6,5-9,5	6,5-9,5	6.5 - 8.5	
EC(µs/cm)	2500	2500		
F(mg/L)	1.5	1.5	4	1,5
Cl(mg/L)	250	250	250	
NO_2(mg/L)	0,5	0,5	1	3
NO_3(mg/L)	50	50	10	50
SO_4(mg/L)	250	250	250	
NH_4(mg/L)	0,5	0,5		

TABLE 3
Result of Microbiological analysis

	Total coliform			*E.coli*		
Fountain number	**June**	**July**	**August**	**June**	**July**	**August**
1	abs	abs	abs	abs	abs	abs
2	abs	abs	abs	abs	abs	abs
3	abs	abs	abs	abs	abs	abs
4	**7**	**9**	abs	**4**	abs	abs
5	**3**	**30**	**14**	abs	abs	abs
6	**15**	**16**	abs	abs	abs	abs
7	**90**	**40**	**35**	**11**	**20**	**10**
8	abs	abs	abs	abs	abs	abs
9	abs	abs	abs	abs	abs	abs
10	abs	abs	abs	abs	abs	abs

TABLE 4
Result of statistical analysis

Parameter	Months	Average	Standard Deviation	Median	Minimum	Maximum	Shapiro test (P value)	Student t-test	Friedman test
pH	June	7,84	0,31	7,73	7,45	8,25	0,12		
	July	7,41	0,44	7,17	7,04	8,15	0,00		0.0012
	August	7,49	0,08	7,49	7,37	7,63	0,99	0.0027	
EC	June	340,00	223,57	236,50	96,00	678,00	0,06		
	July	335,80	207,76	241,00	121,00	662,00	0,06		
	August	318,40	228,66	199,50	119,00	655,00	0,01		
F	June	0,27	0,07	0,24	0,20	0,40	0,03		
	July	0,24	0,09	0,20	0,16	0,39	0,02		
	August	0,23	0,06	0,21	0,16	0,35	0,15		
Cl	June	18,95	18,12	15,22	1,00	50,80	0,07		
	July	19,48	18,84	15,85	0,84	50,25	0,07		
	August	21,10	19,65	16,20	1,18	52,62	0,11		
NO_3	June	24,67	30,63	3,24	2,23	82,79	0,00		
	July	24,28	30,42	3,31	1,54	80,79	0,01		
	August	26,27	32,79	3,00	1,03	83,85	0,00		
SO_4	June	29,20	27,52	18,92	3,02	73,91	0,06		
	July	27,88	27,86	13,90	2,98	72,01	0,03		
	August	29,55	28,93	18,62	2,95	83,85	0,09		
NH_4	June	0,11	0,03	0,12	0,06	0,18	0,02		
	July	0,10	0,03	0,10	0,05	0,15	0,50		
	August	0,11	0,03	0,11	0,08	0,19	0,02		

TABLE 5
Some studies on physical analysis in spring waters

Year	Author	Region/Analyzed spring water number	Parameters	In our study
2002-2005	Khashman O.A. [27]	Petra Region(Jordan) 1008	Turbidity: Acceptable, Odor: Acceptable Color: Acceptable, Taste: Acceptable pH: 7,54-8,14, EC: 488-1059 µs/cm	Turbidity: Acceptable Odor: Acceptable Color: Acceptable Taste: Acceptable pH: 7,14-8,25 EC: 96-662 µs/cm
2009	Dombaycı K. [15]	Erzurum(Turkey) 4	pH: 7.15-7,71, EC: 399-824 µs/cm	
2009	Dönderici Z. [30]	Mediterranean and Internal Anatolia Region (Turkey) 63	Colorless, odorless, normal taste pH 6,71-8,21, EC: 25,9-195,5 µs/cm	
2010	Odeyemi et. al. [31]	Nigeria 6	Colorless, odorless, clear pH: 4,8-6,8	
2012	Glevitzky et. al. [32]	Romania 7	Clear, colorless, without particles and without sediment impurities. No foreign taste or smell (except for one sample). pH 6,9-7,4	
2014	Gültekin et. al. [33]	Istanbul(Turkey) 10	Odor: No abnormal change, Turbidity: Acceptable to consumers. Clear. Without sediment impurities. No foreign matter. pH 5,8-7,6 (except for two sample) EC: 71,8 - 427 µS/cm	
Sept 2015-Febr 2016	Wotchoko et. al. [34]	Bafia-Muyuka(Africa) 5	Odorless, colorless, normal taste and appearence pH: 6,70-7,55 (except for one sample) EC: 180-302 µS/cm	

Results of Physico-Chemical Parameters Turbidity, Appearance, Odor, and Taste; The provision of drinking water is not only safe but also acceptable in appearance, taste, and odor. Changes in the normal appearance, taste or odor of drinking-water may signal to changes in the quality of raw water [26]. Normal appearance of water does not mean that the water is drinkable. In terms of aesthetics, it is desirable that the drinking water should be clear [15]. In our study, turbidity, odor, appearance, and taste are found acceptable to the consumers for all fountains.

pH. pH value does not have a direct effect on human health, but it is important in terms of water quality. Low pH causes bitter metallic taste and corrosion while high pH causes slippery feeling and soda taste. In our study, pH values are found between 7,14 and 8,25 for all fountains.

Electrical conductivity (EC). Electrical conductivity (EC) is known as one of the main physical properties of water [25]. This parameter is taken as a measure of dissolved solids and it reveals the status of pollution from inorganic ions [28]. Dissolved matters in water affect electrical conductivity. Recommended value is between 300 and 400 µS/cm [29]. In our study, electrical conductivity (EC) values are found between 96 and 662 µS/cm for all fountains. The results of the organoleptic analysis, pH, and electrical conductivity (EC) values are in line with Turkısh national standards and EC, EPA ve WHO standards.

The spring waters examined in our study are similar to spring waters examined in other studies in terms of physical properties.

Today, industrialization, fertilizers, and chemicals used in agriculture and industry pollute waters in these regions and they cause important health problems. For this reason, chemical pollution in the waters will be one of the most important problems of water pollution in the future [35].

Results of Chemical Parameters. Fluoride (F). Fluoride (F), like most of the trace elements, is one of the main trace elements in groundwater, which generally occurs as a natural constituent, and ıt is widely used to combat dental caries, but is of ambivalent nature, meaning that when present in high concentration it is toxic, while in lower concentration it is essential [36, 37]. WHO guideline value is 1.5 mg/l. Concentrations above this value carry an increased risk of dental fluorosis [26].

In our study fluoride (F) concentrations are found between 0,16-0,40 mg/L for all fountains. These concentrations are lower than recommended concentrations and in line with Turkish national standards and EC, EPA ve WHO standards.

Chloride (Cl). Chloride (Cl) in drinking-water originates from natural sources, sewage and industrial effluents, urban runoff containing deicing salt and saline intrusion.

Not of health concern at levels found in drinking water [26]. High concentrations of chloride give a salty taste to water. In our study chloride (Cl) concentrations are found between 0,84-52,62 mg/L for all fountains. These concentrations are in line with Turkısh national standards and EC, EPA standards. There is no recommended chloride value in WHO.

Nitrite (NO_2) and Nitrate (NO_3). Nitrite (NO_2) sources in waters are the organic matter, fertilizers, and some of the minerals. The nitrite (NO_2) concentration in surface waters higher than 1 mg/L indicates the presence of pollution and nitrite can be formed by the microbial reduction of nitrate [26, 38].

Nitrate (NO_3) is the final product of nitrogenous organic matters and commonly occurs naturally in groundwater, but high concentration might be associated with animal and human waste, open septic or sewage systems and fertilization of farms [38, 13]. Nitrite (NO_2) may cause toxic effects by converting hemoglobin to methemoglobin and enlarges vein smooth muscles and reduces systemic arterial blood pressure and may cause circulation disorder and shock [10]. Excessive nitrate in drinking water can cause a number of disorders including methemoglobinemia in infants, gastric cancer, goiter, birth malformations and hypertension [13].

In our study nitrite (NO_2) concentrations are not found for all fountains. The results are in line with Turkish national standard and EC, EPA ve WHO standards.

In our study nitrate (NO_3) concentrations are found between 1,03-3,27 mg/L for six fountains and are found between 39,49-48,18 mg/L for number 2 and 3 fountains. These concentrations are in line with Turkısh national standards and EC, EPA ve WHO standards, but they are found 64,19-83,85 mg/L for number 1 and 4 fountains. These concentrations are higher than Turkısh national standards and EC, EPA ve WHO standards. It is thought that there may be fecal pollution in number 1, 2, 3 and 4 fountains and snow water and rainwater may cause that contaminants transported into groundwater.

Sulfate (SO_4); Sulfate (SO4) could derive from a natural source such as sulfate minerals common in igneous rocks [34]. Not of health concern at levels found in drinking water, but very high levels might cause a laxative effect in unaccustomed consumers [26].

In our study sulfate (SO_4) concentrations are found between 3,02-83,85 mg/L for all fountains. These concentrations are in line with Turkish national standards and EC, EPA standards. There is no recommended sulfate value in WHO.

Ammonia (NH_4); Ammonia (NH_4) in the environment originates from metabolic, agricultural and industrial processes. Natural levels in groundwater and surface water are usually below 0.2 mg/l. Ammonia (NH_4) in water is an indicator of possible bacterial, sewage and animal waste pollution. Toxicological effects are observed only at exposures above about 200 mg/kg body weight. Ammonia (NH_4) in drinking-water is not of immediate health relevance, and therefore no health-based guideline value is proposed by WHO, EPA [26].

In our study ammonia concentrations are found between 0,05-0,19 mg/L for all fountains. These concentrations are in line with Turkısh national standards and EC standards.

TABLE 6
Some studies on chemical analysis in spring waters

Year	Author	Region/Analyzed Spring water number	Parameters	
2005-2006	Bhat and et al. [39]	Kashmir (India) 3	Cl: 14-39 mg/L NO_3: 2,5-3,9 mg/L SO_4: 1-9,9 mg/L NH_4: 0,01-0,58 mg/L	Results are complied with WHO. It is stated that presence of ammonia in water indicates pollution of recent origin as a result of ammonification. Chloride and nitrate (except for 4 samples) results of our study are comply within this study. Ammonia results of our study are lower than this study, sulfate results of our study are higher than this study
2007	Koçak and et al. [40]	Erzurum (Turkey) 25	**F:** 0.79±0,02 mg/L **NO_2**: 0.044±0,02 mg/L **NO_3**: 47.62±5,67 mg/L	Fluoride, nitrite, and nitrate (except for 4 samples) results of our study are generally lower than this study. 4 fountains in our study and 7 fountains in this study have high nitrate contents. This situation indicates fecal pollution in this region.
2009	Dombaycı K. [15]	Erzurum (Turkey) 4	**Cl**: 15,65-58,24 mg/L **NO_3**: 33,43-27,11 mg/L **SO_4**: 48,02-68,33 mg/L **NH_4**: 0,01-0,03 mg/,	It is stated that nitrate results are higher than Turkish national standards (except for one sample) Chloride, nitrate, sulfate and ammonia results of our study generally comply within this study. Both in our study and in this study same fountains have low ammonia concentration and high nitrate concentration. This situation indicates fecal pollution in this fountains
2009	Ansari et al. [41].	Himalayas (India) 4	**Cl**: 0,8-5,3 mg/L **NO_3**: 1,6-20,1mg/L **SO_4**: 35,1-116,4mg/L	Results comply with WHO. It is stated that this spring water is drinkable. The sulfate in spring water may be due to the interaction of water with the sedimentary rock and may also come from the breakdown of organic matters in the soil and from fertilizer used in cultivation. Nitrate in spring water may be due to the agricultural practices at recharge area. Sulfate results of our study are generally lower, chloride and nitrate results of our study are higher than this study.
2010	Aghazadeh et al. [6]	Ardabil (Iranian) 77	**F**: 0,15-1,18 mg/L **Cl**: ; 9-667 mg/L **NO_3**: 2,26-130 mg/L SO_4: 4,2-1286 mg/L	Results generally comply with WHO. It is stated that fluoride concentrations in spring water are limited. High nitrate concentration in some spring water indicates groundwater can be contaminated by fertilizer application, human and livestock sewage, deposition of plants and other wastes rich in nitrates. Fluoride, chloride, nitrate and sulfate results of our study are generally lower than this study.
2011	Sheikh et al. [42]	Kashmir (India) 3	**Cl**: 15,7-17,99 mg/L **NO_2**: 2,40-3,87 mg/L **NH_4**: 1,48-6,07 mg/L	It is stated that higher values of different forms of nitrogen in water may be due to domestic sewage, washing, and other agricultural activities within the catchment of these fresh water bodies. Nitrate, ammonia results of our study are generally lower, chloride results of our study are higher than this study.
2011-2013	Szczucin´ska A. [43]	Polonya 20	**Cl**: 3,7-20,5 mg/L **NO_2**: 0-0,03 mg/L **NO_3**: 0,29-37,13 mg/L **SO_4**: 12-82 mg/L **NH_4**: 0-0,26 mg/L	It is stated that groundwater of the study area is not greatly polluted. Sulfate and ammonia results of our study comply with in this study and chloride and nitrate (4 fountains) results of our study are higher than this study.
2013-2014	Jebreen et al. [44]	Soreq-Catchment 10	Dry season-Wet season **Cl**: 31-219-88-230 mg/L **NO_3**: 18-49-2,5-39 mg/L **SO_4**: 18-110-18-112mg/L	It is stated that results comply with WHO. Chloride, nitrate, and sulfate results of our study (except for 4 fountains) are generally lower than this study.
2014	Gültekin et al. [33]	Istanbul (Turkey) 10	**F**: 0-0,46 mg/L **Cl**: 15,9-78,1mg/L **NO_2**: abs **NH_4**: abs	It is stated that fluoride levels are very low. Results of our study comply with this study
Sept 2015-Febr 2016	Wotchoko et al. [34]	Muyuka (Africa) 5	Dry season-Rainy season **Cl**: 5,80-4,80-mg/L **NO_3**: 2,54-3,12-mg/L **SO_4**: 0,72-1,28 mg/L **NH_4**: 0,12-0,54-mg/L	It is stated that the rainy season values are higher than dry seasons (except for chloride parameter), ammonia values in the rainy season result from fertilizer application and are higher than WHO limits. Ammonia results of our study are generally lower, chloride, nitrate, and sulfate results of our study are higher than this study.
2015 In this study	Tuluk B. and Orhan F.	Erzurum (Turkey) 10	**F**: 0,16-0,40 mg/L **Cl**: 0,84-52,62 mg/L **NO_2**: abs **NO_3**: 1,03-83,85 mg/L **SO_4**: 3,02-83,85 mg/L **NH_4**: 0,05-0,19 mg/L	In our samples, low ammonia, high nitrate presence in the water samples indicates an outdated fecal contamination.

Results of Microbiological Parameters. Microbiological pollution of groundwater leads to various environmental and public health problems [12]. Microbiological analyses of drinking water show the hygienic quality of the water. Identification and evaluation of coliform microorganisms in drinking water are easy. For this reason, they are used as indicator microorganisms to determine the microbiological quality of drinking water [14]. Coliform bacteria may not cause disease, but can be indicators of pathogenic organisms that cause diseases. Coliform bacteria originate in the intestinal tract of warm-blooded animals and can be found in their wastes. Coliform bacteria can also be found in soil and on vegetation. The EPA Maximum Contaminant Level (MCL) for coliform bacteria in drinking water is zero (or no) total coliform per 100 ml of water. *E.coli* that live in the intestines of warm-blooded animals. When *E.coli* bacteria present in high numbers in a water sample, it means that the water has received fecal matter from one source or another. Although not necessarily agents of disease, fecal coliform bacteria may indicate the presence of disease-carrying organisms, which live in the same environment as the fecal coliform bacteria [45].

One of the most important water-related hazards is an infection due to fecal contamination in the water. Disinfection is not applied to spring water. For this reason, gastroenteritis cases which are caused by spring waters are frequently observed especially in summer [46]. When the microbiological analyses of our study are evaluated; It was observed total coliform and *E.coli* in number 4 and number 7 fountains in different months. It is observed total coliform in number 5 and number 6 fountains in different months. The highest bacterial count is observed in number 7 fountain. These fountains are not suitable for human consumption.

Sezen et al. microbiologically examined the public fountains of Yakutiye district (Erzurum/Turkey) where numerous individuals complained gastroenteritis in 2012 and total coliform (38-300/100ml) and *E.coli* (22-198/100ml) are observed in fountains waters. They stated that cause of epidemic were public fountains waters which were contaminated. [47].

Barlas et al. examined 684 people complaining of gastroenteritis in Tavsanlı district (Kutahya/ Turkey) in 2014. They stated that cause of epidemic were public fountains waters which were contaminated after heavy rains [48].

Kosekahya et al. examined the case of gastroenteritis in Kütahya city center(Turkey) in 2014. They stated that cause of epidemic were public fountains waters which were contaminated [49].

Kocak et al. examined tap waters and public fountains waters in Erzurum(Turkey) in 2009. They observed total coliform in all of the public fountain's water [50].

Alisarlı et al examined tap waters and public fountains waters in Van (Turkey) in 2007. They observed total coliform %56 of city center water samples and % 76 of Van districts water samples and they observed *E.coli* %13 of city center water samples and % 11 of Van districts water samples [51].

Burkowska-But et al. examined unchlorinated four fountains water in Torun city center (Poland) in 2013. They stated that three fountains water were not suitable for human consumption in terms of microbiologically [52].

In our study, we observed that number 7 fountain (during the working period) and number 4,5,6 fountains (in different months) are not suitable for human consumption in terms of microbiological parameters. but number 1, 2, 3, 8, 9, 10 fountains are suitable.

When the statistical analysis of our study are evaluated; there is no significant difference between June, July and August months in all chemical parameters except for pH parameter. There is a significant difference (p0,05) between June and July and between June and August in pH parameter.

CONCLUSIONS

Spring water is preferable than tap water due to beautiful taste, but especially nitrate (NO_3) and microbiologically pollution may be in city center fountains.

Public fountains should be monitored continuously to use as drinking water especially in the summer season in which snow water is at a high rate and in the rainy season in which rainwater is at a high rate.

When control parameters in public fountains exceed the limits, these fountains should not be used as drinking water.

ACKNOWLEDGEMENTS

Part of this article was presented as a poster in 2015 National Water and Health Congress in Antalya/Turkey.

REFERENCES

[1] Ogundana, A.K., Aladejana, J.A. (2014) Geophysical and Hydrochemical Evaluation of Springwater Potential and Quality within the Basement Complex of Southwestern Nigeria. The International Journal of Engineering and Science. (IJES). 3(5), 45-55.

[2] Dede, O.T., Polat, M. (2010) Şebeke Suyu Kalitesi ile Kaynak Suyu Kalitesinin Karşılaştırılması. DSİ Teknik Bulteni. 107, 22-26 (In Turkish).
[3] Glevitzky, M., Dumitrel G.A., Popa, M., Todoran, A. (2013) Study on the Quality of Spring Waters from Ocna Mures Area, Romania. Chemical Bulletin of "Politehnica" Univ. (Timisoara). 58(72), 1-5.
[4] Bariki, S.K. (2017) Physico-Chemical Quality of Some Spring Water Samples Through Correlation Studies in Four Mandals of Tribal Area of Visakhapatnam District, Andhra Pradesh, India. International Journal of Scientific Engineering and Research (IJSER). 5(3), 33-41.
[5] Tubman, S.C. (2013) Spring Discharge Monitoring in Low-Resource Settings: A Case Study of Concepción Chiquirichapa, Guatemala, Michigan Technological University Department of Geological and Mining Engineering and Sciences, Master of Science Thesis. 58p.
[6] Aghazadeh, N., Chitsazan, M., Golestan, Y. (2017) Hydrochemistry and Quality Assessment of Groundwater in The Ardabil Area, Iran. Appl Water Sci. 7(7), 3599-3616.
[7] Vilane, B.R.T., Dlamini, J. (2016) An Assessment of the Mhlambanyoni Spring Water Quality at Sigombeni, Swaziland. Journal of Agricultural Science and Engineering. 2(5), 40-45.
[8] Mwaniki, S.N., Wanjau, T.W., Njeru, S.N., Mavura, J.W. (2013) Physico-Chemical Properties of Spring Water in Kabare and Baragwi Locations, Gichugu Division Kirinyaga County of Kenya. International Journal of Science and Research (IJSR). 2(7), 280-285.
[9] Michalik, A. (2008) The Use of Chemical and Cluster Analysis for Studying Spring Water Quality in Świętokrzyski National Park. Polish J. of Environ. Stud. 17(3), 357-362.
[10] Ağoğlu, S., Ekici, K., Alemdar, S., Dede, S. (1999) Van ve Yöresi Kaynak Sularının Mikrobiyolojik, Fiziksel ve Kimyasal Kaliteleri Üzerine Araştırmalar. Van Tıp Dergisi. 6(2), 30-33 (In Turkish).
[11] Sekerci, P. (2012) Microbiological, Physical, Chemical Analysis And Molecular Typing Of E.Coli Isolates From Fountaın Waters, Erzurum, Master Thesis, Ataturk University Natural and Applied Science Department of Food Engineering. 82p. (In Turkish).
[12] Tunc, M.S., Tepe, O., Unlu, A., Dursun, A.Y., Yaman, M. (2017) Assessment of Groundwater Quality In Uluova, Elazig, Turkey. Fresen. Environ. Bull. 26, 5092-5102.
[13] Shigut, D.A., Liknew, G., Irge, D.D., Ahmad, T. (2017) Assessment of Physico-Chemical Quality of Borehole and Spring Water Sources Supplied to Robe Town, Oromia Region, Ethiopia. Appl Water Sci. 7(1), 155–164.
[14] Oğur, R., Tekbaş, Ö. F. (2005) Temel Su Analiz Teknikleri, GATA Halk Sağlığı AD, Ankara, 64s. (In Turkish).
[15] Dombaycı, K. (2009) A Monitoring and Evaluation of Erzurum City's Drinking Water With Respect to Some Physical Chemical Quality Parameters, Master Thesis, Ataturk University Natural and Applied Sciences Department of Environmental Science. 86p. (In Turkish).
[16] URL 1. T.C. Çevre ve Şehircilik Bakanlığı. Retrieved May 15, 2017, from https://www.csb.gov.tr /db/ced/editordosya/ Erzurum2015.pdf (In Turkish).
[17] Soylak, M., Divrikli, Ü., Elçi, L., Dogan, M. (2001) Iodine Levels of Drinking Water Samples Collected from Kayseri-Turkey. Fresen. Environ. Bull. 10, 595-597.
[18] TS EN ISO 10523, Turkish Standard, Water quality–Determination of pH. (2013) 12p. (In Turkish).
[19] APHA – AWWA - WEF (2005) Standard Methods for the Examination of Water and Wastewater, 21st edition, American Public Health Association, Washington, D.C.
[20] US EPA (The United States Environmental Protection Agency) (1999), Determination of Inorganic Anions in Drinking Water by Ion Chromatography, EPA 300.1. Washington DC.
[21] Spectroquant UV/VIS Spectrophotometer Pharo 300 Operating manual (2010) Merck, Darmstadt (Germany).
[22] TS EN ISO 9308-1 (2014) Turkish Standard, Water quality- Enumeration of Escherichia coli and coliform bacteria -Part 1: Membrane filtration method for waters with low bacterial background flora. 21p (In Turkish).
[23] SB (2005) İnsani tüketim amaçlı sular hakkında yönetmelik (in Turkish), Official Gazette dated on 17 February 2005 and numbered 25730, Turkey.
[24] Council of the European Communities (1998) Council Directive 98/83/EC of 3 November 1998 on the quality of water intended for human consumption. Official Journal L. 330, 32-54.
[25] URL 2. The United States Environmental Protection Agency. Retrieved June 15, 2017, from https://www.epa.gov/sites/production/files/2016-06/documents/npwdr_ complete _table. pdf.
[26] WHO (2011) Guidelines for drinking-water quality, 4th Edition, World Health Organisation, Geneva.

[27] Khashman, O.A. (2007) Study of Water Quality of Springs in Petra Region, Jordan: A Three-Year Follow-Up. Water Resources Manage. 21, 1145–1163.
[28] Elipek, B.C., Guher, H., Oterler, B., Divrik, M.T., Mimiroglu, P.A. (2017) Determining of Water Quality by Using Multivariate Analysis Techniques in A Drinking/Using Water Reservoir in Turkey. Fresen. Environ. Bull. 26, 5007-5012.
[29] Bariki, S.K., Reddy, T.B., Saramanda, G. (2015) Assessment of Physico- Chemical Quality of Drinking Water in Araku Valley Mandal of Visakhapatnam District, Andhra Pradesh, India. The International Journal of Science & Technoledge. 3(3), 177-183.
[30] Donderici, Z.S., Donderici, A., Basarı, F. (2010) An Investigation on Physical and Chemical Quality of Spring Waters. Turk Hijyen ve Deneysel Biyoloji Dergisi. 67(4), 167-172 (In Turkish).
[31] Odeyemi, A.T., Dada, A.C., Ogunbanjo, O.R., Ojo, M.A. (2010) Bacteriological, Physicochemical and Mineral Studies on Awedele Spring Water and Soil Samples in Ado Ekiti, Nigeria. African Journal of Environmental Science and Technology. 4(6), 319-327.
[32] Glevitzky, M., Dumitrel, G.A., Popa, M., Todoran, A. (2013) Study on the Quality of Spring Waters from Ocna Mures Area, Romania. Chemical Bulletin of "Politehnica" The University of Timisoara. 58(72), 1-5.
[33] Gultekin, S., Sesal, C., Kayhan, F.E. (2016) Chemical Analysis Evaluation of Natural Spring Water in Anatolian Side of Istanbul Province. Marmara Fen Bilimleri Dergisi. 4, 132-140 (In Turkish).
[34] Wotchoko, P., Tita, M.A., Kouankap, N.G.D, Alice, M., Nkemnji, J.Z., Guedjeo C.S., Kamgang, K.V. (2016) Physico-Chemical Analysis of Water Quality of Springs in Bafia-Muyuka, North-Eastern Flank of Mount Cameroon (South West Region, Cameroon Volcanic Line). American Journal of Water Resources. 4(5), 111-120.
[35] Ozaslan A. (2009) Determınetıon of Fecal Colıform Levels and Antıbıotıcs Resıstence Frequency Of Adana Drınkıng Water, Master Thesis, Çukurova University and Department Of Bıotechnology Instıtute Of Natural And Applıed Scıences. 64 p. (In Turkish).
[36] Ramesh, K., Thirumangai, V. (2014) Trace Metals Contamınatıon of Groundwater in and Around Tannery Industrıal Area of Pallavaram, Chennaıcity, India, International Journal of Research in Engineering and Technology. 3(5), 163-169.
[37] Mitrakas, M. (2001) A Survey of Arsenic Levels in Tap, Underground and Thermal Mineral Waters of Greece. Fresen. Environ. Bull. 10, 717-721.
[38] Mutlu, E., Kurnaz, A. (2017) Determination of Seasonal Variations of Heavy Metals and Physicochemical Parameters in Sakiz Pond (Kastamonu-Turkey). Fresen. Environ. Bull. 26, 2807-2816.
[39] Bhat, S.U., Pandit, A.K. (2010) Limnochemistry of Three Freshwater Springs of Kashmir Himalaya. Hydro Nepal. 7, 54-59.
[40] Kocak, O., Guner, A. (2009) Chemical, Physical and Microbiological Qualities of Tap Water in Erzurum City. Atatürk Üniversitesi Vet. Bil. Derg. 4(1), 9-22 (In Turkish).
[41] Ansari, A., Deodhar, A., Kumar, U.S., Khatti, V.S. (2015) Water Quality of Few Springs in Outer Himalayas–A Study on The Ground Water–Bed Rock Interaction Sand Hydro Chemical Evolution. Groundwater for Sustainable Development. 1, 59–67.
[42] Sheikh, M.A., Dar, I.Y., Yaseen, S., Pal, A., Pandit, A.K. (2013) A Study of Physico-Chemical Characteristics of Three Fresh Water Springs of Kashmir Himalaya, India. International Journal of Water Resources and Environmental Engineering. 5(6), 328-331.
[43] Szczucinska, A. (2016) Spring Water Chemistry in a Formerly Glaciated Area of Western Poland: The Contribution of Natural and Anthropogenic Factors. Environ Earth Sci. 75(712), 1-15.
[44] Jebreen, H., Ghanem, M. (2015) Spring Water Qualitative Assessment in Mountainous Areas, Case Study: Soreq Catchment/Ramallah/West Bank. Journal of Water Resource and Protection. 7, 851-859.
[45] URL 3. www.water-research.net. Retrieved June 15, 2017, from http://www.water-research.net/index.php/bacteria.
[46] Yalvac, S., Aydın, A. (2000) Fluoride Levels İn Public Waters Open Purchased Waters Well Waters and Spring Waters Collected from Different Districts of Istanbul. Turkish Archives of Pediatrics. 35(2), 78-86 (In Turkish).
[47] Sezen, F., Aval, E., Agkurt, T., Yılmaz, S. (2015) A Large Multi-Pathogen Gastroenteritis Outbreak Caused by Drinking Contaminated Water from Antique Neighbourhood Fountains, Erzurum City, December 2012, Epidemiology and Infection. 143(4), 704-710.
[48] Barlas, G., Tozan, E., Altuğ, Y., Aktas, D., Temel, F., Korukluoğlu, G., Sucaklı, M. (2016) An İnvestigation of an Outbreak of Gastroenteritis in the Tavsanli District of Kutahya Province, July 2014, A Case-Control Study. Turk J Public Health. 14(2), 81-94 (In Turkish).

[49] Kösekahya, A., Özarslan, F., Çoban, S.C., Altuğ, Y., Levent, B., Yılmaz, M., Temel, F., Sucaklı, M.B., Musaonbaşıoglu, S. (2015) Kütahya İl Merkezinde Su Kaynaklı Gastroenterit Salgını, Ekim 2014, 18. Ulusal Halk Sağlığı Kongresi Kongre Kitabı, 05-09 Ekim Konya. 203-204 (In Turkish).
[50] Koçak, O., Güner, A. (2009) Chemical, Physical and Microbiological Qualities of Tap Water in Erzurum City, Atatürk Üniversitesi Vet Bil Derg. 1, 22 (In Turkish).
[51] Alişarlı, M., Ağaoğlu, S., Alemdar, S. (2007) The Evaluation of Microbiological Quality of Van Region Waters in Terms of Public Health, Yüzüncü Yıl Üniversitesi Veteriner Fakültesi Dergisi. 18(1), 67-77 (In Turkish).
[52] Burkowska-But, A., Swiontek Brzezinska, M., Walczak M. (2013) Microbiological Contamination of Water in Fountains Located in The City of Toruń, Poland. Annals of Agricultural and Environmental Medicine. 20(4), 645–648.

Received: **08.07.2017**
Accepted: **21.10.2017**

CORRESPONDING AUTHOR

Banu Tuluk
Atatürk Univesity,
Faculty of Engineering,
Department of Environmental Engineering,
25240, Erzurum – Turkey

e-mail: nbtuluk@hotmail.com

© by PSP Volume 27 – No. 2/2018 pages 982-988 Fresenius Environmental Bulletin

EFFECTS OF SHORT-TERM HIGH-SALT STRESSES ON PHOTOSYNTHETIC CHARACTERISTICS, ACTIVITIES OF PROTECTIVE ENZYME AND COPPER UPTAKE OF ACORUS CALAMUS IN MICROCOSM SUBMERGED WETLANDS

Jianqiu Han*, Yumei Zhou, Dandan Li, Guangqiang Zhai

College of Ecological Technology and Engineering, Shanghai Institute of Technology, 201418 Shanghai, China

ABSTRACT

Seven microcosm submerged wetlands were built to evaluate the physiological characteristics and copper uptake performance of *Acorus calamus* after short-term high-salt stresses. Each microcosm was equipped with plastic pipes and three plants were planted in each pipe. The artificial copper-containing wastewater of different salt concentrations was added in microcosm wetlands once a week., only at the first week, it was added 0 (as control), 1, 2, 4, 6, 8, and 10 % (by weight) of NaCl respectively. Leaf chlorophyll content, photosynthetic parameters of *Acorus calamus* did not be inhibited when salt concentrations were below 2 %, could restore to normal level after some time under 4 % salt concentration, significantly dropped over 6 % concentrations. *A. calamus* could reduce the damage of salt stresses by generating protective enzymes (mainly SOD), but this ability decreased even disappear when salt concentrations were over 6%. Short-term lower salt stresses of 1 to 4 % did not inhibit copper uptake and transportation in *Acorus calamus*, but higher salt stresses of 6 to 10 % could inhibit the growth of the plants, and decreased the Cu uptake.

KEYWORDS:
Photosynthetic characteristic, Activities of protective enzyme, Submerged wetland, High-salt, *Acorus calamus*, Cu uptake

INTRODUCTION

Copper (II) (Cu^{2+}) is among the most common heavy metals found in wastewater discharges of many industries including surface treatment, metal plating facilities, tanneries, and mining operations [1]. Although copper is a necessary trace element in animal metabolism, excessive amounts of it lead to various health problems such as headache, nausea, dizziness, hemolytic anemia, and so on [2]. Some studies have investigated Cu removal efficiency of submerged bed [3, 4]. Macrophytes have been considered as promising material for remediation of heavy-metal contaminated sites, but availability of Cu to aquatic plants and translocation from roots and rhizomes to shoots leaves depend upon plant species, growth stages of plants, Cu concentration in water, presence of competing metals, temperature, and pH [3, 5, 6].

High-salt wastewater (>1 % salinity by weight) is generated in manufacturing of pharmaceuticals, pesticides and herbicides, and so on [7]. High salt contents are also found in the landfill leachates [8]. Rising sea levels and stronger storm surges may expose tidal fresh water wetlands to saline waters [9]. And salinization poses one of the greatest threats to our rivers and wetlands and has the potential to cause irreversible damage to the structure and function of aquatic communities in arid regions of the world [10].

Some study reported that high salt content in wastewater could alter the biodiversity, species composition and function of the aquatic ecosystems [11], and significantly decreased the treatment efficiency of conventional activated sludge, attached growth, anaerobic, nitrification and denitrification processes [12]. Although the influence of salt on Cu absorption has been exhaustively considered in cyanobacteria [13], marine in vertebrates [14, 15], and algae [16], data concerning aquatic macrophyte after short-term stress are crucially missing when salt content is super high.

Acorus calamus is perennial aquatic herb, widely distributing in South Chin. It is a powerful macrophyte for wetland sewage treatment because of its extremely fast growth rate under optimal conditions and sorption effects on heavy metals [17].

The objectives of this study were to (1) investigate the photosynthetic characteristics and protective enzyme activities of *A. calamus* after short-term high-salt treatments in wastewater; (2) evaluate copper uptake performance of *A. calamus* under short-term high-salt stresses.

MATERIALS AND METHODS

Experimental design. The experiments were carried out in a greenhouse of Shanghai Institute of Technology (Shanghai, China) from 16 October to

21 November 2015). 21 microcosm submerged wetlands were built with 7 plastic pipes (500 mm tall, inner diameter 155 mm). Each pipe was packed with 400 mm of mixture of marble chips (effective chip size 10.1 mm and uniformity coefficient 2.1) and sand, then a 50mm layer of marble chips (effective chip size 13.1mm and uniformity coefficient 0.87) was put on the upper of the mixture beds used for minimizing evaporation and maintaining air diffusion (Figure 1).

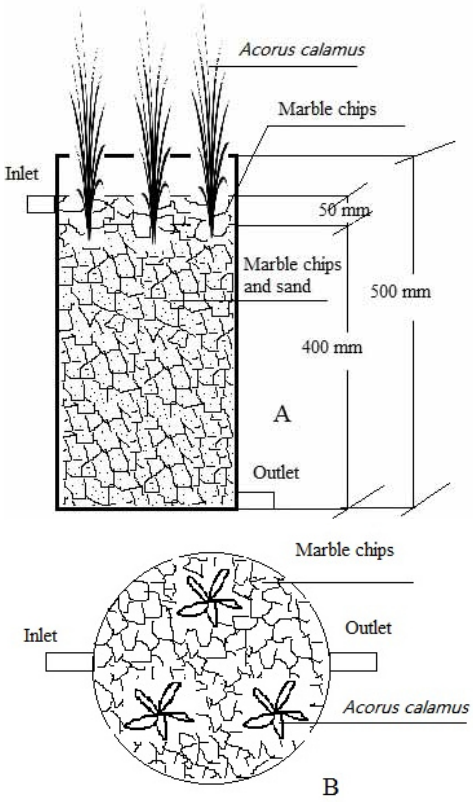

FIGURE 1
The section (A) and plan (B) of the microcosm submerged wetland used in this experiment.

Plants treatment. The *A. calamus* plants were dig from a brook flowing through the campus of Shanghai Institute of Technology. Prior to the experiment,21 seedlings with good shapes, similar sizes, and vigorous growth were selected, and cultivated directly in tap water for 14 days. Then they were planted in the submerged wetlands with 3 plants per pipe.

Experimental methods. There were seven NaCl contents treatments in this experiment, every treatment was repeated three times, so 21 submerged bed wetlands were used. Each pipe of the treatments and control was loaded with artificial Cu wastewater (1 L each), and was operated in a greenhouse. The Cu wastewater was made of 1/2-strength Hoagland solution and $CuSO_4$. The composition of the solution was as follows (1 L):472.5 mg $Ca(NO)_3$, 57.5 mg $(NH_4)_3PO_4$, 303.5 mg KNO_3, 246.5 mg $MgSO_4$, and ultra-pure water as solvent. Only at the first 7 days, 0, 10, 20, 40, 60, 80, 100 g NaCl was added in every 1 L wastewater as influents to the 7 microcosm submerged wetlands respectively. So influents loaded to the 7 microcosm submerged wetlands had 0 (as control), 1, 2, 4, 6, 8, and 10 % (by weight) of NaCl respectively, and Cu 4 mg/L ($CuSO_4$ 10 mg/L). After that, the influents was replaced one time with new Cu wastewater at every first day of the next 5 weeks, no NaCl was added in it again. Ultra-pure water was added every three days to compensate for water loss due to evaporation.

Analytical methods. Leaf chlorophyll relative content (expressed by SPAD value), photosynthetic characteristics, chlorophyll fluorescence characteristics were determined at end of every 7 days during the experiment. SPAD value was measured by SPAD-502 plus (Japan), a portable chlorophyll meter which can measure an index related to the chlorophyll content of a leaf [18]. The photosynthetic characteristics were detected by photosynthetic measurement system (LI-6400XT, LI-COR, USA). The fully expanded new leaves on the top of the plants were selected at 9:30-11:30 am for detection. All the detections were carried out in duplicate 3 times among different plants in same wetlands. The activities of superoxide dismutase (SOD) was determined according to the method of Jiang and Zhang [19]; Peroxidase (POD) and malondialdehyde (MDA) were estimated using the NBT photochemical reduction, Guaiacol and Thiobarbituric acid colorimetry methods described by Li [20] respectively. At the end of the experiment, whole plants were dig out and washed with ultra pure water three times to eliminate the adhering contaminants and soil and metal ions. Absorbent towels were then put on the plants to absorb surface water on them. This process was repeated for 3-5 times. After that, the washed plants were cut into underground parts (roots) and aboveground parts (leaves and shoots). They were dried at 85 ℃ for 48 h to constant weight, then were crushed and mixed thoroughly. About 0.2 g triturated plant tissue was digested with 15 ml mixture of H_2SO_4 and H_2O_2 (1:2, by volume) that was heated in an oven for 2 h at 380℃. After cooling, the digested samples were diluted to a volume of 100 m L using ultra pure water. The Cu contents in digestion solutions were determined using atomic absorption spectrophotometer (S7-AA-7000, Shimadzu, Japan).

Statistical analysis. Statistical analyses were performed using SPSS software version 17.0 developed by Statistical Software Package (SPSS Inc., Chicago, USA). One-way ANOVA were used to analyze the difference among different salt treatments. Differences were considered to be statistically significant at 0.05 level.

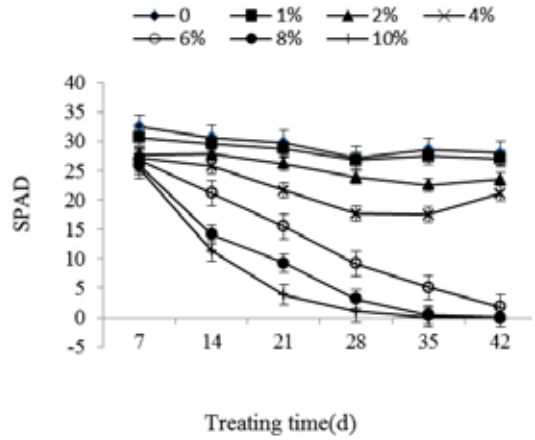

FIGURE 2
Leaf chlorophyll relative content of *A. calamus* after short-term high-salt tress

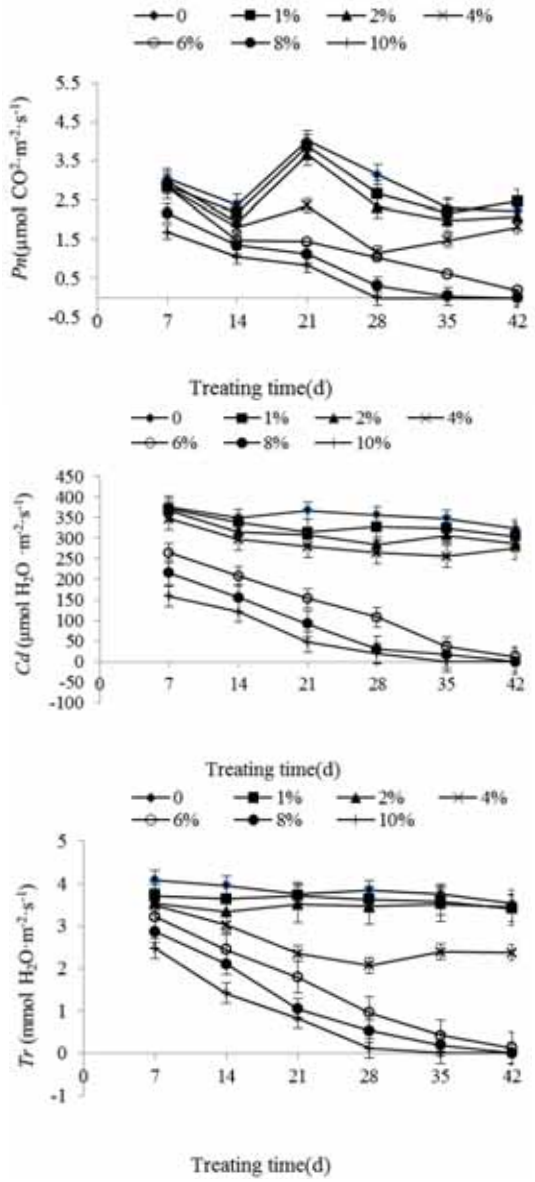

FIGURE 3
The net photosynthetic rate (*Pn*), stomatal conductance (*Cd*), and transpiration rate (*Tr*) of *A. calamus* after short-term high-salt stress

RESULTS AND DISCUSSION

Effects of short-term high-salt stress on the SPAD of *A. calamus.* SPAD values of A. *calamus* under short-term high-salt stress were presented in Fig. 2. At the 7th day, SPAD values of all salt treatments were close to that of the control. At the 14th day, SPAD values of A. *calamus* under 1 %, 2 % and 4 % salt treatments were also remained same level as the control, but those of 6%, 8%, and 10% treatments decreased by 21.27 %, 45.44 % and 57.09 % compared with the control, respectively. From the 21st to 42nd day, SPAD values of 1 %, 2 % were lower than the control, but no significant differences were found between them. 6 %-10 % treatments decreased seriously by 74.45-95.88 %, 84.54-100 % and 94.98-100 %, even no SPAD values were detected out in 8 % at the 35th day and 10% treatments at the 35th and 42nd day because the A. *calamus* plants were withered or dead. SPAD values of 4 % kept the trend of decrease before the 28th day, but it increased after that time, and close to level of the control at the end of this experiment.

High-salt stress decreases chlorophyll content of leaves because of inhibiting chlorophyll biosynthesis or accelerating degradation [21]. Our results are consistent with these previous studies of Hayat et al. [22], Ghogdi et al. [23] and Ahmad et al. [24], indicating that short-term high-salt stress in wetlands could damage chlorophyll or inhibit the synthesis. But the SPAD value could restore to normal level for plants grown under lower salt (1 to 4 %) after two weeks treatment.

Effects of short-term high-salt stress on the photosynthetic characteristics of *A. calamus.* The photosynthetic characteristics of *A. calamus* after short-term high-salt stress were presented in Fig. 3. The results revealed that the net photosynthetic rate (*Pn*) of lower salt treatments (1 %, 2 %, 4 %, 6 %) were close to the control at the 7th day, but that of 8% and 10% salt treatments decreased by 28.62 % and 44.74 % compared to the control ($p < 0.05$). In the subsequent phase, the *Pn* of all salt treatments were lower than the control, no significant differences were found between 1 %, 2 % and the control, but significant differences were found between 6 %, 8 % and 10 % salt treatments and the control ($p < 0.05$). The *Pn* of 4 % kept the same trend as SPAD value after the 7th day. At last term (35-42 days), the aboveground tissues of higher salt treatments (6 %, 8 % and 10 %) wilted or died so *Pn* was very low or could not be detected out. During the experiment, the stomatal conductance (*Cd*) of 1 % and 2 % salt treatments keep same level as the control, no differences were found between them. *Cd* of 4 % salt treatment declined below the control, but it restored to high level as the control at the 42nd day. The *Cd* of 6 % to 10 % salt treatments decreased gradually during the whole time, even no value was detected out at the

end of this experiment because of the up-ground parts of *A. calamus* wilting or death, and serious differences were found between them and the control ($p < 0.05$). At the 7th day, the transpiration rate (*Tr*) of *A. calamus* under high-salt stress was below compared to the control, and the higher the salt content, the more the *Tr* decreased. After then, *Tr* of 1 % and 2 % salt treatments restored close to the level of the control during the all experiment time, that of 4 % salt treatment dropped until to the 28th day, then rise slowly. Other salt treatments (6 %, 8 % and 10 %) remained the downward trend to end of this experiment.

Yusuf et al. [25] and Hayat [26] reported that all gas exchange parameters (*Pn*, *Cd*, *Ci*, *Tr*) of plants could be changed by salt in irrigation water. Stomatal functioning, structure and function of thylakoids, pigment content, electron transport and activity of enzymes may be the one cause of salt damages [27]. Damages to plants caused by salt stress can be attributed to a kind of physiological drought generated by NaCl [28], because of the stomatal closure thereby decreasing the partial CO_2 pressure [29] as well as internal CO_2 concentration [25]. Nilratnisakorn et al. [30] found that the inhibition of photosynthesis of *Typha angustifolia* was due to the precipitation of Na salt crystals in leaves and roots that caused the obstruction of the solute transportation. In our work, *Pn* of *A. calamus* could be inhibited by short-term high-salt stress, and the higher the salt content, the greater the decrease of *Pn*, but they increased again after some time when the salt contents were lower (1-4 %). This result could be explained by *Cd* and *Ci* changes. *Cd* and *Ci* remained higher level close to the the control when salt content were lower (1-2 %), *Pn* remained high level either. All of them decreased at 4-6% salt content, may be because stomatal closure of *A. calamus* leaves, *Cd* decreased, and *Ci* was lower, so the limiting of CO_2 supply caused con-siderable reduction in *Pn*, a result consistent with reported in *Phragmites australis* [31]. From the results of *Tr* of *A. calamus* we also concluded that the decrease of *Pn* mainly resulted from water deficit due to the osmotic stress caused by high salt contents. Our results were in agreement with Munns et al. [32] who observed that growth of *Typha domingensis* under salinity is inhibited through two phases. Initially, growth is affected because of cellular responses to the osmotic effects. In the subsequent phase, growth is reduced due to the toxic effects of accumulated salts.

Effects of short-term high-salt stress on activities of SOD, POD, and content of MDA in *A. calamus*. The activities of superoxide dismutase (SOD), Peroxidase (POD), and malondialdehyde (MDA) content in *A. calamus* were showed in Fig. 4. At the 7th day, SOD activities in *A. calamus* leaves generally increased from salt content of 0 to 10%. At the 14th day, SOD activities remained high level at 1-4 % salt contents, but they decreased sharply at 6-10 % salt contents. From the 21st day to the end of this experiment, SOD activities decreased gradually at 4-10 % salt contents, but they remained higher level at 1-2 % than the control. During the experiment time, POD activities in *A. calamus* leaves showed no obvious changes at 1-4 % salt contents and close to the control, but they constantly decreased at higher salt contents (6-10 %), and the higher the salt contents, the lower the POD activities. MDA contents increased at low salt contents (1 % and 2 %) during the experiment period, but no differences were found between them and the control. When salt contents were higher (4 %-10 %), MDA contents sharply increased and remained high level during the experiment time, very significant differences were found between the salt treatment and the control.

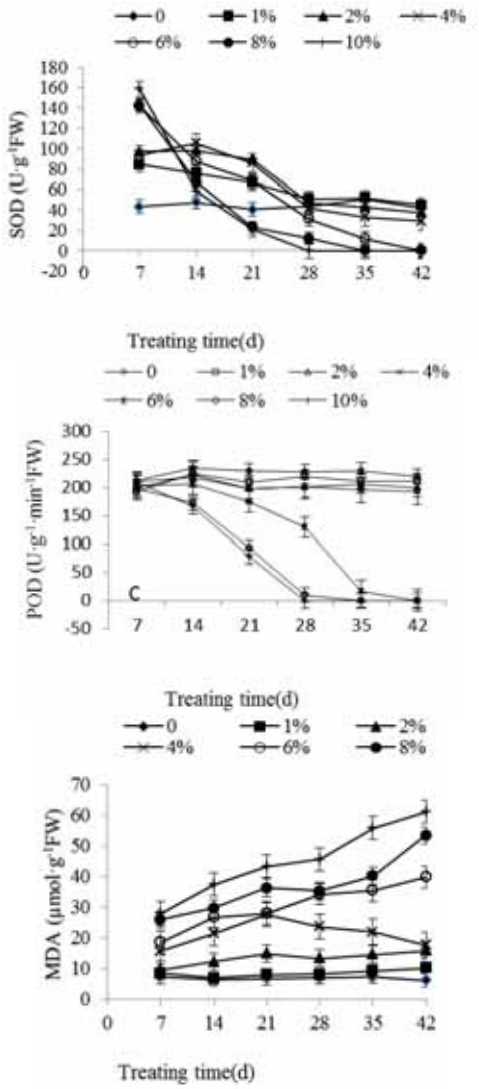

FIGURE 4
The activities of superoxide dismutase (SOD), Peroxidase (POD), and malondialdehyde (MDA) content in *A. calamus* after short-term high-salt stress

TABLE 1
Cu contents in different parts of *A. calamus* plants

Item		0	1%	2%	4%	6%	8%	10%
Cu content (mg/kg)	Leaves	1.24 0.002a	1.41± 0.003b	1.56± 0.003b	1.17± 0.007a	1.26± 0.005a	1.39± 0.005a	1.19± 0.008a
	Roots	3.48 0.011a	3.44± 0.008a	2.89± 0.008a	3.27± 0.010a	2.98± 0.008a	2.99± 0.008a	3.59± 0.012a

Data are the means ± SE of three replications
Values with same small letters mean no differences and different small letters mean significant differences at 5% level ($p < 0.05$) in a same row

Plants can generate reactive oxygen species (ROS), such as hydroxyl radicals (OH^-), superoxide radicals (O_2^-), and hydrogen peroxide (H_2O_2) during normal metabolism, but ROS are overproduced in plants under stress, including salt stress, drought and desiccation, heavy metals, air pollutants, and so on [33,34,35]. It is known that ROS can cause injury by oxidative stress [36]. Plants have defense systems against ROS, involving both enzymatic and non-enzymatic mechanisms [37]. SOD, POD are two important protective enzymes generated against cellular oxidative damage under stress [38]. MDA is a final decomposition product of lipid peroxidation induced by oxidative stress, and has been used as an indicator of lipid peroxidation. The results in our work suggested that *A. calamus* plants could be damaged by high-salt stresses, they could reduce the damage by generating protective enzymes (mainly SOD), but this ability would decrease or disappear when salt contents were higher (6-10 %). From the changes of MDA, we could conclude that the *A. calamus* plants would be injured by excessive ROS caused by higher salt stress, and this damage could not be reversed, because the generating protective enzymes of the plants could not clear the excessive ROS due to their activities decreased.

Effects of short-term high-salt stresses on Cu contents in different parts of *A. calamus.* Cu contents in leaves and roots of *A. calamus* plants were showed in Table 1. Cu accumulations in leaves of *A. calamus* plants were different. They increased by 12.06% and 25.81 % under low salt stresses (1-2 %). When salt contents were higher (4 %, 6 %, 8 %, 10 %), Cu accumulations rescore to normal level as the control. Cu accumulations in roots of *A. calamus* plants were same under all salt stresses as the control, and no significant differences were found among them ($p > 0.05$), but they all were higher than that in leaves. Mónica et al. [39] reported that the ability of the *Sargassum sinicola* to absorb copper was slightly affected by increased salinity, this conclusion was inconsistent with our results when salt contents were at 4 % and below. The results in our work suggested that *A. calamus* plants could restore gradually from short term damage, so the copper accumulation in *A. calamus* did not decrease. But the damage caused by higher salt contents (6-10 %) could not be reversed.

CONCLUSIONS

Short-term high-salt stresses (6-10 %) could damage chlorophyll and inhibit photosynthesis of *A. calamus*, and these damages could not be reversed even if the stresses disappeared.

Short-term high-salt stresses could induce SOD increase in *A. calamus* plants, and elevated activities of SOD could play as important factors of antioxidative defense mechanism against oxidative injury, but too high salt contents (6-10 %) would cause this ability lost.

Roots of *A. calamus* could absorb Cu from wastewater and transport to leaves, and roots were the main parts for Cu accumulation in *A. calamus*.

ACKNOWLEDGEMENTS

This paper was supported by undergraduates design fund from Shanghai Institute of Technology. The authors are grateful to the stuff in the laboratory of Plant Physiology for providing help and assistance. And thanks to Dr. Haiyan Wang in Beijing Forestry University for modifying this paper.

REFERENCES

[1] Marta, I., Paula, M., Piet, Lens, N.L. (2013) Effect of Organic Ligands on Copper(II) Removal from Metal Plating Wastewater by Orange Peel-based Biosorbents. Water Air Soil Pollut. 224, 1507.

[2] Dameron, C., Howe, P.D. (1998) Copper. World Health Organization, Geneva.

[3] Galletti, A., Verlicchi, P., Ranieri, E. (2010) Removal and accumulation of Cu, Ni, and Zn in horizontal subsurface flow constructed wetlands: contribution of vegetation and filling medium. Sci. Total Environ. 408, 5097-5105.

[4] Vymazal, J., Kröpfelová, L., Švehla, J., Chrastný, V., Štíchová, J. (2009) Trace elements in *Phragmites australis* in constructed wetlands for treatment of municipal wastewater. Ecol. Eng. 35, 303-309.

[5] Baldantoni, D., Ligrone, R., Alfani, A. (2009) Macro-and trace-element concentrations in leaves and roots of *Phragmites australis* in a volcanic lake in Southern Italy. J. Geochem. Explor. 101, 166-174.

[6] Du Laing, G., Van de Moortel, A.M.K., Moors, W., De Grauwe, P., Meers, E., Tack, F.M.G., Verloo, M.G. (2009) Factors affecting metal concentrations in reed plants (*phragmites australis*) of intertidal marshes in the Scheldt estuary. Ecol. Eng. 35, 310-318.

[7] Henze, M., Harremoës, P., Jansen, J., Arvin, E. (1995) Wastewater treatment --Biological and Chemical Processes. Springer-Verlag, Berlin, Heidelberg, New York. 509-555.

[8] Ellouze, M., Aloui, F., Sayadi, S. (2008) Detoxification of Tunisian landfill leachates by selected fungi. J. Hazard. Mater. 150, 642-648.

[9] Robert, I., Melody, J., Stuart, E.G., (2015) Changes in Nitrogen Cycling Processes Along a Salt Gradient in Tidal Wetlands of the Hudson River, New York, USA. Wetlands.

[10] Ghassemi, F., Jakeman, A.J., Nix, H.A., (1995) Salinisation of Land and Water Resources: Human Causes, Extent, Management and Case Studies. University of New South Wales Press Ltd., Sydney, Australia. 581-594.

[11] Halse, S.A., Ruprecht, J.K., Pinder, A.M. (2003) Salinisation and prospects for biodiversity in rivers and wetlands of south-west Western Australia. Australian Journal of Botany. 51, 673-688.

[12] Bassin, J.P., Pronk, M., Muyzer, G., Kleerebezem, R., Dezotti, M., and van Loosdrecht, M.C.M. (2011) Effect of elevated salt concentrations on the aerobic granular sludge process: Linking microbial activity with microbial community structure. Appl. Environ. Microbiol. 77, 7942-7953.

[13] Surosz, W., Palinska, K.A. (2000) Ultrastructural changes induced by selected cadmium and copper concentrations in the cyanobacterium-Phormidium: interaction with salt. Journal of Plant Physiology. 157, 643-650.

[14] Grosell, M., Blanchard, J., Brix, K.V., Gerdes, R. (2007) Physiology is pivotal for interactions between salt and acute copper toxicity to fish and invertebrates. Aquatic Toxicology. 84, 162-172.

[15] Lee, J.A., Marsden, I.D., Glover, C.N. (2010) The influence of salt on copper accumulation and its toxic effects in estuarine animals with differing osmoregulatory strategies. Aquatic Toxicology. 99, 65-72.

[16] Ratkevicius, N., Correa, J.A., Moenne, A. (2003) Copper accumulation, synthesis of ascorbate and activation of ascorbate peroxidise in Enteromorpha compressa (L.) Grev. (Chlorophyta) from heavy metal-enriched environments in northern Chile. Plant, Cell and Environment. 26, 1599-1608.

[17] Chang, J., Liu, D., Cao, H., Chang, S.X., Wang, X., Huang, C., Ge, Y., (2010) NO_3^-/NH_4^+ ratios affect the growth and N removal ability of *A. calamus* and Irispseudacorus in a hydroponic system. Aquat. Bot. 93, 216-220.

[18] Marenco, R.A., Antezana-vera, S.A., Nascimento, H.C.S. (2009) Relationship between specific leaf area, leaf thickness, leaf water content and SPAD-502 readings in six Amazonian tree species. Photosynthetica. 47 (2), 184-190.

[19] Jiang, M.Y., Zhang, J.H. (2001) Effect of abscisic acid on active oxygen species, antioxidative defence system and oxidative damage in leaves of maize seedlings. Plant Cell Physiol. 42, 1265-1273.

[20] Li, C.X., Jiang, L.N., Dai, X.M., Shang, Y.L., Hong, Z.X. (2000) The Relationship between Nitrogen Nutrition and Leaf Senescence in the Later Stage of Wheat. Journal of Triticeae Crops. 20(2), 39-41.

[21] Khripach, V.A., Zhabinskii, V.N., Khripach, N.B., (2003) New practical aspects of brassinosteroids and results of their 10 year agricultural use in Russia and Balarus, In: Hayat, S., Ahmad, A. (Eds.), Brassinosteroids: Bioactivity and Crop Productivity, Kluwer Academic Publisher, The Netherlands. 189-230.

[22] Hayat, S., Ali, B., Hasan, S.A., Ahmad, A. (2007) Effect of 28-homobrassinolide on salinity induced changes in growth, ethylene and seed yield in mustard. Indian J. Plant Physiol. 12, 207-211.

[23] Ghogdi, E.A., Izadi-Darbandi, A., Borzouei, A. (2012) Effects of salinity on some physiological traits in wheat (*Triticum aestivum* L) cultivars. Indian J. Sci. Tech. 5(1), 1901-1906.

[24] Ahmad, P., Hakeem, K.U.R., Kumar, A., Ashraf, M., Akram, N.A. (2012) Salt-induced changes in photosynthetic activity and oxidative defense system of three cultivars of mustard (*Brassica juncea* L). Afr. J. Biotechnol. 11 (11), 2694-2703.

[25] Yusuf, M., Hasan, S.A., Ali, B., Hayat, S., Fariduddin, Q., Ahmad, A., (2008) Effect of salicylic acid on salinity induced changes in *Brassica juncea*. J. Integ. Plant Biol. 50, 1-4.

[26] Hayat, S., Mir, B.A., Wani, A.S., Hasan, S.A., Irfan, M., Ahmad, A. (2011) Screening of salt tolerant genotypes of *Brassica juncea* based on photosynthetic attributes. J. Plant Interact. 6, 53-60.

[27] Geissler, N., Hussin, S., Koyro, H.W., (2009) Elevated atmospheric CO_2 concentration ameliorates effects of NaCl salinity on photosynthesis and leaf structure of Astertripolium. J. Exp. Bot. 60, 137-151.
[28] Hopkins, W.J. (1995) Physiology of plant under stress. In: Introduction to Plant Physiology. John Wiley & Sons Inc. New York. 438p.
[29] Iyengar, E.R.R., Reddy, M.P. (1996) Photosynthesis in high salt-tolerant plants. In: Pesserkali, M. (Ed.) Hand Book of Photosynthesis, Marcel Dekkar, Baten Rose, USA. 897-910.
[30] Nilratnisakorn, S., Thiravetyan, P., Nakbanpote, W. (2007) Synthetic reactive dye wastewater treatment by narrow-leaved cattails (*Typha angustifolia* Linn.): effects of dye, salinity and metals. Sci Total Environ. 384, 67-76.
[31] Choi, W.J., Ro, H.M., Chang, S.X. (2005) Carbon isotope composition of *Phragmites australis* in a constructed saline wetland. Aquat. Bot, 82, 27-38.
[32] Munns, R., Greenway, H., Kirst, G.O. (1993) Halotolerant eukaryotes. In: Lange, O.L., Nobel, P.S., Osmond, C.B., Ziegler, H.H. (eds.) Encyclopedia of Plant Physiology (New Series, Vol. 12C). Springer Verlag, Berlin, 59-135.
[33] Dat, J., Vandenabeele, S., Vranova, E., Van Montagu, M., Inze, D., Van Breusegem, F. (2000) Dual action of the active oxygen species during plant stress responses. Cell. Mol. Life Sci. 57, 779-795.
[34] Noctor, G., Foyer, C.H. (1998) Ascorbate and glutathione: keeping active oxygen under control. Annu. Rev. Plant Physiol. Plant Mol. Biol. 49, 249-279.
[35] Desikan, R., Mackerness, S.A., Hancock, J.T., Neill, S.J. (2001) Regulation of the Arabidopsis transcriptome by oxidative stress. Plant Physiol. 127, 159-172.
[36] Bowler, C., Van Montagu, M., Inze, D. (1992) Superoxide dismutases and stress tolerance. Annu. Rev. Plant Physiol. Plant Mol. Biol. 43, 83-116.
[37] Alscher, R.G., Hess, J.L. (1993) Antioxidants in Higher Plants. CRC Press, Boca Raton.
[38] Halliwell, B., Gutteridge, J.M.C. (1999) Free Radicals in Biology and Medicine. 3rd ed. Oxford University Press, New York. 372-375.
[39] Mónica, P.P., Baudilio, A.V., Elisa, S.Z., Lía, C.M.R. (2010) Copper and Cadmium Biosorption by Dried Seaweed Sargassum sinicola in Saline Wastewater. Water Air Soil Pollut. 210, 197-202.

Received: **13.07.2017**
Accepted: **30.08.2017**

CORRESPONDING AUTHOR

Jianqiu Han
College of Ecological Technology and Engineering,
Shanghai Institute of Technology,
Shanghai 201418 – China

e-mail: jianqiu_han@163.com

© by PSP Volume 27 – No. 2/2018 pages 989-995 Fresenius Environmental Bulletin

THE EFFECT OF DIFFERENT ENVIRONMENTAL CONDITIONS ON YIELD AND OIL RATES OF SAFFLOWER (*CARTHAMUS TINCTORIUS* L.)

Ismail Demir[1,*], Kamil Kara[2]

[1]Ahi Evran University Faculty of Agriculture, Department of Field Crop, Kırşehir, Turkey
[2]Kırıkkale University, Delice Vocational School, Kırıkkale, Turkey

ABSTRACT

Safflower (*Carthamus tinctorius* L.) is an important vegetable oil plant for human consumption and alternative bioenergy source. Also, this plant is used for the evaluation of fallow and marginal land areas in the world.

This study was carried out to determine the yield traits of 8 safflower cultivars (Yenice, Dinçer, Remzibey, Balcı, Linas, Ayaz, Olas and Asol) in two marginal locations (Kırşehir and Kırıkkale) in the Central Anatolia Region of Turkey in 2015.

According to the results, yield and oil rates of safflower cultivars varied significantly in different ecologies with respect to yield and oil rate parameters. Results showed that plant height, head diameter, number of seeds per head and 1000-grain weight varied between 54.09- 81.00 cm, 2.05 - 2.33 cm, 16.27 - 31.03 and 36.00 - 46.74 g, respectively. Crude oil rate and crude oil yield ranged from 27.93- 38.91% and 394.8 – 744.3 kg ha^{-1}. Dinçer variety had the highest seed yield with 2.08 t ha^{-1}, followed by Linas cultivar with 1.85 t ha^{-1} for both environmental conditions. In marginal areas, Remzibey (2.07 t ha^{-1}) and Yenice (2.06 t ha^{-1}) cultivars also produced higher yields nearly similar to those of Dinçer and Linas cultivars. To conclude, Dinçer and Linas cultivars can be suggested for both dry and marginal environmental conditions, while Remzibey and Yenice cultivars can be offered for salty marginal conditions.

KEYWORDS:
Safflower, seed yield, oil content, dry conditions

INTRODUCTION

Safflower production area in the world has been very low compared to the other oil plants. This plant has been an important plant in the agricultural system with 870 million tons of production in 1.01 million hectares [1]. Approximately 95% of safflower production has been occurred in Kazakhstan, Mexico, India, USA, Russia, Argentina, Turkey, China and Uzbekistan. Turkey, having the 7th place in safflower production, has met 7% of safflower production of the world [1]. Safflower sowing area in Turkey has expanded after 2008 and reached to 43000 hectares in 2015 with 70000 tons of safflower production [2]. Especially with the state support program carried out for putting fallow lands in dry agricultural areas in use, safflower production has increased in Central Anatolia Region.

Safflower, also known as false saffron [3], is an important industrial plant [4], which has yellow, red, orange and cream colored flowers with thorny and thornless forms, and it has been used for the production of edible oil and biofuels having 30-45% fat on average in its seeds. Due to its high tolerance to drought and salinity, safflower has great importance in terms of reducing fallow land, economical evaluation and prevention erosion in dry agricultural areas where rainfall is particularly low [5, 6, 7]. Safflower grown wherever wheat and barley are cultivated has the capacity of providing higher yield in dry conditions only by supplied natural precipitation. Being less selective regarding climate and soil requirements compared to the other oil plants, safflower can be cultivated in different conditions. Furthermore, safflower has the potential to get into rotation with wheat in Central, Eastern and Southeastern Anatolian Regions [8]. Due to its capability of having place in crop rotations particularly in dry areas, safflower is one of the most important plant that needs to be focused on for compensating the deficiency of vegetable oil [9].

Sunflower one of the most important industrial oil crop in Turkey has been commonly cultivated in Central Anatolia [10, 11] under low precipitation during the summer. Sunflower yield and yield parameters are dependent on rainfall during growing season [12]. Especially in marginal areas, safflower has been an important alternative oil crop for supplying the vegetable oil requirement of Turkey, also, of the world.

Determination of performances of safflower varieties and candidate varieties in different ecologies are so important, especially for wide spreading its cultivation and compensating the deficiency of vegetable oil. Therefore, this study was carried out in the ecological conditions of Kırşehir and Kırıkkale

with the aim of determining the yield and yield components of safflower varieties having great capacity to increase sowing areas in Central Anatolia.

MATERIALS AND METHOD

This study was carried out in two locations (Kırşehir, Kırıkkale) in Randomised Complete Block Design with 8 genotypes (Yenice, Dinçer, Remzibey, Balcı, Linas, Ayaz, Olas and Asol) in 2015. The trials were established in the first week of April in both locations in 6 rows with the length of 5 m and the row spacing of 25 cm and 50 kg of seeds per hectare. Plots were fertilized at seeding time with 80 kg N ha^{-1} and 60 kg P_2O_5 ha^{-1}. For the trial, the experimental fields at Bağbaşı Campus of Ahi Evran University in Kırşehir and at Delice Vocational School of Kırıkkale University in Kırıkkale were used. The following parameters were determined; plant height, number of lateral branches, number of head on branches, head diameter, number of seed per head, 1000-seed weight, crude oil ratio, seed yield, hull ratio, oil yield and protein ratio.

Before the trial, soils in both locations were analyzed. According to soil analysis, experimental soil in Kırşehir was salt-free and clayed-loamy textured, low in organic matter and slightly alkaline reaction in terms of soil characteristics. It was classified as poor soil in terms of available phosphorus, but rich in potassium. Kırıkkale soil was moderately salty, slightly alkaline, too limy, clayed, moderate in terms of organic substance content, available phosphorus level was low and potassium level was quite high (Table 1).

Mean temperature was close to the long-term average in Kırıkkale in 2015, and it was higher than the average temperature in Kırşehir. The minimum and maximum temperatures were above the long-term average. Relative humidity values were close to the average. Precipitation, being one of the most

TABLE 1
Physical and chemical properties of soils in trial areas

Locations	Texture	pH	EC (mmhos/cm)	Salinity (%)	Available P_2O_5 (kg ha^{-1})	$CaCO_3$ %	Available K_2O (kg ha^{-1})	OM (%)
Kırşehir	Clayed-Loamy	7.59	0.52	0.02	21.4	27.90	666.2	1.81
Kırıkkale	Clayed	7.70	6.62	0.42	45.2	16.44	1275.4	2.42

TABLE 2
Kırşehir and Kırıkkale climate parameters (1950-2015 and 2015)*

Locations	Month	Temperature (°C) Mean		Minimum		Maximum		Relative Humidity (%)		Precipitation (mm)	
		1950-2015	2015	1950-2015	2015	1950-2015	2015	1950-2015	2015	1950-2015	2015
KIRIKKALE	January	0.5	0	-2.9	-2.4	4.1	2.7	77.8	86	43	32.1
	February	2.3	2.9	-1.8	-0.7	6.7	7.5	72.9	74.8	31.9	62.3
	March	6.8	7.1	1.4	2.6	12.5	13	64.9	68.7	35.5	85.6
	April	12.2	9.7	6.1	3.3	18	15.7	60.8	55.4	45.5	11.5
	May	16.9	17.1	10.2	10.6	23	23.8	58.6	56.2	50.8	45.1
	June	21.2	19.5	13.8	13.6	27.5	25.6	52.3	62.6	37.1	112
	July	24.6	24.9	16.7	16.8	31	31.3	46.5	40.5	11.1	-
	August	24.2	25.4	16.4	18	30.9	32.2	46.5	42.7	9.6	20.8
	September	19.6	23.5	12.2	15.7	26.7	31.5	50.7	39.4	13.5	2.6
	October	13.6	14.7	7.4	9.7	20.5	21.1	60.9	63.0	29.4	36.3
	November	6.9	8.3	2.2	2.1	12.6	15.7	71.5	59.1	31.8	4.5
	December	2.6	-0.2	-0.7	-3.3	6.2	3.7	78.0	76.6	43.4	6.7
	Mean	12.6	12.7	6.8	7.2	18.3	18.7	61.8	60.4		
	Total									382.6	419.5
KIRŞEHİR	January	-0.1	1.3	-4.1	-2.8	4.7	5.9	78.2	84.2	46.2	35.2
	February	1.3	3.4	-3.2	-0.4	6.5	8.6	74.3	77.5	35.2	38.3
	March	5.3	6.9	0	2.4	11.3	12.8	67.4	75.3	39.2	89
	April	10.7	8.8	4.6	2.9	17.1	15.1	63.7	64.3	43.7	26.8
	May	15.4	16	8.6	8.9	21.8	22.9	60.8	58.7	44.3	39.2
	June	19.6	18.4	12.4	12.8	26.1	25	54.0	66.9	36.8	161.4
	July	23.1	23.5	15.7	15.9	29.7	30.2	48.1	44.7	6.8	20.6
	August	22.9	24.9	15.6	17.9	29.9	32.1	48.4	45.8	4.9	11.8
	September	18.2	22.8	11	14.8	25.9	31.2	53.1	40.7	11.6	1
	October	12.3	14.2	6.1	9.2	19.8	21.1	63.5	62.5	27.8	30.8
	November	6.2	7.2	1.1	0.6	12.8	15.7	72.8	57.5	36.4	6.2
	December	1.9	-1.1	-2	-4.8	6.7	3.8	78.7	78.9	47.0	9.1
	Mean	11.40	12.19	5.48	6.45	17.69	18.70	63.58	63.08		
	Total									379.9	469.4

*Reference: General Directory of State Meteorological Services.

important factors affecting yield in dry agricultural areas, was observed as heavier (rainy) than the average. In particular, in the vegetation period of safflower (March - September), precipitation was found out as higher than the average values in both locations (Table 2). Although the high precipitation in June in both locations had positive effects on surface waters, it caused little sunshine and low temperature due to cloudy days.

Data were analyzed according to completely randomized block design over locations, and Duncan's Multiple Range Test was used to determinate the significant differences among means. MSTATC statistical program was used for analyses [13].

RESULTS AND DISCUSSION

Based on the observations, variations of plant heights between locations and genotypes were significant (P<0.01). The average heights of safflower varieties ranged between 46.67 and 94.36 cm. Means of plant heights in Kırıkkale (71.17 cm) was higher than in Kırşehir (51.80 cm). While variety Yenice was the highest plant in both locations, variety Balcı was the shortest one (Table 3).

Differences in the plant heights might be due to the differences in climatic factors and physical & chemical properties of soil between two locations. Plant heights were higher than the findings of Yılmazlar [14] who observed the values between 45.64-47.00 cm. There are similarity with the results obtained by [15, 16, 17, 18]. In those studies, plant heights changed between 36.73 and 90.07 cm.

In terms of lateral branches, the differences between location and genotypes were significant at the probability levels 1% and %5, respectively. The location x genotypes interaction was also significant (P<0.01). Number of lateral branches was higher in Kırıkkale ecology than Kırşehir. According to the interaction of location x variety, Olas variety, which had the highest number of lateral branches with the value of 9.01 in Kırıkkale ecology, was intermediary in Kırşehir. The lowest one was variety Ayaz in Kırşehir with the value of 4.18 and Dinçer variety in Kırıkkale with the value of 5.83. Regarding the average number of lateral branches of varieties, Olas was the highest with the value of 6.90, and variety Dinçer was the lowest with the value of 5.53 (Table 3). Number of lateral branches per plant was similar to the results of [4, 14, 17, 18].

For the number of heads, being one of the most important yield criteria, differences between locations and varieties, and interaction of location x variety were found statistically significant at the 1% probability level. Number of heads in Kırıkkale (11.69) was higher than Kırşehir ecology (7.00). Regarding the interaction of varieties according to the locations, varieties having the highest number of heads were detected in Kırıkkale as Ayaz, Olas and Asol with the values of 14.92, 13.88 and 13.87, respectively; variety Balcı was the highest with the values of 8.27 number of heads in Kırşehir, while it was the lowest in Kırıkkale. The lower number of heads were determined in Kırşehir from Ayaz, Yenice and Remzibey with the values of 6.27, 6.17 and 6.03 respectively (Table 3). The number of heads obtained in this study support the findings of many studies carried out in different ecologies [14, 17].

Regarding to the head diameter observations, the significance level of variation between locations and varieties was 5%. The highest head diameter was observed in Dinçer cultivar with the value of 2.33 cm while the lowest value was 2.05 cm for Balcı cultivar. In Kırıkkale ecology, the mean head diameter (2.26 cm) was higher than that of Kırşehir ecology (2.14 cm) (Table 4). The data regarding head diameter were similar to the results of Çamaş et al [19] (2.067-2.114 cm), Keleş [17] (1.39-1.84 cm) and Sirel [18] (1.80-2.53 cm).

Besides number of heads, number of seeds per head is also an important yield criterion. In this study, number of seeds per head was significant at the 1% level regarding variety and interaction of location x variety. The highest number of seeds per head was obtained from variety Yenice (31.03) while the lowest number of seeds per head was produced a candidate variety Ayaz (16.27) in Kırşehir ecology.

TABLE 3
Plant heights, number of lateral branches and number of heads of safflower varieties.

	Plant Height (cm)			Number of lateral branches			Number of head		
Genotypes	**Kırşehir**	**Kırıkkale**	**Average**	**Kırşehir**	**Kırıkkale**	**Average**	**Kırşehir**	**Kırıkkale**	**Average**
Asol	46.67	63.14	54.90CD	4.90ac	7.73ab	6.32AC	7.47ac	13.87a	10.67A
Ayaz	47.00	66.24	56.62CD	4.18c	8.04ab	6.11AC	6.27cd	14.92a	10.59A
Balcı	46.93	61.25	54.09D	5.73a	7.07bc	6.40AC	8.27a	8.23c	8.25D
Dinçer	53.47	68.96	61.21BC	5.23ab	5.83c	5.53C	7.70ab	9.79b	8.75CD
Linas	54.87	75.38	65.13B	5.73a	7.57b	6.65AB	7.73ab	11.00b	9.37BC
Olas	47.03	71.47	59.25BD	4.80bc	9.01a	6.90A	6.40bd	13.88a	10.14AB
Remzibey	50.77	68.54	59.65BD	4.67bc	7.04bc	5.85BC	6.03d	10.91b	8.47CD
Yenice	67.63	94.36	81.00A	4.80bc	6.80bc	5.80BC	6.17cd	10.93b	8.55CD
Mean*	51.80ii	71.17i	61.48	5.01ii	7.39i	6.20	7.00ii	11.69i	9.35
LSD(P<0.05)	5.67		2.04	0.,874	1.429	0.80	1.413	1.323	0.92
CV (%)	8.13			10.92			8.36		

* No significant differences between the means with the same letter.

TABLE 4
Head diameter, seed number per head and 1000-grain weights of safflower varieties.

	Head diameter (cm)			Seed number per head			1000-grain weights (g)		
Genotypes	Kırşehir	Kırık-kale	Average	Kırşehir	Kırıkkale	Average	Kırşehir	Kırıkkale	Average
Asol	1.99	2.28	2.14BD	20.00de	17.13d	18.57C	41.64de	40.93bc	41.29B
Ayaz	2.01	2.19	2.10CD	16.27f	21.84bc	19.05C	45.09ac	39.69c	42.39B
Balcı	1.97	2.13	2.05D	19.63ef	19.73cd	19.68C	42.86cd	41.75bc	42.30B
Dinçer	2.32	2.33	2.33A	29.90ab	28.71a	29.30A	46.44a	44.68a	45.56A
Linas	2.28	2.35	2.32AB	17.73ef	20.10cd	18.92C	46.74a	42.43b	44.58A
Olas	2.20	2.22	2.21AD	23.30cd	18.38d	20.84C	45.55ab	44.72a	45.14A
Remzibey	2.21	2.28	2.25AC	26.87bc	25.01b	25.94B	43.44bd	40.39bc	41.92B
Yenice	2.16	2.26	2.21AD	31.03a	28.93a	29.98A	39.47e	36.00d	37.74C
Mean*	2.14ii	2.26i	2.20	23.09	22.48	22.79	43.90i	41.32ii	42.62
LSD(P<0.05)	0.10		0.17	3.58	3.20	2.29	2.37	2.07	1.50
CV (%)	6.09			8.51			2.98		

* No significant differences between the means with the same letter.

According to the means of varieties regarding number of seeds per head, Yenice (29.98) and Dinçer (29.30) were high, but Asol (18.57), Linas (18.92), Ayaz (19.05), Balcı (19.68) and Olas (20.84) were low (Table 4). Variations in the number of seeds per head might be most likely depending on climate and physical & chemical composition of soils in different ecologies. Consequently, it was, of course, expected the variations in the performances of varieties [14, 19, 20].

Differences between locations and varieties for 1000-grain weight were significant at the 1% level while location x variety interaction was found significant at the 5% level. 1000-grain weight in Kırşehir ecological conditions (with the average of 43.90 g) was higher than Kırıkkale ecology (41.32 g). The highest 1000-grain weight was obtained from variety Linas (46.74 g), followed by Dinçer (46.44 g) in Kırşehir location while the lowest value was obtained from variety Yenice (36.00 g) in Kırıkkale location. According to the averages of 1000-grain weight of the varieties, Linas (45.58 g), Dinçer (45.56 g) and Olas (45.14 g) had higher values, but Yenice (37.74 g) had the lowest value (Table 4). Knowles [21] remarked that 1000-grain weight depending on seed plumpness was directly related to climatic conditions at flowering stage. When climatic characteristics of locations were compared, it was observed that, Kırşehir got more rain and had higher humidity compared to Kırıkkale (Table 2) during flowering stage (June). In similar studies at different ecologies, 1000-grain weights were changed from 22.95 to 53.13 g [4, 14, 16, 17, 22, 23, 24, 25].

Data analysis showed that the differences in crude oil ratio were statistically significant at 5% level between locations and at 1% level between genotypes. Mean crude oil ratios of varieties were 35.77% in Kırşehir, and 32.55% in Kırıkkale. The highest crude oil ratio was obtained from variety Linas (38.91%) and the lowest one from Yenice (27.93%) (Table 5). Higher crude oil ratio in Kırşehir could be attributed to the more rainfall and higher humidity during the growing period of safflower. In both locations, the oil ratios of spineless varieties (Dinçer and Yenice) were lower than spiny varieties. Spiny safflower is known as containing high amount of oil as well as having resistance to drought and cold conditions [24]. According to the study carried out in Erzurum under irrigated and non-irrigated conditions by Öztürk et al. [26], changes in oil rates depending on years and varieties, increase in oil ratio by irrigation was very difficult or quite low and crude oil ratio was higher in the year with higher precipitation. While crude oil ratio obtained in this study was lower than that of Yılmazlar and Bayraktar [20] obtained in Konya which was 40.10-48.33%, it is compatible with those of Uysal et al. [24] (23.7-26.9%), Karaaslan et al. [27] (19.59-22.16%), Yau [29] (25.1-26.5%), Erbaş and Tonguç [25] (24.1-31.4 %), Tonguç and Erbaş [16] (22.5-33.3%), Beyyavas et al. [4] (25.80-34.90 %), Keleş [17] (25.60-31.83%) and Sirel [18] (22.9-33.0 %).

Seed yield between locations was significant at the 5% level and variety and interaction of location x variety were significant at the 1% level. Mean seed yield in Kırıkkale location (1.75 t ha^{-1}) was higher than that of Kırşehir (1.48 t ha^{-1}). The highest seed yield was obtained in Kırıkkale from variety Dinçer with the value of 2.23 t ha^{-1}, and the lowest one was obtained in Kırşehir from variety Ayaz with the value of 1.14 t ha^{-1}. According to the mean seed yields in both locations, Dinçer had the highest value with 2.08 t ha^{-1}, but Ayaz cultivar had the lowest yield as 1.25 t ha^{-1} (Table 5). It can be said that the present differences in seed yields of varieties in different locations might be due to the physical & chemical properties of soils as well as climatic factors. While rainfall, which was more than the long-term average, affected the yield positively in both locations, regularity of rainfalls in growing season of safflower could increase this positive affect. Especially, as usually known, at the stages of flowering and seed filling period, regular rainfall increases plant growth and yield considerably. In a three-year study conducted by Bayraktar et al. [28] in Eskişehir conditions, it was emphasized that depending on climate conditions, seed yields of varieties of safflower varied yearly; it was 1.83-2.48 t ha^{-1} in the first year, 0.45- 1.29 t ha^{-1} in the second year and 1.63-2.97 t

ha^{-1} in the third year. As a result of Öztürk et al [30] study, seed yield of safflower varied depending on variety and location. The variety having the highest seed yield in the first year was Remzibey-05 with the value of 1.72 t ha^{-1}, in the second year it was Dinçer with the value of 2.09 t ha^{-1}. Seed yield was determined as 1.1-1.2 t ha^{-1} by Çamaş et al. [19], 1.33-2.39 t ha^{-1} by Koutroubas ve Papakosta [23], 0.52-0.80 t ha^{-1} by Uysal et al. [24], 0.62-1.66 t ha^{-1} by Yau [29], 0.83-1.73 t ha^{-1} by Yılmazlar [14], 0.62-2.31 t ha^{-1} by Nikabadi et al. [31] and 0.54-2.78 t ha^{-1} by Erbaş and Tonguç [25]. The results of previous studies regarding seed yields are compatible with the results of this study.

Variation in oil yield between varieties was significant at the 1% level and location x variety interaction was significant ($P<0.05$). The highest oil yield was obtained from Linas in Kırıkkale with the value of 0.74 t ha^{-1}, while the lowest oil yield was obtained from Ayaz with the value of 0.40 t ha^{-1} in Kırıkkale. The highest oil yield was for Linas (0.72 t ha^{-1}) and the lowest was for variety Ayaz (0.42 t ha^{-1}) (Table 5). Oil yield was determined between the range of 0.42-0.70 t ha^{-1} by Koutroubas and Papakosta [23]. Oil yield is directly related to crude oil rate and seed yield, since it is calculated by the multiplication of them. These two parameters depend on climate, soil properties and cultural operations as well as genetic differences.

Variation between varieties in hull ratio, one of the important quality criteria of safflower, was significant at the 5% level. The highest hull ratio was obtained from variety Yenice (51.67%), and the lowest was from variety Balcı (43.45%) (Table 6). High hull ratio, which is undesirable trait for vegetable oil production, is inversely proportional to kernel ratio and has directly negative effect on oil ratio. According to the studies on same varieties, high hull ratio of Yenice variety was emphasized by different researchers [32, 14]. Variations in the hull ratio of safflowers depend on climate conditions, soil structure, sowing frequency, genetic difference and sowing date.

While variation in the protein content of safflower varieties between locations was significant at the 1% level but differences between varieties and interactions were not significant. Protein content ranged between 14.73% (Remzibey) and 17.24% (Balcı). Protein contents of varieties were higher in Kırıkkale ecology (Table 6) compared to Kırşehir. Variation in the protein content between locations can be explained by the existence of more organic substances in the soil of Kırıkkale compared to Kırşehir (Table1). Obtained protein content in the present study is in line with the findings of previous studies [14 and 17].

TABLE 5
Crude oil ratio, seed yield and oil yield of safflower varieties.

	Crude oil ratio (%)			Seed yield (t ha^{-1})			Oil yield (t ha^{-1})		
Genotypes	**Kırşehir**	**Kırıkkale**	**Average**	**Kırşehir**	**Kırıkkale**	**Average**	**Kırşehir**	**Kırıkkale**	**Average**
Asol	38.07	36.44	37.26A	1.36c	1.55b	1.45D	0.52bc	0.57bc	0.54BC
Ayaz	37.80	29.08	33.44B	1.14d	1.36bc	1.25E	0.43c	0.40d	0.42D
Balcı	39.58	37.22	38.40A	1.61b	1.52b	1.57CD	0.64ac	0.57bc	0.60B
Dinçer	30.36	27.45	28.91C	1.93a	2.23a	2.08A	0.59ab	0.61b	0.60B
Linas	40.45	37.37	38.91A	1.71b	1.99a	1.85B	0.69a	0.74a	0.72A
Olas	38.16	37.28	37.72A	1.31cd	1.19c	1.25E	0.50bc	0.44cd	0.47CD
Remzibey	31.39	30.07	30.73BC	1.40c	2.07a	1.74BC	0.44c	0.62ab	0.53BC
Yenice	30.36	25.51	27.94C	1.39c	2.06a	1.73BC	0.42c	0.53bc	0.48CD
Mean*	35.77i	32.55ii	34.16	1.48	1.75	1.62	0.53	0.56	0.54
LSD(P<0.05)	1.99		3.57	0.19	0.30	0.17	0.11	0.13	0.08
CV (%)	8.83			8.78			12.70		

* No significant differences between the means with the same letter.

TABLE 6
Hull ratio and protein content of safflower varieties.

	Hull ratio (%)			Protein content (%)		
Genotype	**Kırşehir**	**Kırıkkale**	**Average**	**Kırşehir**	**Kırıkkale**	**Average**
Asol	48.53	47.26	47.90ABC	14.85	17.93	16.39
Ayaz	50.47	47.63	49.05AB	15.65	15.94	15.80
Balcı	45.52	41.39	43.45 C	17.12	17.36	17.24
Dinçer	48.86	47.72	48.29AB	15.28	17.07	16.18
Linas	47.14	43.74	45.44 BC	15.73	17.11	16.42
Olas	48.85	42.30	45.57 BC	14.62	17.16	15.89
Remzibey	50.45	45.85	48.15ABC	14.24	15.23	14.73
Yenice	51.22	52.12	51.67A	14.23	17.85	16.04
Ortalama[1]	48.88	46.00	47.44	15.22ii	16.96i	16.09
LSD(P<0.05)			4.28	0.99		
CV (%)	7.63			8.43		

[1] Indicated with same letter.

CONCLUSION

Even though the climatic differences was present between the research areas of this study, dry conditions and moderately salty soil structure, especially in Kırıkkale location, had the potential for cultivation of safflower in marginal areas. When yield and oil ratios for the cultivation of safflower under dry conditions are evaluated as a whole, variety Dinçer was observed as the most productive cultivar in both locations. Like variety Dinçer, varieties Linas for dry conditions and varieties Remzibey and Yenice for salty marginal conditions are promising varieties and can be recommended for cultivation.

REFERENCES

[1] Anonymous. (2016) Food and Agriculture Organization of The United Nations (FAO) Available online. (access 07.07.2016).

[2] Anonymous. (2016) Turkish Statistical Institute Data. Available online. (access 05.07.2016).

[3] Weiss, E.A. (1971) Castrol oil, sesame and safflower. Barnes and noble. Inc. New York. 529-744.

[4] Beyyavas, V., Haliloglu, H., Copur, O. and Yilmaz, A. (2011) Determination of seed yield and yield components of some safflower (Carthamus tinctorius L.) cultivars, lines and populations under the semi-arid conditions. Afr. J. Biotech. 10, 527-534.

[5] Weiss, E.A. (2000) Oilseed Crops. Chapter 4. 2nd Edition, Blackwell Science. Oxford, 93-129.

[6] Vorpsi, V., Harizaj, F., Bardhi, N., Vladiand, V. and Dodona, E. (2010) *Carthamus tinctorius* L., the quality of safflower seeds cultivated in Albania. Research Journal of Agricultural Science. 42 (1), 326-331.

[7] Kaya, M.D, İpek, A. and Özdemir, A. (2003) Effects of different soil salinity levels on germination and seedling growth of safflower (Carthamus tinctorius L.). Tr. J. Agri. and Forestry. 27, 221-227.

[8] Atakişi I.K. (1991) Yağ Bitkileri Yetiştirme ve Islahı. Trakya University, Faculty of Agriculture, Press no: 148, Lesson book number: 10. 181p, (Tr).

[9] Kolsarıcı, Ö., Gür, A., Başalma, D., Kaya, M.D. and İsler, N. (2005) Production of oily plants. TMMOB Board of Agricultural Engineering, Turkey Agriculture Engineering VI. Technical Congress Proceedings Book, Ankara. 1, 411-415.

[10] Day, S. (2016) Determining the diversity among four sunflower (Helianthus annuus L.) cultivars among boron stress. Fresen. Environ. Bull. 25, 4944-4951.

[11] Day, S. (2016) Determining the impact of excessive boron on some growth characters and some nutrients at the early growth stage of sunflower (Helianthus annuus L.). Fresen. Environ. Bull. 25, 4294-4298.

[12] Kaya, M.D., Bayramin, S. and Kaya, G. (2015) The effect of planting geometry and seed priming on sunflower yield under rain-fed conditions. Fresen. Environ. Bull. 24, 4095- 4101.

[13] Russel, D.G. (1986) MSTAT-C Package Program. Crop and Soil Science Department, Michigan State University, USA.

[14] Yilmazlar, B. (2008) The effect of different sowing dates on important agricultural characters and yield of some safflower (*Carthamus tinctorius* l.) cultivars in Konya conditions, ph.D. Thesis in Turkish, Graduate School of Natural and Applied Sciences of Ankara University, 83p.

[15] Yıldırım, B., Tunçtürk, M., Dede, Ö. and Okut, N. (2005) Okut: Effect of Different Doses of Nitrogen and Phosphorus on the Yield and Quality of Safflower (*Carthamus tinctorius* L.). Yuzuncu Yıl University Journal of Agricultural Sciences (J. Agric. Sci.). 15(2),113-117.

[16] Tonguç, M. and Erbaş, S. (2009) Determination of Yield and Yield Components of Domestic and Foreign Safflower (*Carthamus tinctorus* L.) Cultivars and Lines. VIII. Field Crops Congres of Turkey, Hatay, Turkey, 115-119.

[17] Keles, R. (2010) Effects of different sowing dates on the yield, yield components and quality on some safflower (*Carthamus tinctorius* L.) cultivars, Master Thesis in Turkish, Graduate School of Natural and Applied Sciences of Selçuk Üniversity, 123p.

[18] Sirel, Z. (2011) Agricultural features of some safflower (*Carthamus tinctorius* L.) cultivars and lines, Master Thesis in Turkish, Graduate School of Natural and Applied Sciences of Eskişehir Osmangazi Üniversity, 79p.

[19] Çamaş, N., Ayan, A.K. and Cırak, C. (2005) Relationships Between Seed Yield and Some Characters of Safflower (*Carthamus tinctorius* L.) Cultivars Grown in the Middle Black Sea Conditions.VI. International Safflower Conference, İstanbul (6-10 June), 193-198.

[20] Yılmazlar, B. and Bayraktar, N. (2009) The Effects of Different Sowing Dates on Important Agricultural Characters and Yield of Some Safflower (*Carthamus tinctorius* L.) Cultivars in Konya Conditions. VIII. Field Crops Congres of Turkey, Hatay, Turkey, 172-177.

[21] Knowles, P.F. (1958) Safflower. Advances in Agronomy. 10, 289-323.

[22] Kaya, M.D., İpek A., Uranbey, S. and Kolsarıcı, Ö. (2004) The effects of ethephone on yield and yield componentes of safflower. University of Ankara, J. Faculty Agric. 10(2), 182-186.

[23] Koutroubas, S. and Papakosta, D.K. (2005) Adaptation, grain yield and oil content of safflower in Greece.VI th International Safflower Conference, İstanbul.
[24] Uysal, N., Baydar, H. and Erbaş, S. (2006) Determination of agricultural and technological properties of safflower (*Carthamus tinctorius* L.) lines developed from ısparta population. Suleyman Demirel University Journal of the Faculty of Agriculture. 1(1),52-63.
[25] Erbaş, S. and Tonguç, M. (2009) Determination of Yield and Yield Components of Domostic and Foreign Safflower (*Carthamus tinctorius* L.) Accessions. VIII. Field Crops Congres of Turkey, Hatay, Turkey, 120-124.
[26] Öztürk, Ö., Uyanöz, R., Karaca, Ü. and Ada, R. (2009) Growth and Yield of Safflower Genotypes Grown Under Irrigated and Non Irrigated Conditions in a Highland Environment. Plant Soil Environ. 54(10), 453–460.
[27] Karaaslan, D., Tonçer, Ö. and Söğüt T. (2007) Evaluation of In Terms of Yield and Yield Properties of Some Sunflower (*Helianthus annuus* L.) Cultivars in Southeastern Anatolia Region Conditions. Harran University J. of Agric. Faculty. 11(1:2), 31-38.
[28] Bayraktar, N., Can, O., Koşar, F.Ç., Balcı, A. and Uranbey, S. (2005) Production and Development Potential of Oil Crops in Central and Transitional Anatolia Zone. VI. International Safflower Conference (6-10 June). 257-260, İstanbul.
[29] Yau, S.K. (2007) Winter versus spring sowing of rain-fed safflower in a semi-arid, high elevation Mediterranean environment. European Journal of Agronomy. 3(26), 249-256.
[30] Öztürk, Ö., Uyanöz, R., Karaca, Ü. and Ada, R. (2009) The investigation of yield, yield components and oil contents of some safflower cultivars under Konya ecological conditions. 1st National Symposium on Oil Seed Plants and Biofuel, 28-30 May 2007 Samsun-Turkey. Vol 1, 191-202, ISBN 978-975-407-234-1 (Tr).
[31] Nikabadi, S., Soleimani, A., Dehdashti S.M. and Yazdanibakhsh, M. (2008) Effect of Sowing Dates on Yield and Yield Components of Spring Safflower in Isfahan Region. Pakistan Journal of Biological Sciences. 11(15), 1953-1956.
[32] Eren, K., Başalma, D., Uranbey, S. and Er, C. (2005) Effect of growing in Winter and Spring on Yield Components and Quality of Some Safflower (*Carthamus tinctorius* L.) Cultivars in Ankara. VIth International Safflower Conference, Istanbul 6-10 june, 2005. 154-161.

Received: **15.07.2017**
Accepted: **09.12.2017**

CORRESPONDING AUTHOR

Ismail Demir
Ahi Evran University, Faculty of Agriculture,
Department of Field Crop
40100, Kırşehir – Turkey

e-mail: İsmail.demir@ahievran.edu.tr

© by PSP Volume 27 – No. 2/2018 pages 996-1005 Fresenius Environmental Bulletin

EXOGENOUS HYDROGEN PEROXIDE ALLEVIATES COPPER TOXICITY BY STIMULATING ANTIOXIDANT SYSTEM AND INCREASES PHOTOSYNTHESIS EFFICIENCY IN MAIZE SEEDLINGS

Rabiye Terzi[1], Neslihan Saruhan-Guler[2,*], Nihan Biskin[1], Asim Kadioglu[1]

[1]Department of Biology, Faculty of Science, Karadeniz Technical University, 61080, Trabzon, Turkey
[2]Department of Nutrition and Dietetics, Faculty of Health Sciences, Karadeniz Technical University, 61080, Trabzon, Turkey

ABSTRACT

Heavy metal contamination of agricultural soils is a serious environmental problem that negatively affects plant growth and development. In recent years, it is known that hydrogen peroxide (H_2O_2) enhances tolerance to various abiotic stresses but response of exogenous H_2O_2 in plants exposed to excess Cu is poorly investigated. This study provides an insight into the effects of exogenous H_2O_2 on two maize cultivars, Pegaso (tolerant to water deficit) and Akpınar (sensitive to water deficit) exposed to Cu toxicity. Chlorophyll content of maize seedlings was reduced by Cu stress and lipid peroxidation was increased in Cu stressed seedlings. Exogenous H_2O_2 almost totally prevented the increase in lipid peroxidation and reversed changes caused by Cu toxicity in pigment contents and photosystem II efficiency. Antioxidant enzyme activities were more induced and H_2O_2 content was less in H_2O_2 pretreated seedlings under Cu stress than those of excess Cu pretreated seedlings in both cultivars. Of the two maize cultivars, Pegaso cv. exhibited better tolerance to Cu toxicity in terms of lesser membrane damage and H_2O_2 accumulation, higher photosystem II efficiency and further induction of antioxidant enzymes, especially catalase and guaiacol peroxidase activities. Taken together, the results indicate that exogenous H_2O_2 could diminish the hazardous effects of excess Cu and might have a function against the stress by inducing antioxidant machinery and provide higher photosynthetic potential in the tolerant and sensitive maize cultivars exposed to excess copper.

KEYWORDS:
Copper toxicity, H_2O_2 application, antioxidant enzymes, photosynthetic efficiency

INTRODUCTION

Heavy metal contamination is a serious environmental problem that limits plant productivity and threatens human health [1] Copper (Cu) contamination is one of the major environmental hazards in contaminated areas. Cu is an essential micronutrient for the normal growth and development of all living organisms due to its crucial role in various processes such as photosynthesis, respiration, protein metabolism, reactive oxygen metabolism, ion metabolization, nitrogen fixation, ethylene sensing and cell wall remodeling [2]. However, excessive concentrations of Cu in plant tissue are a potential hazard for plants due to its ability to catalyze the formation of active oxygen species or lipid peroxidation [3]. Cu toxicity may result from the binding of metals to sulfhydryl groups in the protein, leading to the inhibition of activity or disruption of the structure. As an active redox metal, high Cu concentration in plants induces oxidative stress by generating reactive oxygen species (ROS) such as singlet oxygen, hydrogen peroxide (H_2O_2), superoxide, and hydroxyl radicals, which can damage biological molecules and membranes by lipid peroxidation [4].

Plants possess several potential cellular mechanisms that may be involved in the detoxification of heavy metals to tolerate metal stress. This mechanism is known as the plant antioxidant defense system that regulates ROS levels in the cellular system. An antioxidant system comprises two types of components: enzymatic antioxidants such as superoxide dismutase (SOD), peroxidase (POD), catalase (CAT) and ascorbate–glutathione cycle enzymes (ascorbate peroxidase (APX), glutathione reductase (GR), dehydroascorbate reductase (DHAR) and monodehydroascorbate reductase (MDHAR) and non-enzymatic antioxidants such as glutathione (GSH) and ascorbate (ASC). It has also been shown that plant tolerance to heavy metal stress was closely related with activities of antioxidant enzymes [5]. Additionally, excess Cu concentration can damage photosynthetic apparatus and disturb the integrity of thylakoid membranes [6]. It has been shown that decreased photosynthetic competence, low quantum

efficiency of PSII, and reduced cell elongation are also associated with Cu toxicity [7].

To overcome the negative effects of metal toxicity, it is necessary to look for alternative ways to improve the soil fertility and stimulate the growth of crop plants. Thus, there is a need for various amendments that may help to ameliorate adverse effects of metal stress. In recent years, exogenous applications of phytohormones (abscisic acid, gibberellic acid and jasmonic acid) and signaling molecules (salicylic acid, nitric oxide and hydrogen peroxide) have been found to be effective in mitigating heavy metal stress-induced damage in plants [8, 9, 10]. Hydrogen peroxide, one of these signal molecules, plays an important role in regulating a number of physiological processes and plant resistance to biotic and abiotic stresses. H_2O_2 directly regulates the expression of numerous genes involved in plant defense and the related pathways such as antioxidant enzymes, defense proteins and transcription factors. Several reports supported that pretreatment with H_2O_2 increased antioxidant activities of plants and thereby ameliorated the damage from various environmental stresses [8, 11]. As mentioned above, the regulatory role of exogenous applications of phytohormones and signal molecules on heavy metal toxicity in plants has been continuously demonstrated. However, reports on the responses of H_2O_2 in plants exposed to copper stress, especially maize, is lacking in the literature. Our previous study on this topic indicated that exogenous H_2O_2 might alleviate the hazardous effect of copper stress by increasing mineral ion distribution, total sugar, proline and soluble protein levels in maize seedlings [12]. Therefore, the aim of this study was to investigate if exogenous H_2O_2 was involved in coordination between antioxidant enzymes and photosynthesis in two maize cultivars differing in water deficit tolerance, in order to better understand the mechanisms of action of exogenous H_2O_2 application to increase copper tolerance.

MATERIALS AND METHODS

Plant material and growth conditions. Two *Zea mays* L. cultivars differently sensitive to water deficit (cv. Pegaso more tolerant than cv. Akpınar) were provided from Black Sea Agricultural Research Institute, Eskisehir, Turkey and Limagrain Seed Production Company, Istanbul, Turkey. Seeds were surface sterilized with 0.1% $HgCl_2$ for 3 min followed by repeated washings with sterilized distilled water. Seeds were sown in pots (14 cm height, 16 cm top and 11 cm bottom diameter) containing sterilize water washed sand. Seedlings were grown in a growth chamber with the following parameters: 16 h light and 8 h darkness at 25°C ± 2, relative humidity 60% ± 5, photon flux density of at the surface of the leaves 400 µmol m^{-2} s^{-1} and were watered once per two days with Hoagland nutrient solution (pH 6.0).

Copper and hydrogen peroxide treatments. When the second leaves were fully expanded, the pots were divided into four groups for each maize cultivar. Two groups were watered with Hoagland nutrient solution, and the other two groups were watered with freshly prepared Hoagland nutrient solution containing 0.5 mM H_2O_2. The H_2O_2-applied plants were watered with either the Hoagland nutrient solution only or Hoagland nutrient solution containing 0.5 mM $CuSO_4$ for additional five days and were designated as "H_2O_2 treatment (H_2O_2)", and "Cu + H_2O_2 pretreatment (Cu + H_2O_2)", respectively. The other two groups of the pots were separately watered with either of the two types of nutrient solutions and were named "control (C)," and Cu stress (Cu)". After two days of the treatments, samples of the third leaf were used for the following analyses.

Hydrogen peroxide content. Hydrogen peroxide concentration was measured using the method of Velikova et al. [13] with minor modifications. Leaf samples (0.25 g) were grounded in 3 ml of 5 % trichloroacetic acid with 0.1 g of charcoal at 0 °C. 0.5 ml of 10 mM potassium phosphate buffer (pH 7.0) and 0.75 ml of 1 M KI were transferred to the 0.5 ml aliquot of the supernatant. Then, absorbance was determined at 390 nm and the concentration of H_2O_2 was given as µmol g^{-1} FW.

Lipid peroxidation. The assay was conducted in terms of malondialdehyde (MDA) content measurement (e = 155 mM^{-1} cm^{-1}), based on Heath and Packer [14]. Leaf samples of 0.5 g were grounded in 10 ml of 0.1 % (w/v) trichloroacetic acid (TCA). 4 ml of 0.5 % (w/v) thiobarbituric acid containing 20 % (w/v) TCA was transferred to 1 ml of supernatant. The supernatant was read to have absorbance values at 532 and 600 nm and the MDA concentration was indicated as nmol MDA g^{-1} FW.

Determination of chlorophyll pigment content. Total Chl concentration was determined with the basic method of Arnon [15]. Leaf samples from the top of different plants of the same age were selected at random and homogenized in 80 % acetone with a mortar. The homogenate was centrifuged at 5000g for 5 min. Supernatant was removed and absorbance was read at 663 and 645 nm by spectrophotometer. Chl content was specified as mg g^{-1} FW.

Chlorophyll a fluorescence parameter. Chlorophyll a fluorescence measurements were performed by pulse modulated fluorimeter (OS1-FL, OptiScience Corporation, Tyngsboro, MA, USA) according to Nar et al. [16]. For each treatment, the 6th leaf from six different plants was selected and

clamped at the center point with the OS1-FL leaf clip holder. Leaves were dark-adapted for 20 min and the Chl fluorescence was then measured. Minimum Chl fluorescence yield (F_o) was determined under weak modulated λ660 irradiation (< 0.1 μmol m^{-2} s^{-1}). Maximum Chl fluorescence yield (F_m) was reached by exposing PSII to saturating λ690 pulse (0.8 s) of white light (8,000 μmol m^{-2} s^{-1}). After dark measurements, the leaves were exposed to the red actinic light of the fluorimeter together with the sunlight functioning as actinic light source. Steady state Chl fluorescence (Fs) was achieved after exposure to the actinic light. A simultaneous saturating pulse (0.8 s) of white light (8,000 μmol m^{-2} s^{-1}) was applied to determine maximum Chl fluorescence in the light (F_m'). Maximum quantum yield of PSII photochemistry (F_v/F_m) and effective quantum yield of PSII photochemistry (Φ_{PSII}) were calculated according to the following equations ($F_v/F_m = (F_m - F_o)/F_m$ and $\Phi_{PSII} = (F_m' - F_s)/F_m'$). Non-photochemical quenching (NPQ) was calculated according to the equation, $NPQ = (F_m - F_m')/F_m'$. Electron transport rate (ETR) was calculated according to following equation, $ETR = (\Phi_{PSII} \times PAR \times 0.5 \times 0.84)$. PAR was measured with a PAR clip. Value 0.5 indicates partitioning of energy between PSII and PSI, while value 0.84 presents proportional light absorbance by photosynthetic tissue.

Antioxidant enzyme assays. Enzyme extraction was performed at 0–4 °C. Leaves (0.5 g) were grounded into powder with a mortar and pestle with the help of liquid nitrogen. Sample was mixed in 5 ml of 50 mM phosphate buffer (pH 7.0) containing 1 % polyvinylpyrrolidone and 1 mM EDTA, with 5 mM ascorbic acid (ASC) only for APX assay. The mixture was centrifuged at 20.000g for 20 min at 4 °C and the aqueous supernatant was stocked for further enzyme experiments.

Superoxide dismutase (SOD, EC 1.15.1.1) activity was determined with the procedure of Beauchamp and Fridovich [17]. In the spectrophotometric assay, the 1 ml reaction mixture contained 50 mM phosphate buffer (pH 7.8), 0.1 mM EDTA, 13 mM methionine, 75 μM nitro blue tetrazolium, 2 μM riboflavin and 50 μl extract. The reaction was continued for 10 min, lighted with two 20 W (watt) lamps. The reaction was read at 560 nm. For all enzyme assays, blanks consisted buffer and no extract. One unit (U) of SOD activity was described as the amount of enzyme required for 50 % inhibition of the NBT photo-reduction rate.

Guaiacol peroxidase (GPX, EC 1.11.1.7) activity was measured by monitoring the increase in absorbance at 470 nm (25 °C, e = 26.6 mM^{-1} cm^{-1}) in 100 mM potassium phosphate buffer (pH 7.0) containing 0.1 mM EDTA, 5 mM guaiacol, 15 mM H_2O_2, and 50 μl of the enzyme extract [18].

Catalase (CAT, EC 1.11.1.6) activity was measured by the depletion of H_2O_2 (25 °C, e = 39.4 mM^{-1} cm^{-1}) at 240 nm [19]. The reaction mixture contained 50 mM potassium phosphate buffer (pH 7.0), 10 mM H_2O_2 and stocked extract (10 μl) for 1 ml of total volume. The reaction was initiated by adding H_2O_2.

Ascorbate peroxidase (APX, EC 1.11.1.11) activity was calculated by tracking ascorbate oxidation at 290 nm (25 °C, e = 2.8 mM^{-1} cm^{-1}) [20]. 1 ml of the reaction consisted of 50 mM phosphate buffer (pH 7.0), 0.25 mM ASC, 5 mM H_2O_2 and 20 μl previously stocked enzyme extract. The reaction was initiated by adding H_2O_2.

Glutathione reductase (GR, EC 1.6.4.2) activity was obtained with the decrease in absorbance at 340 nm (25 °C, e = 6.22 mM^{-1} cm^{-1}), based on Foyer and Halliwell [21]. 1 ml of reaction contained 150 μM NADPH, 500 μM oxidized glutathione (GSSG), 50 mM Tris–HCl (pH 7.8), and 50 μl of extract. The NADPH was the reaction initiator.

All enzyme activities were given on a protein basis. Protein content was specified according to Bradford [22].

Statistical Analysis. Data were assessed with SPSS Ver. 15.0 (SPSS Inc., USA). Duncan's Multiple Range Test was used for analysis of mean values. The statistical significance of differences between treatments was considered as significant at 5 % ($P < 0.05$). All analyses were repeated by three biological and three technical replicates.

RESULTS

H_2O_2 content and lipid peroxidation. Excess copper caused a severe H_2O_2 accumulation up to 2.39 fold for tolerant cv. Pegaso and 2.26 fold for sensitive cv. Akpınar in comparison with their controls. This indicated that an evident oxidative stress occurred in Cu-stressed maize seedlings. In addition, endogenous H_2O_2 concentration after exogenous application of H_2O_2 increased in two cultivars in comparison with the untreated seedlings under unstressed conditions. However, pretreatment with H_2O_2 also reduced the overproduction of H_2O_2 in both cultivars under copper stress. The decrease induced by exogenous H_2O_2 was relatively more pronounced in cv. Pegaso than cv. Akpınar, up to 1.39 fold and 1.18 fold, respectively (Figure 1A).

To test the hypothesis that excess Cu can induce oxidative stress, the content of MDA was measured as an indicator of oxidative stress. As shown in Figure 1B, in comparison with untreated seedlings (control), exogenous application of H_2O_2 alone increased the MDA content in both cultivars. Copper stress immensely increased the MDA content in both cultivars of maize seedlings. However, exogenous application of H_2O_2 mitigated the membrane damage under excess copper in both cultivars. The reduction

in membrane damage was higher in cv. Pegaso than cv. Akpınar, 1.50 fold and 1.21 fold, respectively.

Chlorophyll content. The results relating to the outcome of copper stress and H_2O_2 pretreatment on total chlorophyll are demonstrated in Figure 2. Chlorophyll content was significantly decreased under Cu stress in both cultivars. The decreases were recorded by 1.01 and 1.06-folds in total chlorophyll contents of Cu stressed cv. Pegaso and cv. Akpınar, respectively. However, chlorophyll content of H_2O_2-applied seedlings increased in comparison with control seedlings under unstressed condition in both cultivars. When the Cu+H_2O_2 seedlings were compared with the Cu seedlings, chlorophyll content of Cu+H_2O_2 seedlings was higher than Cu ones in two cultivars. The increases were similar in both cultivars (1.02-fold).

Chlorophyll a fluorescence measurement. As shown in Figure 3A, Cu stress and H_2O_2 applications did not cause a significant change in maximum quantum yield of PS II photochemistry (F_v/F_m) of the tolerant cv. Pegaso. There was a similar change in effective quantum yield of PS II photochemistry (Φ_{PS2}) of tolerant maize seedlings. Conversely, Cu stress inhibited F_v/F_m and Φ_{PSII} of sensitive cv. Akpınar. However, the decreases in these characteristics in response to Cu stress were reversed by the application of H_2O_2 (Figure 3A-B). Non-photochemical quenching (NPQ) increased in both maize seedlings under Cu stress as compared to the control ones. However, NPQ values decreased in Cu+H_2O_2 seedlings in comparison with Cu seedlings in two maize cultivars (Figure 3C). Photochemical quenching (qP) decreased under Cu stress in comparison with their controls in both cultivars. Exogenous application of H_2O_2 alleviated the decrease in the qP value of cv. Pegaso. On the other hand, qP value of cv. Akpınar decreased under the stress in comparison with Cu group seedlings after H_2O_2 application (Figure 3D). The exposure of maize seedlings to Cu stress decreased the electron transport rate (ETR) value. However, this effect removed by using exogenous H_2O_2 in both cultivars (Figure 3E).

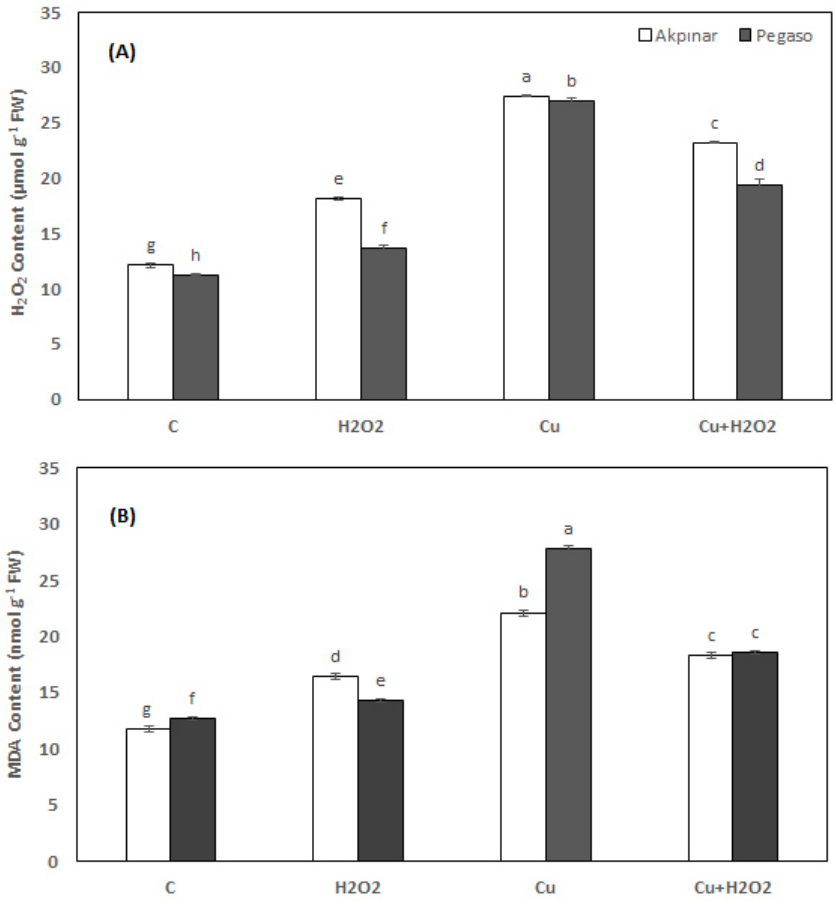

FIGURE 1
The effect of H_2O_2 application on H_2O_2 (A) and lipid peroxidation (B) contents under excess copper in maize cultivars. Vertical bars represent standard deviation. Different letters denote significant differences between the two cultivars along with different treatments at $p<0.05$.

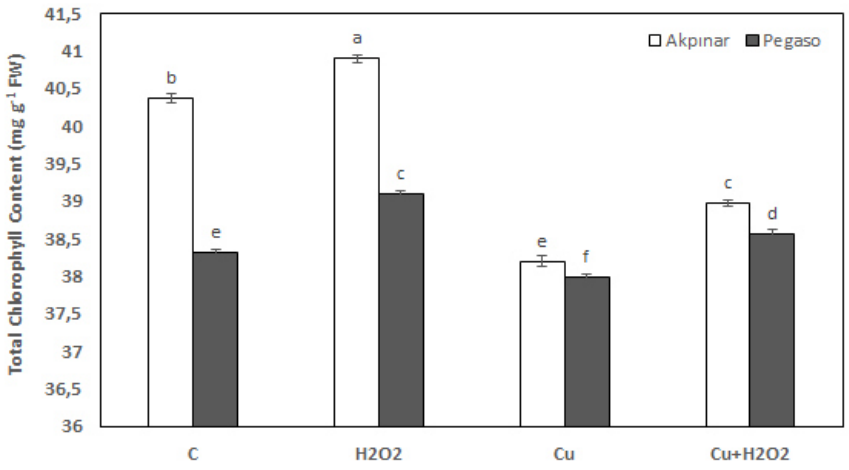

FIGURE 2
The effect of H_2O_2 application on total chlorophyll content under excess copper in maize cultivars. Vertical bars represent standard deviation. Different letters denote significant differences between the two cultivars along with different treatments at $p<0.05$.

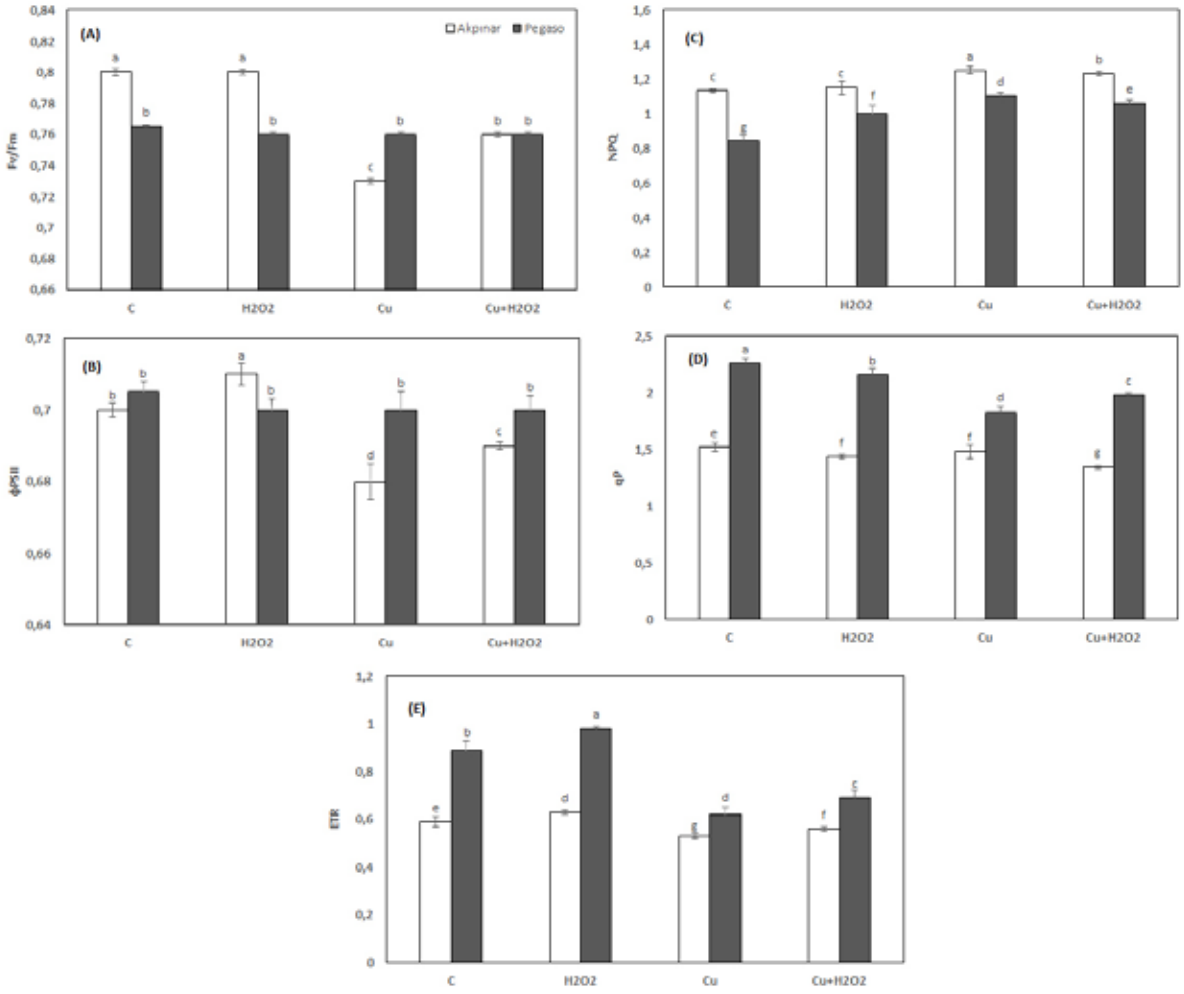

FIGURE 3
The effect of H_2O_2 application on chlorophyll a fluorescence parameter (F_v/F_m (A), Φ_{PSII} (B), NPQ (C), qP (D), ETR (E) under excess copper in maize cultivars. Vertical bars represent standard deviation. Different letters denote significant differences between the two cultivars along with different treatments at $p<0.05$.

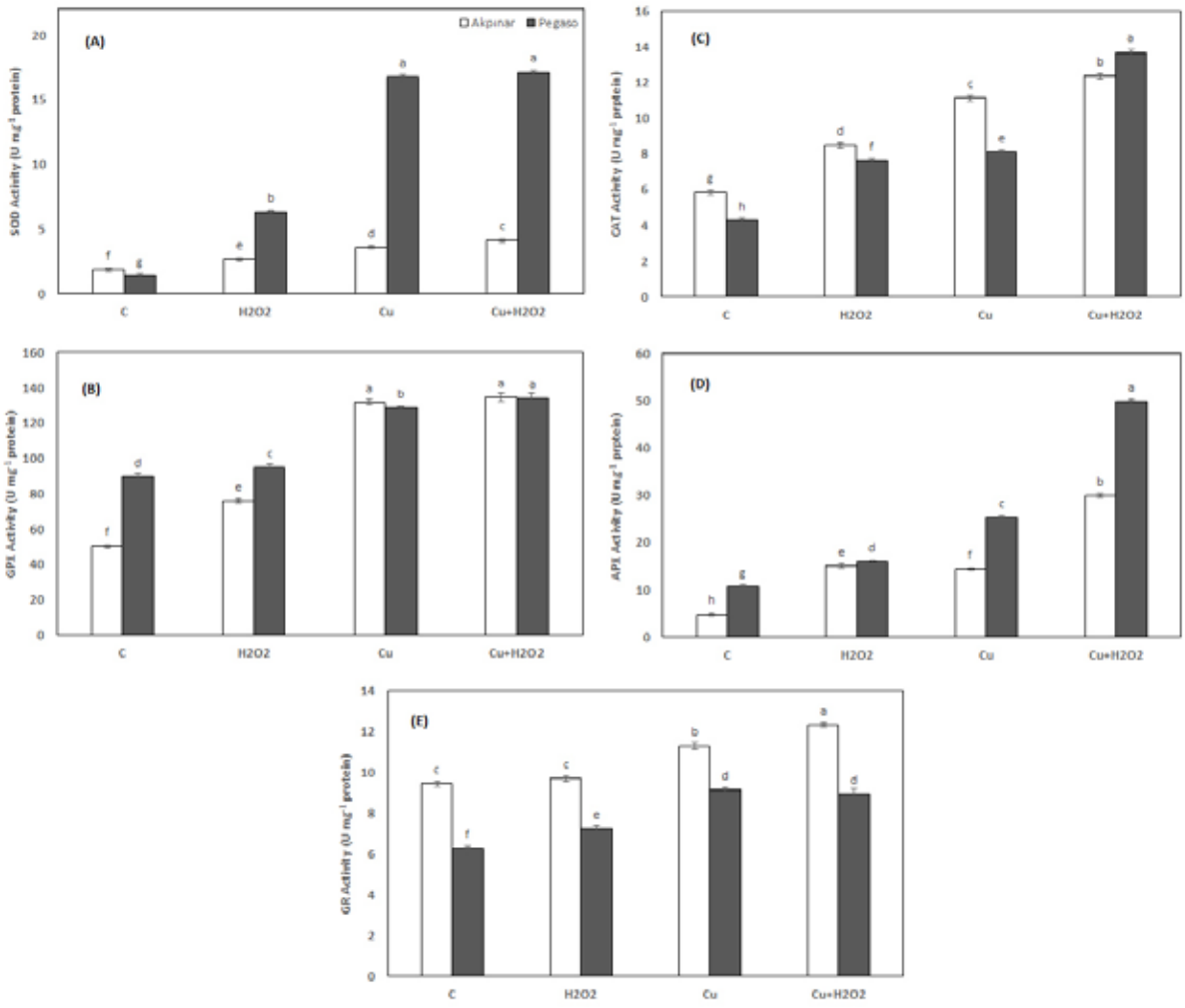

FIGURE 4
The effect of H_2O_2 application on antioxidant enzyme activities (SOD (A), GPX (B), CAT (C), APX (D), GR (E) under excess copper in maize cultivars. Vertical bars represent standard deviation. Different letters denote significant differences between the two cultivars along with different treatments at $p<0.05$.

Antioxidant enzymes. All antioxidant enzyme activities increased under Cu toxicity in both cultivars, and this increase was generally higher in the H_2O_2 pretreated seedlings. The increases in SOD activity were recorded by 1.96-fold and 12-fold under Cu stress in cv. Akpınar and cv. Pegaso in comparison with their controls, respectively. Under Cu stress, exogenous application of H_2O_2 significantly increased SOD activity of sensitive cv. Akpınar in comparison with Cu group seedlings. The increase was recorded by 1.15-fold. Conversely, the activity of SOD in Cu+H_2O_2 seedlings did not change significantly in cv. Pegaso as compared with Cu-group seedlings (Figure 4A).

As similar to SOD acidity, GPX activity increased under the stress conditions in both maize seedlings. Cu-induced increase in GPX activity was relatively more pronounced in cv. Akpınar (2.62-fold) than the cv. Pegaso (1.43-fold). Exposure to H_2O_2 also resulted in a rise in GPX activity of tolerant cv. Pegaso under Cu stress. The increase was recorded by 1.04-fold. On the contrary, GPX activity of cv. Akpınar did not change significantly by exogenous H_2O_2 in comparison with the Cu pretreated seedlings (Figure 4B).

Excess copper also caused increases in CAT activities of cv. Akpınar and cv. Pegaso. Similar increases were recorded by 1.90-fold in both cultivars. The H_2O_2 application under Cu stress more increased CAT activity than Cu group seedlings in two cultivars. The increases in the activity were recorded by 1.11-fold and 1.69-fold in cv. Akpınar and cv. Pegaso, respectively (Figure 4C).

As similar to the other enzymes, Cu stress resulted in higher APX activity in both cultivars as compared to their controls. The increases in the activity were recorded by 3.02-fold and 2.35-fold in cv. Akpınar and cv. Pegaso, respectively. However,

when Cu+H_2O_2 group seedlings were compared with the Cu group seedlings, there was a higher increase in APX activity of H_2O_2 pretreated seedlings under Cu stress. APX activity in H_2O_2 pretreated seedlings of cv. Pegaso increased 1.98-fold while there was 2.07-fold increase in cv. Akpınar (Figure 4D).

GR activity also increased under Cu stress in both maize seedlings. The increases were recorded by 1.20-fold and 1.46-fold in cv. Akpınar and cv. Pegaso, respectively. The activity of Cu+H_2O_2 seedlings showed a higher increase than Cu seedlings and the increase was recorded by 1.09-fold in cv. Akpınar. Conversely, GR activity did not change significantly in cv. Pegaso after H_2O_2 application (Figure 4E).

DISCUSSION AND CONCLUSION

As a crucial signaling molecule in plants, H_2O_2 plays significant roles in regulating many key physiological processes. In recent studies, H_2O_2 has been established as a central player in the responses of plants against heavy metals, including cadmium [8], aluminum [11] and chromium [23]. Our previous study reported that osmotic regulation might be involved in the alleviation of Cu toxicity of maize leaves caused by pretreatment of H_2O_2 [12]. In this work, the effect of H_2O_2 on Cu-induced changes in the chlorophyll fluorescence parameters and antioxidant system were investigated in two maize cultivars, Akpınar and Pegaso differently sensitive to water stress. Our findings suggest that exogenous H_2O_2 may help reducing detrimental effects of Cu stress by inducing antioxidant enzyme activities and maintain photosynthetic activity in maize seedlings.

It is well known that heavy metal stress affects negatively photosynthetic apparatus in an array of plant species. The photosynthetic pigment, chlorophyll plays an important role in light absorption and energy transduction and is essential for photosynthesis. The reduction of leaf chlorophyll under heavy metal stress has been attributed to the destruction of pigments and the instability of the pigment-protein complex. In this study, Cu stress reduced the chlorophyll content of both maize seedlings. Research in this field [24] in Brassica demonstrated that excess copper causes a reduction in chlorophyll content of plants. The decline in chlorophyll content is believed to be due to inhibition of enzymes associated with chlorophyll biosynthesis and/or inhibition of uptake and transportation of other metal elements such as Mn, Zn, and Fe by antagonistic effects [25]. Indeed, in previous study, we demonstrated that ion concentrations decreased significantly in Cu-stressed maize cultivars. Conversely, exogenous application of H_2O_2 improved the ion concentrations in both cultivars [12]. Additionally, the application of H_2O_2 to Cu-stressed seedlings markedly increased the chlorophyll content, suggesting that the increase in chloroplast pigments under the H_2O_2 pretreatment might be due to the ability of H_2O_2 to increase the activity of certain enzymes, thereby stimulating chlorophyll biosynthesis or reducing chlorophyll degradation, leading to increased photosynthesis under Cu stress.

F_v/F_m is a favorable parameter which allows detection of any damage on PSII and possible photoinhibition. In the current study, Cu stressed cv. Akpınar showed a remarkable decrease of the F_v/F_m ratio but exogenous H_2O_2 under the stress caused less reduction in F_v/F_m. Conversely, the stress did not cause significant changes in F_v/F_m of cv. Pegaso. Low F_v/F_m values in plants under stress generally indicate some detrimental effects to the PSII reaction center [16]. In our case, less decreases observed in F_v/F_m ratio in H_2O_2 applied plants indicate that the damage on the cell membrane is minimized and the injury caused by ROS is prevented [26]. F_v/F_m and Φ_{PSII}values of tolerant cv. Pegaso did not change significantly with Cu stress and H_2O_2 applications. These results pointed out that the photochemical activity and electron transport chain of tolerant cv. Pegaso was capable of maintaining well under Cu stress and thus cv. Pegaso could be resistant to Cu stress.

In our investigation, NPQ increased under Cu toxicity in both maize seedlings. Changes in NPQ between Cu group and Cu+H_2O_2 group were noticed. In this case, both maize cultivars might protect themselves from detrimental effects of Cu toxicity through increased NPQ, which has dissipated light energy and decreased the efficiency of photochemical reactions of photosynthesis. On the other hand, Cu-induced photo-inhibition and reduced photosynthetic efficiency was reversed by exogenous H_2O_2. This result showed that H_2O_2 protected photosynthetic activation centers against Cu-induced photoinhibition damage by enhancing energy dissipation process, namely, non-photochemical quenching progress. ETR results were in accordance with qP measurements in tolerant cv. Pegaso. H_2O_2 pretreated seedlings under Cu stress showed an increase in qP, which indicate that exogenous H_2O_2 alleviated the damage of the photoinhibition and improved the photochemical efficiency of cv. Pegaso. Additionally, decreases in F_v/F_m and $\Phi_{PSII}$of cv. Akpınar under Cu stress were mitigated with H_2O_2 application while these values did not change in cv. Pegaso seedlings exposed to copper stress and exogenous H_2O_2 applications. These findings indicated that cv. Akpınar may be more prone to Cu toxicity than cv. Pegaso. As similar to our findings, Khan et al. [27] reported that application of H_2O_2 regulated PS II activity and stomatal movement under Ni stress for maintaining higher photosynthetic potential in high photosynthetic capacity cultivar (Varuna) of mustard.

As an active redox metal, Cu can catalyze the overproduction of ROS, such as singlet oxygen, hydrogen peroxide, superoxide, and hydroxyl radicals by Haber-Weiss reaction [28], and leading to an increase in lipid peroxidation as biomarkers of oxidative markers. The primary site of Cu toxicity was probably the cell membrane. Results of the present study indicated that Cu induced substantial damage to cell membranes in terms of higher cellular levels of MDA and H_2O_2 in both cultivars. However, exogenous application of H_2O_2 at low concentration resulted in a significant reduction in the endogenous levels of H_2O_2 and MDA by inducing antioxidant system. Results obtained from ryegrass showed that Cu stress induced over accumulation of MDA and H_2O_2 in leaves, leading to the oxidative injury and inhibiting plant growth [29]. Our result is in good agreement with the decreased H_2O_2 accumulation in H_2O_2-pretreated seedlings, suggesting that exogenous application of H_2O_2 may decrease lipid peroxidation in both maize cultivars by reducing ROS accumulation under Cu stress. Similarly, H_2O_2 has been reported to decrease the cellular levels of MDA and H_2O_2 in rice seedlings exposed to heavy metal stress [8]. From the results of the present study, we think that the reduction of MDA content was due to increased antioxidative enzyme activities, which reduced H_2O_2 levels and membrane damage. Moreover, the reduction in MDA content of cv. Pegaso was more than in cv. Akpınar. This result implies that cv. Pegaso is better protected from oxidative damage, and can rapidly up-regulate the antioxidative system.

The activation of antioxidant system is an important adaptive strategy to reduce ROS production and minimize oxidative damage under stress conditions. In the present study, we found that excess Cu increased the activities of antioxidant enzymes in both maize cultivars (Figure 4). cv. Pegaso exhibited higher activities of SOD and GR whereas lower activities of APX and GPX as compared with cv. Akpınar. The rate of increase in CAT activity was equal in both cultivars (1.90-fold). According to these results, it can be said that tolerant cv. Pegaso is more resistant to stress especially due to its high SOD and GR activity. Moreover, exogenous application of H_2O_2 under Cu stress further increased the activities of all these enzymes in both cultivars, with the increases in CAT and GPX activities being greater in cv. Pegaso than cv. Akpınar (Figure 4). SOD and GR activities with higher rates of increase under Cu stress in cv. Pegaso did not change in H_2O_2 applied seedlings under excess copper. Thus, application of H_2O_2 to the tolerant cv. Pegaso exposed to copper stress may not significantly affect antioxidant enzymes such as SOD and GR with high activity under the stress. These results suggested that H_2O_2 pretreatment improved Cu-induced ROS scavenging activity in both cultivars. There are supporting data claim that exogenous application of H_2O_2 rises the activity of antioxidant enzymes [8,11], which consecutively protect plants against ROS formation and membrane damage under stress. Indeed, enhanced H_2O_2-scavenging enzyme activities efficiently removed H_2O_2 (Figure 1A) and alleviated Cu-induced lipid peroxidation (Figure 1B). These results are identical with those of Hu et al. [8], who suggested that pre-treatment with 100 μM H_2O_2 for 1-day mitigated Cd stress and increased the levels of the antioxidant enzymes (SOD, CAT, GPX, APX, and GST). Yıldız et al. [23] also reported that H_2O_2 pretreatment caused an increase in the activities of APX and POD in response to Cr stress, but CAT and SOD activities remained unchanged. In this context, our findings can be explained in two ways. First, exogenous H_2O_2 may act as a signal that triggers defense mechanisms that in turn protect plants from ROS-induced damage caused by excess Cu. Secondly, exposure to Cu may induce antioxidant enzymes which play important role in reducing Cu toxicity. Hence, our previous study has shown that maize cultivars exposed to excess Cu accumulated substantial amounts of Cu in their leaves but this increase was further elevated by the application of H_2O_2 [12]. In fact, previous reports demonstrated that it was observed an excess Cu in plants inducing defense genes responsible for antioxidant enzymes, including SOD, POD, and CAT, which contribute to the removal of ROS [30].

In conclusion, findings of this study displayed the positive effects of exogenous H_2O_2 in alleviating Cu toxicity, which was reflected in the growth, photosynthetic efficiency, and antioxidant system of the Cu-exposed seedlings. Exogenous H_2O_2 successfully decreased Cu-induced ROS and MDA levels, providing strong evidence that H_2O_2 protects maize seedlings against oxidative stress. H_2O_2 may be also considered as a potential signaling molecule for augmenting photosynthetic potential of maize plants under Cu stress conditions. Of the two maize cultivars, tolerant cv. Pegaso performed better when exposed to Cu stress. Additionally, application of exogenous H_2O_2 might be a basis for developing strategies to improve risks associated with Cu-induced toxicity in contaminated areas.

REFERENCES

[1] Afrousheh, M., Tehranifar, A., Shoor, M., Safari, V.R. (2005) Salicylic acid alleviates the copper toxicity in *Zinnia elegans*. J. Orna. Plants. 5, 51–59.

[2] Kamali, M., Pour, M.S., Moud, A.A.M. (2012) Copper effects on growth parameters of hollyhock (*Althaea rosea* L.). J. Orna. Horti. Plants. 2, 95–101.

[3] Yu, Z.L., Zhang, J.G., Wang, X.C., Chen, J. (2008) Excessive copper induces the production of reactive oxygen species, which is mediated by phospholipase D, nicotinamide adenine dinucleotide phosphate oxidase and antioxidant systems. J. Integr. Plant Biol. 50, 157–167.
[4] Drazkiewicz, M., Skórzyńska-Polit, E., Krupa, Z. (2004) Cu-induced oxidative stress and antioxidant defence in *Arabidopsis thaliana*. Biometals. 17, 379–387.
[5] Fidalgo, F., Azenha, M., Silva, A.F., de Sousa, A., Santiago, A., Ferraz, P., Teixeira, J. (2013) Copper-induced stress in *Solanum nigrum* L. and antioxidant defense system responses. Food and Energy Security. 2, 70–80.
[6] Yruela, I. (2009) Copper in plants: acquisition, transport and interactions. Funct. Plant Biol. 36, 409–430.
[7] Alaoui- Sossé, B., Genet, P., Vinit-Dunand, F., Taussaint, M.L., Epran, D., Badot, P.M. (2004) Effect of copper on growth in cucumber plants (*Cucumis sativus*) and its relationships with carbohydrate accumulation and changes in ion contents. Plant Sci. 166, 1213–1218.
[8] Hu, Y., Ying, G., Zhang, C., Ju, T., Cheng, W. (2009) Cadmium toxicity and translocation in rice seedlings are reduced by hydrogen peroxide pretreatment. Plant Growth Regul. 59, 51–61.
[9] Wang, Q.H., Liang, X., Dong, Y.J., Xu, L.L., Zhang, X.W., Hou, J., Fan, Z.Y. (2013a) Effects of exogenous nitric oxide on cadmium toxicity, element contents and antioxidative system in perennial ryegrass. Plant Growth Regul. 69, 11-20.
[10] Mei, L., Daud, M.K., Ullah, N., Ali, S., Khan, M., Malik, Z., Zhu, S.J. (2015) Pretreatment with salicylic acid and ascorbic acid significantly mitigate oxidative stress induced by copper in cotton genotypes. Environ. Sci. Pollut. Res. 22, 9922–9931.
[11] Xu, F.J., Jin, C.W., Liu, W.J., Zhang, Y.S., Lin, X.Y. (2011) Pretreatment with H_2O_2 alleviates aluminum-induced oxidative stress in wheat seedlings. J. Integr. Plant Biol. 53, 44–53.
[12] Guzel, S., Terzi, R. (2013) Exogenous hydrogen peroxide increases dry matter production, mineral content and level of osmotic solutes in young maize leaves and alleviates deleterious effects of copper stress. Bot. Stud. 54, 26.
[13] Velikova, V., Yordanov, I., Edreva, A. (2000) Oxidative stress and some antioxidant systems in acid rain-treated bean plants: protective roles of exogenous polyamines. Plant Sci. 151, 59-66.
[14] Heath, R.L., Packer, L. (1968) Photoperoxidation in isolated chloroplasts. I. kinetics and stoichiometry of fatty acid peroxidation. Arch. Biochem. Biophys. 125, 189–198.
[15] Arnon, D. (1949) Copper enzymes in isolated chloroplasts: polyphenol oxidases in *Beta vulgaris*. Plant Physiol. 24, 1–15.
[16] Nar, H., Saglam, A., Terzi, R., Varkonyi, Z., Kadioglu, A. (2009) Leaf rolling and photosystem II efficiency in *Ctenanthe setosa* exposed to drought stress. Photosynthetica. 47, 429–436.
[17] Beauchamp, C., Fridovich, I. (1971) Superoxide dismutase: improved assays and an assay applicable to acrylamide gels. Anal. Biochem. 44, 276-287.
[18] Urbanek, H., Kuzniak-Gebarowska, E., Herka, K. (1991) Elicitation of defense responses in bean leaves by *Botrytis cinerea* polygalacturanase. Acta Physiol. Plant. 13, 43–50.
[19] Aebi, H. (1983) Catalase. In: Bergmeyer, H. (ed.), Methods of Enzymatic Analysis. Weinheim: Verlag Chemie. 3, 273–277.
[20] Nakano, Y., Asada, Y. (1981) Hydrogen peroxide is scavenged by ascorbate-specific peroxidase in spinach chloroplasts. Plant Cell Physiol. 22, 867–880.
[21] Foyer, C.H., Halliwell, B. (1976) Presence of glutathione and glutathione reductase in chloroplast: a proposed role in ascorbic acid metabolism. Planta. 133, 21–25.
[22] Bradford, M.M. (1976) Rapid and sensitive method for the quantitation of microgram quantities of protein utilizing the principle of protein-dye binding. Anal. Biochem. 72, 248–254.
[23] Yıldız, M., Terzi, H., Bingül, N. (2013) Protective role of hydrogen peroxide pretreatment on defense systems and BnMP1 gene expression in Cr(VI)-stressed canola seedlings. Ecotoxicology. 22, 1303–1312.
[24] Xiong, Z.T., Liu, C., Geng, B. (2006) Phytotoxic effects of copper on nitrogen metabolism and plant growth in *Brassica pekinensis* Rupr. Ecotox. Environ. Safe. 64, 273–280.
[25] John, R., Ahmad, P., Gadgil, K., Sharma, S. (2009) Heavy metal toxicity: effect on plant growth, biochemical parameters and metal accumulation by *Brassica juncea* L. Int. J. Plant Prod. 3, 65–76.
[26] Hashem, A., Abd Allah, E.F., Alqarawi, A.A., Al Huqail, A.A., Egamberdieva, D. (2014) Alleviation of abiotic stress in *Ochradenus baccatus* (Del.) by *Trichoderma hamatum* (Bonord.) Bainier. J. Plant Interact. 9, 857–868.
[27] Khan, M.I.R., Khan, N.A., Masood, A., Per, T.S., Asgher, M. (2016) Hydrogen peroxide alleviates nickel-inhibited photosynthetic responses through increase in use-efficiency of nitrogen and sulfur, and glutathione production in mustar. Front. Plant Sci. 7, 1–20.
[28] Halliwell, B., Gutteridge, J.M.C. (1984) Oxygen toxicity, oxygen radicals, transition metals and disease. Biochem. J. 219, 1–14.

[29] Dong, Y., Xu, L., Wang, Q., Fan, Z., Kong, J., Bai, X. (2014) Effects of exogenous nitric oxide on photosynthesis, antioxidative ability, and mineral element contents of perennial ryegrass under copper stress. J. Plant Interact. 9, 402–411.

[30] Wang, H., Shan, X.Q., Wen, B., Zhang, S., Wang, Z.J. (2004) Responses of antioxidative enzymes to accumulation of copper in a copper hyperaccumulator of *Commoelina communis*. Arch. Environ. Con. Tox. 47, 185–192.

Received: **21.07.2017**
Accepted: **02.12.2017**

CORRESPONDING AUTHOR

Neslihan Saruhan-Guler
Department of Nutrition and Dietetics,
Faculty of Health Sciences,
Karadeniz Technical University,
61080, Trabzon – Turkey

e-mail: neslihansaruhan@hotmail.com

© by PSP Volume 27 – No. 2/2018 pages 1006-1012 Fresenius Environmental Bulletin

DETERMINATION OF SERA NGAL LEVELS IN PATIENTS WITH LUNG CANCER AND ITS RELATION WITH APOPTOSIS

Bahadır Ozturk[1], Harun Ciftci[2,*], Husamettin Vatansev[1], Fatma Gul Gun[1], Guven Sami Sunam[3], Murat Oncel[3], Pinar Karabagli[4]

[1]Selcuk University, Faculty of Medicine, Department of Biochemistry, Konya, Turkey
[2]Ahi Evran University, Faculty of Medicine, Department of Biochemistry, Kirsehir, Turkey
[3]Selcuk University, Faculty of Medicine, Department of Thorax Surgery, Konya, Turkey
[4] Selcuk University, Faculty of Medicine, Department of Medical Pathology, Konya, Turkey

ABSTRACT

The NGAL synthesis induces in neoplasms; therefore, probably, it is benefited from the level of this protein for the determination of carcinogenesis and the progress stages of human tumors. In this study, it was aimed to investigate the expression of NGAL (neutrophil gelatinase associated lipocalin) in lung cancer patients and its relation with apoptosis. The study was conducted on the patients between the ages of 40 and 70 years accepted by the Thoracic Surgery Clinic (Selçuk University, Faculty of Medicine) based on their lung cancer diagnosis. The patients aged between 40 and 70 were included in the study from the thoracic surgery clinic of the Selçuk University as they were administered into the clinic based on their lung cancer diagnosis and had operation before. Patients who have acute stroke, rheumatic diseases, chronic kidney disease, congestive heart failure, chronic infection and other organ and system cancers (except lung cancer) were excluded from the study. Two groups including a lung cancer group (N=40) and a normal group (N=40) were formed to determine the NGAL and M30 levels in sera of patients using the ELISA method. According to the analysis results, the NGAL levels for the lung cancer group and the normal group were observed as 424.03±74.49 and 374.04±90.34 ng/mL, respectively. This increase in the lung cancer group was found statistically significant according to the normal group ($p<0.01$). The M30 levels, marker for apoptosis in circulation, were obtained as 144.08±45.91 and 118.76±46.16 U/L for the lung cancer group and the normal group, respectively. This increase in the lung cancer group was found statistically significant according to the normal group ($p<0.01$). A positive correlation was obtained between the NGAL and M30 data by means of Spearman's correlation test ($r(40)=0.58$, $p<0.01$).

The antigen levels of caspase 3, 8 and 9 were determined by the immunohistochemical staining methods in the samples of cancerous tissues and normal tissues adjacent to the cancerous tissue, and the apoptotic indexes were calculated. The apoptotic indexes of the cancerous tissues were significantly lower than the normal tissues ($p<0.01$). This result demonstrates that the predominant type of cell death might be other cell death pathways rather than the apoptotic pathways in lung cancer. In addition, these results support the opinion about the fact that apoptosis may be inhibited by cancer cells in cancerous tissues. The significant increase in the M30 and NGAL levels supports the claims of the previous studies about the fact that it causes the consumption of cellular iron reserves and NGAL induced apoptosis in cancer patients.

KEYWORDS:
Lung cancer, NGAL, Apoptosis, M30, Caspase

INTRODUCTION

Incidence rates of different kinds of cancer have increased besides genetic factors, pollution due to growing industry, various chemicals, agricultural materials, additional agents in nutrition, smoking, alcohol consumption, radiation, some viruses and poor diet habits [1]. Cancer is a complex disease that may be caused by many factors. The role of various organic and inorganic materials in the development or suppression of cancer was investigated [2]. To prevent deaths caused by cancer, early diagnosis is required to enable treatment; increasing amounts of research on some biomarkers including various parameters are being carried out. Tumor biomarkers produced by tumors or relevant tissues at supraphysiological levels can be measured quantitatively using the biochemical or immunochemical methods in tissue, blood and body fluids such as hormones, enzymes, metabolites, proteins or metalloproteins. Also, the antigens related to tumors can include oncogene and the products of oncogene [3]. If biomarkers can be detected before clinical symptoms, or a response to the medical treatment can be seen, a meaningful clinical oncology therapeutic activity can be provided [4].

Apoptosis, a morphological form of cell death, is controlled by extrinsic and intrinsic molecular

mechanisms. Apoptosis is not only a process controlled genetically in organisms, but also a physiological process that has an important role in the developmental and tissue homeostasis. Disorders in the apoptosis mechanisms can cause many diseases including cancer [5].

Various hormonal active substances, ionized radiation and cellular lesions that formed via agents including traumatic chemotherapy or the cellular death program activated by genetic factors can cause apoptosis. As a physiological process, apoptosis is responsible for losses of specific cells during normal development and the destruction process of several cell types in mature organisms. The amount of apoptotic cells defines whether a person is healthy or not, and the functional mechanism of apoptosis is an important part of the balance in cells [6]. There is concrete evidence to prove that apoptosis plays an important role in balancing the productivity of mammals, including human beings [7,8].

In multicellular organisms, the blocking of cell damage occurring genetically or destroying cells completely occurs via apoptosis. Thus, the harmful possibilities like spreading the damage and formation of tumors can be blocked. Before the apoptosis, the cellular replication process stops (DNA repair), and if DNA repair does not occur, some serial incidents that end with apoptosis starts. Whether apoptosis starts or not depends on the size of damage, the type of cell and tumor development risk which is the productivity potential of cell. Apoptosis is not only essential for organogenesis and synaptogenesis occurrence in the intrauterine development, but also essential for the maturation of differentiated tissues because apoptosis stabilizes numbers of cells all around the body and immune system activities [9].

In biological processes including the activation or inhibition of biochemical reactions, bioorganic molecules such as NGAL (neutrophil gelatinase associated lipocalin) play an important role. NGAL is a protein which has a molecular weight of 25 kDa, and it is also known as oncogene 24p3, uterokalin and lipokalin 2 [10]. NGAL synthesis occurs at trace level in healthy people. Its main source is neutrophils in circulation. At the same time, it is expressed in very low amounts in the kidney, prostate, lungs, liver, thymus, gastrointestinal tract epithelial, and postpartum uterus tissues. During the transition period to supplementary foods, it is also seen in the breast and involuted tissues. The factors that regulate NGAL expression are various, such as interleukin, tumor necrosis factor (TNF) and interferon, which includes pro-inflammatory cytokines and vitamins like retinoic acid [11].

NGAL synthesis can be induced in neoplasia, so the level of this protein can be used to obtain the development of tumors and cancerogens in human body. In the studies carried out in the past, it was shown that NGAL expression increased in some cancer types. Studies have shown that NGAL expression increases in malignant tumors which originate in different organs such as thyroid, skin, breast, ovaries, endometrium, colon, lung, liver, biliary tract, esophagus, stomach and pancreas, as well as inflammatory, ischemic and metabolic disorders in body fluids and tissues [12].

The increasing NGAL expression as a response to acute and chronic kidney damage has gained importance in recent years. NGAL expression increases significantly due to several reasons from contrast agent till postoperative stress in acute kidney damage. The many studies carried out in this area have proved that to diagnose kidney damage early and predict prognosis, urine and serum NGAL measurements might become a standard biomarker [13].

NGAL induces cell proliferation by inducing the iron dependent metabolism of nucleoids for DNA synthesis. These features show that detecting NGAL levels is important for carcinogenesis and apoptosis processes. In this study, it is aimed to investigate the expression of NGAL in lung cancer patients and its relation with apoptosis.

MATERIALS AND METHOD

Selection of patients. The patients aged between 40 and 70 were included in the study from the Thoracic Surgery Clinic of the Selçuk University as they were administered into the clinic based on their lung cancer diagnosis and had operation before.

Patients who have acute stroke, rheumatic diseases, chronic kidney disease, congestive heart failure, chronic infection and other organ and system cancers (except lung cancer) were excluded from the study. The study protocol was reviewed and approved by the Selçuk University Ethics Committee for Clinical Research (Protocol No: 2012/108).

Study Protocol of Sera Samples. Two groups were made for serum NGAL and M30 analysis. Group 1 (n=40) (Normal group): The group consisted of people who did not have health problems like rheumatological diseases, chronic kidney disease, congestive heart failure, chronic infection, organ or system cancers. Group 2 (n=40): This group consisted of patients diagnosed with lung cancer, and their blood samples were taken before the surgery.

The average age of the normal group (Group 1) was 51 ± 10 years, and 28 of them were male. In Group 2, the average age was 55 ± 9 years, and 26 of them were male.

Blood samples and isolation of serum. Blood samples were obtained from in-patients at the Thoracic Surgery Clinic (Selçuk University, Faculty of

Medicine, Konya, Turkey). Whole blood was transferred from an anticoagulant citrate dextrose solution formula A-capped tube (ACD-A) to a conical tube (Nalgene, Rochester, NY, USA). The samples were centrifuged for 10 min at 1000 g in a swing bucket rotor at +4 ºC, and the serum was stored in cryovials at -80ºC.

Determination of NGAL. The concentration of NGAL in the serum of patients was determined by using the NGAL Rapid ELISA Kit (BioVendor GmbH, D-69120 Heidelberg, Germany). Serum from patients with lung cancer (n=40) were tested. Serum from healthy donors (n=40) were chosen as the control. Each sample was diluted 100-fold using the sample diluent provided with the kit. A volume of 50 ml horseradish peroxidase-conjugated detection antibody was added to each well of a 96-well plate precoated with NGAL antibody. Thereafter, 50 ml each of the calibrator (provided by the manufacturer), sample (lung cancer, or healthy control serum sample), or sample diluent alone (blank) was rapidly added to the corresponding wells. After incubating at room temperature for 30 min with agitation (200 min^{-1}), the contents of the microwell were aspirated and replaced with 100 ml of the chromogenicperoxidase substrate tetramethylbenzidene (TMB). After the plate was incubated for 15 min in the dark, the reaction was stopped by adding a stop solution, and the absorbance was read at 450nm with a microplate reader.

M30 antigen detection. To detect the M30 antigen, an ELISA assay (a solid phase, two-site immunosorbent assay) was used. The kit (M30-Apoptosense ELISA kit, Peviva, Sweden) for the assay was obtained commercially. Briefly, samples were placed into wells coated with a mouse monoclonal antibody used as catcher. A horseradish peroxidase conjugated monoclonal antibody (M30) was used as detecting antibody (conjugate). Following the sandwich formation, excess unbound conjugate was removed, and then TMB substrate was added. The absorbance was finally measured in a microplate reader at 450 nm. By plotting a standard curve from known concentrations versus measured absorbances, the amount of M30 antigen in the sample was estimated. The concentration of M30 antigen was expressed as units per liter (U/L), according to the manufacturer's instructions. One unit (U) corresponds to 1.24 pmol of a synthesized peptide containing the M30 recognition motif according to the manufacturer.

Immunohistochemical Analysis. Discrimination of cancerous tissues and normal tissues adjacent to the cancerous tissue were identified with the macroscopic method. The samples were stored at -80ºC. The frozen sections (4-6 micron thickness) were taken to polylysine slides from lung tissue samples. After the various washing process, the primer anticores (active caspase 3, 8 and 9) and the seconder solutions (Texas Red) were applied. The DAPI (4',6-Diamidino-2-phenylindole dihydrochloride) as a mounting medium was added on the sections and closed down with slides. The samples were kept at 4 ºC until further processing. Apoptotic and viable cells were counted by fluorescence microscope.

Statistical Analysis. Data were analyzed by using a statistical software application and presented as mean ± standard deviation for normally distributed variables and median (min-max) for non-parametric values. The distribution of the variables was analyzed with the Kolmogorov-Smirnov Test. The results of NGAL were presented as mean ± standard deviation and analyzed using the Independent-Samples T-Test. Due to the non-parametric values, the M30 levels and apoptotic indexes were given as median (min-max) and analyzed using the Mann-Whitney-U Test. Correlation analysis was carried out using the Spearman's correlation test. A value of $p<0.01$ was considered statistically significant.

RESULTS

The calibration equations, linear dynamic range and correlation coefficients (R^2) for NGAL and M30 determination using the ELISA method were detailed in Table 1.

TABLE 1
Analytical parameters for NGAL and M30 determination

Analyte	Calibration equation	Linear dynamic range	R^2
NGAL	A= 0.0022xC+0.202	50- 500 ng L^{-1}	0.9940
M30	A= 0.0014xC+0.022	75- 500 U L^{-1}	0.9948

A=Absorbance, C=Concentration

TABLE 2
NGAL levels in serum samples

Group	Mean (ng/L)	Std. Deviation	Min.	Max.
Lung Cancer (LC)	424.03*	74.49	282.52	551.68
Normal (N)	374.04	90.34	240.27	523.51

*Statistical significance compared to the control group (p<0.01).

TABLE 3
M30 levels in serum samples

Group	Median (U/L)	Mean (U/L)	Std. Deviation	Min.	Max.
Lung Cancer (LC)	136.74 *	144.08	45.91	87.01	266.45
Normal (N)	109.35	118.76	46.16	54.59	266.45

*Statistical significance compared to the control group (p<0.01).

TABLE 4
Apoptotic indexes for caspase 3, caspase 8 and caspase 9 in tissues

	Normal group (N=14)			Tumor group (N=14)		
	Caspase 3	**Caspase8**	**Caspase 9**	**Caspase 3**	**Caspase 8**	**Caspase 9**
Apoptotic index*	1.05[a]	0.40[b]	0.45[c]	0.08[a]	0.02[b]	0.04[c]

[a,b,c] The statistical differences between the tumor group and the normal group ($p<0.01$) are identified with the same characters in the same line.

The serum levels of NGAL and M30 in the lung cancer and normal groups were given in Table 2 and Table 3, respectively. Apoptotic cells and viable cells in cancerous tissues and normal tissues adjacent to the cancerous tissues obtained by the immunohistochemical staining methods were shown on Fig 1-4.

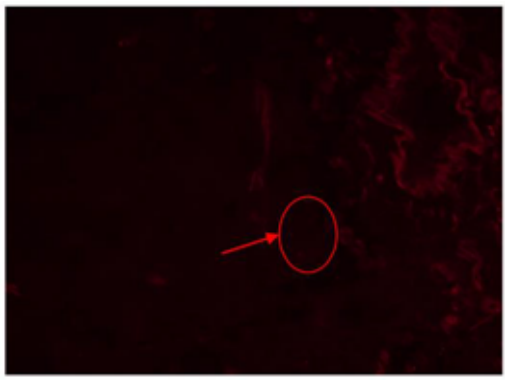

FIGURE 1
Apoptotic cells in cancerous tissues

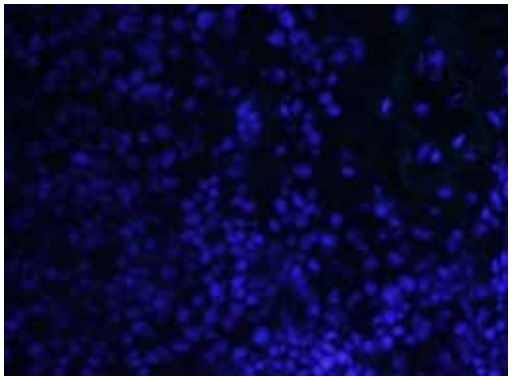

FIGURE 2
Viable cells in cancerous tissues

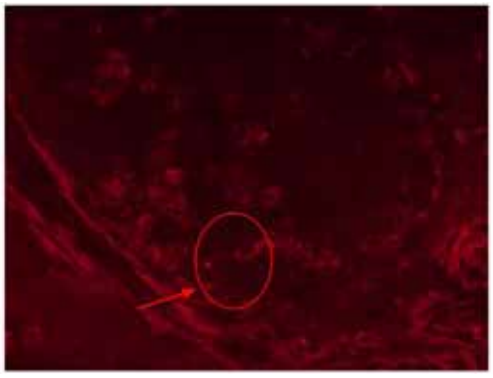

FIGURE 3
Apoptotic cells in normal tissues adjacent to cancerous tissue

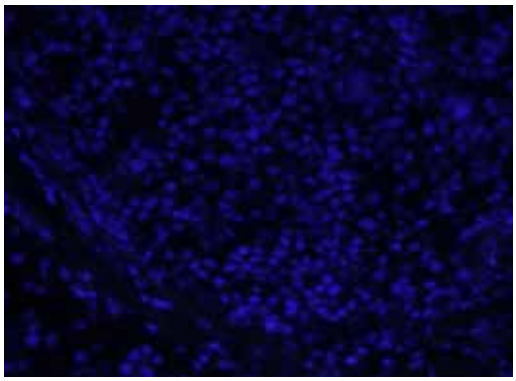

FIGURE 4
Viable cells in normal tissues adjacent to cancerous tissue

The intensity of apoptosis or its rate was histologically explained with the apoptotic index. This index was obtained by calculating the rate (percentage) of the apoptotic cells and the cells that were able to live. Normal and apoptotic cells were counted on 8 different random parts of the tissue using a fluorescent speckle microscope magnifying them 40 times. Apoptotic indexes were calculated by considering the average numbers of cell count. The apoptotic indexes for caspase 3, caspase 8 and caspase 9 were detailed in Table 4, and the correlation results between M30 and NGAL in patients with lung cancer were given in Table 5.

TABLE 5
Spearman's correlation results between M30 and NGAL

M30	Correlation Coefficient	1.000	0.58
	Sig. (2-tailed)	.	0.00
	N	40	40
NGAL	Correlation Coefficient	0.58	1.000
	Sig. (2-tailed)	0.00	.
	N	40	40

DISCUSSION

Cancer can be described as disordered cell proliferation that happens with serial somatic changes in DNA molecules. It mostly takes root in one cell. However, for a normal cell, it can occur by incremental mutation to gain malignant phenotype characteristics. Basically, cancer may develop as a result of exposure to carcinogens or due to random replication errors caused by errors in DNA repair mechanisms [14,15].

The following factors are defined as carcino-

gens; pollution as a result of industrialization, some chemical materials that are used in agriculture, additional agents in nutrition, smoking, alcohol consumption, ionized radiation that causes translocation and typical breakdown of chromosomes, some viruses and poor diet habits [16].

In cancer-based deaths, while lung cancer is the most frequently seen cancer type among men, it is the second cancer type that most commonly affects women. Studies carried out in recent years have stated that lung cancer is responsible for 18% of all cancer-related deaths. 13% of all cancer diagnoses are lung cancer as well [17].

Lung cancer is commonly diagnosed while it is in the metastatic phase or locally advanced-phase in the thorax because of its natural progress. Therefore, there is no operation chance for 70% of patients. Mortality rate for lung cancer in 5 years after the diagnosis is between 85 and 90%. 80% of the patients with lung cancer become already inoperative during the diagnosis. Besides, normal chemotherapy cannot prevent tumors from getting bigger [18].

The markers of tumors regarding the disease such as oncofetal antigens (CEA: carcinoembryonic antigen), growth hormones, alkaline phosphatase, creatine kinase BB isoenzyme (CK-BB), neurophysin and cytokeratin 19 fragment (CYFRA 21-1) are significant markers in diagnosis [19]. However, since majority of these markers have low sensitivity and specificity in the determination of existence of cancer cells, they are insufficient in detecting and monitoring cancer cells at the early phase [20]. Accordingly, the development of molecular techniques, prognosis assessment and alternative treatment methods are needed to facilitate diagnose and the treatment of cancer at the early phase. It is thought that the proposed study serves this purpose by measuring serum NGAL, serum M30, and caspase 3, 8 and 9 levels in tissues.

M30 levels were found as 144.08±45.92 and 118.76±46.16 U/L in the lung cancer group and in the control group, respectively. Compared to the normal group, the increase in the group composed of the patients having cancer is statistically significant ($p<0.01$).

As stated by the studies in literature regarding other organ and tissue cancers, a significant increase in the levels of serum M30 was observed in the cancer groups compared to the control group. According to the research conducted by Ozturk et al. (2009) concerning the patients with local head and neck cancers, it was stated that when the serum M30 levels of the cancer group patients was compared to the control group, they came to the conclusion that M30 level has a prognostic meaning in head and neck cancer types [19].

In another study, it was found that the serum M30 levels of patients who had breast cancer were higher than the levels of healthy people. In addition, they were also observed that the patients were more critical and had even higher M30 levels compared to the other patients [21].

In the study carried by Kramer et al. (2004), the serum M30 levels of patients who had liver and lung cancer were higher than the levels of healthy people [22].

As well as many other factors inducing apoptosis, the medicines administered to patients during their treatments are an important factor. Thus, it is known that cellular lesions which occur as a result of traumatic agents including several hormonal substances activated by hormones, ionized radiation and chemotherapy or cellular suicide program activated by the genetic factors cause apoptosis [23].

Histologically, apoptotic index in tumor tissue is the rate of apoptotic cells to viable cells, and this index defines the intensity of apoptosis. This index helps to detect the level of prognosis and to predict the response to treatment. For this purpose, the antigen levels of caspase 3, 8 and 9 identified with the immunohistochemical staining methods in the samples were observed from the cancer tissues and the adjacent healthy tissues of lung cancer patients, and apoptotic indexes were calculated. It was detected that the apoptotic indexes of the lung cancer tumor tissues were statistically lower than the adjacent healthy tissues ($p<0.01$). We interpret the fact that the quantity of cells going to apoptosis in the cancerous tissues are less than the quantity of cells in the healthy tissues as that cancer cells in cancerous tissue block apoptosis.

The development of cancer depends on an increase in the proliferation of cells and an increase in apoptosis. When the death of cells is inhibited, damaged cells accumulate and cause damage in the tissue. It was discussed that during carcinogenesis, the suppression of apoptosis plays a central role in the development of some cancer types [24]. There are several molecular mechanisms of tumor cells to suppress apoptosis. Tumor cells gain resistance against apoptosis with the expression of anti-apoptotic proteins like Bcl-2, the mutations of pro-apoptotic proteins like Bax, or down regulation [25].

Furthermore, we believe that the dominant type of cellular death in parenchyma occurs as a result of other deaths causing the apoptosis. The proposed research supports the studies which assume an apoptotic impact that can be transformed into necrosis after the combination of the posterior effects of chemotherapeutic agents administered to the patients with the effect of hypoxia. Whether a cell dies by necrosis or apoptosis depends on the signals of cell killers, the type of tissue and the development levels of tissue, and also partly depends on physiological environment [26].

We think that the apoptotic indexes, determined for caspase 3, 8 and 9 antigens in the tissues, induced apoptosis in lung cancer both with the re-

ceptor pathways and with the mitochondrial pathways.

Since cytokeratins released into the serum reflect the post mortal period for cells, it is concluded that the high M30 levels in sera of cancer patients determine the late phases of apoptotic effect.

Furthermore, the high levels of M30 in lung cancer patients can be interpreted as preventing the spread of cancer around other tissues with apoptosis.

In this study, the NGAL levels were 424.03±74.49 in the lung cancer group and 374.04± 90.34 mg/L in the normal group. This increase in the lung cancer group compared to the control group is considered as statistically significant ($p<0.01$).

This increase in the NGAL levels gave information about bad prognoses since it facilitates invasion and the metastasis of cancer patients [27].

According to the studies in literature, it was discovered that the serum NGAL levels of the cancer patients group increased compared to the normal group. In a study with ovarian cancer cells, the levels of NGAL increased 2-2.6 times more in cancer patients who had benign tumors and grade 1 tumors compared to the control group. NGAL expression regulated mesenchymal-epithelial transition in ovary tumor cell lines downwards by epidermal growth factor. It was reported that the downregulation of NGAL expression showed a correlation with strengthened cell dispersion and the downregulation of E-cadherin expression. This information shows that NGAL can be a good biomarker in the distinction of benign, pre-malignant and malignant ovary tumors [28].

In another study, the biological activity of NGAL was characterized in the human endometrial carcinoma cells where cell apoptosis was induced with NGAL. While a reduction in the endometrial cancer cells was observed, an increase in interleukin-8 mRNA and protein levels was detected. It was suggested that NGAL plays an important role in the woman reproduction system or endometrial cancer [29].

Through Spearman's correlation test between the NGAL and M30 data, a positive correlation was observed ($r(40)=0.58$, $p<0.01$). The significant increase in the M30 and NGAL levels in the cancer patients supports the claims of the previous studies about the fact that it causes the consumption of cellular iron reserves and NGAL induced apoptosis.

With regards to NGAL levels in lung cancer caused by various factors because of blocked apoptosis by several mechanisms, it was assumed that it could be related with the process which causes long-living cancer cells.

ACKNOWLEDGEMENTS

The authors have no conflicts of interest to disclosure.

REFERENCES

[1] Ciftci, H., Bakal, U. (2009) The Effect of Lipoic Acid on Macro and Trace Metal Levels in Living Tissues Exposed to Oxidative Stress. Anti Cancer Agents in Medicinal Chemistry. 9(5), 560-569.

[2] Cunzhi, H., Jiexian, J., Xianwen, Z., Jingang, G., Shumin, Z., Du, L. (2003) Serum and tissue levels of six trace elements and copper/zinc ratio in patients with cervical cancer and uterine myoma. Biol Trace Elem Res. 94, 113-122.

[3] Maggino, T., Gadducci, A. (2000) Serum markers as prognostic factors in epithelial ovarian cancer: an overview. Eur J Gynaecol Oncol. 21, 64-9.

[4] Strimbu, K., Jorge, T. (2010) What are Biomarkers?. Curr Opin HIV AIDS. 5(6), 463–466.

[5] Akgul, C. (2009) Manipulation of the Bcl-2 family proteins as potential therapeutic targets in multiple types of cancer. Turk J Bioch. 34(11), 41-42.

[6] Thompson, E.B. (1994) Apoptosis and steroid hormones. MolEndocrinol. 8, 665-673.

[7] Ballian, N., Hu, M., Liu, S.H., Brunicardi, F.C. (2007) Proliferation, hyperplasia, neogenesis, and neoplasia in the islets of Langerhans. Pancreas. 35(3), 199-206.

[8] Schwartzman, R.A., Cidlowski, J.A. (1993) Apoptosis: the biochemistry and molecular biology of programmed cell death. Endocrine Review. 14, 133-150.

[9] Evan, G., Littlewood, T.A. (1998) Matter of life and cell death. Science. 281, 1317-1321.

[10] Hanai, J., Mammoto, T., Seth, P., Kiyoshi, Mori., S. Ananth, Karumanchi., Jonathan, B., Vikas P.S., (2005) Lipocalin 2 diminishes invasiveness and metastasis of ras-transformed cells. J Biol Chem. 280, 3641-3647.

[11] Singan, S. (2012) Lipocalin-2 (Neutrophil Geletinase-Associated Lipocalin (NGAL)) Düzeyinin Akut Koroner Sendromlu Hastalarda Prognostik Önemi. İstanbul Üniversitesi, Dissertation. 45-52.

[12] Chakraborty, S., Kaur, S., Guha, S., Batra, S.K. (2012) The multifaceted roles of neutrophil gelatinase associated lipocalin (NGAL) in inflammation and cancer. Biochim Biophys Acta. 1826, 129–169.

[13] Schmidt-Ott, K.M., Mori, K., Kalandadze, A., Li, J.Y., Paragas, N., Nicholas, T., Devarajan, P., Barasch, J. (2006) Neutrophil gelatinase-associated lipocalin-mediated iron traffic in kidney epithelia. Curr Opin Nephrol Hypertens. 15, 442–449.
[14] Jemal, A., Bray, F., Center, M.M., Ferlay, J., Ward, E., Forman, D. (2011) Global cancer statistics. CA Cancer J Clin. 61, 134.
[15] Lynch, M.D. (2006) How does cellular senescence prevent cancer? DNA Cell Biol. 25(2), 69–78.
[16] Rustagi, T., Dasanu, C.A. (2012) Risk Factors for Gallbladder Cancer and Cholangiocarcinoma: Similarities, Differences and Updates. J Gastrointest Cancer. 43(2), 137–147.
[17] Youlden, D.R., Cramb, S.M., Baade, P.D. (2008) The international epidemiology of lung cancer – geographical distribution and secular trends. J Thorac Oncol. 3, 819–831.
[18] Herbst, R.S., Heymach, J.V., Lippman, S.M. (2008) Molecular origins of cancer: lung cancer. N Engl J Med. 359, 1367–1380.
[19] Ozturk, B., Coskun, U., Sancak, B., Yaman, E., Buyukberber, S., Benekli, M. (2009) Elevated serum levels of M30 and M65 in patients with locally advanced head and neck tumors. Int Immuno pharmacol. 9, 645–648.
[20] Sheng, S.L, Huang, G., Yu, B. and Xin Qin, W. (2009) Clinical Significance and Prognostic Value of Serum Dickkopf-1 Concentrations in Patients with Lung Cancer. Clinical Chem. 55(9), 1656–1664.
[21] Ueno, T., Toi, M., Biven, K., Bando, H., Ogawa, T., Linder, S. (2003) Measurement Of An Apoptotic Product In The Sera of Breast Cancer Patients. Eur J Cancer. 39, 769-74.
[22] Kramer, G., Erdal, H., Mertens, H.J., Nap, M., Mauermann, J., Steiner, G., Marberger, M., Bivén, K., Shoshan, M.C., Linder, S. (2004) Differentiation Between Cell Death Modes Using Measurements Of Different Soluble Forms Of Extracellular Cytokeratin 18. Cancer Res. 64, 1751-6.
[23] Kaufmann, S.H., Vaux, D.L. (2003)Alterations in the apoptotic machinery and their potential role in anticancer drug resistance. Oncogene. 22, 7414-30.
[24] Turunen, N., Paakko, P. and Solni, Y. (2000) Apoptosis in gall bladder carcinomas and dysplasias, its relation of the expression of caspases 3, 6 and 8 and apoptosis regulating proteins bcl-2, mcl-l and bax. Histol Histopathol. 15, 53-60.
[25] Miyashita, T., Krajewski, S., Krajewska, M., Wang, H.G., Lin, H.K., Liebermann, D.A., Hoffman, B., Reed, J.C. (1994) Tumor suppressor p53 is a regulator of bcl-2 and bax gene expression in vitro and in vivo. Oncogene. 9, 1799–805.
[26] Zeiss, C.J. (2003) The apoptosis-necrosis continuum: insights from genetically altered mice. Vet Pathol. 40, 481–95.
[27] Silva Da, F., Nizet, V. (2009) Cell death during sepsis: Integration of disintegration in the inflammatory response to overwhelming infection. Apoptosis. 14, 509-521.
[28] Lim, J., Gasson, C., Kaji, D.M. (1995) Urea inhibits NaK2Cl cotransport in human erythrocytes. J Clin Invest. 96, 2126–2132.
[29] Lin, H.H., Liao, C.J., Lee, Y.C., Hu, K.H., Meng, H.W., Chu, S.T. (2011) Lipocalin-2-induced cytokine production enhances endometrial carcinoma cell survival and migration. Int J Biol Sci. 18, 74-86.

Received: **27.07.2017**
Accepted: **22.11.2017**

CORRESPONDING AUTHOR

Harun Ciftci
Ahi Evran University, Faculty of Medicine
Department of Biochemistry,
Kirsehir – Turkey

e-mail: harunciftci@yahoo.com

© by PSP Volume 27 – No. 2/2018 pages 1013-1021 Fresenius Environmental Bulletin

ANTIOXIDANT AND IMMUNOSTIMULANT EFFECTS OF *ORIGANUM MINUTIFLORUM* O. SCHWARZ ET. P.H. DAVIS IN RAINBOW TROUT

Ataman Bilge Sari*, Oya Ustuner-Aydal

Department of Veterinary Pharmacology and Toxicology, Istanbul University, Istanbul, Turkey

ABSTRACT

This study was aimed to evaluate the effects of dietary supplementation of different extracts of *Origanum minutiflorum* O. Schwarz et. P.H. Davis on nonspecific immune system and antioxidant parameters in rainbow trout. The rainbow trouts were given feeds containing crude plant, lyophilized water extract, and essential oils at three different concentrations for 8 weeks. The nonspecific immune system, antioxidant, and weight performance parameters were evaluated at the end of feeding period. The respiratory burst, lysozyme and phagocytic activities increased significantly as an indicator of immunostimulant activity in the experiment groups fed 1000 and 500 mg/kg essential oil. The feed containing 1000 and 500 mg/kg lyophilized extract was found to increase respiratory burst and phagocytic activities. The malondialdehyde levels decreased significantly in the experiment groups fed all the essential oils concentrations and 1000 mg/kg lyophilized extract. The superoxide dismutase activity in the liver increased in 1000 mg/kg lyophilized extract and 1000 mg/kg essential oil groups; glutathione peroxidase increased in groups fed all the essential oils and lyophilized extract; glutathione S-transferase activity showed no change, and the catalase activity increased statistically in 1000 mg/kg essential oil and 1000 mg/kg lyophilized extract groups. The findings of this study suggested that *O. minutiflorum* could be used in the feed for the rainbow trout considering that the plant extract and essential oils of the plant had positive effects on the nonspecific immune system and antioxidant activity.

KEYWORDS:
Antioxidant, nonspecific immune system, *Origanum minutiflorum*, rainbow trout

INTRODUCTION

Rainbow trout farming is the fastest growing aquaculture system in Turkey, and it is widely cultured as fish species [1]. The main objective of fisheries production is protecting fish health with the highest efficiency. Although disinfectants and antibiotics have been used effectively for many years in treating fish diseases, the use of these substances poses potential risks, such as residual problems in food and development of resistance to microorganisms against antibiotics. Because of these disadvantages, the search for natural feed additives and organic fish farming has focused on plant and plant extracts [2, 3]. Since it is difficult to treat diseases after they emerge in aquaculture, the prophylactic use of natural immunostimulants is a promising method to strengthen the defense mechanisms. Also, many studies have reported that plant extracts increase the resistance against disease and protect meat quality during storage of fish meat due to the antioxidant properties [4].

Origanum species are mostly used in food products and alcoholic beverages as well as perfumery because of their spicy fragrance. They have been of great interest because of antioxidant and antimicrobial activities of their essential oils [5]. *Origanum minutiflorum* (O. Schwarz et. P.H. Davis) is an endemic plant known locally as “Toga kekik,” “Dağ kekik,” or “Çıngıllı kekik” [6]. Although it is used for flavoring of foods and antimicrobial purposes in folk medicine, it is not widely used in Turkey and largely exported to European countries where it is used in spices and animal feed additives to improve performance and protect against diseases [7, 8].

Therefore, this study was performed to investigate the possible effects of different extracts of *O. minutiflorum* on antioxidant enzyme systems, lipid peroxidation, nonspecific immune system, and weight gain in rainbow trout.

MATERIALS AND METHODS

Plant materials and extraction processes. *O. minutiflorum* O. Schwarz et. P.H. Davis plants were collected from Sütçüler and Kesme district of Isparta (37.433683/31.115605, 37.433751/31.117901) at the end of August 2013 in the flowering stage [9]. The plant samples were identified in Gül Herbarium of Süleyman Demirel University with voucher number 94.28.16.04.01. The essential oils of the plant

(EO) were extracted according to the European Pharmacopoeia 5.0. For this purpose, 100 g of the plant was distilled in 2 L of distilled water for 3 h using the Clevenger apparatus, and the essential oils were dried over anhydrous sodium sulfate. For making lyophilized extract (LE) hot water maceration of the plant samples was performed according to the method reported by Teixeira et al. [10]. 50 g of aerial parts of the plant were extracted for 3 h in 1 L of distilled water with continuous stirring at 100°C. After filtering through Whatman (no. 1), the hot water extracts were freeze-dried (lyophilized) at –60°C (Christ, Alpha 2-4 LD plus). The aerial parts of the plant were ground to powder using a high-speed laboratory rotor mill (Ultra Centrifugal Mill ZM-200; Retsch) for making powdered plant (PP).

Preparation of feed. Commercial feed for rainbow trout fry containing 54% protein, 14% lipids, 1.5% cellulose, 11% ash, and 3800 kcal/kg energy was obtained from Çamlı Feed Industry and Trading Company. It was ground to powder and used as base feed. The essential oils were mixed with phosphate-buffered saline (PBS) to obtain a homogenous mixture. Then, 250, 500, and 1000 mg/kg *O. minutiflorum* essential oils (EO) and 250, 500, and 1000 mg/kg lyophilized powder of hot water extract (LE) were mixed with the base feed. The plant's powder (PP) was mixed with the commercial feed at the concentrations of 0.5%, 1%, and 2%. Rainbow trouts were given the prepared feed 2% of their body weight once a day for 8 weeks.

Animals. 150 rainbow trout (40–60 g) were supplied by Sapanca Aquaculture Department, Istanbul University, Turkey. The fish were divided into 10 groups in 250-L aquariums equipped with a continuous–water flow external filter and air supply. Fish were kept for 2 weeks for adaptation. The water of the aquariums was changed with fresh spring water three times a week. Water temperature, pH, chloride levels, nitrite levels, fish behavior, and mortality were followed throughout the experiment. After 2 weeks of adaptation, the fish were given experimental feed 2% of their body weight once a day for 8 weeks [11]. The study was approved by the İstanbul University Animal Experiments Local Ethics Committee (İÜ-HADYEK/2013-89).

Sample collection. After the 8-week feeding period, blood samples from caudal vein and tissue samples were collected under sedation with 25 mg/L benzocaine (Sigma). The liver samples were stored at –80°C until the analyses. Liver tissues were homogenized in cold 20mM PBS (1:9, pH 7.4, 1mM ethylenediaminetetraacetic acid and 0.1% Triton X-100) with ULTRA-TURRAX. After the homogenates were centrifuged at 2000*g* for removing the debris, the supernatants were used for determining the antioxidant activity [12, 13].

Respiratory burst activity [14], lysosomal activity [15], and phagocytic activity [16] were analyzed on the blood sample to evaluate the effects of *O. minutiflorum* on the nonspecific immune systems.

Nonspecific immune system parameters. The total blood was mixed with 150-U heparin/mL in the Eppendorf tubes to determine respiratory burst activity. 275 µl of blood was diluted (1:200) in Hanks' Balanced Salt Solution (0.1% gelatin, 5 U/ml of heparin, 100 I.U./ml of penicillin/streptomycin, 5 µg/ml of oxytetracycline, 0.19 mM luminol, pH 7.4). The samples were put in triplicate into white flat-bottomed enzyme-linked immunosorbent assay (ELISA) plates (Nunc cat. # 236105), which were incubated at room temperature for 10 min for fixing the background. Then, 25 µl of zymosan (Sigma, USA) were added at 5 mg/ml in each well. Chemiluminescence emission was monitored using a ELISA microplate reader at 5-min intervals for 120 min, and maximum chemiluminescence values were expressed as relative lumen unit (RLU) [14].

The serum lysozyme activity was analyzed in accordance with the method developed by Ellis [15]. Then, 0.2 mg/mL lyophilized *Micrococcus lysodeikticus* was prepared in 0.06 M sodium phosphate buffer (pH 6.2). Further, 190 µL of bacterial suspension and 10 µL of plasma were added in triplicates into microplate wells. The decrease in absorbance caused by the lysis of bacteria by lysozymes found in plasma was measured spectrophotometrically in 96-well ELISA plates between 1 and 5 min with 30-s intervals at 450 nm.

Phagocytic activity levels were determined based on the method reported by Ispir [16]. 0.1 mL of PBS containing *Staphylococcus* spp. (1×10^8 cells/mL) was added to 0.1 mL of blood sample. After 30-min incubation, 0.05 mL of the suspension was smeared on a slide. The slides were dried and fixed with ethanol (95%) for 5 min and stained with Giemsa (7%). A total of 100 phagocytes were counted, and the percentage of phagocytosed cells was determined.

Antioxidant parameters. Malondialdehyde (MDA) was analyzed according to the method reported by Zhu et al. [13] using liver samples. After taking 500 µL of homogenate from the liver samples into glass tubes, 400 µL of 15% trichloroacetic acid and 800 µL of thiobarbituric acid (0.67% in 0.3M NaOH) were added. After centrifugation (2000*g*, 4°C, 10 min), the absorbance of supernatants was read at 532 nm using the spectrophotometer (Agilent, Carry 60). MDA concentrations of the samples were determined from a standard curve with thiobarbituric acid, and the results were expressed as µmol MDA/mg protein. Superoxide dismutase (SOD) is an important enzyme that catalyzes the conversion of superoxide anion into hydrogen peroxide and oxygen. The total SOD activity was measured using the

BioVision "SOD Activity Assay Kit" (Cat #K335-100). Liver homogenates were centrifuged at 14000*g* for 5 min at 4°C. The activity of glutathione peroxidase (GPx) was assayed on liver samples using a commercial kit (Cayman, Cat. No. 703102). After centrifuging liver homogenates at 10000*g* for 15 min, the supernatants were assayed for GPx activity in accordance with the commercial kit method, and the 96-well ELISA plate was read at 340 nm using a microplate reader (Molecular Devices, Filtermax F5). The activity of glutathione S-transferase (GST) was measured according to the method described by Habig et al. [17]. 2.5 mL of 120mM potassium phosphate buffer (pH 6.5), 100 µL of glutathione (GSH), 100 µL of 1-chloro-2,4-dinitrobenzene, and 50 µL of the sample were added to the spectrophotometer cuvettes. The absorbance was recorded at 340 nm for 3 min at 20°C, and GST was calculated using 9.6 mM^{-1} cm^{-1} extinction coefficient [17]. Catalase (CAT) activity in liver samples was determined according to the method reported by Cuellar-Cruz et al. [18]. Further, 20 µL of liver supernatant was diluted with 980 µL of phosphate buffer. Then, 1 mL of diluted sample, 1 mL of phosphate buffer, and 1 mL of diluted sample were added to the spectrophotometer cuvettes. The reaction was initiated by adding 1 mL of H_2O_2. After mixing the samples, the change in absorbance was measured at 240 nm. CAT activity values were calculated using the extinction coefficient 0.043 mM^{-1} [18]. One unit of CAT activity was defined as the amount of H_2O_2 decompounded by the enzyme per mg protein of liver. The total protein content of liver samples was determined using the micro Lowry method for determining MDA and enzyme specific activities of GPx, GST, and CAT [19].

Effect on weight performance. The fish were individually weighed in a container filled with water at the beginning and at the end of the experiment. The percentage of weight gain was calculated using the formula 1 [20]. The specific growth rate was determined using the formula 2 according to Company et al. [21]. The specific growth rate was calculated by dividing the natural logarithm of the final weighted average by the experimental day. The condition factor was calculated using the formula 3 according to the method reported by Caballero et al. [22]. The total length was measured between the tip and the end of the long lobe of the tail.

$$(1)\ \text{Weight gain percentage } (\%) = \frac{\text{Final weight (g)} - \text{Initial weight (g)}}{\text{Initial weight (g)}} \text{x} 100$$

$$(2)\ \text{Spesific growth rate, } (\%/\text{day}) = \frac{\text{Ln (Mean of final weight)} - \text{Ln (Mean of initial weight)}}{\text{Total experiment day}} \text{ x } 100$$

$$(3)\ \text{Condition factor (CF)} = [100 \text{ x (Live weight (g) x (Length (cm)}^{1/3}]$$

Statistical analysis. One-way analysis of variance and post hoc tests of Tukey honestly significant difference were performed using SPSS (SPSS, IL, USA) for the statistical evaluation of the results obtained from different groups. The confidence factor was determined as 95%.

RESULTS

Body performance. The yield performance of *O. minutiflorum* lyophilized extracts was found to be 11.50%, and the extraction efficiency of essential oils was determined as 2.4%. The differences in the growth performance and condition factor were not found to be statistically significant between experiment and control groups (Table 1).

Nonspecific immune system parameters. The nonspecific immune system parameters are shown in Table 2. The respiratory burst activity was significantly enhanced in the EO500, EO1000, LE500, and LE1000 groups ($P < 0.05$). Serum lysosomal activities increased in the EO1000 (590.37 U ± 34.21) and EO500 groups (424.81 U ± 19.21), and the differences were statistically significant compared with the control group (294.68 U ± 21.87) ($P < 0.05$). Despite a general increase in serum lysozyme activity in the experimental group fed lyophilized extract and crude plant, the difference was not significant. The phagocytic activities increased significantly in the EO1000 (53.9% ± 2.9), EO500 (49.8% ± 1.1), LE500 (49.9% ±1.3), and LE1000 groups (50.4% ± 1.9), and the differences were statistically significant compared with the control group (37.2% ± 1.8) ($P < 0.05$).

MDA levels and antioxidant enzyme activities. MDA levels of the experiment groups are given as µmol/mg protein in Table 3. A significant decrease in MDA levels was determined as 45.47 µmol/mg ± 5.78 for EO1000, 50.76 µmol/mg ± 5.36 for EO500, and 49.49 µmol/mg ± 6.12 for EO250. The SOD inhibition value was found to be 57.2% ± 3.6 for LE1000 and 54.7% ± 2.2 for EO1000, and the differences were statistically significant compared with the control group ($P < 0.05$). The SOD inhibition value increased in all experimental groups, but the difference was not statistically significant except for LE1000 and EO1000. The GPx activity increased significantly in the EO1000, EO500, EO250, LE1000, LE500, and LE250 groups. The GST enzyme activity of the experimental groups showed no statistically significant change. For the CAT activity, significant differences were found in the EO1000 and LE1000 groups ($P < 0.05$). GST and liver protein levels showed no statistically significant differences between the experimental groups.

TABLE 1
Body performance parameters

Experiment groups	Weight Gain(g)± SE	Condition factor	Specific Growth Percentage (%/day)
Control	84.6 ± 4.2	0.91	1.58
250 mg essential oil/kg feed (EO250)	86.0 ± 3.7	0.95	1.65
500 mg essential oil/kg feed (EO500)	90.1 ± 3.9	0.99	1.61
1000 mg essential oil/kg feed (EO1000)	92.3 ± 5.2	0.96	1.63
250mg lyophilized extract/kg feed (LE250)	77.9 ± 6.2	0.98	1.60
500 mg lyophilized extract/kg feed (LE500)	85.0 ± 7.3	0.98	1.70
1000 mg lyophilized extract/kg feed (LE1000)	84.7 ± 7.3	1.05	1.66
0.5% plant powder/kg feed (PP0.5)	81.6 ± 5.9	0.98	1.58
1% plant powder/kg feed (PP1)	79.4 ± 4.8	0.91	1.62
2% plant powder/kg feed (PP2)	82.5 ± 3.5	0.86	1.63

TABLE 2
Non-specific immune system parameters

Experiment groups	Respiratory burst activity (RLU) ± SD	Lysozyme Activity (unit) ± SE	Phagocytic activity (%) ± SE
Control	10453 ±3511	294.68 ±21.8	37.2 ±1.8
EO250	13925 ±3038	379.64 ±22.6	44.0 ±2.2
EO500	15469 ±3212 *	424.81 ±19.2*	49.8 ±1.1*
EO1000	16623 ±5875 **	590.37 ±34.2 ***	53.9 ±2.9**
LE250	11026 ±4942	338.72 ±37.8	46.7 ±3.9
LE500	15825 ±3448 *	340.00 ±33.5	49.9 ±1.3*
LE1000	15245 ±2691 *	370.78 ±33.1	50.4 ±1.9*
PP0.5	13756 ±3391	337.10 ±33.7	35.0 ±3.0
PP1	12097 ±3695	342.21 ±18.7	41.9 ±3.6
PP2	12542 ±4505	339.10 ±18.2	48.9 ±3.6

*: $P<0.05$ **: $P<0.01$ ***: $P<0.001$ confidence factor 95% One way ANOVA- Tukey HSD Post-Hoc n=15

TABLE 3
Antioxidant Activity Parameters

Experiment group	MDA (µmol/mg protein) ± SE	SOD (% inhibition) ± SE	GPx Activity (U/mg protein) ± SE	GST activity (U/mg protein) ± SE	CAT activity (U/mg protein) ± SE
Control	78.15 ±4.53	40.2 ±2.4	7.62 ±1.34	3.73 ±0.35	10.01 ±0.67
EO250	49.49 ±6.12*	51.1 ±1.8	14.87 ±1.86*	4.48 ±0.40	12.30 ±0.93
EO500	50.76 ±5.36*	50.2 ±1.8	14.84 ±1.13*	4.49 ±0.45	10.24 ±0.50
EO1000	45.47 ±5.78**	54.7 ±2.2*	20.34 ±2.22***	4.57 ±0.52	13.42 ±0.42*
LE250	71.17 ±4.85	52.6 ±0.9	14.37+2.08*	4.16 ±0.45	11.59 ±0.73
LE500	55.18 ±5.67	50.7 ±2.8	15.29 ±1.01*	4.41 ±0.49	12.10 ±0.68
LE1000	52.55 ±5.91*	57.2 ±3.6**	14.89 ±0.96*	4.51 ±0.39	13.26 ±0.56*
PP0.5	80.36 ±6.73	53.4 ±4.9	12.21 ±1.28	3.61 ±0.47	10.91 ±0.79
PP1	71.03 ±4.42	52.8 ±4.5	11.85 ±0.92	3.67 ±0.49	10.45 ±0.92
PP2	75.30 ±5.19	52.7 ±3.6	11.96 ±1.11	3.72 ±0.36	11.20 ±0.66

*: $P<0.05$ **: $P<0.01$ ***: $P<0.001$ confidence factor 95% One way ANOVA- Tukey HSD Post-Hoc n=15

DISCUSSION

The fast development and increasing demands in rainbow trout farming have led to intensive stocking and stress for fish, increasing the risk of disease outbreaks. Enhancement of immunity is one of the most promising methods for preventing fish diseases [23]. As an alternative to chemical use that has multiple environmental and health disadvantages**,** the interest has grown in the prophylactic use of plant products. Plant additives contain active molecules such as alkaloids, terpenoids, saponins, and flavonoids that positively affect weight gain, immune system, and antioxidant activity. In this study, *O. minutiflorum* and its extract and essential oils, which have multiple bioactivities, were evaluated *in vivo* for drawing attention to the use of natural products in fish health. Also, the study aimed to optimize dietary concentrations in the presence of biological effects on growth-promoting, immunostimulant, and antioxidative activities.

Although plant additives generally decrease the growth rate related to the decrease in the protein ratio in the feed, feed additives including *Origanum* species, carvacrol and thymol showed positive effects on growth performance and feed utilization in rainbow trout [24]. The growth-promoting effects of essential oils could be linked to the strong appetizing flavor and increase in the feed intake. It is also suggested that the secretion of digestive enzymes is induced by bioactive compounds, increasing the absorption and consumption of food [25].

O. minutiflorum lyophilized extract and essential oils showed positive effects on growth parameters, but the differences were not found to be statistically significant. Diler et al. reported that the essential oils of *O. vulgare* increased weight performance parameters in rainbow trouts at 1.5, 2.5, and 3 mL/kg concentrations [25]. The highest concentration of essential oils was 1 g/kg in the present study. The concentrations used in this study could be low for growth promotion in fish, and also, it is thought that these differences could be due to different plant species, fish species, composition of the extracts, and physiological differences in different *stages* of fish life cycle. Condition factor is a widely used parameter in evaluating nutrition and growth in fish. Condition factor values were found to be between 0.86 and 1.05 in this study, which were consistent with the values in other studies on rainbow trout [26].

Immunity is of two types: nonspecific and specific. The nonspecific immune system is considered as the first line of defense in fish, which is more important than in mammals [27]. With the activation of nonspecific immune system, phagocytic cells such as neutrophils and macrophages remove bacteria mainly by producing free radicals and reactive oxygen species (ROS) during high oxygen consumption, which is a process called respiratory burst activity [28]. Additionally, neutrophils kill the bacteria by the halogenation of bacterial cell wall or with the help of lysozymes [25].

Respiratory burst activity of macrophages, which is measured as an increase in oxidation levels in phagocytes stimulated by foreign agents, is considered as an important indicator of the nonspecific immunity [29]. The present work also demonstrated that *O. minutiflorum*'s essential oils and lyophilized extract at 500 and 1000 mg/kg concentrations had the ability to enhance the respiratory burst activity of macrophages significantly ($P < 0.05$). The capacity of phagocytic cells to produce superoxide—one of the most potent microbicidal molecules—also increases with the increase in respiratory burst [30]. Superoxide is the precursor of other oxidants, such as H_2O_2 and $OH,^-$ and it has high microbicidal effects [31]. The increase in respiratory burst activity is as an indicator of nonspecific immunostimulant activity at the indicated concentrations of essential oils and lyophilized extract of *O. minutiflorum* [32-34].

Phagocytic activity is a primitive defense mechanism that is generally enhanced by oral administration of immunostimulants [3, 35]. Because phagocytes act as dominant defense cells, an enhancement of phagocyte function is expected to cause an increase in the resistance against microbial infections [36]. The increase in phagocytic activity in the EO500, EO1000, LE500 and LE1000 groups was found to be consistent with that in the other *Origanum* species [32, 37].

Lysozyme, which is secreted by leukocytes, is accepted as the humoral component of nonspecific defense that prevents the growth of bacteria by hydrolysis of β-1,4-glycosidic bonds of bacterial cell wall peptidoglycan. Serum lysozyme levels of EO500 and EO1000 increased significantly in the present study ($P < 0.05$). Lysozyme is accepted as a marker of leukocyte activity, which increases together with phagocytic activity [38]. In this study, the augmentation of lysozyme activity in fish fed essential oils (EO500 and EO1000) resulted from the increment in the number of phagocytic cells and their stimulation, leading to the secretion of more lysozymes, as in the case of most immunostimulants [39, 40]. Yılmaz et al. [41] reported that lysozyme levels in rainbow trout improved with the dietary supplementation of carvacrol. As a major component of essential oil, carvacrol is thought to be responsible for the increase in lysozyme activity [42].

The plant extract and essential oils used in this study could increase the immunological capacity of fish by enhancing respiratory burst activity, phagocytosis, and lysozyme activity. Also, the ethanolic percolation extract of *O. vulgare* has been reported to increase respiratory burst and lysosomal and phagocytic activities activity [32, 37]. Similar studies in tilapia have shown that carvacrol, thymol, and major components of the essential oils of

oregano can augment immunity directly with the primary immunostimulant effect on the host tissue or adjust microbial changes via immunity-relieving effects. Oral administration of *O. minutiflorum* essential oils and lyophilized extract to rainbow trouts led to an immunostimulant activity in parallel with one or more phytoconstituents including carvacrol, thymol, α- terpinene, γ-terpinene, *p*-cymene, and borneol [9]. These phytoconstituents, especially found in essential oils alone or synergistically, might activate the nonspecific immune system by not only acting on receptors on the cell surface and triggering gene activation with the primary immunostimulant effect on the host tissue but also adjusting microbial changes via immunity-relieving effects that can increase immune response such as respiratory burst and phagocytic and lysozyme activities [43]. However, it has been found that the crude plant does not have growth-promoting, immunostimulant, and antioxidant effects on its own, which might be related to the fact that the concentrations of active ingredients in the crude plant are not sufficient to stimulate nonspecific immune activity.

Immune system cells contain a high percentage of polyunsaturated fatty acids in their cell membranes. As part of immune system functions especially phagocytosis and respiratory burst, the cells are exposed to high levels of ROS that damage inhibit the expression of membrane-related signaling and gene expression which participate in normal functions of the cells and protection against foreign antigens [44]. Fish are highly susceptible to oxidative stress due to the richness of polyunsaturated fatty acids. Thus, lipid peroxidation is a basic cellular deterioration process induced by oxidative stress, leading to a decrease in the overall quality of health and meat quality [45, 46]. In relation to the immune system with the antioxidant defense, the antioxidant activity in the liver was evaluated. The liver was chosen as the specimen because it is the site of multiple oxidative reactions and it has the highest SOD and CAT activities among all tissues [47]. Malondialdehyde (MDA) level is a widely used parameter for determining lipid peroxidation in tissues [48]. MDA levels decreased in a concentration-dependent manner in liver samples from groups treated with all concentrations of essential oils and 1000 mg/kg lyophilized extract. Terenina et al. [49] suggested that carvacrol and thymol are the components responsible for the antioxidant activity of *Origanum* essential oil. Phenolic substances such as carvacrol and thymol in the essential oils and lyophilized extract are considered to counteract oxidative stress by neutralizing free radicals, blocking peroxidation catalysis by iron, chain-breaking activity, and radical-scavenging effect [9, 50, 51].

The antioxidant enzymes highly important for aquatic organisms are SOD, CAT, and enzymes dependent on glutathione such as GPx, glutathione reductase, or GST [46]. SOD is an enzyme that catalyzes the dismutation of superoxide radicals into oxygen and hydrogen peroxide. Although the SOD activity increased in all the experimental groups, the activities for only EO1000 and LE1000 were found to be significantly different ($P < 0.05$). The dietary use of *O. heracleoticum* essential oil has been reported to increase SOD, CAT, and lysozyme activities in channel catfish [8]. The increased SOD activity could be related to the increase in a respiratory burst in which reactive superoxide anions were excessively produced in the EO1000 and LE1000 groups. GPx is involved in protection against oxidative stress by degrading hydrogen peroxide together with the catalase enzyme. It was determined that a significant increase in liver GPx activity was observed in the groups given feeds containing all concentrations of essential oils and lyophilized extract. The catalase enzyme (CAT), together with GPx, catalyzes the conversion of hydrogen peroxide into oxygen and water. When CAT in the liver tissue was examined, a statistically significant increase was observed in the EO1000 and LE1000 groups fed essential oils compared with the control group, but the increases in the other groups were not statistically significant. Increases in liver GPx occurring in *O. minutiflorum* essential oil and lyophilized extract groups could be due to radical-scavenging effects of chemical components and protection of the levels of enzymatic antioxidants that are inactivated by ROS. Giao et al. [52] and Urso and Clarkson [53] suggested that the unchanged CAT activity was the result of increased GPx activity. YEH et al. [54] showed that phenolic acid supplement increased mRNA expression levels of SOD, GPx, and CAT in liver tissues in rats.

Briefly, essential oil and lyophilized extract supplementation showed improvements in antioxidant activity directly with antioxidant effect or indirectly increased the activity or expression of antioxidant enzymes. It is suggested that phenolic compounds and flavonoids of essential oils play an important role in antioxidant activity, and the antioxidant activity may result from carvacrol, thymol, rosmarinic acid, and polyphenols present in essential oils and water extract of *Origanum* [55].

CONCLUSIONS

The present study suggested that feeding rainbow trouts with feeds containing essential oils or lyophilized extract of *O. minutiflorum* at the concentrations of 500 and 1000 mg/kg for 8 weeks could increase nonspecific immune system parameters and antioxidant activity. Since this activity can not only be linked to the basic chemical components and the chemical components in the essential oils and lyophilized extract may act synergistically, further studies are needed to determine the efficacy in experimental

infections under field conditions and reveal the responsible components.

ACKNOWLEDGEMENTS

This work was supported by Scientific Research Projects Coordination Unit of Istanbul University. Project number 38930.

REFERENCES

[1] TUIK (2013) Fishery Statistics. Turkish Statistical Institute, Publication Number: 4349.
[2] Gabor, E.F., Ichim, O. and Şuteu, M. (2012) Phyto-additives in rainbow trout (Oncorhynchus mykiss) nutrition. Biharean biol. 6, 134-139.
[3] Siwicki, A.K., Morand, M., Klein, P., Studnicka, M. and Terech-Majewska, E. (1998) Modulation of nonspecific defence mechanisms and protection against diseases in fish. Acta Vet Brno. 67, 323-328.
[4] Citarasu, T. (2010) Herbal biomedicines: a new opportunity for aquaculture industry. Aquaculture International. 18, 403-414.
[5] Altundağ, S., Aslım, B. and Öztürk, S. (2011) In vitro antimicrobial activities of essential oils from Origanum minutiflorum and Sideritis erytrantha subsp. erytrantha on phytopathogenic bacteria. JEOR. 23, 4-8.
[6] Vardar-Ünlü, G., Ünlü, M., Dönmez, E. and Vural, N. (2007) Chemical composition and in vitro antimicrobial activity of the essential oil of Origanum minutiflorum O Schwarz & PH Davis. J Sci Food Agric. 87, 255-259.
[7] Walter, B. and Bilkei, G. (2004) Immunostimulatory effect of dietary oregano etheric oils on lymphocytes from growth-retarded, low-weight growing-finishing pigs and productivity. Tijdschr Diergeneeskd. 129, 178-181.
[8] Zheng, Z.L., Tan, J.Y.W., Liu, H.Y., Zhou, X.H., Xiang, X. and Wang, K.Y. (2009) Evaluation of oregano essential oil (Origanum heracleoticum L.) on growth, antioxidant effect and resistance against Aeromonas hydrophila in channel catfish (Ictalurus punctatus). Aquaculture. 292, 214-218.
[9] Baydar, H. (2005) Yayla kekiği (Origanum Minutiflorum O. Schwarz Et. Ph Davis)'nde farklı toplama zamanlarinin uçucu yağ içeriği ve uçucu yağ bileşenleri üzerine etkisi. Akdeniz Univ Zir Fak Dergi. 18, 175-178.
[10] Teixeira, B., Marques, A., Ramos, C., Serrano, C., Matos, O., Neng, N.R., Nogueira, J.M.F., Saraiva, J.A. and Nunes, M.L. (2013) Chemical composition and bioactivity of different oregano (Origanum vulgare) extracts and essential oil. J Sci Food Agric. 93, 2707-2714.
[11] Anlaş, C. and Üstüner, O. (2016) Genotoxic assessment of amoxicillin in rainbow trout (Oncorhynchus mykiss) by comet assay and micronucleus test. Fresen. Environ. Bull. 25, 5358- 5364.
[12] Sargent, J.R., Tocher, D.R. and Bell, J.G. (2003) The Lipids. In: Halver, J.E. and Hardy, R.W. (Eds.) Fish Nutrition. 3rd ed, Elsevier, California, 181-257.
[13] Zhu, Y., Chen, Y., Liu, Y., Yang, H., Liang, G. and Tian, L. (2012) Effect of dietary selenium level on growth performance, body composition and hepatic glutathione peroxidase activities of largemouth bass Micropterus salmoide. Aquac Res. 43, 1660-1668.
[14] Rigos, G., Samartzis, A., Henry, M., Fountoulaki, E., Cotou, E., Sweetman, J., Davies, S. and Nengas, I. (2010) Effects of additive iron on growth, tissue distribution, haematology and immunology of gilthead sea bream, Sparus aurata. Aquac Int. 18, 1093-1104.
[15] Ellis, A.E. (1990) Lysozyme assays. In: Stolen J.S., Fletcher D.P., Anderson B.S. and Roberson B.S. (Eds.) Techniques in fish immunology. 1st ed, SOS Publications, New Jersey, 101-103.
[16] İspir, U. and Yonar, M.E. (2007) Effects of levamisole on phagocytic activity of rainbow trout (Oncorhynchus mykiss W.). Acta Vet Brno. 76, 493-497.
[17] Habig, W.H., Pabst, M.J. and Jakoby, W.B. (1974) Glutathione S-transferases the first enzymatic step in mercapturic acid formation. J Biol Chem. 249, 7130-7139.
[18] Cuéllar-Cruz, M., Castaño, I., Arroyo-Helguera, O. and De Las Peñas, A. (2009) Oxidative stress response to menadione and cumene hydroperoxide in the opportunistic fungal pathogen Candida glabrata. Mem Inst Oswaldo Cruz. 104, 649-654.
[19] Lowry, O.H., Rosebrough, N.J., Farr, A.L. and Randall, R.J. (1951) Protein measurement with the Folin phenol reagent. J Biol Chem. 193, 265-275.
[20] Saether, B.S. and Jobling, M. (1999) The effects of ration level on feed intake and growth, and compensatory growth after restricted feeding, in turbot Scophthalmus maximus L. Aquacult Res. 30, 647-653.
[21] Company, R., Calduch-Giner, J.A., Kaushik, S. and Pérez-Sánchez, J. (1999) Growth performance and adiposity in gilthead sea bream (Sparus aurata): risks and benefits of high energy diets. Aquaculture. 171, 279-292.

[22] Caballero, M.J., Obach, A., Rosenlund, G., Montero, D., Gisvold, M. and Izquierdo, M.S. (2002) Impact of different dietary lipid sources on growth, lipid digestibility, tissue fatty acid composition and histology of rainbow trout, Oncorhynchus mykiss. Aquaculture. 214, 253-271.

[23] Harikrishnan, R., Balasundaram, C., Kim, M.-C., Kim, J.-S., Han, Y.-J. and Heo, M.-S. (2009) Innate immune response and disease resistance in Carassius auratus by triherbal solvent extracts. Fish Shellfish Immunol. 27, 508-515.

[24] Giannenas, I., Triantafillou, E.l., Stavrakakis, S., Margaroni, M., Mavridis, S., Steiner, T. and Karagouni, E. (2012) Assessment of dietary supplementation with carvacrol or thymol containing feed additives on performance, intestinal microbiota and antioxidant status of rainbow trout (Oncorhynchus mykiss). Aquaculture. 350, 26-32.

[25] Diler, Ö., Görmez, Ö., Metin, S., İlhan, İ. and Diler, İ. (2017) Origanum vulgare L. uçucu yağının gökkuşağı alabalıkları (Oncorhyncus mykiss)'nda büyüme, lizozim ve antioksidan aktivite ve Vibrio anguillarum'a karşı direnç üzerine etkisi. SDÜ Eğirdir Su Ür Fak Der. 13, 42-57.

[26] Özoğul, Y. (2000) The possibility of using crustacean waste products (CWP) on rainbow trout (Oncorhynchus mykiss) feeding. Turk J Biol. 24, 845-854.

[27] Jothi, G.E.G., Deivasigamani, B., Priyadarshini, P., Kumaran, S., Balamurugan, S., Rajasekar, T. and Sakthivel, M. (2012) Immune response against Aeromonas Hydrophila in estuarine catfish (Mystus Gulio, Hamilton 1822) Ofkollidam Estuary: an assessment on Non Specific Immune Parameters. IJFB. 2, 1-7.

[28] Bulfon, C., Volpatti, D. and Galeotti, M. (2014) Modulation of respiratory burst and proliferation activity of rainbow trout (Oncorhynchus mykiss) head kidney leukocytes by medicinal plant extracts, University of Udine, Fish Pathology Division, Department of Food Science, Udine

[29] Akhlaghi, M., Hoseini, A., Nematollahi, A. and Hoseini, S.M. (2011) Humoral and non-specific immune responses in rainbow trout (Oncorhynchus mykiss) naturally exposed to and immunized with Streptococcus iniae. IJVM. 5, 218-224.

[30] Secombes, C.J. and Fletcher, T.C. (1992) The role of phagocytes in the protective mechanisms of fish. Annu Rev Fish Dis. 2, 53-71.

[31] Sharp, G.J.E. and Secombe, C.J. (1993) The role of reactive oxygen species in the killing of the bacterial fish pathogen Aeromonas salmonicida by rainbow trout macrophages. Fish Shellfish Immunol. 3, 119-129.

[32] Pourmoghim, H., Haghighi, M. and Rohani, M.S. (2015) Effect of dietary inclusion of Origanum vulgare extract on non-specific immune responses and hematological parameters of rainbow trout (Oncorhynchus mykiss). Bull Env Pharmacol Life Sci. 4, 33-39.

[33] Soltani, M., Sheikhzade, N., Ebrahimzad, H.A. and Zargar, A. (2010) Effects of Zataria multiflora essential oil on innate immune responses of common Carp (Cyprinus carpio). J Fish Aquat Sci. 5, 191-199.

[34] Sheikhzadeh, N., Soltani, M., Ebrahimzadeh-Mousavi, H.A., Shahbazian, N. and Norouzi, M. (2011) Effects of Zataria multiflora and Eucalyptus globolus essential oils on haematological parameters and respiratory burst activity in Cyprinus carpio. Iran J Fish Sci. 10, 316-323.

[35] Neumann, N.F., Stafford, J.L., Barreda, D., Ainsworth, A.J. and Belosevic, M. (2001) Antimicrobial mechanisms of fish phagocytes and their role in host defense. Dev Comp Immunol. 25, 807-825.

[36] Wang, T., Sun, Y., Jin, L., Xu, Y., Wang, L., Ren, T. and Wang, K. (2009) Enhancement of non-specific immune response in sea cucumber (Apostichopus japonicus) by Astragalus membranaceus and its polysaccharides. Fish Shellfish Immunol. 27, 757-762.

[37] Haghighi, M. and Rohani, M.S. (2015) Non-Specific immune responses and heamatological parameters of rainbow trout (Oncorhynchus mykiss) fed with Origanum Vulgare extract diets. AAJBS. 1, 1-9.

[38] Paulsen, S.M., Engstad, R.E. and Robertsen, B. (2001) Enhanced lysozyme production in Atlantic salmon (Salmo salar L.) macrophages treated with yeast β-glucan and bacterial lipopolysaccharide. Fish Shellfish Immunol. 11, 23-37.

[39] Amar, E.C., Kiron, V., Satoh, S. and Watanabe, T. (2004) Enhancement of innate immunity in rainbow trout (Oncorhynchus mykiss Walbaum) associated with dietary intake of carotenoids from natural products. Fish Shellfish Immunol. 16, 527-537.

[40] Sakai, M. (1999) Current research status of fish immunostimulants. Aquaculture. 172, 63-92.

[41] Yılmaz, E., Ergün, S. and Yılmaz, S. (2015) Influence of carvacrol on the growth performance, hematological, non-Specific immune and serum biochemistry parameters in rainbow trout (Oncorhynchus mykiss). Food Nutr Sci. 06, 523-531.

[42] Can Başer, K.H. (2008) Biological and pharmacological activities of carvacrol and carvacrol bearing essential oils. Curr Pharm Des. 14, 3106-3119.

[43] Sutili, F.J., Gatlin, D.M., Rossi, W., Heinzmann, B.M. and Baldisserotto, B. (2016) In vitro effects of plant essential oils on non-specific immune parameters of red drum, Sciaenops ocellatus L. J Anim Physiol Anim Nutr. 100, 1113-1120.
[44] Nootash, S., Sheikhzadeh, N., Baradaran, B., Oushani, A.K., Moghadam, M.R.M., Nofouzi, K., Monfaredan, A., Aghebati, L., Zare, F. and Shabanzadeh, S. (2013) Green tea (Camellia sinensis) administration induces expression of immune relevant genes and biochemical parameters in rainbow trout (Oncorhynchus mykiss). Fish Shellfish Immunol. 35, 1916-1923.
[45] Chaiyapechara, S., Casten, M.T., Hardy, R.W. and Dong, F.M. (2003) Fish performance, fillet characteristics, and health assessment index of rainbow trout (Oncorhynchus mykiss) fed diets containing adequate and high concentrations of lipid and vitamin E. Aquaculture. 219, 715-738.
[46] Martínez-Álvarez, R.M., Morales, A.E. and Sanz, A. (2005) Antioxidant defenses in fish: biotic and abiotic factors. Rev Fish Biol Fish. 15, 75-88.
[47] Sağlam, D., Atlı, G., Doğan, Z., Baysoy, E., Gürler, C., Eroğlu, A. and Canlı, M. (2014) Response of the antioxidant system of freshwater fish (Oreochromis niloticus) exposed to metals (Cd, Cu) in differing hardness. Turk J Fish Aquat Sci. 14, 43-52.
[48] Giera, M., Lingeman, H. and Niessen, W.M.A. (2012) Recent advancements in the LC- and GC-based analysis of malondialdehyde (MDA): A brief overview. Chromatographia. 75, 433-440.
[49] Terenina, M.B., Misharina, T.A., Krikunova, N.I., Alinkina, E.S., Fatkulina, L.D. and Vorob'yova, A.K. (2011) Oregano essential oil as an inhibitor of higher fatty acid oxidation. Appl Biochem Microbiol. 47, 445-449.
[50] Cervato, G., Carabelli, M., Gervasio, S., Cittera, A., Cazzola, R. and Cestaro, B. (2000) Antioxidant properties of oregano (Origanum vulgare) leaf extracts. J Food Biochem. 24, 453-465.
[51] Amarowicz, R., Żegarska, Z., Rafałowski, R., Pegg, R.B., Karamać, M. and Kosińska, A. (2009) Antioxidant activity and free radical-scavenging capacity of ethanolic extracts of thyme, oregano, and marjoram. Eur J Lipid Sci Technol. 111, 1111-1117.
[52] Gião, M.S., Pestana, D., Faria, A., Guimarães, J.T., Pintado, M.E., Calhau, C., Azevedo, I. and Malcata, F.X. (2010) Effects of extracts of selected medicinal plants upon hepatic oxidative stress. J Med Food. 13, 131-136.
[53] Urso, M.L. and Clarkson, P.M. (2003) Oxidative stress, exercise, and antioxidant supplementation. Toxicology. 189, 41-54.
[54] Yeh, C.-T. and Yen, G.-C. (2006) Induction of hepatic antioxidant enzymes by phenolic acids in rats is accompanied by increased levels of multidrug resistance–associated protein 3 mRNA expression. J Nutr. 136, 11-15.
[55] García-Beltrán, J.M. and Esteban, M.A. (2016) Properties and applications of plants of Origanum Sp. Genus. SM. J Biol. 2, 1006.

Received: **01.08.2017**
Accepted: **04.12.2017**

CORRESPONDING AUTHOR

Ataman Bilge Sari
Department of Veterinary Pharmacology
and Toxicology
Istanbul University,
Faculty of Veterinary Medicine,
34320, Avcılar, Istanbul – Turkey

e-mail: atamanbilge.sari@istanbul.edu.tr

© by PSP Volume 27 – No. 2/2018 pages 1022-1030 Fresenius Environmental Bulletin

METHANE OXIDATION BACTERIA COMMUNITY STRUCTURES IN NANLING MOUNTAIN FOREST SOIL OF CHINESE CLIMATIC ECOTONE

Lile Zeng[1,2,3], Huai Chen[1,*], NingWu[1,4], Zhiying Yan[5], Linfang Du[2], Yan Shen[6], Xu Wang[7], Jianqing Tian[8], Yunpeng Luo[9], Wei Li[1,3], Yixin He[1], Dan Zhu[1]

[1]Key Laboratory of Mountain Ecological Restoration and Bioresource Utilization & Ecological Restoration Biodiversity Conservation Key Laboratory, Chengdu Institute of Biology (CIB), Chinese Academy of Sciences (CAS), Chengdu 610041, China
[2]College of Life Sciences, Sichuan University, Chengdu 610064, China
[3]University of Chinese Academy of Sciences, Beijing 100049, China
[4]International Centre for Integrated Mountain Development, GPO Box 3226, Khumaltar, Kathmandu, Nepal
[5]Key Laboratory of Environmental and Applied Microbiology, CIB, CAS, Chengdu 610041, China
[6]Central South University of Forestry and Technology, Changsha 410004, China
[7]Research Institute of Tropical Forestry, Chinese Academy of Forestry, Guangzhou 510520, China
[8]Institute of Microbiology, CAS, Beijing 100101, China
[9]Northwest Agriculture and Forestry University, Yangling 712100, China

ABSTRACT

Microbial oxidation is regarded as the only biological sink for atmospheric methane (CH_4). The operators of methane oxidation in forest soils are still poorly understood, especially for forests in China. This study investigated the soils from Nanling Mountain forest near the Tropic of Cancer. All together 10 OTUs (Operational Taxonomic Unit) were obtained, with the ratio of type I /type II methanotrophs higher in the forest soil of south plot (~1.6) than that of the north plots (0-0.9). *Methylocaldum*, *Methylobacter*-like /Upland Soil Cluster α Rold1 (USCα R1), Tropical Upland Soil Cluster1 (TUSC1) dominate methane oxidation bacteria (MOB) community. Among them USCα contributed a bigger part in the north plots (about 50%) comparing with south plot (about 7%). The *pmo*A genes of dominant *Methylocaldum* MOB and those closely related to sequences of *Methylocystis* and *Methylosinus* MOB were detected in the south plot did not in the north plots. USCα R1, USCα R3 and *Methylobacter*-like methanotrophs tended to prefer soil environment of higher acidity. On the contrary, Upland Soil Cluster γ methanotrophs tended to prefer neutral comparatively easier. The Shannon diversity index of methanotrophic community was positively related to pH but negatively related to bulk density ($P < 0.05$ for both), and the Simpson diversity index showed the similar tendency. The results indicate that there is heterogeneity of methanotrophic community in the Nanling climatic transition region.

KEYWORDS:
CH_4 oxidation, Forests soil, Methanotrophic community, *Methylocaldum*, climatic transition

INTRODUCTION

Methane (CH_4) is a powerful long-lived greenhouse gas, with 25 times Global Warming Potential to carbon dioxide (CO_2) during the time horizon of 100 years. The atmospheric CH_4 concentration began to rise severely since the start of the industrial era reaching 260% of that level, to a new high of 1813 ppb in 2012 [1], due to an increasing imbalance between the production and consumption of CH_4 [2].

Soils provide the largest terrestrial CH_4 sink [3]. Among them, forest soil that covers about 30% of Earth's land surface accounts for about 60% of terrestrial CH_4 sink through oxidization by methanotrophic bacteria in forest soils [4, 5]. CH_4 consumption is reported to be seriously decreased by destruction of native woodland [3, 6], but increased by forestation [3, 7]. China has the biggest area of planted forest and contributes the biggest increasing forest area from 1990-2010 in the world [8]. The sink of forest in China was estimated as 0.675 Tg CH_4 yr^{-1} [9].

However, compared with many studies about methanotrophs in forest soil of Europe and North America [10, 11] , very little study has paid attention to the soil methane oxidation about forests in China. Researches about methane consumption in forest soil are mostly related to its temporal flux [12], spatial character [13] and influencing factors [14, 15]. So far we are lacking in understanding of the reactors (methanotrophs) and mechanism of this process. Methanotrophs are the key role of methane oxidation, usually classified as Type I and Type II, based on intermembrane pattern and physiological characteristics [16]. The main difference between the two types lies in the carbon assimilation strategy. So far to the best of our knowledge, only three studies were concerned about methanotrophs in

Chinese forest soil at the Changbai Mountain [17], Tianshan [18] and Shengnongjia [19]. both didn't tell apart which kinds of methanotrophs these communities are consist of.

The Nanling Mountains are located in the middle and south subtropical transition region and are the watershed of the Yangtze and Pearl River systems. Because of its position near the Ocean, there are abundant of heat, light, and water resources [20]. Therefore, forests in this region deserve research attention with respect to climate change [21]. Nanling Mountainous forest is located in an area near the Tropic of Cancer, of which a large part is covered by deserts globally. The Eastern Humid and Semi-humid Domains where it is located in account for about 82% of the whole forest CH_4 uptake of China [9].

This study hoped to give the original and direct presentation about the structure of methanotrophic community in this transitional forest soil of China. The objective of this study was to understand the characteristics of methanotrophic community in forest soil of the Nanling mountain forest and possible differences in methanotrophic communities in the north and south parts of Nanling Mountain in the special climatic ecotone.

MATERIALS AND METHODS

Site description and soil sampling. The experiment sites are located in the Nanling Mountain of subtropical monsoon climate. Our sites are dominated by tree species of *Catanopsis eyrei* Tutch, *Catanopsis fargesii* Franch, *Loropetalum chinense* Oliv and *Pinus kwangtungensis*. We chose three forest plots (24°56-58′ N, 112°55-59′ E) with details shown in Table 1 and Figure 1. Among the three plots, Plot N was in the north part of Nanling Mountain, covered by coniferous forest; the other two plots (Plot M and S) were set in the broadleaf forest. Soil samples to the depth of 15 cm were collected in early November 2013. The samples were placed in an ice box and transported to the laboratory for immediate processing. The remaining samples were stored in -20°C refrigerator.

Soil characteristics test. Soil pH was determined with a ratio of 2:5 (W/V) of soil to 1 mol/L KCl. Soil samples were tested for total carbon and nitrogen by vario MACRO cube Elemental Analyzer. Gravimetric soil moisture was determined by drying soil samples for 48 h at 105°C.

WFPS (%) $=\omega \times W_S/(1-W_S/S_S)$, ω (kg kg^{-1}) is gravimetric soil moisture, Ws (Mg m^{-3}) is bulk density, and S_S (2.6 mg m^{-3}) is particle density, based on the quartz [22].

DNA extraction and clone libraries. Soil total DNA was extracted with the E.Z.N.A™ soil DNA kit according to the instructions of manufacturer and was collected in 80 μl Elution Buffer. The concentration of DNA was tested by NanoDrop 2000 (Thermo, Scientific).

Semi-nested PCR amplification method [23] was adopted to amplify the *pmo*A gene fragments which as the functional gene encode the methane monooxygenase (MMO). Primer A189, A682 and mb661 [24, 25] were used in PCR. Amplicons of the correct size purified by cycle-pure kit (Omega) were analyzed by RFLP (Restriction Fragment Length Polymorphism). Purified amplicons were digested by MspI /HpaII (Thermo, Scientific, Germany) at 37°C for 3h and inactivated at 65°C [26]. The products were analyzed through a 2% (w/v) agarose gel electrophoresis.

For all libraries, at least 10% *pmo*A clones within each OTU were sequenced (>500 bp) to verify that the restriction pattern represented a single sequence type [27]: DNA sequences of multiple clones from each library and OTU were >93% identical [28].

Statistics and calculations. The SAS software (Version 9.1) was applied for statistical analyses. Results of analysis of variance (ANOVA) and correlation analysis (Spearman) were regarded statistically significant when $P<0.05$.

The coverage of clone library (C) was calculated using the equation: $C = [1- (n/N_t)] \times 100$. Where n is the number of OTU containing only one *pmo*A gene sequence; N_t is the total number of sequences analyzed.

TABLE 1
Environment and soil physicochemical properties of the plots

Plot	Forest type	Altitude /m	pH	TN (%)	TC (%)	Moisture m/M	Bulk density g.cm^{-3}	WFPS
S	Broadleaf	1300	3.75±0.09^{a}	0.66±0.07^{a}	6.34±0.89^{a}	0.52±0.02^{a}	0.58±0.09^{a}	0.39±0.10^{b}
M	Broadleaf	1300	3.11±0.27^{b}	0.39±0.09^{b}	4.52±1.74^{b}	0.43±0.21^{a}	1.11±0.29^{a}	0.79±0.02^{a}
N	Coniferous	800	3.58±0.06^{ab}	0.36±0.05^{b}	4.92±0.79^{b}	0.29±0.02^{a}	0.82±0.05^{a}	0.40±0.06^{b}

S: southern plot of Nanling; M: plot 1 of mangshan at northern Nanling; N: plot 2 of mangshan at northern Nanling. Each plot has two- four replicate samples. Lowercase letters indicate significant difference ($P < 0.05$).

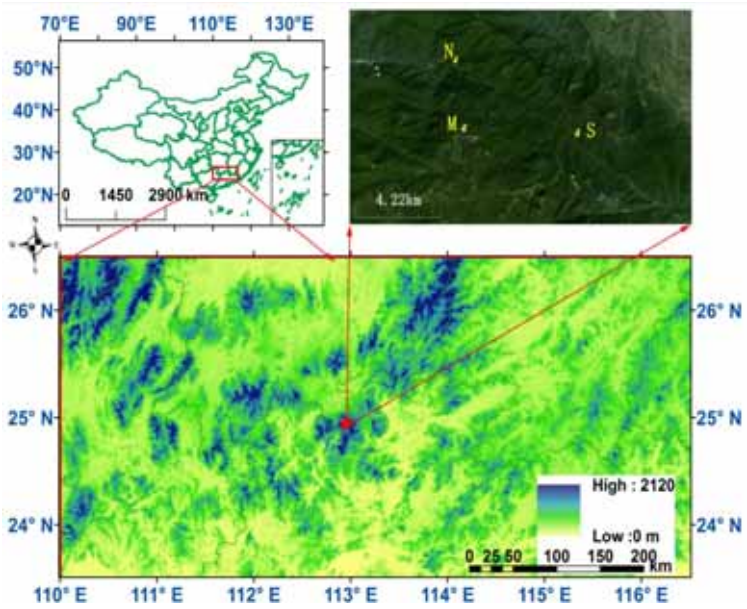

FIGURE 1
Geographical site of experimental plots. The data set is provided by International Scientific & Technical Data Mirror Site, Computer Network Information Center, Chinese Academy of Sciences and Google Earth.

The Shannon diversity index (*H'*) and Gini-Simpson diversity index (*D*) were used to portray the diversity and probability of interspecific encounter of methanotrophic community:

$$H' = -\sum_{i=1}^{S} p_i \ln p_i \, , \; D = 1 - \sum_{i=1}^{S} p_i^2 \, , \; p_i = N_i / N_t,$$

Where N_t is the total number of individuals in the samples and N_i is the number of OTU i in the samples.

The Canonical correspondence analysis (CCA) ordination patterns of *pmo*A gene were applied using CANOCO for Windows 4.5 software (Microcomputer Power, Ithaca, NY).

RESULTS AND DISCUSSION

Soil physical and chemical characteristics. The total nitrogen and carbon of forest soil in the south plot of Nanling Mountain were significantly higher than the north plots ($P< 0.05$). At the same altitude of 1300 m, the pH and WFPS of soil between the north and south parts of Nanling Mountain were also significantly different ($P< 0.05$). However, other environmental factors did not show significant difference among the three sampling plots.

Clone libraries and RFLP. One clone library of methanotrophic community *pmo*A gene was constructed for each plot, containing 60 clones for S, 52 clones for M, and 48 clones for N. RFLP Analysis showed that there were 7 OTUs in S, 3 OTUs in M, 3 OTUs in N. Both γ- and α- subclasses of the Proteobacterial methanotrophs in samples of soil taken from Nanling Mountain were identified (Figure 2).

Analysis of derived PmoA sequences showed that the methanotrophic community consist of *Methylocaldum*, *Methylobacter*-like, Upland Soil Cluster α Rold1 (USCα R1), *Methylocystis*, Upland Soil Cluster α Rold3 (USCα R3), Methylocystaceae (*Methylocystis* or *Methylosinus*-like), USCγ (Upland Soil Cluster γ), SCα (Soil Cluster α), and other uncultured soil methanotrophs cluster, such as: TUSC1 and TUSC2 (Tropical Upland Soil Cluster 1 and 2) (Figure 2). The sequences of the *pmo*A gene from the representative clones based on RFLP in this study were deposited in NCBI database (accession numbers KR139764-139780).

The relative abundances of the methanotrophic community members were estimated using RFLP analysis. The dominant groups were different in different plots. *Methylocaldum*, *Methylobacter*-like/ USCα R1 and TUSC1 were the dominant methanotrophs in each plots respectively. The *pmo*A genes of dominant *Methylocaldum* MOB and those closely related genera of MOB (*Methylocystis*, *Methylosinus*) found in Plot S were not present in the plots in northern Nanling Mountain. USCα contributed a bigger proportion in the northern plots than the southern plot of Nanling Mountain. Most of the Type I cultured MOB were very scarce in Plot N, but at least a half in the communities of the other two plots (Figure 3).

The Shannon index and Gini-Simpson index was 1.30 and 0.63 in Plot S, 0.77 and 0.52 in Plot M,

0.99 and 0.59 in Plot N respectively. There seemed to be a tendency of diversity index decreasing with the lowering of pH and moisture (P<0.05). On the contrary, the diversity index showed an increasing tendency with the lowing of bulk density.

CCA analysis. As seen in the CCA analysis, all the Type I methane-oxide bacteria distributed below the first CCA axis. Each environment factor had almost equal influence to the methanotrophic community. USCα R1, *Methylobacter*-like MOB and USCα R3 seemed to prefer living in more acid soil environment. On the contrary, Upland Soil Cluster γ tended to show in soils of neutral pH (Figure 4).

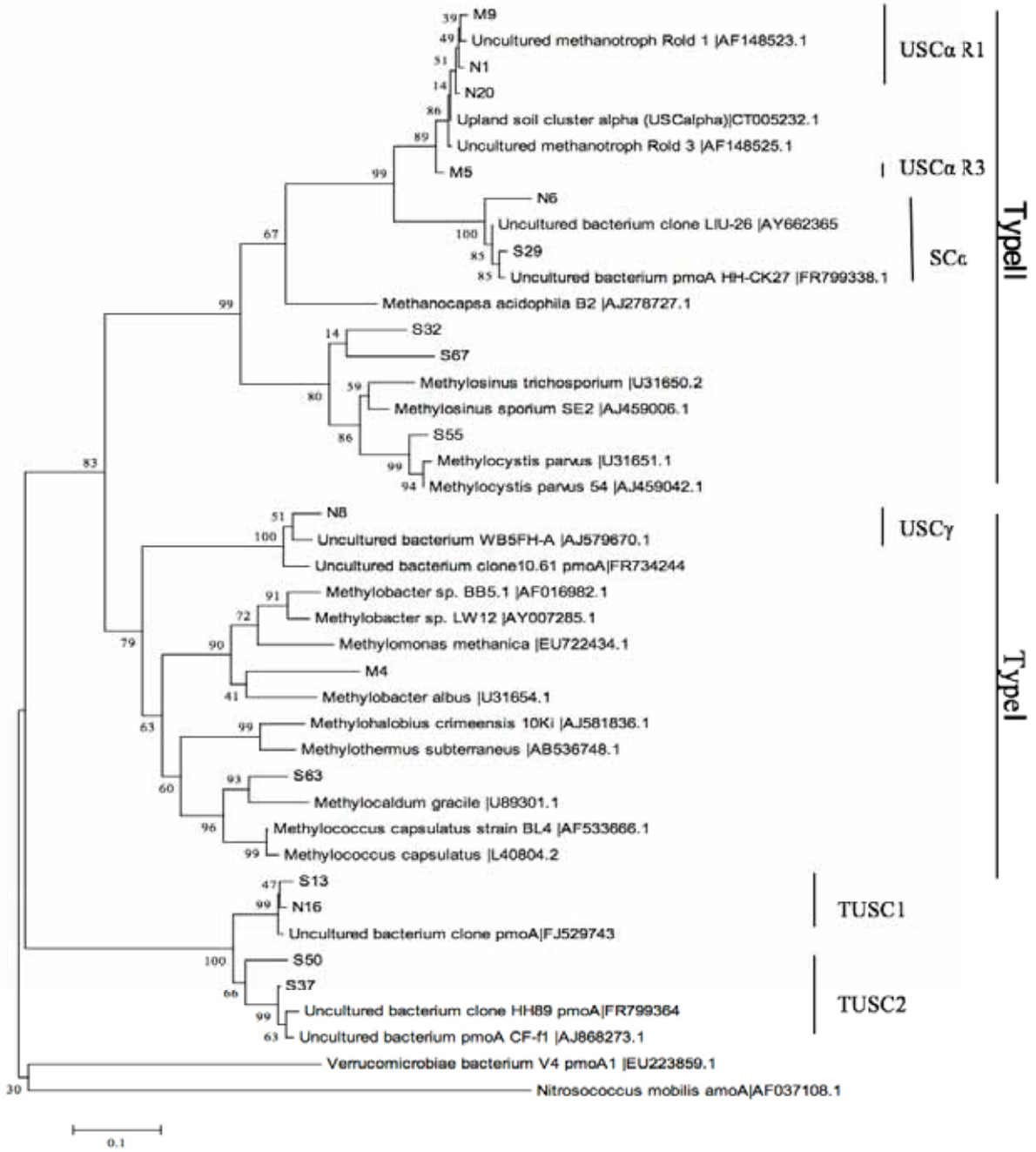

FIGURE 2
Phylogenetic tree among methanotrophic PmoA retrieved from Nanling forest soil. The tree is based on the derived amino acid sequence of a filter (151 amino acids) excluding the primer sequences and alignment positions with sequence ambiguity or missing data Bootstrap values are indicated at branch points.

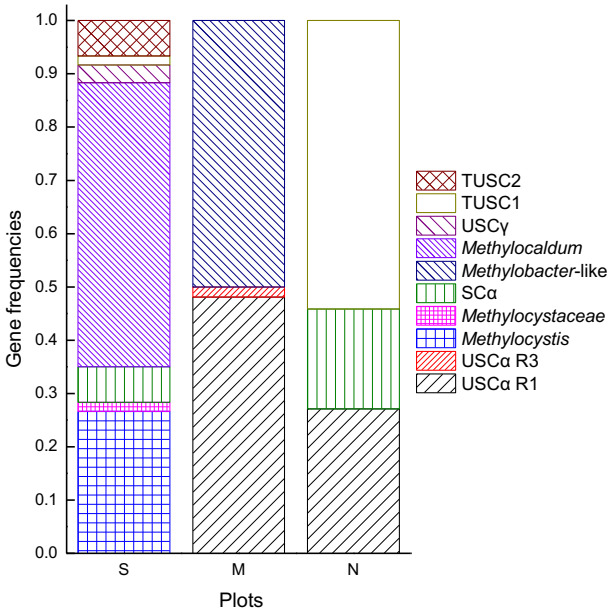

FIGURE 3
Relative abundance of individual OTU from RFLP analysis targeting pmoA genes amplified from DNA extracted from Nanling soil

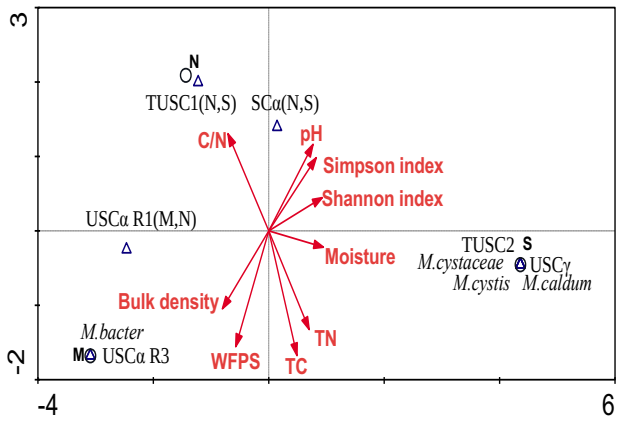

FIGURE 4
Relationship between the samples, the species and the environment variable based on CCA. The arrow stands for physicochemical factors; the circular stands for the samples; the triangle stands for the OTUs.

TABLE 2
Dominant MOB in similar studies

Dominant MOB	Site	Location	Forest zone	Reference
Methylococcus sp., distant relatives of USCα	39°05′ S, 175°45′ E	New Zealand	Temperate	[29]
USCα	38°26′ S, 176°13′ E	New Zealand	Temperate	[29]
USCα	51°00′ N, 9°51′ E	Germany, northern Hesse	Temperate	[30]
Cluster I	51°34′ N, 10°1′ E	Germany, southern Lower Saxony	Temperate	[30]
USCα	23°39′- 23°47′S, 46°55′-47°06′W	Brazil to the west of Sao Paulo	Sub-tropical	[31]
USCα, TUSC and *Methylocystis*	3°26′00″ S, 60°23′00″ W	Caldeirao, Brazilian Central Amazon	Tropical	[32]
USCα, TUSC and *Methylocystis*	3°18′12″ S, 60°31′45″ W	Barro Branco, Brazilian Central Amazon	Tropical	[32]

MOB community composition and its influential factors. This study found the dominant MOB in the soil of Nanling Mountain as USCα, TUSC, *Methylocaldum* and *Methylobacter*-like methanotrophs. This was similar to forest soils in New Zealand, Brazil, Germany within temperate zone with USCα or the relatives of USCα methanotrophs were the dominant groups [29, 30]. This group and TUSC MOB were found to predominated methanotrophic communities in the soil of subtropical and tropical forests (Table 2) [31, 32]. One special finding of this study was *Methylocaldum* as the dominant MOB accounting for 53% of methanotrophic community in the forest soil of southern Nanling Mountain but was very scarce in other two plots. *Methylocaldum* is often found in tropical paddy soil regionally typical of globe rice field [33, 34]. *Methylocaldum*-like sequences are also one of the three main groups in temperate deciduous forest and meadow soils [35]. Therefore our result showing *Methylocaldum* as the dominant MOB could be explained by the location of our plot in the middle region between tropical and temperate zones. *Methylocaldum* usually has a strong tolerance of high temperature, it can grow at 30-62°C [36]. *Methylobacter,* however, favors lower temperatures [37, 38], which could explain why they only appeared in Plot M on the northern Nanling Mountain with high altitude .

The TUSC that was related to both MMO (methane monooxygenase) and AMO (ammonia monooxygenase) clusters was often not sure in phylogenetic systematics. Some researchers consider it as a part of MMO in methanotrophs [39, 40]. However, some others classify them as pXMO [41-43]. pXMO was a new kind of sequnce-divergent particulate monooxygenase first put forward in 2011 [42]. It is considered to be encoded by Gamma MOB in the genera *Methylomonas*, *Methylobacter* and *Methylomicrobium*. The existence of pxmA (the gene encoding a subunit of pXMO) was detected in many environment samples including freshwater creek sediments, peatland soil and paddy soil[41-43]. So far, no clear systematic detail or physiological information was known about this group [41]. In our study, this kind of organisms took a bigger part (~50%) in Plot N, which suggested that the forest soil in this part of Nanling Mountain is still a “grey box” on methane oxidation.

The existence of methanotrophs and consumption of atmospheric CH_4 could be observed frequently in soils over a wide range of pH values, i.e. pH between 3.5-8.0 [11]. In our study, the Upland Soil Cluster γ was detected only in Plot S with higher pH. This was probably because that USCγ are adapted to higher pH values and might represent primary CH_4-consuming methanotrophs in pH-neutral soils [11].

In our study, USCα R1, USCα R3 and *Methylobacter*-like MOB seemed to prefer living in more acid soil environments. It was consistent with previous findings that USCα are significantly more frequently detected in acidic soils with pH values of <6 [30, 35] .They constitute the majority of total MOB communities [44], even to 95% in some forests [30].

The radio of type I /type II methanotrophs in forest soil was higher in the southern plot than the northern plots. This was probably related to the significant difference in total nitrogen between the southern and northern Nanling Mountain soil, because the total nitrogen was shown by CCA analysis to have a strong effect on community composition. N addition stimulates the consumption of methane and the subsequent growth of type I methanotrophs, but generally inhibits that of type II methanotrophs [45, 46]. In short, different kinds of methanotrophs have different optimum environment and oxidation character. The methanotrophic community is the base of methane oxidation.

Relativity between environmental factors and α-diversity index. This study found a positive relationship between Shannon diversity index of methanotrophic community and pH at acid environment and Simpson diversity index showed the similar tendency (Figure 4). The microflora involved in CH_4 metabolism is not well adapted to low pH [47]. The bacteria showed pH responses typical of known MOB [48]. Therefore, it was understandable that there were only a few kinds of acidophilic or acid-tolerable MOB with low diversity in low pH circumstance.

On the other hand, we found a negative relationship between α-diversity index and bulk density, the other main soil property related to CH_4 consumption rates than WFPS [49], which also affects CH_4 oxidation by changing gas diffusion rates [6]. When the bulk density is high, the limited methane and oxygen can get into soil. Low available substrates and energy source restrict the life of MOB that are not adapted to low methane concentrations [50] and reduce the diversity of methanotrophic community. Our result was consistent with previous findings. In the PCA analysis of methanotrophic community with different land use, there were significant relationships between the scores for PC 1 and bulk density, showing bulk density as one of the most influential factors affecting the methanotrophic community structure [51].

CONCLUSIONS

In conclusion, *Methylobacter*-like/ USCα R1, *Methylocaldum* and TUSC1 dominate methanotrophic community in forest soils of the Nanling Mountain. The gene encoding pXMO was also detected. With USCα contributing a bigger part in the northern Nanling Mountain than the southern

mountain. The dominant MOB *Methylocaldum* and those closely related to the genera (*Methylocystis, Methylosinus*) are present in the southern plot but not in the northern ones. USCα R1, USCα R3 and *Methylobacter*-like MOB seem to prefer living in more acidic soil environment. On the contrary, Upland Soil Cluster γ MOB tends to show in pH-neutral soil. There is a positive relationship between Shannon diversity index of methanotrophic community and pH, WFPS and Simpson diversity index, but a negative relationship between Shannon index and bulk density. Our study suggest heterogeneity of methanotrophic community in the Nanling climatic transition region.

ACKNOWLEDGEMENTS

This study was supported by the International S&T Cooperation Program of China (S2013GI0408). The authors give special thanks to Ms. Wan Xiong for her editing and valuable comments on the manuscript, to Mr Zhijun Qiu and Wenqiang Hu for their help in samples collection and to Mrs. Dan Xue and LiFan Xiao for some soil chemical characteristics test.

REFERENCES

[1] Atmospheric Environment Research Division R.D. (2013) The State of Greenhouse Gases in the Atmosphere Using Global Observations through 2012. Geneva: World Meteorological Organization (WMO).

[2] Liang, W., Liu, H., Li, J., He, H. (2017) Ventilation air methane combustion in a flow reversal catalytic reactor: effect sf catalyst, reactor properties and humidity. Fresen Environ Bull. 26, 2302-2313.

[3] Livesley, S.J., Kiese, R., Miehle, P., Weston, C.J., Butterbach-Bahl, K., Arndt, S.K. (2009) Soil–atmosphere exchange of greenhouse gases in a Eucalyptus marginata woodland, a clover-grass pasture, and Pinus radiata and Eucalyptus globulus plantations. Global Change Biol. 15(2), 425-440.

[4] Price, S.J., Sherlock, R.R., Kelliher, F.M., McSeveny, T.M., Tate, K.R., Condron, L.M. (2004) Pristine New Zealand forest soil is a strong methane sink. Global Change Biol. 10(1), 16-26.

[5] Dutaur, L., Verchot, L.V. (2007) A global inventory of the soil CH_4 sink. Global Biogeochem Cy. 21(4).

[6] Dalal, R.C., Allen, D.E., Livesley, S.J., Richards, G. (2008) Magnitude and biophysical regulators of methane emission and consumption in the Australian agricultural, forest, and submerged landscapes: a review. Plant Soil. 309(1-2), 43-76.

[7] Hiltbrunner, D., Zimmermann, S., Karbin, S., Hagedorn, F., Niklaus, P.A. (2012) Increasing soil methane sink along a 120‐year afforestation chronosequence is driven by soil moisture. Global Change Biol. 18(12), 3664-3671.

[8] Smith, R. (2010) Global Forest Resources Assessment 2010: Main report. Rome: Food and Agriculture Organization of the United Nations (FAO).

[9] Wang, Y.F., Chen, H., Zhu, Q., Peng, C.H., Wu, N., Yang, G., Zhu, D., Tian, J.Q., Tian, L.X., Kang, X.M., He, Y.X., Gao, Y.H., Zhao, X.Q. (2014) Soil methane uptake by grasslands and forests in China. Soil Biol Biochem. 74, 70-81.

[10] Lau, E., Ahmad, A., Steudler, P.A., Cavanaugh, C.M. (2007) Molecular characterization of methano-trophic communities in forest soils that consume atmospheric methane. Fems Microbiol Ecol. 60(3), 490-500.

[11] Kolb, S. (2009) The quest for atmospheric methane oxidizers in forest soils. Environ Microbiol Rep. 1(5), 336-346.

[12] Borken, W., Davidson, E.A., Savage, K., Sundquist, E.T., Steudler, P. (2006) Effect of summer throughfall exclusion, summer drought, and winter snow cover on methane fluxes in a temperate forest soil. Soil Biol Biochem. 38(6), 1388-1395.

[13] Amaral, J.A., Knowles, R. (1997) Inhibition of methane consumption in forest soils and pure cultures of methanotrophs by aqueous forest soil extracts. Soil Biol Biochem. 29(11), 1713-1720.

[14] Aronson, E.L., Dubinsky, E.A., Helliker, B.R. (2013) Effects of nitrogen addition on soil microbial diversity and methane cycling capacity depend on drainage conditions in a pine forest soil. Soil Biol Biochem. 62, 119-128.

[15] Tate, K.R. (2015) Soil methane oxidation and land-use change – from process to mitigation. Soil Biol Biochem. 80, 260-272.

[16] Shukla, P.N., Pandey, K.D., Mishra, V.K. (2013) Environmental Determinants of Soil Methane Oxidation and Methanotrophs. Crit Rev Env Sci Tec. 43(18), 1945-2011.

[17] Guan, J., Zhang, Y., Shi, R.J., Li, H., Qin, H.S., Hui, X. (2012) Effects of elevated CO_2 on forest soil CH_4 consumption in Changbai Mountains. Chinese Journal of Applied Ecology. 23(2), 328-334 (In Chinese with an English abstract).

[18] Wu, Z., Shi, Y., Zeng, J., Zhang, T., Mu, W., Deng, L., Zhang, Q., Lou, K. (2013) Pattern of soil methanotrophs on the natural vertical zones of the North Tianshan Mountain. Acta Ecologica Sinica. 33(2), 80-86.

[19] Zhang, Y.G., Cong, J., Lu, H., Yang, C.Y., Yang, Y.F., Zhou, J.H., Li, D.Q. (2014) An Integrated Study to Analyze Soil Microbial Community Structure and Metabolic Potential in Two Forest Types. PLoS One. 9(4), Artn e93773.

[20] Ding, M.M., Sandra, B., Lugo, A.E. (2001) A continental subtropical forest in China compared with an insular subtropical forest in the Caribbean. Río Piedras, Puerto Rico: USDA (United States Department of Agriculture) Forest Service, International Institute of Tropical Forestry.

[21] Tang, X.L., Liu, S.G., Zhou, G.Y., Zhang, D.Q., Zhou, C.Y. (2006) Soil-atmospheric exchange of CO_2, CH_4 and N_2O in three subtropical forest ecosystems in southern China. Global Change Biol. 12(3), 546-560.

[22] Konda, R., Ohta, S., Ishizuka, S., Arai, S., Ansori, S., Tanaka, N., Hardjono, A. (2008) Spatial structures of N_2O, CO_2, and CH_4 fluxes from Acacia mangium plantation soils during a relatively dry season in Indonesia. Soil Biol Biochem. 40(12), 3021-3030.

[23] Di, H., Cameron, K., Shen, J.-P., Winefield, C., O'Callaghan, M., Bowatte, S., He, J.-Z. (2011) Methanotroph abundance not affected by applica-tions of animal urine and a nitrification inhibitor, dicyandiamide, in six grazed grassland soils. J Soil Sediment. 11(3), 432-439.

[24] Holmes, A.J., Costello, A., Lidstrom, M.E., Murrell, J.C. (1995) Evidence that participate methane monooxygenase and ammonia monooxygenase may be evolutionarily related. Fems Microbiol Lett. 132(3), 203-208.

[25] Costello, A.M., Lidstrom, M.E. (1999) Molecular characterization of functional and phylogenetic genes from natural populations of methanotrophs in lake sediments. Appl Environ Microb. 65(11), 5066-5074.

[26] Shrestha, P.M., Kammann, C., Lenhart, K., Dam, B., Liesack, W. (2012) Linking activity, composition and seasonal dynamics of atmospheric methane oxidizers in a meadow soil. Isme J. 6(6), 1115-1126.

[27] Hutchens, E., Radajewski, S., Dumont, M.G., McDonald, I.R., Murrell, J.C. (2004) Analysis of methanotrophic bacteria in Movile Cave by stable isotope probing. Environ Microbiol. 6(2), 111-120.

[28] Hu, B., Shen, L., Lian, X., Zhu, Q., Liu, S., Huang, Q., He, Z., Geng, S., Cheng, D., Lou, L., Xu, X., Zheng, P., He, Y. (2014) Evidence for nitrite-dependent anaerobic methane oxidation as a previously overlooked microbial methane sink in wetlands. P Natl Acad Sci Usa. 111(12), 4495-4500.

[29] Nazaries, L., Tate, K.R., Ross, D.J., Singh, J., Dando, J., Saggar, S., Baggs, E.M., Millard, P., Murrell, J.C., Singh, B.K. (2011) Response of methanotrophic communities to afforestation and reforestation in New Zealand. Isme J. 5(11), 1832-1836.

[30] Kolb, S., Knief, C., Dunfield, P.F., Conrad, R. (2005) Abundance and activity of uncultured methanotrophic bacteria involved in the consumption of atmospheric methane in two forest soils. Environ Microbiol. 7(8), 1150-1161.

[31] Dorr, N., Glaser, B., Kolb, S. (2010) Methanotrophic Communities in Brazilian Ferralsols from Naturally Forested, Afforested, and Agricultural Sites. Appl Environ Microb. 76(4), 1307-1310.

[32] Lima, A.B., Muniz, A.W., Dumont, M.G. (2014) Activity and abundance of methane-oxidizing bacteria in secondary forest and manioc plantations of Amazonian Dark Earth and their adjacent soils. Front Microbiol. 5, Artn 550.

[33] Yun, J.L., Wang, Y.F., Zhang, H.X. (2013) Ecology of aerobic methane oxidizing bacteria (methanotrophs). Acta Ecologica Sinica. 33(21), 6774-6785 (Chinese with English abstract).

[34] Vishwakarma, P., Singh, M., Dubey, S.K. (2010) Changes in methanotrophic community composition after rice crop harvest in tropical soils. Biol Fert Soils. 46(5), 471-479.

[35] Knief, C., Lipski, A., Dunfield, P.F. (2003) Diversity and Activity of Methanotrophic Bacteria in Different Upland Soils. Appl Environ Microb. 69(11), 6703-6714.

[36] Trotsenko, Y.A., Medvedkova, K.A., Khmelenina, V.N., Eshinimayev, B.T. (2009) Thermophilic and thermotolerant aerobic methanotrophs. Mikrobiologiia. 78(4), 387-401.

[37] Ho, A., Kerckhof, F.M., Luke, C., Reim, A., Krause, S., Boon, N., Bodelier, P.L.E. (2013) Conceptualizing functional traits and ecological characteristics of methane-oxidizing bacteria as life strategies. Environ Microbiol Rep. 5(3), 335-345.

[38] Liebner, S., Rublack, K., Stuehrmann, T., Wagner, D. (2009) Diversity of Aerobic Methanotrophic Bacteria in a Permafrost Active Layer Soil of the Lena Delta, Siberia. Microb Ecol. 57(1), 25-35.

[39] Knief, C., Vanitchung, S., Harvey, N.W., Conrad, R., Dunfield, P.F., Chidthaisong, A. (2005) Diversity of methanotrophic bacteria in tropical upland soils under different land uses. Appl Environ Microb. 71(7), 3826-3831.
[40] Levine, U.Y., Teal, T.K., Robertson, G.P., Schmidt, T.M. (2011) Agriculture's impact on microbial diversity and associated fluxes of carbon dioxide and methane. Isme J. 5(10), 1683-1691.
[41] Luke, C., Frenzel, P. (2011) Potential of pmoA Amplicon Pyrosequencing for Methanotroph Diversity Studies. Appl Environ Microb. 77(17), 6305-6309.
[42] Tavormina, P.L., Orphan, V.J., Kalyuzhnaya, M.G., Jetten M.S.M., Klotz M.G. (2011) A novel family of functional operons encoding methane/ammonia monooxygenase-related proteins in gammaproteo-bacterial methanotrophs. Environ Microbiol Rep. 3(1), 91-100.
[43] Deng, Y.C., Cui, X.Y., Luke, C., Dumont, M.G. (2013) Aerobic methanotroph diversity in Riganqiao peatlands on the Qinghai-Tibetan Plateau. Environ Microbiol Rep. 5(4), 566-574.
[44] Jaatinen, K., Knief, C., Dunfield, P.F., Yrjala, K., Fritze, H. (2004) Methanotrophic bacteria in boreal forest soil after fire. Fems Microbiol Ecol. 50(3), 195-202.
[45] Mohanty, S.R., Bodelier, P.L.E., Floris, V., Conrad, R. (2006) Differential effects of nitrogenous fertilizers on methane-consuming microbes in rice field and forest soils. Appl Environ Microb. 72(2), 1346-1354.
[46] Noll, M., Frenzel, P., Conrad, R. (2008) Selective stimulation of type I methanotrophs in a rice paddy soil by urea fertilization revealed by RNA-based stable isotope probing. Fems Microbiol Ecol. 65(1), 125-132.
[47] Dunfield, P., Dumont, R., Moore, T.R. (1993) Methane production and consumption in temperate and subarctic peat soils: response to temperature and pH. Soil Biol Biochem. 25(3), 321-326.
[48] Amaral, J.A., Ren, T., Knowles, R. (1998) Atmos-pheric methane consumption by forest soils and extracted bacteria at different pH values. Appl Environ Microb. 64(7), 2397-2402.
[49] Werner, C., Kiese, R., Butterbach-Bahl, K. (2007) Soil-atmosphere exchange of N_2O, CH_4, and CO_2 and controlling environmental factors for tropical rain forest sites in western Kenya. Journal of Geophysical Research-Atmospheres. 112(3).
[50] Semrau, J.D., DiSpirito, A.A., Yoon, S. (2010) Methanotrophs and copper. Fems Microbiol Rev. 34(4), 496-531.
[51] Singh, B.K., Tate, K.R., Ross, D.J., Singh, J., Dando, J., Thomas, N., Millard, P., Murrell, J.C. (2009) Soil methane oxidation and methanotroph responses to afforestation of pastures with Pinus radiata stands. Soil Biol Biochem. 41(10), 2196-2205.

Received: **05.08.2017**
Accepted: **20.10.2017**

CORRESPONDING AUTHOR

Huai Chen
Chengdu Institute of Biology,
Chinese Academy of Sciences
9th, block 4, South Ren Min Road
Chengdu 610041 – China

e-mail: chenhuai@cib.ac.cn

© by PSP Volume 27 – No. 2/2018 pages 1031-1037 Fresenius Environmental Bulletin

A NEW WIRELESS BOLUS SENSOR WITH ACTIVE RFID TAG TO MEASURE RUMEN pH

Habib Dogan[1], Musa Yavuz[2,*]

[1]Suleyman Demirel University, Graduate School of Natural and Applied Science, Isparta, Turkey
[2]Suleyman Demirel University, Faculty of Agriculture, Animal science Department, Isparta, Turkey

ABSTRACT

Radio Frequency Identification (RFID) systems have been used commonly in different areas in the last decades. Identification of animals has been done for a long time by using passive RFID tags and also some digestive system parameters have been monitored trough sensors equipped with active RFID tags. The aim of this study is to develop a bolus that can accurately measure the rumen pH which has higher length of frequency. Three cannulated local breed steers were used for this study. The Hanna 1270 pH sensor was added to the active RFID tags. The buffer (Operational Amplifier) OPAMP was equipped with the pH sensor outputs which were sent to the analogue digital converter. Either the PCB (Printed Circuit Board) helical or a quarter wave monopole antennas connected to a laptop computer were used with UDEA RFID software. The active PCB helical antenna in the active RFID tags was weaker in signaling than a quarter wave monopole antennas. Despite power supply can be extended to nearly a year when it is recorded in 30 minutes intervals, the accuracy of the pH probe is to loss in forty-five days.

KEYWORDS:
Rumen, pH measurement, RFID, precision livestock farming

INTRODUCTION

Feeding patterns can lead to changes in the pH of the digestive system of the animals and the rumen pH should ideally be maintained between 5.5 and 7.0 [1]. The pH plays a key role in optimal digestion of feed components in the cow's rumen. Sub-acute ruminal acidosis (SARA) is regarded one of the most significant nutrition-related problem for the high producing animals [2,3]. SARA usually develops upon high starch diet and subsequently the rumen pH falls below pH 5.5 [3]. SARA related total annual economic loss was reported around $1 billion in the USA dairy industry [2]. Monitoring and detecting SARA before it starts has a high priority in developing an efficient strategy for the ruminant feeding and production system.

Oro-ruminal probes [4], via rumenocentesis [5] and rumen cannula methods were used to measure momentarily the pH of rumen. The rumen pH has dynamic pattern and it is affected by many factors. Thus, continuous measurement of the ruminal pH has become of interest for the many researchers [6]. First continuous measurement of pH was done in cannulated sheep and cattle by pH electrode and external cable [7, 8]. Later, electrode systems were developed to measure rumen pH and data was transferred to a cordless data logger [9]. The disadvantages of this method were cleaning and recalibration requirement of the electrode after using even for a short period of time and the data must be manually transferred to a data logger at each read-out to see the rumen fluid pH changes. A bolus prototype was then developed which can measure rumen pH and enable to transfer data to receiver without a cable [1, 10]. These devices enable to record data from a distance by means of an antenna and the pH changes could be monitored continuously with minimal disturbance of animal. This system also had some problems such as pH electrode was required to be cleaned and re-calibrated 40 days after insertion to animal and radio transmitter to a remote receiver is short ranged. For example at 433 MHz wavelength, signal could be received from a distance of several meters [1]. In another study, rumen pH boluses were designed to work at 429 MHz and remote pH measurements were performed [11]. However, this system requires high power to continuously send the data to the receiver. Farmers who were remotely monitored rumen pH by a bolus had 60% monetary and 100% commercial benefit [12]; however, the usage of these devices did not become widespread because of the high price tags.

The aims of our study were to develop an active RFID-based bolus that can accurately measure the rumen pH and to ensure these data could be measured in a longer distance from the animal.

MATERIALS AND METHODS

The study was conducted at Suleyman Demirel University, Agriculture Research Farm, Isparta, Turkey in 2016. Three 16 months old local breed steers

were used and cannulated, by the approval of the Süleyman Demirel University, Animal Ethics and Welfare Committee (Approval date: 21.05.2015 No:05). Animals were fed ad-libitum twice a day. The ration composed of 30% wheat straw, 35% alfalfa hay and 35% concentrate feed to compensate growth and maintenance requirement based on NRC dairy requirements [13]. They had free access to water at all the time.

The Hanna 1270 pH sensor added to the active RFID tags of UDEA Company and the sensors were selected by taking into account the economical and dimensional aspects. The buffer OPAMP was attached to the bolus to enable the data transfer to the analogue digital converter. The buffer voltage required for the OPAMP and pH sensor is provided using the voltage regulator Figure 1 and 2. The power unit used 3.6 lithium batteries available on RFID tags.

In the first design, a polyamide sheath was used to seal the system. Due to leakage of liquid after one week the whole structure was taken into epoxy as sealant (Figure 3). A steel block of 40 g was attached to the bolus to allow it to stay at the bottom of the rumen.

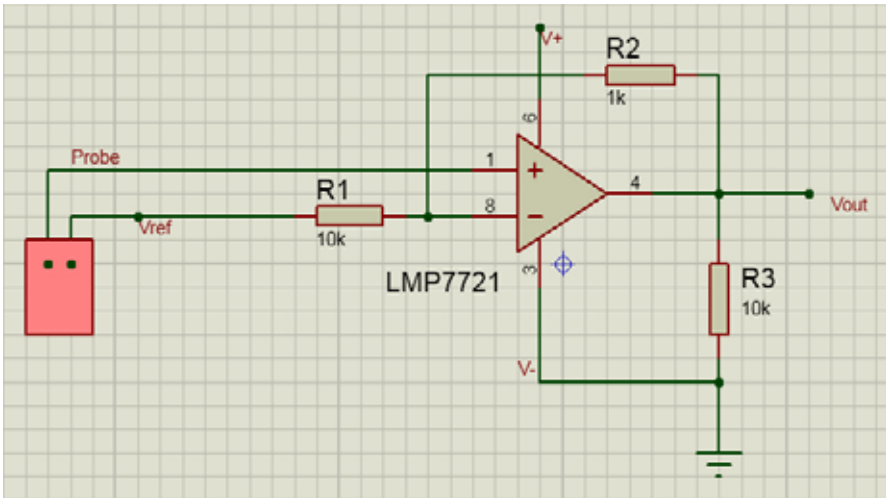

FIGURE 1
Buffer OPAMP used at pH probe output

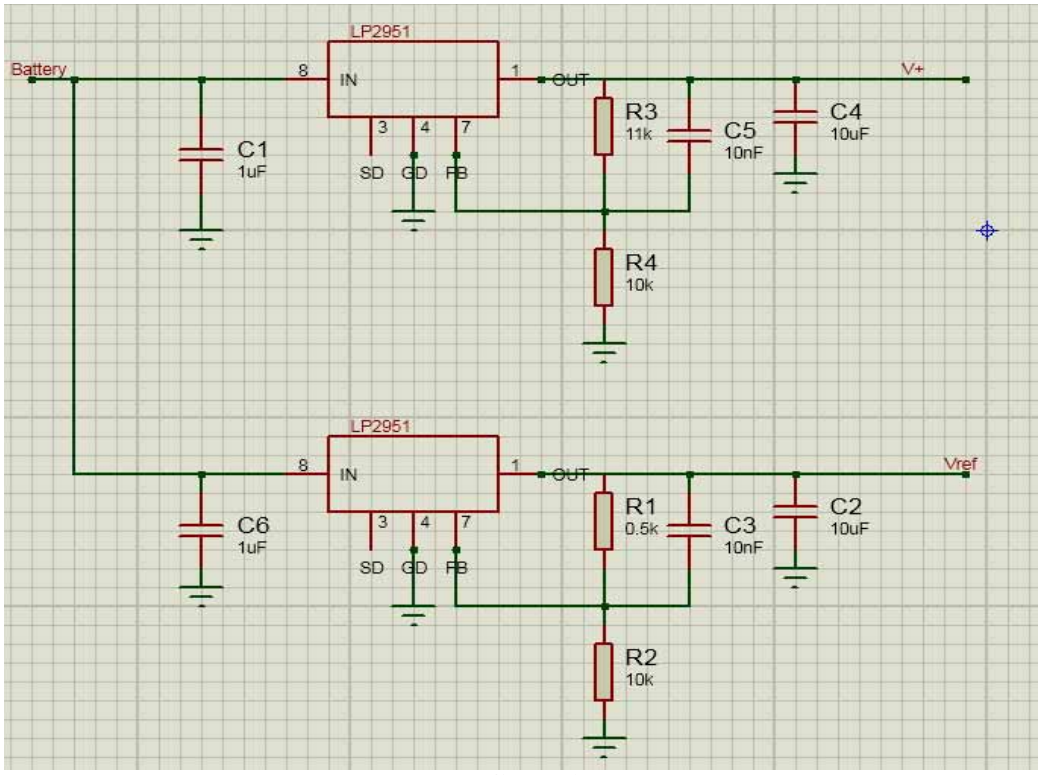

FIGURE 2
Use of voltage regulator for reference voltage

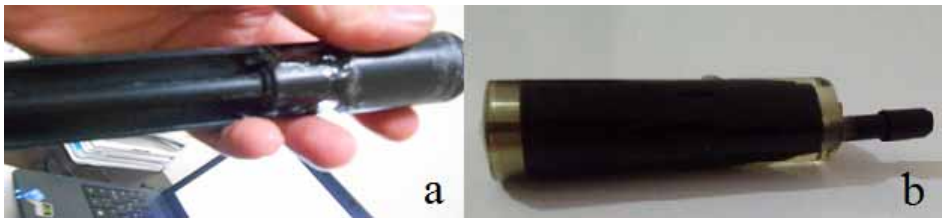

FIGURE 3
Bolus with a polyamide (a) and an epoxy sheath (b)designs

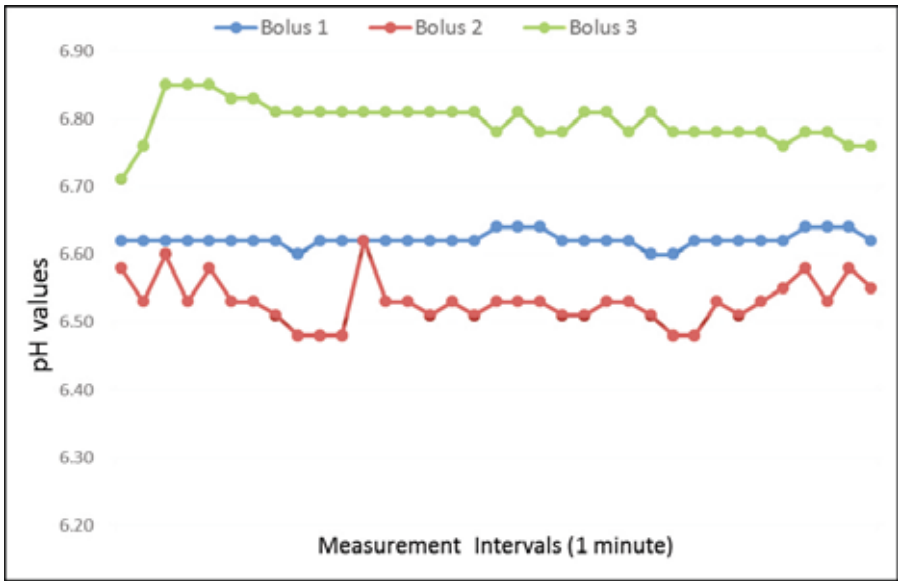

FIGURE 4
Comparisons of pH bolus values of three cattle

The resulting structure is 29mmX150mm in size and weighs 140 g as shown in Figure 3. The length of the bolus could be further reduced with removal of the plastic sheath. In the first design the PCB helical antenna on the active RFID tags gave off weaker signals inside of the animal. Thus in the second set-up the antenna was replaced with a quarter wave monopole antenna. The antenna was connected to a laptop computer by using UDEA RFID software. Calibrated pH boluses were inserted directly into the rumen ventral sac region of three cannulated cattle. Short and long interval (3, 5, 10, 15 and 30 minutes) recordings were set to measure duration of the battery power. Three bench top pH meters (Hanna Edge S600 type) and the sensors were placed into cranial sac of the rumen from the cannula plugs. Bench top pH meter was used as a control in the same area of the rumen boluses. The pH meters were calibrated each time before use. The data of the boluses were compared with each other and with the bench top pH meters.

RESULTS AND DISCUSSION

In the first antenna design, PCB helical antenna structure on the active RFID tags used was failed to produce strong signals. In the second antenna design, a quarter wave monopole antenna signals were received at longer distances from rumen boluses. This design enabled 100% reading rate within the first 10 m. This rate decreased down 80% accurate and precise signals at 20 m. Despite it was possible to receive signals as far as 30 m their accuracy and precision reduced. Mottram [1] reported that 433 MHz frequency signals could be received from several meters. A longer distance was achieved with our design. The reading distance increased when the animals were at standing position, and the signal reception decreased when they were in lying position. When the left side of the animals was facing to antenna signal receival was higher than those of either right site or backward of the animals depending on the absorbance of the signals by the higher muscle and tissue density.

There were some differences between steers' pH (6.48, 6.62 and 6.81) results probably because of pH boluses' locations [14] and animal preferences for diet. However the overall results, as reported by Mottram et al. [1], were well in the acceptable range of the normal rumen environments (Figure 4).

The values in Figures 5 and 6 show that there were as small as 0.03-0.12 pH unit deviations between the boluses and the bench top pH meters measurements. The bench top pH meter electrode was

placed possible adjacent location to the bolus; however, the electrode eventually positioned a bit more inside the rumen. Therefore aforementioned small differences between two measurement methods can appear due to heterogeneity of the rumen at different locations or calibration differences of the two electrodes. Results reported by Mottram [14] support our findings that rumen pH can change as high as 2.5 unit during the day and 0.5 unit in the different regions of the rumen.

Both bolus and bench top pH meters were consistent for the first 40-50 days; but after this time, the bolus pH sensor had higher read-outs of pH due possibly to contamination with rumen content [2] (Figure 7). Comparing our results to grazing cows, ruminal pH measured by pH probes for 40 days shifted after 28 days [15].

To obtain accurate and precise measurements the pH sensor must be cleaned and re-calibrated after 40 days. In fact this easy in-situ operation under experimental conditions, removing boluses from the rumen and cleaning and recalibrating the electrode, may not be possible under farmer conditions. Because of this the bolus measured rumen pH (7.36) required a software adjustment by considering the external pH (6.68) meter readings (Figure 8).

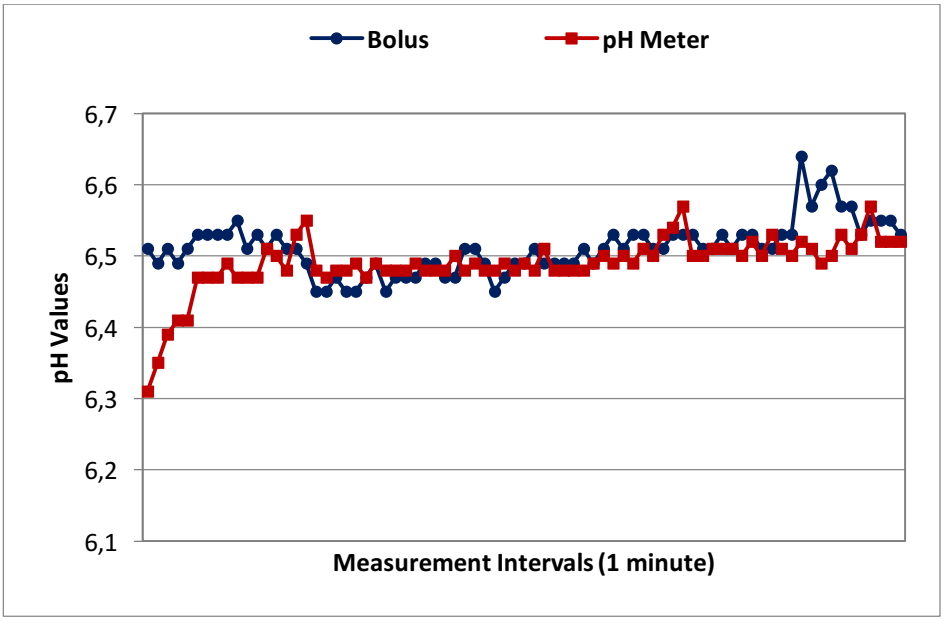

FIGURE 5
Comparisons of pH recordings on the eleventh day

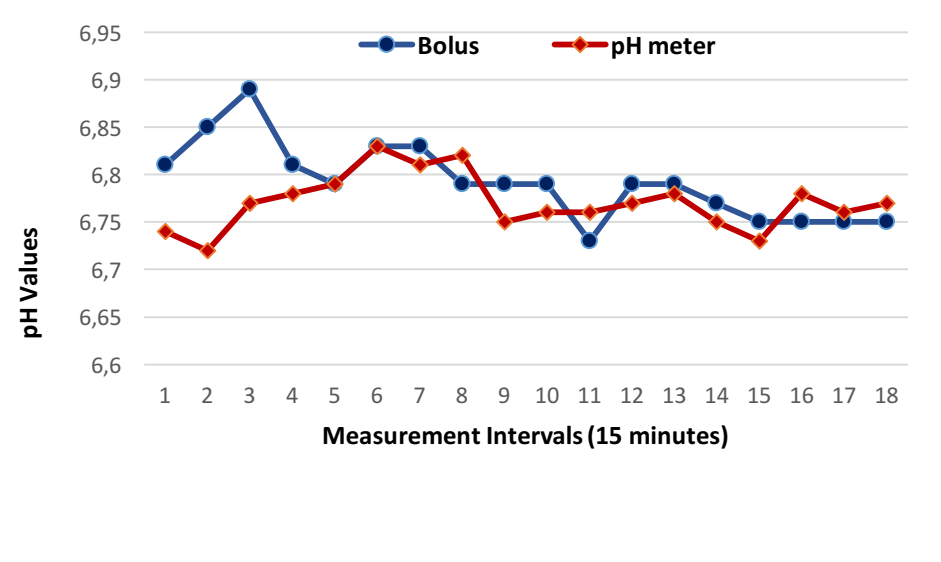

FIGURE 6
Comparisons of pH recordings on the thirty-fourth day

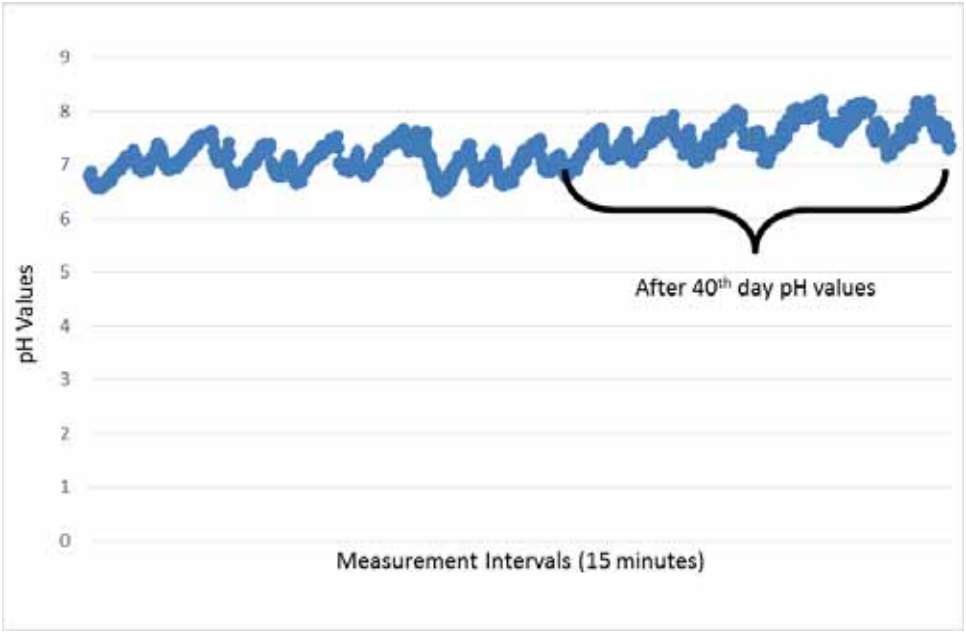

FIGURE 7
Inaccurate pH readings after the fortieth day

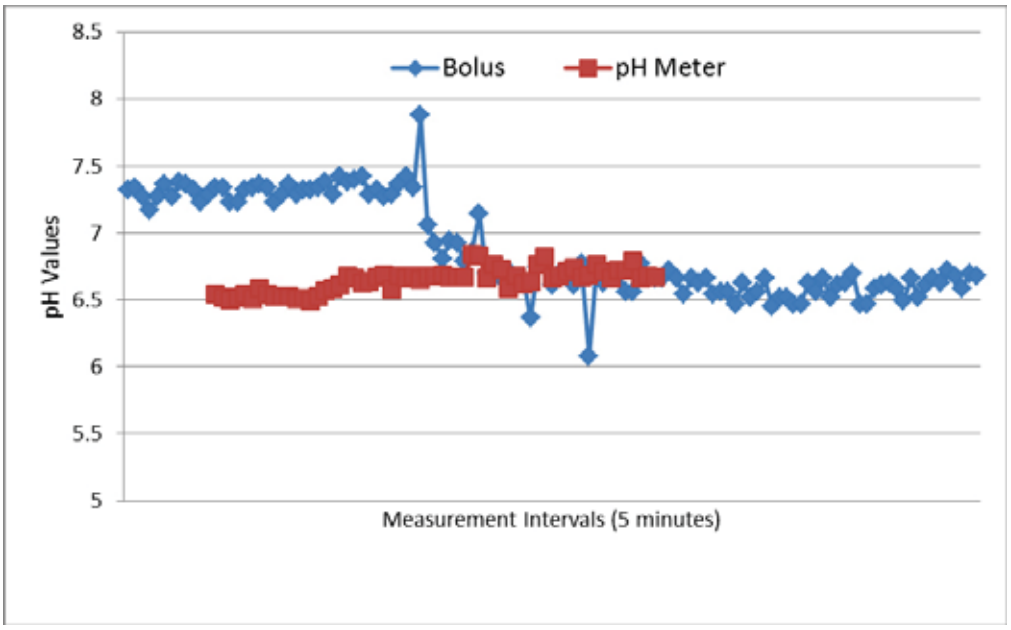

FIGURE8
Calibration of bolus's pH reading with the software on the forty-eight day

It was possible to get a reliable signal for a maximum of additional 15-20 days with the calibration made via software program. At the end of this period, the incorrect pH values were inevitably recorded. Different pH sensors might have been solution to this problem. For example, ISFET (ion-sensitive field-effect transistor) type pH electrodes are expected to have a longer lifetime in terms of contamination [16]. However these types of probes are more expensive than the conventional ones. Continuous measurement of the rumen pH data showed apparent fluctuations in 24 hours period (Figure 9). We have not observed an excessive pH drop in animals that could cause SARA; however, there were pH fluctuations between the feeding time and fermentation period.

When we started to record the data in shorter intervals (3, 5, 10 and 15 min), the power supply of the boluses were lasted about four months. If it was recorded at 30 min intervals, it may enable to measure pH for nearly a year. Also, the operation times of the boluses can be extended by using more powerful buttery supplies instead of 3.6 V/1000 mAh providing that no-increase in the bolus dimensions.

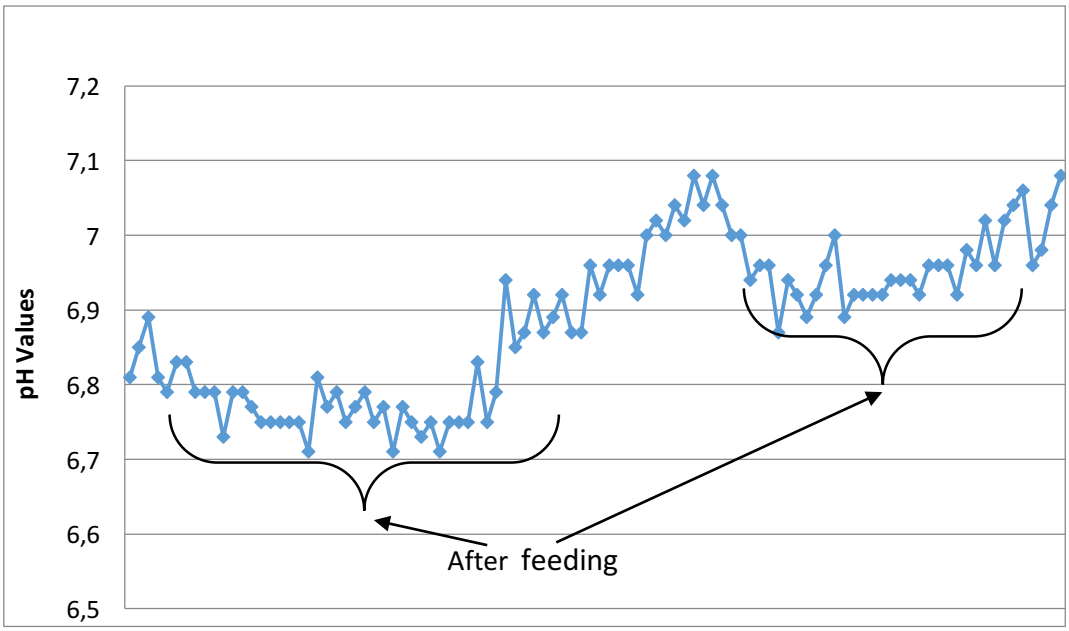

FIGURE 9
pH value fluctuations before and after feeding times

CONCLUSION

Minimal variations between boluses and bench top pH meter values were identified during the first 40-50 days of insertion and the accurate and precise reading period can be extended up to 15-20 days by the readjustment of pH values via software program. The system allowed us to remotely monitor rumen pH over the internet. The monitoring system can give a dairy or feedlot nutritionist to correct SARA-related or other feeding problems.

The optimum location and configuration of antenna are important for getting reliable readings; however, the suggested new bolus systems need to be tested in different situations and animals. Therefore further research is needed to improve this preliminary product.

ACKNOWLEDGEMENTS

This work is supported by Suleyman Demirel University Scientific Research Project Coordination (SDU BAP 4391-D2-2015) and we would like to thank UDEA Company (METU Tecnocity) for their technical assistants.

REFERENCES

[1] Mottram, T., Lowe, J., McGowan, M. and Philips, N. (2008) Technical note: A wireless telemetric method of monitoring clinical acidosis in dairy cows. Computers and Electronics in Agriculture. 64, 45–48.

[2] Philips, N. and Mottram, T. (2010) Continuous Monitoring of Ruminal pH using Wireless telemetry. Animal Production Science. 50, 72-77.

[3] Zosel, J., Kadena, H., Peters, G., Hoffmannc, M., Rudisch, P., Jäkel, L. Lauckner, G., Grodriane, A. and Gutha, U. (2010) Continuous long-term monitoring of ruminal pH. Sensors and Actuators. 144(B), 395–399.

[4] Geishauser, T. (1993) An instrument for collection and transfer of rumen fluid and for administration of water and soluble drugs in adult cattle. The Bovine Practitioner. 27, 38–42.

[5] Duffield, T., Plaizier, J.C., Fairfield, A., Bagg, R., Vessie, G., Dick, P., Aramini, J. and McBride, B. (2004) Comparison of techniques for measurement of rumen pH in lactating dairy cows. Journal of Dairy Science. 87, 59–66.

[6] Doğan, H., Çağlar, M. F., Yavuz, M. and Gözel M. A. (2016) Use of Radio Frequency Identification Systems on Animal Monitoring. SDU International Journal of Technological Sciences. 8(2), 38-53.

[7] Lampila, M. (1955) Preliminary studies on the variations of pH and volatile fatty acid concentration in the rumen contents of the cow. Journal of the Scientific Agricultural Society of Finland. 27, 142–153.

[8] Dado, R.G. and Allen, M.S. (1993) Continuous computer acquisition of feed and water intakes, chewing, reticular motility, and ruminal pH of cattle. Journal of Dairy Science. 76(6), 1589–1600.

[9] Beauchemin, K.A. and Yang, W.Z. (2005) Effects of physically effective fiber on intake, chewing activity, and ruminal acidosis for dairy cows fed diets based on corn silage. Journal of Dairy Science. 88, 2117–2129.
[10] Lowe, J.C., Abeyesinghe, S.M., Demmers, T.G.M., Wathes, C.M. and McKeegan, D.E.P. (2007) A novel telemetric logging system for recording physiological signals in unrestrained animals. Computers and Electronics in Agriculture. 57, 74–79.
[11] Sato, S., Kimura, A., Anan, T., Yamagishi, N., Okada, K., Mizuguchi, H. and Ito, K. (2012) A radio transmission pH measurement system for continuous evaluation of fluid pH in the rumen of cows. Veterinary Research Communi-cations. 36(1), 85–89.
[12] Nogues, A. (2013) Commercial Benefits of Routine Monitoring of Rumen pH in Dairy Cows in South West England.
[13] National Research Council (NRC) (2001) Nutrient Requirements of Dairy Cattle. Seventh Revised Edition. National Academic Press, Washington, D.C.
[14] Mottram, T. (2016) Animal board invited review: precision livestock farming for dairy cows with a focus on oestrus detection. Animals. 10, 1575-1584.
[15] Gasteiner, J., Guggenberger, T., Häusler, J. and Steinwidder, A. (2012) Continuous and Long-Term Measurement of Reticuloruminal pH in Grazing Dairy Cows by an Indwelling and Wireless Data Transmitting Unit, Veterinary Medicine International. 2012(2), 236956.
[16] Anonymous (2016) ISFET pH sensors. http://www.sentron.nl/sensors/isfet-ph-sensors/Accessed date: 28.06.2017.

Received: **10.08.2017**
Accepted: **20.11.2017**

CORRESPONDING AUTHOR

Musa Yavuz
Suleyman Demirel University,
Agricultural Faculty,
Animal Science Department,
East Campus 32260 Isparta – Turkey

e-mail: musayavuz@sdu.edu.tr

© by PSP Volume 27 – No. 2/2018 pages 1038-1042 Fresenius Environmental Bulletin

APHICIDAL ACTIVITY OF ORANGE OIL TO THE GREEN PEACH APHID *MYZUS PERSICAE* SULZER (HOMOPTERA : APHIDIDAE)

Tawfiq M Al-Antary[1,*], Mazen A Ateyyat[2], Idres H Belghasem[1], Salaheddin A Alaraj [1]

[1]Department of Plant Protection, Faculty of Agriculture, University of Jordan, Amman 11942, Jordan
[2]Plant Production and Protection Department, Faculty of Agricultural Technology, Al Balqa' Applied University, Al Salt 19117, Jordan

ABSTRACT

Efficacy of orange essential oil, with four different solvents namely: acetone, ethanol, n-hexane and chloroform screened against the green peach aphid, *Myzus persicae*, for their aphicidal effects under lab conditions. The aphid was reared in special insectary until reaching sensitive strain after ten generations, bioassay was then applied, to find lethal concentration, after three various times; 24, 48 and 72 hours, using four types of solvents. Results showed that orange oil with acetone was the most effective against first and second nymphal instars (early nymphal instars) of *M. persicae*. Orange oil showed effectiveness with LC_{50} of 0.003, and 0.004 (v/v) with acetone and n- hexane solvents, respectively, and LC_{90} of 0.187, and 0.196 (v/v) with acetone and ethanol. Results indicated significant differences in mean percentage mortalities after 24, 48, and 72 hours of the exposure at 10% concentration. Orange oil showed mortality, which ranged between 69.30 to 47.82%. None of the orange extracts was as effective as Calypso insecticide in controlling the insect pest. The study showed that orange essential oil is promising insecticide that provides effective management of *M. persicae* to provide safe environment and crops with high quality.

KEYWORDS:
Essential oils, Botanical insecticides, IPM, Bioassay, Biorational insecticides

INTRODUCTION

Aphids are polyphagous agricultural pests with worldwide distribution, among which the green peach aphid (GPA), *Myzus persicae* (Sulzer) (Homoptera : Aphididae), is considered a key insect pest on several crops. GPA can develop many population densities on young plant tissues as it has short life cycle and tremendous fecundity [1, 2]. It causes severe damage to the attacked host plant through sucking sap of plant tissues resulting in depriving its essential nutrients. Damage leads to deformation and premature leaf senescence. The insect also produces a huge amount of honeydew that encourages sooty mold growth and retards growth rate that causes wilting of the host plant [3, 4, 5, 6]. Severe damage of aphids including GPA results in transmission of over 100 plant viruses by both nymphs and adults [7,8]. Farmers rely mainly on chemical option to control aphids, particularly under outbreak of populations. The extensive use of pesticides has many drawbacks including development of resistance, resurgence of pest population, negative effect on natural enemies, killing non-target organisms, residual effects of pesticides and environmental pollution [9, 10, 11, 12, 13].

Due to these negative impacts of pesticides, growers showed shift to environmentally friendly control tactics [14, 15, 16, 17, 18, 19]. Botanical insecticides represent an attractive alternative to synthetic insecticides and can be used as part of both integrated pest management programs and organic agriculture as botanicals pose low or no negative impact to the environment or to human health [15, 20, 21, 22, 23, 24, 25].

The present research aimed to investigate the toxicity of the oil and different solvent extracts of orange peel (*Citrus sinensis* L) on green peach aphid.

MATERIALS AND METHODS

The Insectary. The insectary was a room of 4×3×3m in dimensions. It contained three rows of frame stands, containing four cages. The frame consisted of two floors. This room provided with air conditions to keep temperature about 22°C and relative humidity percentage about 55 ±5. In addition, light provided with timer to give the needed 16:8 L: D photoperiod regime. The walls of this insectary lined with wood.

Rearing of the Aphid. *M. persicae* adults reared in the laboratory at 22±2°C. Prof. Tawfiq Al-Antary at the University of Jordan according to Blackman and Eastop [26] identified the aphid. The GPA was collected from unsprayed area in Ghore Al Safi region. Apterous individuals obtained from a continuously maintained culture in an insectary in

Department of Plant Protection at the School of Agriculture in the University of Jordan used to establish a colony of GPA, which kept in cages with a wooden frame of (60 × 40 × 45) dimension, with four (20x30cm) fine mesh doors. A continuous supply of new plants of sweet pepper provided as needed for the colony replenishment. Sweet pepper seeds Super Lamuyo (Scanttin seed company) were pre-germinated for three days in plastic Petri dish (9 x1.5 cm) lined on the bottom with wet filter paper before being planted in plastic seedling trays (50 × 30 × 60 cm, 50 seeds/tray) containing commercial potting soil peat moss (Kasvuturvas). After growing for 10 days under greenhouse conditions, seedlings in the primary leaf stage individually transplanted into a plastic pot (15 cm diameter) filled with the soil. Plants kept in a greenhouse at 22 ± 4°C in the campus of the University of Jordan. These plants regularly irrigated. The pots of plants placed on eight plastic cages in the insectary. Each cage contained twelve plant pots, supplemented with 16: 8 L: D average of temperature 22±2°C regime and irrigated as needed.

TABLE 1
Means of essential oil% and water content% for orange oil

Oil	Name	Part of the plant	Essential oil %	Water content %
Orange oil	*Citrus sinensis*	Peel	24.11	2.66

Oil Extracts. The orange oil bought from Talya Bitkisel Company (Amman-Jordan). Orange oil analyzed to determine the active ingredient percentage in the Laboratory of Fruits and Vegetables Processing at Department of Nutrition and Food Technology the University of Jordan as shown in (Table 1). The quantity of essential oil carried out as following. Five milliliters of oil taken in triplicates and placed into a previously weighed glass Petri dishes (12cm). Then placed in an oven at 75°C for 2 hours. After that, they taken from the oven, placed in desiccators to cool down for15 minutes and weighed. The difference between the first weight and the second was calculated and considered as the essential oil weight in grams. To determine the water contained in oil, the glass Petri dish with the oil again placed in the oven at 105°C for 3hr. Calculations for the water content percentage done for oil. Three replications for oil used each time.

Bioassays. In order to test the toxicity of the essential oil against *M. persicae*, the late (3rd and 4th) nymphal instars, and the early (1st& 2nd) nymphal instars of apterous aphid were placed on sweet pepper leaves in Petri dishes (9cm in diameter). The essential oil diluted with distilled water and Tween 20 (0.005 ml) (adjuvant). There were four concentrations for orange oil. Four solvents for each oil were bio-assayed. The used solvents were n- hexane (purity 99.5%), chloroform (purity 99.5%), ethanol (purity 99.9%), and acetone (purity 99.5%) and distilled water with tween 20 used as negative control. Four replicates used for each treatment. Oil diluted separately with the four solvents in four replicates. In addition, each solvent (four replicates) in each treatment tested separately against the green peach aphid. Each replicate had from 35to 50 aphids. The diluted oil with solvent shaken for 5 minutes by hand. A sprayer consisted of 18 ml glass container provided with an atomizer used for applying the treatments. One sprayer fixed for each concentration for each solvent. After application, Petri dishes left to dry for 15 minutes. Mortality rate of the aphids recorded after 24, 48, and 72h. Petri dishes sprayed with Calypso (neonicotinoid) insecticide at the recommended rate of the application considered as a positive control. Four replicates used for each concentration and/or treatment.

Statistical Analysis. Statistical Analysis Software (SAS, version 2014) used to analyze the obtained data from which both LC_{50} and LC_{90} executed from probit analysis.

RESULTS

Lethal Concentrations of Orange Oil. Orange oil with different solvents showed significantly the highest toxicity with both chloroform and ethanol solvents; the LC_{50} values were 0.005 and 0.008, respectively. The LC_{90} in case of acetone and n-hexane with orange oil showed significantly the least activity; the LC_{90} were 0.101and 0.097, respectively (Table 2).

TABLE 2
Concentration (v/v)-mortality data for the different solvents of orange oil on early nymphal instars of *M. persicae* after 24 hours of treatment.

Solvent	Slope	LC_{50}*	95%CL***	LC_{90}**	95%CL***	Chi-Square	Pr> Chi-Square
Ethanol	28.26	0.008^{a}	-0.019 - 0.027	0.086^{a}	0.055 - 0.196	13.70	0.0002
Acetone	30.10	0.028^{b}	0.008 -0.053	0.101^{c}	0.070 - 0.180	21.73	<.0001
n-hexane	25.87	0.012^{bc}	0.009 - 0.014	0.097^{b}	0.092 - 0.102	973.21	<.0001
Chloroform	26.95	0.005^{a}	-0.015 - 0.022	0.086^{a}	0.059 - 0.161	20.76	<.0001

*LC_{50} values sharing the same letters do not differ significantly (95%of CL aren't overlapping).
**LC_{90} values sharing the same letters do not differ significantly (95%of CL aren't overlapping).
***95% confidence limit for LC_{50} and LC_{90}.

TABLE 3
Concentration (v/v)-mortality data for the different solvents of orange oil on late nymphal instars of *M. persicae* after 24 hours of treatment.

Solvent	Slope	LC_{50}**	95%CL***	LC_{90}**	95%CL***	Chi-Square	Pr> Chi-Square
Ethanol	20.24	0.001^{b}	-0.025 - 0.018	0.110^{b}	0.071 -0.249	12.95	0.0003
Acetone	20.01	0.014^{c}	-0.007 - 0.031	0.124^{c}	0.096 -0.178	47.36	<.0001
n-hexane	23.80	0.0005^{a}	-0.007 - 0.007	0.092^{a}	0.075 - 0.120	76.59	<.0001
Chloroform	26.18	0.0004^{a}	-0.077 - 0.030	0.084^{a}	0.045 - 0.484	7.00	0.0081

*LC_{50} values sharing the same letters do not differ significantly (95%of CL aren't overlapping).
**LC_{90} values sharing the same letters do not differ significantly (95%of CL aren't overlapping).
***95% confidence limit for LC_{50} and LC_{90}.

TABLE 4
Effect of different solvent on efficacy of orange oil against early nymphalinstars of *M. persicae* using 100,000 ppm concentration after three times of treatment.

Solvents	Percentage Mortality ±SE		
	After 24h	After 48h	After 72h
Ethanol	$83.75^{c} \pm 2.17$	$89.00^{b} \pm 2.27$	$90.75^{b} \pm 1.88$
Acetone	$87.00^{bc} \pm 1.22$	$88.50^{b} \pm 1.32$	$89.75^{b} \pm 1.25$
Chloroform	$84.00^{c} \pm 1.08$	$87.50^{b} \pm 1.50$	$88.75^{b} \pm 1.25$
n-Hexane	$89.25^{b} \pm 1.15$	$89.75^{b} \pm 0.25$	$91.50^{ab} \pm 0.95$
Calypso	$94.00^{a} \pm 0.57$	$94.00^{a} \pm 0.57$	$94.75^{a} \pm 1.18$
Control	$4.00^{d} \pm 0.70$	$4.50^{c} \pm 1.19$	$6.75^{c} \pm 0.75$

Means within the same column sharing the same letters do not differ significantly at 5% level using LSD test.

TABLE 5
Effect of different solvent on efficacy of orange oil against late nymphal of *M. persicae* using 100,000 ppm concentration after three times of treatment.

Solvents	Percentage Mortality ±SE		
	After 24hours	After 48hours	After 72hours
Ethanol	$80.00^{d} \pm 1.08$	$84.75^{b} \pm 2.95$	$88.00^{b} \pm 3.10$
Acetone	$83.50^{bc} \pm 0.64$	$84.75^{b} \pm 1.03$	$86.75^{b} \pm 1.10$
Chloroform	$81.75^{dc} \pm 0.62$	$84.50^{b} \pm 1.19$	$85.25^{b} \pm 0.75$
n-Hexane	$85.25^{b} \pm 0.85$	$86.25^{b} \pm 0.94$	$87.25^{b} \pm 0.62$
Calypso	$94.00^{a} \pm 0.57$	$94.00^{a} \pm 0.57$	$96.00^{a} \pm 1.22$
Control	$4.00^{e} \pm 0.70$	$4.50^{c} \pm 1.19$	$6.75^{c} \pm 0.75$

Means within the same column sharing the same letters do not differ significantly at 5% level using LSD test.

Orange oil with chloroform and n-hexane showed significantly the most potent activity against the late nymphal instars of *M. persicae* at 10% concentration with LC_{50} of 0.0004 and 0.0005, respectively, and with LC_{90} of 0.084 and 0.092, respectively. The lowest significant activity obtained by using ethanol and acetone; the LC_{50} were 0.001 and 0.014, respectively and the LC_{90} were 0.110 and 0.124, respectively (Table 3).

Orange with Different Solvents. The acetone solvent with orange showed significantly the highest effect against the early nymphal GPA compared with the other different solvents that caused mortality ranged from 87 to 89.75%, but n-hexane caused higher mortality after 72 hours of the exposure (91.50%) (Table 4). There were significant differences between Calypso and all other solvents.

Table 5 shows that orange oil with n- hexane did cause significantly the highest mortality for the late nymphal instar of the GPA compared with the other tested solvent. Mortality ranged from 85.25 to 87.25%. Using acetone solvent resulted in mortalities 83.50, 84.75 and 86.75% after 24, 48 and 72h of exposure, respectively. None of the used solvents was as effective as the positive control, Calypso in controlling GPA.

DISCUSSION

Extensive use of insecticides in agriculture for controlling insect pests posed various problems, such as the environmental pollution [27]. Toxic hazards to human and other non- target organisms due to the broad spectrum of activity of insecticides were recorded [26, 27, 28, 29, 30]

and development of physiological resistance in major insect species including aphids [31, 32, 33]. The use of natural plant products is more sustainable, cheaper and safer [34,35]. Natural pesticides are preferred for many reasons. Of these, they are cheap compared with the chemical pesticides. In addition, they are made from local resources and safer to humans than chemical pesticides [36, 16, 17, 18, 19]. Several workers

[37, 38, 16, 17, 18, 19] studied their biological effects. Use of essential oils of many plants are effective natural insecticidal products to be included in the integrated pest management programs [39, 16, 17, 18, 19].

The present study showed that orange essential oil is promising insecticide that provides effective management of *M. persicae* to provide safe environment and crops with high quality.

ACKNOWLEDGEMENTS

The authors would like to thank the Deanship of Scientific Research at the University of Jordan, Agriculture Research Center of Libya and ICARDA for funding this research.

This work was supported by the University of Jordan under Deanship of Scientific Research Grant; Agriculture Research Center of Libya under ICARDA Grant.

REFERENCES

[1] Williams, I.S., Dixon, A.F.G. (2007) Life cycles and polymorphism. In: Van Emden, H.F., Harrington, R. (eds.) Aphids as crop pests. Wallingford: CAB International. 69–8.

[2] Al Antary, T.M. and Khader, B. (2013) Toxicity of four insecticides on longevity and fecundity of three populations of the green peach aphid Myzus persicae Sulzar (Homoptera : Aphididae) for three generations. Jordan Journal of Agricultural Sciences. 9(1), 52-62.

[3] Gray, S.M. and Gildow, F. (2003) Luteovirus-aphid interactions. Ann Rev Phytopathol. 41, 539-566.

[4] Girousse, C., Moulia, B., Silk, W., Bonnemain, J.L. (2005) Aphid infestation causes different changes in carbon and nitrogen allocation in alfalfa stems as well as different inhibitions of longitudinal and radial expansion. Plant Physiol. 137, 1474–1484.

[5] Pegadaraju, V., Knepper, C., Reese, J.C. and Shah, J. (2005) Premature leaf senescence modulated by the Arabidopsis thaliana PAD4 gene is associated with defense against the phloem-feeding green peach aphid. Plant Physiol. 139, 1927–1934.

[6] AL-Momany, A. and Al-Antary, T.M. (2008) Pests of Garden and Home, 2nd edition. Publications of University of Jordan, Amman. 518pp

[7] Kennedy, J.S., Day, M.F. and Eastop, V.F. (1962) A Conspectus of Aphids as Vectors of Plant Viruses. Commonwealth Institute of Entomology, London. 114 pp.

[8] Namba, R. and Sylvester, E.S. (1981) Transmission of cauliflower mosaic virus by the green peach, turnip, cabbage, and pea aphids. J Econ Entomol.74, 546-551.

[9] Shaaya, E., Kostjukovsky, M., Berg, J.E.H. and Sukprakarn, C. (1997) Plant oils as fumigants and contact insecticides for the control of stored-product Insects. J Stored Prod Res. 33(1), 7-15.

[10] Leake, A. (2000) The development of integrated crop management in agricultural crops: comparisons with conventional methods. Pest Manag Sci. 56(11), 950–953

[11] Ogend, J.O., Kostyukovsky, M., Ravid, U., Matasyoh, J.C., Deng, A.L., Omolo, E.O., Kariuki, S.T. and Shaaya, E. (2003) Bioactivity of Ocimumgratissimum oil and two constituents against five insect pests attacking stored food products. Stored Food Prod J. 44, 328-334.

[12] Bass, C., Alin, M.P., Christoph, T.Z., Lan, D., Linda, M.F., Stephen, P.F., Oliver, G., Ralf, N., Russell, S., Martin, S. and Williamson, S. (2014) The evolution of insecticide resistance in the peach potato aphid, Myzuspersicae. Insect Biochem. Mol Biol. 51, 41- 51

[13] Al Antary, T.M. and Khader, B. (2011) Susceptibility of three strains of green peach aphid Myzuspersicae Sulzar (Homoptera : Aphididae) for four pesticides. Advances in Environmental Biology. 5(11), 3599-3604.

[14] Al Antary, T.M., Alawi, M., Abu Othman, M. and Hadad, N. (2017) Levels of organochlorine pesticides residues in human breast milk from the northern districts in Jordan in 2013/2014. Fresen. Environ. Bull. 26, 4711-4715.

[15] Ateyyat, M. and Abu Darwish, M.S. (2009) Insecticidal activity of different extracts of Rhamnusdispermus (Rhamnaceae) against green peach trunk aphid, Pterochoroidespersicae (Homopetra: Lachinidae). Span J Agric Res. 7(1), 160-164.

[16] Mdanate, H., Al Antary, T.M. and Abu Zarka, M. (2016) Toxicity of six ethanol plant extracts against the green peach aphid Myzus persicae-Sulzar (Homoptera : Aphididae). Fresen. Environ. Bull. 25, 706-718.

[17] Mdanate, H., Al Antary, T.M. and Abu Zarka, M. (2017) Bioactivity of six acetone plant extracts against the green peach aphid Myzus persicae Sulzar (Homoptera : Aphididae). Fresen. Environ. Bull. 26, 3340-3349.

[18] Al Antary, T.M., Belqasim, I. and Araj, S. (2017) Toxicity of anise oil against the green peach aphid Myzus persicae Sulzar (Homoptera : Aphididae) using four solvents. Fresen. Environ. Bull. 26, 3705-3710.

[19] Antary, T.M., Belqasim, I. and Araj, S. (2017) Effect of mint oil against the green peach aphid Myzus persicae Sulzar (Homoptera : Aphididae) using four solvents. Fresen. Environ. Bull. 26, 61-67.

[20] Hori, M. (1999) Antifeeding, settling inhibitory and toxic activities of labiate essential oils against the green peach aphid, Myzus persicae (Sulzer) (Homoptera : Aphididae). Appl. Entomol. Zool. 34, 113-118.

[21] Abu-Darwish, S.M. and Ateyyat, A.M. (2008) The pharmacological and pesticidal actions of naturally occurring 1,8-dihydroxyantra-quinones derivatives. World J Agric Sci. 4, 495–505.

[22] Ateyyat, M.A., Al-Mazra'awi, M., Abu-Rjai, T. and Shatnawi, M.A. (2009) Aqueous extracts of some medicinal plants are as toxic as Imidacloprid to the sweet potato whitefly, Bemisiatabaci. J Insect Sci. 9,15–21.
[23] Ateyyat, M., Al-Antary, T.M., Al Mazrawi, M. and Abu-Romman, S. (2012) Efficacy of different extracts of Rhamnusdispermus Ehrenb. (Rhamnales: Rhamnaceae) as aphicides against Eriosomalanigerum (Hausmann) (Homoptera: Aphididae) and its parasitoid, Aphelinusmali (Hald.) (Hymenoptera: Aphelinidae). Adv Environ. Biol. 74, 39-45.
[24] Hakimi, S., Ateyyat, M. and Bounechada, M. (2015) Insecticidal activity of five essential oils of algerian medicinal plants on peach-potato aphid, Myzuspersicae (Homoptera: Aphididae). Adv. Environ. Biol. 9(2), 89-95.
[25] Alawi, M., Al Antary, T.M., Hussein, E. and Al-Oqlah, K. (2012) Comparison study of pesticides residues in agricultural crops in Jordan for seven studies between 1993 and 2008. Fresen. Environ. Bull. 21, 927-934.
[26] Blackman, R.L. and Eastop, V.F. (2000) Aphids on the World's Crops: An Identification and Information Guide (2nd). John Wiley and Sons Ltd, Chichester, UK. 466p.
[27] WHO (1992) Vector Resistance for Pesticides. World Health Organization Technical Report Serial 818, WHO, Geneva. 62p.
[28] Andrews, N., Miller, E., Grant, A., Stowe, J., Osborne, V. and Taylor, B. (2004) Thimerosal exposure in infants and developmental disorders: a retrospective cohort study in the United Kingdom does not support a causal association. Pediatr. 114(3), 584-91.
[29] Igbedioh, S.O. (1991) Effects of agricultural pesticides on humans, animals and higher plants in developing countries. Arch Environ Health. 46, 218.
[30] Jeyaratnam, J., Seneviratne, R.S. and Copplestone, J.F. (1982) Survey of pesticide poisoning in Sri Lanka. Bull World Health Organ. 60(4), 615–619.
[31] Ateyyat, M.A. and Hoy, M. (2015) Selection for resistance to spiromisifen in the predatory mite Metaseiulusoccidentalis (Acari: Phytoseiidae). Adv. Environ. Biol. 9(23), 388-392.
[32] Devonshire, A.L. (1998) Resistance of Aphids to Insecticides. PP.123-139. In: Minks, A.K. and Harrewijn, P. (eds.) Aphids Their Biology, Natural Enemies and Control, World Corp Pests. Elsevier, New York. Crop Prot. 19, 603–608.
[33] Koul, O., Walia, S. and DhlIwal, G. (2008) Essential oils as green pesticides: potential and constraints. Biopestic Int. 4(1), 63 – 84.
[34] Jiang, Z., Akhtar, Y., Bradbury, R., Zhang, X. and Isman, M.B (2009) Comparative toxicity of essential oils of *Litseapungens* and *Litseacubeba* and blends of their major constituents against the cabbage looper, Trichoplusiani. J Agric Food Chem. 57, 4833-4837
[35] Ben-Guo, Z., Wang, S., Dou, T., Liu, S., Mao, Y., Mao, H., Guang, L.and Feng, L. (2016) Aphicidal activity of *Illiciumverum* fruit extracts and their effects on the acetylcholinesterase and glutathione S-transferases activities in Myzuspersicae (Hemiptera: Aphididae). J. Insect Sci. 16(1), 11.
[36] Sharaby, A., Montasser, S.A. Mahmoud, Y.A. and Ibrahim, S.A. (2012) Plant extracts as alternative botanical insecticides for control the grasshopper *Heteracris littoralis* Ramb. (Orthoptera: Acrididae) with reference to histological changes on the reproductive system. J. Basic Appl.Sci. Res. 1(9), 1031-1038.
[37] Akhtar, Y., Yeoung, R.and Isman, M.B. (2008) Comparative bioactivity of selected extracts from Meliaceae and some commercial botanical insecticides against two noctuid caterpillars, *Trichoplusia ni* and *Pseudaletia unipuncta*. Phytochem Rev. 7, 77-88.
[38] Bakkali, F., Averbeck, S., Averbeck, D.and Idaomar, M. (2008) Biological effects of essential oil: A Review. Food Chem. Toxicol. 46, 446-475.
[39] Siskos, E.P., Konstantopoulou, M.A., Mazomenos, B.E. and Jervis, A.M. (2008) Insecticidal activity of citrus aurantium fruit, leaf, and shoot extracts against adult olive fruit flies (Diptera: Tephritidae). J. Econ. Entomol. 100, 1215-1220.

Received: **21.08.2017**
Accepted: **23.11.2017**

CORRESPONDING AUTHOR

Tawfiq M Al-Antary
Department of Plant Protection,
Faculty of Agriculture,
University of Jordan,
Amman 11942 – Jordan

e-mail: tawfiqalantary@yahoo.com

© by PSP Volume 27 – No. 2/2018 pages 1043-1052 Fresenius Environmental Bulletin

PORE STRUCTURES CHARACTERISTICS AND POROSITY EVOLUTION OF TIGHT SANDSTONE RESERVOIR: TAKING THE CHANG 6_3 TIGHT SANDSTONES RESERVOIR OF HUAQING AREA IN ORDOS BASIN AS AN INSTANCE

Dengke Liu[1,*], Wei Sun[1], Danchen Li[1], Jianchao Shi[2], Dazhong Ren[3]

[1]State Key Laboratory for Continental Dynamics, Department of Geology in Northwest University, Xi'an, P.R. China
[2]Exploration and Development Research Institute of Changqing Oilfield Company in Petro China, Xi'an, P.R. China
[3]Engineering Research Center of Western Low & Ultra-low Permeability Oilfield Development & Management in Xi'an Shiyou University, Xi'an, P.R. China

ABSTRACT

The tight sandstone reservoir of Chang 6_3 Formation of Huaqing Area in Ordos Basin were divided into three types based on its different pore types: formation with intergranular pore type, dissolved-intercrystalline pore type and pore plus fracture type reservoirs, which were dominated by casting thin sections, scanning electron microscope(SEM), granularity image, high-pressure mercury injection, constant-rate mercury injection, nuclear magnetic resonance and real sandstone micromodel experiment, and the porosity evolution path in each type were studied. The study shows that: The physical property, pore structure, and type of displacement in each reservoir type have obvious differences, which indicate that the reservoir classification evaluation which is based on pore assembly type has its own applicability in research region. Combined with parameters such as buried depth and temperature, the porosity evolution path has apparent control on pore structure. The porosity evolution of reservoirs with different pore types reveals the effect of increased and decreased porosity on the reservoir's quality. Pore structures have close relationship with productivity law.

KEYWORDS:
tight sandstone reservoir, Huaqing Area, pore and fissure assembly, porosity evolution, pore structures

INTRODUCTION

The exploration and development of tight sandstone reservoirs is an important part of oil and gas field production and storage, which has been paid more and more attention by scholars [1-3]. In recent years, there have been many studies on the depositional environment, macroscopic features including the lithologic and physical properties of the sediments, the diagenesis, the microscopic pore structure, and the distribution law of oil and water at home and abroad [4-6].

In China, the tight sandstone reservoirs are mainly distributed in the Mesozoic strata of the Ordos, Songliao, Sichuan and Junggar basins. And the fluvial facies, braided river delta facies, meandering river delta facies and shore-shallow lacustrine sand bar and beach facies are the main types of sedimentary facies [7]. According to the previous results, the feldspar and detritus contents of the tight sandstone reservoirs are relatively high compared with the conventional reservoirs. Meanwhile, the secondary pore is the main pore type, with the relatively complex pore-throat tortuosity, low porosity and the poor connectivity [7]. Thus, recognizing the development of pore structure is of great significance to develop the tight sandstone reservoirs.

At present, the research on the pore structure of the tight sandstone reservoir is focused on the pore type, pore-throat size and pore-throat sorting [5, 8-9], but pays less attention to the division of the tight sandstone reservoirs via the sedimentary, diagenetic and multi-parameter integrated way, and to the influence of porosity evolution history on the pore structure. In view of the above problems, this paper has carried on the related research on the Chang 6_3 tight sandstones reservoir of Huaqing Area in Ordos Basin in order to provide a reference for the production.

RESEARCH SITUATION

Research basic data and experimental data. In this paper, the study about the reservoir of Chang 6_3 Formation in Huajing Area is mainly based on the understanding of the analysis data of 39 coring wells in this area. Its physical properties are mainly determined by 115 pieces of pore permeability samples measured by gas. The analysis of the rock type, component characteristics, clay content and its distribution in pores and throats are mainly based on 50

pieces casting thin sections and 40 samples for scanning electron microscopy analysis. And the study on the pore-throat types and its morphological features is also based on 50 pieces casting thin sections and 40 samples for scanning electron microscopy analysis. Meanwhile, there are 20 granularity image samples used to analyze the distribution characteristics of granularity. The application of high-pressure mercury injection with 25 samples and constant-rate mercury injection with 10 samples is to determine the microscopic pore structure characteristics of the reservoir. The results of the nuclear magnetic resonance experiments with 10 samples are used to determine the development of the pores in different sizes. And the application of the microscopic displacement experiment using 10 real sandstone samples is to simulate the characteristics of development.

Regional geologic background. The Huafeng area of the Ordos Basin is located in the southwest of Yishan Slope, and is constructed with a gentle western-leaning monoclinic slope and even a nasal uplift caused by the differential compaction. Triassic Chang6_3 reservoir is the main oil production position, and the sedimentary environment of it includes the braided river delta front and semi-deep lake-deep lake facies (Fig. 1).

The porosity measured by helium is between 4.22% and 13.97%, with an average of 9.08%. The measured permeability is 0.02 ~ 3.11mD, with an average of 0.25mD, which indicates that the reservoir is the typical tight sandstone reservoir [10-12]. The lithology of reservoir is chiefly fine-grained feldspar sandstone and lithic feldspar sandstone with medium-poor sorting and sub-prism roundness. Then the second largest component is feldspar lithic sandstone.

RESERVOIR CLASSIFICATION BASED ON PORE TYPES

The pore type is an important parameter of the microcosmic characteristics of the reservoir, which is a comprehensive characterization of the microscopic pore structure [8, 13-14]. Therefore, the classification of reservoirs based on the pore type combination is an important reference for the rational development of reservoirs which takes full advantage of micro-parameters and macroscopic properties. In this study, the reservoirs of the study area were divided into three types based on its different pore types: formation with intergranular pore type, dissolved-intercrystalline pore type and pore plus fracture type reservoirs, which were dominated by casting thin sections, scanning electron microscope, granularity image, high-pressure mercury injection, constant-rate mercury injection, nuclear magnetic resonance and real sandstone micromodel experiment, (Table 1, Figure 2, and Figure 3).

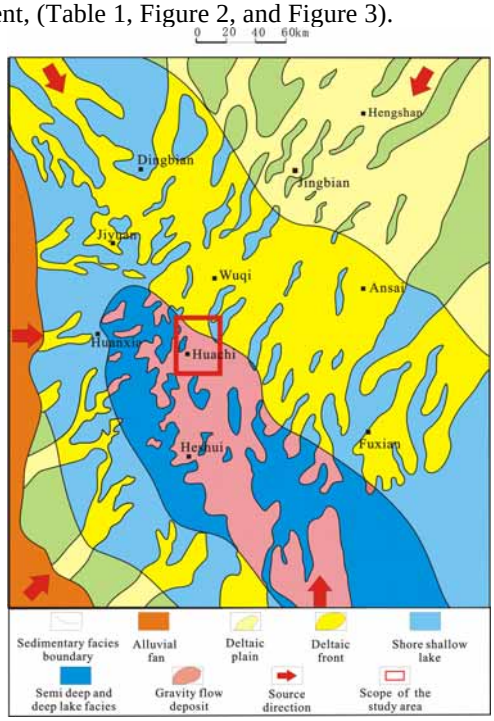

FIGURE 1
Ordos Basin geographical locations [10]

Reservoirs with the intergranular pore type. The study of the length of the reservoir 63 is the accumulation of intergranular pores, which has undergone mechanical compaction and cementation. The mechanical compaction makes the particles tend to be tightly arranged, the porosity decreases and the permeability becomes worse. The main manifestations are particles arranged in a certain degree of orientation, contact from the point of contact into the line contact, mica and other soft components of mineral pseudo-heterogeneous and occupy the pore space, occasionally particles rupture (Figure 2 (a1)). The type of reservoir interstitial is mainly chlorite (Fig. 2 (a2)). On the one hand, the cementite cement occupies a certain pore space, but at the same time, the development of chlorite leaking prevents the cementation of other clay minerals, Preserves the pores [15-17]. The overall porosity of the residual pelletized reservoir is high, and the pore size and connectivity are good.

The average porosity of the samples with the intergranular pore type is 10.55% and the average permeability is 0.63mD. The capillary pressure curve shows that the threshold pressure and the median pressure of the reservoir are both low. The platform segment of the curve is clear, and the final mercury saturation is high (Table 1, Figure 3 (a1)). The distribution of throat radius obtained by constant-rate mercury injection shows that the distribution of the throat in this kind of reservoir is more homogeneous. There are mainly the small-middle throats with a small amount of large throats. The heterogeneity of the throat is medium, but the distribution is

homogeneous with the large average throat radius. (Table 1, Figure 3 (a2)).

The state of nuclear magnetic resonance T_2 spectrum is bimodal which is high in right and low in left or bimodal with double peaks, with <10ms, 10 ~ 100ms and> 100ms as the threshold of clay mineral micropores, mesopores and macropores [18-19]. The fluid saturation of these samples is relatively low, and the movable fluid saturation is relatively high. The movable fluid mainly occurs in the mesopores and a small amount of macropores (Table 1, Figure 3 (a3)). The experimental results show that this kind of pore type has high oil displacement efficiency, and the water phase displaces evenly with less residual oil (Table 1, Fig. 2 (a3)).

Reservoirs with the dissolved pore type. The dissolution of the study area is common, the feldspar dissolution is the main, the erosive dissolution is the second, the dissolution of the hybrid and the cement is less, and the dissolution of the grain and grain edge is more common, which indicates that the study area is mainly acidic hydrocarbon (Fig. 2 (b1), Fig. 2 (b2)). The effect of dissolution on the reservoir properties is improved to a certain extent, and the porosity is increased. But the secondary dissolution has increased the non-homogeneity of the reservoir to a certain extent and provided the material basis for the later clay mineral cementation to form intergranular micropores that have no reservoir and seepage capacity (Fig. 2 (b1)).

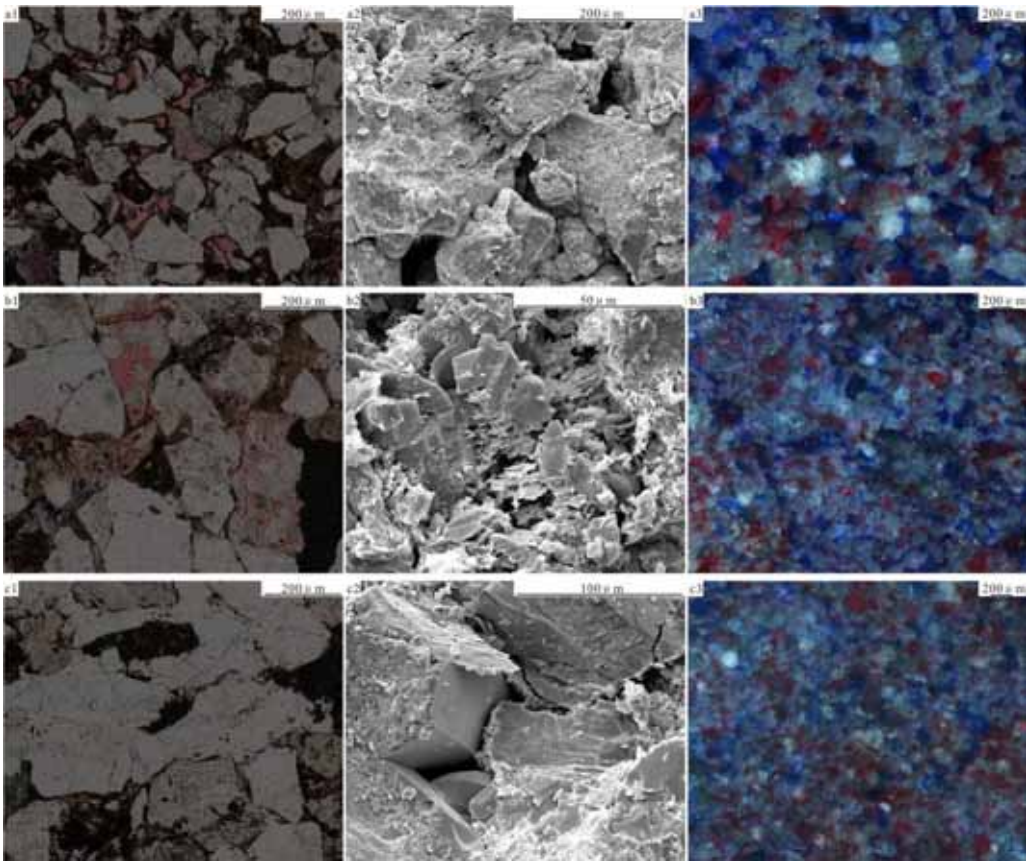

(a1) Particle semi-directional arrangement, residual intergranular pore, the chlorite film wraps the debris particles, casting thin section, B427, 1938.25m；(a2) Residual intergranular pore, the chlorite film wraps the debris particles, B427, 1938.25m；(a3)The final stage picture of displacement of oil by water, homogeneous displacement style, B427, 1938.25m(water started from the left and ended in the right, water liquor is blue, simulated oil is red)；(b1) Particle semi-directional arrangement, feldspar dissolved pore with carbonate cement, casting thin section, S156, 2171.45m；(b2) feldspar dissolved pore, SEM, S156, 2171.45m；(b3) The final stage picture of displacement of oil by water, reticular displacement style, S156, 2171.45m(water started from the left and ended in the right, water liquor is blue, simulated oil is red)；(c1)Increasing shaped quartz, poorly developed secondary pores, casting thin section, B483, 2012.78m；(c2)Fracture, SEM, B483, 2012.78m；(c3) The final stage picture of displacement of oil by water, reticular and fingerlike displacement style, B483, 2012.78m(water started from the left and ended in the right, water liquor is blue, simulated oil is red)

FIGURE 2

The microscopic photos in casting thin sections, scanning electron microscope and water-flooding experiments with the real sandstone micromodel in research area

TABLE 1
Statistics of macro and micro parameters in research area

Well	Depth /m	Lithology	Φ /%	K /mD	P_c /MPa	P_{50} /MPa	S_{max} /%	R /μm	S_m /%	Reser-voir type
B259	2187.3	Medium and fine-grained feldspar lithic sandstone	12.51	0.56	0.72	4.05	82.47	0.57	46.55	A
B427	1938.3	Fine-grained lithic feld-spathic sandstone	10.27	0.85	0.95	3.77	83.63	1.28	55.94	A
B465	2090.3	Fine-grained feldspar lithic sandstone	8.88	0.48	0.73	3.36	89.81	0.83	45.67	A
B168	2087.9	Fine-grained lithic feld-spathic sandstone	8.74	0.17	1.16	5.49	85.78	0.91	36.42	B
B480	2004.4	Medium and fine-grained lithic feld-spathic sandstone	10.05	0.06	1.81	7.15	87.57	0.34	32.11	B
S156	2171.5	Fine-grained lithic feld-spathic sandstone	8.97	0.14	1.15	11.78	79.65	0.96	29.48	B
Y414	1999.2	Fine-grained lithic feld-spathic sandstone	8.25	0.10	1.75	15.16	89.46	0.33	25.58	B
B269	1943.9	Fine-grained lithic feld-spathic sandstone	6.42	0.35	2.05	10.54	77.08	0.20	2.16	C
B463	1984.3	Fine-grained feldspar lithic sandstone	11.63	0.44	1.35	8.15	89.50	0.30	6.02	C
B483	2012.8	Fine-grained lithic feld-spathic sandstone	8.02	0.19	1.81	7.48	83.84	0.26	20.98	C

*Φ=porosity, K=permeability, P_c=threshold pressure, P_{50}=median pressure, S_{max}=maximum mercury saturation, R=throat radius, S_m= movable fluid saturation; In reservoir type: A=reservoirs with the intergranular pore type, B=reservoirs with the dissolved pore type, C=reservoirs with pore plus fracture.

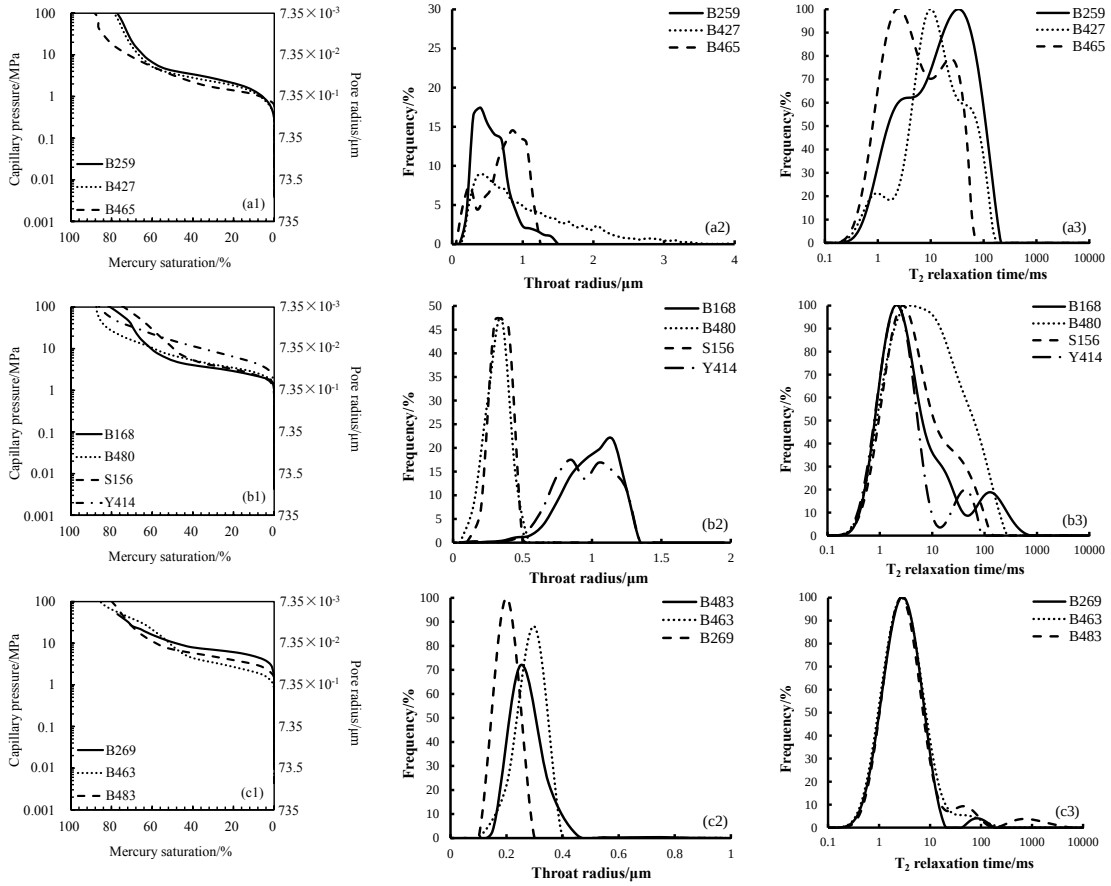

FIGURE 3
The curves of capillary pressure, throat radius and T_2 spectrum distribution

The average porosity of these samples in the study area is 9.00% and the average permeability is 0.12mD. The capillary pressure curve shows that there is an increase both in the threshold pressure and median pressure of the reservoir with the dissolved pores compared with the reservoir with intergranular pores. Meanwhile, it has a shorter and less obvious platform segment, and the final mercury saturation is slightly reduced (Fig. 3 (b1)).

The distribution of throat radius obtained by constant-rate mercury injection shows that the distribution of the throat is simpler with regard to this kind of reservoir mainly consisting of small throats, and relatively rare throats with the radius longer than 1μm (Fig. 3 (b2)). The magnetic resonance T_2 spectrum is bimodal which is high in left and low in right or singlet. Meanwhile, the irreducible water saturation is higher than that of the residual particles and the fluid content of the reservoir is reduced. This kind of reservoir is mainly composed by micro-small pore. Medium pores can be found sometimes but large pores are really rare to see (Figure 3 (b3)). The microscopic displacement experiment of the real sandstone samples indicates a reticular displacement. The water phase flows circuitously and the displacement is not as effective as the first kind with a certain amount of residual oil (Fig. 2 (b3)).

Reservoirs with pore plus fracture. The fractures of the Chang 6_3 reservoir in Huaqing area are almost diagenetic fractures, which are usually caused by strong mechanical compaction, so the quality and the porosity of the rock samples which have developed fractures are pretty low (Fig. 2 (c1)). During the development of reservoirs, it is very important to study the influence of fractures on the seepage flow, which has a positive effect on the increase of the water absorption coefficient of injection wells but increases the heterogeneity oh the reservoir, causing the water channeling in the development process at the same time [20-21] (Fig. 2 (c2)).

Through the microscopic displacement experiment of the real sandstone samples, this kind of reservoirs shows a finger-like displacement.

The average porosity of this type in the study area is 8.69% and the average permeability is 0.33mD. The threshold pressure and median pressure of it are further increased, and the curve platform section becomes shorter. Some samples have two platform sections, and the change of the final mercury saturation is not obvious (Fig.3 (c1)). The distribution of throat radius shows that this kind of samples has a simpler distribution of throats, and the radius of them do not exceed 1μm. But the crack does not respond in the throat radius distribution (Fig. 3 (c2)). Meanwhile, the magnetic resonance T_2 spectrum is in the multimodal state, and the saturation of the irreducible water is the highest. The movable fluid content is further reduced, and the pores are mainly belongs to the micropore interval which is less than 10ms. The pores between the 10 ~ 100ms interval are less, and the peak which is more than 100ms belongs to the response of the crack (Figure 3 (c3)). Through the microscopic displacement experiment of the real sandstone samples, this kind of reservoirs shows a finger-like displacement. The water phase moves along the cracks, so the area affected is very small. As a result, the effect of the displacement for this kind of reservoirs is low and most of the residual oil still remains in the pores (Fig. 2 (c3)).

STUDY ON POROSITY'S DENSITY EVOLUTION OF DIFFERENT TYPES OF RESERVOIR POROSITY

Diagenesis is an important factor to cause the deformation of original porosity. Different pore types have different evolution processes, which lead to the characteristics of the pore structure. The Chang 6_3 reservoir in Huaqing area mainly experienced the early mechanical compaction → quartz overgrowth stage I → chlorite coating → dissolution stage I → late chlorite coating → dissolution stage II → oil and gas filling → siliceous overgrowth → the diagenetic evolution of Carbonate, illite, kaolinite cementation. The diagenesis now is in the middle diagenetic stage B [22].

TABLE 2
Quantitative calculation method of porosity evolution in sandstone reservoir

Porosity evolution parameters (%)	Formula	Comments
Initial porosity	$\Phi_1=20.91+22.90/S_d$	Φ_1=initial porosity (%); S_d=sorting coefficient ($S_d=(P_{25}/P_{75})^{1/2}$), P_{25} and P_{75}=grain size in 25% and 75% of grain size accumulation curve
Reduction of porosity because of compaction	$\Phi_2=\Phi_1 exp^{nh}$	Φ_2=The residual porosity after compaciton (%), exp=exponent, n=fitting constants, h=burial depth(m)
Reduction of porosity because of cementation	$\Phi_3=C$	Φ_3= reduction of porosity because of cementation (%), C=cement content (%); It can be separated from $\Phi_{3\text{-}e}$ for early cementation and$\Phi_{3\text{-}e}$ for late cementation
Increase of porosity because of dissolution	$\Phi_4=P_1\times P_2/P_3$	Φ_4=increase of porosity because of dissolution (%), P_1=surface porosity because of dissolution (%), P_2=porosity measured by helium (%), P_3=total surface porosity (%)

In this study, the diagenesis characterization of the porosity takes use of literature reference [23-25] and the physical parameters to screen the porosity evolution parameters (Table 2). Combined with the burial depth, the porosity varies with the changes of the temperature affected by the stratigraphic chronology and depth. And the B427, S156 and B483 were used as the samples of residual intergranular pore reservoirs, dissolution pore-intergranular pore type reservoirs and pore plus fracture reservoirs respectively to do the contrastive research of these three reservoirs.

Initial reduction of porosity because of mechanical compaction. The history of sedimentation lasts for 203.5Ma, and its burial depth is about 885m. The sediments are buried quickly and are strongly compacted. The initial porosity decreases from 37.97% ~ 39.00% to about 25.62% ~ 28.24%, and then a small uplift erosion occurs at about 197.5Ma (Fig. 4). The weak effect of it on the porosity is negligible.

The subsidence is keeping during 197.5 ~ 180.0Ma, and the depth of burial is up to about 1165m. The compaction continues to play the role of reducing the hole, and the early cementation begins to work. The porosity decreases to about 13.00% ~ 17.14% because of these two effects. The small uplift erosion event around 180.0 to 176.0 Ma also has a negligible effect on porosity (Figure 4).

The original porosity of these three kinds of reservoirs are close, indicating that their mineral compositions and structures belong to the same deposition system. In the period of mechanical compaction, the loss of porosity affected by the three types of compaction is about 21.87%, 22.92% and 25.45% respectively. The compaction has the greatest effect on the decrease of the porosity, and it is also the most important diagenetic effect on the reservoir. The mechanical compaction is the major factor for fractured reservoirs to be tight. The preservation of porosity in the residual intergranular reservoirs is related to the weaker mechanical compaction closely (Figure 4, Table 3).

Early reduction of porosity because of cementation. About 176.0~150.5 Ma ago, the depth of the burial was up to 1669m, so the porosity kept further reducing because the compaction caused by the formation pressure. Then the standard could be divided according to different stages. In this stage, the diagenesis included the early cementation of chlorite, calcite, the secondary quartz increases and others besides compaction. And the weak dissolution also occurred at this stage. The porosity decreased to about 8.00%~11.14% because of all these effects. Meanwhile, the changes of the porosity caused by uplift erosion around 150.5 ~ 146.0Ma could be ignored (Fig. 4).

The loss of porosity due to early cementation in the reservoirs with intergranular pore type, dissolved-intercrystalline pore type and pore plus fracture type is 6.00%, 7.00% and 5.00% respectively. The early cementation is one of the most important factors for the densification of the dissolved-intercrystalline pore type reservoir. However, the clay minerals produced by early cementation are mainly porous lined chlorite and the sparry calcite. Although the chlorite accounts for some of the pore space, it also sets obstacles for the subsequent compaction, late quartz secondary increase, microcrystalline calcite cementation and other kinds of destructive diagenetic effects [15-17]. Compared with the microcrystalline calcite, the sparry calcite has a weaker degree of densification, and the damage of it is relatively smaller (Figure 4, Table 3).

Porosity's increase stage because of dissolution. From 150.5 to 139.0Ma, the depth of burial was around 1798m, the pyrolysis of kerogen formed the carboxylic acid which leaded to the selective dissolution of some soluble components (feldspar, cuttings, etc.). At this stage, the quartz secondary increase was continuing, and compaction was also keeping with the increase of the depth. But the reduction in porosity caused by total compaction and cementation could be negligible compared to the strong dissolution (porosity increases to 12.12% ~ 13.70%) (Fig. 4).

The increase of porosity due to the dissolution in the reservoirs with intergranular pore type, dissolved-intercrystalline pore type and pore plus fracture type is 2.57%, 4.19% and 4.12%, respectively. The content of quartz is relatively high but the content of the soluble fraction, for example, fissile, is relatively low, and the fracture becomes a favorable channel for the acid fluid to enter the pore plus fracture type reservoir (Fig. 4, Table 3).

TABLE 3
Statistics of porosity evolution parameters of representative samples in various reservoir types

Well	Depth/m	Φ_1/%	Φ_2/%	L_1/%	$\Phi_{3\text{-}e}$/%	L_2/%	Φ_4/%	L_3/%	$\Phi_{3\text{-}e}$/%	L_4/%	P/%
B427	1938.25	39.00	21.87	17.14	6.00	11.14	2.57	13.70	3.00	10.70	10.27
S156	2171.45	37.97	22.92	15.05	7.00	8.05	4.19	12.23	3.00	9.23	8.97
B483	2012.78	38.45	25.45	13.00	5.00	8.00	4.12	12.12	5.00	7.12	8.02

*L_1=residual porosity after compaction, L_2=residual porosity after early cementation, L_3==residual porosity after dissolution, L_4==residual porosity after late cementation, P=porosity measured by helium

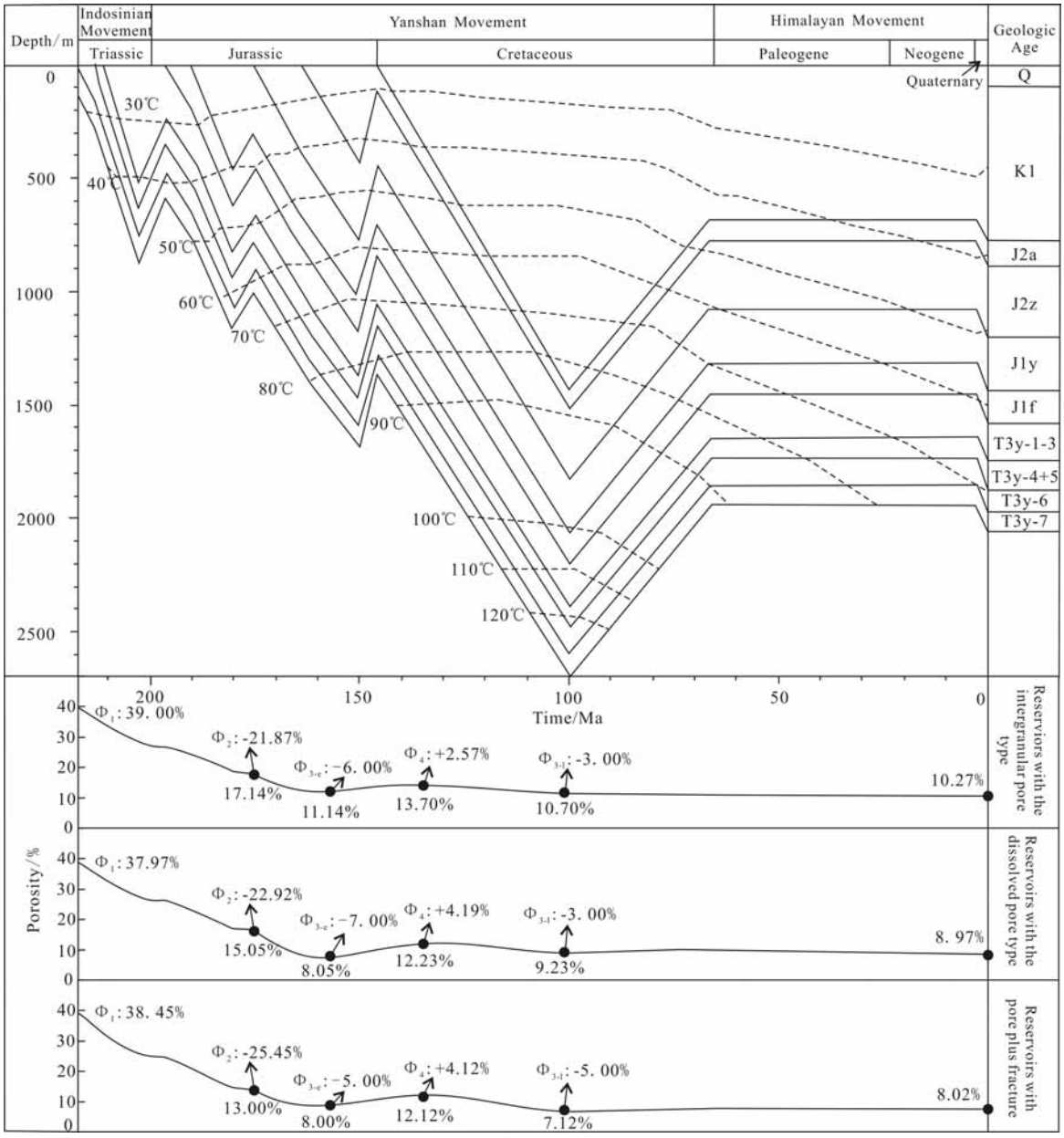

FIGURE 4
Porosity evolution history of different reservoirs in research area

Hydrocarbon charging and middle-late porosity reduction because of cementation. From 139.0 to 100.0Ma, the formation continued to be buried quickly, about 2709m at maximum. A large number of oil and gas charged into the reservoir, inhibited the cementation and dissolution effectively, and the fluid environment gradually transferred to alkaline environment. The degree of mineral cementation (calcite, chlorite, etc.) increased (Fig. 4), and the porosity caused by late cementation decreased to about 7.12% ~ 10.70%.

From 100.0Ma to now, the stratum slowly uplifted to 2055m, then the oil and gas charging was gradually stopped, and the erosion occurred. Alkaline authigenic minerals kept cementing and filling the pores. The final porosity measured by the gas is around 8.02% ~ 10.27%, matching well with the results of porosity evolution simulation (Figure 4, Table 3).

At this stage, the reduction of porosity in the reservoirs with intergranular pore type, dissolved-intercrystalline pore type and pore plus fracture type is 3.00%, 3.00% and 5.00%, respectively. Compared with the early cementation, the authigenic minerals produced under the alkaline environment during the late period have greater reduction and destructive effect on the porosity. The carbonate minerals such as the calcite are mostly microcrystalline, and the chlorite lining is replaced by pompon-like filling. The late cementation is developed in the pore plus fracture type reservoir, so the reduction of the porosity during the late cementation is more obvious than other two kinds of reservoirs (Fig. 4 and Table 3).

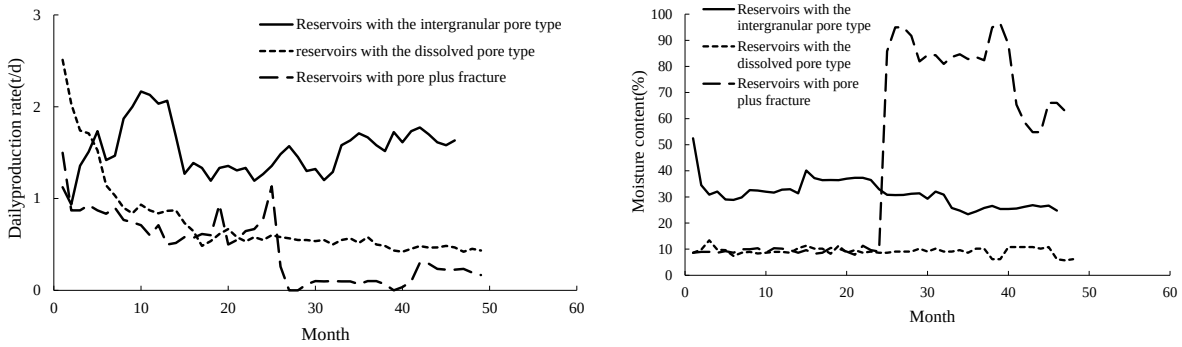

FIGURE 5
Production performance of different reservoir types

THE TYPE AND CAPACITY RESPONSE OF RESERVOIRS

The dynamic response of single well production in Huaqing area can objectively evaluate the relationship between different reservoir types, daily oil production of single well and moisture content. Figure 5 shows that the intergranular pore type reservoir has a high and stable production of the oil with a stable content of the water. But the oil production of reservoir with dissolved-intercrystalline pore type is depleted, and its water content is less stable. For the pore plus fracture reservoir, its initial production of oil keeps in a stable condition, but due to the existence of cracks and the occurrence of water channeling, the production plummeted and the water content soared until almost no capacity. The relationship between different reservoir types and the reservoir's productivity shows that the division of reservoirs based on the pore type is a favorable parameter that reflects the dynamics of reservoir production and can be used to characterize the production capacity.

CONCLUSION

According to the type of pore assemblage, the reservoirs in the study area can be divided into intergranular pore reservoirs, dissolved-intercrystalline pore reservoirs and pore plus fracture reservoirs. Because of different petrological characteristics, mineral compositions and arrangements, the characteristics of the pore structure and the effect of water-oil displacement in the real sandstone are obviously different. Therefore, the reservoir classification and evaluation based on the type of pore assemblages have certain practical value.

Through the simulation of porosity evolution based on the buried history of the Chang6 formation of the Quaternary, the evolution of the porosity can be divided into initial reduction of porosity because of mechanical compaction, early cementation, dissolution, hydrocarbon charging and middle-late porosity reduction due to cementation. Meanwhile, the path of porosity evolution in the three types of reservoirs at different stages is different. This difference is an important factor influencing the different macroscopic and microscopic characteristics of different types of reservoirs.

The dynamic characteristics of reservoirs are closely related to the reservoir types. The macroscopic and microscopic properties of reservoirs are important factors influencing the change of oil production and the water content of reservoirs. The mathematical model of reservoir characteristics and porosity evolution is used to characterize oil and gas production and it does have a positive meaning.

ACKNOWLEDGEMENTS

Foundation item: Project (2011ZX05044) supported by the National Science and Technology Major Program of China; Project (2015KTCL01-09) supported by the Innovation Project of Science and Technology of Shaanxi Province; Project (2015M582699) supported by the China Postdoctoral Science Foundation; Project (2016JQ4022) supported by the Natural Science Foundation Research Project of Shaanxi Province.

REFERENCES

[1] Zou, C.N., Zhu, R.K., Wu, S.T., Yang, Z., Tao, S.Z., Yuan, X.J., Hou, L.H., Yang, H., Xu, C.C., Li, D.H., Bai, B., Wang, L. (2012) Types, characteristics, genesis and prospects of conventional and unconventional hydrocarbon accumulations: taking tight oil and tight gas in China as an instance. Acta Perolei Sinica, 33(2), 173-187.

[2] Jia, C.Z., Zou, C.N., Li, J.Z., Li, D.H., Zheng, M. (2012) Assessment criteria, main types, basic features and resource prospects of the tight oil in China. Acta Perolei Sinica. 33(3), 343-350.

[3] Zhao, J.Z., Bai, Y.B., Cao, Q., Er, C. (2012) Quasi-continuous hydrocarbon accumulation: A new pattern for large tight sand oilfields in the Ordos Basin. Oil&Gas Geology. 33(6), 811-827

[4] Chen, S.J., Zhang, H.X., Lu, J.G., Yang, Y.M., Liu, C.W., Wang, L., Zou, X.L., Yang, J.J., Tang, H.P., Yao, Y.T., Huang, Y.L., Ni, S., Chen, Y.Y. (2015) Controlling factors of Jurassic Da'anzhai tight oil accumulation and high production in central Sichuan Basin, China. Petroleum Exploration and Development. 42(2), 186-193.

[5] Wang, M.L., Zhang, S.A., Zhang, F., Liu, Y.T., Guan, H., Li, J., Shao, L.Y., Yang, S., She, Y.Q. (2015) Quantitative research on tight oil microscopic state of Chang 7 Member of Triassic Yanchang Formation in Ordos Basin, NW China. Petroleum Exploration and Development. 42(6), 1-5.

[6] Cai, L.X., Lu, S.F., Huang, W.B., Li, A., Ren, H.S. (2016) Controlling function of overlying high-quality source rocks on above-generation and below-storage tight oil reservoir: taking mudstone in Q_{n1} formation at central depression in southern Songliao basin as an instance. Journal of China University of Mining& Technology. 45(2), 270-282.

[7] Zou, C., Tao, S., Hou, L. (2011) Unconventional Petroleum Geology. Beijing: Geological Publishing House. 103-117.

[8] Zhu, H.H., Zhong, D.K., Zhang, Y.X., Sun, H.T., Du, B.Q., Meng, H., Zhang, C.W., Yang, Z. (2014) Pore types and controlling factors on porosity and permeability of Upper Triassic Xujiahe tight sandstone reservoir in Southern Sichuan Basin. Oil & Gas Geology. 35(1), 65-76.

[9] Zhu, H., Xu, X., Gao, Y., Hu Y., An, L., Guo, C. (2014) Occurrence Characteristics of Tight Sandstone Pore Water and Its Influence on gas seepage: A case study from the Denglouku gas reservoir in the Changling Gas Field, southern Songliao Basin. Natural Gas Industry. 34(10), 54-58.

[10] Yang, H., Fu, J.H., He, H.Q., Liu, X.Y., Zhang, Z.Y., Deng, X.Q. (2013) Formation and distribution of large low-permeability lithologic oil regions in Huaqing. Ordos Basin. Petroleum Exploration and Development. 39(6), 641-648.

[11] Guo, Y.R., Liu, J.B., Yang, H., Liu, Z., Fu, J.H., Yang, J.L., Xu, W.L., Zhang, Y.L. (2012) Hydrocarbon accumulation mechanism of low permeable tight lithologic oil reservoirs in the Yanchang Formation, Ordos Basin, China Petroleum Exploration and Development. 39(4), 417-425.

[12] Yang, Y.Y., He, K.N., Ren, Y.S. (2015) The Internal Structure Pattern Analysis of Chang 6_3 Reservoirof Huaqing Area. Acta Sedimentologica Sinica. 33(2), 357-363.

[13] Ren, D.Z., Sun, W., Wei, H., Zhou, S.X., Zhang, Y.G., Zhang, X. (2014) Types of Sandstone Reservoir Diagenetic Facies and Microscopic Pore Structure Characteristics of Chang 8_1 Reservoir in Huaqing Oilfield. Geoscience. 28(2), 379-387.

[14] Zhou, X., He, S., Liu, P., Ju, Y.J. (2016) Characteristics and classification of tight oil pore structure in reservoir Chang 6 of Daijiaping area, Ordos Basin. Earth Science Frontiers. 23(3), 253-265.

[15] Huang, H. (2010) Experimental study on the factors of influencing the seepage feature of the fluid in Xifeng extra -low permeability reservoir. Journal of Xi an Shiyou University (Natural Science Edition). 25(6), 35 -37.

[16] Wen, X.H., Zhou, T., Hu, Y., Zhu, H.Y., Wang S.Y. (2010) Experimental study of properties and influencing factors of gas flow in tight core. Petroleum Geology & Experiment. 32(6), 592 - 595.

[17] Zhu, H.Y., Fu, D.Q., Zhuo, X.J., Ben, Y.M (2009) Experimental study on special percolation mechanism of low-permeability gas reservoir. Natural Gas Exploration and Development. 32(3), 39 -41.

[18] Li, H.B., Guo, H.K., Liu, Q., Meng, Z.Q., Wang, X.W., Sun, Y.P. (2014) NMR experimental study of water displacing oil of tight oil reservoir. Journal of Central South University (Science and Technology). 45(12), 4370-4376.

[19] Su, J.L., Sun, J.M., Wang, T., Zhang, S.W. (2011) An improved method of evaluating reservoir pore structure with nuclear magnetic log data. Journal of Jilin University (Earth Science Edition). S1, 380-386.

[20] Ju, W., Hou, G.T., Feng, S.B., Zhao, W.T., Zhang, J.Z., You, Y., Zhan, Y., Yu, X. (2014) Quantitative prediction of the Yanchang Formation Chang 6_3 reservoir tectonic fracture in the Qingcheng-Heshui Area, Ordos Basin. Earth Science Frontiers. 21(6), 310-320.

[21] Yang, D., Zhao, Y.S., Hu, Y.Q., Chang, Z.X. (2005) Theoretical and experimental studies on gas seepage law in a single fracture under 3D stresses. Chinese Journal of Rock Mechanics and Engineering. 24(6), 999-1003.

[22] State Economic and Trade Commission (2003) SY/T 5477-2003, Petroleum and gas industry standard, People's Republic of China. Beijing: Petroleum Industry Press.

[23] Schmid, S., Worden, R.H, Fisher, Q.J. (2004) Diagenesis and reservoir quality of the Sherwood Sandstone (Triassic), Corrib Field, Slyne Basin, West of Ireland. Marine & Petroleum Geology. 21(3), 299-315.

[24] Gier, S., Worden, R.H., Johns, W.D., Kurzweil, H. (2008) Diagenesis and reservoir quality of Miocene sandstones in the Vienna Basin, Austria. Marine & Petroleum Geology. 25(25), 681-695.
[25] Wu, X.B., Hou, J.G., Sun, W. (2011) Microstructure characteristics and quantitative analysis on porosity evolution of ultra-low sandstone reservoir. Journal of Central South University (Science and Technology). 42(11), 3438-3446.

Received: **28.08.2017**
Accepted: **03.12.2017**

CORRESPONDING AUTHOR

Dengke Liu
State Key Laboratory for Continental Dynamics, Department of Geology in Northwest University, Xi'an – P.R. China.

e-mail: liudengke02@stumail.nwu.edu.cn

© by PSP Volume 27 – No. 2/2018 pages 1053-1059 Fresenius Environmental Bulletin

COMPARATIVE ANALYSIS OF ENERGY USE EFFICIENCY IN FOOD GRAIN PRODUCTION SYSTEMS OF PAKISTAN

Adnan Abbas[1], Minli Yang[1,2,*], Khurram Yousaf[3], Khurshied Ahmed Khan[4], Tahir Iqbal[5], Shahbaz Gul Hassan[6]

[1]College of Engineering, China Agricultural University, Beijing 100083, China
[2]China Research Center for Agricultural Mechanization Development, China Agricultural University, Beijing 100083, China
[3]College of Engineering, Nanjing Agricultural University, Nanjing, China
[4]College of Water Resources and Civil Engineering, China Agricultural University, Beijing 100083, China
[5]School of Renewable Energy, North China Electric Power University, Beijing 102206, China
[6]College of Engineering, South China Agriculture University, China

ABSTRACT

Energy sustainable crops are the requirement of the modern era, where highly populated world requires an intensive supply of food grains. This study deals with the evaluation of energy consumption pattern in food grain production systems of Pakistan. A cross sectional data of 240 food grain farmers (corn and wheat growers) were collected for investigation. Results revealed that the total inputs energy to corn and wheat were 48904.80 and 27635.50 MJ ha^{-1} with an output energy of 116188.8 and 57798.0 MJ ha^{-1}, respectively. Fertilizer, diesel fuel, and water were the main energy consuming inputs in grain production systems of Pakistan, contributing 85% of total input energy. Moreover, energy efficiency, specific energy, energy productivity and net energy gain in corn and wheat production were calculated as 2.38 and 1.86, 6.19 and 6.99 MJ Kg^{-1}, 0.16 Kg MJ^{-1} and 0.14 Kg MJ^{-1}, and 67284.00, 23740.50 MJ ha^{-1} respectively. It was ensued that corn using 1.77 times more input energy than wheat and produced 2.26 times higher than that of wheat. The energy use efficiency based conclusion was drawn that corn production found more sustainable as compared to wheat, so corn could be prioritized as a more suitable planting crop in the selected area of study.

KEYWORDS:
Energy use efficiency, sustainable crop production, energy consumption pattern in corn and wheat, energy productivity

INTRODUCTION

Agriculture has always play an imperative role in the economy of Pakistan, irrespective of hasty urbanization and economic discrepancy, it still provides 42% employment of the total labor and contributes 19.8% in gross domestic product (GDP) [1]. Considering the backbone of Pakistan's economy, agriculture heavily relies on its major crops e.g., wheat, rice, cotton, corn and sugarcane. Wheat and corn are two important cereal crops for many countries, where it is consumed as a staple food**.** Moreover, sustainability and efficient use of available resources (energy) are very important for the production of these crops.

Energy use per unit area in agriculture is directly related to the consumption of inputs and the production level, associated energy could be categorized as direct and indirect energy. The direct energy required for on-farm activities, particularly the energy required from field preparation to harvesting and transportation. While indirect energy required for off-farm activities such as manufacturing, packing, and transportation of fertilizer, pesticides, and farm machines [2]. Furthermore, it has been heightened in light of intensive growing populaces, inadequate supply of cultivated land and desire of high living standard, that energy use is one of the key indicators for developing more sustainable agricultural practices [3]. In all social orders, these components have fortified an increase in energy inputs (e.g., agriculture machinery, fertilizer, pesticide and irrigation) to enhance output (e.g., yields), lessen the labor work (mechanization) or both [4]. Moreover, energy input-output offers a significant understanding of the agriculture as a producer and user of energy [5] and it can prompt more effectual and environment friendly production [6]. Sufficient supply of the right amount of energy inputs is necessary for an improved agricultural production [7]. However, the lack of technical knowledge/ awareness of modern agriculture, lead to inefficient use of inputs and energy [8]. Additionally, the exorbitant use of specific agriculture inputs has not only repressed the increase in production, but in few cases, can also reduce it [9]. Hence, the effective use of energy inputs in agriculture is essential for sustainable agriculture production, renewable assets preservation, fiscal saving and reduction in air pollution [10].

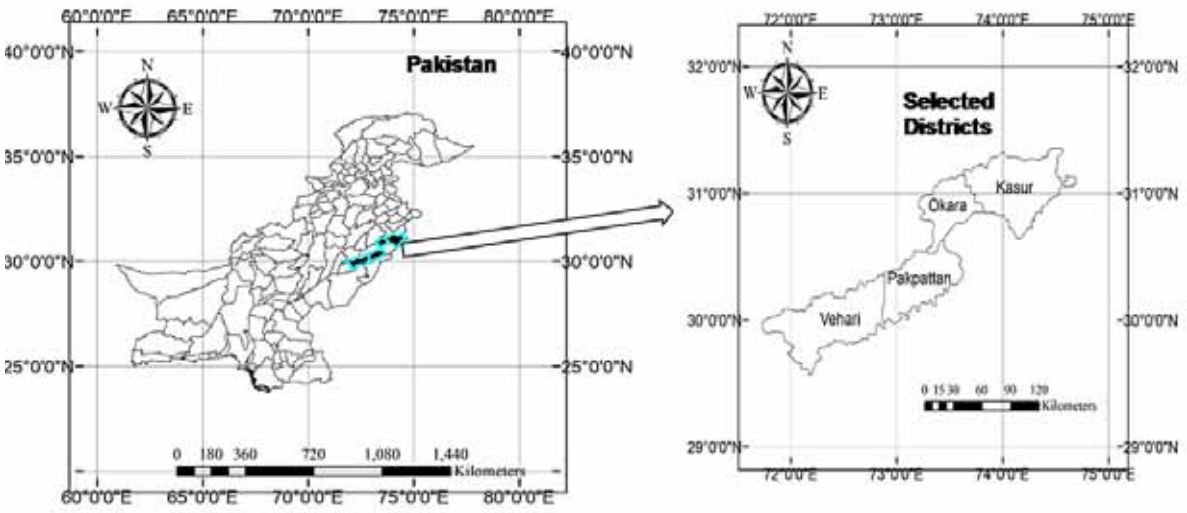

FIGURE 1
Selection of study area

TABLE 1
Energy equivalents of inputs and outputs in grain production systems

Input-output (unit)	Energy equivalent (MJ per unit)	References
1. Inputs		
1. Labor (h)	1.96	[21]
2. Seed (kg)		
Corn	14.7	[15]
Wheat	13	[21]
3. Fertilizer (kg)		
Nitrogen (N)	78.1	[21]
Phosphate (P_2O_5)	17.4	[21]
Potassium (K_2O)	13.7	[21]
4. Machinery (h)	62.7	[21]
5. Chemicals (Kg)		
Insecticides	199	[21]
Herbicide/Weedicide	238	[21]
Fungicides	92	[21]
6. Diesel fuel(L)	47.8	[27]
7. Water (m3 ha-1)	1.02	[21]
2. Output (kg)		
Corn Yield	14.7	[15]
Wheat Yield	13	[21]

Since a balance use of energy is one of the key challenge in agriculture, so, the study of energy balance for various crops could significantly help to identify the existing potential in any country, and a comparative study of energy productivity of the different crops is one of the methods used in ranking the cultivation of different crops [10, 11]. A plethora of research has been carried out in various regions of the world to investigate the energy use efficiency in different crops, including, wheat [12, 13], cotton [14], corn [15], sugar cane [16], vetch [17], barley [18], tomato [19], peach [20] and greenhouse cucumber [3].

To the best of authors knowledge, the comparison of the energy use in different crops in Pakistan is still lacking in the literature, hence, the scarcity of energy resources, significant dependency on agriculture sector and necessity of the evaluation of agricultural system that involves sustainable energy use, has lead this study to prioritize the grain production systems of Pakistan. Particular objective of this study entails the comparative analysis of energy use efficiency in corn and wheat productions, to provide an opportunity for planners and policy makers to evaluate the economic interactions of energy use in agriculture.

MATERIALS AND METHODS

Study area. Agriculture is an important sector of Pakistan's economy, wheat, rice, cotton, maize

and sugarcane are the main contributing crops. Moreover, agriculture sector has two main seasons for crops production, named as Rabi and Kharif, Rabi extends from November to April, while Kharif season starts in May and end in November. In green revolution (1960s) advancement in crop production system of Pakistan was mainly focused. However, despite the improvement, sustainable crop production still remained the primary focus of Pakistan's agriculturists. Hence, quantifiable evaluation is necessary to assess the current status of energy use efficiency in food grain production system of Pakistan.

For current study, we selected four districts (Figure 1) from Punjab, which is the main agriculturist province dominant to all provinces in crop production specially, in wheat and corn production, was selected purposely. Furthermore, the basic input data was collected conveniently followed by a multistage sampling procedure. In sampling process, about 60 farmers from each district and commutatively 240 farmers in whole were interviewed using a well-structured questionnaire. Questionnaire containing information regarding inputs used in field activities (from seedbed preparation to harvesting and threshing) and output gained (crop yield) was used in this study.

Research methodology. This study was carried out in four districts of Punjab province, the amount of inputs (labor, seed, fertilizers, machinery, chemicals, diesel fuel and water for irrigation) used in corn and wheat production and output gained (crop yield) were quantified (per acre latterly converted to per hectare) in order to compute the energy equivalences. Then energy consumption and gained in each crop was calculated by multiplying the calculated amount of inputs-output with their relevant energy equivalent coefficients Table 1. Data concerning energy consumption was entered in excel and SPSS 16. Furthermore, based on the input and output energy, energy use efficiency, energy productivity, specific energy and net energy gain were assessed by using following equations.

$$\eta_{EU} = \frac{O_E}{I_E} \quad (1)$$

$$E_{specific} = \frac{I_E}{Y} \quad (2)$$

$$E_{productivity} = \frac{Y}{I_E} \quad (3)$$

$$N_E = O_E - I_E \quad (4)$$

Where η_{EU} is the energy use efficiency, O_E , I_E are the output and inputs energies (MJ ha^{-1}) respectively, $E_{specific}$ is specific energy (MJ Kg^{-1}), Y is the yield (kg ha^{-1}), $E_{productivity}$ energy productivity (Kg MJ^{-1}) and N_E is the net energy gain (MJ ha^{-1}).

RESULTS AND DISCUSSIONS

Analysis of energy inputs and outputs in corn and wheat production. The questionnaire based information resulted average yield of food grains as 7904 kg ha^{-1} corn and 4446 Kg ha^{-1} wheat, and the inputs consumed in the production of said amounts have shown in Figure 2. Figure 2 depicted the average value of inputs e.g., labor value of 553, and 155.05 h ha^{-1}, and 180 L ha^{-1} and 122 L ha^{-1} diesel etc. for corn and wheat respectively. Hereupon, based on the protocols of energy equivalents derived from previous studies (Table 1), the amount of energy inputs and outputs per unit area were calculated and presented in Table 2. Total input energy for corn and wheat was resulted as 48904.80 and 27635.50 MJ ha $^{-1}$ with an output energy of 116188.8 and 57798.0 MJ ha $^{-1}$, respectively. Furthermore, we found a higher amount of energy consumed and gained in corn production. Moreover, the share of each input to the total input energy (Table 2), ensued that fertilizer, diesel fuel and water were the most demanding energy inputs for both the production systems, while seed and human labor were the least demanding inputs to corn and wheat crops respectively. Similar results were stated by Banaeian and Zangeneh, and Nabavi-Pelesaraei et al., [15, 21] in their studies of energy usage pattern in corn and wheat respectively. Banaeian and Zangeneh, [15],

TABLE 2
Energy consumption and input–output relationship in corn and wheat production

Input-output	Total energy equivalent Corn (MJ ha^{-1})	Percentage in total input (%)	Total energy equivalent Wheat (MJ ha^{-1})	Percentage in total input (%)
1. Inputs				
1. Labor	1083.90	2.22	303.89	1.10
2. Seed	295.88	0.61	1741.97	6.30
3. Fertilizers	23308.40	47.66	15672.45	56.71
4. Machinery	1315.45	2.69	770.58	2.79
5. Chemicals	4275.60	8.74	1094.80	3.96
6. Diesel	8643.20	17.67	5874.62	21.26
7. Water	9982.38	20.41	2177.19	7.88
Total energy input (MJ ha^{-1})	48904.80	—	27635.50	—
2. Output				
Yield	116188.80	—	51376.00	—

reported the energy consumption in corn production as 52.57 GJ ha^{-1} with fertilizer, diesel fuel and machinery as the major energy consuming inputs, and Nabavi-Pelesaraei et al. [21] quantified the energy consumption in wheat production as 39890.2 MJ ha^{-1} with fertilizer, diesel fuel and water for irrigation as leading energy inputs. Houshyar [22] and Tipi [23] also found the similar results in their study for energy efficiency in wheat production of Iran and Turkey respectively, that fertilizer, diesel fuel and electricity consumed about 80% of total input energy. It seems that production of corn in more sustainable than wheat in the studied area. Corn using 1.77 times more input energy than wheat and produced 2.26 times higher than that of wheat. Additionally, fertilizers, water for irrigation and diesel fuel were the most demanding energy inputs in both production systems, contributing more than 85% of total input energy. Furthermore, energy efficiency, specific energy, energy productivity and net energy gain were calculated. Energy efficiency in corn and wheat production was resulted 2.38 and 1.86 respectively, that means corn production system is 1.28 times more efficient than wheat, so production of corn seems more suitable for the studied area. The difference between energy used efficiency can be due to surplus and uneven usage of inputs in wheat production.

Another interpretation revealed that energy use efficiency of wheat can be increased by efficient utilization of fertilizer and diesel fuel, that had a major role in the energy consumption. So, there is a dire need to modify the tillage, harvest and other agronomic operations. Moreover, it can be remarked conclusively that improvements in fertilizer application, productivity level of consumed power and crop irrigation efficiency can have a significant effect on the energy use efficiency in Pakistani agriculture. Employment of advanced production methods with intensive crop management techniques can lead to efficient resource utilization and ultimately will have higher energy use efficiency.

The specific energy was estimated 6.19 and 6.99 MJ Kg^{-1} for corn and wheat respectively. This implies that a total of 6.19 and 6.99 MJ energy is required to produce a kilogram of corn and wheat respectively. Canakci et al. [24] described the specific energy for different field crops and vegetable production in Turkey, such as 16.21 for sesame, 11.24 for cotton, 5.24 for wheat, 3.88 for maize, 1.14 for tomato, 0.98 for melon, and 0.97 MJ Kg^{-1} for watermelon. Energy productivity was 0.16 Kg MJ^{-1} in corn and 0.14 Kg MJ^{-1} in wheat production. Many researchers specified energy productivity in different field crops such as in stake tomato 1.0 [19], cotton 0.06 [25], and sugar beet 1.53 Kg MJ^{-1} [26]. Net energy gain was 67284.00 and 23740.50 MJ ha^{-1} in corn and wheat production respectively, which is almost 3 times higher than wheat, that is another reason for recommendation of corn production in said area.

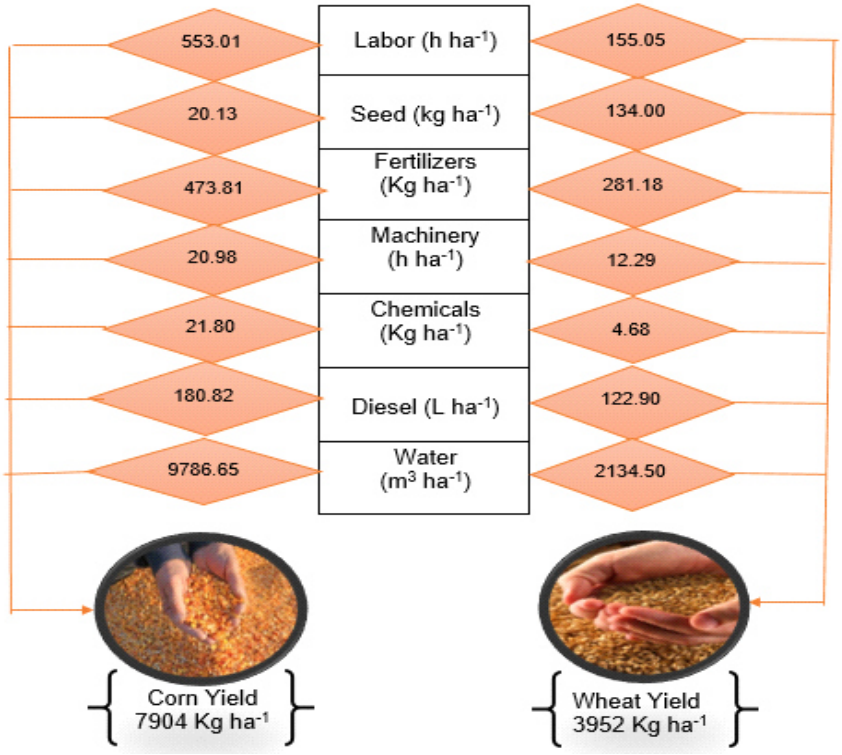

FIGURE 2
Mass balance of corn and wheat production systems in Pakistan

TABLE 3
Energy input–output ratio in corn and wheat production systems

Items	units	**Corn** (value)	**Wheat** (value)
Energy input	MJ ha^{-1}	48904.80	27635.50
Energy output	MJ ha^{-1}	116188.80	51376.00
Energy use efficiency	—	2.38	1.86
Specific energy	MJ kg^{-1}	6.19	6.99
Energy productivity	kg MJ^{-1}	0.16	0.14
Net energy gain	MJ ha^{-1}	67284.00	23740.50

Hence, as wheat crop was found less efficient as compared to corn, this inferred that the existing amount of wheat output can be achieved with less quantity of inputs if inputs were utilized at frontier. Another interpretation revealed that resources could be saved or production can be increased with better management and improved production methods. Over utilization of resources threatens fertility of soil and economic independence of farmer, that signposts the requirement of energy conservation in agriculture sector of Pakistan.

Due to oversight consumption, the farmers of target area do not take the benefit of conserved energy. Energy conservation aims to increase energy use efficiency through waste reduction. So, reduction in the use of fertilizer, diesel fuel and water can play a vital role in the improvement of efficiency.

CONCLUSIONS

The sustainability of the conventional cropping system is vulnerable and deteriorating energy resources. For this reason, resource-saving technologies need to be developed and promote for crop production. Moreover, it is believed that farmers' socio-economic situations and their perceptions of knowledge about the current status of energy use efficiency is of great importance for a sustainable agriculture and food production**.** Likewise, developed countries farmers of Pakistan are also inclined towards commercial farming, however, still there is need to launch new strategies and programs for providing better understanding about balanced use of energy. In this perspective, an energy balance analysis can provide a clear picture of current status and future guidelines for efficient energy use.

Hence, a comparative energy use analysis between food grain production systems (corn and wheat) of Pakistan were carried out and resulted the total input energy of 48904.80 and 27635.50 MJ ha^{-1} for corn and wheat with an average yield of 7904 and 3952 Kg ha^{-1}, respectively. Moreover, fertilizers, diesel fuel and water for irrigation were the most energy consuming inputs in corn and wheat production systems of Pakistan by contributing more than 85% of total input energy. Energy use efficiency, specific energy, energy productivity and net energy gain were 2.38, 6.19 MJ Kg^{-1}, 0.16 Kg MJ^{-1} and 67284.00 MJ ha^{-1}, and 1.86, 6.99 MJ Kg^{-1}, 0.14 Kg MJ^{-1} and 23740.50 MJ ha^{-1} for corn and wheat productions respectively. Moreover, it was ensued that corn using 1.77 times more input energy than wheat and produced 2.26 times higher than that of wheat. Furthermore, energy use efficiency based conclusion was drawn that corn production found more sustainable compared to wheat, so corn could be prioritized as a more suitable planting crop in selected area of study. In addition to above. we found an unproductive energy balance trend in both of the crop as compared to other developed and even under develop countries, which resulted that there is a need to increase the efficiency of irrigation systems, utilization of better machinery management practices and productivity of fertilizer application through precision agriculture, these may be the options to increase energy efficiency and promote environment friendly agriculture.

ACKNOWLEDGEMENTS

This study is part of PhD dissertation. We are thankful to China Scholarship council (CSC-reference number 2014GXZA87.) for providing PhD scholarship funding.

REFERENCES

[1] Government of Pakistan (GOP) (2016) Pakistan Economic Survey 2015-16. Economic Advisor's Wing, Finance Division, Islamabad, Pakistan.

[2] Kazemi, H., Shahbyki, M. and Baghbani, S. (2015) Energy analysis for faba bean production: A case study in Golestan province, Iran. Sustainable Production and Consumption. 3, 15-20.

[3] Mohammadi, A. and Omid, M. (2010) Economical analysis and relation between energy inputs and yield of greenhouse cucumber production in Iran. Applied Energy. 87, 191–196.

[4] Gokdogan, O., Erdogan1, O., Eralp O. and Zeybek A. (2016) Energy efficiency analysis of cotton production in Turkey: a case study from Aydin province. Fresen. Environ. Bull. 25, 4959-4964.

[5] Risoud, B. (2000) Energy efficiency of various French farming systems: questions and sustainability. In: International conference ‘‘Sustainable energy: new challenges for agriculture and implications for land use’’. Organized by Wageningen University, Netherlands, May 18–20.
[6] Moreno, M.M., Lacasta, C., Meco, R. and Mor, C. (2011) Rainfed crop energy balance of different farming systems and crop rotations in a semi-arid environment: Results of a long-term trial. Soil & Tillage Research. 114, 18-27.
[7] Baran, M.F. (2017) Energy and economic analysis of vetch production in Turkey: a case study from Thrace region. Fresen. Environ. Bull. 26, 1966-1972.
[8] Abbas, A., Minli, Y., Elahi, E., Yousaf, K., Ahmad, R. and Iqbal, T. (2017) Quantification of mechanization index and its impact on crop productivity and socioeconomic factors. International Agricultural Engineering Journal. 26(3), 49-54.
[9] Omani, A. and Chizari, M. (2008) Analysis of farming system sustainability of wheat farmers in Khuzestan province of Iran. Green Farming an International Journal of Agricultural Science. 6, 5–8.
[10] Sahabi, H., Feizi, H. and Amirmoradi, S. (2013) Which crop production system is more efficient in energy use: wheat or barley? Environment, Development and Sustainability. 15(3), 711-721.
[11] Ziaei, S.M., Mazloumzadeh, S.M. and Jabbary, M. (2015) A comparison of energy use and productivity of wheat and barley Agricultural Sciences. 14, 19-25.
[12] Marakoglu, T. and Carman, K. (2017) A comparative study on energy efficiency of wheat production under different tillage practices in middle Anatolia of Turkey. Fresen. Environ. Bull. 26, 3163-3169.
[13] Abbas, A., Yang, M., Ahmad, R., Yousaf, K. and Iqbal, T. (2017). Energy use efficiency in wheat production, a case study of Punjab Pakistan. Fresen. Environ. Bull. 26, 6773-6779.
[14] Gokdogan, O., Erdogan, O., Eralp O. and Zeybek A. (2016) Energy efficiency analysis of cotton production in Turkey: a case study from Aydin province. Fresen. Environ. Bull. 25, 4959-4964.
[15] Banaeian, N. and Zangeneh, M. (2011) Study on energy efficiency in corn production of Iran. Energy. 36, 5394-5402.
[16] Karimi, M., RajabiPour, A., Tabatabaeefar, A. and Borghei, A. (2008) Energy analysis of sugarcane production in plant farms a case study in Debel Khazai Agro-industry in Iran. American-Eurasian Journal of Agricultural and Environmental Science. 4, 165–171.
[17] Baran, M.F. (2017) Energy and economic analysis of vetch production in Turkey: a case study from Thrace region. Fresen. Environ. Bull. 26, 1966-1972.
[18] Mobtaker, H.G., Keyhani, A., Mohammadi, A., Rafiee, S. and Akram, A. (2010) Sensitivity analysis of energy inputs for barley production in Hamedan Province of Iran. Agriculture, Ecosystems & Environment. 137, 367–372.
[19] Esengun, K., Erdal, G., Gunduz, O. and Erdal, H. (2007) An economic analysis and energy use in stake tomato production in Tokat province of Turkey. Renewable Energy. 32, 1873–1881.
[20] Yildiz, T., Hazneci, K., Hazneci, E. and Ozkaraman, F. (2016) The Energy Use Efficiency determinants of peach Production in Samsun Province of Turkey. Fresen. Environ. Bull. 25, 4685-4694.
[21] Nabavi-Pelesaraei, A., Hosseinzadeh Bandbafha, H., Qasemi-Kordkheili, P., Kouchaki-penchah, H. and Riahi-Dorcheh, F. (2016) Applying optimization techniques to improve of energy efficiency and GHG (greenhouse gas) emissions of wheat production. Energy. 103, 672-678.
[22] Houshyar, E., Davoodi, S. and Nassiri, S.M. (2010) Energy efficiency for wheat production using data envelopment analysis technique. Journal of Agricultural Technology. 6, 663-672.
[23] Tipi, T., Cetin, B. and Vardar, A. (2009) An analysis of energy use and input costs for wheat production in Turkey. Journal of food agriculture and environment. 7(2), 352-356.
[24] Canakci, M., Topakci, M., Akinci, I. and Ozmerzi, A. (2005) Energy use pattern of some field crops and vegetable production: case study for Antalya region, Turkey. Energy Conversion and Management. 46, 655–666.
[25] Yilmaz, I., Akcaoz, H. and Ozkan, B. (2005) An analysis of energy use and input costs for cotton production in Turkey. Renew Energy. 30, 145–155.
[26] Erdal, G., Esengun, K., Erdal, H. and Gunduz, O. (2007) Energy use and economical analysis of sugar beet production in Tokat province of Turkey. Energy. 32, 35–41.
[27] Elhami, B., Akram, A. and Khanali, M. (2016) Optimization of energy consumption and environmental impacts of chickpea production using data envelopment analysis (DEA) and multi objective genetic algorithm (MOGA) approaches. Information processing in agriculture. 3(3), 190-205.
[28] Shah, Z., Shah, S.H., Herriedge, D.F., Peoples, M.B., Aslam, M., Ali, S. and Tariq, M.T. (1995) Pakistan's agriculture-cereal and legume production. J. Agric. Univ. Wales Aberyswyth. U.K. 75, 89-98.

Received: **29.08.2017**
Accepted: **26.10.2017**

CORRESPONDING AUTHOR

Minli Yang
College of Engineering
China Agricultural University,
Beijing 100083 – China

e-mail: qyang@cau.edu.cn

© by PSP Volume 27 – No. 2/2018 pages 1060-1068 Fresenius Environmental Bulletin

AN EXPERIMENT STUDY OF EFFECTS OF FREEZING-THAWING CYCLES ON WATER AND SALT MIGRATION OF SALINE SOIL

Gang Wang[1], Qing Wang[1,*], Xudong Zhang[1], Wenhua Wang[2], Chaoyue Li[1]

[1]College of Construction Engineering of Jilin University, Changchun, Jilin, China
[2]College of Civil Engineering of Changchun Institute of Technology, Changchun, Jilin, China

ABSTRACT

To study the characteristics of water and salt migration in the process of freezing and thawing cycles for the saline soil of Nong'an, Western Jinlin Province, physicochemical tests in laboratory and indoor experiments of water and salt migration is carried out with the equipment "Rock & Soil Freezing-Thaw Trial and Error Imitating Comprehensive Experimental Platform with Ultra Cold Condition" invented by Jilin University. The remolded soil samples had the same size, initial water content, initial salt content, compaction degree, and temperature. These samples were used to investigate the characteristics of water and salt migration at different times of the freezing and thawing cycle. The water and salt contents at different positions of the soil specimens are tested for comparison with the initial data of water and salt contents. The variation characteristics of the pores are analyzed based on mercury intrusion porosimetry. The freezing and thawing cycles in an open system increases macropore content but decreases the mesopore content, thereby resulting in a layer of water and salt accumulation. The unidirectional freezing results in upward migration of water to the frozen zone, and the unidirectional thawing results in water migration from the ends to the middle part. The water and salt contents at different positions increase with increasing times of freezing and thawing cycles.

KEYWORDS:
Saline soil, Freezing-thawing cycles, Water and salt migration, Water content

INTRODUCTION

Salinized soil is influenced by salt and alkali; these soils include saline, alkali, and other soils at different degrees of salinization [1]. In engineering, salinized soil is defined as soil with more than 0.3 % soluble salt [2]. In a salinized soil region, dissolve settlement, salt expansion, and corrosion always occur. Soil salinization can not only reduce crop output but also cause the highway tympanites, frost heave, differential settlement of the subgrade, and the corrosion of buildings. The study of salinized soil started more than a century ago. With knowledge development, the transportation characteristics of the salt became the focus of research in the 1920s and 1930s [3]. Western Jilin is a region where saline soil is widely distributed. Seasonally frozen soil is also present, which is influenced by seasonally freezing. During the process of freezing, water always migrates under a temperature gradient, and salt transport is mainly dependent on water migration. Thus, some studies have been conducted to investigate water migration during freezing. In the early 1980s, the cold region research and engineering laboratory of America carried out a series of laboratory experiments to explore the mechanism of water migration [4]. In the 1990s, the Chinese academy of sciences studied water migration, salt transport, ice formation, frost heave, and the salt heave of the soil [5, 6]. In a previous research on salinized soil in Western Jilin, Wang [7] studied the rise of capillary water in normal temperature and water migration under freezing and thawing conditions, respectively. The mechanism of the water and salt migration are discussed by comparing the experimental results. Wang [8] also analyzed the frost heaving characteristics of saline soil in Western Jilin by conducting laboratory experiments. Li [9] studied the property of the frost heave of the soil and analyzed the attenuation of soil strength during the freezing and thawing process based on sonic wave test. Zhang [10] predicted the frost heave behavior of saline soil using nonlinear analysis method. Yuan [11] and Yu [12] developed the multi-field coupled model to simulate the interaction of water and heat. Zhang [13] established the mathematical model that included water, heat, and salt by considering the salt crystallization and also validated such model's effectiveness by laboratory experiment.

In the viewpoint of thermodynamics, the water migration of the soil is caused by the unbalanced state, which is induced by the physical chemistry effects, including temperature gradient, pressure gradient, moisture gradient, and the concentration gradient [14]. The water migration in the frozen soil involves migration of the capillary water and bound water under an external force [15]. Salt transport in

the soil has two modes, as follows: molecular diffusion that is affected by the concentration gradient; and convection and mechanical dispersion caused by water migration. Previous studies indicated that the salt transport is mainly induced by the convection flux; thus, water migration is the main factor of salt transport [16].

Western Jilin soil is distributed in a typical seasonally frozen zone, in which a large area comprises salinized soil. The salinization of the soil in this region has a great harm to the agriculture. The water migration of seasonally frozen soil can cause an engineering problem, such as frost heave. Thus, it is necessary to investigate the water and salt transfer characteristics under freezing and thawing conditions [17, 18]. In this study, the soils studied are collected from Nong'an, Western Jilin. The soil samples at 40 cm depth are typical in terms of salt content and other aspects and are influenced little by artificial disturbance. Thus, soil samples were collected at 40 cm depth for the experiments. Remolded soil samples are prepared at different water contents and compaction degrees. Then, the water migration characteristics and salt transport characteristics under the freezing and thawing conditions are studied, thereby providing reference to solve the problems of the salinization and engineering issues in the study area.

STUDY AREA

Western Jilin is located in the southwest of Songnen plain, China. It is a typical seasonally frozen area, in which salinized soil is distributed. The soil in this research is collected from southeast of the Aobaotu in Nong'an County, which is shown in Fig. 1. The groundwater depth in the study area is shallow, and its degree of mineralization is relatively high.

In this area, the long cold winter results in migration of water upward along the temperature gradient in the freezing process. The salt in the soil is also transported upward. Spring and autumn seasons are always dry and windy, thereby leading to intensive evaporation, and high moisture gradient is formed on the soil surface. The salt is transported upward with water migration. Thus, these two processes play important roles in soil salinization.

BASIC PROPERTIES OF THE SOIL

The sampling time of the soil in this paper is in April. The soil samples on the surface are relatively dry because of the strong evaporation of the soil surface in spring, and the graniphyric white salt crystal can be observed on the soil surface. Then, a small soil pit is dug and the soil samples at the depth of 40 cm are collected for experiments. The basic properties of the soil sample are as follows.

Material composition. Soil is a construction material that is always composed of solid particles, liquid water, and air. The frozen salinized soil in the seasonally frozen region contains the soil grains, ice, and crystalloid salt. Salt is dissolved in the liquid water [19]. The soil from 40 cm depth was tested for particle size distribution and mineral component using hydrometer method and X-ray scattering techniques, respectively. The results of particle size distribution and the mineral component are shown in Tables 1 and 2.

Soil consists of silt and clay particles. According to the rules of geotechnical testing DT-92, this soil is recognized as silty clay. Table 2 indicates that the original mineral of the soil sample is dominant, and the content of secondary mineral is relatively low.

Physicochemical property. In the laboratory, the water content of the soil samples is tested. The soil density of the soil sample is tested using cutting-ring method. The limit of moisture content is tested by using the liquid-plastic limit combined method, through which the liquidity and plasticity indexes are obtained. All results of tests for the physical properties are listed in Table 3. The chemical properties of the soil samples include salt content, salt components, pH, organic matter, and cation exchange capacity (CEC). The results of tests for the chemical properties are listed in Table 4.

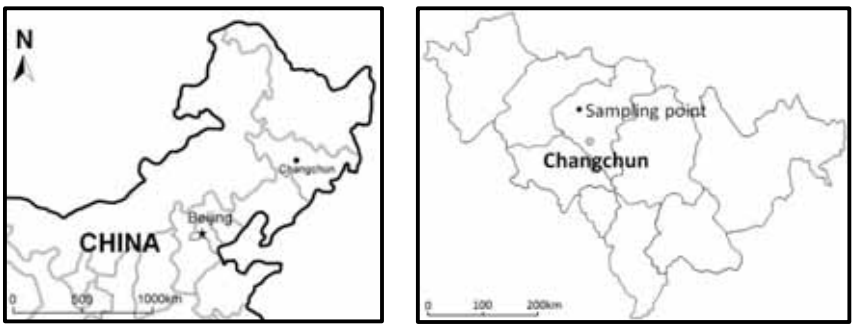

FIGURE 1
Location of the sampling point

TABLE 1
Grain-size distribution and naming of original sample

Particle distribution proportion (%)			Naming
Sand	Slit	Clay	
3.66	58.61	37.73	Silty clay

TABLE 2
The mineralogical compositions of original sample

Volumetric content (%)							Original mineral (%)	Secondary mineral (%)
fs	Q	PI	Cc	I/S	K	I		
17	44	23	5	2	6	3	84	16

Note: fs, alkali feldspar; Q, quartz; PI, plagioclase; Cc, calcite; I/S, illite/smectite formation; K, kaolinite; I, illite

TABLE 3
Basic physicochemical properties of original sample

Natural water content (%)	Natural density (g/cm^3)	Liquid limit (%)	Plastic limit (%)	liquidity index	Plasticity index
23.85	1.92	55	15	0.22	40

TABLE 4
Chemical properties of original sample

Soluble salt composition content (mmol/kg)								Total soluble salt (%)	pH	Organic matter	CEC (mmol/100g)
Na^+	K^+	Ca^{2+}	Mg^{2+}	CO_3^{2-}	HCO_3^-	Cl^-	SO_4^{2-}				
98.5	3	4.4	3.2	0	9.12	7	7	0.681	8.05	0.996	13

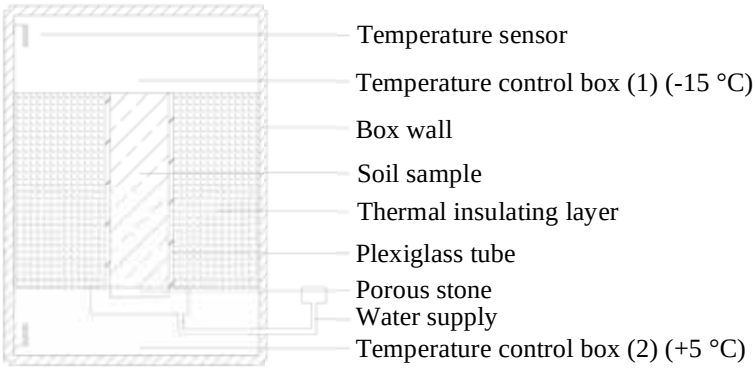

FIGURE 2
Schematic diagram of the test apparatus

EXPERIMENT DESIGN

Experimental apparatus. The experimental apparatus is designed by the supervisor's research team, which is named "Rock & Soil Freezing-Thaw Trial and Error Imitating Comprehensive Experimental Platform with Ultra Cold Condition." The apparatus contains two temperature boxes and one thermal insulating course, as shown in Fig. 2. The cylindrical channel is 6 cm in diameter and 20 cm in height, and this channel connects the two temperature control boxes. In the channel, an organic glass column is fixed. The remolded soil is compacted in the glass column. In the freezing process of the experiment, the temperature of the box (1) is adjusted to -15 °C, and the temperature box (2) was adjusted to +5 °C. During the melting process, the temperature of box (1) is adjusted to +5 °C, and the temperature box (2) is kept as +5 °C.

Experimental program. (1) Soil sample preparation. Based on the moisture-density test in the laboratory, the maximum dry density is 1.63 g/cm^3. In the experiment, all the remolded soil samples are designed with the optimum water content and a compaction degree of 85%. The water content is 22.5%, and the dry density is 1.39 g/cm^3. In this

experiment, 5 soil columns are prepared, which are marked as Sample 1, Sample 2, Sample 3, Sample 4, and Sample 5. Sample 1 is subjected to only the freezing process, whereas the others are subjected to the freezing and melting cycles. Sample 2 is subjected to one time of freezing and melting cycle. Sample 3 is subjected to three times of freezing and melting cycles. Sample 4 is subjected to five times of freezing and melting cycles. Sample 5 is subjected to seven times of freezing and melting cycles. The details of the experimental conditions are listed in Table 5.

(2) Experimental procedure. Firstly, both ends of the soil columns are hermetic. All soil columns are in box ①, and the temperature is adjusted to +5 °C. Storage under these conditions lasted 24 h to ensure that the temperature of the whole soil column is +5 °C. Then, the soil column is fixed in the cylindrical channel between the temperature boxes. The bottom of the columns is supplied with the groundwater sample from the study area. The top surface is maintained as hermetic. After installing the soil samples, the freezing experiment is carried out. The top temperature is -15 °C, whereas the bottom temperature is +5 °C. Thus, a unidirectional freezing process ensues from top to the bottom. The freezing time is 48 h. During melting, the top temperature changed to +5 °C, which ensures that the melting process is also a unidirectional process from top to the bottom. The melting time is 24 h. A cycle of one freezing process and one melting process lasts for 72 h. After the required processes, the soil columns are cut into slices (2 cm thickness) to test the water content, porosity, and salt content. The temperature settings for the ends of the columns are shown in Fig. 3.

TEST RESULTS AND ANALYSIS

Analysis of temperature filed in the sample. Three temperature probes are placed at 5, 10, and 15 cm depth from the top of sample 5 during the test, and the temperatures are recorded every few hours until the test ended. The temperature distribution curve at various depth of sample 5 is shown in Fig. 4. When the freezing starts, temperatures at three depths decreased gradually. Temperatures of samples near the top are lower. At the end of the first freezing process (48 h), temperatures reach below zero degrees at depths of 5 and 10 cm, whereas temperatures reach above zero degrees at a depth of 15 cm. When the temperature of the sample at the top is set at 5 °C, the soil sample begins to thaw. At 24 hours after thawing, temperatures at the abovementioned three depths are above zero, thereby showing that the soil sample has thawed completely after 24 hours. Then, the sample undergoes a complete freezing-thawing process. The trend of temperature variation in subsequent six freezing-thawing cycles is similar to the trend of the first cyclical process. From the figure, we can see that the position of 0 °C inside the sample is at a depth of 13 cm after each 48-hour freezing process. Soil above 13 cm depth is the frozen zone, and the soil below 13 cm depth is the unfrozen zone.

TABLE 5
Test conditions for freezing-thawing in soil samples

Sample number	Freezing time (h)	Thawing time (h)	Time of cycles
1	48	-	-
2	48	24	1
3	48	24	3
4	48	24	5
5	48	24	7

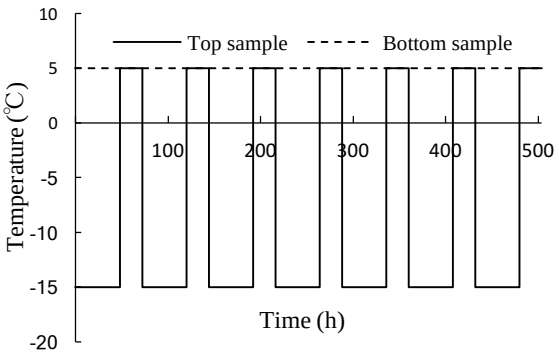

FIGURE 3
Temperature setting curves of two ends of the samples

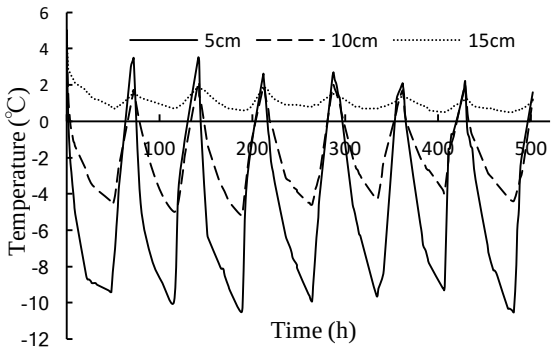

FIGURE 4
Temperature-time curves at various depth of the sample 5

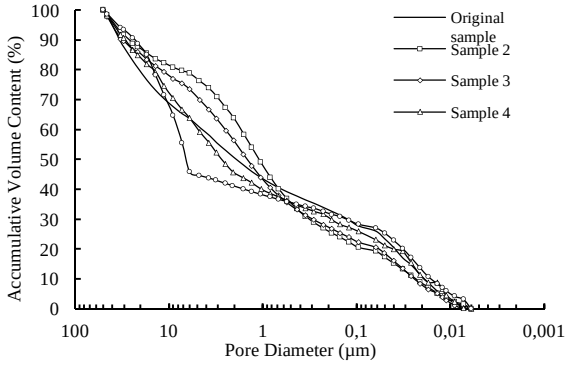

FIGURE 5
Semi-logarithmic curve of pore size and cumulative volume content

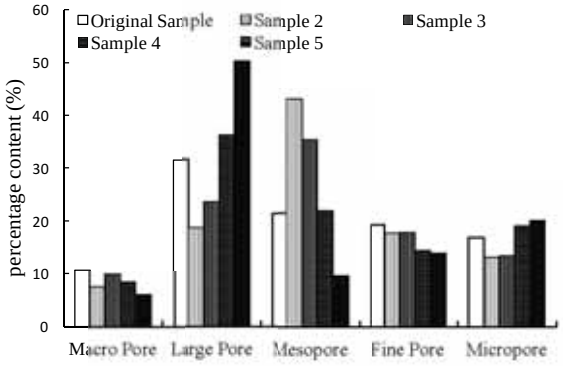

FIGURE 6
The pore distribution with various freezing-thawing cycles

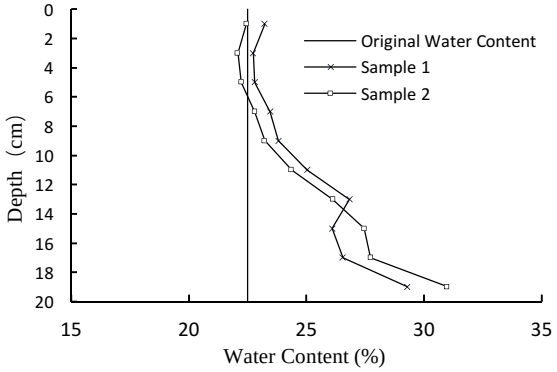

FIGURE 7
Water content of samples 1 and 2 along the directions of depth

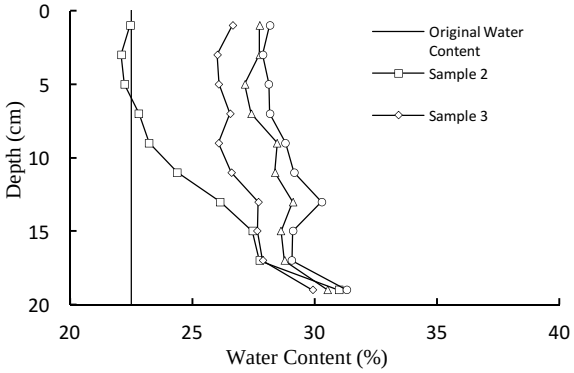

FIGURE 8
Water content curves of the samples for freezing-thawing cycles

Pore distribution characteristics of the sample. After different freezing-thawing cycles, the soil samples at 3 cm depth in the frozen zone are selected for the mercury intrusion test, and results were compared with those from the original sample, which did not undergo freezing-thawing process. The semi-logarithmic curve of pore size and cumulative volume content are obtained (Fig. 5). With four nodes of pore sizes 0.04, 0.4, 4, and 40 μm, the curves in Fig. 5 were designated as follows: micropore, fine pore, mesopore, large pore, and macro pore [20]. According to the above-mentioned division principle, the pore distribution with various freezing-thawing cycles is shown in Fig. 6. Fig. 6 shows that mesopore and large pore have distinct regularity with increasing times of freezing-thawing cycle. After the first freezing-thawing process, mesopore and large pore distinctly redistribute compared with the original sample. The proportion of mesopore increases, whereas that of the large pore decreases. In subsequent freezing-thawing cycles, the proportion of mesopore decreases, and the proportion of large pore increases with increasing times of freezing-thawing cycle. The water inside the sample expands as it freezes, thereby destroying part of the pore structure among soil particles and increases this part of pore size. The above-mentioned effect can be recovered partly when the sample thaws [21]. The effect on the expansion of ice crystals makes the corresponding pore size larger with increasing times of freezing-thawing cycle. However, this effect of expansion squeezes other parts of the pore, thereby reducing the proportion of the corresponding pore size. From the Fig. 6 we can see that the mesopore has been squeezed and the large pore has been expended. No significant effect was found on the other three sections and the proportions have slight variation.

Characteristics of water migration. (1) Freezing and thawing effects on water migration. Fig. 7 is the water content of the samples 1 and 2 along the direction of depth. Fig. 7 shows that water contents of every depth in sample 1 increase compared with the original water content after being frozen for 48 hours. Water content increases with increasing depth in the sample. A special position at 13 cm depth exists, in which the water content is higher than around its adjacent positions. This position is exactly the frozen and unfrozen zone interface. This special position appears because when the freezing starts, freezing front is formed and moves down gradually. The water below the freezing front migrates constantly toward the freezing front. As the freezing front moves down, the water of the upper

sample does not have enough time to migrate. In addition, water supply of upper sample comes mainly from the sample itself, which results in a lower water content at the upper part. Freezing front continues to move down until it remains at about 13 cm depth. This position is close to the bottom of the water supply, and the water has enough time to migrate toward the freezing front. Moreover, the rise of capillary water contributes to the increase in the water content of the lower sample. There is enough time for water to gather below the freezing front; thus, the water content at depth of 13 cm is higher than that around the adjacent positions.

Samples thaw 24 hours after a 48-hour freezing process. Water content above 14 cm depth decreases compared with those before thawing (sample 1), whereas at below 14 cm depth, water content increases. Water content along the direction of depth generally increases, especially below 10 cm depth. Fig. 4 shows that parts of negative temperature in soil sample still exist 17 hours after thawing. As sample thaws from top to bottom, upper and lower samples are unfrozen, but middle of sample is still frozen. There are two different temperature gradients in the sample and both point to the frozen section, thereby resulting in water of the upper sample migrating downward and water of the lower sample migrating upward. This is the reason upper water contents decrease and lower water contents increase in sample 2, compared with water content of sample 1. Because the temperature gradient is a constant presence in the lower sample, water supply flows continuously to the bottom of sample, and the water content of sample 2 is higher than that of sample 1.

(2) Water content variation of samples for freezing-thawing cycles. Water content curves of samples 2, 3, 4 and 5 for different times of freezing-thawing cycle are shown in Fig. 8. The following characteristics are shown in Fig. 8. First, with increasing times of freezing-thawing cycle, the water content of samples also increases. Second, an obvious regularity is found below the depth of 14 cm for each sample, i.e., the water content increases along direction of depth. Third, a high water content position is found at 13 cm depth in samples 3, 4, and 5.

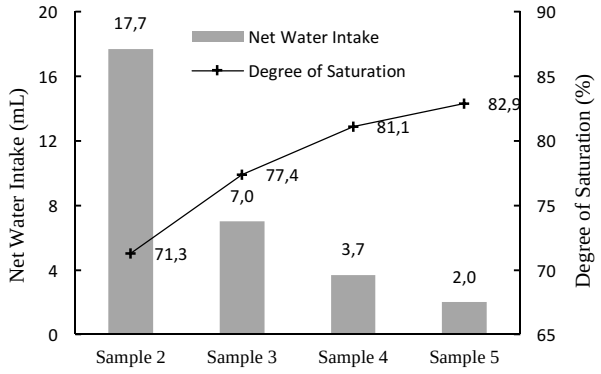

FIGURE 9
Net water intake and degree of saturation with various freezing-thawing cycles

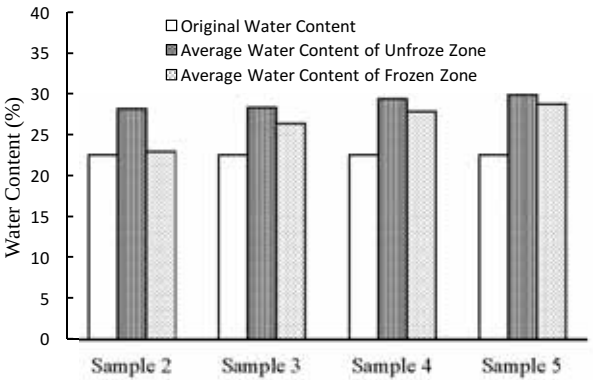

FIGURE 10
Average water content in frozen zone and unfrozen zone for freezing-thawing cycles

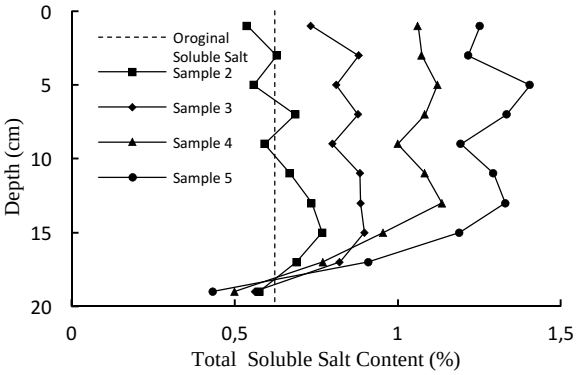

FIGURE 11
Total Salt content curves of the samples for freezing-thawing cycles

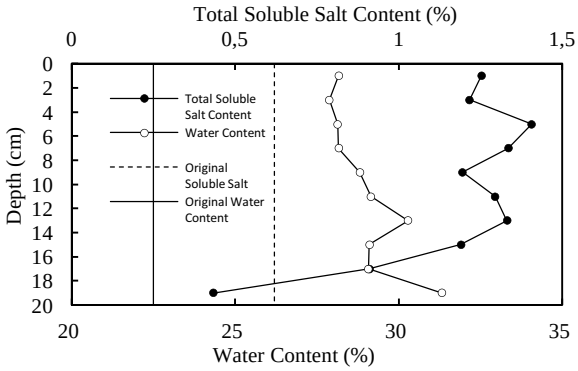

FIGURE 12
Total soluble salt content and water content curves of the sample 5

(3) Water intake and degree of saturation. After each time of freezing-thawing cycle, water intake of lower water supply is recorded, and an average degree of saturation of each sample is calculated at the same time (see Fig. 9). A large amount of water (17.7 mL) migrates from the bottom of the sample in the first freezing-thawing process. This phenomenon is determined by the grain size: When grain size is greater than 2 mm, the pore connectivity of soil is good, but capillary effect is particularly weak. Very little water migrates in the process of freezing. When the grain size is less than 0.005 mm, the clay particle has a large specific surface, strong surface adsorptive ability, and good water holding capacity. However, poor pore connectivity hinders the migration of water in denser soil. As shown in Table 1, the experimental soil in the study has high content of silt particles, which possess not only clay's good water holding capacity but also coarse particles' good pore connectivity, thereby facilitating the migration of water. With increasing freezing-thawing cycles, water intake decreases gradually in each freezing-thawing process. This occurs as a result of a lower degree of saturation and high suction before the test. Degree of saturation increases and suction decreases gradually as the water intake increases. Thus, the net water intake decreases gradually.

(4) Water content variation in frozen zone and unfrozen zone. According to the above-mentioned definition of frozen and unfrozen zones, Fig. 10 shows the average water content in frozen zone and unfrozen zone for freezing-thawing cycles. Fig. 10 shows that after the first freezing-thawing process, the average water content of unfrozen increases by 5.6%, but rarely increases in subsequent freezing-thawing cycles. Average water content of frozen zone increases by just 0.3%, while increases by 3.8%, 5.3%, and 6.2% after the third, fifth, and seventh freezing-thawing cycle. Substantial increment in average water content of frozen zone is caused by the existence of unfrozen water. During the process of freezing, not only the molecular attraction between the liquid water molecules but also the molecular attraction from the soil particle surface needs to be overcome. Strongly bound water still does not freeze at -78 °C, whereas loose bound water (film water) fully freezes from -20 °C to -30 °C. The freezing point of capillary water is slightly under 0 °C. The temperature of the test could not freeze all the loose bound water in the frozen zone of soil sample (whereas almost all capillary water freeze), the water content of frozen zone increases because of the migration of loose bound water. The average water content of the unfrozen zone is larger than that of the frozen zone because the capillary water migrates.

Characteristics of solute transport. Salt content curves of samples 2, 3, 4, and 5 for different times of freezing-thawing cycle are shown in Fig. 11. The following characteristics are observed from Fig. 11. First, with increasing times of freezing-thawing cycle, the salt content of the sample also increases. Second, an obvious regularity exists below the depth of 13 cm for each sample, i.e., the salt content decreases along direction of depth. However, salt content showed an irregular change above the depth of 13 cm. Third, a high salt content position exists at 13 cm depth in samples 4 and 5.

The water and salt content variation of sample 5 after the seventh freezing-thawing cycle is observed, and the regularities of water and salt migration are analyzed. As shown in Fig. 12, the bottom sample's (12–20 cm) water content increases along the direction of depth, whereas salt content decreases. The reason is when the freezing front stays around the depth of 13 cm. The water below the freezing front migrates constantly toward the freezing front. Water transport causes convection and mechanical dispersion of solute, which encourages the transport of solute toward the freezing front. The concentration gradient caused by aqueous solution of water supply and aqueous solution of soil sample leads to the transport of salt from the soil sample to the water supply. This phenomenon is called molecular diffusion in physics. Convection, mechanical dispersion, and molecular diffusion of solute are factors that result in high salt content above the sample and low salt content below the sample at about 12–20 cm depth. Both water and salt contents are high at a depth of 13 cm, because the water that carries salt below the freezing front migrates constantly toward the freezing front when the freezing front stays at 13 cm depth. At 3 cm depth of the top sample, the solute content significantly decreases. At the early stage of freezing, supplements of water and salt at the top only come from the sample itself. Solute is transported from 3 cm to 1 cm in the sample. Because of the lower top temperature (-15 °C), the freezing front moves down quickly, and the speed is more rapid than that of the lower solute transport up to the top. Top soil sample freezes quickly, after which the unfrozen water content on the top decreases rapidly. Meanwhile, the solubility of salt decreases with decreasing temperature. Thus, the solute at the bottom of the sample is difficult to transport to the depth of 3 cm.

CONCLUSION

Based on the experiments on water and salt migration at different times of freezing and thawing cycles in the soil samples, the characteristics of water migration and salt transport have been addressed. The mechanism is discussed along with pore size

distribution. Some of the conclusions drawn are as follows:

(1) With the supplement of water at the bottom of the soil sample, the average water content and the salt contents of the sample increase constantly as the times of freezing and thawing cycles increase. The freezing thawing cycles contributes to the migration of unfrozen water and transport of the salt.

(2) The redistribution of the pore size is the effect of the freezing and melting cycles. The unidirectional freezing results in the migration of water upward to the frozen part, while melting leads to downward water migration results from the gravitational potential. The process of the freezing and melting can comprehensively influence the pore size distributions, which leading to the mesopore squeezed and the large pore expended.

(3) During the process of freezing and melting cycles, the amount of water migration in the unfrozen zone is greater than that in the frozen zone because the degree of saturation of the unfrozen zone increases constantly during this process. And the amount of water migration in the first cycle of freezing and melting is obvious, but the increment becomes smaller with the times of the freezing and cycles increasing.

(4) In the first cycle of freezing and melting, an accumulation zone of salt is observed around the position of freezing front, the salt content at which is larger than other positions. With the times of freezing and melting cycles increasing, the salt accumulates in the whole frozen zone gradually, resulting from the salt transport upwards during the process.

ACKNOWLEDGEMENTS

The authors are grateful for the financial support from the financial support for the study presented in this paper from the State Key Program of the National Natural Science Foundation of China (Grant No. 41430642), the National Natural Science Foundation of China (Grant No. 41372267), and Special Fund for Major Scientific Instruments of the National Natural Science Foundation of China (Grant No. 41627801). The work is also supported by Graduate Innovation Fund of Jilin University (No. 2017067) and China Postdoctoral Science Foundation Funded Project (Grant No. 2017M621212).

REFERENCES

[1] Wang, Z.Q., Zhu, S.Q. and Yu, R.P. (1993) Saline Soil in China. Science Press, Beijing.

[2] Ministry of Housing and Urban-Rural Construction of the People's Republic of China. (2014) GB/T 50942-2014. Technical Specification for Construction of Saline Soil Area. China Planning Press, Beijing.

[3] Yang, J.S. (2008) Development and Prospect of the Research on Salt-affected Soils in China. Acta Pedologica Sinica. 05, 837-845.

[4] Zhao, G., Tao, X.X. and Liu, B. (2009) Experimental Research on Water Migration in Remoulded Soil during Freezing and Thawing Process. Journal of Central South University (Science and Technology). 2, 519-525.

[5] Deng, Y.S. and Xu, X.Z. (1991) Hydraulic Conductivity of Unsaturated Soil and Its Changing Regularity in Saturated Soil After Freezing-thawing Cycles. Journal of Glaciology and Geocryology. 1, 51-59.

[6] Zhang, L.X., Xu, X.Z. and Deng, Y.S. (1995) Unfrozen Water Content of Soil Containing NaCl Relating to Freezing-thawing Processes. Journal of Glaciology and Geocryology. 17(3), 258-262.

[7] Wang, W.H., Wang, Q., Zhang, J. and Chen, H.E. (2011) Research on Basic Properties Test of Carbonate-saline Soil in Western Jilin Province. Journal of Beijing Technology University. 37(2), 217-223.

[8] Wang, W.H., Wang, Q., Zhang, X.D., Zhao, W.D., Yan, H., Zhang, J. (2017) Analysis of Frost Heaving Characteristics of Carbonate-Saline Soil in Western Jilin Province, China. Fresen. Environ. Bull. 26, 4170-4179.

[9] Li, D.G. (2015) Study on Frost Heaving and Intensity Attenuation Characteristics due to Repeated Freezing-Thawing of Saline Soil in Nong'an County. Changchun, Jilin University.

[10] Zhang, X.D., Wang, Q., Huo, Z.S., Yu, T.W., Wang, G., Liu, T.B. and Wang, W.H. (2017) Prediction of Frost-Heaving Behavior of Saline Soil in Western Jilin Province, China by Neural Network Methods. Mathematical Problems in Engineering. 2017(4), 1-10.

[11] Yuan, G.H. (2006) The Mechanism and Numerical Simulation of Water Transfer in Seasonal Freezing Soil. Changchun, Jilin University.

[12] Yu, T.W. (2016) Numerical Analysis of Coupled Water Heat Salt and Stress of Saline Soil in Western Jilin Province. Jilin University, Changchun.

[13] Zhang, X.D., Wang, Q., Wang, G., Wang, W.H., Chen, H.E., and Zhang, Z.Q. (2017) A Study on the Coupled Model of Hydrothermal-Salt for Saturated Freezing Salinized Soil. Mathematical Problems in Engineering. 2017(2), 1-12.

[14] Xu, X.Z., Wang, J.C. and Zhang, L.X. (2010) Physics of Frozen Soils. Science Press, Beijing, China.

[15] Xu, X.Z. and Deng, Y.S. (1995) Experimental Study on Water Migration in Freezing and Frozen Soils. Science Press, Beijing.
[16] Zhang, W.Z., Yang, J.Z., Zhang, Y.F. and Cai, S.Y. (1992) A Sample Forecasting Method of Regional Water and Salt Movement. Solis and Fertilizers. 5, 11-14.
[17] Wang, Q., Liu, Y.F., Liu, S.W., Zhang, X.D., Peng, W., Li, C.Y., Xu, X.C., Fan, J.H. (2017) Evolution Law of the Properties of Saline Soil in Western Jilin Province under Multi Field Effect. Journal of Jilin University (Earth Science Edition). 47(3), 807-817.
[18] Yu, H.B., Song, Y.H., Liu, J., Xi, B.D., He, X.S., Peng, J.F. (2012) UV Spectroscopic Deconvolution (UVSD) Method for Simultaneous Evaluation of Humification and Salinization Processes of Saline Soils. Fresen. Environ. Bull. 21, 2010-2016.
[19] Wang, Q., Kong, Y.Y., Zhang, X.D., Ruan, Y.K., Chen, Y. (2016) Mechanical Effect of Pre-consolidation Pressure of Structural Behavior Soil. Journal of Southwest Jiaotong University. 51(05), 987-994.
[20] Wang, Q. and Wang, J.P. (2000) A Study on Fractal of Porosity in the Soils. Chinese Journal of Geotechnical Engineering. 22(4), 496–498.
[21] Wang, J.C., Cheng, G.D., Zhang, H.D. and Liu, J.M. (1992) Experimental Study on Conditions for Ice Formation of Saturated Sand in Freezing and Thawing Cycles. Journal of Glaciology and Geocryology. 2, 101-106.

Received: **30.08.2017**
Accepted: **07.12.2017**

CORRESPONDING AUTHOR

Qing Wang
College of Construction Engineering of
Jilin University,
Changchun, Jilin – China

e-mail: wangqing@jlu.edu.cn

© by PSP Volume 27 – No. 2/2018 pages 1069-1075 Fresenius Environmental Bulletin

ANALYSIS OF BACTERIAL COMMUNITY IN SEDIMENT FROM DALIAN MARINE AREA BY PCR-DGGE

Jianfang Yan[1,2], Zhiheng Liu[1], Baixia Zhao[3], Qiu Liu[2,*], Jicheng Yu[2], Xiaohui Qi[2], Changjian Liu[2], Xiang Li[4]

[1]Plant Protection College, Shenyang Agricultural University, Shenyang, 110161, China
[2]College of Life Science, Dalian Minzu University, Dalian, 116600, China
[3]Institute of Pomology, Dalian Academy of Agriculture Sciences, Dalian, 116036, China
[4]Water Quality Monitoring Center, Environmental Monitor Station of Yinchuan, Yinchuan, 750002, China

ABSTRACT

8 marine sediment samples were collected from Dalian marine area and Dandong marine area in China respectively. The bacterial community structures of sediments from Dalian and Dandong marine area were analyzed by denaturing gradient gel electrophoresis (DGGE). Our results showed that the total Gel bands remained relatively stable among all collected sediment samples. The bacterial communities of the sediments could be divided into two groups according to the cluster analysis based on DGGE patterns, and the bacterial community structures were different according to the geographical origins of samples. Moreover, the bacterial communities in sediment samples were consistently different within the different Dalian marine functional zones. The bacterial communities of four mariculture zones were clustered into one sub-group, and conservation district and port area were clustered into another sub-group. Analysis of nucleotide sequence of the dominant bands demonstrated that the major phylogenetic groups identified by DGGE belonged to Proteobacteria, Bacteroidete and Actinobacteria, of which *Salinimicrobium* sp., *Nitrosospira* sp. and *Methylophaga* sp. were the predominant bacteria communities in mariculture zone samples, in addition, *Methylophaga* sp. were widely distributed in the sediment samples. However, the DGGE gel band which were closely related with uncultured Actinobacteria were detected as one of the predominant species in Y2 samples from Dandong marine sample but not present in other samples.

KEYWORDS:
Bacterial community, Dalian marine area, DGGE, Marine sediment

INTRODUCTION

Bacteria play important ecological and biogeochemical roles in marine ecosystems [1-3]. They have functions of regulating the transformation of biogenic elements such as C, N, P, Fe, O in marine ecosystems, and S [4]. Several factors have been described to influence the sediment bacterial communities: salinity [5, 6], water chemistry [7], locations [8] organic matter quality [9, 10] and plant cover type [11]. However, it's difficult to determine which factors are most important due to the interactions among them. In addition, the sediment microbial diversity was influenced by different types of activities all the time. One approach to address this difference is to compare the changes of bacteria community structure along an environmental gradient and functional zones of sea area.

It has been estimated that less than 1% of the total microbial population have been successfully isolated in pure culture in land environment and even less in marine environment [12].

So, many environmental microorganisms cannot be cultured using traditional methods. Fortunately, with the development of molecular techniques, the knowledge on the population structure in natural microbial communities has been greatly enhanced. Correlative techniques include amplified rRNA gene restriction analysis (ARDRA) [13], terminal-restriction fragment length polymorphism (T-RFLP) [14] and 16S rDNA clone library [9]. Compared with conventional culture approaches, these new methods provided a more precise picture of microbial communities, including cultured and uncultured organisms. As a new culture-independent genetic fingerprinting technique, denaturing gradient gel electrophoresis (DGGE) of PCR-amplified partial 16S rRNA gene sequences has been used to investigate microbial community structure and diversity in different samples [15]. Studies on the diversity of microbiology have been widely carried out, particularly for describing predominant microbial communities in recent years [16-18]. The changes in microbial diversity along sediment depth [16] and bacterial community composition in deep-sea sediments [19] were also revealed by DGGE. To date, there were few studies on the diversity of predominant bacterial community in different marine functional zones by using the DGGE technique.

Dalian is located at the boarder of the Yellow Sea and Bohai Sea, which has the most cold sea water in Yellow-Bohai sea region with strongest sea

water exchange ability. So, marine organisms in sediment from Dalian sea area may be different from that in sediment from other sea area, especially the microorganisms may be unique. In this study, we aimed to explore the bacterial community composition through investigating the dominate species in such ecosystem by DGGE, and our results revealed the distribution of bacterial community in different sea functional zones. To our knowledge, it is the first study which elucidated the composition of bacterial communities in marine sediment from Dalian sea area.

MATERIALS AND METHODS

Sample collection and description. The marine sediments were collected from eight sites of 5-50 m water depth in Dalian sea area and Dandong sea area in October 2010 (Table 1). The sediments were transferred to a separate sterile centrifuge tube and stored at -80℃ in laboratory for further analysis. Total organic carbon was analyzed in every sample by oxidation with dichromate under external heating [20]. Total N was determined by the Kjeldahl method after sulfuric digestion [21].

DNA extraction and PCR amplification. Total genome DNA was extracted from 10 g sediment samples using alkaline lysis method [22]. The 16S rDNA genes were amplified using universal primer pairs 27F and 1492R [23] in the first step of PCR. Subsequently, the initial PCR product in the first step was used as a template for a nested PCR amplification targeting the V3 region of the 16S rRNA gene with primers 338F with the GC clamp and 518R [15], and the DNA fragments which were suitable for DGGE analysis were obtained. Amplification was performed with TC-512 system in a total volume of 50 μL. The reaction mixture contained 5 μL 10 × buffer, 4 μL 2.5 mM dNTPs, 1 μL 10 μM of each PCR primer, 0.5 μL 5 U Taq DNA polymerase (TaKaRa Taq^{TM}), and 6μL DNA template (50-100 ng), and double-distilled water was added up to 50 μL. Amplification conditions were as follows: 94℃for 5 min, and 21 cycles consisting of 94℃ for 30 s, 63℃ for 30 s, 72℃ for 30 s. with a touchdown of 0.5℃ every cycle until the annealing temperature dropped down to 53℃. The next 20 cycles was consisted of 94℃ for 30 s, 53℃ for 30 s, 72℃ for 30 s, and the final step was 7 min extension at 72℃. Amplification products were analyzed by electrophoresis in 1.2% (w/v) agarose gels using ethidium bromide staining.

DGGE analysis. DGGE analysis was performed with Dcode Universal Mutation Detection System (Bio Rad). A total volume of 30 μL PCR products was added into a 8% (w/v) acrylamide gel (acrylamide/N,N'-methylene bisacrylamide ratio, 37.5:1) in 1×TAE buffer. The gels contained a linear gradient of denaturant from 30-60% (100% denaturant is 7 M urea plus 40% formamide). Electrophoresis was performed at a constant voltage of 80V at 60℃ for 8h. Afterwards, gels were stained in a solution of 1×TAE which contained ethidium bromide for 20min, and photographed.

Recovery, Cloning and sequencing of excised DGGE bands. Dominant fragments were excised from the DGGE gel with a sterile scalpel, dipped in 100 μL sterile distilled water, and stored at -20℃ overnight. After that, they were incubated at 65℃ for 20 min. After centrifugation at 6000 rpm for 5 min, the supernatant was served as template DNA for re-amplification with the V3 region primers without GC clamp. PCR conditions for re-amplification of dominant fragments from the DGGE gel included an initial denaturation step of 5 min at 95℃, followed by 35cycles of 94 ℃ for 30 s, 55 ℃ for 30 s, 72 ℃ for 1 min, and the final extension was performed at 72℃ for 7 min. Then the amplification fragments were cloned into pMD 19-T (TaKaRa pMD19-T Vector) Vector and transformed into *E. coli* JM109 after being purified by 1.0% agarose electrophoresis and recovered by TaKaRa Agarose Gel DNA Purification Kit ver. 2.0. The positive clones from dominant gel fragrant from DGGE bands were selected randomly for sequence analysis which was performed by Shanghai Sangon Biological Engineering Technology & Service Co., Ltd.

TABLE 1
General information of samples studied

No.	Sampling Sites	longitude and latitude	Functional Zones
Y1	Dandong	39°44′ N, 123°31′ E	Conservation district
Y2	Dandong	39°47′ N, 123°41′ E	Conservation district
Y3	Dalian	39°02′ N, 121°54′ E	Mariculture zone
Y4	Dalian	38°48′ N, 121°19′ E	Mariculture zone
Y5	Dalian	39°14′ N, 122°09′ E	Mariculture zone
Y6	Dalian	39°18′ N, 122°07′ E	Mariculture zone
Y7	Dalian	38°55′ N, 121°36′ E	Port area
Y8	Dalian	38°53′ N, 121°42′ E	Conservation district

TABLE 2
Physico-chemical characteristics of the eight investigated samples

samples	Y1	Y2	Y3	Y4	Y5	Y6	Y7	Y8
pH	7.58	7.76	7.72	7.95	8.02	7.81	7.21	7.81
organic C ($g \cdot kg^{-1}$)	6.08	1.46	7.54	2.34	8.56	3.62	11.89	22.12
Total N ($g \cdot kg^{-1}$)	0.35	0.63	0.07	0.21	0.84	0.49	0.7	1.05
C: N	17.37	2.32	107.71	11.14	10.19	7.39	16.99	21.07

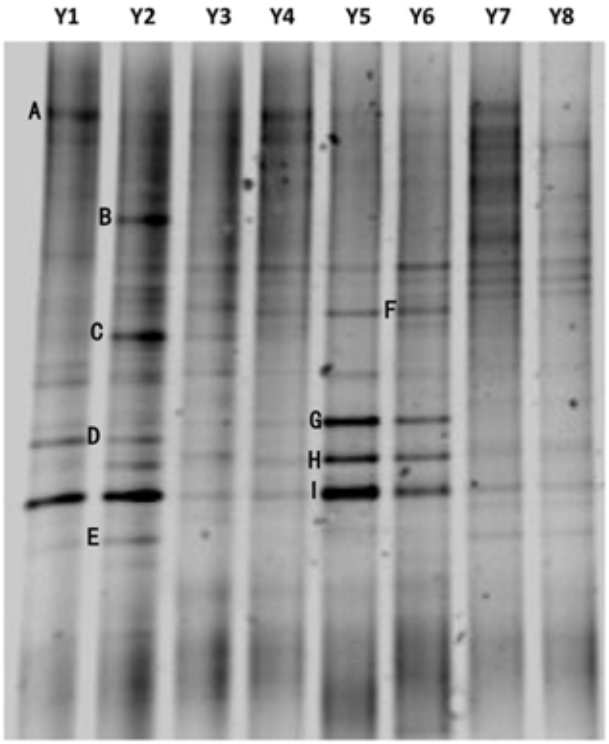

FIGURE 1
The DGGE profiles of bacterial V3 16S rDNA gene fragments amplified from sediment samples. Lanes Y1-Y2: Dandong marine, conservation district. Lane Y3-Y8: Dalian marine, belong to mariculture zone, mariculture zone, mariculture zone, mariculture zone, port area and conservation district, respectively. The DNA bands which were excised from the gel, cloned and sequenced were indicated. The letters of the bands corresponds to that of the clones showed in Table 3.

Data analysis and phylogenetic tree construction. The partial bacterial 16S rDNA gene sequences homology searches were carried out using BLAST in NCBI (http://www.ncbi.nlm.nih.gov/BLAST/). Then Neighbor-Joining phylogenetic tree was constructed with MEGA 5.0 by using Tajima-Nei model, 1000 bootstrap replicates were performed.

A scanned image of DGGE gel was performed using BIO-RAD software Quantity One version 4.6.2. DGGE fingerprints were automatically scored by the presence or absence of co-migrating bands. The number and the similarity of band patterns in DGGE gel were comparatively analyzed among different sediment samples. Dendrograms were constructed using the complete linkage method with arithmetic averages (UPGMA).

Nucleotide sequence accession numbers. All the nucleotide sequences in this study have been deposited in the NCBI nucleotide sequence database under accession numbers (JN853593-JN853600).

RESULTS

Sediment properties. All the sediment samples were weakly alkaline (pH values were 7.21 to 8.02). Table 2 showed the other main physical and chemical properties of sediments. The marine sediment samples showed obvious differences in organic carbon and total nitrogen.

Community structure of soil microorganisms. Microbial community structure in marine sed-

iment samples from Dalian marine and Dandong marine were investigated based on the V3 regions of 16S rDNA gene fragment analysis. The number in DGGE gel bands and relative brightness in DGGE gel from each sample were analyzed by Quantity One software. Eight samples in this study had different band numbers. The band number was 21, 23, 22, 19, 15, 22, 25 and 20 (Figure 1). The representative bands which were clear and had high intensity were excised and recovered from acrylamide gel. These bands were indicated in Figure 1 with arrows in the gel lanes and the band profiles were analyzed by clustering methods to examine the homology. Similar community structures were observed in sample Y1 and Y2, and they were clustered into one group, which both were from Dandong marine region. Other samples were included into another group, in which they were all from Dalian marine region. Composition of bacterial communities in Y7 sample and Y8 sample showed the most similarities (Figure 2), which came from conservation district and port area.

Identification of dominant bacterial species. Nine dominant 16S rDNA DGGE bands (A, B, C, D, E, F, G, H, I) were excised from the gels, cloned and sequenced as described above. After band sequences analysis, we found that the main bacteria in the sea sediment were *Bacteroidetes*, *Actinobacteria*, *β-proteobacteria* and *γ-proteobacteria* (Table 3). Half of the sequences showed the highest similarities with those of uncultured organisms from other environment samples, including sea sediment, lake and soil (Figure 3). *Bacteroidetes* and *γ-proteobacteria* were the most abundant ones in Y5 and Y6 sediment, which came from mariculture zone. The bands C, E, F and G were similar with *Salinimicrobium* sp. and *Sphingobacteria* sp., which were affiliated with *Bacteroidetes*. Clones, which were closely related with uncultured *Actinobacteria* (band B) were detected as unique and predominant species in Y2 sample. Uncultured *Sphingobacteria*, *Salinimicrobium* sp., uncultured *Nitrosospira* sp. and *Methylophaga* sp. were widely distributed in every sediment samples.

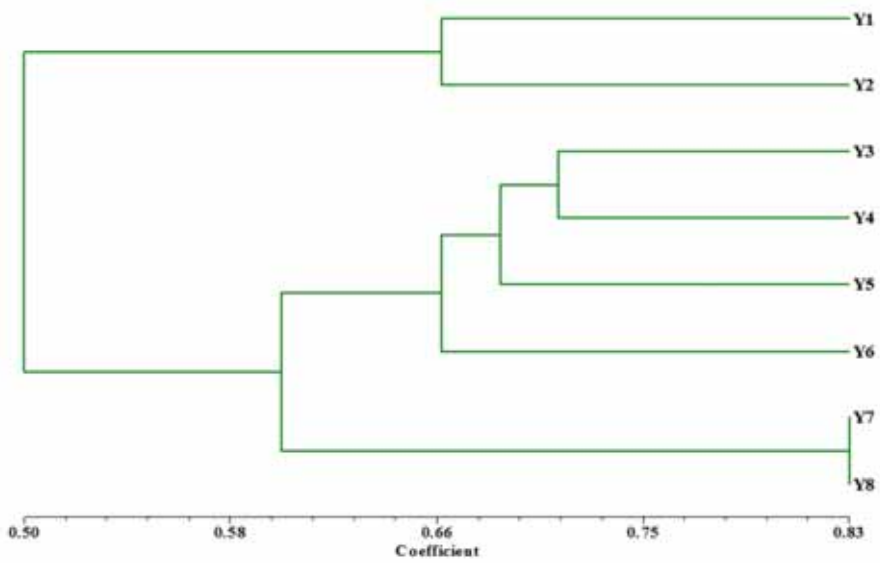

FIGURE 2
UPCMA dendrogram analysis of profiles obtained from DGGE banding patterns for bacteria from sediment samples. Lanes Y1-Y2: Dandong sea. Lane Y3-Y8: Dalian sea.

TABLE 3
The sequencing analysis results of selected DGGE bands

Sequenced clones	GenBank Accession no.	Similarity rate (%)	the most similar GenBank sequence	Division
DLY1-1(A)	JN853600	100	*Escherichia coli*	γ-Proteobacteria
DLY2-1(B)	JN853597	98	Uncultured Actinobacteria	Actinobacteria
DLY2-2(C)	JN853598	93	Uncultured *Sphingobacteria*	Bacteroidetes
DLY2-4(E)	JN853599	98	*Salinimicrobium* sp.	Bacteroidetes
DLY5-1(F)	JN853593	98	*Salinimicrobium* sp.	Bacteroidetes
DLY5-3(G)	JN853594	94	Uncultured *Sphingobacteria*	Bacteroidetes
DLY5-4(H)	JN853595	96	Uncultured *Nitrosospira* sp.	β- Proteobacteria
DLY5-5(I)	JN853596	92	*Methylophaga* sp.	γ-Proteobacteria

D: sequencing failure.

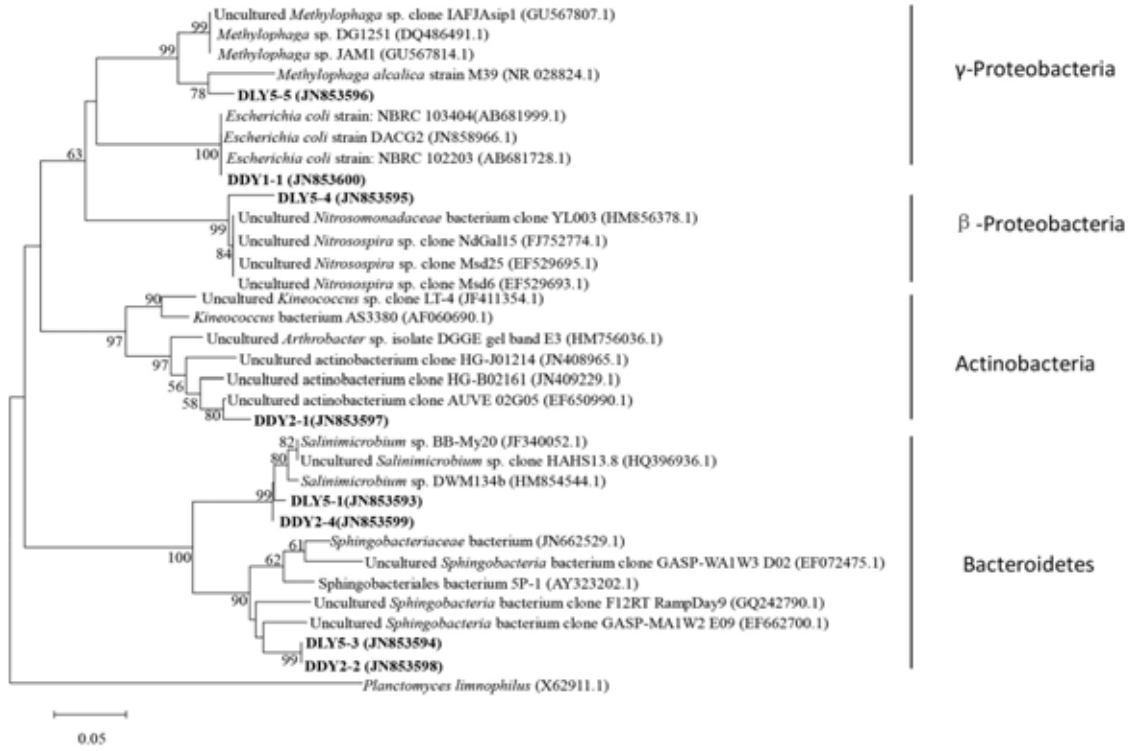

FIGURE 3
Phylogenetic tree show the relationship of retrieved clones in this paper with references from GenBank closest sequences. The phylogenetic tree was constructed as described in the materials and methods. Clones derived in this study were marked with boldface. The number of sequences in parentheses following the clone name and GenBank accession number. The sequence of 16S rDNA gene from *Planctomyces limnophilus* (X62911) served as outgroup.

DISCUSSION

Dalian sea area is one of the special scientific interesting sites. The bacterial communities and the impacts of marine functional zones on the bacterial community in the sea sediments were investigated in this study. The microbial communities in the sediments were analyzed by molecular approaches targeting the 16S rDNA gene sequences. DGGE profiles were used to analyze bacterial community among samples. About 15 to 25 DGGE bands in DGGE gel were detected wintin the different sediment samples. The number of bands was similar to those in deep-sea sediments and Yellow Sea Cold Water Mass [19, 24]. All bands in DGGE gel had the most similarities to sequences from other environment samples. In the sediment from Dalian and Dandong sea areas, the bacterial communities included *γ-Proteobacteria*, *Bacteroidetes*, *β- Proteobacteria* and *Actinobacteria*. Consistent with previously studies [19, 25], *γ-Proteobacteria* and *Bacteroidetes* were found to be abundant and widely distributed in sediment samples.

It has been reported that the major bacterial processes in marine sediments were methane metabolism and sulfate reduction [26, 27]. With the exception of two recent isolates, all known methanotrophs belong to two monophyletic families: type I/X methanotrophs belong to the family *Methylococcaceae* within the γ-Proteobacteria, and type II methanotrophs which belong to the family *Methylocystaceae* within the α-Proteobacteria [28]. The *α-Proteobacteria* were not detected in this study. However, the DGGE gei band I was retrieved, and had a 92% sequence similarity with *Methylophaga* sp., which was affiliated with *γ-Proteobacteria*, a type of I methanotroph [29]. In this study, sequences from the *Cytophaga- Flavobacteria- Bacteroides* (CFB) division were found to be abundant. Bands C and D showed 93% similarity with uncultured *sphingobacteria*, bands E and F had a similarity of 98% with uncultured *salinimicrobium*, which were commonly referred as CF cluster [30]. Similar results were also found from the study on permanently cold marine sediments [31]. Previous study had shown that CFB played important roles in carbon cycling of organic substances deposited in deep-sea sediments [32].

Bands B showed 98% similarity with uncultured *Actinobacteria* clone, and Y2 sample from Dandong sea area was unique. A*ctinobacteria* groups were not detected in the sediments samples of South China Sea [19], however it's a major lineage of the domain bacteria in the glacial meltwater lake sediment in Antarctica [17, 25].

It is an effective and convenient method using DGGE technique to determine community structures in sea sediments. DGGE analysis method was used to detect the bacterial communities in the marine sediment samples from Dalian sea area and Dandong sea areas, and the major members of the microbial communities were identified in this study. Among the 4 major domain bacteria, *γ-Proteobacteria* and *Bacteroidetes* were predominant in 8 samples. The main bacterial communities are similar among each sample in the same area, and the bacterial community structure including predominant species was related with geographical location and functional zones. However, no significant relationship was found between the bacterial community and physico-chemical characteristics of sediment samples. To the best of our knowledge, this study was the first report to reveal the microbial diversity in various functional zones in Dalian sea area by DGGE analysis methods. Usually, the sediment bacterial communities' changes could be driven by the salinity, nutrients and vegetation type. All these factors are affected by the special actions engaged by humans for many years. In the future, studies should focus on the interactions among these factors as well as the way they affect the structure of sediment microbial communities.

ACKNOWLEDGEMENTS

This work was supported by the National Natural Science Foundation of China (30671398, 31070005), the Fundamental Research Funds Central Universities (DC10030102, DC10030106) and Liaoning Provincial Natural Science Foundation (20062189).

The authors declare no conflict of interest.

REFERENCES

[1] Cammen, L.M. (1982) Effect of particle size on organic content and microbial abundance within four marine sediments. Mar Ecol Prog Ser. 9, 273-280.

[2] Montagna, P.A. (1982) Sampling design and enumeration statistics for bacteria extracted from marine sediments. Appl Environ Microbiol. 43(6), 1366-1372.

[3] Danovaro, R., Manini, E. and Dell'Anno, A. (2002) Higher abundance of bacteria than of viruses in deep Mediterranean sediments. Appl Environ Microbiol. 68(3), 1468-1472.

[4] Nealson, K.H. (1997) Sediment bacteria: who's there, what are they doing, and what's new? Annu Rev Earth Planet Sci. 25, 403-434.

[5] Bordalo, A.A. (1993) Effects of salinity on bacterioplankton, field and microcosm experiments. J. Appl. Bacteriol. 75, 393-398.

[6] Crump, B.C., Hopkinson, C.S., Sogin, M.L. and Hobbie, J.E. (2004) Microbial biogeography along an estuarine salinity gradient: combined influences of bacterial growth and residence time. Appl Environ Microbiol. 70(3), 1494-1505.

[7] Zhao, D.Y., Huang, R., Zeng, J., Yan, W.M., Jiang, C.L., Ma, T. and Wang, M. (2012) Bacterioplankton Community Composition and the Influence of Water Chemistry in Small Lakes of Nanjing City, China. Fresen. Environ. Bull. 21, 960-966.

[8] Sivri, N., Balci, M., Durmus, T., Seker, D.Z. and Balkis, N. (2012) Analysis of Enteric Bacteria Distribution in the Gulf of Gemlik (Marmara Sea) by Means of Gis. Fresen. Environ. Bull. 21, 3224-3232.

[9] Powell, S.M., Bowman, J.P., Snape, I. and Stark, J.S. (2003) Microbial community variation in pristine and polluted nearshore Antarctic sediments. FEMS Microbiol Ecol. 45(2), 135-145.

[10] Bissett, A., Burke, C., Cook, P.L. and Bowman, J.P. (2007) Bacterial community shifts in organically perturbed sediments. Environ Microbiol. 9(1), 46-60.

[11] Jensen, S.I., Kuhl, M. and Prieme, A. (2007) Different bacterial communities associated with the roots and bulk sediment of the seagrass Zostera marina. FEMS Microbiol Ecol. 62(1), 108-117.

[12] Amann, R.I., Ludwig, W. and Schleifer, K.H. (1995) Phylogenetic Identification and in-Situ Detection of Individual Microbial-Cells without Cultivation. Microbiological Reviews. 59(1), 143-169.

[13] Webb, V.L. and Maas, E.W. (2002) Sequence analysis of 16S rRNA gene of cyanobacteria associated with the marine sponge Mycale (Carmia) hentscheli. FEMS Microbiol Lett. 207(1), 43-47.

[14] Lee, E.Y., Lee, H.K., Lee, Y.K., Sim, C.J. and Lee, J.H. (2003) Diversity of symbiotic archaeal communities in marine sponges from Korea. Biomol Eng. 20(4-6), 299-304.

[15] Muyzer, G., de Waal, E.C. and Uitterlinden, A.G. (1993) Profiling of complex microbial populations by denaturing gradient gel electrophoresis analysis of polymerase chain reaction-amplified genes coding for 16S rRNA. Appl Environ Microbiol. 59(3), 695-700.

[16] Koizumi, Y., Kojima, H. and Fukui, M. (2003) Characterization of depth-related microbial community structure in lake sediment by denaturing gradient gel electrophoresis of amplified 16S rDNA and reversely transcribed 16S rRNA fragments. FEMS Microbiol Ecol. 46(2), 147-157.

[17] Ikenaga, M., Guevara, R., Dean, A.L., Pisani, C. and Boyer, J.N. (2010) Changes in community structure of sediment bacteria along the Florida coastal everglades marsh-mangrove-seagrass salinity gradient. Microb Ecol. 59(2), 284-295.

[18] Tian, Y., He, X., Torralba, M., Yooseph, S., Nelson, K.E., Lux, R., McLean, J.S., Yu, G. and Shi, W. (2010) Using DGGE profiling to develop a novel culture medium suitable for oral microbial communities. Molecular Oral Microbiology. 25(5), 357-367.

[19] Lai, X.T., Zeng, X.F., Fang, S., Huang, Y.L., Cao, L.X. and Zhou, S.N. (2006) Denaturing gradient gel electrophoresis (DGGE) analysis of bacterial community composition in deep-sea sediments of the South China Sea. World Journal of Microbiology & Biotechnology. 22(12), 1337-1345.

[20] Nelson, D.W. and Sommers, L.E. (1996) Total carbon, organic carbon, and organic matter. Methods of Soil Analysis, Part 3. Chemical Methods. Madison: Soil Science Society of America Inc. 961-1010.

[21] Bremner, J.M. (1996) Nitrogen-total. Methods of Soil Analysis, Part 3. Madison: Soil Science Society of America Inc. 1085-1121.

[22] Hu, Y., Liu, Z., Yan, J., Qi, X., Li, J., Zhong, S., Yu, J. and Liu, Q. (2010) A developed DNA extraction method for different soil samples. J Basic Microbiol. 50(4), 401-407.

[23] Lane, D.J. (1991) 16S/23S rDNA sequencing. In: Stackebrandt, E., Goodfellow, M. (eds.) Nucleic acid techniques in bacterial systematics. Chichester, United Kingdom: John Wiley and Sons. 115–175.

[24] Liu, M., Zhu, K.L., Li, H.B., Zhang, T. and Xiao, T. (2008) Bacterial community composition of the Yellow Sea Cold Water Mass studied by PCR-denaturing gradient gel electrophoresis. Huan Jing Ke Xue. 29(4), 1082-1091.

[25] Li, S., Xiao, X., Yin, X. and Wang, F. (2006) Bacterial community along a historic lake sediment core of Ardley Island, West Antarctica. Extremophiles. 10(5), 461-467.

[26] Ravenschlag, K., Sahm, K., Knoblauch, C., Jorgensen, B.B. and Amann, R. (2000) Community structure, cellular rRNA content, and activity of sulfate-reducing bacteria in marine arctic sediments. Appl Environ Microbiol. 66(8), 3592-3602.

[27] Parkes, R.J., Cragg, B.A. and Wellsbury, P. (2000) Recent studies on bacterial populations and processes in subseafloor sediments: A review. Hydrogeology Journal. 8(1), 11-28.

[28] Gulledge, J., Ahmad, A., Steudler, P.A., Pomerantz, W.J. and Cavanaugh, C.M. (2001) Family- and genus-level 16S rRNA-targeted oligonucleotide probes for ecological studies of methanotrophic bacteria. Appl Environ Microbiol. 67(10), 4726-4733.

[29] Inagaki, F., Suzuki, M., Takai, K., Oida, H., Sakamoto, T., Aoki, K., Nealson, K.H. and Horikoshi, K. (2003) Microbial communities associated with geological horizons in coastal subseafloor sediments from the sea of okhotsk. Appl Environ Microbiol. 69(12), 7224-7235.

[30] Chen, X.H., Zeng, Y.H. and Jiao, N.Z. (2006) Development and evaluation of specific 16S rDNA primers for marine Cytophaga-Flavobacteria cluster. Molecular Ecology Notes. 6(4), 1278-1281.

[31] Ravenschlag, K., Sahm, K., Pernthaler, J. and Amann, R. (1999) High bacterial diversity in permanently cold marine sediments. Appl Environ Microbiol. 65(9), 3982-3989.

[32] O'Sullivan, L.A., Weightman, A.J. and Fry, J.C. (2002) New degenerate Cytophaga-Flexibacter-Bacteroides-specific 16S ribosomal DNA-targeted oligonucleotide probes reveal high bacterial diversity in River Taff epilithon. Appl Environ Microbiol. 68(1), 201-210.

Received: **01.09.2017**
Accepted: **09.11.2017**

CORRESPONDING AUTHOR

Qiu Liu
Dalian Minzu University,
No. 18 West Liaohe Road,
Dalian Development Zone,
Dalian, 116600 – China

e-mail: qiuliu2017@qq.com

© by PSP Volume 27 – No. 2/2018 pages 1076-1080 Fresenius Environmental Bulletin

EFFICIENT PROTOCOL FOR MULTIPLE MICRO-SHOOT REGENERATION FROM ENDANGER, ENDEMIC AND ORNAMENTAL PLANT *CENTAUREA FENZLII* REICHARDT.

Nalan Turkoglu[1], Fethi Ahmet Ozdemir[2,*], Nurhan Keskin[1], Khalid Mahmood Khawar[3]

[1]Department of Horticulturae, Faculty of Agriculture, Van Yuzuncu Yıl University, 65090, Van, Turkey
[2]Department of Molecular Biology and Genetics, Faculty of Science and Art, Bingol University, 12000, Bingol, Turkey
[3]Department of Field Crops, Faculty of Agriculture, Ankara University, Diskapi, 06110, Ankara, Turkey

ABSTRACT

Environment damage has brought about the elimination of many plant species, and numerous more are endangered. Similarly, ornamental and endemic *Centaurea fenzlii* Reichardt that grows in Turkey is threatened that necessities measures for its immediate conservation. *In vitro* culture techniques are widely used to conserve uncommon, threatened plants. This study reports a proficient technique for multiple micro-shoot regeneration of *C. fenzlii*. A low recurrence (35%) germination was acquired on MS medium supplemented with 2.60 µM GA_3. Juvenile leaves were utilized as an explants source. The leaves were regenerated on MS medium that contained 1.11, 2.22, 4.44, 8.88 µM BAP + 2.685, 5.37, 10.64 µM NAA. The best callus regeneration percentage was seen on MS medium that used 4.44 µM BAP + 10.64 µM NAA. Callus regeneration percentage extended between 21.33 to 66.87. The most noteworthy micro-shoot regeneration percentage was gotten on MS medium containing 8.88 µM BAP + 2.685 µM NAA. Micro-shoot regeneration percentage run between 5.66 to 36.87%. The highest number of micro-shoots per explants was noted on MS medium containing 4.44 µM BAP + 10.64 µM NAA. Also number of micro-shoots per explants extended between 1.66 to 5.87. The rooting percentage of *C. fenzlii* was low with a few roots. The best rooting was noted following seven weeks of culture on 4.90 µM IBA. IBA appears to act as stimulant in rooting of *C. fenzlii.*

KEYWORDS:
Centaurea fenzlii, endemic, multiple micro-shoot regeneration, BAP, NAA, IBA

INTRODUCTION

The genus *Centaurea L.* distributed all around the world [1, 2] and grows on a huge variety of geological, orographical and geographical diverse landscapes and environments. Numerous species among these are endemic or threatened and need appropriate management for conservation due to anthropogenic practices that more often jeopardize their existence along with incredible number of other plant species [3]. Turkey is one of main region with largest genetic diversity in the family *Centaurea* with 209 taxa [1, 4]. Destruction of habitats, and careless unlawful gatering of plants growing in wild for use in flower industry are the fundamental reasons undermining the existence of any of the Centaureas including endemic *Centaurea fenzlii*. Reichardt that has high ornamental potential [5, 6, 7]. It is found in Agri, Erzurum, Malatya, Mus, Tunceli provinces of Eastern Anatolia at altitudes of 1150-1820 m above sea level. Proper management of plant diversity through effective protection measures is required.

Conservation of the endemic plant species is completed utilizing distinctive procedures. Micropropagation constitutes an effective instrument for *ex situ* protection of this plant, that has diminished populaces and low seed yield and germination [8, 9].

This paper present results of a showing recovery, conservation and protection of this plant and other endangered plant species with in this genera. The purpose and objective of this study was to develop an *in vitro* micropropagation protocol using juvenile leaf explants of *C. fenzlii*. Formation of an appropriate strategy towards this end will encourage laying of foundation to conserve this endemic endangered plant species.

MATERIALS AND METHODS

Plant material. Matured seeds of *C. fenzlii* were gathered from eastern Turkish province of Tunceli during July - August (2016) and stored in paper packs at 23-25 ˚C under cold, dry and dark conditions.

Seed viability test. Seeds of *C. fenzlii* were soaked in water overnight. Thereafter the sseeds were dissected, longitudinally after removing seed coats, with a scalpel exposing embryo to the 1% tetrazolium chloride solution (1 mg/ml) taking care not to damage any part of embryo when peeling the seed coat and imbibing in colorless tetrazolium solution.

Seed sterilization and germination. The seeds were disinfected with 100 % commercial bleach for 10 min taken after by 5×5 min flushing with sterilized distilled water. The initial experiments confirmed dormancy in the seeds of *C. fenzlii* as they failed to germinated on MS medium that was supplemented with 30 g/l sucrose. Therefore, they were cultured on petri dishes containing 0.65% (w/v) plant agar (Duchefa) set on MS medium [10] that contained 2.60 µM giberellic acid (GA_3, Duchefa) supplemented with 3% sucrose cultured for 18 days by incubating at 24±1 °C.

The multiple Micro-shoot regeneration. Leaves of sprouted seeds were utilized as an explant. They were cultured on 0.65% (w/v) plant agar (Duchefa) gelled with MS medium containing 1.11, 2.22, 4.44, 8.88 µM BAP (6-benzylaminopurine - Duchefa) + 2.685, 5.37, 10.64 µM NAA (1-Naphthaleneacetic acid Duchefa) in Petri dishes (15 combinations) supplemented with 3% sucrose. All cultures were kept up under 16 h light photoperiod (35 μmol m^{-2} s^{-1}) in Aralab flexible development chamber (Praha, Czech Republic) at 24±1°C. All cultures used as a part of this study were subjected to autoclave for 20 min at 120 °C, 1.42 kg cm^{-2}. The pH of all media was adjusted to 5.8 ± 0.1 with 1N NaOH or 1 N HCl.

Micro-shoot rooting and acclimatization of plantlets. Developing micro-shoots were removed from the stock culture, and transferred to MS medium containing 4.90 µM IBA for rooting and a control treatment without using auxin treatments was included. Following root induction, the plants were transferred to MS medium so as to provide opportunity to roots the micro shoots to reach a desirable size for transfer to pots containing 3:1 ratio of soil: sand for acclimatization.

Statistical analysis. Each treatment contained 30 explants divided into 3 replications with equal numbers of explants. The experimental data was analyzed using One-way ANOVA subjected to Post hoc Tukey's b test was obtained utilizing IBM SPSS v. 22 computer software for Windows.

RESULTS

Randomly selected 85 seeds out of 100 seeds of *C. fenzlii* showed high viability using tetrazolium test by reduction of dehydrogenase enzyme present in all living tissues to create formazan, a reddish water insoluble compound. The rate of hydrogen released in viable tissue is slow compared to the dead tissues. No seed induced abnormal red colour showing week living tissues. Similarly, no seed showed White or dead tissues that showed lack of respiration and inhibition of formazan formation [11].

It was noted that the seeds could be disinfected using commercial, mercantile bleach for 10 min. The seeds sprouting was made on MS medium containing 2.60 µM GA_3; as the seeds failed to germinate without GA_3 treatment as indicated earlier. The leaf explants were collected from six days old germinated seedlings. Different combinations and concentrations of phytohormones influenced rate of callus regeneration variably. Callus and shoot regeneration was accomplished on all regeneration treatments (Table 1).

The maximum callus regeneration (86.67%) was seen on 4.44 µM BAP + 10.64 µM NAA followed 63.33% callus induction using 8.88 µM BAP + 10.64 µM NAA in MS medium. All leafs explants regenerated callus on MS medium four weeks later after culture initiation. Callus regeneration percentage ranged between 21.33 to 66.87. The findings showed that the concentrations and combinations of BAP and NAA affected callus regeneration percentage. Callus regeneration percentage decreased with decrease of both BAP and NAA concentrations.

The most elevated micro-shoot regeneration percentage was noted on 8.88 µM BAP + 2.685 µM NAA (Table 1) trailed by MS medium that contained 4.44 µM BAP + 2.685 µM NAA in MS medium. Micro-shoot regeneration percentage extended between 5.66 to 36.87. Furthermore, the results showed that micro-shoot regeneration percentage decreased with an increased NAA concentrations. No regeneration was noted on the control treatments. An increase in the micro-shoot regeneration percentage was observed at high concentrations of BAP+NAA.

The results indicated that increased BAP+NAA concentrations played a key role in Micro-shoot regeneration on leaf explants of *C. fenzlii*. Both BAP+NAA are most commonly used phytohormones used in tissue culture of most of the plants. It is assumed that high concentrations of these phytohormones act as stimulants to induces micro-shoot induction on endangered *C. fenzlii*. No callus and micro-shoots were reported on MS medium. Results further illustrated that concentrations and combinations of BAP-NAA used in the study important factors to effectuate micro-shoot induction. Number of micro-shoots per explants ranged 1.66 to 5.87 (Table 1). Maximum number of micro shoots per explants were borne or regenerated on MS medium containing 4.44 µM BAP + 10.64 µM NAA followed closely by 4.33 and 4.13 micro-shoots per explants on 2.22 µM BAP+ 5.37 µM NAA and 2.22 µM BAP + 10.64 µM NAA respectively.

TABLE 1
Effect of different concentrations of BAP +NAA on micro-shoot regeneration from leaf explants of *C. fenzlii*.

Treatments		Callus regeneration percentage (%)	Micro-shoot regeneration percentage (%)	Number of Micro-shoots per explant
BAP (µM)	NAA (µM)			
1.11	2.685,	31.66i	21.13d	2.13i
2.22	2.685,	28.87k	24.66c	3.67d
4.4	2.685,	23.33l	29.33b	1.87k
8.88	2.685,	21.33m	36.87a	2.66h
1.11	5.37	57.87e	11.13h	3.13f
2.22	5.37	51.66f	12.33g	4.33b
4.4	5.37	47.33g	14.87f	2.66h
8.88	5.37	36.87h	18.66e	1.66l
1.11	10.64	61.66c	3.87m	3.33e
2.22	10.64	60.33d	5.66l	4.13c
4.4	10.64	66.87a	7.87k	5.87a
8.88	10.64	63.33b	10.33i	2.87g
MS medium (control)		0.00	0.00	0.00

All values in a single column showed by different small letters are statistically different at 0.05 level of significance.

The rooting ability of *C. fenzlii* was very low. *In vitro* regenerated micro-shoots induced a very few roots only after five weeks of culture. The best rooting responses after seven weeks of culture was obtained using 4.90 µM IBA. This concentration of IBA seems to have a stimulatory role during root formation in *C. fenzlii.* Besides this auxin concentration was beneficial for root system development and micro-shoot quality. All micro plantlets with well developed root systems on transferrance to plastic pots. 60 % of the plantlets survived in the green house and showed no sign of water stress. Thereafter, the regenerated plants showed normal growth.

DISCUSSION

The method described here offers a simple, efficient and rapid procedure to micropropagate the endangered, endemic and ornamental plant *C. fenzlii* using juvenile leaves as explants. The viability of any species relies upon the harmony among annihilation and colonization. In view of this it could be rightly said that the surviving of species depends in all on the survival of the populace and its seed germination. The utilization of seeds is for the most part an ideal way to conserve plant species and the variation in hereditary pattern of local species. In the event that plants are multiplied from seeds, the variation among local ecotypes could be increased to the maximum [12, 13]. Every species has specific prerequisites for seed germination [14, 15]. Conservation of seeds by their propagation cheap and effective methodology. Poor seed germination is in concurrence with past studies [16, 17, 18, 19, 20]. It was observed that seeds of *C. fenzlii* [16, 17, 18, 19, 20].

The study positively utilised 13 distinct combinations of plant hormones for regeneration from leaf explants of *in vitro* regenerated seedlings. The results showed that MS medium was not useful for regeneration that failed to induce any swelling actuation of any callus. The results are in concurrence with the past studies [17, 21, 22, 23, 24, 25].

The study demonstrated that micro-shoot recovery was mostly hindered by callus recovery. The most noteworthy micro-shoot regeneratin percentage was instigated on 8.88 µM BAP + 2.685 µM NAA. The treatments including distinctive BAP concentrations used in this study were helpful to induce micro-shoot regeneration. This BAP has already been viewed as an appropriate phytohormone for regeneration of *C. spachii* [23], *C. paui* [24], *C. zeybekii* [21], *C. ultreiae* [25], *C. tchihatcheffii* [17], *C. rupestris* [26], *C. arifolia* [27], *C. ragusina* [28].

CONCLUSIONS

To finish up, a fruitful, quick regeneration and propagation tecnique has been developed for endangered *Centaurea fenzlii* from juvenile leaf explants for utilization in future conservation programs that would definitley help in conservation of rare and wild plant species in future.

REFERENCES

[1] Wagenitz, G. (1975) Centaurea L. In: Davis, P.H. (ed.) Flora of Turkey and the East Aegean Islands. vol 5. Edinburgh: Edinburgh University Press, 465-585.

[2] Davis, P.H., Mill, R.R. and Tan, K. (1988) Centaurea L. In: Davis, P.H., Mill, R.R., Tan, K. (eds.) Flora of Turkey and the East Aegean Islands. Vol. 10 (Supplement). Edinburgh: Edinburgh University Press, 166-169.
[3] Ozdemir, F.A. and Yildirim, M.U. (2016) *Scilla siberica* subsp. armena yaprak sapindan *in vitro* çoklu sürgün rejenerasyonu. Y.Y. Uni. J. of Agri. Sci. 26(2), 215-220.
[4] Guner, A. (2000) Centaurea L. In: Güner, A., Özhatay, N., Ekim, T., Başer, K.H.C. (eds.) Flora of Turkey and the East Aegean Islands. Vol. 11 (Supplement). Edinburgh: Edinburgh University Press, 163-164.
[5] Ekim, T., Koyuncu, M., Vural, M., Duman, H., Aytac, Z. and Adiguzel, N. (2000) Red data book of Turkish plants. In: Turkish Association for the conservation of nature, Ankara, Turkey. 221, 1-41 (In Turkish).
[6] Garcia-Jacas, N., Susanna, A., Garnatje, T. and Vilatersana, R. (2001) Generic delimitation and phylogeny of the subtribe Centaureinae (Asteraceae): A combined nuclear and chloroplast DNA analysis. Annals of Bot. 87, 503-515.
[7] Wagenitz, G. and Hellwig, F.H. (1994) Evolution of characters and thephylogeny of the Centaureinae. In: Hind, D.J.N., Beentje, H.G. (eds.) Compositae: Systematics. - Proceedings of the International Compositae Conference, Kew. Kew: Royal Botanical Gardens, 491-510.
[8] Fay, M.F. (1994) In what situation is *in vitro* culture appropriate to plant conservation? Biodiversity and Conservation. 3, 176-183.
[9] Krogstrup, P., Baldursson, S. and Norgaard, J.V. (1992) *Ex situ* genetic conservation by use of tissue culture. Opera Botanica Belgica. 113, 49-53.
[10] Murashige, T. and Skoog, F. (1962) A revised medium for rapid growth and bioassays with tobacco tissue cultures. Physio. Plant. 15, 473-497.
[11] Ista. (1966) International rules for seed testing. Proceedings of the International Seed Testing Association. 31, 92-106.
[12] Fay, M.F. and Muir, H.J. (1990) The role of micropropagation in the conservation of European plants. In: Hernández Bermejo, J.E., Clemente, M., Haywood, V. (eds.) Conservation techniques in botanic gardens. Koeltz Scientific Books, Koenigstein, 27-32.
[13] Fay, M.F. (1992) Conservation of rare and endangered plants using *in vitro* methods. *In Vitro* Cel. & Develop. Bio.-Plant. 28, 1-4.
[14] Harper, J.L., Lovell, P.H. and Moore, K.G. (1970) The shapes and sizes of seeds. Annual Review of Ecology. Evolution and Systematics. 1, 327-356.
[15] Schutz, W. and Milberg, P. (1997) Seed dormancy in *Carex canescens*: regional differences and ecological consequences. Oikos. 78, 420-428.
[16] Koller, D., Poljakoff-Mayber, A., Breg, A. and Diskin, T. (1963) Germination regulating mechanisms in *Citrullus colcynthis*. Am. J. of Bot. 50, 597-603.
[17] Ozel, C.A., Khawar, K.M., Mirici, S., Ozcan, S. and Arslan, O. (2006) Factors affecting *in vitro* plant regeneration of the critically endangered Mediterranean knapweed (*Centaurea tchihatcheffii* Fisch et. Mey). Naturwissenschaften. 93, 511–517.
[18] Celik, S. (2006) Studies on the germination of three endangered *Centurea* species. Pak. J. of Bot. 38(5), 1431-1437.
[19] Okay, Y. and Gunoz, A. (2009) Golbasi's endemic *Centaurea tchihatcheffii* Fisch. et. Mey. The effect on germination of seeds of some applications. J. of Agri. Sci. 15(2), 119-126.
[20] Okay, Y. and Demir, K. (2010) Critically endangered endemic *Centaurea tchihatcheffii* Fisch. and Mey. and its propagation possibilities. African J. of Agri. Research. 5(25), 3536-3541.
[21] Kurt, S. and Erdag, B. (2009) *In vitro* germination and axillary shoot propagation of *Centaurea zeybekii*. Biologia. 64(1), 97-101.
[22] Ozel, C.A., Khawar, K.M., Mirici, S., Arslan, O. and Ozcan, S. (2006) Induction of *ex vitro* adventitious roots and soft wood cuttings of *Centaurea tchihatcheffii* Fisch. et Mey. using Indole 3-Butyric and α-Naphthalene acetic acid. Inter. J. of Agri. and Bio. 8(1), 66-69.
[23] Cuenca, S. and Amo-Marco, J.B. (2000) *In vitro* propagation of *Centaurea spachii* from inflorescence stems. Plant Growth Regulation. 30, 99-103.
[24] Cuenca, S., Amo-Marco, J.B. and Para, R. (1999) Micropropagation from inflorescense stems of the Spanish endemic plant *Centaurea paui* Loscos ex Wilk. (Compositae). Plant Cell Rep. 18, 674-679.
[25] Mallon, R., Oubina, J.R. and Gonzalez, M.L. (2010) *In vitro* propagation of the endangered plant *Centaurea ultreiae*: assessment of genetic stability by cytological studies, flow cytometry and RAPD analysis. PCTOC. 101, 31–39.
[26] Perica, M.C. (2003) *In vitro* propagation of *Centaurea rupestris* L. Acta Bio. Cracoviensia Series Bot. 45(2), 127-130.
[27] Yuzbasioglu, E., Dalyan, E., Bona, M. and Oz, G. (2012) *In vitro* propagation of endemic plant *Centaurea arifolia* Boiss. Taxa, IUFS J. of Bio. 71(2), 121-127.
[28] Pevalek-Kozlina, B. (1998) *In vitro* propagation of *Centaurea ragusina* L. a Croatian endemic species. Acta Biologica Cracoviensia. 40, 21-24.

Received: **05.09.2017**
Accepted: **03.12.2017**

CORRESPONDING AUTHOR

Fethi Ahmet Ozdemir
Department of Molecular Biology and Genetics,
Faculty of Science and Art,
Bingol University,
12000, Bingol – Turkey

e-mail: ozdemirfethiahmet23@yahoo.com

© by PSP Volume 27 – No. 2/2018 pages 1081-1085 Fresenius Environmental Bulletin

ENHANCED SIMULTANEOUS SEPARATION OF H_2S AND CO_2 BY AN AMINO ACID SALT-PROMOTED POTASSIUM CARBONATE SOLUTION IN A HOLLOW FIBER MEMBRANE CONTACTOR

Pengrui Jin[1,2], Chuan Huang[1,2,*], Yadong Shen[1,2], Liao Wang[1,2]

[1]State Key Laboratory of Coal Mine Disaster Dynamics and Control, Chongqing University, Chongqing 400044, People's Republic of China.
[2]College of Resources and Environmental Science, Chongqing University, Chongqing 400044, People's Republic of China

ABSTRACT

An aqueous solution of potassium carbonate is a low-cost suitable absorbent for the simultaneous separation of CO_2 and H_2S from biogas. The promoted potassium carbonate with amino acid salt has the potential to combine the advantages of these two kinds of absorbents. In this communication, potassium glycinate (PG), potassium sarcosine (PS) and potassium L-proline (PLP) were considered promoters. The absorption performance of CO_2 and H_2S in promoted potassium carbonate was compared with non-promoted potassium carbonate. The results indicated that the CO_2 absorption performance of the promoted potassium carbonate with various amino acid salts was much higher than that of the aqueous potassium carbonate solution. Furthermore, among three solutions, the promoted K_2CO_3 with PS had the highest CO_2 and H_2S absorption flux. The promoted K_2CO_3 with various amino acid salts and non-promoted K_2CO_3 had approximately the same H_2S absorption flux, since the H_2S removal rates of both can reach nearly 100%.

KEYWORDS:
Amino acid salts, Potassium Carbonate, H_2S, CO_2, Simultaneous separation, Hollow fiber membrane contactor

INTRODUCTION

Biogas is a source of sustainable energy that is produced by anaerobic fermentation of organic materials. In general, the original biogas consists of methane (CH_4, 40%-75%), carbon dioxide (CO_2, 15%-60%) and traces of hydrogen sulphide (H_2S) [1]. A large amount of acidic CO_2 in biogas will reduce the heating value of biogas as well as lead to corrosion in equipment. H_2S is a very harmful pollutant that can endanger human health and corrode equipment [2-4]. Therefore, CO_2 and H_2S in biogas must be removed before biogas can be used as a fuel for vehicles [5].

Gas-liquid membrane contactors (GLMCs) are a hybrid and effective strategy for gas absorption that integrates membrane separation and liquid absorption.[6-8] From the theoretical and practical point of view, CO_2- and H_2S-absorbing liquid is an important variable in the GLMC process.[9] In recent years, various absorption liquids, including aqueous solutions of Na_2CO_3, [10] monoethano-lamine (MEA), [2, 11, 12] methyldiethanolamine (MDEA), [11] and potassium carbonate (K_2CO_3) [12] have been used in simultaneous separation of CO_2 and H_2S. However, the performance of amines as the absorbent is limited by amine loss, amine degradation, high reaction heat and corrosion [8]. Compared with MEA, the main advantages of aqueous K_2CO_3 are low cost and easier regeneration. However, the reaction rate of K_2CO_3 in the liquid phase is very low, but can be increased with addition of a promoting agent. [14] The amino acid absorption solution has an amino functional group, so it can act as an activator for the potassium carbonate solution. In addition, Yan et al. [15] reported that aqueous amino acid salts can provide high reactivity to CO_2. Thus, promoted carbonate solutions with amino acid salts can provide a favorable condition for absorbing CO_2 and H_2S. The effect of adding the amino acid salt to the carbonate solution in the wetted wall column has been studied by previous researchers [16-18]. However, to the best of our knowledge, there is no published work involving theoretical analysis of the simultaneous absorption of CO_2 and H_2S using an amino acid salt-promoted carbonate solution in a GLMC. In this communication, three kinds of amino acid salts, including PG, PS and PLP, were used to enhance a potassium carbonate solution in a GLMC for simultaneous separation of CO_2 and H_2S.

MATERIALS AND METHODS

The characteristics of the PVDF hollow fiber membrane are shown in Table 1. The pH value,

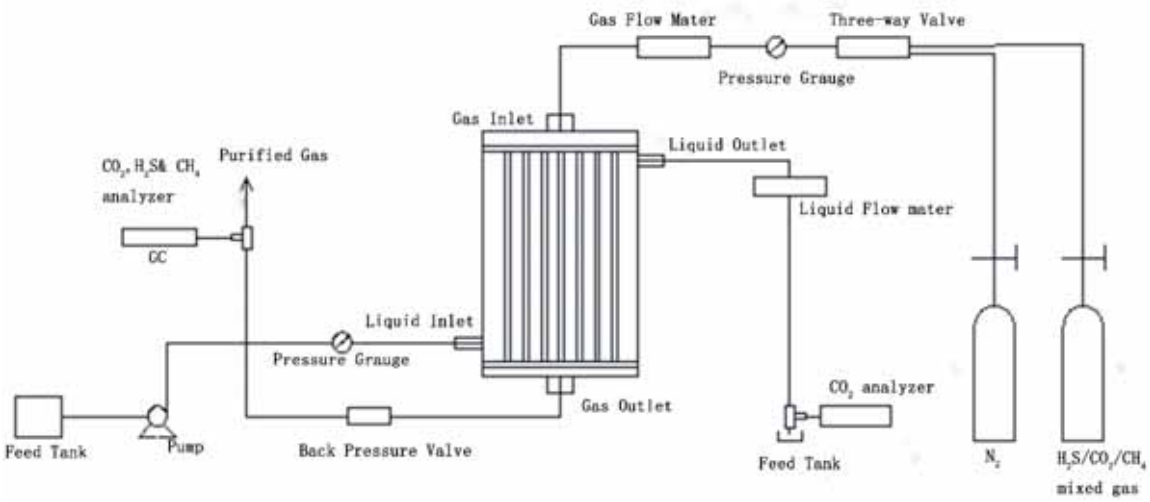

FIGURE 1
Flow diagram of experimental setup for simultaneous absorption of CO_2 and H_2S

surface tension and viscosity were measured with a pH meter (IP67, Mettler), surface tension meter (K11, Kruss) and rotary rheometer (Anton Paar MCR302), respectively. These measurements are shown in Table 2. The schematic diagram of the experimental set up is shown in Figure 1. A gas mixture of CO_2 40% v/v and H_2S 300 ppm in the balance of CH_4, which is in the composition range of biogas, was fed through the shell side of the GLMC module while PG, PS, PLP and their blended solutions as absorbents were fed into the lumen side of the PVDF hollow fiber membrane. The gas phase flow rate was fixed at 250 ml/min, whereas the liquid phase flow rate varied from 50 to 140 ml/min.

TABLE 1
Specifications of PVDF hollow fiber membrane used in this study

Parameter (unit)	PVDF hollow fiber membrane
Fibre o.d. (mm)	1.1
Fibre i.d. (mm)	0.8
Module i.d. (mm)	15
Membrane pore size (μm)	0.2
Membrane porosity	0.70
Effective module length	500
Number of fibres	37

TABLE 2
pH, surface tensions and viscosities of the various absorbents

Membrane	pH	Viscosity (mPa·S)	Surface tension (mN/m)
PG 0.05M	10.59	0.991	71.25
PS 0.05M	10.83	0.984	71.07
PLP 0.05M	11.41	1.133	71.39
K_2CO_3 0.05M	11.07	1.535	71.61
K_2CO_3 0.025M + PG 0.025M	10.95	1.17	71.33
K_2CO_3 0.025M + PS 0.025M	10.99	1.055	71.29
K_2CO_3 0.025M + PLP 0.025M	11.06	1.133	72.42

RESULTS AND DISCUSSION

Gas absorption flux. In this study, CO_2 and H_2S absorption flux was used to indicate the separation properties of the hollow fiber membrane module, which can be calculated using the following equation: [19,20]

$$J_{CO_2} = \frac{\left(Q_{g,in} \times C_{g,in} - Q_{g,out} \times C_{g,out}\right) \times 273.15 \times 1000}{22.4 \times T \times S} \quad (1)$$

Where J_{CO2} is the CO_2 absorption flux [mol $(m^2 \cdot s)^{-1}$], $C_{g,in}$ and $C_{g,out}$ represent the inlet and outlet gas-phase CO_2 concentrations, respectively (%), $Q_{g,in}$ and $Q_{g,out}$ are the gas volumetric flow rate at the inlet and outlet, respectively (m^3/s), T is temperature (K) and S is the gas-liquid interfacial area (m^2).

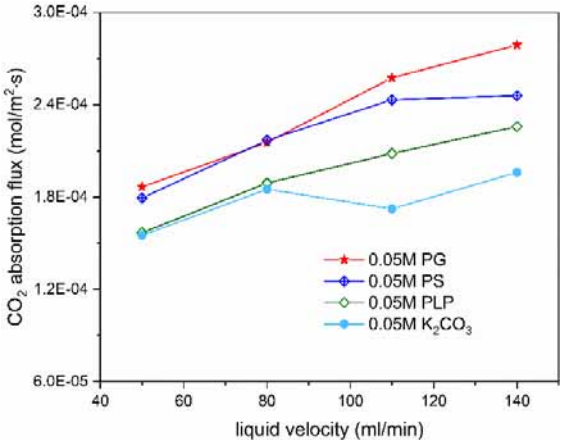

FIGURE 2
Effect of liquid velocity and types of amino acid salts solutions on CO_2 absorption flux.

Absorption performance of single absorbents. The effects of liquid flow rate and types of amino acid slat used are shown in Figure 2. It was found that the CO_2 absorption flux increases as the liquid flow rate increases. This is because the liquid

mass transfer resistance decreases as the liquid velocity increases. Many studies have reported a similar trend demonstrating that the mass transfer process of CO_2 absorption in the membrane contactor is controlled by the mass transfer coefficient of the liquid phase [21, 22]. In contrast, as shown in Figure 3, the liquid velocity has little effect on the H_2S absorption flux.

As shown in Figure 2, the CO_2 absorption flux of the different absorbents at a 0.05M concentration in decreasing order was PG > PS > PLP > K_2CO_3. These results can be explained by the difference in the viscosity of the various absorbents. The greater the viscosity of the absorbent, the lower diffusion coefficient of CO_2 and the lower theCO_2 absorption flux [23]. It was found that the viscosity of the different absorbents was ordered as follows: K_2CO_3(1.535) > PLP(1.133) > PG(0.991) > PS(0.984) (see Table 2). Although the liquid viscosity of PG is slightly higher than PS, the reaction rate constant between PS and CO_2 was lower than the reaction rate constant between PG and CO_2 at 35°C as reported by Zhou et al. [24]. Thus, the CO_2 absorption flux of PG is slightly higher than the that of PS.

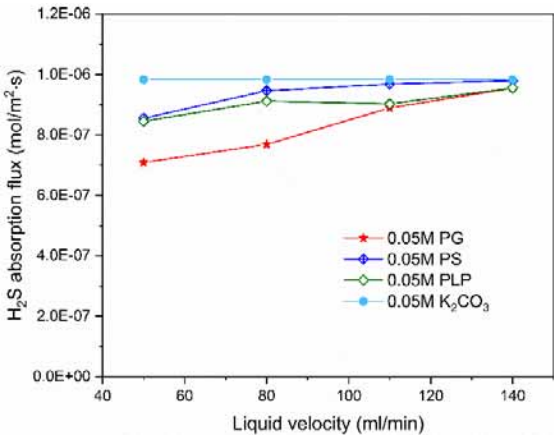

FIGURE 3
Effect of liquid velocity and types of amino acid salts solutions on H_2S absorption flux.

Figure 3 shows the H_2S absorption flux of different absorbents, and the removal efficiency of H_2S by different absorbents is ordered as K_2CO_3 > PS > PLP > PG. In the case of the K_2CO_3 solution, the H_2S removal percentage is approximately 100%. Therefore, the increase of liquid flow rate in the K_2CO_3 absorption solution did not affect the H_2S absorption flux. Figure 2 shows an obvious the increase of the CO_2 absorption flux with the increase of the liquid flow rate. On the contrary, liquid velocity had little effect on the H_2S absorption flux. Similar results have been reported in the literature [2, 11].

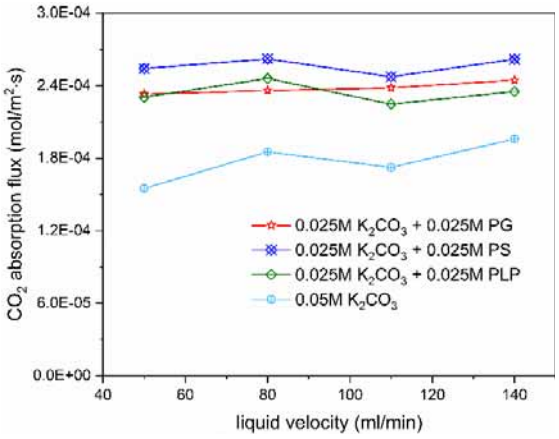

FIGURE 4
Experimental results for K_2CO_3 solutions promoted with various amino acid salts on CO_2 absorption flux.

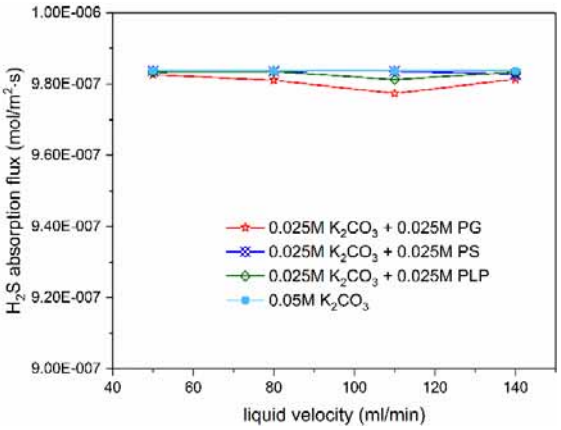

FIGURE 5
Experimental results for K_2CO_3 solutions promoted with various amino acid salts H_2S absorption flux.

Absorption performance of promoted K_2CO_3 solutions. Figure 4 compares the CO_2 absorption performance of aqueous K_2CO_3 and promoted K_2CO_3 with various aqueous amino acid salt solutions. This figure indicates that the CO_2 absorption performance of the promoted K_2CO_3 with different amino acid salts was much higher than that of the aqueous K_2CO_3 solution. This is due to the low reaction rate of non-promoted K_2CO_3.[25] The promoted K_2CO_3 with amino acid salt solutions provides higher CO_2 absorption fluxes, improved approximately 2-fold over non-promoted K_2CO_3. It can be found that promoted K_2CO_3 with amino acid salts has even better performance than single amino acid salts by comparing Figure 2 with Figure 4. To explain this result, it should be noted that the surface tension of amino acid salt/K_2CO_3 in a 1:1 mole ratio at 0.05M total concentration is higher than that of 0.05M amino acid salt solution (see Table 2); thus, the promoted K_2CO_3 with amino acid salts had better resistance to membrane wetting compared to the single amino acid salts. Zhao et al. have reported that

the high surface tension of the absorbent will improve the pore-wetting resistance of the membrane [8].

As can be seen from Figure 5, the H_2S absorption flux performance of the promoted K_2CO_3 with different amino acid salts was nearly identical to the non-promoted K_2CO_3, which is due to a H_2S removal rate of nearly 100%. Furthermore, the results shown in Figure 5 indicate that the promoted K_2CO_3 with amino acid salts has an excellent H_2S absorption performance as well as the non-promoted K_2CO_3 solution.

CONCLUSIONS

In summary, the present study was conducted to analyze simultaneous separation of CO_2 and H_2S using solutions of K_2CO_3 promoted with various amino acid salts (i.e., PG, PS and PLP). We believe that this is the first demonstration of the use amino acid salts to enhance K_2CO_3 solutions in GLMC for the simultaneous separation of CO_2 and H_2S. The results of this communication show that the CO_2 absorption performance of the promoted K_2CO_3 with different amino acid salts was much higher than that of the aqueous K_2CO_3 solution. In addition, among three solutions, the K_2CO_3 promoted with PS had the highest CO_2 and H_2S absorption flux. The H_2S absorption flux performance of the promoted K_2CO_3 solutions promoted with different amino acid salts was very similar to the non-promoted K_2CO_3, which was due to a H_2S removal rate of almost 100%.

ACKNOWLEDGEMENTS

This work was supported by the Chinese National Science and Technology Support Program (Contract No. 2014BAC29B01) for which due acknowledgement is given.

REFERENCES

[1] Tilahun, E., Bayrakdar, A., Sahinkaya, E., Calli, B. (2017) Performance of polydimethylsiloxane membrane contactor process for selective hydrogen sulfide removal from biogas. Waste management. 61, 250-257.

[2] Rongwong, W., Boributh, S., Assabumrungrat, S., Laosiripojana, N. Jiraratananon, R. (2012) Simultaneous absorption of CO_2 and H_2S from biogas by capillary membrane contactor. Journal of Membrane Science. 392–393(2), 38-47.

[3] Ceper, B.A., Uysal, M., Kahraman, N., Akansu, S.O. (2017) Investigation of enging performance and emissions of an si engine using biogas-hydrogen mixtures. Fresen. Environ. Bull. 26, 5556-5563.

[4] Song, X., Li, K., Ning, P., Tang, L., Sun, X., Ruan, H., Mei, Y., Wang, C. (2016) Optium reaction conditions, pathways and kinetic model of hydrolysis of carbon disulfide over modified lake sedment biochar. Fresen. Environ. Bull. 25, 4952.

[5] Deublein, D., Steinhauser, A. (2010) Biogas from waste and renewable resources: An introduction. Wiley. 2011(9), 8.

[6] Mansourizadeh, A., Ismail, A.F. (2009) Hollow fiber gas-liquid membrane contactors for acid gas capture: a review. Journal of Hazardous Materials. 171(1-3), 38

[7] Zhang, Z.E., Yan, Y.F., Zhang, L., Ju, S.X. (2014) Hollow fiber membrane contactor absorption of CO_2 from the flue gas: review and perspective. Glob. Nest J. 16, 355-374.

[8] Zhao, S., Feron, P.H.M., Deng, L., Favre, E., Chabanon, E., Yan, S., Hou, J., Chen, V., Qi, H. (2016) Status and progress of membrane contactors in post-combustion carbon capture: A state-of-the-art review of new developments. Journal of Membrane Science. 511, 180-206.

[9] Li, J.L., Chen, B.H. (2005) Review of CO_2 absorption using chemical solvents in hollow fiber membrane contactors. Separation & Purification Technology. 41(2), 109-122.

[10] Wang, D., Teo, W.K., Li, K. (2004) Selective removal of trace H_2S from gas streams containing CO_2 using hollow fibre membrane modules/contractors. Separation & Purification Technology. 35(2), 125-131.

[11] Hedayat, M., Soltanieh, M., Mousavi, S.A. (2011) Simultaneous separation of H_2S and CO_2 from natural gas by hollow fiber membrane contactor using mixture of alkanolamines. Journal of Membrane Science. 377(1), 191-197.

[12] Faiz, R., Al-Marzouqi, M. (2009) Mathematical modeling for the simultaneous absorption of CO_2 and H_2S using MEA in hollow fiber membrane contactors. Journal of Membrane Science. 342(1–2), 269-278.

[13] Faiz, R., Al-Marzouqi, M. (2011) Insights on natural gas purification: Simultaneous absorption of CO_2 and H_2S using membrane contactors. Separation & Purification Technology. 76(3), 351-361.

[14] Benson, H.E., Field, J.H., Jimeson, R.M. (1954) CO_2 Absorption Employing Hot Potassium Carbonate Solutions. Chemical Engineering Progress. 7, 356-364.

[15] Yan, S., He, Q., Zhao, S., Wang, Y., Ai, P. (2014) Biogas upgrading by CO_2 removal with a highly selective natural amino acid salt in gas–liquid membrane contactor. Chemical Engineering and Processing: Process Intensification. 85, 125-135.
[16] Kohl, A.L., Nielsen, R.B. (1997) Chapter 5–Alkaline Salt Solutions for Acid Gas Removal. Gas Purification. Houston, Texas: Elsevier. 330-414.
[17] Thee, H., Nicholas, N.J., Smith, K.H., Silva, G.D., Kentish, S.E., Stevens, G.W. (2014) A kinetic study of CO_2 capture with potassium carbonate solutions promoted with various amino acids: Glycine, sarcosine and proline. International Journal of Greenhouse Gas Control. 20(2), 212-222.
[18] Shen, S., Feng, X., Ren, S. (2013) Effect of Arginine on Carbon Dioxide Capture by Potassium Carbonate Solution. Energy & Fuels. 27(10), 6010-6016.
[19] Yan, S.P., Fang, M.X., Zhang, W.F., Wang, S.Y., Xu, Z.K., Luo, Z.Y., Cen, K.F. (2007) Experimental study on the separation of CO_2 from flue gas using hollow fiber membrane contactors without wetting. Fuel Processing Technology. 88(5), 501-511.
[20] Jin, P., Huang, C., Shen, Y., Zhan, X., Hu, X., Wang, L., Wang, L. (2017) Simultaneous separation of H2S and CO2 from biogas by gas-liquid membrane contactor using single and mixed absorbents. Energy & Fuels. 31(10), 11117-11126.
[21] Rahbari-Sisakht, M., Ismail, A.F., Rana, D., Matsuura, T., Emadzadeh, D. (2013) Effect of SMM concentration on morphology and performance of surface modified PVDF hollow fiber membrane contactor for CO 2 absorption. Separation & Purification Technology. 116(37), 67-72.
[22] Mansourizadeh, A. (2012) Experimental study of CO_2 absorption/stripping via PVDF hollow fiber membrane contactor. Chemical Engineering Research & Design. 90(4), 555-562.
[23] Rongwong, W., Jiraratananon, R., Atchariyawut, S. (2009) Experimental study on membrane wetting in gas–liquid membrane contacting process for CO_2 absorption by single and mixed absorbents. Separation & Purification Technology. 69(1), 118-125.
[24] Zhou, X.P., Fang, M.X., Xiang, Q.Y., Cai, D.Y., Wang, T., Luo, Z.Y. (2016) Characteristics of mass transfer in various aqueous amino acid salt solutions for CO_2 capture. Journal of Zhejiang University (Engineering Science). 50(2), 312-319.
[25] Scholes, C.A., Simioni, M., Qader, A., Stevens, G.W., Kentish, S.E. (2012) Membrane gas–solvent contactor trials of CO_2 absorption from syngas. Chemical Engineering Journal. 195–196, 188-197.

Received: **06.09.2017**
Accepted: **06.11.2017**

CORRESPONDING AUTHOR

Chuan Huang
College of Resources and Environmental Science, Chongqing University,
Chongqing 400044 – P.R. China

e-mail: hclsjb@163.com

© by PSP Volume 27 – No. 2/2018 pages 1086-1094 Fresenius Environmental Bulletin

DIFFERENT EFFECTS OF HEAVY METALS ON PHYSIOLOGICAL AND BIOCHEMICAL PARAMETERS IN WHEAT VARIETIES

Ayse Ak[1,*], Ersin Yucel[2]

[1]Erzincan University, Engineering Faculty, Biomedical Engineering, Erzincan, Turkey.
[2]Anadolu University, Biology Department, Eskisehir, Turkey.

ABSTRACT

Heavy metal pollution threatens all living organisms in worldwide. Serious health problems can be induced in human being, when they enter food chain by plants. Heavy metals can result in adverse effect in plant physiologic and biochemical process. These effects differ between plant species as well as their varieties depending on several factors such as heavy metal types, concentration, plant parts and growth stage. To assess different toxic effects of zinc, cadmium and lead applied at 100, 200 and 300 μM, we investigated physiologic and biochemical parameters of three wheat varieties. As a result, all applied heavy metals led to different effects in germination, mitotic index, photosynthetic pigments and antioxidant enzyme levels of wheat varieties. Well-tolerated variety was found as *T. a.* cv. 'Sönmez-2001'variety. *T. a.* cv. 'Sultan-95' variety was also moderate-tolerated variety. *T. a.* cv. 'Altay-2000' variety was more susceptible to heavy metal applications. Among applied heavy metals, high concentrations of Cd and Pb are most toxic elements in all varieties. In order to gain better crop productivity in heavy metal polluted area, selection of tolerated variety is a suitable approach. Therefore, evaluation of physiologic and biochemical parameters of any variety provides a valuable information to choose most suitable genotype for polluted area.

KEYWORDS:
Antioxidant enzymes, germination, heavy metals, mitotic index, photosynthetic pigments, wheat varieties

INTRODUCTION

Nowadays, metal industries, mining, pesticides usage lead to serious problems in environment and public health. It is important to know that consuming food contaminated with heavy metals is related to prevalence of cancer [1]. Heavy metals produced by natural processes or anthropological activities induce oxidative stress in all forms of life [2, 3]. High levels of heavy metals in soil and water also result in loss of crop production by interacting physiological and biochemical process in plants [3, 4].

Excessive heavy metal exposure affects seed morphology and physiology, such as chromosomal abnormalities, decrease in germination, reduced root and shoot elongation, dry weight, oxidative stress, nutrient loss, etc. For instance, Zinc (Zn), Cadmium (Cd) and Lead (Pb) have been shown to cause inhibition of germination, root elongation, seedling development, DNA synthesis, photosynthesis and impairment of antioxidant enzymes and molecules in seeds, finally leading to lower yield [5, 6, 7, 8, 9, 10]. Heavy metal toxicity also influences photosynthetic pigments by reducing contents of chlorophylls and carotenoids. Photosynthetic pigments play role in the protection from degenerative stresses. Especially, carotenoids have their antioxidant function by acting quenchers of the high Reactive Oxygen Species (ROS) levels [4]. It has been reported that these photosynthetic pigments have been inhibited by exposure of Pb and Cd [9, 11]. Responses of heavy metal are also different between plants and their cultivars [5, 11, 12, 13].

In order to provide protection from oxidative stress, plants have several mechanisms. One of them is antioxidative defense mechanism that includes enzymatic antioxidants such as superoxide dismutase (SOD), catalase (CAT), peroxidase (POD), glutathione reductase (GR), ascorbate peroxidase (APX), guaiacol peroxidase (GPX) and non-enzymatic antioxidants such as ascorbic acid, glutathione and tocopherol. SOD in all cellular compartments and CAT in peroxisomes that are key enzymes, are required for ROS detoxification in plants [3, 6, 14, 15]. Previous studies found specific correlation between upregulation of several enzyme activities, especially SOD and CAT, and exposure of heavy metals in plant tissues. It can be concluded that antioxidant enzymes play a role in tolerance mechanism to heavy metals and uptake of heavy metal. Therefore, in order to reduce heavy metal toxicity and to provide successful germination, they can be important in the technique termed as phytoremediation [3,16]. Under environmental conditions with excessive heavy metal, if plants have high level antioxidant enzyme activities, they also have elevated germination and growth. Therefore,

selection of suitable plant and its varieties will provide us to gain better agricultural product with resistance to heavy metal stress. Therefore, in the present study, we have selected three heavy metals namely cadmium, lead and zinc (Zn). Cd and Pb are both non-essential metals and most common contaminants [1], whereas Zn is essential micronutrient for plant growth and development [2]. Three of them can be toxic if they are present high concentrations in soil and water [4, 17]. In order to investigate ecotoxicological effects of heavy metals, Wheat that is the most produced cereal in worldwide, has been widely used [18]. Therefore, we aim to determine that which varieties of wheat have more high germination rate and chlorophyll content, mitotic index level and antioxidant enzymes when they are exposed to different heavy metals such as zinc (Zn) and cadmium (Cd) and lead (Pb).

MATERIALS AND METHODS

Seeds of three bread wheat varieties (*Triticum aestivum* L. cv. 'Altay-2000', *Triticum aestivum* L. cv. 'Sönmez-2001', and *Triticum aestivum* L. cv. 'Sultan-95') were provided by Anatolian Agricultural Research Institute, Eskişehir, Turkey. These three varieties are widely cultivated in Anatolia.

Seed germination. Different concentrations (100, 200 and 300 µM) of ZnCl2, CdCl2 and PbCl2 on seed germination were evaluated. The concentrations of heavy metals were prepared freshly by dissolving with deionized water. In order to observe seed germination, a piece of filter paper was placed on a Petri dish (9 cm) and moistened with 10 mL aqueous mixture of ZnCl2, CdCl2 and PbCl2. Controls were maintained by moistening the filter paper with 10 mL deionized water. One hundred seeds of each variety were placed on Petri dish and incubated in dark at 22±2°C. Each treatment was replicated four times.

Mitotic index (MI) in wheat root tip cells. The roots (1.5-2 cm) were cut and fixed immediately in mixture of absolute ethyl alcohol and glacial acetic acid [3:1 (v/v)] for 24 hours. The fixed root tips were hydrolyzed in 1N hydrochloric acid at 60ºC then stored in 70% ethyl alcohol. Cytological preparations were prepared by use of the Feulgen squash technique [19]. For each treatment, 3000–4000 mitotic cells were counted. Each treatment was replicated four times.

Chlorophyll measurement. For the chlorophyll (Chl) measurement, 100 mg of leaf from fresh samples was used. Samples were homogenized in 1-2 mL of 80% acetone and centrifuged at 3000 rpm for 5 minutes. Extract was transferred to cuvette and measured on spectrophotometer. The chlorophyll a, chlorophyll b and carotenoid contents were measured absorbance at 662, 645 and 470 nm respectively and were calculated using the three "trichromatic equations" [20]. Each treatment was replicated four times.

Assays of SOD and CAT enzyme activities. Wheat seedlings were homogenised in extraction buffer 50 mM sodium phosphate buffer (pH 7,6) containing 10 mM EDTA and 10% (w/v) PVPP. Homogenates were centrifuged at 12000 g for 15 minutes. The samples were collected for protein estimation following the method of Bradford (1976) using BSA as standard [21].

SOD activity was measured by the percentage reaction inhibition rate of enzyme with WST-1 substrate (a water soluble tetrazolium dye) and xanthine oxidase using a SOD Assay Kit (Fluka, 19160) according to the manufacturer's instructions. Absorbance of the formazan dye was read at OD 450 nm after 20 min of reaction time at 37°C. Each treatment was replicated three times.

Catalase (CAT) activity was determined spectrophotometrically as a decrease in absorbance at 240 nm for 1 minutes following the decomposition of H_2O_2. The 1 mL of reaction mixture contained 50 mM phosphate buffer (pH 7.0), 100 mM H_2O_2 and 20-60 mL of enzyme extract at 25°C. The activity was calculated using the extinction coefficient ($40 mM^{-1}cm^{-1}$) for H_2O_2 [22]. Each treatment was replicated three times.

Statistics. Data were subjected to One-Way analysis of variance (ANOVA) using Statistica Software. Post-hoc testing was carried out using the Duncan test. A significant level of 0.05 was used for all statistical tests.

RESULTS

Seed Germination. In this study, germination rates were observed under heavy metal treatments. In order to accept germination, its radicula should touch filter paper. Approximately 2-5 mm primary root was used as the operational definition of germination [69, 70]. Of the 3 wheat cultivars, only *T.a.*cv 'Altay-2000' showed significantly decreased germination rates compared to control ($p<0.05$) (Figure 1).

Mitotic index in wheat root tip cells. The influence of heavy metals on mitotic activity of wheat varieties, expressed as mitotic index, is shown in Figure 2. Mitotic index was significantly different among wheat varieties. Difference was statistically significant ($p<0.05$) in terms of cell division in wheat varieties (Figure 2). Mitotic index of control was higher in *T.a.* cv. 'Sönmez-2001' than other varieties.

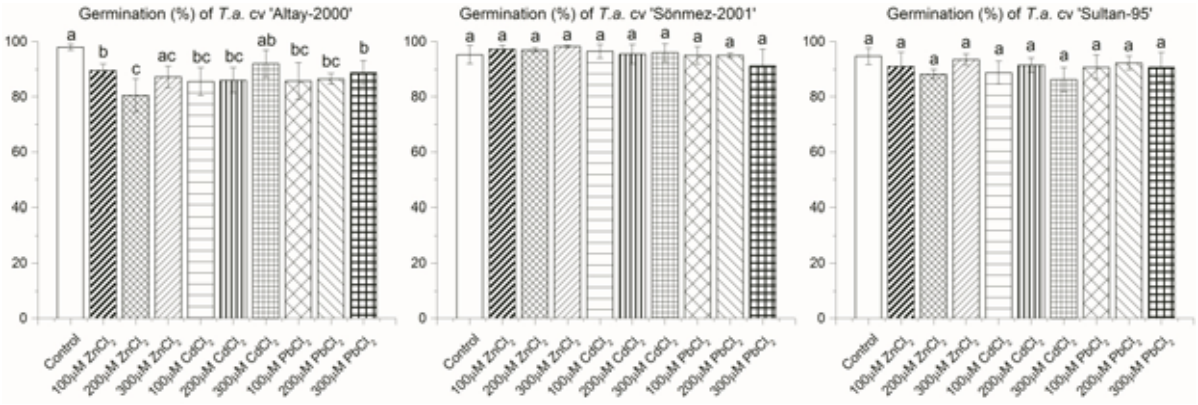

FIGURE 1

Germinations of three varieties exposure to100, 200 and 300µM Zn, Cd and Pb. Values represent the means of at least four replicates for each treatment. Bars with different letters are significantly different at the 0.05 level.

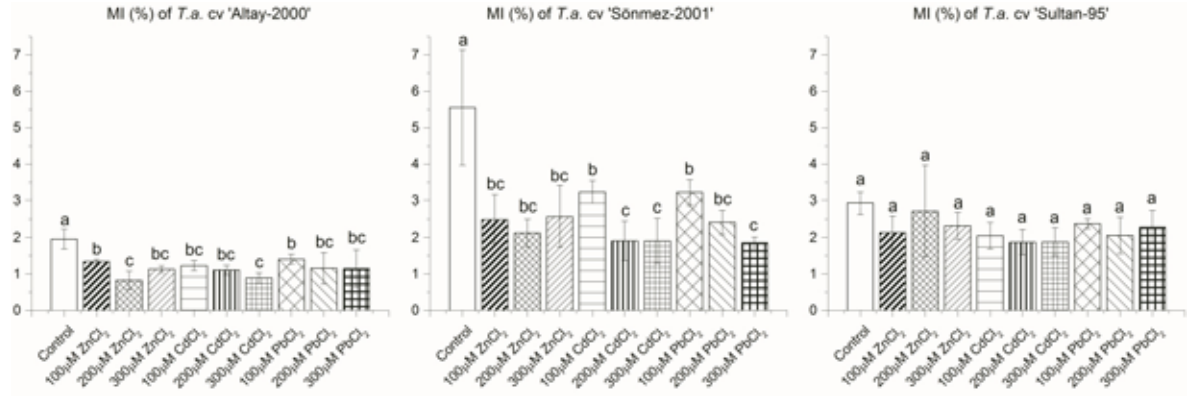

FIGURE 2

Mitotic index (MI) of three varieties exposure to 100, 200 and 300µM Zn, Cd and Pb. Values represent the means of at least four replicates for each treatment. Bars with different letters are significantly different at the 0.05 level.

TABLE 1

Photosynthetic pigments of three varieties exposure to100, 200 and 300 µM Zn, Cd and Pb. Values represent the means of at least four replicates for each treatment. Distinct different letters are significantly different at the 0.05 level.

	***T. a.* cv 'Altay-2000'**			***T. a.* cv 'Sönmez-2001'**			***T. a.* cv 'Sultan-95'**		
	Chl a	**Chl b**	**Carotenoid**	**Chl a**	**Chl b**	**Carote-noid**	**Chl a**	**Chl b**	**Carotenoid**
Control	3.07^{abc}	2.40^{abcd}	1.15^{ab}	11.65^{a}	6.66^{a}	2.87^{a}	9.50^{cd}	7.72^{d}	3.46^{bc}
100 µM Zn	5.60^{d}	4.42^{e}	1.19^{b}	10.38^{a}	6.16^{a}	4.49^{ab}	4.98^{ab}	3.77^{ab}	2.41^{ab}
200 µM Zn	4.82^{cd}	3.68^{de}	3.23^{c}	9.76^{a}	7.46^{a}	4.22^{ab}	6.31^{abc}	5.10^{bc}	2.60^{ab}
300 µM Zn	3.41^{bc}	2.46^{abcd}	1.31^{ab}	10.56^{a}	6.23^{a}	4.58^{ab}	6.08^{abc}	2.84^{a}	1.58^{a}
100 µM Cd	1.58^{ab}	1.27^{ab}	0.54^{a}	11.90^{a}	7.16^{a}	3.45^{ab}	8.24^{bcd}	7.00^{cd}	3.43^{bc}
200 µM Cd	1.26^{a}	0.83^{a}	0.50^{a}	11.10^{a}	7.20^{a}	4.43^{ab}	10.45^{de}	8.28^{d}	3.79^{c}
300 µM Cd	2.48^{ab}	1.51^{ab}	1.35^{ab}	12.83^{a}	7.87^{a}	4.44^{ab}	13.28^{e}	8.79^{d}	3.20^{bc}
100 µM Pb	4.59^{cd}	3.32^{cde}	1.77^{ab}	12.04^{a}	8.38^{a}	3.95^{ab}	4.40^{a}	3.97^{ab}	1.98^{a}
200 µM Pb	2.53^{ab}	2.57^{bcd}	0.91^{ab}	12.87^{a}	8.11^{a}	5.20^{b}	5.59^{ab}	3.59^{ab}	1.95^{a}
300 µM Pb	2.23^{ab}	1.81^{abc}	1.04^{ab}	12.01^{a}	7.56^{a}	3.65^{ab}	5.36^{ab}	3.98^{ab}	2.13^{a}
	$P < 0.05$	$P < 0.05$	$P < 0.05$	$P > 0.05$	$P > 0.05$	$P < 0.05$	$P < 0.05$	$P < 0.05$	$P < 0.05$

Mitotic index is reduced due to heavy metal treatment when compared to control groups in each wheat varieties. On the other hand, it was statistically significant in *T.a.*cv. 'Altay-2000' and *T.a.*cv. 'Sönmez-2001' ($p<0.05$), not in *T.a.*cv. 'Sultan-95' ($p>0.05$). Cd and Pb caused decreases of MI in dose-dependent manner in *T.a.* cv. 'Altay-2000' and *T.a.* cv. 'Sönmez-2001' when compared to control (Figure 2).

Photosynthetic pigments in wheat seedlings. In *T. a.* cv. 'Altay-2000' variety, 100 µM and 200 µM Zn induced chlorophyll a and carotenoid level, respectively ($p<0,05$). Only 200 µM Pb induced

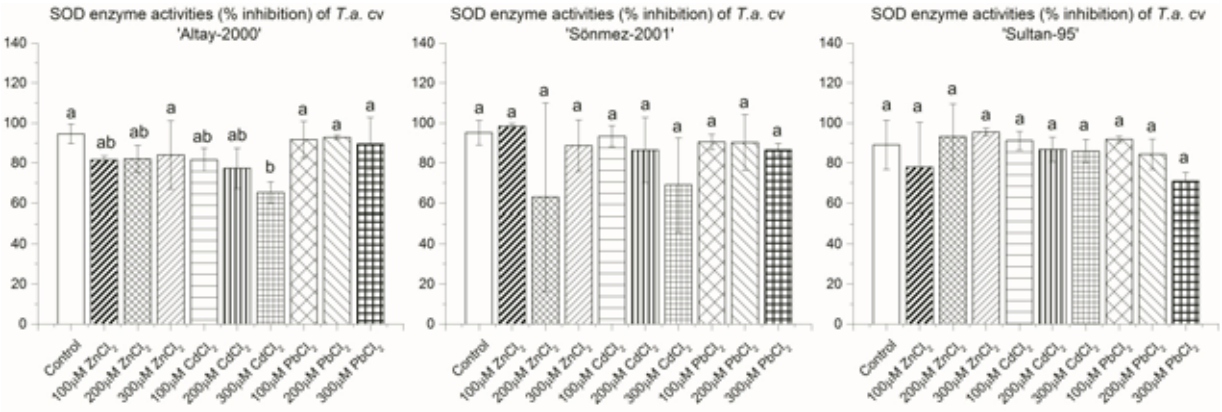

FIGURE 3
SOD enzyme activities of three varieties exposure to100, 200 and 300µM Zn, Cd and Pb. Values represent the means of at least three replicates for each treatment. Bars with different letters are significantly different at the 0.05 level.

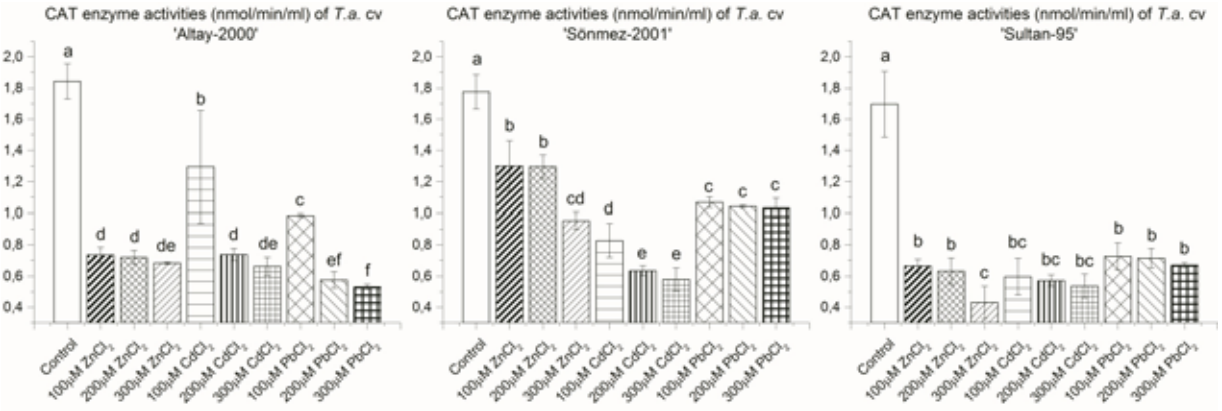

FIGURE 4
CAT enzyme activities of three varieties exposure to100, 200 and 300µM Zn, Cd and Pb. Values represent the means of at least three replicates for each treatment. Bars with different letters are significantly different at the 0.05 level.

significantly carotenoid level of *T. a.* cv. 'Sönmez-2001' ($p<0.05$). 100 µM Zn and all applied Pb concentrations reduced chlorophyll a level, 300 µM Zn and all applied Pb concentrations caused loss of chlorophyll b level and carotenoid level of *T. a.* cv. 'Sultan-95' ($p<0.05$) (Table 1).

Assays of SOD and CAT enzyme activities

All applied concentrations of heavy metals had no statistically significant effect on SOD enzyme activities of *T. a.* cv. 'Sönmez-2001' and *T. a.* cv. 'Sultan-95'. However, 100, 200 µM Zn and all Cd concentrations reduced SOD enzyme activities of *T. a.* cv. 'Altay 2000' ($p<0.05$) (Figure 3).

CAT activities of all varieties were decreased at all concentrations of Zn, Cd and Pb as compared to control ($p<0.05$). As seen in Figure 4, 100 and 200 µM Zn had same inhibitory effect in CAT enzyme activity of all wheat varieties, while 300 µM Zn had more inhibitory effect when compared to other concentrations of Zn and control. All Cd concentrations had significant inhibitory effect in dose-dependent. All Pb concentrations also reduced CAT enzyme activities of wheat varieties ($p<0.05$) (Figure 4).

DISCUSSION

In present study, all applied Zn concentrations (100 µM, 200 µM, 300 µM) had no adverse effects on germinations of *T. a.* cv. 'Sönmez-2001' and *T. a.* cv. 'Sultan-95' except for *T. a.* cv. 'Altay-2000' variety. Zn concentrations inhibited germination dose-dependent manner in *T. a.* cv. 'Alta-2000' variety. Mitotic cell division in roots was also inhibited in *T. a.* cv. 'Sönmez-2001' and *T. a.* cv. 'Altay-2000' varieties. While this inhibition was dose-dependent in *T. a.* cv. 'Altay-2000', inhibition level of cell division was same for all applied Zn concentrations in *T. a.* cv. 'Sönmez-2001'. It is well known that roots are primary contact site for heavy metals. Therefore, roots are more sensitive than shoots and loss of cell viability may cause reduction of root growth [6, 7, 17, 23]. Zinc accumulation in plant parts may differ between wheat varieties [13].

For this reason, responses of plants to heavy metals may be different between species as well as their varieties [24, 25]. Adverse effects of Zn on germination and root cell viability have been well-documented by several studies [7, 26, 27]. There are several reports that germination and mitotic index are reduced as zinc concentrations increase, although wheat variety and zinc concentrations are different from we used [28, 29, 30, 31]. In present study, most heavy metal sensitive variety is *T. a.* cv. 'Altay-2000' variety in terms of germination and mitotic index level.

Chlorophyll content is also another important parameter that can be affected by Zn applications [32, 33]. Zinc applied at higher concentrations leads to inhibition of photosynthetic pigments in wheat [28, 33]. In order to prevent several degenerative stresses in plants, carotenoids are also in important role by playing as quenchers of the high ROS levels [4]. It was shown that chlorophyll a and b contents were induced by Zn applications in *T. a.* cv. 'Altay-2000' variety, while carotenoid content was induced by only 200µM Zn concentration. In *T. a.* cv. 'Sönmez-2001' variety, Zn application had no effect significantly on its chlorophyll a, chlorophyll b and carotenoid contents, while, in *T. a.* cv. 'Sultan-95' variety, these pigments were affected negatively by Zn applications. Zn concentrations may cause reduction of chlorophyll synthesis, or increase of their degradation or suppression of photosynthetic electron transport [33]. This is a valuable result for *T. a.* cv. 'Altay-2000' and *T. a.* cv. 'Sönmez-2001' varieties because of applied Zn had no negative effects.

In the literature, little is known about the effects of Zn toxicity on antioxidant enzyme activities of wheat roots and seedlings [4, 7, 23, 27, 28, 33, 34]. Superoxide dismutase (SOD) in all cellular compartments is the key enzyme that quenches superoxide radicals [35, 36]. There are controversial studies in the literature regarding the inhibition [23, 28, 37] or stimulation of SOD enzyme [7, 27, 31, 34] when applied Zn in different wheat varieties. Zn is a cofactor that is required for antioxidant enzymes, especially Cu/Zn-SOD [33, 34, 38]. In a study, it was shown that different genotypes of wheat exhibited different activity of SOD enzyme in response to zinc concentrations (Hacisalihoglu et al. 2003 [38]). In the present study, low Zn concentrations we used, had no alterations on SOD enzyme activities. These results are in accordance with those of Li et al. [33]. Catalase (CAT) is another important enzyme required for decomposing of H2O2 to water and molecular oxygen. Effects of Zn on CAT enzymes are also contradictory because of different plant organs studied, plant growth conditions, durations and concentrations [2, 4]. In our study, all Zn concentrations led to loss of CAT enzyme activities of three varieties in dose-dependent manner. On the other hand, *T. a.* cv. 'Sönmez-2001' varieties had more CAT enzyme activity than other varieties, *T. a.* cv. 'Sultan-95' and *T. a.* cv. 'Altay-2000'. Cherif et al. (2011) [39] and Saifullah et al. (2014) [40] reported that high level of zinc concentrations led to inhibition of antioxidative enzyme activity. It is important to select wheat varieties with high antioxidant enzyme activity and low H2O2 levels for more successful germination in polluted soils [7, 16]. In Zn-polluted growth conditions, *T. a.* cv. 'Sönmez-2001' variety will have more germination ability when compared to other varieties.

Cd and Pb that are two of most common heavy metals, have no function as nutrients in plant cell growth [1, 41]. Both of Cd an Pb have been shown to inhibit seed germination percentage, mitotic index, chlorophyll content [1, 18, 41, 42, 43, 44]. In present study, Cd and Pb had no effect on germination of *T. a.* cv. 'Sönmez-2001' and *T. a.* cv. 'Sultan-95' varieties except for *T. a.* cv. 'Altay-2000'. In *T. a.* cv. 'Altay-2000' variety, both of Cd and Pb concentrations led to decline of germination. When we observed result of mitotic index, all concentrations of heavy metals reduced percentage of mitotic index except for *T. a.* cv. 'Sultan-95' variety. *T. a.* cv. 'Altay-2000' was found to be more Cd sensitive to heavy metal stress. Similar findings in different cultivars treated with Cd and Pb have been observed by Yang et al. (2010) [6], Chen et al. (2010) [18], Liu et al. (2015) [44], Ahmad et al. (2012) [45], and Sheng et al. (2005) [46]. In order to evaluate Cd toxicity in soil, plant germination level may not be a suitable indicator. Wheat roots are likely to undergo Cd damage first. Therefore, mitotic index may be considered as a bioindicator for Cd pollution [18, 47]. Alterations of biochemical parameters occur before any visible symptom of Cd toxicity, assessing of enzyme activities may be more sensitive or indicative than growth parameters in Cd toxicity [47].

It was also found that applied Cd and Pb had no significant inhibitory effect on photosynthetic pigments of *T. a.* cv. 'Altay-2000' variety. Only 200 µM Pb induced carotenoid level in *T. a.* cv. 'Sönmez-2001', meanwhile 300 Cd induced chlorophyll a level in *T. a.* cv. 'Sultan-95' variety. All Pb concentrations caused loss of photosynthetic pigments in *T. a.* cv. 'Sultan-95' variety in agreement with the findings by Wang et al (2011) [32], Dar et al. (2010) [42], Khan et al. (2008) [48], Ci et al. (2010) [49], and Nabiha et al (2015) [50]. It is well known that the uptake and distribution of Cd and Pb differ among plants as well as their varieties, therefore, their effects also vary in physiological processes of plants [6, 11, 13, 45, 51, 52, 53]. Different uptake and accumulation of Cd and Pb in parts of wheat varieties and different SH (sulphydryl) group levels in roots are important factors in explaining genotypic variations [35, 54, 55, 56, 57]. The effects of heavy metal exposure also depend on

duration time, composition, concentration of heavy metal, forms of heavy metal as with salt, sulphate, acetate or nitrate and plants used [17, 32, 35, 58].

Cd and Pb also influence antioxidant enzymes activities [31, 37, 53, 59]. In agreement with the studies of Lin et al. (2007) [60], Benavides et al. (2005) [61], Liu et al (2007) [62], Ci et al. (2009) [63], our results indicated that SOD activity of *T. a.* cv. 'Altay-2000' variety had been negatively influenced by only Cd exposure, while there was no significant difference in SOD enzyme activities of other varieties, *T. a.* cv. 'Sönmez-2001' and *T. a.* cv. 'Sultan-95'. Activities of CuZn-SOD and Fe-SOD isoforms are more sensitive to high Cd concentrations, but Cd concentrations may cause no inhibition in total SOD activity, because of unaffected Mn-SOD [64]. Yadav and Singh (2013) [65] demonstrated that Cd treatment had no effect on SOD and CAT enzymes of wheat seedlings. The lack of SOD activity stimulation in Cu- or Cd-treated wheat varieties indicates that SOD enzyme has no role in the defense mechanism of used varieties [14,63]. Similar with these findings, SOD enzyme may not be an effective role in *T. a.* cv. 'Sönmez-2001' and *T. a.* cv. 'Sultan-95' under Cd and Pb toxicity. Free radicals triggered by heavy metals may not have caused elevation of antioxidant enzyme levels in wheat cultivars [66].

In contrast to findings of Kaur et al. (2013) [10], Lamhamdi et al. (2013) [67], we observed that CAT activity were inhibited by all Cd and Pb concentrations in all variety, although heavy metal treatment groups of *T. a.* cv. 'Sönmez-2001' had more CAT activity than other varieties. Our results support the findings of Dey et al. (2007) [59] and Liu et al. (2007) [62] who showed inhibition of CAT enzymes under Cd and Pb stress. In parallel with our findings, Sandalio et al. (2001) [68] showed that acidic CAT isoenzymes were inhibited in *Pisum sativum* plants when applied 50 µM CdCl2. Degradation of NO accumulation may be the cause of CAT enzyme depletion [27].

CONCLUSIONS

In conclusion, antioxidant enzyme activities may not relate with germination of wheat varieties at low concentrations of applied heavy metals, since germination is not related to enzyme activities especially in *T. a.* cv. 'Sönmez-2001' and *T. a.* cv. 'Sultan-95' varieties. *T. a.* cv. 'Altay-2000' variety is also more susceptible to metal concentrations in terms of germination, mitotic index and enzyme activity. Our study shows that genotypic differences and heavy metal types may cause different response to stress conditions. Future researches are necessary to investigate reasons under these genotypic differences when applied different heavy metals. Selection of heavy metal tolerated wheat genotypes with high levels of germination rate, mitotic index, photosynthetic pigments and antioxidant enzymes will contribute to higher agricultural productivity.

REFERENCES

[1] Liu, W., Liang, L., Zhang, X., Zhou, Q. (2015a) Cultivar variations in cadmium and lead accumulation and distribution among 30 wheat (Triticum aestivum L.) cultivars. Environ Sci Pollut Res. 22, 8432–8441.

[2] Bhaduri, A.M., Fulekar, M.H. (2012) Antioxidant enzyme responses of plants to heavy metal stress. Rev Environ Sci Biotechnol. 11, 55–69.

[3] Ovečka, M., Takáč, T. (2014) Managing heavy metal toxicity stress in plants: Biological and biotechnological tools. Biotechnology Advances. 32, 73–86.

[4] Sytar, O., Kumar, A., Latowski, D., Kuczynska, P., Strzałka, K., Prasad, M.N.V. (2013) Heavy metal-induced oxidative damage, defense reactions, and detoxification mechanisms in plants. Acta Physiol Plant. 35, 985–999.

[5] Zhang, G., Fukami, M., Sekimoto, H. (2000) Genotypic differences in effects of cadmium on growth and nutrient compositions in wheat. Journal of Plant Nutrition. 23(9) 1337-1350.

[6] Yang, Y., Wei, X., Lu, J., You, J., Wang, W., Shi, R. (2010) Lead-induced phytotoxicity mechanism involved in seed germination and seedling growth of wheat (Triticum aestivum L.) Ecotoxicology and Environmental Safety. 73, 1982–1987.

[7] Li, X., Yang, Y., Zhang, J., Jia, L., Li, Q., Zhang, T., Qiao, K., Ma, S. (2012) Zinc induced phytotoxicity mechanism involved in root growth of Triticum aestivum. Ecotoxicology and Environmental Safety. 86, 198–203.

[8] Kaur, G., Singh, H.P., Batishi, D.R., Kohli, R.K. (2012) A time course assessment of changes in reactive oxygen species generation and antioxidant defense in hydroponically grown wheat in response to lead ions (Pb2+). Protoplasma. 249, 1091–1100.

[9] Sethy, S.K., Ghosh, S. (2013) Effect of heavy metals on germination of seeds. J Nat Sci Biol Med. 4(2), 272–275.

[10] Kaur, G., Singh, H.P., Batish, D.R., Kohli, R.K. (2013) Lead (Pb)-induced biochemical and ultrastructural changes in wheat (Triticum aestivum) roots. Protoplasma. 250, 53–62.

[11] Eker, S., Erdem, H., Yazıcı, M.A., Barut, H., Heybet, E.H. (2013) Effects of cadmium on growth and nutrient composition of bread and durum wheat genotypes. Fresen. Environ. Bull. 22, 1779-1786.

[12] Belimov, A.A., Safronova, V.I., Tsyganov, V.E., Borisov, A.Y., Kozhemyakov, A.P., Stepanok, V.V., Martenson, A.M., Gianinazzi-Pearson, V., Tikhonovich, I.A. (2003) Genetic variability in tolerance to cadmium and accumulation of heavy metals in pea (Pisum sativum L.). Euphytica. 131, 25–35.

[13] Alybayeva, R.A., Kenzhebayeva, S.S., Atabayeva, S.D. (2014) Resistance of winter wheat genotypes to heavy metals. IERI Procedia. 8, 41-45.

[14] Sgherri, C., Milone, M.T.S., Clijsters, H., Navari-Izzo, F. (2001) Antioxidative enzymes in two wheat cultivars, differently sensitive to drought and subjected to subsymptomatic copper doses. J. Plant Physiol. 158,1439–1447.

[15] Verma, S., Dubey, R.S. (2003) Lead toxicity induces lipid peroxidation and alters the activities of antioxidant enzymes in growing rice plants. Plant Sci. 164, 645–655.

[16] Jiang, P., Wan, Z., Wang, Z., Li, S., Sun, Q. (2013) Dynamic QTL analysis for activity of antioxidant enzymes and malondialdehyde content in wheat seed during germination. Euphytica .190, 75–85.

[17] El Rasafi, T., Nouri, M., Bouda, S., Haddioui, A. (2016) The effect of Cd, Zn and Fe on seed germination and early seedling growth of wheat and bean. Ekológia (Bratislava). 35, 213–223.

[18] Chen, C., Zhou, Q., Bao, Y., Li, Y., Wang, P. (2010) Ecotoxicological effects of polycyclic musks and cadmium on seed germination and seedling growth of wheat (Triticum aestivum). Journal of Environmental Sciences. 22(12), 1966–1973.

[19] Darlington, C.D., La Cour, L.F. (1976) The Handling of Chromosomes. 6th Ed. George Allen & Unwin Ltd., London.

[20] Costache, M.A., Campeanu, G., Neata, G. (2012) Studies concerning the extraction of chlorophyll and total carotenoids from vegetables. Romanian Biotechnological Letters. 17, 7702-7708.

[21] Bradford, M.M. (1976) A Rapid and sensitive method for the quantitation of microgram quantities of protein utilizing the principle of protein-dye binding. Analytical Biochemistry. 72, 248-254.

[22] Chance, B., Maehly, A.C. (1955) Assay of catalase and peroxidases. Methods Enzymol. 2, 764-775.

[23] Yang, Y., Ma, T., Ding, F., Ma, H., Duan, X., Gao, T., Yao, J. (2017) Interactive zinc, iron, and copper-induced phytotoxicity in wheat roots. Environ Sci Pollut Res. 24, 395–404.

[24] Stefanović, V.Z., Filipovi, N.K., Jovanović, B.M. (2008) Undesirable metals content in wheat of different wheat varieties. APTEFF. 39, 69-76.

[25] Glińska, S., Gapińska, M., Michlewska, S., Skiba, E., Kubicki, J. (2016) Analysis of Triticum aestivum seedling response to the excess of zinc. Protoplasma. 253(2), 367-77.

[26] Nagajyoti, P.C., Lee, K.D., Sreekanth, T.V.M. (2010) Heavy metals, occurrence and toxicity for plants: a review. Environ Chem Lett. 8, 199-216.

[27] Duan, X., Li, X., Ding, F., Zhao, J., Guo, A., Zhang, L., Yao, J., Yang, Y. (2015) Interaction of nitric oxide and reactive oxygen species and associated regulation of root growth in wheat seedlings under zinc stress. Ecotoxicology and Environmental Safety. 113, 95–102.

[28] Panda, S.K., Chaudhury, I., Khan, M.H. (2003) Heavy metal induce lipid peroxidation and affect antioxidants in wheat leaves. Biologia Plantarum. 46(2), 289-294.

[29] El-Ghamery, A.A., El-Kholy, M.A., Abou El-Yousser. M.A. (2003) Evaluation of cytological effects of Zn2+ in relation to germination and root growth of Nigella sativa L. and Triticum aestivum L. Mutation Research. 537, 29-41.

[30] Stanković, M., Topuzović, M., Marković, A., Pavlović, D., Delić, G., Bojović, B., Branković, S. (2010) Influence of zinc (Zn) on germination of wheat (Triticum aestivum L.). Biotechnology & Biotechnological Equipment. 24, 236-239.

[31] Naguib, D.M. (2016) Enzymatic status of germinating wheat grains under heavy metals stress. International Journal of applied and Pure Science and Agriculture. 2, 61-69.

[32] Wang, H., Zhong, G., Shi, G., Pan, F. (2011) Toxicity of Cu, Pb, and Zn on seed germination and young seedlings of wheat (Triticum aestivum L.). In: Li D., Liu Y., Chen Y. (eds.) Computer and Computing Technologies in Agriculture IV. CCTA 2010. IFIP Advances in Information and Communication Technology, vol. 346. Springer, Berlin, Heidelberg.

[33] Li, X., Yang, Y., Jia, L., Chen, H., Wei, X. (2013) Zinc-induced oxidative damage, antioxidant enzyme response and proline metabolism in roots and leaves of wheat plants. Ecotoxicology and Environmental Safety. 89,150–157.

[34] Zhao, Z-Q., Zhu, Y-G., Kneer, R., Smith, S.E. (2005) Effect of zinc on cadmium toxicity-ınduced oxidative stress in winter wheat seedlings. Journal of Plant Nutrition. 28,1947-1959.

[35] Lamhamdi, M., Bakrim, A., Aarab, A., Lafont, R., Sayah, F. (2011) Lead phytotoxicity on wheat (Triticum aestivum L.) seed germination and seedlings growth. C R Biol. 334(2), 118-26.

[36] Hossain, Z., Hajika, M., Komatsu, S. (2012) Comparative proteome analysis of high and low cadmium accumulating soybeans under cadmium stress. Amino Acids. 43(6), 2393-416.
[37] Shafi, M., Bakht, J., Hassan, M.J., Raziuddin, M., Zhang, G. (2009) Effect of cadmium and salinity stresses on growth and antioxidant enzyme activities of wheat (Triticum aestivum L.). Bull Environ Contam Toxicol. 82,772-776.
[38] Hacisalihoglu, G., Hart, J.J., Wang, Y-H., Cakmak, I., Kochian, L.V. (2003) Zinc efficiency is correlated with enhanced expression and activity of zinc-requiring enzymes in wheat. Plant Physiology. 131, 595-602.
[39] Cherif, J., Mediouni, C., Ammar, W., Jemal, F. (2011) Interactions of zinc and cadmium toxicity in their effects on growth and in antioxidative systems in tomato plants (Solanum lycopersicum). J Environ Sci. 23,837–844.
[40] Saifullah A.N., Sarwar, N., Bibi, S., Ahmad, M., Ok, Y.S. (2014) Effectiveness of zinc application to minimize cadmium toxicity and accumulation in wheat (Triticum aestivum L.). Environ Earth Sci. 71,1663-1672.
[41] Hu, K-D., Bai, G-S., Li, W-J., Yan, H., Hu, L-Y., Li, Y-H., Zhang, H. (2015) Sulfur dioxide promotes germination and plays an antioxidant role in cadmium-stressed wheat seeds. Plant Growth Regulation. 75, 271–280.
[42] Dar, S.H., Agnihotr, R.K., Sharma, R., Ahmad, S. (2010) Nickel and lead ınduced variations in pigment composition of Triticum aestivum L. Research Journal of Agricultural Sciences. 1(2), 128-131.
[43] Bhatti, K.H., Anwar, S., Nawaz, K., Hussain, K., Siddiqi, E.H., Sharif, R.U., Talat, A., Khalid, A. (2013) Effect of heavy metal lead (pb) stress of different concentration on wheat (Triticum aestivum L.), Middle-East Journal of Scientific Research. 14(2), 148-154.
[44] Liu, J., Hu, Q-P. (2015b) Effect of Bacillus subtilis QM3 on morphology parameters during germination of wheat seeds under lead stress. International Journal of Current Advanced Research. 4, 64-70.
[45] Ahmad, I., Akhtar, M.J., Zahir, Z.A., Jamil, A. (2012) Effect of cadmium on seed germination and seedling growth of four wheat (Triticum aestivum L.) cultivars. Pak. J. Bot. 44(5), 1569-1574.
[46] Sheng, Z., Jin, H., Zhen-Hua, C., Jiang-feng, C., Yun-Ye, Z., Wen-Jian, S. (2005) Effects of Pb pollution on seed vigor of three rice cultivars. Rice Science. 12(3), 197-202.
[47] An, Y-J. (2004) Soil ecotoxicity assessment using cadmium sensitive plants. Environmental Pollution. 127, 21–26.
[48] Khan, N.A., Singh, S., Anjum, N.A., Nazar, R. (2008) Cadmium effects on carbonic anhydrase, photosynthesis, dry mass and antioxidative enzymes in wheat (Triticum aestivum) under low and sufficient zinc. Journal of Plant Interactions. 3, 31-37.
[49] Ci, D., Jiang, D., Wollenweberi, B., Dai, T., Jing, Q., Cao, W. (2010) Cadmium stress in wheat seedlings: growth, cadmium accumulation and photosynthesis. Acta Physiol Plant. 32, 365–373.
[50] Nabiha, B., Noureddine, Z., Réda, D.M. (2015) Lead induced oxidative stress and antioxidant defense response in durum wheat (Triticum durum Desf.). Int. J. Pharm. Sci. Rev. Res. 32(2), 28-33.
[51] Sharma, V., Parmar, P., Kumari, N. 2016. Differential cadmium stress tolerance in wheat genotypes under mycorrhizal association. Journal of Plant Nutrition. 39, 2025-2036.
[52] Zhang, G., Fukami, M., Sekimoto, H. (2002) Influence of cadmium on mineral concentrations and yield components in wheat genotypes differing in Cd tolerance at seedling stage. Field Crops Research. 77, 93–98.
[53] Yang, Y., Zhang, Y., Wei, X., You, J., Wang, W., Lu, J., Shi, R. (2011) Comparative antioxidative responses and proline metabolism in two wheat cultivars under short term lead stress. Ecotoxicology and Environmental Safety. 74, 733–740.
[54] Grant, C.A., Buckley, W.T., Bailey, L.D., Selles, F. (1998) Cadmium accumulation in crops. Can. J. Plant Sci. 78, 1-17.
[55] Ozturk, L., Eker, S., Ozkutlu, F. (2003) Effect of cadmium on growth and concentrations of cadmium, ascorbic acid and sulphydryl groups in durum wheat cultivars. Turk J Agric For. 27, 161-168.
[56] Guilherme, M.F.S., Oliveira, H.M., Silva, E. (2015) Cadmium toxicity on seed germination and seedling growth of wheat Triticum aestivum, Acta Scientiarum. Biological Sciences Maringá. 37, 499-504.
[57] Saifullah, A.N., Rehman, M.Z., Akhtar, T., Ok, Y.S., Renge, Z. (2016) Genetic variation in cadmium accumulation and tolerance among wheat cultivars at the seedling stage. Communications in soil Science and Plant Analysis. 47(5), 554-562.
[58] Olteanu, Z., Oprica, L., Truta, E., Zamfirache, M.M. (2011) Behaviour of antioxidative enzymes and of soluble protein in wheat seedlings after lead-induced stress. Analele tiinifice ale Universitii Alexandru Ioan Cuza", Seciunea Genetic Biologie Molecular, TOM XII.

[59] Dey, S.K., Dey, J., Patra, S., Pothal, D. (2007) Changes in the antioxidative enzyme activities and lipid peroxidation in wheat seedlings exposed to cadmium and lead stress. Braz. J. Plant Physiol. 19(1), 53-60.
[60] Lin, R., Wang, X., Luo, Y., Du, W., Guo, H., Yin, D. (2007) Effects of soil cadmium on growth, oxidative stress and antioxidant system in wheat seedlings (Triticum aestivum L.). Chemosphere. 69, 89–98.
[61] Benavides, M.P., Gallego, S.M., Tomaro, M.L. (2005) Cadmium toxicity in plants. Braz. J. Plant Physiol. 17(1), 21-34.
[62] Liu, X., Zhang, S., Shan, X-Q., Christie, P. (2007) Combined toxicity of cadmium and arsenate to wheat seedlings and plant uptake and antioxidative enzyme responses to cadmium and arsenate co-contamination. Ecotoxicology and Environmental Safety. 68, 305–313.
[63] Ci, D., Jiang, D., Dai, T., Jing, Q., Cao, W. (2009) Effects of cadmium on plant growth and physiological traits in contrast wheat recombinant inbred lines differing in cadmium tolerance. Chemosphere. 77,1620–1625.
[64] Milone, M.T., Sgherri, C., Clijsters, H., Navari-Izzo, F. (2003) Antioxidative responses of wheat treated with realistic concentration of cadmium. Environmental and Experimental Botany. 50, 265-276.
[65] Yadav, K., Singh, N.B. (2013) Effects of benzoic acid and cadmium toxicity on wheat seedlings. Chilean J. Agric. Res. 73, 168-174.
[66] Rodríguez-Serrano, M., Romero-Puertas, M.C., Zabalza, A., Corpas, F.J., Gómez, M., Del Río, L.A., Sandalio, L.M. (2006) Cadmium effect on oxidative metabolism of pea (Pisum sativum L.) roots. Imaging of reactive oxygen species and nitric oxide accumulation in vivo. Plant Cell Environ. 29(8), 1532-44.
[67] Lamhamdi, M., Bakrim, A., Bouayad, N., Aarab, A., Lafont, R. (2013) Protective role of a methanolic extract of spinach (Spinacia oleracea L.) against Pb toxicity in wheat (Triticum aestivum L.) seedlings: beneficial effects for a plant of a nutraceutical used with animals. Environ Sci Pollut Res Int. 20(10), 7377-85.
[68] Sandalio, L.M., Dalurzo, H.C., Gómez, M., Romero-Puertas, M.C., del Río, L.A. (2001) Cadmium-induced changes in the growth and oxidative metabolism of pea plants. J Exp Bot. 52(364), 2115-26.
[69] Rehman, S., Park, I.H. (2000) Effect of scarification, GA and chilling on the germination of goldenrain-tree (Koelreuteria paniculata Laxm.) seeds. Scientia Horticulturae. 85, 319-324.
[70] Talebi, S., Nabavi Kalat, S.M., Sohani Darban, A.L. (2014) The Study Effects of Heavy Metals on Germination Characteristics and Proline Content of Triticale (Triticoseale Wittmack). Intl J Farm & Alli Sci. 3(10), 1080-1087.

Received: **08.09.2017**
Accepted: **17.11.2017**

CORRESPONDING AUTHOR

Ayse Ak
Erzincan University,
Engineering Faculty,
Biomedical Engineering,
Erzincan – Turkey

e-mail: ayseak@erzincan.edu.tr

© by PSP Volume 27 – No. 2/2018 pages 1095-1103 Fresenius Environmental Bulletin

A RESEARCH ON THE DETERMINATION OF MOLECULAR GENETIC CHARACTERISTICS OF SOME *BEMISIA TABACI* (GENN.) (HEMIPTERA:ALEYRODIDAE) POPULATIONS

Nurdan Topakci[1,*], Huseyin Gocmen[2,3]

[1]Akdeniz University, Vocational Higher School of Technical Sciences, 07058, Antalya, Turkey
[2]Akdeniz University Faculty of Agriculture. Plant Protection Department 07058, Antalya, Turkey
[3]Kyrgyz-Turkish Manas University, Faculty of Agriculture, Department of Plant Protection , Bishkek, Kyrgyzstan

ABSTRACT

The whitefly *Bemisia tabaci* (Gennadius) (Hemiptera, *Aleyrodidae*) is one of the most crucial agricultural pests in tropical and subtropical regions. The pest is a species complex which contain morphologically indistinguishable biotypes or genetic groups. The aim of the present study is to examine *B. tabaci* populations collected from Aydın, Antalya, Mersin, Adana and Hatay regions in 2004 and 2005. Prior to analysis, as the first step, the biotypes were determined by considering molecular differences among populations. In addition , the differences among populations were determined by means of biochemical analysis, namely, by conducting esterase enzyme analysis. Nucleotide variation in mitochondrial cytochrome oxidase I (mtCOI) showed that a total of 32 nucleotide variations were present in 617 basepair sequence of mtCOI. Dendogram constructed based on phylogenetic analysis indicated that *B. tabaci* populations consisted of B and Q biotypes. Furthermore, the findings revealed that there were no nucleotid differences within B and Q biotype populations. In terms of the spread of the biotypes, it is found that while B biotypes were settled in Dörtyol and Harbiye regions in Hatay province, Q biotypes were found in Kırıkhan and Hassa regions. Likewise, while B biotypes were found in Tarsus, Q biotypes were seen in Ceyhan and Havutlu in Çukurova region (Mersin and Adana provinces). In Antalya province, Q biotype was found in Campus area, whereas B biotype was present in Gazipasa. On the other hand, it is found that all samples from Aydin province were biotype Q. Concerning the findings, it can be claimed that Polyacrylamide gel electrophoresis results clearly distinguished the two genetic types.

KEYWORDS:
Bemisia tabaci, mtCOI, Q biotype, B biotype, PAGE

INTRODUCTION

Bemisia tabaci (Genn.) (Hemiptera: Aleyrodidae) is one of the most crucial agricultural pests for vegetables and ornamental plants in the vast majority of tropical and subtropical regions in the world[1]. The pest causes damages to crops by feeding on phloem sap, producing sticky honeydew as well as vectoring plant viruses [2].

The genetic complexity of *B. tabaci* was initially recognized in the late 1950s [3]. Several morphologically indistinguishable populations were identified differing in the host range, fecundity, insecticide resistance, host plant adaptability, and capability to transmit begomoviruses [4, 5, 6, 7, 8, 9]. To date, various genetic groups of the *B. tabaci* have been attempted to define by some alternative molecular techniques such as the esterase or isoenzymes [10,11,12,13], Restriction Fragment Length Polymorphism-RFLP [14], Random Amplification of Polymorphic DNA-RAPD [15,16,17,18], Amplified Fragment Length Polymorphism-AFLP [19] and mitochondrial COI (mtCOI) sequence analyses [6, 20, 21]. In the recent studies; however, *Bemisia tabaci* has been reported to be a sort of species complex composed of at least 34 different morphologically undistinguished genetic groups [22, 23].

In Turkey, the epidemic of the *B. tabaci* was first found in Cukurova region in 1974 [24] and this insect has become the prominent pest since then. As it was reported in a study [5] *B. tabaci* population, which was called as the M (Turkish Cotton) biotype and collected from Turkey, has not been discovered yet in the conducted studies. However, the existence of the B and Q biotypes was identified [25, 26, 27, 28, 29, 30, 31] in various studies conducted on genetic diversity of *B. tabaci* populations in Turkey. *B. tabaci* Middle East – Minor Asia 1 genetic group (biotype B) and Mediterranean genetic group (biotype Q) are the two most invasive and widely spread whiteflies around the World [32].

In the present study, the data of which was gathered between 2004 – 2008, the differences between various *B. tabaci* populations were demonstrated via a polyacrylamide gel electrophoresis method and utilizing the sequences of Mitochondrial Cytochrome Oxidase I (MtCOI) gene region.

MATERIALS AND METHODS

***Bemisia tabaci* populations sampling:** *B. tabaci* populations were collected from Adana, Mersin, Hatay, Aydın and Antalya provinces in 2004 and 2005. The locations where the populations were collected, and the host plants are presented in Table 1. The adults were collected by a mouth aspirator, placed in 80% alcohol, and kept at -20 °C in order to use as the supplementary material. The samples, which were kept as the supplementary material in the laboratory and taken into the eppendorf tubes, were used for biochemical analyses and their protein structure was maintained by keeping them at -80 ºC.

TABLE 1
Sampling locations and host plants of the cotton whitefly (*Bemisia tabaci*)

Location	Host Plant	Date
Mersin (Tarsus)	Cotton	29.08.2004
Hatay (Hassa)	Cotton	30.08.2004
Hatay (Kırıkhan)	Cotton	30.08.2004
Hatay (Dörtyol)	Eggplant	31.08.2004
Adana (Ceyhan)	Cotton	31.08.2004
Adana (Havutlu)	Eggplant	01.09.2004
Hatay (Harbiye)	Eggplant	01.09.2004
Aydın (Söke)	Cotton	18.09.2004
Aydın (Centre)	Cotton	18.09.2004
Aydın (Nazilli)	Cotton	18.09.2004
Antalya (Gazipaşa)	Cucumber	30.09.2005
Antalya (Campus)	Cotton	30.09.2005

DNA Extraction: Except for a few modifications, the DNA extraction was performed by the DNA isolation kit (EZNA SQ Tissue DNA Kit D5040-02) produced by Omega Company, in line with the manufacturer protocol. Differently from the manufacturer protocol, the DNA samples were kept in isopropanol for on average 12 hours and at -20 °C instead of keeping the samples in room temperature during DNA precipitation phase.

Additionally, a fragment of Mitochondrial Cytochrome Oxidase Subunit I (MtCOI) gene region was amplified by A and B primer sets (Table 2), and the optimized PCR conditions were used [20]. Each PCR reaction was performed in the final total volume of 12.5 µl containing 0.2 mM dNTP (Larova), 3 mM $MgCl_2$, 2 pmol primer (iontek), 0.4 unit of *Taq* DNA Polymerase Enzyme (Bioron), 1.25 µl of reaction buffer solution and 1 µl of DNA sample. The PCR was conducted by using a thermal cycler PCR machine (Primus 96 Advanced Gradient, PeqLab, Germany), and the PCR conditions used for 30 cycles were as follows; initial incubation step at 94 °C for 2 min, denaturation at 94 °C for 60 sec, annealing at 48 °C for 60 sec, and extension at 72 °C for 60 sec. The amplified products were size separated and visualized on 1% agarose gel containing 10 mg/l of ethidium – bromide. The amplified products, approximately 800 bp in size, were reamplified with the combination of B and C primer sets (Table 2) using the same PCR conditions as stated above. The reamplified DNA products were run on agarose gel and size separated. The one – band – PCR – products with the expected fragment size (760 bp) were kept in -20 °C for sequencing procedure.

TABLE 2
Primer sequences used in the amplification of the sequence region of mtCOI gene and the expected amplification fragment sizes

Primer	DNA	Primer B
Primer A (Forward)	5' TTGATTTTTTGGT CATCCAGAAGT 3'	~ 800 bp
Primer B (Reverse)	5' TCCAATGCACTAA TCTGCCATATTA 3'	---------
Primer C (Forward)	5'ATAGCAGTGAGG CTGGAAAA 3'	760 bp
Primer D (Forward)	5' GGGTATAATTTAT GCTATA 3'	720 bp

DNA Sequencing and Phylogenetic Analysis: A minimum of three different PCR products obtained from various individuals were sequenced for each population. For sequencing process, the Beckman 8000 CEQ Genetic Analyzer and the manufacturers chemical kit were used. The PCR conditions for sequencing recommended in the manufacturer protocol were modified as follows; the D primer given in Table 2 and the reaction volume of 10 µl instead of 20 µl were used for the PCR reactions; the chemicals were reduced in half for the sequence cleaning process; and the sequencing products were dissolved in 30 µl of deionized formamide instead of 40 µl before the loading process. The PCR conditions were as follows; denaturation at 96 °C for 20 sec, annealing at 50 °C for 20 sec, and extension at 60 °C for 4 min. The sequencing products were incubated in a bath tub at 90 °C for 120 sec, and the single stranded DNA was generated. These products were loaded into the device initially run at 2000 Volts for 30 sec, and then the products were run for size separation at 4200 Volts for 100 minutes.

The raw fluorescence data in the DNA analyzer were subjected to sequence analysis in the Beckman Sequence Analysis program, and the automated – sequences obtained were checked by a manual ocular control so that the sequences of each individual sample were finalized. The sequences were recorded in FASTA format and aligned in the 'CLUSTAL W' program, and analyzed using the 'Unweighted Pair Group Method with Arithmetic Mean' (UPGMA) option of the 'MEGA 4' program. The genetic distances between analyzed populations were also calculated by the 'Maximum Composite Likelihood' option of the same program. The individuals of population resulting in dendrograms were compared with both reference B and Q biotypes and MtCOI sequence information available in the Genbank (http://www.ncbi.nlm.nih.

gov/Genbank/), and the biotype distribution was identified based on their proximity to the defined reference sequences.

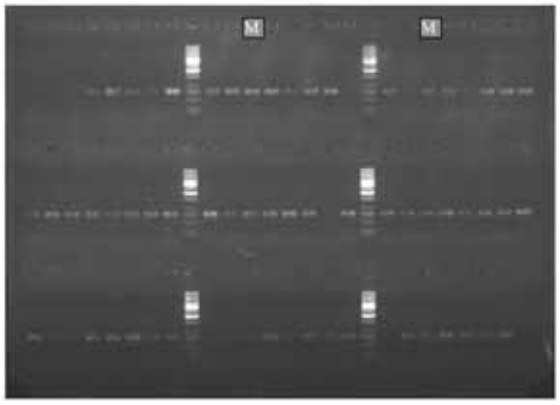

FIGURE 1
The image of the mtCOI gene region with 760 bp in size (M: 1 kb Marker) products amplified by second PCR from individuals of different *Bemisia tabaci* populations

Polyacrylamide gel electrophoresis studies: The female whiteflies (individual) were homogenized in 15 µl of native sample buffer (11.1 µl of deionized water, 2.5 µl of 0.5 M Tris HCl (pH 6.8), 6 µl of glycerol, 0.4 µl of 0.5% Bromophenol blue, 20.0 µl solution in total) (Bio-Rad, 161-0738). After centrifuging the mixtures for about 2 minutes, the entire sample extract in each tube was loaded into a 6% vertical native gel (PAGE) (polyacrylamide gel electrpforesis) and run at 220 Volts for 2 and a half hours at 4 °C in running buffer (Tris -glycine, pH 8.3). Alpha- and beta-naphthyl acetates were used as substrates. The gel was initially preincubated in the phosphate buffer (KH_2PO_4 (0.175 M), Na_2PO_4 (0.025 M)/l, pH 6) for 10 min, and then it was transferred into a phosphate buffer plate, which was kept waiting in an incubator for about 25 min (37 °C). Substrates, 100 mg alpha-naphthyl acetate and 50 mg beta-naphthyl acetate (in acetone) and 1 ml of the Fast Blue RR Salt were added into 150 ml of phosphate buffer. Gel was incubated at 37 °C until the bands were observed, visualized by a scanner, and the images were stored digitally (modified Wool et al.) [33]

RESULTS

Sequence studies: An agarose gel image of approximately 760 bp products obtained from the MtCOI gene region amplified by the PCR conditions, and representing the individuals from populations were given in Figure 1. The sequence alignment and the following phylogenetic analyses were

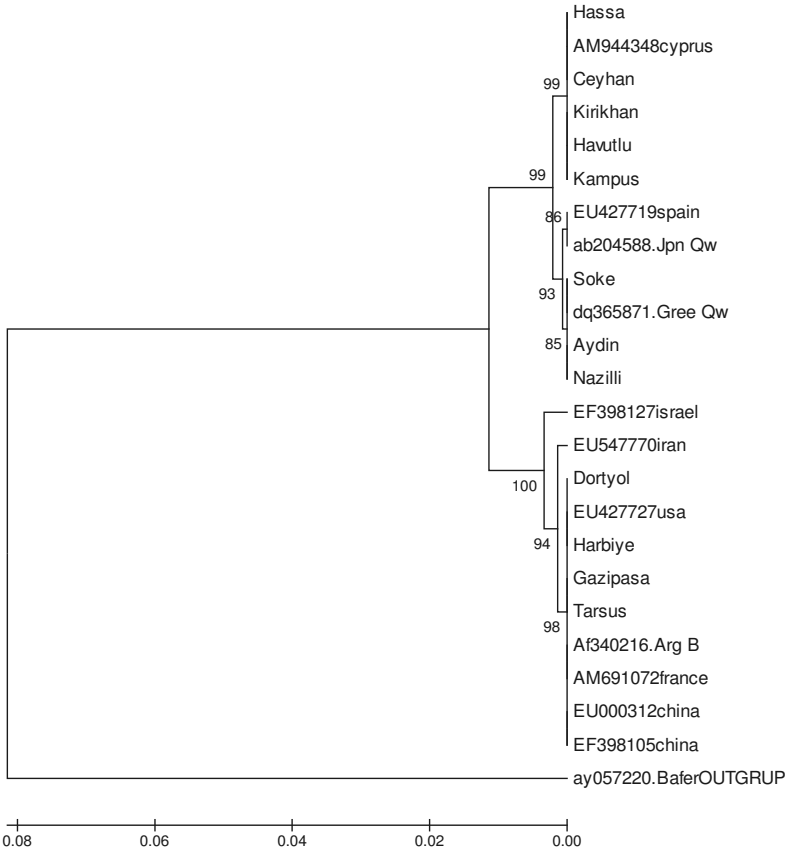

FIGURE 2
The phylogenic tree generated by the MEGA 4 Phylogenic Analysis Program under the UPGMA option using the mtCOI sequences of the reference samples taken from Genbank on cotton whitefly samples

performed based on the data obtained from 617 bp of MtCOI gene region, since the first and last 40 – 50 bp fragments of the fluorescent products, which were generated by sequencing chemistry, were not separated sufficiently during the capillary electrophoresis. When the alignment was performed with the CLUSTAL W program, the obtained in population samples were observed as homogenous and contained the same sequences (single haplotype).

The analysis revealed that a total of 32 different nucleotides showed polymorphism among the analyzed 617 bp fragments in sizes. These nucleotide polymorphisms were identified as in the forms of either change of one nucleotide to another or, in one case, replacement of three nucleotides between each other. Hence, these conditions resulted in formation of three different haplotype groups. Consistent with phylogenetic tree, the samples located into three different clusters (Figure 2). The populations were also clustered around the B and Q biotypes along with the reference population sequences pulled out of the Genbank. Additionally, Dörtyol, Harbiye, Tarsus and Gazipaşa populations were clustered within the same haplotype group of the B biotype, and the remaining eight populations were clustered with the Q biotype. Populations of Aydin province shared one – to – one similarity with the Greece – type Q biotype; however, the other Q biotypes were clustered under the group of a Q biotype, which shared a similarity with Cypriot referenced sample. In order to make a distinction between these two haplotypes, the identified haplotype populations in Aydın region and other populations were denominated as Qw and Qe, respectively.

When the genetic distances among the three clusters generated by the populations were analyzed; the distances of the Qe and Qw biotypes form the B biotype were 0.021 and 0.023 respectively On the other hand, the genetic distance between the Qe and Qw biotypes was only 0.004. It is also found in the present study that no nucleotide polymorphism was identified between the four B biotype populations found in this study. All populations clustering around the B biotype showed 100% nucleotide identity. As Bayhan et al. [26] reported that populations were highly homogeneous in terms of nucleotide polymorphism among the B biotype samples. Similarly, no nucleotide polymorphism was identified among five populations of the Qe biotype and three populations of the Qw biotype groups.

Biochemical Studies: In the present study, individually extracted female whiteflies were analyzed on the polyacrylamide gel electrophoresis, and esterase bands of each population were determined (Figure 3). As a result, two different banding patterns were generated. One of these patterns was the first group of populations, in which three main bands could be detected, and the other one was the second group of populations, in which a single band detected. The first group consisted of Tarsus, Dortyol, Harbiye and Gazipaşa populations and the second group was in Hassa, Kırıkhan, Ceyhan, Soke, Aydın, Nazilli and the Campus populations. In general, it was determined that the first group of B biotype populations was strongly dyed; however, the second group of Q biotype populations was weakly dyed.

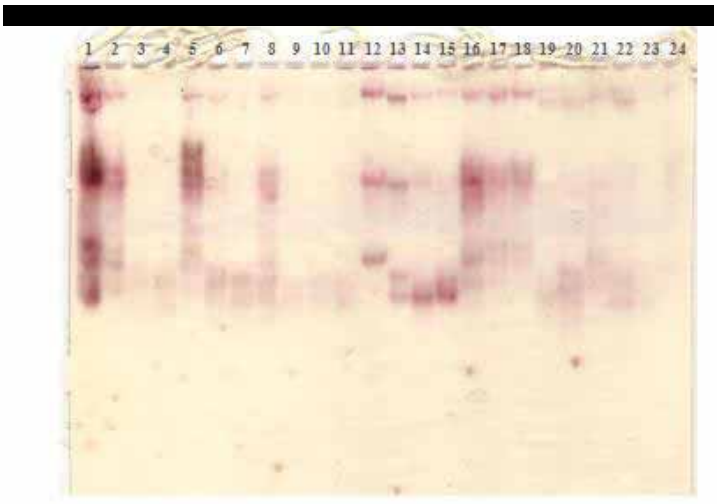

FIGURE 3
The esterase band profiles of *Bemisia tabaci* populations

1	Positive control	2	Tarsus	3	Hassa	4	Kırıkhan	5	Dörtyol
6	Ceyhan	7	Havutlu	8	Harbiye	9	Söke	10	Aydın
11	Nazilli	12	Gazipaşa	13	Nazilli	14	Kampus	15	Kampus
16	Gazipaşa	17	Gazipaşa	18	Gazipaşa	19	Nazilli	20	Gazipaşa

FIGURE 3
The esterase band profiles of *Bemisia tabaci* populations

DISCUSSION

The use of polyacrylamide gel electrophoresis (PAGE) was a preferred and reliable method in identification of esterase – enzyme – band – patterns for determination of species and biotypes. The B biotype within the *B. tabaci* populations collected from Aegean and Mediterranean Regions in Turkey was identified via using this method, and it was determined that the esterase bands varied in densities depending on populations [34]. In a similar study, it was determined by the PAGE method that the samples collected from cotton alleys in Adana, Antalya, İzmir and Tarsus showed B biotype characteristics [28]. Analyses of one of the cassava whitefly race on the gel electrophoresis revealed three bands, one small and two large; however, the sweet potato race demonstrated four bands, two small and two large, in sizes [35]. The B and Q biotypes generated three esterase band groups in the gel electrophoresis, and the Q biotype bands in the 3rd group were closer to the anodal pole in comparison to the B biotype bands. In addition, they reported that the Q biotype bands were dyed weaker than the B biotype bands [36]. The B and Q biotypes generated three esterase band groups on the gel, and these two biotypes might be distinguished from each other by the esterase band patterns [37].

In the esterase enzyme studies, it was determined that the populations from different hosts could take place in the same group in terms of their esterase profiles. This result was in compliance with the study performed by Wool et al. [12], and the differences observed among esterase allele frequencies were not related to the host plants or their geographies. Wool et al.'study [12] also confirmed that the esterase allele frequencies were related to whether or not individual pests were collected from commercial areas treated with insecticides. Indeed, Gocmen et al. [27] identified in their study that the populations of the Q biotype had a very low level of esterase activities as compared to the B biotype; however, the Q biotype, which was exposed to excessive insecticide, had higher esterase activity than other Q biotypes. It has also been stated that the esterase enzyme profiles on polyacrylamide gels might be used to distinguish between B and Q biotypes; however, there was no linear relationship between the quantities or profiles of esterase activity and the resistance to insecticide. Regarding the findings of the present study, it can be claimed that, the presence of two genetic types was clearly distinguished in the surveyed areas in terms of the esterase. As a result, it was determined that the esterase enzyme profiles on the polyacrylamide gel might be used to distinguish between B and Q biotypes.

In this study present study which was conducted with the MtCOI gene region, the *B. tabaci* populations collected from Antalya during the years of sampling were determined as B (cucumber) and Q biotype (cotton). In another study that was performed on even dates [27], Antalya province populations were identified as the B (mostly vegetables) and Q (vegetable) biotypes. In the light of these results, it is possible to draw a conclusion that the B and Q biotypes coexist in Antalya province when the study was conducted. However, in the different molecular studies carried out after these dates, the collected samples from Antalya province appeared to be the B biotype [34, 38, 39, 40]. In addition, in some other studies performed outside the province of Antalya, it was determined that the B was the dominant biotype among the samples obtained from the vegetable fields [26, 27, 28, 34, 31, 39].

Additonally, the three samples collected from Aydın province (Centre, Soke and Nazilli) within the present study appeared as the Qw biotype that showed similarity to the Q biotype found in Greece. This finding shows similarity with the findings of Gocmen et al.' [27] study which also determined that the samples collected from Aydın province were the Qw biotype.

It was reported that the B biotype was the sole species identified in whitefly survey studies conducted in Adana, Mersin and Hatay provinces between the years of 2000 and 2002 [26]. Likewise, in another study carried out by sampling method within these regions in 2004 – 2005, both the B and Q biotypes were detected in Mersin, Adana and Hatay regions, and the Q biotype was determined as the dominant species [27]. In the present study; however, both the B and Qe biotypes were found to have coexisted in Adana, Mersin and Hatay regions, and three populations out of seven and four populations out of seven detected within this region were identified as the B and Qe biotypes, respectively. Similarly, the majority of the *B. tabaci* samples collected from Adana province were determined as the Q biotype (MED) [29, 30]. As Satar and Ulusoy [39] reported that the majority of the samples collected from Adana, Mersin and Hatay provinces were determined as the B biotype, and this suggested that these two biotypes (B and Q) partly preferred different habitats. They also indicated that the B biotype was intensively identified in vegetable areas; however, the Q biotypes were predominantly detected among biennial plants. Similarly, Charaabi et al. [41] determined that the MEAM1 and MED species were found in different ratios and on different hosts; and the MEAM1 was dominant on vegetable hosts, while the MED species was most prevalent on the ornamental species.

Pascual and Callejas [42] found that the B biotype substituted the Q biotype under the laboratory conditions. The main reason for high competitiveness of the B biotype was that it was able to reproduce itself at a faster rate than the Q biotype [43, 44]. However, insecticide resistance also played an important role in *B. tabaci* distribution. As Horo-

witz et al. [45] reported applications of the pyriproxyfen might have led to the selection of a more viable Q biotype against this insecticide. Similarly, Yukselbaba and Gocmen's study [46] showed that the Q biotype of *B. tabaci* has developed more resistance to spiromesifen than B biotype and EST activity plays a major role in the resistance mechanism. In fact, Karut et al. [30] stated that the Q biotype (MED) was the predominant species in cotton fields in Cukurova Region, and its reason for that might be the wide use of neonicotinoid insecticides. Indeed, they identified that the B biotype was still present in the regions where neonicotinoids were not commonly used. It can be claimed that the resistance levels to insecticides varied among the whiteflies found in open fields and on plants grown in greenhouses, and there was higher resistance in the greenhouse condition due to more exposure to insecticides [47, 48]. Therefore, it is believed that The B biotype was highly adapted to the open fields, whereas the Q biotype was gradually dominated crops that were grown under protected conditions [49]

CONCLUSIONS

Earlier it was reported that the whiteflies, which were collected from cotton plants in Adana in 1985, were encoded as TC, and they were defined as having an MtCOI nucleotide profile very similar to the Q biotype [5]. Apart from this, there was no other verified data on the status of *B. tabaci* biotypes in Turkey before 2000. However, studies on biotypes and their distribution have been examined since 2000. For instance, in the present study, which examined the *B. tabaci* biotypes in some regions of Turkey, it was identified that the samples collected in 2004 and 2005 from Aydın, Antalya, Adana and Hatay regions were the the samples of B and Q biotypes. In this context, In this context, based on the findins of the present study it can be claimed that the biotypes may vary over time.

ACKNOWLEDGEMENTS

This study comprises part of the project numbered 2004.0121.011, supported by the Scientific Research Projects Management Unit of Akdeniz University. We thank the Scientific Research Projects Management Unit of Akdeniz University for their support.

This Study is a part of Ph.D. thesis. It was presented in the congress entitled 'The International Conference on Agriculture, Forest, Food Sciences and Technologies (ICAFOF) on 15 – 17 May 2017 and published as an Abstract.

REFERENCES

[1] Oliveira M.R.V., Henneberryand T.J. and Anderson, P. (2001) History, current status and collaborative research projects for *Bemisia tabaci*. Journal of Crop Protection. 20, 709-723.

[2] Powell, M.E., Cuthbertson, A.G.S., Boonham, N., Morris, J., Bell, H.A. and Northing, P. (2012) First record of the Q Biotype of the sweetpotato whitefly, *Bemisia tabaci*, intercepted in the UK. Eur. J. Plant Pathol. 133, 797-801.

[3] Bird, J. (1957) A Whitefly transmitted mosaic of Jatropha gossypifolia. Tecnical paper. Agricultural Experiment Station Poerto Rico. 22, 1-35.

[4] Costa, H.S. and Brown, J.K. (1991) Variation in biological characteristics and esterase patterns among populations of *Bemisia tabaci* and the association of one population with silverleaf symptom induction. Entomol. Exp.App. 61,211-219.

[5] Bedford, I.D., Briddon, R.W., Brown, J.K., Rosell, R. and Markham, P.G. (1994) Geminivirus transmission and biological characterisation of *Bemisia tabaci* (Gennadius) biotypes from different geographic regions. Ann.Appl. Biol. 125, 311-325.

[6] Brown, J.K., Frohlich, D.R. and Rosell, R.C. (1995) The sweetpotato or . silverleaf whiteflies:Biotypes of *Bemisia tabaci* or a species complex? Annu. Rev. Entomol. 40, 511-534.

[7] Perring, T.M. (2001) The *Bemisia tabaci* species complex. Crop Protection. 20,725-737.

[8] Jones, D.R. (2003) Plant viruses transmitted by whitefies, European Journal of Plant Pathology. 109,195-219.

[9] Boykin, L.M., Shatters, R.G., Rosell, R.C., McKenzie, C.L., Bagnall, De Barro, P. and Frohlich, D.R. (2007) Global relationships of *Bemisia tabaci* (Hemiptera: Aleyrodidae) revealed using Bayesian analysis of mitochondrial COI DNA sequences. Mol Phylogenet Evol. 44(3), 1306-1319.

[10] Perring, T.M., Cooper, A.D., Rodriguez, R.J., Farrar, C.A. and Bellows, T.S. (1993) Identification of a whitefly species by genomic and behavioral studies. Science. 259, 74-77.

[11] Costa, H.S., Johnson, M.W., Uilman, D.E., Omer, A.D. and Tabashnik, B.E. 1993. Sweetpotato whitefly(Homoptera: Aleyrodidae). Analysis of biotypes and distribution in Hawaii. *Environ. Entomol*. 22(1), 16-20.

[12] Wool, D., Gerling, D., Bellotti, A.C. and Morales, F.J. (1993) Esterase electrophoretic variation in *Bemisia tabaci* (Genn.) (Hom: Alayrodidae) among host plants and localities in Israel. Zeitschrift für Angewandte Entomologie. 115(2),185-196.

[13] Brown, J.K., Coats, S.A., Bedford, I.D., Marcham, P.G., Bird, J. and Frohlich, D.R. (1995) Characterization and distribution of esterase electromorphs in the whitefly, *Bemisia tabaci* (Genn.) (Homoptera:Aleyrodidae). Biochemical Genetics. 33(7/8),205-214.

[14] Abdullahi, I., Winter, S., Atiri, G.I. and Thottappilly, G. (2003). Molecular characterization of whitefly, *Bemisia tabaci* (Hemiptera: Aleyrodidae) populastions infesting cassava. Bulletin of Entomological Research. 93(2), 97-106.

[15] Gawell, N.J. and Barlett, A.C. (1993) Characterization of differences between whiteflies using RAPD-PCR. Insect Molecular Biology. 2(1), 33-38.

[16] Bellows, T.S., Perring, T.M., Gill, R.J. and Headrick, D.H. (1994) Description nof a species of *Bemisia* (Homoptera:Aleyrodidae). *Ann. Entomol. Soc. Am.* 87(2), 195-206.

[17] De Barro, P.J. and Driver, F. (1997) The use of RAPD-PCR to distinguish the B biotype from other biotypes of *Bemisia tabaci* (Genn.) (Hemiptera:Aleyrodidae). Australian J. of Entomology. 89, 1038-1043.

[18] Moya, A., Guirao, P., Cifuentes, D., Beitias, F. and Cenis, J.L. (2001) Genetic diversity of Iberian populations of *Bemisia tabaci* (Hemiptera:Aleyrodidae) based on RAPD-PCR. Molecular Ecology. 10,891-897.

[19] Cervera, M.T., Cabezas, J.A., Simon, B., Martinez-Zapater, J.M., Beitia, F. and Cenis, J.L. (2000) Genetic relationships among biotypes of *Bemisia tabaci* (Hemiptera: Aleyrodidae) based on AFLP analysis. Bulletin of Entomological Research. 90, 391-396.

[20] Frohlich, D.R., Torres-Jerez, I., Bedford, I.D., Markham, P.G., Brown, J.K. (1999). A phylogeographical analysis of the *Bemisia tabaci* species complex based on mitochondrial DNA markers. Moluculer Ecology. 8, 1683-1691.

[21] Kirk, A.A., Lacey, L.A., Brown, J.K., Ciomperlik, M.A., Goolsby, J.A., Vacek, D.C., Wendel, L.E. and Napompeth B. (2000) Variation in the *Bemisia tabaci* species complex (Hemiptera:Aleyrodidae) and its natural enemies leading to successful biological control of *Bemisia* biotype B in the USA. Bulletin of Entomological Research. 90, 317-327.

[22] Boykin, L.M., De Barro, P.J. (2014) A practical guide to identifying members of the *Bemisia tabaci* species complex: and other morphologically identical species. Frontiers in Ecology and Evolution. 2, 1-5.

[23] Boykin, L.M., Bell, C.D., Evans, G., Small, I., De Barro, P.J. (2013) Is agriculture driving the diversification of the *Bemisia tabaci* species complex (Hemiptera: Sternorrhyncha: Aleyrodidae): dating, diversification and biogeographic evidence revealed. BMC Evololutionary Biology. 13, 228.

[24] Sengonca, C. (1975) Beitrag zum epidemischen Auftreten von Tabakmottenschildlaus, *Bemisia tabaci* Genn., an Baum-wollpflanplanzen in Südanatolien. Anz. Schädlingsk. Pflanzensch., Umweltsch. 48**,** 140–142.

[25] Ulusoy, R.. and Bayhan, E (2003) A new whitefly species on vegetable fields in the east mediterranean region of Turkey: Silverleaf whitefly, *Bemisia argentifolii* Bellows and Perring (Homoptera: Aleyrodidae). Turkish Journal of Entolomogy. 27(1), 51-60.

[26] Bayhan, E., Ulusoy, M. and Brown, J.K. (2006) Host range, distribution and natural enemies of *Bemisia tabaci* B biotype (Homoptera:Aleyrodidae) in Turkey. J Pest Sci, 79, 233-240.

[27] Gocmen, H., Ikten, C., Dagli, F., Topakci, N. (2007). Pamuk Beyazsineği (*Bemisia tabaci* Genn.) Populasyonlarının Moleküler Genetik ve Biyokimyasal Özellikleri ile Pestisitlere Direnci Arasındaki İlişkilerinin Araştırılması. TUBITAK TOVAG Sonuç Raporu. Antalya. (In Turkish).

[28] Erdogan, C., Moores, G.D., Gurkan, M.O., Gorman, K.J. and Denholm, I, (2008) Insecticide resistance and biotype status of populations of the tobacco whitefly *Bemisia tabaci* (Hemiptera: Aleyrodidae) from Turkey. Crop Protection. 27(3-5), 600–605.

[29] Karut, K., Malik, A.A.Y., Kazak, C., Kamberoglu, M.A, Ulusoy, M.R. (2012) Determination of biotypes of *Bemisia tabaci* Gennadius 1889 (Hemiptera: Aleyrodidae) on different host plant in Adana (Balcalı) by using two different molecular methods. Turkish Journal of Entomology. 36, 93-100.

[30] Karut, K., Kaydan, M.B., Castle, S.J., Kazak, C, Ulusoy, M.R. (2014) Study on species composition of *Bemisia tabaci* (Gennadius, 1889) (Hemiptera: Aleyrodidae) on cotton in Çukurova plain, Turkey. Turkish Journal of Entomology. 38 (1), 43-50.

[31] Karut, K., Kaydan M.B., Tok, B., Doker, I. and Kazak, C. (2015). A new record for *Bemisia tabaci* (Gennadius) (Hemiptera: Aleyrodidae) species complex of Turkey. Journal of Applied Entomology. 139(1-2). 158-160.

[32] De Barro, P.J., Liu, S.S., Boykin, L.M. and Dinsdale, A.B. (2011) *Bemisia tabaci*: a statement of species status. Annu Rev Entomol. 56,1–19.

[33] Wool, D., Gerling, D., Nolt, B.L., Constantino, L.M., Bellotti, A.C. and Morales, F.J. (1989). The use of electrophoresis for identification of adult whiteflies (Homoptera, Aleyrodidae) in Israel and Columbia. Journal of Applied Entomology. 107, 344 -350.

[34] Erdogan, C., Velioglu, A.S., Gurkan, M.O., Moores, G.D and Denholm, I. (2011) Determination of *Trialeurodes vaporariorum* (Westw.) and *Bemisia tabaci* (Genn.) (Hemiptera:Aleyrodidae) species collected from greenhouses by using polyacrylamide gel electrophoresis. Plant Protection Bulletin. 51(4), 373-385.

[35] Lisha, V.S., Anthony, B., Palaniswami M.S. and Henneberry, T. J. (2003). *Bemisia tabaci* (Homoptera:Aleyrodidae) biotypes in India. J. of Econ. Entomol. 96(2),322-327.

[36] Naunen, R., Benting, J., Elbert, A., Rogers, D. and Denholm, I. (2006). Incidence and mechanisms of resistance in *Bemisia tabaci* with special referance to biotype Q. *Bemisia tabaci* Q Biotype Symposium. April 3.

[37] Dennehy, T.J., Degain, B.A., Harpold, V.S., Zaborac, M., Morin, S., Fabrick, J.A., Nichols, R.L., Brown, J.K., Byrne, F.J. and Li, X. (2010) Extraordinary resistance to insecticides reveals exotic Q biotype of *Bemisia tabaci* in the New World. J. Econ.Entomol, 103, 2174-2186.

[38] Yukselbaba, U., Ikten, C., Gocmen, H. (2012) Determination of the biotypes of *Bemisia tabaci* (Gennadius) (Hemiptera: Aleyrodidae) populations from Antalya Province of Turkey by sequence analysis of mitochondrial cytochrome oxidase I (mtCOI) gene region. QBOL-EPPO Conf-DNA Barcoding and Diagnostic Methods for Plant Pests,21-25.05.2012; Haarlem, Holland. pp: 29.

[39] Satar, G. and Ulusoy, M.R. (2016) Biotype detection of *Bemisia tabaci* (Gennadius) (Hemiptera:Aleyrodidae) populations collected from Mediterranean Region.Turkish Bulletin of Entomology. 6(3),205-212.

[40] Sahin, I. And Ikten, C. (2017) Neonicotinoid resistance in *Bemisia tabaci* (Genn., 1889) (Hemiptera: Aleyrodidae) populations from Antalya, Turkey. Turkish Journal of Entomology. 41(2),169-175.

[41] Charaabi, K., Guerfali, M.M., Belgacem, A.B., Saidi, M., Bel-Kadhi, M.S. and Makni, M. (2015) Species diversity and distribution patterns of *Bemisia tabaci* (Gennadius) (Hemiptera: Aleyrodidae) from various agricultural crops in Tunisia. Journal of Entomology and Zoology Studies. 3(4), 32-41.

[42] Pascual, S. and Callejas, C. (2004) Intra- and interspecific competition between biotypes B and Q of *Bemisia tabaci* (Hemiptera: Aleyrodidae) from Spain. Bull. Entomol. Res. 94(4), 369-75.

[43] Sun, D.B., Xu, J., Luan, J.B. and Liu, S.S. (2011) Reproductive incompatibility between the B and Q biotypes of the whitefly *Bemisia tabaci* in China: genetic and behavioural evidence. Bulletin of Entomological Research. FirstView: 1-10.

[44] Crowder, D.W., Horowitz, A.R., De Barro, P.J., Liu, S.S., Showalter, A.M., Kontsedalov, S., Khasdan, V., Shargal, A., Liu, J. and Carrière, Y. (2010) Mating behaviour, life history and adaptation to insecticides determine species exclusion between whiteflies. Journal of Animal Ecology. 79,563-570.

[45] Horowitz, A.R., Kontsedalov, S., Khasdan, V., Ishaaya, I. (2005) Biotypes B and Q of *Bemisia tabaci* and Their Relevance to Neonicotinoid and Pyriproxyfen Resistance. Archives of Insect Biochemistry and Physiology. 58, 216–225.

[46] Yukselbaba, U., Gocmen, H. (2016) Determination of the resistance development potential to spiromesifen and the enzym activities of the B and Q biotypes of cotton whitefly *Bemisia tabaci* (Genn.) (Hemiptera: Aleyrodidae), Fresen. Environ. Bull. 25, 2461-2465.

[47] Dagli, F., Gocmen, H., Ikten, C., Yukselbaba, U. ve Topakci, N. (2007) *Bemisia tabaci* (Genn.) Akdeniz ve Ege Bölgesi Populasyonlarının Bazı İnsektisidlere Duyarlılığı Üzerinde Araştırmalar. Türkiye II. Bitki Koruma Kongresi Bildirileri, 27-29 Ağustos, Isparta.

[48] Roditakis, E., Roditakis, N.E., Tsagkarakou, A. (2005) Insecticide resistance in *Bemisia tabaci* (Homoptera: Aleyrodidae) populations from Crete. Pest Manag Sci. 61, 577-582.

[49] Kontsedalov, S., Abu-Moch, F., Lebedev, G., Czosnek, H., Horowitz, A.R. and Murad Ghanim, M. (2012). *Bemisia tabaci* Biotype Dynamics and Resistance to Insecticides in Israel During the Years 2008-2010. Journal of Integrative Agriculture. 11 (2), 312-320.

Received: **12.09.2017**
Accepted: **20.11.2017**

CORRESPONDING AUTHOR

Nurdan Topakci
Akdeniz University Vocational Higher School of Technical Sciences 07058 Antalya / Turkey

e-mail: ntopakci@akdeniz.edu.tr

© by PSP Volume 27 – No. 2/2018 pages 1104-1121 Fresenius Environmental Bulletin

HEAVY METAL ACCUMULATION IN THE *MICROTUS GUENTHERI* (DANFORD AND ALSTON, 1880) LIVING NEAR THE MINES AS A BIOMONITOR

Mustafa Yavuz[1,*], Ozgur Aktas[2]

[1]Department of Biology, Akdeniz University, 07058 Antalya, Turkey
[2]Mediterranean Fisheries Research, Production and Training Institute, Antalya, Turkey

ABSTRACT

In this study, the levels of some heavy metals (B, Al, Cr, Mn, Fe, Co, Ni, Cu, Zn, As, Cd, Hg, ^{206}Pb and ^{208}Pb) in the muscle tissues of *Microtus guentheri* (Danford and Alston 1880) from the Çaltepe at Burdur Province (Turkey), were investigated. Prior to study there was no information available on the heavy metal accumulation in this species at this region. The muscle tissues sample from the legs were analysed. The mean concentrations of the metals accumulated in *M. guentheri* on the localities, as follows: B;0.18±0.001, Al;72.65±1.16, Cr;0.56±0.003, Mn;3.19±2.02, Fe;137.14±0.55, Co;0.21±0.04, Ni;1.21±0.02, Cu;1.91±0.003, Zn;24.26±1.17, As;0.12±0.01, Cd;0.69±0.02, Hg;0.76±0.02, ^{206}Pb;0.38±0.001, ^{208}Pb;0.28±0.002 ppm. The order of mean value in samples was Fe>Al>Zn>Mn>Cu>Ni>Hg>Cd>Cr>^{206}Pb>^{208}Pb> Co>B>As. Almost all of the heavy metals studied (except As and Cd) are below the world average. These results indicate relatively low concentrations of some heavy metals (Cu and Zn) in the vole samples collected in polluted localities. But, the concentrations found quite high value (especially Al, Mn, Cd and Hg) in a significant proportion of the muscles of individuals. The accumulation values obtained for B, Al, Co, Ni, Cd, Hg and 206Pb and 208Pb are higher than the reference area. The accumulation values for Co in the soil and muscle are increasing as the mine resources are approached. The toxic heavy metal pollution began at the vicinity of Çaltepe which is approximately 1200 m altitude. Case, is thought to be due to mine sources, like marble and stone quarries and maybe agricultural activities.

KEYWORDS:
Heavy metal accumulation, *Microtus guentheri*, Co, Biomonitor, Burdur

INTRODUCTION

In our time, at the first of the most important dangers affecting to the ecosystem, comes from environmental pollution. After the industrial revolution, it is a known fact that increased environmental pollution and heavy metal pollution. There are different sources for environmental pollution and heavy metals in the environment. These sources can be both of natural or anthropogenic origin [1]. Among them, perhaps the most important factor is anthropogenic. Anthropogenic activities may generate metal pollution of the environment, where soil is often the major receptacle of these elements. Indeed, metals are retained in soil profiles and thence transferred into aquatic and/or terrestrial ecosystems, thereby increasing their bioavailability and consequent ecological risk for the environment [2]. Also, for the most heavy metals, their solubility in soil and water is very toxic. "Even low concentrations of heavy metals have damaging effects to man and animals because there is no good mechanism for their elimination from the body". The analysis of pollution through the accumulation of of toxic elements and the toxic effects as pollutants on wild animals is very important for the assessment of environmental quality and to understand tolerance capacity of the wild or natural populations to pollutant contamination [3].

The pollution in the environment, which is accumulate in soil and water goes up to plants and animals, last stage up to vertebrates may indicate the values resulting from the pollution source. Such ecological risks can be studied by focusing on small mammals due to their numerous advantages in comparison with other target animal species. While plant and soil analyses give principally report about the presence of contaminants in the rooting zone (while most of the contaminants are also found on the leaves and surface of body), small mammals (esp. rodents) satisfy with larger areas and sites because of their high mobility and reproductive capacity [4]. In addition, relatively easy capture of small rodents, the population density is much more than from other vertebrate, contain widely distributed species, rapid growth, short life span and etc., is among the advantages.

"Therefore, rodents are usually used as indicators of pollution, with elements being determined in either whole body or in specific organs", generally the liver, kidney or muscles [4]. Terrestrial and subground ecosystems, which include wild populations

of small mammals (bushy lands, steppes, plains, forests, hollows and caves etc.) are usually contaminated with probably heavy metals, toxic pollutants and very hazardous trace elements are based on agricultural activities (the accumulation of pesticides or fertilizers) or industrial and military waste and pollutants on the ground [5]. These wastes contains usually high concentrations of heavy metals which can be taken up by plants and then pass on to the various tissues of the animals, being toxic and hazardous for small herbivores at the vicinity, their predators and at last humans. For this reason, knowing the effects of different human activities (road construction, factory management, thermal and nuclear power plants etc.) on natural wild populations of plants and animals in general, and especially in small mammals such as rodents, is of very importance for wildlife conservation planning as well as for site management objectives [6]. Moreover, the predators which are consume rodents as food, may be affected and through the food chain is affected to the other vertebrate species, is important to note that.

Nowadays, heavy metals are almost everywhere because of their increasingly and immoderate use in agricultural activities, industrial applications and mining activities [7, 8]. Some of the heavy metals, such as lead (Pb) and cadmium (Cd; non-essential and xenobiotic) often cause acute and chronic environmental contamination. As a commonly analyzed element from environment is Pb accumulates mainly in bone and teeth but the critical organs for Pb intoxication are kidneys, muscles, nervous system, and bone marrow [9]. Similar to this effect, Cd causes damage primarily to kidneys, bone, digestive system and lungs. It also alters the calcium (Ca) metabolism that leads to osteomalacia [10]. These non-essential metals are toxic to humans and other animals, even if very low concentrations [11]. In contrast, nickel (Ni), iron (Fe), copper (Cu), and zinc (Zn) are essential for the some of proper functioning of the living organisms. Because these elements as they participate in the structure of the enzyme, they carry through to such as significant metabolites. However, "essential metals can also produce toxic effects when metals intake high concentrations" [12, 13]. Small mammals (mainly rodents) are sensitive and accurate monitors of exposure to environmental pollution by heavy metals which almost originates from whatever source. In addition, the pattern of heavy metal distribution and levels of heavy metals in their tissues are similar to those found in human studies [14]. Therefore, small mammals frequently serve as mammalian surrogate for humans in research [15]. Therefore, in this study *Microtus guentheri* (Danford and Alston 1880) which is a subterranean small mammal and same time a rodent is preferred as a bioindicator species.

Small mammals, especially rodents, have spread over large areas of the earth. Small mammals are found in abundance on many hazardous waste sites in The World. Their close association with the soil, large populations, small home ranges, relatively short life span, and position within the food web make them good sentinels of contaminant exposures and effects [16]. Many small mammal species have been used in field studies to effectively monitor potential exposure of resident wildlife to environmental contaminants [17] and a number of studies have focused on contaminant exposure and health effects in small mammals inhabiting large hazardous waste sites [18]. In fact that, the use of wild and natural animal models provides predictable insight into potential pollutant exposure and accumulation scenarios on contaminated sites.

The aim of this study was to determine heavy metal levels in *Microtus guentheri* (Levant Vole) near the city of Burdur/Çaltepe, located in the west of the Mediterranean Region of Turkey. Prior to this study there was no information available about the heavy metal levels of small mammals in this region. In this region, numerous marble quarries and mines are located. Thus, the primary objective of this study was to measure in the present levels of heavy metal accumulation that could be used to examine future environmental effects of bioaccumulation from the mines and marble quarries. In addition they are our other goals; to investigate the effect of distance from mines on the accumulation of heavy metals in voles muscle tissue and the impact of gender on the accumulation of heavy metals in voles, and determination of heavy metal accumulation values in soil and individuals. Besides it was investigated how much the accumulation values in the soil were transfer from soil to levant vole individuals.

Our results are the first record for this species living in this region. The results obtained from this study can be used as a reference in case bioaccumulation observations occur in the future. The species examined in this case can be used as a biomonitor for long-term and large-scale studies in the future.

METHODS

Study area. Turkey has very diverse and large amounts of marble and mines reserves. The important Turkish marble and mine reserves are found in Afyon, Bilecik, Burdur, Denizli, Muğla, Elazığ, Balıkesir and Eskişehir. Turkey is also one of the world's most important natural stone producers. Turkey's natural stone and marble production has increased tremendously in the last few years and Turkey has become one of the most important natural stone producers in the world. Therefore, especially the large number of mines and marble quarries in Burdur, located in the west of the Mediterranean Region of Turkey. In this study three localities are investigated in the Burdur/Çaltepe region (Fig. 1). Placemarks (Loc 1, 2 and 3) on the map shown that studied localities, red circles shown that the location

of the mine resources. In addition, the average distance as the bird flight distance which the mine is located at nearest between the locality are as follows; Loc. 1- Mine 1: 1.500 m, Loc. 2-Mine 2: 750 m, Loc. 3-Mine 2: 1.400 m. As a reference area, a 37.24.08.35 N, 29.42.22.90 E coordinated (altitude: 1664 m) site was chosen at the geographical borders of Dereköy village province, which is far away from the mines (about 10 km with bird flight distance). This area, which is quite deserted among the mountains, has only one non-functioning pathway and there are no other polluting artificial effectors.

Sampling and Chemical analysis. This research is based on 68 dead individuals (31♀♀;37♂♂) for voles, taken from the various habitats (close to agricultural lands and bush) found within Çaltepe at Burdur Province (Turkey), during June 2011. Field studies and observations voles were caught in various habitats are close to mine resources in trapping areas. Fifty snaptraps were placed at each site with the habitat features at each trapsite being specified. Also, 24 dead individuals (13♀♀;11♂♂) were taken from the reference area. Snaptraps were set at suitable locations two hours before sunset on the day of arrival in the field, and checked the following morning one hour before sunrise or at sunrise (snaptrapping). Only one trap was placed in 10 m^2, approximately. Captured specimens were identified as to species and transported to the laboratory, where the femoral muscles were removed, weighed and frozen prior to chemical analysis. All muscle samples placed in polystyrene tubes and stored at -20 °C until analysis.

Then, the samples were brought to the laboratory. Muscle tissues of the samples (68 samples in total) that were dissected were dried till and comes to constant weight at 80 °C. Also, microwave method was applied for the digestion produce of samples. Samples homogenized by milling prior to analyses. Acid microwave digestion was carried out in a Milestone Ethos Plus microwave. From each tissue, 0.5 g homogenates were placed in a teflon digestion vessel with mix: 8 mL 65% nitric acid (HNO_3) and 2 mL 30% hydrogen peroxide (H_2O_2). Similarly, for soil, five soil samples were taken (15 samples in total) from each site where vole samples were captured. Then, the soil samples were brought to the laboratory. For digestion of this soil samples, an acid mixture (8 mL 65% nitric acid (HNO_3) and 2 mL 2 ml 40% HF) was added. The samples in the vessels were then digested using an optimized microwave method. After digestion the samples were cooled to room temperature and diluted with ultra-pure water (optimized from [19]). Then, samples were analysed by Inductively Coupled Plasma Mass Spectroscopy (ICP-MS 7500ce-Agilent). The accuracy of the chemical analyses for muscle tissues was checked using mice (balb/c) fed with heavy metal-free foods at the laboratory. Recoveries ranged from 95–100 % for all investigated elements. The analytical accuracy of the method was 10%. The concentrations of heavy metals were expressed for the muscle as milligrams per kilogram (ppm) dry weight.

FIGURE 1
Map of investigated polluted area (Loc 1: 37°26'28.88"K, 29°49'35.56"D; Loc 2: 37°26'49.06"K, 29°47'28.37"D; Loc 3: 37°27'59.98"K, 29°47'23.40"D) in Çaltepe/Burdur.

Statistical analyzes. All statistical analyses were carried out by using SPSS Statistics Software Package V.21 (IBM 2013). Data were tested with the use of Levene's test (homogeneity of variance) and Shapiro–Wilk test (normality). Additionally, the parametric ANOVA test for depended samples was used to compare the differences in heavy metal levels between the localities, reference area and genders. Due to normal distribution and homogeneity of variance of metal levels in the samples, parametric statistics were employed for data. In the tables where the values of the accumulation are compared and the values of the reference area are examined; for Multiple Comparison Test, the statistically similar values of the reference area and the values obtained from the examined localities are marked with the same letters and statistically different ones with different letters.

In addition, to investigate the level of the mine resources on the samples, have been identified distances of the localities which are captured the samples. This was examined by Pearson Correlation Test whether there is a correlation between heavy metal accumulation levels of depending on distance from the source by gender. Moreover, inclusion rates (the value at the muscle tissue corresponds to the percentage of the value of the soil) were evaluated on heavy metal accumulation levels from the soil for each locality.

In this study, the results were given on dry weight (dry wt.) basis. However, some studies in the literature are given as wet weight (w wt.). In this case the necessity to convert these values has arisen. In accordance with this objective for comparative purposes (with the results of other studies), the 29.3% ratio in muscle is used to convert wet weight to dry weight, as [20] have indicated. Hence, wet values are multiplied by 3.413 (100/29.3). In comparison for mean values; some studies on muscle tissues of small rodents have been evaluated as reference values on literature.

From the final data, descriptive statistical characteristics were calculated (mean, standard error, variance, standard deviation, minimum, maximum) for *M. guentheri*. Analysis of Independent Samples *t* Tests were used to identify the gender-specific differences in heavy metal accumulation at. In addition, the heavy metal accumulation by each individual separately for genders are given.

RESULTS AND DISCUSSION

Heavy metal accumulation in muscle tissue by localities. The values measured from examined three localities and reference area in Burdur/Çaltepe region are given in the below (Table 1). The accumulation values of B ranged from 0.17 to 0.18 ppm. For Al from 62.02 to 79.99 ppm, Cr from 0.52 to 0.60 ppm, Mn from 2.15 to 13.84 ppm, Fe from 130.07 to 144.96 ppm, Co from 0.14 to 0.30 ppm, Ni from 1.18 to 1.25 ppm, Cu from 1.88 to 1.96 ppm, Zn from 22.08 to 26.39 ppm, As from 0.10 to 0.14 ppm, Cd from 0.66 to 0.72 ppm, Hg from 0.73 to 0.79 ppm, ^{206}Pb from 0.35 to 0.40 ppm, ^{208}Pb from 0.26 to 0.31 ppm. Otherwise, the accumulation values in the reference area; for B ranged from 0.13 to 0.16 ppm, Al from 23.61 to 40.29 ppm, Cr from 0.49 to 0.60 ppm, Mn from 1.11 to 1.48 ppm, Fe from 117.08 to 182.53 ppm, Co from 0.04 to 0.19 ppm, Ni from 1.03 to 1.24 ppm, Cu from 1.79 to 2.84 ppm, Zn from 24.45 to 44.41 ppm, As from 0.10 to 0.15 ppm, Cd from 0.28 to 0.99 ppm, Hg from 0.48 to 0.79 ppm, ^{206}Pb from 0.23 to 0.33 ppm, ^{208}Pb from 0.15 to 0.20 ppm. When the results among the muscle samples collected from Çaltepe at Burdur Province are analyzed; the highest B accumulation mean value was found at Loc.3 as 0.18 ppm, the lowest mean value was found at Loc. 2 as 0.18 ppm. For the highest Al value was found at Loc.3 as 74.56 ppm, the lowest value at Loc. 1 as 68.97 ppm. For the highest Cr value was found at Loc.2 as 0.56 ppm, the lowest value at Loc. 1 as 0.56 ppm. For the highest Mn value was found at Loc.1 as 4.17 ppm, the lowest value at Loc. 2 as 2.17 ppm. For the highest Fe value was found at Loc.3 as 137.34 ppm, the lowest value at Loc. 1 as 136.77 ppm. For the highest Co value was found at Loc.2 as 0.23 ppm, the lowest value at Loc. 1 as 0.20 ppm. For the highest Ni value was found at Loc.1 as 1.22 ppm, the lowest value at Loc. 2 as 1.21 ppm. For the highest Cu value was found at Loc.2 as 1.92 ppm, the lowest value at Loc. 3 as 1.91 ppm. For the highest Zn value was found at Loc.3 as 24.42 ppm, the lowest value at Loc. 2 as 24.09 ppm. For the highest As value was found at Loc.2 as 0.118 ppm, the lowest value at Loc. 1 as 0.116 ppm. For the highest Cd value was found at Loc.2 as 0.69 ppm, the lowest value at Loc. 3 as 0.68 ppm. For the highest Hg value was found at Loc.2 as 0.7632 ppm, the lowest value at Loc. 1 as 0.7629 ppm. For the highest ^{206}Pb value was found at Loc.2 as 0.38 ppm, the lowest value at Loc. 1 as 0.37 ppm. For the highest ^{208}Pb value was found at Loc.1 as 0.29 ppm, the lowest value at Loc. 2 as 0.28 ppm.

When the localities and the reference fields examined are evaluated together; with the exception of Cr, Mn, Fe and As, the difference between the localities and the reference area in terms of their accumulation values is statistically significant. That is, while the values of Cr, Mn, Fe and As accumulation are similar to the reference area, the accumulation values of B, Al, Co, Ni, Cd, Hg, ^{206}Pb and ^{208}Pb are considerably higher than the reference area. However, interestingly, Cu and Zn values are lower than the reference field (Table 1).

TABLE 1
Descriptive statistics of heavy metal concentrations by localities and comparison with the reference area for *M. guentheri.*

Loc	Gender		B	Al	Cr	Mn	Fe	Co	Ni	Cu	Zn	As	Cd	Hg	^{206}Pb	^{208}Pb
1	Female	Mean	0.18	64.74	0.56	4.17	134.87	0.20	1.22	1.92	24.24	0.11	0.68	0.77	0.37	0.28
		Min	0.17	0.62	0.52	1.15	130.07	0.14	1.19	1.90	22.32	0.10	0.66	0.74	0.35	0.26
		Max	0.19	78.05	0.60	13.84	143.30	0.29	1.25	1.96	26.28	0.13	0.72	0.79	0.40	0.30
		N	9	9	9	9	9	11	9	9	9	9	9	9	9	9
	Male	Mean	0.18	72.42	0.55	2.17	138.33	0.20	1.21	1.92	24.33	0.12	0.68	0.76	0.37	0.29
		Min	0.17	67.69	0.52	2.15	130.48	0.15	1.18	1.88	22.53	0.10	0.66	0.73	0.36	0.26
		Max	0.19	79.80	0.59	2.49	144.92	0.25	1.24	1.94	26.13	0.14	0.71	0.79	0.40	0.31
		N	11	11	11	11	11	13	11	11	11	11	11	11	11	11
	Total	Mean*	^{a}0.18	^{b}68.97	^{a}0.56	^{a}2.86	^{a}136.77	^{a}0.20	^{a}1.22	^{a}1.92	^{a}24.29	^{a}0.12	^{a}0.68	^{a}0.76	^{a}0.37	^{a}0.29
		Min	0.17	0.62	0.52	1.15	130.07	0.14	1.18	1.88	22.32	0.10	0.66	0.73	0.35	0.26
		Max	0.19	79.80	0.60	13.84	144.92	0.29	1.25	1.96	26.28	0.14	0.72	0.79	0.40	0.31
		N	20	20	20	20	20	24	20	20	20	20	20	20	20	20
2	Female	Mean	0.18	74.48	0.56	2.18	137.86	0.22	1.21	1.92	23.68	0.12	0.69	0.76	0.37	0.28
		Min	0.17	69.65	0.53	2.16	131.25	0.15	1.18	1.88	22.26	0.11	0.66	0.73	0.35	0.26
		Max	0.19	79.96	0.60	2.20	144.96	0.27	1.24	1.96	25.75	0.14	0.72	0.79	0.40	0.29
		N	11	11	11	11	11	9	11	11	11	11	11	11	11	11
	Male	Mean	0.18	73.21	0.56	2.17	136.72	0.25	1.21	1.92	24.43	0.12	0.69	0.76	0.38	0.29
		Min	0.17	69.45	0.52	2.15	130.48	0.19	1.19	1.88	22.08	0.10	0.66	0.73	0.36	0.26
		Max	0.19	78.49	0.60	2.20	144.78	0.30	1.25	1.95	26.39	0.14	0.72	0.79	0.40	0.31
		N	13	13	13	13	13	11	13	13	13	13	13	13	13	13
	Total	Mean*	^{a}0.18	^{ab}73.79	^{a}0.56	^{a}2.17	^{a}137.25	^{b}0.23	^{a}1.21	^{a}1.92	^{a}24.09	^{a}0.12	^{a}0.69	^{a}0.76	^{a}0.38	^{a}0.28
		Min	0.17	69.45	0.52	2.15	130.48	0.15	1.18	1.88	22.08	0.10	0.66	0.73	0.35	0.26
		Max	0.19	79.96	0.60	2.20	144.96	0.30	1.25	1.96	26.39	0.14	0.72	0.79	0.40	0.31
		N	24	24	24	24	24	20	24	24	24	24	24	24	24	24
3	Female	Mean	0.18	73.79	0.56	2.17	137.25	0.23	1.21	1.92	24.09	0.12	0.69	0.76	0.38	0.28
		Min	0.17	69.45	0.52	2.15	130.48	0.15	1.18	1.88	22.08	0.10	0.66	0.73	0.35	0.26
		Max	0.19	79.96	0.60	2.20	144.96	0.30	1.25	1.96	26.39	0.14	0.72	0.79	0.40	0.31
		N	11	11	11	11	11	11	11	11	11	11	11	11	11	11
	Male	Mean	0.18	73.98	0.56	2.18	137.36	0.21	1.21	1.91	24.83	0.11	0.68	0.76	0.38	0.28
		Min	0.17	67.27	0.53	2.16	130.33	0.16	1.18	1.89	22.74	0.10	0.66	0.73	0.36	0.26
		Max	0.19	79.03	0.60	2.20	144.16	0.29	1.24	1.96	26.26	0.13	0.71	0.79	0.40	0.31
		N	13	13	13	13	13	13	13	13	13	13	13	13	13	13
	Total	Mean*	^{a}0.18	^{a}74.56	^{a}0.56	^{a}2.18	^{a}137.34	^{ab}0.20	^{a}1.21	^{a}1.91	^{a}24.42	^{a}0.12	^{a}0.68	^{a}0.76	^{a}0.38	^{a}0.28
		Min	0.17	67.27	0.52	2.15	130.33	0.14	1.18	1.88	22.28	0.10	0.66	0.73	0.35	0.26
		Max	0.19	79.99	0.60	2.20	144.54	0.29	1.24	1.96	26.26	0.14	0.71	0.79	0.40	0.31
		N	24	24	24	24	24	24	24	24	24	24	24	24	24	24
Total	Female	Mean	0.18	71.93	0.56	4.10	136.80	0.21	1.21	1.92	23.94	0.12	0.69	0.77	0.37	0.28
		Min	0.17	62.02	0.52	2.15	130.07	0.14	1.18	1.88	22.26	0.10	0.66	0.73	0.35	0.26
		Max	0.19	79.99	0.60	13.84	144.96	0.29	1.25	1.96	26.28	0.14	0.72	0.79	0.40	0.31
		N	31	31	31	31	31	31	31	31	31	31	31	31	31	31
	Male	Mean	0.18	73.25	0.56	2.17	137.42	0.22	1.21	1.92	24.54	0.12	0.69	0.76	0.38	0.29
		Min	0.17	67.27	0.52	2.15	130.33	0.15	1.18	1.88	22.08	0.10	0.66	0.73	0.36	0.26
		Max	0.19	79.80	0.60	2.20	144.92	0.30	1.25	1.96	26.39	0.14	0.72	0.79	0.40	0.31
		N	37	37	37	37	37	37	37	37	37	37	37	37	37	37
	Total	Mean	**0.18**	**72.65**	**0.56**	**3.19**	**137.14**	**0.21**	**1.21**	**1.92**	**24.26**	**0.12**	**0.69**	**0.76**	**0.38**	**0.28**
		Min	0.17	62.02	0.52	1.15	130.07	0.14	1.18	1.88	22.08	0.10	0.66	0.73	0.35	0.26
		Max	0.19	79.99	0.60	13.84	144.96	0.30	1.25	1.96	26.39	0.14	0.72	0.79	0.40	0.31
		N	68	68	68	68	68	68	68	68	68	68	68	68	68	68
Ref	Female	Mean	0.15	32.44	0.55	1.20	132.13	0.10	1.10	2.18	32.94	0.12	0.51	0.66	0.25	0.17
		Min	0.14	23.61	0.49	1.11	117.08	0.04	1.03	1.79	27.43	0.10	0.30	0.48	0.23	0.15
		Max	0.16	40.29	0.60	1.45	142.37	0.19	1.21	2.84	44.41	0.15	0.99	0.79	0.27	0.20
		N	13	13	13	13	13	13	13	13	13	13	13	13	13	13
	Male	Mean	0.15	30.44	0.56	1.21	139.21	0.13	1.12	2.08	31.56	0.13	0.44	0.66	0.26	0.17
		Min	0.13	23.66	0.52	1.17	121.62	0.05	1.04	1.79	24.45	0.11	0.28	0.48	0.23	0.15
		Max	0.16	39.05	0.59	1.48	182.53	0.19	1.24	2.25	38.88	0.15	0.56	0.78	0.33	0.19
		N	11	11	11	11	11	11	11	11	11	11	11	11	11	11
	Total	Mean*	^{b}**0.15**	^{c}**31.52**	^{a}**0.55**	^{a}**1.21**	^{a}**135.38**	^{c}**0.11**	^{b}**1.11**	^{b}**2.13**	^{b}**32.31**	^{b}**0.13**	^{b}**0.48**	^{b}**0.66**	^{b}**0.25**	^{b}**0.17**
		Min	0.13	23.61	0.49	1.11	117.08	0.04	1.03	1.79	24.45	0.10	0.28	0.48	0.23	0.15
		Max	0.16	40.29	0.60	1.48	182.53	0.19	1.24	2.84	44.41	0.15	0.99	0.79	0.33	0.20
		N	24	24	24	24	24	24	24	24	24	24	24	24	24	24
ANOVA (df_1=3, df_2=88) **			F= 101.036 p= 0.0001	F= 137.406 p= 0.0001	F= 0.213 p= 0.887	F= 1.202 p= 0.314	F= 0.344 p= 0.794	F= 31.182 p= 0.0001	F= 47.103 p= 0.0001	F= 12.053 p= 0.0001	F= 45.773 p= 0.0001	F= 3.204 p= 0.027	F= 51.718 p= 0.0001	F= 15.868 p= 0.0001	F=320.284 p= 0.0001	F=335.982 p= 0.0001

* The Multiple Comparison Test (Duncan Test) results are indicated on the table using letters, i.e. within in the same letter are statistically not different from one another, whereas groups with different letters do differ. Those which have more than one letter resemble the groups so designated.

** df_1= Degrees of Freedom for between groups, df_2= Degrees of Freedom for within group

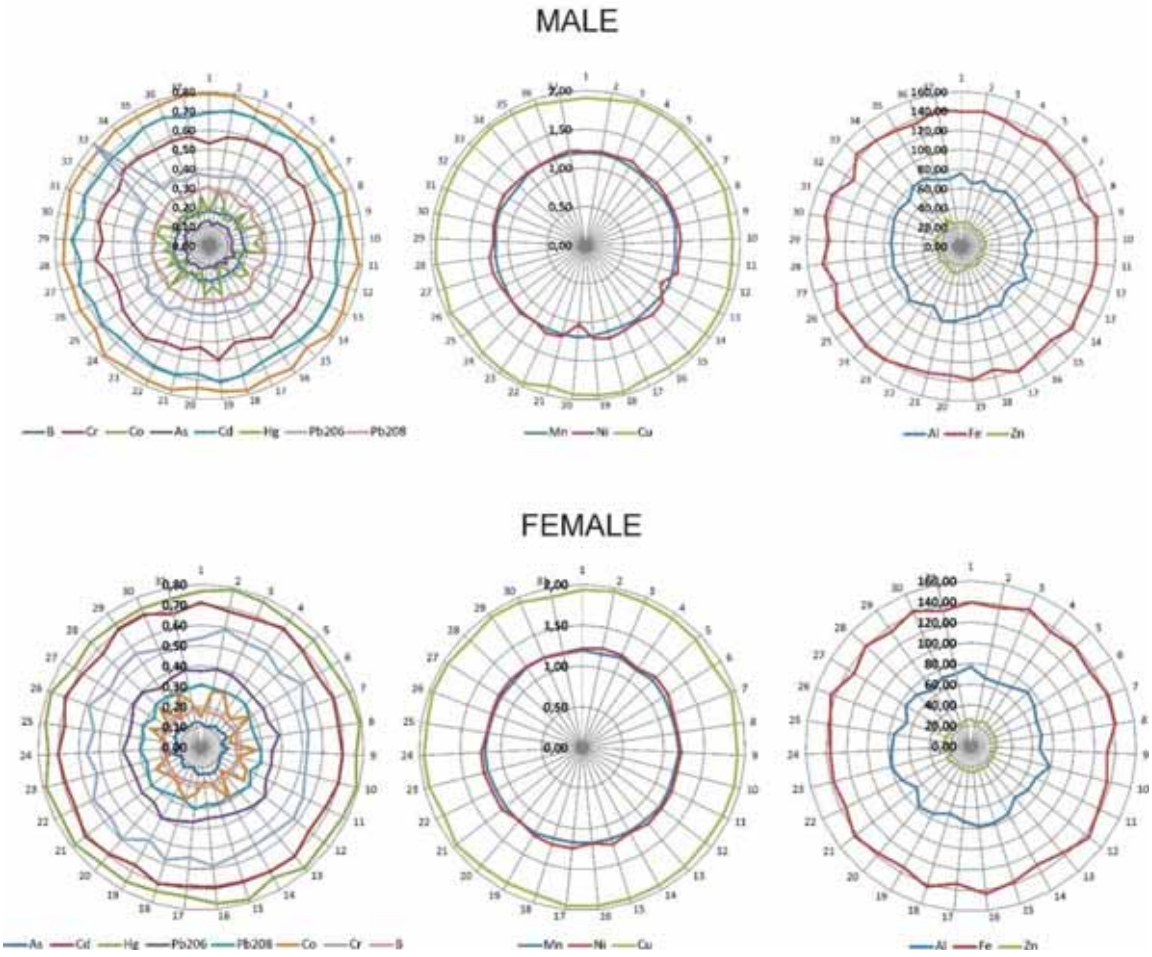

FIGURE 2
Distributions of the concentration values for individuals by gender
(values around the circle show the numbers of individual)

Heavy metal accumulation in muscle tissue by genders. Moreover, our results are analyzed depend on genders; the highest B accumulation mean value was found at Loc.1 as female is 0.18 ppm, the lowest mean value was found at Loc. 2 as male is 0.176 ppm. For the highest Al value was found at Loc.3 as female is 75.26 ppm, the lowest value at Loc. 1 as female is 64.74 ppm. For the highest Cr value was found at Loc.1 as female is 0.56 ppm, the lowest value at again Loc. 1 as male is 0.55 ppm. For the highest Mn value was found at Loc.1 as female is 4.17 ppm, the lowest value at again Loc. 1 as male is 2.17 ppm. For the highest Fe value was found at Loc.1 as male is 138.33 ppm, the lowest value at again Loc. 1 as female is 134.87 ppm. For the highest Co value was found at Loc.2 as male is 0.25 ppm, the lowest value at Loc. 3 as female is 0.20 ppm. For the highest Ni value was found at Loc.1 as female is 1.22 ppm, the lowest value at Loc. 2 as female is 1.21 ppm. For the highest Cu value was found at Loc.1 as female is 1.92 ppm, the lowest value at Loc. 3 as female is 1.91 ppm. For the highest Zn value was found at Loc.3 as male is 24.83 ppm, the lowest value at Loc. 2 as female is 23.68 ppm. For the highest As value was found at Loc.3 as female is 0.12 ppm, the lowest value at Loc. 1 as female is 0.11 ppm. For the highest Cd value was found at Loc.2 as male is 0.69 ppm, the lowest value at Loc. 3 as male is 0.68 ppm. For the highest Hg value was found at Loc.3 as female is 0.77 ppm, the lowest value again at Loc. 3 as male is 0.76 ppm. For the highest ^{206}Pb value was found at Loc.2 as male is 0.38 ppm, the lowest value at Loc. 1 as female is 0.37 ppm. For the highest ^{208} Pb value was found at Loc.1 as male is 0.29 ppm, the lowest value at Loc. 2 as female is 0.28 ppm.

Otherwise, reference area results are analyzed depend on genders; the highest B accumulation mean value was found as female is 0.153 ppm. For the highest Al value was found as female is 32.44 ppm, for the highest Cr value was found as male is 0.55 ppm, for the highest Mn value was found as male is 1.21 ppm, for the highest Fe value was found as male is 139.21 ppm, for the highest Co value was

found as male is 0.13 ppm, for the highest Ni value was found as male is 1.12 ppm, for the highest Cu value was found as female is 2.18 ppm, for the highest Zn value was found as female is 32.94 ppm, for the highest As value was found as male is 0.12 ppm, for the highest Cd value was found as female is 0.51 ppm, for the highest Hg value was found at Loc.3 as female is 0.6638 ppm, for the highest ^{206}Pb value was found as male is 0.26 ppm, for the highest ^{208} Pb value was found as male is 0.1727 ppm.

When evaluated individually for each metal; There is no statistically significant difference between the gender groups in terms of heavy metal accumulation values for both for localities and reference area.

Heavy metal accumulation in muscle tissue by distance from mines. The mean concentrations of the metals accumulated in *M. guentheri* on the sites which is close to mine resources, as follows: B: 0.18±0.001, Al: 72.65±1.16, Cr: 0.56±0.003, Mn: 3.19±2.02, Fe: 137.14±0.55, Co: 0.21±0.04, Ni: 1.21±0.02, Cu: 1.91±0.003, Zn: 24.26±1.17, As: 0.12±0.01, Cd: 0.69±0.02, Hg: 0.76±0.02, ^{206}Pb: 0.38±0.001, ^{208}Pb: 0.28±0.002 ppm. The order of mean concentration of the heavy metals in samples from the areas was Fe>Al>Zn>Mn>Cu>Ni>Hg> Cd>Cr>^{206}Pb>^{208}Pb>Co>B>As. Moreover, heavy metal accumulation measured from each individual was given in the graphics depending on gender (Fig. 2). Also, the differences between the two gender groups for concentrations of the total heavy metals accumulation were not statistically significant (Table 2). Moreover similarly, the differences between the two gender groups for concentrations of the total heavy metals accumulation on reference area were not statistically significant (Table 3).

TABLE 2
ANOVA results and significance values of concentrations depend on gender groups for samples near mines

		Sum of Squares	df	Mean Square	F	Sig.
	Between Groups	0.00	1	0.00	.835	.364
B	Within Groups	0.00	66	0.00		
	Total	0.00	67			
	Between Groups	90.71	1	90.71	.985	.325
Al	Within Groups	6080.58	66	92.13		
	Total	6171.29	67			
	Between Groups	0.00	1	0.00	.014	.907
Cr	Within Groups	0.05	66	0.00		
	Total	0.05	67			
	Between Groups	329.93	1	329.93	1.195	.278
Mn	Within Groups	18217.38	66	276.02		
	Total	18547.31	67			
	Between Groups	1.28	1	1.28	.060	.807
Fe	Within Groups	1398.14	66	21.18		
	Total	1399.42	67			
	Between Groups	0.00	1	0.00	1.994	.163
Co	Within Groups	0.13	66	0.00		
	Total	0.14	67			
	Between Groups	0.00	1	0.00	.015	.902
Ni	Within Groups	0.03	66	0.00		
	Total	0.03	67			
	Between Groups	0.00	1	0.00	1.060	.307
Cu	Within Groups	0.04	66	0.00		
	Total	0.04	67			
	Between Groups	0.24	1	0.24	.128	.722
Zn	Within Groups	124.37	66	1.88		
	Total	124.61	67			
	Between Groups	0.00	1	0.00	.002	.964
As	Within Groups	0.01	66	0.00		
	Total	0.01	67			
	Between Groups	0.00	1	0.00	.182	.671
Cd	Within Groups	0.02	66	0.00		
	Total	0.02	67			
	Between Groups	0.00	1	0.00	.128	.722
Hg	Within Groups	0.02	66	0.00		
	Total	0.02	67			
	Between Groups	0.00	1	0.00	1.646	.204
Pb206	Within Groups	0.01	66	0.00		
	Total	0.01	67			
	Between Groups	0.00	1	0.00	.033	.857
Pb208	Within Groups	0.01	66	0.00		
	Total	0.01	67			

TABLE 3
ANOVA results and significance values of concentrations depend on gender groups for samples of reference area

		Sum of Squares	df	Mean Square	F	Sig.
B	Between Groups	0.00	1	0.00	0.643	0.279
	Within Groups	0.00	22	0.00		
	Total	0.00	23			
Al	Between Groups	23.96	1	23.96	0.772	0.389
	Within Groups	682.83	22	31.04		
	Total	706.78	23			
Cr	Between Groups	0.00	1	0.00	0.171	0.683
	Within Groups	0.02	22	0.00		
	Total	0.02	23			
Mn	Between Groups	0.00	1	0.00	0.038	0.846
	Within Groups	0.17	22	0.01		
	Total	0.17	23			
Fe	Between Groups	298.54	1	298.54	1.953	0.176
	Within Groups	3362.61	22	152.85		
	Total	3661.15	23			
Co	Between Groups	0.01	1	0.01	2.633	0.119
	Within Groups	0.05	22	0.00		
	Total	0.05	23			
Ni	Between Groups	0.00	1	0.00	0.852	0.366
	Within Groups	0.08	22	0.00		
	Total	0.09	23			
Cu	Between Groups	0.06	1	0.06	0.687	0.416
	Within Groups	1.89	22	0.09		
	Total	1.95	23			
Zn	Between Groups	11.24	1	11.24	0.411	0.528
	Within Groups	601.81	22	27.36		
	Total	613.05	23			
As	Between Groups	0.00	1	0.00	0.545	0.468
	Within Groups	0.01	22	0.00		
	Total	0.01	23			
Cd	Between Groups	0.03	1	0.03	1.929	0.179
	Within Groups	0.37	22	0.02		
	Total	0.40	23			
Hg	Between Groups	0.00	1	0.00	0	0.997
	Within Groups	0.30	22	0.01		
	Total	0.30	23			
Pb206	Between Groups	0.00	1	0.00	2.411	0.135
	Within Groups	0.01	22	0.00		
	Total	0.01	23			
Pb208	Between Groups	0.00	1	0.00	0.004	0.953
	Within Groups	0.01	22	0.00		
	Total	0.01	23			

On the other hand, a negative and comparatively weaker correlation ($r_{distance}$= -0.298; n:68, p<0.014) was found between the average Co accumulation and the distance from mine resources (Fig. 3), no relationship could be found between other metals and the distance. But, the differences between the two gender groups for concentrations of Co accumulation (for Female= 0.22±0.009 and Male= 0.21±0.007, respectively) were not statistically significant (F=1.994; df_1=1, df_2=66, p=0.163). In addition, mean concentrations of Co accumulation depending on multiple comparison tests (Duncan, Tukey) were different from each other for the localities. According to this; while Loc. 1 and Loc. 2 different from each other, Loc. 3 is similar to both (Table 4). But, for other heavy metals accumulation, there is no difference among the localities. Also can be seen descriptive statistics of heavy metal concentrations for *M. guentheri* from the Table 1.

Heavy metal accumulation in soil of localities and possible inclusion rates in muscle tissue. The mean concentrations of the metals accumulated in soil of the localities which was investigated as follows: B: 28.23±1.15, Al: 9625.36±23.52, Cr: 10.03± 1.24, Mn: 163.94±08.86, Fe: 38929.74±205.43, Co: 6.61±1.34, Ni: 23.99±1.04, Cu: 36.21±1.63, Zn: 59.77±1.46, As: 13.44±0.79, Cd: 2.06±0.72, Hg: 2.34±0.71, ^{206}Pb: 22.18±1.44, ^{208}Pb: 19.33±0.52

ppm. The order of mean concentration of the heavy metals in the soil was taken from the localities was Fe>Al>Mn>Zn>Cu>B>Ni>^{206}Pb>^{208}Pb>As>Cr>Co>Hg>Cd. In addition to, just as muscle tissue samples of *M. guentheri*, a negative and comparatively weaker correlation ($r_{distance}$= -0.264; n:15, p<0.038) was found between the average Co accumulation and the distance from mine resources, no relationship could be found between other metals and the distance. But, the differences for the reference area between the two gender groups for concentrations of Co accumulation (for Female= 0.10±0.044 and Male= 0.13±0.046, respectively) were not statistically significant (independent t test, t= -1.623; df=22, p=0.119 sig. 2 tailed). This may indicate that the soil (except cobalt) is regularly affected by the mines. Mean concentrations of Co accumulation depending on multiple comparison tests (Duncan, Tukey) were different from each other for the localities. According to this; while Loc. 1 and Loc. 2 different from each other, Loc. 3 is similar to both. But, for other heavy metals accumulation, there is no difference among the localities. Also can be seen descriptive statistics of heavy metal concentrations for soil of the localities from the Table 5.

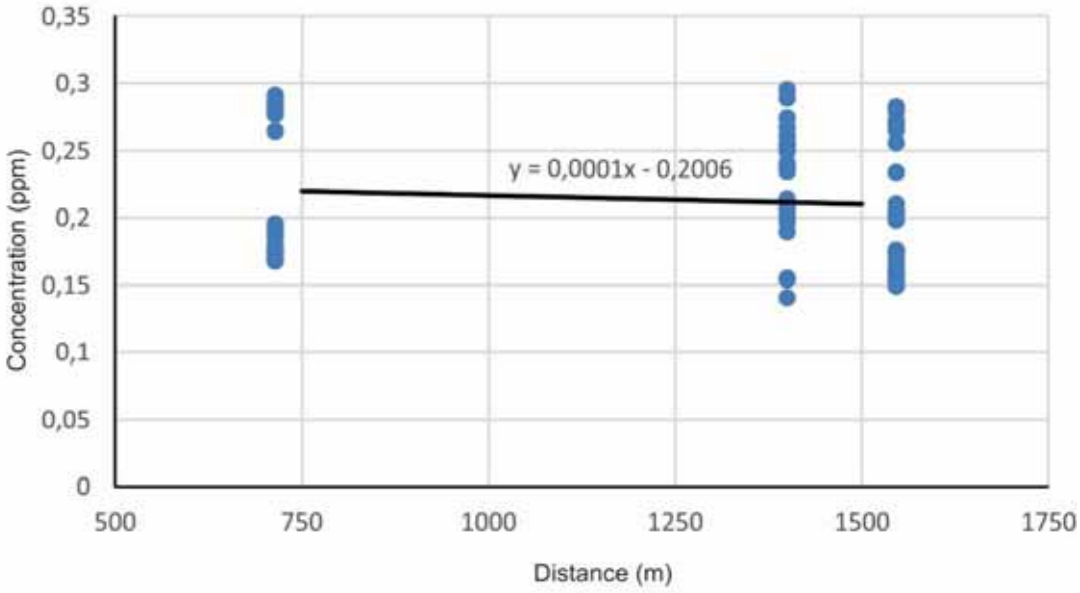

FIGURE 3
Values of Co concentrations and distance (Loc. 1- Mine 1: 1.500 m, Loc. 2-Mine 2: 750 m, Loc. 3-Mine 2: 1.400 m) from mine resource as a function of tendency.

TABLE 4
Results of Multiple Comparison Tests for Co accumulation in muscle tissue of samples

Multiple Comparison Tests	Localities	N	Subset for alpha = 0.05	
			1	2
Tukey HSD[a,b]	1	24	.2014	
	3	24	.2046	.2046
	2	20		.2337
	Sig.		.968	.072
Duncan[a,b]	1	24	.2014	
	3	24	.2046	
	2	20		.2337
	Sig.		**.810**	**1.000**

Means for groups in homogeneous subsets are displayed.
a. Uses Harmonic Mean Sample Size = 22,500.
b. The group sizes are unequal. The harmonic mean of the group sizes is used. Type I error levels are not guaranteed.

TABLE 5
Descriptive statistics of heavy metal concentrations (ppm) for soil of the localities and results of Multiple Comparison Tests

Loc		B	Al	Cr	Mn	Fe	Co	Ni	Cu	Zn	As	Cd	Hg	Pb206	Pb208
1	Mean*	[a]27.61	[a]9585.69	[a]9.38	[a]165.35	[a]39241.11	[a]5.85	[a]23.04	[a]37.53	[a]59.34	[a]12.87	[a]1.93	[a]2.36	[a]22.56	[a]20.04
	Min	20.42	8423.92	6.12	133.66	28123.34	3.92	13.82	23.40	56.94	10.51	1.75	1.89	20.19	17.30
	Max	36.74	10767.78	12.93	209.40	48765.85	7.66	31.83	44.86	61.27	15.60	2.27	2.62	23.57	22.90
	N	5	5	5	5	5	5	5	5	5	5	5	5	5	5
2	Mean*	[a]27.44	[a]9716.05	[a]10.50	[a]174.67	[a]33835.65	[b]6.61	[a]25.06	[a]35.67	[a]59.35	[a]13.38	[a]2.11	[a]2.29	[a]2179	[a]18.02
	Min	20.40	8663.88	10.27	120.38	27832.70	3.79	18.40	30.91	57.53	10.85	1.80	2.00	19.01	17.35
	Max	35.82	10736.03	12.08	206.00	39588.87	8.36	31.10	41.49	61.79	15.87	2.39	2.59	23.26	20.39
	N	5	5	5	5	5	5	5	5	5	5	5	5	5	5
3	Mean*	[a]29.06	[a]9650.33	[a]10.27	[a]151.51	[a]43712.64	[ab]5.94	[a]23.33	[a]35.99	[a]60.61	[a]14.53	[a]2.14	[a]2.38	[a]22.40	[a]19.94
	Min	22.55	8204.23	9.01	130.06	30846.82	3.06	17.82	26.75	57.69	9.37	1.73	1.87	19.13	17.41
	Max	36.99	10944.25	14.11	181.65	52359.37	8.23	28.72	40.04	61.57	18.06	2.52	2.71	23.62	22.36
	N	5	5	5	5	5	5	5	5	5	5	5	5	5	5
Total	Mean	**28.23**	**9625.36**	**10.03**	**163.94**	**38929.74**	**6.61**	**23.99**	**36.21**	**59.77**	**13.44**	**2.06**	**2.34**	**22.18**	**19.33**
	Min	20.40	8204.23	6.12	120.38	27832.70	3.06	13.82	23.40	56.94	9.37	1.73	1.87	19.01	17.30
	Max	36.99	10944.25	14.11	209.40	52359.37	8.36	31.83	44.86	61.79	18.06	2.52	2.71	23.62	22.90
	N	15	15	15	15	15	15	15	15	15	15	15	15	15	15
Average of the World ***		42	71000	59.5	488	56000	11.3	29	38.9	70	6.83	0.41	0.07	27	27
By Cambisol **** min-max (mean)		<1-128 (40)	-	4-1100 (51)	45-9200 (525)	-	3-58 (10)	3-10 (26)	4-100 (23)	9-362 (60)	1.3-27 (8.4)	0.08-1.61 (0.45)	0.01-1.1 (0.1)	1.5-70 (28)	1.5 (28)
ANOVA (df_1=2, df_2=12) ****		F=0.782 p= 0.479	F=0.021 p= 0.980	F= 2.568 p= 0.118	F= 0.734 p= 0.500	F= 2.322 p= 0.140	F= 3.148 p= 0.022	F= 0.251 p= 0.782	F= 0.082 p= 0.922	F= 0.813 p= 0.467	F= 0.420 p= 0.666	F= 0.929 p= 0.422	F= 0.143 p= 0.868	F=0.171 p= 0.845	F=1.924 p= 0.188

* The Multiple Comparison Test (Duncan Test) results are indicated on the table using letters, i.e. within in the same letter are statistically not different from one another, whereas groups with different letters do differ. Those which have more than one letter resemble the groups so designated.
** df_1= Degrees of Freedom for between groups, df_2= Degrees of Freedom for within groups
*** From [58] (But, Al and Fe from [58])
**** Soil type from Burdur Provincial Environmental Situation Report [60] and values from [58].

Almost all of the heavy metals studied (except Cd and Hg) are below the world average. According to the type of soil (cambisol) in the area studied; Only values of the Cd and Hg are above the upper limit. This may be indicative of Cd and Hg contamination, especially from mines.

When inclusion rates (the value at the muscle tissue corresponds to the percentage of the value of the soil) were evaluated (Table 6); It is seen that the highest value is Zn with 40.59% and the lowest value is Fe with 0.35%. If the inclusion rates are ordered from highest to lowest, then the situation is Zn>Cd>Hg>Cr>Cu>Ni>Co>Mn>^{206}Pb>^{208}Pb>As>Al>B>Fe. As can be seen, there is no linear relationship between the amount of metal found in the soil and its accumulation in muscle. Some metals (such as Cd, Cr, Hg), which are found less in the soil, but accumulate in the muscle tissue much higher than those in abundance metals (such as Al, Fe).

Heavy metal accumulation in rodent muscle tissue and the general situation in the world. This study obtained accumulation concentrations of most of the heavy metal, which are in the samples, lower than the values found in other studies with muscle from rodents (Table 7). For Cu, the accumulation concentration value ($\bar{X}$=1.92±0.003 ppm) is lower than the literature values: the values are 6.02 ppm for muscle from *Rombomys opimus* and 7.57 ppm from *Rattus norvegicus* on different localities at city in Iran [21], 9.66 ppm from *Peromyscus maniculatus* and 7.99 ppm from *Microtus pennsylvanicus* from oil sands and surface mines in Canada [22], 9.56 ppm from *Acomys cahirinus* on polluted areas from Egypt [23], 32.40 ppm from *Meriones persicus* on polluted areas in Iran [24], 4.25 ppm from *Peromyscus gossypinus* on different contaminated areas in USA [25] and 8.80 ppm from *Heliophobius argenteocinereus* trapped from City's different habitats in Malawi [26]. As can be seen, our values are much lower than the values obtained from other

studies by rodent muscle. Similarly, for as values obtained from the other elements of the metabolic importance for animals; values obtained for Zn, the accumulation concentration value ($\bar{X}$=24.26±1.170 ppm) is lower than the values of other studies with muscle from rodents at literature (Table 7): the values are 40.74 ppm for muscle from *Rombomys opimus* and 63.76 ppm from *Rattus norvegicus* on different localities at city in Iran [21], 48.29 ppm from *Peromyscus maniculatus* and 47.82 ppm from *Microtus pennsylvanicus* from oil sands and surface mines in Canada [22], 55.97 ppm from *Acomys cahirinus* on polluted areas from Egypt [23], 111.12 ppm from *Meriones persicus* on polluted areas in Iran [24], 51.90 ppm from *Clethrionomys glareolus* on abandoned lead mine in UK [27], 101.23 ppm from *Heliophobius argenteocinereus* trapped from City's different habitats in Malawi [26] and 101.23 ppm from *Clethrionomys glareolus* from near active mine sites at Ireland [28]. As expected, Zn concentration is quite lower than the literature values for liver (70.65 ppm for *Microtus agrestis* and 76.79 ppm for *Microtus arvalis*) in the study by [29] in Slovenia, also for the present study the value is 24.26±1.170 ppm at Burdur, Turkey. In fact that, this results "might be mainly due to the good homeostatic mechanisms of this metal in mammalian tissues" [30]. The lower values of the essential elements in contaminated areas are usually related to the interaction between essential and non-essential metals. In mammalian tissues, this metal is effectively controlled by homeostatic mechanisms such as enzimal activities [30, 31] that may be disrupted by high exposure to Pb and Hg [32]. Same way; for As, the accumulation concentration value ($\bar{X}$=0.12±0.001 ppm) is lower than a few literature values. The values are 0.75 ppm for muscle from *Apodemus sylvaticus* and 0.72 ppm from *Clethrionomys glareolus* on the near abandoned mines in UK [33]. But, the value is 0.10 ppm for game animal and small mammal's whole body in the study by [34] in Bulgaria. Moreover, the values are higher as 0.06 ppm for kidney from white-footed mice and 0.05 ppm from rice rats in the study by [35] in USA. The mine impacted sites are significantly elevated arsenic concentrations in both the soil and plant samples when compare with the back ground site. "This is an indication that arsenic is being transported from the soil to the plants. Furthermore, this plant arsenic has the potential to adversely affect herbivores (i.e. meadow voles, mice, rabbits, etc.)" [36]. Here it is the most important fact is, As, Hg and Cd known to be very toxic metals [2]. Compared with literature, there's much more concentration in this study, it reveals the extent of the potential hazardous. In addition to; for values obtained for Cr, the accumulation concentration value ($\bar{X}$=0.56±0.003 ppm) is lower than one of the literature values for rodents: The value is 0.61 ppm from *Peromyscus maniculatus* from oil sands and surface mines in Canada [22], but the accumulation concentration value in this study very little higher than 0.34 ppm from *Microtus pennsylvanicus* from Canada and 0.50 ppm from *Peromyscus gossypinus* on different contaminated areas in USA [25]. As expected from the other side: the value is fairly lower than 1.12 ppm for liver from *Crocidura russula*'s liver in the study by [3] in Portugal. In fact, "Chromium levels are mainly influenced by natural content of parent rocks on a regional scale" [37, 38]. Consequently, Cr was not significantly correlated with the altitude and distance of localities from mine. Same way, for values obtained for Co, the accumulation concentration value ($\bar{X}$=0.21±0.04) is lower than the literature values for rodent muscle: The values are 4.07 ppm from *Peromyscus maniculatus* and 2.28 ppm from *Microtus pennsylvanicus* from oil sands and surface mines in Canada [22], and 0.22 ppm from *Peromyscus gossypinus* on different contaminated areas in USA [25]. As expected from the other side: the value is fairly lower than the values are 11.91 ppm for liver from shrews's whole body in the study by [39] in Spain. For values obtained for B, the accumulation concentration value ($\bar{X}$=0.18±0.001) is very lower than the literature value: the value are 21.73 ppm for liver from shrews's whole body in the study by [39] in Spain. As known, some trace elements (e.g. Cu, Co, Se, Mn) are essential to correct biological function but outside required ranges, abstinence problems or toxicities lead to health problems. Non-essential metals (e.g. Pb, Hg, Cd, Cr and Al) have no known biological function, and become very toxic and hazardous when they exceed tolerance limits. Interactions among essential and non-essential elements are complex with unpredictable dose-response relationships, affecting toxic levels with safe dose level [40]. Even, Cobalt an essential nutrient for vertebrates, "becomes toxic at high exposures increasing reproductive problems, genetic disruptions, and cardiovascular pathologies" [41]. Otherwise, for values obtained for Ni, the accumulation concentration value ($\bar{X}$=1.21±0.02 ppm) is mostly lower than the literature values: the values are 7.95 ppm from *Peromyscus maniculatus* and 10.63 ppm from *Microtus pennsylvanicus* from oil sands and surface mines in Canada [22], 9.56 ppm from *Acomys cahirinus* on polluted areas from Egypt [23], 28.60 ppm from *Meriones persicus* on polluted areas in Iran [24]. Unlike, our value is higher than the some values: the values are 0.78 ppm for muscle from *Rombomys opimus* and 0.48 ppm from *Rattus norvegicus* on different localities at city in Iran [21] and 0.22 ppm from *Peromyscus gossypinus* on different contaminated areas in USA [25]. The accumulation concentration of Ni value for different tissue types, is shown remarkable similarly to the literature values: the values are 1.17 ppm for kidney from white-footed mice and 1.11 ppm from rice rats for similar rodents in the study by [35] in USA. Also, the value is 1.48 ppm for *Crocidura russula*'s liver

in the study by [3] in Portugal. This is because, Al and Ni are common natural constituents of soils and sediments, are poorly absorbed with limited accumulation in tissues like muscles and kidneys, do not biomagnify in food webs, and tissue concentrations are highly variable in healthy populations [42]. From this point on, it is inevitable that the similar accumulation depending on the specific tissue type.

The data obtained in this study is higher than some other studies but is rather low. For values obtained for Fe, the accumulation concentration value ($\bar{X}$=137.14±0.55 ppm) is lower than the literature values: the values are 148.05 ppm from *Peromyscus maniculatus* caught from Canada and quite lower than 187.37 ppm from *Acomys cahirinus* on polluted areas from Egypt [23]. But, slightly higher than, 117.65 ppm from *Microtus pennsylvanicus* from oil sands and surface mines in Canada [22]. Also, as expected our values are much lower than other tissues (such as the liver, kidney and bone) where the bioaccumulation is high. The values are 455.23 ppm for liver from yellow-necked mouse and 461.77 ppm from bank vole; 506.90 ppm for kidney from yellow-necked mouse and 394.73 ppm from bank vole; for bone 156.61 ppm from yellow-necked mouse and 138.98 ppm from bank vole, |for similar rodents in the study by [43] in Slovakia, the value is 203.40 ppm for *Microtus guentheri*'s whole body in the study by [44] in Bulgaria. "There are several cellular detoxification mechanisms involving iron, such as the induction of synthesis of proteins like cytochromes and ferritin, that protect mammalian cells from the toxic effects of both essential and non-essential metals" [45, 46], cytochromes are proteins that bind to it because they are necessary for metabolic processes in mammals and not to protect the organism from the harmful action of the metal. Unlike ferritin as it is a reserve protein, it may also exert a protective action on organisms against the possible deleterious effects of iron, which might explain our findings about to insignificant difference for localities. Indeed, in our study there was no significant difference between localities according to genders.

TABLE 6
Descriptive statistics of heavy metal concentrations and inclusion rates for soil of the localities

Loc.	Means and Ratio	B	Al	Cr	Mn	Fe	Co	Ni
	Soil	27.61	9585.69	9.38	165.35	39241.11	5.85	23.04
1	Muscle of the samples	0.18	68.97	0.56	2.86	136.77	0.20	1.22
	Inclusion rate (%)	**0.65**	**0.72**	**5.97**	**1.73**	**0.35**	**3.42**	**5.30**
	Soil	27.44	9716.05	10.50	174.67	33835.65	6.61	25.06
2	Muscle of the samples	0.18	73.79	0.56	2.17	137.25	0.23	1.21
	Inclusion rate (%)	**0.66**	**0.76**	**5.33**	**1.24**	**0.41**	**3.48**	**4.83**
	Soil	29.06	9650.33	10.27	151.51	43712.64	5.94	23.33
3	Muscle of the samples	0.18	74.56	0.56	2.18	137.34	0.20	1.21
	Inclusion rate (%)	**0.62**	**0.77**	**5.45**	**1.44**	**0.31**	**3.37**	**5.19**
	Soil	28.23	9625.36	10.03	163.94	38929.74	6.61	23.99
Total	Muscle of the samples	0.18	72.65	0.56	3.19	137.14	0.21	1.21
	Inclusion rate (%)	**0.64**	**0.75**	**5.58**	**1.95**	**0.35**	**3.18**	**5.04**

Loc.	Means and Ratio	Cu	Zn	As	Cd	Hg	^{206}Pb	^{208}Pb
	Soil	37.53	59.34	12.87	1.93	2.36	22.56	20.04
1	Muscle of the samples	1.92	24.29	0.12	0.68	0.76	0.37	0.29
	Inclusion rate (%)	**5.12**	**40.93**	**0.93**	**35.23**	**32.20**	**1.64**	**1.45**
	Soil	35.67	59.35	13.38	2.11	2.29	21.79	18.02
2	Muscle of the samples	1.92	24.09	0.12	0.69	0.76	0.38	0.28
	Inclusion rate (%)	**5.38**	**40.59**	**0.90**	**32.70**	**33.19**	**1.74**	**1.55**
	Soil	35.99	60.61	14.53	2.14	2.38	22.40	19.94
3	Muscle of the samples	1.91	24.42	0.12	0.68	0.76	0.38	0.28
	Inclusion rate (%)	**5.31**	**40.29**	**0.83**	**31.78**	**31.93**	**1.70**	**1.40**
	Soil	36.21	59.77	13.44	2.06	2.34	22.18	19.33
Total	Muscle of the samples	1.92	24.26	0.12	0.69	0.76	0.38	0.28
	Inclusion rate (%)	**5.30**	**40.59**	**0.89**	**33.50**	**32.48**	**1.71**	**1.45**

Inclusion rate: the value at the muscle tissue corresponds to the percentage of the value of the soil (%)

TABLE 7
Comparison of studies from the World by heavy metal accumulation in rodent muscle tissue.

Lit. [a]	Description of Location	Species [b]	B	Al	Cr	Mn	Fe	Co	Ni	Cu	Zn	As	Cd	Hg	^{206}Pb	^{208}Pb
ITS.	Near active mine sites/Turkey	*Microtus guentheri*	**0.18**	**72.65**	**0.56**	**3.19**	**137.14**	**0.21**	**1.21**	**1.92**	**24.26**	**0.12**	**0.69**	**0.76**	**0.38**	**0.28**
S1	Different land uses with city/Iran	*Rombomys opimus*	-	-	-	-	-	-	0.78	6.02	40.74	-	0.47	-	2.14	2.14
		Rattus norvegicus	-	-	-	-	-	-	0.48	7.57	63.76	-	-	-	2.51	2.51
S2	Oil sands and surface mines/Canada	*Peromyscus maniculatus*	-	9.86	0.61	1.23	148.05	4.07	7.95	9.66	48.29	-	-	-	32.63	32.63
		Microtus pennsylvanicus	-	7.00	0.34	1.26	117.65	2.28	10.62	7.99	47.82	-	-	-	44.95	44.95
S3	Polluted areas/ Egypt	*Acomys cahirinus*	-	-	-	2.05	187.37	-	9.56	9.56	55.97	-	-	-	7.17	7.17
S4	Polluted areas/ Iran	*Meriones persicus*	-	-	-	-	-	-	28.60	32.40	111.12	-	-	-	-	-
S5	Near abandoned mines/UK	*Apodemus sylvaticus*	-	-	-	-	-	-	-	-		0.75	-	-	-	-
		Clethrionomys glareolus	-	-	-	-	-	-	-	-		0.72	-	-	-	-
S6	Abandoned Lead Mine/UK	*Clethrionomys glareolus*	-	-	-	-	-	-	-	-	51.90	-	0.00	-	3.60	3.60
S7	Polluted areas/USA	*Peromyscus gossypinus*		12.02	0.50	0.97	-	0.22	0.22	4.25	-	-	0.04	0.04	0.13	0.13
S8	City's different habitats/Malawi	*Heliophobius argenteocinereus*	-	-	-	-	-	-	-	8.80	101.23	-	0.07	-	0.25	0.25
S9	Forest containing ash/ Finland	*Clethrionomys glareolus*	-	-	-	-	-	-	-	-	-	-	0.13	-	-	-
		Sorex araneus	-	-	-	-	-	-	-	-	-	-	0.41	-	-	-
S10	Near active mine sites/ Ireland	*Clethrionomys glareolus*	-	-	-	-	-	-	-	-	46.20	-	0.03	-	0.13	0.13
Ref.	No heavy metal pollution, relatively clean/Turkey	*Microtus guentheri*	**0.15**	**31.52**	**0.55**	**1.21**	**135.38**	**0.11**	**1.11**	**2.13**	**32.31**	**0.13**	**0.48**	**0.66**	**0.25**	**0.17**

[a] Literature are given according to date order and new ones are written on the top rows (ITS: In this study, S1: [21], S2: [22], S3: [23], S4: [24], S5: [33], S6: [27], S7: [25], S8: [26], S9: [49], S10: [28], Ref: Reference Area)
[b] The target organisms in all studies are rodent species.
All data in ppm (mg kg^{-1}) dry wt. When comparing in table, wet weight (w wt.) are converted to dry weight (dry wt.).
Also, if values are given separately for gender, as the mean of values are taken. Same way; Age groups, locality groups, etc. if they are, their arithmetic means are evaluated.

When the values for lead and cadmium, the most important pollutants, are examined: For values obtained for Pb (^{208}Pb and ^{206}Pb), the accumulation concentration values (respectively, $\bar{X}$=0.38±0.001 and 0.28±0.002 ppm) is higher than the most literature values for muscle. 0.13 ppm from *Peromyscus gossypinus* on different contaminated areas in USA [25] and 0.25 ppm from *Heliophobius argenteocinereus* trapped from City's different habitats in Malawi [26] and 0.13 ppm from *Clethrionomys glareolus* from near active mine sites at Ireland [28]. But, our value is lower than a few literature values. 32.63 ppm from *Microtus pennsylvanicus* and 44.95 ppm from *Peromyscus maniculatus* caught from oil sands and surface mines in Canada [22], 7.17 ppm from *Acomys cahirinus* on polluted areas from Egypt [23] and 3.60 ppm from *Clethrionomys glareolus* on abandoned lead mine in UK [27]. Also, the value is very lower than some literature values for other tissues. The value is 1.70 ppm for *Microtus guentheri*'s whole body in the study by [44] in the value is 1.0 ppm for game animal and small mammal's whole body in the study by [34] in Bulgaria, but higher than 0.37 ppm for *Microtus arvalis* and 0.27 ppm for *Microtus agrestis* in the study (for liver) by [29] in Slovenia. According to [47]: "It is also important to note

that the relationships between Cd and Pb residues in soil and in small mammals appear to be robust. The data were derived from several independent studies and included sites contaminated from a variety of sources. Despite this, the relationships between Cd and Pb residues in soil and in the body organs of rodents and shrews were mostly highly significant. This suggests that these relationships accommodate, to some extent, differences in Cd and Pb bio-availability which may occur because of inter-site variation in contaminant source or form". In future studies, small mammals may be suitable organisms possible for metals other than Cd and Pb and for non-metallic compounds which bio-accumulate. In his study; this has already been shown that antimony, selenium, mercury, arsenic, chromium residues in small mammal tissues are elevated above background levels on contaminated sites [48]. Results from present this study indicate that, the contamination which may from polluted areas and mines are much higher than the international reports. Even, for values obtained for Cd, the accumulation concentration value ($\bar{X}$=0.69±0.02 ppm) is higher than the most literature values: the values are 0.47 ppm for muscle from *Rombomys opimus* caught from different localities at city in Iran [21], 0.001 ppm from *Clethrionomys glareolus* on abandoned lead mine in UK [27], 0.04 ppm from *Peromyscus gossypinus* on different contaminated areas in USA [25] and 0.07 ppm from *Heliophobius argenteocinereus* trapped from City's different habitats in Malawi [26], 0.13 ppm from *Clethrionomys glareolus* and 0.41 ppm from *Sorex araneus* trapped on forest containing ash in Finland [49] and finally, 0.03 ppm from *Clethrionomys glareolus* from near active mine sites at Ireland [28]. Other studies on other tissues are as follows: the values are 0.02 ppm for liver from yellow-necked mouse and 0.05 ppm from bank vole; 0.07 ppm for kidney from yellow-necked mouse and 0.08 ppm from bank vole; for bone 2.53 ppm from yellow-necked mouse and 4.61 ppm from bank vole for similar rodents in the study by [43] in Slovakia. However, Cd concentration is absolutely higher than the literature: For liver value 0.10 ppm for *Microtus arvalis* in the study by [29] in Slovenia. Moreover, the value is lower than some literature values: the value is 1.40 ppm for *Microtus guentheri*'s whole body in the study by [44] in Bulgaria. But, the value is very higher than 0.1 ppm for game animal and small mammal's whole body in the study by [34] in Bulgaria. Similarly, for values obtained to Hg, the accumulation concentration value ($\bar{X}$=0.76±0.02 ppm) is very higher than the literature values for muscle and the other tissues: 0.04 ppm from muscle of *Peromyscus gossypinus* on different contaminated areas in USA [25]. Moreover, the values are 0.03 ppm for *Microtus agrestis* and similarly 0.03 ppm for *Microtus arvalis* for liver in the study by [29] in Slovenia. Also, the value is 0.05 ppm for game animal and small mammal's whole body in the study by [34] in Bulgaria. The available evidence from the literature indicates that toxic effects, "including reproductive changes, can be produced through exposure to some mercury types. Methyl mercury has been found to be more toxic than inorganic mercury in these terrestrial mammals. It has been shown to be a potent neurotoxin to most vertebrates, because they lack external barriers or internal detoxification systems" [50].

According to our data we obtained in the study areas; the values of Al and Mn are higher than world values. For values obtained for Al, the accumulation concentration value ($\bar{X}$=72.65±1.16 ppm) is quite higher than the literature values for rodent muscle: The values are 9.86 ppm from *Peromyscus maniculatus* and 7.00 ppm from *Microtus pennsylvanicus* from oil sands and surface mines in Canada [22] and 12.02 ppm from muscle of *Peromyscus gossypinus* on different contaminated areas in USA [25]. For other tissues, the values are aprox. 70-75 ppm for kidney from white-footed mice and aprox. 60-65 ppm from rice rats for similar rodents in the study by [35] in USA. Same way, for values obtained to Mn, the accumulation concentration value ($\bar{X}$=3.19±2.02 ppm) is higher than the literature values: the values are 1.23 ppm from *Peromyscus maniculatus* and 1.26 ppm from *Microtus pennsylvanicus* from oil sands and surface mines in Canada [22], 2.05 ppm from *Acomys cahirinus* on polluted areas from Egypt [23] and finally, 0.97 ppm from muscle of *Peromyscus gossypinus* on different contaminated areas in USA [25]. For other tissues, the value is 2.60 ppm for *Microtus guentheri*'s whole body in the study by [44] in Bulgaria. These results support hypotezis of "Mn levels are physiologically regulated in mammals and environmental increases are not generally related to high levels in tissues" [51].

As can be seen in Table 1; When the reference area and the examined localities are compared, the low reference values for B, Al, Co, Ni, Cd, Hg and Pb are statistically significant. On the other hand, the high reference values for Cu and Zn are statistically significant too. Moreover, for Cr, Mn and Fe there are no statistical difference between examined localities and reference area. According to these results, the accumulation values obtained for B, Al, Co, Ni, Cd, Hg and ^{206}Pb and ^{208}Pb are higher than the reference area.

CONCLUSIONS

Heavy metals detected in variable-valence and high quantity, it is natural origin, but should not be ignored that the accumulation in their living organism increase due to human activities. In particular, uncontrolled mining, construction and road constractions and inexperienced use of pesticides increases the value of this accumulation.

On the basis of the presented results of our study, the following conclusions can be made:

(a) These results indicate relatively low concentrations of some heavy metals (Cu and Zn) in the muscle tissues of levant voles collected in Çaltepe/Burdur at Turkey. The mines in the vicinity of the studied localities are considerable source of metals, especially of Pb, As, Co, Fe, Hg, Ni, Cu, Cr, Zn and Cd which are accumulated in the muscles of the small mammals inhabiting that area. In fact, this type of mining is considered the source of the most heavy metals [52]. Fact that the localities and the reference fields examined are evaluated together; with the exception of Cr, Mn, Fe and As, the differences between the localities and the reference area in terms of their accumulation values are statistically significant. Especially, accumulation values of B, Al, Co, Ni, Cd, Hg, ^{206}Pb and ^{208}Pb are considerably higher than the reference area, It is attracting attention for this toxic metals. In this case, total heavy metal accumulation values generally appear to be higher than the reference area. The concentrations found to be higher than similar studies in the world (especially Al, Mn, Cd, Hg) and reference area (B, Al, Co, Ni, Cd, Hg, ^{206}Pb and ^{208}Pb) in a significant proportion of the muscles of small mammal individuals. Furthermore, the most of these elements are known to be very toxic metals. These findings indicate that the majority of small mammals trapped in the vicinity of the mines are at risk from toxic effects due to high bioaccumulation of heavy metals in the subterranean vertebrate organism. The accumulation concentration of some metals is lower than the reference values. This may be due to the inhibition of the metabolism of these low-abundance metals and the uptake of tissue by other metals which may be toxic.

(b) Otherwise, when evaluated individually for each metal; there is no statistically significant difference between the gender groups in terms of heavy metal accumulation values for both for localities and reference area. This shows us that the genders are exposed to similar effects in every way. Perhaps it can be said that there is no significant difference between genders, especially in terms of accumulating toxic metals.

(c) Another important point for this study, a negative and comparatively weaker correlation was found between the average Co accumulation and the distance from mine resources for individuals and soil samples. The pollution of cobalt, the closer to the mine resource substantially increase is remarkable. Especially when considered for Co, the accumulation values in the soil and muscle are increasing as the mine resources are approached. As soon, there has been considerable research where small mammals are utilized as sentinels of environmental metal exposure for resident wildlife on both active and former smelting and mining sites. Metal and metalloid levels measured in select tissues and whole bodies of small mammals living in proximity to smelting sites [53] active mining sites [54], abandoned mining sites [55] mine tailing piles [56] and sewage sludge-treated mine waste [57], indicate wildlife living in proximity to metal-contaminated areas are more likely to have elevated levels of metals in their tissues. Similar to literature, it has been determined only for Co. But, for other heavy metals accumulation, there is no difference among the individuals and soils.

(d) According to the type of soil (cambisol) in the area studied; Almost all of the heavy metals studied (except Cd and Hg) are below the world average. This situation should not create the illusion that these lands may be clean. Values of the Cd and Hg are above the upper limit. This may be indicative of Cd and Hg contamination, especially from mines. As is known, marble mines can be a source of Cd in particular.

(e) When we look at the transition from soil to organism; Some metals (such as Cd, Cr, Hg), which are found less in the soil on study areas, but accumulate in the muscle tissue much higher than those in abundance metals (such as Al, Fe). When inclusion rates (the value at the muscle tissue corresponds to the percentage of the value of the soil) were evaluated; the highest value is Zn with 40.59% and the lowest value is Fe with 0.35%. These ratios are not surprising, as these metals are necessary for metabolic activities. However, it is remarkable that toxic metals such as Cd, Hg and Cr are high (respectively, 33.50%, 32.48 and 5.58 for total). The reasons for the transition presence of such toxic metals in from soil to organisms at such high rates should be investigated with larger scale and interdisciplinary studies.

(f) Finally, on the basis of the results from the first record for heavy metal levels in this species living in this region and from soils. The values show that, the heavy metal pollution (especially Al, Mn, Cd, Hg) began at the vicinity of Çaltepe which is approximately 1200 m altitude. In this case, probably, is thought to be due to industry (especially mine sources, like large marble quarries and stone quarries) and maybe agricultural activities (like pesticides and engine oil). For better understanding of the situation of the region it will be appropriate to follow the target species *M. guentheri* and its ecological relations for many years.

ACKNOWLEDGEMENTS

This work was partly supported by the Akdeniz University Scientific Research Projects Coordination Unit.

REFERENCES

[1] Siegel, F.R. (2002) Environmental Geochemistry of Potentially Toxic Metals. Berlin, Heidelberg: Springer.

[2] Sánchez-Chardi, A., López-Fuster, M., Nadal, J. (2007) Bioaccumulation of lead, mercury, and cadmium in the greater white-toothed shrew, *Crocidura russula*, from the Elba Delta (NE Spain): sex- and age-dependent variation. Environmental Pollution. 145, 7-14.

[3] Sánchez-Chardi, A., Marques C.C., Nadal, J., Mathias, M.L. (2007) Metal bioaccumulation in the greater white-toothed shrew, *Crocidura russula*, inhabiting an abandoned pyrite mine site. Chemosphere. 67, 121-130.

[4] Mertens, J., Luyssayert, S., Verbeeren, S., Vervaeke, P., Lust, N. (2001) Cd and Zn concentrations in small mammals and willow leaves on disposal facilities for dredged material. Environmental Pollution. 115, 17-22.

[5] Cooke, J.A., Andrews, S.M., Johnson, M.S. (1990) Lead, zinc, cadmium and fluoride in small mammals from contaminated grassland established on fluorspar tailings. Water Air and Soil Pollution. 51, 43-54.

[6] Schleich, C.E., Beltrame, M.O., Antenucci, C.D. (2010) Heavy metals accumulation in the subterranean rodent *Ctenomys talarum* (Rodentia: Ctenomyidae) from areas with different risk of contamination. Folia Zoologica. 59(2), 108-114.

[7] Yuan, C.G., T.F. Wang, Song, Y.F., Chang, A.L. (2010) Total mercury and sequentially extracted mercury fractions in soil near a coal-fired power plant. Fresen. Environ. Bull. 19, 2857-2863.

[8] Jusufi, K., Stafilov, T., Vasjari, M., Korça, B., Halili, J., Berisha, A. (2016) Determination of heavy metals by ICP-AES in the agricultural soils surrounding Kosovo's power plants. Fresen. Environ. Bull. 25, 1313-1321.

[9] Riberg, L., Nordberg, G.F., Vouk, V.B., Kessler, E. (1986) Handbook on the toxicology of metals. Amsterdam: Elsevier.

[10] Ido, T., Nogawa, K., Hochi, Y., Hayano, M., Honda, R., Tsuritani, I., Ishizaki, M. (1993) The renal handling of calcium and phosphorus in environmental cadmium-exposed subjects with renal dysfunction. Journal Applied Toxicology. 13(1), 43-47.

[11] Haider, S., Naithani, V., Barthwal, J., Kakkar, P. (2004) Heavy metal content in some therapeutically important medicinal plants. Bulletin of Environmental Contamination and Toxicology. 72(1), 119-127.

[12] Angelova, V., Ivanova, R., Delibaltova, V., Ivanov, K. (2004) Bio-accumulation and distribution of heavy metals in fiber crops (flax, cotton, and hemp). Industrial Crops and Products. 19(3), 197-205.

[13] Jusufi, K., Stafilov, T., Vasjari, M., Korça, B., Halili, J., Berisha, A. (2017) Measuring the presence of heavy metals and their bioavailability in potato crops around Kosovo's power plants. Fresen. Environ. Bull. 26, 1682-1686.

[14] Amek-Poprawa, M., Sawicka-Kapusta, K. (2003) Damage to the liver, kidney, and testis with reference to burden of heavy metals in yellow-necked mice from areas around steelworks and zinc smelters in Poland. Toxicology. 186(1-2), 1-10.

[15] Hore, R.F., Rattner, B.A. (2001) Ecotoxicology of wild mammals. London: John Wiley & Sons.

[16] Thompson, R.A., Schroder, G.D., Conner, T.H. (1988) Chromosomal aberrations in the cotton rat, *Sigmodon hispidus*, exposed to hazardous waste. Environmental and Molecular Mutagenesis. 11, 359-367.

[17] Sheffield, S.R., Sawicka-Kapusta, K., Cohen, J.B., Rattner, B.A. (2001) Rodentia and Lagomorpha. In: Ecotoxicology of Wild Mammals. Shore, R.F. and Rattner, B.A. (Eds.) England, Chichester: John Wiley & Sons, 215-314.

[18] McMurry, S.T., Lochmiller, R.L., McBee, K., Qualls, Jr., C.W. (1999) Indicators of immunotoxicity in populations of cotton rats (*Sigmodon hispidus*) inhabiting an abandoned oil refinery. Ecotoxicology and Environmental Safety. 42(3), 223-235.

[19] Minamia, T., Yamazakia, H., Ohamab, N. (2009) Accumulation of heavy metals in the organs of wild rodents. Annual reports by Research Institute for Science and Technology. 1(21), 11-17.

[20] Millán, J., Mateo, R., Taggart, M.A., López-Bao, J.V., Viota, M., Monsalve, L., Camarero, P.R., Blázquez, E., Jiménez, B. (2008) Levels of heavy metals and metalloids in critically endangered Iberian lynx and other wild carnivores from Southern Spain. Science of the Total Environment. 399, 193-201.

[21] Zarrintab, M., Mirzaei, R. (2017) Evaluation of some factors influencing on variability in bioaccumulation of heavy metals in rodents species: *Rombomys opimus* and *Rattus norvegicus* from central Iran. Chemosphere. 169, 194-203.

[22] Rodriguez-Estival, J. and Smits, J.E. (2016) Small mammals as sentinels of oil sands related contaminants and health effects in northeastern Alberta, Canada. Ecotoxicology and Environmental Safety. 124, 285-295.

[23] Mohallal, E.M.E. and Younes, M.I. (2015) Concentration of Heavy Metals in The Tissues of Spiny Mouse As Bio-Indicators Of Pollution Under Different Environmental Conditions In Egypt. Egyptian Journal of Desert Research. 65(1), 63-76.

[24] Okati, N. and Rezaee, M. (2013) Heavy Metals Concentrations in Different Tissues of Persian Jird (*Meriones persicus*) In Sistan Region. International Research Journal of Applied and Basic Sciences. 5(10), 1272-1276.

[25] Reinhart, B.D. (2003) The use of small mammals as indicators of heavy metal bioavailability in a contaminated riparian zone. Master of Science Thesis, University of South Carolina-Aiken, Athens, Georgia, 1-50.

[26] Umbera, R., Baruš, V., Tenora, F. (2003) Heavy metals in the silvery mole-rat, *Heliophobius argenteocinereus* (Bathyergidae, Rodentia) from Malawi. Folia Zoologica. 52(2), 149-153.

[27] Milton, A., Cooke, J.A., Johnson, M.S. (2003) Accumulation of lead, zinc, and cadmium in a wild population of *Clethrionomys glareolus* from an abandoned lead mine. Archives of Environmental Contamination and Toxicology. 44(39), 405-411.

[28] Milton, A. and Johnson, M. (1999) Biomonitoring of contaminated mine tailings through age accumulation of trace metals in the bank vole (*Clethrionomys glareolus*). Journal of Environmental Monitoring. 1(3), 219-225.

[29] Al Sayegh Petkovšek, S., Kopušar, N., Kryštufek, B. (2014) Small mammals as biomonitors of metal pollution: a case study in Slovenia. Environmental Monitoring and Assessment. 186, 4261-4274.

[30] Goyer, R.A. (1997) Toxic and essential metal interactions. Annual Reviews of Nutrition. 17, 37-50.

[31] López Alonso, M., Prieto Montana, F., Miranda, M., Castillo, C., Hernandez, J., Benedito, J.L. (2004) Interactions between toxic (As, Cd, Hg and Pb) and nutritional essential (Ca, Co, Cr, Cu, Fe, Mn, Mo, Ni, Se, Zn) elements in the tissues of cattle from NW Spain. Biometals. 17, 389-397.

[32] Lavado, R., Ureña, R., Martin-Skilton, R., Torreblanca, A., del Ramo, J., Raldúa, D., Porte, C. (2006) The combined use of chemical and biochemical markers to assess water quality along the Ebro River. Environmental Pollution. 139(2), 330-339.

[33] Erry, B.V., Macnair, M.R., Meharg, A.A., Shore, R.F. (2005) The distribution of arsenic in the body tissues of wood mice and bank voles. Archives of Environmental Contamination and Toxicology. 49(4), 569-576.

[34] Metcheva, R., Teodorova, S., Topashka-Ancheva, M. (2003) A comparative analysis of the heavy metal loading of small mammals in different regions of Bulgaria I: monitoring points and bioaccumulation features. Ecotoxicology and Environmental Safety. 54(2), 176-87.

[35] Smith, P.N., Cobb, G.P., Harper, F.M., Adair, B.M., McMurry, S.T. (2002) Comparison of white-footed mice and rice rats as biomonitors of polychlorinated biphenyl and metal contamination. Environmental Pollution. 119, 261-268.

[36] Saunders, J.R., Knopper, L.D., Koch, I., Reimer, K.J. (2010) Arsenic transformations and biomarkers in meadow voles (*Microtus pennsylvanicus*) living on an abandoned gold mine site in Montague, Nova Scotia, Canada. Science of the Total Environment. 408(4), 829-835.

[37] Klein, D.H. (1972) Mercury and other metals in urban soils. Environmental Science & Technology. 6(6), 560-562.

[38] Rodríguez Martín, J.A., Arias, M.L., Grau Corbí, J.M. (2006) Heavy metals contents in agricultural topsoils in the Ebro basin (Spain) Application of the multivariate geostatistical methods to study spatial variations. Environmental Pollution. 144(3), 1001–1012.

[39] Sánchez-Chardi, A. and Lopez-Fuster, M.J. (2009) Metal and metalloid accumulation in shrews (Soricomorpha, Mammalia) from two protected Mediterranean coastal sites. Environmental Pollution. 157, 1243-1248.

[40] Nordberg, G.F., Gerhardson, L., Broberg, K., Mumtaz, M., Ruiz, P., Fowler, B.A. (2007) Interactions in metal toxicology. In: Nordberg, G.F., Fowler, B.A., Nordberg, M., Friberg, L. (Eds.) Handbook on the Toxicology of Metals, 3rd. Ed. Amsterdam: Elsevier, 117-145.

[41] Gál, J., Hursthouse, A., Tatner, P., Stewart, F., Welton, R. (2008) Cobalt and secondary poisoning in the terrestrial food chain: Data review and research gaps to support risk assessment. Environment International. 34(6), 821-838.

[42] Jarzyńska, G. and Falandysz, J. (2011) Selenium and 17 other largely essential and toxic metals in muscle and organ meats of Red Deer (*Cervus elaphus*)-Consequences to human health. Environment International. 37(5), 882-888.

[43] Martiniaková, M., Omelka, R., Grosskopf, B., Jančová, A. (2010) Yellow-necked mice (*Apodemus flavicollis*) and bank voles (*Myodes glareolus*) as zoomonitors of environmental contamination at a polluted area in Slovakia. Acta Veterinaria Scandinavica. 52(1), 52-58.

[44] Chassovnikarova, T., Metcheva, R., Dimitrov, K. (2005) *Microtus guentheri* (Danford & Alston) (Rodentia, Mammalia): a bioindicator species for estimation of the influence of polymetal dust emissions. Belgian Journal of Zoology. 135(2), 135-137.
[45] Lopes, P.A., Viegas-Crespo, A.M., Nunes, A.C., Pinheiro, T., Marques, C., Santos, M.C., Mathias, M.L. (2002) Influence of age, sex, and sexual activity on trace element levels and antioxidant enzyme activities in field mice (*Apodemus sylvaticus* and *Mus spretus*) Biological Trace Element Research. 85, 227-239.
[46] Pereira, R., Pereira, M.L., Ribeiro, R., Gonçalves, F. (2006) Tissues and hair residues and histopathology in wild rats (*Rattus rattus* L.) and Algerian mice (*Mus spretus* Lataste) from an abandoned mine area (southeast Portugal). Environmental Pollution. 139(3), 561-575.
[47] Shore, R.F. (1995) Predicting cadmium, lead and fluoride levels in small mammals from soil residues and by species-species extrapolation. Environmental Pollution. 88(3), 333-340.
[48] Ainsworth, N., Cooke, J.A., Johnson, M.S. (1990) Distribution of antimony in contaminated grassland: 2--Small mammals and invertebrates. Environmental Pollution. 65(1), 79-87.
[49] Lodenius, M., Soltanpour-Gargari, A., Tulisalo, E., Henttonen, H. (2002) Effects of ash application on cadmium concentration in small mammals. Journal of Environmental Quality. 31(1), 188-192.
[50] Klaassen, C.D., Amdur, M.O., Doull, J. (1986) Toxicology, III ed. The Basic Science of Poisons, New York NY: Macmillan.
[51] Beardsley, A., Vagg, M.J., Beckett, P.H.T., Sansom, B.F. (1978) Use of field vole (*M. agrestis*) for monitoring potentially harmful elements in environment. Environmental Pollution. 16(1), 65-71.
[52] Martin, M.H. and Coughtrey, P.J. (1982) Biological Monitoring of Heavy Metal Pollution. London: Applied Science Publishers.
[53] Ismail, A., Roberts, R.D. (1992) Arsenic in small mammals. Environmental Technology. 13, 1091-1095.
[54] Smith, G.J., Rongstad, O.J. (1982) Small mammal heavy metal concentrations from mined and control sites. Environmental Pollution (Series A). 28, 121-134.
[55] Erry, B.V., Macnair, M.R., Meharg, A.A., Shore, R.F. (2000) Arsenic contamination in wood mice (*Apodemus sylvaticus*) and bank voles (*Clethrionomys glareolus*) on abandoned mine sites in southwest Britain. Environmental Pollution. 110, 179-187.
[56] Cloutier, N.R., Clulow, F.V. (1985) Metal (Cu, Ni, Fe, Co, Zn, Pb) and Ra-226 levels in meadow voles *Microtus pennsylvanicus* living on nickel and uranium mine tailings in Ontario, Canada: environmental and tissue levels. Environmental Pollution. 10(1), 19-46.
[57] Alberici, T.M., Sopper, W.E., Storm, G.L., Yahner, R.H. (1989) Trace metals in soil, vegetation, and voles from mine land treated with sewage sludge. Journal of Environmental Quality. 18, 115-120.
[58] Kabata-Pendias, A. (2011) Trace elements in soils and plants. CRC Press, Taylor & Francis Group, NW. 1-505.
[59] Lepp, N.W. (2012) Effect of Heavy Metal Pollution on Plants: Effects of Trace Metals on Plant Function. Springer Science & Business Media. 1-352.
[60] Burdur Provincial Environmental Situation Report (2009) Republic of Turkey, Burdur Governorship Provincial Environment and Forestry Directorate. Burdur/Turkey, 1-386.

Received: **14.09.2017**
Accepted: **10.11.2017**

CORRESPONDING AUTHOR

Mustafa Yavuz
Department of Biology,
Akdeniz University,
07058 Antalya – Turkey

e-mail: myavuz2006@gmail.com

© by PSP Volume 27 – No. 2/2018 pages 1122-1130 Fresenius Environmental Bulletin

ADSORPTION REMOVAL OF METHYLENE BLUE FROM AQUEOUS SOLUTION USING CORNCOB ACTIVATED CARBON: EQUILIBRIUM AND KINETICS STUDIES

Xuefeng Wei[1,2,*], Xiaoyang Wan[1], Fangzhou Liu[1], Juan Miao[1], Shufa Zhu[1], Qingshan Niu[1,2]

[1]College of Chemical Engineering & Pharmaceutics, Henan University of Science and Technology, Luoyang 471003, P.R. China
[2]Luoyang key laboratory of industrial waste resource, Henan University of Science and Technology, Luoyang 471003, P.R. China

ABSTRACT

The activated carbon was prepared from corncob using H_3PO_4 as chemical activating reagent. The H_3PO_4 activated corncob carbon (HACC) was characterized by nitrogen adsorption instrument, infrared spectrum (FTIR) and Boehm titration method. The optimum conditions of methylene blue (MB) sorption on HACC were found to be: 0.025g HACC in 50 mL of 25mg·L^{-1} with contact time of 3h and pH 7. According to adsorption isotherm studies, the Frumkin, Freundlich and D-R, isotherms were proved to be the best fit for our experimental data, in comparison to Langmuir and Temkin models. The mean free adsorption energy was 16.0~18.1 kJ·mol^{-1}, indicating it was a feasible, spontaneous and chemical adsorption process. Four equations, namely Morris-Weber, Pseudo-first-order, Pseudo-second-order and Elovich have been used in order to determine the kinetics of removal process. The collected kinetic data showed that pseudo-second-order equations controlled the adsorption process.

KEYWORDS:
corncob, activated carbon, methylene blue, isotherm, adsorption kinetics

INTRODUCTION

Dyes have been extensively used in industrial fields, including paper, textile, printing, wools, etc. In general, effluents containing such dye are difficult to deal with, where there are great varieties of dyestuffs, complex composition, high COD and poor biodegradability. The wastewater may be carcinogens and toxic which are of serious health risk to human beings. There are various methods used for the removal of dyes including electrolysis[1], biodegradation [2], adsorption [3] etc. The adsorption process, among all above-mentioned methods, is an effective means for the dye removal due to its ease of operation, simple equipments, low cost of application and insensitivity to toxic substances.

Activated carbon (AC) is the most common adsorbent for removing varieties of organic contaminants. However, the raw materials of commercially activated carbon are from coal, petroleum, fossil sources and other non-renewable energy, which limits its application. Therefore, there is a need to utilize readily alternative and less expensive materials to manufacture activated carbon. In the past years, a number of workers have found out the feasibility of using agricultural or industrial wastes, for instance, wood apple outer shell [4], silkworms feces [5], rice husk [6], sewage sludge [7], olive stones [8], olive mill waste [9] and leaves [10] as cheap adsorbents.

Over the years, several attempts have been made to produce adsorbents from different waste materials for dye removal. Methylene blue (MB) is selected as a target contaminant for evaluating the potential of biomass-based activated carbon to remove dye from wastewater. MB is a textile azo (cationic) dye. The maximum removal of MB from waste water was 98.9% on activated carbon prepared from wood apple carbon (ZAWAC) by chemical activation with $ZnCl_2$ [4]. Bamboo was used to produce activated carbon by physiochemical activation with KOH. The maximum monolayer adsorption capacity of MB was 454.2 mg·g^1[11]. The removal of MB was 96.7 % on activated carbon derived from pomelo peel by activation with water vapor [12].

In this work, we used H_3PO_4 activated corncob carbon (HACC) as adsorbent to remove the MB dye from waste water. The main objects of this paper are: (i) to evaluate the feasibility of employing HACC as an adsorbent for the removal of MB dye; (ii) to characterize the activated carbon developed from corncob; (iii) to determine the applicability of various isotherm and kinetics models based on R^2 value to find out the best-fit equation and describe the rate controlling mechanism. This work could significantly contribute towards the application of biomass-based activated carbon to remove dye from waste water.

MATERIALS AND METHODS

Preparation of the activated carbon. Raw material (corncob) was procured locally, washed, dried, and sieved to desired mesh size (1-2 mm). A

certain amount of corncob was soaked with 50% H_3PO_4 at impregnation ratio of 1:3. The sample was held at the activation temperature (70℃) for 24 h. The mixture after drying was carbonized in an oven at 450℃ for 2 h. Thus, the activated product was cooled to room temperature and washed with 0.1mol·L^{-1} HCl in an oven at 70℃ for 3 h. Finally, the carbon was repeatedly washed with deionized (DI) water until the pH of the washings reach 7.

Characterization of the activated carbon. Textural characterization of the HACC was carried out by N_2 adsorption at 77K using Autosorb-iQ (Quantachrome Corporation, USA). The Brunauer-Emmett-Teller (BET) surface area and pore structure were then determined. The surface functional groups were detected by Fourier transform infrared spectroscope (FTIR) using Nicolet IS10 (Thermo Electron Corporation, USA). Boehm titrations (Boehm, 2002) were employed for determining acidic and basic surface oxides. The iodine number was measured by GB/T12496.8-1999 (China).

Batch equilibrium studies. The adsorption of methylene blue (MB) from aqueous solution was conducted in 250 mL flasks with 100 mL MB solution, and weighted HACC were added. The mixture was stirred in thermostated water bath at temperature of the experiment at 160 rpm. The concentration of MB after adsorption was measured using spectrophotometer (722N, Shanghai Precision Scientific Instrument Company, China) at λ_{max} of 665nm.

The amount of MB adsorbed, q_t (mg·g^{-1}) and removal efficiency (R) attained by the corncob activated carbon were calculated as:

$$q_t = \frac{C_0V_0 - C_tV_t}{m} \quad (1)$$

$$R = \frac{C_e}{C_0} \times 100\% \quad (2)$$

where q_t is the amount of MB adsorbed per unit weight of HACC at time t (mg·g^{-1}) , C_0, C_t and C_e are the initial, t time and equilibrium concentrations, respectively (mg·L^{-1}). V_0 and V_t are the volumes at the initial and t time of the MB concentrations in solution, respectively (L). m is the weight of HACC used (g).

RESULTS AND DISCUSSION

Characterization of the prepared activated carbon. Surface area and porosity characteristics of the corncob activated carbon. The results for pore structure parameters of the HACC and commercial activated carbon (CAC) are presented in Table 1. That most of the CAC pores are in the misoporous range. The specific surface area of HACC sample was determined as1160.838 m^2·g^{-1}, which was greater than that of CAC. HACC had lager macropore and mesopore volume.

TABLE 1
Pore structure parameters of HACC and CAC.

Sample	$S_{B.E.T.}$/ m^2·g^{-1}	V_{total}/ cm^3·g^{-1}	$V_{micropore}$/ cm^3·g^{-1}	$V_{mesopore}$/ cm^3·g^{-1}	$V_{macropore}$/ cm^3·g^{-1}	Microporosity (%)
CAC	122.303	0.107	0.044	0.024	0.038	41.12
HACC	1160.838	0.823	0.186	0.342	0.295	22.60

Fig.1 shows the nitrogen adsorption-desorption isotherms of HACC and CAC at 77 K. It was clear that the amount of nitrogen adsorbed by the HACC was higher than CAC due to its high total pore volume and porosity. The isotherm of CAC adjusted to type I isotherm, indicating the presence of microporous [13]. The isotherm of the HACC exhibited type IV isotherm. The isotherm presented a noticeable increase in the N_2 adsorption capacity throughout the pressure range. The step in the adsorption branch combined with the decline in the desorption branch is an indication of mesoporosity. There was a hysteresis, which indicated capillary condensation. This phenomenon is related to wall destruction, turning micropores into mesopores, and not to the creation of new pores [14]. High BET surface area and well developed pore structure and affluent inner pores obtained from HACC is promising compared to CAC.

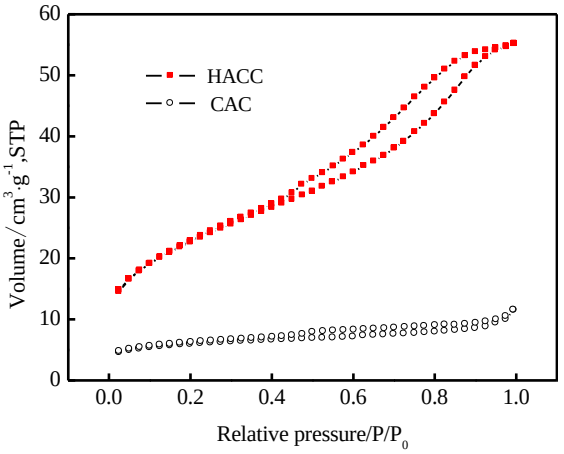

FIGURE 1
Nitrogen adsorption/desorption isotherms

IR spectroscopy. Fig.2 illustrates the FT-IR spectra of HACC and CAC. For the CAC, it was noted that in Fig.2 (a) the absorption band at 1029cm^{-1} was due to the C-O stretching vibration. O-H bending C-O stretch of dimmers was around 1423 cm^{-1}[15]. For HACC, it can be observed from Fig.2 (b) that C-O-C of aliphatic ethers was about 1213cm^{-1}. The band at 1583cm^{-1} was assigned to the carboxylate ion groups stretching vibration. The band at 1695cm^{-1} was associated with C=C stretching vibration in aromatic rings. The band at 1022cm^{-1} was attributed to the C-H out-of-plane bending vibrations, with C=C stretching [4, 13]. The FTIR analysis indi-

cated that hydroxyl, carbonyl or aromatic rings compounds may exist on the surface of HACC.

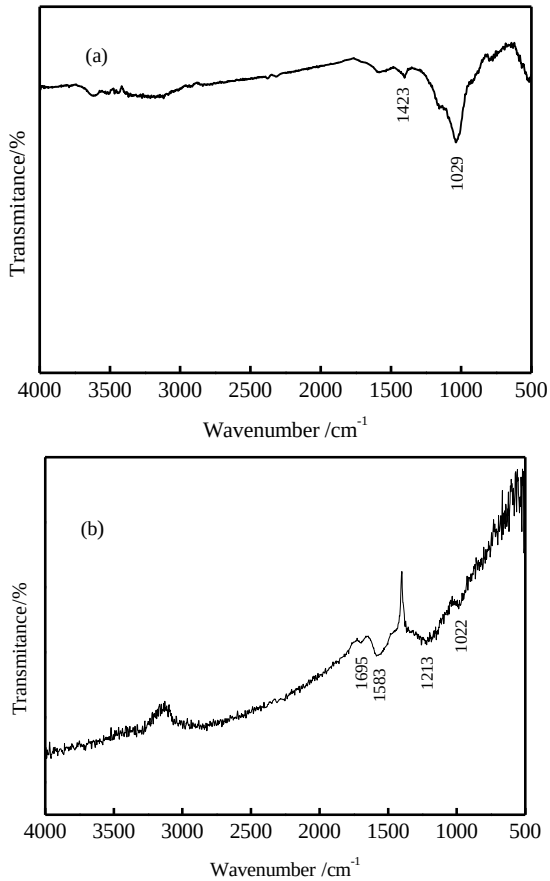

FIGURE 2
Infrared spectrum of CAC (a) and HACC (b)

Oxygen functional groups content (Boehm). Quantitative analysis of the acidic surface groups was conducted by Boehm's titration. The results of Boehm titrations for HACC and CAC are listed in Table 2. It was demonstrated from Table 2 that the negligible presence of acidic functional groups on the surface of commercial activated carbon. The results were in agreement with the FTIR data, since no absorption peaks associated with acidic functional groups were detected. Compared with CAC, the remarkable increase in the amount of acidic type (0.500mmol·g^{-1}), especially the carboxylic groups, is probably responsible for the relatively high hydrophilicity and cation exchange capacity and adsorption mechanism may based on ionic interaction [16].

Iodine number. The iodine numbers of CAC and HACC are presented in Table 2. Furthermore, the higher value in Table 2 in case of HACC is an additional evidence for deciding that this sample is a successful result of the activation process [5].

Study of adsorption parameters. Initial dye concentration and temperature. Fig.3 shows the effect of temperature on the adsorption of MB dye at different initial dye concentration onto HACC. It can be noticed that the removal of dye by adsorption on HACC was found to be increased with increased temperature (303.15K~323.15K) and then to slow-down with increased temperature (323.15K~343.15K). It may due to the increase of the rate of diffusion of the adsorbate molecules across the external boundary layer and the internal pores of the adsorbent particle, whose decreases in case viscosity of the solution for high temperature. In fact, a possible mechanism of interaction is the reaction between the functional groups such as lactonic and carbonylic of the corncob activated carbon and the cationic group in the dye molecule, hydrogen bond may occur on this reaction, such a reaction could be affected by temperature [17].

TABLE 2
The results of iodine adsorption value and Boehm titration of CAC and HACC.

Sample	Carboxylic groups /mmol·g^{-1}	Lactonic groups /mmol·g^{-1}	Phenolic groups /mmol·g^{-1}	Iodine numbers /mg·g^{-1}
CAC	—	0.102	0.126	750.2
HACC	0.256	0.244	—	141.2

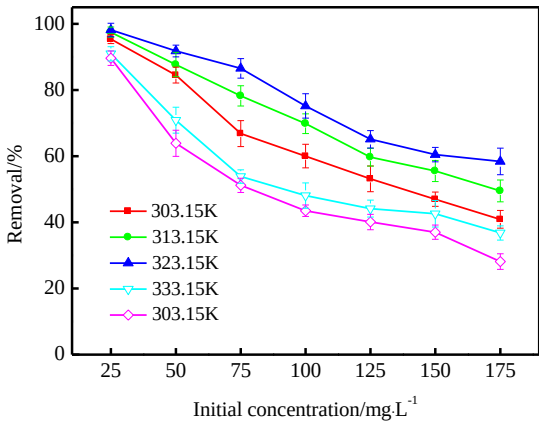

FIGURE 3
Effect of temperature and initial concentration on adsorption efficiency of MB (adsorption time of 3h)

Effect of initial solution pH. Change of the adsorption removal of MB on HACC with pH is represented in Fig. 4. It was observed that the maximum adsorption occurred at pH 7and 8. MB is a basic dye. In water, it produces cation (C^+) and reduced ions (CH^+). In lower pH, the low adsorption of dye displays possibility of development of positive charge at activated carbon surface, which subdues the adsorption of MB [18]. In addition, the lower adsorption capacity of corncob activated carbon observed at acidic pH is due to the competition between the excess H_3O^+ ions and the positively charged dye ions for the adsorption sites [15]. Generally, the adsorption of organic molecules by activated carbon is difficult to adsorb when pH is greater than 9, a similar result was reported in our study. However, in the neutral medium the formation of electric double

TABLE 3
Regression equations for isotherms

T/K		303.15	313.15	323.15	333.15	343.15
Langmuir	q_{max}/mg·g^{-1}	131.6	139.3	150.8	107.6	100.3
	K_L/L·mg^{-1}	0.048	0.083	1.012	0.311	0.299
	R_L	0.106	0.064	0.006	0.018	0.019
	R^2	0.8914	0.8712	0.9314	0.8213	0.8177
Freundlich	1/n	0.28	0.27	0.24	0.28	0.267
	K_F/L·g^{-1}	45.09	53.06	63.99	33.90	32.97
	R^2	0.9615	0.9634	0.9434	0.9363	0.9182
D–R	$q_m \times 10^4 / mol \cdot g^{-1}$	9.37	10.10	10.39	8.31	7.22
	$k' \times 10^4 / mol^2 \cdot kJ^2$	19.6	18.3	15.4	18.0	16.2
	E/kJ·mol^{-1}	15.97	16.53	18.20	16.67	17.57
	R^2	0.9688	0.9436	0.9114	0.9103	0.8933
Temkin	B_1	26.66	27.61	25.43	23.07	20.66
	K_T/L·mg^{-1}	3.53	5.56	12.71	2.01	2.21
	R^2	0.8513	0.8339	0.8282	0.8146	0.7906
Frumkin	α	0.68	0.65	0.62	0.81	0.97
	lnk	7.64	7.65	7.55	7.71	7.79
	ΔG/kJ·mol^{-1}	19.26	19.91	20.29	21.37	22.21
	R^2	0.9901	0.9928	0.9951	0.9718	0.9413

layer changes its polarity and consequently the dye may uptake increases [18]. At neutral and alkaline pH, corncob activated carbon surface charge may be deprotonated, it could be inferred that there was an interaction between MB and adsorbent [15].

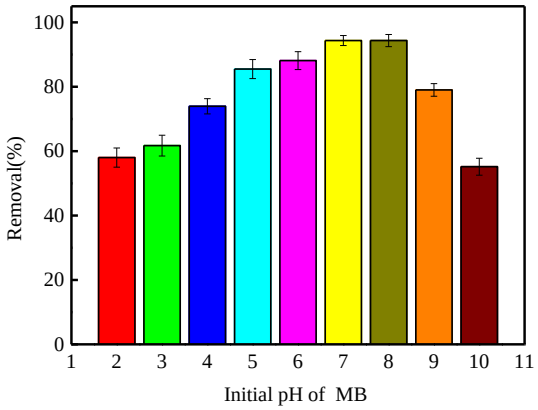

FIGURE 4
Removal of methylene blue with different pH (temperature of 313.15K)

Isotherm analysis. In this work, the equilibrium data for MB on HACC was fitted with the Langmuir, Freundlich, D-R, Temkin and Frumkin models. The constant parameters and correlation coefficient (R^2) were summarized in Table 3.

Langmuir isotherm. Langmuir isotherm is based on the assumption of a monolayer adsorption by the adsorbent with the same energy of active sites and there is no interaction between the adsorbed species. Langmuir isotherm is calculated as:

$$\frac{1}{q_e} = \frac{1}{q_{max}} + \frac{1}{K_L q_{max} C_e} \quad (3)$$

where q_e is the amount of adsorbate adsorbed at equilibrium (mg·g^{-1}), q_{max} is the maximum monolayer adsorption capacity of the adsorbent (mg·g^{-1}), Ce is the equilibrium concentration of adsorbate (mg·L^{-1}) and K_L is the Langmuir adsorption constant related to the free energy adsorption (L·mg^{-1}) [19]. Fig. 4 shows the Langmuir plots for the removal of MB at different temperatures.

A further analysis of the Langmuir model could be made on the basis of a dimensionless constant separation factor or equilibrium parameter R_L, given by:

$$R_L = \frac{1}{1 + K_L C_0} \quad (4)$$

where C_0 is the initial MB concentration (mg·L^{-1}). The value of R_L indicates the adsorption process which is unfavorable ($R_L > 1$), linear ($R_L = 1$), favorable ($0 < R_L < 1$), or irreversible (RL = 0) [17,19]. The constants and R_L values are listed in Table 3.

Jaynes and Boyd [20] suggested that the adsorption satisfy with the isotherm model when the value of the correlation coefficient is greater than 0.89. The R^2 values in Table 3 were less than 0.89, indicating that the isotherms were not fit with Langmuir model. The R_L values were in between 0 and 1, demonstrating that the adsorption of MB on corncob activated was favorable.

Freundlich isotherm. The Freundlich isotherm utilizes for adsorption on a heterogeneous surface energy system where the binding sites are not equivalent. The equation could be conveyed as:

$$\lg q_e = \lg K_F + (1/n) \lg C_e \quad (5)$$

where K_F ($L \cdot g^{-1}$) and n are isotherm constants which indicate the capacity and intensity of the adsorption, respectively [19]. Fig. 6 shows the fitting curve to Freundlich isotherm. The isotherm parameters and the correlation coefficient are shown in Table 3.

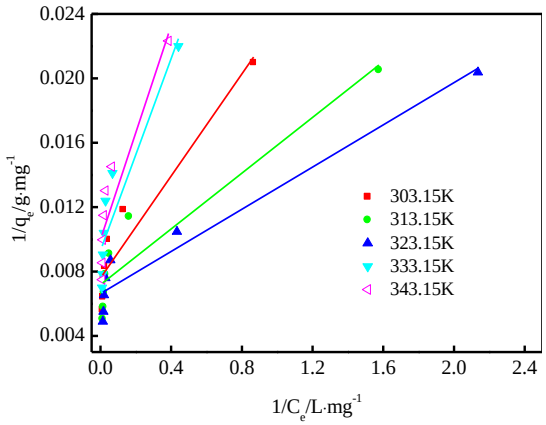

FIGURE 5
Langmuir isotherm plots for the removal of MB (adsorption time of 3 h).

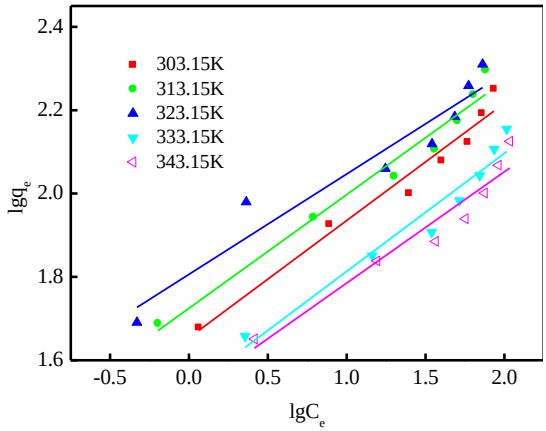

FIGURE 6
Freundlich isotherm plots for the removal of MB (adsorption time of 3 h).

From Table 3, it can be seen that the R^2 values (R^2>0.92) indicated that the isotherm data was fitted with Freundlich isotherm model. The value of K_F from the Freundlich model increased with the rise in temperature (303.15K~ 323.15K) and then to descend with increased temperature (323.15K~343.15K). It was in agreement with the experimental result, giving the information about adsorption of MB mechanism may contain chemical and physical sorption process. K_F value reached a maximum when the temperature was 323.15K, indicating that highest interaction between MB and adsorbent. Besides that, values of 1/n less than 1 showed the adsorption was favorable. It can be inferred that the active sites of activated carbon have a heterogeneous distribution of adsorption energy.

Dubinin-Radushkevick (D–R) isotherm. The Dubinin-Radushkevick (D–R) isotherm is employed to specify the nature of the adsorption through physical or chemical processes. The equation of this model is described as:

$$\ln q_e = \ln q_m - K'\varepsilon^2 \qquad (6)$$

Where ε (Polanyi potential) is equivalent to RT $\ln(1 + 1/C_e)$, q_e is the amount of the dye adsorbed per unit dosage of activated carbon ($mol \cdot g^{-1}$), q_m is the adsorption capacity ($mol \cdot g^{-1}$), C_e is the equilibrium concentration of the dye solution ($mol \cdot L^{-1}$), K′ is activity coefficient pertinent of the mean sorption energy ($mol^2 \cdot kJ^{-2}$). R is the gas constant ($8.314 J \cdot mol^{-1} \cdot K^{-1}$), and T is the temperature (K) [21]. The fitting of the experimental date to this model is displayed in Fig. 7.

K′ is connected with mean adsorption energy E ($kJ \cdot mol^{-1}$) as:

$$E = \frac{1}{\sqrt{2K'}} \qquad (7)$$

This value of E gives information about the mechanisms of adsorption process. If E value is range between 8 and 16 $kJ \cdot mol^{-1}$, the type of adsorption is chemical process, if E <8 $kJ \cdot mol^{-1}$, the process is physisorption [8, 21]. The isotherm constants are offered in Table 3. E values were calculated in the range of 16.0~18.1 $kJ \cdot mol^{-1}$ from Table 3, suggesting that the type of adsorption of MB on HACC was classified as chemical adsorption.

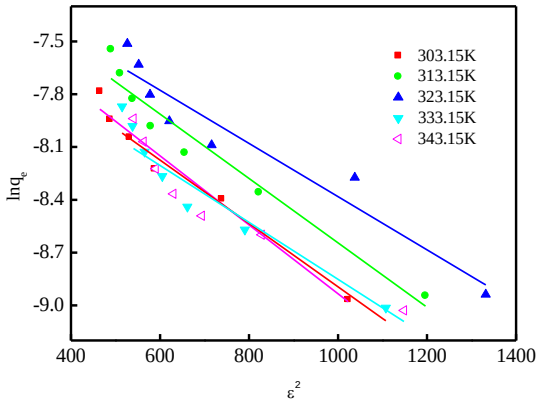

FIGURE 7
Freundlich isotherm plots for the removal of MB (adsorption time of 3 h).

Temkin isotherm. Temkin model accepts that the decrease in the heat of sorption is linear with coverage due to adsorbent-adsorbate interactions. The Temkin isotherm equation may be expressed as:

$$q_e = \frac{RT}{b} \ln K_T C_e \qquad (8)$$

where B_1=RT/b, B_1 is involved with the heat of adsorption, K_T is the equilibrium binding constant ($L \cdot mg^{-1}$) [22]. The parameters are given in Table 3. The fitted equilibrium data to this model is offered in Fig. 8.

From Table 3, it was apparent that the fitting to Temkin model is poor, as the values of R^2 lied below 0.89. The values of K_T were high, meaning that there were strong interaction between MB and adsorbent. This was consistent with the conclusion obtained from the D-R isotherm that the adsorption is chemical process.

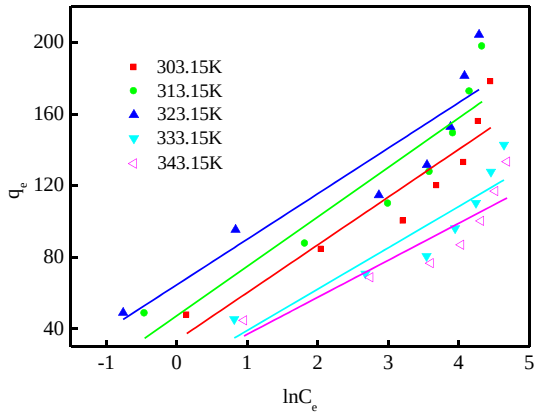

FIGURE 8
Temkin isotherm plots for the removal of MB (adsorption time of 3 h).

Frumkin isotherm. Frumkin model takes into account the case of interaction between the adsorbed species. The equation is presented as:

$$\ln\left[\left(\frac{\theta}{1-\theta}\right)\frac{1}{C_e}\right] = \ln k + 2a\theta \qquad (9)$$

where $\theta = q_e / q_m$, θ is the fractional occupation, q_e is the adsorption capacity in equilibrium ($mg \cdot g^{-1}$), q_e is the theoretical monolayer saturation capacity ($mg \cdot g^{-1}$), which is obtained from D-R isotherm. The constant k is related to adsorption equilibrium, $\ln k = \frac{-\Delta G}{RT}$, ΔG is Gibbs free energy. a is the interaction coefficient, if a>0 indicates there is attraction, if a<0 means repulsion, if a=0 indicates no interaction between the adsorbate species [22]. The fitting curve was given in Fig. 9.

From Table 3 it was apparent that the adsorption followed Frumkin isotherm. There was attractive interaction between the adsorbed species, as the values of a were positive. In general, attractive interaction increased with increasing temperature. The negative values of ΔG suggested the spontaneous nature of the adsorption. ΔG was more negative with temperature increased, showing a better adsorption was obtained.

As it can be concluded from Table 3, the suitable isotherm models were Frumkin, Freundlich and D-R, as the high value of R^2. The negative values of ΔG and a obtained from Frumkin isotherm, confirming that the process of MB adsorption was spontaneous and there was attractive interaction between the adsorbed species. The adsorption of MB onto corncob activated carbon was found to be multilayer and favorable adsorption according to Freundlich model. The E values of D-R isotherm indicated the chemical adsorption in nature.

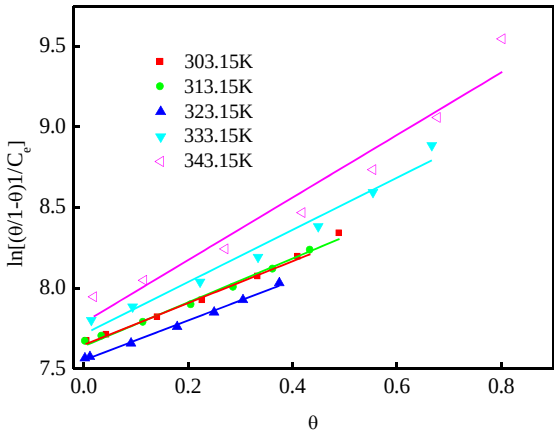

FIGURE 9
Frumkin isotherm plots for the removal of MB (adsorption time of 3 h).

Kinetic models. The adsorption of MB on HACC was analyzed with Morris-Weber, Pseudo-first-order Pseudo-second-order and Elovich models respectively to determine the rate-controlling step and mechanism of adsorption process. Kinetic parameters are collected in Table 4.

Morris-Weber kinetic model. Morris-Weber kinetic model accepts that the rate of adsorption is only under the control of intra-particle diffusion and can be given as:

$$q_t = K_{id} t^{0.5} + C_i \qquad (10)$$

where q_t ($mg \cdot g^{-1}$) is the concentration of MB adsorbed at time t (min), K_{id} is the intra-particle diffusion rate constant ($mg \cdot g^{-1} \cdot min^{-0.5}$), C_i is the intercept, the larger intercept means the effect of boundary layer is greater [18]. Fig. 10(a) shows the curve-fitting plot of this model.

Fig. 10(a) shows the curve was not pass through the origin, indicating intra-particle diffusion would not be the only controlling step. Moreover, the process of MB adsorption was dominated by boundary layer control to a certain degree [17]. The fitting curve was nonlinear relationship and there were two sections of straight lines. This further displayed that there may exist the other processes controlling the rate of adsorption. The first step exhibited a steep slope and occupied most of the whole adsorption curve, indicating the boundary layer diffusion of solute molecules and chemical adsorption may occur. The second step was a gradual adsorption stage, where intra-particle diffusion may be rate limiting step and then reached the final equilibrium stage [20]. C_i increased with increasing MB initial concentration, meaning that the boundary layer effect was greater.

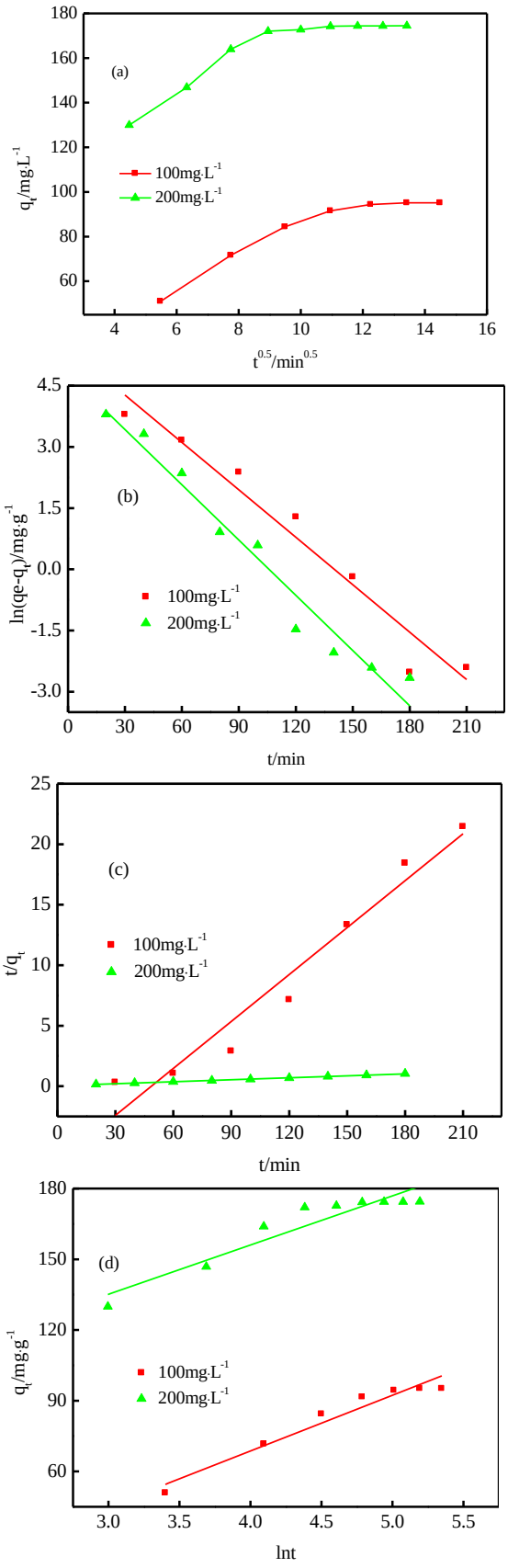

FIGURE 10
Morris-Weber(a), pseudo-first-order (b), pseudo-second-order(c) and Elovich (d) plots of methylene blue sorption onto corncob activated carbon

Pseudo-first-order kinetic model. The pseudo-first-order model supposes that the rate of adsorption is proportional to the amount of unoccupied active sites on the adsorbent and can be represented as:

$$\ln(q_e - q_t) = \ln q_e - k_1 t \quad (11)$$

where q_e is the sorbed concentration at equilibrium ($mg \cdot g^{-1}$), k_1 is the first order rate constant (min^{-1}) [21]. The fitting curve of this model was in Fig. 10(b).

Pseudo-second-order kinetic model. The Pseudo-second-order kinetic model investigates that the adsorption rate is controlled by the adsorption mechanism and can be written as:

$$\frac{t}{q_t} = \frac{1}{k_2 q_e^{\,2}} + \frac{1}{q_e} t \quad (12)$$

where k_2 is the second order rate constant ($g \cdot mg^{-1} \cdot min^{-1}$) [5,17]. The linear plot of pseudo-second-order equation is in Fig. 10(c). From the Table 4, adsorption of MB belonged to pseudo-second-order model, suggesting that the process of MB uptake is due to chemisorptions. K_2 decreases with the initial concentration of MB increased, showing that a decrease in adsorption rate. This may be that the surface of the adsorption sites were limited, MB solution increased from 100 $mg \cdot L^{-1}$ to 200$mg \cdot L^{-1}$, the competitive behavior of MB molecules made a decrease in the adsorption rate.

Elovich kinetic model. Elovich kinetic model considers that the surface energy distribution of the adsorbent is not uniform and can be given as:

$$q_t = \frac{1}{\beta}\ln(\alpha\beta) + \frac{1}{\beta}\ln t \quad (13)$$

where α is the initial adsorption rate($mg \cdot g^{-1} \cdot min^{-1}$), β is the desorption constant($g \cdot mg^{-1}$), which is related to the extent of surface coverage and activation energy for chemisorption [20]. The fitting of the Elovich model is presented in Fig. 10(d).

It could be seen from Table 4, Elovich model had the poor fitting at low concentration(100$mg \cdot L^{-1}$) but performed reasonably well at higher MB concentration (200$mg \cdot L^{-1}$). It was found that the initial rate of adsorption (α) increased with increasing the initial MB concentration, while calculated value of the desorption constant (β) decreased. That may due to the driving force of mass transfer increased with increasing initial concentration [18], while the degree of adsorbent surface coverage and chemical adsorption activation energy was changed.

It was clear from Table 4 that adsorption process was better represented by the pseudo-second-order model, meaning that chemical reaction played a significant role in the rate-controlling step. In the adsorption of MB onto HACC, basic dye in contact with water solution to form positive ion, so it was probably that a chemical reaction may occur on the

surface of corncob activated carbon containing oxygen functional groups, involving the electronic exchange between adsorbate and adsorbent [20]. The adsorption process depended on the availability of active sites. Intra-particle diffusion was involved in the adsorption process, however, it would not be the only rate controlling mechanism.

TABLE 4
Linear regression fitting parameters for kinetic equations

C_0/mg·L^{-1}		100	200
Morris–Weber model	K_{id}/mg·g^{-1}·min$^{-0.5}$	4.85	4.71
	C_i	32.16	119.60
	R^2	0.8486	0.7576
Pseudo-first-order model	K_1/min^{-1}	0.04	0.45
	R^2	0.9446	0.9596
Pseudo-second-order model	K_2/g·mg^{-1}·min^{-1}	2.66×10^{-3}	7.25×10^{-5}
	R^2	0.9444	0.9991
Elovich model	α/mg·g^{-1}·min^{-1}	70.74	671.73
	β/g·mg^{-1}	0.042	0.047
	R^2	0.9400	0.8794

CONCLUSION

The present investigation revealed that the activated carbon was prepared from corncob is an effective adsorbent for removal of MB from aqueous solution. The BET surface area of the HACC was 1160.838 m^2·g^{-1}. Nitrogen adsorption-desorption isotherm showed that the HACC was porous with well developed pores. The main surface functional groups present on HACC were hydroxyl, carbonyl and aromatic rings. The amount of MB adsorbed was found to vary with initial of MB concentration and contact temperature and pH.

The adsorption data fitted with the Langmuir, Freundlich, D-R, Temkin and Frumkin models. Frumkin, Freundlich and D-R isotherms displayed a better fitting model, indicating the adsorption of MB as a favorable, multilayer, chemical and spontaneous adsorption. Batch MB uptake capacity tests have shown that the adsorption process can be better described by pseudo-second-order model, meaning that chemical reaction played a significant role in the rate-controlling step. The intra-particle diffusion may be one of the determining step in the adsorption process.

ACKNOWLEDGEMENTS

This work was supported by National Natural Science Foundation of China (21403058), and Research Foundation for the Young Core Instructor Program of Henan Province, China (2016GGJS-058).

REFERENCES

[1] Zhang, F., Feng, C., Li, W., Cui, J. (2014) Indirect electrochemical oxidation of dye wastewater containing acid orange 7 oak Ti/RuO_2-Pt electrode. Int. J. Electrochem. Sci. 9(2), 943-954.

[2] Daneshvar, N., Ayazloo, M., Khataee, A., Pourhassan, M. (2007) Biological decolorization of dye solution containing malachite green by microalgae cosmarium sp. Bioresour. Technol. 98(6), 1176-1182.

[3] Khattri, S.D., Singh, M.K. (2009) Removal of malachite green from dye wastewater using neem sawdust by adsorption. J. Hazard, Mater. 167(1), 1089-1094.

[4] Bhadusha, N., Ananthabaskaran, T. (2011) Adsorptive removal of methylene blue onto $ZnCl_2$ activated carbon from wood apple outer shell: kinetics and equilibrium studies. J. Chem. 8(4), 1696-1707.

[5] Elshafei, G.M.S., Elsherbiny, I.M.A., Darwish, A.S., Philip, C.A. (2014) Silkworms' feces-based activated carbons as cheap adsorbents for removal of cadmium and methylene blue from aqueous solutions. Chem. Eng. Res. Des. 92(3), 461-470.

[6] Altintig, E., Acar, I., Altundag, H., Ozyildirim, O. (2015) Production of activated carbon from rice husk to support Zn^{2+} ions. Fresen. Environ. Bull. 24, 1499-1506.

[7] Meng, G., Liu, B., Tao, D., Li, P., Wan, T. (2012) Ammonium nitrogen adsorption from biologically pretreated coking wastewater by sewage sludge based activated carbon. Fresen. Environ. Bull. 21, 2536-2543.

[8] El-Sheikh, A.H., Newman, A.P., Al-Daffaee, H.K., Phull, S., Cresswell, N. (2004) Characterization of activated carbon prepared from a single cultivar of Jordanian olive stones by chemical and physicochemical techniques. J. Anal. Appl. Pyrolysis. 71(1), 151-164.

[9] Guneysu, S., Aydin, S., Arayici, S. (2004) Removal of some organic acids from water using olive mill wastes as adsorbent. Fresen. Environ. Bull. 13, 1006-1009.

[10] Ackacha, M.A. (2013) Removal of Pb(II) from Aqueous Solution by Portulaca oleracea leaves: kinetic, equilibrium and thermodynamic studies. J. American Journal of Analytical Chemistry. 4(7A), 27-32.

[11] Hameed, B.H., Din, A.T.M., Ahmad, A.L. (2007) Adsorption of methylene blue onto bamboo-based activated carbon: Kinetics and equilibrium studies. J. Hazard. Mater. 141(3), 819-825.

[12] Zhou, Y., Hu, C.W., Li, J.L. (2008) Study on the biosorption mechanism of methylene blue in aqueous solution using pummelo peel. Res. Environ. Sci. 21(5), 49-54.

[13] Rincón-Silva, N.G., Moreno-Piraján, J.C., Giraldo, L.G. (2015) Thermodynamic study of adsorption of phenol, 4-chlorophenol and 4-nitrophenol on activated carbon obtained from eucalyptus seed. J. Chem. 2015(5), 1-12.
[14] Chen, C., Zhao, P., Huang, Y., Tong, Z., Li, Z. (2013) Preparation and characterization of activated carbon from eucalyptus sawdust I. activated by NaOH. J. Inorg. Organomet. Polym. Mater. 23(5), 1201-1209.
[15] Gobi, K., Mashitah, M.D., Vadivelu, V.M. (2011) Adsorptive removal of methylene blue using novel adsorbent from palm oil mill effluent waste activated sludge: equilibrium, thermodynamics and kinetic studies. Chem. Eng. J. 171(3), 1246-1252.
[16] Yang, Y., Li, L., Sun, Z.Y. (2012) The research on the surface oxidation modification of activated carbon and its adsorption mechanisms of organic matter and heavy metal ions. J. Sci. Technol. Eng. 12(24), 6132-6138.
[17] El-Latif, M.M.A, Ibrahim, A.M., El-Kady, M.F. (2010) Adsorption equilibrium, kinetics and thermodynamics of methylene blue from aqueous solutions using biopolymer oak sawdust composite. J. Am. Sci. 6(6), 267-283.
[18] Hameeda, B.H., El-Khaiary, M.I. (2008) Equilibrium, kinetics and mechanism of malachite green adsorption on activated carbon prepared from bamboo by K_2CO_3 activation and subsequent gasification with CO_2. J. Hazard. Mater. 157(2–3), 344-351.
[19] Mahmoud, D.K., Salleh, M.A.M. (2014) Adsorption isotherm and kinetic studies of methylene blue dye on leucaena leucocephala wood char as bioenergy by-product. J. Purity Utility React. Environ. 3(6), 114-127.
[20] Alzaydien, A.S. (2009) Adsorption of methylene blue from aqueous solution onto a low-cost natural Jordanian tripoli. Am. J. Environ. Sci. 5(3), 179-208.
[21] Javadian, H., Ghorbani, F., Tayebi, H.A., Asl, S.M.H. (2015) Study of the adsorption of Cd (II) from aqueous solution using zeolite-based geopolymer, synthesized from coal fly ash; kinetic, isotherm and thermodynamic studies. J. Arab. J. Chem. 8(6), 837-849.
[22] Başar, C.A. (2006) Applicability of the various adsorption models of three dyes adsorption onto activated carbon prepared waste apricot. J. Hazard. Mater. 135(1-3), 232-241.

Received: **14.09.2017**
Accepted: **22.11.2017**

CORRESPONDING AUTHOR

Xuefeng Wei
College of Chemical Engineering & Pharmaceutics
Henan University of Science and
Technology
Kaiyuan Avenue 263, Luolong District,
Luoyang 471023 – P.R. China

e-mail: xfwei@haust.edu.cn

© by PSP Volume 27 – No. 2/2018 pages 1131-1137 Fresenius Environmental Bulletin

STATISTICAL EVALUATION OF WATERMELON GENOTYPES EXHIBITING DIFFERENT FEATURES UNDER STRESS CONDITIONS

Muhemet Zeki Karipcin*

Department of Horticulture, Agriculture Faculty, University of Siirt, Siirt, Turkey

ABSTRACT

It is impossible to obtain results for genetic sources reflecting phenotypic differences and dissimilar groups. Thus, in addition to applying a standard statistical model using different watermelon genotypes under drought stress, a new formula was also used. The present study also suggests that according to the groupings in the statistical evaluation, the genotypes in the top groups did not yield positive results; thus, the parcel data may change according to the evaluation criteria. The use of a new evaluation model comprising comparative changes in these respective studies is more accurate. In the present study, the data for TSS (total soluble solids), average fruit weight and total yield values were evaluated using both methods of analysis. In conclusion, as a result of the standard statistical analysis, genotype nos. 325 and 26 have the best group, while the evaluation according to comparative variation criteria demonstrated that genotype nos. 24, 25, 27 and 218 have the best group. Thus, the most reliable evaluation method was to use the new evaluation model comprising comparative variations.

KEYWORDS:
Abiotic, Statistical evaluation and grouping, Watermelon genotypes.

INTRODUCTION

Academic research in the field of science varies from engineering research based on the presence of objectives and a timeline. Academic research is rarely conducted in the field of industry. Therefore, the expression "of academic interest," unfortunately, is used as a euphemism for "useless" [1]. Statistics, which is the only subject matter in the science of data, has shown tremendous growth over the last 50 years. Today, developments in information technology provide statisticians with even more opportunities, such as studies on climate change, health, environmental and genetic research, policy-making areas and social survey activities, enabling scientists in those fields to interpret complex data using powerful computational tools [2].

Researchers often perceive statistics as simple calculations and graphics or assign statistics too many roles in the research process. However, according to a number of studies, statistics is a tool that helps people to understand a complex world [3]. Statistics is an important method of comparison that can provide direction to subsequent programs. In most scientific literature, there are few details concerning contradictions in statistics. Thus, the primary objective of the present study was to determine the tolerances of watermelon genotypes to stress conditions, specifically, the conditions of abiotic stress, particularly drought. The results describe the statistical evaluation of the genotypes, all of which have genetically different properties (even in terms of phenotypic characteristics). The present study was conducted to demonstrate that evaluations using standard statistical models, ignoring genetic characteristics, do not reflect reality. Rather, it would be more effective to use a new evaluation model that includes comparative changes. Statistics have a significant impact on the lives of many people. For example, because statistics are often biased, government health policies are frequently enacted incorrectly [4]. With the development of modern computer programs, the selection of the most appropriate multivariate statistical technique, the correct interpretation of the results obtained using appropriate statistical techniques and the knowledge of the advantages and disadvantages of the multivariate techniques, have gained more importance. Statistical analysis is required for the evaluation of research trials.

The verification of theories is thus an endless process, since scientists can never assume that all possibilities have been evaluated [5]. Statistical analysis methods are some of the most effective tools to accurately detect the positive or negative impact of each application on the material studied and to analyse and interpret the data obtained from scientific studies to develop suitable models for the solution of each problem [6]. Different from methods frequently encountered in the past, and from different methods of data analysis based only on descriptive statistics, multivariate analysis methods

are currently used more frequently [7]. Each study, of course, has its own unique evaluation. Exchange, distribution, standard deviation and median absolute distribution are the foursome by which variability is measured. The purpose of measuring the variation is two-fold: 1) to determine the accuracy of each measurement as close to the value measured within the redistribution and to determine the highest value among the values that are different from each other; and 2) to determine the accuracy of each measurement as close to the values measured within the redistribution. In addition, change is accepted as the measurement of the usable variability for the given values [8]. Moreover, the dynamics affecting any case are complex, and the factors affecting the flow of events in each area are multidimensional, as these factors are determined by several (usually infinite) characteristics. It is inevitable, therefore, to treat the phenomena in a multidimensional manner. Thus, it is necessary to use multivariate statistical techniques in research; otherwise, a great number of variables and their joint effects would not be considered but rather would have been defined simply and far from the actual images of the event. In exceptional cases, however, when the number of variables is stable and in controlled environments where the actual effect can be obtained by criteria that are not so complex, many variables among the groups, and their joint effects within the unique groups should be discussed such that the results of the present study can closely reflect the actual image and be clearly defined. Descriptive statistics and reliability analysis have been the most widely used methods in most studies. Furthermore, correlation analysis, regression analysis and factor analysis have drawn considerable attention as the most preferred analysis techniques. The scientists participating in the discussions on this topic arrived at a consensus as to the need to reform social and non-social issues in statistics [9]. Cumming's article, titled "From Null Hypothesis Significance Testing to Effect Sizes", in the second volume of his book, *Understanding the New Statistics* (10), has provided vast literature on the subject and has skillfully summarized the findings. Approximately 35 years ago, Rosenthal [11] published an article with a provocative title: "How Often Are Our Numbers Wrong?" This article focuses on the frequency of errors of recorded data, and the shift of these errors in the direction the researchers would prefer.

Rosenthal's results were encouraging because only one percent of all of the observations were incorrect. In addition, Rosenthal observed that two-thirds of the errors were used to verify the hypotheses of the researchers. Similar to Rosenthal's discourse, other researchers rightly posed the question: "How often are our statistical results incorrect?" [12] Statistical contradictions have also attracted the attention of many researchers, such as Novella [13]. As a result of improved formulas, the results (without a need to comment or to be specialized on the subject) can be directly observed. The groupings clearly reflect the actual results. The formula developed to determine the effects of different applications (e.g., mechanical, biotic and abiotic stress) on genotypes with different genetic structures (also people of various races) is more accurately based on the comparison of genotypes among different applications. The new methods, developed as a result of trusting the statistical applications, performed similarly to the present study, and as Waller [14] confirms, these methods are attempts to reduce the error covariation with more accurate determinations using our own opinions and comments.

MATERIALS AND METHODS

Plant Material Properties Used in the Present Study. In the present study, we used a total of 9 genetic resources: one wild species, three *Citrullus* species other than *Citrullus lanatus* and four old and one new cultigen Figure 1 illustrates the differences between some genotypes used in the research as a result of their fruit characteristics. As shown in Figure 1, the physiological and morphological characteristics of native and wild genotypes and other commercial varieties, such as the flesh colour, peel thickness, number of seeds, fruit size, fruit size (aspect ratio) and TSS (total soluble solids), have values that significantly differ.

Field Trial Methods and Issues. To determine the drought tolerance of domestic and wild watermelon genotypes, the trial subjects used in this two-year project are explained below.

I_1: Full irrigation (bringing the missing moisture level to that of the field capacity)

I_2: Deficit irrigation (implementation of half of the water used in I_1)

There were no water applications in the I_1 and I_2 trial subjects. The irrigation was performed in experimental plots during the period in which the plant formed leaves in a manner in which the water requirement of the plant was precisely met. Subsequently, 50% of the water used in the I_1 trial subject was applied to I_2. For the I_1 trial subject, the crop water requirement was fully met until the harvest. The seeds were planted in both 2007 and 2008 with a row space of 3.00 m x 0.6 m in a raised bed. In I_1 and I_2, the seeds were sown on the same date as that of the direct seeding to 45 vials. The seedlings grown in the vials were planted in the field on June 12. A total of 12 plants were grown in the plot, and three plants were removed for biomass measurements every month, beginning in October (three months in total). The remaining nine plants were

used to obtain other measurements and observations and to perform additional analyses.

Statistical Analysis. The research was performed in a split plot design with three replications. The plots to be irrigated were placed in the main plots, while the watermelon genotypes examined for their performance under drought conditions were placed in the lower plots.

Analysis Using a Standard Statistical Model. The obtained data were analysed using the JUMP package, and the LSD test was used to compare the averages.

Analysis Using a New Evaluation Model Comprising Comparative Changes. The formula for Drought Tolerance $(DT\%) = (I_2 / I_1) * 100$ and $(I_0 / I_1) * 100$ was used as the basis for the new evaluation model, which comprises comparative changes. The following formulas were used to determine the drought tolerance for each genotype:

$DT_{0\,(X)} = I_0 / I_1$ or I_2 / I_1 (1)

$DT_{1\,(X)} = 100 - \{(I_0 / I_1) * 100\}$ (2)

$DT_{2\,(X)} = 100 - \{(I_2 / I_1) * 100\}$ (3)

In these equations, X *is* the number of genotypes; I_1 is the 100% water parcel data; I_2 is the 50% water cut parcel data, and *100* is the fixed number in the formula. As the DT_0 value of the draught-tolerant genotype gets closer to 1, its ability to resist high-stress conditions increases. In addition, the DT_1 and DT_2 values (particularly DT_1) of the drought-tolerant genotypes are smaller than those of the other genotypes. The sole purpose of this comparative analysis methodology is to demonstrate the true response of each genotype to stress conditions. According to Dembélé and Kastner [15], who suggested the same logic, the results are more realistic compared with the control result. In this model, using the Excel programme to prepare the data for the analysis, we calculated the overall standard deviation for all genotypes and for each data point, the joint standard deviation for the overall data, and finally, the standard deviation for the overall trial. The average of the three replications, whose standard deviation was previously calculated, was used as a data point. The formula of I_2 (or I_0) data / / I_1 data x was applied, calculated and compared, resulting in a percentage value (%). The percentages (%) of all the genotypes could also be obtained through the remaining variations from 100%. Covariance analysis of the data was performed in Excel to complete the analysis. Similarly, the correlation analysis can also be performed using Excel. Creating conditional formatting and colour groups in Excel, the obtained DT_0 data and the percentage of changes for the DT_1 and DT_2 tables, in which differences can easily be observed, were formed.

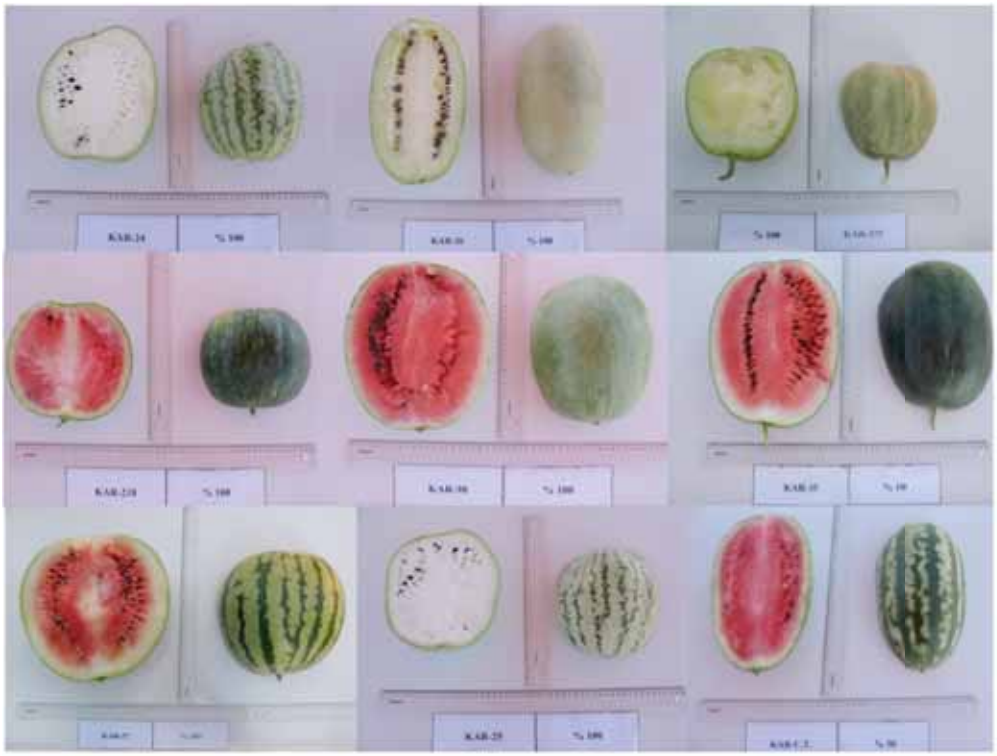

FIGURE 1
Thickness of the exocarp, fruit colour, fruit dimension and seed features of the watermelon genetic resources used in the present study.

TABLE 1
Effect of the irrigation x genotype interaction on the total soluble solid contents (%)

GNT	Irrigation	LSD Gr.	TSS	GNT	Irrigation	LSD Gr.	TSS
98	I_1	A	9.3	27	I_2	F	6.3
218	I_1	AB	8.7	325	I_1	G	4.7
98	I_2	ABC	8.5	325	I_2	G	4.4
218	I_2	ABC	8.4	25	I_1	GH	4.3
27	I_1	BCD	7.8	25	I_2	GH	4.0
35	I_1	CDE	7.6	24	I_1	GHI	3.8
35	I_2	DEF	7.2	26	I_1	GHI	3.7
CT	I_1	EF	6.7	24	I_1	HI	3.4
CT	I_2	F	6.4	26	I_1	I	2.9

TABLE 2
Effect of the irrigation x genotype interaction on the total yield (tons/da)

GNT	Irrigation	LSD Gr.	Yield	GNT	Irrigation	LSD Gr.	Yield
325	I_1	A	12.6	35	I_1	F	5.3
26	I_1	AB	11.6	27	I_1	FG	4.8
25	I_1	B	11.2	26	I_2	GH	3.7
218	I_1	C	9.2	98	I_1	H	3.4
24	I_1	CD	8.8	CT	I_2	H	3.1
CT	I_1	CDE	8.4	27	I_2	H	2.9
25	I_2	DE	7.5	35	I_2	H	2.9
218	I_2	E	7.4	325	I_2	H	2.5
24	I_2	E	7.2	98	I_2	I	0.4

Features Studied TSS (%). TSS measurements of three fruit randomly collected from each plot were observed as the % brix and presented as an average value.

Average Fruit Weight (kg). Three pieces of fruit randomly collected from each plot were weighed on a scale, and the average fruit weight was determined.

Total Yield (for Each Ton). The fruits reaching maturity were harvested at the optimum time. The resulting amount of total fruit yield was calculated by dividing the number of harvested fruit by the total plot area.

RESULTS

The results obtained from the experiment and the results of the two analysis models are provided in separate tables.

Analysis Findings Using the Standard Statistical Model (JUMP Package Programme). The TSS values measured in watermelon genotypes were calculated as the % brix and presented in Table 1. When the effects of the water application x genotype interaction to TSS values were examined, the highest TSS value (9.3%) was identified in the No. 98 genotype x 100% water application interaction, while the lowest TSS value (2.9%) was identified in the No. 26 genotype x 100% water application interaction (Table 1).

The total yield values obtained from watermelon genotypes are present in Table 2. When the effects of the water application x genotype interaction to the total yield values were examined, the highest value was identified (12.6 per ton) in the No. 325 wild genotype x 100% water application interaction. The lowest value (0.4 per ton) was identified in the No. 98 wild and intolerant genotype x 50% water application interaction (Table 2).

The average fruit weights of the watermelon genotypes are present in Table 3. The highest average fruit weight (9.6 kg) was identified in the 100% water application x No. 325 intolerant genotype interaction, and the lowest value (1.2 kg) was identified in the 50% water application x No. 24 tolerant genotype interaction (Table 3).

In the groupings using the standard statistics model, the highest values showed parallelism with the genetic features: the yield values, average fruit weight and TSS values of the large-fruited genotypes had better groups than those of the small-fruited genotypes in 100% water application parcels, and even in 50% water applications. Similarly, the TSS values are *genetically* low, and the 50% water application values of the wild genotypes with TSS averages of 1-3 brix, which were not used for feeding animals because of their bitterness, have lower values than those of the genotypes with sugar in their natural genetic structure.

TABLE 3
Effect of the irrigation x genotype interaction on the mean fruit weight (kg)

GNT	Irrigation	LSD Gr.	Mean fruit weight	GNT	Irrigation	LSD Gr.	Mean fruit weight
325	I_1	A	9.6	325	I_2	EF	4.1
218	I_1	B	7.9	CT	I_2	EFG	3.9
27	I_1	BC	7.8	98	I_2	HI	3.1
35	I_1	C	6.9	25	I_1	FGH	3.5
218	I_2	CD	6.4	35	I_2	GH	3.2
27	I_2	CD	6.1	25	I_2	HI	2.7
98	I_1	D	5.9	26	I_2	I	2.4
CT	I_1	D	5.8	24	I_1	J	1.3
26	I_1	E	4.7	24	I_2	J	1.2

TABLE 4
Total yield, total soluble solid contents and mean fruit weight of fully irrigated (control) watermelons and the rate of reduction with a 50% irrigation level in watermelon genotypes.

	Yield (ton/ha)		TSS (%)		Mean fruit weight (kg)	
Genotypes	Control	Disparity at 50%	Control	Disparity at 50%	Control	Disparity at 50%
24	8.8	17.9	3.8	10.3	1.3	5.7
25	11.2	33.2	4.3	5.3	3.1	14.6
26	11.6	62.6	3.8	21.4	5.2	54.4
27	4.8	38.0	7.8	18.6	7.8	21.5
35	5.3	46.1	7.6	4.6	6.9	53.5
98	3.4	87.2	9.3	8.3	5.9	33.7
218	9.2	19.4	8.7	3.6	7.9	19.0
325	12.7	80.3	4.7	6.4	9.6	57.6
CT	8.4	63.1	6.7	4.4	5.8	32.1

Analysis Using the New Evaluation Model Comprising Comparative Changes. The rates of the comparative variations are shown in Table 4. When the TSS values were analysed according to a 50% water cut, the lowest TSS change rate was identified in the No. 218 genotype, 3.6% from the negative direction, while the highest rate was obtained from the No. 26 intolerant genotype (21.4%). The rate of variation of the average fruit weight is another feature associated with genetic features and TSS. The lowest yield rate detected between the plots with 50% water cut and the plot with no drought was identified in the No. 24 tolerant genotype (17.9%), while the highest rate was obtained from the No. 98 and 325 intolerant genotypes (87.2%, 80.3%, shown in Table 4). In the comparative analysis model, in which the reactions of the genotypes to abiotic stress conditions were clearly revealed, the lowest variation rate of the average fruit weight averages in 50% water cut plots was observed for the No. 24 wild and tolerant genotype with Egyptian origin, which yields abundant but small fruits (5.7%). The highest rate, however, was obtained from the No. 325 intolerant genotype (57.6%).

DISCUSSION

Belief, confirmation, evidence and subsequent integration into a better understanding of personal and scientific epistemologies are important [16]. The average fruit weight of genetically small-fruited genotypes is, without the necessity of examining, generally higher than that of genetically large-fruited genotypes. As for showing the effect of the stress applications, however, evaluations using standard analysis methods resulted in many more errors. When the same example was considered, the average fruit weight of the large-fruited genotypes, even in stress applications, represented a statistically better group than that of the small-fruited genotypes in parcels with no stress application, which causes more chaos during an assessment. Significant errors of assessment arise in assessing the genetic characteristics and stress applications, such as TSS (total soluble solids). Similarly, for the fruit flesh determination of genetically white, orange, light pink or yellow flesh (wild genotypes)-coloured genotypes and genotypes with genetically red fruit flesh and the determination of their TSS, the parcels with and without

(control parcels) stress application should be considered as the basis, otherwise there will be errors before the transition. Using the new formula, a clearer evaluation can be achieved, avoiding potential errors. When the effects of the application are examined, we observed an erroneous evaluation, not only for the abovementioned criteria but also for all evaluations. "*Without a good model, parameter estimation will be faulty"* [17]. Studying with genetically wide genotypes especially on abiotic stress is not easy to explain result very well [18, 19, 20]. However, the formula described in the present study, when applied, closely reflected an accurate assessment. These results were in keeping with the ideas of Kempthorne [21] as the source of inspiration. Similarly, Dembélé and Kastner [15], in studies parallel to the present study, examined new statistical methods to determine the difference that arises from genetic distinctions between genes. In the present study, we examined the statistical evaluation of the reactions of morphologically, pomologically and phenotypically different genotypes under stress conditions in terms of genetics. According to Kempthorne [21], who was the first to examine genetic statistics and is considered an expert in the field, when applying the standard statistical evaluation, it is impossible to obtain results for phenotypically different genetic sources that do not share the same group. Thus, in addition to applying one of the standard statistical models of the trial using different watermelon genotypes under drought stress, the new formula developed by Karipçin et al. [22] was also used. The study suggests that according to the groupings made in the statistical evaluation, the genotypes in the top groups did not yield positive results, and thus the parcel data may change according to the evaluation criterion, explaining why both results of the trials in the present study have been discussed in terms of their causes and effects. The evaluation of standard statistical models ignores the genetic characteristics and did not reflect reality. The use of the new evaluation model comprising comparative changes in the respective studies has been identified as more accurate. In the present study, the data concerning TSS, average fruit weight and total yield values were evaluated using both methods of analysis. When the genotypes were examined in terms of their lowest yield values, the average fruit weight values of the wild genotypes with naturally small fruits were at low levels. However, in addition to detecting no excessive difference among the water levels in tolerant genotypes, a stable variation between the values was also observed. While a high yield was obtained in intolerant genotypes, as the water content decreased, yield values were adversely affected, as in other features. In the performance of genotypes with genetically distinct features in terms of their average fruit height under abiotic stress conditions using the standard analysis, the variation rates of the values of the genotypes for different applications located in the subgroups according to LSD groupings can neither be identified nor misinterpreted. In the comparative analysis model, the features of the genotypes of fruits adapting to the stress conditions were realized, as shown in Table 4.

CONCLUSION

In conclusion, as a result of the standard statistical analysis, genotype nos. 325 and 26 had the best group, whereas in the evaluation according to comparative variation criteria, genotype nos. 24, 25, 27 and 218 had the best group. While examining the effects of different applications, such as abiotic stress, it was concluded that the most reliable method of evaluation was the new evaluation model comprising comparative variations. Thus, according to Taper et al. [17] "never fall in love with our model—it should not be a long relationship."

ACKNOWLEDGEMENTS

The author would like to thank the GAP Agriculture Research Institute (Turkish Ministry of Agriculture and Rural Affairs in Sanliurfa-Turkey) – GAPTAEM and SODES (Social Support Program).

REFERENCES

[1] Mujumdar, A.S. (2013) Editorial: On Citation Statistics-What Do They Really Mean? Drying Technology. 16, 1897-1898.
[2] Fu, W. (2013) A Celebration of Statistics and its Applications. Ann Biom Biostat. 1, 1008.
[3] Rolka, K., Bulmer, M. (2005) Picturing student beliefs in statistics. ZDM. 37, 412 417.
[4] Baranowski, T. (2014) Lying (or Maybe Just Misleading) With (or Without) Statistics. Games for Health: Research, Development, and Clinical Applications. 3, 1-2.
[5] Pidwirny, M. (2006) Scientific Method. Fundamentals of Physical Geography. 2, 66.
[6] Yıldırım, N. (2013) Devlet Üniversiteleri Strateji ve Yapılarında Yenilikçilik, Girişimcilik, ÜSİ ve Bölgesel Kalkınma Yönelimi, ÜSİMP (Üniversite Sanayi İşbirliği Merkezleri Platformu) VI. Ulusal Kongresi, Düzce.
[7] Ozen, S. (2002) Türkiye'deki Örgütler / Yönetim Araştırmalarında Törensel Görgülcülük Sorunu. Yönetim Araştırmaları Dergisi. 2, 7.
[8] Barragués, J.I, Morais, A., Guisasola, J. (2014) Probability and statistics - A didactics introduction. Boca Raton (Florida, USA): CRC Press Taylor & Francis Group.

[9] Hak, T. (2014) After statistics reform: should we still teach significance testing? Paper for the Ninth International Conference on Teaching Statistics (ICOTS) Flagstaff (AZ), 5.
[10] Cumming, G. (2013) Understanding the new statistics: Effect sizes, confidence intervals, and meta-analysis. New York, NY: Routledge.
[11] Rosenthal, R. (1978) How often our number wrong? American Psychologist. 33. 1005-1008.
[12] Rossi, J.S. (2000) How often are our statistics wrong? A statistics class exercise. In: Ware, M.E., Johnson, D.E. (Eds.) Handbook of demonstrations and activities in the teaching of psychology. I: Introductory, statistics, research methods, and history (2nd ed.) Mahwah, NJ: Lawrence Erlbaum Associates, 101-105
[13] Novella, P.R. (2013) Official Statistics after Statistics 2013: facing a challenging future. Boletin de Estadistica e Investigacion Operativa. 29, 199-213.
[14] Waller, J.A., Dance, S.L. Lawless, A.S. Nichols, N.K., Eyre, J.R. (2012) Representativity error for temperature and humidity using the Met Office high resolution model. Quarterly Journal of the Royal Meteorological Society. 140(681), 1189-1197.
[15] Dembélé, D., Kastner, P. (2014) Fold change rank ordering statistics: a new method for detecting differentially expressed genes. BMC bioinformatics. 15(1), 14.
[16] Bandyopadhyay, P.S., Brittan, G., Taper, M.L. (2016) Belief, evidence, and uncertainty: problems of epistemic inference. Springer Briefs in Philosophy of Science.
[17] Taper, M.L., Ponciano, M. (2016) Evidential statistics as a statistical modern synthesis to support 21st century science. Population Ecology. 58, 9-29.
[18] Barutcular, C., Yıldırım, M., Koc, M., Akıncı, C., Tanrıkulu, A., EL-Sabagh, A., Albayrak, O. (2016) Quality traits performance of bread wheat genotypes under drought and heat stress conditions. Fresen. Environ. Bull. 25, 1-7.
[19] Ahmad, P., Ozturk, M., Gucel, S. (2012) Oxidative damage and antioxidants induced by heavy metal stress in two cultivars of mustard (Brassica juncea L.) plants. Fresen. Environ. Bull. 21, 2953-2961.
[20] Uncumusaoglu, A.A., Sengul, U., Akkan, T. (2016) Environmental Contamination of Heavy Metals in The Yaglidere Stream (Giresun), Southeastern Black Sea. Fresen. Environ. Bull. 25, 5492-5498.
[21] Kempthorne, O. (1957) An introduction to genetic statistics. Oxford, England: Wiley. Xvii, 545.
[22] Karipcin, M.Z., Sarı, N., Kırnak, H. (2008) Preliminary research on drought resistance of wild and domestic Turkish watermelon genotypes, Cucurbitaceae, Proceedings of the IXth EUCARPIA Meeting on Genetics and Breeding of Cucurbitaceae, INRA, Avignon-France, 493-499.

Received: **16.09.2017**
Accepted: **06.11.2017**

CORRESPONDING AUTHOR

Muhemet Zeki Karipcin
University of Siirt
Agriculture Faculty
Department of Horticulture
Siirt – Turkey

e-mail: zkaripcin@gmail.com

© by PSP Volume 27 – No. 2/2018 pages 1138-1144 Fresenius Environmental Bulletin

STUDY ON THE CHARACTERISTICS OF WATER - SOLUBLE ION POLLUTION IN $PM_{2.5}$ IN FULING DISTRICT

Xianghong Wang[1,2,3,*], Qiong Luo[1,2], Lin Qin[1], Huanbo Wang[2], Fumo Yang[1,2]

[1]The Research Center for Ecological Environment Monitoring and Disaster Control of the Three Gorges Reservoir, Yangtze Normal University, Fuling, Chongqing, 408100, China
[2]Chongqing Institute of Green and Intelligent Technology, Chinese Academy of Sciences, Chongqing, 400714, China
[3]Collaborative Innovation Center for Green Development in Wuling Mountain Areas, Yangtze Normal University, Chongqing, 408100, China

ABSTRACT

$PM_{2.5}$ was collected at the atmospheric observatory (located at the campus of Chongqing Yangtze Normal University in Fuling District in January and July of 2015 respectively. The variation of the mass concentration characteristics and the water-soluble ions variation of $PM_{2.5}$ were analyzed. The pollution characteristics was found as follows: The average mass concentration of $PM_{2.5}$ was 116.28μg•m^{-3}, 46.80μg•m^{-3} respectively in January and July, and the mass concentration ranged from 23.21 μg•m^{-3} to 216.61μg•m^{-3} during the sampling period. The obvious seasonal characteristics were observed. Nine water-soluble ions (F^-, Cl^-, NO_3^-, SO_4^{2-}, K^+, Na^+, NH_4^+, Mg^{2+}, Ca^{2+}) were measured using the ion chromatography (ICS-600). The concentration of water-soluble ions ranged from6.37μg•m^{-3} to 86.30μg•m^{-3}, accounted for 42.28% in $PM_{2.5}$ samples. Average mass concentration of SO_4^{2-}, $NO_3^-$and NH_4^+ was 30.53μg•m^{-3}, accounted for 87.99% of the total soluble ions. There existed a good correlation among SO_4^{2-}, $NO_3^-$and NH_4^+ distribution and variation. The analysis of equilibrium between cation and anion indicated a good correlation(R^2=0.95) with weak alkaline in winter and weak acidic in summer.

KEYWORDS:
$PM_{2.5}$, water-soluble ions, seasonal variation

INTRODUCTION

The research on atmospheric particles of Chongqing was mainly concentrated in the main city and Wanzhou District. The main contents mainly concentrated on concentration level, pollution characteristics, source analysis and chemical composition of total suspended particulate (TSP), PM_{10} and $PM_{2.5}$ [1-4]. However, study of particulate pollution in Fuling District of Chongqing is still blank. Chongqing Fuling is located in the hinterland of Three Gorges reservoir, and the Interchange of the Yangtze River and Wujiang, which is the central city of Chongqing. Systematic research on Water soluble components of particulate matter in Fuling, which is important to study the characteristics of air pollution in Fuling area, and to provide scientific basis for the improvement of atmospheric visibility and the control of acid rain.

Water-soluble ionic component is one of the most important chemical constituents in airborne particles, and it is also one of the most studied components. There are more and more researches on water-soluble ions at home and abroad. Water-soluble components mainly include sulfate, nitrate, ammonium salt and sodium chloride, etc., generally accounted for 30% to 50%of $PM_{2.5}$ mass [5]. SO_4^{2-}, NO_3^- and NH_4^+ are mainly composed of secondary particles, which are formed by physical condensation of nuclei in the atmosphere. The concentrations of SO_4^{2-}, NO_3^- and NH_4^+ are related to the concentrations and Conversion rate of SO_2, NO_x and NH_3 in the atmosphere, while being affected by temperature and humidity. SO_4^{2-} is mainly from fossil fuel combustion, SO_2 through oxidation reaction generated SO_4^{2-} and H_2SO_4 (including gas phase oxidation and liquid oxidation, ozone and peroxide as catalyst) [6]. NO_3^- is mainly from nitrogen oxides generated by oxidation reaction and motor vehicle exhaust emissions [7]. Gaseous precursor of NH_4^+ is gaseous ammonia, mainly from plant and soil microbial release and use of farm chemical fertilizers. The CI^- ,K^+,Na^+,Mg^{2+},Ca^{2+} in water-soluble ions come from sea salt and coal combustion [8], biomass combustion, marine source, soil dust, building dust and soil [9].

EXPERIMENTAL

Sample collection. The sampling point of this study is in the administrative building roof of Changjiang Normal University, Fuling District of Chongqing (E 106 ° 56'-107 ° 43 ', N 29 ° 21'-30 ° 01'). Changjiang Normal University is located in the northwest direction of Fuling District, surrounded by

the high-speed of Change Fu and South Fu, mixed with cultural and residential areas. The sampling point is about 20m above the ground, the surrounding terrain is flat, there is no obvious pollution source, the environment quality is good, can objectively represent the Fuling District atmospheric environmental pollution level and change regularity.

Sampling of the $PM_{2.5}$ is divided into two phases, respectively, January 6, 2015 - February 5,2015 and July1, 2015 - July 31,2015. Daily continuous collection of 23 hours, the sampling period for the day 11:00 am to 10:00 am the next day, an interval of 1 hour for membrane exchanging, flow monitoring and calibration or instrument cleaning and maintenance.

The sampler used to collect the samples was a multi-channel chemical species sampler manufactured by Met One Instruments of America. Equipped with $PM_{2.5}$ cutting head, and the sampler flow rate is 6.7L / min. The instrument also equipped with temperature and pressure sensor. The sampling volume can be converted into the standard volume according to the real-time temperature and pressure. And the instrument can set sampling time and date. Water-soluble ion analysis of atmospheric particulates is carried out using quartz membranes. In this study, atmospheric fine particles were collected by inertial collision using φ47mm quartz film (Whatman). Teflon filter (Whatman) made of PTFE film, blank value is low, non-hygroscopic, non-adsorption of inorganic and organic gases, usually used for $PM_{2.5}$ mass concentration analysis.

Sample analysis. After sampling, open 1/2 of the filter box lid put it into the tray, and then into the balance tank, filter into the balance chamber at least 24h.

Cut 1/4 of the filter using knife, and then cut into pieces with scissors, put these pieces into 50ml centrifuge tube, add about 10ml of ultra-pure water, ultrasound 20minute in Ultrasonic oscillator, oscillation is completed, according to the number Filter with 0.45μm filter to 25ml volumetric flask, repeat the two ultrasonic oscillation and filtration, constant volume to the scale line, placed in 4 ℃ under refrigeration, to be measured.

The cationic column is CS12A column and the anion column is AS11 (superscript -) column. The cationic column is composed of two kinds of ions, -HC and AG11-HC guard columns and ASRS suppressors. The anion and cation eluents were analyzed for 30 mm KOH and 20 mm methanesulfonic acid (MSA), respectively.

RESULTS AND DISCUSSION

Characteristics of $PM_{2.5}$ mass concentration. $PM_{2.5}$ daily average concentration (24h average) changes, as shown in Figure 1.

The peak of $PM_{2.5}$in winter was on January 15, January 19 and January 25, the concentration values were 204.35μg•m^{-3}, 190.92μg•$m^{-3}$and 216.61μg•m^{-3}, respectively. It appears valley in January 28, and the value was 27.40μg • m^{-3}. The concentration of $PM_{2.5}$ in summer was on July 10, July 19 and July 25, the concentration values were 83.33μg•m^{-3}, 66.47μg•$m^{-3}$and 62.07μg•m^{-3}, respectively. It appears valley in July 3, and the value was 23.21μg•m^{-3}.

The concentration of $PM_{2.5}$ in winter ranges from 27.40μg•m^{-3} to 216.61μg•m^{-3} with an average value of 116.28μg•m^{-3}. The concentration of $PM_{2.5}$ in summer ranges from 23.21 to 83.33μg • m^{-3} with an average value of 46.80μg • m^{-3}. Winter $PM_{2.5}$ concentration was significantly higher than the summer, about 2.5 times than summer. As the Fuling is located in the mountain city of Chongqing, the static wind day is more, followed by winter fog weather is more frequent, is not conducive to the proliferation of pollutants, and more rain in summer, is conducive to the removal of particulate matter, resulting in $PM_{2.5}$ concentration in winter higher than summer.

According to Chinese current Ambient Air Quality Standard (GB3095-2012) [10], the average mass concentration of $PM_{2.5}$ in January and July 2015 is 81.54μg • m^{-3}, which is 2.3 times of the average annual upper limit. In the year of 2015, 62 samples of effective samples were collected, among which 21 exceeded the standard of $PM_{2.5}$ in the winter and exceeded rate 67.7% and 1.08 to 2.89 times exceeded. In summer the number of the upper limit of the secondary standard about the day average concentration is 2. Thus, winter atmospheric fine particulate pollution is much higher than in summer.

Seasonal variation of water-soluble ionic. In this study, F^-, Cl^-, SO_4^{2-}, NO_3^-, K^+, Ca^{2+}, Na^+, Mg^{2+} and NH_4^+ were analyzed by ICS-600 ion chromatograph, as shown in Table 1. In Fuling, The total concentration of water-soluble ions in $PM_{2.5}$ ranges from 6.37 to 86.30μg•m^{-3} with an average of 34.69μg • m^{-3}. Water-soluble ionic components accounted for 42.28% of the total mass of $PM_{2.5}$ sample, showing that the water-soluble ionic component is an important component of $PM_{2.5}$.

From Table 1, the average values of water-soluble ions in Fuling area in January and July are:SO_4^{2-}>NO_3^->NH_4^+>Cl^->Na^+>K^+>Ca^{2+}>F^->Mg^{2+}, the concentration values are14.48, 8.27, 8.00, 1.63, 1.28, 0.76, 0.41, 0.24 and 0.07μg•m^{-3}, Water-soluble ions accounted for 41.43%, 23.66%,

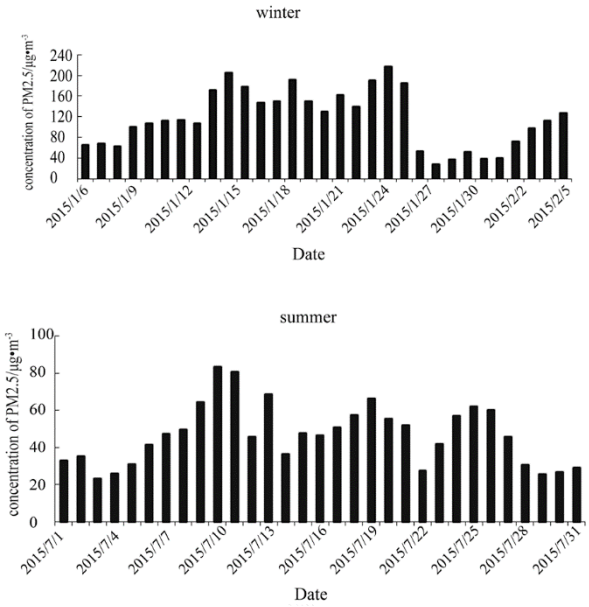

FIGURE 1
Mean daily variation of $PM_{2.5}$ concentration in urban area of Fuling in 2015

TABLE 1
Concentration levels of water-soluble ions in $PM_{2.5}$ (Unit: μg•m^{-3})

	winter			summer		
Analyzed series	maximum	minimum	average	maximum	minimum	average
Na^+	4.45	0.68	1.91	1.59	0.02	0.41
NH_4^+	20.27	2.30	12.00	10.40	0.30	3.86
K^+	2.88	0.16	1.29	0.48	0.05	0.21
Mg^{2+}	0.31	0.01	0.09	0.11	0.01	0.05
Ca^{2+}	2.34	0.01	0.55	0.44	0.07	0.18
F^-	1.20	0.02	0.38	0.30	0.01	0.09
Cl^-	12.71	0.12	2.94	3.69	0.32	0.95
SO_4^{2-}	43.91	3.86	18.63	26.51	3.30	10.20
NO_3^-	31.06	2.46	14.01	4.55	0.52	2.33

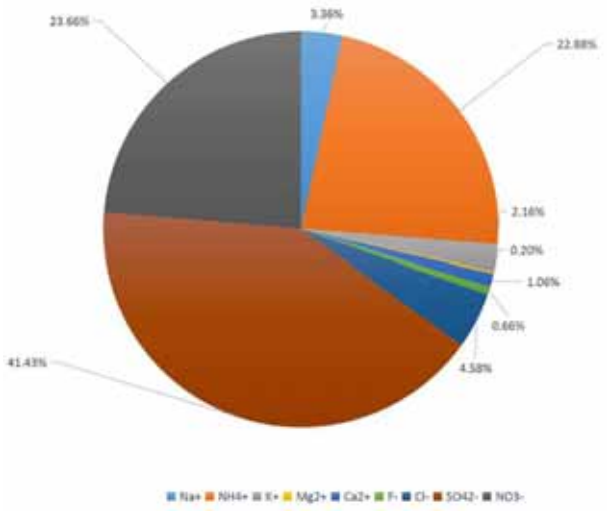

FIGURE 2
Percentage of water-soluble ions in total ions

22.88%, 4.58%, 3.36%, 2.16%, 1.06%, 0.66%, 0.20% of total water-soluble ions, respectively. Figure 2 shows the percentages of water-soluble ions in the total ions. The total mass concentration of SO_4^{2-}, NO_3^- and NH_4^+ was 30.53μg • m^{-3}, accounting for 87.99% of total water-soluble ions and 35.97% of $PM_{2.5}$, indicating that SO_4^{2-}, NO_3^- and NH_4^+ were the most important water-soluble ingredients in $PM_{2.5}$, but also that more serious secondary pollution.

The concentrations of SO_4^{2-}, NO_3^- and NH_4^+ were the highest in winter, which appeared on Feb. 5, Jan. 16 and Jan. 25, whose value were 43.91,31.06 and 20.27μg • m^{-3}, respectively. Mass concentrations of $PM_{2.5}$were 126.87,178.18 and 216.61μg • m^{-3}, respectively. The formation of SO_4^{2-} and NO_3^- is mainly due to the photo-chemical oxidation of SO_x and NO_x, which is susceptible to temperature, humidity and light intensity. Therefore, in contrast to the coastal city of Tianjin [11], (the secondary aerosol composition is summer> winter), while Fuling is winter> summer. In winter, the atmosphere structure is stable, the mixing layer height is relatively low, the cumulative effect is obvious, the pollutants accumulate in the atmosphere and spread slowly. Pollutant retention time is longer, but also makes primary pollutants prone to secondary transformation [12]. Fuling is located in the edge of Sichuan Basin, mostly mountainous, less rainfall and relatively high temperature in winter, is not conducive to the proliferation of pollutants, conductive to the formation of SNA.

Similar to water-soluble ion concentrations of $PM_{2.5}$ in Wanzhou, the seasonal distributions of water-soluble ionic components in $PM_{2.5}$ were all in winter> summer, and the average concentrations of SO_4^{2-}, NO_3^- and NH_4^+ are higher, about 1.12, 2.32, 1.30 times of Wanzhou, respectively [13]. This shows that pollution is more serious than Fuling, on the one hand is due to its serious pollution, on the other hand because of the main city of Fuling close to Chongqing, more vulnerable to the impact of the main city of pollutants.

The concentrations of Cl^-, Na^+ and Ca^{2+} in the primary aerosols were less than 2.5% of $PM_{2.5}$, which could reflect the characteristics of the source emission, and less rainfall in winter, the construction dust and ground dust caused by human activities, and long-distance dust lead to the three ions in winter are greater than the summer. The change of K^+ in $PM_{2.5}$ is mainly biomass burning, in winter (1.29μg•m^{-3}) which is about 6.14 times of that in summer (0.212μg•m^{-3}), which is related to the agricultural production in Fuling area. The maximum value of K^+ is 2.88μg•m^{-3} on January 26, the day Cl^-, Na^+ also has a higher value, most likely there is a straw burning activity. The total concentration of water-soluble ions in winter ranges from 10.82 to 86.30μg•$m^{-3}$with an average value of 51.08μg•m^{-3}. Figure 3 shows the daily variation of water-soluble ion concentration about $PM_{2.5}$ in winter.

The average daily average concentration of water-soluble ions in $PM_{2.5}$ was 85.66μg•m^{-3} on January 16 and 86.30μg•m^{-3} on January 25, and the $PM_{2.5}$ concentration was 178.18μg•m^{-3} and 216.61μg•m^{-3} respectively, which accounted for 48.08 and 39.84% of the $PM_{2.5}$ concentration on the same day. The minimum value was 10.82μg•m^{-3} on January28, accounting for 39.49% of the $PM_{2.5}$ concentration. The concentration of $PM_{2.5}$ on the day of sampling was 27.40μg•m^{-3}. Since February 6, no sampling, it cannot determine the February 5 water-soluble ions are peak, but the day the proportion of water-soluble ions accounted for the largest concentration of $PM_{2.5}$, about 62.18%, concentration of $PM_{2.5}$ on the day was 126.87μg·m^{-3}.

Figure 4 shows the ratio of water-soluble ions in $PM_{2.5}$ in winter. The concentration of water-soluble ions in winter is in the order of SO_4^{2-}>NO_3^->NH_4^+>Cl^->Na^+>K^+>Ca^{2+}>F^->Mg^{2+}, and the values are 18.63, 14.01, 12.00, 2.30, 1.91, 1.29, 0.59, 0.38, 0.09μg • m^{-3}, the percentages of the ions are 36.48%, 27.44%, 23.50%, 4.36%, 3.73%, 2.52%, 1.08%, 0.73% and 0.17% respectively. So the proportion of SO_4^{2-}, $NO_3^-$and respectively, is 86.53%, which is the biggest contribution of water-soluble ions. Water-soluble ions on January 27, a sharp decline, mainly rainy weather on the role of pollutants removal, so that rapid reduction.

The total concentration of water-soluble ions in summer ranges from 6.37μg•m^{-3} to 43.48μg•m^{-3}, with an average of 18.30μg•m^{-3}. Figure 5 shows the daily variation of water-soluble ion concentration in $PM_{2.5}$ in summer.

In summer the daily maximum concentration of water-soluble ions in $PM_{2.5}$ was 43.48μg•m^{-3} on July 10, accounting for 52.18% of $PM_{2.5}$ concentration, and the $PM_{2.5}$ concentration on the day was 83.33μg•m. The lowest concentration of $PM_{2.5}$ on July 29 was 6.37μg•m^{-3}. On the day of sampling, the mass concentration of $PM_{2.5}$ was 25.62μg•m^{-3}., accounting for 24.82% of the mass concentration of $PM_{2.5}$ on the same day.

In the summer, the water-soluble ions were in the order of SO_4^{2-}>NH_4^+>NO_3^->Cl^->Na^+>Ca^{2+}>K^+>F^->Mg^{2+}, the average concentration values were 10.20, 3.86, 2.33, 0.95, 0.50, 0.22, 0.21, 0.09 ,0.05μg•m^{-3}, The percentages of water-soluble ions were 55.72%, 21.11%, 12.75%, 5.21%, 2.29%, 1.13%, 1.02%, 0.47% and 0.28% respectively. Figure 6 shows the proportion of water-soluble ions in $PM_{2.5}$ in summer. It can be seen, SO_4^{2-}, NH_4^+ and NO_3^- are still the main component of water-soluble ions. The water-soluble ions decreased sharply on July 12, mainly due to rainfall and rainfall, which was favorable for the removal of particulate pollutants.

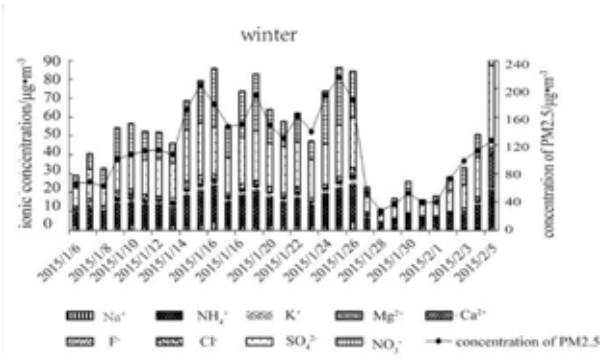

FIGURE 3
Daily variation of water-soluble ion concentration about $PM_{2.5}$ in winter

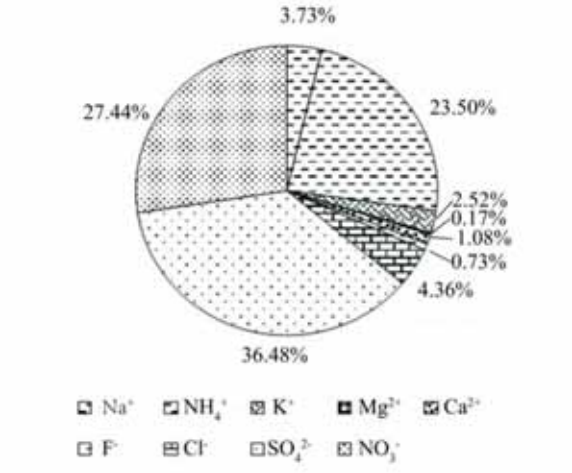

FIGURE 4
Percentage of water-soluble ions in winter

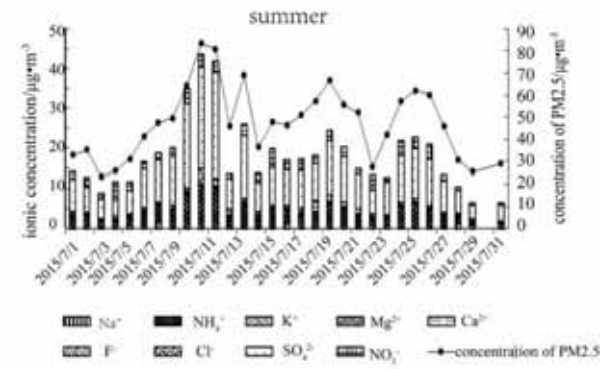

FIGURE 5
Daily average of water-soluble ions in summer

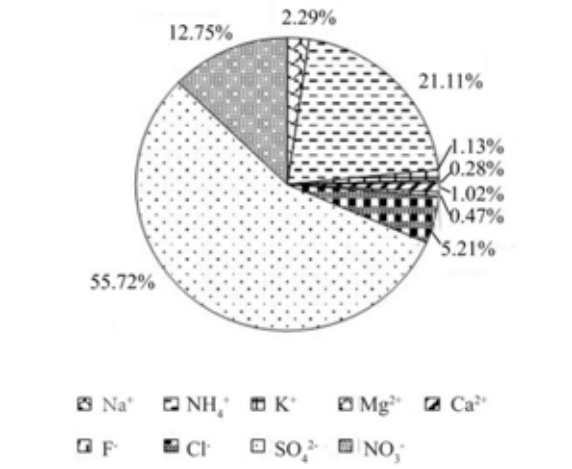

FIGURE 6
Percentage of water-soluble ions in summer

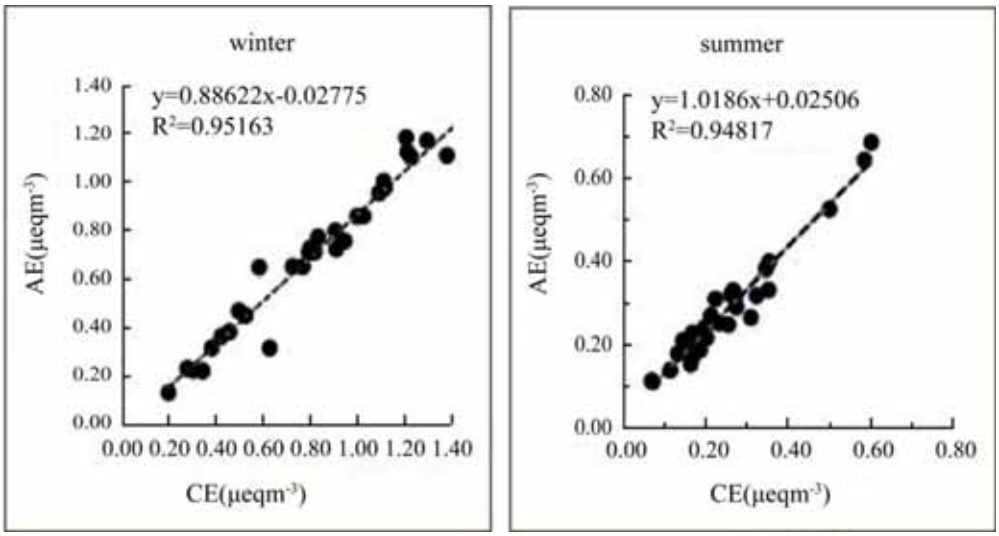

FIGURE 7
Balance of anions and cations

TABLE 2
Correlation of water-soluble ion

	Na^+	NH_4^+	K^+	Mg^{2+}	Ca^{2+}	F^-	Cl^-	SO_4^{2-}	NO_3^-
Na^+	1	-0.314	-0.301	0.174	0.399	0.051	-0.278	-0.257	-0.365
NH_4^+	0.539	1	0.840	-0.006	-0.359	-0.203	0.583	0.983	0.509
K^+	0.658	0.900	1	0.067	-0.393	-0.167	0.510	0.843	0.362
Mg^{2+}	0.774	0.555	0.580	1	0.317	-0.587	-0.198	-0.033	0.109
Ca^{2+}	0.473	-0.003	0.092	0.359	1	0.011	-0.450	-0.413	-0.003
F^-	0.178	0.320	0.147	0.131	-0.051	1	0.018	-0.173	-0.376
Cl^-	0.371	0.227	0.239	0.286	0.474	0.082	1	0.571	0.137
SO_4^{2-}	0.401	0.926	0.724	0.384	-0.076	0.442	0.180	1	0.395
NO_3^-	0.566	0.869	0.889	0.670	0.110	0.101	0.156	0.634	1

Note: the lower left corner for the winter, the upper right corner for the summer

Balance of anions and cations and acidity and alkaline of particular matter.

$$\text{Cation(CE)}=\frac{Na^+}{23}+\frac{NH_4^+}{18}+\frac{K^+}{39}+\frac{Mg^{2+}}{12}+\frac{Ca^{2+}}{20}$$

$$\text{Anion(AE)}=\frac{SO_4^{2-}}{48}+\frac{NO_3^-}{62}+\frac{Cl^-}{35.5}+\frac{F^-}{19}$$

It can be seen from Figure 7 that the correlation of anions and cations is very good, and R^2 in both winter and summer is equal to 0.95, indicating that the sample data are valid and the ions analyzed are the main components of $PM_{2.5}$. According to the slope of the equation, the slope is less than 1 in winter, the overall level of ions is alkaline; the slope is greater than 1 in summer, the overall is acidic. Although the average concentration of SO_4^{2-}, NO_3^- and NH_4^+ in winter is higher than that in summer, the dust is not conducive to the diffusion due to the less rain and windy days in winter, and the dust, soil dust and crop incineration are not conducive to diffusion and can neutralize the acid aerosol, resulting in the ions are alkaline in winter. In summer, the temperature is high and rainy, and the weather changes frequently, which is favorable for the chemical reaction of SO_x and NO_x, resulting in the ions are acidity in summer.

The relationship between the water-soluble ions. Table 2 for the water-soluble ion correlation coefficient matrix. The correlation between SO_4^{2-} and NO_3^- in winter (0.634) is better than summer (0.395) indicates that the two have good homology in winter, both from the combustion of fossil fuels and the conversion of SO_x and NO_x from motor vehicles. The correlation between NH_4^+ and SO_4^{2-} was good in winter and summer, but it was slightly higher in summer than in winter, 0.983 in summer and 0.926 in winter. Indicating that the meteorological conditions in summer, the source of emission characteristics more conducive to their formation. The correlation between NH_4^+ and NO_3^- was less obvious in winter than in winter. Thus, NH_4^+ in the winter and easy to NO_3^- combination; in the summer and SO_4^{2-} priority.

The correlation between Cl^- and NH_4^+ in the summer was 0.583, indicating that excess NH_4^+would combine with $Cl^-$to form NH_4Cl. Cl^- and Na +, SO_4^{2-}, NO_3^- are poor, indicating that the homology is not obvious, and Cl^- not from coal and motor vehicle emissions, may come from biomass combustion. The correlation between Cl^- and K^+ in summer is 0.51, indicating that KCl exists in summer $PM_{2.5}$.

CONCLUSIONS

In this paper, the data in two seasons of Chongqing Fuling in 2015 were collected to study the water-soluble ions in Fuling area. The diurnal and seasonal changes of water-soluble ions, the anion and cation balance, and correlation of water-soluble ions were analyzed. The results reflected in a certain extent that $PM_{2.5}$ pollution characteristics. Mastering the $PM_{2.5}$ pollution status, distribution characteristics and temporal and spatial variation of Fuling $PM_{2.5}$ are of great significance to comprehensively understand the atmospheric pollution in Fuling area.

ACKNOWLEDGEMENTS

This work was supported by Chongqing Municipal Commission of social and livelihood projects [Grant No. cstc2015shmszx20010], Scientific and Technological Research Program of Chongqing Municipal Education Commission [Grant No. KJ1401205] as well as Fuling District Science and technology research projects [Grant No. FLKJ2015ABB1097].

The authors declare no conflict of interest.

REFERENCES

[1] Zhang, D., Zhou, Z.E., Zhang, C., Meng, X.X., Bai, Z.P. (2011) The PM_(2.5) Source Profile in the Chongqing Urban Areas. Environment & Ecology in the Three Gorges. 33, 14-18.

[2] Chen, K., Chen, G., Wang, D., Meng, X., Tao, J., Jiang, W. (2003) Analysis of TSP Character in Chongqing. Chongqing Environmental Science. 25, 43-46.

[3] Ren, L.H., Zhou, Z.E., Zhao, X.Y., Yang, W., Yin, B.H., Bai, Z.P. (2014) Source apportionment of PM10 and $PM_{2.5}$ in urban areas of chongqing. Research of Environmental Sciences. 27, 1387-1394.

[4] Zhang, L.Y., Liu, Y., Qiao, B.Q., Fu, C., Wang, H.B., Huang, Y.M. (2016) Characteristics of Atmospheric Dry and Wet Deposition of Trace Metals in the Hinterland of the Three Gorges Reservoir. China. Environmental science. 37, 466-474.

[5] He, K.B., Yang, F.M., Duan, F.K., Ma, Y.L. (2011) Atmospheric Particles and Regional Compound Pollution. Beijing: Science Press. 5, 135-142.

[6] Geng, Y.H., Wei, L., Jian, S., Jian, Y., Fan, X.B., Wei, N.N. (2010) Characterization of major water-soluble ions in size-fractionated particulate matters in Shanghai. China Environmental Science. 30, 1585-1589.

[7] Ma, J.Z., Liu, Y.C., Ma, Q.X. (2011) Atmopheiuc heterogeneous reactions and their environmental effects. Environmental Chemistry. 30, 97-119.

[8] Su, B.B., Zhang, Z.S., Tao, J., Tao, J., Xu, J.Y., Ji, X.X., Liu, X.D. (2015) Characteristics of Water-soluble Inorganic Ions in $PM_{2.5}$ and $PM_{2.5}$ -10 in Mountain Background Region of East China in Spring. Environmental Science. 36, 1195.

[9] Jia, Y.T. (2008) Study on Formation Mechanism of Regional Pollution of Atmospheric Particles in Beijing. 6, 25-26.

[10] People's Republic of China (1996) Ambient air quality standard. Environmental Protection of Oil & Gas Fields.2.

[11] Sun, R., Zhang, W.J., Dong, H.Y., Bian, W.L., Chen, K. (2014) Chemical Character and Source Analysis of Water-Soluble Irons in PM_(10) and PM_(2.5) in Tianjin City. Environmental Monitoring China. 30, 145-150.

[12] Cao, J.J. (2014) $PM_{2.5}$ and environment. Beijing: Science Publishing. 67-154.

[13] Li, H.L. (2014) Research of the Chemical Composition Characteristics of $PM_{2.5}$ in Wanzhou City in Summer and Winter, Chongqing. 4, 3-5.

Received: **18.09.2017**
Accepted: **26.11.2017**

CORRESPONDING AUTHOR

Xianghong Wang
The Research Center for Ecological Environment Monitoring and Disaster Control of the Three Gorges Reservoir, Yangtze Normal University,
No. 16 Li Du Juxian Road,
Fuling District,
Chongqing, 408100 – China

e-mail: mikeue@sina.com.

© by PSP Volume 27 – No. 2/2018 pages 1145-1151 Fresenius Environmental Bulletin

EFFECT OF HEAT STABILIZED WHEAT GERM ON SOME PROPERTIES OF COOKIES

Hulya Gul[1,*], Fatma Hayit[2], Songul Bicakci[1], Sultan Acun[3]

[1]Department of Food Engineering, Faculty of Engineering, Suleyman Demirel University, 32260, Isparta, Turkey
[2]Bogazliyan Vocational School, Bozok University, Yozgat, Turkey
[3]Suluova Vocational School, Amasya University, 05500, Amasya, Turkey

ABSTRACT

The aim of this study was to evaluate the impact of heat stabilized wheat germ addition (HSWG) on the some chemical, physical and sensory quality of wheat flour cookies as well as to investigate the consumer's acceptability and purchasability of these cookies. For this purpose, wheat germ, after inactivation of its enzymes by heat treatment, was added at 0, 10, 20 and 30% levels replacement with wheat cookie flour. The incorporation of the HSWG in increasing amounts lead significant changes on thickness and spread ratio of cookies. After 10% addition level of HSWG, the thickness of the cookie samples were decreased and accordingly the spread ratios were increased. At the same time cookies were became darker as the HSWG ratio was increased. The results showed that the cookies favoured by consumers could be produced by adding maximum 10% of HSWG without affecting negatively their technological quality. Thus the usage of raw wheat germ after limiting its enzymatic activity by heat treatment (roasting) will increase both the shelf life and acceptability of cookies.

KEYWORDS:
Wheat germ, heat stabilization, cookie, quality, consumer acceptance, purchasability

INTRODUCTION

Wheat grain morphologically consists of three basic parts: germ, bran and endosperm. Due to its rich nutrient content, it is one of the most produced and consumed grains in Turkey and in the world [1], [2]. Whole grains contain phytochemicals such as lignin, phenolic acids and nutrients such as phytic acid, tannins and enzyme inhibitors. The separation of germ and bran by grinding causes the loss of these important components [1]. The germ has more protein, fat, sugar, mineral matter, thiamine and riboflavin when compared to wheat flour [3]. During processing of wheat to the flour, it was determined that calcium content decreased by 35%, iron content decreased by 80%, bran and germ separation resulted in a decrease of 60% in B1 and B2, 85% in content of B6 and niacin [4].

Germ is the part which makes 2.5-3.5% of the wheat and allows the formation of a new plant from the body [5]. Germ contains approximately 52% carbohydrates, 23% protein, 11% water, 10% fat, and 4% mineral matter and the proportion of these components is better than endosperm [5], [6]. Germ oil is rich in polyunsaturated fatty acids and 70% is essential fatty acid [7], [8], [6]. It is also a rich source of antioxidants such as tocopherols, phenolic substances, carotenoids, important bioactive compounds such as sterols, and phytosterols [6], [9].

Germ contains high amounts of lysine, aspartic acid and arginine, 8 different minerals including 18 kinds of amino acids, more than 10 vitamins including high amount of vitamin E, pantothenic acid and vitamin B1, phosphorus, potassium and magnesium and omega-3, Omega-6 contains omega-9 fatty acids [10], [11], [3]. Along with all these beneficial ingredients, about 15% of the recommended dietary fiber for healthy eating is available in germ [10]. Consumption of dietary fibers provides weight control, regulation of blood sugar, protection against cancer and heart disease [12]. In addition to its high nutritional value and taste and flavour, wheat germ is a very suitable source for the enrichment of protein and vitamins of foodstuffs [3]. Also it is used in the cosmetics, chemical and pharmaceutical industries as well as food industry because of the abundance of germ-rich biologically active ingredients [7], [11]. Atalay [13] reported that wheat germ oil accelerated wound healing when working on rats.

Wheat germ is quite amenable to oxidation in the free state [14]. The low stability of the wheat germ reduces the shelf life of germ-containing wheat flour and related bakery products, which limits the use of wheat germ in the bakery industry. Germ is the living part of the grain, which is responsible for the development of the plant because of the oxdidative and hydrolytic enzymes, in particular lipase and lipoxygenase activity, and the susceptibility of the free fatty acids to oxidation and ultimately in the products [15]. Because of its high content of unsaturated lipids and an important enzymatic activity being lipases and lipoxygenase, cause the highest impact in the reduction on the shelf life of wheat germ to only few days. There are several methods such as; continuous microwave [16], infrared radiation [17],

gamma irradiation [18], heat-treatment or sourdough fermentation [19] to increase the storage stability and shelf life of wheat germ.

Wheat germ is a valuable by-product of the flour industry with its rich nutrient content. Therefore it is a unique source of concentrated nutrients, highly valued as food supplement [20]. Unfortunately, it must be separated from the wheat flour because of its adverse effect on storage stability of flours. The reason of limited keeping quality and utilization of wheat germ in bakery products can be attributed the presence of large amount of unsaturated fatty acids as well as hydrolytic enzymes causes the product highly susceptible to rancidity. For this reason in the present study raw wheat germ was subjected to heat treatment before adding in to cookies.

Cookies are widely consumed all around the word because of their lots of variety, preference by all age groups, relatively long shelf life and ready to eat form. Gül et al. [21] found that 97.21% of consumers consume cookies and the frequency of cookie consumption of interviewed consumers varies between once a week and every 15 days. They [21] determined that monthly consumption of cookie was calculated as 1649.81 grams and sweet cookies were more preferred by consumers, cookies consumed along with afternoon tea by 59% of the interviewed households.

There has been a particularly noteworthy increase at consumer demand for "healthy" in other words "functional" foods. Therefore, in the present study, it was aimed to investigate the effect of HSWG which has high functional quality as mentioned above, on physical, technological and sensory properties of cookies.

MATERIALS AND METHODS

Materials. The cookie flour used in the production of cookies was obtained from Sosyete Milling Factory (Karaman) and the wheat germ was supplied from Berberoğlu Milling Factory (Burdur). Sodium bicarbonate from Şişecam Chemicals Group Soda Industry (Mersin, Turkey), corn syrup (HFCS 42%) was from Sunar Corn Integrated Plant Inc. (Adana, Turkey), hydrogenated vegetable oil and powdered sugar was supplied from Mustanoğlu Gıda (Isparta, Turkey). All chemicals used were of analytical grade.

Preparation of HSWG samples. Wheat germ was taken during the day of production from the factory, then brought to the laboratory and subjected to heat treatment at 130 ° C for 20 minutes to limit enzyme activity in a natural flow type oven (Daihan, WiseVen Won, South Korea). Then, HSWG was grounded with a hummer mill (Tekpa, Ankara) and sieved. Samples which had particle size between 125-200 μm was collected and stored in an airtight plastic bags and kept in a freezer (− 18 ◦C) until it was further used for different experiments.

Preparation of cookie samples. The cookies were prepared by AACC 10-50.05 [22] method with slight modifications. The cookie formula is given in Table 1. There is an increasing trend to consume more healthy foods such as which contain less fat and sugar by consumers. Thus, many manufactures altered the saturated fat and sugar composition of cookies to address policy requirements and hedonic properties demanded by consumers [23]. Therefore, in the present study to produce more healthy cookies, shortening and powdered sugar in cookie formulation was reduced by 50%, 23% respectively. These reduction rates were determined as a result of the preliminary tests performed (data was not given) from us.

TABLE 1
Cookie formula

Ingredients, at 23.9° (75 °F)	*Weight (g)*
Shortening(1)	64.0
Powdered Sugar (2)	130.0
NaCl	2.1
Sodium bicarbonate	2.5
Dextrose solution (HFCS 42%)	33 ml
Distilled water (3)	*
Flour (based on 14% moisture basis)	225 g

(1): Shortening in the formulation is reduced by 50%.
(2): The sugar in the formulation is reduced by 23%.
(3):* Determined by the Consisto-Alveograph for each formulation.

HSWG was added to the cookie formulation at different ratios (0%, 10, 20, 30) on the basis of displacement with wheat cookie flour. Cookie dough was prepared by using Hobart N50 mixer (Hobart, Troy, OH, USA). After mixing dough was gently scraped from bowl and placed six portions at well-spaced points on lightly greased cookie sheet. Then dough was sheeted to 5 mm by rolling pin and cut into circular shapes with a circular scone cutter having an internal diameter of 60 mm. The cut-out pieces of dough were baked on greased pans at 205 ºC for 10 min in a conventional oven. After cooling to room temperature, it was packaged hermetically in high density polyethylene bags and stored until analysis was performed.

Chemical analyses. Cookie flour was analysed for moisture by AACC Method 44-01.01 [24], wet and dry gluten by AACC Method 38-12.02 [25], sedimentation by AACC Method 56-60.01 [26], Alveo-consystograph parameters by AACC Method 54-30.02 [27] 54-50.01 [28]. In wheat germ, moisture was analysed by AACC method 44-01.01 [24], total oil by AOAC [29] and ash by AACC method 08-01.01 [30].

Physical characteristics of cookies. In the experiments, the width (W) and the thickness (T) of

the cookies produced using germ at various ratios (6 cookie samples taken at each trial) were measured using digital callipers. The spread ratio (W/T) was calculated by the ratio of the cookie width to the thickness (AACC Method, 10-50.05) [22]. The colour values; L * value [(0) black- (100) white], a * value [(+) red- (-) green] and b * value [(+) yellow -(-) blue] of the cookie samples were determined with Minolta CR 400 (Konica Minolta Sensing, Inc., Osaka, Japan) [31].

Sensory analysis and purchasability. Sensory analysis was done 4 hours after the cookies were produced. Cookies were evaluated by 15 trained panellists in terms of appearance (brightness, surface colour and surface smoothness), inner structure (cross section structure, pore distribution, crust thickness) taste (hardness, chewiness, dispersion in the mouth) and flavour.

A 5-point hedonic scale was used to determine the sensory quality criteria. "Dislike extremely" and "like extremely" were scored in order from lowest point to highest point. The same scale was applied when the purchasability was determined. 1 point "definitely would not buy" and 5 points "definitely would buy" was expressed as. The purchasability test was conducted with a total of 30 volunteer cookie consumers, 15 males and 15 females aged between 17 and 62 years.

Statistical analysis. The trials were conducted in triplicate. The data obtained at the end of the study were compared with the analysis of variance. Analysis of variance (ANOVA) was performed using the SPSS 16.0 program. Averages of the sources of principal variation, whose differences are statistically significant, were determined by the Duncan multiple comparison test.

RESULTS AND DISCUSSION

Some Properties of Cookie Flour. The moisture, wet gluten, dry gluten, sedimentation and alveo-consistogram values of cookie wheat flour used in cookie production are given in Table 2. Cookie wheat flour is in the category of special purpose flour in the Turkish Food Codex Wheat Flour Association No: 2013/9 [32].

The moisture content of the cookie flour used in the experiments was 14.2%, the wet gluten value was 28%, the dry gluten value was 9%, the sedimentation value was 21 ml and the water absorption was 54.9%. Demir [33] reported that moisture content of cookie flour was 11.71%, wet gluten value was 23.5%, selenium sedimentation value was 20.5 ml; Sertakan [34] reported the moisture content of wheat flour as 13.8% and the wet gluten content as 23%, the sedimentation value as 21 ml and the water absorption as 49.4%; Levent [35] found that the wet gluten content of cookie flour was 22.75%, the sedimentation value was 18.61 ml, the water absorption rate was 51.80%, Svoboda and Barier [36] measured the sedimentation value of 2 different wheat cultivars as 30 ml and 25 ml. Atli et al. [37] determined the sedimentation value of 20 wheat cultivars as 18.8-57.6 ml.

Since cookie wheat flours' quality are affected considerably by factors such as the variety, location, and climate, it may be normal to find that there are limited differences between the results of different researchers and the results of the present study.

As can be seen from the alveogram values (Table 2), cookie flour has the ability to spread because of its low gluten content. The fine granulation structure of the cookie flours is associated with low protein content and low water absorption ability to provide the desired spreading rate and uniform internal structure in products made from soft wheat.

TABLE 2
Some properties of cookie flour

Properties	Cookie flour
Moisture (%)	14.2
Wet gluten (%)	28
Dry gluten (%)	9
Sedimentation (ml)	21
Delayed sedimentation (ml)	14
Alveo-Konsistograph parameters	
Water absorption (%)	54.9
P: Resistance to extension (mmH_2O)	57
L: Extensibility (mm)	44
G: Expansion index	14.8
W: Area under the curve ($10^{-4}J$)	83
RP/L: Ratio of curve height to length	1.3
Ie: Elasticity index (%)	24.3

Some properties of wheat germ. The moisture content of HSWG was 11.02% and the total fat content was 20.94%. As seen from these results, the fat content of wheat germ is quite high. Germ oil is rich in essential fatty acids. However, it contains B1, B2, B6, PP and D vitamins and other biologically active compounds [38]. Germ ash value was calculated to be 4.56. This value was in agreement with the values determined by Appelt [10] (4-5%) and Çakmaklı [39] (4.82%).

Some properties of cookie samples. The moisture values of the cookies were 9.6% in control and 8% in germ-added samples. Moisture content of cookies made by various researchers were reported to vary from 2.1% to 9.47% [40], [41], [42].

The physical properties of cookies containing HSWG at different ratios are given in Table 3. There was no statistically significant difference in widths with increasing HSWG supplementation ratio ($p > 0.05$). After 10% substitution level, thickness was decreased and spread ratio was increased. However, no statistically significant difference was found between 20% and 30% addition levels in terms of both

thickness and spread ratio (p> 0.05). Due to the increase in the HSWG supplementation rate, the decrease in the thickness of the cookies and the increase in the spread ratio were expected, due to the dilution of the gluten by the germ particles. These results were similar to those reported for cookies prepared from defatted wheat germ –wheat flour blends [43].

Contrary to these results, Acun [41] found no significant change in width and thickness at 5% addition of grape seed flour, but reported that the addition of more than 7.5% led to a decrease in cookie width. Similarly, it was reported that the spread ratio of cookies decreased as the contribution rate increased in different studies; such as lemon fiber-wheat bran [42], wheat-rice bran [44], palm plant residue [45], pea flour [46], rye flour - buckwheat flour [42], apples, oranges, lemons, grapefruits, carrots, oranges fibers [47].

This study suggests that the increase in the rate of spread ratio by HSWG addition is due to the decrease in hydrophilic areas due to the decreasing gluten content in the germ. It was reported that the cookies with a high spread ratio were preferred most [48], and high quality cookies was obtained [34]. Ertop et al. [49] found that the germ generally contained 9% fat and they suggested that this fat may be prevent the mass formation between starch and gluten thus it leads the product to become soft. In the present study higher spread ratio of cookies with high amounts of HSWG may be attributed the higher fat content of HSWG so it may cause the dough become softer.

TABLE 3
Physical properties of cookies containing HSWG at different ratios ([1])

HSWG level (%)	W mm)	T (mm)	(W/T)	L	a	b
0	59.5^{a}	12.3^{a}	4.8^{b}	63. 9^{a}	6.9^{d}	17.6^{a}
10	59.8^{a}	12.1^{a}	4.9^{b}	56.0^{b}	8.9^{c}	15. 9^{b}
20	60.1^{a}	11.7^{b}	5.1^{a}	52.1^{c}	9.8^{b}	14.5^{c}
30	59.9^{a}	11.7^{b}	5.1^{a}	48.7^{d}	11.1^{a}	13.3^{d}

[(1)]: There is no statistically significant difference between the averages indicated by the same letter in the same column (p <0.05).
W: Width, T: Thickness, W/T: Spread Ratio
L:Brigtness, a: redness, b:yellowness

Colour values of cookie samples. Colour is one of the important factors affecting consumer choice. Especially in cereal products, colour is gaining more importance because it gives an idea about freshness of the product. When Table 3 is considered, the values of L, a and b of cookies produced by adding HSWG and were observed statistically different from each other and from control samples.

The L value, indicator of the brightness, was decreased significantly as the level of HSWG increased. As can be seen from Figure 1, cookies were become darker with the increasing levels of HSWG. In contrast the L value a value (redness) was increased significantly from 6.94 to 8.92, 9.77 and 11.06 for control and for 10, 20 and 30% usage levels of HSWG respectively. On the other hand b value (yellowness) of HSWG containing cookies were gradually decreased with the addition of higher levels of HSWG.

Increase at the browning of cookies might be due to maillard reactions and sugar caramelization. Maillard reaction occurs between compounds with amino groups and carbonyl groups present in foods and lysine provided the majority of free amino groups in proteins, which were the main participant in this reaction [50]. Wheat germ has well-balanced amino acid profiles and relatively rich in lysine, which is the first limiting amino acid in the wheat grain [51]. The lysine content would increase proportionally as the amount of HSWG added to the cookies and as a result more darker cookies were obtained.

Also the acidic character of the lysine is due to the presence of two amino groups, might be resulted in a faster reaction [52] so more browning.

Furthermore, the addition of HSWG at the 30% level was caused to form cracks on the surface of the cookies (Fig. 1).

FIGURE 1
Overall view of cookie samples produced with different levels of HSWG

Demir [33] reported that the L * and b * values of the cookies produced with full wheat flour decreased, while the a * value increased [53].

Sensory properties of cookies. The cookies produced in the experiments were subjected to sensorial evaluation and results are shown in Figure 2. Sensorial test revealed that sudden drop was noted after the 10% addition level in the crust thickness value were taken significantly high scores than control and other germ added cookies by means of brightness, surface colour and inner pore distribution. Panellists found the surface smoothness of the HSWG cookies significantly lower than the control. In addition cookies containing more than 20% HSWG were taken least surface smoothness scores because of cracks on their surface.

Although a slight decrease was observed at the cross section structure after addition of HSWG, there is no statistical difference was detected between cookies. A sudden drop at crust thickness was noted after the 10% addition level of HSWG.

Increasing levels of HSWG (0–30%) were caused a significant decrease at the hardness value of

cookies while hardness of 10 % containing HSWG cookies were closely resembled the control (100% wheat flour) cookies with 20 and especially 30% HSWG was found difficult to bite because of their higher hardness. Dough became harder and denser as a result of competition between non-starch polysaccharides such as cellulose and hemicellulose with gluten for water through HSWG addition [54]. Thus when HSWG was added more than 10% level this might cause the firm and hard structure on final product. The force applied during the bite increased as the germ addition rate increased, and the cookies displayed a harder structure.

Chewiness is a dependant on hardness parameter; therefore, its behaviour will follow a similar tendency. But chewiness of 10% HSWG cookies were scored a little more than control. On the other hand further increasing the supplementation amount of HSWG up to 30% was lead to drop chewiness, distribution in the mouth and flavour points of cookies. 10% HSWG added cookies received almost similar flavour scores when compared with control. Heat treatment was provide a roasted taste to wheat germ. Therefore addition of this roasted germ in to cookies was found acceptable and pleasant up to 10% level. But increasing the usage level of it at 20% and 30% levels were brought an unpleasant flavour to cookies.

Highest sensorial scores was reported by Tyagi et al. [55] and Tiwari et al. [46] for cookies with 15% non-fat mustard seed flour and 15% pea flour, respectively.

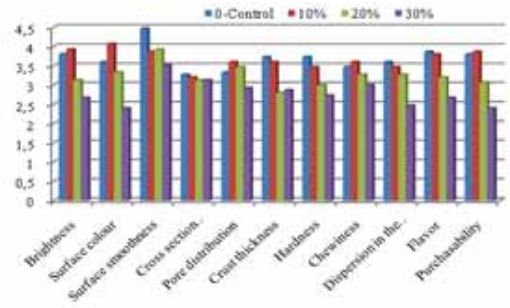

FIGURE 2
Sensory evaluation and purchasability of cookie samples produced with different levels (0-control, 10, 20 and 30%) of HSWG

Purchasability of cookies. The purchasability test of the produced cookies was carried out with an equal number of men and women aged between 17 and 62 years with 30 volunteer cookie consumers. As a result of scores given by different consumers at income level and education level, the findings obtained were given in Fig. 2. %10 HSWG cookies were received more point than others. It was not noteworthy that these cookies were got a little bit more score than the control samples. The control group and the 10% germ added cookie group generally received "definitely would buy" points and no statistically significant difference was found between them ($p > 0.05$). When the HSWG supplementation level was increased to 20%, the availability scores decreased, and at 30% there was a further decrease in this parameter. Therefore, we suggest that the HSWG cookies can be prepared with up to 10% addition level of it to maintain the sensory acceptability for the consumers. According to the findings, 10% germ added cookies were preferred over 20% and 30% added levels. That is, the consumer will tend to buy cookies containing 10% germ.

CONCLUSION

The conversion of food industry by-products to valuable food ingredients is important both in terms of contributing to the economy and increasing the functional characteristics of food in which they used. Wheat germ, an important by-product of flour industry is generally used as an animal feed. Therefore in the present study it was aimed to gain wheat germ as a value-added food ingredient by investigating its effect on the quality of cookies. Raw wheat germ was subjected to heat treatment. To increase its keeping quality and pleasant flavour that gives to cookies.

The addition of increasing amounts of HSWG was not caused a significant difference on moisture content and widthness of the cookies, while the thickness, brightness and yellowness were reduced. In contrast spread ratio and redness were shown an increase with the increasing rates of HSWG. When the supplementation level of it was raised to 30%, the surface of the cookies were began to crack. This data is important to put forward the impact of HSWG on cookie quality from the technological point of view.

The results showed a higher sensorial scores and acceptability for the cookies with 10% of HSWG, with the lower scores for the cookies with 20 and 30%. So in order to improve functional properties of cookies with reduced fat and sugar content and acceptable quality in terms of technological and sensorial viewpoint, raw germ after roasting can be used up to 10% level.

REFERENCES

[1] Slavin, J.L., Jacobs, D., Marquart, L. and Wiemer, K. (2001) The role of Whole grains in disease prevention. Food Science and Nutrition. 101, 780-785.

[2] Gül, H., Acun, S., Türk, S., Öztürk, A. and Kara, B. (2012) Physical characteristics of some wheat genotypes cultivated in Lake district of Turkey (in Turkish). Batı Akdeniz Araştırma Enstitüsü, Derim Dergisi. 29, 21-32.

[3] Demir, M.K. and Elgün, A. (2015) Importance of wheat germ in nutrition (in Turkish). 1. Ulusal Helal ve Sağlıklı Gıda Kongresi, 19-20 November 2015, Ankara. 184-185.
[4] Şanal, T. (2009) White gold flour. Standard. 48, 32-35 (in Turkish).
[5] Baysal, A. (2009) Beslenme. (16th edition) Hatipoğlu Yayınları, Ankara.
[6] Gelmez, N., Kıncal, N.S. and Yener, M.E. (2009) Optimization of Supercritical carbon dioxide extraction of antioxidants from roasted wheat germ based on yield, total phenolic and tocopherol contents, and antioxidant activities of extracts. J. Supercrit. Fluids. 48, 217-224.
[7] Karwowska, K. and Kostrezewa, E. (1998) A new technology, for the production of valuable vitamin extracts from wheat and rye germs. Die Nahrung. 32, 491-495.
[8] Çiftci, V. (2002) Effect of wheat germ addition on the selected properties of bread. University of Gaziantep Food Engineering, Gaziantep.
[9] Zhu, K. Lian, C. Guo, X. Peng, W. and Zhou, H. (2010) Antioxidant activities and total phenolic contents of various extracts from defatted wheat germ. Food Chem. 126, 1122 -1126.
[10] Appelt, G. (1986) Nutritional value and stability of extruded wheat germ product. Getreide Mehl Brot. 40, 176-180.
[11] Hışıl, Y. and Ötleş, S. (1991) Vitamin and mineral contents of wheat germ. Gıda. 16, 303-306.
[12] Gül, H., Yanık, A. and Acun, S. (2013) Effects of white cabbage powder on cookie quality. J Food Agric Environ. 11, 68-72.
[13] Atalay, C. (2013) Assessment of the effects of quince seed mucilage and wheat germ oil on wound healing in rats. Marmara University Graduate School of Health Sciences, İstanbul.
[14] Yazıcıoğlu, B. (2013) Encapsulation of wheat germ oil. Orta Doğu Teknik University Graduate School of Natural and Applied Sciences, Ankara.
[15] Rizzello, C.G., Nionelli, L., Coda R., Cagno, R.D. and Gobbetti, M. (2010) Use of sourdough fermented wheat germ for enhancing the nutritional, texture and sensory characteristics of the white bread. Eur Food Res Technol. 230, 645–654.
[16] Xu, B., Zhou, S.L., Miao, W.J., Gao, C., Cai, M.J. and Dong, Y. (2013) Study on the stabilization effect of continuous microwave on wheat germ. J Food Eng. 117, 1–7.
[17] Gili, R.D., Palavecino, P.M., Penci M.C., Martinez, M.L. and Ribotta, P.D. (2017) Wheat germ stabilization by infrared radiation. J Food Sci Technol. 54, 71–81.
[18] Jha, P.K., Kudachikar, V.B. and Kumar, S. (2013) Lipase inactivation in wheat germ by gamma irradiation. Radiat Phys Chem. 86, 136–139.
[19] Marti, A., Torri, L., Casiraghi, M.C., Franzetti, L., Limbo, S., Morandin, F., Quaglia, L. and Pagani, M.A. (2014) Wheat germ stabilization by heat-treatment or sourdough fermentation: Effects on dough rheology and bread properties. LWT - Food Sci Technol. 59, 1100-1106.
[20] Brandolini A. and Hidalgo A. (2012) Wheat germ: not only a by-product. Int J Food Sci Nutr. 63, 71–74.
[21] Gül, H., Özmen, C., Ak Metin, S. and Gül, M. (2016) Consumption and preferences of cookie products of consumers: a case in the city of Isparta" XII. Ulusal Tarım Ekonomisi Kongresi Kitabı. 3, 1903-1912. (in Turkish).
[22] AACC Method 10-50.05. (2000) Baking quality of cookie flour. 11th ed. St. Paul: AACC International [cit. 1 July 2017]. ISBN: 9781891127682.
[23] Hooker, N., Spees, C., Watowicz, R. and Taylor C. (2015) From shelf to health: product reformulations in cookies impacts the public health consumption estimates of saturated fat and sugar intakes. The FASEB Journal. 29, 272-2.
[24] AACC Method 44-01.01. (1999) Calculation of percent moisture. 11th ed. St. Paul: AACC International. [cit. 1 July 2017]. ISBN 978-1-891127-68-2.
[25] AACC Method 38-12.02. (2000) Wet gluten, dry gluten, water-binding capacity, and gluten index. 11th ed. St. Paul: AACC International. ISBN: 978-1-891127-68-2.
[26] AACC Method 56-60.01. (1999) Sedimentation test for flour. 11th ed. St. Paul: AACC International. ISBN: 978-1-891127-68-2.
[27] AACC Method 54-30.02. (1999) Alveograph method for soft and hard wheat flour. 11th ed. St. Paul: AACC International. ISBN: 978-1-891127-68-2.
[28] AACC Method 54-50.01. 11th ed. (1999) Determination of the water absorption capacity of flours and of physical properties of wheat flour doughs, using the consistograph. St. Paul: AACC International. ISBN: 978-1-891127-68-2.
[29] AOAC (1990) Official Methods of Analysis of the Association of the Official Analysis Chemists. Association of Official Analytical Chemists, (15th edition), Washington, DC.
[30] AACC Method 08-01.01. (1999) Total Ash—Basic Method. 11th ed. St. Paul: AACC International. ISBN 978-1-891127-68-2.
[31] Francis, F.J.C. (1998) Colour Analysis. In: Nielsen, S.S. (ed.) Food Analysis. An Aspen Publishers, Gaithersnurg. 599-612.
[32] TGK, Turkish Food Codex-Notification of Wheat Flour (Notification No: 2013/9). 2013.
[33] Demir, M.K (2015) Utilization of whole wheat flour and its blends in cookies production (in Turkish). Tarım Bilimleri Dergisi (Journal of Agricultural Sciences). 21, 100-107.

[34] Sertakan, G.S. (2006) Possibilities of using triticale flour at producing cookie and cracker. Trakya University Graduate School of Natural and Applied Sciences, Edirne.
[35] Levent, H.U. (2005) Comparison of the effect of dietary fibers from different sources on cookie quality. Selcuk University Graduate School of Natural and Applied Sciences, Konya.
[36] Svoboda, L.H. and Baier, A.C. (1990) Comparison of quality parameters in triticale and wheat. In: Proceedings of The Second International Triticale Symposium. 456-459.
[37] Atli, A., Kocak, N. and Ozan, A.N. (1993) Investigations on cookie quality of bread wheat varieties grown in Central Anatolia Region (in Turkish). Un Mamulleri Dünyası. 44-48.
[38] Yuldasheva, N.K., Ul'henko, N.T. and Glushenkova, A.I. (2010) Wheat germ oil. Chem Nat Compd. 46, 97-98.
[39] Çakmaklı, Ü., Köse, E. and Kemahlıoğlu, K. (1995) Effects of the addition of crude and stabilized wheat germ together with a mixture of improvers on dough and bread characteristics. Gıda. 20, 243-248 (Turkish).
[40] Özkaya, H., Seçkin, R. and Ercan, R. (1984) Investigation of chemical properties, mineral and vitamin contents of some cookie varieties. Gıda. 9, 245-251 (in Turkish).
[41] Acun S. (2011) The grape wine waste pomace and grape seed enterprises on the quality of cookies. Süleyman Demirel University Engineering Faculty, Isparta.
[42] Flipcev, B., Šimurina, O., Sakac, M., -Sedej, I., Jovanov, P., Pestoric, M. and Bodroza-Solarov, M. (2011) Feasibility of use of buckwheat flour as an ingredient in ginger nut cookie formulation. Food Chem. 125, 164–170.
[43] Arshad, M.U., Anjum, F.M. and Zahoor, T. (2007) Nutritional assessment of cookies supplemented with defatted wheat germ. Food Chem. 102, 123- 128.
[44] Sudha, M.L., Vetrimani, R. and Leelavathi, K. (2007) Influence of fibre from different cereals on the rheological characteristics of wheat flour dough on cookie quality. Food Chem. 100, 1365-1370.
[45] Vieira, M.A., Tramonte, K.C., Podesta, R. Avancini, S.R.P., Amboni, R.D.de M.C. and Amante, E.R. (2008) Physicochemical and sensory characteristics of cookies containing residue from king palm (*Archontophoenix alexandrae*) processing. IJFST. 43, 1534–1540.
[46] Tiwari, B.K., Brennan, C.S., Jaganmohan, R., Surabi, A., Alagusundaram, K. (2011) Utilisation of pigeon pea (*Cajanus cajan L*) by products in biscuit manufacture. Food Sci Technol. 44, 1533-1537.
[47] Türksoy, S. (2011) Effects of fruit and vegetable fibre concentrates addition on the rheological properties of dough and quality of cookie. Ankara University Graduate School of Natural and Applied Sciences, Ankara,
[48] Kirssel, L. and Prentice M. (1979) Protein and fibre enrichment of cookie flour with brewer's spent grains. Cereal Chem. 50, 261-265.
[49] Ertop, M.H., Kutluk, K., Coşkun, K. and Canlı, S. (2016) A new approach for production of chips with food industry by-products: gluten enriched chips. Akademik Gıda. 14, 398-406 (in Turkish).
[50] Eskin, N.A.M., Ho, C.T. and Shahidi F. (2013) Browning reactions in foods. In: Eskin, N.A.M., and Shahidi, F. (eds.) Biochemistry of Food. (Third Edition) Elsevier Inc., ProQuest Ebook Central. 245-281.
[51] Zhu, K.X., Zhou, H.M. and Qian, H.F. (2006) Comparative study of chemical composition and physicochemical properties of defatted wheat germ flour and its protein isolate. J Food Biochem. 30, 329–341.
[52] Daniel, J.R. and Whistler, R.L. (1985) Carbohydrates In: Fennama, O.R. (ed) Food Chemistry. Marcel Dekker, New York, 70-137.
[53] Namiki, M. (1988) Chemistry of maillard reactions: recent studies on the browning reaction mechanism and the development of antioxidants and mutagens In: Chichester, C.O., and Schweigert, B.S. (eds.) Advances in Food Research. Academic Press, London, 116-184.
[54] Gül H. and Şen H. (2017) Effects of pomegranate seed flour on dough rheology and bread quality. CyTA - J Food. 15, 622-628.
[55] Tyagi, S.K., Manikantan, M.R., Oberoi, H.S. and Kaur, G. (2007) Effect of mustard flour incorporation on nutritional, textural and organoleptic characteristics of cookies. J Food Eng. 80, 1043-1050.

Received: **20.09.2017**
Accepted: **03.12.2017**

CORRESPONDING AUTHOR

Hulya Gul
Department of Food Engineering,
Faculty of Engineering,
Suleyman Demirel University,
32260, Isparta - Turkey

e-mail: hulyagul@sdu.edu.tr

© by PSP Volume 27 – No. 2/2018 pages 1152-1156 Fresenius Environmental Bulletin

STUDY ON COLONIZATION ABILITY IN PLANTS OF ENDOPHYTIC *BACILLUS AMYLOLIQUEFACIENS* HT-Q6 ISOLATED FROM WALNUT

Mei-qin Wang*, Xiao-juan Hao, Yan-ping Yao, Min Xu

College of Agronomy, Shanxi Agricultural University, Taigu Shanxi 030801, China

ABSTRACT

In this study, the strain Ht-q6-Rif was inoculated with different inoculation methods on the young stem and leaf of walnut, and the colonization sites of the strain were obtained by scanning electron microscopy combined with the resistant strain. Colonization dynamics: Ht-q6-Rif can be colonized on the surface and internal of walnut leaves after inoculation, and the number of bacteria after successful colonization is stable. As the sampling time is 28 days, the size of the young stem and leaf of the walnut plant is very different from that of the previous sampling.

KEYWORDS:
Ht-q6, walnut, colonization ability, Endophytic *Bacillus amyloliquefaciens*

INTRODUCTION

Chemical fungicides, available for the management of plant diseases, present many adverse effects on humans and environment especially with the emergence of the phenomenon of resistance of fungi to these pesticides [1]. Consequently, increasing agricultural productivity using friendly andenvironmentally products depends largely on the development of new and potent biocontrol strategies to a variety of currently usedchemical fungicides [2-4].

Biological control basis in the use of natural antagonistic organisms to combat pests or suppress plant diseases, offers an interesting alternative to the use of chemicals [5-9]. *Bacillus* spp. are among the beneficial bacteria exploited as biocontrol agents [10-12]. These Gram positive and spore-forming bacteria are able to colonize the roots or the rhizosphere with beneficial effects on plants from which they were designated as Plant Growth Promoting Rhizobacteria (PGPR) [13-15].

In this context, the colonization ability and colonization of Ht-q6-Rif obtained from Ht-q6 were studied by the method of scanning electron microscopy (TEM) and scanning electron microscopy (TEM). The strain Ht-q6 provides more theoretical data and guidance for improving crop disease resistance in practical applications, and lay the foundation for its development and application.

EXPERIMENTAL

Material. Test plant material and biocontrol strain: Thin shell incense 3 walnut seedlings (Horticultural College of Shanxi Agricultural University); *Bacillus amyloliquefaciens* Ht-q6.

Test medium: NA medium, PDA medium, LB medium (yeast extract 5 g, tryptone 10 g, NaCl 10 g, distilled water 1000 mL, pH 7.2).

Major reagents. pH 7.17, 0.2 mol/L PBS buffer: 0.2 mol/L KH_2PO_4 and 0.2 mol/L K_2HPO_4 3: 7 were mixed and sterilized before use.

Rifampicin (Sigma): 250 mg was dissolved in 25 mL of 95% alcohol to give 10 mg/mL mother liquor and stored at 4℃.

Main instrument. Japan JEOL JSM-6490LV scanning electron microscope, SW-CJ-2FD clean bench, GSP-9270MPE incubator, ZWYR-211C oscillation incubator, Thermo Sorvall ST refrigerated centrifuge, Haier BCD-579WE refrigerator.

Method. Screening of rifampicin - resistant strains. Detection of Sensitivity of Ht-q6 Strain to Rifampicin. The sensitivity of the Ht-q6 strain to rifampicin was first detected. The NA medium was cooled to about 50°C and the diluted rifampicin mother liquor was mixed in such a proportion that the rifampicin concentration was 0,0.5 μg/mL, 1 μg/mL, 2 μg/mL, 4 μg/mL and 8 μg/mL. After mixing the tablet containing the tablet, each concentration of 3 repeat. 100 μL of Ht-q6 bacteria was cultured on each treatment plate for 12 h, and the growth of colony was observed after incubation at 30℃ for 36 h.

Screening of Trifferrine Strains of Ht-q6 Strains. The sensitivity of the Ht-q6 strain to rifampicin was 1 μg/mL. According to the results, 2 μg/mL,4 μg/mL, 10 μg/mL, 20 μg/mL, 50 μg/mL, 100 μg/mL, 200 μg/mL, 300 μg/mL, respectively.

After incubation for 36 h, Containing the same concentration of rifampicin on the plate and then cultured for 2 passages in the next induction concentration LB medium. The labeled strain, which was stably grown on NA plates containing 300 μg/mL rifampicin, was screened as Ht-q6-Rif.

Construction of rifampicin strains in walnut plants. Anti - rifampicin strain deals with young plants of walnut. Two days after germination of walnut seedlings. Sprayed with 70% ethanol sprayed sterile water 3 times, until the surface of the fresh water after the natural air dry and then sprayed by two ways to deal with each treatment of three walnut seedlings to sterile water as a control. The concentration of the suspension was 10^8 cfu/mL, sprayed 3 times, and the whole plant was sprayed with sterile water after drying the bacteria suspension. Soak for 2 h in the beaker, and finally spray the whole plant with sterile water.

Recipe strains containing drug plate test. The leaves of the treated walnut plants were treated at 1, 3, 5, 7, 10, 14, 21 and 28 d after treatment. The samples were weighed 0.3-0.5 g each, and 75% alcohol wiped the surface and dried with sterile water. A sample was added to the sterilization column, 9.5 mL of PBS buffer and a little sterile quartz sand were thoroughly ground. The grinding fluid and its 10-fold, 100-fold dilutions were applied to NA plates containing 300 μg/mL Rif, respectively. On each of the three gradients of each gradient. (cfu/g) per gram of plant tissue (fresh weight), and the number of bacteria per gram of plant tissue (fresh weight) was counted.

Preparation and Observation of Electron Microscope. The young leaves of walnut were cut at 12 h, 24 h, 36 h and 48 h after spraying and soaking, and cut into small pieces in 3% glutaraldehyde solution and fixed at 4℃ for 24 h. After the fixation was done, the sections were washed with 0.1 mol / L PBS buffer and the sections were washed for 15 min each time. The gradient was then dewatered with 50%, 70%, 80%, 95% and 100% ethanol for 15 min at each gradient, where 100% ethanol was treated twice. After dehydration, the samples were treated with tert-butanol and the samples were freeze-dried. Freeze-dried paste the sample, spray gold, electron microscopy to observe the camera.

RESULTS AND DISCUSSION

Colonization of Spray and Immersion Treatment in Young Leaves of Walnut. The samples of walnut leaves treated at 12 h, 24 h, 36 h and 48 h were observed by scanning electron microscopy. The results are shown in Figure 1. The attachment of endophytic bacteria Ht-q6-Rif to the young leaves of walnut was shown in Fig. 1 A. The number of bacteria attached to the leaves was very large, and the leaves of the leaves. The volume is much more than the soaking treatment of leaves. Walnut leaf cross section of the scanning electron microscopy can be clearly seen that a small number of bacteria have successfully invaded walnut leaves inside.

Figure 1 B and 1 C were colonization of the walnut leaf at 24 h and 36 h after inoculation: the amount of bacteria attached to the leaf surface was reduced compared to 12 h after inoculation Trend, the amount of leaf spray treated with the amount of bacteria is still more than soaking treatment. Leaf surface of the bacteria and more bacteria in the form of bacteria, there are a few single bacteria exist alone, and more in the leaf surface depression at the site of the bacteria attached to the site. The amount of bacteria in the invaded leaves increased with the increase of 12 h after inoculation, and the vascular bundles could be invaded, which indicated that the strain might be transferred by means of vascular bundles, and further confirmed by the experiment.

It can be seen from Fig. 1D that after 48 h of colonization, some bacteria and granules appeared in the leaf table, indicating that the strain had been adapted to the leaf environment and began to propagate on the leaf surface. At the same time, the bacteria were successfully present, Ht-q6-Rif has been successfully colonized within the walnut leaves and begins to propagate the cells. No significant increase or decrease was observed at 36 h after inoculation compared with the amount of internal bacteria.

The results of scanning electron microscopy showed that the adsorption capacity of endophytic bacteria on the leaf surface was inoculated within 36 h after inoculation, and the foliar cells were reduced. 48 hours after inoculation, the results showed that the amount of leaf surface did not decrease continuously. In addition, the results of leaf cross section scanning showed that the cells could invade the leaves within 12 h after inoculation, and the cells were clustered at 48 h after inoculation. In addition, the cells showed that the strain Ht-q6-Rif could be invaded from the follicular glands and stomata in the walnut leaf and the presence of the leaves in the walnut leaf.

Colonization and immersion in the colonization of young leaves of walnut. Stems and leaves of the walnut were collected by the immersion and incubation of the Ht-q6-Rif suspension and the stems and leaves were collected. Results As shown in Figure 2, the strain recovered from the plant can be grown on an NA plate containing rifampicin at a concentration of 300 μg / mL, whereas no bacterial colonies were found on the plate of the control plant abrasive, indicating that the strain was successful in walnut plants Colonization, while the control can be excluded by other bacteria on the impact of the amount of bacteria.

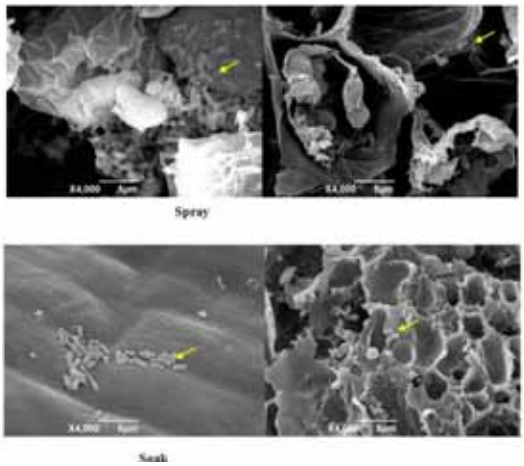

FIGURE 1 A
The attachment of endophytic bacteria Ht-q6-Rif to the young leaves of walnut for 12 h

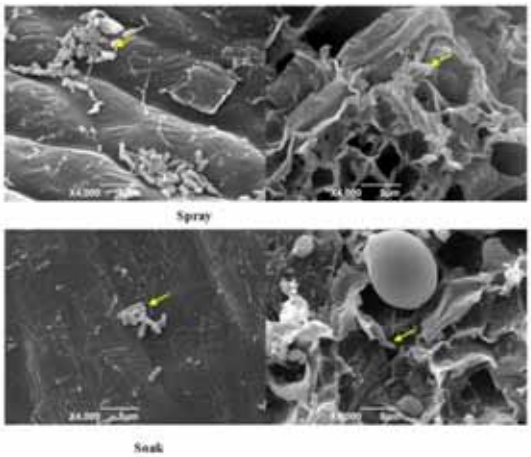

FIGURE 1 B
The colonization of Ht-q6-Rif in the walnut leaves at 24 h after inoculation

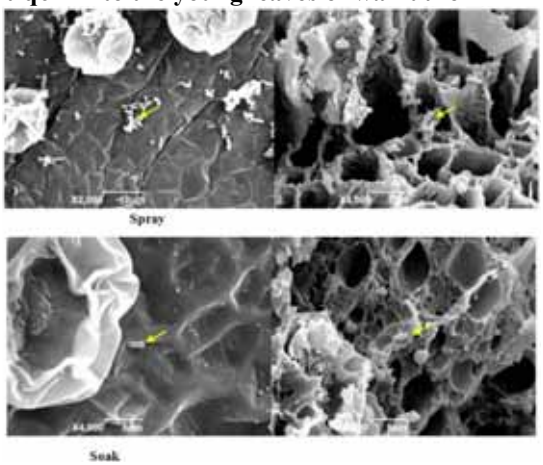

FIGURE 1 C
The colonization of Ht-q6-Rif in the walnut leaves at 24 h after inoculation

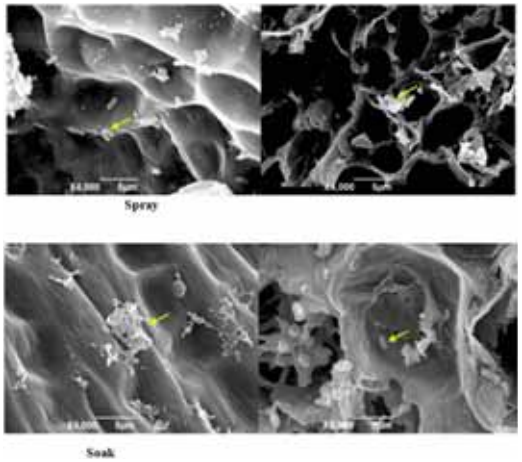

FIGURE 1 D
The colonization of Ht-q6-Rif in the walnut leaves at 48 h after inoculation

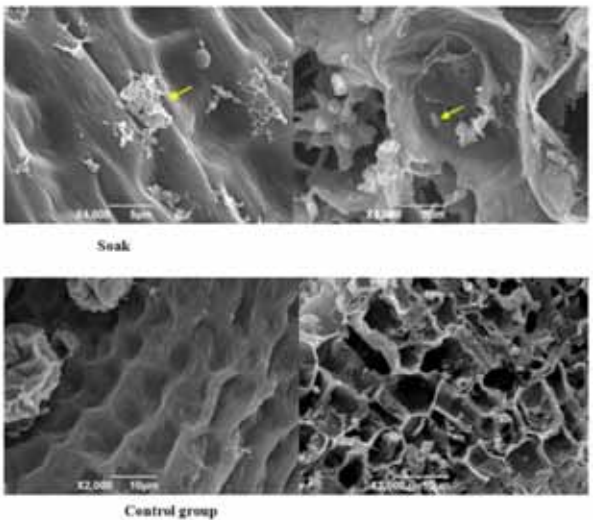

FIGURE 1E
Control group

FIGURE 1
Colonization of GHt-q6-Rif on leaf of walnut (spray and soak)
Note: left: the SEM photos of leaf surface, right: the SEM photos of leaf inside. A:12 hours after inoculation, B:24 hours after inoculation, C:36 hours after inoculation, D:48 hours after inoculation, E: Control group

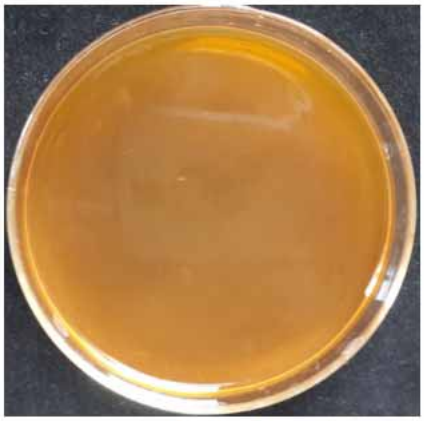

Control group

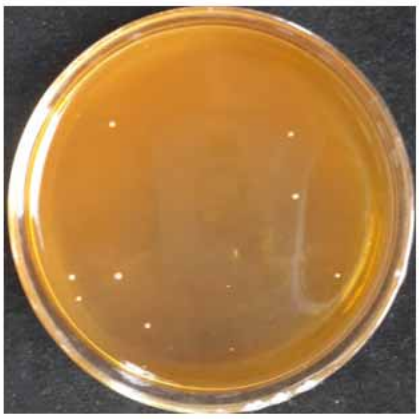

Treating

FIGURE 2
The growth of strain recovered from walnut

Two strains were inoculated with Ht-q6-Rif, and the colonization of the strain in the leaves and stems of walnut was observed at 1, 3, 5, 7, 10, 14, 21 and 28 days after inoculation. Of the stems and leaves can be detected in the Ht-q6-Rif, spray inoculation in the walnut leaves and stems colonization is greater than the soaking inoculation. The amount of bacteria in the stems and leaves of walnut was always decreased, and the final colonies became stable after 21 days of inoculation. The colonies in the stems and leaves were about 3.86×10^2 cfu / g and 2.96×10^2 cfu / g.

The results showed that the number of bacteria in the walnut stems and leaves decreased gradually within 7 days after inoculation, and then the trend of "increasing first and then decreasing" was observed. The amount of bacteria in the later plant was basically stable , And the number of colonies in stem and leaf were about 9.45×10^3 cfu / g and 2.81×10^3 cfu / g, respectively. In addition, 28 days after colonization, a considerable amount of bacteria was recovered from the walnut green skin, indicating that the Ht-q6-Rif strain could not only colonize the walnut, but also in the walnut plant. But also that the bacteria can be long-term colonization in the walnut body without causing damage to walnut tissue.

The results of the colonization dynamics and the results of scanning electron microscopy showed that the amount of spray inoculated with Ht-q6-Rif was higher than that of soaking inoculation. However, the colonization curve shows that the strain can not distinguish between the surface and the internal colonization of the strain. Therefore, the colonization of the strain Ht-q6-Rif in walnut plants is more intuitively demonstrated by scanning electron microscopy combined with the recovery of plate count.

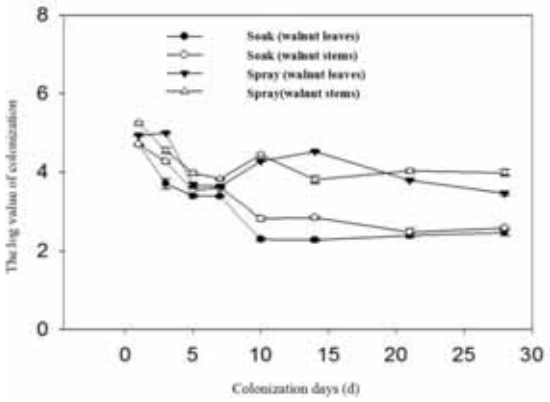

FIGURE3
The colonization of Ht-q6-Rif in stems and leaves of walnut

CONCLUSIONS

In this study, the strain Ht-q6-Rif was inoculated with different inoculation methods on the young stem and leaf of walnut, and the colonization sites of the strain were obtained by scanning electron microscopy combined with the resistant strain. Colonization dynamics: Ht-q6-Rif can be colonized on the surface and internal of walnut leaves after inoculation, and the number of bacteria after successful colonization is stable. As the sampling time is 28 days, the size of the young stem and leaf of the walnut plant is very different from that of the previous sampling. The stem and leaf of the later stage are the newly growing part after inoculation, and the strain is also isolated from the newly grown green walnut, indicating that the strain Ht-q6-Rif can be transported in walnut plants after successful colonization.

ACKNOWLEDGEMENTS

Research Fund for the Doctoral Program of Shanxi Agricultural University (No. 2013YJ10) and Key Programs of Shanxi Province (No. 201703D221010-2).

REFERENCES

[1] Imen, Z., Lobna, J., Slim, T., and Mohamed, T. (2016) Biocontrol activity of the endophytic *Bacillus amyloliquefaciens* strain CEIZ-11 against Pythium aphanidermatum and purification of its bioactive compounds. Biological Control. 100, 54 – 62.

[2] RadjaCommare, R., Nandakumar, R., Kandan, A., Suresh, S., Bharathi, M. (2002) Pseudomonas fluroscences based bioformulation for the management of sheath blight disease and leaf folder insect in rice. Crop Prot. 21, 671 – 677.

[3] Choudhary, D.K., Johri, B.N. (2009) Interactions of Bacillus spp. and plants with special reference to induced systemic resistance (ISR). Microbiol. Res. 164, 493 – 513.

[4] Chung, S.H., Kong, H.S., Buyer, J.S., Lakshman, D.K., Lydon, J., Kim, S.D., Roberts, D.P., (2008) Isolation and partial characterization of *Bacillus subtilis* ME488 for suppression of soilborne pathogens of cucumber and pepper. Appl. Microbiol. Biotechnol. 80, 115 – 123.

[5] El Arbi, A., Rochex, A., Chataign, G., Bechet, M., Lecouturier, D., Arnauld, S., Gharsallah, N., Jacques, P. (2016) The Tunisian oasis ecosystem is a source of antagonistic *Bacillus* spp. producing diverse antifungal lipopeptides. Res. Microbiol. 167(1), 46-57.

[6] Geetha, I., Manonmani, A.M., Paily, K.P., (2010) Identification and characterization of a mosquito pupicidal metabolite of a *Bacillus subtilis* subsp. subtilis strain. Appl. Microbiol. Biotechnol. 86, 1737 – 1744.

[7] Tan, S., Jiang, Y., Song, S., Huang, J., Ling, N., Xu, Y., Shen, Q. (2013) Two *Bacillus amyloliquefaciens* strains isolated using the competitive tomato root enrichment method and their effects on suppressing Ralstonia solanacearum and promoting tomato plant growth. Crop Prot. 43, 134 – 140.

[8] Weller, D.M. (1988) Biocontrol of soilborne plant pathogens in the rhizosphere with bacteria. Annu. Rev. Phytopathol. 26, 379 – 407.

[9] Oliveira, C.A., Alves, V.M.C., Marriel, I.E., Gomes, E.A., Scotti, M.R., Carneiro, N.P., Guimaraes, C.T., Schaffert, R.E., Sa, N.M.H. (2009) Phosphate solubilizing microorganisms isolated from rhizosphere of maize cultivated in an oxisol of the Brazilian Cerrado Biome. Soil Biol. Biochem. 41, 1782 – 1787.

[10] Tang, J.S., Zhao, F., Gao, H., Dai, Y., Yao, Z.H., Hong, K., Li, J., Ye, W.C., Yao, X.S. (2010) Characterization and online detection of surfactin isomers based on HPLC-MSn analyses and their inhibitory effects on the overproduction of nitric oxide and the release of TNF-a and IL-6 in LPS-induced macrophages. Mar. Drugs. 8(10), 2605-2618.

[11] Wang, S.L., Shih, I.L., Liang, T.W., Wang, C.H. (2002) Purification and characterization of two antifungal chitinases extracellularly produced by *Bacillus amyloliquefaciens* V656 in a shrimp and crab shell powder medium. J Agric Food Chem. 50, 2241 – 2248

[12] Yu, G.Y., Sinclair, J.B., Hartman, G.L., Bertagnolli, B.L. (2002) Production of iturin A by *Bacillus amyloliquefaciens* suppressing Rhizoctonia solani. Soil Biol Biochem. 34, 955 – 963

[13] Ryan, R.P., Germaine, K., Franks, A., Ryan, D.J., Dowling, D.N. (2008) Bacterialendophytes: recent developments and applications. FEMS Microbiol. Lett. 278 (1), 1 – 9.

[14] Strobel, G., Daisy, B., Castillo, U., Harper, J. (2004) Natural products from endophytic microorganism. J. Nat. Prod. 67(2), 257 – 268.

[15] Srinivasan, K., Mathivanan, N. (2009) Biological control of sunflower necrosis virus disease with powder and liquid formulations of plant growth promoting microbial consortia under field conditions. Biol. Control. 51, 395 – 402.

Received: **XX.XX.201X**
Accepted: **XX.XX.201X**

CORRESPONDING AUTHOR

Mei-qin Wang
College of Agronomy,
Shanxi Agricultural University,
Taigu Shanxi 030801 – China

e-mail: mgq2020@126.com

© by PSP Volume 27 – No. 2/2018 pages 1157-1163 Fresenius Environmental Bulletin

COMPARISON OF MAXIMUM RANGE OF POLLUTANTS

Ljiljana Takic[1], Sonja Ketin[2,*], Ranko Marjanovic[3], Adem Preljevic[4], Selim Sacirovic[5]

[1]University in Nis, Faculty of Technology, Leskovac, Serbia
[2]University of Novi Sad, Faculty of Technical Science, Environmental Engineering, Novi Sad, Serbia
[3]University of Donja Gorica, Faculty of Sports Management, Podgorica, Montenegro
[4]State University in Novi Pazar, Novi Pazar, Serbia
[5]University of Nis, Faculty of Sciences and Mathematics, Nis, Serbia

ABSTRACT

Paper present modeling for max range of nitrogen oxide in the fertilizer plant (FP). Based on the results of modeling and analysis of aggregate data it can be concluded that the application of software ALOHA (model) it is possible to plan and manage the set limit values for concentrations of pollutants in industrial plants along with monitoring the dispersion of pollutants in the fertilizer plant. The model was applied, which based on Gaussian distribution calculates maximum range of pollutants and pollutant concentrations. These researches are specific and using the model of NO_2 dispersion, the dominant pollutants in the fertilizer industry. The modeling for the control and reduction of pollution (MCRP) can be used in case of chemical accidents.

KEYWORDS:
max range, accident, chemical

INTRODUCTION

The modeling for the control and reduction of pollution (MCRP) can be determinated max range and vulnerable zone. The model based on Gaussian distribution calculates maximum range of pollutants and concentrations. Paper presents experiment and results for FP.

EXPERIMENTAL

The experimental part consists of analytical consideration and graphical display of high emitters - sources of NO_2 in plants FP. As IPP1 presented are the plants for the production of fertilizers. To obtain accurate data the used model is licensed ALOHA®5.4.1. programme of the U.S. National Agency for Environmental Protection EPA. The analysis included a mathematical calculation of maximum range of pollutants for different boundary conditions (U.S. EPA and national standards). The ratio of the results was calculated and the analysis of each particular high emitter. Model testing is an integral part of the experimental work.

Emitters. The overview of high emitters in the FP (based on the Register of pollution sources of national importance) is presented. In addition to analytical outline also presented was the graphical display of emissions in the plants of FP Table 1. shows all high emitters of the plants FP (A1-A10), Mentioned are the geographical positions of each emitter (GPRS) and plants in which there is each high emitter. In FP the plants from PA1 to PA4 are located.

Figure 1 shows the spatial distribution of high emitters for FP. Emitters A1-A10 are presented in plants that is are marked on the satellite view.

TABLE 1
List of high emitters FP

Items	Plant	GPS	
		N	E
A1	PA1	44 °50 25.23	20 °39 59.16
A2	PA1	44 °50 25.15	20 °39 59.35
A3	PA1	44 °50 25.40	20 °39 59.45
A4	PA2	44 °50 26.10	20 °39 57.65
A5	PA2	44 °50 25.06	20 °39 59.06
A6	PA2	44 °50 25.26	20 °39 57.06
A7	PA3	44 °50 25.37	20 °40 03.60
A8	PA3	44 °50 25.85	20 °40 03.07
A9	PA3	44 °50 25.58	20 °40 03.33
A10	PA4	44 °50 24.02	20 °39 55.70

GPS geographical position of emitters, N-latitude, E-longitude
A1-A10 - high emitters in plants FP

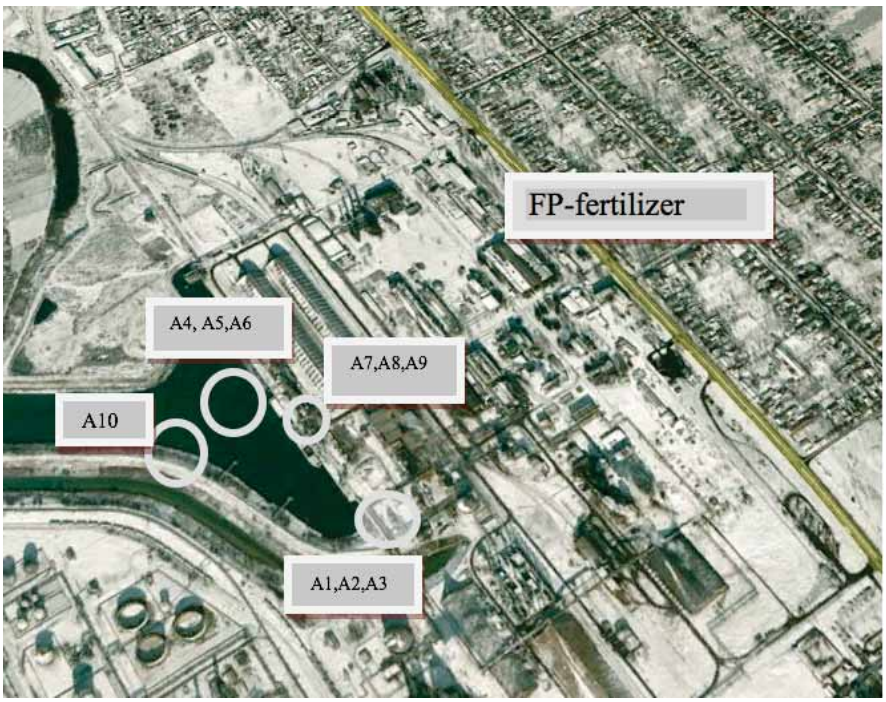

FIGURE 1
The spatial representation of FP with high emitters

TABLE 2
The input data of modeling for FP

Emitters	Mass flow (kg⁄h)	Height releases (m)	Mass flow (kg⁄min)	Quantity (kg)	The share of emitters (%)
A1	36.2	45	0.603	36.2	5.55
A2	0.54	20.8	0.009	0.540	0.083
A3	0.02	9.3	0.00333	0.020	0.0031
A4	83.4	82	1.39	83.4	12.78
A5	62.6	82	1.04	62.6	9.59
A6	213.21	82	3.55	213	32.64
A7	46.3	18	0.772	46.3	7.09
A8	116.8	18	1.95	117	17.93
A9	72.5	18	1.21	72.5	11.11
A10	21	46	0.350	21	3.22

TABLE 3
Summary view of emitters and % share of pollutants in emerging pollution

Emitters	Mass flow (kg⁄h)	Height releases (m)	Mass flow (kg⁄min)	Quantity (kg)	The share of emitters (%)
A1	36.2	45	0.603	36.2	1.386
A2	0.54	20.8	0.009	0.540	0.02
A3	0.02	9.3	0.00333	0.020	0.0007
A4	83.4	82	1.39	83.4	3.19
A5	62.6	82	1.04	62.6	2.40
A6	213.21	82	3.55	213	8.156
A7	46.3	18	0.772	46.3	1.77
A8	116.8	18	1.95	117	4.48
A9	72.5	18	1.21	72.5	2.776
A10	21	46	0.350	21	0.804

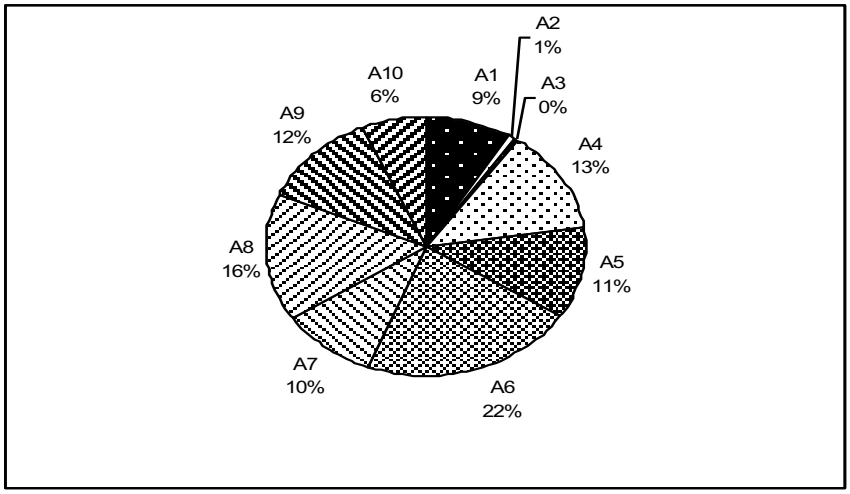

FIGURE 2
Percentage share of high emitters for FP [1]

Studied pollutants can be found at 10 emitters mentioned in Table 1. (A1-A10). The emitters A1, A2, A3 are located in the plant PA1. The emitters A4, A5, A6 are located in the plant PA2. The emitters A7, A8, A9 are located in the plant PA3. The emitters A10, are located in the plant PA4.

Characteristics of high emitters are shown in Tables of calculations (height, diameter of emitter, fluid flow). The input data of the model that is used for calculation of the maximum range of pollutants are:

1. Physical and chemical characteristics of the pollutants NO_2
2. The mass flow on the emitter,
3. Continual/discontinual emitter characteristic

There are three possibilities of calculation: Gaussian method, "heavy gas" method and letting the program itself to choose the model. The final result also depends on the choice of limit values of the model.

The total aggregate amount of pollutants is 2611.47 kg10 emitters are defined that make up the largest share in emerging of the pollutants: A4, A6, A8. The largest share was detected in three emitters from FP.

In Figure 2. the percentage of the overall pollution for the high emitters of FP is shown where it can be seen that the largest percentage share is of the emitter A6 (22%).

The atmospheric conditions that were used as input data and did not change during the experiment are listed. Values were used for the worst case scenario ("worst case"): wind speed of 2 m/s, wind direction southeast, urban area, temperature 15° C, stability class F, relative humidity 50%. The limit values of Serbia (for NO_2 limit values are 0.15 mg/m^3; 700 mg/m^3, 2 mg/m^3) and Russia (for NO_2 limit values are 0.25 mg/m^3; 0:04 mg/m^3; 0.002 mg/m^3).

METHODS

Developed model for the control and reduction of pollution presents results of the research by application of licensed U.S. program ALOHA (Area Locations of Hazardous Atmospheres) developed by the U.S. Agency for Environmental Protection EPA (Environmental Protection Agency) for the pollution distribution at the given input data.

The developed model considers four cases - scenarios for different input values (limit values of pollutants) in three industrial plants (plant for the production of nitrogen FP) The results of modeling were analyzed in order to recommend the operation by which the required emission limits will be satisfied.

The model application requires entering the data (fixed and variable), the formation of graphics and tabulation of results. Fixed parameters of the model are the physical characteristics of the model (height, diameter and pollutants of the model); the variable parameters are the mass flow, the total amount of pollutants and meteorological data. The pollutants for all high emitters were modeled and the obtained values varied depending on the defined limit values of pollutants.

Application of the model is simple, accurate and allows prediction of pollutant emissions in all conditions. The most important consideration is the so-called "worst case" that shows the model results for the worst case. The developed model of integrated pollution control and prevention uses the diffusion equations of emissions during the continuous operation of the plant as well as the equations for the plant operation during the irregular operation.

Diffusion equation for routine emission.

$$C(x,y,z)= \frac{Q}{2\pi\sigma_y\sigma_z u}\exp\left(\frac{-1}{2}\frac{y^2}{\sigma_y^2}\right)\left\{\exp\left[\frac{-1}{2}\frac{(z-H)^2}{\sigma_z^2}\right]+\exp\left[\frac{-1}{2}\frac{(z+H)^2}{\sigma_z^2}\right]\right\} \quad (1)$$

Equation (1) represents the calculation of the concentration at the continual work of broadcasters and is dependent on the emission rate of pollutant Q, the effective source height H, the wind speed u and standard-deviation of the concentration of pollutant.

The parameters in equation (1) and equation (2):

C (x,y,z) - the concentration at the point (x,z,y)

Q - emission rate of pollutant

H - effective source height

σ_y σ_z - standard deviation of the concentration of pollutant in the horizontal and vertical direction

u - wind speed

Diffusion equation for accidental emission.

$$C(x,y,z)= \frac{q}{\sqrt[3]{2\pi}\sigma_x\sigma_y\sigma_z}\exp\left\{-\left[\frac{(x-u)^2}{2\sigma_x^2}+\frac{y^2}{2\sigma_y^2}\right]\right\}\times\left\{\exp\left[-\frac{(z-H)^2}{2\sigma_z^2}\right]+\exp\left[\frac{(z+H)^2}{2\sigma_z^2}\right]\right\} \quad (2)$$

Equation (2) represents the calculation of the concentration of high emitters in accidental emission and is dependent on the emission rates of pollutant q, the effective source height H, the wind speed u and standard deviation of the pollutant concentration. Fixed input data are the physical characteristics of the emitters (height, diameter, pollutant) [2, 3, 5, 8].

Modeling of Scenario 1, 2, 3 and 4 for FP. Modeling for scenario 1 (modeling according to the limit values of ALOHA model) on an industrial example IPP1 is shown. By modeling the result is obtained showing the three areas of vulnerability, which is indicated in the table with the colors of red, orange and yellow. Modeling for scenario 2 (modeling according to national limit values) on an industrial example FP is shown. Modeling for scenario 3 (potentially worst case of pollution) on an industrial example FP is shown. Modeling for scenario 4 (modeling according to limit values in Russia) on an industrial example FP is shown.

Modeling for scenario 1: The red color shows the area for concentration of pollutant NO_2 (20 ppm), the orange for the concentration (12.5 ppm) and yellow for the concentration (0.5 ppm).

Modeling for scenario 2: The red color shows the area for concentration of pollutant NO_2 (2 mg/m^3), the orange for concentration (700 mg/m^3) and yellow for concentration (0.15 mg/m^3).

Modeling for scenario 3: The red color shows the area for concentration of pollutant NO_2 (2 mg/m^3), the orange for concentration (700 mg/m^3) and yellow for concentration (0.15 mg/m^3).

Modeling for scenario 4: The red color shows the area for concentration of pollutant NO_2 (250 mg/m^3), the orange for concentration (40 mg/m^3) and yellow for concentration (2 mg/m^3). The result obtained by modeling was the maximum range of pollutants or the maximum distance the pollutant can reach. Gauss and "Heavy gas" models are used to calculate the dispersion of pollutants [4, 6].

RESULTS AND DISCUSSION

Table 5. shows the modeling results for FP for vulnerable zones by models at limit values of ALOHA model, national limit values and Russian literature data.

TABLE 4
Modeling values for FP at limit values of ALOHA model

Emitters	The mass flow (kg/h)	The mass flow (kg/min)	Total quantity (kg)	Height releases (m)
A1	36.2	0.603	36.2	45
A2	0.54	0.009	0.540	20.8
A3	0.02	0.00333	0.020	9.3
A4	83.4	1.39	83.4	82
A5	62.6	1.04	62.6	82
A6	213.21	3.55	213	82
A7	46.3	0.772	46.3	18
A8	116.8	1.95	117	18
A9	72.5	1.21	72.5	18
A10	21	0.350	21	46

TABLE 5
The modeling results for FP for vulnerable zones [4]

Emitter	Vulnerable zones by models, (km)			
	Scenario 1	Scenario 2	Scenario 3	Scenario 4
A1	0.097 0.125 0.673	0.031 0.931 37		1.4 3.6 10
A2	0.011 0.013 0.075	0.011 0.098 0.394		0.151 0.395 1.9
A3	0.011 0.013	0.011 0.018 0.067		0.028 0.011
A4	0.149 0.191 1.0	0.045 1.4 5.7	0.969 10 10	2.1 5.5 10
A5	0.130 0.165 0.896	0.039 1.2 4.9	0.969 10 10	1.8 4.7 10
A6	0.244 0.312 1.700	0.067 2.3 9.3	1.4 10 10	3.4 8.9 10
A7	0.111 0.142 0.764	0.0 34 1.1 4.2		1.6 4.0 10
A8	0.178 0.228 1.200	0.052 1.7 6.8		2.5 6.5 10
A9	0.141 0.178 0.968	0.042 1.3 5.3		2.0 5.1 10
A10	0.074 0.093 0.506	0.022 691 2.7		1.0 2.7 10

TABLE 6
Comparison of the obtained maximum range of pollutants for calculated, modeled and design values [4]

Emitter	"Worst case" value (km)	Modeled value (km)			Design (Theoretical-licensing) value (km)
		Foreign		National	
		EPA	Russia		
A1	10	0.67	10	3.7	-
A2	1.9	0.075	1.9	0.394	-
A3	0.338	0.013	0.338	0.067	-
A4	10	1.00	10	5.7	10.00
A5	10	0.896	10	4.9	10.00
A6	10	1.7	10	9.3	10.00
A7	10	0.764	10	4.2	-
A8	10	1.2	10	6.8	-
A9	10	0.968	10	5.3	-
A10	10	0.506	10	2.7	-

A1-A10 - high emitters in plants FP

Table 6. shows the comparison of the obtained maximum ranges of pollutants for the modeled values (EPA, national and Russian concentration limit values) and the design of values of pollutants' range. Modeled value is the column originated as the result of research of Scenario 1 and Scenario 4, the design value of pollutants range is the result of research of Scenario 3. Whereas the column "worst case" emerged as the highest score of all four Scenarios. "Worst Case" is necessary in research and modeling as the highest values are obtained.

Graphic representation of the results of modelling. Graph 1 and 2 present results for scenario 1 for FP; graph 3 and 4 present results for scenario 2; graph 5 and 6 presents results for scenario 3 and graph 7 and 8 presents results for scenario 4 for FP. It is methods for determinated max range and vulnerability for zones [1, 6].

Graphs of the scenario 1 for FP

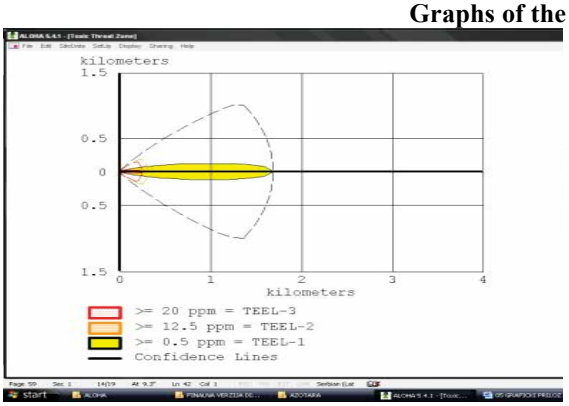

GRAPH 1
Graphical representation of the dispersion of NO_2 measurement point A6

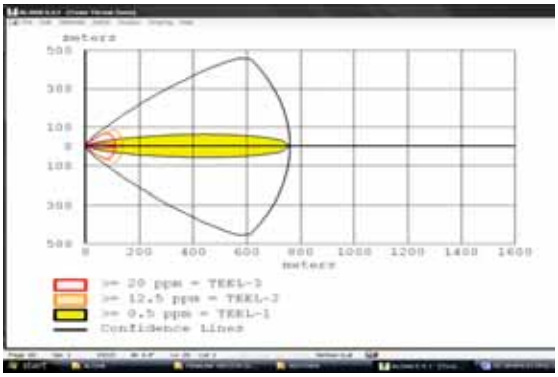

GRAPH 2
Graphical representation of the dispersion of NO_2 measurement point A7

Graphs of the scenario 2 for FP

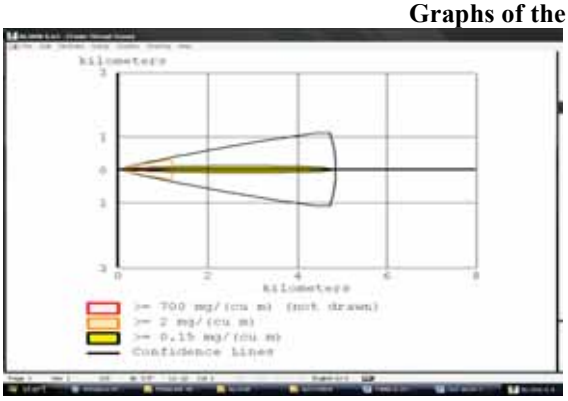

GRAPH 3
Graphical representation of the dispersion of NO_2 measurement point A5

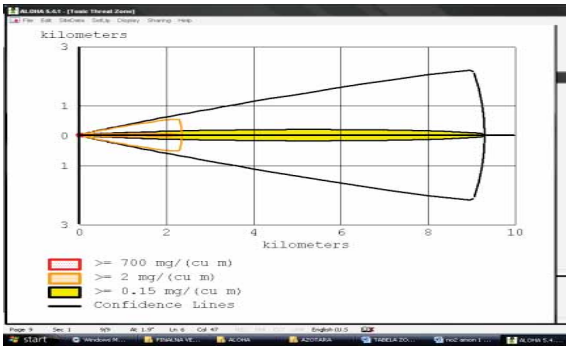

GRAPH 4
Graphical representation of the dispersion of NO_2 measurement point A6

Graphs of the scenario 3 for FP

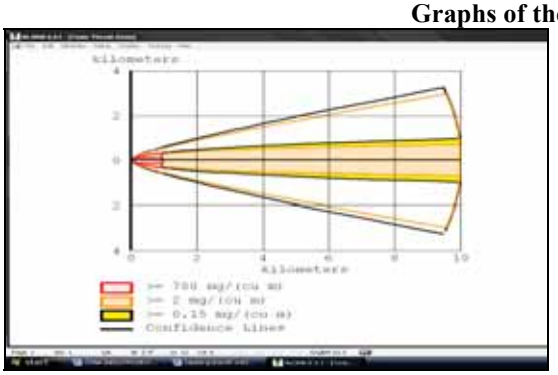

GRAPH 5
Graphical representation of the dispersion of NO_2 measurement point A4

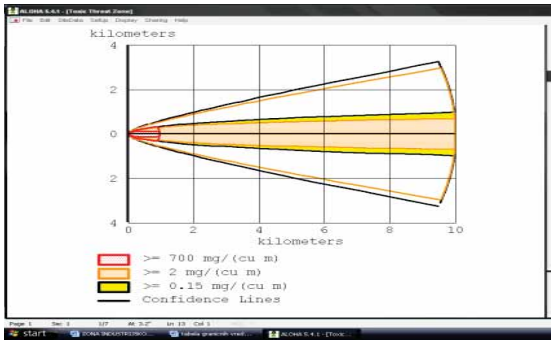

GRAPH 6
Graphical representation of the dispersion of NO_2 measurement point A5

Graphs of the scenario 4 for FP

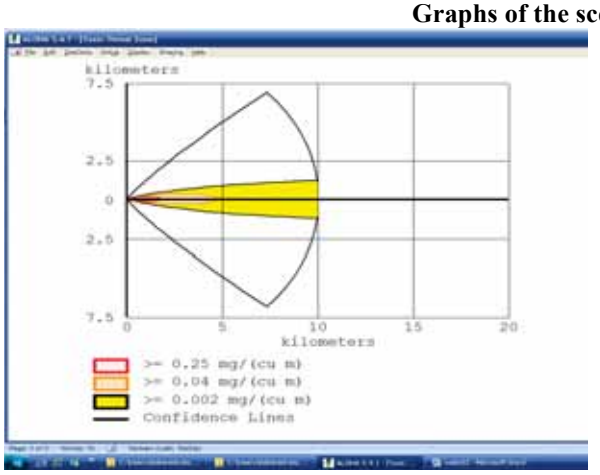

GRAPH 7
Graphical representation of the dispersion of NO_2 measurement point A5

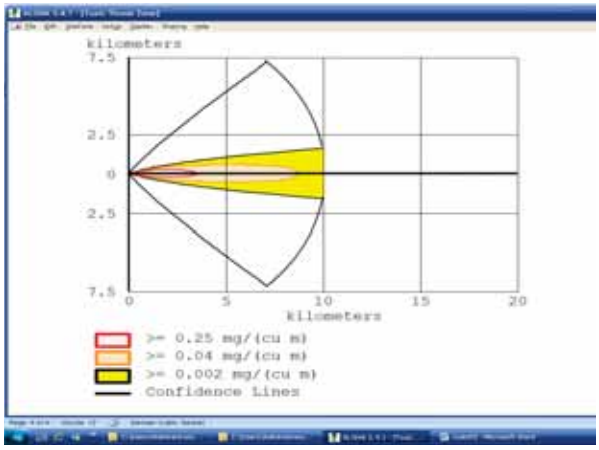

GRAPH 8
Graphical representation of the dispersion of NO_2 measurement point A6

CONCLUSION

Paper analyzes the FP and the model which based on Gaussian distribution calculates maximum range of pollutants and pollutant concentrations. For the first time in a unique way the cumulative effect of pollutants NO_2 for existing modes of operation are shown. Based on the application of the models and their analyses as well as by varying variables the planning of optimal modes of fertilizer is enabled. Presented operating mode with constant control of parameters reduces pollution. The modeling for the control and reduction of pollution (MCRP) can also be used in case of chemical accidents.

REFERENCES

[1] Stefanov, S., Biočanin, R., Vojinović Miloradov, M. (2012) Ecological modeling of industrial pollutants-Serbian case, Journal of Environmental Protection and Ecology. Bulgaria. 13, 75-86.

[2] Stefanov, S., Biočanin, R., Vojinović Miloradov, M., Sokolović, S. (2013) Ecological modeling of pollutants in accidental fire at the landfill waste. Thermal Science, Serbia. 17(3), 903-913

[3] Biocanin, R., Stefanov, S., Urosevic, S., Mekic, S. (2012) Modeling of pollutants in the air in terms of fire on dumps. Ecol Chem Eng S. 19(4), 609-616

[4] Ketin, S., Sacirovic, S., Sacirovic, S., Plojovic, S., Skrijelj, R., Biocanin, R. (2014) Method for comparison of the maximum range of chemical pollutants. Russian Journal of General Chemistry. 84(13), 2677-2680.

[5] Stefanov, S., Cvejic, R., Biocanin, R. (2011) Modeling of pollutants at the landfill waste, International scientific and methodological conference. "Quality of education" management, certification, recognition. Kramatorsk, Ukraine. 152-159.

[6] Stefanov, S. (2014) New model for Intergrated control and Reduced Pollution for Example Oil-Petrochemical Plant. PhD Thesis, University of Novi Sad, Environmental Engineering Department, Novi Sad, Serbia.

[7] Stefanov, S., Vojinovic Miloradov, M., Sokolovic, S., Bancov, S. (2009) Monitoring of industrial pollutants in oil and petrochemical industry. Proceedings of the Romanian Academy Serial B: Chemistry, Life Science and Geoscience. Chemistry. 2-3, 77-84

[8] Stefanov, S., Biočanin, R., Mehic, S., Adamovic, D. (2012) Modeling Of Pollutants CO, PM, PAH In Accidental Fire at The Landfill Waste, GCGW-12, Istanbul. 840-849.

Received: **24.09.2017**
Accepted: **02.12.2017**

CORRESPONDING AUTHOR

Sonja Ketin
University of Novi Sad
Faculty of Technical Science
Environmental Engineering Department
Novi Sad 21000 – Serbia

e-mail: ketin.sonja@gmail.com

© by PSP Volume 27 – No. 2/2018 pages 1164-1168 Fresenius Environmental Bulletin

THE EFFECTS OF MANNAN OLIGOSACCHARIDE (MOS) AND VITAMIN B_{12} ADDITIVES ON THE LIVER AND INTESTINE HISTOLOGY OF THE CARP FRY *(CYPRINUS CARPIO L. 1758)*

Mehmet Ates[1,*], Hasan Huseyin Atar[2]

[1]Munzur University, Faculty of Engineering, Department of Bioengineering, Tunceli, 62000, Turkey
[2]Ankara University, Faculty of Agriculture, Department of Fisheries and Aquaculture, Ankara 06110, Turkey

ABSTRACT

In this study, four hundred (400) carp frys (*Cyprinus carpio* L. 1758) were fed for 90 days with commercial feed containing Mannan oligosaccharide (MOS) and Vitamin B_{12}. The effects of feeding with MOS and Vitamin B_{12} additives in different proportions on the parameters on intestine and liver histology of the carps were studied. As a result of this particular study, no pathological disorder was observed in the liver cells based on histologic reviews. The villi in the intestine showed slight increase both in terms of length and thickness within the group fed with MOS, while the other groups fed without MOS showed no alteration for this particular organ.

KEYWORDS:
Mannan oligosaccharide, Vitamin B_{12}, Carp (*Cyprinus carpio)*, Histology, Liver, Intestine

INTRODUCTION

Hygiene and fish health are important factors which have impact on the fishery production. The feeds and feed quality should be standardized at the highest level for the application of hygienic fishery techniques. It can be argued that the key to success for the health of the fishes in aquacultural applications depends on the quality of the water and use of high quality feeds. Although all health and hygienic conditions are fully satisfied, the pathogenic effects of the bacteria and parasites are inevitable. Therefore, in order to protect the fishes against diseases, particular importance should be given primarily to the stress factor as well as the stock density, nutrition type, cleanliness of the tools and kits used and the training of the personnel while protective measures should be taken [1, 2].

The various probiotics produced for defined purposes and several feeds with additives and vitamins which develop immune system are important protective action in aquaculture. Probiotic feed additives have proven successful in functional and prophylactic nutrition. These additives increase the strength of fish against diseases, stress and provide optimal dietary intake with improving gastro intestinal morphology [3]. It has been observed that the fishes showed resistance against various bacterial, viral and parasitic diseases with the help of the immunostimulants in aquaculture. The rate of death caused by opportunist pathogens during larval period gradually decreased, the effects and growth of the antimicrobial substances have increased while the negative effects of the stress have been reduced [4, 5].

Mannan oligosaccharides (MOS) are the natural cellulose polysaccharides which include cross ties. They are obtained through the cell walls of the *Saccharomyces cerevisiae* yeast. With terminal mannose units in MOS structure, it establishes adhesion with fimbriae in the pathogenic bacteria, comprises lecithin and provides excretion without negative impact on the fish. Vitamin B_{12} is of particular importance because this vitamin is necessary for usual growth and supports immune system and acts as a coenzyme for metabolic events. The Vitamin B_{12} deficiency leads to decrease in anorexia and growth in the fishes. After the injection of folic acid and xanthopterin, which are ingredients of the crystallized Vitamin B_{12} into anemic salmon fish produced, affirmative progresses were observed in the blood cells within several days and the salmon fish showed recovery from anemia rapidly [6].

Carp (*Cyprinus carpio* L. 1758*)* is worldwide the most cultured fish species and also produced on large scale in Turkey. The wild carps and culture carps which are species of economic value for people raised in temperate climates are also resistant against cold. They need less oxygen and have a wide range of tolerance for oxygen. They are not hooked up or caught through dip net and not easily wounded. They can also live under a wide range of temperatures from 0°C to 30°C. The carps have strong adaptability to culture conditions and develop in highly variable conditions. These carps are preferred not only for their faster growth than a normal carp but also for easy impregnation and breeding [7]. In this study, the effects of MOS and Vitamin B_{12} which are

TABLE 1
Experimental plan for raising carp frys

Carp frys	Control	Group A	Group B	Group C
Weight of the stocked fish (g)	~1	~1	~1	~1
Number of fishes within the group	30	30	30	30
Number of replications	3	3	3	3
MOS (Kg^{-1})*	0	5 g	0	0
Vit-B_{12} (Kg^{-1})**	0	0	0.5 mg	0
MOS + Vit-B_{12} (Kg^{-1})***	0	0	0	5 g + 0.5 mg

*Rate of **MOS** in the feed (MOS/Kg^{-1} Feed)
Rate of **Vit-B_{12} in the feed (Vit-B_{12}/Kg^{-1} Feed)
***Rate of **MOS + Vit-B_{12}** in the feed (MOS+Vit-B_{12}/Kg^{-1} feed)

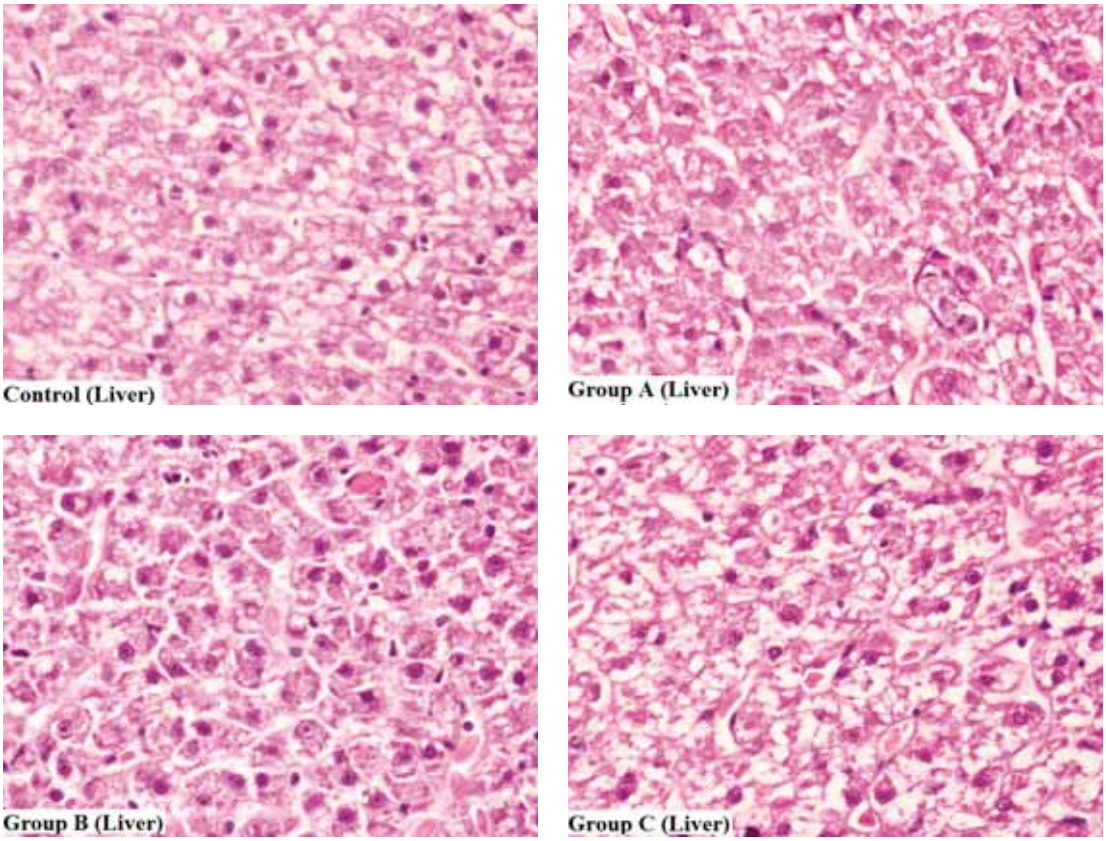

FIGURE 1
Liver [Hamatoxylen-Eosin (H+E X350)] section for carp (*Cyprinus carpio*) fish, usual and vacullary distribution of the hepatocytes in all groups (liver cell), under usual cases light necrosis is observed in group C where MOS was solely used.

considered to increase the performance of the carp were investigated. The changes in intestine and liver histology with particular emphasis on the structural features of the intestinal microvilli on the digestion were examined.

MATERIALS AND METHODS

Empirical conditions. The carp frys used in this study were supplied from Mediterranean Aquaculture Research, Production and Training Institute, Kepez Station, Antalya, Turkey. The fishes were brought to the Ankara University, Faculty of Agriculture, Department of Aquaculture, Inland Water Fishes Research and Application Unit through carrying bags with oxygen support. Following adaptation phase, lasting 15 days, all fishes were individually weighed and measured length wise. The average initial weight and total length were measured as 1.11±0.05 g and 4.04±0.04 cm, respectively. The fishes were stocked with an empirical application plan that the details are specified in Table 1.

Diets. The feeds used in the study were supplied from Pınar Feed Company, Izmir, Turkey. The granulated feed produced specifically for the freshwater fishes with 55 % crude protein, 12 % crude fat and metabolic energy of 4900 kcal was used during the experiments. The other additives, MOS (Aqua-

Myces, Vitomix, CO, USA) and Vitamin B_{12} (Sigma Aldrich St. Lo. Mo, USA) were also added to the trial feed. During the experimental period, the feeding rate of 3 % of their body weight was applied 3 times a day manually [8]. The MOS and Vitamin B_{12} additives were dissolved in water prior to addition of mixed feed for both groups. The additives were added to the feed through spray method and homogenously mixed for 5 minutes. The feeds were placed in different cups as granule powder and the remaining feeds were re-weighed within each period to calculate the consumed feed. The MOS and Vitamin B_{12} ratio arrangement within trial feeds for each group was planned as given in Table 1.

Liver and intestine histology. For histological study, tissue samples with a size of 0.5 cm^3 from the liver and intestine tissues of the carp frys were fixed for a period of 48 hours in 10 % neutral formaldehyde solution. Then, the tissues were prepared in compliance with the histopathological techniques outlined by Culling [9]. The fixed tissue particles were casted on the paraffin blocks subsequent to dehydration, transparency and paraffin embedment processes. The sample tissues were then placed on the slides after they were cut in 5µ thickness using rotary microtome (RM2255, Leica, Wetzlar, Germany). Such sections were painted with hematoxylin-eosine method and transferred into a fixed preparate. The preparates have then been examined by means of light microscope. Any pathological change in the tissues could be defined by examining the epithelium tissue of the small intestines along with the structural features of the villi.

RESULTS

Liver histology. When the enteric tissue sections of the carp fishes were examined, it has been noted that the pancreatic tissue and liver tissue form primary part of the hepatopancreas. The liver is the organ where the digested materials, vitamins and minerals are metabolized. This tissue is the depot where the fats in glycogen form are collected. The formation of the nutritional pathogens is related with the vascular problems due to the fatty microvescilar droplets within the tissue. In order to examine the occurrence of the pathologic changes in this particular organ, the sections painted with hematoxylen-eosine have been examined. It has been noted that the fishes fed with commercial feed containing MOS and vitamin B_{12} showed no pathologic disorder compared to the fishes in other groups. The photographs representing various groups included in this study are given in Figure 1.

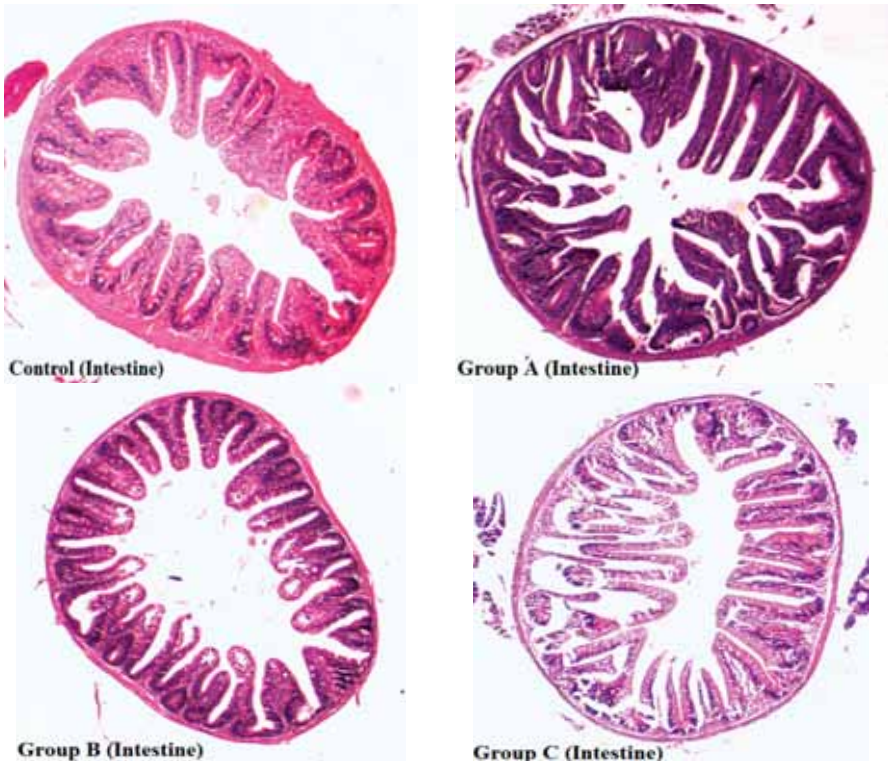

FIGURE 2
Small intestine section [Hamatoxylen-Eosin (H+E X350)] of carp (*Cyprinus carpio*) fish. Intestine epithelia tissue and villi display usual morphology in all groups however in Group A and C, slight increases in the length and thickness of the intestine villi were observed.

Intestine histology. There exist villus - like patterns which are particularly effective in the digestion and absorption of the nutrients on longitudinal intestine section. For the fishes included in MOS, Vitamin B_{12} and control groups, the cross sections prepared from the intestines starting from the posterior Pylorus section have been examined subsequent to hematoxylen-eosin painting process. As a result of the examination of the intestine sections of the carp fishes in all groups, it has been observed that the epithet structures of the intestine are normal in all samples (Figure 2). However, for Groups A and C where MOS is added, slight increases were observed in the length and thickness of the intestine villi.

DISCUSSION

In this study, the carp frys have been fed for a period of 90 days with the commercial feed MOS and vitamin B_{12} addition. The effects of MOS and vitamin B_{12} addition in different rates to commercial feed on intestine and liver histology were assessed. The obtained results showed that the epithelium is normal histologically in all samples when the intestinal sections of the carp fish are thoroughly examined. However, in the Groups A and C where MOS added to the trial feed, slight increases were observed in the lengths and thickness of the carp fishes. But no pathologic disorder was observed in the liver cells of the trial fishes in all of the groups.

The results of this study are in line with the results obtained from the studies on different fish like Salmon (*S. salar* L.) [10]; Trout (*O. mykiss)* [11-12]; Sole (*S. solea*) [13]; Catfish (*I. punctatus*) [14]; Carp (*C. carpio)* [15]; European Catfish (*S. glanis*) [16]; Sea Bass (*D. labrax)* [17]; Blackspot Seabream *(D. sargus)* [18]; Atlantic Sturgeon (*A. oxyrinchus*) [19]. These studies also reported that MOS has substantial effect on the increase of density, length and thickness of intestine microvillus and it also decreases the observation of any damage to the intestine microvillus. The majority of the studies focus on the growth and resistance of the fishes fed with prebiotic diets against pathogenic bacteria as well as feed efficiency. It has been proven that alimentation through MOS encourages growth of the fishes. Fewer studies mention the influence of different probiotics on the growth of the fishes.

As a result, the use of MOS and Vitamin B_{12} has no adverse effect on the vitality and physiology of the carp fishes and no pathological disorder has been observed in the intestines and livers. The fats on the liver are usual. The lengthened and thickened villi of the intestines prove that this particular study has achieved a success. Although the advantages of the feed additives have long been examined, the studies for the use of the utterly natural MOS in the field of fishery are quite limited in Turkey. More comprehensive studies should be made for such products in order to increase the efficiency of the fishes and improve their health wise condition. Also the effects of such products should be defined and in case the natural feed additive is to be used widely, it is considered that it will be beneficial for cultivation.

ACKNOWLEDGEMENTS

Authors acknowledge help of Agriculture Engineer Soner Sezen from Mediterranean Aquaculture Research, Production and Training Institute, Kepez Station (AKSAM) Antalya, Turkey in providing the fish used in this experiment and Dr. Tülay AKAYLI (Istanbul University, Faculty of Aquaculture) and Prof. Dr. Erol Rüştü BOZKURT (Istanbul Research and Examination Hospital) for providing help in pathologic analysis for the intestines and livers.

This paper is summarized from a part of the doctorate thesis of Mehmet Ates.

REFERENCES

[1] Lawrence, C. (2007) The husbandry of zebrafish (*Danio rerio*): A review. Aquaculture. 269, 1–20.

[2] Masser, M.P., Rakocy, J. and Losordo, T.M. (1999) Recirculating aquaculture tank production systems: Management of recirculating systems. College Station TX: Southern Regional Aquaculture Center; Southern Regional Aquaculture Center Publication No. 452.

[3] Sweetman, J. and Davies, S. (2006) Improving growth performance and health status of aquaculture stocks in europe through the use of biomos. web page: http://www.aquafeed. com/article.php.

[4] Yano, T., Mangindan. E.P. and Matsuyama, H. (1989) Enhacement of resistance of carp (*Cyprinus carpio*) to experimental *edwardsiella tarda* infection. by some β-1,3 glucans. Nippon Suisan Gakkaishi. 55, 1815-1819

[5] Raa, J. (2000) The use of immune-stimulants in fish and shellfish feeds. pages 47-56 in L. E. Cruz-Suàrez, D. Ricque-Marine, M. Tapia-Salazar, M. A. Olvera-Novoa, R. Civera-Cerecedoi editors. Avances en nutrición acuícola V. memorias del V sisposium internacional de nutrición aquícola, 19-22 Noviembre, 2000.Mérida, Yucatán, Mexico.

[6] Halver, J.E. and Hardy, R.W. (2002) Fish nutrition, 3rd edition, academic press ISBN: 9780080494920. San Diego, California. 500 pp.

[7] Routray, P., Verma, D.K., Sarkar, S.K., and Sarangi, N. (2007) Recent advances in carp seed production and milt cryopreservation. Fish Physiology and Biochemistry. 33(4), 413–427

[8] Bryant, P.L., and Matty, A.J. (1981) Adaptation of carp (*Cyprinus carpio*) larvae to artificial diets: 1. Optimum feeding rate and adaptation age for a commercial diet. Aquaculture. 23(1-4), 275-86.

[9] Culling, F.A. (1963) Handbook of histopathological techniques, second edition, Butterworth & Company Publishers Ltd., London. 553p.

[10] Dimitroglou, A., Sweetman, J. and Morkore, T. (2007) Influence of Bio-Mos on salmon (*Salmo salar*, L) gut morphology, in commercial rearing conditions, using electron microscopy. Poster presented at Alltech's 23rd Annual Symposium, May 20-23, 2007, Lexington, KY, USA.

[11] Dimitroglou, A. (2007) Influence of Bio-Mos on rainbow trout (*Oncorhynchus mykiss*) gut integrity in commercial rearing conditions. Poster presented at Alltech's 23rd Annual Symposium, May 20-23, 2007, Lexington, KY, USA.

[12] Staykov, Y., Spring, P. and Denev, S. (2005) Effects of dietary Bio-Mos on growth rate and immunity of rainbow trout (*Salmo gairdneri irideus* G.) grown in raceways. Poster presented at Alltech's 21st Annual Symposium, May 22-25, 2005, Lexington, KY, USA.

[13] Dimitroglou, A., Janssens, T. and Davies, S. (2006) Effect of Bio-Mos on sole (*Solea solea*) gut integrity (histological perspectives). Poster presented at Alltech's 22nd Annual Symposium, April 24-26, 2006, Lexington, KY, USA.

[14] Peterson, B.C., Quiniou, S., Manning, B.B., and Bramble, T.C. (2007) Effects of Bio-Mos on growth and survival of channel catfish challenged with *Edwardsiella ictaluri*. Poster presented at Alltech's 23rd Annual Symposium, May 20-23, 2007, Lexington, KY, USA.

[15] Culjak, V., Bogut, I., Has-Schon, E., Milakovic, Z. and Canecki, K. (2006) Effect of Bio-Mos on performance and health of juvenile carp. Poster presented at Alltech's 22nd Annual Symposium, April 24-26, 2006, Lexington, KY, USA.

[16] Bogut, I., Milakovic, Z. Pavlicevic, J., and Petrovic, D. (2006) Effect of Bio-Mos on performance and health of european catfish (*Silirus glanis*). Poster presented at Alltech's 22nd Annual Symposium, April 24-26, 2006, Lexington, KY, USA.

[17] Torrecillas, A., Caballero, M.J., Sweetman, J., Makol, A., and Izguierdo, M.S. (2006) Effect of Bio-Mos on european sea bass (*Dicentrarchus labrax*) juveniles: growth performance and feed utilization. Poster presented at Alltech's 22nd Annual Symposium, April 24-26, 2006, Lexington, KY, USA.

[18] Dimitroglou, A., Davies, S., Divanach, P., and Chatzifotis, S. (2005) The role of Bio-Mos on the gut development of white sea bream (*Diplodus sargus*). Poster presented at Alltech's 21st Annual Symposium, May 22-25, 2005, Lexington, KY, USA.

[19] Pryor, G.S., Royes, J.B., Chapman, F.A. and Miles, R.D. (2003) Mannan oligosaccharides in fish nutrition: effects of dietary supplementation on growth and gastrointestinal villis structure in gulf of mexico sturgeon. North Am. J. Aquac. 65(2), 106-111.

Received: **01.10.2017**
Accepted: **02.12.2017**

CORRESPONDING AUTHOR

Mehmet Ates
Munzur University,
Faculty of Engineering,
Department of Bioengineering,
Tunceli, 62000 -Turkey

e-mail: mehmetates@munzur.edu.tr

© by PSP Volume 27 – No. 2/2018 pages 1169-1175 Fresenius Environmental Bulletin

INVESTIGATION OF *DESMODESMUS ARMATUS* FOR LEAD (Pb^{+2}) AND NICKEL (Ni^{+2}) REMOVAL CAPACITY FROM METAL POLLUTED WATER

Cigdem Acar, Ozden Fakioglu*

Ataturk University, Faculty of Fisheries, Erzurum, Turkey

ABSTRACT

This research was carried out in order to investigate the lead and nickel removal of *Desmodesmus armatus. D.armatus* was applicated three doses (0.025 mg L^{-1}, 0.21 mg L^{-1}, 0.25 mg L^{-1}) lead and three doses (0.02 mg L^{-1}, 0.05 mg L^{-1}, 0.3 mg L^{-1}) nickel. As a result of the experiment, it was determined that the highest absorbance was 0.023 ± 0.0 mgL^{-1} on the 13th day of lead application with 0.025 mgL^{-1} dose. In this study has been found that *D.armatus* removes about 80% of the lead in the water. The live cells of *D.armatus* were able to remove about 50% of the nickel in the water but nickel retained back to the water by die cell of *D.armatus.* As a result of in this research, *D.armatus* was found to be effective in lead elimination, but nickel removal was determined to be possible only with living cells.

KEYWORDS:
Lead, Nickel, Removal, *Desmodesmus armatus*

INTRODUCTION

The accumulation of domestic and industrial heavy metal wastes in aquatic systems bring about not only increased environmental pollution but also reduced biodiversity [1]. The rate of accumulation of heavy metals in aquatic ecosystems has changed to the industrial activities in the region, human activities and human literacy rates [2].

Microalgae represent in a particular area of ecosystems [3]. These organisms are preferred studies of heavy metal removal in the wastewater, because they are to be susceptible, grow fast and have low cost of breeding [4-5]. However, they are effected on heavy metal removal by some factors such as algae cell size, morphology, physiology, pH, temperature, metal specificity, metal concentration and biomass density [6-7].

The metal ions included Al^{+3}, Cu^{+2}, Pb^{+2}, Cd^{+2}, Ni^{+2}, Co^{+2}, Zn^{+2}, Fe^{+3}, Be^{+2} and UO_2^{+2}. The cations of this groups are also compatible with the pH, binding sites in the cell wall, and cationic properties of metals [6]. The pH of the solution is an important indication for the heavy metals bioabsorption by algae. Generally, when the pH is increased, the cationic metals absorption is increased, but the anion metals absorption is decreased. The leads to positively charge surfaces in excess of the acidic environment and increases the metal bonding of the electrostatic attraction between the cations and the surface [7-8].

Nickel concentrations in rivers and lakes are fairly low (below 10 μgL^{-1} on average). The amount of nickel in drinking water is usually below 0.02 mgL^{-1}. Higher concentrations can also be seen in special cases where nickel accumulation is due to natural or industrial sources. Nickel is an element with low toxicity when compared to materials such as zinc, manganese and chromium. Nickel does not accumulate in tissues [9].

The zinc removal capacity of *Acutodesmus obliquus*, *Desmodesmus subspicatus* and *D.armatus* was investigated. The highest percentage of zinc removal was found in *D. subspicatus* (40%), and followed by *A. obliquus* (30%) and *D. armatus* (18%) [10].

The aim of in this study was investigate the lead and nickel remove capacity of *D. armatus* that It can grow rapidly and live in different temperature range.

MATERIALS AND METHODS

The *D.armatus* used in this study was obtained from the SAG microalgae culture unit of Göttingen University (Germany) under the code SAG 276-13.

Cultures. The algae were inoculated into 100 ml Erlenmeyer flask and multiplied in the incubator and then the algae were inoculated into 5 L glass containers (15x103 $cellsml^{-1}$ in each sample) applied with Bold Basal 11 medium [11]. Nutrient application was discontinued after heavy metal addition to sample containers. Lead standard solutions (commercial name Merck 6080-56-4; formula is (CH3COO) $2Pb.3H_2O$) were prepared to be final concentration as 0.025 mgL^{-1} (P1), 0.21 mgL^{-1} (P2), 0.25 mgL^{-1} (P3) doses. The final concentration of nickel (commercial name is Merck 6080-56-4; formula is CH3COO) $2Pb.3H_2O$) were prepared to be final concentration as 0.02 mgL^{-1} (N1), 0.05 mgL^{-1} (N2), 0.3 mgL^{-1} (N3) doses. Both solutions were stored in the refrigerator at +4ºC.

Laboratory Studies. During the experiment, temperature, pH and light measurements were measured daily in the morning. In order to determine the amounts of dry matter, 50 micrograms of microalgae were taken from all cultures and analyzed every three days. The dry matter quantities were calculated % values by subtraction wet weighed from dry weighed [12].

Chlorophyll-a was determinate each sample has been taken 100 ml every three days [13]. Samples were filtered through a Wathman GF/6 filter paper and then allowed to dry in the dark at room temperature for 2-4 hours. The dried filter papers were placed in test tubes (10 ml of 90% acetone). The agitated test tubes have been kept in the refrigerator (+4 °C) for 24 hours in the dark. Centrifugation of the samples and optical density of the extract were then carried out in spectrophotometers at 630, 645, 665 nm wavelengths.

The samples were then homogenously mixed and counted under a microscope by dropping 2 drops onto both sides of the Thoma lamina [4]. At the same time, cultures were mixed homogeneously on a daily basis to detect microalgae biomass, and then 3 ml samples were taken with a pipette. Samples were placed in quartz tubes and read at 680 nm wavelength in spectrophotometer. The biomass is calculated according to this formula [14];

Dry cell weight (gL^{-1}) = $0.668 \times OD_{680}$

Lead and Nickel Concentration. Lead and nickel concentration was determinate with ICP-MS. The Inductively Coupled Plasma-Mass Spectrometry (ICP-MS) analysis was carried out in the Eastern Anatolia High Technology Application and Research Center (DAYTAM) of the Atatürk University.

Statistical Analysis. One-Way (ANOVA) test using SPSS was applied to statistical analyzes of *D.armatus* cell count, biomass, chlorophyll-a, pH, temperature, dry matter and concentrations of lead and nickel in the medium. The difference was evaluated according to the DUNCAN test. Calculations and controls were made according to [15].

RESULTS AND DISCUSSION

In this study, pH was found statistically significant ($p < 0.05$) the relationship between lead and nickel applied *D.armatus* cultures and control group. In cultures with lead application, the highest value for Pb1 (0.025 mg L^{-1}) was 7.77 ± 0.08 at 2nd day and the lowest was 7.32 ± 0.49 at 8th day. The lowest and highest values of Pb2 (0.21 mgL^{-1}) were found to be 5.59 ± 0.07 and 7.58 ± 0.16, respectively. The highest value of Pb3 (0.25 mgL^{-1}) was found to be 7.57 ± 0.03 at the 1st day. The pH value in the nickel-treated cultures, the highest value for Ni1 (0.02 mgL^{-1}) was measured as 7.53 ± 0.02 at 4th day and the lowest value at 11th day with 6.57 ± 0.28. In the application of Ni2 (0.05 mgL^{-1}), the lowest and highest values were determined as 6.91 ± 0.08 and 7.36 ± 0.05, respectively. In the case of Ni3 (0.3 mgL^{-1}), the highest value was determined as 7.37 ± 0.17 at 1st day (Figure 1). The pH limit value in ideal culture media ranges from 7 to 9 [16]. The mean of pH values for nickel application were measured to the limit values for the ideal culture medium, whereas the mean of pH value for lead-treated cultures was lower than the ideal value. Two resins [(Dowex HCR S/S (strong cationic) and Dowex Marathon C (strong cationic)] were chose for the purpose of copper removal from aqueous solutions, and maximum effect of these resins on copper removal was observed pH 5.5 value so the effect of pH also changes with respect to the adsorbent type [17].

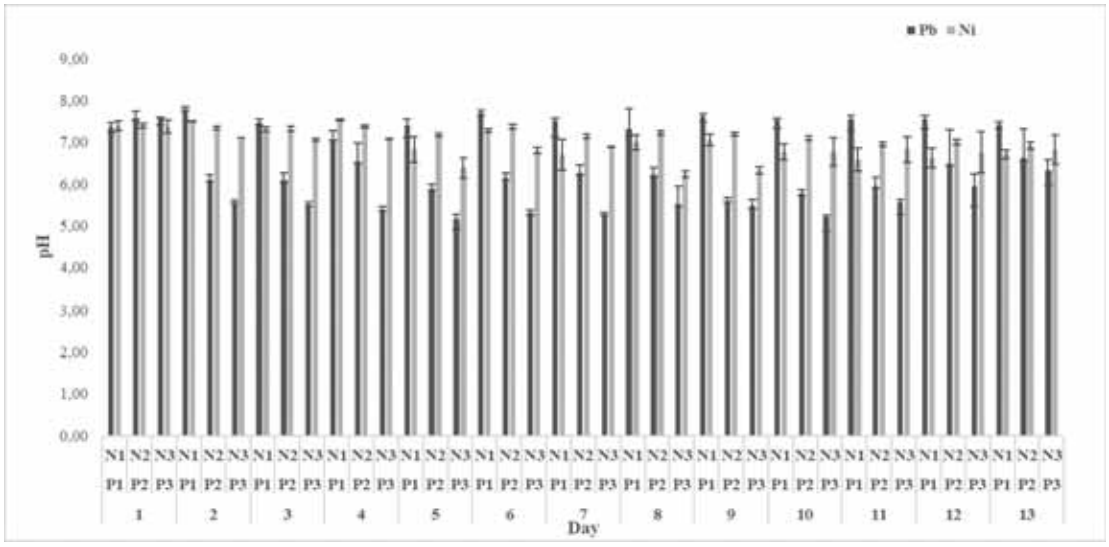

FIGURE 1

Change of pH value for lead and nickel applied on *D.armatus* (Pb1=0.025 mgL^{-1} Pb^{+2}; Pb2 =0.21 mgL^{-1} Pb^{+2}; Pb3=0.25 mgL^{-1} Pb^{+2}; Ni1=0.02 mgL^{-1} Ni^{+2}; Ni2=0.05 mgL^{-1} Ni^{+2}; Ni3=0.3 mgL^{-1} Ni^{+2})

When pH value is low, the cell surface is more positively charged. The optimum pH value for the metal-algae interaction in the removal of heavy metals is among 5.5 to 7 [18]. The more increase the pH value, the more increase the removal of cationic metals [8]. For cultures with nickel application, daily changes in pH value were measured among 7.53 to 6.23. It was determined that the nickel binding capacity of *D. armatus* increased by 20% by decreasing the pH value.

Water temperature of algae culture samples was measured at 9:00 a.m. every morning. The relationship between lead and nickel applied *D.armatus* culture and non-applied cultures was statistically significant ($p<0.05$). In cultures with lead application; the lowest value was measured at application of P2 (0.21 mgL^{-1}) with 24.87 ± 1.75 °C and the maximum value was measured at 35.70 ± 3.08 °C at application of Pb1 (0.025 mgL^{-1}). In the case of nickel application, the lowest and highest values were determined as 24.40 ± 1.73 °C and 35.70 ± 0.46 °C, respectively (Figure 2). Some scholars have reported that high temperatures enhance heavy metal adsorption, while others have suggested that high temperatures reduce heavy metal absorption. In the common sight absorption case, pH is more influenced than the rate of temperature [18]. During in this study, it was determined that the change in pH was more effect on absorption than the change in water temperature.

Chlorophyll-a was measured at the 9th and the end of this experiment and chlorophyll-a were found statistically significant ($p<0.05$) between groups and days. The mean chlorophyll-a in the lead applied (P1, P2 and P3) was calculated 0.2 ± 0.05 μgL^{-1}; 0.05 ± 0.0 μgL^{-1} and 0.1 ± 0.00 μgL^{-1}, respectively. In nickel applications [Ni1 (0.02 mgL^{-1}), Ni2 (0.05 mgL^{-1}), Ni3 (0.3 mgL^{-1})] were found 0.03 ± 0.01 μgL^{-1}; 0.095 ± 0.01 μgL^{-1} and 0.03 ± 0.01 μgL^{-1}, respectively (Table 1). However, it has been reported that the same species does not change chlorophyll-a in Cd application [19]. In the terrarial plants, Ni ion might play an important role in the water balance of plants, so that plants uses even a small amount of nutrient element like a nickel. However, Pb ion was found no significant differences between the level of irrigation and the amount of Pb removed from the soil by the plant [20-21].

TABLE 1
Change of chlorophyll-a depend on between groups and days in *D.armatus* of lead and nickel applied cultures

Day	Control (mgL^{-1})	Ni1 (0.02mgL^{-1})	Ni2 (0.05mgL^{-1})	Ni3 (0.3 mgL^{-1})	Pb1 (0.025mgL^{-1})	Pb2 (0.21 mgL^{-1})	Pb3 (0.25 mgL^{-1})
9	$0,55±0,25^{Aa}$	$0,05±0,01^{Ad}$	$0,12±0,05^{Ac}$	$0,05±0,04^{Ac}$	$0,21±0,04^{Ab}$	$0,10±0,0^{Ac}$	$0,19±0,05^{Ab}$
13	$0,12±0,13^{Ba}$	$0,01±0,01^{Bc}$	$0,07±0,05^{Bb}$	$0,01±0,0^{Bc}$	$0,19±0,07^{Ba}$	$0,00±0,00^{Bc}$	$0,00±0,00^{Bd}$

AB The different capital letters in the same **COLUMN** show the differences of days and different capitalization is statistically significant ($p<0.05$).
abcd The different lower-case letters in the same **ROW** show the differences of groups and different capitalization is statistically significant ($p<0.05$).

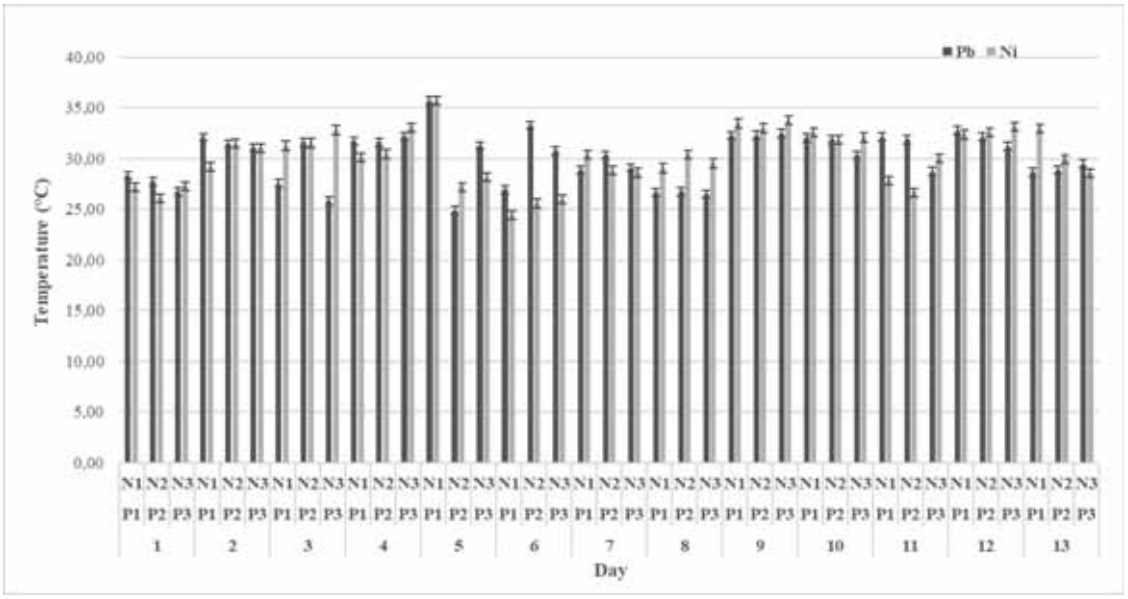

FIGURE 2
Change of temperature value for lead and nickel applied on *D.armatus*
(Pb1=0.025 mgL^{-1} Pb^{+2}; Pb2 =0.21 mgL^{-1} Pb^{+2}; Pb3=0.25 mgL^{-1} Pb^{+2}; Ni1=0.02 mgL^{-1} Ni^{+2}; Ni2=0.05 mgL^{-1} Ni^{+2}; Ni3=0.3 mgL^{-1} Ni^{+2})

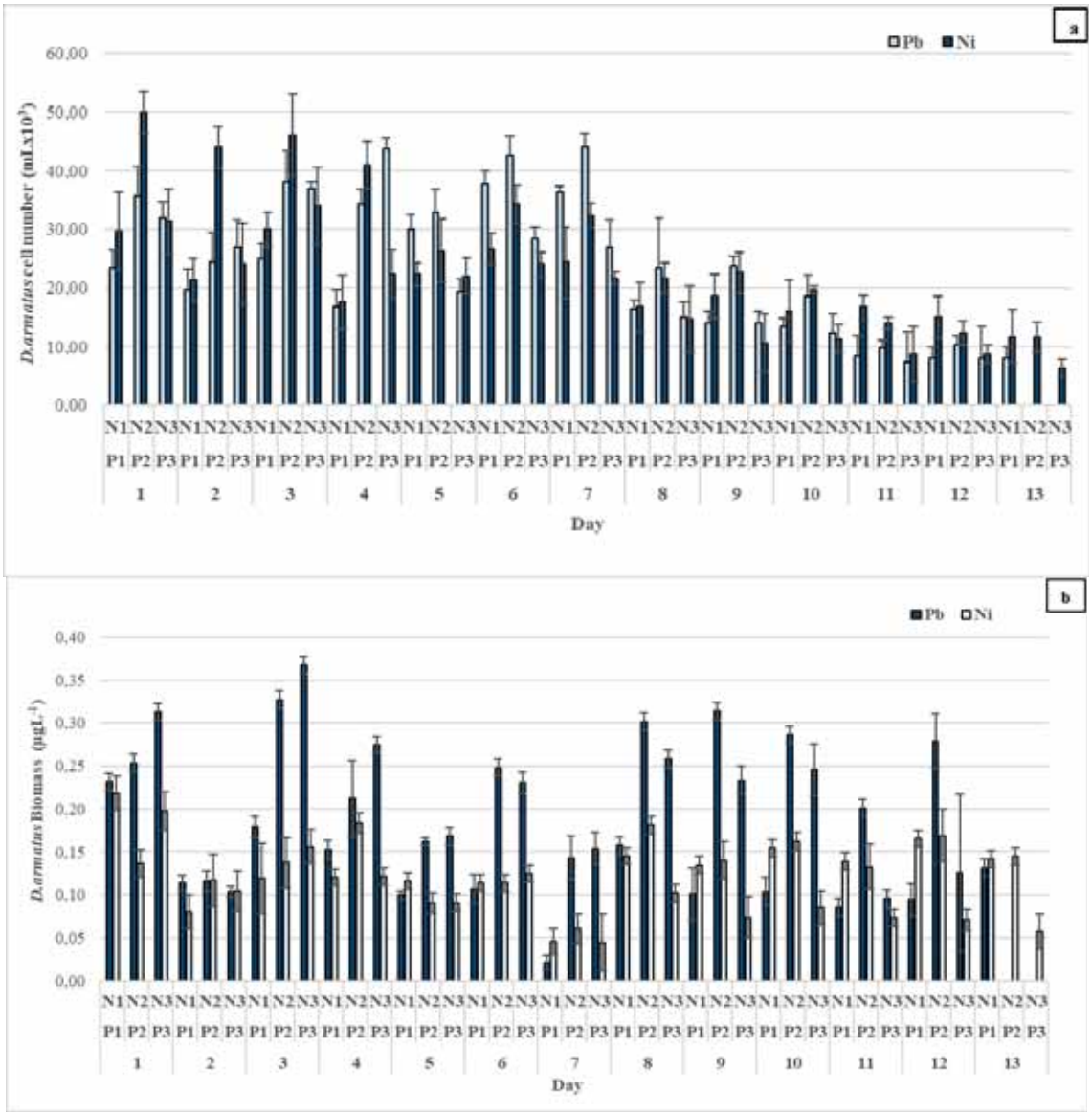

FIGURE 3
Change of cell number (a) and biomass (b) for lead and nickel applied on *D.armatus* (Pb1=0.025 mgL^{-1} Pb^{+2}; Pb2 =0.21 mgL^{-1} Pb^{+2}; Pb3=0.25 mgL^{-1} Pb^{+2}; Ni1=0.02 mgL^{-1} Ni^{+2}; Ni2=0.05 mgL^{-1} Ni^{+2}; Ni3=0.3 mgL^{-1} Ni^{+2})

TABLE 2
Variation of lead and nickel concentrations in water of lead and nickel applied *D.armatus* cultures with days

Day	Lead*			
	Control (mgL^{-1})	Pb1 (0.025 mgL^{-1})	Pb2 (0.21 mgL^{-1})	Pb3 (0.25 mgL^{-1})
1	0.00±0.0^{Ad}	0.005±0.0^{Ab}	0.001±0.0^{Cc}	0.120±0.01^{Aa}
7	0.00±0.0^{Ad}	0.001±0.0^{Bc}	0.018±0.0^{Bb}	0.020±0.0^{Ba}
13	0.00±0.0^{Ad}	0.0003±0.0^{Cc}	0.085±0.01^{Aa}	0.002±0.01^{Cb}
	Nickel*			
	Control (mgL^{-1})	Ni1 (0.02 mgL^{-1})	Ni2 (0.05 mgL^{-1})	Ni3 (0.3 mgL^{-1})
1	0.0001±0.0^{Ad}	0.016±0.0^{Cc}	0.03±0.0^{Bb}	0.199±0.0^{Ba}
7	0.0002±0.0 ^{Ad}	0.006±0.0^{Bc}	0.010±0.0^{Cb}	0.071±0.0^{Ca}
13	0.0001±0.0 ^{Ad}	0.032±0.0^{Ac}	0.055±0.0^{Ab}	0.380±0.0^{Aa}

***Lead and nickel concentrations were assessed within themselves**
ABC: The different capital letters in the same **COLUMN** show the differences of days and different capitalization is statistically significant ($p<0.05$).
abcd: The different lower-case letters in the same **ROW** show the differences of groups and different capitalization is statistically significant ($p<0.05$).

Spirulina platensis did not affect the growth of chromium and zinc application [22]. Nevertheless, many factors such as the type of organism, lethal and sublethal doses, metal-species interaction have been reported to affect the growth of heavy metal-applied microalgae [17, 23].

The relationship between the application of lead and nickel cultures and control group were found statistically significant ($p<0.05$). The number of *D.armatus* and biomass in the cultures where lead is applied; all of the *D.armatus* cells died in the P2 and P3 specimens on the 13th day, although occasional increases were observed in the advancing days, which increased until about the 6th day. In cultures with nickel application, the lowest-highest The number of *D.armatus* and biomass values were measured 10.67 ± 4.93 μgL^{-1}, 0.04 ± 0.01 μgL^{-1}, 50.00 ± 9.54 μgL^{-1} and 0.22 ± 0.04 μgL^{-1}, respectively (Figure 3).

Biomass and cell number tend to similar have been changed in this study. Biomass and cell number of *D. armatus* application of heavy metal were identified to increase on the seven days long, but they suddenly decreased on the 13th day. Nickel, however, is a necessary element for plants and is an element with low toxicity when compared to materials such as zinc, manganese and chromium and does not accumulate in tissues. Besides, single-celled creatures and fish are influenced on inorganic lead, which is concentration among 0.04 mgL^{-1} to 0.02 mgL^{-1} [24]. The accumulation of Pb concentrations in the freshwater ecosystem is primarily in sediment, followed by plankton and fish.

Water samples were taken from the culture of lead and nickel applied on *D.armatus* and untreated culture on 1st, 7th and 13th days. The lead and nickel concentrations in these samples were analyzed and relationship between treated and untreated *D.armatus* cultures was found statistically significant ($p<0.05$).

In lead application, the lowest value for Pb1 (0.025 mgL^{-1}) was 0.0003 ± 0.0 mgL^{-1} on 13th day and the highest value was 0.0044 ± 0.0 mgL^{-1} on 1st day. In the application of Pb2 (0.21 mgL^{-1}), the lowest and highest values were determined as 0.0013 ± 0.0 mgL^{-1} and 0.085 ± 0.0 mgL^{-1}, respectively. In the case of Pb3 (0.25 mgL^{-1}), the lowest value was found to be 0.002 ± 0.01 mgL^{-1} on 13th days and the highest value on 1st day (0.12 ± 0.01 mgL^{-1}) (Table 2). Dead cells of *Scenedesmus obliguus* are more effective in removing heavy metals than living cell of *S.obliguus* [10].

In nickel-enriched cultures was measured the lowest and the highest values for Ni1 (0.02 mgL^{-1}), 0.016±0.0 mgL^{-1} and 0.016 ± 0.0 mgL^{-1}, respectively. The lowest and highest values were found 0.01 ± 0.0 mgL^{-1} and 0.055 ± 0.0 mgL^{-1} in Ni2 (0.05 mgL^{-1}) application. In the N3 (0.3 mgL^{-1}) application was calculated the lowest and highest values as 0.071 ± 0.0 mgL^{-1} and 0.38 ± 0.0 mgL^{-1}, respectively (Table 2). It was observed that the nickel retained at the end of the assay again.

It has been reported that nickel is not toxic among 1 mgL^{-1} to 10 mgL^{-1} concentration in water [25-26]. However, nickel use production of battery and as a result of the water mixing of the pillars, many aquatic creatures lose their life. *Chlorella miniata* is the most suitable algal for the removal of nickel [27]. In this study was determinate that *D.armatus* is not suitable to removal nickel from waste water.

D. armatus has been found to be effective in Pb removal, but it not to be effective nickel removal. It has been reported that *D. armatus* is used to be Cd and Zn removal to the metal-pollution site [28]. *Desmodesmus subspicatus* is to be a useful algal for removal of zinc [19]

CONCLUSIONS

The effects of heavy metals (Cd, Co, Cr, Cu, Ni, Pb, Zn) on green algae (*C. vulgaris*, *C. sorokiniana* and *S. quadricauda* etc.) and blue-green algae (*Spirulina platensis*) were investigated to bioabsorption capacity. In these studies, they reported that algae could be used for heavy metal removal [10, 19, 22, 29].

In this study was found that *D. armatus* use to be effective on lead elimination in metal-pollution area, but it uses to be possible only live cells for nickel removal.

As a result, it is thought that microalgae can be used for heavy elimination due to rapid developments, cell structures and cell building materials. In addition, microalgae to be able to retain heavy metals in more constituents by diversifying the chemical substances used in culture media and/or by changing the pH value.

ACKNOWLEDGEMENTS

We would like to thank Eastern Anatolia High Technology Application and Research Center (DAYTAM), who helped in the analysis during our scientific work.

This article is produced from a master thesis.

REFERENCES

[1] Pena-Castro, J.M., Martinez-Jeronimo, F., Esparza-Garcia, F., Canizares-Villanueva, R.O. (2004) Heavy metals removal by the microalga *Scenedesmus incrassatulus* in continuous cultures. Bioresource Technology. 94, 219-222.

[2] Chipasa, K.B. (2003) Accumulation and fate of selected heavy metals in a biological wastewater treatment system. Waste Management. 23(2), 135-143.
[3] Rojickova-Padrtova, R. and Marsalek, B. (1999) Selection and sensitivity comparisons of algal species for toxicity testing. Chemosphere. 38(14), 3329-3338.
[4] Komarek, J and Et Marvan, P. (1979) Selection and registration of strains of algae as assay organisms. – In: Marvan, P. Algal Assays, Stuttgart. 87-102,.
[5] Rioboo, C., Gonzalez, O., Herrero, C., Cid, A. (2002) Physiological response of freshwater microalga (*Chlorella vulgaris*) to triazine and phenylurea herbicides. Aquatic Toxicology. 59, 225-235.
[6] Wase, J. and Forster, C. (1997) Biosorbents for metal ions. UK: CRC Press, London. 1-238.
[7] Mehta, S.K. and Gaur, J.P. (2005) Use of algae for removing heavy metal ions from wastewater: process and prospects. Critical Reviews in Biotecnology. 25(3), 113-152.
[8] Arief, V.O., Trilestari, K., Sunarso, J., Indraswati, N., Ismadji, S. (2008) Recent progress on biosorption of heavy metals from liquids using low cost biosorbents: characterization, biosorption parameters and mechanism studies. Clean. 36(12), 937-962.
[9] World Health Organization-WHO. (2011) Guidelines for drinking water quality. 4th edn. Geneva: World Health Organization.
[10] Guclu, Z., and Ertan, Ö.O. (2012) Toxicity and removal of zinc in the three species (*Acutodesmus obliquus, Desmodesmus subspicatus* and *Desmodesmus armatus*) belonging to the Family, Scenedesmaceae (Chlorophyta). Turkish Journal of Fisheries and Aquatic Sciences. 12(2), 309-314.
[11] Andersen, R.A. (2005) Algal culturing techniques. Elsevier Academic Press, California, USA, 578 p.
[12] Vonshak, A. (1997) Outdoor mass production of spirulina: The Basic Consept. *Spirulina platensis* (Arthrospira) physiology. Cell- Biology and Biotechnology. Great Britain.79-99.
[13] Strickland, J.D.H. and Parsons, T.R. (1972) A practical handbook of seawater analysis. Fisheries Research Board Of Canada. 94-167.
[14] Kang, C.D., Lee, J.S., Park, T.H. and Sım, S.J. (2005) Comparison of hetetrophic and photoautotrophic induction on astaxanthin production by *Haematococcus pluvialis.* 68, 237-241.
[15] Kesici, T., Kocabas, Z. (2007) Biostatistics, Ankara University, Faculty of Pharmacy Biostatistics Press No:94, Turkey, Ankara, 1-369.
[16] Sukatar, A. (2002) Alg kültür yöntemleri (Prosedüre of algae culture). Ege Universitesi Fen fakültesi Kitaplar Serisi No:184, İzmir, 1-168.
[17] Veli, S., and Pekey, B. (2004) Removal of copper from aqueous solution by ion exchange resins. Fresen. Environ. Bull. 13, 244-250.
[18] Kumar, K.S., Dahms, H.U., Won, E.J., Lee, J.S., Shin, K.H. (2015) Mikroalgae – a promising tool for heavy metal remediation. Ecotoxicology and Environmental Safety. 113, 329-352.
[19] Pokora, W., Bascik-Remisiewicz, A., Tukaj, S., Kalinowska, R., Pawlik-Skowronska, B., Dziadziuszko, M. and Tukaj, Z. (2014) Adaptation strategies of two closely related *Desmodesmus armatus* (green alga) strains contained different amounts of cadmium: A study with light-induced synchronized cultures of algae. Journal of Plant Physiology. 171, 69-77.
[20] Onder, D., Onder, S., Daghan, H., and Uygur, V. (2016) Influence of different irrigation level and different nickel (Ni) doses on phytoremediative capacity of *Tagetes erecta* l. Fresen. Environ. Bull. 25, 191-199.
[21] Onder, D., Onder, S., Daghan, H., Uygur, V. (2016) The ability of *Brassica napus* l. to remove lead (Pb) from the soil at different irrigation levels and Pb concentrations. Fresen. Environ. Bull. 25, 200-209.
[22] Dogru, F. (2010) Determination of binding capacity of Cr (III) and Zn (II) ions of *Spirulina platensis*. Master Thesis, Institute of Science and Technology. Turkey, Adana.
[23] Wang, W. (1984) Enteraction of iron and zinc toxcity on algal community. ASTM STP 854. Am. Soc. Testing Mater. 1987-2001.
[24] Pulatsu, S., Topcu, A. ve Atay, D. (2014) Water Pollution and Control. Ankara University Agriculture Faculty Press No:432, Turkey. Ankara,1-384 (Turkish).
[25] Prasad, P.V. and Prasa, P.S. (1982) Effect of cadmium, lead and nickel on three freshwater green algae. Water, Air, And Soil Pollution. 17(3), 263–268.
[26] Muyssen, B.T.A, Brix, K.V, Deforest, D.K., Janssen, C.R. (2004) Nickel essentiality and homeostasis in aquatic organisms. Environmental Review. 12(2), 113-131.
[27] Chong, A.M.Y., Wong, Y.S., Tam, N.F.Y. (2000) Performance of different.microalg species in removing nickel and zing from industrial wastwater. Chemosphere. 41, 251-257.
[28] Bascik-Remisiewicz, A., Tomaszewska, E., Labuda, K. and Tukaj Z. (2009) The effect of Zn and Mn on the toxicity of Cd to the green microalga *Desmodesmus armatus* cultured at ambient and elevated (2%) CO_2 concentrations. Polish J. of Environ. Stud. 18(5), 775-780.
[29] Das, D., Chakraborty, S., Bhattacharjee, C., Chowdhury, R. (2015) biosorption of lead ions (Pb^{+2}) from simulated wastewater using residual biomass of microalgae. Desalination and Water Treatment. 57(10), 4576-4586.

Received: **03.10.2017**
Accepted: **09.12.2017**

CORRESPONDING AUTHOR

Ozden Fakıoglu
Ataturk University,
Faculty of Fisheries,
Department of Basic Science,
Erzurum – Turkey

e-mail: ozden.fakioglu@atauni.edu.tr

© by PSP Volume 27 – No. 2/2018 pages 1176-1182 Fresenius Environmental Bulletin

DETERMINATION OF PHENOLIC COMPOUNDS OF *STACHYS RUPESTRIS* MONTBRET ET AUCHER EX BENTHAM BY LC-MS/MS AND ITS BIOLOGICAL ACTIVITIES

Bulent Ergun[1], Fatih Goger[2], Yavuz Bulent Kose[3,*], Gokalp Iscan[2,4]

[1]Anadolu University, Faculty of Pharmacy, Department of Toxicology, 26470 Eskisehir, Turkey
[2]Anadolu University, Faculty of Pharmacy, Department of Pharmacognosy, 26470 Eskisehir, Turkey
[3]Anadolu University, Faculty of Pharmacy, Department of Pharmaceutical Botany, 26470, Eskisehir, Turkey
[4]Anadolu University, Yunus Emre Vocational School, 26470 Eskisehir, Turkey

ABSTRACT

One of the largest genus of Lamiaceae, *Stachys,* extended from south western part of Asia to America, represented in Turkey with % 48 endemism rate. In this presented study LC-ESI-MS/MS properties, anticandidal, antioxidant and cytotoxic activity of methanol extract of an endemic *Stachys rupestris* Montbret et Aucher ex Bentham was determined. Total phenol content, Trolox Equivalent Antioxidant Capacity assay (TEAC), 1,1-Diphenyl-2-picrylhydrazyl (DPPH) radical scavenging activity tests were made for antioxidant activity. Phenolic compounds determination were performed with LC- MS/MS. Extract was further investigated against thirteen selected human pathogenic *Candida* strains. Additionally, cytotoxic effect of the extract was determined against NIH3T3 mouse embryonic fibroblast cell lines by MTT assay. Total phenol content was found as 18.90 ± 0.54 mg GAE. IC_{50} value of DPPH radical scavenging activity was determined as 0.04 ± 0.003 mg/ml. TEAC activity was found as 0.7 ± 0.02 mM while IC_{50} value of Gallic acid = 0.002 ± 0.0001 mg/ml and TEAC of gallic acid 2.47 ± 0.07 mM. Hydroxybenzoic acid derivatives and flavonoids were identified as main compounds Anticandidal activity of the extract was evaluated with CLSI M27-A2 protocol against 13 *Candida* strains. Remarkably, two strains of *Candia krusei* were inhibited by *S. rupestris* extract, with the concentrations of 31.25 and 62.5 µg/mL. Cytotoxicity test showed that *S. rupestris* extract does not possess a cytotoxic activity against NIH3T3 cell lines at these concentrations.

KEYWORDS:
Stachys, Lamiaceae, LC-MS/MS, Anticandidal, Antioxidant, Cytotoxicitiy

INTRODUCTION

Labiatae (Lamiaceae) which is a cosmopolitan family showing wide distribution in tropical and subtropical areas including the Mediterranean region and consist of aromatic plants that contain the essential oils usually a different composition with a high amount.

Stachys is a genus of annual or perennial herbaceous and small shrubs in the number of species represented by over 300 of the World [1-5].

In Turkey, there are 91 species (116 taxa) belonging to genus *Stachys*. Endemism ratio of the genus is 48% with 55 taxa [6]. *Stachys* has some traditional therapeutic uses such as sedative, antispasmodic, diuretic, emmenagogue, stomachic, digestive, carminative, tonic and throat pain reliever [7, 8]. Several *Stachys* species have also been reported for uses on genital tumours, sclerosis of the spleen, inflammatory tumours and cancerous ulcers [9].

Candida species are being developed resistance to common antifungals such as amphotericin B and flucytosine [10]. There is a big need to screen potential antifungal natural compounds against multidrug-resistant fungal pathogens such as *Candida* spp.

Free radicals are the substances that would cause many diseases like cancer, diabetes and arthritis [11]. Antioxidants are important for human body to scavenge free radicals. Chemical preservatives such as BHT, BHA are used to ensure food quality and longer shelf life by food industry. Most people are consuming such kind of preservatives even though they are not realised. However it is well known that synthetic antioxidants are very dangerous for human health.

Finding new sources of natural antioxidants, used widely from beauty to health care, are getting importance. For this purpose, *S. rupestris* one of the endemic species from the genus investigated for its antioxidant and anticandidal activity. Previous investigation shown that secondary metabolites of *Stachys* are generally phenyl ethanol glycosides, flavonoids, phenolic acids, fatty acids, essential oils and diterpenes [12].

The aim of this study was to investigate anticandidal, antioxidant and cytotoxic activity of the *S. rupestris*. Phytochemical characterization of the extract determined by LC-ESI-MS/MS.

MATERIALS AND METHODS

Plant Material. Samples collected from, Turkey: İçel, around Namrun castle, stony places. [17 V 2014).Voucher specimen (ESSE: 15005) is kept at the herbarium of Faculty of Pharmacy of Anadolu University, Eskisehir, Turkey.

LC-MS/MS analysis. Experiments were performed with a Shimadzu 20A HPLC system coupled to an Applied Biosystems 3200 Q-Trap LC- MS/MS instrument equipped with an ESI ion source was used in the negative ionization mode. Separations were performed on an ODS 150 x 4,6 mm, i.d., 3 µm particle sizes, octadecyl silica gel analytical column operating at 40 ºC at a flow rate of 0.3 ml/min. The mobile phase was used Methanol: Water: Formic acid (10:89:1) (solvent A) and Methanol: Water: Formic acid (89:10:1) (solvent B). The composition of B was increased from 15% to 40% in 15 min, increased to 45% in 3 min and held for 12 min, and increased to 75% in 5 min; then the composition of B was increased to 100% in 10 min.

Anticandidal Assay. Anticandidal effect was evaluated by using partly modified CLSI (formerly NCCLS) methods for broth dilution antifungal susceptibility testing of yeasts (M27-A2) [39]. Clinically isolated (Osmangazi University, Faculty of Medicine, Department of Microbiology) and standard strains (ATCC and NRRL) of *Candida* strains were used as the test microorganisms. Amphotericin-B (Sigma-Aldrich) and Ketoconazol (Sigma-Aldrich) were used as standard antifungal agents.

TEAC assay (Trolox Equivalent Antioxidant Capacity). This test measures the ability of a compound to scavenge the ABTS (2, 2′-azinobis-(3-ethyl-benzothiazoline-6-sulphonate) radical in comparison to the antioxidant activity of Trolox which is a water-soluble form of vitamin E, used as a standard. The blue–green ABTS radical was formed through the reaction of 7 mM ABTS with 2.5 mM sodium persulfate ($Na_2S_2O_8$) in the dark at room temperature for 12–16 h before use. ABTS solution was diluted with ethanol to a final absorbance of 0.7–0.8 at 734 nm. 10 µl portion of sample was added to 990 µl of ABTS solution, and the reduction in absorbance was measured 1 min after addition of Trolox up to 40 min after addition of the extract. The stock solution of Trolox (2.5 mM) was prepared in ethanol. Absorbance was measured on a UV/spectrophotometer [40].

1,1-Diphenyl-2-picrylhydrazyl (DPPH) radical scavenging activity. Serial dilutions were prepared with the stock solutions (4 mg/ml) of the extract to get the half concentrations of previous one. Diluted solutions were added with DPPH• (equal amounts). After 30 min UV absorbance was recorded at 517 nm. The experiment was performed in triplicate for extract and positive standard control, BHT (Butylated hydroxyl toluene). The average of the absorptions was noted for each concentration. The percentage inhibition was calculated using Eqn. 1. The IC_{50} value, which is the concentration of the test material that inhibits 50% of the free radical concentration, was calculated as mg/ml using Sigma Plot statistical program [41].

$$\text{Percentage Inhibition} = \left[\frac{(\text{Abs}_{\text{control}} - \text{Abs}_{\text{sample}})}{\text{Abs}_{\text{control}}}\right] x100 \quad (1)$$

Total phenolics. Total phenols were estimated as Gallic acid equivalents (GAE), expressed as mg Gallic acid/g extract [42].

Cytotoxicity test. NIH3T3 cell line is frequently used to determine cytotoxic effects of compounds [43-47]. NIH/3T3 mouse embryonic fibroblast cell line (ATCC® CRL-1658™, London, UK) was incubated to the Dulbecco's Modified Eagle's Medium (DMEM). NIH/3T3 cells were plated on 96-well culture plates as 10000 cells per well and were then treated with the compounds at concentrations ranging from 500 µg/ml to 3.90625 µg/ml (500, 250, 125, 62.5, 31.25, 15.625, 7.8125, 3.90625 µg/ml). MTT assay was performed as previously described [48-49]. Dose-response curves were plotted against compound concentrations applied to determine IC50 values. The following formula was used to calculate the inhibition percentage for each concentration.

% inhibition = 100 - (mean sample*100 / mean solvent)

RESULTS AND DISCUSSION

Anticandidal assay. *In vitro* anticandidal evaluation of the extract were performed by CLSI microdilution broth method. 13 different *Candida* strains were tested in comparison with standard antifungal agents. The extract showed moderate to strong effects on tested strains between 4000 to 31.25 µg/mL (MIC). Notably, *Candida krusei* ATCC 6258 and 34135 strains were inhibited by the extract having MIC values of 31.25 and 62.5 µg/mL (Table 1). Previous activity studies were generally reported the bioactivity of *S. rupestris* essential oil [5, 13-15]. This is the first study on *S.rupestris* crude extract and its anticandidal activity. According to our results *C. krusei* is most sensitive fungi to *S. rupestris* extract *in vitro*.

TABLE 1
Anticandidal activity results of *Stachys rupestris* extract (MIC, µg/mL)

Candida spp.	*Source*	*SRE*	*S1*	*S2*
Candida albicans	*CI*	*250*	*0.25*	*0.06*
Candida albicans	*ATCC 90028*	*250*	*0.12*	*0.5*
Candida albicans	*ATCC 10231*	*1000*	*0.5*	*0.06*
Candida albicans	*ATCC 24433*	*500*	*0.25*	*0.12*
Candida glabrata	*CI*	*500*	*0.25*	*0.06*
Candida glabrata	*ATCC 2001*	*250*	*1*	*0.5*
Candida glabrata	*ATCC 66032*	*4000*	*1*	*0.12*
Candida tropicalis	*ATCC 1369*	*250*	*0.5*	*0.06*
Candida tropicalis	*ATCC 750*	*250*	*0.25*	*0.06*
Candida krusei	*ATCC 6258*	***31.25***	*1*	*0.5*
Candida krusei	*ATCC 34135*	***62.5***	*2*	*0.5*
Candida parapsilosis	*ATCC 22019*	*125*	*0.25*	*0.06*
Candida zeylanoides	*NRRL Y-1774*	*250*	*1*	*0.25*

SRE: Methanolic extract of *S. rupestris*, S1: Amphotericin-B; S2: Ketoconazole, CI: Clinically isolated (Osmangazi University, Faculty of Medicine, Department of Microbiology, Eskisehir, Turkey)

Apart from *C. albicans*, *C. krusei* is one of the most common pathogenic fungi for female genital tract [16] and it causes several infections on patients with hematologic malignancies and transplant recipients. After further studies *S. rupestris* extract may be considered as potential anticandidal natural product.

Cytotoxicity assay. As known, biochemical similarity of the human cell and fungi forms is a handicap for selective activity. Therefore, we evaluated to selectivity of inhibitory activity by MTT assay on healthy NIH3T3 mouse embryonic fibroblast cell lines (ATCC CRL165), which is recommended for cytotoxicity screening by ISO (10993-5, 2009) [50]. The IC50 value of the extract (241.57 µg/mL) against NIH3T3 cells was higher than its MIC values (31.25 and 62.5 µg/mL) against *Candida krusei* ATCC 6258 and 34135. Furthermore, it may be concluded that the extract is not cytotoxic, because its MIC values against *Candida krusei* ATCC 6258 and 34135 strains are about 3 and 7 folds lower than IC_{50} values against NIH3T3 cells.

Antioxidant assay. Extract yield of dried plant material was obtained as 27 %. As far as we know this is the first report on *S. rupestris* antioxidant activity.

Total Phenolic compound was determined as 143.826 ± 12.4685 mgGAE in 1gr extract. Result can be also explain as 3,95 gr in 100 gr dried plant material which was coherent with previously reported from *Stachys persica* [17] and *S. alpina* [18].

Hydrogen atom or electron transfer is the main reason for the antioxidant capacity so we determine antioxidant activity by using ABTS and DPPH radical scavenging methods. DPPH is the method related to capacity of a compound's hydrogen donating ability while the second one is related electron transfer capacity.

DPPH radical scavenging activity was determined as 0.04 ± 0.003 mg/ while positive control gallic acid was determined as 0.002 ± 0.00 mg/ml and Butylated hydroxytolune (BHT) showed 0,01± 0.00. It is reported similar activity from *Stachys schtschegleevii* [19] and *S. lavandulifolia* [20]. Delazar and colleagues was reported acetylated flavanoid glycosides of *S. bombycina* was showed prominent DPPH radical scavenging activity [21]. It is reported to similar antioxidant activity in another study of *Stachys* [18].

TEAC activity was found as 0.7 ± 0.02 mM TEAC however positive control gallic acid showed more activity with the score 2.47 ± 0.07 mM and BHT showed 1,75± 0.01 mM TEAC antioxidant activity. In a previous study of *S. lavandulifolia* we reported that water extract was presented 0.5 mM TEAC [20]. Leporini and colleagues reported significant ABTS radical scavenging activity from *S. glutinosa* [22].

Based on the antioxidant activity results previously published we determined the more active antioxidant activity results than other *Stachys* species but not as good antioxidant activity as positive control gallic acid and BHT.

Based on the antioxidant activity results previously published we determined the more active antioxidant activity results than other *Stachys* species but not as good antioxidant activity as positive control gallic acid and BHT.

LC-MS/MS characterization of the extract. According to LC-MS/MS identification 16 compounds were determined (Table 2).

Compounds 1, 2, 5 were showed characteristic molecular ion peaks and fragments of hydroxy cinnamic acid derivatives.

Compound 1 and 2 showed the same molecular ion peak at m/z 353 $(M-H)^-$ same base peak at m/z 191 and the same low abundance product ion at m/z 179. According to Clifford and colleagues previous studies Compound 1 and 2 must be 5-caffeoylquinic acid and 1-caffeoylquinic acid [23] which can be differ from each other according to their elution time [24].

Compound 1 was identified as 1-caffeoylquinc acid which was previously determined in *S. glutinosa* [22] and compound 2 was identified as 5-caffeoylquinic acid.

TABLE 2
LC-MS/MS analysis results of the *S. rupestris* methanolic extract

No	Rt	M-H	B.P	MS^2	Identification
1	5.5	353	191	179	1-Caffeoylquinic acid
2	9.3	353	191	179	5-Caffeoylquinic acid
3	10.1	461	415	339, 293, 149, 121	Unknown
4	11.5	337	191		5-Coumaroylquinic acid
5	12.0	755	593	461, 315, 297, 179, 161, 135	Forsythoside B
6	12.2	623	161	461, 305, 179	Verbascoside
7	13.3	609	285	447, 429, 213	Isoscutellarin 7-O-allosyl (1-2) glucoside
8	14.3	637	461	315, 297, 175, 135	leucosceptoside A
9	15.5	651	285	609, 591, 447, 429	Isoscutellarein 7-O-[6’’’-O-acetyl]-allosyl(1-2) glucoside
10	17.4	623	299	443, 284	4'-O-Methylisoscutellarein 7-O-allosyl(1-2) glucoside
11	19.9	665	299	623, 503, 461, 443, 299, 284	4’-O-Methylisoscutellarein 7-O-[6’’’-O-acetyl] -allosyl(1-2)glucoside
12	20.7	285	133	175	Isoscutellarein
13	21.3	315	300	271, 255, 243	Methylquercetin
14	30.2	343	328	313, 298, 270	Xanthomicrol
15	26.2	359	344	329, 314, 299	Sideritiflavon

RT: Retention time, M-H: deprotonated molecular ion peak, MS^2: MS/MS fragment ions

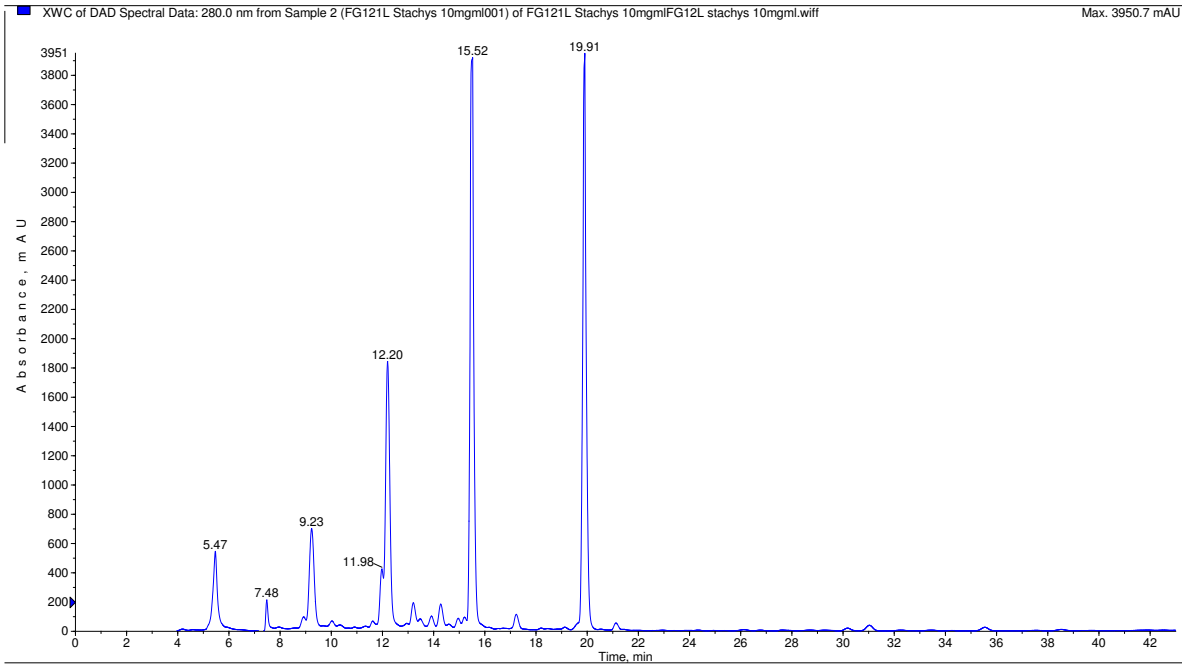

FIGURE 1
280 nm HPLC chromatogram of the extract

Compound 4 was identified as 5-coumaroylquinic acid based on the previous study of Clifford [25].

Compound 5 presented pseudo molecular ion at m/z 755 and gave the base peak ion at m/z 593 owing to the loss of a caffeoyl moiety. Other ion were observed at m/z 461 (M-H-132) due to a loss of a pentose moiety. Than losing of a rhamnose gave rise to an ion at m/z 315 (M-H-132-146). m/z 297 ion produced by the loss of the H_2O. Other ions at m/z 179 161 and 135 closely related with caffeic acid. This fragmentation behaviour was led us to understand that compound 5 is a molecule of caffeoyl phenylethanoide glycoside. Forsythoside B is the compound was previously determined at *Stachys* and its MS fragmentation being in agreement with that reported by Mitreski and Kırmızıbekmez [26, 27].

Compound 6 presented a deprotonated molecular ion peak at m/z 623 (M-H) which yielded four major fragments at m/z 461, 305, 179 and 161. The MS fragmentation was found to similar with phenylethanoide glycosides described above. Verbascoside is the compound previously identified in several *Stachys* and gives the same mass fragments thus compound 6 was identified as verbascoside [28-30].

Compound 7, 9, 10, 11 were determined as O-glycosylated isoscutellarein derivatives which were reported in genus *Stachys* several times [28, 31-34].

Compound 7 showed a $[M-H]^-$ ion at m/z 609 and its MS^2 spectrum showed a base peak ion at m/z 285 due to the loss of 324. amu, probably a diglucose moiety. Presence of an ion at m/z 429 (M-H-180) indicates that glycosylation was occurred in position 1-2 between the sugars [35]. So compound 7 was identified as Isoscutellarin 7-O-allosyl (1-2) glucoside

which is previously determined in *Stachys*. [28].

Compound 9 showed the similar fragmentation behaviour but 42 amu higher molecular ion peak than compound 7 which indicate that compound 9 is acetylated derivative of compound 7. So Compound 9 was identified as Isoscutellarein 7-O-[6'''-O-acetyl]-allosyl (1-2) glucoside [36]. Acetyl loss and other fragments can be seen in Table 1.

Compound 8 showed a precursor ion at m/z 637 [M - H]- and its MS/MS spectrum presented base peak at m/z 461 due to the loss of a feruloyl moiety the feruloyl part also observed at m/z 175 . Further fragmentation of compound was resulted in ions at m/z 315 because of the elimination rhamnose unite. Compound 8 was identified as Leucoseptoside A which displayed the same fragmentation pattern with previous report [26].

Compound 10 was identified as 4'-O-Methylisoscutellarein 7-O-allosyl (1-2) glucoside. Methylated isoscutellarein at m/z 299 and (1-2) linkage position of sugars can be seen at m/z 443 (M-H-180).

Compound 11 deprotonated molecular ion at *m/z* 665, was 42 amu higher (an acetyl moiety) than compound 10 and exhibited similar MS fragmentation. Thus compound 11 was labelled as 4'-O-Methylisoscutellarein 7-O-[6'''-O-acetyl]-allosyl (1-2) glucoside. Isoscutellarein which was determined as aglycon of compounds described above was also determined as compound 12.

Compound 13 eluted after isoscutellarein, its deprotonated molecular ion was observed at m/z 315 which yielded a base peak at m/z 300 due to the loss of a methyl unit further fragmentation of this ion was resulted in ions at m/z 271, 255, 243. Similar MS fragmentation pattern of compound 13 and quercetin indicate that compound 13 is methyl ether of quercetin which is also known as rhamnetin or isorhamnetin correspond to methyl position. Because of the unknown methyl position, compound 13 was just identified as methylquercetin.

Compound 14 showed a precursor ion at *m/z*343 $[M - H]^-$ and other product ions at m/z 328, 313, 298, were formed after elimination of three methyl group. After a comparing the literature data about previously identified *Stachys* compounds that included three methyl unıt and the same molecular ion with compound 14, xhantomicrol was determined which was agreement with our MS data. Thus compound 14 was identified as xhantomicrol tentatively [37].

Compound 15 presented MS/MS spectrum characteristics of a trihydroxy-trimethoxyflavone with product ion at *m/z* 359. Other ions related to methyl loss was observed at m/z 344, 329, 314 Determination of compound was performed in similar way to compound 14. After a comparing the literature data about previously identified *Stachys* compounds that include three methyl unıt and the same molecular ion, sideritiflavon was matched with compound 15 [38].

It is the first report on detailed phytochemical characterization of *S. rupestris* by LC-MS/MS. CLSI protocol of *S. rupestris* extract was screened for its *in vitro* inhibitory effect on several *Candida* strains for the first time here. The extract was demonstrated moderate to strong inhibitory effects against tested *Candida* strains. Both strains of *C. krusei* were determined as susceptible. Furthermore, anticandidal activity of the extract is not due to general toxicity, but can be ascribed to its selective action against *C. krusei* strains. The antioxidant activity was determined moderate.

ACKNOWLEDGEMENTS

This work was partially supported by Anadolu University Research Fund (1404S135)

REFERENCES

[1] Dundar, E., Akcicek, E., Dirmenci, T. and Akgun, S. (2013) Phylogenetic analysis of the genus Stachys sect. Eriostomum (Lamiaceae) in Turkey based on nuclear ribosomal ITS sequences. Turk J Bot. 37(1), 14-23.

[2] Piozzi, F., Bruno, M. (2011) Diterpenoids from Roots and Aerial Parts of the Genus Stachys. Rec Nat Prod. 5(1), 1-11.

[3] Radulovic, N., Lazarevic, J., Ristic, N. and Palic, R. (2007) Chemotaxonomic significance of the volatiles in the genus Stachys (Lamiaceae): Essential oil composition of four Balkan Stachys species. Biochem Syst Ecol. 35(4), 196-208.

[4] Serbetci, T., Demirci, B., Guzel, C.B., Kultur, S., Erguven, M., Baser, K.H.C. (2010) Essential Oil Composition, Antimicrobial and Cytotoxic Activities of Two Endemic Stachys cretica Subspecies (Lamiaceae) from Turkey. Nat Prod Commun. 5(9), 1369-1374.

[5] Ugur, A., Sarac, N. and Varol, O. (2013) Antimicrobial activities of the essential oils of endemic Stachys rupestris and Stachys amanica against multi-resistant bacteria. Indian J Pharmacol. 45(2), 201-U211.

[6] Baştürk, K., Dinç, M. and Doğu, S. (2015) Anatomical characteristics of Turkish endemic Stachys rupestris Montbret et Aucher ex Bentham (Lamiaceae). Mod Phytomorphol. 8, 37-40.

[7] Baytop, T. (1999) Geçmişte ve Bugün Türkiye'de Bitkiler ile Tedavi, Nobel Tıp Kitabevi Ltd Şti, İstanbul.

[8] Dulger, B., Ugurlu, E., Aki, C., Suerdem, T.B., Camdeviren, A. and Tazeler, G. (2005) Evaluation of antimicrobial activity of some endemic Verbascum, Sideritis, and Stachys species from Turkey. Pharm Biol. 43(3), 270-274.

[9] Morteza-Semnani, K., Saeedi, M. and Shahani, S. (2006) Antioxidant activity of the methanolic extracts of some species of Phlomis and Stachys on sunflower oil. Afr J Biotechnol. 5(24), 2428-2432.
[10] Pfaller, M., Diekema, D., Gibbs, D., Newell, V., Nagy, E. and Dobiasova, S., (2008) Candida krusei, a multidrug-resistant opportunistic fungal pathogen: geographic and temporal trends from the ARTEMIS DISK Antifungal Surveillance Program, 2001 to 2005. J Clin Microbiol. 46(2), 515-521.
[11] Tepe, B., Degerli, S., Arslan, S., Malatyali, E. and Sarikurkcu, C. (2011) Determination of chemical profile, antioxidant, DNA damage protection and antiamoebic activities of Teucrium polium and Stachys iberica. Fitoterapia. 82(2), 237-246.
[12] Tundis, R., Peruzzi, L. and Menichini, F. (2014) Phytochemical and biological studies of Stachys species in relation to chemotaxonomy: A review. Phytochemistry. 102, 7-39.
[13] Singleton, V.L., Orthofer, R. and Lamuela-Raventos R.M. (1999) Analysis of total phenols and other oxidation substrates and antioxidants by means of Folin-Ciocalteu reagent. Methods Enzymol. 299, 152-178.
[14] Papandreou, M.A., Kanaki, C.D., Polissiou, M.G., Efthimiopoulos, S., Cordopatis, P. and Margarity, M. (2006) Inhibitory activity on amyloid-β aggregation and antioxidant properties of Crocus sativus stigmas extract and its crocin constituents. J of Agri and Food Chem. 54(23), 8762-8768.
[15] Kumarasamy, Y., Byres, M., Cox, P.J., Jaspars, M., Nahar, L. and Sarker, S.D. (2007) Screening seeds of some Scottish plants for free radical scavenging activity. Phytother Res. 21(7), 615-621.
[16] M27-A2 CN. Reference Method for Broth Dilution Antifungal Susceptibility Testing of Yeasts; Approved Standard, Second Edition.
[17] Erdogan, E.A., Everest, A., De Martino, L., Mancini, E., Festa, M. and De Feo, V. (2013) Chemical Composition and In vitro Cytotoxic Activity of the Essential Oils of Stachys rupestris and Salvia heldreichiana, Two Endemic Plants of Turkey. Nat Prod Commun. 8(11), 1637-1640.
[18] Işcan, G., Köse, Y.B, and Demirci, B. (2015) Stachys rupestris (Lamiaceae)'İn Uçucu Yağ Bileşimi Ve Antimikrobiyal Etkileri. Anadolu University Journal of Science and Technology–C Life Sciences and Biotechnology. 4(1), 41-47.
[19] Cellat, K., Gül, Ş. and Everest, A. (2011) Mersin'deki Stachys rupestris Montbret et Aucher ex Bentham Türünün Eterik Yağ İçeriğinin Araştırılması. Lokman Hekim Journal. 7, 11-14.
[20] Singh, S., Sobel, J.D., Bhargava, P., Boikov, D. and Vazquez, J.A. (2002) Vaginitis due to Candida krusei: epidemiology, clinical aspects, and therapy. Clinical infectious diseases. 35(9), 1066-1070.
[21] Khanavi, M., Hajimahmoodi, M., Cheraghi-Niroomand, M., Kargar, Z., Ajani, Y. and Hadjiakhoondi, A. (2009) Comparison of the antioxidant activity and total phenolic contents in some Stachys species. Afr J Biotechnol. 8(6), 1143-1147.
[22] Kukic, J., Petrovic, S. and Niketic, M. (2006) Antioxidant activity of four endemic Stachys taxa. Biol Pharm Bull. 29(4), 725-729.
[23] Abichandani, M., Nahar, L., Singh, P., Chitnis, R., Nazemiyeh, H. and Delazar, A. (2010) Antibacterial and Free-Radical-Scavenging Properties of Stachys Schtschegleevii (Lamiaceae). Arch Biol Sci. 62(4), 941-945.
[24] Iscan, G., Demirci, B., Demirci, F., Goger, F., Kirimer, N. and Kose, Y.B. (2012) Antimicrobial and Antioxidant Activities of Stachys lavandulifolia subsp lavandulifolia Essential Oil and its Infusion. Nat Prod Commun. 7(9), 1241-1244.
[25] Delazar, A., Celik, S., Gokturk, R.S., Unal, O., Nahar, L. and Sarker, S.D. (2005) Two acylated flavonoid glycosides from Stachys bombycina, and their free radical scavenging activity. Pharmazie. 60(11), 878-880.
[26] Leporini, L., Menghini, L., Foddai, M., Petretto, G.L., Chessa, M. and Tirillini, B. (2015) Antioxidant and antiproliferative activity of Stachys glutinosa L. ethanol extract. Nat Prod Res. 29(10), 899-907.
[27] Clifford, M.N., Knight, S. and Kuhnert, N. (2005) Discriminating between the six isomers of dicaffeoylquinic acid by LC-MS. Journal of Agricultural and Food Chem. 53(10), 3821-3832.
[28] Jaiswal, R., Kiprotich, J. and Kuhnert, N. (2011) Determination of the hydroxycinnamate profile of 12 members of the Asteraceae family. Phytochemistry. 72(8), 781-790.
[29] Clifford, M.N., Kirkpatrick, J., Kuhnert, N., Roozendaal, H. and Salgado, P.R. (2008) LC–MSn analysis of the cis isomers of chlorogenic acids. Food Chem. 106(1), 379-385.
[30] Mitreski, I., Stanoeva, J.P., Stefova, M., Stefkov, G. and Kulevanova, S. (2014) Polyphenols in representative Teucrium species in the flora of R. Macedonia: LC/DAD/ESI-MS (n) profile and content. Nat Prod Commun. 9(2), 175-180.
[31] Kırmızıbekmez, H., Montoro, P., Piacente, S., Pizza, C., Dönmez, A. and Çalış, İ. (2005) Identification by HPLC-PAD-MS and quantification by HPLC-PAD of phenylethanoid glycosides of five Phlomis species. Phytochem Analysis. 16(1), 1-6.

[32] Karioti, A., Bolognesi, L., Vincieri, F.F. and Bilia, A.R. (2010) Analysis of the constituents of aqueous preparations of Stachys recta by HPLC-DAD and HPLC-ESI-MS. J Pharmaceut Biomed. 53(1), 15-23.
[33] Asnaashari, S., Delazar, A., Alipour, S.S., Nahar, L., Williams, A.S. and Pasdaran, A. (2010) Chemical Composition, Free-Radical-Scavenging and Insecticidal Activities of the Aerial Parts of Stachys byzantina. Arch Biol Sci. 62(3), 653-662.
[34] Ahmad, V.U., Arshad, S., Bader, S., Ahmed, A., Iqbal, S. and Tareen, R.B. (2006) New phenethyl alcohol glycosides from Stachys parviflora. J Asian Nat Prod Res. 8(1-2), 105-111.
[35] Demirtas, I., Gecibesler, I.H. and Yaglioglu, A.S. (2013) Antiproliferative activities of isolated flavone glycosides and fatty acids from Stachys byzantine. Phytochem Lett, 6(2), 209-214.
[36] Savic, M.M., Kukic, J.M., Grayer, R.J., Milinkovic, M.M., Marin, P.D. and Divljakovic, J. (2010) Behavioural Characterization of Four Endemic Stachys Taxa. Phytother Res. 24(9), 1309-1316.
[37] Marin, P.D., Grayer, R.J., Grujic-Jovanovic, S., Kite, G.C. and Veitch, N.C. (2004) Glycosides of tricetin methyl ethers as chemosystematic markers in Stachys subgenus Betonica. Phytochemistry. 65(9), 1247-1253.
[38] Murata, T., Endo, Y., Miyase, T. and Yoshizaki, F. (2008) Iridoid Glycoside Constituents of Stachys lanata. J Nat Prod. 71(10), 1768-1770.
[39] Petreska, J., Stefova, M., Ferreres, F., Moreno, D.A., Tomas-Barberan, F.A. and Stefkov, G. (2011) Potential bioactive phenolics of Macedonian Sideritis species used for medicinal "Mountain Tea". Food Chem. 125(1), 13-20.
[40] Pereira, O.R., Domingues, M.R., Silva, A. and Cardoso, S.M. (2012) Phenolic constituents of Lamium album: Focus on isoscutellarein derivatives. Food Res Int. 48(1), 330-335.
[41] Ulubelen, A., Topcu, G. and Kolak, U. (2005) Labiatae flavonoids and their bioactivity. In: Attaur, R. (ed.) Studies in Natural Products Chemistry, Elsevier. 233-302.
[42] Ruiu, S., Anzani, N., Orrù, A., Floris, C., Caboni, P. and Alcaro, S. (2015) Methoxyflavones from Stachys glutinosa with binding affinity to opioid receptors: in silico, in vitro, and in vivo studies. J Nat Prod. 78(1), 69-76.
[43] Brunner, T.J., Wick, P., Manser, P., Spohn, P., Grass, R.N., Limbach, L.K. and Stark, W.J. (2006) In vitro cytotoxicity of oxide nanoparticles: comparison to asbestos, silica, and the effect of particle solubility. Environ Sci Technol. 40(14), 4374-4381.
[44] Danihelová, M., Veverka, M., Šturdík, E. and Jantová, S. (2013) Antioxidant action and cytotoxicity on HeLa and NIH-3T3 cells of new quercetin derivatives, Interdisciplinary Toxicology. 6(4), 209-216. Orsine, J.V., Marques Brito, L., Silva, R.C., Santos Almeida Mde, F. and Novaes, M.R. (2013). Cytotoxicity of Agaricus sylvaticus in non-tumor cells (NIH/3T3) and tumor (OSCC-3) using tetrazolium (MTT) assay. Nutr Hosp. 28(4), 1244-1254.
[45] Theiszova, M., Jantova, S., Dragunova, J., Grznarova, P. and Palou, M. (2005). Comparison the cytotoxicity of hydroxyapatite measured by direct cell counting and MTT test in murine fibroblast NIH-3T3 cells. Biomed Pap Med Fac Univ Palacky Olomouc Czech Repub. 149(2), 393-396.
[46] Can, O.D., Osmaniye, D., Ozkay, U.D., Saglik, B.N., Levent, S., Ilgin, S. and Kaplancikh, Z.A. (2017). MAO enzymes inhibitory activity of new benzimidazole derivatives including hydrazone and propargyl side chains. European Journal of Medicinal Chemistry. 131, 92-106.
[47] Gencer, H.K., Cevik, U.A., Cavusoglu, B.K., Saglik, B.N., Levent, S., Atli, O. and Kaplancikli, Z.A. (2017). Design, synthesis, and evaluation of novel 2-phenylpropionic acid derivatives as dual COX inhibitory-antibacterial agents. Journal of Enzyme Inhibition and Medicinal Chemistry. 32(1), 732-745.
[48] Ozkay, U.D., Can, O.D., Saglik, B.N., Cevik, U.A., Levent, S., Ozkay, Y. and Atli, O. (2016). Design, synthesis, and AChE inhibitory activity of new benzothiazole-piperazines. Bioorganic & Medicinal Chemistry Letters. 26(22), 5387-5394.
[49] International Organization for Standardization (2009) Biological Evaluation of Medical Devices-Part 5: Tests for In Vitro cytotoxicity. ISO-10993-5 (3rd ed.).

Received: **09.10.2017**
Accepted: **03.12.2017**

CORRESPONDING AUTHOR

Yavuz Bulent Kose
Anadolu University,
Faculty of Pharmacy,
Department of Pharmaceutical Botany,
26470, Eskisehir – Turkey

e-mail: ybkose@anadolu.edu.tr

© by PSP Volume 27 – No. 2/2018 pages 1183-1190 Fresenius Environmental Bulletin

NUMERICAL COMPARISON OF ANATOMICAL FEATURES IN SOME *ALLIUM* L.

Ali Ozdemir[1], Canan Ozdemir[2,*]

[1]Manisa Celal Bayar University, Faculty of Art and Science, Department of Mathematics, Manisa, Turkey
[2]Manisa Celal Bayar University, Faculty of Art and Science, Department of Biology, Manisa, Turkey

ABSTRACT

In this study, the anatomical features of some members of the *Allium* L. (*A. karsianum* Fomin, *A. kunthianum* Vved., *A. rupestre* Steven, *Allium armenum* Boiss. Et Kotschy and *Allium djimilense* Boiss. Ex Rege) were compared numerically. The values produced by analysis of the root, stem and leaf anatomical characters are compared both with one another and with those produced by analysis of all characters. The results showed that investigated species also could be distinguished from each other not only by their morphological features but numerical anatomical characters as well.

KEYWORDS:
Numerically, *allium*, anatomy

INTRODUCTION

The genus *Allium* L., with more than 850 species [1, 2] is one of the most diverse and taxonomically difficult groups of monocots [3, 4]. This genus is naturally distributed in the Northern Hemisphere [3,5] and its main center of diversity is in the mountainous areas of southwestern and central Asia [3, 6,7]. The species from genus *Allium* are morphologically very diversified, therefore, many taxonomical problems remain unsolved [8]. In the 19th century, the *Allium* genus was divided into 6 groups. In the second half of the 20th century, first 3 subgenera and 12 sections were separated, next – 5 subgenera and 16 sections and, later on – 6 subgenera and 54 sections and subsections [9].

Systematics was based on the origin of plants as well as morphological, anatomical, cytological and serological traits. Among others, numerical taxonomy was applied [10, 11]. The present study is based on some wild species of *Allium* which can be eaten as folk vegetable [12]. Although, in recent years, numerous researchers have investigated this area, we have not found any studies on statistical comparisons of numerical anatomical features, such as this one we have just done. In this study, five selected *Allium* species belonging to Codonoprasum section were compared statistically regarding their numerical anatomical characters. The purpose is to determine statistically the closeness of the species investigated with the help of numerical anatomical features. In addition we assessed the numerical anatomical characters to answer the following question; Which anatomical characters are useful between species determination and which characters have diagnostic value?

MATERIALS AND METHODS

The plants were collected from natural populations of East Anatolia. Specimens were kept in the herbarium at Celal Bayar University. For anatomical studies, the plant specimens were fixed in 70% ethanol. Transverse sections were made using a sliding microtome and the cross sections were drawn after stained with safranin-Fast Green [13].

Anatomical measurements were taken using ocular-micrometer of root, stem and leaf cell sizes of the species. The minimal and maximal values of characteristics as well as arithmetical means were calculated. For the nümerical analysis, 16 anatomical characters were selected. This selection was based on the variations of the anatomical data. Characters were coded as 1, 2, 3, 4, 5, 6, 7, 8, 9, 10, 11, 12, 13, 14, 15, 16 and the taxa were coded as A, B, C, D, E (*A. karsianum A. kunthianum A. rupestre, A. armenum* and *A. djimilense*, respectively). Significance of the differences between the taxa and characters were evaluated by Analysis of variance (Regression Analysis) and Pearson's correlation. The differences were assessed by the one–way ANOVA test. Pearson's correlation coefficients were also calculated. Statistical analysis were performed using the MINITAB software package.

RESULTS AND DISCUSSION

Anatomical findings. Roots. *A. kunthianum* has two layered epidermis. Other species have single layered epidermis. Cortex is 2-5 layered in *A. djimilense.* Other species have 3-7 layered cortex. Three-sided endodermis wall thickening was present in all root cross sections except for *A. armenum* which has single-sided endodermis wall thickening. *A. kunthianum* and *A. armenum* have 1-2 metaxylem. Other

species have single big metaxylem. 3-4 xylem strands were present in all roots (Figure 1).

Stems. A thin cuticle surrounds the one layered epidermis in stem cross sections of *A. armenum* and *A. djimilense*. Other species have one layered epidermis with a thick cuticle. The cortex consists of orbicular shaped cells in all species and cortex cell row numbers range from 6 to 12. Vascular bundles are arranged in 2 rows in all species. The inner ring is formed by 3-5 big bundles in *A. rupestre* and *A. armenum*. Starch grain were present in the stem cortex of *A. Kunthianum* (Figure 2).

Leaves. In all species the epidermis of the leaf is covered by well developed cuticle with prominent ridges at vascular bundles. Palisade tissue 1-2, 1, 2-3, 2 and 1-2 layered in *A. karsianum A. kunthianum A. rupestre, A. armenum* and *A. djimilense*, respectively. The spongy tissue is limited to a peripheral belt around the central part in *A. armenum* (Figure 3).

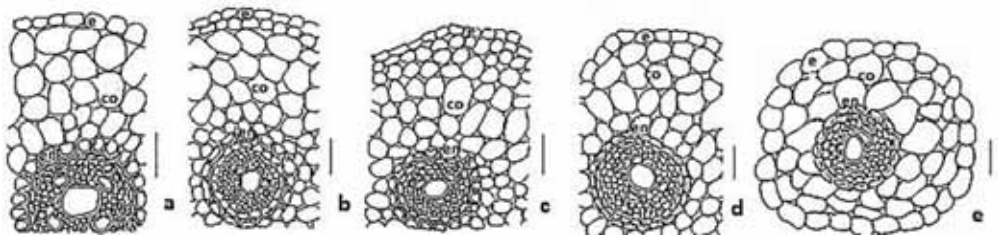

FIGURE 1
Cross-section of roots of *Allium karsianum* (a), *A. kunthianum* (b), *A. rupestre* (c), *A. armenum* (d), *A. djimilense* (e) e. epidermis, co. cortex, en. Endodermis. Bars = a : 40 µm; b: 20 µm; c,d: 30 µm e:15 µm

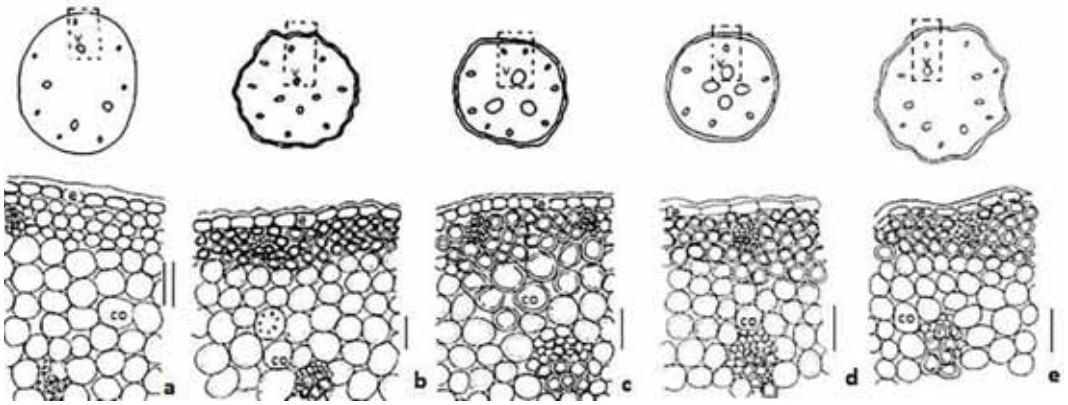

FIGURE 2
Cross-section of a stem showing gross morphology and part enlarged of *A. karsianum* (a), *A. kunthianum* (b), *A. rupestre* (c), *A. armenum* (d), *A. djimilense* (e) e. epidermis, co. cortex, v. vascular bundle). Bars = a, b, c: 70 µm d: 30 µm e:65 µm.

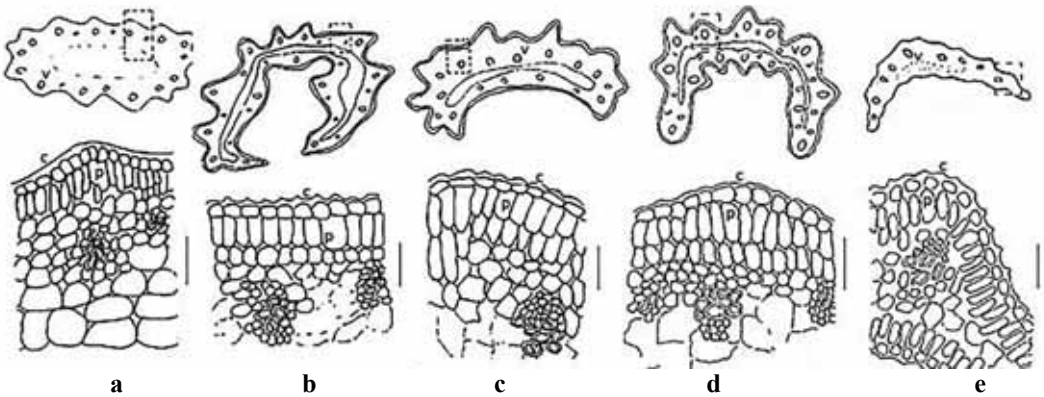

FIGURE 3
Cross-section of leaves showing gross morphology and part enlarged of *A. karsianum* (a), *A. kunthianum* (b), *A. rupestre* (c), *A. armenum* (d), *A. djimilense* (e) c, cuticle; p, palisade parenchyma; v, vascular bundle. Bars = 50 µm

TABLE 1
Anatomical measurements of the investigated taxa

		A		B		C	
		A. karsianum		***A. kunthianum***		***A. rupestre***	
		min.-max.	mean±S.D	min.-max.	mean±S.D	min.-max.	mean±S.D
		Root					
1	Epidermis Width	7.0 - 19	13 ± 1.3	10 - 29	20 ± 2.4	9.0 - 28	18 ± 10
2	Epidermis Length	5.0 - 12	8.5 ± 1.2	7.0- 20	14 ± 5.3	7.0 -19	13 ± 10
3	Cortex (diameter)	17 - 45	31 ± 5.2	10 - 36	33 ± 1.9	11 - 42	26 ± 12
4	Endodermis Width	8.0 - 14	11 ± 1.5	7.0- 10	8.5 ± 2.7	9.0 - 21	15 ± 11
5	Endodermis Length	7.0 - 10	8.5 ± 1.2	2.0- 10	6.0 ± 1.2	4.0 - 11	7.5 ± 7.5
6	Pericycle Width	5.0 - 10	7.5 ± 1.0	7.0 -10	8.2 ± 4.6	4.0 - 10	7.0 ± 1.4
7	Metaxylem (diameter)	24 - 40	32 ± 8.0	14 -19	16 ± 6.6	17 - 19	18 ± 12
		Stem					
8	Epidermis Width	12 - 5.5	8.0 ± 2.2	12 - 21	15 ± 1.5	12 - 14	10 ± 5.5
9	Epidermis Length	20 - 33	26 ± 4.8	7.0 - 11	10 ± 2.1	5.0 -10	12 ± 1.9
10	Cortex (diameter)	7.0 - 83	45 ± 1.2	7.0 - 71	46 ± 16	10 - 33	21 ± 12
11	Trachea (diameter	12 - 24	17 ± 2.4	10 - 70	40 ± 11	25 - 35	30 ± 16
		Leaf					
12	Cuticle	5.0 - 12	8.1 ± 2.8	1,0 – 4,0	7.0 ± 1,2	5.0- 10	4.8 ± 8.5
13	Epidermis Width	7.0 - 12	10 ± 2.8	10 - 17	10 ± 0,9	7.0 - 19	12 ± 9.0
14	Epidermis Length	6.0 - 17	11 ± 2.1	15 - 20	9.5 ± 2,2	5.0 - 7.0	12 ± 1.7
15	Palisade Width	8.0 - 23	16 ± 2.2	10 - 15	12 ± 1,5	5.0 - 10	8.0 ± 1.2
16	Palisade Length	28 - 53	44 ± 4.7	25 - 35	30 ± 2,8	20 - 33	24 ± 3.7

		D		E	
		A. armenum		***A. dijimilense***	
		Root			
1	Epidermis Width	12 - 29	22 ± 5.0	3.0 - 31	17 ± 5.2
2	Epidermis Length	7.0 - 19	14 ± 4.2	7.0 - 10	8.5± 2.3
3	Cortex (diameter)	10 - 36	23 ± 6.2	12 - 24	18 ± 0.8
4	Endodermis Width	7.0 - 17	12 ± 5.0	7.0 - 17	12 ± 1.2
5	Endodermis Length	8.0 - 14	11 ± 3.8	5.0 - 10	7.5± 0.9
6	Pericycle Width	7.0 - 10	8,5 ± 5.0	6.0 - 10	8.0± 0.8
7	Metaxylem (diameter)	17 - 31	24 ± 2.8	12 - 29	21 ± 9.2
		Stem			
8	Epidermis Width	10 - 17	13 ± 2.2	7.0 - 14	11 ± 0.8
9	Epidermis Length	4.0 – 7,0	5,5 ± 2.0	2.0 - 10	6.0± 1.8
10	Cortex (diameter)	7.0 - 33	20 ± 5.2	7.0 - 36	22 ± 1.8
11	Trachea (diameter)	15 - 30	22 ± 1.8	25 - 32	26 ± 1.9
		Leaf			
12	Cuticle	4.0 – 7.0	5,5 ± 1.2	7.0 - 21	14 ± 1.8
13	Epidermis Width	10 - 33	22 ± 2.0	14 - 29	22 ± 3.4
14	Epidermis Length	10 - 17	13 ± 2.3	10 - 24	17 ± 1.5
15	Palisade Width	15 - 30	26 ± 3.2	10 - 16	12 ± 1.7
16	Palisade Length	54 - 87	34 ± 2.2	53 - 89	74 ± 4.7

SD: Standart Deviation. 1-16: Character Codes. A-E: Taxa Codes

The results of the study show that three-sided endodermis wall thickening was present in all root cross sections except for *A. armenum* which is the most distant taxa as systematically among the investigated has single-sided endodermis wall thickening.

On the other hand, the spongy tissue is limited to a peripheral belt around the central part only in the leaf of *A. armenum.* Similarly another the study showed the importance of numerical analysis of the anatomy characters of the leaf for systematically in the some *Crocus* and *Salvia* L. species [14, 15].

Statistical analysis. The anatomical measuments of the investigated taxa, the minimal and maximal values of characteristics as well as arithmetical means are shown in Table 1. Significance of the differences and similarities between the *Allium* taxa was evaluated by Pearson's correlation (Correlation) and Analysis of variance (Regression Analysis). The statistical analysis of the results are shown in Tables 2, 3, 4, 5 and 6.

TABLE 2
Pearson's correlation between the investigated taxa based on nümerical anatomical characters

Taxa	A	B	C	D
B	0,542			
	0,030*			
C	0,641	0,767		
	0,007**	0,001**		
D	0,588	0,382	0,645	
	0,057	0,144	0,240	
E	0,628	0,740	0,567	0,785
	0,009**	0,001**	0,022*	0,166

*Significant at the level of 0.05 A-B: Investigated taxa
**Significant at the level of 0.01

TABLE 3
Pearson's correlation based on numerical anatomical characters of the investigated taxa

Characters	1	2	3	4	5	6	7	8	9
2	0,896								
	0,040*								
3	0,183	0,048*							
	0,769	0,775							
4	0,034*	0,024*	0,031*						
	0,957	0,969	0,401						
5	0,330	0,116	0,535	0,400					
	0,588	0,852	0,353	0,505					
6	0,793	0,048*	0,385	0,303	0,535				
	0,043*	0,416	0,523	0,030*	0,353				
7	0,624	0,674	0,065	0,070	0,397	0,181			
	0,261	0,213	0,918	0,911	0,508	0,770			
8	0,846	0,764	0,101	0,495	0,124	0,708	0,686		
	0,071	0,132	0,872	0,396	0,842	0,181	0,201		
9	0,822	0,568	0,611	0,112	0,237	0,725	0,707	0,696	
	0,087	0,318	0,274	0,858	0,701	0,166	0,182	0,192	
10	0,411	0,203	0,860	0,765	0,653	0,338	0,229	0,054	0,645
	0,491	0,744	0,061	0,132	0,232	0,578	0,711	0,944	0,240
11	0,334	0,663	0,572	0,196	0,158	0,085	0,090	0,131	0,189
	0,583	0,223	0,314	0,752	0,800	0,893	0,885	0,834	0,761
12	0,424	0,056	0,904	0,206	0,688	0,725	0,058	0,171	0,697
	0,477	0,993	0,035*	0,739	0,200	0,165	0,990	0,783	0,191
13	0,041*	0,379	0,956	0,024*	0,331	0,288	0,008**	0,144	0,516
	0,009**	0,529	0,010**	0,594	0,586	0,039*	0,970	0,817	0,373
14	0,035*	0,774	0,740	0,151	0,261	0,038*	0,423	0,477	0,044*
	0,464	0,125	0,153	0,809	0,671	0,042*	0,478	0,416	0,944
15	0,386	0,172	0,149	0,222	0,797	0,731	0,472	0,194	0,124
	0,521	0,782	0,811	0,720	0,106	0,061	0,422	0,755	0,843
16	0,482	0,617	0,303	0,265	0,657	0,069	0,911	0,732	0,452
	0,411	0,267	0,620	0,667	0,228	0,913	0,061	0,159	0,445

* Significant at the level of 0.05. ** Significant at the level of 0.01. 1- 16: Characters coda (Continued)

TABLE 3 (Continued)
Pearson's correlation based on numerical anatomical characters of the investigated taxa

Characters	10	11	12	13	14	15
11	0,089					
	0,886					
12	0,757	0,474				
	0,139	0,420				
13	0,684	0,785	0,834			
	0,203	0,116	0,079			
14	0,347	0,860	0,500*	0,864		
	0,567	0,051*	0,270	0,050*		
15	0,149	0,165	0,507	0,022*	0,047*	
	0,810	0,791	0,384	0,973	0,914	
16	0,190	0,146	0,302	0,276	0,588	0,509
	0,760	0,815	0,621	0,653	0,297	0,381

* Significant at the level of 0.05. ** Significant at the level of 0.01. 1- 16: Characters coda

In the Study, according to both the method, for investigated taxa coded as A-E, positive statistically significant correlations between A and B, A and C, A and E, B and C, B and E, C and E, as well as negative correlations between A and D, B and D, C and D, D-E were observed (Table 2,4). The highest similarity (Pearson's correlation 0.01p and 0.05p) was revealed between *A. kunthianum* and *A. rupestre, A. kunthianum* and *A. djimilense,* while the lowest (Pearson's correlation 0.01p and 0.05p) was found for *A. armenum* and *A. djimilense* (Table 2).

According to the mentioned statistical results derived, there is a considerable relation between the investigated taxa which are close taxa as systematically, except for *A. armenum* which is the most distant taxa as systematically among the investigated.

Also it is mentioned that there are close relationships among *A. rupestre, A. djimilense, A. kunthianum, A. karsianum.* On the other hand *A. armenum* is the most distant species systematically

TABLE 4
Correlation between the investigated Allium taxa (Regression Analysis)

Species	DF	SD	MS	F- Value	Probability	Significance
	1	746,5	746,5	5,81	0,030	*
A-B	14	1797,4	128,4			
	15	2543,9				
	1	1046,6	1046,6	9,79	0,007	**
A-C	14	1497,3	107,0			
	15	2543,9				
	1	108,4	108,4	8,54	0,061	NS
A-D	14	38,6	12,9			
	15	2543,9				
	1	1004,0	1004,0	9,13	0,009	**
A-E	14	1539,9	110,0			
	15	2543,9				
	1	1299,0	1299,0	19,94	0,001	**
B-C	14	912,0	65,1			
	15	2211,0				
	1	322,6	322,6	2,39	0,144	NS
B-D	14	1888,4	134,9			
	15	2211,0				
	1	328,52	328,52	9,78	0,007	**
B-E	14	470,42	33,60			
	15	798,94				
	1	62,0	62,0	0,40	0,535	NS
C-D	14	2149,0	153,5			
	15	2211,0				
	1	256,71	256,71	6,63	0,022	*
C-E	14	542,23	38,73			
	15	798,94				
	1	579,40	579,4	9,40	0,057	NS
D-E	14	1664,6	118,9			
	15	2543,9				

DF : Degree of freedom SD : Standart Deviation MS: Mean square. NS: Not significant. *p<.05. **p<.01.

TABLE 5
The correlation between the characters of the investigated species compared to two different methods

Pearson's correlation							Analysis of variance (Regression Analysis)						
1	2	3	4	6	13	14	1	2	3	4	6	13	14
*	*	**	*	*	**	*	**	**	**	*	*	**	*
*	*	*	*	*	*	*	*	*	*	*	*	*	*
*	*	*	*	*	*	*	*	*	*	*	*	*	*
*	*	*	*	*	*	*	*	*	*	*	*	*	*
*			*	*	*	*	*	*	*		*	*	
*				*	*	*							
					*	*							
					*	*							

* Significant at the level of 0.05. ** Significant at the level of 0.01. 1- 4,6,13,14: Characters coda

TABLE 6
Correlation (Regression Analysis) between numerical anatomical characters of the investigated taxa

character	MS	F-Value	Probability	Significance	character	MS	F-Value	Probability	Significance
1-2	36,8	12,1	0,04	**	5-11	0,32	0.08	0,80	NS
1-3	1,53	0,10	0,76	NS	5-12	6,04	2,69	0,20	NS
1-4	0,05	0,00	0,95	NS	5-13	1,40	0,37	0,58	NS
1-5	5,00	0,37	0,58	NS	5-14	0,87	0,22	0,67	NS
1-6	28,9	5,08	0,05	*	5-15	8,13	5,24	0,10	NS
1-7	17,9	1,91	0,26	NS	5-16	5,52	2,28	0,22	NS
1-8	32,9	7,54	0,05	*	6-7	0,09	0,10	0,77	NS
1-9	31,1	6,27	0,05	*	6-8	1,40	3,01	0,18	NS
1-10	7,78	0,61	0,49	NS	6-9	1,47	3,32	0,05	*
1-11	5,12	0,38	0,58	NS	6-10	0,31	0,39	0,57	NS
1-12	8,26	0,66	0,47	NS	6-11	0,02	0,02	0,89	NS
1-13	0,00	0,00	1,00	NS	6-12	1,47	3,33	0,05	*
1-14	8,70	0,70	0,04	*	6-13	0,23	0,27	0,03	*
1-15	6,86	0,53	0,52	NS	6-14	0,00	0,00	0,92	NS
1-16	10,6	0,91	0,41	NS	6-15	1,49	3,44	0,04	*
2-3	1,04	0,10	0,05	*	6-16	0,01	0,01	0,91	NS
2-4	0,01	0,00	0,96	NS	7-8	73,7	2,66	0,20	NS
2-5	0,45	0,04	0,85	NS	7-9	78,3	3,00	0,18	NS
2-6	7,55	0,88	0,04	*	7-10	8,24	0,17	0,71	NS
2-7	15,0	2,49	0,21	NS	7-11	1,28	0,02	0,88	NS
2-8	19,3	4,22	0,13	NS	7-12	0,00	0,00	0,99	NS
2-9	10,7	1,43	0,31	NS	7-13	0,08	0,00	0,97	NS
2-10	1,36	0,13	0,74	NS	7-14	28,0	0,65	0,47	NS
2-11	14,5	2,35	0,22	NS	7-15	34,9	0,86	0,42	NS
2-12	0,01	0,00	0,99	NS	7-16	130	14,7	0,03	*
2-13	4,76	0,50	0,05	*	8-9	14,1	2,81	0,19	NS
2-14	19,8	4,47	0,04	*	8-10	0,05	0,01	0,94	NS
2-15	0,97	0,09	0,78	NS	8-11	0,50	0,05	0,83	NS
2-16	12,6	1,85	0,26	NS	8-12	0,85	0,09	0,78	NS
3-4	35,4	0,95	0,40	NS	8-13	0,60	0,06	0,81	NS
3-5	42,0	1,20	0,35	NS	8-14	6,64	0,88	0,41	NS
3-6	21,7	0,52	0,52	NS	8-15	1,09	0,12	0,75	NS
3-7	0,61	0,01	0,91	NS	8-16	15,6	3,47	0,15	NS
3-8	1,49	0,03	0,87	NS	9-10	113	2,14	0,24	NS
3-9	54,7	1,78	0,27	NS	9-11	9,68	0,11	0,76	NS
3-10	108	8,54	0,05	*	9-12	132	2,84	0,19	NS
3-11	48,0	1,46	0,31	NS	9-13	72,4	1,09	0,37	NS
3-12	120	13,4	0,03	*	9-14	0,52	0,01	0,94	NS
3-13	134	31,9	0,01	**	9-15	4,15	0,05	0,84	NS
3-14	80,3	3,62	0,05	*	9-16	55,5	0,77	0,44	NS
3-15	3,25	0,07	0,81	NS	10-11	5,70	0,02	0,88	NS
3-16	13,4	0,30	0,62	NS	10-12	414	4,02	0,13	NS
4-5	3,00	0,57	0,50	NS	10-13	338	2,64	0,20	NS
4-6	1,72	0,30	0,03	*	10-14	87,1	0,41	0,56	NS
4-7	0,09	0,01	0,91	NS	10-15	16,1	0,07	0,81	NS
4-8	4,60	0,97	0,05	*	10-16	26,0	0,11	0,76	NS
4-9	0,23	0,04	0,85	NS	11-12	11,2	0,87	0,42	NS
4-10	11,0	4,24	0,05	*	11-13	30,8	4,82	0,11	NS
4-11	0,72	0,12	0,75	NS	11-14	37,0	8,55	0,06	NS
4-12	0,80	0,13	0,73	NS	11-15	1,35	0,08	0,79	NS
4-13	1,97	0,35	0,05	*	11-16	1,06	0,07	0,81	NS
4-14	0,42	0,07	0,80	NS	12-13	108	6,83	0,07	NS
4-15	0,92	0,15	0,72	NS	12-14	59,2	1,82	0,27	NS
4-16	1,31	0,23	0,66	NS	12-15	40,2	1,04	0,38	NS
5-6	3,65	1,20	0,35	NS	12-16	14,3	0,30	0,62	NS
5-7	0,02	0,56	0,50	NS	13-14	21,7	8,81	0,05	*
5-8	0,19	0,04	0,84	NS	13-15	0,01	0,00	0,97	NS
5-9	0,72	0,18	0,70	NS	13-16	2,22	0,25	0,65	NS
5-10	5,45	2,23	0,23	NS	14-15	8,81	0,01	0,91	NS
					14-16	48,9	1,05	0,04	*

DF : Degree of freedom SD : Standart Deviation MS: Mean square. NS: Not significant. *p<.05. **p<.01.

within such investigated species [16-17]. So the above data were confirmed by the statistically results of this study.

According to Table 3,5 based on the Pearson's correlation method (Correlation), there are important correlations among the anatomical characters which shown as coded with 1-16 (1-2,4,6,13,14; 2-3,4,6; 3-4,12,13; 4-6,13; 6-13,14; 7-13; 9-14; 11-10-4; 12-14; 13-14,15; 14-15) the anatomical characters of the investigated taxa at levels of 0.01 and 0.05 (Table 3,5). On the other hand, according to Table 5, based on Analysis of variance (Regression Analysis), there are important correlations among (1-2,6,8,9,14; 2-3,6,13,14; 3-10,12,13,14; 4-6,8,10,13; 6-9,12,13,15; 7-16; 13-14; 14-16) the investigated taxa at levels of 0.01 and 0.05 (Table 5, 6). Statistical analyses indicate that, in the case of the examined *Allium* species, the epidermis width (13) and epidermis length (14) of leaf have the highest significant at level of 0.01p and 0.05p according to both statistical methods. So the feature exhibiting the highest diagnostic values are the epidermis width (13) and epidermis length (14) of leaf (Table 1, 3, 6).

In this study, numeric anatomical features of all of investigated taxa have also the smallest and similar variability and there are positive statistically significant, correlations between them. These results are normal because they belong to the same section (section *Codonoprasum*).

In the present study, 5 *Alium* taxa were compared statistically regarding numeric anatomical characters. We aimed to find statistically and anatomical differences in addition to morphological characters to distinguish these taxa.

Since *Allium* is systematically a problematic genus, it is necessary to use alternative methods to distinguish its taxa. Numerical anatomical features and statistical evaluations of the taxa can be used to distinguish these taxa. It has been also found that the results from can provide additional evidences that correspond to the anatomy for the recognition of the taxa.

REFERENCES

[1] Wheeler, E.J., Mashayekhi, S., McNeal, D.W., Columbus, J.T. and Pires, J.C. (2013) Molecular systematics of *Allium* subgenus Amerallium (Amaryllidaceae) in North America. Am. J. Bot. 100, 701–711.

[2] Lin, C-Y. and Tan, D-Y. (2017) Seed testa micromorphology of thirty-eight species of *Allium* (Amaryllidaceae) from central Asia, and its taxonomic implications. Nordic Journal of Botany. 35, 189–200.

[3] Friesen, N., Reinhard, M.F., Frank, R. (2006) Phylogeny and new intrageneric classification of *Allium* (Alliaceae) based on nuclear ribosomal DNA its sequences. Aliso. 22, 372–395.

[4] Fritsch, R.M., Blattner, F.R., Gurushidze, M. (2010) New classification of *Allium* L. subg. Melanocrommyum (Webb & Berthel) Rouy (Alliaceae) based on molecular and morphological characters. Phyton. 49, 145–220.

[5] Stearn, W.T. (1980) *Allium* L. In: Tutin, T.G., Heywood, V.H., Burges, N.A., Moore, D.M., Valentine, D.H., Walters, S.M. and Webb, D.A. (eds.) Flora Europaea, Vol. 5. Cambridge University Press, Cambridge, 49–69.

[6] Matin, F. (1992) The genus *Allium* in Iran, diversity, distribution and endemism. In: Hanelt, P., Hammer, K., Knupffer, H. (eds.) The genus *Allium*-taxonomic problems and genetic resources. Gatersleben. 193–194.

[7] Fritsch, R.M., Friesen, N. (2002) Evolution, domestication, and taxonomy. In: Rabinowitch, H.D., Currah, L. (eds.), *Allium* Crop Science: Recent Advances. CABI Publishing, New York, pp. 5–30.

[8] Gurushidze, M., Mashayekhi, S., Blattner, F.R., Friesen, N., Fritsch, R.M. (2007) Phylogenetic Relationships of wild and cultivated species of *Allium* section Cepa inferred by nuclear rDNA ITS sequence analysis. Plant Syst. Evol. 269, 259–269.

[9] Kamenetsky, R., Rabinowitch, H.D. (2004) The genus *Allium*: A development and horticultural analysis. Hortic. Rev. 32, 329–390.

[10] El-Gadi, A., and Elkington, T.T. (1977) Numerical taxonomic studies on species in Allium subgenus Rhizirideum. New Phytol. 79, 183–201.

[11] Fritsch, R.M., Friesen, N. (1996) Evolution, domestication and taxonomy. In: Evolution und Taxonomie von Pflanzengenetischen Ressourcen. Allium crop science – recent advances. 2002. Rabinowitch, H.D., Currah, L. (eds.) CABI Publishing, Oxon, 5–30.

[12] Baytop, T. (1984) Türkiye'de Bitkiler ile Tedavi. I.Ü. Yay. No: 3255, Ecz. Fak., Y.N: 40, Istanbul

[13] Bozdağ, B., Kocabaş, O., Akyol, Y., Özdemir, C. (2016) New Dyeing Method for Hand Sections in Plant Anatomy Studies. Marmara Pharmaceutical Journal. 20, 184-190.

[14] Ozdemir, A.Y. Özdemir. A, Özdemir, C. (2010) Statistical Comparative Leaf Anatomy of Some *Crocus* L. Taxa. Asian journal of Mathematics and Statistics. 3(1), 16-24.

[15] Ozdemir, A.Y. Özdemir A, Yetişen, K. (2016) Statistical Comparative Petiol Anatomy Of *Salvia* sp. Planta Daninha. Viçosa-MG. 34(3), 465-474.

[16] Cullen, J. (1984) *Ornithogalum* L. In: Davis, P.H. (ed.) Flora of Turkey and the East Aegean Islands. Edinburgh: Edinburgh University Press. v.8. 227-244.

[17] Davis, P.H., Mill, R.R., Tan K. (1988) *Ornithogalum* L. In: Davis, P.H. (ed.) Flora of Turkey and the East Aegean Islands. Edinburgh: University Edinburgh. v.10 (Supplement), 225-6.

Received: **09.10.2017**
Accepted: **07.12.2017**

CORRESPONDING AUTHOR

Canan Ozdemir
Manisa Celal Bayar University,
Department of Biology
Manisa – Turkey

e-mail: cozdemir13@gmail.com

© by PSP Volume 27 – No. 2/2018 pages 1191-1195 Fresenius Environmental Bulletin

THE USE OF ANALYTICAL HIERARCHY METHOD IN FACTORY ESTABLISHMENT PLACEMENT TO PREVENT ENVIRONMENTAL POLLUTION IN FURNITURE INDUSTRY

Yildiz Cabuk*

Bartin University, Faculty of Forestry, Department of Forest Industrial Engineering, 74100 Bartin, Turkey

ABSTRACT

The all variables should be taken into consideration when determining the location of factories which are the most important source of industrial wastes in the prevention of environmental pollution. Enterprises around the world have been subject to several problems in today's conditions of competition. Effective supplier selection is among these problems for enterprises to achieve their market goals, a vast number of qualitative and quantitative methods and conservation of natural environmental conditions from furniture industrial pollutant have been developed in this context. One of these methods is the Analytical Hierarchy Process (AHP) as a multi-criteria decision making method.

With its numerous inputs used in the manufacturing process, furniture industry has a vast supplier network. Accordingly, while selecting their suppliers, it is essential for furniture enterprises to evaluate their strengths and weaknesses and to take optimal decisions in line with their goals, as during the supplier selection process enterprises seek to choose among the suppliers that are capable of constantly supplying their demands with desired price, in desired quality and quantity, and in a timely fashion.

In this research, an AHP application was implemented for addressing the supplier selection problem in a furniture enterprise operating in Marmara Region of Turkey. In this context, a number of criteria, selected on the basis of their significance levels, were organized in a hierarchical form, and comparisons were made to scientifically determine the optimal supplier alternative upon a reliable evaluation process.

KEYWORDS:
Environmental pollution**,** AHP, Supplier Selection, Furniture Industry, Decision Making.

INTRODUCTION

The level of pollution caused by industrial wastes arising from industrial installations and which is quite dangerous is increasing rapidly all over the world. The level of pollution caused by industrial wastes arising from industrial installations and which is quite dangerous is increasing rapidly all over the world. This is the case in Turkey. Today, many natural agriculture and pasture lands and drinking water resources in Turkey are contaminated as a result of the erroneous establishment of industrial sites that have been selected for the site and become useless. In this context, the majority of the factory establishments which cause widespread industrial pollution in Turkey are caused by furniture and paper factories in the country.

Enterprises seek to profit from properly and effectively planned activities. One of the main constituents of planning activities is the supplier selection process. Enterprises encounter and interact with several suppliers throughout their lifetime. Upon a proper evaluation, enterprises may not be obliged to work with a multiple number of suppliers, which in turn paves the way for long term partnerships. Long term partnerships bring along provision of low cost and high quality raw materials. This also results in reduced lead times, thus providing the customers with their orders in shorter terms [1].

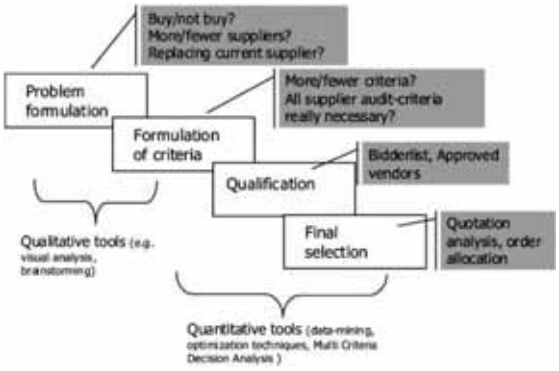

FIGURE 1
Illustration of the use of decision making methods in supplier selection [2]

In the simplest term, supplier selection can be defined as the process of determination of the supplier from which the raw materials, semi-products and other goods will be purchased for manufacturing [3]. Basically, supplier selection is implemented in

two ways. In the first alternative, all suppliers are capable of fulfilling the requirements of delivery, quality, etc. demands and here the purchaser is only required to make a decision. The other way of supplier selection is implemented when a number of limitations in terms of capacity, quality, etc. come into question. This type of selection differs from the other with the requirement to choose more than one supplier [4]. The stages of supplier selection, widely adopted in the literature, are given in Figure 1.

As a multi-criteria decision making problem, supplier selection is among the most important problems in the fields of decision analysis and operational research. Making precise and timely decisions brings along several advantages for professionals working in related fields. Several numerical methods have been developed for solution of multi-criteria decision making problems. One of the most commonly used methods for solution of these problems is Analytical Hierarchy Process (AHP) [5]. AHP is a systematical method used for determination of multi-criteria factors of a problem in a hierarchical structure and on the basis of their priority. AHP separates a problem into smaller sub-divisions, subjects them to paired comparisons, sets the priorities for each hierarchical step, thus organizing a specific logical process [6]. In decision making, AHP is a mathematical method that takes into account the individual's or group's priorities with the capability to make a collective evaluation of qualitative and quantitative variables [7]. As a system based on the principle of dividing and synthesizing the elements of a problem, AHP aims to logically determine and classify the superiority and significance levels of the compared alternatives or elements [8]. In the last two decades, AHP method has been widely implemented in almost all applications related to multi-criteria decision making problems [9]. AHP is applicable for the multi-purpose structure of supplier selection problem. This method also allows a trade-off among the significance levels of criteria used by decision maker in supplier selection. As a result of these mentioned advantages, AHP has been applied by a vast number of researchers in supplier selection problems [10].

MATERIALS AND METHODS

The furniture enterprise, subject of the present research, aimed to choose among the 4 suppliers which would provide them with the operational inputs they need. For this purpose, the prominent criteria for supplier selection and alternative suppliers were determined by the enterprise's own experts. Criteria evaluation form was prepared for the experts to determine the significance level of criteria and alternatives.

The problem was considered as a multi-criteria decision making problem for selection of the most suitable supplier. In this context, a six-phase approach was implemented to build an AHP supplier selection model for use by the enterprise and to gather the qualitative and quantitative data required to successfully accomplish the research. These phases are also the general phases of AHP as stated by Saaty [11]:

- Definition of the problem
- Organizing the decision criteria and building the hierarchical structure
- Building the paired comparison matrices on the basis of the criteria
- Calculation of the priority vectors of the matrices
- Verification of consistency
- Synthesizing the weights to achieve the results.

Expert Choice 11.5 software package was used for implementation of the AHP method. This software is an effective tool that significantly facilitates multi-criteria decision making processes as a means to achieve the results in a quick and simple way. Expert Choice is also used for investment portfolio analysis and making joint decisions.

The expert group was asked questions by survey method for application of AHP method and the obtained survey data were then transferred to the software. The opinions of the expert staff were taken separately to enable unbiased evaluations. The questions were prepared in accordance with 1-9 evaluation scale to determine the relative significance of the criteria and alternatives.

The existing criteria used in the literature for supplier selection process were implemented to determine the research criteria. As the first step of the hierarchy, alternative suppliers were determined by the expert staff of the enterprise. After determination of the alternatives and criteria, hierarchy building phase started.

The main criteria affecting the supplier selection process were determined by the expert staff as quality, price, reliability, size, delivery, distance and novelty. Four alternatives were present in the hierarchy for supplier selections defined by the same group.

TABLE 1
Basic Scale [12]

Significance Values	Value Definitions
1	Equal importance
3	Moderate importance (slight precedence)
5	Strong importance (strong precedence)
7	Very strong importance (very strong precedence)
9	Extreme importance (absolute precedence)
2, 4, 6 and 8	Intermediate values (mediating values)

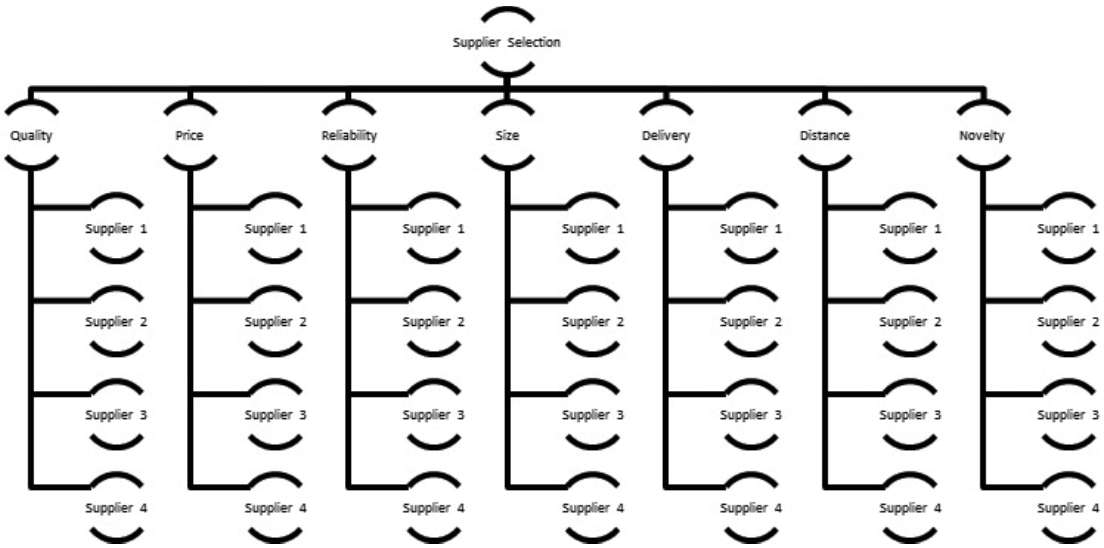

FIGURE 2
Hierarchy interface of EC software for supplier selection

TABLE 2
Column totals of the criteria

Criteria	Quality	Price	Reliability	Size	Delivery	Distance	Novelty
Quality	**1**÷117/20= 0.17094	**1/3**÷37/15= 0.135	**1**÷117/20= 0.17094	**4**÷77/4= 0.207792	**5**÷17= 0.294117	**5**÷119/6= 0.2521	**5**÷26= 0.1923
Price	**3**÷117/20= 0.51282	**1**÷37/15= 0.405	**3**÷117/20= 0.51282	**5**÷77/4= 0.25974	**5**÷17= 0.294117	**5**÷119/6= 0.2521	**5**÷26= 0.1923
Reliability	**1**÷117/20= 0.17094	**1/3**÷37/15= 0.135	**1**÷117/20= 0.17094	**4**÷77/4= 0.207792	**5**÷17= 0.294117	**5**÷119/6= 0.2521	**5**÷26= 0.1923
Size	**1/4**÷117/20= 0.042735	**1/5**÷37/15= 0.081	**1/4**÷117/20= 0.042735	**1**÷77/4= 0.051948	**1/3**÷17= 0.047619	**1/2**÷119/6= 0.02521	**4**÷26= 0.153846
Delivery	**1/5**÷117/20= 0.034188	**1/5**÷37/15= 0.081	**1/5**÷117/20= 0.034188	**3**÷77/4= 0.155844	**1**÷17= 0.05882	**3**÷119/6= 0.15126	**3**÷26= 0.11538
Distance	**1/5**÷117/20= 0.034188	**1/5**÷37/15= 0.081	**1/5**÷117/20= 0.034188	**2**÷77/4= 0.103896	**1/3**÷17= 0.047619	**1**÷119/6= 0.05042	**3**÷26= 0.11538
Novelty	**1/5**÷117/20= 0.034188	**1/5**÷37/15= 0.081	**1/5**÷117/20= 0.034188	**1/4**÷77/4= 0.012987	**1/3**÷1= 0.0476197	**1/3**÷119/6= 0.0168	**1**÷26= 0.03846
TOTAL	**1**	**1**	**1**	**1**	**1**	**1**	**1**

The expert personnel were asked questions with the evaluation for to specify the significance levels of these criteria. Afterwards, the definitions and significance values corresponding to these values were organized. The basic 1-9 scale applied by Saaty [11] and adopted by the AHP experts were used during the implementation of AHP.

Expert Choice (EC) software was effectively used for implementation of AHP method and related calculations. The data entered in the forms were transferred to the software environment upon one-by-one verification of the consistency ratios. The basic purpose was to determine the best alternative for the enterprise using these criteria and related suppliers. The criteria and alternatives were entered in EC software environment and the hierarchy model, given in Figure 2, was built accordingly.

FINDINGS

The values of paired comparison matrix, built in accordance with expert opinions, were determined as a means for comparing each criterion or alternative. Column totals were obtained by adding the table values in each column of the matrix. These total values were divided by their respective values and the obtained results were converted to decimal fractions. The sum of each column was divided by 7 to find the mean value.

TABLE 3
Weight Values of Criteria

Criteria	Weights (W)
Quality	0.209
Price	0.354
Reliability	0.209
Size	0.053
Delivery	0.086
Distance	0.057
Novelty	0.032
Inconsistency (T.O.) = 0.09	**Total = 1**

As seen in Table 3, weight values of the criteria add up to "1". The comparison is consistent as the T.O. value, given in the last row of the table, is equal to 0.09 < 0.1. In the following stages, each criterion

TABLE 4
Decision Matrix

Criteria / Alternatives	Quality	Price	Reliability	Size	Delivery	Distance	Novelty	W	**Inconsistency (T.O.)**
Supplier 1	0.525	0.197	0.430	0.212	0.210	0.124	0.542	0.328	0.08
Supplier 2	0.273	0.084	0.215	0.603	0.437	0.571	0.269	0.241	
Supplier 3	0.153	0.186	0.304	0.145	0.297	0.241	0.137	0.219	
Supplier 4	0.048	0.534	0.051	0.040	0.056	0.065	0.052	0.212	
W	0.209	0.354	0.209	0.053	0.086	0.057	0.032		
Inconsistency (T.O.)	0.05	0.05	0.05	0.07	0.04	0.05	0.06		

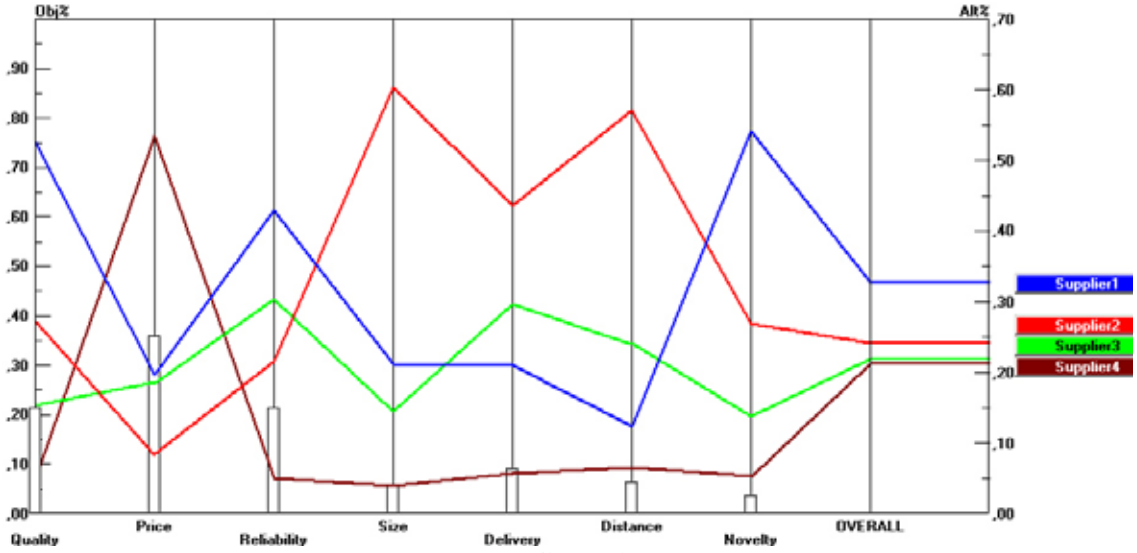

FIGURE 3
Performance sensitivity graph

was evaluated along with the alternatives by use of paired comparison matrices and the same operations were applied. In the last calculations, criterion based value of each alternative in the supplier alternatives matrix was multiplied with the weighted scores of those alternatives to calculate the sum of their respective rows. Following the calculations, existing supplier alternatives were found to gain different weights, and the most suitable supplier for the enterprise was determined accordingly.

As indicated by the values of relative significance vectors, the values of price, quality, and reliability factors hold particular importance for supplier selection. As seen in Table 4, quality, reliability and novelty criteria are gathered in supplier 1, whereas supplier 2 becomes prominent in terms of size, delivery and distance criteria. As for the price criterion, supplier 4 is distinguished from the others. In terms of price, quality and reliability criteria, supplier 1 can be regarded as the most suitable supplier.

The performance sensitivity graph given in Figure 3 shows how all other criteria and alternatives, thus the overall result is affected when the priority of a given criteria changes. In other words, the extent of the change likely to occur in other criteria and alternatives as a result of the changes in each criteria, in addition the information as to which alternative under which main criterion takes higher precedence, are indicated.

CONCLUSION

The problem of determination of the most suitable supplier among a series of suppliers has been an important issue for enterprises. Consideration of multiple criteria during supplier selection renders the decision making process even more difficult. However, as a multi-criteria decision making method, Analytical Hierarchy Method significantly facilitates addressing this problem, thus enabling decision makers to make correct decisions. By means of AHP method, it becomes possible to choose the most suitable alternative among a group of alternatives with the help of paired comparisons, and consequently favorable results can be achieved.

In this study, a sample model for supplier selection in an enterprise was established by application of AHP method which is one of the multi-criteria decision making techniques. While making paired comparisons during the application, the following considerations were taken in account and afterwards the obtained results were compared with the expectations. Inconsistency ratios were found to be lower than 0.1 for all criteria and alternatives. Consequently, the results were found to be in agreement with the estimations of the decision makers. Estimations were found to be consistent and the results were accepted.

During the evaluation of the criteria, price criterion was found to hold the highest weight. Price

and quality criteria hold particular importance in terms of economy. High price and low quality are likely to have adverse effects on the enterprise. In this context, supplier 1 became prominent on the basis of economy criterion. On the basis of delivery, distance and size criteria, supplier 2 became the most suitable alternative. According to the price criterion, however, supplier 2 ranked last.

According to the general results; the paired comparison matrix, built for comparison of all criteria, was found to be sufficiently consistent within the frame of AHP method. As indicated by overall results, supplier 1 has the highest significance weight with 0.328, which is followed by supplier 2 (0.241), supplier 3 (0.219) and supplier 4 (0.212). The most important criterion, among all criteria, is the price criteria with the significance weight of 0.354. According to the sensitivity graph, the ranking changed with the increase in the weight of the price criterion, and supplier 4 ranked first in the general ranking. Economy criterion's high priority in supplier selection decisions is also indicated in other literature studies.

The model built in the present research constitutes a sample application for use of AHP method, a multi-criteria decision making technique, in the furniture industry. By use of the model built for the mentioned problem, decision makers will be allowed to make modifications in their hierarchy by adding or eliminating alternatives or criteria, and in turn they will be able to establish suitable models for their own decision problems. On the other hand, the choice of location in factories by the AHP method is very important to prevent environmental problems caused by the pollution caused by furniture factories and other forest industry facilities. This is because the sources of agriculture, drinking and potable water that are of common interest to the community in the AHP method and that are concerned with the health of the community are assessed as variables in independent data inputs and analyzes. As a matter of fact, within the scope of the findings obtained from this survey, Turkish furniture and other forest products factories should never be established in the pit locations where the base land is located, near the agricultural areas and especially in the natural spring water resources.

REFERENCES

[1] Soner, S., Önüt, S. (2006) Çok Kriterli Tedarikçi Seçimi: Bir Electre-AHP Uygulaması. Mühendislik ve Fen Bilimleri Dergisi Sigma. 4, 110-120.

[2] De Boer, L., Labro, E. and Morlacchi, P. (2001) A Review of Methods Supporting Supplier Selection. European Journal of Purchasing & Supply Management. 7, 75-89.

[3] Güner, H., Mutlu, Ö. (2005) Bulanık AHP İle Tedarikçi Seçim Problemi ve Bir Uygulama. V. Ulusal Üretim Araştırmaları Sempozyumu. İstanbul Ticaret Üniversitesi, 25-27 November.

[4] Cedimoğlu, İ.H., Tunacan, T. (2004) Örüntü Tanıma Sistemiyle Tedarikçi Seçimi, Yöneylem Araştırması/ Endüstri Mühendisliği. - XXIV Ulusal Kongresi, 15-18 Haziran, Gaziantep–Adana.

[5] İmren, E., Can A., Kurt, R., Kurban, H. (2016) The Selection of Samples with AHP Method in the Experimental Study: Bending Strength Test Sample. International Forestry Symposium IFS 2016, Kastamonu University, 7-10 December.

[6] Saat, M. (2000) Çok Amaçlı Karar Vermede Bir Yaklaşım: Analitik Hiyerarşi Yöntemi. Gazi Üniversitesi İ.İ.B.F Dergisi. 2, 149-162.

[7] Dağdeviren, M., Eraslan, E., Kurt, M. (2004) Çalışanların Toplam İş Yükü Seviyelerinin Belirlenmesine Yönelik Bir Model ve Uygulaması. Gazi Üniversitesi Müh. Mim. Fak. Dergisi. 20(4), 518-519.

[8] Yılmaz, H., Surat, H. (2015) Determination of the Most Convenient Ecotourism Activity by Using Analytic Hiyerarchy Process. Turkish Journal of Forestry. 164-175.

[9] Ho, W. (2008) Integrated Analytic Hierarchy Process and Its Applications-A Literatüre Review. European Journal of Operational Research. 211-228.

[10] Barbarosoğlu, G., Yazgaç, T. (1997) An Application of the Analytic Hierarchy Process to the Supplier Selection Problem. Production and Inventory Management Journal. 38(1), 14-17.

[11] Saaty, T.L. (1994) How to Make a Decision: The Analytic Hierarchy Process. Interfaces. 24(6), 19-43.

[12] Saaty, T.L. (1990) Physics As a Decision Theory. European Journal of Operational Research. 48(1), 98-104.

Received: **13.10.2017**
Accepted: **02.12.2017**

CORRESPONDING AUTHOR

Yildiz Cabuk
Bartin University, Faculty of Forestry,
Department of Forest Industrial Engineering,
Bartin – Turkey

e-mail: yildizcabuk74@gmail.com

© by PSP Volume 27 – No. 2/2018 pages 1196-1201 Fresenius Environmental Bulletin

STUDY ON BIODEGRADATION OF CHLORPYRIFOS AND UTILIZATION OF A CHLORPYRIFOS DEGRADING BACTERIUM, *BACILLUS AMYLOLIQUEFACIENS* CZ-5

Jiangwei Zhu[1], Yan Zhao[2], Kun Xie[3,*], Xiaolou Li[4], Yi Chen[5]

[1]Collaborative Innovation Center of Sustainable Forestry in Southern China of Jiangsu Province, Nanjing Forestry University, Nanjing 210037, China
[2]Shanghai Institute of Quality Inspection and Technical Research, Shanghai 200233, China
[3]Key Laboratory of Crops with High Quality and Efficient Cultivation and Security Control, Yunnan Higher Education Institutions, College of Life Science and Technology, Honghe University, Mengzi 661100, China
[4]Architecture and Environmental Engineering Department, Sichuan Vocational and Technological College, Suining 629000, China
[5]Pudong Agrotechnology Extension Center, Shanghai 201201, China

ABSTRACT

A strain CZ-5 capable of highly degrading chlorpyrifos was isolated from soil. The strain CZ-5 was identified as *Bacillus amyloliquefaciens* based on 16S rRNA and analysis of morphology, physiological and biochemical characters. The optimal pH value and temperature were 7.0-7.5 and 30-35℃. The 7d degradation rate of 100 mg/L chlorpyrifos by strain CZ-5 was at about 99.5% in inorganic salt medium. The strain CZ-5 could hydrolyze chlorpyrifos to 3,5,6-trichloro-2-pyridinol(TCP), but could not degrade TCP as the sole carbon source for its growth. The combined applications of the strain CZ-5 and the strain TR-16 was considered an effective means for degrading chlorpyrifos, because the strain TR-16 could degrade TCP. The degradation rate of chlorpyrifos (100mg/L) by the strain CZ-5 and the strain TR-16 could reach about 99.2% in 6d. This study may provide theoretic basis and reference for prevention and control of pesticides pollution.

KEYWORDS:
Chlorpyrifos, 3,5,6-trichloro-2-pyridinol, biodegradation, *Bacillus amyloliquefaciens*

INTRODUCTION

Chlorpyrifos(O,O-diethyl O-(3,5,6-trichloro-2-pyridyl)-phosphorothioate) was a broad-spectrum moderately toxic organophosphate insecticide and acaricide, and was widely used in the prevention of agriculture pests [1]. The chlorpyrifos residue in soil or water might bring some trouble to environmental health and public health [2-4]. The major metabolite of chlorpyrifos was reported to be 3,5,6-trichloro-2-pyridinol(TCP), which was more hazardous pollutants than the parent. TCP was more mobile in soil and more leachable into groundwater and surface water [5, 6], and it causes the widespread contamination in soils and in the aquatic environment [7]. Half-life of TCP ranges from 65 to 360 days in soil and was considered as persistent pollutant by US EPA [8]. Both chlorpyrifos and TCP have been reported to be responsible for contamination of varied ecosystems; decline in diversity of essential microflora (that decreases soil productivity); disruption of biogeochemical cycles; and death of non-target macroscopic life forms [9, 10]. Therefore, the biodegradation of chlorpyrifos and TCP were paid close attention. The microbial degradation was considered the most important degradation method because it was the main factor impacting degradation of chlorpyrifos and TCP [11, 12]. Isolation and application of chlorpyrifos degrading bacteria was considered to be an effective way to treat chlorpyrifos contamination.

In this study, *Bacillus amyloliquefaciens* CZ-5, a strain that could degrade chlorpyrifos was isolated, its degradation potential and the application for environment protection were studied. The strain CZ-5 could degrade chlorpyrifos to TCP, but could not degrade TCP as the sole carbon source for its growth. Some TCP degrading bacteria had been isolated previously. Li et al. isolated a highly efficient TCP degrading bacterium *Ralstonia* sp. T6 [6]. Abraham et al. isolated *Sphingobacterium sp.* JAS3, which could hydrolyze TCP utterly [13]. Therefore, although the strain CZ-5 could not degrade TCP, it might still be used for the treatment of chlorpyrifos pollution. The combined applications of the strain CZ-5 and TCP degrading bacteria was considered an effective means for degrading chlorpyrifos.

MATERIALS AND METHODS

Chemicals and Media. Chemicals: chlorpyrifos (99.8%) was purchased from Dow Chemical Company. All other chemicals used were of analytical grade and commercially available.

Culture media: (1). Inorganic salt medium: $(NH_4)_2SO_4$ 0.1 g, $MgSO_4 \cdot 7H_2O$ 0.2 g, K_2HPO_4 0.1g, $CaSO_4$ 0.05 g, $FeSO_4 \cdot 7H_2O$ 0.01 g, water 1 L, pH 7.0. (2). Isolation medium: inorganic salt medium containing 100 mg/L chlorpyrifos was used to isolate chlorpyrifos degrading bacteria. (3). Enrichment medium: peptone10 g, yeast extract powder 5 g, beef extract powder 3 g, sodium chloride 5 g, water 1 L, pH7.0.

Isolation and identification of chlorpyrifos degrading bacteria. The soil sample was collected from farmland in Zhenjiang City, China, in which chlorpyrifos has been used for more than 6 years. 5.0 g soil sample was placed in 100ml isolation medium for shaking culture at 30℃ (120 rpm). The concentration of the residual chlorpyrifos was determined every 24h [14]. 5ml culture solution with 3d degradation rate >70% was transferred to enrichment medium containing same concentration of chlorpyrifos, and continuously transferred for more than 5 times. After the degradation effect was verified again, the above enrichment medium was coated on inorganic salt culture plate containing chlorpyrifos for inverted culture at 30℃. The eugonic bacterial colonies were selected and repeatedly streaked on the culture plate to obtain the pure culture. The new isolates were identified by using 16SrRNA sequence analysis. At the same time, the optimum pH and temperature of the strain CZ-5 were tested.

Degradation of chlorpyrifos by strain CZ-5. Inoculums of chlorpyrifos degrading bacteria were prepared in advance [15]. 6% strain CZ-5 inoculum was inoculated in inorganic salt culture medium containing 100mg/L chlorpyrifos, and then place it in the shaker (120rpm, 30℃). The concentration of chlorpyrifos and TCP were determined every 24h [14, 16].

Degradation of TCP by strain CZ-5. The inorganic salt culture medium containing 15 mg/L TCP was inoculated with 6% strain CZ-5 inoculum, and then place it in the shaker (120rpm, 30℃). The concentration of TCP was determined regularly.

Degradation of chlorpyrifos by combining strain CZ-5 and strain TR-16. The strain TR-16 was a triclopyr degrading bacterium deposited in our laboratory. It was identified as *Lactobacillus brevis* according to 16S analytical method (GenBank accession number KY682075). The strain TR-16 could effectively degrade TCP, and could degrade triclopyr into carbon dioxide and water completely. Because the strain CZ-5 could not degrade TCP, the combined applications of the strain CZ-5 and the strain TR-16 was considered an effective means for degrading chlorpyrifos.

3% strain CZ-5 inoculum and 3% strain TR-16 inoculum were inoculated simultaneously in inorganic salt culture medium containing 100mg/L chlorpyrifos, and then place it in the shaker (120rpm, 30℃). The concentration of chlorpyrifos and TCP were determined every 24h

Degradation of chlorpyrifos by strain TR-16. In order to find out whether both strains have played a role in the combined degradation process, the ability of the strain TR-16 to degrade chlorpyrifos was tested. 6% strain TR-16 inoculum was inoculated in inorganic salt culture medium containing 100mg/L chlorpyrifos, and then place it in the shaker (120rpm, 30℃). The concentration of chlorpyrifos was determined regularly.

Phosphoesterase activity of the strain CZ-5 and the strain TR-16. Take 100ml of CZ-5 (or TR-16) culture medium, then add protease inhibitor mixture, centrifuge at 10000r / min for 5min, the precipitate(α) and supernatant(I) were collected separately. The precipitate(α) was washed twice with 50 mmol/L Tris-HCl buffer, the wash solution was added to the supernatant (I), freeze-dried to near dry, and constant volume to 20ml for testing the extracellular enzyme. The precipitate(α) was set to 20 ml with Tris-HCl buffer, the appropriate amount of protease inhibitor was added, and sonicated in an ice bath (200W, broken for 5s, interval 4s, total 4min), then centrifuged at 10,000 r/min for 10min, supernatant (Ⅱ) was the crude enzyme solution (set to 20ml for determinating enzyme activity). The crude enzyme solution was centrifuged at 18,000 r/min for 30 min and the supernatant(β) was resuspended in 20 ml Tris-HCl buffer for the determination of membrane-bound enzyme. Supernatant (III) was re-set to 20 ml with Tris-HCl buffer for intracellular enzyme [17, 18].

Phosphoesterase enzymatic reaction system (3 ml): 2.8 ml glycine-sodium hydroxide buffer (0.05 mol / L, pH 9.0), 0.19 ml of enzyme solution, 10μl of p-nitrophenyl phosphate disodium salt (40 mmol/L), 37 ℃ water bath for 1h, take 0.5ml of reaction solution into the test tube, add 3.5ml glycine-sodium hydroxide buffer (pH10.0), OD_{405} and the amount of p-nitrophenol in solution were determined (colorimetric determination). The unit of enzyme activity (U) was defined as the amount of enzyme required to convert p-nitrophenyl phosphate disodium salt to 1 μmol of p-nitrophenol in 1 min.

RESULTS AND DISCUSSION

Identification and characterization of chlorpyrifos degrading bacteria. A bacterium capable of degrading chlorpyrifos was isolated from soil, named CZ-5. The strain CZ-5 was gram-positive, aerobiotic, mobile, spore-forming, rod-shaped,

0.5-1.0×2.0-3.0 um in size. It formed white, smooth, non-pigmented colonies on the nutrient agar plate. The optimum growth was at 30-35℃ and pH 7.0-7.5. It was positive for catalase, starch hydrolysis and VP test, but negative for oxidase test, gelatin liquefaction and indole test [19, 20].

A 1507 base pairs long sequence of 16S rRNA was amplified and submitted to NCBI GenBank (Accession no. KY682074). Blastn of 16S rRNA sequence indicated that strain CZ-5 showed nearly 99% similarity with 16S rRNA sequence *Bacillus amyloliquefaciens*. The identification result was consistent with that of Biolog^{TM} microorganisms identification system.

Degradation of chlorpyrifos and TCP by the strain CZ-5. The results in Fig. 1 showed that the chlorpyrifos could be rapidly degraded by the strain CZ-5. The degradation rate of chlorpyrifos (100mg/L) by the strain CZ-5 could reach about 99.5% in 7d. The degradation law of chlorpyrifos under the experimental conditions accorded with the first order kinetic model ($C=C_0 \cdot e^{-kt}$), ("C_0" was initial concentration, "k" was the degradation rate constant, "t" was the degradation time.) $C=100e^{-0.4272t}$, $R^2=0.9897$, half life=1.69d. At the same time, it was found that TCP concentration continued to increase in the degradation process of chlorpyrifos. In addition, TCP could not be degraded by the strain CZ-5 (Fig. 2). These results suggested that the strain CZ-5 could not completely degrade chlorpyrifos into CO_2 and H_2O. If the strain CZ-5 was used for the degradation of chlorpyrifos, it was necessary to consider degradation of TCP. It was believed that the combination of the strain CZ-5 and a TCP degrading bacterium may be an effective means.

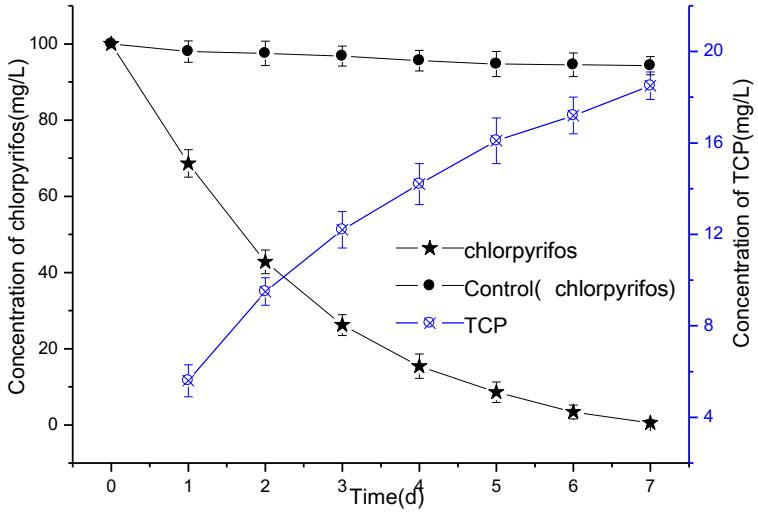

FIGURE 1
The curve on degradation of chlorpyrifos by the strain CZ-5 and the concentration of TCP

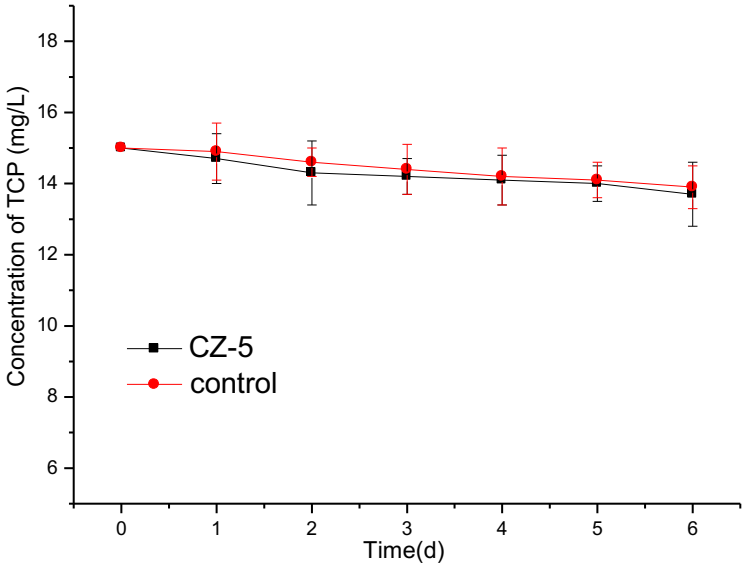

FIGURE 2
The curve on degradation of TCP by the strain CZ-5

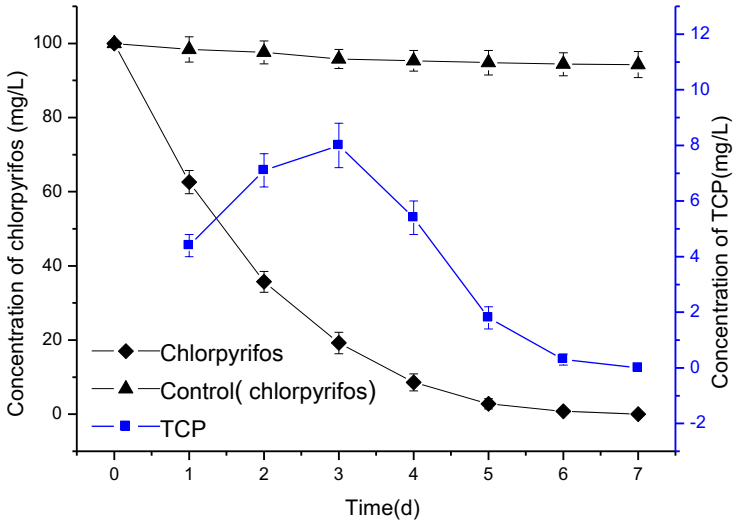

FIGURE 3
The curve on degradation of chlorpyrifos by combining strain CZ-5 and strain TR-16

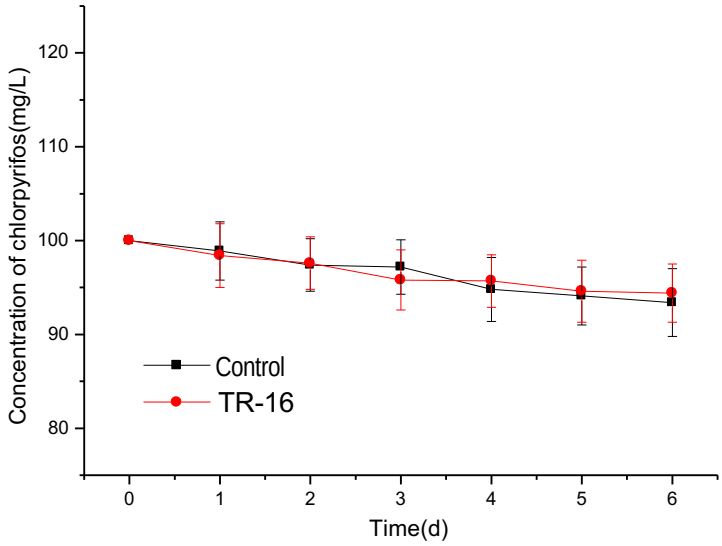

FIGURE 4
The curve on degradation of chlorpyrifos by the strain TR-16

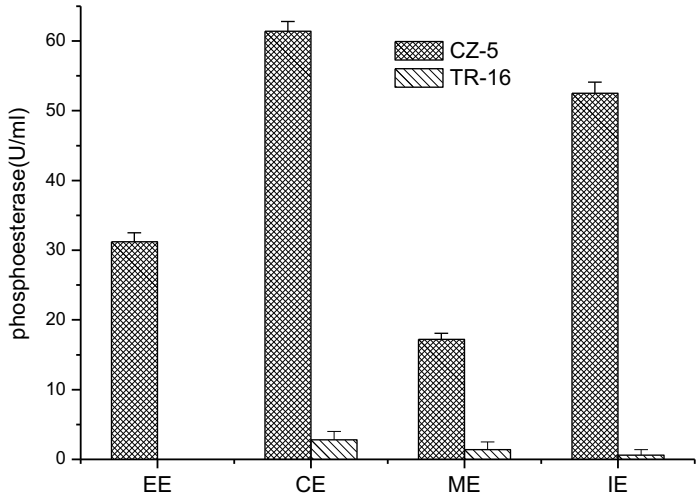

FIGURE 5
Activity of phosphoesterase enzyme
(EE-extracellular enzyme, CE-crude enzyme, ME-membrane-bound enzyme, IE- intracellular enzyme)

Degradation of chlorpyrifos by combining strain CZ-5 and strain TR-16. Because the strain CZ-5 could not degrade TCP, the combined applications of the strain CZ-5 and TCP degrading bacteria was considered an effective means for degrading chlorpyrifos. The results in Fig. 3 showed that the chlorpyrifos could be rapidly degraded by the strain CZ-5 and the strain TR-16 (the strain TR-16 could degrade TCP). The degradation rate of chlorpyrifos (100mg/L) by the strain CZ-5 and the strain TR-16 could reach about 99.2% in 6d. The fitted equation was $C=100e^{-0.5118t}$, $R^2=0.9886$, half life=1.35d. These data indicated that the degradation rate was faster when combined with the strain CZ-5 and the strain TR-16. Because the results in Fig. 4 showed that the strain TR-16 could not degrade chlorpyrifos alone, the increase in degradation rate was considered to be the result of the combined action of the two strains. So it was speculated that the strain CZ-5 first degrades chlorpyrifos into TCP, then TCP was degraded by strain TR-16. Degradation of TCP could help to reduce feedback suppression, and promote degradation of chlorpyrifos [21-23].

Phosphoesterase activity of the strain CZ-5 and the strain TR-16. The phosphoesterase activity of the two strains were shown in Fig. 5. It could be seen from the data that the phosphoesterase activity of the two strains was very different. The strain CZ-5 has a high phosphoesterase (> 30U/ml) in its extracellular enzyme, but the strain TR-16 did not have phosphatase activity. In addition, the phosphoesterase activity of strain CZ-5 in the intracellular enzyme and membrane-binding enzyme were 52.5 U/ml and 17.2 U/ml respectively, but the strain TR-16 was only 0.6 U/ml and 1.4 U/ml. This might be the reason that the strain CZ-5 could rapidly degrade chlorpyrifos and the strain TR-16 could not degrade chlorpyrifos alone. In general, the phosphoesterase could hydrolyze the phosphate bond of most organophosphorus pesticides, which could break down chlorpyrifos into TCP [24-26].

CONCLUSION

In this study, *Bacillus amyloliquefaciens* CZ-5 was isolated from soil, which could degrade chlorpyrifos. The optimal pH value and temperature of strain CZ-5 were 7.0-7.5 and 30-35℃. The strain CZ-5 has a high phosphoesterase activity (> 30U/ml) in its extracellular enzyme, which was considered to be the reason that the strain CZ-5 could rapidly degrade chlorpyrifos into TCP. The degradation rate of chlorpyrifos (100mg/L) by the strain CZ-5 could reach about 99.5% in 7d, but TCP could not be degraded by the strain CZ-5. The strain CZ-5 could not completely degrade chlorpyrifos into CO_2 and H_2O. Because the strain TR-16 could degrade TCP, the combined applications of the strain CZ-5 and the strain TR-16 was considered an effective means for degrading chlorpyrifos. The degradation rate of chlorpyrifos (100mg/L) by the strain CZ-5 and the strain TR-16 could reach about 99.2% in 6d. So it was speculated that the strain CZ-5 first degrades chlorpyrifos into TCP, then TCP was degraded by strain TR-16. Degradation of TCP could promote degradation of chlorpyrifos.

ACKNOWLEDGEMENTS

This study was funded by the China Postdoctoral Science Foundation (No.2017M611827) and Applied Science Research Project of Honghe University (No.XJY15Z07 to K.X.), and partially by the Priority Academic Program Development of Jiangsu Higher Education Institutions and Ph.D Specific Research Project of Honghe University (No.XJ15B13 to K.X.).

REFERENCES

[1] Dubey, K.K., Fulekar, M.H. (2012) Chlorpyrifos bioremediation in pennisetum rhizosphere by a novel potential degrader *stenotrophomonas maltophilia mhf* env20. World Journal of Microbiology and Biotechnology. 28, 1715-1725.

[2] Liu, R., Jiang, H., Xu, P., Qiao, C., Zhou, Q., Yang, C. (2014) Engineering chlorpyrifos-degrading *stenotrophomonas* sp. yc-1 for heavy metal accumulation and enhanced chlorpyrifos degradation. Biodegradation. 25, 903-910.

[3] Zhu, J., Zhao, Y., Qiu, J. (2011) Isolation and utilization of a chlorpyrifos degrading bacterium, *pseudomonas fluorescens* ZHU-6. Fresen. Environ. Bull. 20, 962-968.

[4] Yu, Y.L., Fang, H., Wang, X., Wu, X.M., Shan, M., Yu, J.Q. (2006) Characterization of a fungal strain capable of degrading chlorpyrifos and its use in detoxification of the insecticide on vegetables. Biodegradation. 17, 487-494.

[5] Abraham, J., Shanker, A., Silambarasan, S. (2013) Role of gordonia sp jaas1 in biodegradation of chlorpyrifos and its hydrolysing metabolite 3,5,6-trichloro-2-pyridinol. Letters in Applied Microbiology. 57, 510-516.

[6] Li, J., Liu, J., Shen, W., Zhao, X., Hou, Y., Cao, H. (2010) Isolation and characterization of 3,5,6-trichloro-2-pyridinol-degrading ralstonia sp. strain t6. Bioresource Technology. 101, 7479-7483.

[7] John, E.M., Shaike, J.M. (2015) Chlorpyrifos: pollution and remediation. Environmental Chemistry Letters. 13, 269-291.

[8] Armbrust, K.L. (2001) Chlorothalonil and chlorpyrifos degradation products in golf course leachate. Pest Management Science. 57, 797-802.

[9] Aktar, W., Sengupta, D., Chowdhury, A. (2009) Impact of pesticides use in agriculture: their benefits and hazards. Interdisciplinary Toxicology. 2, 1-12.
[10] Latifi, A.M., Khodi, S., Mirzaei, M., Miresmaeili, M., Babavalian, H. (2012) Isolation and characterization of five chlorpyrifos degrading bacteria. African Journal of Biotechnology. 11, 3140-3146.
[11] Sasikala, C., Jiwal, S., Rout, P., Ramya, M. (2012) Biodegradation of chlorpyrifos by bacterial consortium isolated from agriculture soil. World Journal of Microbiology and Biotechnology. 28, 1301-1308.
[12] Yang, L., Zhao, Y.H., Zhang, B.X., Yang, C.H., Zhang, X. (2005) Isolation and characterization of a chlorpyrifos and 3,5,6-trichloro-2-pyridinol degrading bacterium. Fems Microbiology Letters. 251, 67-73.
[13] Abraham, J., Silambarasan, S. (2013) Biodegradation of chlorpyrifos and its hydrolyzing metabolite 3,5,6-trichloro-2-pyridinol by sphingobacterium, sp. jas3. Process Biochemistry. 48, 1559-1564.
[14] Prodhan, M.D.H., Papadakis, E.N., Papadopoulou-Mourkidou, E. (2015) Determination of multiple pesticide residues in eggplant with liquid chromatography-mass spectrometry. Food Analytical Methods. 8, 229-235.
[15] Zhu J.W., Wu, L., Yang, N. (2016) Study on utilization of a nicosulfuron degrading bacterium, *Bacillus pumilus* ZHU-11. Fresen. Environ. Bull. 25, 3796-3801.
[16] Koch, H.M., Angerer, J. (2001) Analysis of 3,5,6-trichloro-2-pyridinol in urine samples from the general population using gas chromatography-mass spectrometry after steam distillation and solid-phase extraction. Journal of Chromatography B Biomedical Sciences & Applications. 759, 43-49.
[17] Das, S., Singh, D.K. (2006) Purification and characterization of phosphotriesterases from pseudomonas aeruginosa f10b and clavibacter michiganense subsp. insidiosum sbl11. Canadian Journal of Microbiology. 52, 157-168.
[18] Bhadbhade, B.J., Sarnaik, S.S., Kanekar, P.P. (2002) Biomineralization of an organophosphorus pesticide, monocrotophos, by soil bacteria. Journal of Applied Microbiology. 93, 224-234.
[19] Kaynar, P., Beyatli, Y. (2008) Protein profiles and biochemical characterizations of Bacillus spp. strains isolated from fishes. Fresen. Environ. Bull. 17, 1316-1321.
[20] Ersoy Omeroglu, E., Karaboz, I., Sukatar, A., Uzel, A., Sayan, M., Sanlidag T. (2008) Phenotypic and molecular characterization of luminous bacteria isolated from Izmir Gulf in Turkey: Vibrio harveyi TEM O5 and TEM S1 strains. Fresen. Environ. Bull. 17, 506-510.
[21] Li, C., Liu, H., Hao, Z., Ke, H., Tao, G., Ni, H. (2012) Characterization of a newly isolated highly effective 3,5,6-trichloro-2-pyridinol degrading strain cupriavidus pauculus, p2. Current Microbiology. 65, 231-236.
[22] Silambarasan, S., Abraham, J. (2014) Efficacy of ganoderma sp. jas4 in bioremediation of chlorpyrifos and its hydrolyzing metabolite tcp from agricultural soil. Journal of Basic Microbiology. 54, 44-55.
[23] Anwar, S., Liaquat F., Khan Q.M. (2009) Biodegradation of chlorpyrifos and its hydrolysis product 3,5,6-trichloro-2-pyridinol by bacillus pumilus strain C2A1. Journal of Hazardous Materials. 168, 400-405.
[24] Pailan, S., Sengupta, K., Ganguly, U., Saha, P. (2016) Evidence of biodegradation of chlorpyrifos by a newly isolated heavy metal-tolerant bacterium acinetobacter, sp. strain memcl4. Environmental Earth Sciences. 75, 1-10.
[25] Gilani, R.A., Rafique, M., Rehman, A., Munis, M.F., Rehman, S.U., Chaudhary, H.J. (2016) Biodegradation of chlorpyrifos by bacterial genus pseudomonas. Journal of Basic Microbiology. 56, 105-119.
[26] Thengodkar, R.R.M., Sivakami, S. (2010) Degradation of chlorpyrifos by an alkaline phosphatase from the cyanobacterium spirulina platensis. Biodegradation. 21, 637-644.

Received: **26.10.2017**
Accepted: **02.12.2017**

CORRESPONDING AUTHOR

Kun Xie
Key Laboratory of Crops with High Quality and Efficient Cultivation and Security Control,
Yunnan Higher Education Institutions
College of Life Science and Technology
HongHe University
Mengzi 661100 – China

e-mail: xk_017@hotmail.com

© by PSP Volume 27 – No. 2/2018 pages 1202-1209 Fresenius Environmental Bulletin

PRODUCTION OF GHK TRIPEPTIDE EMBEDDED POLY VINYL ALCOHOL-NANOFIBERS

Yasemin Budama-Kilinc[1,*], Rabia Cakir-Koc[1], Guncem Ozgun Eren[1], Perihan Kubra Akman[2], Mustafa Tahsin Yilmaz[2]

[1]Department of Bioengineering, Yildiz Technical University, Istanbul, Turkey
[2]Department of Food Engineering, Yildiz Technical University, Istanbul, Turkey

ABSTRACT

Nanofibers fabricated by the electrospinning process demonstrate excellent surface area, high porosity, phase purity, and good chemical composition. In this study, we fabricated pure poly vinyl alcohol (PVA) nanofiber and glycyl-L-histidyl-L-lysine (GHK) embedded PVA nanofibers by using the electrospinning technique and characterized the fibers using relevant methods. Scanning electron microscopic images demonstrated that the average dimensions of the fabricated PVA fibers at 20 and 25 wt% were 100 and 200 nm, respectively, and they possessed equivalent diameters. In contrast, GHK embedded PVA nanofiber dimensions varied between 50 and 250 nm. The Fourier transform-infrared spectrophotometry results revealed the bonds related to PVA and GHK-PVA conjugation. In addition cell culture studies showed that the nanofibers were non-toxic. Growth-modulating peptide (GHK) embedded poly vinyl alcohol was electrospun to yield nanofibers that can be used for wound dressing applications.

KEYWORDS:
tripeptide, GHK, nanofiber, electrospinning, cell culture.

INTRODUCTION

One-dimensional materials, such as nanowires, nanorods, nanotubes, and nanobelts, have received attention due to their high electrical, thermal conductivity, high optical density, and flexibility properties [1, 2]. In addition, these materials show good thermal stability, good chemical resistance, and are cost-effective [3]. They have been produced using different methods, such as the hydrothermal-solvothermal process [4] and electron beam [5] and electrospinning techniques etc [6]. The electrospinning process is more easily controlled compared to the others, due to the ability to adjust the process parameters, such as viscosity, concentration, voltage, current, flow rate, and the distance between the capillary and collector. Hence, they have a wide range of applications in medicine, such as wound-dressing, scaffold design, filtration, and drug delivery [7]. Tissue engineering applications represent a new era of medicine, and electrospun nanofibers have become important in this area.

Tissue engineering is a new medical therapy and it is an alternative to conventional transplantation methods. Scaffolds, cells, and biochemical stimuli are the three main elements of tissue engineering [8]. Polymeric nanofiber-based scaffolds serve as a support for tissue regeneration. A scaffold must possess high surface area, interconnected pores, and be suitable for cell growth [9, 10]. Hence, many biocompatible polymers are used in this field as mimics of the extracellular matrix [11-13].

GHK is a tripeptide consisting of glycyl-histidyl-lysine that naturally occurs in human plasma, saliva, and urine [14]. GHK-Cu was isolated from human plasma by Pickart and Thaler [15]. It is present in plasma at approximately 200 mg/mL (10^{-7} M) by age 20 years, but decreases with aging. GHK has a high affinity for copper, and the copper complex accelerates wound healing and skin repair[14]. In addition, GHK has been reported as a therapeutic agent [16].

In this study, we fabricated pure poly(vinyl alcohol) (PVA) nanofibers and biocompatible GHK embedded PVA nanofibers by using electrospinning, investigated their toxicity in cell culture, and characterized the material using morphological and analytical methods.

MATERIALS AND METHODS

Methods. All chemicals were used as received without further purification. PVA powder [Mw = 31,000–50,000 Da; degree of hydrolysis = 87–89 mol%] was purchased from Aldrich (Munich, Germany). GHK (Gly-His-Lys., purity > 98%) was purchased from Active Peptide (Cambridge, MA, USA). An electrospinning unit (model No: HONFES-043U/ Holmarc, Kochi, Kerala, India) was used in these experimental studies.

Production of 20 and 25 wt% PVA and GHK embedded PVA solution and the electrospinning process. In the experimental studies, 1 g and 1.25 g

PVA were dissolved in 5 ml pure water each. Solutions of 20 wt% PVA and 25 wt% PVA were prepared in pure water and mixed at 80°C. The process was repeated at the same concentrations to prepare the GHK-embedded PVA solutions. The GHK peptide was added to the solutions at a concentration of 0.02% (w/v) and electrospinning was performed. The polymer solutions were placed in a 5 ml syringe with a capillary tip whose inner diameter was 0.3 mm. Stainless steel wrapped with aluminum foil was used as the collector. A high voltage supply (HMPSKV30/0-30 kV) was used to generate an electric field with voltage of 15–18 kV. The distance from the tip to the collector was 14 cm, and flow rate was 0.3 mL/h, respectively.

Scanning electron microscopy (SEM) and energy dispersive X-ray spectroscopy (EDX) analysis. SEM (Supra 50 V; Zeiss, Jena, Germany) was used to observe the structure of the pure PVA nanofibers and GHK embedded PVA nanofibers. The morphologies and chemical composition of the samples was determined by EDX [17].

Fourier transform-infrared (FT-IR) spectroscopy. The IR Prestige21 FT-IR spectrophotometer (Shimadzu, Tokyo, Japan) was used for the chemical analysis of the functional groups which present in the samples. Measurements were carried out on PVA nanofibers and GHK embedded PVA nanofibers in universal attenuation total reflectance mode. The FT-IR spectra were obtained from four scans per sample ranging from 4000 to 750 cm^{-1} at a resolution of 4 cm^{-1}.

Determination of Cytotoxicity. The L929 cell line was used to determine if the GHK embedded PVA nanofibers were cytotoxic. L929 cells were cultured in DMEM-F12 medium (including 10% fetal bovine serum, penicillin-streptomycin, and L-glutamine) at 37°C (5% CO_2). The cultured cells were trypsinized and seeded (10^4 cells/well) in 96-well flat bottom microplates. Electrospun nanofibers (1.5 mg) were added to 10 ml of cell culture medium and vortexed until they dissolved. The 150 µg/ml dissolved nanofibers were added to cultured cells at different concentrations (1.5, 3, 7.5, 15, 30, 45, and 60 µg/ml) after a 24 hour incubation. Medium alone was used as the negative control.

After the 24 hour incubation, the medium was aspirated and 100 µL of 2,3-bis-(2-methoxy-4-nitro-5-sulfophenyl)-2H-tetrazolium-5-carboxanilide solution was added in fresh medium to the wells at a concentration of 0.5 mg/ml (with 7.5 µg/mL phenazine methosulfate). The plates were incubated for 3 h at 37°C and optical density was measured at 450 nm with a multiplate reader (Multiskan Ascent 354 Microplate Photometer; Thermo Labsystems, Mumbai, India).

RESULTS

Concentrations of 20% and 25% PVA with or without GHK were electrospun and characterized. The optimum amount of PVA was 20% or 25% to achieve electrospinning without any bead formation. The SEM images of the electrospun PVA (20 wt%) polymer are shown in Figure 1. PVA nanofibers were successfully obtained with average dimensions of 100 nm. They possessed identical fiber diameters, and no beads formed.

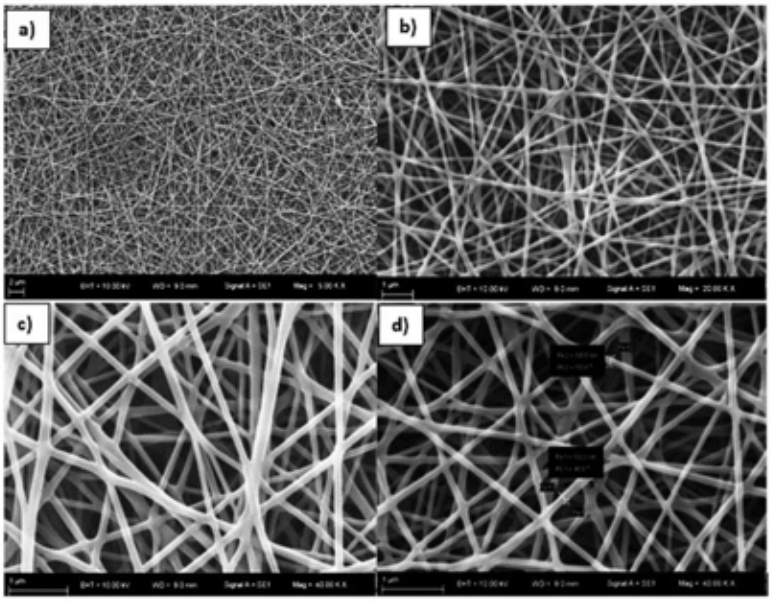

FIGURE 1
(a–d)- Scanning electron microscopic images of the PVA(20 wt%) nanofibers.

The EDX analysis results of the pure PVA nano fibers (20 wt%) are shown in Figure 2. The high intensity carbon peak and oxygen peak belong to the PVA polymer, which has the molecular formula $[CH_2CH(OH)]_n$ [18].

Some peaks in the graph were related to gold and palladium used in the coating treatment before the SEM analysis. The aluminum peak likely belonged to the grid.

Figure 3 shows the SEM results of PVA nanofibers at a concentration of 25 wt%. The nanofibers had average diameters of 200 nm. Increasing the concentration of the PVA solution proportionally increased the diameter of the nanofibers. In addition, the formation of beads has not occurred.

Figure 4 reveals that the PVA nanofiber peaks were similar with those of the electrospun PVA (20 wt%) polymer.

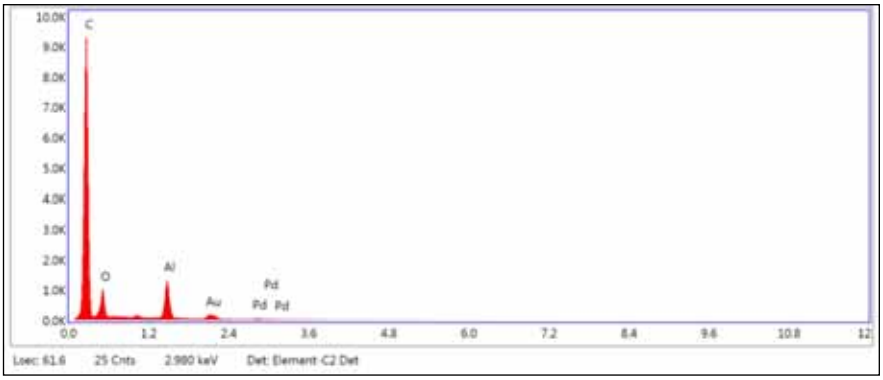

FIGURE 2
Energy dispersive X-ray results of the PVA(20 wt%) nanofibers.

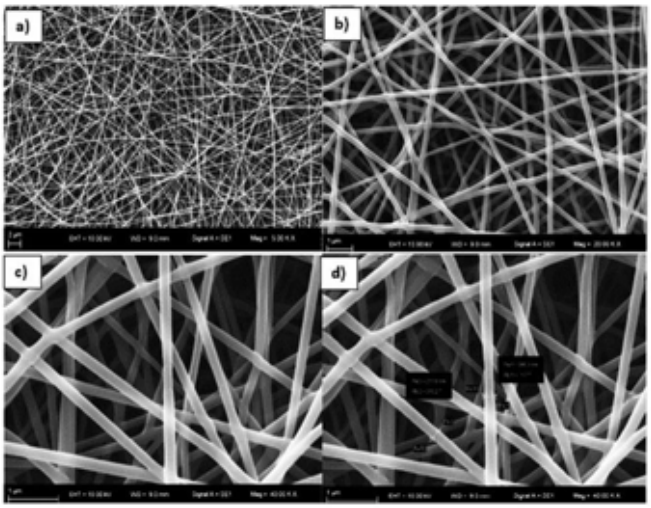

FIGURE 3
(a–d)- Scanning electron microscopic images of the PVA (25 wt%) nanofibers.

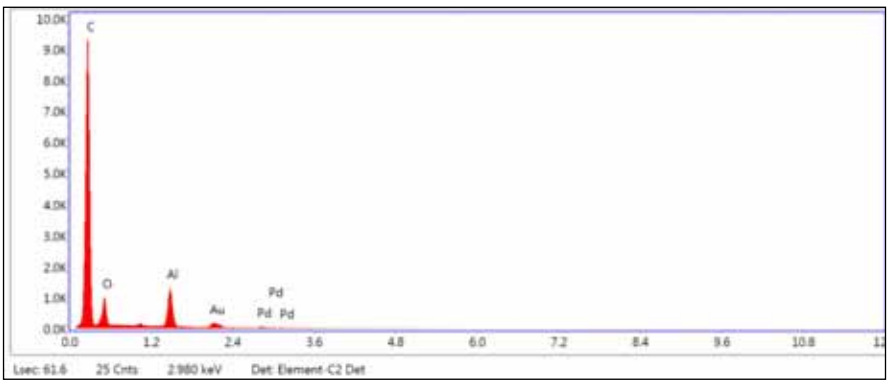

FIGURE 4
Energy dispersive X-ray results of the PVA(25 wt%) nanofibers.

Figure 5 (a) and (b) shows the characteristic FT-IR bands of PVA and their assignments. The bands observed between 3,604 and 3,724 cm^{-1} were associated with stretching O-H bonds [19]. The bands at 1,750 and 1,730 cm^{-1} referred to water absorption in the initial PVA spectra, as reported previously [20]. In addition, the peaks at 1,356 cm^{-1} demonstrate C-H stretching of aliphatic groups [21].

The SEM images of GHK embedded PVA (20 wt%) nanofibers are shown in Figure 6 (a–d). As indicated, the morphology consisted of nanofibers with diameters of 50–250 nm. Although the conditions and spinning parameters were the same, the diameters of the fibers decreased compared to pure PVA nanofibers due to the presence of the GHK-peptide. Adding the peptide changed the fiber diameter due to changes in the charge characteristics, as reported previously [22, 23]. In contrast, the EDX analysis revealed the presence of peptide–nitrogen on the surface of the PVA–GHK peptide (Fig. 7), specifically agglomeration regions, which were absent in the PVA nanofibers.

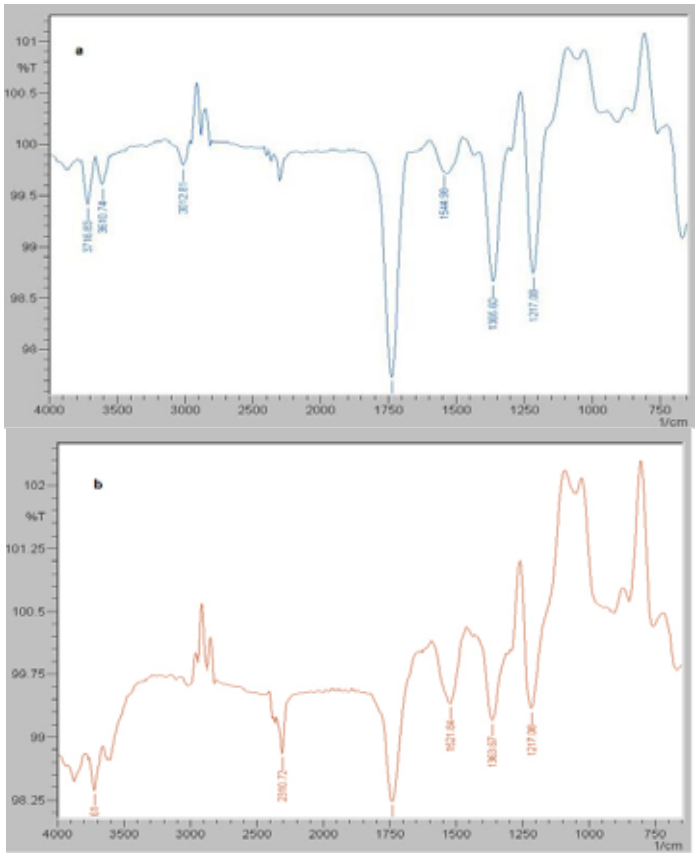

FIGURE 5
Fourier transform-infrared results of PVA (a) 20 wt% and (b) 25 wt%.

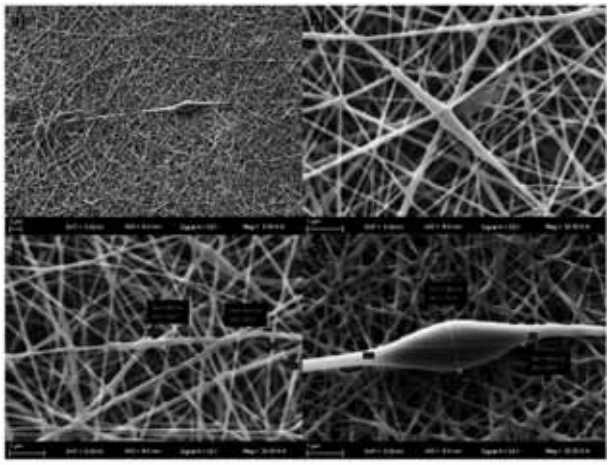

FIGURE 6
(a–d)- Scanning electron microscopic images of the GHK embedded PVA(20 wt%) nanofibers.

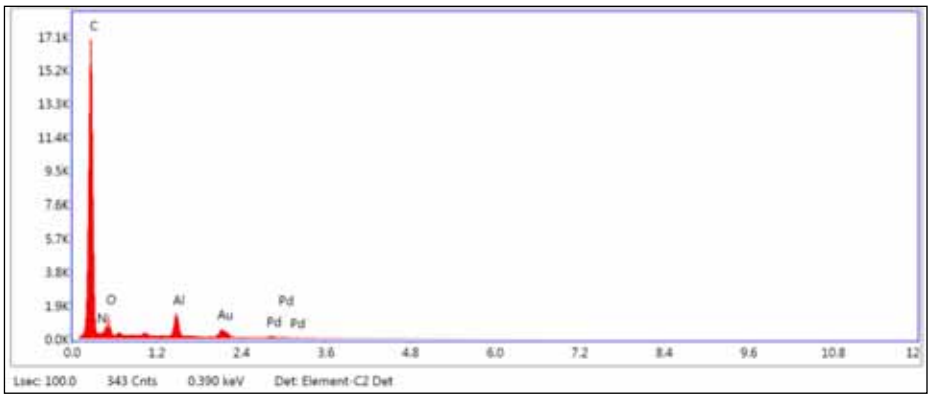

FIGURE 7
Energy dispersive X-ray results of the PVA-GHK (20 wt%) nanofibers.

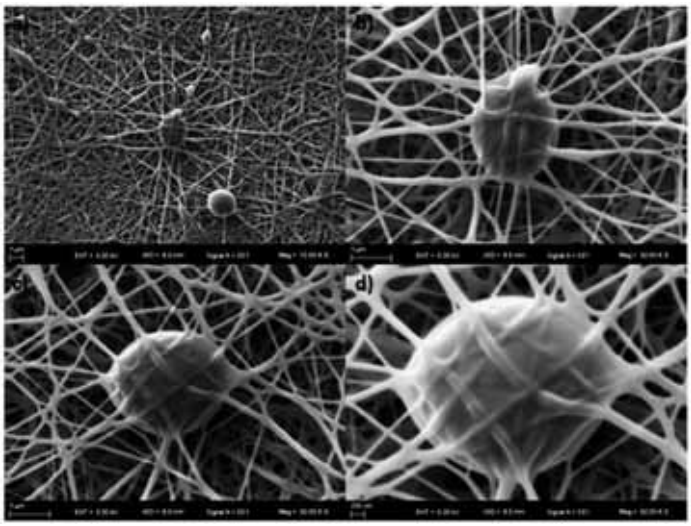

FIGURE 8
(a–d)- Scanning electron microscopic images of the GHK embedded PVA (25 wt%) nanofibers.

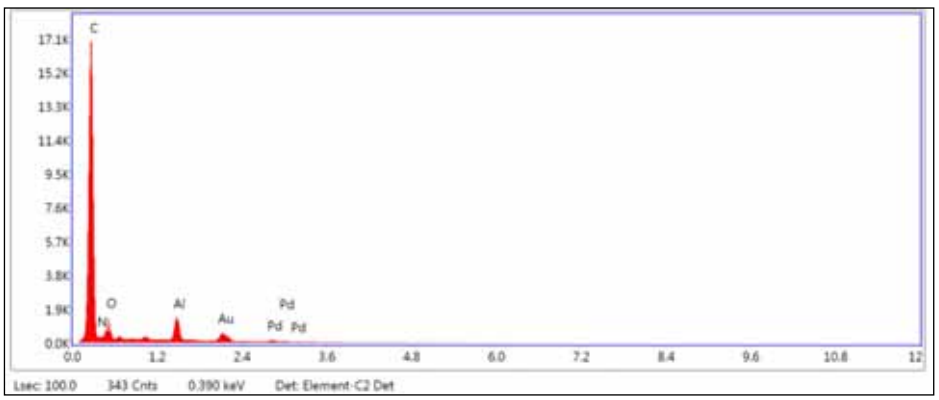

FIGURE 9
Energy dispersive X-ray results of the PVA-GHK (20 wt%) nanofibers.

As shown in Figure 7, the peptide–nitrogen peak was low because the GHK peptide consists of three amino acids comprised of small protein fragments. Peptide molecules can penetrate the polymer chains resulting in interactions. Figure 8 shows the GHK embedded PVA (25 wt%) nanofiber morphology. According to the results, the fibers had diameters of 50–200 nm, and the diameters decreased due to the presence of GHK peptide. In contrast, a non-uniform structure was observed for PVA-GHK (25 wt%). We inferred that when the PVA concentration was increased, agglomerations occurred in some locations and their dimensions reached micrometer size due to changes in viscosity of the polymer solution. The EDX analysis revealed the presence of the peptide–nitrogen complex on the surface of the PVA–GHK peptide (Fig. 9).

Figure 10 (a) and (b) shows the characteristics of the PVA-GHK peptide bands (20 and 25 wt%) and their assignments. The band observed at 3,724 cm^{-1} was associated with stretching O-H bonds. The C=O stretching has a strong band in the 1,660–1,730 cm^{-1} region [24, 25]. Our results demonstrate that C=O stretching of the carboxyl group of the GHK peptide was observed at the peak at 1,743 cm^{-1}. The C-O stretching vibration of the carboxyl group was observed in the 1,340–1,440 region, according to the literature. In this regard, the 1,363 cm^{-1} peak referred to C-O stretching, and confirmed the GHK peptide [26].

The toxicity results of the GHK-PVA nanofibers are shown in Figure 11. PVA is not normally a toxic polymer and GHK is normally found in humans and is nontoxic[14]. Our results showed that GHK-PVA was not toxic to L929 cells.

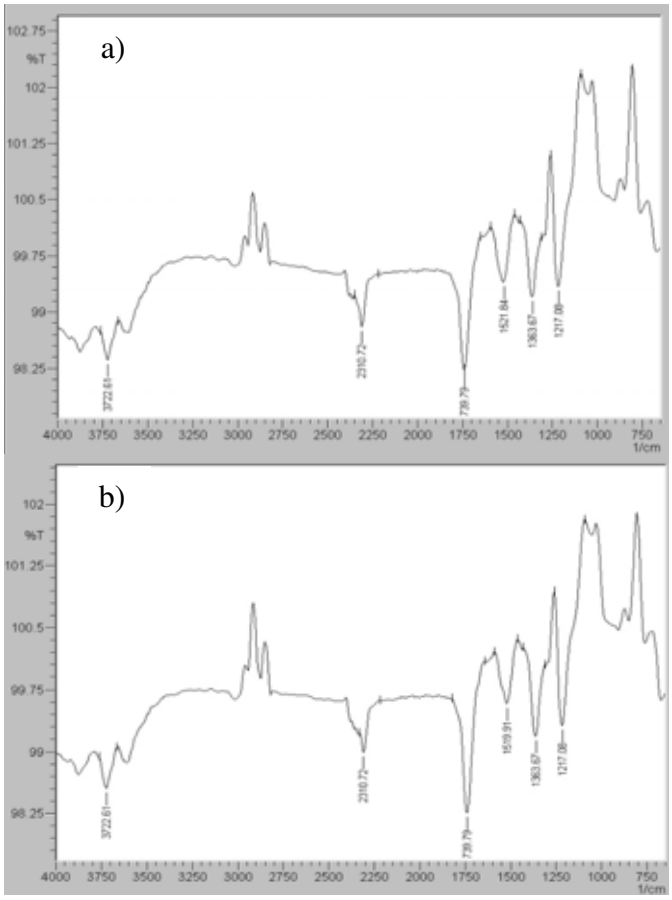

FIGURE 10
Fourier transform-infrared results of (a) 20 wt% and (b) 25 wt% PVA-GHK peptide.

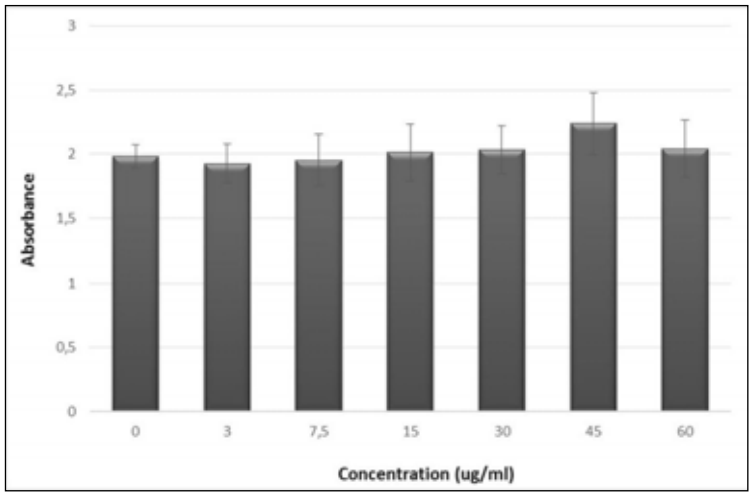

FIGURE 11
Cell toxicity of the GHK-PVA nanofibers.

DISCUSSION AND CONCLUSION

In this study, pure PVA nanofibers with a uniform morphology were synthesized. The FT-IR and EDX results confirmed that the GHK peptide was embedded successfully in the PVA fiber structure. However, structural uniformity changed after adding the GHK-peptide to the PVA solution due to changes in the charge characteristics between the GHK-peptide and the PVA polymer chain. In addition, as the concentration of the GHK peptide was increased, polymer fiber diameter decreased. GHK-PVA was not toxic to L929 cells. Non-toxic, nano-dimensional fibers were successfully fabricated, and the nanofibers could be useful in future tissue engineering studies.

No potential conflicts of interest are reported by the authors.

REFERENCES

[1] Xia, Y., Yang, P., Sun, Y., Wu, Y., Mayers, B., Gates, B., Yin, Y., Kim, F., Yan, H. (2003) One-dimensional nanostructures: synthesis, characterization, and applications. Advanced materials. 15, 353-389.

[2] Jahangiri, M., Shahtaheri, S.J., Adl, J., Rashidi, A., Kakooei, H., Rahimi Forushani, A., Ganjali, M.R., Ghorbanali, A. (2011) The adsorption of benzene, toluene and xylenes (BTX) on the carbon nanostructurs: the study of different parameters. Fresen. Environ. Bull. 20, 1036-1045.

[3] Supaphol, P., Chuangchote, S. (2008) On the electrospinning of poly (vinyl alcohol) nanofiber mats: a revisit. Journal of Applied Polymer Science. 108, 969-978.

[4] Zhang, Y., Wang, J., Yang, P. (2013) Convenient synthesis of Ag nanowires with tunable length and morphology. Materials Research Bulletin. 48, 461-468.

[5] Gibson, J. (1996) Phys. Today 1997, October, 56. b) S. Matsui, Y. Ochiai. Nanotechnology. 7, 247.

[6] Li, D., Xia, Y. (2004) Electrospinning of nanofibers: reinventing the wheel? Advanced materials. 16, 1151-1170.

[7] Li, W.J., Laurencin, C.T., Caterson, E.J., Tuan, R.S., Ko, F.K. (2002) Electrospun nano-fibrous structure: a novel scaffold for tissue engineering. Journal of biomedical materials research. 60, 613-621.

[8] Ghasemi-Mobarakeh, L., Prabhakaran, M.P., Morshed, M., Nasr-Esfahani, M-H., Ramakrishna, S. (2008) Electrospun poly (ε-caprolactone)/gelatin nanofibrous scaffolds for nerve tissue engineering. Biomaterials. 29, 4532-4539.

[9] He, W., Yong, T., Teo, W.E., Ma, Z., Ramakrishna, S. (2005) Fabrication and endothelialization of collagen-blended biodeg-radable polymer nanofibers: potential vascular graft for blood vessel tissue engineering. Tissue engineering. 11, 1574-1588.

[10] Dahlin, R.L., Kasper, F.K., Mikos, A.G. (2011) Polymeric nanofibers in tissue engineering. Tissue Engineering Part B: Reviews. 17, 349-364.

[11] Shrestha, B.K., Mousa, H.M., Tiwari, A.P., Ko, S.W., Park, C.H., Kim, C.S. (2016) Development of polyamide-6, 6/chitosan electrospun hybrid nanofibrous scaffolds for tissue engineering application. Carbohydrate polymers. 148, 107-114.

[12] Agrawal, P., Pramanik, K. (2016) Chitosan-poly (vinyl alcohol) nanofibers by free surface electrospinning for tissue engineering applications. Tissue Engineering and Regenerative Medicine. 13, 485-497.

[13] Yoshimoto, H., Shin, Y., Terai, H., Vacanti, J. (2003) A biodegradable nanofiber scaffold by electrospinning and its potential for bone tissue engineering. Biomaterials. 24, 2077-2082.

[14] Pickart, L., Vasquez-Soltero, J.M., Margolina, A. (2015) GHK peptide as a natural modulator of multiple cellular pathways in skin regeneration. BioMed research international 2015.

[15] Pickart, L., Thaler, M. (1973) Tripeptide in human serum which prolongs survival of normal liver cells and stimulates growth in neoplastic liver. Nature: New biology. 243, 85-87.

[16] Meiners, S., Eickelberg, O. (2012) Next-generation personalized drug discovery: the tripeptide GHK hits center stage in chronic obstructive pulmonary disease. Genome medicine. 4, 70.

[17] Aravindh, S., Periasamy, P., Kalirajan, M., Indumathy, K., Venkatachalam, R. (2016) Efficacy Of Bacterial Biopolymeric (EPS) Liganded Silver Mesocage Complexes For Hexavalent Chromium Adsorption. Fresen. Environ. Bull. 25, 6030-6037.

[18] Bunn, C. (1948) Crystal structure of polyvinyl alcohol. Nature. 161, 929-930.

[19] Coates, J. (2000) Interpretation of infrared spectra, a practical approach. Encyclopedia of analytical chemistry.

[20] Anicuta, S-G., Dobre, L., Stroescu, M., Jipa, I. (2010) Fourier transform infrared (FTIR) spectroscopy for characterization of antimicrobial films containing chitosan. University Politehnica of Bucharest, Faculty Applied Chemistry and Material Science.

[21] Jia, Y-T., Gong, J., Gu, X-H., Kim, H-Y., Dong, J., Shen, X-Y. (2007) Fabrication and characterization of poly (vinyl alcohol)/chitosan blend nanofibers produced by electrospinning method. Carbohydrate Polymers. 67, 403-409.
[22] Zeng, J., Aigner, A., Czubayko, F., Kissel, T., Wendorff, J.H., Greiner, A. (2005) Poly (vinyl alcohol) nanofibers by electrospinning as a protein delivery system and the retardation of enzyme release by additional polymer coatings. Biomacromolecules. 6, 1484-1488.
[23] Viana, J.F., Carrijo, J., Freitas, C.G., Paul, A., Alcaraz, J., Lacorte, C.C., Migliolo, L., Andrade, C.A., Falcão, R., Santos, N.C. (2015) Antifungal nanofibers made by controlled release of sea animal derived peptide. Nanoscale. 7, 6238-6246.
[24] Roeges, N.P. (1994) A guide to the complete interpretation of infrared spectra of organic structures. Chichester: Wiley & Sons.
[25] Kecel, S., Ozel, A.E., Akyuz, S., Celik, S., Agaeva, G. (2011) Conformational analysis and vibrational spectroscopic investigation of l-proline–tyrosine (l-Pro–Tyr) dipeptide. Journal of Molecular Structure. 993, 349-356.
[26] Mansur, H.S., Oréfice, R.L., Mansur, A.A. (2004) Characterization of poly (vinyl alcohol)/poly (ethylene glycol) hydrogels and PVA-derived hybrids by small-angle X-ray scattering and FTIR spectroscopy. Polymer. 45, 7193-7202.

Received: **27.10.2017**
Accepted: **19.11.2017**

CORRESPONDING AUTHOR

Yasemin Budama-Kilinc
Chemical and Metallurgy Faculty,
Bioengineering Department
Yildiz Technical University
Istanbul – Turkey

e-mail: yaseminbudama@gmail.com

© by PSP Volume 27 – No. 2/2018 pages 1210-1213 Fresenius Environmental Bulletin

THE GENETIC VARIATION OF SEVEN NATURAL CRIMEAN JUNIPER (*JUNIPERUS EXCELSA* BIEB. M.) POPULATIONS AND ITS GROWING ENVIRONMENTAL CONDITIONS IN TURKEY

Cengiz Yucedag[1], Halil Baris Ozel[2,*]

[1]Department of Landscape Architecture, Mehmet Akif Ersoy University, Burdur, Turkey
[2]Department of Forest Engineering, Bartin University, Bartin, Turkey

ABSTRACT

The aim of this study was to determine the genetic variation in one-year-old seedling characters of seven Crimean juniper populations naturally distributing in the Lakes District of Turkey. For this purpose, totally 70 families (10 per population) were used to estimate the amount of genetic variation and heritability among individuals within and among populations. Genetic variation among individuals within populations was found to be higher than that among populations. It was detected that seedling fresh weight had the highest coefficient of both genetic and phenotypic variations. On the contrary, the lowest coefficients of genetic and phenotypic variations were the shoot height. Individual heritability ranged from 0.08 (shoot height and the longest root length) to 0.13 (seedling fresh weight), whereas family heritability varied from 0.82 (the longest root length) to 0.91 (seedling fresh weight). In conclusion, it can be recommended to select family within the population rather than population in the context of breeding strategies of the species.

KEYWORDS:
Crimean juniper, genetic variation, heritability, seedling

INTRODUCTION

Genetic variation is a raw material to be shaped for breeding work. For this reason, research on genetic variation is among the priority areas of forestry rehabilitation programs [1]. In this sense, morphological variation studies have also provided an estimate of relatedness among populations within species [2]. Likewise, the characterization of local genetic resources is often based on the knowledge of variation in morphological characters [3].

Juniperus excelsa Bieb. M. is one of the major species for afforestations as it is resistant to drought, frost damages and poor soils growing at the boundaries of steppe in the interior parts of the mountains in its distribution areas [4, 5, 6, 7]. In Turkey, it has a wide natural distribution in northern, western, central, and southern Anatolia, especially in the Taurus and Anti- Taurus Mountains [8]. It has economical functions due to the durability of its timber [9], and organic and inorganic components in their cones [10].

Despite being a valuable species, so far the amount of genetic variation based on cone, seed and juvenile seedling characters [6] and via genetic markers [7, 11, 12, 13, 14] and also morphological dissimilarities among seven populations of Crimean juniper [15] were studied. So, in this study genetic variations in one-year-old seedling characters of seven Crimean juniper populations were investigated.

MATERIALS AND METHODS

70 open-pollinated parent trees (10 from each of seven populations) sampled from the Lakes District of Turkey were used (Table 1). In order to represent gene poll of the populations, the parent trees were sampled at random with the following restrictions: 1) they were to be separated by at least 50 m, 2) the range of elevation of the parent trees had to be not greater than 100 m within any population, 3) they were to be approximately of the same age (± 10 years), ranging from 130 to 140 years. The coarse and healthy cones were collected from the middle part of the crown during November of 2006.

Seeds were sown in polyethylene tubes with 13 x 25 cm dimensions in Eğirdir Forest Nursery (45 km northeast of Isparta, at 920 m a.s.l.) in February 2007. As a growing medium, the mixture containing 50% of silt and forest soil respectively was used. The sowing depth was 2 mm. The layout of the experiment was a randomized complete block design with three replications. Seedlings were irrigated based on the operational regime for this nursery, but not fertilized. For measurements, 15 one-year-old seedlings per parent tree were used.

TABLE 1
Locations of The Studied Populations

No	Forest District	Location	Altitude (m)	Exposure	Latitude (°)	Longitude (°)
1	Eğirdir	Barla	1027	SE	37°58'162"	30°46'289"
2	Eğirdir	Balkırı	1493	E	37°47'101"	30°48'981"
3	Bucak	Kestel	1197	SE	37°24'863"	30°21'036"
4	Aksu	Sorgun	1416	NE	37°50'488"	31°05'782"
5	Eğirdir	Y. gökdere	1150	SE	37°40'558"	30°50'570"
6	Gölhisar	Gölhisar	1413	SE	36°57'115"	29°27'236"
7	Sütçüler	Tota	1546	NE	37°34'678"	31°04'306"

TABLE 2
Components of total variance (%) and genetic parameters for all the characters

Characters	$\bar{x} \pm SE$	σ_P^2	$\sigma_{F(P)}^2$	σ_e^2	CV_g	CV_f	h^2	h_f^2
SH	33.75±0.15	2.00	24.00	74.00	12.59	7.97	0.08±0.17	0.83±0.12
LRL	26.86±0.15	0.00	23.00	77.00	14.81	9.46	0.08±0.17	0.82±0.11
RCD	1.85±0.01	1.00	29.00	70.00	22.16	13.78	0.10±0.18	0.86±0.08
RFW	1.67±0.02	4.00	38.00	58.00	38.81	23.51	0.13±0.20	0.91±0.05

Shoot height (SH, cm), the longest root length (LRL, cm), root collar diameter (RCD, mm) and seedling fresh weight (SFW, g) of seedlings were evaluated.

All the characters were analyzed by using the model of two level nested ANOVA given below through SPSS program [16]:

$Y_{ijk} = \mu + P_i + F(P)_{j(i)} + e_{k(ij)}$

Where; Y_{ijk} is the phenotypic value of the k_{th} tree [i: population (1-7); j: each parent tree (1-70); k: replication (1-15)]; μ is the overall mean; P_i is the effect of i_{th} population; $F(P)_{j(i)}$ is the effect of j_{th} parent tree in i_{th} population; $e_{k(ij)}$ is the residual. In model, while populations were fixed variables parent trees were random variables. Besides, replications were not analyzed as a variable.

Individual heritability for each character were calculated equation given below [17].

$$h^2 = \frac{k\sigma_{F(P)}^2}{\sigma_T^2}$$

Where; h^2 = individual heritability; $\sigma_{F(P)}^2$ = genetic variance from family; σ_T^2 = total phenotypic variance and k= the similarity ratio. In here, we used 1/3 for the similarity ratio because of the natural Crimean juniper populations.

$$h_f^2 = \frac{\sigma_{F(P)}^2}{\frac{\sigma_e^2}{n} + \sigma_{F(P)}^2}$$

Where; h_f^2 = family heritability; σ_e^2 = variance among individual trees within family (sampling error) and n= the replication number.

On the other side, the coefficients of genetic (CV_g) and phenotypic (CV_f) variation for each population were calculated to be able to compare the genetic variances of characters defined by different units. For this purpose, equations below were used.

$$CV_g = \frac{\sqrt{3\sigma_{F(P)}^2}}{\bar{x}} . 100$$

$$CV_f = \frac{\sqrt{\sigma_{F(P)}^2 + \frac{\sigma_e^2}{n}}}{\bar{x}} . 100$$

Where;

$\bar{x}$ = Arithmetic means of seedling characteristics

RESULTS AND DISCUSSION

The component of the total variance attributed to variation among populations was less than 4%. The components of the total variance attributed to variation among families within populations ranged from 23% in the longest root length to 38% in root fresh weight (Table 2). Generally, the family variance components were estimated with higher precision than the population components.

According to Table 2, individual heritability (h^2) for all the characters was low (0.08-0.13) but family heritability (h_f^2) was high (0.82-0.99). High family heritability of one-year-old seedling characters showed that an important genetic gain using selective improvement methods could be provided in this species. Heritability of root collar diameter was higher than that of shoot height. This case indicated that the root collar diameter of seedling was of higher importance in the seedling growing and selection studies than the rootstock diameter. On the contrary, Bilir et al. [18] reported that shoot height was more important than root collar diameter in the seedling growing and selection studies of *Pinus pinea* L.

Moreover, the coefficients of genetic and phenotypic variation have showed significant differences among populations (Table 2). While root fresh weight has the highest value of the coefficient of

both genetic (CV_g=38.81) and phenotypic variations (CV_f=23.51). In turn, it was determined that shoot height has both the low genetic (CV_g=12.59) and phenotypic (CV_f=7.97) variations. As seen, the coefficients of genetic variation for both characters were high. This may be explained that genetic factors were more effective on those characters.

According to the result of the current study, the Crimean juniper populations in Lakes District of Turkey were genetically variable and a greater amount of genetic variation resided within populations. The increment of family heritability has supported the increment of the genetic variation regarding families within populations. It was likely that selection within populations would be much more effective than those among populations. This result drawn from the seedling characters was congruent with the morphological variation estimated within and among natural *J. excelsa* populations [6, 11] and genetic variation estimated using microsatellite markers in 12 *J. excelsa* populations from Lebanon, Turkey, Greece and the Ukraine [7], in seven *J. excelsa* populations from Lakes District of Turkey [13], in six *J. excelsa* populations from Crimean Mountains and one population from Lebanon [12] and in three *J. excelsa* populations from Pakistan [14].

It was predicted that low genetic variation among populations was observed due to limited geographic sampling. Consequently, future studies should broaden the geographic range of populations to be tested and establish the pattern of variation in relation to geographic and climatic variables. The results of this study are only representative for the populations from Lakes District of Turkey. As common garden studies show genetic differences in fitness-related traits (e.g. growth, drought tolerance, insect resistance), the determination of genetic variation and estimation of genetic parameters for *J. excelsa* populations in common gardens pre-established before about 10 years will be more useful to carry out the breeding strategies of the species.

REFERENCES

[1] Işık, F. (1998) Kızılçamda (*Pinus brutia* Ten.) genetik çeşitlilik, kalıtım derecesi ve genetik kazancın belirlenmesi. Batı Akdeniz Ormancılık Araştırma Enstitüsü Yayınları, Yayın No: 7, Antalya.

[2] Gezer, A., Yücedağ, C., Carus, S. (2006) Rehabilitation the Juniper Forest Ecosystems in Terms of Their Present Silvicultural Situation in Turkey, IUFRO Division 2 Joint Conference: Low Input Breeding and Genetic Conservation of Forest Tree Species, October 9-13, 2006, Antalya–Turkey, 65-79.

[3] Delgado J.V., Barba C., Camacho M.E., Sereno F.T.P.S., Martinez A., Vega-Pla, J.L. (2001) Caracterización de los animales domésticos en Espańa. Animal Gen. Res. Infor. 29, 7-18.

[4] Saatçioğlu F. (1969) Silvikültürün biyolojik esasları ve prensipleri. İstanbul University Forestry Faculty Pub. İstanbul.

[5] Browicz K., Zieliński, J. (1982) Chorology of trees and shrubs in south-west Asia and adjacent regions. Warszawa–Poznań, Polish Scientific Pub. Poland.

[6] Yücedağ, C., Gezer, A., Orhan, H. (2010) The genetic variation in Crimean juniper populations from the Lakes District of Turkey. Romanian Biotech. Lett. 15, 5487-5492.

[7] Douaihy, B., Vendramin, G.G., Boratyński, A., Machon, N., Dagher-Kharrat, M.B. (2011) High genetic diversity with moderate differentiation in *Juniperus excelsa* from Lebanon and the eastern Mediterranean region. AoB Plants. 2011, 1-14.

[8] Yaltırık, F. (1993) Dendroloji ders kitabı I. Gymnospermae (açık tohumlular). İstanbul University Forestry Faculty Pub. İstanbul.

[9] Uçar, G., Balaban, M. (2002) The composition of volatile extractives from the wood of *Juniperus excelsa, Juniperus foetidissima* and *Juniperus oxycedrus*. Holz als Roh und Werkstoff. 60, 356-362.

[10] Baytop, T. (1999) Türkiye'de Bitkilerle Tedavi, Nobel Tıp Kitapevleri Yayını, 2. edition, Istanbul, 321-324.

[11] Douaihy B., Sobierajska K., Jasinska AK., Boratynska K., Ok T., Romo A., Machon A., Didukh Y., Bou Dagher-Kharrat M., Boratynski A. (2012) Morphological versus molecular markers to describe variability in *Juniperus excelsa* subsp. *excelsa* (Cupressaceae). AoB Plants. 2012, pls13.

[12] Korshikov, I.I., Nikolaeva, A.V. (2013) Genetic variability of juniper tall (*Juniperus excelsa* Bieb.) in the northern and southern limits of the natural distribution. Tsitol Genet. 47, 33-41.

[13] Yücedağ, C., Gailing, O. (2013) Genetic variation and differentiation in *Juniperus excelsa* M. Bieb. Populations in Turkey. Trees- Structure and Func. 27, 547-554.

[14] Saeed, S., Barozai, M.Y.K., Ahmed, A., Tareen, R.B., Begum, S., Ali, G.M. (2017) Impact of ecological diversity on genetic and phytochemical variation in *Juniperus excelsa* from high elevation zones of Quetta Valley, Pakistan. Pakistan J. of Bot. 49, 201-206.

[15] Yücedağ, C., Gailing, O. (2013) Differences among *Juniperus excelsa* populations as revealed at morphological traits. Dendrobiology. 70, 65-72.

[16] SPSS Inc. (2011) SPSS 20.0 guide to data analysis. Prentice Hall Public. New Jersey.

[17] Falconer, D.S. (1989) Introduction to Quantitative Genetics, Third Edition, Longman, London, 340p.
[18] Bilir, N., Kaya, C., Ulusan, M.D. (2010) Aydın Orijinli Fıstıkçamı (*Pinus pinea* L.) Fidanlarında Morfolojik Özellikler ve Fidan Kalitesi. Kastamonu University Orman Fak. Dergisi. 10, 37-43.

Received: **06.11.2017**
Accepted: **03.12.2017**

CORRESPONDING AUTHOR

Halil Baris Ozel
Bartin University,
Faculty of Forestry,
Department of Silviculture,
Bartin – Turkey

e-mail: halilbarisozel@gmail.com

© by PSP Volume 27 – No. 2/2018 pages 1214-1225 Fresenius Environmental Bulletin

SPATIOTEMPORAL CHARACTERISTICS OF HOURLY RAINFALL IN THE UPPER REACHES OF HANJIANG RIVER BASIN

Mingyuan Wang[1], Weihong Liao[2], Xiaohui Lei[2,*], Yongguang Hu[3], Tao Qin[2]

[1]College of Civil Engineering, Tianjin University, Tianjin 300072, P.R. China
[2]State Key Laboratory of Simulation and Regulation of Water Cycle in River Basin, China Institute of Water Resources and Hydropower Research, Beijing, 100038, P.R. China
[3]Hanjiang Water Resource & Hydropower Group, Co., Ltd, Wuhan 430001, P.R. China

ABSTRACT

The spatiotemporal distribution of rainfall in mountainous area has great importance in the prediction and prevention the natural rainfall hazard, such as, flash flood, landslides and debris flow. In the Hanjiang River Basin, rainfall variation patterns, especially the variations of hourly rainfall have not been examined in detailed. This study aims to analysis the spatial patterns of hourly rainfall by a number of statistics, thereby, demonstrating the correlations with the time-scale and geographical features. The result indicates that the frequency of hourly rainfall has significant positive with all the geographical features. The monsoon climate and local terrain information both affect the local short-time scale rainfall, especially in the Northeast part of the watershed. For temporal variations, the shorter time scale rainfall occurs in the midnight on the South part of the watershed, and rainfall from monsoon season dictates the distribution of yearly rainfall. Statistically, the result showed that, the season factor plays an important role in the spatial correlation, based on the empirical model. The spatial correlation coefficients are also increase with the increase of accumulate rainfall time scale. In summary, the results presented in this article demonstrates the distributions of the rainfall regime from the viewpoints of quantitative and qualitative in the upper reaches of Hanjiang River Basin.

KEYWORDS:
Hourly rainfall, Spatiotemporal characteristics, Upper Reaches of Hanjiang River Basin, Pearson correlation coefficient, Spearman rank correlation coefficient

INTRODUCTION

Rainfall is a key input component of watershed hydrological system [1, 2]. Quantitative analysis of spatiotemporal characteristics of precipitation is one of the basic elements of hydrological research and vital for natural hazards such as flash flood, landslides, debris flow and urban water-logging which are caused by extreme rainfall [3, 4]. Previous rainfall studies were based on daily temporal data and the spatial scale varying from hundreds of kilometres to global. Because of data limitations, few previous researchers focused on small-scale variations of rainfall [5, 6]. Some of latest studies, however, have revealed that small scale rainfall study is beneficial to analyse the land surface changes, and rainfall distribution may also influence the land surface process [7].

Despite being a critical variable to hydrological system, the study of rainfall spatiotemporal characteristics is a daunting challenge, because of its diversity over space and time [8-10]. In generally, measurement of rainfall is subjected to errors from gauge station, especially, in the mountainous areas. Most of the quantitative rainfall estimation often have significant inaccuracies, due to various reasons [11]. In additionally, the hourly rainfall which are caused by terrain is difficult to forecast and even to measure at an hourly scale [12, 13]. The analysis of the hourly rainfall can benefit the flash flood prediction and surveillance of extreme rainfall [14]. Previous research results have showed that in different climatic and terrain conditions, the spatial and temporal variability of rainfall on small scale also has obvious differences, so it is necessary to carry out statistical analysis of the specific research area [15, 16].

In climate research, experts have studied a variety of complex models to study and simulate rainfall [17, 18]. It is known that most numeric weather and climate models tend to under predict in intensity, but over predict in frequency of occurrences even though precipitation amount is reasonable and this will cause hydrological model instability [19, 20]. Small scale spatial and temporal variability of rainfall has its unique features different from large scale rainfall in terms of analysis and simulation, which can show the change in much finer detail. The drastic change of rainfall intensity at finer scales may cause different kinds of flood disaster, especially in the mountain area [21]. The spatial analysis of fine-scale rainfall allows up to detect the defects in the distribution of rainfall station, such as mal-functioned stations, misaligned data etc.

This study analysed different kinds of hourly data in upper reaches of Hanjiang River Basin. This basin is located in the humid subtropical monsoon climate zone edge [22].Despite the influence from mountainous terrain, it is a warm temperate mountain climate, with the rainy season appearing in the summer and autumn. In Summer, it is governed by the low pressure Southwest warm and the high pressure Western Pacific subtropical wind. In Autumn, it is also influenced by the Northwest cold and high pressure. Previous studies show that the runoff from different tributaries of the upper reach of the Hanjiang River Basin rainfall is differs greatly and largely influenced by climate and topography [23]. Accordingly, it is of prime significance for flush flood simulation and prediction to be able to represent the regional hourly rainfall variability in particular areas of this region. Past reports had explored the climate effect of this watershed, including annual, seasonal, monthly and daily rainfall variations [24, 25]. However, hourly rainfall regimes have never been represented, mainly because of the lack of data. In this paper, close attention is paid to the following two aspects: (i) the characteristics of the hourly rainfall variations in both space and time; (ii) the defects of existing gauge network in different tributaries.

The objective of this study is to resolve the following two questions: 1) What is the main features of the hourly rainfall changes in time and space; 2) What is the most appropriate gauge station distance for monitoring the hourly rainfall in the upstream of Hanjiang river basin. To answer the first question, hourly gauge rainfall data in the recent four years were collected to analyse the spatial distribution of hourly rainfall and rainfall temporal distribution for each day. To solve the second question, the gauge station information and the rainfall of different time scales can be approximated as a spatial distribution function and the parameters of the function can show the most appropriate gauge station distance.

The paper is organized as follows: the study area and datasets are described in section 2; Section 3 presents the statistical method of the rainfall data; Section 4 gives the results and some discussions; followed by summary and conclusions in Section 5.

STUDY AREA AND GAUGE DATA

Study area. The study area showed in Figure 1 is known as the upper reaches of Hanjiang River Basin. This area is located between 106° 12′ E and 110° 07′ E, 31° 50′ N and 34° 05′ N, and the Danjiangkou reservoir is located at the downstream this watershed. The total catchment area is 59155 km2, and the elevation ranges from 107m to 3365m above sea level.

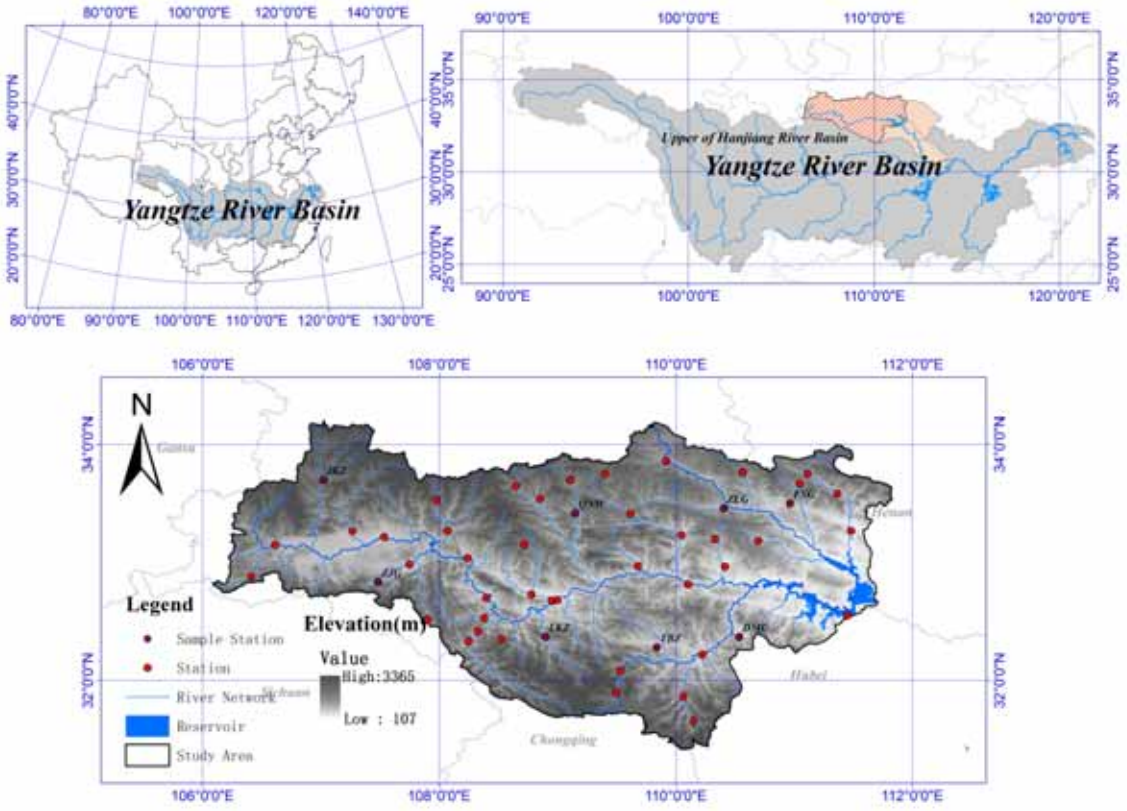

FIGURE 1
The location of the upper reaches of Hanjiang River Basin, and the basic details of the research watershed, including river, reservoir, terrain, and rainfall stations.

This watershed contains Micang Mountains and Daba Mountains which are the famous storm centers in Qinling South Mountain, as the noted in the earlier studies [26, 27].The main stream is known as the Hanjiang River, and it is the largest tributary of the Yangtze River, originating from south of Qinling Mountains. Most part of the terrains are mountains and sloping fields, and the river flows through the Hanzhong plain. Therefore, the complex terrain gives rise to a lot of small tributaries, which directly generated floods into the main Hanjiang River. The rainfall distribution is very different from the west to the east. For example, the annual rainfall of Lengshuihe station in the west varies from 1500 ~1700mm and the annual rainfall in the east varies from only 800 ~ 900mm. Generally, the flood season in upper reaches of Hanjiang River Basin starts in May and ends in October. During July to September, local precipitation is dominated by the Pacific subtropical high pressure zones, and influenced by Southwest China Vortex. Rainfall during the flood season contributes to 82% of total annual rainfall [28].

Gauge data. There are two types of rain gauge data used in this study. Thirty of the 48 rainfall stations are of funnel These gauge stations were in operation since 2010. The other eighteen rainfall stations were from the local meteorological rainfall stations in the national meteorological system. Four years of hourly rainfall data (from September 2012 to August 2016) was used to ensure that these two data sets are compatible, a cross-validation test was carried out to compare accumulated daily rainfall using the accumulated 6 hours rainfall from the two different gauges system the nearby. The result showed that the correlation coefficient between two kinds of gauge station was more than 0.90 average, indicating that the data can be used together.

METHOD

The spatiotemporal characteristics of rainfall is always based on classic probability and statistics as rainfall processes are stochastic processes. The parameters of the distribution functions can be calculated by limited historical observation data. Based on existing data and different aspects of the problems, the analysis can be separated into three steps:

(A) Spatial distribution of rainfall: This section can focus on the spatial variation of rainfall over the whole basin, without considering the changes over time. The statistics information can be computed from the historical data.

(B) Rainfall temporal distribution within the day: The whole basin will be separated in different parts. In each unique part, the rainfall data of different stations can be added up by different hours of the day. This kind of analysis will show the unique daily rainfall process in different areas

(C) Spatial correlation analysis of rainfall: In this section, the rainfall stations should be paired and their correlation coefficient can be computed. The function of the distance and the coefficient can then be fitted. The parameters of the function will reveal the optimum distance of the different two stations. Using the optimum distance, the density of the rainfall station in the whole basin can be calculated and the districts which have inadequate rainfall station coverage can also be detected.

In the analysis of the whole spatiotemporal characteristics, the following basic statistic indices are introduced and utilized.

(i) Pearson correlation coefficient. Pearson correlation coefficient [29]describes the close relationship between 2 fixed variables, which is used to measure the correlation between 2 variables X and Y (linear correlation), and its value is between -1 and 1, which lies generally expressed by r_{xy}.

$$r_{xy} = \frac{\sum(X-\bar{X})(Y-\bar{Y})}{(\sqrt{\sum_{i=1}^{n}(X_i-\bar{X})^2})(\sqrt{\sum_{i=1}^{n}(Y_i-\bar{Y})^2})}$$

In this formula, n is the sample size, X, Y were 2 variables of the observed value. If $r_{xy} > 0$, it is showed that the 2 variables are positively correlated, that is the value of a variable is larger, another variable value will be greater; if $r_{xy} < 0$, showed that the 2 variables are negatively correlated, that is the value of a variable is the value of another variable, but will be smaller. The greater the absolute value of r_{xy}, the stronger the correlation.

(ii) Spearman rank correlation coefficient. The spearman rank correlation coefficient [30] is a nonparametric rank statistic parameter, proposed by Spearman in 1904, to measure the relationship between the two variables. Spearman rank correlation coefficient can be expressed as ρ_s.

$$\rho_s = 1.0 - \frac{6\sum {d_i}^2}{N^3 - N}$$

In this formula, d_i is the rank difference of the two variables. Spearman rank correlation coefficient is often referred to as the no a parametric correlation coefficient, which has two meanings. Firstly, if the relationship between Y and X is monotonic, X and Y are completely Spearman dependent, which is different from the Pearson Correlation Coefficient. The latter is completely related to the linear relationship between variables. What is more, nonparametric means that the exact distribution of the samples can be obtained when the joint probability density function of Y and X is not known.

The largest difference between the two coefficients is the requirements for variable distribution. Pearson correlation coefficient needs the variables to obey normal distribution or approximately normal distribution, but Spearman rank correlation coeffi-

cient need not. In this study, Pearson correlation coefficient is used in the space and time variations to test the correlation between hourly rainfalls data and spatial information. Spearman rank correlation coefficient is used in the analysis of hourly rainfall for two different stations, to detect the distance between the rainfall station pairs. Two kinds of data use two different coefficients, because the hourly rainfall data does not obey the normal distribution, but the statistical information of hourly rainfall obey the normal distribution.

The correspondence of coefficient and relationship is shown in Table 1 [31].

TABLE 1
The correspondence of coefficient and relationship

relation	negative	positive
No relevance	−0.09～0.0	0.0～0.09
Little relevance	−0.3～−0.1	0.1～0.3
Middle relevance	−0.5～−0.3	0.3～0.5
Significant relevance	−1.0～−0.5	0.5～1.0

SPACE AND TIME VARIATIONS RESULT IN UPPER REACHERS OF HANGJIANG RIVER BASIN

Most of the analysis in the Upper reaches of Hanjiang River Basin are focused in mechanism and influence of local climate, temporal variation of rainfall characteristics of year and spatiotemporal characteristics of rainfall in month and day. In this research, the focus is on the diurnal cycle and its spatial dependence within the study area, using hourly continuous observation rainfall data from September 2012 to August 2016.

Results. A. Spatial distribution of hourly rainfall. Eight statistical indices were extracted from the spatial variations analysis, including the mean, median, standard deviation, interquartile range, coefficient of variance, conditional mean rainfall (the total rainfall amount divided by the rainy hours), rainfall occurrence percentage (the rainy hours divided by the total hours of the 4-yr gauge records), and maximum rainfall accumulated with four different time scales (1,6,12,24h). All the eight stations are all in the mountain area, to analyze the spatial distribution in mountainous region which do not have rainfall station coverage

The summary statistics of hourly rainfall from eight sample rainfall gauges (Figure 1) are shown in Table 2. The median takes the 0 and no rain data into consideration to reflect the intermittence of natural rainfall. The hours without rain are excluded from the analysis in the other seven indices. The values of skewness, kurtosis, CV and CS suggest that hourly rainfall in the whole watershed instability and high temporal variability.

From the result in Table 2, the sample station showed that the mean rainfall increases with increase in altitude, but the number of rainfall hours decreases with increase in altitude. Secondly, it became evident that the stations located in the northern side of the river show lower mean rainfall, which suggested the southern part in the watershed had a higher-intensity rainfall than the northern part. All these results showed that the geographic information has influence on the spatial distribution of short-time rainfall, in the upper reaches of Hanjiang River Basin.

This part focuses on the analysis of the influence of geographical factors on the spatial distribution of short-time hourly rainfall. The elevation, latitude and longitude characterize the geographical features, to a certain extent. The rainfall significant property can be represented by the hourly mean, Cv, Cs and frequency. The Pearson coefficients of geographical features and rainfall property are shown in the Table 3. The result shows that the frequency has a significant negative correlation with longitude, latitude and elevation of the location of the stations. There is no significant correlation between the other rainfall properties and the geographical features. And the average of hourly rainfall has minor positive correlation with these three geographical features.

TABLE 2
Statistics of conditional hourly rainfall (eight representative gauges) in the reach. (The locations associated with the site identifiers are given in Fig. 1.)

	JKZ	LKZ	QNW	ZJG	TBZ	DMC	ZLG	FSG
Long (°)	107.02	108.90	109.15	107.48	109.84	110.54	110.41	110.97
Lati (°)	33.70	32.37	33.42	32.83	32.28	32.37	33.46	33.50
Elev (M)	1145	630	833	664	590	311	663	549
Mean (mm)	1.61	1.23	1.32	1.33	1.13	1.07	1.27	1.03
Median (mm)	0.4	0.4	0.8	0.4	1	1	0.8	0.4
Std dev (mm)	2.07	2.19	1.33	2.47	2.47	2.54	1.22	2.451
Kurtosis (mm)	16.87	36.34	0.84	18.7	23.2	75.27	2.02	115.53
Skewness	0.73	2.46	-0.4	0.68	1.42	9.2	-0.34	21.4
Cv	1.84	1.78	1	1.85	1.54	1.62	0.96	2.38
Cs	0.82	1.74	0.06	0.8	1.2	4.23	0.16	7.57
No. of hours	2545	2629	1158	3304	2241	1897	984	1396

TABLE 3
The Pearson correlation coefficient of geographical features and rainfall properties

Pearson	coefficient	Mean(mm)	CV	CS	Frequency
	Long	0.23	-0.18	-0.01	-0.58
1 hr.	Lati	0.42	-0.21	0.14	-0.6
	Elev	0.21	-0.15	-0.14	-0.52
	Long	0.25	-0.2	0.07	-0.52
2 hr.	Lati	0.24	-0.22	0.26	-0.45
	Elev	0.23	-0.23	0.03	-0.57
	Long	0.29	-0.26	0.2	-0.62
3 hr.	Lati	0.25	-0.28	0.26	-0.54
	Elev	0.28	-0.29	0.03	-0.56
	Long	0.29	-0.32	0.28	-0.59
6 hr.	Lati	0.19	-0.31	0.37	-0.47
	Elev	0.33	-0.29	0.22	-0.56

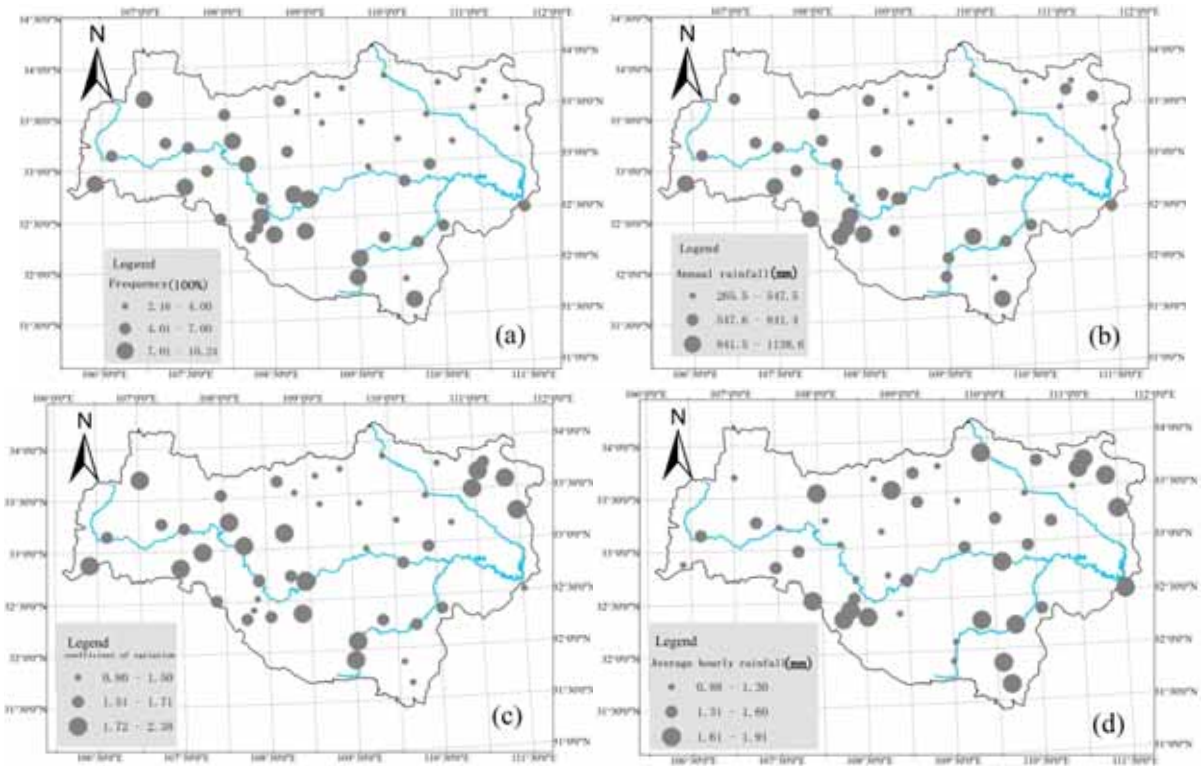

FIGURE 2(2)
Summary statistics of hourly rainfall during 2012–2016, including (a) annual rainfall (mm), (b) frequency (%), (c) rainfall coefficient of variation and (d) average hourly rainfall (mm).

Figure 2 depicts the spatial distribution of the rainfall frequency (ratio of the total number of hours of rainfall and the total number of hours), annual rainfall, ratio of variation coefficient (ratio of the standard deviation and mean value) and the average hourly rainfall in the rainfall hours. As shown in the Fig 2(a), rainfall frequency ranges from 2.16% to10.24%, and most stations with high rainfall frequency is located in the southwest of the watershed. Annual rainfall is presented in Fig 2(b). It can be founded that small rainfall amounts (less than 548 mm) can be observed on the north side of middle watershed. Conversely, large rainfall amounts (more than 841 mm) can be observed on the south mountainous side of the watershed. In Fig 2(d), we can find that the middle reaches in the watershed have the highest average hourly rainfall station. and in the north mountainous watershed, the same conclusion can be reached. Combining the results in Fig 2(a), 2(b) and 2(d)suggests that, the west plain has frequent light rainfall, the south mountain has high intensity rainfall, but its accumulated mount is less than the north side. The CV values varies from 0.8 to 2.8, suggesting that the mountainous areas always have lower CV values than the other region in the whole watershed. All these conclusions match the data in the Table 3.

Flash floods are usually produced by continuous high strength precipitation process, so the results of accumulated hourly rainfall can guide us to study

particular flash floods and torrential rain. Accordingly, the spatial distribution of maximum accumulated rainfall at different time scales (1, 6, 12 and 24h; all mean consecutive hours) are shown in the Fig 3. From 1 to 6h, the maximum rainfall shows large values in the upper reaches of the whole watershed and the northeast mountains, suggesting that local short-duration storms could occur in these areas of the watershed. On the other hand, in 12h and 24h analysis, larger values of maximum rainfall intensities occur uniformly in many places of the study area. This result indicates that it is key to strengthen local storm flood monitoring and warning, to increase new rainfall gauges in the southwest mountains and northeast mountains.

B. Rainfall temporal distribution within the day. In the resolution of the rainfall temporal distribution in the whole day, the focus was on the three indices: precipitation amount (PA), precipitation intensity (PI), and precipitation frequency (PF). If the gauge data is more than 0, this hour is denoted as the rainy hour, and a dry hour is denoted by 0 value. PA is defined as the accumulated precipitation amount for all the hours averaged over the 1461 days of the study period. PI is defined as the average accumulated precipitation amount for rainy hours PF is defined as the rainy hours proportion of the whole year hours [32].

In this part, the hourly peaks of PA, PF, and PI within the day, which were indicated by MPA, MPF, MPI separately, are shown in the Figure 4. It shows the spatial distribution and the occurrence time of the MPA, MPF and MPI. The peak times are indicated by an arrow pointer on a circular clock dial. The spatial distributions are interpolated by gauge statistics with the method of inverse distance weighting considering the elevation, because the mean hourly rainfall and the frequency have relevance to the elevation as mentioned before.

Figure 4a shows the spatial distribution of MPA and its occurrence time. The large MPA values mainly appears in the southwest and northeast mountainous regions, and the small MPA values mostly occurs due north. The result indicates that the north of the watershed, is the driest place of the whole watershed, especially in the Guan River reach. This could be caused by the topography. The occurrence of the MPA has its own regular pattern. The occurrences of the MPA in the West part are mostly in the middle night (00:00-03:00), but in the Eastern region, it tends to be in the morning or afternoon.

It is shown in the Figure 4b, that large frequency values are located in the southwest region with the due North and Northeast region having mainly low values. This means that the Northeast part have a big possibility of encountering a sudden storm and that the southwest have the most abundant rainfall. So, the two mountainous regions have the highest possibility of a flash flood. In the occurrence time aspect, it is similar to the MPA distribution.

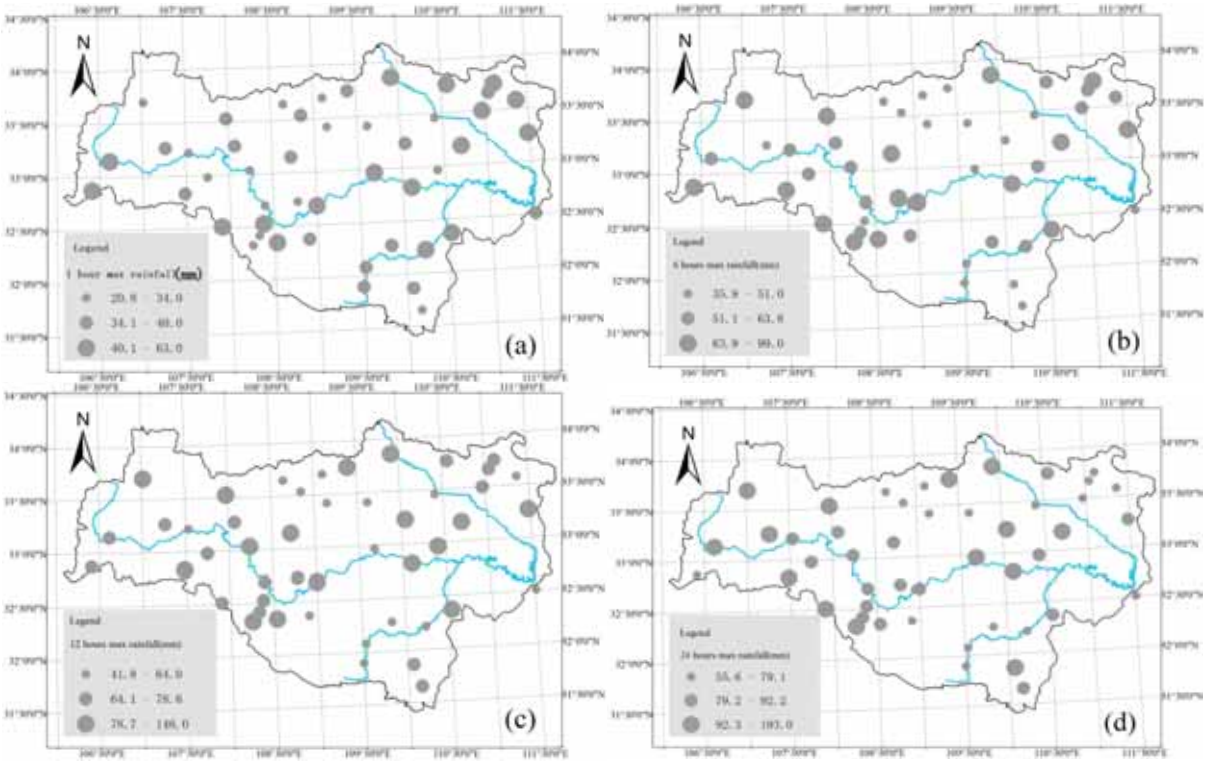

FIGURE 3
Spatial maps of 1, 6, 12, 24h maximum rainfall in the study area during 2012–2016

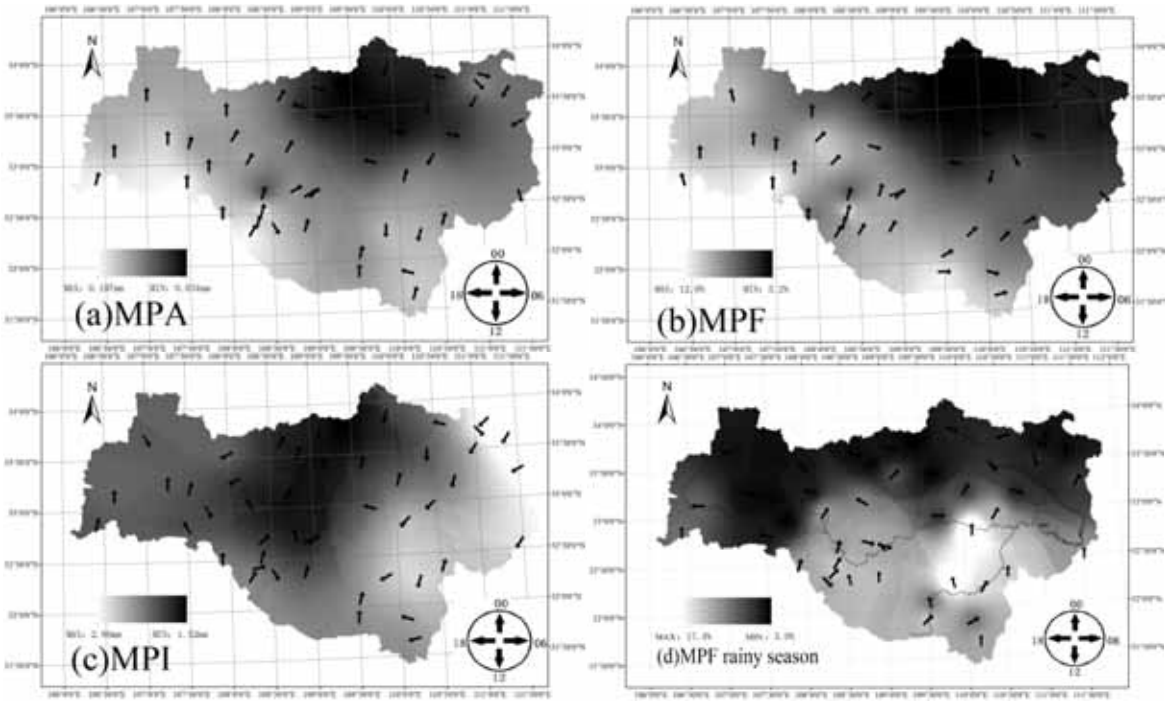

FIGURE 4
Spatial distribution of (a) MPA (mm), (b) MPI (mm), (c) MPF (%) for the whole year, and (d) MPF (%) for summer (the arrow on a circular clock dial indicates the peak time in Beijing time).

The MPI distribution is depicted in the Figure4(c). As the conclusion, we summarize from the last two figures, the large values of precipitation intensity are in the northeast mountains. Though it has the most accumulated rainfall amount, the average rainfall is in the middle type, in the west part of the watershed. It means the west part contains a long wet time the whole year and that cannot be influenced by the flush flood easily. Different from the previous two figures, the occurrence time is mixed in this figure, thus, it is hard to confirm when the peak time of PI will appear in any region of the whole watershed.

Furthermore, we also separately analyse the spatial distributions of rainy season MPA, MPI, and MPF (i.e., rainy season: May–October). Figure 4(d) is the MPF distribution of the rainy season, as an example. In the north side of the figure, there is no obvious change between the results of rainy season and those of the whole year. In the west side, the MPF in the rainy season has low values than in the whole year, because the rainy season in the west last longer than the whole watershed, but the mainly part of the rain also happens in the rainy season. And this also prove the conclusion from the Figure 4(c).

C. Spatial correlation analysis of hourly rainfall. As mentioned before, spatiotemporal distribution in the upper reaches of Hanjiang river basin is complex. The local weather system is influenced by the monsoon system and the local terrain. Earlier research showed that both the physical hydrological model and the conceptual hydrological model have a significant uncertainty in the model simulation of this watershed[33, 34].

The correlation coefficient between the two observations of rainfall stations is an important part of the spatial statistical analysis in the hourly rainfall [35]. It not only describes the dominating mode in the study area, but it also estimates the underlining factors without the need to use other observations. The analysis of spatial correlation between two rainfall gauge stations, follow the two-step procedure proposed by Ciach and Krajewski [36]. First, the Spearman rank correlations are calculated for each station pair, taking into consideration the time series of rainfall data:

$$\rho_s = 1.0 - \frac{6\sum {d_i}^2}{N^3 - N}$$

The Spearman rank correlation was used to detect the gauge pairs because the hourly rainfall are not normal distribution, in this way, the inter gauge correlation value for each gauge pair [37](separated by a specific distance) may be obtained and then fitted to the correlation model by the correlation-distance data samples:

$$\rho_g(d) = c_0 \exp\left[-\left(\frac{d}{d_0}\right)^{s_0}\right] - a_0$$

In this formula, c_0, d_0, s_0, and a_0 are model parameters to be estimated, and d is the separation distance for the two stations. Parameter c_0 is usually called the nugget parameter, interpreting the correlation value for near-zero distance, and it always approximates but never equals 1 because of measurement noises; d_0 represents the typical correlation scale and is called the scale parameter, and s_0 is the shape parameter. And the negative correlation situation is considered to by parameter a_0.

The separation distance of two different stations ranges from 3 to 475km in the study area. Dynamic programming is used to optimize parameters in the equation above. There are four parameters in the formula. Firstly, the d_0 parameter should less than the max d of the two gauges (about 500km). S_0 parameter should be from 0 to 2 based on the previous studies; A_0 should not be bigger than the absolute value of the minimum value in the correlations. The value of c_0 should not be bigger than the a_0 in order to the crest value of all the correlation values not bigger than 1. All this four parameters are involved in the optimization, and the objective is to minimize the RMSE of model fitting.

The result of the parameter optimization are shown in the Table 4. And the spatial correlation structure in different time scales are shown in the Figure 5, labelled with the optimal parameters.

The optimal result of c_0 is 0.83 and a_0 is 0.1 in the 1 hour precipitation. The 6 hour result of c_0 is 1.01 and a_0 is 0.08. The difference between c_0 and a_0 is about 1.0. This shows the fact that the measurements of precipitation at shorter time scales could contain noise which makes the difference between c_0 and a_0 deflect away from the theoretical value. And this noise can be filtered out with the time intervals of rainfall increasing. Figure 8a shows that the separation distance d_0 of the study watershed of 1 hour precipitation is about 27.6 km and the shape parameter is 0.53. Thus, the fitting correlation curve rapidly fall off with the decreases of distance. The correlation value falls below 0.2 when the distance between two gauges is greater than 100km. It is shown that, the correlation of hourly rainfall is influence by the local terrains. Comparing the fitting results at different selected time scales, it is found that the parameters of the spatial correlation structure will change with the time scale, (Figure 8). With the increase of time scale, the correlation scale of distance parameter d_0 also increased. This shows that the correlation between rainfall gauges of the site will increase with the increase in time scale. The observation of rainfall on finer time scales, would include the influence of many local and short duration rainfall process. With the increasing of accumulate rainfall scale time, the control of the weather process is increased. And the spatial correlation coefficients are also increased accordingly.

TABLE 4
The optimized parameter results of spatial analysis

Time	c_0	d_0(km)	s_0	a_0	RMSE
1 hour	0.83	27.6	0.53	0.10	0.07
6 hour	1.01	79.0	0.58	0.08	0.10
12 hour	1.10	120.1	0.52	0.11	0.11
24 hour	1.24	149.5	0.44	0.26	0.13
1 hour dry season	0.87	23.2	0.52	0.12	0.17
1 hour rainy season	0.72	49.9	0.43	0.09	0.06

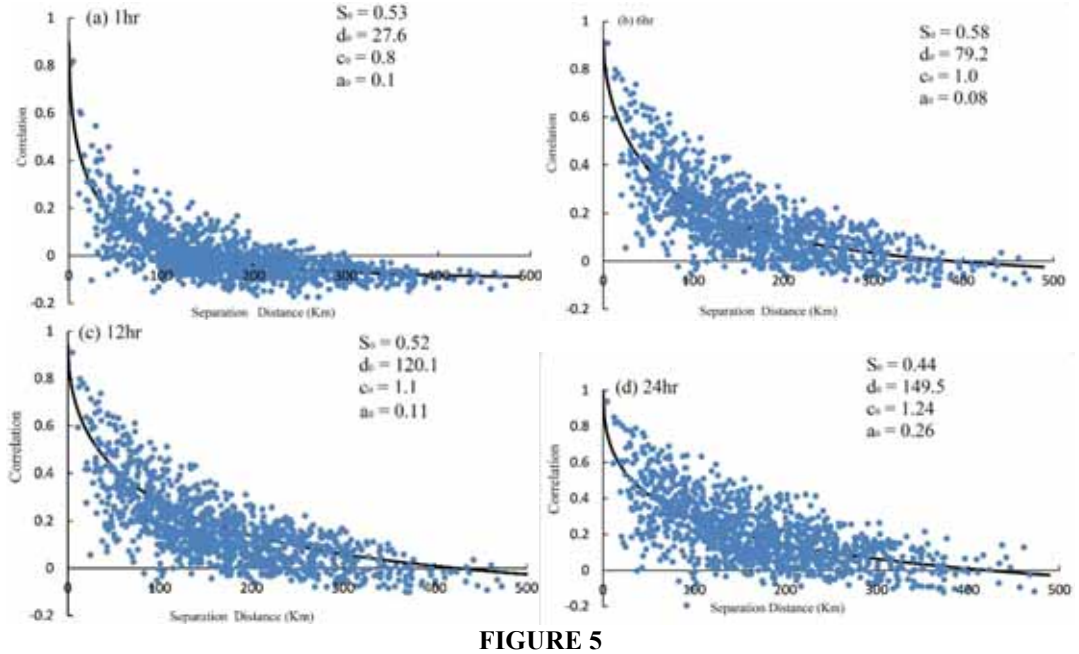

FIGURE 5
Spatial correlation structure of (a) 1-, (b) 6-, (c) 12- and (d) 24-h rainfall in the Upper Reach of Hanjiang River Basin during 2012–2016.

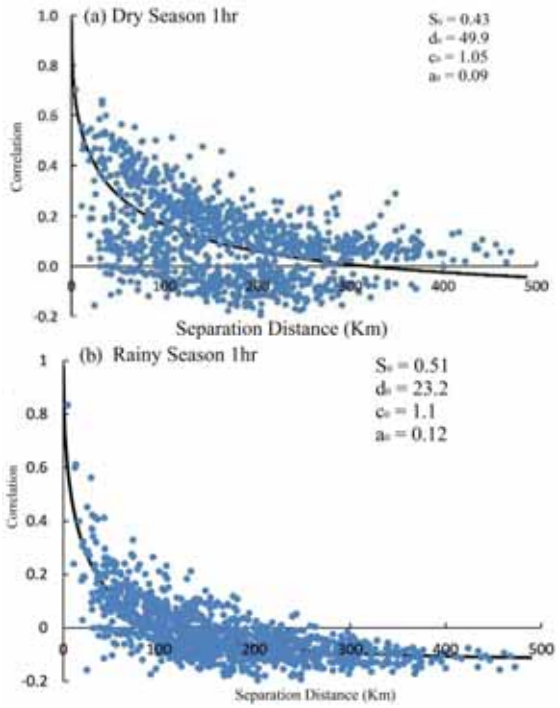

FIGURE 6
Spatial correlation structure of hourly rainfall in the (left) dry season and (right) rainy season

Previous studies have indicated that, rainy season and cold season are usually controlled by different scale weather systems [38, 39]. For example, the rainy season rainfalls are mostly from storm weather process, influenced by the local convective weather process. In the dry season, rainfall is mainly controlled by the strati form cloud, mainly affected by the large scale atmospheric circulation. In this study, rainy season is controlled by the Southwest warm and low pressure and the Western Pacific subtropical high pressure zone. Therefore, by separating the whole year hourly rainfall into two seasons, (rainy season (May-Oct) and dry season (Nov-Apr)) It was possible to analyse the spatial correlation structure of hourly rainfall during two seasons.

As can be seen from Figure 6 and Table 4, the scale parameter (d_0) in the rainy season is less than a half of the scale parameter in dry season. It is 23.2km in the rainy season but 49.9km in dry season. The shape parameter which is 0.51 in the rainy season, is closer to the 1-year shape parameter in the dry season. It can be seen that the difference of the spatial correlation scale between the study watershed in the rainy season and the dry season is very significant and that the weather of rainy season is similar to the whole year weather's distribution. In the rainy season, a lot of prominent local features can be observed, because of the monsoon climate and the convective heavy rainfall.

The whole study area is 59155 km^2, and there are 48 gauge stations in the study. Therefore, the average representative area of the existing ground gauge stations is about 1232 km^2, using the method of average apportionment. The distance between two stations (35.1 km), is bigger than the scale parameter of rainy season (23.2km), but it is less than the other scale parameters. It can be concluded that when the averaging time interval is longer, both shape parameter and correlation distance are larger, (Table 4). The RMSE result of the rainy season in 1 hour is 0.07, and its correlation value is 0.52. Thus, although the existing ground rainfall observation station network has a relatively high density, it may not be able to capture the seasonal rainfall in the study area of the local storm centre. It is necessary to build new gauge stations or develop high resolution remote sensing rainfall monitoring technology.

DISCUSSION

This study detected the spatiotemporal variations of hourly rainfall in the upper reaches of Hanjiang River Basin. It also analysed several features of hourly rainfall, including spatial variations of summary statistics (mean, coefficient of variance, rainfall occurrence, conditional mean rainfall, skewness and kurtosis) and regionalization of the diurnal cycle. To analyse the spatial distribution of the whole watershed, spatial correlation is taken into consideration in this study.

The main findings and conclusions are as follows:

Hourly rainfall in the upper reaches of Hanjiang River Basin must have been influenced by the geographic information, especially the frequency. It has a significant negative correlation with the longitude, latitude and elevation. The whole watershed can be separated into four regions: the upstream mountain area, the downstream mountain area, the north side of the midstream and the south side of the midstream. In the four streams, the upstream and the south of the midstream are confronted with the continuous daily rainfall, especially in the autumn. The other two streams are drier, but they faced the bigger hourly rainfall in summer. It means that the other two streams have the threat from the short time rain storm in summer.

The monsoon climate and local terrain information both affect the local short-time rainfall. From 1 hour to 6 hours, the maximum rainfall shows large values in the upper reaches of the whole watershed and the northeast mountains. The monsoon climate is the primary cause of the continuous rainfall in autumn.

In the rainfall temporal distribution part, the MPA and MPF occurs in the midnight in the south part of the whole watershed. Rainfall from rainy season decides the whole year rainfall distribution. In the summer midnight, the temperature suddenly drops in one or two hours, in the mountainous area. It is the most necessary condition for the formation of rainstorm. It is also the main reason that the storm

centre located in the mountainous area.

The study found that the distance scale parameter d_0 of hourly rainfall is about 30km in the study area. Further, the season factor play important effects in the spatial correlation. The spatial correlation coefficients are also increasing with the increasing of accumulate rainfall scale time. In the past studies, Rebort J. Allen [40] suggested that the ARF (Areal reduction factors) can be satisfactorily transposed to different area. In his study, the optimum value of rain station density in North California and NJ ranged from 200 to 500 Km^2 per station. Anoop Kumar Mishra [41] launches research on the rain gauge density in Bangalore, India. The study finds small errors are reported while considering 4 to 7 in a 50 km×50km box area. They can prove the same conclusion with our study.

The results presented in our article emerge the distributions of the rainfall regime from the viewpoints of quantitative and qualitative in the upper reaches of Hanjiang watershed. Conclusions in this study can be advantageous to the local hydrological applications.

Periodically in more than 4 years and inter annual variation cannot be detected in our study limited to data. We only concern about the recent potential impacts of rainfall in the study area. The shortage of the rainfall data will limit our study in the decadal variations of rainfall and lead to unreasonable assessment. Though the rainfall shows an obvious change from year to year, the analysis method and the spatiotemporal distribution is consistent to a certain extent. The temporal distribution in a day may be changed by a heavy rainfall, but the spatial distribution and spatial correlation analysis is sustainable. This show the rainfall in day timescale should not be depicted comprehensive and intensive only using these four-year data. The sub-daily rainfall distribution is complicated by the alternate monsoon from year to year. However, the analysis methods and the statistic characteristics can be applied to the future study, when the long-term and elaborate data can be used.

ACKNOWLEDGEMENTS

This paper was jointly supported by National Key Technology R&D Program of the Ministry of Science and Technology (2013BAB05B05, 2015BAB07B03), National Natural Science Foundation of China (51579248), Beijing Municipal Science and Technology Project (Z141100006014049) and State Key Laboratory of Simulation and Regulation of Water Cycle in River Basin (2016CG05).

REFERENCES

[1] Gao, J., Holden J. and Kirkby, M. (2016) The impact of land-cover change on flood peaks in peatland basins. Water Resources Research. 52, 3477-3489.

[2] Chen, X., Hao, Z., Devineni, N. and Lall, U. (2013) Climate information based streamflow and rainfall forecasts for Huai River basin using hierarchical Bayesian modeling. Hydrology & Earth System Sciences Discussions. 10(9), 11559-11584.

[3] Li, D., Sun, J., Fu, S., Wei, J., Wang, S. and Tian, F. (2016) Spatiotemporal characteristics of hourly precipitation over central eastern china during the warm season of 1982–2012. International Journal of Climatology. 36(8), 3148-3160.

[4] Jiang, P., Yu, Z., Gautam, M.R. and Acharya, K. (2016) The Spatiotemporal Characteristics of Extreme Precipitation Events in the Western United States. Water Resources Management. 30, 4807-4821.

[5] Zhang, Q., Jiang, T., Gemmer, M. and Becker, S. (2005). Precipitation, temperature and runoff analysis from 1950 to 2002 in the yangtze basin, china. Hydrological Sciences Journal. 50(1), 65-80.

[6] Yang, W., Zhang, L., Shan, L., Chen, X. and Yang, Y. (2015) Spatiotemporal distribution features of extreme hydrological events in the hanjiang river basin. Progressus Inquisitiones De Mutatione Climatis. 11(1) ,15-21.

[7] Morin, E., Goodrich, D.C., Maddox, R.A., Gao, X., Gupta, H.V. and Sorooshian, S. (2006) Spatial patterns in thunderstorm rainfall events and their coupling with watershed hydrological response. Advances in Water Resources. 29(6), 843-860.

[8] Sorooshian, S., Aghakouchak, A., Arkin, P., Eylander, J., Foufoulageorgiou, E., Harmon, R. Hendrickx, Jan, M. H., Bisher, I., Kuligowski, R., Skahill, B., and Gail, S. J., (2011) Advanced concepts on remote sensing of precipitation at multiple scales. Bulletin of the American Meteorological Society. 92(10), 1353-1357.

[9] Aghakouchak, A., Bárdossy, A. and Habib, E. (2010) Conditional simulation of remotely sensed rainfall data using a non-gaussian v-transformed copula. Advances in Water Resources. 33(6), 624-634.

[10] Gao, Y.C., Liu, M.F. (2013) Evaluation of high-resolution satellite precipitation products using rain gauge observations over the tibetan plateau. Hydrology & Earth System Sciences. 17(2), 837-849..

[11] Minjarezsosa, C.M. (2013) Improved quantitative precipitation estimation over complex terrain using cloud-to-ground lightning data. Dissertations & Theses - Gradworks.

[12] Bitew, M.M., Gebremichael, M., Ghebremichael, L.T. and Bayissa, Y.A. (2012) Evaluation of high-resolution satellite rainfall products through streamflow simulation in a hydrological modeling of a small mountainous watershed in ethiopia. Journal of Hydrometeorology. 13(1), 338-350.
[13] Sundriyal, Y.P., Shukla, A.D., Rana, N., Jayangondaperumal, R., Srivastava, P., Chamyal, L.S., Sati, S.P., Juyal, N. (2015) Terrain response to the extreme rainfall event of June 2013: Evidence from the Alaknanda and Mandakini River Valleys, Garhwal Himalaya, India. Episodes. 38(3), 179-188.
[14] Dolciné, L., Andrieu, H., Sempere-Torres, D., Creutin, D. (2001) Flash flood forecasting with coupled precipitation model in mountainous mediterranean basin. Journal of Hydrologic Engineering. 6(6), 1-10.
[15] Guo, J., Guo, S.L., Zhang, J., Chen, H. and Chen, G.Y. (2009) Prediction of rainfall and runoff changes in the hanjiang basin. Journal of China Hydrology. 29(5), 18-22.
[16] Chen, Y.F., Zhang, X. (2011) Distribution of continued rainy days in hanjiang river basin. Resources & Environment in the Yangtze Basin. 20(6), 744-748.
[17] Burton, A., Fowler, H.J., Blenkinsop, S. and Kilsby, C.G. (2010) Downscaling transient climate change using a neyman–scott rectangular pulses stochastic rainfall model. Journal of Hydrology. 381(1–2), 18-32.
[18] Kangas, M., Rontu, L., Fortelius, C., Aurela, M., and Poikonen, A. (2016) Weather model verification using sodankylä mast measurements. Geoscientific Instrumentation Methods & Data Systems. 5(2), 577-598.
[19] Buytaert, W., Celleri, R., Willems, P., Bièvre, B.D., and Wyseure, G. (2006) Spatial and temporal rainfall variability in mountainous areas: a case study from the south ecuadorian andes. Journal of Hydrology. 329(3), 413-421..
[20] Mishra, A.K., and Coulibaly, P. (2009) Developments in hydrometric network design: a review. Reviews of Geophysics. 47(2), 2415-2440.
[21] Braud, I., Ayral, P.-A., Bouvier, C., Branger, F., Delrieu, G., Dramais, G. Le Coz, J., Leblois, E., Nord, G. and Vandervaere, J.-P. (2016) Advances in flash floods understanding and modelling derived from the floodScale project in South-East France. E3S Web of Conferences. 7, 04005, 3-10.
[22] Zhang, Y., Huang, C.C., Pang, J., Zha, X., Zhou, Y. and Gu, H. (2013) Holocene paleofloods related to climatic events in the upper reaches of the hanjiang river valley, middle yangtze river basin, China. Geomorphology. 195(195), 1-12.
[23] Zhang, Y., Huang, C.C., Pang, J., Zha, X., Zhou, Y., Yin, S., and Juan, W. (2012) Comparative study of the modern flood slackwater deposits in the upper reaches of hanjiang and weihe river valleys, China. Quaternary International. 282(60), 184-191.
[24] Zheng, X., Lu, F. and Ma, J. (2013) Hanjiang river basin precipitation multiple time scales characteristics and with circulation factors correlation analysis. Advances in Earth Science. 28(5), 618-626.
[25] An-Yan, H.U., Liu, X.H. and Jiang, L. (2009). Change-points analysis of hydrological series in the hanjiang river basin. Journal of Irrigation & Drainage. 28(6), 128-115.
[26] Zhao, F. and Shepherd, M. (2011). Precipitation changes near three gorges dam, china. part i: a spatiotemporal validation analysis. Journal of Hydrometeorology. 13(2), 735-745.
[27] He, H., Zhou, J., Peart, M.R., Chen, J. and Zhang, Q. (2012) Sensitivity of hydrogeomorphological hazards in the qinling mountains, china. Quaternary International. 282(1), 37-47.
[28] Chen, H., Xu, C.Y. and Guo, S. (2012) Comparison and evaluation of multiple gcms, statistical downscaling and hydrological models in the study of climate change impacts on runoff. Journal of Hydrology. 434–435, 36-45.
[29] Amdisen, A. and Amdisen, A. (1987) Pearson's correlation coefficient, p -value, and lithium therapy. Biological Psychiatry. 22(7), 926-8.
[30] Pirie, W. (2006) Spearman Rank Correlation Coefficient. 285.
[31] Cohen, J. (1988) Statistical power analysis for the behavioral sciences. Journal of the American Statistical Association. 2nd(4), 19–74.
[32] Rouault, M., Roy, S.S., Balling Jr., R.C. (2013) The diurnal cycle of rainfall in South Africa in the austral summer. International Journal of Climatology. 33(3), 770–777.
[33] Tumbo, M. and Hughes, D.A. (2015) Uncertain hydrological modelling: application of the pitman model in the great ruaha river basin, tanzania. Hydrological Sciences Journal. 60(11), 2047-2061.
[34] Balin, D., Hyosang, L., Rode, M. (2010) Is point uncertain rainfall likely to have a great impact on distributed complex hydrological modeling?. Water Resources Research. 46(11), 3439-3445.
[35] Haile, A.T., Rientjes, T., Gieske, A., Gebremichael, M. (2009) Rainfall variability over mountainous and adjacent lake areas: the case of lake tana basin at the source of the blue nile river. Journal of Applied Meteorology & Climatology. 48(8), 1696-1717.
[36] Ciach, G.J., Krajewski, W.F. (2006) Analysis and modeling of spatial correlation structure in small-scale rainfall in central oklahoma. Advances in Water Resources. 29(10), 1450-1463.

[37] Li, Z., Yang, D., Hong, Y., Zhang, J., Qi, Y. (2013) Characterizing spatiotemporal variations of hourly rainfall by gauge and radar in the mountainous three gorges region. Journal of Applied Meteorology & Climatology. 53(4), 873-889.
[38] Mao, H.M. (2008) Trmm rainfall applied in flow prediction of lshm in upper hanjiang river basin. Express Water Resources & Hydropower Information. 29(8), 22-26
[39] Xu, Y.P., Yu, C., Zhang, X., Zhang, Q., Xu, X. (2012) Design rainfall depth estimation through two regional frequency analysis methods in hanjiang river basin, china. Theoretical & Applied Climatology. 107(3-4), 563-578.·
[40] Allen, R.J., Degaetano, A.T. (2005) Areal reduction factors for two eastern united states regions with high rain-gauge density. Journal of Hydrologic Engineering. 10(4), 327-335.1
[41] Mishra, A.K. (2013) Effect of rain gauge density over the accuracy of rainfall: a case study over Bangalore, India. Springerplus. 2(1), 1-7.

Received: **26.05.2017**
Accepted: **09.11.2017**

CORRESPONDING AUTHOR

Xiaohui Lei
State Key Laboratory of Simulation and Regulation of Water Cycle in River Basin,
China Institute of Water Resources and Hydropower Research,
Beijing, 100038 – P.R. China.

e-mail: lxh@iwhr.com

© by PSP Volume 27 – No. 2/2018 pages 1226-1231 Fresenius Environmental Bulletin

EFFECT OF RELATIVE HUMIDITY ON HUMAN INDUCED RESUSPENSION OF PARTICLES

Shuihua Zheng*, Lipan Zhao, Weiyuan Du, Yunqing Gu, Jiegang Mou, Jiaxin Tang

College of Mechanical Engineering, Zhejiang University of Technology, Hangzhou 310014, China

ABSTRACT

In order to study the effect of relative humidity on human induced resuspension of particles, the experimental study was carried out with the resuspension of different size of particles in the laboratory at the relative humidity of 40%, 60% and 80% respectively and the ground material is low level loop pile carpet. The results show that when the relative humidity is 40%, 0~5μm particles suspended concentration and the suspension rate is higher. When the relative humidity increasing continuously, the suspended concentration and the suspension rate of 0~5μm particles decreased and the 5~10μm particles increased. In addition, under the condition of high relative humidity, small particles reduced because of various reasons.

KEYWORDS:
Particulate matter, resuspension, relative humidity, suspension rate, human walking

INTRODUCTION

With the increase of the time of indoor human activity, urban residents spend nearly 90% of their time indoors [1, 2] and pay more attention to indoor air quality. The current domestic and foreign scholars have studied a lot on the factors affecting the air quality and there are many reports on the dynamics of aerosol particles in indoor environment. However, there are few studies on the resuspension of surface sediments. Indoor particulate matter is mainly derived from the infiltration of outdoor environment, ventilation and indoor human and animals' activities. These particles carry viruses, carcinogens and allergens etc. [3, 4], which will cause the body's discomfort. The indoor human walking and cleaning will increase the concentration of indoor particles [5, 6]. In recent years, there are a lot of scholars have found that indoor human walking is an important cause of particle resuspension [7, 8]. Luoma et al. [9] placed a certain amount of particles in a non-smoking room and studied the resuspension of them by human walking. The results showed that walking was the reason for the particle concentration change of 24% ~ 55% particles whose size is 1~25μm. Ferro et al. [10] used five different floor materials and different relative humidity separately to analysis the resuspension of particles induced by human walking. It was found that the difference of resuspension fraction of particles between carpet and floor is not obvious when the particle size in 0.4~3μm and the particle resuspension fraction of carpet is larger than that of the floor when the particle size in 3~10μm. Besides, with the increase of relative humidity, the resuspension rate of particles on the high-density carpet increased.

Although Ferro et al. [10] have studied the resuspension of particles induced by human walking under different relative humidity, but the range of relative humidity is not wide enough and there is no detailed study on the suspension of particulates under high relative humidity conditions. Based on this, this paper expands the range of relative humidity, through experimental method, aiming at high humidity conditions to study the effect of human walking on resuspension of different size of particles deeply on low level loop pile carpet in indoor environment. The results presented here can be used to assess the impact of these factors on human walking caused resuspension of particles. This will provide some experimental basis for improving indoor environment quality.

EXPERIMENTAL EQUIPMENT AND METHODS

Arrangement of experimental area. The experiment was carried out in a closed chamber (length × width × height=6m×3.6m×3.5m), as shown in Figure 1. The entrance of chamber is only one door and no windows and the top of the chamber is equipped with a central air conditioning which is used to regulate the temperature of the chamber. There is a humidity controller in the lower left corner which can automatically adjust the indoor humidity according to setting. The ground of the chamber is divided into three parts on average and the width of every part is 1.2m. The middle area is the experimental area and the rest of the area is non-experimental. The experimental area is placed with low level loop pile carpet and the ground material could be replaced according to the

experiment. Other instruments such as laser dust monitor and humidity controller were placed in the non-experimental area.

The LD-5 Laser Dust Monitor was used in the experiment, it can read out the mass concentration of dust directly. During the experiment, two laser dust monitors were placed on each side of the experimental area, and total four laser dust Monitors. The distance between the two laser dust monitors on each side is 0.5m and the laser dust monitor is 1.75m from the edge of the walking area. Besides, the distance between the four laser dust monitors and the ground is 1m. The cutting heads of PM1, PM2.5, PM5 and PM10 are placed on the laser dust monitors respectively, which can constantly measure the concentration of different particle size in the air of 1m high from the ground.

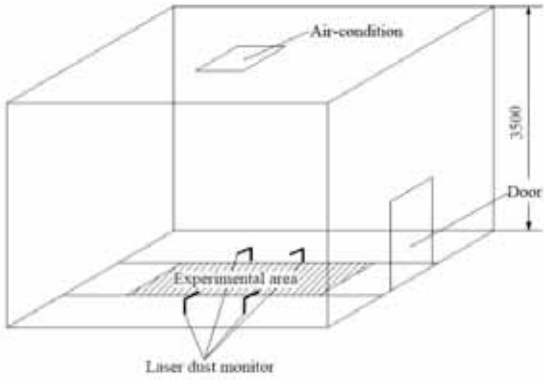

(a) The three-dimensional sketch map of the chamber

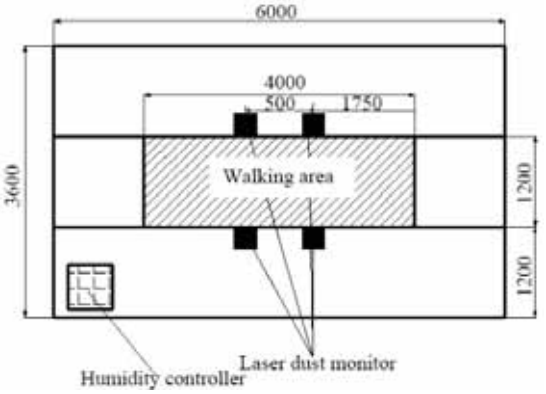

(b) The floor layout of the chamber

FIGURE 1
Layout of the chamber

Experimental scheme design. The experimental procedure is shown in Table 1, the experiment started within 30 minutes before the start of the test without any treatment. It is time to start the timer when opening the laser dust monitor, when t=0~5min, no treatment, the laser dust meter began to monitor the natural state of the particle concentration in the air. When t=5~10min the experimenter started walking around in the experimental area and the experimenter was a male, height 178cm, weight 76kg and walking steps per minute for 90 steps. When t=10~20min, the experimenter left the experimental area to make the particulate matter to settle down. When t=20~25min, the experimenter entered the experimental area again, moving in the same way. When t=25~90min, the experimenter left the experimental area. During the whole process, the temperature was controlled in 25±0.5℃ and the relative humidity was controlled in 40%±0.5%、60±0.5% or 80±0.5% according to the requirements of the experimental conditions. The laser dust detector works continuously when t=0~90min to monitor the concentration of particles in the air.

Ground material arrangement. On the carpet, the particles were broadcast with an improved dust spreading device based on the screen, and the seeding density of the particles on the carpet is 20g/m^2. The particles are hydrophobicity. The relevant parameters of the particles are detailed in Table 2 and Table 3.

Estimation method of suspension rate. In order to quantitatively describe the resuspension of particle, a suspension rate r [11] is introduced. Suspension rate refers to the ratio of the particles in the air which suspended from the naked ground instantly and initial deposition density of ground particles. It describes the process of the change of particle suspension with time relative to a certain deposition density. The formula is:

$$r = \frac{R}{L} \qquad (1)$$

Where R is the resuspension flux and L is the surface concentration of the species. The resuspended flux represents the number or mass of particles suspended from per unit area per unit time.

TABLE 1
Experimental Procedure

t/[min]	Action
-30~0	No walk, no laser dust monitor was started
0~5	No walk, the laser dust monitor was started
5~10	The experimenter walked
10~20	No walk, natural sedimentation
20~25	The experimenter walked
25~90	No walk, natural sedimentation

TABLE 2
The chemical composition of ISO 12103-1 A1 Ultrafine Test Dust A1

Chemical composition	Weight percentage (%)
$Si0_2$	68 - 76
Al_20_3	10 - 15
Fe_20_3	2 - 5
Na_20	2 - 4
Ca0	2.0 - 5.0
Mg0	1.0 - 2.0
$Ti0_2$	0.5 - 1.0
K_20	2.0 - 5.0

TABLE 3
ISO 12103-1 A1 Ultrafine Test Dust A1 Particle Distribution (Volume percentage is less than)

Diameter (μm)	Volume percentage is less than (%)
1	1.0~3.0
2	9.0~13.0
3	21.0~27.0
4	36.0~44.0
5	56.0~64.0
7	83.0~88.0
10	97.0~100

Ethical Statement. All subjects gave their informed consent for inclusion before they participated in the study. The study was conducted in accordance with the Declaration of Helsinki, and the protocol was approved by the Ethics Committee of Zhejiang University of Technology (H15-091021).

RESULTS AND DISCUSSION

As shown in Figure 2, when the RH=80%, the variations of the suspended concentration of particles with different diameter vary with time in the whole experiment process and the C represents the concentration of suspended particles. The reason why there are some particles suspended in air when t=0~5min is that the experimenter placed experimental equipment and materials. The concentration of particles in the air increased rapidly when t=5~10min and t=20~25min because of the movement of researcher in the experimental area. The suspended particle concentrations are higher in the second movement phase of the researcher, relative to the peak of the first movement phase. When the researcher left the experimental area, the concentration of particles decreased rapidly and the rate of decline began to slow down until reached a certain value. Therefore, it is possible for the indoor human body moving to cause the resuspension of the ground particles and increase the concentration of the particles in the air. In addition, the particle concentration of 5~10μm particles was the highest and the concentration of suspended particles increased rapidly when the experimenter was moving. The sedimentation speed of 1.0~2.5μm particles was the fastest. In the case of natural sedimentation, the suspended concentration can rapidly decrease and reach a steady state.

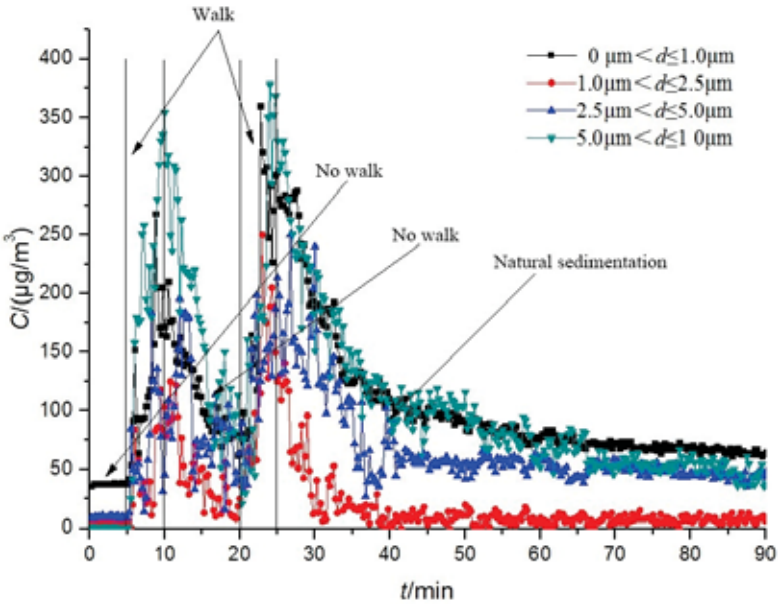

FIGURE 2
Variation of mass concentration of different sizes of particles in air

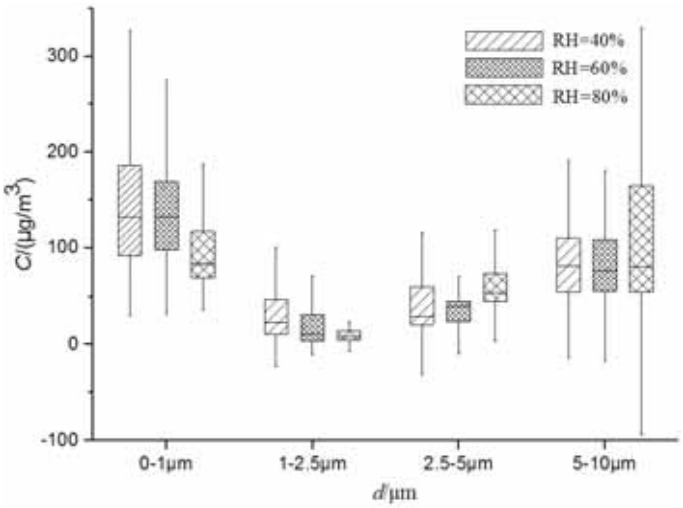

FIGURE 3
Variation of suspended concentration of different sizes of particle caused by human walking under different relative humidity

Figure 3 describes the effects of different relative humidity conditions on the concentration of different size of suspended particles induced by human walking. It took total three different relative humidity RH=40%, RH=60%, RH=80%, the other conditions are the same as before. It can be seen from the figure that under the same relative humidity condition, the particle suspended concentration among the range of particle size d=0~1μm and d=5~10μm is larger than the other size particles. With the increase of relative humidity, the suspended particles concentration in the range of 0~1μm particles decreases and the floating range decreases. On the contrary, the suspended particles concentration among the range of d=2.5~5μm and d=5~10μm increased in varying degrees. From the Figure 4 we can obviously see that in the high relative humidity RH = 80%, the floating range of suspended particles concentration when particle size in d=5~10μm increases a lot. Fig.4 is the variation of concentration of different size of suspended particles under different relative humidity conditions. It can be seen that in the case of high relative humidity, the concentration of 0~1μm particle is lower than that in the case of low relative humidity no matter human walking or natural sedimentation, it changes little when particle size d=1~2.5μm. For large particle size d=2.5~10μm, the change of its suspension concentration with the change of relative humidity is contrary to the particle size d=0~1μm. When the relative humidity is high, the concentration of suspended particles is larger, which decreases with the decrease of relative humidity. It can be seen that with the increase of relative humidity, the suspension concentration of small size of particle will decrease, but the large size of particle will increase. The main reason is that relative humidity affects the surface properties of particles. The main force between particles is changed from weak van der Waals force to strong liquid bridge force. When the particles collide with each other, the phenomenon of coagulation occurs. Small size of the particles will be condensed into larger size of particles. So in the case of high relative humidity, the suspension concentration of big size of particle is larger.

It can be seen from Figure 5 that the order of magnitude of suspension rate r of different size of particles is in the range of 10^{-5} to 10^{-4} hr^{-1}. Thatcher et al. [12] measured the suspension rate of particles in a house where four people were normally active and found that the rate of suspension of very small size of particle was between 10^{-5} and 10^{-4} hr^{-1} and when the particles size is 0.4~1μm, the suspension rate was $10^{-7}hr^{-1}$. Qian et al. [13] measured the suspension rate of PM10 induced by one person walking on the carpet in a house and made 14 experiments with an average suspension rate of 10^{-4}. Thus, the order of magnitude of experimental data is correct. The figure5 show that the suspension rate of particles with particle size d=1~2.5μm is larger than that of the other two groups when RH = 40%. The suspension rate began to decrease when the relative humidity increased, but the suspension rate of particles whose size is d=2.5~5μm and d= 5~10μm increased especially the particle size d=2.5~5μm increased obviously. When RH=80%, the suspension rate of small size of particles is less than the large size of particles. It can be seen that the small size of particles are easy to suspend and when the relative humidity increased, the suspension rate of big size of particles will increase. This result is in agreement with the result of previous analysis. It is basically because of the increase of relative humidity, small size of particles reduced due to various reasons, such as condensed into large particles or sticking on the carpet. The variation range of suspension rate of particles whose size is d=5~10μm is smaller than the particle size is d=2.5~5μm.

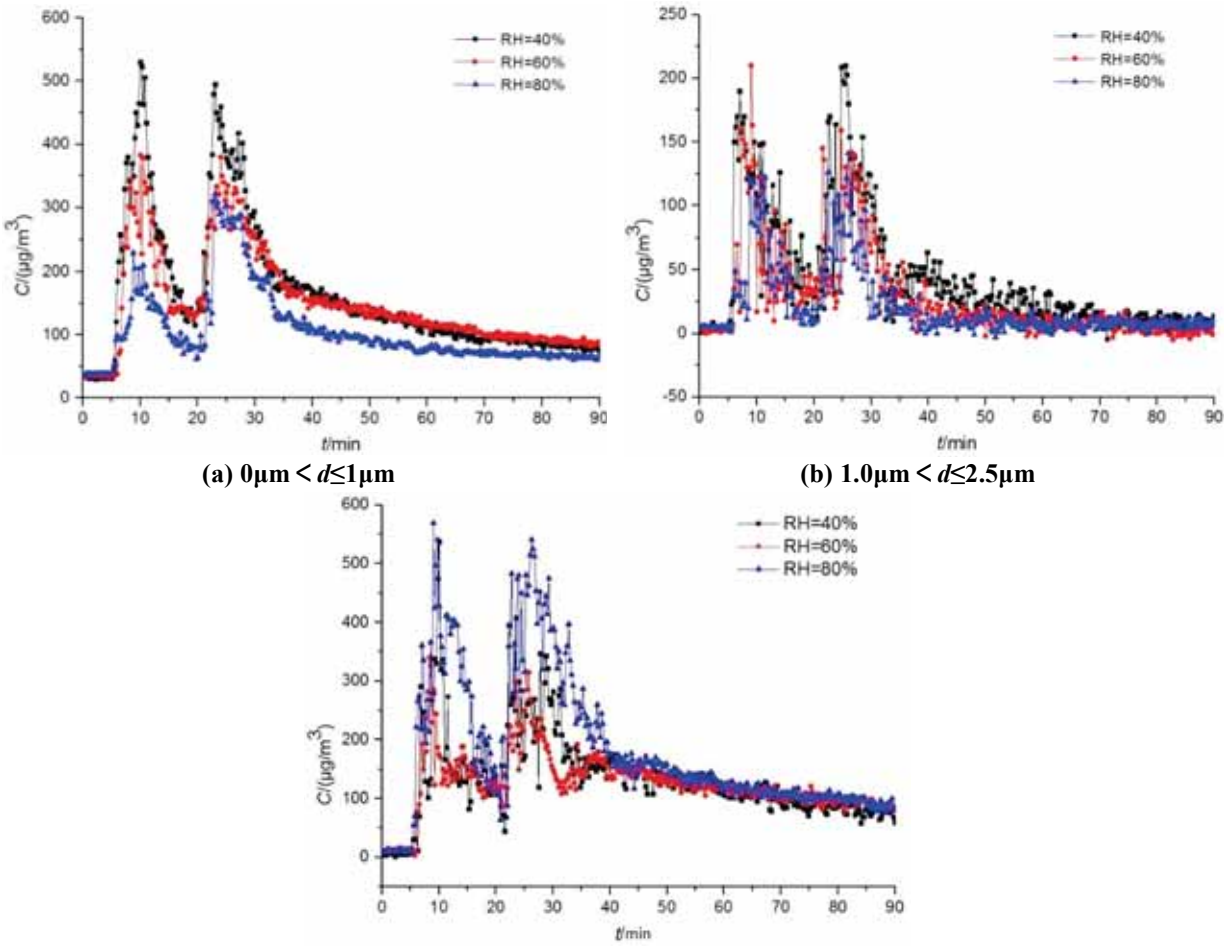

(a) 0μm < *d*≤1μm **(b) 1.0μm < *d*≤2.5μm**

(c) 2.5μm < *d*≤10μm

FIGURE 4
Variation of suspended concentration of particle with time under different relative humidity

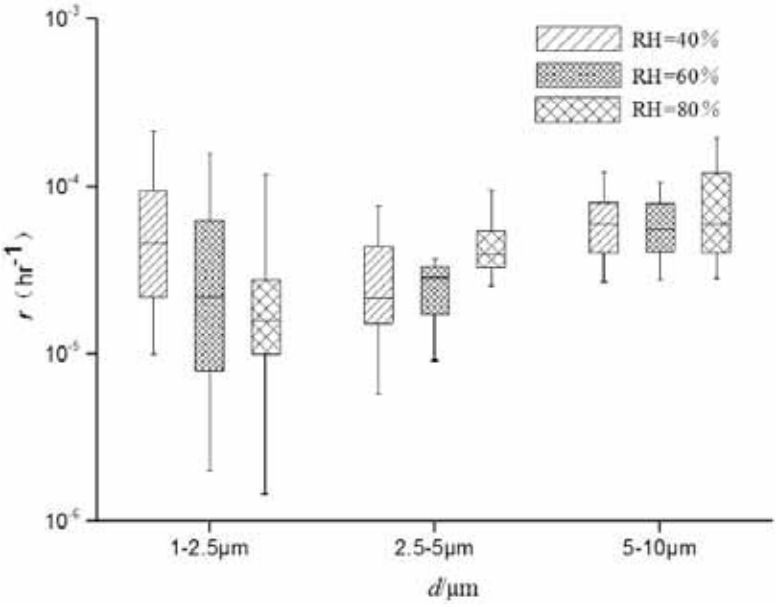

FIGURE 5
Variation of suspension rate of different size of particles induced by human walking under different relative humidity

CONCLUSIONS

Indoor human walking will cause the resuspension of particles, resulting in the increase of concentration of particles in indoor air. In the case of RH = 40%, human walking easily leads to resuspension of 0~5μm particles and the concentration of suspended particles is larger than that of 5~10μm particles. The suspension concentration of small size of particles will decrease when the relative humidity increases. In the case of RH=80%, small size of particles reduced due to various reasons, such as condensed into large size of particles due to the change of the surface property of the particles, resulting in the decrease of the suspension concentration and the suspension rate. When the relative humidity increases, the suspension concentration of 0~5μm particles will decrease, the suspended concentration and suspension rate of 5~10μm particles will increase.

ACKNOWLEDGEMENTS

This work was fully supported by a grant from the Project "Numerical and Experimental Study on Particulate Resuspension and Transport Due to Human Walking in Indoor Environment supported by National Natural Science Foundation of China" [Project number 51476144].

REFERENCES

[1] Jenkins, P.L., Phillips, T.J., Mulberg, E.J., Hui, S.P. (1990) Activity patterns of Californians: use of and proximity to indoor pollutant sources. Atmospheric Environment. part A. general Topics. 26(12), 2141-2148.

[2] Robinson, J., Nelson, W. (1995) National human activity pattern survey data base. U.S. EPA, Research Triangle Park, NC.

[3] Lioy, P.J., Freeman, N.C.G., Millette, J.R. (2002) Dust: a metric for use in residential and building exposure assessment and source characterization. Environmental Health Perspectives. 110(10), 969-983.

[4] Raja, S., Xu, Y., Ferro, A.R., Jaques, P.A., Hopke, P.K. (2010) Resuspension of indoor aeroallergens and relationship to lung inflammation in asthmatic children. Environment International. 36(1), 8-14.

[5] Fish, B.R., Walker, R.L. and Royster, G.W. (1967) Resuspension of settled particulates in Surface Contamination. Gatlinburg, Tennessee, Oxford, 75-82.

[6] Jones, I.S., Pond, S.F. (1967) Surface Contamination: Some experiments to determine the resuspension factor of plutonium from various surfaces. Elsevier Ltd. 83-92.

[7] Choi, S.J. (2008) The effect of outdoor air and indoor human activity on mass concentrations of size-selective particulate in classrooms. Journal of Biological Chemistry. 34(2), 6786-92.

[8] Ferro, A.R., Kopperud, R.J., Hildemann, L.M. (2004) Source strengths for indoor human activities that resuspend particulate matter. Environmental Science & Technology. 38(6), 1759.

[9] Luoma, M., Batterman, S.A. (2001) Characterization of particulate emissions from occupant activities in offices. Indoor Air. 11(1), 35.

[10] Qian, J., Ferro, A.R. (2008) Resuspension of dust particles in a chamber and associated environmental factors. Aerosol Science & Technology. 42(7), 566-578.

[11] Slinn, W.G.N. (1978) Parameterizations for resuspension and for wet and dry deposition of particles and gases for use in radiation dose calculations. Nuclear Safety. 19, 205–219.

[12] Thatcher, T.L., Layton, D.W. (1995) Deposition, resuspension, and penetration of particles within a residence. Atmospheric Environment. 29(13), 1487-1497.

[13] Qian, J., Ferro, A.R., Fowler, K.R. (2008) Estimating the resuspension rate and residence time of indoor particles. Journal of the Air & Waste Management Association. 58(4), 502-516.

Received: **14.07.2017**
Accepted: **12.12.2017**

CORRESPONDING AUTHOR

Shuihua Zheng
College of Mechanical Engineering,
Zhejiang University of Technology,
Hangzhou 310014 – China

e-mail: zneu@zjut.edu.cn

© by PSP Volume 27 – No. 2/2018 pages 1232-1239 Fresenius Environmental Bulletin

DETERMINATION OF MITE SPECIES ON VINEYARDS OF ANKARA, TURKEY

Emre Inak*, Sultan Cobanoglu

Ankara University Agricultural Faculty, Plant Protection Department, Acarology Lab., 06110 Ankara, Turkey

ABSTRACT

Vineyards have a long history for Central Anatolia region with its significant economic importance. Mite biodiversity surveys were carried out for vineyards all around the world but there are limited studies which aim Central Anatolia region. A survey was conducted in vineyards of Ankara during 2015-2016. The samples were collected mainly from the most important grape producing areas of Ankara (Kalecik, Güdül, Çubuk and Beypazarı) at weekly interval. The identified mite species were belonged to herbivory, predatory, detrivor and saprophyte groups. A total of 26 mite species belonging to 13 families were determined. *Tetranychus urticae, Panonychus ulmi, Bryobia rubrioculus* (Acari: Tetranychidae); *Brevipalpus lewisi* and *Cenopalpus pulcher* (Acari: Tenuipalpidae); *Colomerus vitis* and *Calepitrimerus vitis* (Acari: Eriophyidae) were identified as phytophagous mites. Among beneficial mite families, the most common family was Phytoseiidae. Phytoseiid mites constitute 60% of all identified samples and the most common species were *Phytoseius finitimus, Typhlodromus bagdasarjani* and *Euseius finitimus.* The other mite species found belonged to the families Tydeidae, Stigmaeidae, Ascidae, Melicharidae, Laelapidae, Iolinidae, Cunaxidae, Acaridae and Oribatida.

KEYWORDS:
Ankara, Vineyard, Acari, Phytoseiidae, Eriophyidae, *Phytoseius finitimus*

INTRODUCTION

The Anatolia region which includes Turkey is considered as the origin of many plants, including *Vitis vinifera* [1]. Turkey has great potential for growing *Vitis vinifera* L. (Vitales: Vitaceae) with its 467.000 ha (fifth in the world) [2]. Also, Turkey is the second biggest dried grape producer and the biggest dried grape exporter in the world [3]. Furthermore, Ankara region has some special grape cultivars for wine (such as Kalecik Karası). Protection of such local cultivars is crucial for both genetic source and sustainable grape farming all around the world. Determination of biodiversity of mites is vital for designing proper pest management strategies especially in local areas such as Ankara. Although viticulture is common and has a great economic importance all around Turkey, there are limited study available about vineyard mites.

In previous studies about vineyard mites in Turkey; Çobanoğlu [4] has reported phytoseiid species of diverse plants in Thrace including *V. vinifera*. Göven et al. [5] has reported *Colomerus vitis* and *Calepitrimerus vitis* as the most widespread with the highest density among other mite species in Aegean vineyards. *Typhlodromus perbibus* Wainstein &Arutunjan (Acari: Phytoseiidae) and *Tydeus caudatus* (Duges) (Acari: Tydeidae) were reported as the most common with the highest density among other beneficial mite species. Kasap et al. [6] has determined *Tetranychus urticae* and *Colomerus vitis* as important pests for vineyards of Çanakkale. Among predatory mites; *Phytoseius finitimus* has been reported at the highest density. These previous studies related the mites of vineyards were mainly conducted on the western region of Turkey and there is not any study focus on Central Anatolia region.

The aim of this study was identification of mite species belonging to Ankara which is located in Central Anatolia region. To doing this, since now, mite biodiversity of Ankara can be monitored and biological control possibilities of phytophagous mites can be revised for Ankara region.

TABLE 1
Localities and Coordinates of Sampling areas

District	Coordinates
Kalecik	40°12'26.7"W 33°27'29.5"S
	40°11'29.8"W 33°34'23.2"S
	40°06'44.5"W 33°25'43.3"S
	40°08'23.4"W 33°22'36.8"S
Çubuk	40°12'37.3"W 33°07'33.2"S
	40°11'09.4"W 33°06'13.6"S
Güdül	40°07'29.2"W 32°14'04.8"S
	40°12'49.4"W 32°09'35.3"S
	40°12'44.9"W 32°12'39.1"S
Beypazarı	40°13'06.7"W 31°51'50.5"S
	40°07'39.8"W 31°54"31.1"S

MATERIALS AND METHODS

This study was conducted in five different regions of Ankara which represent about 90% of grape production of Ankara (Table 1, Figure 1) [7]. Sam-

pling was done weekly interval during vegetation period of grape in 2015-2016.

FIGURE 1
Sampling vineyards areas of Ankara

Thirty leaves were taken from different height and direction of plants for sampling. Informations such as locations, damage symptoms etc. were recorded and then samples were put in a plastic bag. The mite samples were extracted under a stereo microscope using a brush. Samples were kept in 70% alcohol. For further process, lactophenol was used for clarification and Hoyer's medium was used for preparation. After preparation, slides were placed to hot oven (40-50°C) for about a week. Identification was done by a light microscope (LEICA DM750).

Identification was done according to; Baker (1965) [8] , Karg (1971) [9], Jeppson et al. (1975) [10], Hughes (1976) [11], Hatzinikolis and Emmanouel (1991) [12], Bolland et al. (1998) [13], Amrine et al. (2003) [14], Kalúz and Fend'a (2005) [15], Zhang and Fan (2005) [16], Chant and McMurtry (2007) [17], Papadoulis et al. (2009) [18], Faraji et al. (2011) [19], Tixier et al. (2012) [20], Denizhan et al. (2015) [21], Çobanoğlu et al. (2016) [22], da Silva et al. (2016) [23], Döker et al. (2016) [24].

RESULTS AND DISCUSSION

A total of 26 mite species belonging to 13 different mite families were identified. Some families identified at the family rank. The identified mite samples were belong to; Phytoseiidae, Ascidae, Laelapidae, Tydeidae, Stigmaeidae, Iolinidae, Melicharidae and Cunaxidae which were mainly beneficial species. Tetranychidae, Tenuipalpidae and Eriophyidae families were determinated as phytophagous. Also, Oribatidae and Acaridae were decomposer and saprophyte species.

Family Phytoseiidae Berlese. Subfamily Phytoseiinae Berlese. Genus *Phytoseius* Ribaga, 1904. *Phytoseius plumifer* (Canestrini and Fanzago) 1876

Specimens examined: Keçiören, 7 June 2015 (4♀♀); Kalecik, 9 June 2015 (42♀♀,17♂♂); Kalecik, 2 July 2015 (62♀♀,34♂♂), Keçiören 6 July 2015 (1♀); Çubuk, 10 July 2015 (1♀); Güdül, 24 July 2015 (1♀); Kalecik, 18 August 2015 (57♀♀,22♂♂); Çubuk, 3 September 2015 (1♀); Beypazarı, 7 September 2015 (3♀♀,1♂); Güdül, 7 September 2015 (8♀♀,2♂♂); Güdül, 29 October 2016 (1♀); Güdül, 23 June 2016 (1♀)

Distribution: Algeria, Armenia, Azerbaijan, Brazil, Cyprus, Egypt, France, Georgia, Greece, Hungary, Iran, Israel, Italy, Jordan, Kazakhstan, Lebanon, Moldova, Portugal, Saudi Arabıa, Turkey, Ukraine, USA [25]

Remarks: This species is very common in Turkey and it has been identified from various plants including *V. vinifera* in different parts of Turkey [6, 19, 26]

Subfamily Amblyseiinae Muma. Genus *Euseius* Wainstein, 1962. *Euseius finlandicus*, (Oudemans, 1915)

Specimens examined: Beypazarı, 12 June 2015 (1♀); Keçiören, 7 June 2015 (4♀♀,1♂); Keçiören, 6 July 2015 (3♀♀); Güdül, 7 September 2015 (1♀); Beypazarı, 7 September 2015 (1♀), 28 September 2015 (7♀♀,3♂♂); Beypazarı, 29 October 2015 (11♀♀,5♂♂); Kalecik, 20 May 2016 (1♀); Güdül, 23 June 2016 (2♀♀)

Distribution: Albania, Algeria, Angola, Argentina, Armenia, Austria, Azerbaijan, Belarus, Belgium, Bosnia And Herzegovina, Bulgaria, Canada, China, Croatia, Cyprus, Czech Republic, Czechoslovakia (former), Denmark, England, Finland, France, Georgia, Germany, Greece, Hungary, India , Indonesia, Iran, Italy, Japan, Kazakhstan, Latvia, Lithuania, Macedonia, Mexico, Moldova, Montenegro, Netherlands, Nicaragua, Norway, Poland, Portugal, Russia , Scandinavia, Serbia, Slovakia, Slovenia, South Korea, Spain, Sweden, Switzerland, Turkey, Ukraine, USA [25]

Remarks: *E. finlandicus* were identified on various plants including *V. Vinifera* in almost everywhere in Turkey and also it is very common in Europe [19]

Genus *Kampimodromus* Nesbitt, 1951. *Kampimodromus aberrans*, (Oudemans, 1930)

Specimens examined: Keçiören, 7 June 2015 (8♀♀,4♂♂); Keçiören, 6 July 2015 (5♀♀,2♂♂); Çubuk 3 September 2015 (1♀); Beypazarı, 7 September 2015 (2♀♀,2♂♂)

Distribution: Albania, Algeria, Armenia, Austria, Azerbaijan, Belarus, Bulgaria, Canada, Croatia, Czech Republic, Czechoslovakia (former), England, France, Georgia, Germany, Greece, Hungary, Iran, Israel, Italy, Moldova, Montenegro, Morocco, Netherlands, Norway, Poland, Portugal, Russia , Serbia, Slovakia, Slovenia, Spain, Switzerland, Tunisia, Turkey, Ukraine, USA [25]

Remarks: *K. aberrans* is generalist predator species commonly found in Turkey on different hosts including *V. vinifera* [19, 27]

Genus *Neoseiulus* Hughes, 1948. *Neoseiulus marginatus*, (Wainstein, 1961)

Specimens examined: Grape leaves litter of the vineyards. Kalecik, 21 March 2016 (9♀♀); Çubuk, 15 April 2016 (1♀)

Distribution: Algeria, Armenia, Azerbaijan, France, Georgia, Greece, Hungary, Iran, Israel, Kazakhstan, Kenya, Latvia, Moldova, Russia, Serbia, Turkey, Turkmenistan, Ukraine [25]

Remarks: *N. Marginatus* is firstly recorded on tulip bulbs in Turkey [19]. Reports about this species are quite rare in Turkey. With this study, *N. Marginatus* has been reported on grape producing area for the first time.

Subfamily Typhlodrominae Scheuten. Genus *Paraseiulus* Muma, 1961. *Paraseiulus triporus*, (Chant & Yoshida-Shaul, 1982)

Specimens examined: Keçiören, 7 June 2015 (1♀); Keçiören, 6 July 2015 (1♀); Güdül, 24 July 2015 (1♀); Kalecik, 8 August 2015 (1♀)

Distribution: Czech Republic, Czechoslovakia (former), Denmark, Finland, France, Georgia, Germany, Greece, Hungary, Iran, Italy, Kazakhstan, Moldova, Morocco, Netherlands, Poland, Portugal, Russia, Serbia, Slovakia, Slovenia, Spain, Sweden, Syria, Turkey, Ukraine, USA [25]

Remarks: This species were found in almost all area in Turkey except Blacksea region [19, 27]. Although *P. triporus* is recorded from different hosts, it was first time on vineyards in Turkey with this study.

Genus *Typhlodromus* Scheuten, 1857. Subgenus *Anthoseius* De Leon, 1959. *Typhlodromus (Anthoseius) bagdasarjani* Wainstein & Arutunjan, 1967

Specimens examined: Çubuk, 29 June 2015 (1♀,3♂♂); Güdül, 24 July 2015 (1♀); Çubuk, 18 August 2015 (1♀); Çubuk, 3 September 2015 (2♀♀,3♂♂); Beypazarı, 7 September 2015 (1♀); Çubuk, 28 October 2015 (1♀); Beypazarı, 29 October 2015 (1♀); Kalecik, 20 May 2016 (4♀♀,1♂); Kalecik, 21 July 2016 (13♀♀,4♂♂); Çubuk, 21 July 2016 (2♀♀); Beypazarı, 28 July 2016 (2♀♀); Kalecik, 10 August 2016 (6♀♀,3♂♂)

Distribution: Armenia, Azerbaijan, Iran, Turkey, Turkmenistan [25]

Remarks: *T. bagdasarjani* is determined one of the most common phytoseiid species in this study. This species was also reported in many studies in Turkey [25, 28]. But, it is recorded first time on *V. Vinifera* in this study.

***Typhlodromus (Anthoseius) psyllakisi* Swirski & Ragusa, 1976**

Specimens examined: Güdül, 24 July 2015 (2♀♀); Beypazarı, 24 July 2015 (1♀); Beypazarı, 1 July 2015 (2♀♀)

Distribution: Greece, Turkey [25]

Remarks: *A. psyllakisi* is a recently reported species for Turkey [29]. It was not so abundant in vineyards of Ankara.

***Typhlodromus (Anthoseius) recki* Wainstein, 1958**

Specimens examined: Güdül, 24 July 2015 (2♀♀,1♂); Beypazarı, 23 June 2016 (3♀♀).

Distribution: Algeria, Armenia, Austria, Azerbaijan, France, Georgia, Greece, Hungary, Iran, Israel, Italy, Kazakhstan, Lebanon, Moldova, Morocco, Portugal, Russia, Syria, Tunisia, Turkey, Ukraine [25]

Remarks: This species has been reported on various plants including *V. vinifera* and locations in Turkey [6, 19]. *A. recki* was not so common in vineyards of Ankara.

Family Ascidae Voigts And Oudemans. Genus *Arctoseius* Sig Thor, 1930. *Arctoseius cetratus*, Sellnick 1940

Specimens examined: Grape leaves litter. Kalecik, 21 March 2016 (2♀♀,2♂♂)

Distribution: England, Iceland, Israel, Switzerland, USA [30]

Remarks: *A. cetratus* was found only Ankara and İzmir in Turkey. It has a great potential for biological control on soil ecosystems [31]

Genus *Asca V. Heyden*, 1826. *Asca bicornis*, (Canestrini & Fanzago, 1887)

Specimens examined: Grape leaves litter. Çubuk, 15 April 2016 (2♀♀)

Distribution: All over the European countries [32]

Remarks: *A. bicornis* was only reported in Ankara region in Turkey [33]

Family Melıcharidae. Genus *Proctolaelaps*, Berlese, 1923. *Proctolaelaps pygmaeus*, (Müller, 1859)

Specimens examined: Grape leaves litter. Kalecik, 21 March 2016 (2♀♀)

Distribution: USA, Canada, Oriental, Palaearctic, Afrotropic, Neotropic and Australian regions [34]

Remarks: *P. pygmaeus* has been found in Ankara and İzmir region in Turkey [33]. It may be predator on small arthropods, but also it can be fungivore [34]

Family Laelapidae. Genus *Hypoaspis* Canestri, 1884. *Hypoaspis brevipilis* (Hirchmann, 1969)

Specimens examined: Grape leaves plant litter. Kalecik, 21 March 2016 (1♀)

Distribution: Middle of Europe [32]

Remarks: *H. brevipilis* found only in Ankara region for Turkey. This species is common mainly in bulbaceous plants [32, 35]

Family Tydeidae Kramer. Genus *Tydeus* Koch, 1835. *Tydeus californicus* (Banks, 1904)

Specimens examined: Güdül, 29 October 2015 (5♀♀); Kalecik, 18 August 2015 (3♀♀); Keçiören, 7 June 2015 (2♀♀)

Distribution: Worldwide [23]

Remarks: *T. californicus* is a common species especially for citrus and orchards for Turkey [27-28]

***Tydeus kochi* Oudemans, 1928**

Specimens examined: Grape leaves litter. Kalecik, 21 March 2016 (23♀♀)

Distribution: Worldwide [23]

Remarks: *T. kochi* species is distributed largely in Turkey [26, 28]

Family Iolinidae. Genus *Pronematus* Canestrini, 1886. *Pronematus sextoni* Baker, 1968

Specimens examined: Çubuk, 3 September 2015 (1♀♀); Güdül, 7 September 2015 (3♀♀); Çubuk, 29 June 2015 (2♀♀); Beypazarı, 7 September 2015 (3♀♀)

Distibution: China, India

Remarks: *P. sextoni* has been reported firstly by Çobanoğlu and Kazmierski [36]. This species is rare for Turkey.

Family Stigmaeidae Oudemans. Genus *Zetzellia* Oudemans, 1927. *Zetzellia mali* (Ewing), 1917

Specimens examined: Güdül, 7 September 2015 (3♀♀); Çubuk, 29 June 2015 (2♀♀); Kalecik, 09 June 2015 (1♀); Keçiören, 16 June 2016 (3♀♀)

Distribution: Argentina, Austria, Bulgaria, Canada, China, Czech, France, Germany, Hungary, India, Iran, Italy, Lebanon, Lithuanian, Moldavia, Netherlands, Poland, Serbia, Slovenia, Spain, Switzerland, Tunisia, Turkey, UK, USA, Ussr (former),Yugoslavia (former) [37].

Remarks: *Z. mali* is a common predator species throughout the world. It can be found on numerous hosts [37].

Family Cunaxidae

Specimens examined: Kalecik, 21 March 2016 (4♀)

Family Tetranychidae Donnadieu. Subfamily Tetranychinae Berlese. Genus Tetranychus Dufuor. *Tetranychus urticae* Koch, 1836

Specimens examined: Keçiören, 7 June 2015 (1♀); Kalecik, 9 June 2015 (1♀); Çubuk, 29 June 2015 (3♀♀,1♂); Keçiören, 6 July 2015 (1♀); Çubuk, 10 July 2015 (2♀♀); Güdül, 24 July 2015 (2♀♀); 18 August 2015 (1♂); Çubuk, 3 September 2015 (2♀♀); Beypazarı, 7 September 2015 (1♀); Çubuk, 28 October 2015 (1♀); Beypazarı, 29 October 2015 (1♀,1♂); Keçiören, 16 June 2016 (1♂); Güdül, 23 June 2016 (1♀); Kalecik, 21 July 2016 (6♀♀,2♂♂); Beypazarı, 28 July 2016 (8♀♀,1♂); Kalecik, 10 August 2016 (1♀,1♂)

Distribution: Afrotropical, Australasian, Nearctic, Neotropical, Oriental, Palearctic [38]

Remarks: It is a very cosmopolitan species with its great economic importance [13]

Genus Panonychus Yokoyoma, 1929. *Panonychus ulmi* (Koch), 1836

Specimens examined: Kalecik, 21 July 2016 (1♀)

Distribution: Afrotropical, Australasian, Nearctic, Neotropical, Oriental, Palearctic [38]

Remarks: Although *P.ulmi* is very harmful in vineyards of European [39], it is not so common in Turkey. Although, it was reported on different hosts in Turkey, it was first time on vineyards.

Subfamily Bryobinae. Genus Bryobia Koch 1836. *Bryobia rubrioculus* (Scheuten), 1857

Specimens examined: Çubuk, 18 August 2016 (1♀)

Distribution: Afrotropical, Australasian, Nearctic, Neotropical, Oriental, Palearctic [38]

Remarks: This species is highly polyphagous and can be found mainly on Rosaceae [38]. Although *B. rubrioculus* is common in Turkey, it is recorded for the first time in vineyards of Turkey.

Family Tenuipalpidae Berlese. Subfamily Brevipalpinae Reck. Genus *Brevipalpus* Donnadieu, 1875. *Brevipalpus lewisi* McGregor, 1949

Specimens examined: Çubuk, 29 June 2015 (1♀); Güdül, 24 July 2015 (2♀♀); Kalecik, 18 August 2015 (4♀♀); Çubuk, 03 September 2015 (1♀); Güdül, 07 September 2015 (2♀); Güdül, 29 October 2015 (2♀♀)

Distribution: Australian, Nearctic, Palearctic [40]

Remarks: *B. lewisi* had low density in this study. It was also found in different hosts including *V. vinifera* in Turkey [5, 27].

Genus *Cenopalpus* Pritchard and Baker 1958. *Cenopalpus pulcher* (Canestrini and Fanzago, 1876)

Specimens examined: Kalecik, 20 May 2016 (1♀)

Distribution: Nearctic, Western Palearctic [40]

Remarks: This species was very rare in Ankara vineyards, still it was recorded on many other hosts before in Turkey [41-42].

Family Eriophyidae. Subfamily Cecidophyinae Keifer. Genus *Colomerus* Newkirk & Keifer, 1971. *Colomerus vitis* (Pagenstecher), 1857

Specimens examined: Keçiören, 7 June 2015;

Kalecik, 9 June 2015; Beypazarı, 12 June 2015; Çubuk, 29 June 2015; Kalecik, 2 July 2015; Keçiören, 6 July 2015; Çubuk, 10 July 2015; Güdül, 24 July 2015; Kalecik, 18 August 2015; Çubuk, 18 August 2015; Çubuk, 3 September 2015; Güdül, 7 September 2015; Beypazarı, 7 September 2015; Çubuk, 28 October 2015; Beypazarı, 29 October 2015; Kalecik, 20 May 2016; Güdül, 23 June 2016; Kalecik, 21 July 2016; Beypazarı, 28 July 2016; Kalecik, 10 August 2016.

Distribution: Africotropical, Australian, Nearctic, Neotropical, Palaearctic [21]

Remarks: *Col. vitis* is very common in Ankara vineyards when sulfur is not applied. This species is known in Turkey for many years [43, 44, 21].

Subfamily Phyllocoptinae Nalepa. Genus *Calepitrimerus* Keifer, 1938. *Calepitrimerus vitis* (Nalepa), 1905

Specimens examined: Keçiören, 7 June 2015; Kalecik, 9 June 2015; Beypazarı, 12 June 2015; Çubuk, 29 June 2015; Kalecik, 2 July 2015; Keçiören, 6 July 2015; Çubuk, 10 July 2015; Güdül, 24 July 2015; Kalecik, 18 August 2015; Çubuk, 18 August 2015; Çubuk, 3 September 2015; Güdül, 7 September 2015; Beypazarı, 7 September 2015; Çubuk, 28 October 2015; Beypazarı, 29 October 2015; Kalecik, 20 May 2016; Güdül, 23 June 2016; Kalecik, 21 July 2016; Beypazarı, 28 July 2016; Kalecik, 10 August 2016

Distribution: Africotropical, Antarctic, Australian, Indomalayan, Nearctic, Neotropical, Palaearctic [21]

Remarks: *Cal. vitis* is very common in Ankara vineyards. This species generally was found together with *Col. vitis.*

Family Oribatidae

Specimens examined: Kalecik, 21 March 2016 (70); Çubuk, 15 April 2016 (40)

Distribution: Worldwide

Remarks: These specimens identified at the rank family.

Family Acaridae. Genus *Tyrophagus* Oudemans, 1924. *Tyrophagus putrescentiae* (Schrank), 1781

Specimens examined: Keçiören, 07 June 2015 (1♀); Kalecik, 9 June 2015 (1♀); Beypazarı, 12 June 2015 (4♀♀); Çubuk, 29 June 2015 (1♀); Çubuk, 10 July 2015 (1♀); Beypazarı, 24 July 2015 (1♀); Çubuk, 3 September 2015 (1♀)

Distribution: Cosmopolitan [11]

Remarks: *T. putrescentiae* was found on the foliage of plants.

***Tyrophagus similis* Volgin, 1949**

Specimens examined: Grape leaves litter. Kalecik, 21 March 2016 (5♀♀,6♂)

Distribution: Australia, Belgium, Germany, Iceland, Netherland, New Zealand, UK, USA [11].

Remarks: *T. similis* was found in litters, bulbaceous plants and stored dried fruits in Turkey [45. 35].

***Tyrophagus perniciosus* Zakhvatkin, 1941**

Specimens examined: Grape leaves litter. Kalecik, 21 March 2016 (4♀♀).

Distribution: Australia, Bulgaria, England, USSR (Former) [11].

Remarks: It was found in storages, bulbaceous plants and also houses in Turkey [45, 35, 46,47].

FIGURE 2
Ratio of mite specimens in vineyards of Turkey

CONCLUSION

The identified mites have different feeding types such as herbivory, predatory, detrivor and saprophyte. The distribution and abundance ratio of mite species according to locality is provided (Figure 2). Kalecik has the most mite diversity (22 species) comparing the other localities (Güdül: 13, Beypazarı: 11, Çubuk: 15, Central part of Ankara:10). Because plant litters were sampled mainly in Kalecik, diversity is much more from other districts.

The first infestation of spider mite in European vineyards were detected in the second half of the nineteenth century [39]. *Panonychus ulmi* (Koch), *Tetranychus urticae* Koch and *Eotetranychus carpini* (Oudemans) species are considered the most important spider mite species in European vineyards. And, 19 tetranychid mite species were found in vineyards in Europe until now [38]. *Calepitrimerus vitis* (Nalepa) and *Colomerus vitis* (Pagenstecher) are also very common in viticultural areas of the world [39].

In the sampled grape areas phytophagous mite damage symptoms were not clear except Eriophyids and number of individuals was not high.

B. lewisi can cause yield losses up to 30% [48]. But still, no economic injury levels have been established for *B. lewisi* [39]. For local varieties in Ankara, economic injury levels should be determined.

P. ulmi was reported as one of the most important mite pest in European vineyards [39]. Although *P. ulmi* is common in orchards in Turkey; there isn't any report about *P. ulmi* in vineyards of Turkey. Due to the fact that Turkey is located very close to Europe, researchers should be careful about *P. ulmi*.

Tixier et al. [20] have reported a total of 54 phytoseiid species belonging to 15 genera in European vineyards. Although many species are recorded in vineyards of Europe, five species are reported as the most important; *Kampimodromus aberrans* (Oudemans), *Typhlodromus* (*Typhlodromus*) *pyri* Scheuten, *Typhlodromus* (*Typhlodromus*) *exhilaratus* Ragusa, *Euseius finlandicus* (Oudemans) and *Phytoseius finitimus* Ribaga [49]. But in vineyards of Turkey, only 15 phytoseiid species were reported [4-6].

Eight phytoseiid species were identified (Only *N. marginatus* was found plant litter of vineyard) in this survey. The most common Phytoseiid species were *Phytoseius finitimus*, *Typhlodromus bagdasarjani* and *Euseius finlandicus* in all localities of vineyards (Figure 3). According to McMurtry et al. [50], all of these identified phytoseiids are generalist, so they can survive even with pollen or other food items. Although phytophagous mite density was low in this study, phytoseiid mites were found densely because of generalist dietary features.

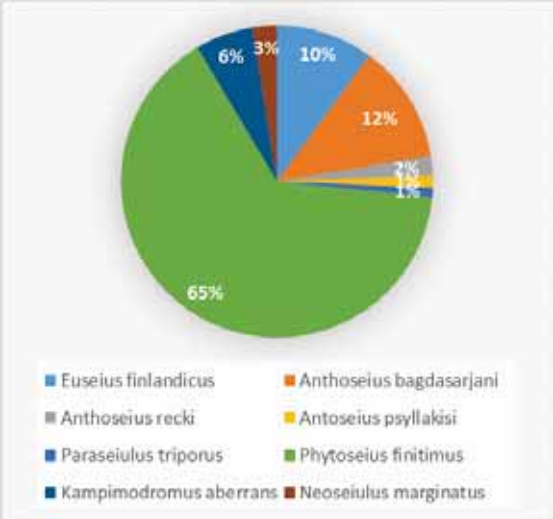

FIGURE 3
Phytoseiid mite species and their ratio

In Turkey; *Paraseiulus triporus, P. soleiger, P. talbii, Euseius scutalis, E. finlandicus, Phytoseius finitimus, Kampimodromus aberrans, Typhlodromus tiliae, T. athiasae, T. rarus, T. cotonesatri, T. (A) recki* and *T. (A) bagdasarjani* were reported from vineyards [4-6]. In this study, *Typhlodromus* (*Anthoseius*) *psyllakisi* and *Neoseiulus marginatus* (obtained from plant litter of vineyards) were recorded the first time in vineyards of Turkey.

8 different mite families were identified from plant litters of vineyards. *Neoseiulus marginatus* (Acari: Phytoseiidae) (Wainstein, 1961), *Tydeus kochi* Oudemans, 1928 (Acari: Tydeidae), *Proctolaelaps pygmaeus* (Muller, 1859) (Acari: Melicharidae), *Hypoaspis brevilipis* (Hirchmann, 1969) (Acari: Laelapidae), *Arctoseius cetratus* (Sellnick, 1940) (Acari: Ascidae) , *Asca bicornis* (Canestrini & Fanzago, 1887) (Acari: Ascidae), *Tyrophagus similis* Volgin, 1949 (Acari: Acaridae) , *Tyrophagus perniciosus* Zakhvatkin, 1941 (Acari: Acaridae) were obtained from plant litter of vineyards. Furthermore, Oribatidae and Cunaxidae family specimen were recorded. Oribatidae was the most common mite group among other mite family members (Figure 4).

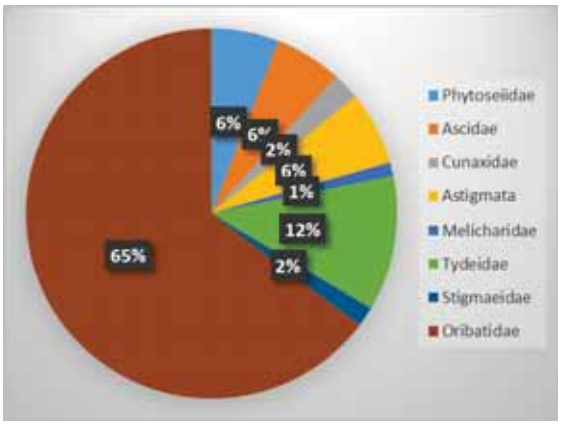

FIGURE 4
Ratio of mite families obtained from plant litters of vineyards

Oribatid mites were found in a conventional grape producing area. Most of soil mites are indicator specimens and susceptible to pesticide application. They have a critical role in decomposing process. For sustainable soil management, protecting of decomposer is essential. For further knowledge, ecotoxicological role of soil mites has been reviewed extensively [51-53].

Further studies should be carried out for monitoring mite diversity change and for assesment of biological control possibilities.

ACKNOWLEDGEMENTS

This work was supported by the Ankara University (Project Number: 16L0447001).

REFERENCES

[1] McGovern, P.E. (2004) Ancient Wine: The Search for the Origins of Viticulture. New Jersey: Princeton University Press. 392p.
[2] FAO (2015) Food and Agriculture Organization of the United Nations [Internet] — [14.11.2016].

[3] USDA (2016). Raisins: World Markets and Trade [Internet]. [02.03.2017] Available from: https://apps.fas.usda.gov/psdonline/circulars/raisins.pdf.
[4] Çobanoglu, S. (2004) Phytoseiid mites (Mesostigmata: Phytoseiidae) of Thrace, Turkey. Isr. J. Entomol. 34, 83-107.
[5] Göven, M.A., Cobanoglu, S., Güven, B. (2009) Predatory mite fauna in Aegean vineyards. Plant Protection Bulletin. 49(1), 1-10.
[6] Kasap, İ., Polat, B., Şahin, K. (2014) The important pest and predatory mites species (Acari) and their population fluctuation in the vineyards of Çanakkale Province. Turkish Journal of Entomology. 38(4), 451-458.
[7] Anonymous (2015) Turkish Statical Institute [Internet]. [11.11.2016].
[8] Baker, E.W. (1965) A review of the genera of the family Tydeidae (Acarina). Advances in acarology. 2, 95-133.
[9] Karg, W. (1971) Acari (Acarina), Milben Unterordnung Parasitiformes (Anactinochaeta). Die freilebenden Gamasina (Gamasides), Raubmilben, in: F. Dahl (Ed.), Die Tierwelt Deutschlands und der angrenzenden Meeresteile. 1-475p.
[10] Jeppson, L.R., Keifer, H.H., Baker, E.W. (1975) Mites injurious to economic plants. USA: Univ of California Press. 528p.
[11] Hughes, A.M. (1976) The mites of stored food and houses. London: Technical Bulletin, Ministry of Agriculture, Fisheries and Food. (9, Ed. 2). 400p.
[12] Hatzinikolis, E.N., Emmanouel, N.G. (1991) A revision of the genus Bryobia in Greece (Acari: Tetranychidae). Entomologia Hellenica. 9(1991), 21-34.
[13] Bolland, H.R., Gutierrez, J., Flechtmann, C.H. (1998) World catalogue of the spider mite family (Acari: Tetranychidae). Netherlands: Brill. 392p.
[14] Amrine, J.W.Jr., Stasny, T.A., Flechtmann, C.H.W. (2003) Revised Keys to World Genera of Eriophyoidea (Acari: Prostigmata). Indira Publishing House, West Bloomfield, Michigan, U.S.A., 244p.
[15] Kalúz, S., Fenďa, P. (2005) Mites (Acari: Mesostigmata) of the family Ascidae of Slovakia. Bratislava: Institute of Zoology Slovak Acedemy of Sciences. 166p.
[16] Zhang, Z.Q., Fan, Q.H. (2005) Revision of Tyrophagus Oudemans (Acari: Acaridae) of New Zeland and Australia. New Zealand: Landcare Research New Zealand Ltd. 189p.
[17] Chant, D.A., McMurtry, J.A. (2007) Illustrated keys and diagnoses for the genera and subgenera of the Phytoseiidae of the world (Acari: Mesostigmata). West bloomfield: Indira Publishing House. 220p.
[18] Papadoulis, G.T., Emmanouel, N.G., Kapaxidi, E. (2009) Phytoseiidae of Greece and Cyprus (Acari: Mesostigmata). West Bloomfield: Indira Publishing House. 200p.
[19] Faraji, F., Çobanoğlu, S., Çakmak, I. (2011) A checklist and a key for the Phytoseiidae species of Turkey with two new species records (Acari: Mesostigmata). International journal of Acarology. 37(sup1). 221-243.
[20] Tixier, M.S., Baldassar, A., Duso, C., Kreiter, S. (2012) Dichotomous key to species of Phytoseiidae mites in European vine fields [Internet]. [23.02.2017] Available from: http://www1.montpellier.inra.fr/CBGP/phytoseiidae/sitewebvineyards2/index.htm
[21] Denizhan, E., Monfreda, R., De Lillo, E., Çobanoğlu, S. (2015) Eriophyoid mite fauna (Acari: Trombidiformes: Eriophyoidea) of Turkey: new species, new distribution reports and an updated catalogue. Zootaxa. 3991(1), 1-63.
[22] Çobanoğlu, S., Ueckermann, E.A., Sağlam, H.D. (2016). The Tenuipalpidae of Turkey, with a key to species (Acari: Trombidiformes). Zootaxa. 4097(2), 151-186.
[23] Da Silva, G.L., Metzelthin, M.H., Da Silva, O.S., Ferla, N.J. (2016). Catalogue of the mite family Tydeidae (Acari: Prostigmata) with the world key to the species. Zootaxa. 4135(1), 1-68.
[24] Döker, İ., Kazak, C., Karut, K. (2016) Contributions to the Phytoseiidae (Acari: Mesostigmata) fauna of Turkey: morphological variations, twelve new records, re-description of some species and a revised key to the Turkish species. Systematic and Applied Acarology. 21(4), 505-527.
[25] Demite, P.R., de Moraes, G.J., McMurtry, J.A., Denmark, H.A., Castilho, R.C. (2016) Phytoseiidae Database [Internet]. [16.02.2017]
[26] Çobanoğlu, S., Kumral, N.A. (2016) The biodiversity, density and population trend of mites (Acari) on Capsicum annuum L. in temperate and semi-arid zones of Turkey 1. Systematic and Applied Acarology. 21(7), 907-918.
[27] Satar, S., Ada, M., Kasap, İ., Çobanoğlu, S. (2013) Acarina fauna of citrus trees in eastern Mediterranean region of Turkey. IOBC-WPRS Bulletin. 95, 171-178.
[28] Kasap, İ., Çobanoğlu, S., Pehlivan, S. (2013) Predatory mite species on pome fruit trees and weeds in the province of Çanakkale and Balıkesir. Turkish Journal of Biological Control. 4(2), 109-124.
[29] Kumral, N.A., Çobanoğlu, S. (2016) The Mite (Acari) Biodiversity and Population Fluctuation of Predominat Species in Eggplant. Journal of Agricultural Sciences. 22(2), 261-274.
[30] Binns, E.S. (1974) Notes on the biology of Arctoseius cetratus (Sellnick) Mesostigmata: Ascidae). Acarologia. 16(4), 577–582.

[31] de Moraes, G.J., Venancio, R., dos Santos, V.L., Paschoal, A.D. (2015) Potential of Ascidae, Blattisociidae and Melicharidae (Acari: Mesostigmata) as biological control agents of pest organisms. In: Carillo, D., de Moraes, G.J., Pena, J.E. (Eds). Prospects for Biological Control of Plant Feeding Mites and Other Harmful Organisms. Cham: Springer International Publishing. 33-75.
[32] Bayram, Ş., Çobanoğlu, S. (2005) Mesostigmata (Acari) of bulbous ornamental plants in Turkey. Acarologia. 45(4), 257–265.
[33] Çakmak, I., Faraji, F., Çobanoğlu, S. (2011) A checklist and key to the Ascoidea and Phytoseioidea (except Phytoseiidae) species of Turkey with three new species records (Acari: Mesostigmata). Turkish Journal of Entomology. 35(4), 575-586.
[34] Connor, B.O., Klimov, P. (2012) North American Bee-Associated Mites [Internet]. [19.11.2016]
[35] Kılıç, T., Çobanoğlu, S., Yoldaş, Z., Madanlar, N. (2012) Mite (Acari) species determined in fresh onion fields in Izmir province. Turkish Journal of Entomology. 36(3), 401-411.
[36] Çobanoglu, S., Kazmierski, A. (1999) Tydeidae and Stigmaeidae [Acari: Prostigmata] from orchards, trees and shrubs in Turkey. Biological Bulletin of Poznań. 36(1), 71-82.
[37] Fan, Q.H., Flechtmann, C.H., de Moraes, G.J. (2016) Annotated catalogue of Stigmaeidae (Acari: Prostigmata), with a pictorial key to genera. Zootaxa. 4176(1), 1-199.
[38] Migeon, A., Nouguier, E., Dorkeld, F. (2011) Spider Mites Web: a comprehensive database for the Tetranychidae. Trends in Acarology. 557-560.
[39] Duso, C., Pozzebon, A., Kreiter, S., Tixier, M.S. and Candolfi, M. (2012) Management of Phytophagous Mites in European Vineyards. In: Bostanian, J.N., Vincent, C. and Isaacs, R. (eds.) Arthropod Management in Vineyards: Pests, Approaches, and Future Directions. Dordrecht, Springer Netherlands. 191-217.
[40] Mesa, N.C., Ochoa, R., Welbourn, W.C., Evans, G.A., De Moraes, G.J. (2009) A catalog of the Tenuipalpidae (Acari) of the World with a key to genera. Zootaxa. 2098, 1-185.
[41] Yeşilayer, A., Çobanoğlu, S. (2011) Deter-mination of Tenuipalpidae (Acari: Prostigmata) species in parks and ornamental plants of Istanbul, Turkey. Plant Protection Bulletin. 51(4), 315-330.
[42] Kasap, İ., Çobanoğlu, S., Pehlivan, S., Şahin, K., Baştuğ, G. (2015) Çanakkale ve Balıkesir illeri yumuşak çekirdekli meyve ağaçları ve yabancı otlar üzerinde bulunan bitki zararlısı akar türleri. Bitki Koruma Bülteni. 55(2), 85-94.
[43] Alkan, B. (1952) Türkiye'nin Zoosesid (zoocecid)'leri (kökeni hayvansal bitki urları) üzerinde çalışmalar I-II. Ankara Üniversitesi Ziraat Fakültesi Yıllığı. 8–3, 185–225.
[44] Bodenheimer, F.S. (1958) A study on insects injurious to crops and trees in Turkey and their control. Ankara: Buyur Matbaası. 346p.
[45] Çobanoğlu, S. (2009) Mite population density analysis of stored dried apricots in Turkey. International Journal of Acarology. 35(1), 67-75.
[46] Zeytun, E., Dogan, S., Aykut, M., Özçiçek, F., Ünver, E., Özçiçek, A. (2015) House dust mites in Erzincan province. Turkish Journal of Parasitology. 39(2), 124.
[47] Bayram, S., Çobanoglu, S. (2006) Astigmata and Prostigmata (Acari) of bulbaceous ornamental plants in Ankara, Turkey. Acta Phytopathologica et Entomologica Hungarica. 41(3-4), 367-381.
[48] Raikov, E., Nachev, P. (1965) Winter control of the vine Phytoptipalpid. Rastitelna Zashchita. 13, 6–8.
[49] Tixier, M.S., Baldassar, A., Duso, C., Kreiter, S. (2013) Phytoseiidae in European grape (Vitis vinifera L.): bio-ecological aspects and keys to species (Acari: Mesostigmata). Zootaxa. 3721(2), 101-142.
[50] McMurtry, J.A., De Moraes, G.J., Sourassou, N.F. (2013) Revision of the lifestyles of phytoseiid mites (Acari: Phytoseiidae) and implications for biological control strategies. Systematic and Applied Acarology. 18(4), 297-320.
[51] Lebrun, P., Straalen, N.M. (1995) Oribatid mites: prospects for their use in ecotoxi-cology. Experimental and Applied Acarology. 19(7), 361-379.
[52] Gergócs, V., Hufnagel, L. (2009) Application of oribatid mites as indicators. Applied ecology and environmental research. 7(1), 79-98.
[53] Huguier, P., Manier, N., Owojori, O.J., Bauda, P., Pandard, P., Römbke, J. (2015) The use of soil mites in ecotoxicology: a review. Ecotoxicology. 24(1), 1-18.

Received: **18.07.2017**
Accepted: **08.12.2017**

CORRESPONDING AUTHOR

Emre Inak
Ankara University,
Faculty of Agriculture,
Departmant of Plant Protection,
06110 Dışkapı – Ankara

e-mail: einak@ankara.edu.tr

© by PSP Volume 27 – No. 2/2018 pages 1240-1247 Fresenius Environmental Bulletin

THE FATTY ACID AND MINERAL COMPOSITIONS OF DIFFERENT CHICKPEA CULTIVARS CULTIVATED

Muharrem Kaya[1,*], Asuman Kan[2], Azime Yilmaz[3], Ruziye Karaman[1], Aykut Sener[1]

[1]Department of Field Crops, Faculty of Agriculture, Suleyman Demirel University, Isparta, Turkey
[2]Food Technology Department, Technical Sciences Vocational School of Higher Education, Selcuk University, Konya, Turkey
[3]Bioengineering Department, Chemical and Metallurgical Engineering Faculty, Yildiz Technical University, Istanbul, Turkey

ABSTRACT

In this study, crude oil content, fatty acid and mineral composition of different chickpea varieties cultivated in Konya were investigated. Fatty acid (saturated and unsaturated) compositions, crude oil and mineral contents were determined; GC-MS, Soxhelet-Henkel and ICP-OES, respectively. There were significant (p<0.01) differences between the chickpea cultivars in view of their crude oil contents and fatty acids (saturated and unsaturated) compositions. The oil yields of the nineteen chickpea cultivars varied between 2.91 and 6.43%. The highest crude oil content was determined in Gökçe (6.43%) cultivar. On the other hand, highest compositions of the unsaturated fatty acids were determined in Uzunlu 99 (88.01%). Furthermore, the total compositions of the highest saturated fatty acids were determined in Canıtez 87 (17.71%). The linolenic (in ILC 482, 2.68%), linoleic (in ILC 482, 57.25%) and oleic (in Gülümser, 42.30%) acids were dominating fatty acids of the cultivars. According to the results, the total macro element composition of the chickpea cultivars were found to range from 16267 to 23634 and K and P were the dominating macro elements of the cultivars. Moreover, the micro element composition of the chickpea cultivars varied from 165.36 to 269.09 Fe and B were the highest micro elements of the cultivars.

KEYWORDS:
Chickpea, crude oil, fatty acid, mineral compositions

INTRODUCTION

Legumes are of great to importance to human nutrition because they are good sources of proteins, carbohydrates, several water-soluble vitamins and minerals. Chickpea (*Cicer arietinum* L.), being one of the oldest and most widely consumed legumes in the world is particularly grown in tropical and subtropical areas [1]. Chickpea is also widely grown and cultivated in Southern Europe, North Africa, India and Middle East countries as well as other countries such as Algeria, Ethiopia, Iran, India Mexico, Morocco, Myanmar, Pakistan, Spain, Syria, Tanzania, Tunisia and Turkey. It was reported to be the second most widely grown legume in the world [2]. In Turkey, it is produced at the level of 530,634 ton on 446,218 ha. This shows that the average yield in Turkey is 1,189 kg ha^{-1}, which is higher than the world average (912 kg ha^{-1}) [3]. In the recent years, chickpea has been immensely produced in Turkey, which can be attributed to three main factors: (a) the development of new chickpea cultivars with higher yields, (b) improved adaptation to local agroclimatic conditions and (c) better acceptability through improved nutritional status. In Turkey, 19 chickpea cultivars is now cultivated [4-5]. For these reasons, the number of the studies on cultivated chickpea production has also considerably increased. Another factor which makes chickpea a well-studied plant is its high carbohydrate and protein contents, which plays a great role for human and animal nutrition, as well. In addition, its rich mineral and trace element content as well as oil content, including essential fatty acids makes it very important food among the legumes [6-7]. The bioactive properties of chickpea should be also noted here, including antioxidant properties of tocotrienols having biologically important properties such as inhibition of cholesterol biosynthesis [8]. Phytosterols having cholesterol-lowering, anti-inflammatory, antibacterial, antifungal, antitumor and antiviral activities are among the other bioactive compounds present in chickpea [9-10]. Since consumers have had a recent tendency towards the healthy foods, chickpea has also taken its place among the most important functional or nutraceutical foods [11]. Furthermore, it has positive effects on soil fertility as it fixes symbiotic nitrogen. Due to above advantages, the cultivation of chickpea is of the same economic level as that of cereals [12]. Depending on genotypic and environmental factors, oil content changes between 3.8 and 10 %. The majority of the fatty acids present in chickpea are linolenic, oleic and palmitic acids [8-13]. In recent years, much work has been done on the oil content of chickpea genotypes grown in the different parts of world. In other a study, it was founded that the fat content of chickpea flour had 4.8 % [1]. For chickpea flour, high oil content

should be taken in to account since this makes it one of the mostly utilized food products. Zia-Ul-Haq et al., (2007) [6] reported that iron and zinc content of four chickpea cultivars were ranged from 2.4 to 4.1% and 3.5 to 6.0 %, respectively.

To our knowledge, data about oil yield, fatty acids composition and mineral contents of the chickpea cultivars cultivated in Turkey are limited. However, genotypes of chickpea cultivars and cultivation conditions would have an important role for composition of fatty acid. Some chickpea genotypes are available for oil yield and composition.

Objectives of this research were (a) to determine the levels crude oil (fat) and (b) to investigate fatty acid compositions and mineral component of 19 chickpea cultivars cultivated in Turkey.

MATERIALS AND METHODS

Seed material. The field trials were conducted during the growing season 2010 at the Experimental Station of Bahri Dağdaş International Agricultural Research Institute, in Konya, Turkey. Nineteen chickpea cultivars were used in this research. The experimental field conditions were (1) dry and hot for summer period and (2) rainy and cold for winter. The soil had a sand-loam characteristic. The planting date was at the end of March in spring, for growing year. The experimental set up was based on completely randomized block design with three replications. Fertilizers, fungicidal or insecticidal treatments were not used in study. The harvesting was harvested in August. Samples were taken randomly from each plot for analyses.

Extraction of seed oils. The oil extraction of dried and powdered chickpea seeds (5 g) were carried out at 40°C for 6 h by Soxhelet extractor using diethil ether as a solvent. The solvent was evaporated by rotary evaporator. The obtained oil was esterified to determine fatty acid composition. Methylation of the fatty acids was carried out according to the AACC Official Method [14].

Fatty acid analysis of seed oil by GC–MS. The fatty acids in the total lipid were esterified into methyl esters by saponification with 0.5 N methanolic NaOH and transesterified with 14 % BF3 (v/v) in methanol (IUPAC, 1979). GC–MS analysis was performed on an Agilent 6890 N Network GC system combined with Agilent 5973 Network Mass Selective Detector. The GC conditions were as follows: column: HP Innowax Capillary (60.0 m × 0.25 mm, 0.25 μm); oven temperature program: the column held initially at 60 °C for 3 min after injection, then increased to 185 °C with 10 °C min–1 heating ramp for 1 min and increased to 200 °Cwith 5 °C min–1 heating ramp for 10 min. Then the final temperature was increased to 220 °C with 5 °C min–1 heating ramp for 20 min; injector temperature: 250 °C; carrier gas: Helium; inlet pressure: 40.65 psi; linear gas velocity: 44 cm s−1; column flow: 2.9 mL min−1; splitless mode; injection volume: 1.0 μL. MS conditions were regulated as follows; ionization energy: 70 eV, ion source temperature: 280 °C; interface temperature: 250 °C; mass range: 35–450 amu.

In order to determine the components, their mass spectra was compared with Wiley and Nist GC–MS Libraries and retention indices, relative to n-alkanes, with corresponding data from relevant literature. The GC peak areas were used to calculate the percentages of the components using the normalization method.

Determination of minerals. Varian Vista-MPX simultaneous ICP-OES (Inductively Coupled Plasma Optical Emission Spectrometry) system with CCD detection was used to analyze mineral compositions in chickpea cultivars as macro element (P, K, Ca, Mg, Na), micro trace elements (Fe, B, Mn, Zn, Cu) and heavy metal (Pb, Ni, Cr, Co) [15-21]. It was used to analyze the elements in nineteen chickpea samples. All experiments were performed qualitatively and quantitatively with statistical data comparison to a certified reference plant material, respectively.

Statistical analysis. Each parameter was tested in triplicate samples with three replications. Conventional statistical methods were used to calculate means. Collected data were subjected to statistical analyses using JMP statistical package software (Version 5.0.1.a, SAS Institute. Inc. Cary, NC). One way ANOVA was used to evaluate the effect of chickpea varieties on the parameters studied. When significant ($P < 0.01$) main effect was found, the mean values were further analyzed using t test.

RESULTS AND DISCUSSION

Crude oil content of the chickpea cultivars. Table 1 indicates that there were significant ($p<0.01$) differences between the chickpea cultivars with respect to their crude oil contents and fatty acids (saturated and unsaturated) compositions. The oil yields of the nineteen chickpea cultivars ranged from 2.91 to 6.43 %. This results revealed that the highest crude oil content was determined in Gökçe (6.43 %) cultivar, followed by İzmir 92 (5.91 %) and ILC 482 (4.91 %) cultivars. On the other hand, the lowest crude oil contents were determined in Küsmen 99 (2.91 %), İnci (3.87%) and Aydın 92 (3.80 %) cultivars. Results also found in agreement with reported oil content of 2.6 to 6,8 % in nine different cultivars of chickpea [16]. Findings of this

TABLE 1
Fatty acid compositions of the cultivated chickpea cultivars in Turkey

Chickpea Cultivars	Crude Oil (%)	Unsaturated fatty acids (UFA) (%)									Saturated fatty acids (SAFA)				
		Palmitoleic acid		Oleic acid		Linoleic acid		Linolenic acid			Palmitic acid		Stearic acid		
		RI	$C_{16:1}$	RI	$C_{18:1}$	RI	$C_{18:2}$	RI	$C_{18:3}$	ΣUFA (%)	RI	$C_{16:0}$	RI	$C_{18:0}$	ΣSAFA (%
Damla 89	4.24^{c}	1296	0.23^{c}	1604	38.03^{f}	1664	47.13^{f}	1742	2.14^{d}	87.53^{b}	1286	9.22^{d}	1572	1.58^{k}	10.81^{ı}
Çağatay	4.08^{c}	1296	0.23^{d}	1598	32.55^{k}	1656	52.25^{b}	1740	2.53^{b}	87.56^{b}	1285	9.51^{b}	1568	1.60^{k}	11.10^{g}
Gülümser	3.93^{c}	1296	0.21^{f}	1602	**42.30^{a}**	1660	**41.25^{n}**	1740	1.76^{j}	85.53^{f}	1286	9.36^{c}	1570	2.14^{f}	11.50^{f}
Menemen 92	4.69^{b}	1296	0.26^{b}	1600	34.79^{ı}	1658	48.19^{d}	1740	2.05^{e}	85.29^{f}	1285	8.51^{j}	1568	1.85^{g}	10.36^{k}
Aydın 92	3.80^{c}	1296	0.29^{a}	1599	35.54^{h}	1658	49.63^{c}	1739	2.29^{c}	87.75^{a}	1285	9.13^{e}	1567	**1.48^{l}**	10.60^{jk}
İzmir 92	5.90^{a}	1296	0.24^{c}	1601	37.09^{g}	1660	48.00^{e}	1740	2.15^{d}	87.49^{b}	1286	8.95^{f}	1569	1.94^{f}	10.90^{h}
Cevdetbey	4.08^{c}	1296	**0.10^{l}**	1600	34.86^{ı}	1658	43.82^{k}	1740	1.97^{g}	80.75^{ı}	1285	8.73^{h}	1570	7.44^{b}	16.18^{b}
Sarı 98	4.02^{c}	1296	**0.29^{a}**	1599	37.26^{g}	1657	47.12^{f}	1740	2.12^{d}	86.80^{d}	1285	**9.63^{a}**	1567	1.75^{g}	11.39^{f}
Akçin 91	4.22^{c}	1296	0.21^{f}	1600	37.14^{g}	1658	47.25^{f}	1740	2.14^{d}	86.33^{e}	1285	9.58^{a}	1569	2.87^{e}	12.45^{e}
Gökçe	**6.43^{a}**	1296	0.22^{f}	1600	42.06^{a}	1656	43.81^{k}	1739	**1.68^{j}**	87.77^{a}	1285	8.68^{ı}	1568	1.98^{f}	10.66^{ı}
Küsmen 99	**2.91^{d}**	1296	0.22^{e}	1598	39.05^{e}	1655	46.13^{h}	1739	2.16^{d}	87.55^{b}	1285	9.12^{e}	1567	1.61^{j}	10.73^{ı}
Uzunlu 99	4.39^{c}	1296	0.11^{ı}	1597	42.17^{a}	1656	43.94^{j}	1738	1.78^{hı}	**88.01^{a}**	1285	8.97^{f}	1565	1.93^{f}	10.90^{h}
Er 99	4.74^{b}	1296	0.22^{e}	1601	39.86^{d}	1659	45.07^{ı}	1741	2.02^{f}	87.18^{c}	1286	9.59^{a}	1570	1.73^{h}	11.32^{f}
İnci	3.87^{c}	1296	0.18^{g}	1597	41.54^{b}	1657	44.06^{j}	1739	1.86^{h}	87.63^{a}	1285	**8.43^{k}**	1568	1.82^{g}	**10.25^{l}**
Canıtez 87	4.03^{c}	1296	0.02^{j}	1597	34.58^{ı}	1656	43.57^{l}	1738	1.79^{h}	**79.96^{j}**	1285	9.06^{e}	1566	**8.66^{a}**	**17.71^{a}**
Aziziye 94	4.89^{b}	1296	0.14^{h}	1598	33.40^{j}	1655	48.01^{e}	1738	2.11^{d}	83.66^{h}	1285	8.83^{g}	1568	5.09^{c}	13.92^{c}
Diyar 98	4.70^{b}	1296	0.19^{g}	1601	40.82^{c}	1658	42.24^{m}	1740	1.81^{h}	85.06^{g}	1286	9.20^{d}	1569	3.77^{d}	12.97^{d}
ILC 482	4.91^{b}	1296	0.19^{g}	1600	**27.55^{l}**	1661	**57.25^{a}**	1741	**2.68^{a}**	87.67^{a}	1286	9.51^{b}	1568	1.65^{i}	11.16^{g}
ESER 87	4.85^{b}	1296	0.14	1600	34.46^{ı}	1655	48.12^{h}	1740	2.14^{d}	84.86^{h}	1286	8.92^{f}	1568	4.12^{d}	13.04^{c}
Max	**6,43**		**0,29**		**42,30**		**57,25**		**2,68**	**88,01**		**9,63**		**8,66**	**17,71**
Min	**2,91**		**0,10**		**27,55**		**41,25**		**1,68**	**79,96**		**8,43**		**1,48**	**10,25**

Common letters in the same column indicate significant differences between the means at p <0.01 level.
ΣUFA, total Unsaturated fatty acids; ΣSAFA, total Saturated fatty acids

study are similar to the values reported for chickpea [1].

Fatty acid composition of the chickpea cultivars. Regarding the fatty acid compositions of the cultivars, according to this results for comparison of the unsaturated fatty acid (palmitoleic, oleic, linoleic and linolenic acids) and saturated fatty acid (palmitic and stearic acids) compositions with respect to the cultivars were also presented in Table 1. and Figure 1. Oil content, comprising of essential fatty acids (FA), is the third important organic component of chickpeas. Chickpea cultivars are rich in point of nutritionally essential lipids [7]. Oil content ranges from 3.8 to 10 % with respect to genotype and environmental factors [8]. In the other study, the oil content was found about 6.58–9.12 % [17]. The fatty acids varied significantly with respect to the genotypes [8]. It can be easily seen in Table 1 that linoleic acid was the dominating fatty acid, followed by palmitic and oleic acids. Most of the fatty acids were unsaturated, while saturated fatty acids (mainly, palmitic acid) contributed little of the total fatty acids content. The high composition of unsaturated fatty acids make chickpea a special legume, suitable for nutritional applications [7]. As far as the fatty acid compositions of the cultivars are concerned, the results can be seen in the Table 1 which shows that the highest compositions of the unsaturated fatty acids were determined in Uzunlu 99 (88,01 %), followed by Gökçe (87,77 %), Aydın 92 (87,75 %), ILC 482 (87,67 %), İnci (87,63 %) and Çağatay (87,56 %), Küsmen 99 (87,55 %), Damla 89 (87,53 %) and İzmir 92 (87,49 %). The lowest total compositions were detected in Canıtez 87 (79,96 %), Cevdetbey (80,75 %) and Aziziye 94 (83,66 %), respectively. In this research, while the oleic and linoleic acids contents ranged between 27.55-42.30 % and 41.25-57.25 %, respectively, according to the other study, major fatty acid contents varied between 18.57 and 35.23 % for oleic acid and 47.15 and 63.44 % for linoleic acid. When the planting time took into account, the mean values for oleic acid changed between 21.23 and 30.52 % and for linoleic acid between 51.77 and 60.79 % [8].

Furthermore, the total composition of the highest saturated fatty acids were determined in Canıtez 87 (17.71 %), Cevdetbey (16.18 %) and Aziziye 94 (13.92 %), respectively. On the other hand, the lowest composition was found in İnci (10.25 %), followed by Menemen 92 (10.36 %) and

Aydın 92 (10.60 %). According to Table 1, the palmitic acid (16:0) content the third major fatty acid of chickpea ranged from 9.78 to 8.43 %, whereas the other study revealed that the content ranged between 10.86 and 12.38 % [8].

According to Table 1 and Figure 1, it can be easily seen that the highest linolenic acid content was detected in ILC 482 (2.68 %), while the lowest content was determined in Gökçe (1.68 %). On the other hand, the highest and lowest linoleic acid contents were found in ILC 482 (57.25 %) and in Gülümser (41.25 %), respectively. The highest oleic acid content was observed to be in Gülümser (41.25 %), whereas the lowest content was investigated in ILC 482 (27.55 %).

Mineral composition of the chickpea cultivars. It is indicated in Table 2 and Figure 2 that the highest K content was detected in Menemen 92 (14370 ppm), whereas the lowest content was determined in Eser 87 (9811 ppm). Furthermore, the highest and lowest P contents were found in Küsmen 99 (5503 ppm) and in Eser 87 (3109 ppm), respectively. On the other hand, it can be easily seen that the Na was the lowest macro element of chickpea cultivars.

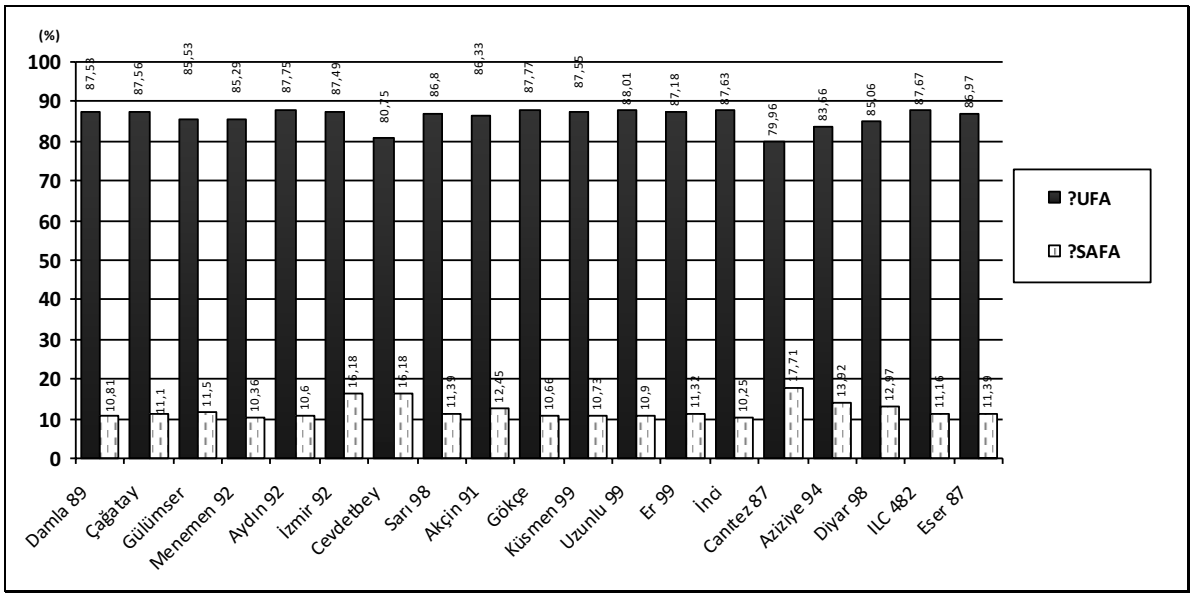

FIGURE 1
Unsaturated fatty acids and saturated fatty acids of compositions the chickpea cultivars cultivated in Turkey

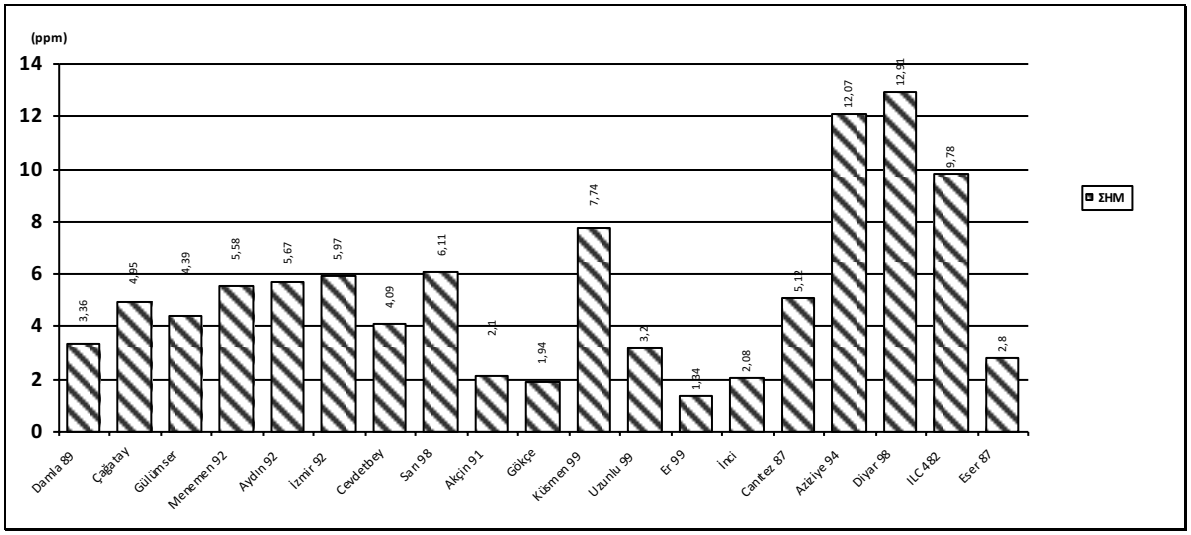

FIGURE 2
Heavy metal contens of the chickpea cultivars cultivated in Turkey

TABLE 2
Mineral contents of the chickpea cultivars cultivated in Turkey

Chickpea	Heavy metals (ppm)						Micro elements (ppm)					
Cultivars	Co	Pb	Cd	Cr	Ni	**ΣHM**	B	Fe	Zn	Cu	Mn	**ΣMIE**
Damla 89	0.51^{d}	0.78^{k}	0.15^{b}	0.43^{f}	1.49^{e}	3.36^{h}	58.17^{k}	52.55^{n}	34.74^{k}	8.75^{h}	49.03^{b}	203.24^{k}
Çağatay	0.23^{h}	Nd	nd	**2.25**^{a}	2.45^{d}	4.95^{f}	32.60^{p}	66.29^{f}	42.84^{e}	8.93^{g}	48.89^{c}	199.55^{l}
Gülümser	nd	Nd	nd	0.39^{f}	3.79^{b}	4.39^{g}	**23.93**^{r}	61.53^{i}	37.18^{h}	8.43^{j}	45.38^{d}	176.45^{q}
Menemen 92	0.30^{f}	1.61^{i}	nd	0.42^{f}	3.25^{c}	5.58^{f}	61.13^{j}	61.75^{h}	31.84^{n}	**0.02**^{q}	44.35^{e}	199.07^{m}
Aydın 92	0.26^{g}	2.45^{g}	nd	0.71^{c}	2.25^{d}	5.67^{f}	75.79^{c}	69.08^{d}	35.46^{i}	9.26^{f}	43.64^{h}	233.23^{d}
İzmir 92	0.18^{i}	3.28^{d}	**0.31**^{a}	0.63^{d}	1.57^{e}	5.97^{f}	81.94^{b}	53.22^{m}	29.46^{q}	11.37^{d}	37.53^{m}	213.53^{g}
Cevdetbey	0.11^{j}	2.54^{f}	**0.13**^{c}	**0.20**^{h}	1.11^{f}	4.09^{g}	68.55^{e}	47.94^{q}	30.30^{o}	7.11^{m}	35.27^{p}	189.17^{o}
Sarı 98	0.17^{i}	2.56^{f}	nd	1.08^{b}	2.30^{d}	6.11^{e}	**86.13**^{a}	73.53^{c}	30.08^{p}	0.35^{p}	36.26^{o}	226.36^{e}
Akçin 91	0.36^{e}	Nd	nd	0.36^{k}	1.38^{e}	2.10^{h}	70.99^{d}	50.17^{p}	34.81^{j}	14.07^{c}	38.12^{l}	208.16^{j}
Gökçe	0.24^{g}	**0.50**^{m}	nd	0.75^{c}	**0.45**^{h}	1.94^{j}	64.14^{h}	58.60^{j}	34.12^{l}	9.45^{e}	44.23^{f}	210.55^{i}
Küsmen 99	2.64^{b}	3.04^{e}	nd	0.30^{g}	1.76^{e}	7.74^{d}	66.25^{f}	56.04^{l}	39.48^{f}	15.01^{b}	34.32^{r}	211.11^{h}
Uzunlu 99	0.55^{c}	0.64^{l}	nd	0.45^{f}	1.56^{e}	3.20^{h}	56.81^{l}	52.52^{n}	**18.71**^{s}	7.81^{l}	40.12^{k}	175.97^{r}
Er 99	nd	Nd	nd	0.34^{g}	1.00^{g}	**1.34**^{k}	36.85^{o}	52.06^{o}	43.76^{d}	8.78^{h}	43.09^{i}	184.54^{p}
İnci	**0.08**^{k}	Nd	nd	0.33^{g}	1.67^{e}	2.08^{i}	28.15^{q}	105.22^{b}	**77.24**^{a}	8.37^{k}	**50.10**^{a}	**269.09**^{a}
Canıtez 87	0.49^{d}	1.84^{h}	nd	0.54^{e}	2.25^{d}	5.12^{f}	65.47^{g}	68.34^{e}	38.23^{g}	**17.97**^{a}	34.41^{q}	224.42^{f}
Aziziye 94	0.26^{g}	3.67^{c}	nd	1.09^{b}	**7.05**^{a}	12.07^{b}	49.98^{m}	**118.31**^{a}	46.76^{c}	8.94^{g}	43.77^{g}	267.76^{b}
Diyar 98	0.34^{e}	**10.86**^{a}	nd	0.26^{h}	1.45^{e}	**12.91**^{a}	46.96^{n}	62.45^{g}	32.11^{m}	8.65^{i}	42.95^{j}	193.12^{n}
ILC 482	**2.73**^{a}	4.52^{b}	Nd	0.28^{h}	2.25^{d}	9.78^{c}	68.55^{e}	57.30^{k}	65.30^{b}	6.50^{n}	36.70^{n}	234.35^{c}
Eser 87	nd	1.37^{j}	nd	0.35^{g}	1.08^{f}	2.80^{i}	63.26^{i}	**43.74**^{r}	26.02^{r}	5.48^{o}	**26.86**^{s}	**165.36**^{s}
Max:	**2.73**	**10.86**	**0.31**	**2.25**	**7.05**	**12.91**	**86.13**	**118.31**	**77.24**	**17.97**	**50.10**	**269.09**
Min:	**0.08**	**0.50**	**0.13**	**0.20**	**0.45**	**1.34**	**23.93**	**43.74**	**18.71**	**0.02**	**26.86**	**165.36**

Common letters in the same column indicate significant differences between the means at p <0.01 level.
ΣHM, total heavy metal content; ΣMIE, total micro element content ΣMAE.
nd: not determined

TABLE 2
Mineral contents of the chickpea cultivars cultivated in Turkey (Following)

Chickpea	Macro elements (ppm)					
Cultivars	K	Ca	Mg	Na	P	**ΣMAE**
Damla 89	14034^{b}	2512^{b}	**2037**^{a}	409^{b}	4465^{h}	23457^{a}
Çağatay	11240^{g}	2238^{c}	1304^{f}	89^{g}	4472^{h}	19343^{f}
Gülümser	12572^{e}	1525^{f}	1613^{b}	**10**^{k}	4721^{f}	20441^{e}
Menemen 92	**14370**^{a}	1520^{f}	1572^{b}	43^{j}	5130^{c}	22635^{b}
Aydın 92	13729^{c}	**3008**^{a}	1822^{a}	**507**^{a}	4568^{g}	**23634**^{a}
İzmir 92	11809^{f}	1635^{f}	1508^{c}	13^{j}	4757^{e}	19722^{f}
Cevdetbey	11126^{g}	1514^{f}	1634^{b}	112^{f}	4483^{i}	18869^{g}
Sarı 98	11158^{g}	1444^{f}	1608^{b}	19^{k}	4454^{i}	18683^{g}
Akçin 91	12542^{e}	1262^{g}	1204^{g}	151e	4471^{h}	19630^{f}
Gökçe	13505^{c}	2151^{d}	1669^{b}	24^{l}	5016^{c}	22365^{b}
Küsmen 99	14023^{b}	**886**^{i}	1545^{c}	87^{g}	**5503**^{a}	22044^{c}
Uzunlu 99	12460^{e}	1232^{h}	1639^{b}	31^{k}	5475^{a}	20837^{d}
Er 99	13165^{d}	1573^{f}	1360^{d}	47^{j}	4921^{d}	21066^{d}
İnci	11814^{f}	2506^{b}	1607^{b}	185^{d}	5167^{c}	21279^{d}
Canıtez 87	13188^{d}	2448^{b}	1574^{c}	64^{h}	5200^{b}	22474^{b}
Aziziye 94	10690^{h}	2462^{b}	1523^{c}	394^{c}	4735^{e}	19804^{f}
Diyar 98	11127^{g}	1219^{h}	1457^{c}	40^{j}	4282^{j}	18125^{h}
ILC 482	10669^{h}	2001^{d}	**1218**^{g}	131^{e}	4807^{e}	18826^{g}
Eser 87	**9811**^{i}	1929^{e}	1367^{e}	51^{i}	**3109**^{k}	**16267**^{i}
Max:	**14370**	**3008**	**2037**	**507**	**5503**	**23634**
Min:	**9811**	**886**	**1218**	**10**	**3109**	**16267**

Common letters in the same column indicate significant differences between the means at p <0.01 level.
ΣMAE; total macro element content.

Furthermore, as can be seen in Table 2 that the composition of heavy metals (ppm), micro and macro elements (ppm) are indicated. According to the study results, the heavy metal composition of the eighteen chickpea cultivars were determined to range from 1.34 to 12.91 % (Figure 2), showing that the highest contents were found in Diyar 98 (12.91 ppm), Aziziye 94 (12.07 ppm) and ILC 482 (9.78 ppm) cultivars. However, the lowest contents were observed in Er 99 (1.34 ppm), Gökçe (1.94 ppm) and Eser 87 (2.80 ppm) cultivars. Concentration of essential elements may vary from one region to other one as a consequence of various agricultural practices, type of soil, type of fertilizer and pesticides/herbicides. Therefore, the increases in major elements (such as Ca, P, Mg, Na and K), some minor elements or trace elements (such as Fe, Ba) and heavy metal (such as Pb, Ni, Cr, Co) in the chickpea under grown conditions could be attributed to the differences in different practices [18-21].

On the other hand, micro element composition (MIEs) of nineteen chickpea cultivars varied from 165.36 to 269.09 ppm. It was observed that the highest MIEs were detected in İnci (269.09 ppm), Aziziye 94 (267.76 ppm) and ILC 482 (234.35 ppm) cultivars. Eser 87 (165.36 ppm), Uzunlu 99 (175.97 ppm) and Gülümser (176.45 ppm) were the cultivars having the lowest MIEs (Figure 3). Significant cultivars differences were also found content of iron and zinc among chickpea cultivars. Iron content ranged from 43.74 to 118.31 ppm. Iron content was found highest (Aziziye 94) and lowest in (Eser 87). Zinc content ranged from 18.71 ppm (Uzunlu 99) to 77.24 ppm (Inci). It was reported that significant varietal differences were found in total content of iron and zinc among chickpea cultivars and results also showed that iron content ranged from 46 to 103 ppm and zinc content from 22 to 62 ppm for nine different chickpea cultivars [16]. The values obtained from this study are similar to the Zn and Fe values reported for chickpea. The macro element compositions (MAEs) of the nineteen chickpea cultivars, compared with each other in the Table 2 and Figure 4. revealed that Aydın 92 cultivar had the highest MAC (23,634

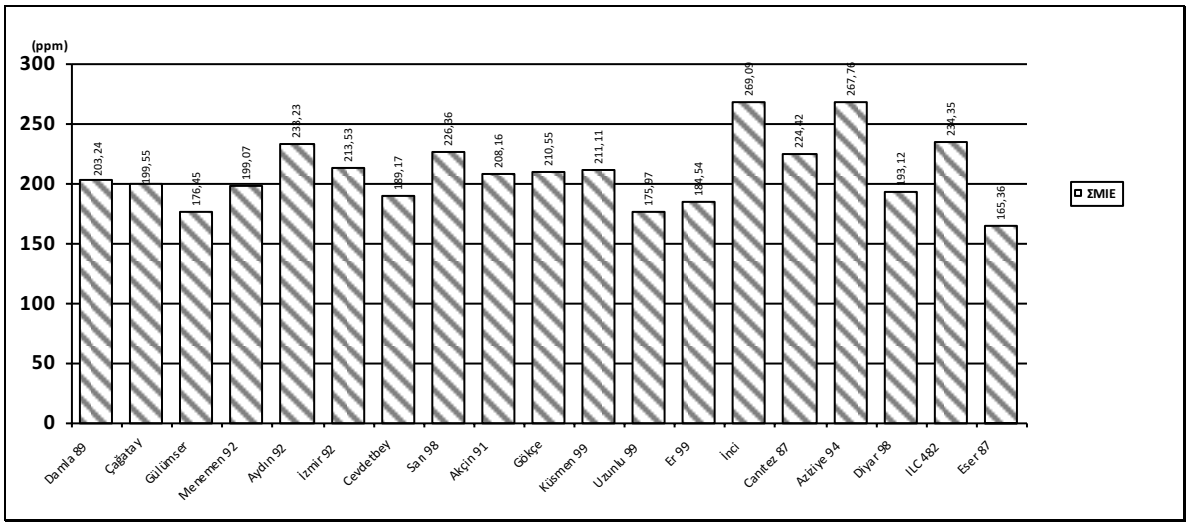

FIGURE 3
Micro elements contents of the chickpea cultivars cultivated in Turkey

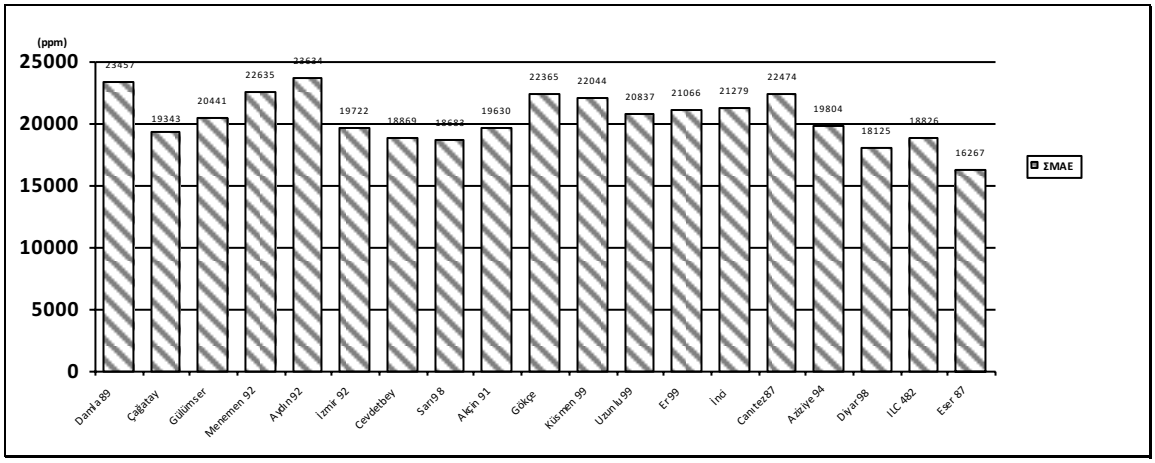

FIGURE 4
Macro elements contents of the chickpea cultivars cultivated in Turkey

ppm), followed by Damla 89 (23457 ppm) and Menemen 92 (22635 ppm). However, the lowest MAE was determined in Eser 87 (16267 ppm), followed by Diyar 98 (18125 ppm) and Sarı 98 (18683 ppm). Another study reported that mineral constituents of chickpea changed between the cultivars (potassium constituted the major mineral), ranging from 9800 to 14366 % [19]. Cultivars soil type, soil conditions, fertilization, irrigation and weather etc. are among the factors affecting the elemental contents of plants [20].

The most abundant minerals in *chickpea cultivars* were potassium (K) phosphorus (P), magnesium (ppm), calcium (Ca) and sodium (Na), while boron (B), zinc (Zn), iron (Fe), manganese (Mn) and copper (Cu) were in minor amount. This study shows a comprehensive presentation of macro and micro elements of chickpea cultivars cultivated in Turkey.

The results of this study indicate that chickpea cultivars are rich in crude oil, unsaturated fatty oil and mineral contents. The results suggested that these chickpea cultivars can be an economic, improving overall nutritional status of functional food in which they will be added. More agronomic and chemical studies should be done on chickpea with a view to cultivating.

ACKNOWLEDGEMENTS

The author would like to thank Ms. S. A. Çelik for her assistance in the experiments.

REFERENCES

[1] Sreerama, Y.N., Sashikala, V.B., Pratape, V.M. and Singh, V. (2012) Nutrients and antinutrients in cowpea and horse gram flours in comparison to chickpea flour: Evaluation of their flour functionality. Food Chemistry. 131, 462-468.

[2] FAO (2012) Food and Agricultural Organization Statistical Database. Rome: FAO (Food and Agricultural Organization)-available at www.faostat.org.

[3] Anonymous (2011) State Statistics Institute, Ankara, Turkey.

[4] Özdemir, S. and Karadavut, U. (2003) Comparison of the performance of autumn and spring sowing of chickpeas in a temperate region. Turkish Journal of Agriculture and Forestry. 27, 345-352.

[5] Gül, M.K., Egesel, C.Ö. and Türk, M.F. (2005) Bazı nohut hatlarının Çanakkale yöresinde kış koşullarına adaptasyonu. Türkiye VI. Tarla Bitkileri Kongresi Bildiriler Kitabı. 1, 267–269 (in Turkish).

[6] Zia-Ul-Haq, M.Z., Ahmad, M., Iqbal, S., Ahmad, S. and Ali H. (2007) Characterization and Compositional Studies of Oil from Seeds of Desi Chickpea (*Cicer arietinum* L.) Cultivars Grown in Pakistan. J Am Oil Chem Soc. 84, 1143–1148.

[7] Zia-Ul-Haq, M.Z., Iqbal, S., Ahmad, S., Imran, M., Niaz, A. and Bhanger, M.I. (2007) Nutritional and compositional study of Desi chickpea *(Cicer arietinum L.)* cultivars grown in Punjab, Pakistan. Food Chemistry. 105, 1357–1363.

[8] Gül, M.K., Egesel, C.Ö. and Turhan, H. (2008) The effects of planting time on fatty acids and tocopherols in chickpea. Eur Food Res Technol. 226, 517–522.

[9] Kan, A., Özçelik, B. and Kartal, A. (2009) In vitro antiviral activities under cytotoxic doses against herpes simples type-1 and parainfluensa-3 viruses of *Cicer arietinum* L. (Chickpea). African Journal of Pharmacy and Pharmacology. 3(12), 627-631.

[10] Kan, A., Özçelik, B., Kartal, M., Özdemir, Z.A. and Özgen, S. (2010) In Vitro Antimicrobial Activities of *Cicer arietinum* L (Chickpea). Tropical Journal of Pharmaceutical Research. 9(5), 475-481.

[11] Akbaba, U., Şahin, Y. and Turkez, H. (2012) The element contents in chickpeas grown under organic and conventional farming regimes using WDXRF analysis for human nutrition and health. Turk J Phys. 36, 279 – 287.

[12] Günes, A., Cicek, N., Inal, A., Alpaslan, M., Eraslan, F., Guneri, E. and Guzelordu, T. (2006) Genotypic response of chickpea *(Cicer arietinum L.)* cultivars to drought stress implemented at pre- and post-anthesis stages and its relations with nutrient uptake and efficiency. Plant Soil Environ. 52(8), 368–376.

[13] Asif, K.H. and Ahsan, S.M. (2011) A Critical Analysis of the Existing Ontology Evolution Approaches. Journal of American Science. 7(7), 145-152.

[14] AACC International Method (1999) Determination of the crude oil in wheat, corn and soy flour, feeds and mixed feeds. AACCI Method 30-25.01

[15] Ficco, D.B.M., Riefolo, C., Nicastro, G., De Simone, V., Di Gesu, A.M., Beleggia, R., Platani, C., Cattivelli, L. and De Vita, P. (2009) Phytate and mineral elements concentration in a collection of Italian durum wheat cultivars. Field Crops Research. 111, 235–242.

[16] Sharma, S., Yadav, N., Singh, A. and Kumar, R. (2013) Nutritional and antinutritional profile of newly developed chickpea *(Cicer arietinum L)* varieties. International Food Research Journal. 20, 805-810.

[17] Lou, Z., Wang, H., Zhang, M. and Wang, Z. (2010) Improved extraction of oil from chick-pea under ultrasound in a dynamic system. Journal of Food Engineering. 98, 13–18.
[18] Setia, N. and Malik, C.P. (1985) Distribution of Mineral Nutrients in Developing Fruits of Chickpea *(Cicer arietinum)*. Phyton. 25(1), 17-21.
[19] Alajaji, S.A. and El-Adaway, T.A. (2006) Nutritional composition of chickpea (*Cicer arietinum* L.) as affected by microwave cooking and other traditional cooking methods. Journal of Food Composition and Analysis. 19, 806-812.
[20] Kan, Y., Kan, A., Ceyhan, T., Sayar, E., Kartal, M., Altun, L., Aslan, S. and Cevheroğlu, Ş. (2005) Atomic Absorbtion Spektrometric analysis of *Trigonella foenum- graecum L.* seeds cultivated in Turkey. Turkish Journal of Pharmalogical Science. 2(3), 187-191.
[21] Arslan, M. (2017) Variation of some seed trace element contents in grass pea (*Lathyrus sativus* L.) Genotypes from Turkey. Fresen. Environ. Bull. 26, 3676-3684.

Received: **02.08.2017**
Accepted: **05.12.2017**

CORRESPONDING AUTHOR

Muharrem Kaya
Department of Field Crops,
Faculty of Agriculture,
Süleyman Demirel University,
Isparta – Turkey

e-mail: muharremkaya@sdu.edu.tr

© by PSP Volume 27 – No. 2/2018 pages 1248-1255 Fresenius Environmental Bulletin

THE USE OF FURFURAL RESIDUE FOR AQUEOUS-PHASE Cr(VI) REDUCTION

Zhili Wang, Huanzhen Zhang*

School of Water Resources and Environment, China University of Geosciences (Beijing), Beijing, 100083, China

ABSTRACT

Hexavalent chromium (Cr(VI)) in environmental systems is an important concern due to its toxicity. The first step in the conventional treatment of Cr(VI)-containing pollutants is the reduction of Cr(VI) to trivalent chromium (Cr(III)), which is less toxic. The objective of this study was to explore the kinetics of Cr(VI) reduction using a cheap, locally available biomass waste, furfural residue (FR). The effects of pH and equilibration time were investigated. The results showed that Cr(VI) was removed (100%) after a shaking time of 18 h: 69.52% of the Cr was reduced by FR and approximately 30% of the Cr was adsorbed by FR. The initial stage (0.5 h) of the reaction process was based on the reduction of Cr(VI), and the adsorption rate of Cr(VI) increased as the reaction time increased in the early stage (6 h). The removal rate for Cr(VI) reached 100% at a pH of 6.5, and half of the Cr was reduced. When the initial pH was less than 6.5, the reduction of Cr(VI) increased as the pH decreased. The reduction rate of Cr(VI) reached 99.9% with an initial pH of 2.5. The Cr(VI) reduction process with FR followed a second-order kinetic model.

KEYWORDS:
Chromium (VI), Reduction, Furfural Residue, Chromium (III).

INTRODUCTION

Cr contamination in ecosystems is a significant global problem. The most stable Cr oxidation states are +3 and +6 in most natural water environments. Hexavalent Cr (Cr(VI)) is highly toxic, mutagenic and potentially carcinogenic to living organisms [1, 2, 3]. In contrast, trivalent Cr (Cr(III)) is less toxic than Cr(VI) and is immobile in aqueous environments because it readily precipitates as $Cr(OH)_3$ or mixed Fe(III)-Cr(III) (oxy) hydroxides in the pH range of natural water [4].

Because of the significant differences in the physical and chemical properties of the two oxidation states of Cr, the reduction of Cr(VI) to Cr(III) is an attractive and useful solution for the remediation of Cr(VI) contamination. Commonly used reducing agents include sulfur dioxide, sodium sulfite and ferrous sulfate [5]. However, these agents introduce other ions that increase the amount of dissolved solids and further complicate the sorption process. In addition to using various inorganic materials, the reduction of Cr(VI) using organic substances [6, 7, 8, 9, 10, 11, 12, 13, 14], agricultural by-products [15, 16, 17], algae [18]and microorganisms [19, 20, 21, 22, 23] has been widely investigated.

Furfural residue (FR) is an industrial waste that is produced during the manufacturing of furfural from corn cobs. China annually generates at least 2~3 million tons of FRs [24, 25, 26]. FR could potentially be used as a reconditioning agent for Cr(VI) pollution. FR has a porous microstructure, is enriched in both cellulose and lignin, and has active functional groups with strong reducibility. Ren Guangjun et al. [27] and Chen Xiaoyan et al. [28] investigated FR for the adsorption of Cr(VI) and Cr(III), respectively. However, no study has previously used FR to reduce Cr(VI). The reduction of Cr(VI) by FR in aqueous solutions was studied in this paper, and the kinetics of the Cr reduction were investigated by eliminating the adsorption influence.

MATERIALS AND METHODS

Raw materials and chemicals. FR was kindly provided by Liangtian Company (Hebei Province, China) and was water-rinsed before use. The main components of FR were hemicellulose, 5.68%; cellulose, 37.33%; lignin, 40.75%; and ash, 13.90% (absolute wt% of the starting material). The raw FR had an initial pH of 2–3 and was washed with deionized water to remove dirt and other impurities. Then, it was dried in a hot air oven at 70°C for 12 h, ground, sieved to obtain a size under 40 mesh and stored in sealed bags at room temperature. The other chemicals used were all analytical grade and used as purchased without further purification.

The Cr(VI) standard solution (1000 mg/L) was purchased from the National Analysis and Testing Center of Nonferrous Metals and Electronic Materials. To eliminate the influence of Cr(VI) adsorption on FR, a KH_2PO_4 solution (0.01 mol/L) was prepared [29]. The working solution of 10 mg Cr(VI)/L was prepared by diluting the Cr(VI) standard solution with the KH_2PO_4 solution (0.01 mol/L).

Reduction experiments. The reduction experiments were performed using a continuously shaken batch system. The FR (0.5 g) and 50 mL of the prepared working solution were added to 150 mL conical flasks without adjusting the pH. The experiments were conducted in an air bath homothermal vibrator at 25°C and 220 rpm. After a predetermined time (0.5 h~24 h), the supernatant solutions were collected by centrifugation (4500 rpm, 10 min) and filtration (0.45 μm) and analyzed for their Cr(VI) and total Cr contents and pH values. In this study, a mixture of 0.5 g of FR and 50 mL of the 10 mg Cr(VI)/L solution diluted with distilled water without KH_2PO_4 was used as the control.

The effects of pH on the Cr(VI) reduction rate were studied by varying the pH from 2 to 10. The pH values of the working solutions were adjusted prior to the reduction experiments to predetermined values using small additions of concentrated HCl or NaOH solution, and the values were confirmed by pH measurements. The concentration of the Cr(VI) solution used in this study was 10 mg/L. The volume of the working solution containing 0.01 mol/L KH_2PO_4 was 50 mL. The FR amount used was 0.5 g dry weight. The vibrator speed was 220 rpm, and the contact time was approximately 150 min at 25°C. FR (0.5 g) and 50 mL of 10 mg/L Cr(VI) solutions without KH_2PO_4 were pH adjusted and used as controls.

Analytical methods. The metal ion concentration was analyzed using a HACH DR6000 UV-vis spectrophotometer. The Cr(VI) concentration was determined using the 1,5-diphenylcarbohydrazide spectrophotometric method (GB7467-87). The total Cr concentration was determined using the potassium permanganate oxidation-1,5-diphenylcarbohydrazide spectrophotometric method (GB7466-87).

In all the aqueous solution samples, the total Cr was assumed to include Cr(VI) and Cr(III). Thus, the Cr(III) concentration in each sample was calculated using the following equation:

$$Cr(III)=\text{Total } Cr - Cr(VI)$$

RESULTS AND DISCUSSION

Effect of the equilibration time. The effect of the contact duration on the rate of Cr(VI) and total Cr reduction was studied at 25°C at a pH of 6.5. The percent decrease in the Cr concentration with respect to time is plotted in a graph in Figure 1. An appreciable difference was observed in the decrease in the Cr concentration between the control and reduction groups. Figure 1 (a) clearly shows that a 100% decrease in Cr(VI) was achieved in the control group with a shaking time of 18 h, and a 69.5% decrease in Cr(VI) was achieved in the reduction group with a shaking time of 24 h. When the contact duration was 18 h, the total Cr removal efficiencies were 56.3% and 26.5% for the control and reduction groups, respectively (Figure 1 (b)). The efficiency increased to 30.2% for the reduction group at a shaking time of 24 h. Based on the data comparison in Figure 1 (a), the initial stage (0.5 h) of the control group mainly included the Cr(VI) reduction reaction. After this stage, the reduction rate gradually decreased, and the adsorption rate substantially increased over time. Figure 1 (b) illustrates that the adsorption rate of Cr(III) on FR did not substantially change over the entire reaction. The adsorption rate of Cr(VI) increased as the reaction time increased in the early stage (6 h).

Figure 2 shows the Cr(III) concentration variations in over time, displaying differences between the control and reduction groups. At the beginning of the reaction (0.5~2 h), the Cr(III) concentration in the control group rapidly increased to 4.12 mg/L from 1.78 mg/L. The Cr(III) concentration in the reduction group increased from 2.78 mg/L to 3.52 mg/L within 0.5~5 h. The equilibrium Cr(III) concentration in the control group was 4.37 mg/L, which was slightly higher than that in the reduction group (4.02 mg/L).

The pH values were different in the two equilibrium solutions, and the values were 4.12 in the control group and 6.18 in the reduction group, indicating that the adsorption process for Cr(VI) on FR consumes hydroxyl ions or hydroxide radicals or causes the release of hydrogen ions.

Effect of the pH. The decreases in the Cr(VI) and total Cr contents with FR at different pH values at an initial concentration of 10 mg/L and an FR dose of 10 g/L are shown in Figure 3. The decrease in Cr(VI) (caused by both reduction and adsorption) in the control group was 100% for pH values under 6.5. However, this value decreased to 95.9%, 92.4% and 88.9% when the initial pH values were 7.5, 8.5 and 9.5, respectively. At a pH of 10.6, the efficiency decreased to 61.6%. In the reduction group, the Cr(VI) reduction efficiency decreased at higher initial pH values, and the efficiencies were 99.9%, 92.5%, 85.6%, 67.2% and 50% for pH values of 2.5, 3.3, 4.5, 5.5 and 6.5, respectively. No appreciable change was observed for the pH values of 7.5, 8.5, 9.5 and 10.6. Figure 3 (b) shows that the decrease in the total Cr (caused by the adsorption of Cr(VI) and Cr(III)) in the control group was steady at 48.59-54.97% in the pH range from 2.5 to 9.5, but the decrease dropped to 27% for the pH value of 10.6. The variation in the decrease in the total Cr (caused by the adsorption of Cr(III)) in the reduction group was similar to the variation observed in the Cr(VI) reduction efficiency (Figure 3 (a)). The highest decrease in the total Cr in the reduction group was 62.29% at a pH value of 2.5, and the decrease gradually fell to 14.21% for a pH value of 6.5. The lowest efficiency was 8.55% for a pH value of 8.5.

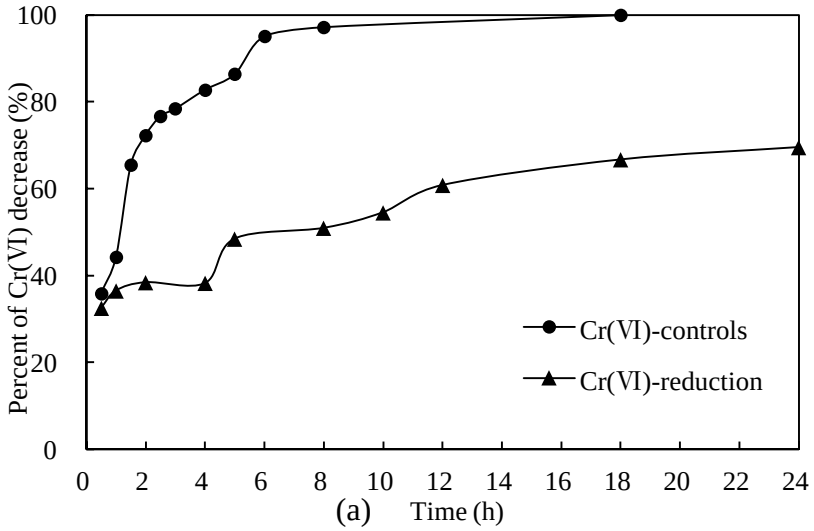

(a)

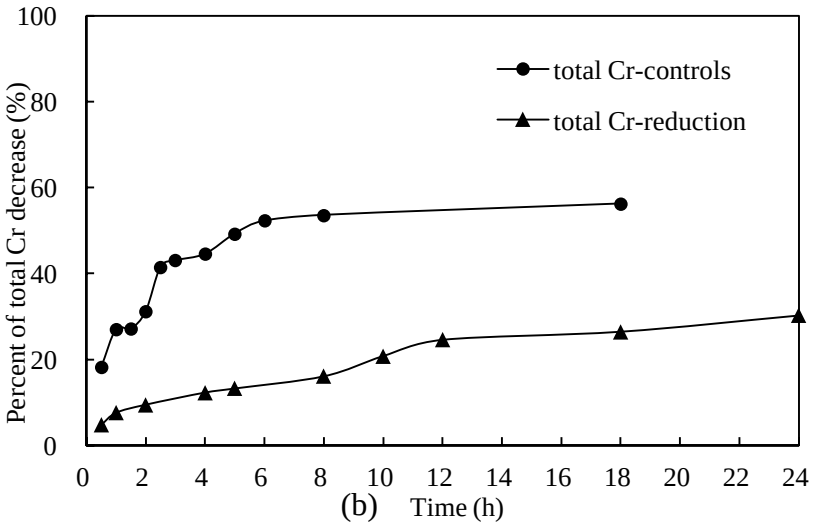

(b)

FIGURE 1
Effect of the equilibration time on the percent decrease of Cr

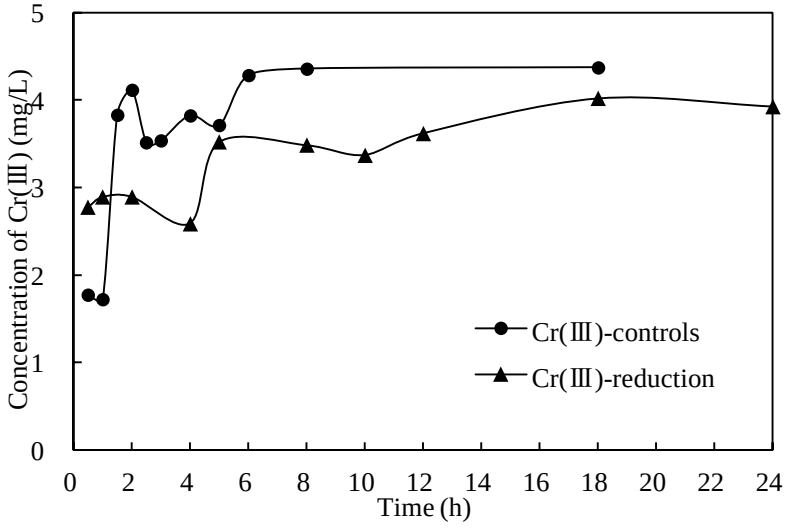

FIGURE 2
Effect of the equilibration time on the Cr(III) concentration

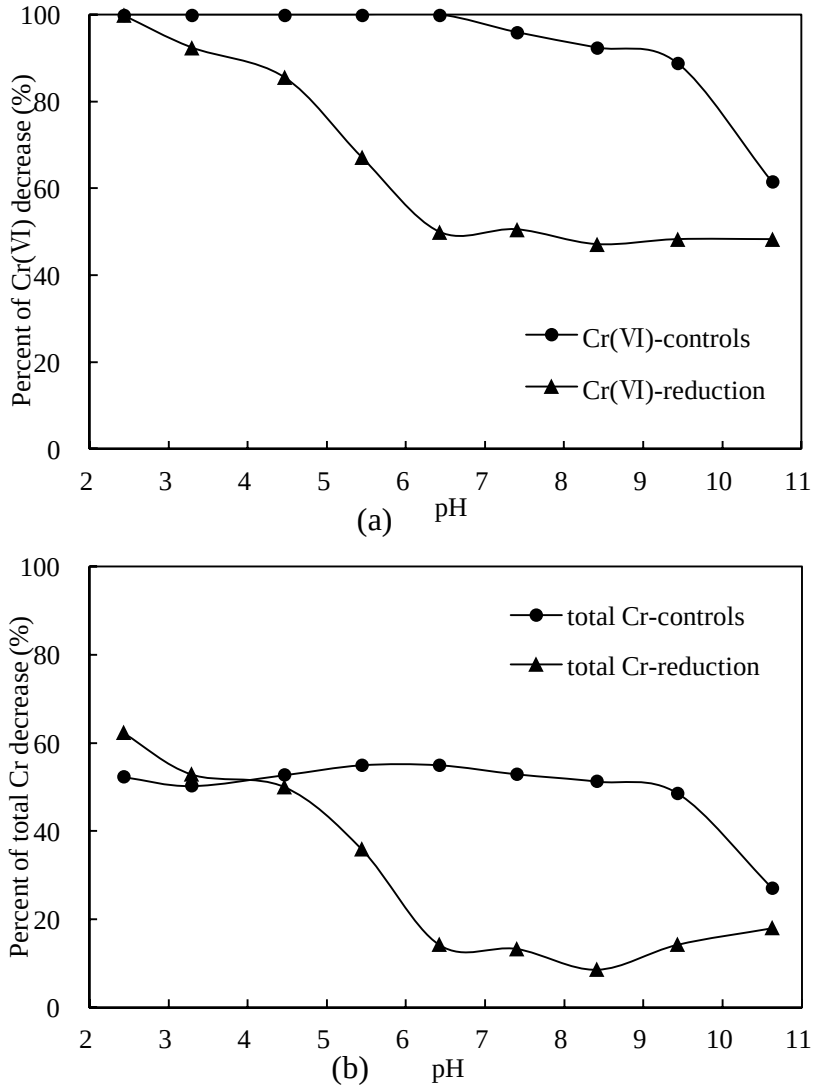

FIGURE 3
Effect of the pH on the decrease in Cr

Figure 3 (a) shows that the reduction of Cr(VI) to Cr(III) by FR gradually decreased as the initial pH increased (2.5~6.5). When the pH value was between 6.5 and 10.6, the adsorption of Cr(VI) on FR gradually weakened as the initial pH increased, whereas no decrease was observed in the reduction of Cr(VI). Figure 3 (b) shows that the initial pH value has a large effect on the adsorption efficiency of Cr(III) by FR, but the initial pH has little influence on the total Cr content.

Figure 4 shows that the Cr(III) concentrations in the reduction and control groups were 3~4 mg/L and 3~4.5 mg/L, respectively. The Cr(III) concentrations in solution depend on the Cr(VI) reduction rate and the Cr(III) sorption rate. In the reduction group, the Cr(VI) concentrations were relatively high since the adsorption of Cr(VI) on FR was inhibited by the KH_2PO_4. The Cr ions in the control group solution were mainly Cr(III), and the Cr(VI) concentration was only greater than 50% when the initial pH was 10.6.

An increase in the pH values can be seen in Figure 5. However, all of the final pH values were lower than the corresponding initial pH values, which is likely due to the production of hydronium ions during the adsorption process. Overall, the final pH values of the reduction group were higher than the equilibrium pH values of the control group, which indicates more hydronium ions were produced during the adsorption process of Cr(VI).

Cr(VI) reduction kinetics model. Experiments on Cr(VI) reduction by FR in aqueous solutions showed that the reduction kinetics are complex. The initial Cr reduction is rapid because a substantial amount of reduction occurs within 30 min of the start of the reaction. After the initial sampling period, the reduction rate gradually slows over time. To determine the reduction rate constants, first-order and second-order kinetic models were applied to the experimental data. The kinetic models can be expressed as follows.

The first-order reaction is:

$$\log(q_e - q_t) = \log q_e - k_1 t/2.303$$

where q_t is the amount of Cr(VI) reduced to Cr(III) at time t per unit weight of FR (mg/g), k_1 is the rate constant of the first-order model (min^{-1}) and t is the time (min). q_e is the amount of Cr(VI) reduced to Cr(III) at equilibrium per unit weight of FR (mg/g). Plotting $\log(q_e - q_t)$ against time creates a straight line with slope $-k_1$. An approximately linear plot was obtained for the Cr (VI) reduction, which is shown in Figure 6. The kinetic constant k_1 and q_e were obtained from the slope of the plot and the fitting formula, which are tabulated in Table 1.

The second-order rate model can be represented as:

$$t/q_t = 1/k_2\, q_e^2 + t/q_e$$

where k_2 is the rate constant for the second-order model (M/min.). The plot of t/q_t versus time should give a straight line if the reaction is of second-order in nature. The plot for the Cr (VI) reduction was found to be linear (Figure 7). The values of k_2 and q_e are tabulated in Table 1.

The plots for the Cr(VI) reduction were both linear (Figure 6 and Figure 7). The regression coefficient was closer to unity in the second-order model (R^2=0.9807) than in the first-order model (R^2=0.9579). Therefore, the reduction of Cr(VI) by FR was more appropriately approximated using the second-order kinetic model.

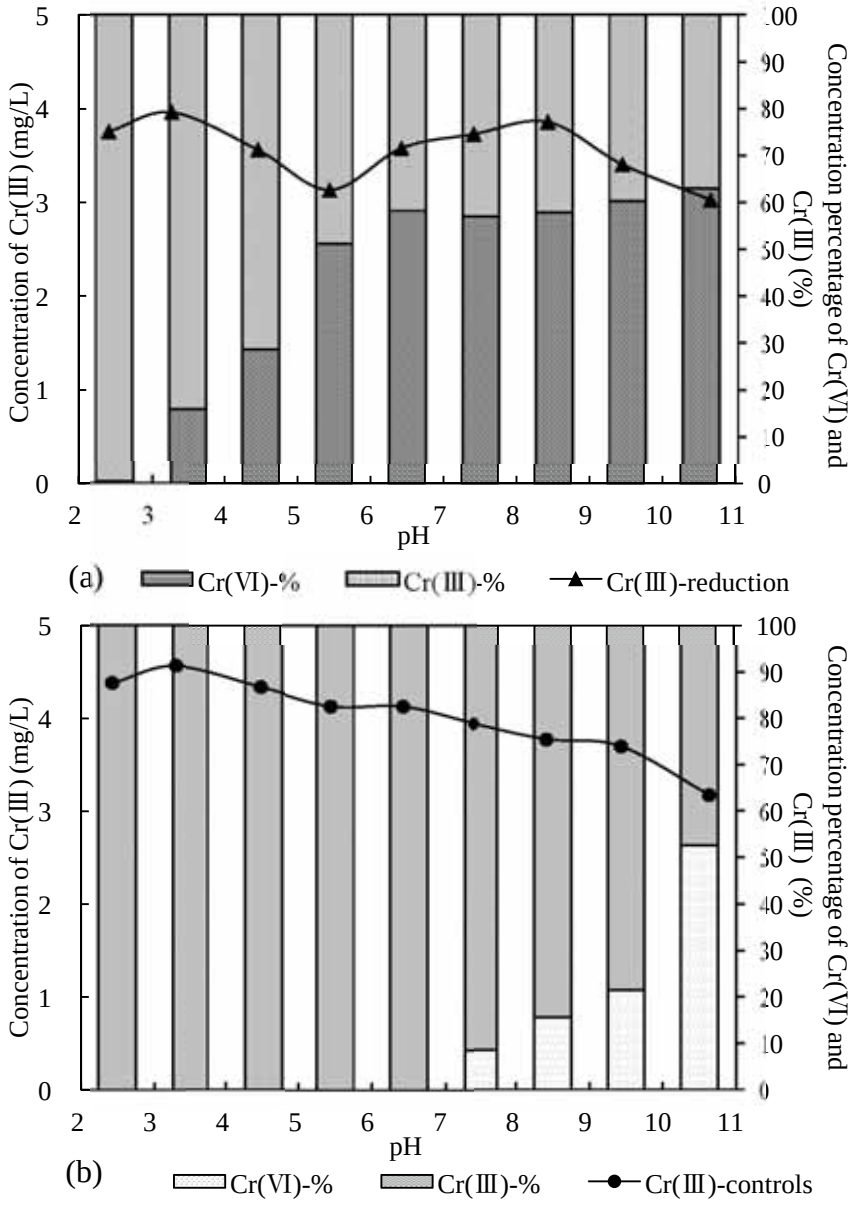

FIGURE 4
Effect of the pH on the Cr(III) concentration and Cr(VI) and Cr(III) concentration percentages

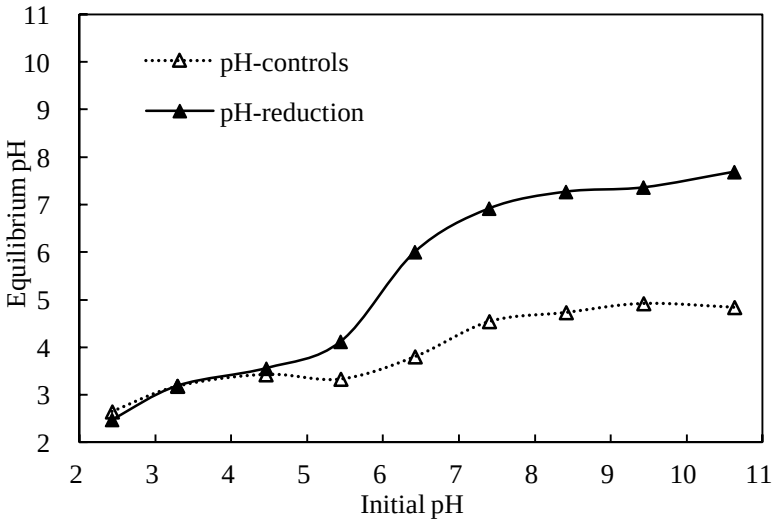

FIGURE 5
Change in the final pH after 150 min of equilibration

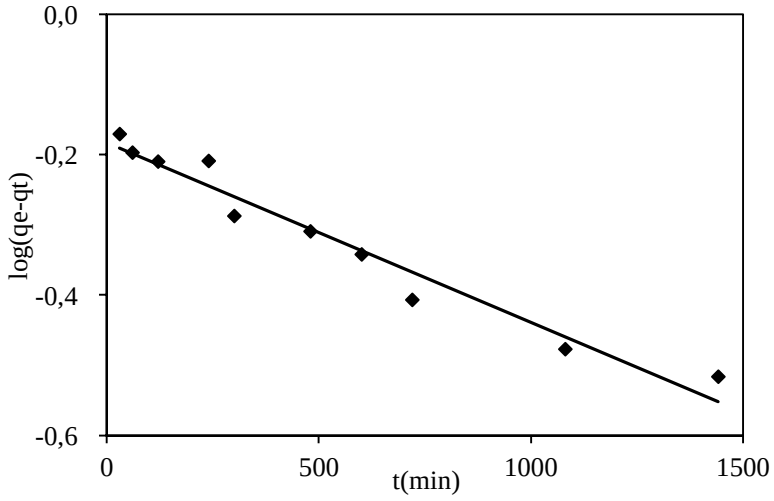

FIGURE 6
First-order kinetics plot for the reduction of Cr(VI)

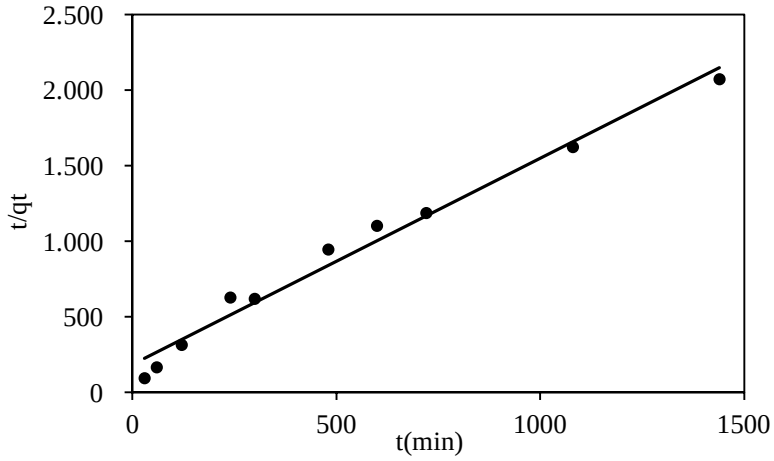

FIGURE 7
Second-order kinetics plot for the reduction of Cr(VI)

TABLE 1
Regression equations and kinetic parameters for the reduction of Cr(VI)

Reaction kinetics model	Regression equation	R^2	k_1 (min^{-1})	k_2 (M/min)	q_e (mg/g)
First-order reaction	y=-0.0003x-0.1828	0.9579	0.0007	_	0.6564
Second-order reaction	y=1.3656x+181.07	0.9807	_	0.0030	0.7323

CONCLUSIONS

FR is very efficient for the removal of Cr(VI) from aqueous solution because of its excellent reduction and adsorption properties. The removal rates for Cr(VI) and the total Cr content were 100% and over 50%, respectively, under both acidic and neutral conditions. The Cr(VI) reduction rate by FR is fast. In the initial stage, reduction is the main mechanism. As the reaction time increases, the adsorption and reduction rates increase. The Cr(VI) reduction process on FR consumes hydrogen ions; therefore, the reduction rate is higher at lower pH values. Under alkaline conditions, the Cr(VI) reduction degree is between 47%~51%. The kinetics of the Cr(VI) reduction process can be described using a second-order rate equation. FR could be utilized for the treatment of wastewater or groundwater contaminated with Cr(VI).

REFERENCES

[1] Puls, R.W., Blowes, D.W. and Gillham, R.W. (1999) Long-term performance monitoring for a permeable reactive barrier at the U.S. Coast Guard Support Center, Elizabeth City, North Carolina. J. Hazard. Mater. 68(1-2), 109-124.

[2] Blowes, D.W., Ptacek, C.J., Benner, S.G., McRae, C.W.T., Bennett, T.A. and Puls, R. (2000) Treatment of inorganic contaminants using permeable reactive barriers. J. Contam. Hydrol. 45(1-2), 123-137.

[3] Yari, A.R., Nasseri, S., Mahvi, A.H., Nabizadeh, R., Kalantari, R.R. and Yunesian, M. (2013) Application of forward osmosis membrane in removal of chromium from aqueous solutions. Fresen. Environ. Bull. 22, 2319-2323.

[4] Rai, D., Sass, B.M. and Moore, D.A. (1987) ChemInform Abstract: Chromium (III) Hydrolysis Constants and Solubility of Chromium (III) Hydroxide. Inorg. Chem. 26(3), 345-349.

[5] Kotaś, J. and Stasicka, Z. (2000) Chromium occurrence in the environment and methods of its speciation. Environ. Pollut. 107(3), 263-283.

[6] Chebrolu, P. and Sharada, P.K. (1993) Reduction of potassium chromate by D-fructose, D-galactose, D-mannose, D-glucose and L-sorbose. Carbohyd. Res. 244(1), 15-25.

[7] Elovitz, M. S. and Fish, W. (1994) Redox interactions of Cr(VI) and substituted phenols: kinetic investigation. Environ. Sci. Technol. 28(12), 2161-2169.

[8] Steams, D.M. and Wetterhahn, K.E. (1994) Reaction of chromium (VI) with ascorbate produces chromium (V), chromium (IV), and carbon-based radicals. Chem. Res. Toxicol. 7(2), 219-230.

[9] Wittbrodt, P.R. and Palmer, C.D. (1995) Reduction of Cr(VI) in the presence of excess soil fulvic acid. Environ. Sci. Technol. 29(1), 255-263.

[10] Deng, B. and Stone, A.T. (1996) Surface-catalyzed chromium (VI) reduction: Reactivity comparisons of different organic reductants and different oxide surfaces. Environ. Sci. Technol. 30(8), 2484-2494.

[11] Hug, S.J., Laubscher, H.U. and James, B.R. (1997) Iron (III) catalyzed photochemical reduction of chromium (VI) by oxalate and citrate in aqueous solutions. Environ. Sci. Technol. 31(1), 160-170.

[12] Jorge, F.S., Santos, T.M., Jesus, J. and Banks, W.B. (1999) Reactions between Cr(VI) and wood and its model compounds. 1. A qualitative kinetic study of the reduction of hexavalent chromium. Wood Sci. Technol. 33(6), 487-499.

[13] Pohlandt-Schwandt, K., Salthammer, T. and Marutzky, R. (2002) Reduction of soluble chromate in wood ash by formaldehyde. Biomass & Bioenergy. 22(2), 139-143.

[14] Yurkow, E.J., Hong, J., Min, S. and Wang, S. (2002) Photochemical reduction of hexavalent chromium in glycerol-containing solutions. Environ. Pollut. 117(1), 1-3.

[15] Wyszkowski, M. and Radziemska, M. (2013) Influence of Chromium (III) and (VI) on the concentration of mineral elements in oat (Avena sativa L.). Fresen. Environ. Bull. 22, 979-986.

[16] Gardea-Torresdey, J.L., Tiemann, K.J., Armendariz, V., Bess-Oberto, L., Chianelli, R.R., Rios, J.G., Parsons, G. and Gamez, G. (2000) Characterization of Cr(VI) binding and reduction to Cr(III) by the agricultural byproducts of Avena monida (oat) biomass. J. Hazard. Mater. 80(1-3), 175-188.

[17] Daneshvar, N., Salari, D. and Aber, S. (2002) Chromium adsorption and Cr(VI) reduction to trivalent chromium in aqueous solutions by soya cake. J. Hazard. Mater. 94(1), 49-61.

[18] Malkoc, E. and Nuhoglu, Y. (2003) The removal of chromium (VI) from synthetic wastewater by Ulothrix zonata. Fresen. Environ. Bull. 12, 376-381.
[19] Shen, H., Pritchard, P.H. and Sewell, G.W. (1996) Microbial reduction of Cr(VI) during anaerobic degradation of benzoate. Environ. Sci. Technol. 30(5), 1667-1674.
[20] Evans, M.N.C. and Wang, Y.T. (1997) Hexavalent chromium reduction by bacillus sp. in a packed-bed bioreactor. Environ. Sci. Technol. 31(5), 1446-1451.
[21] Shakoori, A.R., Makhdoom, M. and Haq, R.U. (2000) Hexavalent chromium reduction by a dichromate-resistant gram-positive bacterium isolated from effluents of tanneries. Appl. Microbio. Biot. 53(3), 348-351.
[22] Wielinga, B., Mizuba, M.M., Hansel, C.M. and Fendorf, S. (2001) Iron Promoted Reduction of Chromate by Dissimilatory Iron-Reducing Bacteria. Environ. Sci. Technol. 35(3), 522-527.
[23] Quilntana, M., Curutchet, G. and Donati, E. (2001) Factors affecting chromium (VI) reduction by Thiobacillus ferrooxidans. Biochemical Engineering Journal. 9(1), 11-15.
[24] Tang, Y., Zhao, D.Q., Cristhian, C. and Jiang, J.X. (2011) Simultaneous saccharification and cofermentation of lignocellulosic residues from commercial furfural production and corn kernels using different nutrient media. Biotechnology for Biofuels. 4(1), 1-10.
[25] Mamman, A.S., Lee, J.M., Kim, Y.C., Hwang, I.T., Park, N.J., Hwang, Y.K., Chang, J.S. and Hwang, J.S. (2008) Furfural: hemicellulose/xylose-derived biochemical. Biofuels Bioproducts & Biorefining. 2, 438-454.
[26] Mandalika, A. and Runge, T. (2012) Enabling integrated biorefineries through high-yield conversion of fractionated pentosans into furfural. Green Chem. 14, 3175-3184.
[27] Ren, G.J., Zhang, C.L., Zhao, J.X. and Gao, X.R. (2009) Adsorption Performance of Furfural Residue for Cr(VI). Plating and Finishing. 31(6), 9-11.
[28] Chen, X.Y., Sun, Y., Wang, D. and Liu, W.Y. (2011) Absorption of Cr3+ from Wastewater by Furfural Residue. Journal of Ningxia University (Natural Science Edition). 32(3), 262-265.
[29] Chen, Y.X., Zhu, Y.M., Yuan, K.N. and Zhu, Z.X. (1989) Adsorption and Reduction of Cr(VI) in Soils. Acta Scientiae Circumstantiae. 9(2), 137-143.

Received: **17.08.2017**
Accepted: **03.12.2017**

CORRESPONDING AUTHOR

Huanzhen Zhang
School of Water Resources & Environment,
China University of Geosciences (Beijing),
Beijing, 100083 – China

e-mail: huanzhen@cugb.edu.cn

© by PSP Volume 27 – No. 2/2018 pages 1256-1263 Fresenius Environmental Bulletin

POST-HARVEST APPLICATION OF SALICYLIC ACID CAN RETAIN THE PHYSICOCHEMICAL ATTRIBUTES OF SWEET ORANGES CV. BLOOD RED

Faheemul Haq[1], Muhammad Sajid[1], Amjad Iqbal[2], Farooq Shah[2,*], Ibadullah Jan[3], Badshah Islam[2], Zafar Hayat Khan[2], Mudassar Iqbal[3], Yousaf Jamal[4]

[1]Department of Horticulture, The University of Agriculture Peshawar, Pakistan
[2]Department of Agriculture, Abdul Wali Khan University Mardan, Pakistan
[3]Department of Agricultural Chemistry, The University of Agriculture Peshawar, Pakistan
[4]Department of Agriculture, University of Swabi, Khyber Pakhtunkhwa, Pakistan

ABSTRACT

Citruses are important, yet perishable fruits that lose its marketability due to pathogens as well as physical losses during storage. A research was, therefore, conducted to treat the sweet oranges, cv. Blood Red with different concentrations of SA (0, 1, 2, and 3 mM). The treated oranges were then stored for 60-days at room temperature and tested for quality attributes at an interval of 15-days. The results revealed that fruits treated with 2 mM SA had retained fruit firmness, total soluble solids (TSS), ascorbic acid (AA) and low disease incidence (DI) to a greater extent. Moreover, 3 mM SA treatment showed higher titratable acidity (TA), lowest weight loss (WL) and TSS:acid ratio, whereas fruits stored for more than 30-days had lower quality. Consequently, it is concluded that the application of SA at the rate of 2 to 3 mM can retain the quality of the fruits till 30-days of storage.

KEYWORDS:
Blood Red, sweet orange, salicylic acid, shelf life and qualitative attributes

INTRODUCTION

Sweet orange (*Citrus sinensis* L.) fruits are classified as non- climacteric fruits belongs to the family Rutaceae. It is cultivated in subtropical, tropical and temperate regions with latitudes of 40 ^{o}N to 40 ^{o}S. In Pakistan, the total area under citrus cultivation is 194.5×10^3 hectares with an average production of 1912×10^3 tones. Furthermore, the area under citrus cultivation in Khyber Pakhtunkhawa is 4×10^3 hectares with an average production of 32.3×10^3 tones [1]. Citrus is having many commercial species, which includes grapefruit (*Citrus paradise*), lemon (*Citrus lemon*), Lime (*Citrus aurantifolia*), mandarin (*Citrus unshi*), tangerine (*Citrus reticulata*), pamelo (*Citrus grandis*), orange (*Citrus sinensis*) [2]. Citrus fruits are considered to be moderately perishable depending upon the variety having a shelf life for about 2-20 weeks. In citrus fruits post-harvest losses are estimated from 20-95%. It may be due to high weight loss from the surface due to poor handling and also the post-harvest insect or fungal attack. Post-harvest treatments are helpful in order to reduce the fungal attack and weight losses of the fruits. Some post-harvest treatments like application of salicylic acid, calcium chloride, coatings and other antioxidants are helpful in reducing the microbial attack and salt stress [3-7]. Such, biosafe treatments reduce the usage of synthetic chemicals e.g. fungicides that can pollute the environment and affect human health [8]. By the application of natural compounds like phenolics etc., one can keep the quality of horticultural crops by diminishing the fungal growth, weight losses and salt stress [4, 9]. Salicylic acid, an important polyphenol in combination with other active compounds is considered safe and effective against various fungal infections in fruits and vegetables [10]. By keeping the role of salicylic acid in minimizing pre and post-harvest losses in mind, the present study was designed to investigate the effect of various concentrations of salicylic acid on fruit quality of sweet orange during storage. Moreover, through this study, we have found the optimum concentration of salicyclic acid to keep the quality of oranges with extended storage time.

MATERIALS AND METHODS

An experiment was conducted to study the influence of salicylic acid on storage of sweet oranges *(Citrus sinensis L)* cv. Blood Red at Post-harvest Laboratory, Department of Horticulture, The University of Agriculture, Peshawar. The experiments were conducted during December 2013 at normal room temperature (12±1 ^{o}C and RH of 70-80%) in an open environment. The experiment was laid out in a Completely Randomized Design (CRD) with two factors and repeated in triplicate (each replicate consists of 10 fruits). Fruits of sweet orange cv. Blood Red were

dipped in salicylic acid at various concentrations (0, 1, 2 and 3 mM) and were stored for 60 days. The representative fruits from each treatment were selected at an interval of 15 days (i.e. 0, 15, 30, 45 and 60 days) and were tested in triplicate for various quality parameters.

Collection of fruit samples. The fruit of sweet oranges, was collected at the Citrus Research Institute (CRI) Sargodha, Punjab, to the Post-harvest Laboratory Peshawar Department of Horticulture, The University of Agriculture Peshawar in December 2013. The fruits with uniform size and maturity were selected for experimental trial, while the injured or diseased fruits were discarded.

Preparation of salicylic acid and treatment of the oranges. A 1, 2, and 3 mM solution of SA was made by dissolving SA in distilled water. As SA is hardly soluble in water, so the solution was mixed till complete dissolution with the help of magnetic stirrer for 24 hours. The fruits were divided into four groups; each group contained 150 fruits that were dipped in their respective solution of SA (0 as a control, 1, 2 and 3 mM) for about 5 minutes. The treated fruits were then air dried for about 30 minutes and finally stored at room temperature (10-15 ^{o}C) with relative humidity of 70-80%) for 60 days.

The following parameters were studied during the course of the experiment.

Weight loss (%). All the sweet orange fruits were weighed after freshly harvested and at the time of testing to calculate any WL (%). The weight of the fruits was expressed in grams and percent WL was determined by using the formula:

$$\%\, WL = \frac{W1 - W2}{W1} \times 100$$

Where,
WL = weight loss
W1 = weight of fruits before storage
W2 = weight of fruits after storage

Fruit Firmness (Kg cm^{-2}). In order to determine the firmness of sweet orange fruit, Penetrometer (Wanges fruit firmness tester model FT-327) equipped with 8 mm tip, suitable for softer fruits were used for the purpose. Thirty fruits form each treatment was randomly selected and the epidermis were removed with the help of a peeler. The fruits were held firmly in one hand and the plunger of the penetrometer was placed on the cut side of the fruit. A force was applied in order to penetrate the plunger inside the fruit and the force (Kg cm^{-2}) of penetration was recorded from the digital dial of penetrometer.

Total soluble solids (^{o}Brix). A digital refrectometer (Kernco, Instruments Co-Texas) was used to compute the TTS of fruit juice. Couple of drops of sweet orange juice was placed on the clean prism of refrectometer and the lid was put back in its original position. Under the bright light the dial of the meter was rotated till blue and white light coincides and the reading was recorded as TSS in fruit juice. The prism was cleaned with damp tissue between each analysis.

Titratable acidity (%). Titratable acidity was determined by the well-established method of AOAC [11]. The results were expressed as gram of citric acid per 100 gram fresh weight of the fruits. The percent TA was computed by the formula:

$$\%\, titratable\ acidity = \frac{N \times T \times F \times 10}{D \times S} \times 100$$

Where
N = Normality of NaOH
T = ml of 0.1 N NaOH used
F = constant acid factor 10.0064 (citric acid)
D = Ml of Sample taken of citrus juice
S = Ml of diluted sample taken for titration

TSS acid ratio. The TSS to acid ratio was estimated as follows:

$$TSS - Acid\ Ratio = \frac{Total\ Soluble\ Solids}{Titrable\ acidity}$$

Ascorbic acid content (mg/100ml). For the measurement of AA contents, a dye method was used [12] and the results were expressed as milligram of citrus per 100 ml. AA content was calculated by using the following formula:

$$Ascorbic\ acid = \frac{F \times T \times 100}{D \times S} \times 100$$

Where
F = factor of standardization $\frac{ml\ of\ ascorbic\ acid\ used}{ml\ of\ dye\ used}$
T = ml of dye used for the sample - ml of dye used for blank
D = ml of sample taken for titration
S = ml of dilute sample taken for titration

Disease Incidence (%). The percent DI of the intact healthy fruits was recorded at 15 days of intervals during 60 days of storage time by means of visual observation and applying the following formula:

$$\%\, DI = \frac{No.of\ fruits\ infected}{Total\ No.of\ fruits} \times 100$$

RESULTS AND DISCUSSION

Weight loss (%). The results revealed that a significant difference existed among the fruits treated with various concentrations of salicylic acid, storage durations and their interaction (Table 1). Highest losses in weight were recorded in untreated/control fruits (15.97%), followed by fruits dipped in 1 (14.07) and 2 mM (10.87%) of SA, respectively. On the other hand, fruits that were treated

with 3 mM of SA resisted the weight loss (9.34%) up to a certain extent. Similarly, weight losses showed a linear relationship with storage duration as was expected. The weight loss in fruits was high, when stored for 60 days as compared to the other storage duration. More interestingly, the interaction effect of SA × storage duration had significantly influenced the losses in fruit weight to a certain limit. The highest percent of weight loss (31.30%) was observed in untreated fruits (control), when stored for 60 days. While a ten times lower loss in weight (3.33%) was noticed in fruits that were dipped in 3 mM of SA before storage for the next 15 days (Figure 1).

The evaporation of moisture from the surface of the fruits and vegetables is basically the main cause of the weight loss during storage [13, 14]. Such losses might be linked to the membrane permeability, cell wall degradation during the fruit ripening and structure of the fruit skin [15]. Principally, weight losses in living cells of fruits are regulated by respiration, transpiration and metabolic activities. The loss of moisture from the cells result in low turgor pressure thus shrinkage and softening of the fruits [16], which significantly affect the consumer's demand. The application of SA can reduce the weight loss in the horticultural commodities by decreasing the respiration rate by keeping the stomata close and inhibiting the ethylene production [17]. Such action can helps in delayed senescence by maintaining the cellular integrity, which helps in minimizing weight losses [18]. Similarly, the application of SA significantly controlled the weight losses in a highly perishable strawberry fruits [19] and peaches [20].

Fruit firmness (kg cm^{-2}). Various concentrations of SA, storage durations and the interaction between SA and storage durations significantly influenced the fruit firmness of the sweet orange (Table 1). The fruits dipped in 2 mM SA were found firmer (3.27 kg cm^{-2}) than the rest of the treatments. The lowest firmness (2.87 kg cm^{-2}) was attained by the fruits that were dipped in a solution of 1 mM SA. Additionally, a significant variation was observed in fruits during the storage, where the highest fruit firmness (3.69 kg cm^{-2}) was found in freshly harvested fruits, closely followed by fruits stored for 15 days (3.34 kg cm^{-2}). A lowest firmness (2.23 kg cm^{-2}) was recorded for fruits stored for 60 days. Concerning the effect of interaction between SA × storage duration, the fruits that were treated with 2 mM SA and stored for 15 days had retained the higher values for fruit firmness (4.10 kg cm^{-2}), while the control fruits stored for 60 days had the lowest values for fruit firmness, i.e. below 1 kg cm^{-2} (Figure 2).

The degradation of insoluble protopectin to soluble pectins tends to decrease the firmness of fruits, though it progresses at slow rate in citruses [21]. Fruit firmness may also be decreased with an increase transpiration that results in significant loss in water and solutes thus shrinkage of cells [22, 23]. Certainly, the losses in firmness of fruit during storage might be associated with the degradation of cellular structures and high respiration and metabolic rate of fresh produce [16]. Salicylic acid can somehow interfere with respiration as well as metabolic rates of the fruits and finally senescence, therefore, confirms the integrity of the cell and the fruit firmness. Beside this, SA can affect the enzymatic activities of the enzymes that are associated with the digestion of cell wall polysaccharides [24]. The findings of our study are in agreement with the previous studies on tomato [25], peach fruit [19], banana [26] and strawberry [27].

TABLE 1
Influence of Salicylic Acid and storage durations on weight loss, fruit firmness and AA in sweet oranges fruit cv. Blood Red

SA (mM)	Parameters		
	WL (%)	Firmness (kg cm^{-2})	AA (mg/100 ml)
0	15.97 a	2.96 b	38.86 b
1	14.07 b	2.87 b	49.67 a
2	10.87 c	3.27 a	49.94 a
3	9.34 d	2.93 b	49.33 a
LSD (P≤0.05)	0.830	0.201	0.818
Storage (days)			
0	0e	3.69 a	48.69 a
15	4.59 d	3.34 b	48.61 a
30	14.50 c	3.00 c	47.37 b
45	19.77 b	2.78 c	45.73 c
60	23.96 a	2.23 d	44.35 d
LSD (P≤0.05)	0.929	0.225	0.914
Interaction effect			
S x D	*** (Fig 1)	*** (Fig 2)	*** (Fig 3)

LSD test at p=0.05 was used to compare the mean values of different treatments. Moreover, the means that are followed by different letters are significantly different from each other at 5% significance level.

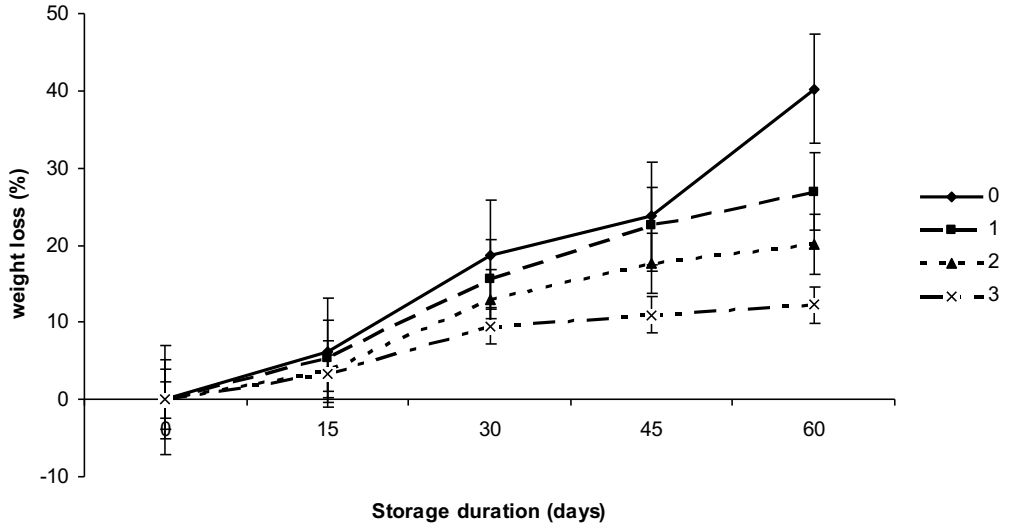

FIGURE 1
Effect of SA on the weight loss of sweet oranges during storage.

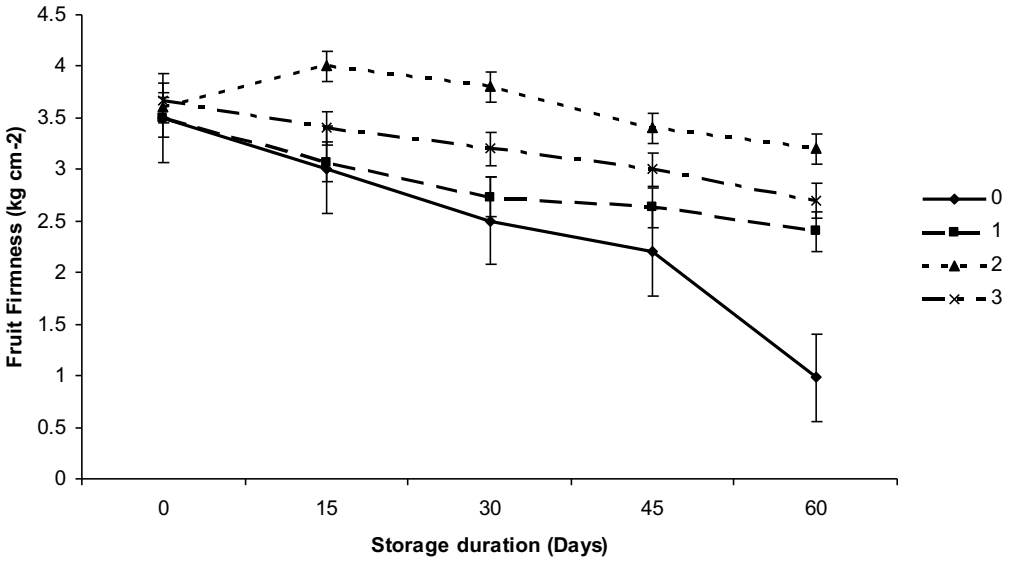

FIGURE 2
Effect of SA on the fruit firmness of sweet oranges during storage.

Ascorbic acid (mg/100 ml). A significant difference in AA was existed among the fruits treated with different concentrations of SA, storage durations and the interaction between the two factors (Table 1). Highest ascorbic acid contents (49.94 mg 100 ml^{-1}) was observed in fruits dipped in 2 mM of SA that was at par with 1 and 3 mM SA treatments, while the lowest ascorbic acid contents was observed in fruits dipped in distill water. The storage durations did affect the AA of the fruits with highest contents was recorded in those that were harvested fresh. The contents of AA in fruits were decreased with time and almost depleted, when the fruits were stored for 60 days. Similarly, the interaction between SA × storage duration demonstrated that fruits dipped in 2 mM SA and stored for 60 days retained two times more the AA, when fruits were dipped in water and stored for 60 days (Figure 3).

Ascorbic acid being a natural antioxidant can play a positive role during oxidative stress. Both kiwi fruit and citrus fruit are known to be the richest sources of AA. It is, indeed, considered as a nutritional indicator of fruit and vegetables, but it is labile to certain external factors (including light, gaseous composition in surroundings, temperature, etc.). It is, therefore, obvious that AA concentration diminishes with the passage of time without taking any further actions to preserve them. Salicylic acids found one of the best solutions to maintain the ascorbic acid

content of the tomato, strawberry, apricot and Chinese water chestnut during storage [27-29]. The preservation of ascorbic acid by SA treatment might be due to strong scavenging properties of reactive oxygen species by SA.

Total soluble solids (^{0}Brix). Salicylic acid and storage durations showed a significant effect on TSS, whereas the interaction of both factors didn't have any effect on TSS of the fruits (Table 2). The fruits that were dipped in 1 mM SA had the highest soluble solids (10.80 ^{o}Brix), followed by 3 and 2 mM treatments, while the lowest soluble contents (9.88 ^{0}Brix) were found in fruits dipped in distill water as a control treatment. Likewise, the fruits stored for 60 days were noticed high in TSS (11.55 ^{0}Brix) that was closely followed by fruits, when stored for 45 days (11.19). These quantities of TSS during storage have been increased significantly from 8.84 ^{0}Brix (as recorded in fresh fruits) (Table 2).

The increase in fruit's TSS during storage might be due to the conversion of starch into sugar or by the hydrolysis of cell wall polysaccharides. According to Lu [30] and Hayat et al. [31], TSS is one of the main indicators of maturity that determine the true quality of the ripe fruits. Total soluble solids increased with the increase in storage duration of orange fruits, which might be due to the digestion of the fruit polymers into readily soluble oligomers and monomers. Salicylic acid helped in slowing down

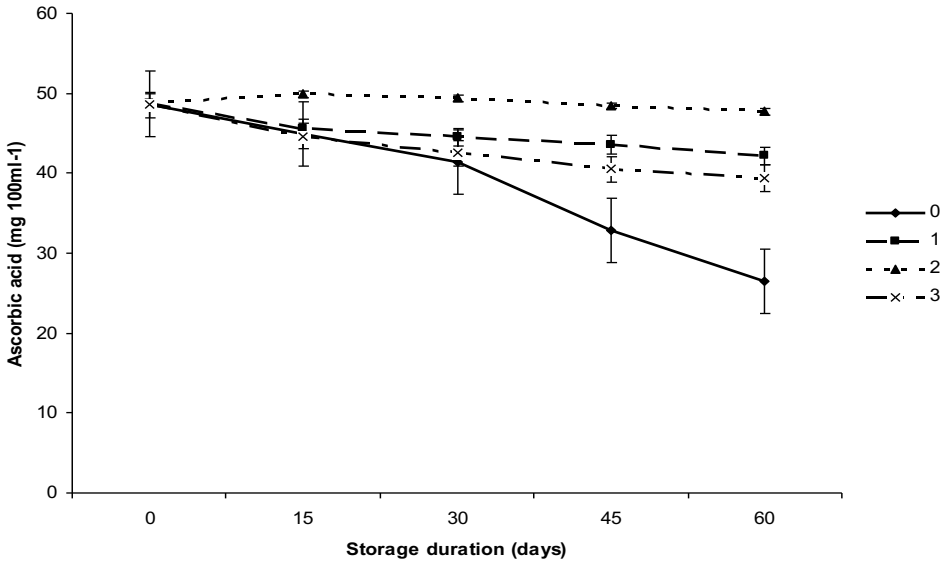

FIGURE 3
Effect of SA on the AA content of sweet oranges during storage.

TABLE 2
Influence of salicylic acid and storage durations on TSS, TA, TSS:acid and DI in sweet oranges cv. Blood Red

Salicylic acid (mM)	Parameters			
	TSS (Brix^0)	TA (%)	TSS:acid	DI (%)
0	9.88 b	1.81 b	13.70 a	18.67 a
1	10.80 a	1.59 b	12.48 b	11.33 b
2	10.41 ab	1.88 ab	11.03 c	3.33 c
3	10.45 ab	2.13 a	9.47 d	6.67 bc
LSD (P≤0.05)	**0.626**	**0.301**	**0.461**	**5.473**
Storage duration (days)				
0	8.84 c	2.2 a	8.86 e	0 d
15	9.82 c	1.98 a	9.99 d	4.17 cd
30	10.52 b	1.95 a	10.58 c	7.50 c
45	11.19 ab	1.59 b	13.78 b	15.00 b
60	11.55 a	1.58 b	15.13 a	23.33 a
LSD (P≤0.05)	**0.699**	**0.337**	**0.515**	**6.119**
Interaction (P≤0.05)				
S x D	**NS**	**NS**	***** (Fig 4)**	**NS**

LSD test at p=0.05 was used to compare the mean values of different treatments. Moreover, the means that are followed by different letters are significantly different from each other at 5% significance level.

the accumulation of TSS during storage, such decrease might be governed by delaying the process of ripening and higher water contents of the cells. It is merely possible that the presence of water in cytoplasm and apoplast might control the enzyme system that can degrade the large molecules into smaller ones.

Titratable Acidity (%) and TSS:acid ratio. The results in Table 2 also revealed that SA and storage duration significantly influenced the TA of sweet oranges, while no significant difference was recorded for the interaction effect of those treatments. A highest TA (2.13%) was recorded in fruits dipped in 3 mM of SA, which was statistically different from the rest of the other treatments. The data regarding the storage duration showed variations in TA, the fruits that were stored for a long time (i.e. 65 days) showed lower amounts of the acids compared to the fruits stored for 15 or 30 days. The highest TA (2.2 %) was noticed in the fresh fruits without experiencing storage. A significant differences regarding TSS:acid ratio of sweet orange was founded among the various levels of applied SA, storage durations and their interaction (Table 2). The maximum TSS:acid ratio (13.70) was found in untreated fruits closely followed by TSS:acid ratio (12.48 and 11.03) of fruits dipped in 1 and 2 mM of SA respectively, while the minimum (9.47) TSS:acid ratio was found in fruits dipped in 3 mM of SA. Additionally, the storage duration also influenced the ratio (TSS:acid) significantly, the maximum TSS:acid ratio (15.13) was found in fruits stored for 60 days that was closely followed by of fruits stored for 45 (13.78) and 30 days (10.58). On the other hand, the minimum TSS:acid ratio (8.86%) was found in freshly harvested fruits. The combined effect of SA × storage duration displayed a significant effect with untreated fruits stored for 60 days had the highest TSS:acid ratio (18.17), while the minimum TSS:acid ratio (7.37) was found in fruits dipped in 3mM without going to storage (Figure 4).

Fruit taste is mainly credited to sugars and acids, fruit having high acidity, retains the flavor [32]. Titratable acidity basically depended upon the organic acid contents present in fruit. Fruit taste is believed to be associated with the combinations of acids and sugars, which can be affected during the ripening process with the depletion of acids [18]. In today's research we found a significant change in the acidity of stored oranges that might be connected to the higher consumption of organic acids [22]. But, SA helped in retaining the acid contents in fruits that might be through delaying the process of ripening and slowing down the respiration rate. The application of SA in past have retained the acids contents in apricot [18] and chest nut [29].

Disease incidence (%). The existence of diseases was strongly related to the application of low concentrations of SA and longer storage durations, while their interaction was found non-significant (Table 2). A highest DI (18.67%) was recorded in untreated fruits, while the lowest percent DI (3.33%) was found in fruits dipped in 2mM SA. The chances of DI were increased during storage for longer time, i.e. (23.33%) was found in fruits stored for 60 days, followed by percent disease incidence (15 and 7.50%) in fruits stored for 45 and 30 days compared to the 0% diseases in the freshly harvested fruits.

Fruits after harvest are susceptible to several diseases because of high water and nutrients. In order to control diseases, various fungicides have been successfully developed in the past to tackle the problem. The production of potent synthetic fungicides revolutionaries the industries, yet on the expense of the environment and issues related to human health. So the need for alternative ways to control the disease in horticultural crops without effecting the environment is demanded. Salicylic acid seems to be one of the best alternatives that can help in minimizing the prevalence of the diseases in fruits. In past, it helped in inducing the defense related genes and thus activating the defense system of the plants to combat the foreign threats [33, 34]. Quiet recently, SA have shown promising results in the reduction of fungal attack during storage of strawberry [35], tomatoes [8], sweet cherry [4] and peaches [36].

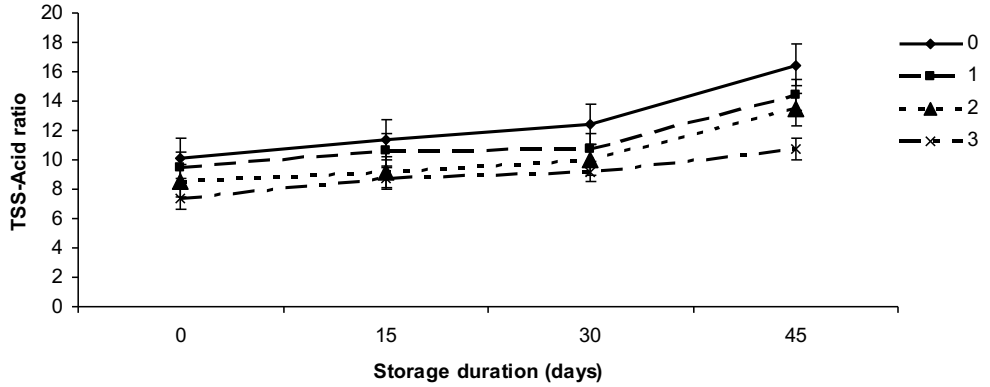

FIGURE 4
Effect of SA on the TSS:acid ratio of sweet oranges during storage.

CONCLUSIONS

Based on the results of our study, it is concluded that the post-harvest application of salicylic acid effectively maintain the quality attributes of sweet oranges (including, fruit volume, fruit firmness, total soluble solids, titratable acidity, ascorbic acid contents, TSS:acid ratio, fruit juice pH, disease resistance). The salicylic acid treatment @ 2 mM was efficient in controlling and minimizing the percent disease incidence, while 3 mM salicylic acid was efficient to minimize percent weight loss of sweet orange fruits during storage. Besides, sweet oranges sustained its quality attributes, when stored up to 30 days at room temperature (12±1^{o}C) and RH of 70-80%, whereas the increase in storage resulted in the gradual declination in all quality parameters.

ACKNOWLEDGEMENTS

The authors confirm that there is no conflict of interest of any kind related to this manuscript.

REFERENCES

[1] MINFA. (2011) Government of Pakistan Statistics Division, Pakistan Bureau of Statistics. 44, 9-89.
[2] Murata, T. (1997) Citrus. In: Mitrae, S.K. (ed.) Post-harvest physiology and storage of tropical and sub-tropical fruits, CAB, UK, 21-40.
[3] Fisk, C.L., Silver, A.M., Strik, B.C. and Zhao, Y. (2008) Postharvest quality of hardy kiwifruit (*Actinidia arguta* 'Ananasnaya') associated with packaging and storage conditions. Postharvest Biol. Technol. 47(3), 338-345.
[4] Yao, H. and Tian, S. (2005) Effects of pre-and post-harvest application of salicylic acid or methyl jasmonate on inducing disease resistance of sweet cherry fruit in storage. Postharvest Biol. Technol.,35(3), 253-262.
[5] Jan, I., Rab, A., Sajid, M., Iqbal, A., Shinawari, Z. and Hamayun, M. (2016) Effect of calcium salt on soft rot, bitter pit and physicochemical properties of stored apples. Pak. J. Bot. 48, 1415-1420.
[6] El-Beltagi, H.S., Ahmed, S.H., Namich, A.A.M. and Abdel-Sattar, R.R. (2017) Effect of salicylic acid and potassium citrate on cotton plant under salt stress. Fresen. Environ. Bull. 26, 1091-1100.
[7] Yigit, E., Akbulut, G.B., Bayram, D., Kaya, A. and Gok, Y. (2016) Effect of salicylic acid and selenium on antioxidant system of Avena sativa L. under fenoxaprop-p-ethyl stress. Fresen. Environ. Bull. 25, 874-884.
[8] Mandal, S., Mallick, N. and Mitra, A. (2009) Salicylic acid-induced resistance to *Fusarium oxysporum* f. sp. lycopersici in tomato. Plant Physiol. Biochem. 47(7), 642-649.
[9] Uysal, D., Ozdener, Y., Aydin, B. and Demir, E. (2009) Determination of ameliorating effect of salicylic acid on toxicity of aluminum in wheat roots. Fresen. Environ. Bull. 18, 32-39.
[10] Aghdam, M., Motallebiazar, A., Mostofi, Y., Moghaddam, J. and Ghasemnezhad, M. (2009) Effects of MeSA vapor treatment on the postharvest quality of 'Hayward' kiwifruit, Acta Hortic. 877, 743-748.
[11] AOAC. (2012) Official methods of analysis, Gaithersburg, Maryland, USA.
[12] Ranganna, S. (1977) Manual of analysis of fruit and vegetable products. McGraw-Hill, New Delhi.
[13] Tareen, M.J., Abbasi, N.A. and Hafiz, I.A. (2012) Postharvest application of salicylic acid enhanced antioxidant enzyme activity and maintained quality of peach cv.'Flordaking'fruit during storage. Sci. Hort. 142221-228.
[14] Sadiq, K., Irfan, U., Nadeem, K., Amjad, I., Tariq, S., Farooq, S., Badshah, I., Arshad, A. Rashad Waseem, Khan, Q. (2016) The role of LTST hot water immersion on quality of peach fruit during storage. Madridge Journal of Food Technology. 15, 131-36.
[15] Lara, I., Belge, B. and Goulao, L.F. (2014) The fruit cuticle as a modulator of postharvest quality, Postharvest Biol. Technol. 87, 103-112.
[16] Paniagua, A., East, A., Hindmarsh, J. and Heyes, J. (2013) Moisture loss is the major cause of firmness change during postharvest storage of blueberry. Postharvest Biol. Technol. 79, 13-19.
[17] Srivastava, M.K. and Dwivedi, U.N. (2000) Delayed ripening of banana fruit by salicylic acid. Plant Sci. 158(1), 87-96.
[18] Ali, S., Masud, T., Abbasi, K.S., Mahmood, T. and Ali, A. (2013) Effect of different concentrations of salicylic acid on keeping quality of apricot cv. Habi at ambient storage. J. Biol. Food Sci. Res. 2(6), 69-78.
[19] Shafiee, M., Taghavi, T. and Babalar, M. (2010) Addition of salicylic acid to nutrient solution combined with postharvest treatments (hot water, salicylic acid, and calcium dipping) improved postharvest fruit quality of strawberry. Sci. Hort. 124(1), 40-45.
[20] Abbasi, N., Hafeez, S. and Tareen, M. (2009) Salicylic acid prolongs shelf life and improves quality of 'Maria Delicia' peach fruit. Acta Hortic. 880, 191-197.

[21] Ladaniya, M. (2004) Citrus: Postharvest cold chain. In: Dris, R., Niskanen, R., Jain, S.M. (eds.) Crop management and postharvest handling of horticultural products: Fruits & Vegetables, vol. 2. Plymouth, UK: Science, 2, 239-276.
[22] Ghafir, S.A., Gadalla, S.O., Murajei, B.N. and El-Nady, M.F. (2009) Physiological and anatomical comparison between four different apple cultivars under cold-storage conditions. Afr. J. Plant Sci. 3(6), 133-138.
[23] Nadeem, K., Irfan, U., Waleed Amjad, K., Rashad, Q., Muhammad Mumtaz, K., Zhang, F., Teng, R., Badshah, I., Farooq, S., Farman, A., Zafar Hayat, K. and Amjad, I. (2017) Effect of harvesting stage on quality losses of persimmon fruits during storage. Madridge Journal of Food Technology. 2, 79-84.
[24] Xu, G., Liu, D., Xio, Y., Liu, P., Gao, P., Cao, L. and Wu, Y. (2015) Effects of exogenous salicylic acid on cell wall polysaccharides and aluminum tolerance of trichosanthes kirilowii. Pak. J. Bot. 47(5), 1649-1655.
[25] Ding, C.-K., Wang, C., Gross, K. C. and Smith, D. L. (2002) Jasmonate and salicylate induce the expression of pathogenesis-related-protein genes and increase resistance to chilling injury in tomato fruit. Planta. 214(6), 895-901.
[26] Kang, G.Z., Wang, Z.X. and Sun, G. (2003) Participation of H_2O_2 in enhancement of cold chilling by salicylic acid in banana seedlings. Acta Bot. Sin. 45(5), 567-573.
[27] Pila, N., Gol, N.B. and Rao, T.R. (2010) Effect of post harvest treatments on physicochemical characteristics and shelf life of tomato (*Lycopersicon esculentum* Mill.) fruits during storage. American-Eurasian J. Agric. Environ. Sci. 9(5), 470-479.
[28] Ali, I., Abbasi, N. A. and Hafiz, I. A. (2014) Physiological response and quality attributes of peach fruit cv. Florida king as affected by different treatments of calcium chloride, putrescine and salicylic acid. Pak. J. Agric. Sci. 5133-39.
[29] Karlidag, H., Yildirim, E. and Turan, M. (2009) Salicylic acid ameliorates the adverse effect of salt stress on strawberry. Sci. Agric. 66(2), 180-187.
[30] Lu, X., Sun, D., Mo, Y., Xi, J. and Sun, G. (2010) Effects of post-harvest salicylic acid treatment on fruit quality and anti-oxidant metabolism in pineapple during cold storage. J. Hort. Sci. Biotechnol. 85(5), 454-458.
[31] Hayat, I., Masud, T. and Rathore, H. A. (2005) Effect of coating and wrapping materials on the shelf life of apple (*Malus domestica* cv. Borkh). Int. J. Food Safety. 5, 24-34.
[32] Ulrich, R. (1970) Organic acids. In: Hulme, A.C. (ed.) The biochemistry of fruits and their products. Academic Press. London and New York, 189-118.
[33] Kuć, J. (1982) Induced immunity to plant disease. Bioscience. 32(11), 854-860.
[34] Malamy, J., Sánchez-Casas, P., Hennig, J., Guo, A. and Klessig, D. F. (1996), Dissection of the salicylic acid signaling pathway in tobacco. Mol. Plant Microbe Interact. 9(6), 474-482.
[35] Babalar, M., Asghari, M., Talaei, A. and Khosroshahi, A. (2007) Effect of pre-and postharvest salicylic acid treatment on ethylene production, fungal decay and overall quality of Selva strawberry fruit. Food Chem. 105(2), 449-453.
[36] Zhang, H., Ma, L., Wang, L., Jiang, S., Dong, Y. and Zheng, X. (2008) Biocontrol of gray mold decay in peach fruit by integration of antagonistic yeast with salicylic acid and their effects on postharvest quality parameters. Biol. Control. 47(1), 60-65.

Received: **04.09.2017**
Accepted: **10.12.2017**

CORRESPONDING AUTHOR

Farooq Shah
Department of Agriculture,
Abdul Wali Khan University
Mardan – Pakistan

e-mail: farooqshah@awkum.edu.pk

© by PSP Volume 27 – No. 2/2018 pages 1264-1268 Fresenius Environmental Bulletin

CHARACTERISTICS OF DEEP SHALE WITH DRILLING FLUID IMMERSION BASED ON RSM

Yuehui Pan[1,*], Jingyun Peng[2]

[1]Zhejiang East China Science and Technology Testing Co., Ltd, No. 16 First Street of Hangzhou Economic and Technological Development Zone, Hangzhou, 310018, China
[2] Taizhou Branch of Zhejiang Dibiao Building Design Co., Ltd. China

ABSTRACT

According to the key technical problem of deep mudstone failure under drilling fluid soaking the weakening law of strength is analyzed by the laboratory test. The result shows that: (1) Under the drilling fluid soaking the mudstone strength increases first and then decreases with increase of coring angle. With the increase of confining pressure the increasing range of strength is lower. (2) The elastic modulus of mudstone decreases with the increase of soaking time and increases first and then decreases with the increase of coring angle. But the change law of the Poisson's ratio is opposite with that of the elastic modulus. (3) Comparing with the internal friction angle the change of mudstone cohesion presents stronger regularity. The decreasing range of cohesion is larger with coring angles of 0^0 and 90^0.

KEYWORDS:
Deep mudstone, soaking time, drilling fluid, strength.

INTRODUCTION

Shale gas has recently received attention in the field of energy production [1-4]. As an effective way to cope with energy shortages and energy security, as previously proven by the USA during the past few decades, shale gas exploration is a viable option in China, especially in the southwest Sichuan Basin [5-8]. Compared with the Mesozoic and Upper Paleozoic erathem as the target stratum for the USA's shale gas industry, the Lower Paleozoic erathem for the Sichuan Basin is deeper [9-11]. To reduce the cost of shale gas production, China still requires fundamental research on the physicochemical properties of shale at increasing depths [12-14]. As a type of mud rock, shale is a fine-grained rock mainly composed of clay mineral flakes [15]. Clay minerals form in the presence of water. The system, consisting of clay minerals and water, has a significant effect on the physicochemical properties of the shale, which has been reported and observed by using modern technologies.

However, under the effect of drilling in deep shale strength characteristics less time effect. The key technical challenges for action under deep shale drilling damage, carry different confining pressures, ask different drilling mud soaked interior strength test, get soaked in the process of drilling deep shale intensity variation and mechanisms for drilling wells in deep shale formations provide a scientific basis to predict stable wall.

MATERIALS AND METHODS

Mineral composition analysis of deep shale. Mudstone samples are taken from a western, sampling depth of 6247.1-6251.9 m. Take three small cuttings carried out with the full depth of the rock-forming minerals and X- diffraction experiments, analyzed the whole rock and mineral composition of clay mineral component content, analyze collected and shown in Table 1 and 2.

TABLE 1
Rock mineral compositions of rock samples

Lithology	Well segment /m	Mineral type and content /%					The total amount of clay minerals /%
		Quartz	Feldspar	Plagioclase	Calcite	Dolomite	
Mudstone	6247.1-6251.9	30.4	1.3	11	12	8.1	37.2
		25	1	10	35	6	33
		31	3	10.9	20.1	7	28

TABLE 2
Relative content of rock samples for clay mineral

Lithology	Well segment /m	Relative content of clay minerals /%				Mixed-layer content /%
		I	K	C	I/S	I/S
Mudstone	6247.1-6251.9	28	7	18	47	29
		24	8	22	46	29
		23	7	19	51	21

Note: S, said montmorillonite: I said that illite: K represents kaolinite: C expressed chlorite: I / S, said Iraq / smectite

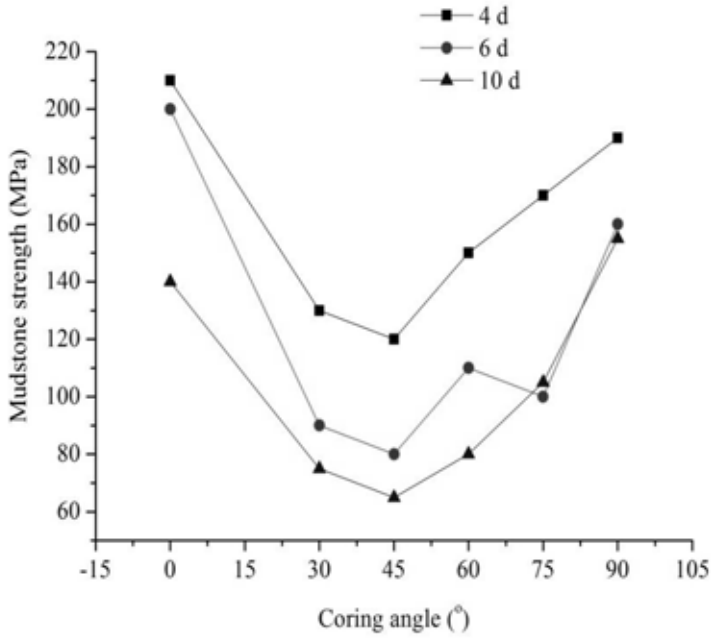

(a) Confining pressure 20MPa

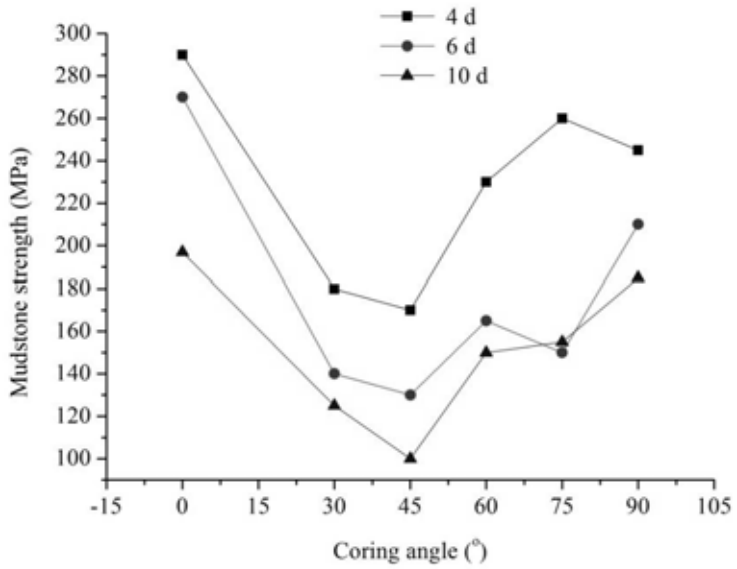

(b) Confining pressure 50MPa

FIGURE 1
Effects of drilling fluid immersion on strength of mudstone under confining pressures of 20 and 50 MPa

Analysis of the test results, the clay mineral content of 30%. Clay minerals are illite / smectite is characterized by the development of the content of 50%, followed by illite, kaolinite and chlorite, and its content was 23% --28%, 18% -22% and 7-8%. According to shale drilling industry classification standard, mudstone belong to the hard - hard and brittle shale.

Experimental Design. General development of brittle shale cracks, micro-cracks and bedding planes, these structures on the surface of the mechanical performance of the weak side, but the strength of the rock is often controlled by the weak nature of the rock face and external fluid. This paper focuses on the weak side and test drilling influence of immersion on the strength characteristics of deep shale sample for 6247.1-6251.9 m at a depth of brittle shale.

Sample equipment using MTS-815 rock mechanics testing machine, a full three-axis device consists of high temperature and pressure chamber, confining pressure pressurization system, the axial pressure system and automatic data acquisition and control system of four major components. Design specifications for high temperature and pressure triaxial chamber: confining pressure 100 MPa, which can accommodate the size of the rock sample is 25 mm; maximum axial compression of 2000 kN. Get into the standard core drilling fluid collected in the field, under different angles coring drilling immersion on rock strength characteristics. Mudstone hydration of drilling fluid under different coring angles is examined. Coring angle is selected for 0-90^0, drilling soaking time 0-10 d, Confining pressure 20-50 MPa(Fig.1).

RESULTS AND DISCUSSION

Under the influence of drilling mud soaked strength characteristics. The results show that, under the same core angle and confining pressures, drilling fluid immersion time increases, the strength of the rock is reduced, resulting in a different angle minimize coring rock strength vary, as confining pressure 20 MPa, the angle between the core 30^o. When rock strength of 130 MPa in 4d from soaking down to soak 10 d of 75 MPa. At the same time, and confining pressure fluids soaking conditions, with the increase in the angle of coring, rock strength after first reducing the increase, there is a minimum threshold intensity, such as the angle between the core 45. At the same angle and core drilling soaking time role with the increase of confining pressure, rock strength increases; different core strength increase under different angles, such as coring angle is 0^o and 90^o.

From the above analysis, the drilling fluid immersion, coring angle and confining pressure on the strength of lower shale plays an essential role, but with different mechanisms of action, the role has changed itself mud soaked rock mechanical properties, while the angle and coring confining pressure is changed inside the rock stress state.

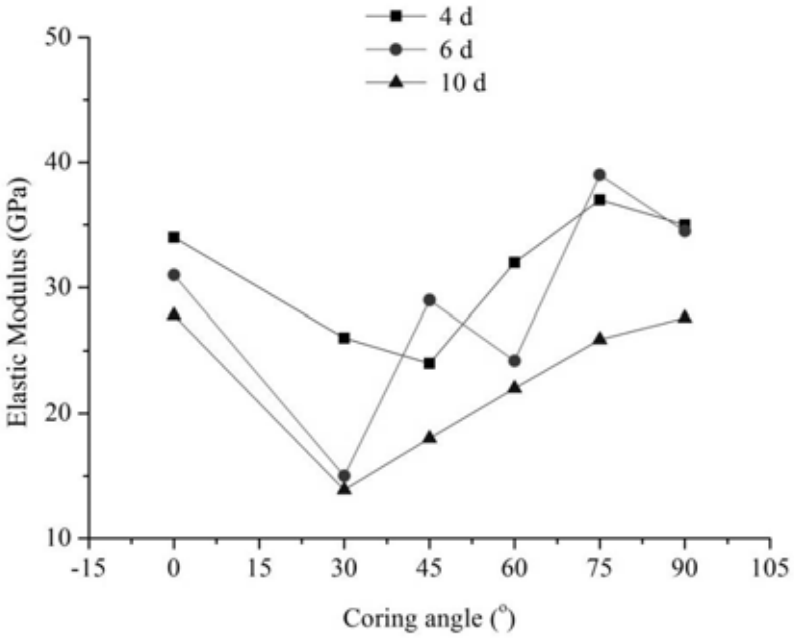

FIGURE 2
Effect of drilling fluid immersion on elastic modulus of mudstone

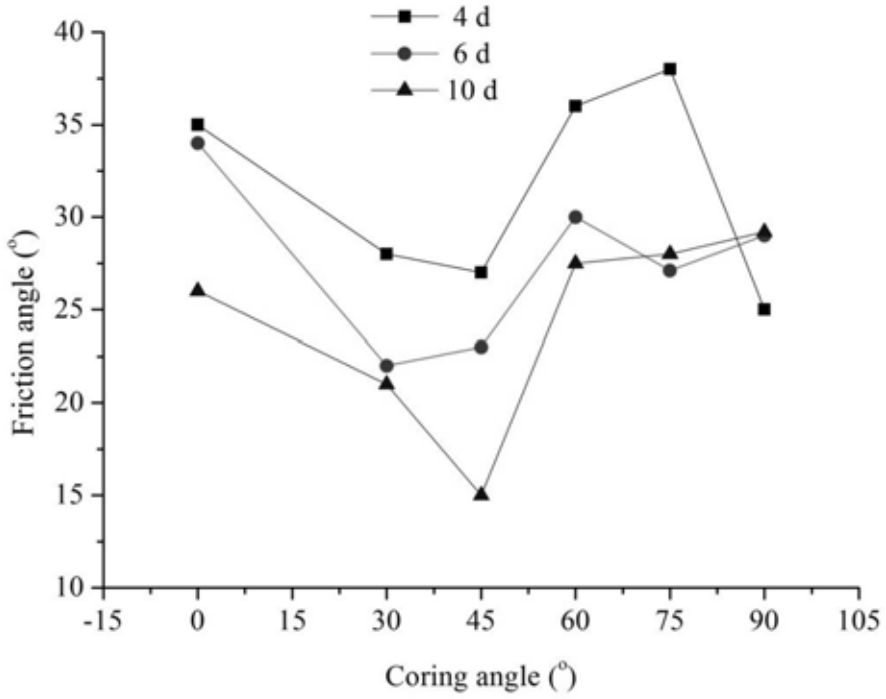

FIGURE 3
Effect of drilling fluid immersion on internal friction angle of mudstone

Drilling mud immersion on the elastic modulus. Analysis of Figure 2 shows that, under the same core angle, with the drilling fluid immersion Q increases, the elastic modulus decreases mudstone, such as coring angle of 90. When the elastic modulus decreased to 35 GPa from 27.6 GPa; at the same time ask soaked mud, coring angle increases, the elastic modulus of the rock first and then reduce the increasing trend. The overall trend of the elastic modulus less regularity.

Effect of drilling fluid immersion on strength parameters of mudstone. Mudstone controlled intensity strength parameters, under the same conditions coring angle, with the increase in drilling fluid immersion time, internal friction angle mudstone occurs in varying degrees to reduce, reduce the degree of the angle between the size of the core, such as when coring angle 0, reduced internal friction angle from 35 to 26; coring angle of 60, the internal friction angle decreased by 23.6%; however, the angle between the core 90, the internal friction angle appears to increase with the sample inside construction and testing related to the operation(Fig.3).

CONCLUSIONS

In this paper, the macro-mechanical tests carried out under the action of the drilling fluid to soak deep shale, on the basis of test results on the analysis of the intensity variation characteristic of deep shale drilling fluid immersion, obtained the following conclusions:

(1) drilling fluid immersion, with coring angle increases, the intensity of the first increased and then decreased after the rock, and there is a critical strength, rock strength decline of more than 50%; with the increase of confining pressure, under different angles coring rock strength different growth, coring angle between 0 and 90, the increase in rock strength is low, only about 20%.

(2) the elastic modulus of shale drilling action when asked increases with decreases with increasing angle coring presented after the first increased and then decreased; internal friction angle with increasing shale drilling action time decreases.

REFERENCES

[1] Ge, X.R. (2008) Deformation control law of rock fatigue failure, real-time X-ray CT scan of geotechnical testing, and new method of stability analysis of slopes and dam foundations. Chinese Journal of Geotechnical Engineering. 30, 1-20.

[2] Josh, M., Esteban, L., Delle, P.C., Sarout, J., Dewhurst, D.N. and Clennell, M.B. (2012) Laboratory characterisation of shale properties.

Journal of Petroleum Science and Engineering. 88–89, 107-124.
[3] Wen, H., Chen, M., Jin, Y., Zhang, Y.Y., Ge, W.F., Du, J.L. and Zeng, C. (2015) Water activity characteristics of deep brittle shale from Southwest China. Applied Clay Science. 108, 165-172.
[4] Chigira, M., Hariyama, T. and Yamasaki, S. (2013) Development of deep-seated gravitational slope deformation on a shale dip-slope: Observations from high-quality drill cores. Tectonophysics. 605, 104-113.
[5] Shivhare, S. and Kuru, E. (2014) A study of the pore-blocking ability and formation damage characteristics of oil-based colloidal gas aphron drilling fluids. Journal of Petroleum Science and Engineering. 122, 257-265.
[6] Gadenne, L., Raimbourg, H., Champallier, R. and Yamamoto, Y. (2014) Mechanical properties and processes of deformation in shallow sedimentary rocks from subduction zones: An experimental study. Geochemistry, Geophysics, Geosystems. 15, 5001–5014.
[7] Thakare, M.R., Wharton, J.A., Wood, R.J.K. and Menger, C. (2007) Exposure effects of alkaline drilling fluid on the microscale abrasion–corrosion of WC-based hardmetals. Wear. 263, 125-136.
[8] Mao, H., Qiu, Z.S., Shen, Z.H. and Huang, W.A. (2015) Hydrophobic associated polymer based silica nanoparticles composite with core–shell structure as a filtrate reducer for drilling fluid at utra-high temperature. Journal of Petroleum Science and Engineering. 129, 1-14.
[9] Zhong, H.Y., Qiu, Z.S., Huang, W.A. and Cao, J. (2011) Shale inhibitive properties of polyether diamine in water-based drilling fluid. Journal of Petroleum Science and Engineering. 78, 510-515.
[10] Qu, Y.Z., Lai, X.Q., Zou, L.F. and Su, Y.N. (2009) Polyoxyalkyleneamine as shale inhibitor in water-based drilling fluids. Applied Clay Science. 44, 265-268.
[11] Guo, J.K., Yan, J.N., Fan, W.W. and Zhang, H.J. (2006) Applications of strongly inhibitive silicate-based drilling fluids in troublesome shale formations in Sudan. Journal of Petroleum Science and Engineering. 50, 195-203.
[12] Li, J., Pan, R., Guo, B.Y. and Shan, J. (2014) Thermal stability of brine foams for shale gas drilling. Journal of Natural Gas Science and Engineering. 17, 131-135.
[13] Xuan, Y., Jiang, G.C., Li, Y.Y., Geng, H.N. and Wang, J.S. (2013) A biomimetic drilling fluid for wellbore strengthening. Petroleum Exploration and Development. 40, 531-536.
[14] Li, J., Guo, B.Y., Yang, S.J. and Liu, G.H. (2014) The complexity of thermal effect on rock failure in gas-drilling shale-gas wells. Journal of Natural Gas Science and Engineering. 21, 255-259.
[15] You, L.J., Kang, Y.L., Chen, Z.X., Chen, Q. and Yang, B. (2014) Wellbore instability in shale gas wells drilled by oil-based fluids. International Journal of Rock Mechanics and Mining Sciences. 72, 294-299.

Received: **12.09.2017**
Accepted: **26.11.2017**

CORRESPONDING AUTHOR

Pan Yuehui
Zhejiang East China Science and Technology Testing Co., Ltd, No. 16 First Street of Hangzhou Economic and Technological Development Zone, Hangzhou, 310018 – China

e-mail: 40453479@qq.com

© by PSP Volume 27 – No. 2/2018 pages 1269-1281 Fresenius Environmental Bulletin

EXPERIMENTAL STUDY ON MECHANICAL PROPERTIES OF HIGH WATER QUICK-SETTING MATERIALS IN MARINE ENVIRONMENT

Bingbing Guo[1,2], Changwu Liu[1,*], Bangwen Lu[1], Hui Xie[3], Defeng Liu[1]

[1]College of Water Resource and Hydropower, Sichuan University, Chengdu 610065, Sichuan, China
[2]College of Safety Engineering, Henan University of engineering, Zhengzhou 451191, Henan, China
[3]Sichuan Electric Power Design &Consulting Co., Ltd, Chengdu 610016, Sichuan, China

ABSTRACT

High water quick setting material is a new type of hydraulic engineering materials. With the expansion of the application field, the mechanical properties of the high water material consolidation body in the special environment are paid more and more attention. In order to explore the application of high water quick setting materials in marine engineering, this paper studies the mechanical properties and mechanism of high water quick setting materials in marine environment. Through the comparison of the peak intensity of the solidified body in different mixing and curing environments, the scanning electron microscopy analysis of consolidation body and the creep experiment of consolidation body under different pressure water environment, this paper analyzed the microscopic mechanism of the deformation of the consolidation body, studied the effect of the main ions on the formation of solidification in seawater, it also compared the differences in the microstructure of the aggregates under different mixing and curing environments and discussed the influence of water pressure on the creep of the solid body and its mechanism. The results show that: (1) the strength of consolidation under artificial seawater mixing is the highest, the strength of consolidation under drinking water mixed artificial seawater is the second and the strength of consolidation under drinking water mixing is the lowest. (2) The concentration of SO_4^{2-} in sea water affects the stability of the main component calcium vanadium in the solidified body. The higher SO_4^{2-} concentration is favorable for the formation and stabilization of calcium vanadium. Cl^- can react with low-sulfur sulphoaluminate in the solidified body to form hydrated calcium chloroaluminate, Cl^- can also be physically adsorbed by ettringite and silicate gel. The formation of hydrated calcium chloroaluminate and the adsorption of Cl^- on silicate gel can cause the change of the microstructure of the solidified body, change the pore structure of the solidified material, reduce the porosity of the solidified body and then improve the consolidation mechanics macro strength. (3) Under the pressure water environment, the water pressure suppresses the creep deformation of the consolidation body and the creep deformation of the solidified body is not controlled by total stress. The water pressure affects the deformation of the solidified body by directly affecting the true stress of the skeleton. With the increase of water pressure, the real stress on the material skeleton decrease, the strain rate and the deformation amount in the creep are reduces and the long - term strength of the consolidation body is improved. High water materials can adapt to the harsh environment of marine salt ion corrosion and water pressure, so it can be used as a good marine engineering reinforcement material.

KEYWORDS:
Marine environment, High water quick setting materials, Calcium vanadium, Pressure water, Creep

INTRODUCTION

High water quick setting material is a new type of hydraulic engineering materials with fast solidification speed, early strength high, and simple construction technology. In recent years, the application areas of high water materials continue to expand. It has been applied in coal mine filling and mining, gas drainage sealing, oil well cementing and water shutoff, marine engineering and soft soil foundation reinforcement [1].

In the past, many scholars have made great achievements in the research of high water materials. With the application field expanding, the application environment is becoming more and more complicated and the engineering characteristics of the consolidation body in the special environment are getting more and more attention. Sun Henghu pioneered a comprehensive study of the basic performance, hardening reaction mechanism and application of high water quick setting materials [2-3]. Gao Meng studied the corrosion of high water materials in coal mine water corrosion environment by experiment [4]. The creep test of the high water quick setting material stone body was carried out in the dry and water environment by the method of gravity contin-

uous loading [5]. The geophysical transient electromagnetic method have been carried out to examine the treatment quality of mined-out voids using super high-water material [6]. The high water quick setting material is suitable for use as a good backfilling material in mining so as to effectively reduce the ground surface subsidence and to conserve the soil and water [7]. The super-high water backfilling with strip mining can ensure the safety of the surface buildings [8]. Wang and Villaescusa studied the influence of water salinity on the properties of cemented tailings backfill by using binders ordinary Portland cement and High Water and Quick Setting cement [9].

The marine environment is a harsh and complex corrosive environment in which the material is affected by seawater salt corrosion, seawater pressure, temperature and marine microbes. The average salinity of the world's oceans is 3.5%. The salt ions in seawater mainly include Cl^- (19.344g / kg), Na^+ (10.773g / kg), SO_4^{2-} (2.712g / kg), Mg^{2+} (1.294g / kg), Ca^{2+} (0.412 g / kg), K^+ (0.399 g / kg). At present, the materials used in marine engineering are mainly concrete and steel. The research on the durability of concrete in marine environment and the research on corrosion of marine engineering metal materials have greatly promoted the development of marine engineering.

High water quick setting material as a new type of engineering materials has been carried out a preliminary application practice in marine engineering, but the research on the mechanical properties of high water material consolidation body in the marine environment remains to be systematically studied.

In this paper, the influence of the main ions in the seawater on the formation and stability of the solidified water material was analyzed by the strength experiment of the solidified water material under different mixing and curing environments. The creep characteristics of high water material consolidation body under pressure water environment are studied by using self-designed rock tri-axial rheological experiment system, and they can also explore the mechanism of water pressure on creep deformation.

The 21st century is the century of the ocean and the oceans will be the main areas of international competition [10]. The dispute between the ocean and the sea depends on the technological innovation capability of the sea. Its strength determines the international voice of a country in the marine field. As an exploratory study, it is expected to draw the attention of peer researchers and jointly promote the popularization and application of high water quick setting materials in marine engineering.

EXPERIMENTAL METHODS AND RESULTS

Sample Preparation. High water quick setting materials mainly composed of a material and b material. There is a small amount of adjustment function of the admixture. A material of Sulfur-aluminum high-water materials is mainly composed of anhydrous calcium sulphoaluminate ($3CaO \cdot 3Al_2O_3 \cdot CaSO_4$) and dicalcium silicate ($2CaO \cdot SiO_2$). The *b* material is mainly lime (CaO) and gypsum ($CaSO_4$).

Uni-axial compression test samples were prepared with drinking water and artificial seawater as mixing water. The water-cement ratio is 5: 1. At room temperature, different samples were treated with drinking water and artificial seawater for soak conservation. Reference to the International Society of Rock Mechanics recommended specimen standards, the sample size is φ50*100mm cylinder [11-14]. The care age is 7 days [11, 12]. The preparation of the sample is shown in Table 1. Artificial seawater is used to refer to the main ion concentration in natural seawater. The composition is shown in Table 2.

Creep test sample preparation with drinking water as mixing water. Water - cement ratio is 3: 1. At room temperature, it uses drinking water for soak conservation [13, 14]. Reference to the Chinese national standard is that "General concrete mechanical performance test method standard" (GB/T50081-2002). The sample size is 100*100 *100 mm and 150*150 *150 mm cubes. The care age is 7 days. The preparation of the sample is shown in Table 1.

TABLE 1
Sample Preparation Table

Group	Mixing Water	Water for Conservation	Sample Size	Water - cement Ratio	Experiment
Group A	Drinking Water	Drinking Water	φ50×100	5:1	Uniaxial compression experiment
Group B	Drinking Water	Artificial Seawater	φ50×100	5:1	Uniaxial compression experiment
Group C	Artificial Seawater	Artificial Seawater	φ50×100	5:1	Uniaxial compression experiment
Group D	Drinking Water	Drinking Water	150×150×150	3:1	Creep experiment
Group E	Drinking Water	Drinking Water	100×100×100	3:1	Creep experiment

TABLE 2
Artificial Seawater Composition Table (g /L)

Ingredients	NaCl	$MgCl_2$	Na_2SO_4	$CaCl_2$	KCl
Content	24.53	5.20	4.09	1.16	0.70

TABLE 3
Uni-axial Compressive Strength and Moisture Content of the Sample

	A-1	A-2	A-3	A-4	B-1	B-2	B-3	B-4	C-1	C-2	C-3	C-4
Strength/MPa	0.46	0.44	0.47	0.46	0.60	0.61	0.58	0.62	0.75	0.71	0.67	0.71
Average Value	0.46				0.60				0.71			
Moisture Content/%	81.8	82.0	81.8	81.9	80.9	80.0	80.8	80.1	77.1	77.3	77.7	77.4
Average Value	81.88				80.45				77.38			

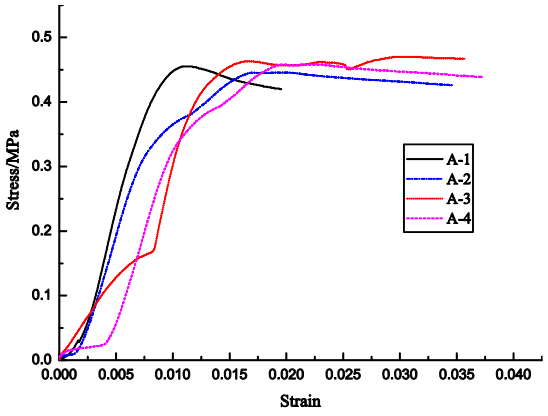

FIGURE 1
Stress-strain curves of group A sample

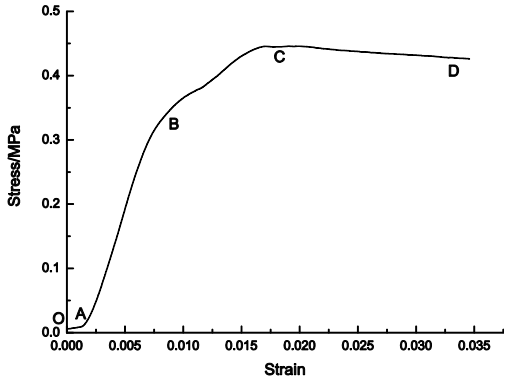

FIGURE 2
The whole process of specimen deformation

Uni-axial Compression Experiment. The uni-axial compression experiments and the moisture content test were carried out on the solidified body of high water material in group A, group B and group C by using MTS815 Flex Test GT Rock and Concrete Mechanics Experiment System [15]. In group A, group B and group C, there were 4 samples in each group. The results are shown in Table 3.

The total stress curve of the single - axis compressive stress - strain of A group is shown in Fig 1. Combined with the change of the specimen morphology during the experiment, the uni-axial compression deformation of the solidified body can be divided into four stages. It is shown in Fig 2.

(1) OA section. The curve convexes and the slope gradually increased. Increased stress increases and strain increases rapidly. There was no significant change in the surface of the specimen.

(2) AB section. The curve is approximately straight, the slope remains basically unchanged. With the increasing stress, strain increases slowly; the sample surface has no significant change.

(3) BC section. The curve began to gradually bend, the slope gradually smaller. The stress rises slowly and the strain begins to increase. Small water droplets appear on the surface of the specimen. Water droplets pooled into small strands of water. The surface of the crack began to expand and gradually began to break. C point reaches the peak point and the specimen is horizontally contracted.

(4) CD segment. The curve began to decline, the stress slowly reduced, strain rapidly increased. The specimen crack develops rapidly, the surface crack extends from the end to the middle and the water is in serious condition. The end of the sample appeared uplift broken; the volume appears to reduce the trend.

Creep Test of High Water Material Consolidation Body under Pressure Water Environment. Whether the marine geotechnical engineering or other areas of geotechnical engineering are all related to the time factor, it is necessary to consider the time effect and rheological properties when we study on the mechanical properties of high water material consolidation body.

(1) Experimental Methods. Experiments were carried out by self-designed pressure water environment rock tri-axial rheological experiment device to carry out creep experiments under different water pressure. The experimental system mainly includes the hydrostatic axial loading system, the hydrostatic

ring loading system, the deformation measuring system, the pressurized barrel and the specimen restraint mold. The loading system principle is shown in Fig 3. The creep characteristics of high water material consolidation body in pressure water environment are mainly studied. Drinking water is used as pressure water. Under the same axial load, the creep process of the solidified body under different water pressure was studied and two groups of experiments were designed. The loading method is shown in Table 4.

(2) Experimental Results. In the first group of experiments, the test piece D-1 was subjected to the axial load of 10 kN and the water pressure of 0.2 MPa. The axial load of 10kN sustained by the D-2 remains unchanged and water pressure increased by 0.2 MPa. The axial load and hydraulic pressure on the D-3 are increased by 0.2MPa. The water pressure application rate is set to 0.2 MPa/min and the axial load loading speed is set to 0.1MPa/min [16]. After reaching the experimental set value, it is necessary to maintain the long-term stability of water pressure and axial load. The experiment time is 500h. The creep curves of the first group's three specimens are shown in Fig 4.

In the second group of experiments, the specimen E-1 was subjected to the axial load of 20 kN and the water pressure of 0.2MPa. E-2, E-3 and E-4 bear the axial load of 20kN remained unchanged, water pressure increased by 0.2MPa in turn and the test time is 1000h. The creep curves of the four specimens are shown in Fig. 5 and the creep characteristics of each stage of the sample are shown in Table 5.

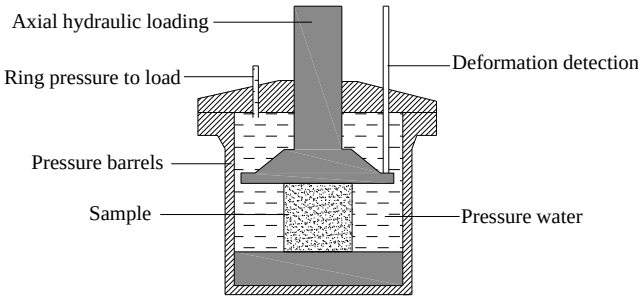

FIGURE 3
Loading System Schematic

TABLE 4
Experimental Loading Method

Group	Specimen number	Axial load / kN	Axial stress / MPa	Water pressure / MPa
Group 1	D-1	10	1.0	0.2
	D-2	10	1.0	0.4
	D-3	12	1.2	0.4
Group 2	E-1	20	0.89	0.2
	E-2	20	0.89	0.4
	E-3	20	0.89	0.6
	E-4	20	0.89	0.8

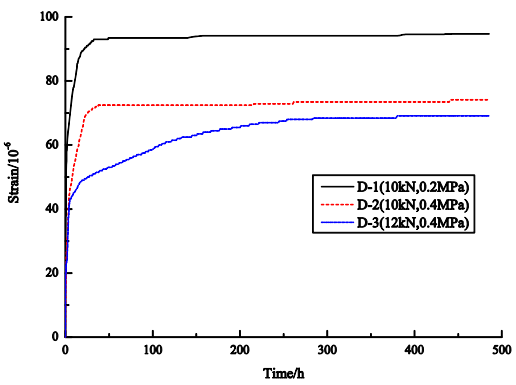

FIGURE 4
Creep Curve of the First Experiment

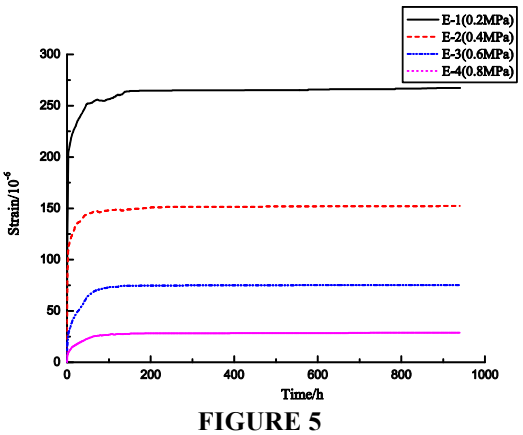

FIGURE 5
Creep Curve for the Second Set of Experiments

TABLE 5
Creep Characteristics of Each Stage of the Sample Parameters

	Elastic stage			Initial creep stage			Constant creep stage		
	Time /h	Strain /10-6	Strain rate /(10-6/h)	Time/ h	Strain / 10-6	Strain rate /(10-6/h)	Time /h	Strain / 10-6	Strain rate /(10-6/h)
E-1	0~1	0~200	198~20	1~42	200~250	20~0.3	42~940	251~267.3	0.3~0
E-2	0~3	0~110	171~10	3~54	110~145	10~0.3	54~940	145~152.3	0.3~0
E-3	0~2	0~23	118~15	2~65	23~70	15~0.3	65~940	70~75.2	0.3~0
E-4	0~2	0~8	55~6	2~70	8~25	6~0.3	71~940	25.6~28.8	0.3~0

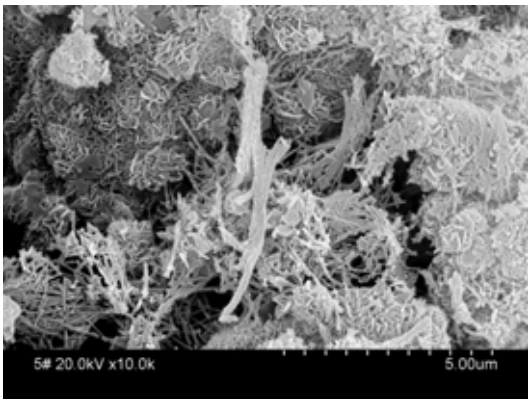

FIGURE 6
Consolidated scanning electron microscopy (10000 times)

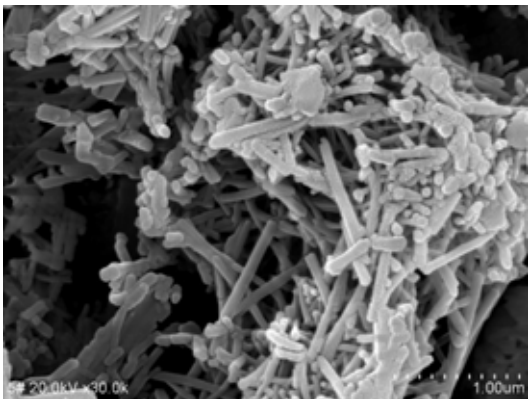

FIGURE 7
Scanning electron microscopy (30000 times)

DISCUSSIONS

Hardening of High Water Quick Setting Material. Now the study is generally believed that the high water material hardening reaction process after a material (b material) hydration dissolved, cementing and hardening of the three stages of hardening. A material (b material) were hydrated and dissolved to form Ca^{2+}, AlO^{2-}, SO_4^{2-}, OH-plasma and the hydration slurry is rapidly reacted between the ions. A large amount of ettringite ($3CaO \cdot Al_2O_3 \cdot 3CaSO_4 \cdot 32H_2O$) is generated in a short time and a large amount of free water is converted into crystallization water of ettringite. So the mixed slurry is rapidly thickened and gelled. The main chemical reaction of ettringite is as follows.

$$6Ca^{2+}+2AlO_2^-+3SO_4^{2-}+30H_2O+4OH^- = 3CaO \cdot Al_2O_3 \cdot 3CaSO_4 \cdot 32H_2O \quad (1)$$

The main components of high water materials hydration products include ettringite, aluminum hydroxide gel and silicate gel. Scanning electron microscopy (SEM) was performed on group A. It can be seen from Fig 6 and Fig 7 that the ettringite morphology is like a bar-like shape [17], the crystal thickness is about 1μm and the crystal is staggered with each other. The internal structure of the consolidation body is dominated by the network structure and the branches are intertwined with each other. The distance between the branches and columns is obvious, and there are a large number of gaps between the network structure and a group of flocculent gels at local space. The silicate gel is in the form of a leaf and the plate-like gel is present in its entirety. The gel makes the structure of the consolidation more compact.

Water in High Water Material Consolidation Body. The presence of water in the consolidation body is mainly crystal water, adsorption water and free water. Crystalline water is a part of the crystal structure of water that is formed by the combination of chemical molecules and other ions. According to the ettringite formula, the water accounts for about 46% in the ettringite crystal. The stability of the crystal water is mainly affected by temperature. When the crystal water overflows, the crystal structure will be destroyed. The adsorbed water is mechanically adsorbed on the surface or pores of the solid particles under the action of the adsorption effect and the capillary force. It does not participate in the crystal structure of the hydrate. Adsorption of water can be divided into gel water and capillary water. Gel water is strongly adsorbed by the gel surface and highly oriented, with a strong difference in bond strength. Capillary water is only affected by the capillary; the binding force is very weak. Free water is mainly present in the voids of the consolidation network. Free water evaporates slowly with the change of ambient humidity and temperature. Free water flow should be accompanied by poor water pressure

and overcome the resistance through the pore channel. Most of the moisture in the consolidation is free water. Experimental data shows that free water and adsorbed water account for 70% of the moisture in the consolidation [18].

High water material is a hydrophilic material. The formation of ettringite requires a lot of water to participate. At the same time the water environment can prevent the solid body directly contact with the air and the loss of internal moisture. The water environment is beneficial to the development and maintenance of high water material's strength.

Microscopic Mechanism of Uni-axial Compression Deformation of Consolidation. The main components of the consolidation body include ettringite, aluminum hydroxide gel and silicate gel. It belongs to the polycrystalline composite medium. The theory of solid-state physics holds that the interior space of the polycrystalline composite media can be divided into three categories such as grain internal, grain interface and grain gap. Different ions form crystal particles with certain structural characteristics under the action of chemical health. Polymorphic interface among the different grain orientations is known as the grain interface. There is a gap among the grains and the grain gap is filled with cement, water or air. The deformation of the crystal material includes the deformation of the grain itself, the slip of the grain boundary and the destruction of the crystal itself. The deformation of the grain, the slip of the grain boundary and the destruction of the crystal can cause changes in the grain gap.

Based on the theory of solid-state physics and combined with the existence of water in the consolidation body, the four stages of the whole process of analyzing the uni-axial compression deformation of stone can be seen in Figure 2.

(1) OA segment is the compaction stage. With the increase in stress and strain increased rapidly, no significant changes in the sample surface. Maybe the sample from the local pressure into all the pressure.

(2) The AB segment is the elastic phase. With the increasing stress, strain increases slowly and the sample surface no significant change. The deformation of the specimen is mainly the compression of the grain itself.

(3) The BC segment is a rupture phase. The stress rise is slow and the longitudinal strain begins to increase. At first the surface of the sample extrusion has small water droplets, and then the water droplets pool into a small flow of water. Longitudinal continuous cracks. Under the action of load, the position of different branches of calcium vanadium in the consolidation body is reoriented, the space staggered overlap is more closely, the free water in the pore of the mesh structure is extruded and the pore compression is deformed. The deformations are mainly grain boundary slip and destruction of alumitic stone crystals.

In the rupture stage, the surface of the solidified body has crack propagation. However, due to the large porosity and the high water content of the material, the free water in the mesh structure was massively extruded in the compression process. The grain gap is compressed and the sample appeared transverse shrinkage deformation. The overall volume has a tendency to decrease.

(4) CD segment is broken after the stage. After the bearing capacity of the material reaches its peak value, the stress value begins to decrease slowly and the material is lost to carry capacity. Specimen cracks continue to expand and the water situation is serious.

The Stability of High Water Material Consolidation in Artificial Seawater Environment. The contents of salt ions in seawater mainly include Cl^- (19.344g/kg), Na^+ (10.773g/kg), SO_4^{2-} (2.712g/kg), Mg^{2+} (1.294g/kg), Ca^{2+} (0.412g/kg) K^+ (0.399 g/kg).

The main component of the consolidation is ettringite. The amount of ettringite, formation rate and stability will directly affect the performance of the solidified body. The main salt ions in seawater will have an effect on the formation and stabilization of ettringite.

(1) Effect of Ca^{2+} and SO_4^{2-} on Ettringite Formation Reaction. According to the formation reaction of ettringite, we can see chemical formula (2). The equilibrium constant of the reaction is shown as follows.

$$K_P = \frac{\left[3CaO \cdot Al_2O_3 \cdot 3CaSO_4 \cdot 32H_2O\right]}{[Ca^{2+}]^6[AlO_2^-]^2[SO_4^{2-}]^3[OH^-]^4[H_2O]^{30}} \quad (2)$$

The formation of ettringite is affected by Ca^{2+}, AlO^{2-}, SO_4^{2-}, OH^- concentration only from the thermodynamic point of view of chemical reaction. The effect of different ions on the experimental response is different. Ca^{2+} is a 6th order relationship. In the composition of ettringite, the amount of Ca^{2+} required is large and Ca^{2+} concentration is the main influencing factor of the reaction.

However, the literature holds that the formation of ettringite reaction is divided into three steps [19]. The three steps are shown in reaction formula (3), reaction formula (4) and reaction formula (5). The formation rate of ettringite is mainly determined by the concentration of AlO^{2-}. When the SO_4^{2-} concentration is lower than a certain degree, the reaction is a third step reaction, which is reaction formula (4). It can be carried out in reverse. The concentration of SO_4^{2-} affects the stability of ettringite. The concentration of Ca^{2+} in the reaction system of high water material has little effect on the reaction.

$$AlO_2^- + 2OH^- + 2H_2O = \left[Al(OH)_6\right]^{3-} \quad (3)$$

$$2\left[Al(OH)_6\right]^{3-} + 6Ca^{2+} + 24H_2O = \left\{\left[Ca_6Al(OH)_6\right]_2 24H_2O\right\}^{6+} \quad (4)$$

$$\left\{\left[Ca_6Al(OH)_6\right]_2 24H_2O\right\}^{6+} + 3SO_4^{2-} + 2H_2O = \left\{\left[Ca_6Al(OH)_6\right]_2 24H_2O\right\}[3SO_4^{2-} 2H_2O] \quad (5)$$

The AlO^{2-} of ettringite is derived from sulphoaluminate, $SO_4^{2-}$is derived from gypsum and sulphoaluminate and Ca^{2+} is provided by lime, sulphoaluminate and gypsum. Despite the large amount of Ca^{2+} required in the reaction of ettringite, it is possible to provide sufficient Ca^{2+} in the raw material. In the whole reaction system, Ca^{2+} is excessive. Ca^{2+} concentration are not a control factor for the reaction rate.

The formation rate of ettringite is mainly determined by the concentration of AlO_2^- and the concentration of SO_4^{2-} affects the stability of ettringite. Literature through experiments shows that the stability of ettringite in solution depends largely on the concentration of SO_4^{2-} in the liquid phase. When the concentration of SO_4^{2-} in the solution is less than 1.0g/L, ettringite is difficult to be formed or it is unstable after formation, it is converted to low sulfur hydrated calcium sulphoaluminate ($3CaO \cdot Al_2O_3 \cdot CaSO_4 \cdot 12H_2O$) [20]. When the concentration of SO_4^{2-} in the solution is higher than 1.0 g/L, ettringite can be stably present and can be continuously produced.

(2) Effect of Cl- on Ettringite Formation Reaction. The highest proportion of seawater salt ions is Cl^- and Cl^- is the most corrosive to marine engineering materials. There are many important results in the study of corrosion of marine engineering concrete and marine metal materials [21-23]. At present, the study of the effect of Cl^- on ettringite is mainly aimed at the study of the durability of sulphoaluminate cement in chloride environment. The effect of Cl^- on ettringite is divided into two cases, one is mixed as a raw material mixture and it known as the inclusion of Cl-; the other is the external environment infiltration and it known as the outer osmosis Cl^- [24].

The general view is that there is a low sulfur type hydrated sulphoaluminate in hydrated products of sulphoaluminate cement in the case of mixed with Cl^-. Low-sulfur hydrated sulphoaluminate can react with Cl- to form hydrated calcium chloroaluminate [25-26].

$$3CaO \cdot Al_2O_3 \cdot CaSO_4 \cdot 12H_2O + Cl^- = SO_4^{2-} + 3CaO \cdot Al_2O_3 \cdot CaCl_2 \cdot 10H_2O + 2H_2O \quad (6)$$

Literature [27-28] holds that ettringite in the chloride salt solution can remain stable because the ettringite crystal lattice constant, functional groups and micro-morphology are not changed after being eroded by the chloride salt solution. The effect of ettringite on Cl^- is only physical adsorption rather than chemical binding. The ettringite is incapable of combining the Cl^- of external solution. However, by comparing X-ray diffraction of hydrated products of sulphoaluminate cement before and after erosion of chloride salt solution, the literature [4, 29-30] holds that Cl^- could replace the SO_4^{2-} of ettringite and produce hydrated chloraluminous acid calcium. The reason for this disagreement may be due to a large difference in Cl^- concentration. The stability of hydrated calcium chloroaluminate depends on the concentration of Cl^- and the pH. In the case of higher Cl^- concentration, hydrated calcium chloroaluminate can be stably present [31]. In addition, the silicate gel in the hydrated product also has a certain physical adsorption capacity for Cl- [32].

In the case of exudation Cl^-, Cl^- in the external environment enters into the interior of the consolidation by means of osmotic action, capillary adsorption, electrochemical migration, diffusion or a combination of the above and it will produce physical and chemical reactions with cement hydration products.

Comparison of three samples of compressive strength and water content can be seen in Table 3. The compressive strength of group A was the smallest and the water content was the highest. The compressive strength of group C was the highest and the water content was the smallest. The water is mainly present in the pores of the solid body and the water content can reflect the size of the porosity of the solid. According to the different water content, it can be considered that the porosity of group A is the largest, the porosity of group C is the smallest and the porosity of group B is centered.

Scanning electron microscopy analysis and comparative observation of samples A, B and C can be seen in Fig. 8. The internal structure of group A is dominated by dendritic structure and each branch is overlapped with each other. The distance between the branches is obvious; there are a lot of pores between the dendrites and some flocculent and filamentous gels. The internal structure of group B was dominated by disorderly dendritic structure and the flocculent and filamentous gels were obviously increased. The whole structure was denser than that of group A and the porosity was reduced. In the C group of samples, it still can see the internal structure of the disorder. The flocculent, filamentous gels are produced in large quantities in the form of pellets, lumps or flakes. And the bonding between the mass material and the mass material or bulk material is more compact. The pore size becomes smaller and the pore network system is more tortuous. The internal pores are less than group A, B and the overall structure is relatively dense. The overall is better.

Through the comparison of the strength and porosity of different samples are combined with the microscopic analysis of scanning electron microscopy, it can be concluded that the solid structure will form different microstructures in different mixing and curing water environment. The difference of pore distribution and quantity will affect the macroscopic mechanical properties of the consolidation.

Artificial seawater mixing and curing can provide adequate SO_4^{2-} and Cl^-. The concentration of SO_4^{2-} affects the stability of ettringite in the solidified body. The higher concentration of Cl^- contributes to the formation and stabilization of hydrated calcium chloroaluminate and Cl^- can also be physically adsorbed by ettringite and silicate gel. Due to the formation of hydrated calcium chloroaluminate and the adsorption of Cl^- on ettringite and silicate gel, the pore structure and pore distribution of the solidified material are changed which reduces the porosity of the solidified body. The change of the microstructure of the solidified body causes the compressive strength to change and the macroscopic mechanical strength of the material is improved. Artificial seawater mixing and curing environment can improve the strength of high water material consolidation body.

Creep of High Water Material Stone Body Artificial under Seawater Pressure Environment. (1) Analysis of Creep Process of High Water Material Consolidation. In the first group of experimental results, the creep curves of different samples are shown in Figure 4.

We can see as follows.

(1) In the pressure water environment, the initial creep development of the sample loading is rapid and the time to reach the relatively stable state is very short. The peristaltic deformation of the high-water consolidation compact is extremely rapid in the early stages of loading. After loading for about 2 hours, the creep amount has reached more than 50% of the relatively stable state. After loading for 24 hours, it reaches more than 90% and then the creep amount enters a relatively stable state.

(2) In the creep curves of the three specimens, the curve approximates a vertical straight line at the beginning of loading and the strain rate increases rapidly with time. The curve then begins to bend downward and the strain rate decreases with increasing time. Finally the strain rate remained essentially unchanged and the curve tends to be gentle. All three samples experienced an instantaneous elastic deformation stage, an initial creep stage and a constant velocity creep stage. Because of the test conditions the loading time is not long enough and the stress applied does not reach the critical stress. None of the three samples showed accelerated creep stages.

(3) The creep curve of sample D-2 is located below the curve of sample D-1 which shows that when the axial stress is the same, the creep deformation decreases with increasing water pressure. Water pressure has a negative effect on creep and water pressure is negatively correlated with creep deformation. The creep curve of sample D-2 is located below the curve of sample D-3 which shows that when the water pressure is the same, the creep deformation increases with the increase of axial stress. The axial stress has a positive effect on the creep and the stress level is positively correlated with the creep deformation. The creep curve of the sample D-3 is located below the curve of the sample D-1. The large difference between sample D-1 and sample D-3 indicates that when the axial stress and water pressure increase at the same time, the role of the promotion of axial stress and water pressure inhibition cannot completely offset each other. The inhibition effect is stronger than the promoting effect, and the creep deformation is decreasing.

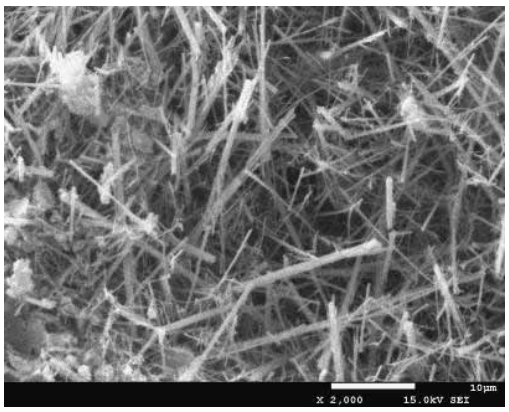

FIGURE 8a
Group A Sample Scanning Electron Microscopy (2000 times)

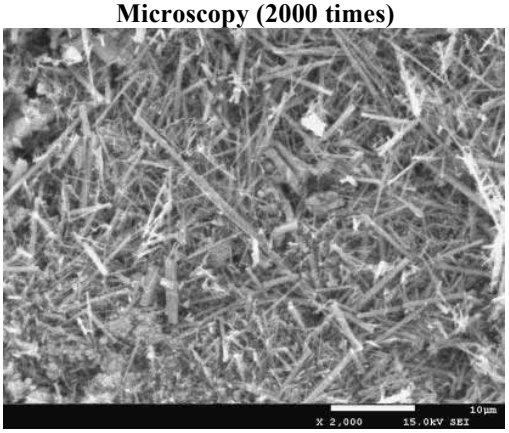

FIGURE 8b
Group B Sample Scanning Electron Microscopy (2000 times)

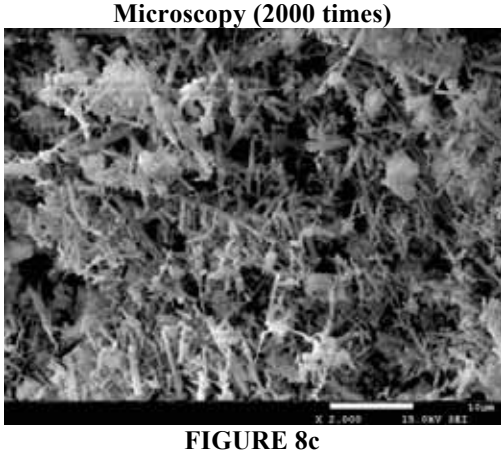

FIGURE 8c
Group C Sample Scanning Electron Microscopy (2000 times)

(4) The creep test results of the three samples were significantly different in different loading modes. It indicates that the creep of the consolidation body in the pressure water environment is affected by the stress level and the water pressure at the same time and the influence degree is different.

In the second experiment, the creep curves of the four different loading modes are shown in Figure 5. And the creep characteristic parameters of each stage are shown in Table 5. We can see as follows.

(1) The creep curves of the four samples have experienced the instantaneous elastic deformation stage. Taking sample E-2 as an example, the instantaneous elastic strain stage is from 0 h to 3 h. The strain curve rises linearly as time goes by. The strain value is increased from 0 to $110*10^{-6}$ and the strain rate is changed from 171×10^{-6}/h to 10×10^{-6}/h. The creep curve gradually decreases from 3h to 54h, the strain value gradually increases from 110×10^{-6} to 145×10^{-6} and the strain rate is gradually reduced to 0.3×10^{-6} / h. The strain rate is from 145×10^{-6} to 151×10^{-6}. There is no tendency to find the sample enters the accelerated creep stage.

(2) The strain rate of four samples is generally similar. The strain rate is rapidly decayed from the beginning of the order of 10^{-4} / h to 10^{-6} / h order of magnitude within 3 h. During the period of 3h ~ 70h, the strain rate gradually changed from 10^{-6} / h to 10^{-7} / h and the deformation increased gradually. After 70 h, the strain rate fluctuates from 0 to 0.3×10^{-6} / h and the strain rate tend to be constant. The sample can be considered to enter the steady-state creep stage. There is no increase in the strain rate during the creep after this stage.

(3) The strain rate of each stage is reduced with the increase of water pressure. The water pressure has a significant effect on the initial strain rate of the high water material creep test. It affects the time required to enter the stable creep stage. When the water pressure is greater, the initial strain rate of the creep test is greater, the creep rate decay time is longer and the time required longer entering the stable creep stage.

(4) The deformation of the stable creep stage decreases with the increase of the water pressure, and the water pressure can inhibit the creep development of the high water material. The water pressure is greater; the limit creep of the stable creep is smaller. The difference in the amount of deformation in the creep test curve is shown from the initial elastic strain stage. The difference in the elastic phase strain is the main reason for the difference in the stability of the creep stage.

(5) At the same stress level, the curve under different water pressure is obviously different. And the total amount of deformation decreases with the increase of water pressure. The water pressure suppresses the creep deformation of the solidified body. In the case of water pressure, the creep deformation of the solidified body is not controlled by total stress.

(2) Analysis of the Mechanism of Water Pressure Affecting the Creep Process of High Water Material. The creep process of the solidified body is studied with the viewpoint of the pore medium. We can make the following basic assumptions such as the pore medium is homogeneous, isotropic. In the structure it is interconnected by the solid skeleton and the pores between skeletons, the pores are filled with fluid. The skeletal particles can be compressed, the fluid in the pores is incompressible and all the pores in the skeleton are connected. The pores are changing during the deformation process.

A representative elemental volume (REV) that defines a physical mechanics feature can represent the pore dielectric space and the mean value of the point is represented by the mean value of the physical mechanical feature on REV. These feature quantities satisfy mathematically continuous conditions throughout the pore media space. Let S_r be the area of REV characteristic length, ΔA_n be the area of the sub-plane, ΔA_{sn} be the area of the skeletal particles corresponding to ΔA_n in the sub-plane and ΔN_n be the component of the internal force acting on ΔA_n. The actual stress of the skeleton is the average of the actual cross-sectional area occupied by the skeletal internal forces in the skeletal particles. It can be defined as follows [33].

$$\sigma_s = \lim_{\substack{\Delta A_{sn} \to S_r \\ S_r \to 0}} \frac{\Delta N_n}{\Delta A_{sn}} \tag{7}$$

The forces acting on the skeleton of the saturated pore medium are that external load (excluding pore fluid pressure), the interaction among the crystal particles caused by the external load, pore fluid pressure and the interaction between the crystal particles caused by the pore fluid pressure. The stress caused by the pore fluid has the properties of hydrostatic pressure. In addition to the volume deformation of the skeletal crystal particles, there is generally no observable skeleton deformation. Pore fluid pressure is a set of self-balanced volumetric forces within the skeleton. If the volume deformation of the skeletal crystal particles can be ignored, it does not cause any volume deformation. The actual stress of the skeleton is the stress that controls the deformation and strength of the skeleton which is the measure of all external forces acting on the skeleton except the pore fluid pressure.

As well as the instantaneous compression deformation of the material, the creep deformation of the pore medium also includes the deformation of the grain itself, the slip of the grain boundary and the destruction of the crystal itself. Creep mechanism and creep deformation is directly related to the actual skeleton stress acting on the material.

After the high-water material consolidation body is subjected to the pressure load, the internal microstructure will be re-adjusted under the actual

stress of the skeleton. The deformation of the instantaneous elasticity stage is mainly its own compressive deformation of the skeleton crystal particles. The initial creep stage and the constant velocity creep stage are mainly the rearrangement of the skeletal crystals caused by the slip of the grain boundary. The deformation of the accelerated creep stage is mainly the grain boundary slip and the destruction of the crystal itself. During the whole creep processes, the micro-porous structure of the solidified body changes under the real stress of the skeleton.

In the initial creep stage and the constant velocity creep stage, the grain gap is compressed and a new crack is produced due to the slip of the grain boundary and the destruction of the crystal itself. But the porosity of the material is large and the volume of grain gap reduced by compression is much larger than the expanded volume produced by the new crack. The pores of the solidified crystals are full filled with free water and the pores are interconnected. Grain gap compression is bound to require free water within the pores to be excluded. The pore water pressure affects the deformation of the solidified body by directly affecting the true stress of the skeleton and it ultimately affects the long-term strength of the solidified body.

Selecting any of the tiny cells in the porous medium, the bottom area of the micro-element is A, the total stress of the position of the micro-element is σ and the selected cross section utilized by the effective principle of too sand is b-b. In Figure 9, pour water pressure acts the space through the pores. The forces of action through the solid particles are P_1, P_2 ..., P_i. The contact area between the particles is A_{c1}, A_{c2} ..., A_{ci}. The effective stress is the average of the micro-particle solid particles in the vertical direction to the bottom area A. It is the virtual physical quantity. With reference to the effective stress of the Taisha basis [34], the cross section c-c is selected. In Figure 10, the cross-sectional area is A, the contact area between the particles is A_{ci}, micro-body internal cross-section c-c on the internal forces are F_1, F_2 ..., F_i. The actual stress σ_s of the skeleton is as follows.

$$\sigma_s = \frac{\sum F_i}{\sum A_{ci}} \tag{8}$$

Consider the balance of the vertical force on the c-c surface:

$$\sigma A = \sigma_s \sum A_{ci} + u(A - \sum A_{ci}) \tag{9}$$

$$\sigma = \sigma_s \frac{\sum A_{ci}}{A} + u(1 - \frac{\sum A_{ci}}{A}) \tag{10}$$

Not considering the microstructure of the material and as long as c-c surface have the average statistical significance. There are: $\frac{\sum A_{ci}}{A} = 1 - n$.

$$\sigma = \sigma_s \frac{\sum A_{ci}}{A} + u(1 - \frac{\sum A_{ci}}{A}) = \sigma_s(1-n) + un \tag{11}$$

$$\sigma_s = \frac{\sigma - un}{1-n} = \frac{\sigma}{1-n} - \frac{n}{1-n}u \tag{12}$$

In the formula: σ_s is the actual stress of the skeleton, u is the pore water pressure, n is the porosity and σ is the total stress.

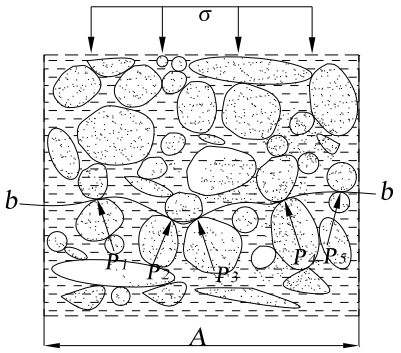

FIGURE 9
Schematic diagram of effective stress calculation

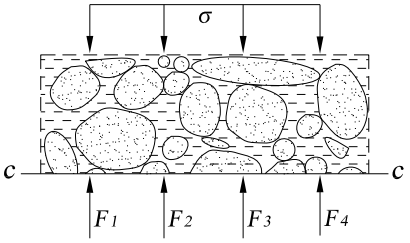

FIGURE 10
Schematic diagram of the actual stress calculation of the skeleton

According to the formula (12), when the total stress σ = 0.89MPa under the condition of certain porosity, the influence of pore water pressure on skeleton stress is investigated. As shown in Fig. 11, the actual stress of the skeleton decreases when the pore water pressure increases. We can analysis combined with Figure 5. At the same stress level, the curves' differences between different water pressures are obvious. With the increase of water pressure, the actual stress on the skeleton of the material decreases and the instantaneous elastic deformation and stable creep deformation are reduced. In the case of water pressure, the water pressure suppresses the creep deformation of the solidified body. The creep deformation of the consolidation is not controlled by total stress.

When the total stress is σ = 0.89MPa and the pore water pressure is constant, the influence of the change of porosity on the stress of the skeleton is investigated. In Figure 12, the actual skeleton stress increase with increasing porosity. According to the analysis of Figure 5, the creep process of the solidified body undergoes instantaneous elastic deformation, initial creep stage and stable creep stage under certain stress level and water pressure. After the

solid body is subjected to axial load and water pressure, grain deformation, grain boundary slip and crystal itself damage will cause changes among the crystal pores. This leads to a change in porosity which in turn causes a change in the actual stress of the skeleton. In the creep process, the porosity changes with time and the porosity can be used as a physical quantity to measure the state of the material structure.

The above analyses are only from the perspective of the fluid pressure affects the solid stress field. According to the fluid-solid coupling, the fluid affects the solid stress field through the pore water pressure. The stress field also affects the fluid through the compressibility of the porous medium and the porosity affects the actual stress of the skeleton. In turn, the porosity is also affected by multiple factors such as the actual stress of the skeleton, the fluid pressure, the volume strain and the compression coefficient of the crystal particles. We do not do in-depth discussion in this paper.

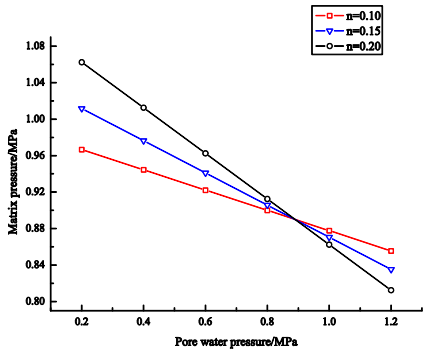

FIGURE 11
The Relationship between the Actual Stress of Skeleton and Pore Water Pressure

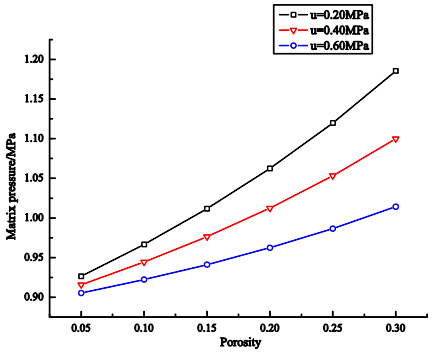

FIGURE 12
The Relationship between the Actual Stress of Skeleton and Porosity

CONCLUSION

Artificial seawater mixing and curing environment can improve the peak strength of the solidified body. Water pressure can change the actual stress of the skeleton to inhibit the creep deformation of the material and improve the long-term strength of the solidified body. High water materials can adapt to the harsh environment of marine salt ion corrosion and water pressure. It can be used as a good marine engineering reinforcement material. In this paper, the mechanical properties of the solidified body are studied in the case of high water-cement ratio and no additional material. The strength of the solidified body is generally not high. In order to be able to use high water materials better in marine engineering, you can reduce the water-cement ratio or add silicon powder, sea sand, gravel and other additives to improve the strength of the consolidation body. This work needs further exploration.

ACKNOWLEDGEMENTS

Supported by the Science & Technology Development Projects of Henan Province (Grant No. 172102310706), the S&T Open Cooperation Projects of Henan Province (Grant No. 172106000073) and the Key S&T Program of Henan Province (Grant No. 172102310643).

REFERENCES

[1] Feng, G.M. (2009) Research on the super high-water packing material and filling mining technology and their application. XuZhou: China University of Ming & technology.

[2] Sun, H.H., Li, S.Q. (1994) A study on the high-water material-a new material. Beijing: Proceedings of the Second Asia-Pacific Symposium on Advances in Engineering Plasticity and Its Applications, 661-666.

[3] Sun, H.H., Liu, W.Y., Huang, Y.C., Yang, B.G. (1998) Use of high-water-rapid-solidifying material as backfill binder and its application in metal mines. Australasian Institute of Mining and Metallurgy Publication Series. 1, 21-24.

[4] Gao, M. (2016) Study on the deterioration mechanism of cement-based rich-water filling material in corrosive environment. Beijing: University of Science & Technology Beijing.

[5] Wang, D., Zeng, J.H., Liu, C.W., Xu, Y.H. (2014) Creep law and rheological model of high-water rapid-setting material in water environment. Journal of Sichuan University (Engineering Science Edition). 46(3), 1-6.

[6] Li, H.J., Zhang, Y.C., Xu, L., Jia, X.G., Gu, X.M. (2017) Examination of the treatment quality of filling mined-out voids using super-high-water material by the TEM technique. Environmental Earth Sciences. 76(3), 115.

[7] Wang, A.L., Ma, L.Q., Wang, Z.W., Zhang, D.S., Li, K., Zhang, Y., Yi, X.J. (2016) Soil and water conservation in mining area based on ground surface subsidence control: development of a high-water swelling material and its application in backfilling mining. Environmental Earth Sciences. 75(9), 779.

[8] Li, H.Z., Guo, G.L., Zhai, S.C. (2016) Mining scheme design for super-high water backfill strip mining under buildings: a Chinese case study. Environmental Earth Sciences. 75(9), 1017.

[9] Wang, C., Villaescusa, E. (2013) Influence of water salinity on the properties of cemented tailings backfill [J]. Mining Technology. 110(1), 62-65.

[10] Rosenfeldt, R.R., Seitz, F., Senn, L., Schilde, C., Schulz, R., Bundschuh, M. (2015) Nanosized Titanium Dioxide Reduces Copper Toxicity the Role of Organic Material and the Crystalline Phase. Environmental science & technology. 49(3), 1815-1822.

[11] MacCallum, N., Howell, C., Kim, P., Sun, D., Friedlander, R., Ranisau, J., Ahanotu, O., Lin, J.J., Vena, A., Hatton, B., Wong, T.S., Aizenberg, J. (2014) Liquid-infused silicone as a biofouling-free medical material. ACS Biomaterials Science & Engineering. 1(1), 43-51.

[12] Lenz, R., Enders, K., Stedmon, C.A., Mackenzie, D.M., Nielsen, T.G. (2015) A critical assessment of visual identification of marine microplastic using Raman spectroscopy for analysis improvement. Marine pollution bulletin. 100(1), 82-91.

[13] Chian, S.C., Nguyen, S.T., Phoon, K.K. (2015) Extended strength development model of cement-treated clay. Journal of Geotechnical and Geoenvironmental Engineering. 142(2), 06015014.

[14] Orani, A.M., Han, E., Mandjukov, P., Vassileva, E. (2015) Marine sediments monitoring studies for trace elements with the application of fast temperature programs and solid sampling high resolution continuum source atomic absorption spectrometry. Spectrochimica Acta Part B: Atomic Spectroscopy. 103, 131-143.

[15] Suwan, T., Fan, M. (2014) Influence of OPC replacement and manufacturing procedures on the properties of self-cured geopolymer. Construction and Building Materials. 73, 551-561.

[16] Füllenbach, C.S., Schöne, B.R., Branscheid, R. (2014) Microstructures in shells of the freshwater gastropod Viviparus viviparus: a potential sensor for temperature change? Acta Biomater. 10, 3911-3921.

[17] Cody, A.M., Leeb, H., Codya, R.D., Sprya, P.G. (2004) The effects of chemical environment on the nucleation, growth, and stability of ettringite $[Ca_3Al(OH)_6]_2(SO4)_3 \cdot 26H_2O$. Cement and Concrete Research. 34, 869-881.

[18] Ouhadi, V.R., Yong, R.N. (2008) Ettringite formation and behaviour in clayey soils. Applied Clay Science. 42(1-2), 258-265.

[19] Peng, J.H., Lou, Z.H. (2000) Study on the mechanism of ettringite formation. Journal of The Chinese Ceramic Society.12, 500-515. (in Chinese).

[20] Yang, N.R., Zhong, B.Q., Dong, P., Wang, J. (1984) Ettringite formation and conditions for its stability. Journal of The Chinese Ceramic Society. 6, 155-165. (in Chinese).

[21] Liu, X., Li, Y., Wu, Y.P., Huang, B.Q., Dai, M.H., Fu, F.X., Hutchins, D.A., Gao, K.S. (2017) Effects of elevated CO2 on phytoplankton during a mesocosm experiment in the southern eutrophicated coastal water of China. Scientific Reports. 7.

[22] Thomas, B.S. and Gupta, R.C. (2016) Properties of high strength concrete containing scrap tire rubber. Journal of Cleaner Production. 113, 86-92.

[23] Hanif, A., Diao, S., Lu, Z.Y., Fan, T.Y., Li, Z.J. (2016) Green lightweight cementitious composite incorporating aerogels and fly ash cenospheres–Mechanical and thermal insulating properties. Construction and Building Materials. 116, 422-430.

[24] Sayadi, A.A., Tapia, J.V., Neitzert, T.R., Clifton, G.C. (2016) Effects of expanded polystyrene (EPS) particles on fire resistance, thermal conductivity and compressive strength of foamed concrete. Construction and Building Materials. 112, 716-724.

[25] Glasser, F., Kindness, A., Stronach, S. (1999) Stability and solubility relationships in AFm phases: Part I. Chloride, sulfate and hydroxide. Cem Concr Res. 29(6), 861-866.

[26] Balonis, M., Lothenbach, B., Le Saout, G., Glasser, F. (2010) Impact of chloride on the mineralogy of hydrated Portland cement systems. Cem Concr Res. 40(7), 1009-1022.

[27] Hirao, H., Yamada, K., Takahashi, H., Zibara, H. (2005) Chloride binding of cement estimated by binding isotherms of hydrates. J Adv Concr Technol. 3(1), 77-84.

[28] Elakneswaran, Y., Nawa, T., Kurumisawa, K. (2009) Electrokinetic potential of hydrated cement in relation to adsorption of chlorides. Cem Concr Res. 39(4), 340-344.

[29] Hong, K., Hooton, R.D (1999) Effects of cyclic chloride exposure on penetration of concrete cover. Cement and Concrete Research. 29(9), 1379-1386.

[30] Sahu, S., Havlica, J., Tomkovà, V., Majling, J. (1991) Hydration Behaviour of Sulphoaluminate Belite Cement in the Presence of Various Calcium Sulphates. Thermo Chimica Acta. 175(1), 45-52.

[31] Suryavanshi, A., Narayan Swamy, R. (1996) Stability of Friedel's salt in carbonated concrete structural elements. Cem Concr Res. 26(5), 729-741.
[32] Wowra, O., Setzer, M.J. (1997) Frost Resistance of Concrete//Sorption of chlorides on hydrat-edcements and C3S pastes. London. 147-153.
[33] Shao, L.T., Sun, Y.Z. (2006) Primary study of stress-strain constitutive relation for porous media. Rock and Soil Mechanics. 27(4), 561-565. (in Chinese).
[34] Xu, X.Z., Li, P.C., Li, C.L. (2001) Principle of effective stress based on porous medium. Mechanics in Engineering. 23(4), 42-45 (in Chinese).

Received: **18.09.2017**
Accepted: **05.12.2017**

CORRESPONDING AUTHOR

Changwu Liu
College of Water Resource and Hydropower,
Sichuan University,
Chengdu 610065, Sichuan – China

e-mail: liuchangwu@scu.edu.cn

© by PSP Volume 27 – No. 2/2018 pages 1282-1288 Fresenius Environmental Bulletin

STUDY ON DIURNAL VARIATION OF METHANE EMISSION FROM DOMESTIC REFUSE LANDFILL

Wu Xiaoyun[1,2], Zheng Youfei[1,2,*], Liu Shengtao[1,3], Lin Kesi[4]

[1]Key Laboratory for Aerosol-Cloud-Precipitation of China Meteorological Administration, Nanjing University of Information Science and Technology, 210044, Nanjing, Jiangsu, China
[2]School of Atmospheric Physics, Nanjing University of Information Science and Technology, 210044, Nanjing, Jiangsu, China
[3]School of Environmental Science and Engineering, Nanjing University of Information Science and Technology, 210044, Nanjing, Jiangsu, China
[4]Nanjing Sanhe Environmental Protection Technology Co., Ltd., 210048 Nanjing, Jiangsu, China

ABSTRACT

In this paper, the daily variation of CH_4 emission in the sealing area of the saddle landfill in Luhe District of Nanjing City was analyzed by static box method, and the possible changes of CH_4 were analyzed. The results showed that the variation range of CH_4 was 1.9-119.7mg / m^3 and the flux range was -20.6-52.6mg / (m^2h) during the whole observation period. The peak of CH_4 concentration in different sampling points is different, the peak concentration difference is large, and the diurnal variation of CH_4 emission in landfill is random. Stable landfill CH_4 emissions are not integral, continuous emissions, but local intermittent emissions, CH_4 emissions shorter duration, most of the time in a non-discharge state, the discharge area is random, and the discharge area small. The results show that there is no significant correlation between the CH_4 emission landfill and the temperature and humidity at the time of the stable landfill.

KEYWORDS:
Landfill, closure area, CH_4, diurnal variation

INTRODUCTION

CH_4 is an important greenhouse gas, according to statistics, the global landfill to the atmosphere emissions of CH_4 amount of 9 × 1012-70 × 1012g / a, accounting for about 1.5% of the world's total emissions of 15%, in CH_4. The third column of the source [1-3]. Carbon dioxide (CO_2) is the main cause of greenhouse gases, but methane (CH_4) is particularly important to note that the power of global warming per tonne of methane is calculated in the latest way in 20 years. The greenhouse effect of methane is 72 times stronger than that of carbon dioxide. There are a lot of research on the CH_4 emissions from landfills. Kumar et al. Pointed out that the landfill's landfill age determines the amount of CH_4 release, and the landfill age enters the CH_4 release peak at 1-2 a, with a duration of up to 1 to 5 years [4]. The peak of gas production in China's landfill is slightly different from that in foreign countries. Many studies have shown that the peak time of gas production in landfills varies from 7 months to 4 years [5-7]. In addition Lohila et al. noted that the landfill gas active collection system can reduce the CH_4 release propulsion and reduce landfill carbon emissions [8]. Landfill cover soil microbes can also oxidize CH_4 to slow its release [9]. Ishigaki et al. Used a static box method to measure the CH_4 release rate on the surface of a private landfill in Japan. The CH_4 release rate on the surface of the landfill was different at different sites in the same field [10]. Borjesson and other static box method to two different landfill measurements, the results found that in some cases the landfill in addition to CH_4 release source, but also become CH_4 sink [11]. However, there are few studies on CH_4 emissions for stable landfills.

At present, there are many controversies about the daily variation of CH_4 emission in landfill. Liu Hongting after a study of a landfill, the night to the early discharge rate of the lowest, the highest at noon, afternoon with the law of decreasing time [12]. Yang Xue et al. through the experiment concluded that the discharge flux afternoon is greater than noon than the morning conclusion, and the release of flux change is small [13]. Ma Zhanyun et al. through long-term observation of methane emissions in the closure area of methane methane daily changes do not exist regular conclusions [14]. To this end, we chose the Nanjing Mahe landfill site closure area, through the static box method to observe the landfill CH_4 discharge diurnal variation in order to provide the landfill CH_4 emission control data base.

The site of this experiment is located in the saddle landfill area of Luhe Landfill in Luhe District, Nanjing, Jiangsu Province. The landfill is a valley landfill site. It is mainly responsible for handling the garbage in Nanjing Luhe District, and completed the closure operation in 2011.

The observation period is from March 2015 to July 2015, and the observation period is sunny. Using static box sampling, static box length 30cm, width 20cm, height 20cm. Static box at the top with a sampling port and temperature test port, the box

wrapped insulation cotton, to avoid direct sunlight affect the temperature inside the box. Sampling will be static box buried in the casing, and water around the wet to ensure that the box closed.

Due to the limitation of landfill conditions, the sampling points of this experiment are located in the central and partial edge areas of the sealing area, with a total of 9 sampling points, as shown in Fig. 1.

Sampling time is 24h, a set of samples is collected per hour. Using a three-way valve syringe sampling, respectively, in the static box sealed after 1,16,31 min sampling 60mL.

The collected samples were analyzed by gas chromatography (Agilent 6890N) and quantified by area normalization:

$$C = \frac{A \cdot C_1}{A_1}$$

Where C is the detection gas concentration, A is the detection gas peak area, C1, A1 are the standard gas concentration and peak area.

Analysis of CH_4 Emission Time and Spatial Characteristics. Each sample point CH_4 concentration changes shown in Figure 2, CH_4 concentration range of 1.9-119.7 mg / m^3.

It can be seen from Fig. 2 that the concentration of CH_4 in the landfill is relatively stable and the concentration is low. The concentration fluctuation in the partial time is large and the time of the fluctuation of the sampling points is inconsistent and there is no regularity.

It can be seen from Fig. 2 (a) that the four sampling points fluctuate in different degrees in 24 h, but the time is different and the concentration is different. The maximum daily concentration of sampling points 2 and 3 appeared at 17:00, 78.3 mg / m^3 and 91.1 mg / m^3 respectively. The maximum daily concentration of sampling point 4 appeared at 5:00 pm and 119.7 mg / m^3 the next day. The maximum daily concentration of point 1 appears at 16:00 and the concentration is only 20.4 mg / m3. Which sampling point 4 from 18:00 to 7:00 the next day are in a large concentration fluctuations, that point from 18:00 to 7:00 the next day there are active CH4 emissions activities. It is worth noting that the sampling point at 19:00, the next day 1: 00,3: 00,4: 00 and 6:00 CH_4 concentration is very low, close to the average concentration of blank, which can be seen CH_4 is not Continuous discharge, but intermittent emissions.

Compared with the sampling point 4, the sampling points 2, 3 is in the 15: 00-17: 00 CH_4 concentration in a high state, although the concentration of other periods of time although a small fluctuations, but the overall smooth. It can be seen that CH_4 emissions from various areas of the landfill show unsatisfactory characteristics, that is, the methane emission from landfills is not the overall discharge of landfills, but the discharge of local areas.

The CH_4 concentration at sampling point 3 is generally higher than that of sampling point 2 and a small peak of concentration is observed at 19:00 and 0:00 the next day. It can be seen that the CH_4 emission in the adjacent area of the landfill may have mutual influence. The impact is not always there. It is speculated that the local area of methane emissions from landfills is not large and may be only a certain period of time, a small area of emissions.

FIGURE 1
Sampling point diagram

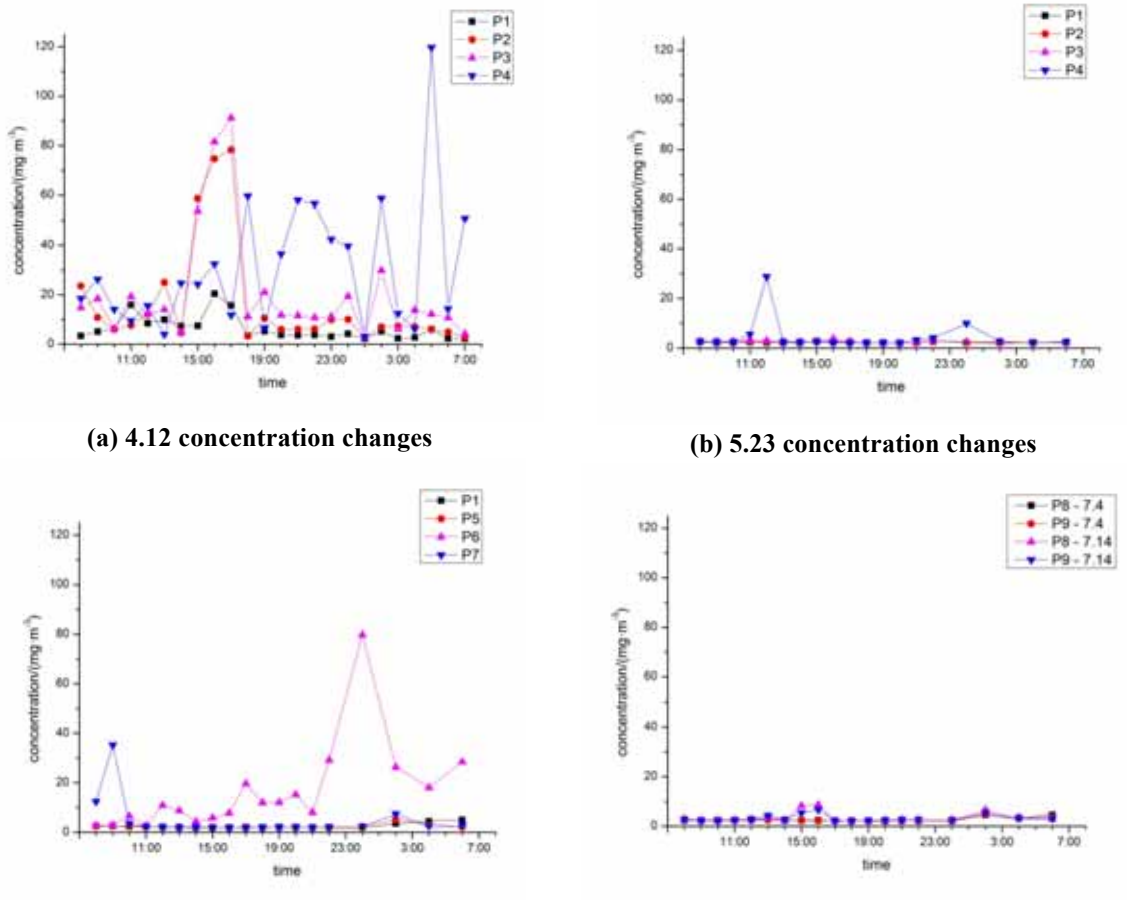

(a) 4.12 concentration changes

(b) 5.23 concentration changes

(c) 6.6 concentration changes

(d) 7.4 and 7.14 concentration changes

FIGURE 2
Diurnal changes in CH_4 concentration

As can be seen from Fig. 2 (b), the same four sampling points show a completely different concentration change from April. Sampling points 1, 2 and 3 CH_4 concentration within 24h no change, the concentration is in the blank sample CH_4 concentration range, that is, the three sampling points in this day there is no CH_4 emissions. And the sampling point 4 appeared two smaller concentration peaks, one at 12:00, the concentration of 28.8mg / m^3, the other appeared in the next day 0:00, the concentration of 9.9mg / m^3, much lower than 4 Month concentration value; other time period and sampling points 1, 2, 3, no methane emissions. This further proves that landfill CH_4 emissions are intermittent emissions and are largely free of emissions.

Figure 2 (c), four sampling points around a gas gathering wells, from the gas wells 2m, respectively, in the gas gathering wells in four directions, close to each other. As can be seen from the figure, even a similar sampling point, but also showed a different CH_4 concentration changes. In general, the concentration of CH_4 in sampling point 6 fluctuated greatly, the maximum concentration appeared at 0:00 on the next day and the concentration was 79.7mg / m^3. At the sampling point 7, the concentration peak was 35.3mg / m^3 at 9:00, There are no CH_4 emissions for other time periods. It is noteworthy that, although the sampling point 6 has a large concentration fluctuation, the sampling points 1, 5, 7 are not synchronized with the CH_4 concentration fluctuations, but also proved that the landfill CH_4 emissions are not a wide range of overall emissions Is limited to only a small area of random emissions.

Analysis of CH_4 Emission Flux Characteristics. The change of CH_4 flux at each sampling point is shown in Fig. 3, and the flux range is -20.6-52.6mg / (m^2h). It is worth noting that CH_4 flux changes are not consistent with changes in CH_4 concentration. In Fig. 3 (a), in Fig. 2 (a), the sampling points 2, 3 show the same CH_4 concentration trend at 14: 00-18: 00, but in Fig. 3 (a), the sampling points 2,3 CH_4 flux changes exactly the opposite. In addition, from 18:00 - 7:00 the next day, the sampling point 4 CH_4 concentration changes violently, but the same time period calculated CH_4 flux is very smooth.

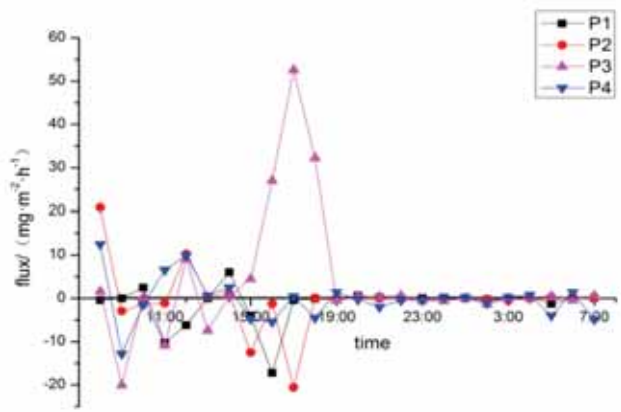

(a) 4.12 Flux changes

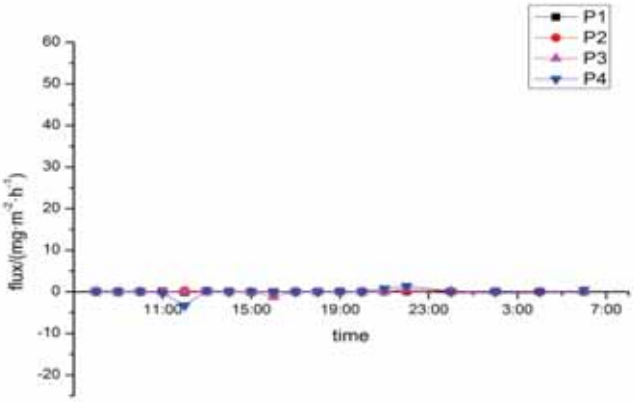

(b) 5.23 Flux changes

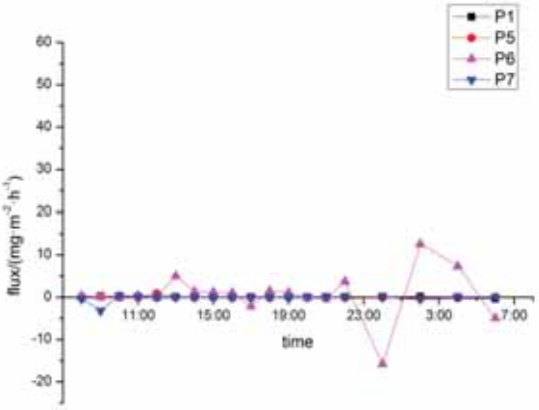

(c) 6.6 Flux changes

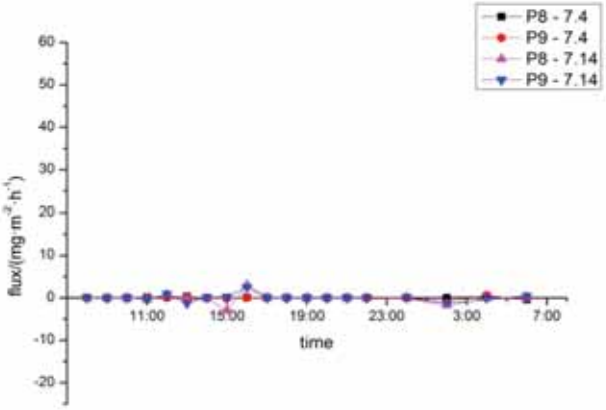

(d) 7.4 and 7.14 Flux changes
FIGURE 3
CH_4 flux diurnal variation

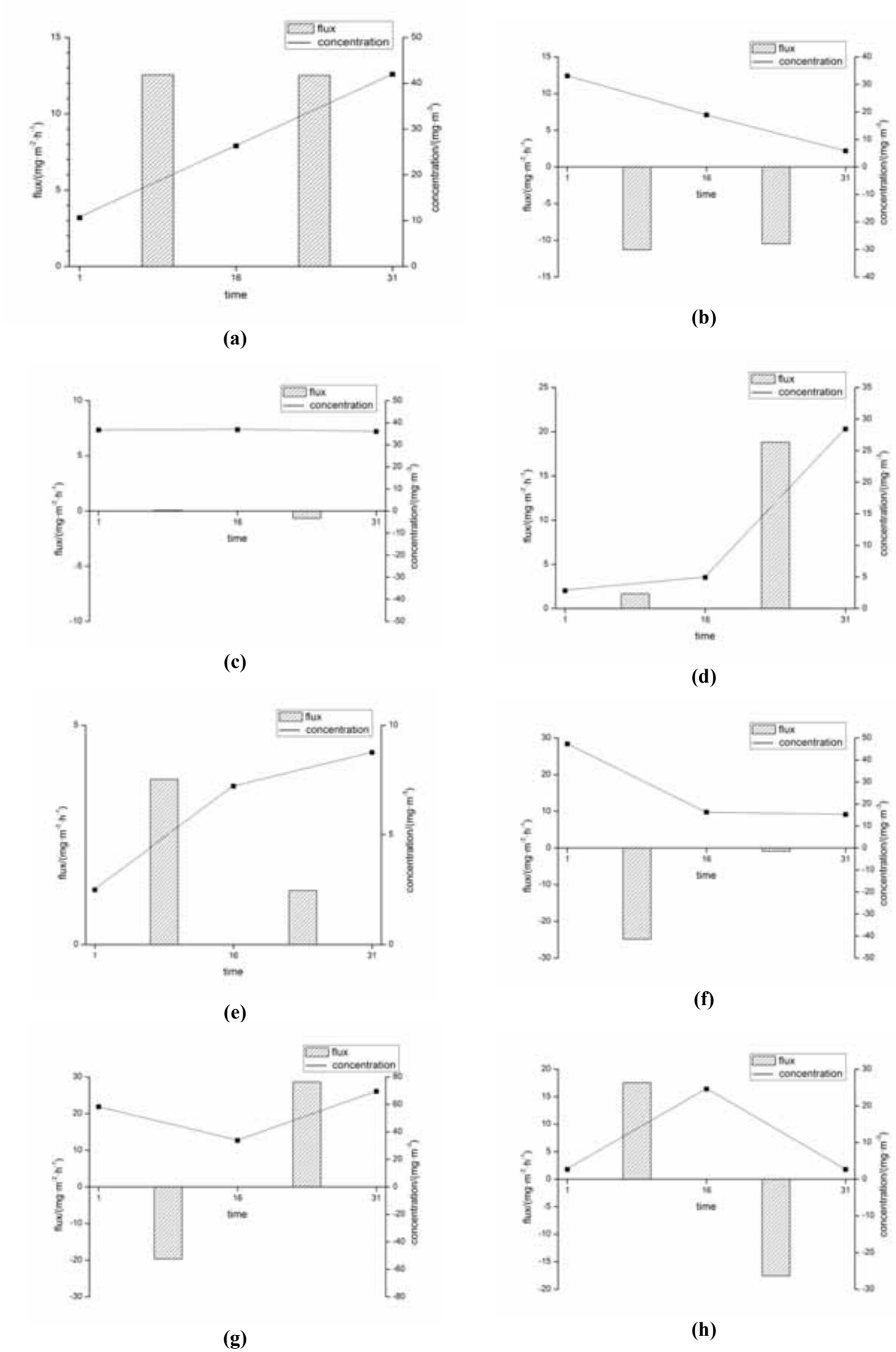

FIGURE 4
CH_4 concentration and flux change mode

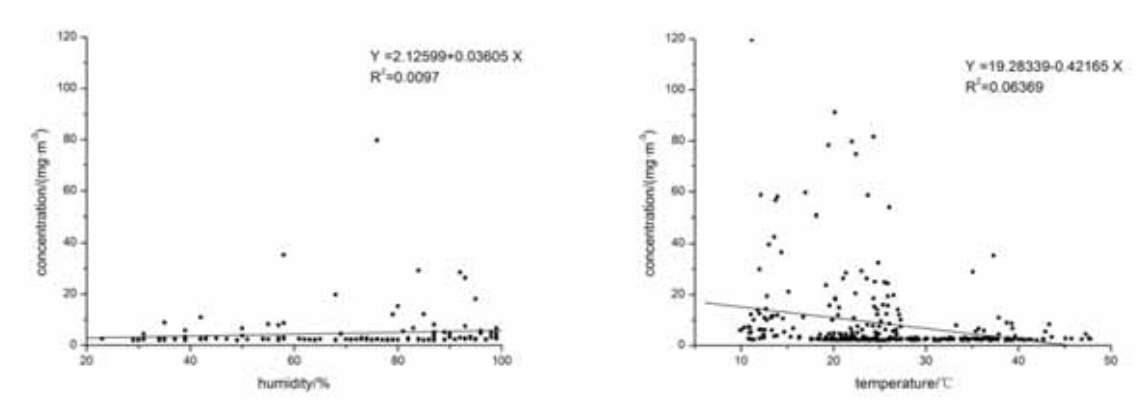

FIGURE 5
CH_4 concentration and temperature and humidity correlation analysis

To this end, we specifically studied the sampling period CH_4 concentration and flux changes, found in the sampling half an hour, CH_4 concentration and flux changes in 8 modes, as shown in Figure 4.

From Figure 4 can clearly see the sampling of 0.5h, the static box CH_4 concentration changes.

We found that CH_4 concentration changes are not uniform. In addition to the three modes of Fig. 4 (a), (b) and (c), ie, uniform rise, uniform decrease and concentration remain unchanged, the other five emission modes have the CH_4 flux in the first 15 min and 15 min after the sampling process Big difference. As shown in Fig. 4 (d), (e), (f), the CH_4 concentration fluctuates less in a 15 min, ie, the flux is very low and the other fluctuates in another 15 min, Large / reduced. Figure 4 (g) and (h) show that the CH4 concentration in the static box will increase and decrease at different times during the 0.5h sampling process. This may be related to the change in the amount of methane oxidizing bacteria and the change in oxidative efficiency caused by changes in CH_4 flux. In fact, the organic matter content in the soil also affects the ability of CH_4 to oxidize [15, 16]. However, studies have shown that 5% of the CH_4 produced by the landfill is oxidized by microbes [17], indicating that short-term CH_4 flux fluctuations are not only affected by methane oxidizing bacteria but also CH_4 emissions. These CH_4 flux fluctuations lead to the final calculation of CH_4 flux deviation, can not accurately reflect the landfill CH4 concentration changes.

However, the short-term fluctuations in CH_4 flux further demonstrate that the CH_4 emission from the stable landfill is not a continuous process but a short period of time. Therefore, to monitor the stability of the landfill CH_4 emissions, the need for automatic observation equipment continuous observation records, in order to truthfully reflect the landfill CH_4 emissions.

Analysis of Correlation between CH_4 Emissions and Temperature and Humidity. Finally, we analyze the correlation between CH_4 emissions and temperature and humidity in landfill, as shown in Figure 5.

The CH_4 concentration and humidity correlation coefficient R2 obtained by linear fitting is only 0.0097, and the correlation coefficient R2 is only 0.06369. This indicates that the CH_4 concentration in this experiment is not significantly correlated with temperature and humidity. This conclusion is consistent with the conclusion that Feng Kui has no significant correlation between CH_4 release flux and casing temperature and water content in Nanjing sedan landfill experiment [18]. Therefore, it is speculated that the CH_4 emission from the landfill is mainly affected by the internal pressure of the landfill, which is related to the gas permeability coefficient of the waste body and the overburden layer.

CONCLUSION

(1) During the whole observation period, the CH_4 concentration range was 1.9-119.7mg / m3, and the flux range was -20.6-52.6mg / (m^2h). The peak value of CH_4 concentration is different and the peak concentration is larger. (2) CH_4 emissions from stable landfills are not continuous emissions, but intermittent emissions, CH_4 emissions are shorter, most of the time in the absence of emissions. (3) CH_4 emission from stable landfill is not an integral one, but there are randomness in the discharge and discharge area of the local area, and the emission area is small. (4) There is no significant correlation between the CH_4 emission landfill and the current temperature and humidity of the stable landfill. (5) For the above stable landfill CH_4 emission characteristics of the causes and potential impact factors, we will further analysis through laboratory experiments.

REFERENCES

[1] Scheutz, C., Mosbaek, H., Kjeldsen, P. (2004) Attenuation of methane and volatile organic compounds in landfill soil covers. Journal of Environmental Quality. 33(1), 1-71.6

[2] De Visscher, A., Thomas, D. (1999) Methane oxidation in simulated landfill cover soil environments. Environmental Science and Technology. 33(11), 1854-1859.

[3] Gao, Q., Du, W., Lu, S., Zhang, Z., Zhang, E., Wu, J., Ren, Z. (2006) Methane Emission from Municipal Solid Waste Treatments in China. Advances in Climate Change Research. 2(6), 269-272.

[4] Kumar, S., Gaikward, A., Shekdar, A. (2004) Estimation method for national methane emission from soil waste landfills. Atmospheric Environment. 38, 3481-3487.

[5] Yu, M., Zhang, F., An, J. (2012) Landfill Gas Generation Model Based on Difference of Gas Generation Rate of Waste. Environmental Sanitation Engineering. 20(4), 45-50.

[6] Dong, X., Shen, G., Li, X. (2010) Variational Characteristics of Methane Concentration after Closure of Waste Landfill Sites. Environmental Sanitation Engineering. 18(6), 53-54.

[7] Zhao, C., Liang, Y., Zhang, L., Wang, H., Li, Z. (2012) Study on methanotrophs and methane fluxes in municipal solid waste landfills. Techniques and Equipment for Environmental Pollution Control. 6(2), 599-604.

[8] Lohila, A., Laurila, T., Tuovinen, J.P. (2007) Micrometeorological measurements of methane and carbon dioxide fluxes at a municipal landfill. Environmental Science and Technology. 41(8), 2717-2722.

[9] Berger, J., Fornés, L.V., Ott, C. (2005) Methane oxidation in a landfill cover with capillary barrier. Waste Management. 25(4), 369-373.

[10] Ishigaki, T., Yamada, M., Nagamori, M. (2005) Estimation of methane emission from whole waste landfill site using correlation between flux and ground temperature. Environmental Geology. 48(7), 845-853.

[11] Borjesson, G., Sundh, I., Tunlid, A. (1998) Methane oxidation in landfill cover soils, as revealed by potential oxidation measurements and phospholipid fatty acid analyses. Soil Biology and Biochemistry. 30(10-11), 1423-1433.

[12] Liu, H., Li, Q., Liu, D., Han, Z. (2009) Study on the Release Rate of Methane from Soild Waste Landfill. Journal of Anhui Agricultural Sciences. 37(23), 11151—11153.

[13] Yang, X., Yue, B., Huang, Z.-C., Yin, Y., Huang, Q.-f., Wang, Q. (2011) Research on CH_4 Emission Fluxes from Active Terrace Surface of MSW Semi-aerobic Landfills. Journal of Environmental Engineering Technology. 1(9), 383-388.

[14] Ma, Z.-y., Li, H.-l., Yue, B., Gao, Q.-x., Dong, L. (2014) Study on Emission Characteristics and Correlation of GHGs CH4 and CO2 in MSW Landfill Cover Layer. Journal of Environmental Engineering Technology. 4(5), 399-405.

[15] Gulledge, J., Hrywna, Y., Cavanaugh, C., Steudler, P.A. (2004) Effects of long-term nitrogen fertilization on the uptake kinetics of atmospheric methane in temperate forest soils. FEMS Microbiology Ecology. 49(3), 389-400.

[16] Saari, A., Rinnan, R., Martikainen, P.J. (2004) Methane oxidation in boreal forest soils: Kinetics and sensitivity to pH and ammonium. Soil Biology and Biochemistry. 36(7), 1037-1046.

[17] Pariatamby, A., Cheah, W.Y., Shrizal, R. Thamlarson, N., Lim, B.T., Barasarathi, J. (2015) Enhancement of landfill methane oxidation using different types of organic wastes. Environmental Earth Sciences. 73(5), 2489-2496.

[18] Feng, K., Huang, T.-y. (2014) Study on the Variation Regularity of Greenhouse Gas Release from Jiaozishan Mountain Municipal Solid Waste Landfill. Research of Environmental Science. 27(12), 1432-1439.

Received: **28.09.2017**
Accepted: **02.12.2017**

CORRESPONDING AUTHOR

Zheng Youfei
Key Laboratory for Aerosol-Cloud-Precipitation of China Meteorological Administration,
Nanjing University of Information Science and Technology,
210044, Nanjing, Jiangsu – China

e-mail: zhengyoufei2008@163.com

© by PSP Volume 27 – No. 2/2018 pages 1289-1298 Fresenius Environmental Bulletin

NOVEL CVD GROWTH OF LARGE AREA GRAPHENE AND CNTS/GRAPHENE COMPOSITE AT LOW TEMPERATURE AND ITS POTENTIAL APPLICATION

Shu Ye[1,2], Won-Chun Oh[2,*]

[1] Department of Materials Science & Chemical Engineering, Bengbu University, Bengbu, China, 233030
[2] Department of Advanced Materials Science & Engineering, Hanseo University, Seosan-si, Chungnam-do, Korea, 356-706

ABSTRACT

Here, we report on the growth of large area graphene (LAG) on copper foil at a low temperature (500 °C) and at atmospheric pressure by using chemical vapor deposition (CVD). Liquid benzene was used as the graphene precursor material by heating below its boiling point to create benzene vapors. The as-prepared LAG with a Raman D band was obtained, and graphene layers can be clearly seen in Field emission scanning electron microscope (FESEM), Raman, Transmission electron microscope (TEM), High-Resolution Transmission Electron Microscopy (HRTEM) and atomic force microscopy (AFM) images. Finally, we suggest potential application of LAG coating on electronic devices.

KEYWORD:
CVD, graphene, CNT, Cu foil, Raman, HRTEM.

INTRODUCTION

Graphene is an ideal one-atom-thick two- dimensional material of sp^2-bonded carbon atoms [1–3], and has been receiving significant attention owing to its exciting characteristics such as quantum Hall effect [4-5], superior thermal conductivity [6], and ultra-high carrier mobility [7-8], etc. The utilization of these outstanding properties of graphene has been screened for a variety of applications: such as transistors [9], sensors [10-11], actuators [12], flexible and transparent conducting films [13]. However, for practical applications, a reproducible and large-scale production of graphene is of vital importance. Graphene can be prepared by mechanical exfoliation of graphite [14], epitaxial growth on SiC surfaces [15–17], reduction of graphene oxide [18-19], and chemical vapor deposition (CVD). Among these strategies, CVD has become the most promising approach because it is inexpensive, transfer- rable and it has the ability to produce high quality and large-area graphene films [20-21]. CVD graphene was first reported in 2008 and 2009, using Ni and Cu as substrates [22-23], which was then followed by an explosion of research activities. To date, many problems still remain, hampering the further development of graphene in fundamental research and practical application.

Here, we report on the deposition of a graphene film and CNTs/Graphene on Cu foil at a temperature as low as 500 °C using CVD for 1, 3 and 5 min. The behavior of the graphene coating layers as an oxidation resistive barrier is then investigated using Raman spectroscopy and `HRTEM. The novel mass production of LAG on Cu foil may be very useful to fabricate the ultrafast charge transfer next generation optical and electronic devices. Finally, we suggest potential application of LAG coating on electronic devices.

EXPERIMENTAL

Experimental materials and method. Benzene used as a carbon precursor material was purchased from Dae-Jung Chemical and Metals Co. Ltd Korea. The Cu foil (99.9 %), annealed uncoated, was used as the substrate material to grow LAG. Argon and Nitrogen gas were purchased from Samchun Pure Chemical Co. Ltd., Korea. A specially designed split Si tube furnace divided into two parts, the inner tube and the outer tube, was used. The dimensions of the tube are 30 cm length and 4 cm outer diameter, with two nozzles, one for the inlet of benzene vapors and the other for the inlet of Ar and N_2 gas. The inner furnace, also called the heating zone, having a 10 cm length and 5 cm diameter, is used to grow the LAG and CNTs/Graphene on Cu foil. The benzene was first heated below its boiling temperature and vapors were produced. The vapors were then transferred to the tube simultaneously with Ar gas which also acts as a carrier for benzene vapors and prevents the Cu foil reacting with water molecules. The vapor flow and the Ar gas ratio were controlled through the control valve. The furnace temperature was increased to 500 °C at the first step and Ar gas was released into the Si furnace. After reaching the temperature to around 500 °C, a Cu foil was inserted in the inner tube followed by controlled amount of Ar gas and

benzene vapors. The growth of LAG was checked at different reaction times (1, 3 and 5 minutes) at 500 °C and the obtained samples were labeled as G1, G3 and G5 respectively. Fig. 1 shows a typical graphene growth process.

Coating graphene on a semiconductor index device (pipe) and measuring its electrical resistance. A semiconductor pipe was coated with graphene by using our CVD technique as introduced previously. After 3 min coating, the electrical resistance of the pipe was measured by 2 probe wired method. The schematic diagram and optical image are shown in Fig.2.

Instrumentation. High resolution transmission electron microscopy (HRTEM) JEOL, JEM-2012, Japan was used to determine the state and the sheet morphology of the prepared graphene. Transmission electron microscope (TEM) at an acceleration voltage of 200 kV was used to investigate the number and the stacking state of the graphene layers on the various samples. Raman analysis was carried out to check the signature of graphene on the metallic substrate. The measurement was performed using a ''labRam Aramis'' Horiba Jobin Yvon spectrometer. A 514 nm argon-ion laser was used for the measurements. The measurements were performed using a backscattering geometry. The Raman excitation beam spot size is about 1 µm diameter. Field emission scanning electron microscopes (FESEM (JSM)-5200 JOEL, Japan) that offer expanded imaging and capabilities customizable to performance requirements were used to carry out the analysis. Atomic force microscopy (AFM) was carried out using Park NX 20 Korea.

RESULTS AND DISCUSSION

Morphological formation and growth of LAG and CNTs/LAG. The FESEM images of the as prepared CVD grown LAG and CNTs/LAG assembly are shown in fig 3(a-f). From this figure, it is obvious that the quantity of large area graphene increases with decreasing reaction time. The figure 3(a-b) describes the FESEM image of G1 sample with 1 minute reaction time. In this figure the G1 sample gives a vibrant picture of the graphene morphology. The graphene sheets mainly multilayers are separated by pores formed on Cu substrate. These pores can be considered as support

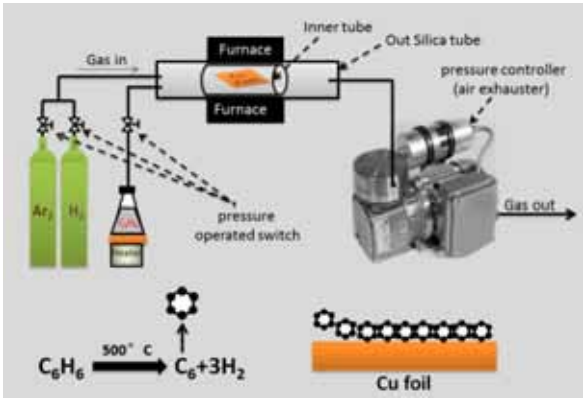

FIGURE 1
Schematic of the LAG and CNTs/LAG on the Cu foil using atmospheric CVD.

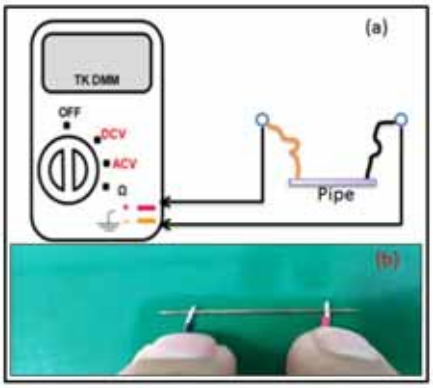

FIGURE 2
(a): Schematic diagram for the electrical resistivity measurement;
(b): Measuring the electrical resistance of the semiconductor pipe.

reaction spaces for the attachment of nanoparticles for device applications. The figure shows that there is no any other spot or mounds were found on the surface of graphene. This gives us the clue that 1 minute reaction time is suitable forLAG layer to grow on copper surface at 500 ºC.

Increasing the reaction time to 3 and half minutes by keeping the temperature at 500 ºC a small dot appears on the surface of LSG these dots are termed as a carbon nanotube seeds as shown in figure 3(c-d). The sample in fig 3(c-d) is labeled as G3 with 3 minute reaction time. From this figure, the small dots can be seen very clearly spotted white in color. These dots are further responsible for the CNTs concentric graphene sheet rolling into a tube format. Figure 3(e-f) depicts the G5sample with 5 minutes reaction time. The CNTs on the Cu substrate are clearly visible in tube type shape. The densities of MWCNTs are quite large so that Cu grains are not visible in the image. From G5 sample, we can say that initially when the reaction time exceeds 3 minutes or higher, the CNTs seeds were grown on the surface of the graphene sheet. These small islands, termed seeds for MWCNTs, expand vertically on the graphene sheet to form CNTs. The large numbers of MWCNTs were wrinkled curled around each other so that the width of MWCNTs also increases as compared to G3 sample. These formed MWCNTs are found to vertical on LAG sheet which are confirmed from AFM images. Our observation further shows that by controlling a number of experimental parameters, these MWCNTs can be grown in a convenient manner on a graphene sheet, which may be beneficial for future graphene based nanoelectronics devices.

The confirmation of LAG and the number of layers has been investigated through the TEM image of the G1 sample shown in Fig. 4(a-b). In Fig. 4(a), a smooth large area graphene with mostly a single layer has been established. The dark region shows the stacked mostly multilayer graphene with the presence of some wrinkles. These wrinkles may be associated with the difference in thermal coefficient between the graphene and Cu film [24]. Fig 4 (b) shows a high quality single layer graphene sheet without any CNTs on the graphene surface. Our results further confirm that benzene vapors flowing through CVD at the low temperature reported here (500 ºC) and normal pressure can produce LSG composites. The LAG sheet in figure 4(b) shows the composition of mostly single layer and multilayer LAG.

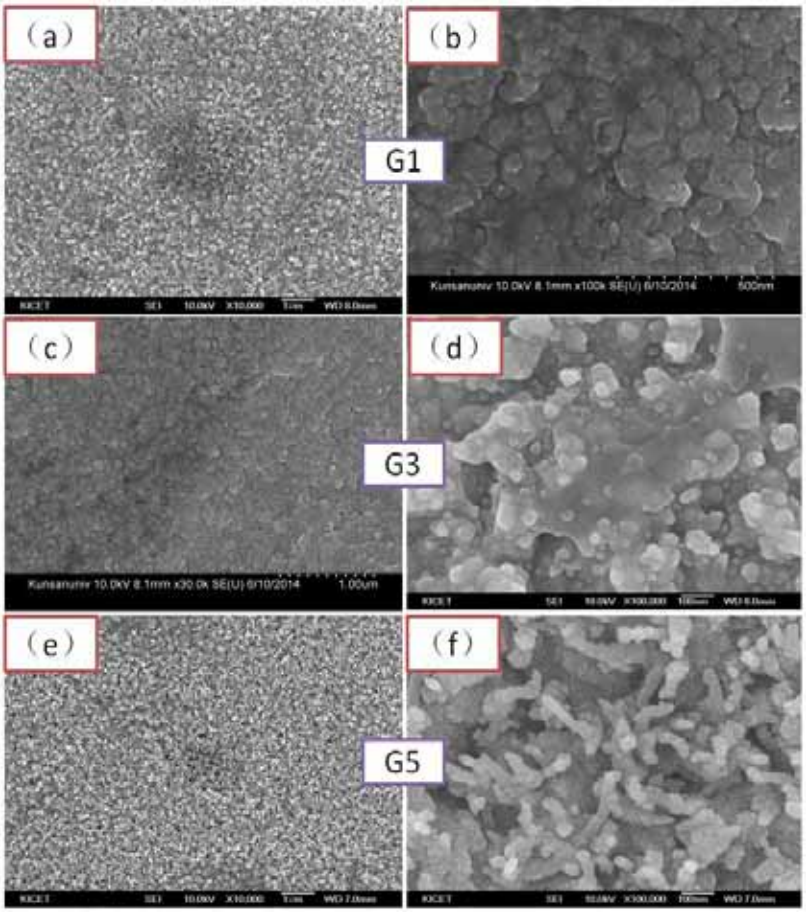

FIGURE 3
FESEM images of as prepared LAG and CNTs/LAG (a-b) G1, 1 minute reaction time (c-d) G3, 3 minute reaction time (e-f) G5, 5 minute reaction time.

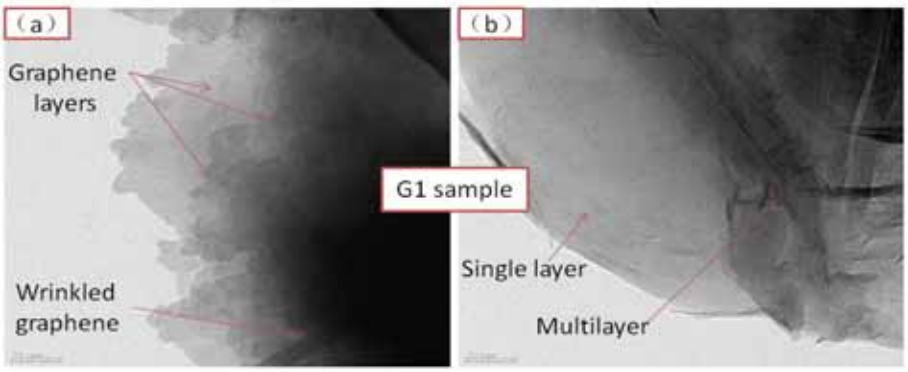

FIGURE 4
TEM images of G3 sample (3minute reaction time) (a) 50nm (b) 50 nm.

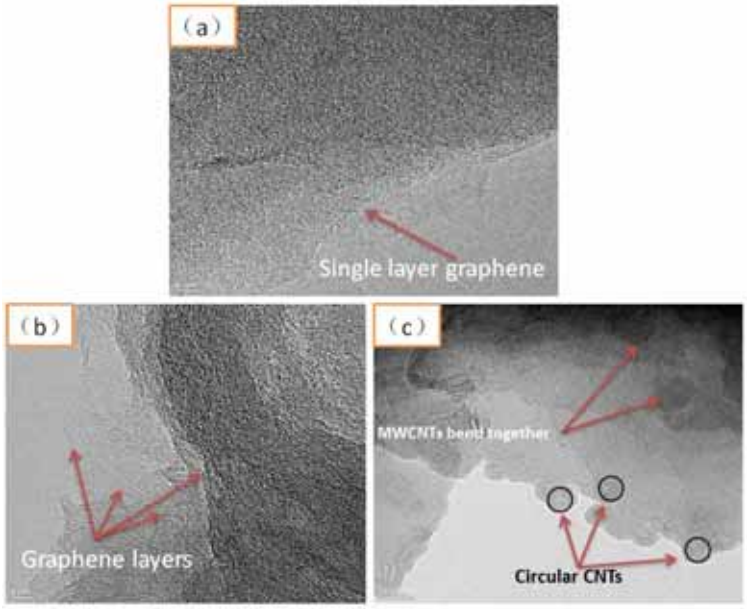

FIGURE 5
HRTEM images of G1, G3 and G5; (a) G1, (b) G3, (c) G5.

Fig.5. show HRTEM images of as-prepared samples. The two-dimensional structure of the LAG sheet is clearly shown to have been retained with partial agglomeration in Fig. 5(a). Multilayer graphene structure could be obviously seemed in Fig. 5(b). The HRTEM image in Fig. 5(c) further confirms the tip type MWCNTs which is closed from the outer end. Here, we can observe that the circular MWCNTs wound together in bundle type shapes. This means that at the edges of our large area graphene, MWCNTs were grown and the density reduces at the interior of the sheet. These results give us new insight into CNTs/LAG composites. The edge CNTs may be very helpful to develop ultrafast nanoelectronics devices by providing sharp anchoring sites.

Physicochemical characterization of LAG and CNTs/LAG. Raman spectroscopy is a powerful technique to study the structure and electronic properties of carbon materials such as graphene/graphite and carbon nanotubes. Fig. 6(a) depicts the Raman spectrum of the G1 sample. The furnace temperature was kept at 500 ºC with a reaction time of 1 minute. The Raman signature for the carbon based materials D band, G band were found in our CVD grown LAG. The mode positioned between 80 and 300 cm^{-1} from the excitation line, are associated with the Cu present in the sample. The Cu arises due to scratching the graphene composite from Cu foil.

In Fig. 6(a), the G1 sample shows unusual results rather than ordinary Raman spectra of LAG and CNTs. From this figure, we found a small intensity peak (inset figure 6) around 2700 cm^{-1} assigned to the 2D peak in graphene. This observed 2D peak was further split into four Raman peaks. The dispersion of the peak yielded information on the number of layers and stacking order in the graphene system. In bilayer graphene, it was reported that 2D peaks were split into four components; the further increase in the

layer and bulk area of graphene leads to lower intensity peaks [25-26]. In our case, we believe that the surface area of graphene is very large and the intensity of the peaks was therefore found to be very low compared to the metallic band in the Raman spectroscopic results.

Fig. 6(b) shows the Raman spectra for G3 sample with the reaction time was kept at 4 minutes at 500 ºC. From the figure, it is clear that small intensity G and D bands were observed (inset (b)). The Cu metallic peaks were also observed. From our study, we found that by increasing the reaction time, the Raman band intensities of G band and D band shift towards a lower frequency. This allows the MWCNTs start growing on LAG sheet. The other reason for the intensity variation is the large number of MWCNTs rolls together, encouraging phonon confinement and thus reducing the intensity [27-28]. These observations show that the attachment of MWCNTs/LAG on Cu during CVD would probably affect the electronic transition and hence the dispersive behaviors of the signature bands were found.

The laser excitation also has an effect on the Raman band shift and intensities variation. In MWCNTs, the bands are attributed to the Raman resonance condition. The incident laser on carbon nanotubes can yield the optical resonance profile for a given mode at a vibrating frequency of their respective modes [29-32]. In Fig. 6(b), the G band frequency was found at 1592 cm^{-1}, while the D band frequency was found at 1352cm^{-1}. In MWCNTs, a large number of CNTs with different diameters affects the characteristic G band and were therefore found close to the graphite G band frequency [33]. The peaks between 300 and 500 cm^{-1} were attributed to the metallic Cu used as a substrate material [34-36].

Fig. 6(c) shows the Raman spectrum of G5 sample with 5 minutes reaction time. The observation of Fig. 6(c) shows that at increasing reaction time there is D band appear in the spectrum. Unlike other samples there is a defect band observed which may be due to large number of MWCNTs grown on LAG sheet. The morphology of G5 sample from FESEM and TEM images are quiet clear that by increasing reaction time there is increased density of MWCNTs. It is because of the formation of CuO on surface increase the grains and thus provides maximum number of reaction sites for growth of CNTs. This produces high surface energy by providing more active sites for MWCNTs on the surface [37].

In Fig.7(a-c) the LAG and MWCNTs/LAG composites has been shown. The G1 sample labeled as 6(a) gives a larger area graphene with some dark region considered to be valleys between the two graphene domains. The depths of these valleys are found to be 350 to 400 nm to minimize the graphene domains. These graphene edges may be very useful for creating Li ion batteries with remarkable storage capacity, as reported elsewhere [38].

A comparison of the obtained MWCNTs/LAG composites with different reaction is depicted in Fig. 7(b-c). The image 7(b) ascribed G3 sample with 3 minutes reaction time while Fig. 7(c) is G5 sample

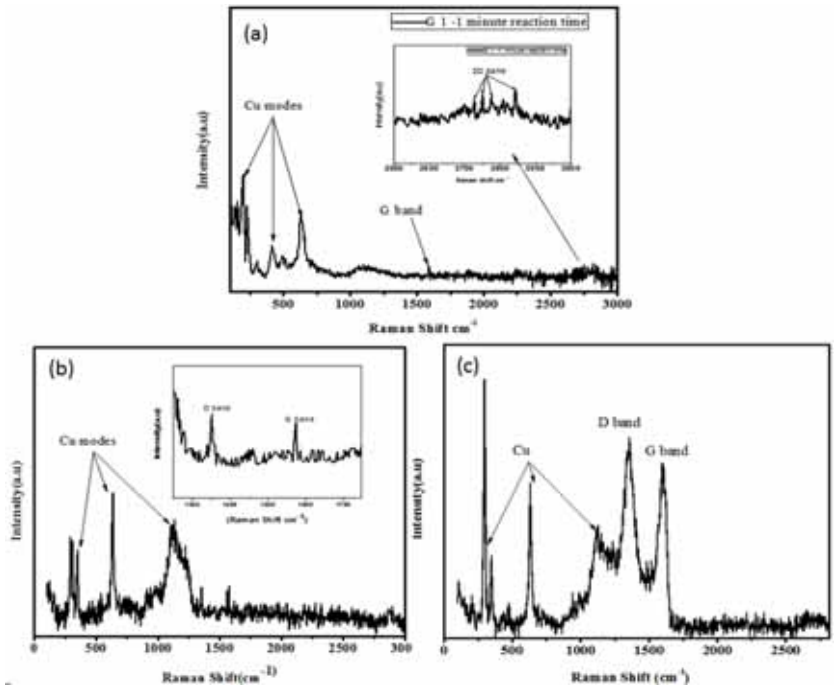

FIGURE 6
Raman spectra of as-prepared samples: (a): G1 sample; (b): G3 sample; (c): G5 sample.

with 5 minute reaction time. These figures show the obvious difference between the heights of MWCNTs due to variation in reaction times. In Fig. 7 (b), the G3 sample shows MWCNTs having a height of around 198 nm, while in Fig. 7 (c), (G5 sample) this height was reported to be ~338 nm. The AFM height images of MWCNTs clearly shows that the CNTs were gathered in a rolled type shape having a sharp tip and close ends. The growth of CNTs shown in Fig. 7 (b-c) was consistently achieved through a large area of the substrate material. Obviously, the surface growth of vertically aligned CNTs on a substrate material at a micrometer scale with nonometric effect is very important for next generation devices.

The surface construction of MWCNTs revealed by AFM leading towards the nanohills formation of carbon nanotubes is unique and its formation may be a complex phenomenon. The formation may be the result of the different competing factors such as temperature, reducing atmosphere, oxide reduction during CVD process, and decomposition of benzene. This elusive and complex phenomenon requires a devoted focus and investigation in the future to explore the outstanding physical and chemical properties of these MWCNTs/LAG composites.

Mechanism of chemical vapor deposition of graphene. In the case of metals having low carbon solubility (such as Cu), carbon atoms will nucleate and laterally expand around the nucleus to form graphene domains with decomposition of hydrocarbon catalyzed by the substrates at high temperature. The growth process will terminate when the substrates are fully covered by the graphene layer, which is usually referred as a "self-limited surface deposition" growth mechanism (Fig. 8a) [41]. Recently, it has been observed that the self-limiting growth process could be broken on Cu and few layer graphene can be produced under special growth conditions, such as CVD growth under atmosphere pressure [42], a very slow cooling rate [43] as well as a high methane concentrations [44].

.

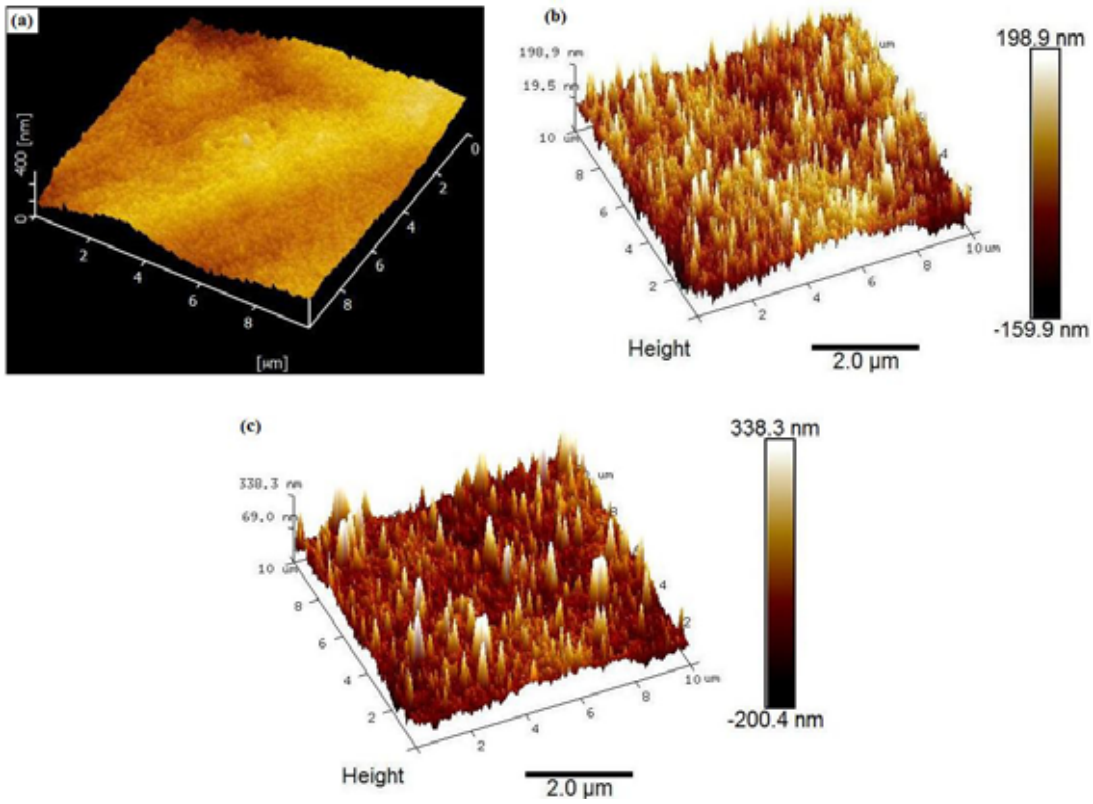

FIGURE 7
AFM images of LAG and MWCNTs/LAG (a) G1 (b) G3 (c) G5

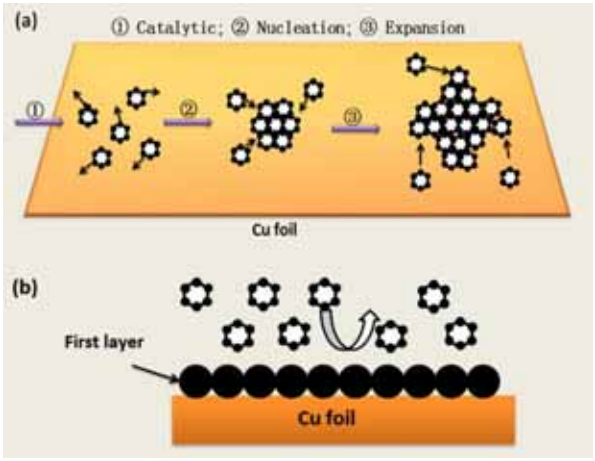

FIGURE 8
Schematics diagram of CVD graphene grown on Cu foil.

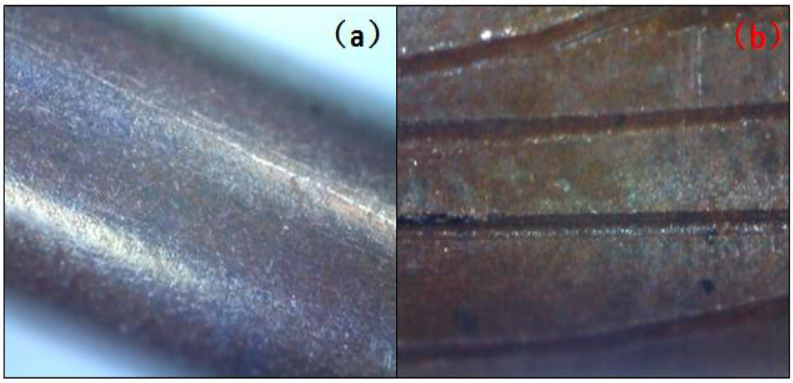

FIGURE 9
Coating of LAG on semiconductor index device using our CVD technique (a): After graphene coating; (b): After scratch with knife.

Despite the low carbon solubility in Cu, several researchers have observed the segregation growth mechanism occurred on Cu enclosure, where carbon species penetrate from one side of the Cu foil to the other side, and then forms the second layer or multilayer graphene underneath the top first layer [45]. This mechanism is denoted as the "penetration" growth mode (Fig. 8b) [46], which favor the production of large scale graphene bilayer or multilayer.

The application of our CVD technique. The semiconductor index device (pipe) has been considered to coat with our introduce CVD method. The actual device picture is shown in Fig.9. After CVD coating the material was found to be a remarkable heat sink source because of large area graphene attachment. This describes the importance of our new method to produce low temperature CVD graphene for device application. Knowing the benefits of CNTs/graphene composites several studies has been devoted to these composites nanostructures [39-40]. In addition, after coating with graphene, the electrical resistance of the semiconduct pipe changed in a certain range (30mΩ-50mΩ), and we can check the inner part by scratching its surface. In light of the above experimental results our work is novel, one step low temperature techniques to produce CNTs/LAG composites structure. The use of a separator between Cu foil and catalyst materials is consider being very important to reduce the interaction between Cu and metallic catalyst materials. In our case the most interesting point is that LAG provided a plate form to grow MWCNTs and also act as separator between Cu foil and MWCNTs.

CONCLUSION

In conclusion, we investigated a new and short route to produce large area graphene. This large area graphene can be produced in industries at a bulk scale by further controlling experimental parameters to optimum values. We demonstrate the production of large area graphene at a very short reaction time in a nitrogen environment using chemical vapor deposition method. The increasing reaction time gives us results that are more interesting by producing ~350 nm (5 minute reaction time) long vertically aligned MWCNTs distributed homogenously

through the copper foil as depicted in AFM images. The FESEM images showed that the island found on the graphene can further give rise to vertical CNTs. The valleys found between graphene domains may be due to the use and handling of very thin copper foil. Thus we believe that our low temperature, normal pressure CVD provides a simple and reproducible way to produce high quality CNTs/LAG for large-scale integration of graphene based next generation devices.

REFERENCES

[1] Ma L., Cheng A., Lu J., Zhang Z., He H., Li C., In situ synthesis of CNTs/Fe–Ni/TiO_2 nanocomposite by fluidized bed chemical vapor deposition and the synergistic effect in photocatalysis. Separation and Purification Technology 116, 360–365 (2013).

[2] Zhao H., Li H., Chang H., Quan X and Chen S. Fabrication and energetic performance in water treatment CNTs–TiO_2/Al_2O_3 composite membrane with a photocatalytic function. Particuology 14, 24–32 (2014).

[3] Ullah K., Ye S., Jo SB., Zhu L., Cho KY., Oh WC. Optical and photocatalytic properties of novel heterogeneous $PtSe_2$–graphene/TiO_2 nanocomposites synthesized via ultrasonic assisted techniques. Ultrasonics Sonochemistry 21, 1849–1857 (2014).

[4] Yan Z., Peng Z., Casillas G., Lin J., Xiang C. Rebar graphene. ACS Nano 8, 5061–5068 (2014).

[5] Rupasinghe C., Rukhlenko I. D. & Premaratne M. Spaser made of graphene and carbon nanotubes.ACS Nano 8, 2431–2438 (2014).

[6] Wei W., Sun K. & Hu Y. H. Synthesis of 3D cauliflower-fungus-like graphene from CO_2 as a highly efficient counter electrode material for dye-sensitized solar cells. J. Mater. Chem. A. 2, 16842–16846 (20140).

[7] Panchal V., Lartsev A., Manzin A., YAkimova R., Tzalenchuk A. Visualisation of edge effects in side-gated graphene nanodevices. Sci. Rep. 4, 5881–5888 (2014).

[8] Maher P., Wang L., Gao Y., Forsythe C1., Taniguchi T., Watanabe K., Abanin D., Papić Z., Cadden-Zimansky P., Hone J., Kim P., Dean CR. Tunable fractional quantum Hall phases in bilayer graphene. Science 345, 61–64 (2014).

[9] Kim KS., Zhao Y., Jang H., Lee SY., Kim JM., Kim Kwang-S., Ahn J-H., Kim P., Choi JY & Hong B.H. Large-scale pattern growth of graphene films for stretchable transparent electrodes. Nature 457, 706–710 (2009).

[10] Wang H., Sun K., Tao F., Stacchiola DJ., Hu YH. 3D Honeycomb-like structured graphene and its high efficiency as a counter-electrode catalyst for dye-sensitized solar cells. Angewandte Chemie International Edition 52, 9210–9214 (2013).

[11] Gao LB., Ren WC., Xu HL., Jin L., Wang ZX., Ma T., Ma L-P., Zhang ZY., Fu Q., Peng LM., Bao XL & Cheng H-M. Repeated growth and bubbling transfer of graphene with millimeter size single-crystal grains using platinum. Nature Commun 3, 699 (2012).

[12] Sutter Peter W., Flege Jan-Ingo & Sutter Eli A. Epitaxial graphene on ruthenium. Nat. Mater. 7, 406–411 (2008).

[13] Yu Q., Lian J., Siriponglert S., Li H. Graphene segregated on Ni surfaces and transferred to insulators. Appl. Phys. Lett. 93, 113103–113106 (2008).

[14] Ohta T., Bostwick A., Seyller T., Horn K. & Rotenberg E. Controlling the electronic structure of bilayer graphene. Science 313, 951–954 (2006).

[15] Reina A., Jia XT., Ho J., Nezich D., Son H., Bulovic V., Dresselhaus M.S & Kong J. Large Area, few-layer graphene films on arbitrary substrates by chemical vapor deposition. Nano Letter. 9, 30–35 (2009).

[16] Coraux J., Diaye A. T. N., Busse C. & Michely T. Structural coherency of graphene on Ir (111).Nano Letter. 8, 565–570 (2008).

[17] Berger C., Song Z., Li X., Wu X., Brown N. Electronic confinement and coherence in patterned epitaxial graphene. Science 312, 1191–1196 (2006).

[18] Emtsev KV., Bostwick A., Horn K., Jobst J., Kellogg GL. Towards wafer-size graphene layers by atmospheric pressure graphitization of silicon carbide. Nat. Mater. 8, 203–207 (2009).

[19] Wang H., Wang G., Bao P., Yang S., Zhu W. Controllable synthesis of submillimeter single-crystal monolayer graphene domains on copper foils by suppressing nucleation. J. Am. Chem. Soc. 134, 3627–3630 (2012).

[20] Sutter P. Epitaxial graphene: How silicon leaves the scene. Nature Mater. 8, 171–172 (2009).

[21] Poirier W., Schopfer F. Can graphene set new standards. Nature Nanotechnology 5, 171–172 (2010).

[22] Ritter KA. & Lyding JW. The influence of edge structure on the electronic properties of graphene quantum dots and nanoribbons. Nat. Mater. 8, 235–242 (2009).

[23] Tao C., Jiao L., Yazyev OV., Cheng Y-C., Feng J., Zhang XW., Capaz RB., Tour JM., Zettl A., Louie SG., Dai HJ。， Crommie MF. Spatially resolving edge states of chiral graphene nano ribbons. Nat. Phys. 7, 616–620 (2011).

[24] Pan M., Girão EC., Jia X., Bhaviripudi S., Li Q. Giopographic and spectroscopic characterization of electronic edge states in CVD grown graphene nano ribbons. Nano Lett. 12, 1928–1933 (2012).
[25] Tao P., Haifeng L., Daping H., Mu P. & Mu S. Direct transformation of amorphous silicon carbide into graphene under low temperature and ambient pressure. Pressure. Sci. Rep. 3, 1148; (2013).10.1038/srep01148
[26] Peng T. Kou Z. K. Wu H. & Mu S. C. Graphene from amorphous titanium carbide by chlorination under 200ºC and atmospheric pressures. Sci. Rep. 4, 5494 (2014).
[27] Muniza A. R., Machadoa A. S. & Maroudas D. Mechanical behavior of interlayer-bonded nanostructures obtained from bilayer graphene. Carbon 81, 663–677 (2015).
[28] Das A., Pisana S. & Chakraborty B. Monitoring dopants by Raman scattering in an electrochemically top-gated graphene transistor. Nature Nanotechnology 3, 210–215 (2008).
[29] Tan PH., Han WP., Zhao WJ., Wu ZH., Chang K. The shear mode of multilayer graphene. Nature Mater. 11, 294–300 (2012).
[30] Malard LM., Pimenta MA., Dresselhaus G. & Dresselhaus MS. Raman spectroscopy in graphene. Phys. Rep. 473, 51–87 (2009).
[31] Reich S. & Thomsen C. Raman spectroscopy of graphite. Phil. Trans. R. Soc. Lond. A 362, 2271–2288 (2004).
[32] Ullah K., Ye S., Zhu L., Sarkar S., Oh WC. Microwave assisted synthesis of a noble metal-graphene hybrid photocatalyst for high efficient decomposition of organic dyes under visible light. Materials Science & Engineering B 180, 20–26 (2014).
[33] Zhang X., Yazyev OV., Feng J., Xie L., Tao C., Chen Y-C., Jiao L., Pedramrazi Z., Zettl A., Louie SG., Dai H and Crommie MF. Experimentally engineering the edge termination of graphene nano ribbons. ACS Nano. 7, 198–202 (2013).
[34] Ferrari AC & Basko DM. Raman spectroscopy as a versatile tool for studying the properties of graphene. Nature Nanotechnology 8, 235–246 (2013).
[35] Ferrari AC & Robertson J. Interpretation of Raman spectra of disordered and amorphous carbon.Phys. Rev. B 61, 14095–14107 (2000).
[36] Li X., Zhu Y., Cai W., Borisiak M., Han B., Chen D., Piner RD., Colombo L and Ruoff RS. Transfer of large-area graphene films for high-performance transparent conductive electrodes. Nano Lett. 9, 4359–4363 (2009).
[37] Cartwright R., Esconjauregui S., Hardeman D., Bhardwaj S., Weatherup R., & Guo Y. Low temperature growth of carbon nanotubes on tetrahedral amorphous carbon using Fe–Cu catalyst. Carbon 81, 639–649 (2015).
[38] Gong L., Kinloch IA., Young RJ., Riaz I., Jalil R., & Novoselov KS. Interfacial stress transfer in a graphene monolayer nanocomposite. Adv. Mater.22, 2694–2697 (2010).
[39] Sprinkle M., Ruan M. & Hu Y. Scalable templated growth of graphene nano ribbons on SiC. Nature Nanotechnology 5, 727–731 (2010).
[40] Sadezky A., Muckenhuber H., Grothe H., Niessner R. & Pöschl U. Raman microspectroscopy of soot and related carbonaceous materials: spectral analysis and structural information. Carbon 43, 1731–1742 (2005).
[41] Li G., Chakrabarti S., Schulz M. & Shanov V. Growth of aligned multiwalled carbon nanotubes on bulk copper substrates by chemical vapor deposition. J. Mater. Res. 24, 2813–2820 (2009).
[42] Wang H., Feng J., Hu X. & Ng K. M. Synthesis of aligned carbon nanotubes on double-sided metallic substrate by chemical vapor deposition. J. Phys. Chem. C 111, 12617–12624 (2007).
[43] Delzeit L., Nguyen CV., Chen B., Steven R., Cassell A., Han J and Meyyappan M. Multiwalled carbon nanotubes by chemical vapor deposition using multilayered metal catalysts. J. Phys. Chem. B 106, 5629–5635 (2002).
[44] Pan D., Wang S., Zhao B., Wu M., Zhang H., Wang Y and Jiao Z. Li storage properties of disordered graphene nanosheets. Chem. Mater. 21, 3136–3142 (2009).
[45] Burda C., Lou Y., Chen X., Samia ACS., Stout J and Gole JL. Enhanced nitrogen doping in TiO_2 nanoparticles. Nano Letters 3, 1049–1051 (2003).
[46] Ullah K., Ye S., Lei Z., Cho K. Y. & Oh WC. Synergistic effect of $PtSe_2$ and graphene sheets supported by TiO_2 as cocatalysts synthesized via microwave techniques for improved photocatalytic activity. Catal. Sci. Technol. 5, 184–198 (2015).

Received : 26.03.2016
Accepted: 18.09.2016

CORRESPONDING AUTHOR

Won-Chun Oh
Department of Advanced Materials Science & Engineering, Hanseo University, Seosan-si, Chungnam-do, Korea, 356-706

e-mail: wc_oh@hanseo.ac.kr

AUTHOR INDEX

A

Abbas, A. 1053
Acar, C. 1169
Acun, S. 1145
Agirbas, E. 871
Ahmad, K. 846
Ak, A. 1086
Akal-Solmaz, S. K. 787
Akib, S. 807
Akman, P. K. 1202
Aktas, O. 1104
Al–Antary, T. M. 1038
Alaraj, S. A. 1038
Altun, S. 787
Arnolds, J. L. 928
Ashfaq, A. 846
Aslam, Z. 846
Atar, H. H. 1164
Atay, E. 921
Ates, M. 1164
Ateyyat, M. A. 1038
Aytan, U. 871

B

Bai, R. 675
Banishoaib, S. A. 910
Basaran, M. 765
Basbag, S. 733
Basir, H. 846
Batool, F. 846
Belghasem, I. H. 1038
Bicakci, S. 1145
Biskin, N. 996
Bordbar, A. 910
Budama-Kilinc, Y. 1202
Buddidathi, R. 838

C

Cabuk, Y. 1191
Canbazoglu, C. 793
Cao, Y. 651, 831
Cevizci, H. 720
Chen, H. 1022
Chen, Y. 1196
Ciftci, H. 1006
Cilli, S. 921
Cobanoglu, S. 1232

D

Dai, X. 938
Dedeoglu, M. 880
Demir, I. 989
Dogan, H. 1031
Dogan, Y. 846
Dogru, M. 793
Dong, C. 651
Du, L. 1022
Du, W. 1226
Duygulu, M. 799

E

Ekinci, R. 733
Erdogan, B. E. 668
Eren, G. O. 1202
Ergun, B. 1176
Ertorun, N. 921
Eskin, B. 668

F

Fakıoglu, O. 1169
Fan, Z. 863
Fang, Y.-M. 771
Feng, K. 658
Fujii, Y. 727

G

Gao, C. 898
Gocmen, H. 1095
Goger, F. 1176
Gokalp, Z. 765, 799
Gu, L. 749
Gu, Y. 1226
Gul, H. 1145
Gun, F. G. 1006
Guo, B. 1269
Guzel, E. 681

H

Han, J. 982
Han, Y. 651
Hao, X.-J. 1152
Haq, F. 1256
Hassan, S. G. 1053
Hayit, F. 1145
He, Y. 1022
He, Z. -X. 898
Heidarnejad, M. 910
Hu, Y. 675, 1214
Huang, C. 1081
Huang, Y. 675

I

Ilter, S. 793
Inak, E. 1232
Iqbal, A. 1256
Iqbal, M. 1256
Iqbal, S. 846
Iqbal, T. 1053
Iscan, G. 1176
Islam, B. 1256

J

Jamal, Y. 1256
Jan, I. 1256
Jin, C. 658
Jin, P. 1081
Jing, Q. 938

K

Kadioglu, A. 996
Kagnici, I. 787
Kamanbedast, A. A. 807, 910
Kan, A. 1240
Kaplan, S. 765
Kara, K. 989
Karaarslan, E. 880
Karaaslan, N. M. 645
Karabagli, P. 1006
Karaceylan, I. B. 703
Karademir, C. 733
Karademir, E. 733
Karaman, R. 1240
Karatepe, S. 793
Karipcin, M. Z. 1131
Kasapoglu, A. 921
Kaya, G. 645
Kaya, M. 1240
Kesi, L. 1282
Keskin, N. 1076
Ketin, S. 1157
Khadem, K. 807
Khan, K. A. 1053
Khan, Z. H. 1256
Khan, Z. I. 846
Khawar, K. M. 1076
Kizil, S. 744
Koc, R. C. 1202
Kokab, R. 846
Kose, Y. B. 1176
Kosteckas, R. 727
Kriauciuniene, Z. 727
Kurmanbekova, G. 668

L

Lei, X. 1214
Lek, S. 947
Li, C. 1060
Li, D. 982, 1043
Li, W. 1022
Li, X. 1069, 1196
Li, Z. 947
Liao, W. 1214
Liu, C. 1069, 1269
Liu, D. 1043, 1269
Liu, F. 1122
Liu, H. 820
Liu, J. 947
Liu, Q. 1069
Liu, S. 658
Liu, X. 749, 938
Liu, Y. 960
Liu, Z. 1069
Lu, B. 1269
Luo, Q. 1138
Luo, Y. 1022

M

Ma, X.-Y. 960
Manikrao, G. 838
Marcinkeviciene, A. 727
Marjanovic, R. 1157
Masjedi, A. 910
Matadha, N. Y. 838
Mazlum, R. E. 871
Mehmood, N. 846
Memoona, H. 846
Miao, J. 1122
Miao, Y. -M. 898
Mohapatra, S. 838
Mou, J. 1226
Munir, B. 846
Munir, M. 846
Muqadas, H. 846
Mutlu, M. B. 921

N

Nadeem, M. 846
Nawaz, K. 846
Ni, H. 651
Niu, Q. 1122
Noorka, I. R. 846

O

Odendaal, J. P. 928
Oh, W. -C. 1289
Oncel, M. 1006
Orhan, F. 971
Ozaytekin, H. H. 880
Ozdemir, A. 1183
Ozdemir, C. 1183
Ozdemir, F. A. 1076
Ozel, H. B. 1210
Ozluoymak, O. B. 681
Ozturk, B. 1006
Ozturk, H. H. 710
Ozyigit, I. I. 668

P

Pan, Y. 1264
Peng, J. 1264
Preljevic, A. 1157

Q

Qi, X. 1069
Qin, L. 863, 1138
Qin, T. 1214

R

Rehman, S. U. 846
Ren, D. 1043

S

Sacirovic, S. 1157
Sahin, S. 757
Sahin-Bal, S. 793
Sajid, M. 1256
Sana, M. 846
Sari, A. B. 1013
Saruhan-Guler, N. 996
Sen, U. 668
Sener, A. 1240
Severoglu, Z. 668
Shad, H. A. 846
Shah, F. 1256
Shaheen, F. 846
Shahriari, T. 779
Shen, Y. 771, 1022, 1081
Shengtao, L. 1282
Sher, M. 846
Shezadi, M. 846
Shi, J. 1043
Shi, T. 938
Shokouhi, M. 779
Siddamallaiah, L. 838
Snyman, R. G. 928
Sogut, T. 744
Sohail, M. 846
Sun, J. 820
Sun, W. 1043
Sunam, G. S. 1006

T

Tabur, M. A. 703
Takic, L. 1157
Tang, J. 1226
Tas, I. 765
Terzi, R. 996
Tian, J. 1022
Tian, L. 658
Tiejun, L. 815
Toncer, O. 744
Topakci, N. 1095
Tuluk, B. 971
Turkoglu, N. 1076

U
Ugulu, I. 846
Ullah, M. F. 846
Ullah, S. 846
Uras, M. E. 668
Ustun, G. E. 787
Ustuner-Aydal, O. 1013
Uysal, M. 757
Uzun, C. 880
Uzun, O. 765

V
Vatansev, H. 1006
Velicka, R. 727

W
Wajid, K. 846
Wan, X. 1122
Wang, G. 1060
Wang, H. 831, 1138
Wang, J. 947
Wang, L. 1081
Wang, M. 1214
Wang, M.-Q. 1152
Wang, Q. 1060
Wang, W. 1060
Wang, X. 1022, 1138
Wang, Y. 938
Wang, Z. 947, 1248
Wei, X. 1122
Wu, C. 820
Wu, L. 960
Wu, N. 1022

X
Xiao, Y. 831
Xiaomin, L. 690
Xiaoyun, W. 1282
Xie, H. 1269
Xie, K. 1196
Xiong, Y. 749
Xu, M. 1152
Xu, S. -C. 898
Xuanxuan, D. 690
Xue, H. 749

Y
Yalcin, I. E. 668
Yaman, M. 645
Yan, J. 1069
Yan, P. 938
Yan, Z. 1022
Yang, F. 1138
Yang, M. 675, 1053
Yang, T. 749
Yao, Y.-P. 1152
Yavuz, M. 1031, 1104
Ye, S. 947
Ye, S. 1289
Yilmaz, A. 1240
Yilmaz, M. T. 1202
Youfei, Z. 1282
Yousaf, K. 1053
Yu, J. 1069
Yuan, F. 815
Yucedag, C. 1210
Yucel, E. 1086
Yurekli, F. 856

Z
Zeng, L. 1022
Zhai, G. 982
Zhang, G. -L. 863
Zhang, H. 1248
Zhang, K.-M. 771
Zhang, L. 960
Zhang, T. 947
Zhang, W. 820
Zhang, X. 651, 1060
Zhang, Y. 938
Zhao, B. 1069
Zhao, C. 831
Zhao, L. 1226
Zhao, W.-G. 960
Zhao, Y. 1196
Zheng, S. 1226
Zheng, W. 863
Zhong, C. 675
Zhou, X. 658
Zhou, Y. 982
Zhu, D. 1022
Zhu, J. 1196
Zhu, S. 1122

SUBJECT INDEX

A

Abiotic 1131
Acari 1232
accident 1157
Acid effect 720
Acorus calamus 982
activated carbon 1122
Activities of protective enzyme 982
Adsorption 690, 765
adsorption kinetics 1122
Aflatoxin 681
AHP 1191
allelopathy 727
allium 1183
Amino acid salts 1081
anatomy 1183
Andisols 880
Ankara 1232
Anticandidal 1176
Antioxidant 1013, 1176
antioxidant enzymes 996, 1086
Apoptosis 1006
Aquatic 928
Arsenic speciation 645
assessment 820
autecology 668

B

B biotype 1095
Bacillus amyloliquefaciens 1196
Bacterial community 1069
BAP 1076
Bemisia tabaci 1095
Bentonite 765
Bidens pilosa 771
Bilimneus 921
Bioassay 1038
Biodegradation 779, 863, 1196
biological quality 820
biological treatment 779
bioluminescent bioassay 658
Biomonitor 1104
Bio-rational insecticides 1038
bioremediation 651
Black Sea 871
Blood Red 1256
BOD5 799
Bohai Bay 820
Botanical insecticides 1038
Burdur 1104

C

Calcium vanadium 1269
carbon source/sink 831
carbonate stones 720
Carp (Cyprinus carpio) 1164
Caspase 1006
Cationic polyacrylamide Modification 675
CCHE2D 807
cell culture 1202
Centaurea fenzlii 1076
CH_4 1282
CH_4 oxidation 1022
chemical 971, 1157
chicken 645
Chickpea 1240
chlorophyll fluorescence 771
Chlorpyrifos 1196
Chromium (III) 1248
Chromium (VI) 1248
Cirsium 668
climatic transition 1022
closure area 1282
CNT 1289
Co 1104
CO_2 1081
CO_2 emissions 710
COD 779
colonization ability 1152
commercial organism 820
common mugwort 727
Community structure 947
Compacted liner 765
conservation 668
constructed wetlands 799
Constructed wetlands 938
consumer acceptance 1145
Contaminated soil 846
cookie 1145
Copper toxicity 996
corncob 1122
cotton 733
Countermeasures 898
Cr(VI) 651
Creep 1269
Crimean juniper 1210
crude oil 1240
ctenophores 871
Cu foil 1289
Cu uptake 982
CVD 1289
Cytochrome C Oxidase 921
Cytotoxicitiy 1176

D
Dalian marine area 1069
Decision Making 1191
Deep mudstone 1264
Desmodesmus armatus 1169
DGGE 1069
Differential evolution (DE) 749
Digital image processing 681
diurnal variation 1282
DNA 703
domestic wastewater 799
Dried fig 681
drilling fluid 1264
dry conditions 989

E
early growth 727
effluent 799
electrolyte leakage 771
electrospinning 1202
endemic 1076
Endophytic Bacillus amyloliquefaciens 1152
energy consumption pattern in 1053
Energy Dissipation 910
energy productivity 1053
Energy use efficiency 1053
Environmental impact 787
Environmental pollution 1191
Epi(groin) 807
Eriophyidae 1232
Erzurum 971
Essential oils 1038
Evolution 898
exposure concentrations 928

F
fatty acid 1240
fatty acid composition 744
feather 703
Flax wastes 690
Flocculation 675
Fluopicolide 838
Forests soil 1022
Freezing-thawing cycles 1060
fruit characteristics 744
fuel consumption 710
Functional group 947
Furfural Residue 1248
Furniture Industry 1191

G
gametophyte 771
Gamma spectrometry 793
Genetic algorithms 960
genetic variation 1210
germination 727, 1086
GHK 1202
glossiness 720
Glycine-betaine 856
Grapevine 757
graphene 1289
growth 658

H
H_2O_2 application 996
H_2S 1081
Half-life 838
Hasandag 880
Health risk index 846
heat stabilization 1145
Heavy metal 765, 820
Heavy metal accumulation 1104
heavy metals 1086
heritability 1210
HG-AAS 645
high temperature tolerance 733
High water quick setting materials 1269
High-salt 982
Histology 1164
Hollow fiber membrane contactor 1081
Hourly rainfall 1214
HRTEM 1289
Ht-q6 1152
Huaqing Area 1043
human walking 1226
Hydraenidae 921

I
IBA 1076
immobilized 863
indole-3-butyric acid 757
Intestine 1164
IPM 1038
isotherm 1122

K
$KHCO_3$ 815

L

Laboratory test results 681
Labyrinth Spillway 910
Lamiaceae 1176
Landfill 1282
lava rock 779
LC-MS/MS 1176
Lead 1169
Life cycle assessment 787
Limnebius 921
Liver 1164
Livestock and poultry breeding 938
Location of Intake 807
low-function plantation 831
Lung cancer 1006

M

M30 1006
Mannan oligosaccharide 1164
Marine environment 1269
Marine sediment 1069
max range 1157
meat 645
Medicinal plants 793
metal bioaccumulation 928
Methanotrophic community 1022
Methyl violet 690
methylene blue 1122
Methylocaldum 1022
microbial biomass carbon 831
microbiological 971
microcystin 658
Microcystis aeruginosa 658, 675
Microtus guentheri 1104
microwave digestion 645
mineral compositions 1240
mineral content 744
mineral nutrition 668
mineral uptake 757
mitotic index 1086
molecular sexing 703
mtCOI 1095
multiple micro-shoot regeneration 1076
multi-subgroup 960

N

NAA 1076
NaCl stress 856
nanofiber 1202
Natural and Artificial Radioactivity 793
NGAL 1006
NGS 703
Nickel 1169
Nitrogen removal 938
nonspecific immune system 1013
numerically 1183

O

oil content 989
oleic and linoleic acids 744
Organic matter 938
Origanum minutiflorum 1013
Orthogonal test 690

P

PAGE 1095
parameter calibration 960
Parameter estimation 749
particle swarm optimization 960
Particulate matter 1226
Pearson correlation coefficient 1214
PET fibre production 787
pH measurement 1031
phenolic compounds 727
Phenolic wastewater 815
Phosphorus 765
photosynthetic bacteria 863
Photosynthetic characteristic 982
photosynthetic efficiency 996
photosynthetic pigments 1086
phycocyanin 658
physical 971
Physical Model 910
Physicochemical parameters 846
physio-morphological traits 733
Phytoplankton 947
Phytoseiidae 1232
Phytoseius finitimus 1232
plants 928
plant-soil interactions 668
Pleurobrachia pileus 871
PM25 1138
p-nitroaniline 863
pollutant 820
pollution 799
pollution event 928
pore and fissure assembly 1043
pore structures 1043
porosity evolution 1043
Potassium Carbonate 1081
precision livestock farming 1031
predation 871
Pressure water 1269
Problems 898
proline 856
Propamocarb 838
Pteris multifida 771
Pumice 765
purchasability 1145

Q
Q biotype 1095
quality 1145

R
Radiation dose 793
rainbow trout 1013
Raman 1289
Reduction 1248
relative humidity 1226
Removal 815, 1169
Removal efficiency 675
resuspension 1226
Retention time 938
RFID 1031
Risk assessment 838
River 749
River Bend 807
River sand 675
root development 757
Rose hip 744
roughness 720
Rumen 1031

S
Safflower 989
salicylic acid 1256
Saline soil 1060
seasonal variation 1138
seed yield 989
seedling 1210
shelf life and qualitative attributes 1256
Simultaneous separation 1081
soaking time 1264
soil 651
Soil Classification 880
Soil Formation 880
soil organic matter 831
Soil weathering 880
Spatiotemporal characteristics 1214
Spearman rank correlation coefficient 1214
Spinning 787
spring water 971
Stachys 1176
Statistical evaluation and grouping 1131
Stepped Spillway 910
stone decay 720
strength 1264
stress 733
Submerged wetland 982
sulfate-reducing bacteria (SRB) 651
sun flower 856
Sunflower cultivation 710
Supercritical water oxidation 815
Supplier Selection 1191
suspension rate 1226
sustainable crop production 1053
SWAT model 960
sweet orange 1256

T
Tadorna ferruginea 703
Tariff policy 898
textile wastewater 779
Three Gorges Reservoir 947
tight sandstone reservoir 1043
trickling filter 779
tripeptide 1202
Triticum aestivum LWastewater 846
Turkey 703, 921, 971

U
Ultrasound 690
Upper Reaches of Hanjiang River Basin 1214
UV 681

V
Vineyard 1232
Vitamin B_{12} 1164

W
walnut 1152
Water and salt migration 1060
Water content 1060
water quality 971
Water quality model 749
Water treatment 799
Watermelon genotypes 1131
water-soluble ions 1138
Wheat germ 1145
wheat varieties 1086
Wind power 898

1,2….,9
2,6-Dichlorobenzamide 838
3,5,6-trichloro-2-pyridinol 1196

FEB – GUIDE FOR AUTHORS

General

FEB accepts original papers, review articles, short communications, research abstracts from the entire sphere of environmental-chemistry,-biology,-microbiology,- technology, -biotechnology and-management, furthermore, about residue analysis/ and ecotoxicology of contaminants.

Acceptance or no acceptance of a contribution will be decided, as in the case of other scientific journals, by a board of reviewers. Papers are processed with the understanding that they have not been published before (except in form of an abstract or as a part of a published lecture, review or thesis);that they are not under consideration for publication elsewhere; that their publication has been approved by all co-authors, if any, as well as-tacitly or explicitly- by the responsible authorities at the institute where the work has been carried out and that, if accepted, it will not be published elsewhere in the same form, in either the same or another language, without the consent of the copyright holders.

Language

Papers must be written in English. Spelling may either follow American (Webster) or British (Oxford) usage but must be consistent. Authors who are less familiar with the English language should seek assistance from proficient colleagues in order to produce manuscripts that are grammatically and linguistically correct.

Size of manuscript

Review articles should not exceed 30 typewritten pages. In addition up to 5 figures may be included.

Original papers must not exceed 14 typewritten pages. In addition up to 5 figures may be included.

Short-Communications should be limited to 4 typewritten pages plus not more than 1 illustration.

Short descriptions of the authors, presentation of their groups and their research activities (with photo) should together not exceed I typewritten page. Short research abstracts should report in a few brief sentences (one-fourth to one page) particularly significant findings. Short articles by relative newcomers to the chemical innovation arena highlight the key elements of their Master and PhD-works in about I page.

Book Reviews are normally written in-house, but suggestions for books to review are welcome.

Preparation of manuscript

Dear authors,

FEB is available both as printed journal and as online journal on the web. You can now e-mail your manuscripts with an attached file. Save both time and money. To avoid any problems handling your text please follow the instructions given below:

When preparing your manuscripts have the formula K/SS (Keep It Simple and Stupid) in mind. Most word processing programs such as MS-Word offer a lot of features. Some of them can do serious harm to our layout. So please do not insert hyperlinks and/or automatic cross-references, tables of contents, references, footnotes, etc.

1. Please use the standard format features of your word processor (such as standard.dot for MS Word).
2. Please do not insert automatisms or secret link-ups between your text and your figures or tables. These features will drive our graphic department sometimes mad.
3. Please only use two fonts for text or tables "Times New Roman" and for graphical presentations "Arial".
4. Stylesheets, text, tables and graphics in shade of grey
5. Turn on the automatic language detection in English (American or British)
6. Please - check your files for viruses before you send them to us!!

Manuscripts should send to:parlar@wzw.tum.de
or:parlar@prt-parlar.de

Thank you very much!

STRUCTURE OF THE MANUSCRIPT

Title page: The first page of the manuscript should contain the following items in the sequence given: A concise title of the paper (no abbreviations). The names of all authors with at least one first name spelled out for every author. The names of Universities with Faculty, City and Country of all authors.

Abstracts: The second page of the manuscript should start with an abstract that summarizes briefly the contents of the paper (except short communications). Its length should not exceed 150-200 words. The abstract should be as informative as possible. An extended repetition of the paper's title is not considered to be an abstract.

Keywords: Below the Summary up to 6 key words have to be provided which will assist indexers in cross-indexing your article.

Introduction: This should define the problem and, if possible, the frame of existing knowledge. Please ensure that people not working in that particular field will be able to understand the intention. The word length of the introduction should be 150 to 300 words.

Materials and methods:
Please be as precise as possible to enable other scientists to repeat the work.

Results: Only material pertinent to the subject must be included. Data must not be repeated in figures and tables.

Acknowledgements: Acknowledgements of financial support, advice or other kind of assistance should be given at the end of the text under the heading "Acknowledgements". The names of funding organisations should be written in full.

References: Responsibility for the accuracy of references rests with the authors. References are to be limited in number to those absolutely necessary. References should appear in numerical order in brackets and in order of their citation in the text. They should be grouped at the end of the paper in numerical order of appearance. Abbreviated titles of periodicals are to be used according to Chemical or Biological Abstracts, but names of lesser known journals should be typed in full. References should be styled and punctuated according to the following examples:

ORIGINALPAPERS:
l. Author, N.N. and Author, N.N. (Year) Full title of the article. Journal and Volume, first and last page.
BOOK OR PROCEEDING:
2. Author, N.N. and Author, N.N. (Year) Title of the contribution. In: Title of the book or proceeding. Volume (Edition of klitor-s, ed-s) Publisher, City, first and last page

DOCTORAL THESIS:
3. Author, N.N. (Year) Title of the thesis, University and Faculty, City

UNPUBLISHED WORK:
Papers that are unpublished but have been submitted to a journal may be cited with the journal's name followed by "in press". However, this practice is acceptable only if the author has at least received galley proofs of his paper. In all other cases reference must be made to “unpublished work" or "personal communication".

Discussion and Conclusion: This part should interpret the results in reference to the problem outlined in the introduction and of related observations by the author/s or others. Implications for further studies or application may be discussed. A conclusion should be added if results and discussion are combined.

Corresponding author: The name of the corresponding author with complete postal address

Precondition for publishing:
A minimum number of 25 reprints must be ordered and prepaid.
1 - 4 pp.: 200,- EURO + postage/handling
5 - 8 pp.: 250,- EURO + postage/ handling
More than 8pp: 1.50 EURO/page x number of reprints +postage/ handling.
The prices are based upon the number of pages in our journal layout (not on the page numbers of the submitted manuscript).
Postage/ Handling: The current freight rate is Germany 10 €, Europe 18,00 €, International 30 €.
VAT: In certain circumstances (if no VAT registration number exists) we may be obliged to charge 7% VAT on sales to other EU member countries.MESAEP and SECOTOX members get a further discountof 20% (postage/ handling full).